Short Papers in the Geological Sciences

Geological Survey Research 1960

GEOLOGICAL SURVEY PROFESSIONAL PAPER 400-B

Scientific notes and summaries of investigations prepared by members of the Geologic Division in the fields of geology and allied sciences

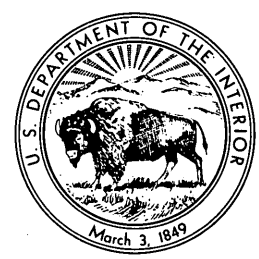

UNITED STATES GOVERNMENT PRINTING OFFICE, WASHINGTON : 1960

UNITED STATES DEPARTMENT OF THE INTERIOR

FRED A. SEATON, *Secretary*

GEOLOGICAL SURVEY

Thomas B. Nolan, *Director*

For sale by the Superintendent of Documents, U.S. Government Printing Office
Washington 25, D.C. - Price $4.25 (paper cover)

CONTENTS

SHORT PAPERS IN THE GEOLOGICAL SCIENCES

GEOLOGY OF METALLIFEROUS DEPOSITS

1. AN HYPOTHESIS FOR THE ORIGIN OF ORE-FORMING FLUID

By J. Hoover Mackin and Earl Ingerson, University of Washington, Seattle, Wash., and University of Texas, Austin, Tex.

It is generally agreed that primary metalliferous veins are genetically related to intrusive igneous bodies, but in most mining districts the field relations demonstrate only that both the magma and the ore-forming fluid originated below the present surface, and it is therefore not possible to determine the nature of the genetic relationship by direct observation. The classical view, based largely on theoretical considerations, holds that "metals and mineralizers," present in minute proportions in the orginal melt, are concentrated in a rest liquid by fractional crystallization of rock-forming minerals devoid of those substances, and that during a late stage in the solidification of the intrusion the rest liquid escapes to form ore deposits. The different hypothesis outlined in this note is based on studies in the Iron Springs district, in southwestern Utah.

In the Iron Springs district replacement ore bodies of magnetite and hematite occur in Jurassic limestone around the borders of early Teritiary laccoliths of granodiorite porphyry. The present erosion surface cuts the laccoliths at a favorable level, and it is possible to prove that the iron in the ore bodies was derived from the immediately adjacent porphyry. Several lines of evidence indicate that the iron was originally incorporated in biotite and hornblende that crystallized in the melt in depth prior to the emplacement of the laccoliths. The outermost part of the typical Iron Springs laccolith—a "peripheral shell" 100 to 200 feet thick—consolidated so rapidly that there was little deuteric alteration; the biotite and hornblende phenocrysts in the peripheral shell rock are fresh, and the field relations indicate that this rock yielded no ore. In the interior of the laccoliths, on the other hand, the biotite and hornblende phenocrysts were largely or completely destroyed by deuteric alteration, and the iron contained in them was released into the interstitial fluid of a slowly consolidating crystal mush. This fluid escaped only from those parts of the laccoliths where renewed intrusion caused outbulging that opened gaping tension joints in the semisolid mush within the peripheral shell. The tension joints are bordered by bleached-appearing "selvages" as much as three or four inches in width; the selvage rock contains about 30 percent less iron than the rock midway between them. The faces of the selvaged joints are encrusted with magnetite and other minerals, and the joint fillings are in a merely descriptive sense fissure veins; they differ in origin from ordinary fissure veins, which are, if we may use a medieval analogy, the branches or leaves of the "mineral tree", whereas the selvaged joints in the Iron Springs laccoliths are the *roots* of the "mineral tree." It is possible to walk across ledge outcrops from the deep interior of the laccoliths, where the interstitial fluid was all retained, upward and outward through the selvaged joint zone, where the iron of the ore deposits originated, and thence along magnetite-impregnated breccias formed by late-intrusive faults, that served as conduits for movement of the ore-forming fluid through the peripheral shell, and finally reach the replacement ore bodies at the contact.

This theory implies that the replacement ore bodies of the Iron Springs district should occur only adjacent to parts of the laccoliths where there are selvaged joints, and, conversely, that the selvaged joints should be present only where there was late-intrusive distension. Ore bodies should therefore be restricted to segments of the contact that are convex outward in section, or in plan, or both; where the contact is planar there should be no selvaged joints in the intrusive rock and no replacement ore in the adjacent limestone. These implications are borne out by the actual distribution of the iron ore bodies.

Crystalline hematite was deposited in cracks in the upper part of a silicic ignimbrite sheet formed by a nueé ardente eruption in the Iron Springs district just prior to emplacement of the laccoliths. As the ignimbrite sheet is almost identical in composition with the intrusions, one can reasonably assume that it was derived from the same magmatic source. The biotite and hornblende phenocrysts in a layer of vitrophyre at the base of the ignimbrite sheet are perfectly fresh, but those in the middle part, where the matrix is stony-textured, are largely or wholly destroyed by deuteric alteration. The mechanics of origin of the ignimbrite sheet virtually rule out the possibility that the fluid which deposited the fumarolic hematite in its upper part was a magmatic rest liquid, enriched in "metals and mineralizers" by fractional crystallization; the relations indicate rather that the iron was released by deuteric alteration of intratelluric hornblende and biotite while the ignimbrite was consolidating at the surface.

The "deuteric release" hypothesis of origin of the ore-forming fluid in the Iron Springs district has thus far been applied only in that district, and its validity depends entirely on specific lines of evidence developed there, but it is worthwhile to consider its possible application to a larger, long-standing geologic problem: Why is it that ore deposits tend to cluster around stocks and other hypabyssal intrusions consisting of porphyry, while the border zones and roof pendants of the great batholiths tend to be relatively barren? This relationship does not comport with the view that the ore metals are concentrated in a rest liquid by fractional crystallization. Slow and complete crystallization in batholithic bodies should be much more favorable for such concentration than the conditions under which hypabyssal bodies consolidate. The poverty of deep-seated bodies as compared with hypabyssal bodies is, on the other hand, a direct and necessary consequence of the "deuteric" release hypothesis, not considered when that hypothesis was being formulated in the Iron Springs district.

Iron is an integral constituent of some rock-forming minerals, and many of the other ore metals are readily accepted into the lattices of many of the rock-forming minerals, particularly biotite. If these minerals crystallize in a batholithic chamber and if the magma consolidates completely in that same chamber, the metals locked up in the rock-forming minerals will not be available to form ore bodies. But if, during the period of crystallization, a phenocryst-bearing magma moves upward from the batholithic chamber to form a hypabyssal body, deuteric decay of those phenocrysts that are unstable under the new conditions will release the metals to the interstitial fluid in the interior of the consolidating body. A second requirement for the production of ore is continued growth of the hypabyssal body, or a renewed upsurging of magma which causes distension in convex parts of the chamber at a time when the crystal mush in those parts is stiff enough to crack but is still chemically reactive; the gaping primary tension joints which will then penetrate into the semisolid mush can become the "roots of the mineral tree". A general prerequisite is, of course, that the original melt shall contain all the substances needed for making ore; we have only iron oxide ore in Iron Springs because the magmas there happen to have been nearly devoid of sulfur, which is a constituent of most ores of other metals.

The "deuteric release" hypothesis is useful because its consequences are readily deducible and very specific, and serve as a basis for diagnostic tests that can be applied wherever the present erosion surface or mine workings cut an intrusive body at the level at which ore was released.

2. VARIETIES OF SUPERGENE ZINC DEPOSITS IN THE UNITED STATES

By A. V. Heyl, Jr., and C. N. Bozion, Beltsville, Md., and Washington, D.C.

Deposits of oxidized zinc minerals are widely distributed throughout the United States, especially in the general region of the Rocky Mountains and Basin and Range provinces, in the principal Mississippi Valley districts, in the Valley and Ridge province, and in the New Jersey Highlands and western Adirondacks.

Most supergene zinc deposits can be classified into three main types in order of their abundance: (a) direct-replacement deposits (fig. 2.1), (c) wallrock deposits (fig. 2.2), and (b) saprolitic (weathered in place) and residual (essentially in place, but compacted) accumulations (fig. 2.3). A few supergene wurtzite de-

posits are known (for example, Horn Silver mine in Utah, Butler, 1913), also placer (Heyl and others, 1959, p. 131), bog (Cannon, 1955), and cave accumulations. Many deposits are combinations of several types.

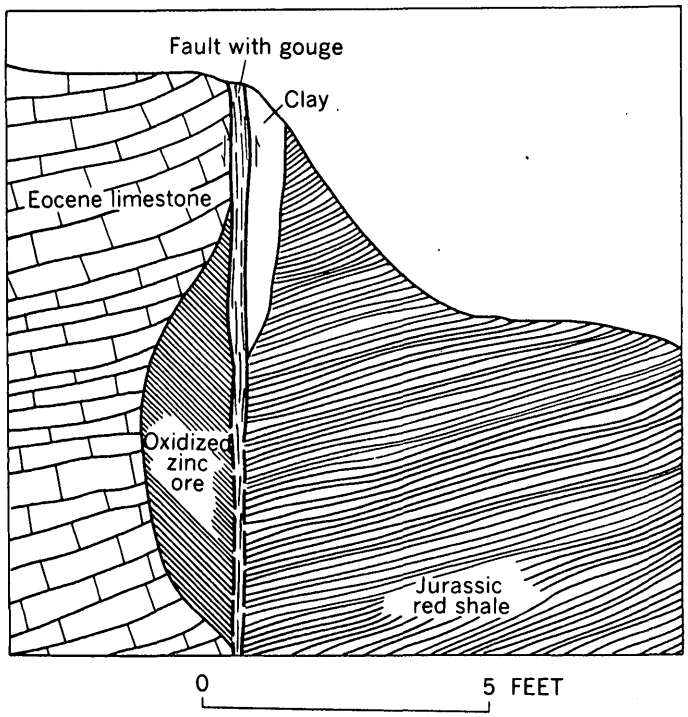

FIGURE 2.1.—Direct-replacement deposit of zinc sulfide vein by oxidized zinc minerals, Redmond, Utah.

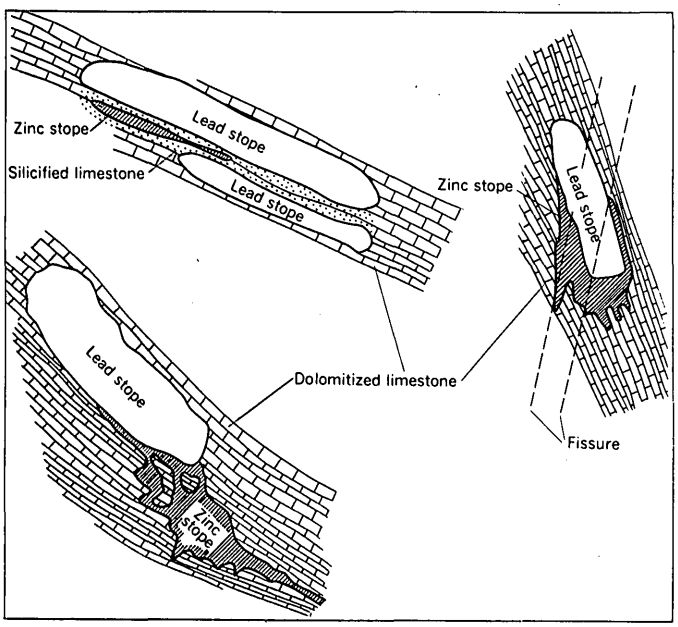

FIGURE 2.2.—Wallrock deposits of oxidized zinc ore (after Loughlin, 1914), Tintic district, Utah.

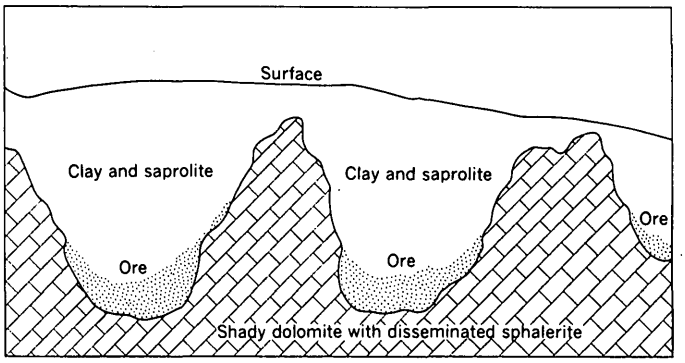

FIGURE 2.3.—Saprolitic and residual accumulation of oxidized zinc ore (after Watson, 1905, fig. 16), Bertha, Va.

DIRECT-REPLACEMENT DEPOSITS

Deposits directly replacing hypogene sulfides are the most abundant. They retain the shape of the original ore bodies, although the metals are redistributed. In areas of slow oxidation and near-neutral conditions (pH 7–8), such as the upper Mississippi Valley (Heyl and others, 1959, p. 164–165), pseudomorphs of smithsonite after sulfides are common; but in areas of deep and rapid oxidation zinc, copper, and iron tend to migrate towards the margins of the deposit where they reconcentrate as smithsonite, hemimorphite, malachite-azurite, and limonite casings, or as kidney-shaped, concentric-shelled masses within the original ore body. Lead, silver, and gold migrate somewhat but redeposit nearly in place as supergene compounds and native gold and silver. Galena, completely replaced by cerussite, anglesite, and plumbojarosite, is typical. Sphalerite is replaced by smithsonite and hemimorphite, and less commonly by hydrozincite, willemite, descloizite, and adamite. Outcrops are leached to a porous gossan of limonite, jasperoid, calcite, and less abundantly cerussite, plumbojarosite, cerargyrite, hemimorphite, and gold.

Although many discussions of zinc oxidation state that supergene zinc deposits of commercial size in rocks lean in carbonate are rare or nonexistent, at least 24 are known. All are in the West, and some are rich and large, such as those in the Warm Springs district, Idaho (Umpleby and others, 1930), Clifton-Morenci (Lindgren, 1905), Globe-Miami (Peterson, 1950, p. 98–112), Silver-Eureka (Wilson, 1951, p. 83–97) districts of Arizona, and the Sedalia mine (Lindgren, 1908, p. 161–166), Salida, Colorado. The "rule" that zinc is usually dispersed in solutions when deposits in noncarbonate rocks are oxidized obviously has many exceptions. The wall rocks include metasedimentary and clastic sedimentary rocks, gneisses, mafic and felsic igneous rocks, and calcareous quartzites. Most districts have under-

gone deep and intense oxidation, usually in areas of arid climate where supergene solutions are so sparse that most metals are redeposited within the original ore bodies as the solutions descend and evaporate.

Descloizite, mottramite, and vanadinite are common as main or accessory minerals throughout the southern part of the Basin and Range province of the United States and Mexico. The source of the vanadium has been attributed by some (Kelly and others, 1958, p. 1596; Fischer, 1959, p. 222–223) to adjacent limestones. Newhouse (1934, p. 209–219) attributed the vanadium to traces in hypogene deposits. The present study shows that vanadium minerals are found in a wide variety of geologic environments throughout metallogenetic provinces irrespective of wallrocks, be they felsic or mafic igneous rocks, gneisses, amphibolites, limestones, or clastic rocks of different ages. Only one of several oxidized zinc deposits in the vanadium-bearing Colorado Plateau province contains vanadium minerals, which supports the ideas of Newhouse.

Willemite is a supergene mineral locally abundant in the West, and mined in at least nine localities; nearly all are in deeply oxidized districts of the Basin and Range province. For reasons unclear, it is restricted to certain deposits within districts.

WALLROCK DEPOSITS

Wallrock deposits (fig. 2.2) are common in the West, but uncommon in the East, except for very small pockets in walls of direct-replacement and saprolitic deposits and a single large supergene willemite ore body at Balmat, N.Y. (Brown, 1936).

Wallrock pockets, casings, blankets, veins, and pipes of supergene zinc ores in carbonate rocks below and adjacent to leached sulfide bodies comprise some of the largest and richest deposits in the West, such as Leadville, Colo. (Loughlin, 1918); Magdalena, N. Mex. (Loughlin and Koschmann, 1942); Goodsprings, Nev. (Hewett, 1931); and Cerro Gordo, Calif. (Knopf, 1918). The main minerals in these bodies commonly are smithsonite, hemimorphite, limonite, calcite, and jasperoid in massive, lamellar, and vuggy masses replacing barren limestones (fig. 2.2). Chalcophanite, hydrohetaerolite, and sauconite are also abundant where manganese and silica are present, as at Leadville, Colo., and Tintic, Utah (Loughlin, 1914). In the Basin and Range province, where oxidation and leaching have been deep and intense over long periods, hydrozincite and aurichalcite occur in commercial quantities; for reasons unknown, hydrozincite is nearly restricted to the northern parts of that province. Wallrock deposits contain very little of the gold, silver, lead, vanadium, molybdenum, antimony, and arsenic typical of direct-replacement deposits. Where leached to a gossan, vuggy and concentrically banded limonite and jasperoid contain a little hemimorphite.

SAPROLITIC ACCUMULATIONS AND RESIDUAL DEPOSITS

Saprolitic accumulations (fig. 2.3) and residual deposits are restricted to the East—the former to the warm and humid Ridge and Valley province. Saprolitic accumulations include residual as well as redeposited masses of smithsonite, hemimorphite, and locally, sauconite collected partly in saprolite and in compacted clay-filled solution pockets between buried pinnacles of unweathered limestone. The supergene minerals are derived from lean disseminated or massive sphalerite in unweathered limestone pinnacles, such as at Austinville and Bertha, Va. (Watson, 1905, p. 78–92). The unfractured sulfide-bearing limestone in the warm, wet climate is rapidly dissolved into pinnacles and pockets by abundant vadose waters (pH 4–5); along fractures residual limestone solution-clay slumps into pockets, intermingled with limestone saprolite still in place. Smithsonite replaces part of the sphalerite and remains as residual masses embedded in the clayey pockets. Some zinc dissolves in vadose waters but is redeposited as smithsonite, hemimorphite, and sauconite near the bottoms of the pockets when accumulated solutions become saturated in zinc.

CONCLUSIONS

The study shows that supergene zinc deposits most commonly directly replace the sulfide deposits, and they show regional patterns of geology dependent on (a) pH, rainfall, and climatic factors; (b) wallrocks and geologic variations between metallogenetic provinces. Deposits in noncarbonate wall rocks are fairly common, and many western deposits contain complex minerals previously thought to be uncommon.

REFERENCES

Brown, J. S., 1936, Supergene sphalerite, galena, and willemite at Balmat, N.Y.: Econ. Geology, v. 31, p. 331–354.

Butler, B. S., 1913, Geology and ore deposits of the San Francisco and adjacent districts: U.S. Geol. Survey Prof. Paper 80.

Cannon, H. L., 1955, Geochemical relations of zinc-bearing peat to the Lockport dolomite, Orleans County, N.Y.: U.S. Geol. Survey Bull. 1000–D, p. 119–185.

Fischer, R. P., 1959, Vanadium and uranium in rocks and ore deposits, *in* Garrels, R. M., and Larsen, E. S., 3d, Geochemistry and mineralogy of Colorado Plateau uranium ores: U.S. Geol. Survey Prof. Paper 320, p. 219–230.

Hewett, D. F., 1931, Geology and ore deposits of the Goodsprings quadrangle, Nevada: U.S. Geol. Survey Prof. Paper 162, 172 p.

Heyl, A. V., and others, 1959, The geology of the upper Mississippi Valley zinc-lead district: U.S. Geol. Survey Prof. Paper 309, p. 131, p. 164–165.

Kelly, W. C., and others, 1958, Progress in studies on leached outcrops [abs.]: Geol. Soc. America Bull., v. 69, p. 1596.

Knopf, Adolph, 1918, A geologic reconnaissance of the Inyo Range and the eastern slope of the Sierra Nevada, Calif.: U.S. Geol. Survey Prof. Paper 110.

Lingren, Waldemar, 1905, The copper deposits of the Clifton-Morenci district, Ariz.: U.S. Geol. Survey Prof. Paper 43, 375 p.

——— 1908, Notes on copper deposits in Chaffee, Fremont, and Jefferson Counties, Colo.: U.S. Geol. Survey Bull. 340, part 1, p. 161–166.

Loughlin, G. F., 1914, The oxidized zinc deposits of the Tintic district: Econ. Geology, v. 9, no. 1, p. 1–19.

——— 1918, The oxidized zinc ores of Leadville, Colo.: U.S. Geol. Survey Bull. 681.

Loughlin, G. F., and Koschmann, 1942, Geology and ore deposits of the Magdalena mining district, N. Mex.: U.S. Geol. Survey Prof. Paper 200.

Newhouse, W. H., 1934, The source of vanadium, molybdenum, tungsten, and chromium in oxidized lead deposits: Am. Mineralogist, v. 19, no. 5, p. 209.

Peterson, N. P., 1950, Arizona zinc and lead deposits; Lead and zinc deposits in the Globe-Miami district, Arizona: Arizona Bur. Mines Bull. 156, Geol. Ser. 18, p. 98–112.

Umpleby, J. B., and others, 1930, Geology and ore deposits of the Wood River region, Idaho: U.S. Geol. Survey Bull. 814.

Watson, T. L., 1905, Lead and zinc deposits of Virginia: Virginia Geol. Survey Bull. 1, p. 78–92, fig. 16.

Wilson, E. D., 1951, Silver and Eureka districts, Chap. 9 *of* Arizona zinc and lead deposits, Pt. 2: Arizona Bur. Mines Bull. 158, Geol. Ser. no. 19, p. 83–97.

3. LITHOFACIES OF THE COPPER HARBOR CONGLOMERATE, NORTHERN MICHIGAN

By Walter S. White and James C. Wright, Beltsville, Md., and Denver, Colo.

The Copper Harbor conglomerate of northern Michigan crops out along the south limb of the Lake Superior syncline from Keweenaw County westward through Gogebic County, Mich. (fig. 3.1), and along its north limb on Isle Royale. The formation, which is of late Keweenawan age, is underlain by the Portage Lake lava series, a thick sequence of flood basalts of middle Keweenawan age, and overlain by the Nonesuch shale and the Freda sandstone of late Keweenawan age. The formation interfingers slightly with both the overlying shale and the underlying lava.

The Copper Harbor conglomerate consists chiefly of red to brown arkosic conglomerate and sandstone, cemented with calcite and laumontite; most of its pebbles are of rhyolite, a few are of mafic lava, and other types are rare. Locally it contains interbedded groups of mafic and rhyolitic lava flows, and a very little red shale and volcanic ash. The ash, which contains montmorillonite and tiny books of biotite, was observed in only seven beds in a series of holes drilled through the formation at Calumet.

The distribution of the principal rock types in the formation is portrayed in figure 3.2. East of Houghton the contacts are based on detailed mapping (much of it by H. R. Cornwall), supported by airborne magnetometer traverses in areas under Lake Superior. The relative proportions of sandstone and conglomerate are not known everywhere east of Houghton, but conglomerate predominates where no pattern is used. The persistent sandstone unit shown in the lower part of the formation throughout Keweenaw County is based on a few outcrops and on prominent topographic expression (Cornwall, 1954).

West of Houghton, exposures are generally poor and only a few small areas have been mapped in detail. The thickness of the formation and of its subdivisions at various places has been determined from breadth of outcrop. Our own field data are supplemented by scattered observations recorded in many published reports, and by the results of an airborne magnetometer survey of part of the area by the U.S. Geological Survey.

The Copper Harbor conglomerate thins markedly at Houghton, where the formation appears to lap up on a ridge of the underlying lavas. This ridge is the product of differential uplift, most of which occurred during the first half of Copper Harbor time; the base of the formation is parallel with the two persistent conglomerate beds in the underlying lava series, but its top is not (see fig. 3.2).

Most of the thick accumulation of rhyolite that makes up a large part of the formation in western Ontonagon County is believed to consist of rhyolite flows that piled up close to their source. The area in which the rhyolite is thick and the overlying conglomerate is thin (as little as 500 feet thick in places) is roughly outlined by a dashed line in figure 3.1; just out-

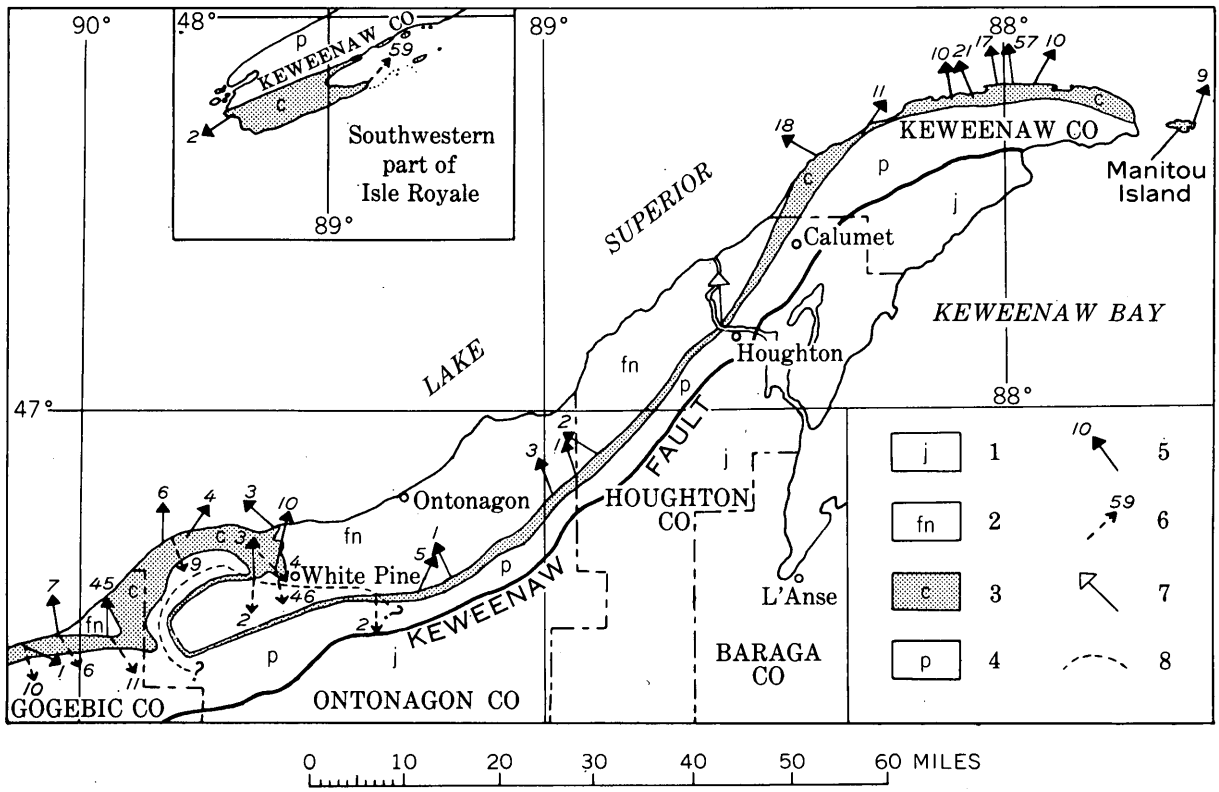

FIGURE 3.1.—Distribution of Copper Harbor conglomerate and its oriented sedimentary structures. 1, Jacobsville sandstone; 2, Nonesuch shale and Freda sandstone; 3, Copper Harbor conglomerate; 4, Portage Lake lava series and lavas in lower part of Copper Harbor conglomerate; 5, average direction of current flow shown by crossbeds in conglomeratic sandstone; number beside each arrow gives the number of individual observations included in average; 6, average direction of current flow shown by crossbeds in "red facies"; 7, direction of current flow indicated by imbrication of pebbles; 8, limit of thick mass of extrusive rhyolite.

side this area, the conglomerate is 2,000 to 3,000 feet thick.

The directions of the currents that deposited the conglomerate were determined from the attitudes of crossbeds, and, at one place near Houghton, from that of imbricated pebbles. Though many of the samplings of attitudes are small, and some are known to be biased because of the nature of the exposures, the measured directions indicate clearly, when taken together, that the conglomerate was deposited by northward flowing currents, in contrast with the rocks to be described next.

A separate facies of the Copper Harbor conglomerate, here designated the "red facies," is exposed in at least the western third of the area shown in figure 3.1. The dominant rock of this facies is platy fine- to medium-grained sandstone, redder than the rocks of the formation as a whole. This red sandstone occurs in thick sequences with very little interbedded conglomerate, and its statigraphic position is not everywhere the same. In Gogebic County it occurs only in the uppermost 200 to 500 feet of the formation (fig. 3.2), but at the Mendenhall location 250 feet or more of red platy sandstone underlies 500 feet of conglomerate and coarse brownish-red sandstone. North of White Pine, north of the line of figure 3.2, rocks of the red facies occur from 300 to at least 1,000 feet below the top of the formation. The currents that deposited the rocks of the red facies flowed southward, as indicated in figure 3.1 by arrows with dashed-line shafts.

The Lake Superior basin was at least 60 or 70 miles across in late Keweenawan time. The conglomerate facies is interpreted as a piedmont fan, deposited by northward-flowing streams at the foot of hills along the southern margin of this basin. The great central expanse of the basin presumably had a more nearly horizontal surface, covered by finer grained sediments deposited on flood plains or in standing water. The red facies is interpreted as a flood-plain deposit, transported by currents that locally, at least, flowed southward on this broad alluvial plain to deposit material against the toe of the fan.

We have suggested previously (White, 1960) that the copper in the base of the Nonesuch shale at White Pine and elsewhere (White and Wright, 1954, p. 715–716)

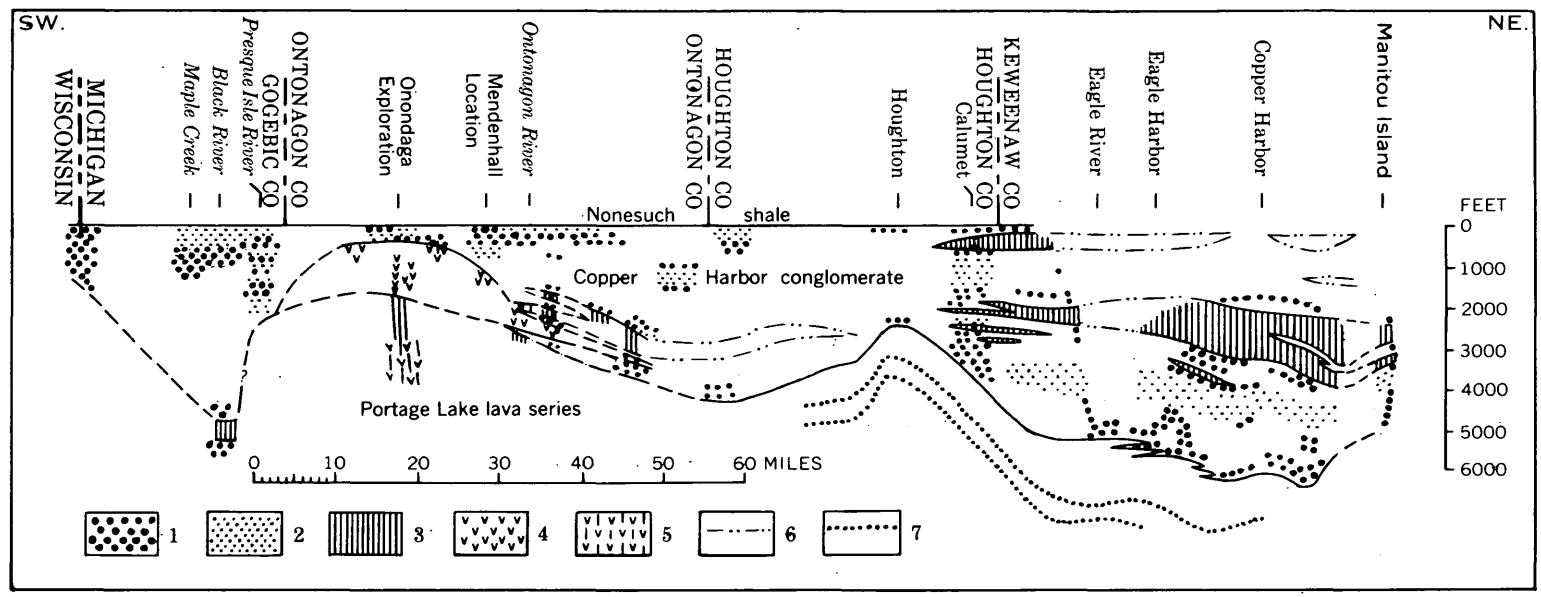

FIGURE 3.2.—Stratigraphic cross-section of the Copper Harbor conglomerate, northern Michigan, looking down dip. Datum is base of Nonesuch shale. Line of section lies 8 to 12 miles south of Lake Superior in western Ontonagon County. 1, Conglomerate; 2, sandstone; 3, basaltic lava; 4, rhyolite; 5, basalt and rhyolite, undifferentiated; 6, contacts of basaltic lava located by aeromagnetic survey; 7, persistent conglomerate bed in Portage Lake lava series.

may have been deposited from connate water, squeezed out of the Keweenawan sedimentary rocks during compaction and diagenesis. This source of water would be very large and suitably located if the coarse-grained facies of the Copper Harbor conglomerate does indeed give way to fine-grained sediments in the central part of the Lake Superior basin, far down the dip from the copper deposits. The thick pile of rhyolite outlined by the dashed line in figure 3.1 may have acted like a buried hill to intensify the flow of water up into the Nonesuch shale; this mechanism could help explain the unusual concentrations of copper close to the border of the thick mass of rhyolite.

REFERENCES

Cornwall, H. R., 1954, Bedrock geology of the Lake Medora quadrangle, Michigan: U.S. Geol. Survey Geol. Quad. Map GQ–52.

White, W. S., 1960, The White Pine copper deposit: Econ. Geology, v. 55, p. 402–410.

White, W. S., and Wright, J. C., 1954, The White Pine copper deposit, Ontonagon County, Michigan: Econ. Geology, v. 49, p. 675–716.

4. RELATION OF THE COLORADO MINERAL BELT TO PRECAMBRIAN STRUCTURE

By Ogden Tweto and P. K. Sims, Denver, Colo.

Work done in cooperation with Colorado State Metal Mining Fund Board

The narrow northeast-trending Colorado mineral belt is characterized by intrusive porphyries and associated ore deposits of Laramide age, and in some places by fissures and faults of northeasterly trend. All the major mining districts of Colorado, except the uranium districts of southwestern Colorado and a few mining districts associated with isolated volcanic centers, such as Cripple Creek, are in this belt.

The mineral belt extends diagonally across the generally north-trending mountain ranges of the State for a distance of 250 miles—from the Front Range in central Colorado southwestward across the Park and Sawatch Ranges to the San Juan Mountains (fig. 4.1). It thus cuts indiscriminantly across the geologic grain of the State, occupies several different geologic environments, and seems to be independent of the present mountain structure.

Although the most conspicuous features of the mineral belt are of Laramide age, the belt follows an ancient zone of weakness defined by northeast-trending shear zones of Precambrian age, which form an echelon pattern in a strip that is nearly coextensive with the mineral belt. Many of these zones have not yet been fully mapped, but major shear zones of this group have been studied in detail in two areas—on the eastern flank of the Front Range (Moench, Harrison, and Sims, 1954, 1958; Sims, Moench, and Harrison, 1959; Harrison and Wells, 1959; J. D. Wells and D. M. Sheridan, oral communication, 1959) and in the northern part of the Sawatch Range (Tweto and Pearson, 1958). In the eastern part of the Front Range is the Idaho Springs-Ralston shear zone, marked by cataclasis and related small-scale cross folds, which lies along the southeastern side of the mineral belt (fig. 4.1). In the Sawatch Range, there is the composite Homestake shear zone which comprises dozens of individual shear zones in a belt 7 or 8 miles wide. In the Park Range, which lies between the Front and Sawatch Ranges, the northeast-trending line of shearing is interrupted by a major cross-trending shear zone, of Precambrian age, which localized the Gore and Mosquito faults in Laramide time. Lesser cross faults of northwest trend are numerous in the Front Range, where they are known as breccia reefs (Lovering and Goddard, 1950). These faults originated in Precambrian time but are in general younger than the northeast-trending shear zones, and many of them were reactivated during the Laramide.

Intermittent movement has occurred in the shear zones through most of the geologic time recorded in the region. Primary folds in the oldest metamorphic rocks, some of them oriented in stress fields confined to the shear zones, indicate that the shear zones existed at the stage of deformation by plastic flow. At a later stage, when pressure was less intense and temperature lower, shearing took place by fracturing and locally by minor cross-folding. Early fracturing occurred before the metamorphic environment had permanently

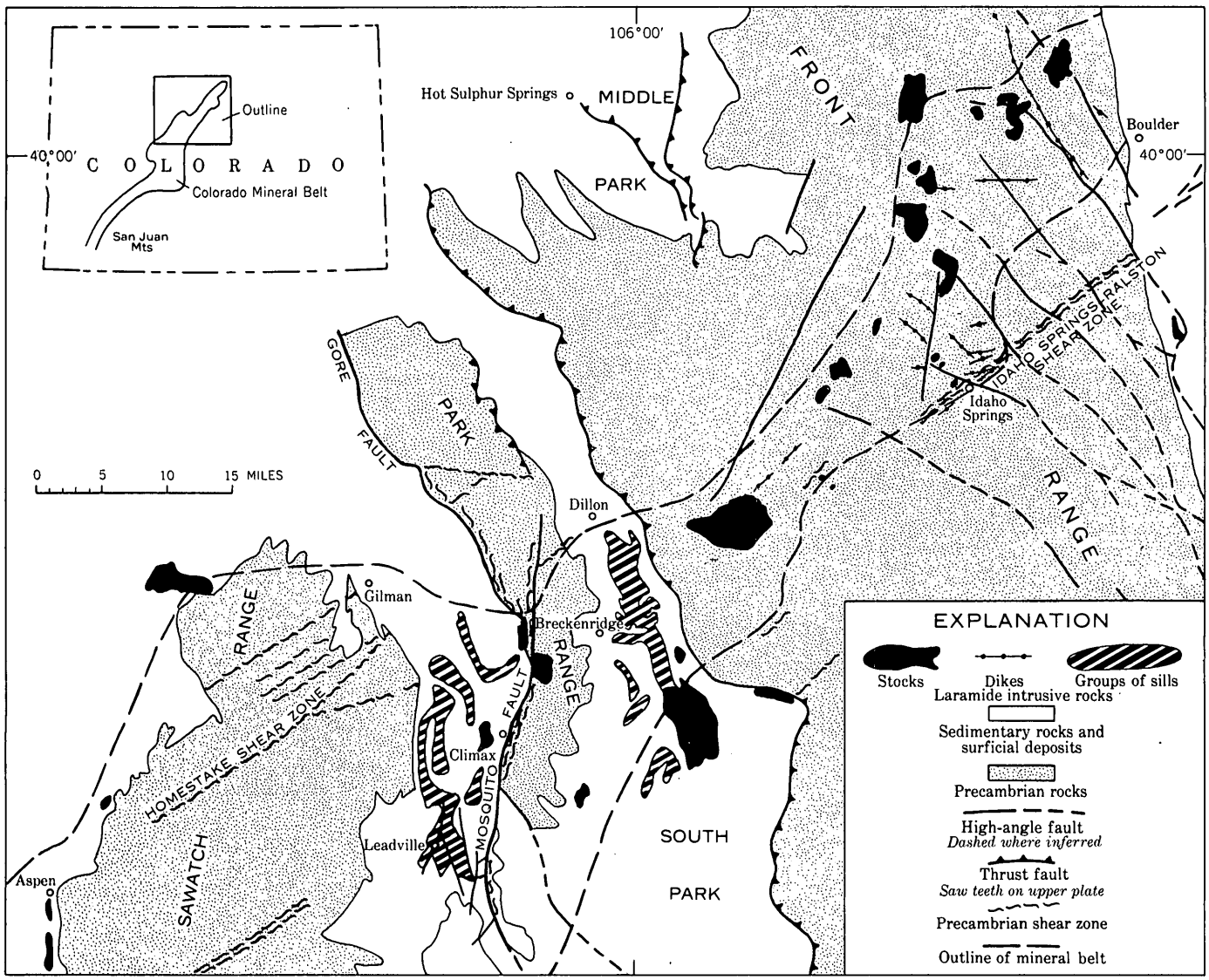

FIGURE 4.1—Geologic setting of Precambrian shear zones and northeastern part of Colorado mineral belt.

disappeared, and rocks formed at this stage are reorganized and recrystallized gneisses. Later shearing yielded cataclastic gneisses, mylonite, broad granulated zones, and locally pseudotachylyte. Still later, but still in the Precambrian, gouge, breccia, and fault zones were formed, partly by the degradation of earlier shear products of higher rank.

Differential movements in parts of the regional zone of shearing continued intermittently through Paleozoic and Mesozoic time, mostly on a minor scale, as recorded by thinning, wedgeouts, and changes in facies of several sedimentary formations along the shear zone. In some places the shear zones formed a sharp border between the persistent positive and negative areas that existed in Colorado during Paleozoic and Mesozoic time.

With the onset of the Laramide orogeny, magma invaded the regional zone of shearing and imparted to it the conspicuous features that characterize the mineral belt—intrusive igneous bodies and ore deposits. Fault movement took place along the zone at this stage also but was in general on a smaller scale than it had been previously. Reasons for the appearance of magma in the ancient zone of weakness at this time, and the processes by which it yielded a large family of porphyries and a remarkable variety of ore deposits, are major problems remaining for investigation.

REFERENCES

Harrison, J. E., and Wells, J. D., 1959, Geology and ore deposits of the Chicago Creek area, Clear Creek County, Colorado: U.S. Geol. Survey Prof. Paper 319.

557753 O—60——2

Lovering, T. S., and Goddard, E. N., 1950, Geology and ore deposits of the Front Range, Colorado: U.S. Geol. Survey Prof. Paper 223.

Moench, R. H., Harrison, J. E., and Sims, P. K., 1954, Precambrian structures in the vicinity of Idaho Springs, Front Range, Colorado [abs.]: Geol. Soc. America Bull., v. 65, p. 1383–1384.

——— 1958, Precambrian folding in the central part of the Front Range mineral belt, Colorado [abs.]: Geol. Soc. America Bull., v. 69, p. 1737.

Sims, P. K., Moench, R. H., and Harrison, J. E., 1959, Relation of Front Range Mineral Belt to ancient Precambrian structures [abs.]: Geol. Soc. America Bull., v. 70, p. 1749.

Tweto, Ogden, and Pearson, R. C., 1958, Great Precambrian shear zone, Sawatch Range, Colorado [abs.]: Geol. Soc. America Bull., v. 69, p. 1748.

5. PRE-ORE AGE OF FAULTS AT LEADVILLE, COLORADO

By Ogden Tweto, Denver, Colo.

Work done in cooperation with Colorado State Metal Mining Fund Board

In the Leadville mining district, Colorado, sedimentary rocks of Paleozoic age dip gently eastward and are broken by many faults, most of which are upthrown to the east. Porphyries of Laramide age form sills, dikes, and irregular bodies that cut the sedimentary rocks in an intricate pattern. Although the porphyries—presumably derived from the same source as the ores—are all older than the ores, they are in general only weakly mineralized; the ore deposits are largely restricted to the sedimentary rocks in layers and blocks between bodies of porphyry. Faults displace many ore bodies, and for this reason many major faults of the district have been regarded as younger than the ores (Emmons, 1886; Emmons, Irving, and Loughlin, 1927). Recent studies within the Leadville district and north of it have revealed, however, that practically all the faults originated before the ore, although many underwent renewed movement during a post-ore stage.

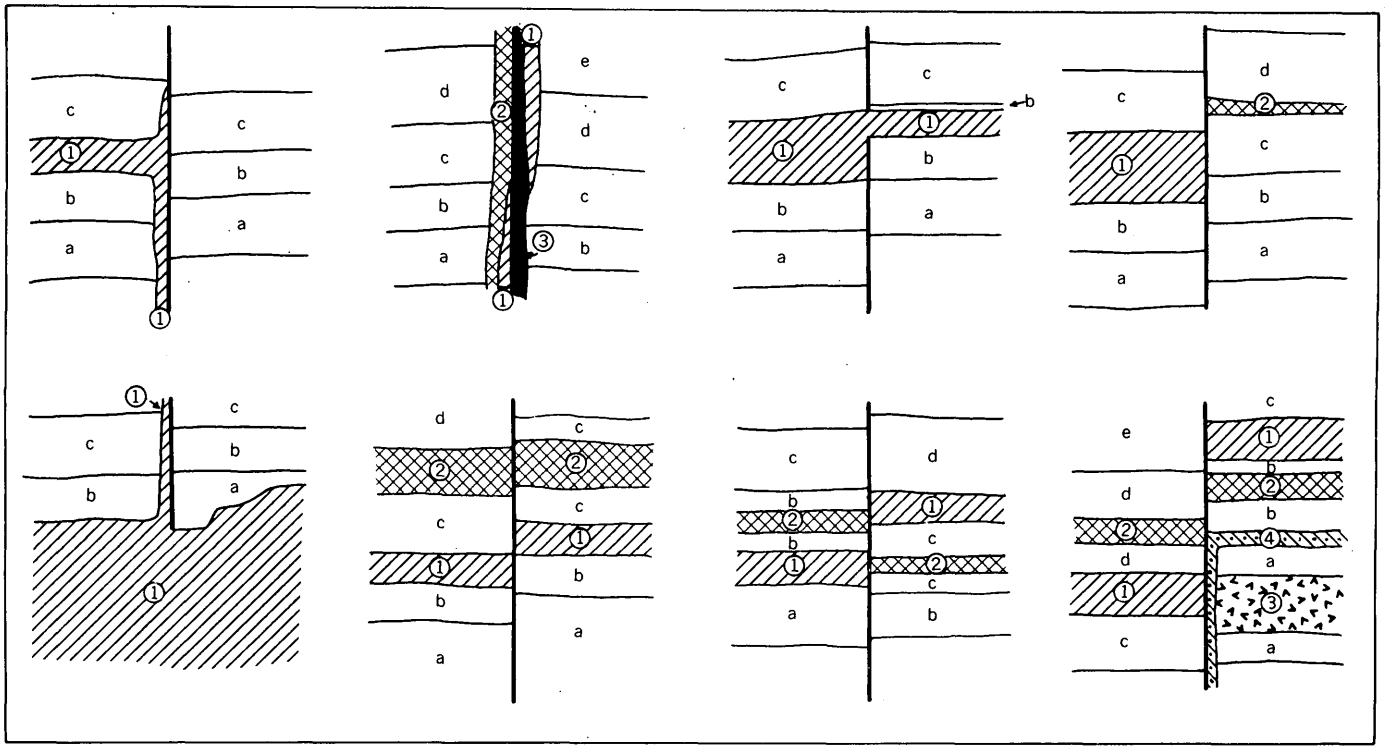

Figure 5.1.—Cross-section sketches of relations between porphyry bodies and faults in the Leadville district, Colorado. Igneous rocks patterned and numbered; sedimentary rock units blank and lettered.

The faults are dated by their relations to intrusive porphyries. Some 25 or 30 distinct varieties of porphyry are recognized in the area, and about 15 of these show clear-cut age relations with respect to one another and hence can be fitted into an age sequence. Members of this sequence show many different kinds of relations to faults. Some varieties of porphyry are displaced by some faults but not by others; others are displaced by almost every fault they intersect, and still others by very few. Similarly, individual faults displace some porphyries but guided the emplacement of others and are cut by still others. Relations such as those sketched in figure 5.1 indicate that many of the faults existed at the time certain porphyries were emplaced, and that movement recurred on some faults during the period of porphyry emplacement. Clearly, both the faults and the porphyry bodies of the areas are products of the same general phase of the Laramide orogeny, and the porphyry sequence can thus be used as a time scale both to determine relative ages of faults and to trace evolution of the fault pattern.

Results of such dating are shown in simplified form in figure 5.2 which illustrates the extent of faulting at four different stages during the period of porphyry emplacement. Some of the faults might be older than the ages assigned them, as they are dated only by relatively young members of the porphyry sequence, but they cannot be younger. On the other hand, the age of many of the faults is closly bracketed; the faults displace certain porphyries but guided the emplacement of other, younger ones.

Except as simplified because of scale, the fault pattern shown in the top diagram of figure 5.2 is the one that exists today. Yet the pattern was achieved before the period of porphyry intrusion came to an end, for some of the youngest porphyries locally obliterate the faults. These youngest porphyries, like the others, are hydrothermally altered and weakly mineralized; they are clearly older than the ore. This being so, the faults all originated before the ore, although many have a history of movement that extends virtually to the present.

Faults that existed at the ore-depositing stage could affect the original distribution of ore, as many obviously did, and yet the resulting ore bodies could later have been displaced by renewed movement on these same faults.

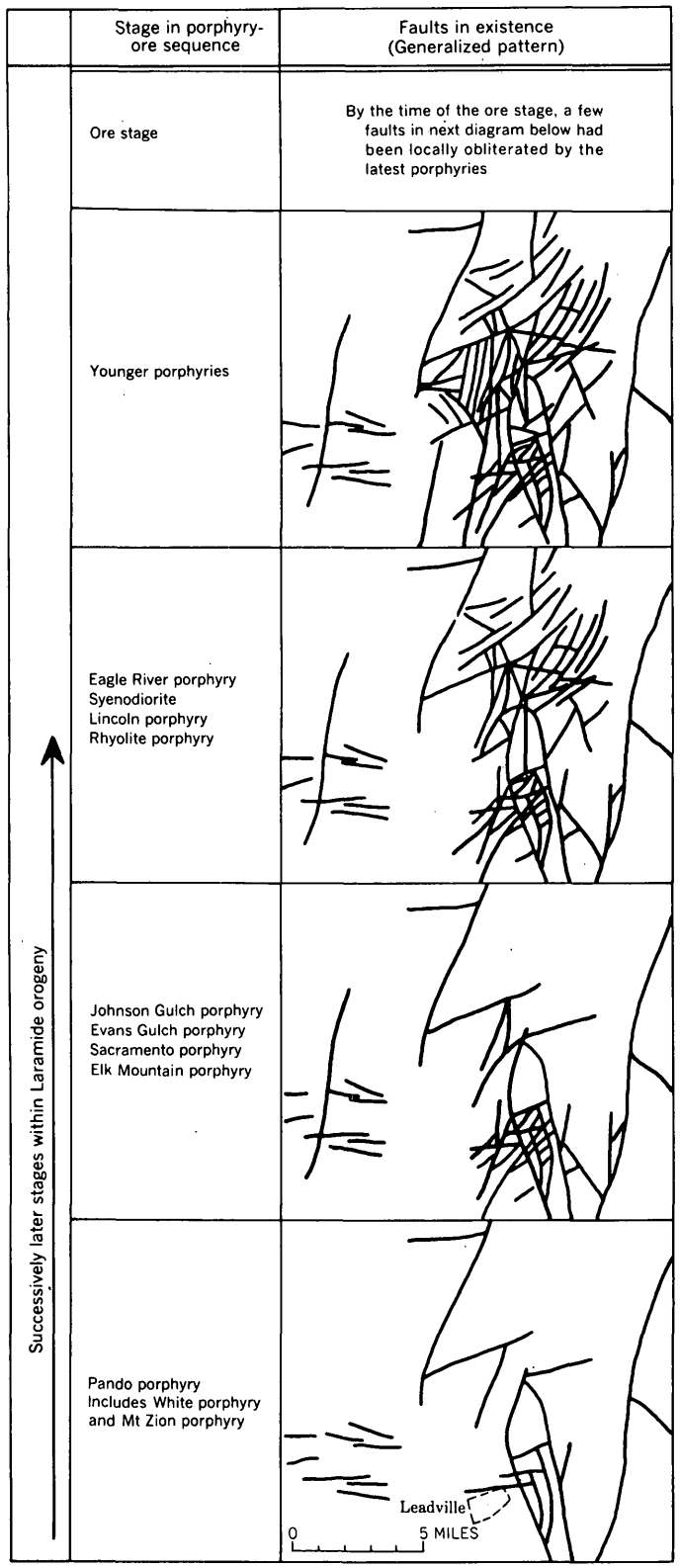

FIGURE 5.2.—Fault pattern in the Leadville district, Colorado, at successive stages defined by the sequence of porphyries.

REFERENCES

Emmons, S. F., 1886, Geology and mining industry of Leadville, Colorado: U.S. Geol. Survey Mon. 12.

Emmons, S. F., Irving, J. D., and Loughlin, G. F., 1927, Geology and ore deposits of the Leadville mining district, Colorado: U.S. Geol. Survey Prof. Paper 148.

6. PRE-ORE PROPYLITIZATION, SILVERTON CALDERA, COLORADO

By WILBUR S. BURBANK, Exeter, N.H.

Work done in cooperation with the Colorado State Metal Mining Fund Board

Several types of rock alteration, such as argillization, sericitization, and silicification that are closely related to ore deposition (Ransome, 1901; Burbank, 1941 and 1950), have been recognized in the Silverton caldera and surrounding area, northwestern San Juan Mountains, Colorado. Some alteration of the layered succession of calc-alkaline lavas and related pyroclastic rocks of late Tertiary age undoubtedly occurred during the period of eruptions. However, of principal concern here is the propylitic or quartz-carbonate-chlorite type of alteration that took place mostly prior to, but in part during, the period of ore deposition. This type of alteration becomes more pronounced with depth in certain parts of the caldera, and grades to a quartz-carbonate-albite-epidote-chlorite type analogous to the albite-epidote hornfels facies of low-grade contact metamorphism. Carbonate is locally either absent or a minor constituent in the albitic type. Pyrite is present in small quantities in much of the propylitized rocks.

Problems involved in the alteration include: (a) the depth and source of the altering agents, (b) the reasons for its post-volcanic and pre-ore position in the sequence of events, and (c) the mechanism of pervasive penetration of altering agents in the pores of many massive rocks whose initial permeability to liquid solutions must have been vanishingly low. Diffusion processes in a static medium occupying the rock pores are tentatively ruled out because of the extreme slowness of such processes, the highly pervasive nature of the alteration, and the belief that except in near-surface positions the pores of the heated volcanic rocks nearby and within the caldera could not have been initially saturated with aqueous liquids.

Propylitic alteration has affected many cubic miles of volcanic rocks throughout and beyond the caldera. Carbon dioxide is believed to have been a major constituent of the agents of rock alteration although other gases undoubtedly were present. Estimates of carbonate formed range from 2 to 5 percent (equivalent to 100 to 250 feet of limestone per mile of rock); this amount is far greater than can be accounted for by thermal metamorphism of any known basement rocks.

During volcanism the gases tended to become dissipated rather than entrapped due to the highly explosive nature of many of the eruptions. Injections of clastic dikes composed of Precambrian rock fragments are indicative that gas pressures in the basement rocks tended to reach culmination during earlier stages of propylitic alteration. Intense propylitic alteration, following cessation of volcanic eruptions, may be attributed in part to final sealing of the vents. The occurrence of a partly carbonatized and mineralized breccia pipe at the edge of a gabbroic and granodioritic stock northwest of the Silverton caldera suggests that the primitive magmas were of similar composition, and that the propylitization was related to deep-seated crystallization and differentitation of such magmas.

The amounts of H_2O, CO_2, and S_2 in basaltic magmas and in their siliceous differentiates suggest that gases rich in CO_2 would be expelled during crystallization (Sheperd, 1938; Rubey, 1951, p. 1136, fig. 4). The expulsion of CO_2 also is suggested by the work of Morey and Fleischer (1940) on the system CO_2–H_2O–K_2O–SiO_2, which shows that the solubility of CO_2 in alkali silicate solutions decreases much more rapidly than that of H_2O as the silica content of the solution increases. They concluded (1940, p. 1056) that this process probably would apply to more complex silicate mixtures. Garrels and Richter (1955) presented data to support the possibility that carbon dioxide could exist as a separate phase in comparatively shallow environments because of the low mutual solubilities of CO_2 and H_2O.

It is postulated that the evolved gases invaded the deeper parts of the caldera and surrounding ground through previously heated rocks deficient in uncombined water, and that the gradients of pressure were established in a pervasive gas phase composed mainly of carbon dioxide. Alteration is inferred to have taken place in an open system by a series of coupled condensations and vaporizations in rock pores under osmotic conditions and under control of physical and chemical adsorption in capillary and sub-capillary spaces. Recurrent actions are interpreted to consist of: (a) condensation of gases in locally adsorbed water films; (b) partial solution of silicate minerals by the condensates; (c) mixing of saturated condensates with other droplets of liquid forced along by gas pressures; and (d) reaction in these mixtures causing precipitation of new

minerals. Continuous attack by new condensates of the active gases would maintain a certain degree of permeability by solution of country rock and re-solution of precipitated material which would allow egress of solutions saturated with products of rock decomposition. These solutions were forced by expanding gases into newly fractured rock and reopened fissure systems in numerous and repetitive stages of adjustment throughout this period of late activity.

The resulting reactions between the gases, liquid condensates, and solids could have caused widespread and highly pervasive propylitic alteration. Most of the propylitized rocks are considered as an arrested stage of development in this reaction. The carbonatized and chloritized breccia pipe possibly represents the end stage of development—the result of long continued and concentrated passage of altering agents within a restricted volume of rock.

REFERENCES

Burbank, W. S., 1941, Structural control of ore deposition in the Red Mountain, Sneffels, and Telluride districts of the San Juan Mountains, Colorado: Colorado Sci. Soc. Proc., v. 14, no. 5, p. 141–261.

——— 1950, Problems of wall-rock alteration in shallow volcanic environments: Colorado School of Mines Quart., v. 45, no. 18, p. 287–319.

Garrels, R. M., and Richter, D. H., 1955, Is carbon dioxide an ore-forming fluid under shallow-earth conditions?: Econ. Geology, v. 50, p. 447–458.

Morey, G. W., and Fleischer, Michael, 1940, Equilibrium between vapor and liquid phases in the system CO_2–H_2O–K_2O–SiO_2: Geol. Soc. America Bull., v. 51, p. 1035–1058.

Ransome, F. L., 1901, A report on the economic geology of the Silverton quadrangle, Colorado: U.S. Geol. Survey Bull. 182, 265 p.

Rubey, W. W., 1951, Geologic history of sea water: Geol. Soc. America Bull., v. 62, p. 1111–1147.

Shepherd, E. S., 1938, The gases in rocks and some related problems: Am. Jour. Sci., 5th ser., v. 35A, p. 311–351.

7. RING-FRACTURED BODIES IN THE SILVERTON CALDERA, COLORADO

By Robert G. Luedke and Wilbur S. Burbank, Washington, D.C. and Exeter, N.H.

Work done in cooperation with the Colorado State Metal Mining Fund Board

The Silverton caldera, in the northwestern part of the San Juan Mountains, Colorado, is a nearly circular volcanic center about 12 miles in diameter, filled with a layered succession over a mile thick of calc-alkaline lavas and related pyroclastic rocks of late Tertiary age. These rocks were complexly faulted and tilted by repeated upthrust and collapse during and after subsidence of the main caldera floor. Within the margin of the caldera is a great zone of ring faults, as much as two miles wide, into which many pipelike bodies of quartz latite, rhyolite, and breccia were intruded, after the main episodes of extrusive activity. The intrusion of these rocks was followed by alteration and mineralization.

Several smaller bodies of ring-fractured rock, each about a mile in diameter, are located in an apparently random fashion within the northern part of the caldera. Discontinuous ring fractures and faults around each of these bodies are superimposed upon pre-existing structural features of the caldera without greatly disturbing them, though some early-formed shear zones and tilted blocks are slightly offset by the faults. Planar flow structures of the volcanic rocks within some of the tilted blocks locally dip inward from the arcuate breaks. Many of the veins and altered zones cross these ring-fractured bodies with little or no deflection in trend.

These ring-fractured bodies are neither volcanic vents nor intrusive plugs; they are cylindrical columns of the country rock that were pushed up by magma, and that collapsed when magma was withdrawn and upward pressure released. The net downward displacement of the layered volcanic rocks amounted to as much as 200 feet. Their collapse was accompanied locally by minor injections of quartz latite and rhyolite into ring fractures and other fissures.

A possible cause for the inferred withdrawal of magma might have been the intrusion of the pipelike bodies into the major ring-fault zone of the caldera.

8. RELATION OF MINERALIZATION TO CALDERA SUBSIDENCE IN THE CREEDE DISTRICT, SAN JUAN MOUNTAINS, COLORADO

By THOMAS A. STEVEN and JAMES C. RATTÉ, Denver, Colo.

Work done in cooperation with the Colorado State Metal Mining Fund Board and U.S. Atomic Energy Commission

Detailed study of the volcanic rocks in the central San Juan Mountains has defined a subcircular caldera about 10 miles in diameter, which we have called the Creede caldera after the nearby town and mining district. The ores in the Creede district are localized along faults in a complex graben that extends outward from the caldera; these faults were active many times while the caldera area was subsiding but mineralization did not take place until the last main period of fault movement.

The volcanic rocks exposed in this area include the upper units of the Potosi volcanic series of Larsen and Cross (1956, p. 30–167), and the younger Fisher quartz latite and Creede formation. The volcanic sequence we have determined, however, differs considerably from that defined previously in the San Juans, and in this paper informal local names are applied to most of the units.

The oldest rocks exposed near Creede formed prior to any known caldera subsidence, and they record concurrent accumulation from several volcanic centers. We have no knowledge of the original extent of any of these formations; only those parts of these and the succeeding formations that we know or can reasonably extrapolate are shown by pattern on figure 8.1. The accumulation centering on Bachelor Mountain (fig. 8.1*A*) is more than 3,500 feet thick, and consists of welded rhyolite tuff grading up into non-welded pumiceous tuff. To the northeast, the Bachelor Mountain rocks intertongue with a great sequence of quartz latitic welded tuffs more than 4,000 feet thick. To the west, Bachelor Mountain rocks overlie a local rhyolitic accumulation, and intertongue with quartz latitic lava flows and breccias derived from a source west of the Creede district.

The pumiceous eruptions of the Bachelor Mountain volcano culminated in the collapse of the probable vent area and in the development of several north-northwest trending normal faults (fig. 8.1*B*). The exposed margin of this early caldera is characterized by pervasively brecciated rock passing outward into strongly sheeted rock.

The early caldera stage was followed by renewed eruptions of rhyolitic magma that deposited great sheets of welded ash flows over most of the Creede area (fig. 8.1*C*). These rocks have a maximum aggregate thickness exceeding 2,500 feet. Southeast of Creede they are interlayered with quartz latitic lava flows and southwest of Creede are intertongued with dacitic flows and breccias. The main Creede caldera probably originated as a result of these rhyolitic eruptions, as some faults along the eastern margin of the caldera were active at this time.

Great volumes of quartz latitic ash (fig. 8.1*D*) were erupted following the rhyolitic intracaldera stage. Outside the main Creede caldera, the quartz latites form widespread sheets of tuff and welded tuff more than a thousand feet thick. Within the caldera, at least 6,000 feet of quartz latitic welded tuff is exposed, and the total thickness may be much greater. Intertongued landslide and talus breccia from the caldera walls indicate that at least the upper several thousand feet, and perhaps all of the observed caldera fill is younger than the welded tuffs of the rhyolitic intracaldera stage.

Caldera subsidence stopped sometime following the quartz latitic eruptions, leaving a broad, flat-floored caldera with outward extending grabens (fig. 8.1*E*). Breccias derived by avalanching from the caldera walls spread over at least part of the caldera floor. The core of the caldera was domed (fig. 8.1*F*), probably by magmatic intrusion, and a complex graben formed along the crest of the arch.

Viscous quartz latitic lava was erupted along the broken margin of the caldera to form local flows and domes of Fisher quartz latite, and stream and lake sediments and travertine accumulated elsewhere around the domed core to form the Creede formation.

Following Fisher volcanism and Creede alluviation, the graben extending northward from the caldera (fig. 8.2) was again broken. This was the last major structural event in the area, and it is of particular importance as the faults active at this time were extensively mineralized to form the major lead-zinc-silver deposits in the Creede district.

The main displacement on the Creede graben has been on two pairs of faults with opposing dips. The core of the graben is bounded on the east by the Amethyst fault, which originated during early caldera sub-

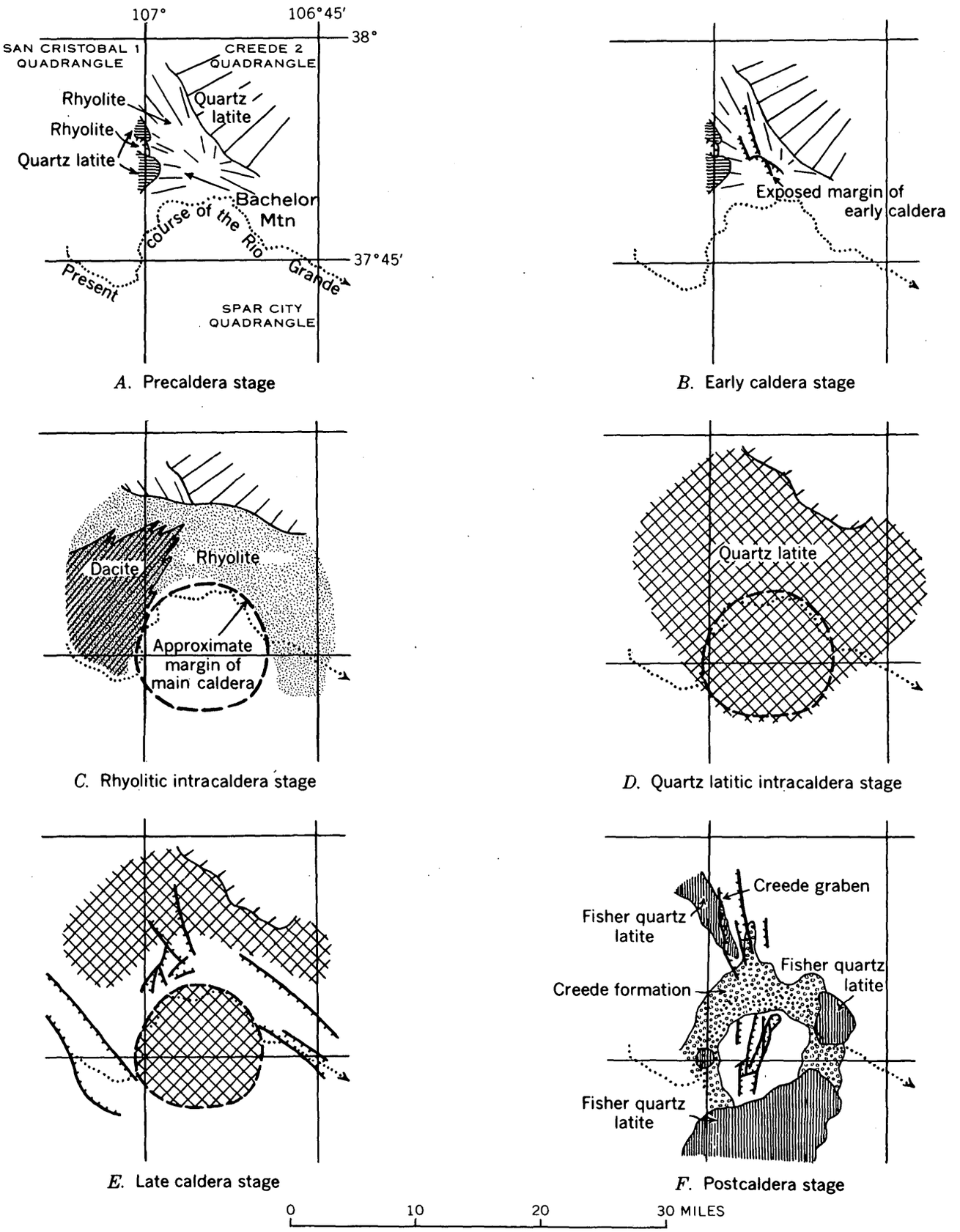

FIGURE 8.1.—Stages in the geologic history of the Creede district, Colorado.

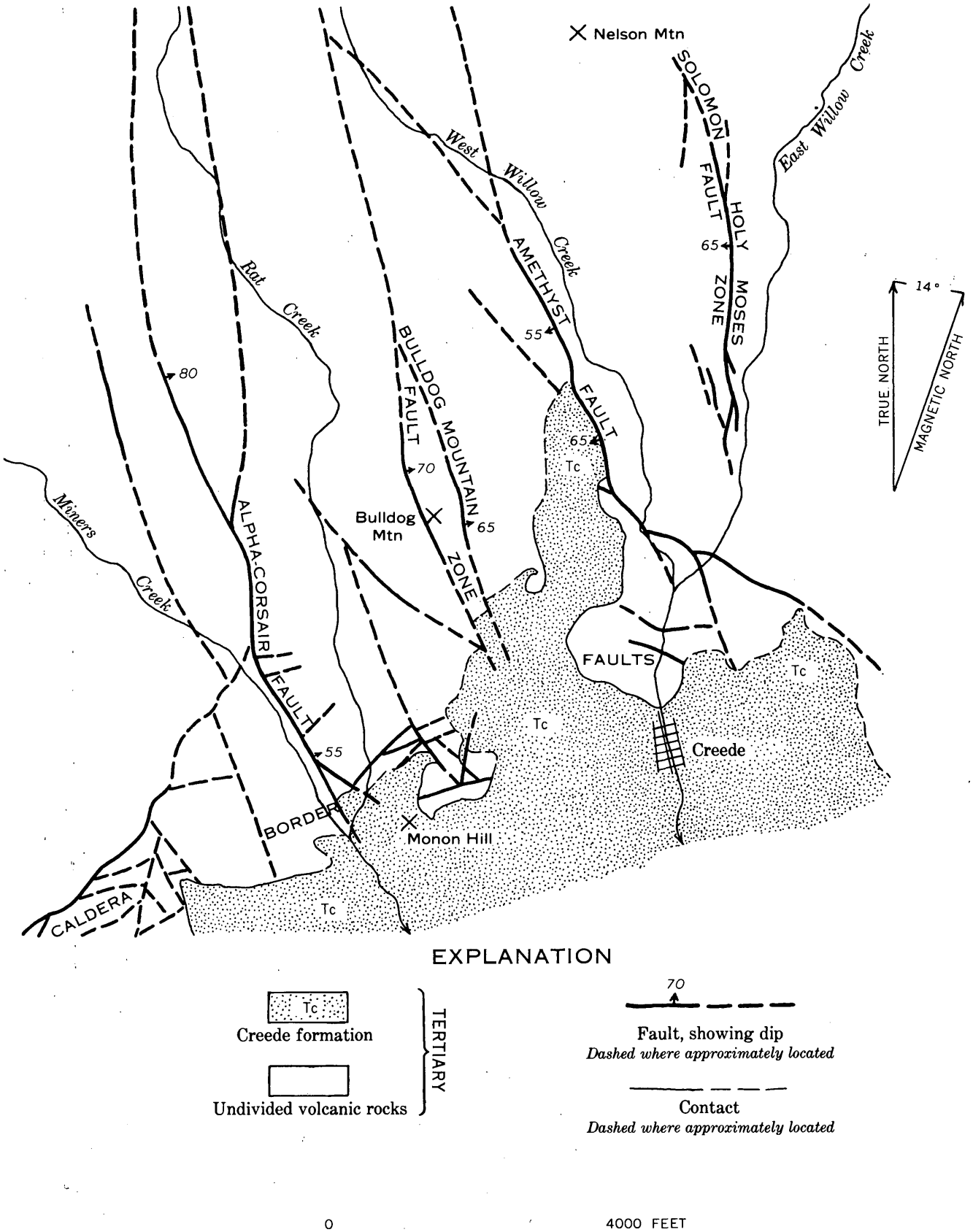

FIGURE 8.2.—Fault pattern in the Creede district, Colorado.

sidence and was recurrently active until after the Creede formation was deposited. The Bulldog Mountain fault zone on the west side of the core apparently originated during early caldera subsidence when the west side was downthrown; later movement reversed the direction of displacement along the mapped faults (fig. 8.2). The Alpha-Corsair fault near the west margin of the graben had its main movement after the Creede formation was deposited, but it followed the trend of an older series of echelon fissures marked by dikes. Movement on the Solomon-Holy Moses fault zone on the east side of the graben cannot be dated closely, nor is it known whether faulting took place during more than one period.

Mine production in the Creede district has come from three of the four main fault zones in the graben, and from disseminated deposits in the Creede formation. The Amethyst fault and related fractures have produced about $55,000,000 worth of metals, and the Alpha-Corsair and Solomon-Holy Moses fault zones about $600,000 and $2,200,000 worth respectively. The Monon Hill area has produced about $800,000 worth of metals from basal beds in the Creede formation where it rests on a highly faulted segment of the caldera margin.

The Bulldog Mountain fault zone appears to be the most favorable structure to prospect in the Creede district. It is a major fault zone with recurrent movement that bounds the west side of the core of the graben, and is thus comparable in several respects with the highly productive Amethyst fault zone. Prospecting to date has been confined to near-surface formations which are underlain by soft tuffs that may have inhibited passage of mineralizing solutions. Important ore bodies are more likely to be found at depth, where the rocks are the same hard rhyolites that enclose the ore bodies on the Amethyst, Alpha-Corsair, and Solomon-Holy Moses fault zones.

REFERENCE

Larsen, E. S., Jr., and Cross, Whitman, 1956, Geology and petrology of the San Juan Region, Southwestern Colorado: U.S. Geol. Survey Prof. Paper 258.

9. ALINEMENT OF MINING DISTRICTS IN NORTH-CENTRAL NEVADA

By Ralph J. Roberts, Menlo Park, Calif.

Work done in cooperation with the Nevada Bureau of Mines

The mining districts of north-central Nevada are localized by major structural features. One of these is the Roberts Mountains thrust fault, on which clastic and volcanic rocks of early and middle Paleozoic age (western assemblage) have ridden eastward over correlative carbonate rocks (eastern assemblage) (Roberts and others, 1958). The thrusting took place in Mississippian time, at the culmination of the Antler orogeny; post-thrust uplift and doming caused the upper plate to be locally removed by erosion, so that carbonate rocks of the lower plate were exposed in windows. As the principal mining districts are in and around these windows, study of the origin and history of the windows will shed light on the regional and economic geology of the area.

Recent mapping in Eureka County and adjacent areas has shown that the windows are alined in two northwest-trending belts, and that they contain many of the intrusive bodies (Roberts, 1957). The western, or Shoshone-Eureka belt, extends from the Shoshone Range southeastward to the Eureka district, and the other, the Lynn-Pinyon belt, from the Lynn district south-southeastward to the Railroad district (fig. 9.1).

SHOSHONE-EUREKA BELT

The Shoshone-Eureka belt includes the Goat Ridge, Red Rock, and Gold Acres windows in the Shoshone Range (J. Gilluly, written communication, 1958), the Cortez window in the Cortez Mountains, the Keystone, Tonkin, J-D, and Windmill windows in the Simpson Park Mountains, and the Roberts Mountains window in the Roberts Mountains. Lone Mountain also appears to be a window (C. W. Merriam, oral communication); and the rocks of the Eureka district may have been partly covered by the Roberts Mountains thrust plate.

Windows in which the ore deposits were mainly in the carbonate rocks of the lower plate are the Cortez and Lone Mountain windows; the ore bodies in the Eureka district also are in carbonate rocks. The Cortez window contains the Cortez district, a major silver-

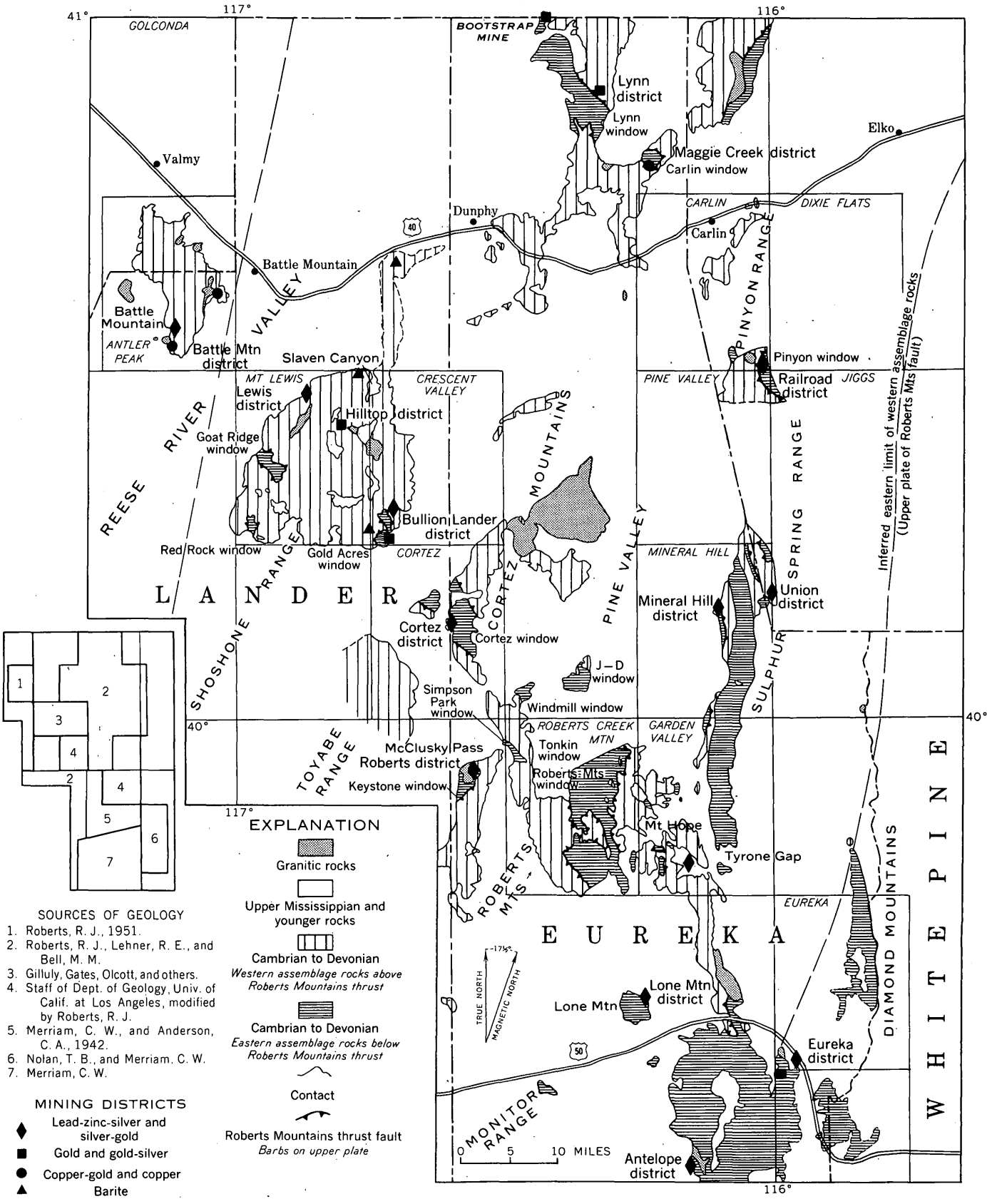

FIGURE 9.1.—Map showing distribution of Paleozoic facies, granitic rocks, and principal mining districts in Eureka County, Nev., and adjacent areas.

lead producer between 1870 and 1920. Most of the ore bodies mined were in or near fault zones that cut carbonate rocks. Lone Mountain, a block of carbonate rocks bordered on the northeast, east, and southeast by rocks of the upper plate, has yielded a small tonnage of zinc carbonate ore from bodies in Devonian limestone. The rocks in the Eureka district may not have been completely covered by the upper plate, but they appear to have been domed like those in the windows along the belt to the northwest. More than $52,000,000 in silver, gold, lead, and zinc ore was produced in this district, mostly between 1870 and 1900; it came chiefly from the Eldorado and Hamburg dolomites, of Cambrian age.

Other windows in the Shoshone Range that contain ore deposits are the Gold Acres window in breccia along the thrust, and the Lewis and Hilltop districts in the upper plate rocks. The Gold Acres window contains the Goldacres mine, which has yielded a significant production in gold beginning in 1934. The ore is mostly in the brecciated zone along the Roberts Mountains thrust (Keith Ketner, oral communication). The Lewis and Hilltop districts are in clastic and volcanic rocks of the upper plate, presumably not far from the thrust. The Battle Mountain district northwest of the Shoshone Range, is also in this belt. It is mainly underlain by western assemblage rocks of early Paleozoic age, presumably exposed by warping of the kind indicated by windows to the southeast.

LYNN-PINYON BELT

The Lynn-Pinyon belt (fig. 9.1) includes the Lynn and Carlin windows in the Tuscarora Mountains and the Pinyon window (formerly called the Bullion window) in the Pinyon Range. The Lynn window contains the Lynn district, which produced a small quantity of gold ore, mostly from veins that cut siliceous shale and chert in the upper plate of the Roberts Mountains thrust. The Bootstrap mine, at the north end of the district and just north of the Eureka County line, has produced gold ore from silicified zones along the thrust, from the carbonate rocks in the lower plate, and from altered dikes that cut these rocks. The Carlin window contains several properties that have yielded small tonnages of silver and copper ores and barite. The Copper King mine is near the window, but is in the upper plate and about 200 feet above the thrust. The Pinyon window contains the Railroad district, which has yielded a small amount of silver-lead and copper ore from veins and replacement ore bodies in carbonate rocks.

The Mineral Hill and Union districts, in carbonate rocks of the lower plate, south of the Pinyon window in the Sulphur Spring Range, have yielded silver-lead-zinc ore. These districts lie between the Shoshone-Eureka and Lynn-Pinyon belts, and possibly are on a separate, less distinct, belt.

ORIGIN AND HISTORY OF THE WINDOWS

The windows are the result of doming of the Roberts Mountains thrust. Part of the doming may have occurred during or shortly after thrusting, but part of it may have occurred much later. Evidence that some doming occurred shortly after the thrusting is found in the north end of the Monitor Range, where coarse clastic rocks of Permian age containing carbonate boulders (eastern assemblage) rest on rocks of the upper plate, and on the south side of Lone Mountain, where similar clastics may rest on rocks of both the upper and the lower plate. The doming was later intensified during the emplacement of igneous bodies in late Mesozoic and early Tertiary time and during the uplift of the ranges in the Tertiary.

The alinement of the windows indicates that the doming occurred in zones of structural weakness in which movement has taken place intermittently. We do not yet fully understand the nature of the deformation or know the precise date of its beginning, but clearly the zones of weakness and the windows along them are penetrated by conduits along which igneous rocks and related ore-bearing fluids rose. The zones probably penetrate to great depths within the crust, and they possibly date back to Precambrian time.

SUGGESTIONS FOR PROSPECTING

In prospecting within the windows and near them, a special effort should be made to explore the lower units in the carbonate sequence, such as the Eldorado and Hamburg dolomites, for lead-zinc-silver ore bodies in promising structural settings such as fault intersections. The rocks of the upper plate close to the thrust may also be locally mineralized, especially near intrusive bodies.

REFERENCES

Roberts, R. J., 1957, Major mineral belts in Nevada: Am. Inst. Mining Metall. Engineers program for Reno meeting.

Roberts, R. J., Hotz, P. E., Gilluly, James, and Ferguson, H. G., 1958, Paleozoic rocks in north-central Nevada: Am. Assoc. Petroleum Geologists Bull., v. 42, no. 12, p. 2813–2857.

10. MINERAL ASSEMBLAGE OF A PYROMETASOMATIC DEPOSIT NEAR TONOPAH, NEVADA

By R. A. Gulbrandsen and D. G. Gielow, Menlo Park, Calif.

Pyrometasomatic deposits in a limestone environment commonly contain andradite and pyroxene (Knopf, 1942, p. 63). A deposit in Paymaster Canyon, about 31 miles southwest of Tonopah, Nevada, is typical in this respect, although the pyroxene is an uncommon manganoan hedenbergite, heretofore found principally in a group of pyrometasomatic zinc deposits that extends from New Mexico to the central part of old Mexico (Allen and Fahey, 1957). The Paymaster deposit also contains an apparently rare zincian nontronite.

The deposit was first examined by J. E. Carlson and R. M. Smith of the U.S. Geological Survey, and a study of one of their specimens led to the identification of the manganoan hedenbergite. Additional samples, on which this preliminary report is based, were collected principally for a detailed study of the hedenbergite and for the identification of the associated minerals. Because of limited sampling, the mineral assemblage described here is probably incomplete.

198 The Paymaster deposit is on the west side of Paymaster Canyon, in sec. 2, T. 1 N., R. 40 E., Esmeralda County, and about a mile south of a contact, shown by Ball (1907, plate 1), between Cambrian sedimentary rocks and the granite of Lone Mountain. The deposit is a dikelike body about 10 to 15 feet wide, and is exposed for about two hundred feet at the surface. It extends along a fault separating Cambrian limestone from Cambrian shale, strikes N. 80° E., and is nearly vertical.

The mineralized zone, where it is exposed in a prospect pit, consists principally of massive dark-green quartz-hedenbergite rock and massive olive quartz-andradite rock. Masses of soft yellow zincian nontronite, as much as 1 or 2 feet across, occur along an irregular limestone contact. The nontronite also forms envelopes around small hedenbergite veins, and pseudomorphs after coarsely bladed clusters of hedenbergite. Some small blocks of limestone appear to be completely enclosed by the rock of the mineralized zone and show sharp contacts with it. The contact between the shale and the hedenbergite and andradite rocks appears sharp, and some of the dark-olive shale is bleached white owing to the destruction of chlorite. Both the hedenbergite rock and the andradite rock contain quartz, sphalerite, galena, magnetite, and calcite, but sphalerite and galena are more abundant in the hedenbergite rock. There is a noteworthy absence of pyrite and other iron sulfides.

The minerals of the deposit have been identified principally by X-ray diffraction and X-ray spectrographic techniques. Table 10.1 shows X-ray diffraction data of the manganoan hedenbergite and of johannsenite, the calcium-manganese analogue of hedenbergite. The johannsenite specimen was kindly lent by D. F. Hewett and is part of one of the type johannsenite specimens (no. 6) described by Schaller (1938). The X-ray data of the two minerals are very similar, but they differ markedly in composition. The johannsenite contains about 23 percent MnO and 5 percent FeO (Schaller, 1938, p. 580), whereas the manganoan hedenbergite contains about 9 percent MnO and 26 percent FeO, as determined by X-ray spectrography. Composition and other properties will be fully reported when the work on the manganoan hedenbergite is finished.

TABLE 10.1.—*X-ray diffraction data of manganoan hedenbergite and johannsenite*

Wide range diffractometer, Ni-filtered Cu-radiation (λ=1.54050 Angstrom units)

Manganoan hedenbergite [a]		Johannsenite [b]	
d[c]	I	d[c]	I
6. 58	25	6. 59	15
4. 76	45	4. 77	35
4. 51	10	4. 54	10
4. 28	5	4. 27	10
3. 34	10	3. 34	20
3. 27	20	3. 28	25
3. 001	100	3. 012	100
2. 910	10	2. 915	15
2. 587	15	2. 595	15
2. 552	20	2. 550	30
[d]2. 381	15	[d]2. 380	10
[d]2. 342	5	[d]2. 343	5
[e]2. 238	5	[d]2. 233	5
2. 181	10	[e]2. 184	10
2. 149	10	2. 155	15
2. 124	10	2. 128	15
Other peaks not measured			

[a] Paymaster Canyon, sec. 2, T. 1 N., R. 40 E., Esmeralda County, Nevada.
[b] Venetia, Italy. Collected by D. F. Hewett. Type specimen no. 6 (Schaller, 1938).
[c] Silicon used as a reference internal standard. Measured in angstroms.
[d] Peak poorly defined.
[e] Broad peak.

The zincian nontronite is a montmorillonite-type clay mineral intermediate in composition between nontronite and sauconite. The basal X-ray diffraction peak expands from about 14.8 A to 18 A after treatment with glycerol, a change typical of the montmorillonites. X-ray spectrography shows more iron than zinc, and the mineral is therefore a nontronite rather than the rarer sauconite. The mean index of refraction of the zincian nontronite is approximately 1.58. Much of the nontronite was undoubtedly derived from hedenbergite, as shown by its occurrence in pseudomorphs after hedenbergite, but some of it may have been derived from andradite, like that occurring in the dry regions of central Kazakhstan (Ginzburg and Vitovskaya, 1956).

The unit cell size of the andradite, carefully measured by X-ray diffraction with silicon as an internal standard, is 12.057 A, with an estimated precision of ±.005 A. It is very close to the values reported by Skinner (1956, p. 429), which were 12.069, 12.064, and 12.048, and indicates that the andradite here described is very near the end member in composition.

The sphalerite of the deposit contains about 7.3 percent iron, as determined by X-ray spectrography with the use of chemically analyzed sphalerite standards. The temperature of formation of this sphalerite cannot be determined accurately from the data of Kullerud (1959, p. 315), because the required iron sulfide phase associated with the sphalerite is not present. The iron content of the sphalerite does make it possible, however, to estimate a minimum temperature of formation that is a little less than 400° C. Stone (1959, p. 1019), using Kullerud's data, found that the sphalerite in a pyrometasomatic deposit in Mexico, which also contains hedenbergite and andradite, formed at a temperature between 500° and 550° C.

The economic value of the Paymaster deposit is not yet known, but an appraisal of the deposit's potential may be aided by noting another similarity between the Paymaster and the deposits in New Mexico and Mexico. This is the tendency for sphalerite and pyroxene to be closely associated. It is so marked in the New Mexico-Mexico deposits that pyroxene appears to be a useful guide to ore (Allen and Fahey, 1957, p. 889).

REFERENCES

Allen, V. T., and Fahey, J. J., 1957, Some pyroxenes associated with pyrometasomatic zinc deposits in Mexico and New Mexico: Geol. Soc. America Bull., v. 68, p. 881–896.

Ball, S. H., 1907, A geologic reconnaissance in southwestern Nevada and eastern California: U.S. Geol. Survey Bull. 308, p. 218.

Ginzburg, I. I., and Vitovskaya, I. V., 1956. Vyvetrivaniye granatovykh aksinitovyhh i tremolitovykh porod v zasushlivykh raionakh tsentral'nogo Kazakhstana [The weathering of garnet, axinite, and tremolite rocks in the dry regions of central Kazakhstan], *in* Kora vyvetrivaniya [Crust of weathering]: Akad. Nauk SSSR [Acad. Sci., U.S.S.R.], no. 2, p. 299–316. Mineralog. Abstracts, 1959, v. 14, p. 124.

Knopf, Adolph, 1942, Ore deposition in the pyrometasomatic deposits, *in* Ore deposits as related to structural features: edited by W. H. Newhouse, p. 63–72.

Kullerud, Gunnar, 1959, Sulfide systems as geological thermometers, *in* Researches in geochemistry: edited by P. H. Abelson, p. 301–335.

Schaller, W. T., 1938, Johannsenite, a new manganese pyroxene: Am. Mineralogist, v. 23, p. 575–582.

Skinner, Brian J., 1956, Physical properties of end-members of the garnet group: Am. Mineralogist, v. 41, p. 428–436.

Stone, J. G., 1959, Ore genesis in the Naica district, Chihuahua, Mexico: Econ. Geology, v. 54, p. 1002–1034.

11. SEDIMENTARY IRON-FORMATION IN THE DEVONIAN MARTIN FORMATION, CHRISTMAS QUADRANGLE, ARIZONA

By Ronald Willden, Menlo Park, Calif.

Sedimentary iron-formation was discovered in July 1959 in the upper part of the Martin formation, of Devonian age, in sec. 19, T. 2 S., R. 16 E., in the northwest part of the Christmas quadrangle, in Gila County, Ariz. (see fig. 11.1). The iron-formation occurs in a bed from 5 to 7 feet thick. This bed is traceable over a strike length of about 2,150 feet on the north side of Limestone ridge, where it dips 40°–50° southwest. The oolitic bed lies at the base of a widespread shale unit that is at the top of the Martin formation in much of the surrounding area, and is underlain by a buff to yellowish-brown fine- to medium-grained silty limestone. Hematite also occurs at approximately the same horizon in much of the northern part of the Christmas quadrangle, forming either crystalline nodules in the buff limestone or a cement in a rather poorly sorted sandstone that intervenes, in some places, between the shale and limestone.

The iron-formation consists of ooliths of hematite and chamosite in a matrix of calcite, dolomite, and quartz silt. Point counts on thin sections of rock from three horizons in the oolitic bed (near the top, at the

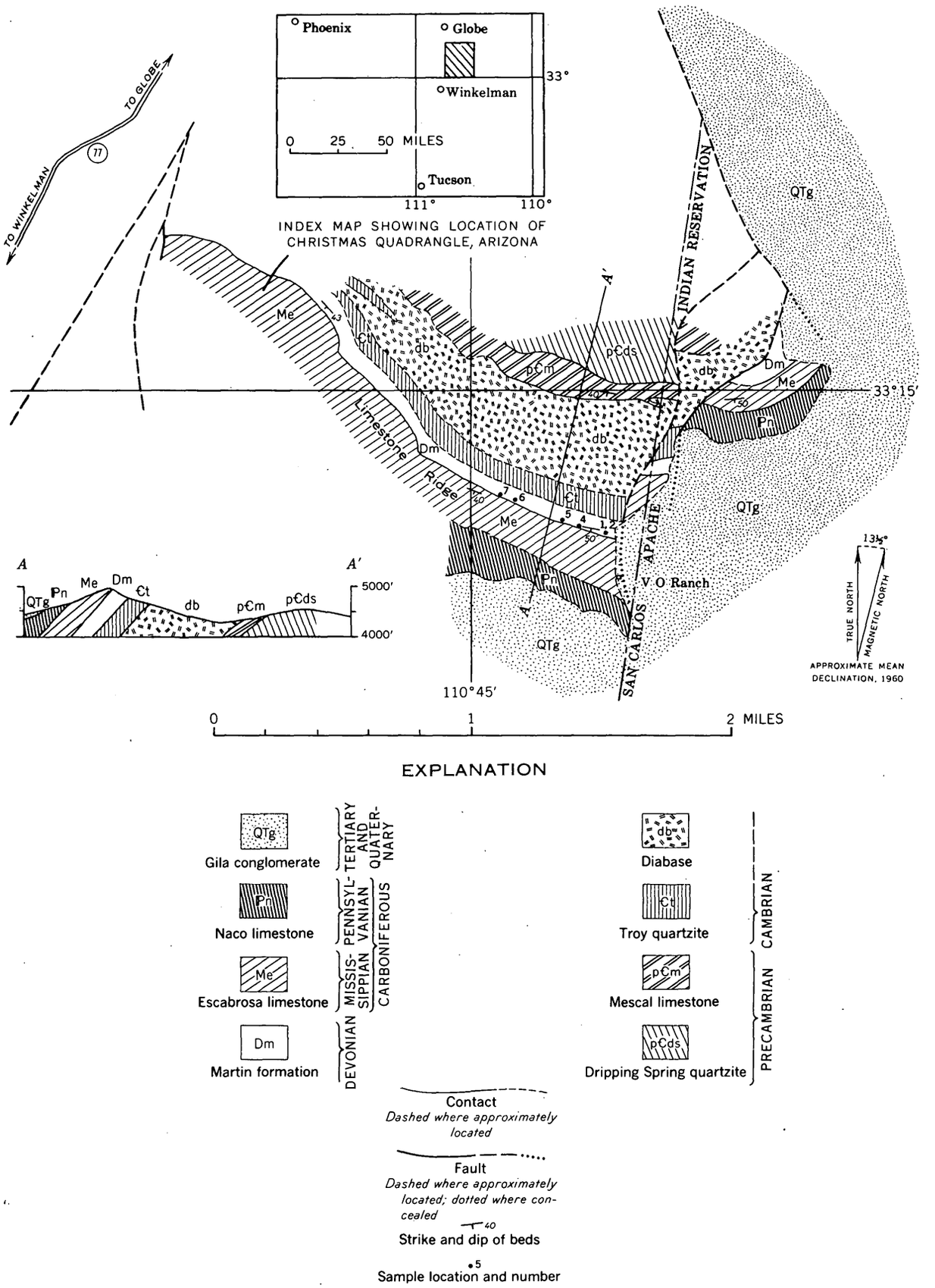

FIGURE 11.1.—Northwest corner of Christmas quadrangle and vicinity, Arizona, showing geology and sample locations.

top of the lower third, and in the lowest 6 inches) show 49 to 58 percent ooliths, 33 to 42 percent carbonates, and 7 to 10 percent quartz. The ellipsoidal ooliths are 0.2 mm long and tend to lie parallel to bedding. X-ray diffraction patterns of the carbonates have characteristic calcite lines, but the principal dolomite line is displaced from the position for pure dolomite by about 0.2° toward a lower 2-theta value, which may be due to some substitution of iron for magnesium.

Partial chemical analyses by D. L. Skinner (written communication, February 1960) of 6 samples, give an iron content of 31.1 to 39.3 percent (table 11.1). X-ray spectographic analyses of 11 chip samples collected at about ½-foot intervals from across the bed at the same locality as sample 1 (fig. 11.1) indicate iron content ranging from about 31 percent in the lower part of the bed to about 40 percent at the top, with a maximum of 46 to 49 percent in a 2-foot zone in the upper half. Assuming that the bed maintains a uniform length and thickness downdip, and that it has an average specific gravity of 3.19, there are about 1,250 tons of iron-formation per foot of depth. Owing to its low grade and small size this deposit probably cannot be profitably mined at the present time, but its existence justifies a hope that other and perhaps larger deposits may be discovered elsewhere in the Martin formation.

TABLE 11.1.—*Iron content of 6 samples of oolitic iron-formation from the Devonian Martin formation*

[Analyses by D. L. Skinner; reported as Fe_2O_3]

Sample [1]	Location	Width (feet)	Total Fe as Fe_2O_3	Total Fe
1	About 210 ft west of alluvial cover	6	56.2	39.3
2	do	1	44.4	31.1
3 [2]	do	7		38.1
4	540 ft west of sample 1	6.2	56.0	39.1
5	360 ft west of sample 4	[3] 3.0	50.5	35.3
6	1,040 ft west of sample 5	5.0	50.9	35.6
7	325 ft west of sample 6	1.2	49.1	34.3

[1] Sample numbers same as on geologic map (fig. 11.1).
[2] Weighted average of samples 1 and 2.
[3] Only lower 3 feet of bed could be sampled because upper part of section was covered with tightly cemented rubble. Bed is probably about 6 feet thick at this point.

12. EARLY TERTIARY VOLCANIC GEOLOGY OF AN AREA NORTH AND WEST OF BUTTE, MONTANA

By HARRY W. SMEDES, Washington, D.C.

Remnants of two unconformable sequences of early Tertiary volcanic rocks rest on the Boulder batholith and older rocks within a belt about 60 miles long and as much as 18 miles wide, which roughly parallels the northeast-trending axis of the batholith. The younger sequence is of rhyolite, and occupies principally the northeastern part of this belt; the older sequence is of quartz latite, and occupies principally the southwestern part. An unconformable contact between the rocks of the two sequences is exposed in the Champion Pass area, about 19 miles north of Butte. Rocks of the older sequence, which are the principal topic of this paper, occupy an area of about 400 square miles and have a composite thickness of more than 6,000 feet. The lithology, and structural and stratigraphic relations of these volcanic rocks, and their known or inferred maximum preserved thickness, are shown diagrammatically in figure 12.1.

Volcanic rocks of the older sequence comprise six major unconformable or disconformable units (II–VII). During the earliest phase of volcanism a mixture of tuff and quartz monzonite detritus (unit II) accumulated on the lower parts of an erosion surface having a relief of about 1,000 or 1,500 feet. Rocks of this unit were slightly tilted and eroded before the extrusion of a thick sequence of ash flows (unit III), most of which are now sheets of welded tuff.

This eruption was followed by block faulting and tilting toward the west-northwest, and subsequent erosion produced a surface of moderate relief upon which rocks of unit IV accumulated. The basal part of this unit commonly consists of moderately well sorted sandstone and granule conglomerate, which grade upward into breccias containing boulders and blocks of quartz monzonite and welded tuff. Higher up, the breccia contains, instead of these, blocks of porphyritic quartz latite up to 20 feet in diameter, which are indistinguishable from the rock of the overlying lava flows. Some of the breccia may be vent agglomerate; all of it was produced by explosive reopening of sealed conduits prior to, or contemporaneous with, the formation of plugs, dikes, and lava flows. Block faulting recurred during deposition of these coarse deposits; as a result,

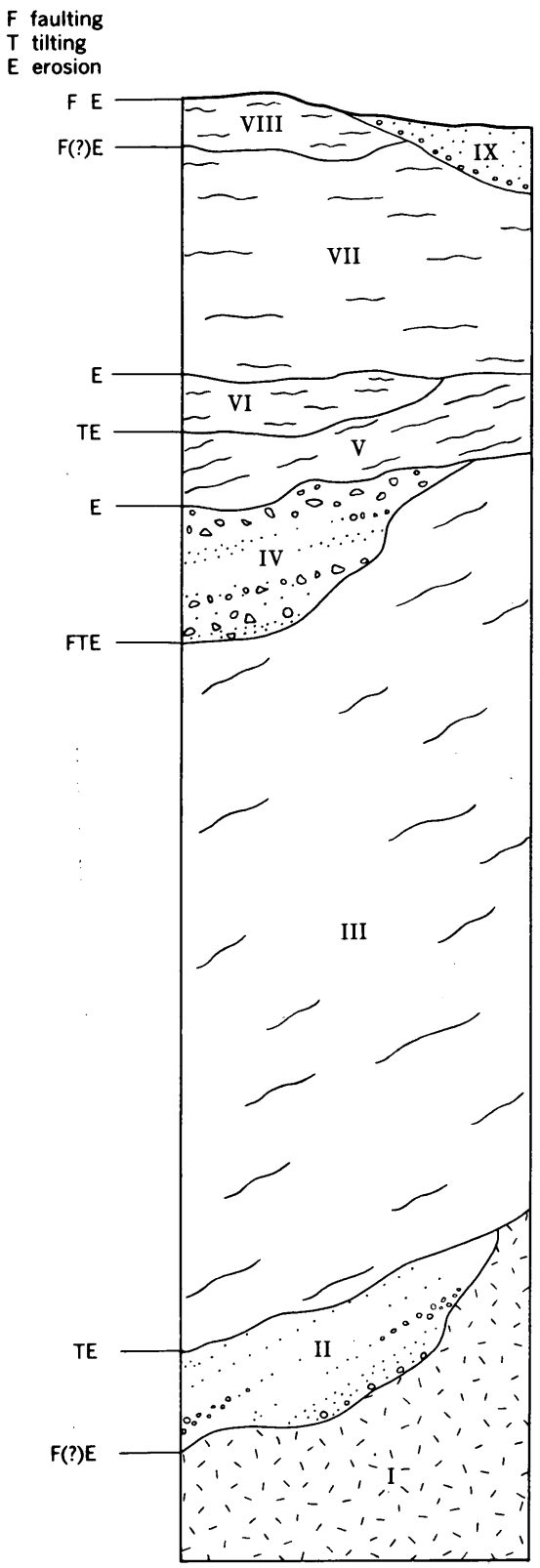

FIGURE 12.1.—Diagrammatic section of early Tertiary volcanic rocks of an area north and west of Butte, Mont.

some breccia deposits abut against fault scarps in breccia or welded tuff.

Breccia of unit IV, and older rocks, are overlain by two unconformable successions of quartz latite lava (units V and VII), locally separated by a vitrophyre (unit VI). Lavas of unit V are preserved only in the western part of the area, where they are overlain with angular discordance of as much as 30° by lavas of unit VII. Many small intrusive bodies were emplaced after and perhaps partly during the extrusion of the lavas of unit V. These lavas, and intrusives which cut them, were eroded before the eruption of the vitrophyre and the lavas of unit VII. In the Champion Pass area the quartz latites of unit VII are unconformably overlain by rhyolite of the younger sequence (unit VIII).

Between almost every one of the volcanic episodes and the next one there was faulting or tilting followed by erosion, and some of the faulting was contemporaneous with the deposition of unit IV. Major faulting and collapse took place after the eruption and welding of the succession of ash flows forming unit III. In the area immediately west of Butte this block faulting produced an L-shaped graben ¾ to 1½ miles wide in quartz monzonite of the Boulder batholith, into which the sheets of welded tuff collapsed. As a result the welded tuff sheets have a chaotic structure, and many of the blocks of tuff are nearly vertical. This fact, and the presence of minor breccia vents and marginal dikes, apparently caused earlier workers to interpret the welded tuff as an intrusive rock. Gravity surveys indicate that the floor of the graben lies at a depth of about 1,200 feet. The volcanic rocks in this graben are probably underlain by segments of truncated metalliferous quartz veins in the manganiferous zone in the quartz monzonite of the Butte district.

Renewed movement along some of the block faults that followed the volcanism produced intermontane basins, which received debris shed from the bounding scarps, and were thus filled with sand, gravel, silt, ash, and tuff (unit IX). These basins may be as old as late Oligocene; basin deposits near Silverbow contain lower Miocene fossils (Konizeski, 1957, p. 145).

Later movement along some of the faults displaced Pleistocene glacial deposits.

The net effect of repeated tilting of fault blocks in the area north of Butte is indicated by west-northwest dips of 15° to 35° in the basal unit and the sheets of welded tuff (units II and III).

REFERENCE

Konizeski, R. L., 1957, Paleoecology of the middle Pliocene Deer Lodge local fauna, western Montana: Geol. Soc. America Bull., v. 68, no. 2, p. 131–150.

13. TECTONIC SETTING OF THE COEUR D'ALENE DISTRICT, IDAHO

By Robert E. Wallace, Allan B. Griggs, Arthur B. Campbell, and S. Warren Hobbs, Menlo Park, Calif., Menlo Park, Calif., Denver, Colo., and Washington, D.C.

In gross structural pattern the Coeur d'Alene district lies at the intersection of the Lewis and Clark line (Billingsley and Locke, 1939, p. 36), represented by the Osburn and related faults, and a broad arch that extends north at least to Kimberly, British Columbia. The rocks of the district have been intensely deformed in a complex pattern that shows a marked discordance of structural elements on opposite sides of the Osburn fault and which well might be referred to as a structural knot (fig. 13.1C).

Dominating this structural knot is the Osburn fault which strikes about N. 80° W. across the area. Strike slip is indicated on the Osburn fault by: (a) the offset of large upwarped blocks more or less delineated by areas of outcrop of the Prichard formation, the oldest unit of the Belt series; (b) the offset of major folds and faults, and the dissimilarity of structural features adjacent to one another on opposite sides of the fault; (c) large-scale drag features; (d) offset of the same sense along parallel or subparallel faults; and (e) the position of major mining areas on opposite sides of the Osburn fault and the pattern of ore and gangue-mineral distribution within the areas. A maximum of about 16 miles of right-lateral strike slip is indicated on the segment of the Osburn fault east of the Dobson Pass fault and about 12 miles displacement in the same sense is indicated west of the Dobson Pass fault. The difference in displacement on these two segments is believed to be principally the result of contemporaneous dip slip on the Dobson Pass fault, which has effectively lengthened the block north of the Osburn fault relative to the block south. A few miles east of the area shown in figure 13.1, in the vicinity of Superior, Mont., the cumulative lateral movement in the Osburn and the related Boyd Mountain fault, as shown by stratigraphic displacement, appears to be approximately 16 miles, which strongly corroborates the suggested displacement on the Osburn fault in the Coeur d'Alene district.

The age of the Osburn fault is known only within broad limits. It cuts rocks of the Belt Series of Precambrian age and is capped by flows of Columbia River basalt of middle Miocene age. The probably contemporaneous Dobson Pass fault cuts the Gem stocks, which have been dated as about 100 million years old (Jaffe and others, 1959, p. 95–96). Other geologic evidence indicates that a lineament in the general position of the Lewis and Clark line may have been in existence since early Precambrian time.

Ages obtained from uraninite from the Sunshine mine (L. R. Stieff and T. W. Stern, written communication, 1957; Eckelmann and Kulp, 1957, p. 1130) indicate that uranium mineralization occurred about 1,250 million years ago. Thus tight folds, such as the Big Creek anticline (fig. 13.1), that are cut by the uraninite veins, must have been developed before that time. In contrast, the principal ore-bearing veins are younger than the Gem stocks of about 100-million-year age.

The overall history of development of the structural knot must have been complex; the following summary of a possible sequence of events is suggested. During an early stage of deformation (fig. 13.1*A*) the principal folds were developed and overturned to the northeast, and reverse faults that strike northwest and dip southwest were formed. A large domelike structure, the Moon Creek-Pine Creek upwarp, was formed west of the reverse faults.

Accompanying a major reorientation of the stress system, the axes of the folds began to bow (fig. 13.1*B*), the southern part of the region moved relatively westward, and incipient strike-slip faults developed. The Mill Creek and Deadman syncline was separated from the Granite Peak syncline and wrapped around the truncated end of the Granite Peak syncline. The northern flank of the Lookout-Boyd Mountain anticline was sliced off by one of the antecedent fractures of the Osburn fault.

Monzonite stocks intruded the structural knot thus produced (fig. 13.1*C*), and the principal period of ore deposition followed. Most of the veins are included in spatial groups that define distinct linear belts trending slightly more northwesterly than the Osburn fault system. The concentration in such belts of veins, which are subparallel but differ in size and orientation, suggests that linear feeders for the mineralizing solutions existed at depth, although no through-going structural elements reflect these feeders in the upper crust.

After the principal period of ore deposition, strike-slip movement along the ancestral Osburn zone of weakness became more through-going than previously, and apparently deep-seated stresses were accommodated at this time by displacement on relatively few faults, most

557753 O—60——3

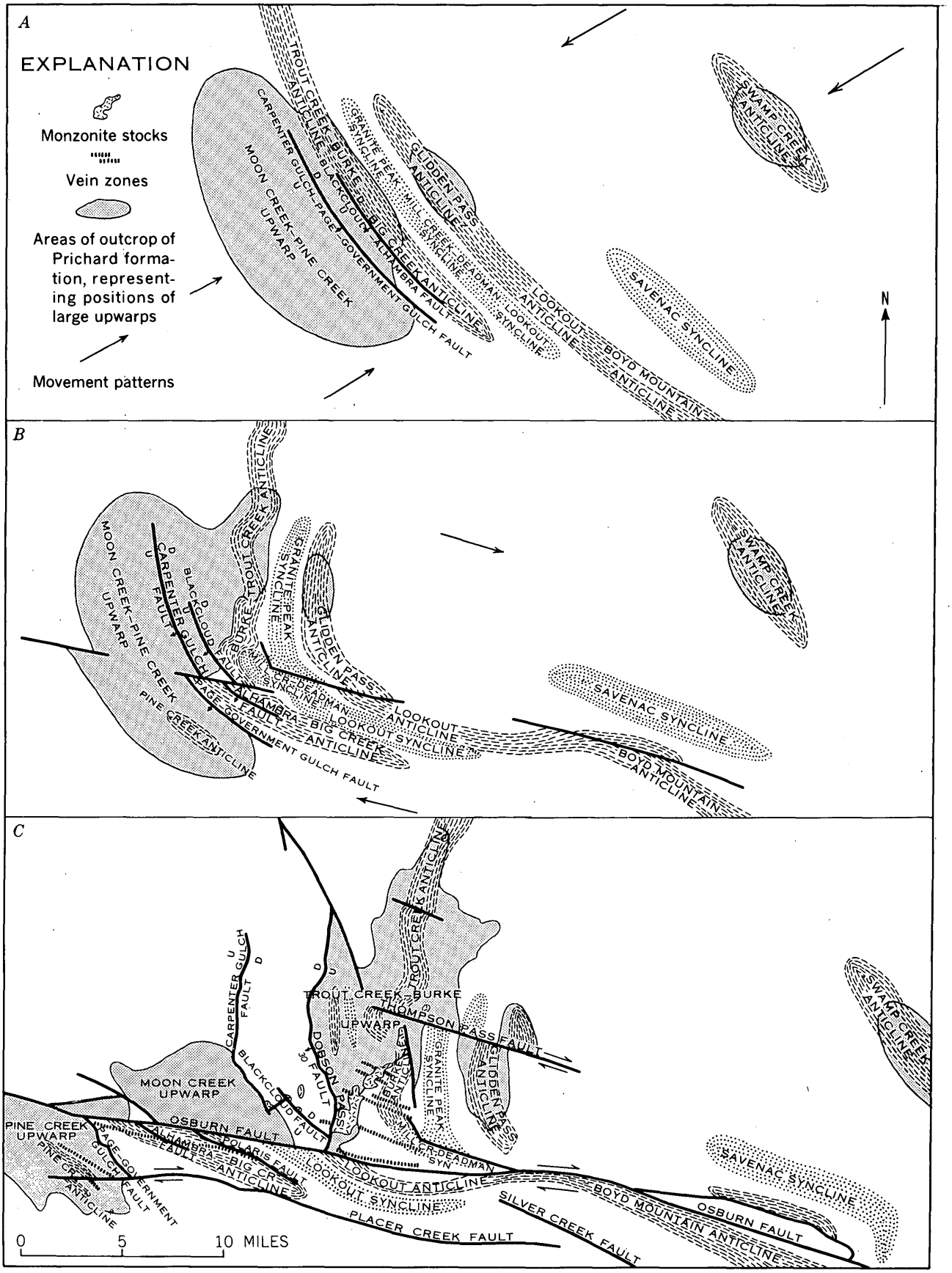

FIGURE 13.1.—Three stages (*A* to *C*) in the development of the tectonic setting of the Coeur d'Alene district, Idaho.

of which were in or parallel to this zone. The Osburn fault offset the major folds and early reverse faults, and separated the northern segment of the ore-bearing area from that to the south. The Thompson Pass fault also offset the major folds, and the Placer Creek fault offset the Pine Creek anticline and vein system. The Dobson Pass fault came into existence concurrently with the Osburn fault. The small stocks a few miles west of the Dobson Pass fault may represent cupolas displaced from the main part of the Gem stocks by dip slip on the Dobson Pass fault.

Some of the early-formed tight folds and strike-slip faults were flexed as later rotational stresses were accommodated along newly developed slip planes. Thus, the east end of the Savenac syncline and the adjacent north branch of the Osburn fault were sharply bent and later movement was "short-circuited" along the south segment of the fault. Likewise, the Polaris fault may have accommodated strike-slip deformation after the Placer Creek fault buckled.

Late normal faults, some resulting from the final stages of strike-slip deformation, and others possibly of Quaternary age (Pardee, 1950), have affected the area.

REFERENCES

Billingsley, Paul, and Locke, Augustus, 1939, Structure of ore districts in the continental framework: New York, Am. Inst. Mining and Metall. Engineers, 51 p.

Eckelmann, W.R., and Kulp, J. L., 1957, Uranium-lead method of age determination, Part II; North American localities: Geol. Soc. America Bull., v. 68, p. 1117–1140.

Jaffe, H. W., Gottfried, David, Waring, C. L., and Worthing, H. W., 1959, Lead-alpha age determinations of accessory minerals of igneous rocks (1953–57): U.S. Geol. Survey Bull. 1097-B, p. 65–148.

Pardee, J. T., 1950, Late Cenozoic block faulting in western Montana: Geol. Soc. America Bull., v. 61, no. 4, p. 359–406.

14. BLEACHING IN THE COEUR D'ALENE DISTRICT, IDAHO

By P. L. Weis, Spokane, Wash.

A striking feature of the Coeur d'Alene district is the presence of large elongated masses of what is commonly called bleached rock, though its color is pale yellowish green rather than white; many of these masses are associated with ore deposits. The bleached rock has been recognized and used as a guide to prospecting for 20 years or more, and those who have worked in the district have generally regarded them as being of hydrothermal origin and related in some way to the ore deposits. The cause of the bleaching, however, is in dispute. Two views have been expressed: (a) A number of workers, among them Shenon and McConnel (1939), believe that the bleached rocks have been sericitized—that is, that they have undergone hydrothermal alteration that converted pre-existing minerals to sericite. (b) Others, notably Mitcham (1952), believe that the bleached zones are places where certain of the pigmenting minerals have been replaced or removed. The present investigation is principally an effort to decide between these views.

The rocks involved in the bleaching are a part of the Belt series, of late Precambrian age. All are thin-bedded, fine-grained, slightly metamorphosed, quartz-rich rocks. They include quartzites, phyllites, slates, and all the many intermediate types. Adjacent beds may differ widely in composition, mainly because they contain different proportions of the two principal minerals, quartz and sericite. Quartz content ranges from about 10 percent to 90 percent, and the sericite varies essentially inversely through about the same range. The rocks also contain about 5 to 10 percent of other material—rock fragments, carbonates (including calcite, dolomite, ferrodolomite, ankerite, and siderite), plagioclase and potassium feldspar, chlorite, hematite, magnetite, pyrite, zircon, tourmaline, rutile, carbonaceous (?) material, and probably leucoxene and goethite. The bleached rocks contain the same minerals, except that hematite, chlorite, carbonaceous (?) material and in places pyrite are absent.

One way to approach the problem is to consider what characteristics the bleached rocks should have if they were sericitized. Those that come to mind are as follows:

1. Sericitized rocks should contain more sericite than unbleached rocks—which should be apparent both in thin sections and in chemical analyses.
2. Sericitized rock should contain veinlets of sericite and pseudomorphs of sericite after other minerals,

especially detrital feldspar; it should show replacement textures where the process was incomplete.

3. Introduced sericite should have random orientation, in contrast to sericite formed under stress during metamorphism. Some pre-existing flakes of sericite might be enlarged.
4. Progressive, systematic differences in sericite content from place to place should be recognizable, especially where such differences are related to structural features.
5. Ore deposits and zones of sericite-rich rock should bear some recognizable relation to each other as well as to structural features.

If sericitization were responsible for the color changes that define the bleached zones, then one or more of these features should be readily identified in any specimen of strongly bleached rock. Not one of these features was found, however, in the bleached rocks of the Coeur d'Alene district.

Specimens that contained both bleached and unbleached parts of the same bed were studied with particular care. Without exception, these specimens showed no difference between altered and unaltered rock in content of sericite, carbonates, and detrital feldspars. Other evidences of sericitization are similarly lacking in the bleached rocks. The conclusion is inescapable: the bleached rocks do not owe their color to sericitization.

The mineralogical changes that accompanied the bleaching are simple. Hematite, carbonaceous (?) material, and green chlorite, the principal pigmenting minerals, are absent from the bleached rocks; otherwise the mineralogy of bleached and unbleached rocks is identical. It should be emphasized that the proportion of sericite has not been increased by bleaching. The intimate association of bleached zones to faults and areas of more disturbed rocks. and generally close relation to ore deposits clearly points to a hydrothermal origin. The problem, then, is to define the probable range in temperature and chemical composition of a solution that will attack hematite, carbonaceous material, and green chlorite without attacking such relatively susceptible minerals as carbonates and feldspars. The solutions cannot have been strongly acid, or they would have attacked the carbonates. Nor can they have been strongly alkaline, for feldspars, especially plagioclases, are attacked by strongly alkaline solutions and hematite is not. Their temperature range can also be roughly bracketed within the limits 110° and 150° C, for although hematite can be hydrolized to goethite in nearly neutral solutions within that approximate range (Smith and Kidd, 1949, p. 411), it is stable at higher and lower temperatures. The effect of such a solution on chlorite and carbonaceous material is unknown; one can only assume that because in the bleached rock the supposedly carbonaceous material is absent and the chlorite is altered to a colorless though apparently sheeted mineral, their behavior in the bleaching solution was similar to that of hematite.

Although the precise chemical composition of the bleaching solution is not known, the solution apparently need not have contained anything other than nearly neutral warm water. It may have contained a little CO_2 or H_2S, but these evidently were not essential. The solution may have removed the pigmenting minerals, or have caused them to recombine with other minerals in the rock, or have aggregated some of them into such large grains that they were no longer effective as coloring agents; in some places the rock may have been affected by any one of these changes or by two or three of them. The final result, at any rate, was the destruction of disseminated dark-colored pigmenting minerals, apparently without any other change.

Hydrothermal solutions consisting merely of warm water are a far cry from the solutions that many geologists envision as agents that deposited the ores. Such apparently great differences between the two solutions indicate that they must have been separated both in time and in source, but further work will be necessary to provide the details of origin and age of the bleaching solutions.

REFERENCES

Mitcham, T. W., 1952, Indicator minerals, Coeur d'Alene silver belt: Econ. Geology, v. 47, no. 4, p. 415–450.

Shenon, P. J., and McConnel, R. H., 1939, The Silver Belt of the Coeur d'Alene district, Idaho: Idaho Bur. Mines and Geology Pamph. 50, 9 p.

Smith, F. G., and Kidd, D. J., 1949, Hematite-goethite relations in neutral and alkaline solutions under pressure: Am. Mineralogist, v. 34, nos. 5 and 6, p. 403–412.

15. ORIGIN OF THE MAIN PERIOD VEINS, COEUR D'ALENE DISTRICT, IDAHO

By VERNE C. FRYKLUND, JR., Spokane, Wash.

The Coeur d'Alene district, in Shoshone County, Idaho, is part of what I have called the Coeur d'Alene mineral belt. This belt is about 95 miles long, its west end being near Coeur d'Alene, Idaho, and its east end near Superior, Mont. The Coeur d'Alene district lies about midway between the ends of the belt, at its intersection with a northeast-trending fracture zone containing a row of monzonite stocks, two of which are exposed in the northern part of the district. The country rocks are quartzitic formations in the Belt series, of late Precambrian age cut by monzonite and lamprophyric dikes.

Although six periods of mineralization, of Precambrian to Tertiary age, are recognized, the following remarks relate only to the possible sources of the vein minerals formed during the Main period of mineralization, which occurred in Cretaceous time.

The zonal patterns of ore and gangue minerals formed during the several stages of the Main period could mean that those minerals came from three sources, at least two of them magmatic; the isotope composition of the lead, however, suggests that one source was nonmagmatic.

A crucial point in considering the origin of the Main period veins is the time relation of those veins to the monzonite stocks, which are believed to be of Cretaceous age (Larsen and others, 1958, p. 54). Only one period of monzonite intrusion has been recognized, and most previous workers believe, as I do, that the principal veins were formed while the monzonite was being intruded or shortly thereafter (Hershey, 1916, p. 20; Crosby, 1959, p. 700; Ransome and Calkins, 1908, p. 135 ff.; Umpleby and Jones, 1923, p. 18; Griggs, 1952, p. 102).

The distribution and possible sources of the major vein minerals are considered below in the paragenetic order of those minerals.

The silicate minerals of the first stage—green biotite, garnet, and amphiboles—are found in minor amounts in the veins in monzonite and in the contact aureoles, and also in veins as much as 5,000 feet outside those aureoles. This restriction of silicates to veins around the stocks strongly indicates a genetic connection between the stocks and the silicates (Umpleby and Jones, 1923, p. 149).

Siderite, ankerite, and barite were next deposited. Veins whose gangue consists mainly of carbonate minerals are characteristic of the great Coeur d'Alene mineral belt. As the carbonate-rich veins are very much more widely distributed than those containing silicates, their source was probably not the monzonite magma. It may have been an underlying batholith.

Specular hematite, which followed the carbonate minerals and barite, has the same general distribution in the mineral belt as the carbonate minerals, and probably had the same source.

Euhedral magnetite was deposited later than the hematite. It is concentrically zoned around the stocks, and it may have been the last mineral contributed by the monzonite magma.

Although minor amounts of many sulfide minerals are found in veins throughout the mineral belt, the only deposits in the belt that are known to contain sulfide-rich ore are in the 25-mile segment within the Coeur d'Alene district. It therefore seems unlikely that the sulfides came from the same source as the much more widespread carbonate minerals. But as the sulfides are more widespread than the silicate minerals, and are not zoned around the stocks, it does not seem probable that they came from the monzonite magma.

The isotopic composition of the lead in the galena of the Main period is apparently uniform throughout the district; this lead, moreover, contains much less of the radiogenic isotopes than the lead from feldspar in the south stock (data contained in written communication, L. Stieff and T. Stern, 1959). Long and others (1959) have interpreted the isotopic ratios as indicating a Precambrian age of 1,250 million years for the mineralization, but this interpretation is inconsistent with the fact that some of the Main period veins cut monzonite and that the silicate-bearing veins are zoned around the stocks. There is little possibility, however, that galena of this isotopic composition came from the stocks, or from any granitic magma of similar age that contains what are generally regarded as normal, or average, amounts of uranium and thorium.

Possibly the lead was separated from a normal granitic magma, and thus removed from further contamination by radiogenic lead, in Precambrian time, and brought into the upper part of the crust in Cretaceous time. This concept, however, is hard to accept, for it would imply that the mechanism by which the ore deposits of the Coeur d'Alene district were formed was unusual if not unique. The Coeur d'Alene district is

not unique, however, in its geologic relations, its mineralogy, or the isotopic composition of its lead. Butte ores show a difference in isotopic composition between vein lead and wall-rock lead (Murthy, 1959, p. 1649). The Sullivan ore body at Kimberly, British Columbia, is mineralogically identical with the productive silicate-bearing veins of the Coeur d'Alene district (Schofield, 1915, p. 133–135; Rice, 1937, p. 43), and according to Long and others (1959) the Sullivan lead has the same isotopic composition as Coeur d'Alene lead.

A more likely supposition is that the Coeur d'Alene lead, together with other valuable metals, was brought from some deep source that contained only insignificant amounts of uranium and thorium. This source might have been a granitic magma in which uranium and thorium were abnormally scarce; or it may have lain much deeper, in the mantle, where it is generally believed on geochemical grounds that neither uranium nor thorium is present in significant amount.

REFERENCES

Crosby, G. M., 1959, The Gem stocks and adjacent ore bodies, Coeur d'Alene district, Idaho: Mining Eng., v. 11, no. 7, p. 697–700.

Griggs, A. B., 1952, Geology and notes on ore deposits of the Canyon-Nine Mile Creeks area, Shoshone County, Idaho: U.S. Geol. Survey open-file report, 108 p., 23 pls., Oct. 27, 1952.

Hershey, O. H., 1916, Origin and distribution of ore in the Coeur d'Alene, Idaho: Published by the author, 32 p.

Larsen, E. S., Jr., Gottfried, David, Jaffe, H. W., and Waring, C. L., 1958, Lead-alpha ages of the Mesozoic batholiths of western North America: U.S. Geol. Survey Bull. 1070–B, p. 35–62.

Long, Austin, Silverman, Arnold, and Kulp, J. L., 1959, Precambrian mineralization of the Coeur d'Alene district, Idaho (abs.): Jour. Geophys. Research, v. 64, no. 8, p. 1114.

Murthy, V. R., 1959, Lead isotopic study of ore and igneous minerals at Butte, Montana (abs.): Geol. Soc. America Bull., v. 70, no. 12, pt. 2, p. 1649–1650.

Ransome, F. L., and Calkins, F. C., 1908, The geology and ore deposits of the Coeur d'Alene district, Idaho: U.S. Geol. Survey Prof. Paper 62, 203 p.

Rice, H. M. A., 1937, Cranbrook Map-Area, British Columbia: Canada Geol. Survey Mem. 207.

Schofield, S. J., 1915, Geology of the Cranbrook Map-Area, British Columbia: Canada Geol. Survey Mem. 76.

Umpleby, J. B., and Jones, E. L., 1923, Geology and ore deposits of Shoshone County, Idaho: U.S. Geol. Survey Bull. 732, 156 p.

16. GEOLOGIC AND ECONOMIC SIGNIFICANCE OF SOME GEOCHEMICAL RESULTS OBTAINED FROM STREAM SEDIMENT SAMPLES NEAR NOME, ALASKA

By C. L. Hummel and Robert M. Chapman, Menlo Park, Calif., and Denver, Colo.

During recent areal geologic investigations, thirty samples of sediments were obtained from streams throughout a 500-square-mile area near Nome, Alaska. They were collected primarily to test the efficacy of this method of geochemical exploration in the part of the metamorphic terrane of the Seward Peninsula that is best known geologically. In general, the sediment samples contained meaningful quantities of a number of metals; anomalously high amounts of copper, zinc, bismuth, and molybdenum in samples collected from Thompson Creek in the Kigluaik Mountains located 30 miles north of Nome are of particular geologic and economic significance as indicators of metalliferous lodes in an area not formerly known to contain them.

The geochemical sediment samples were collected and processed according to procedures developed by the U.S. Geological Survey. The samples were selected to include mainly the finest and lightest stream sediments and some organic material, wherever it was present. Although sediment sampling was designed as a field method for determining the heavy metal content of sediments by colorimetric techniques, all of the determinations reported here were made in a Survey laboratory as part of a continuing program to develop and improve geochemical exploration methods (Chapman and Shacklette, Art. 49). F. N. Ward was a constant source of advice and assistance.

The amounts of antimony, arsenic, bismuth, copper, lead, molybdenum, tungsten, and zinc were determined in all samples. Useable quantities were obtained of all metals except tungsten, whose level of detection (20 ppm) is still too high to be of value by this method in the Nome area.

All of the bedrock of the Nome area has been regionally metamorphosed; high-grade metamorphic rocks occur only in the Kigluaik Mountains while metamorphic rocks of considerably lower grade form the bedrock of the area between the Kigluaik Moun-

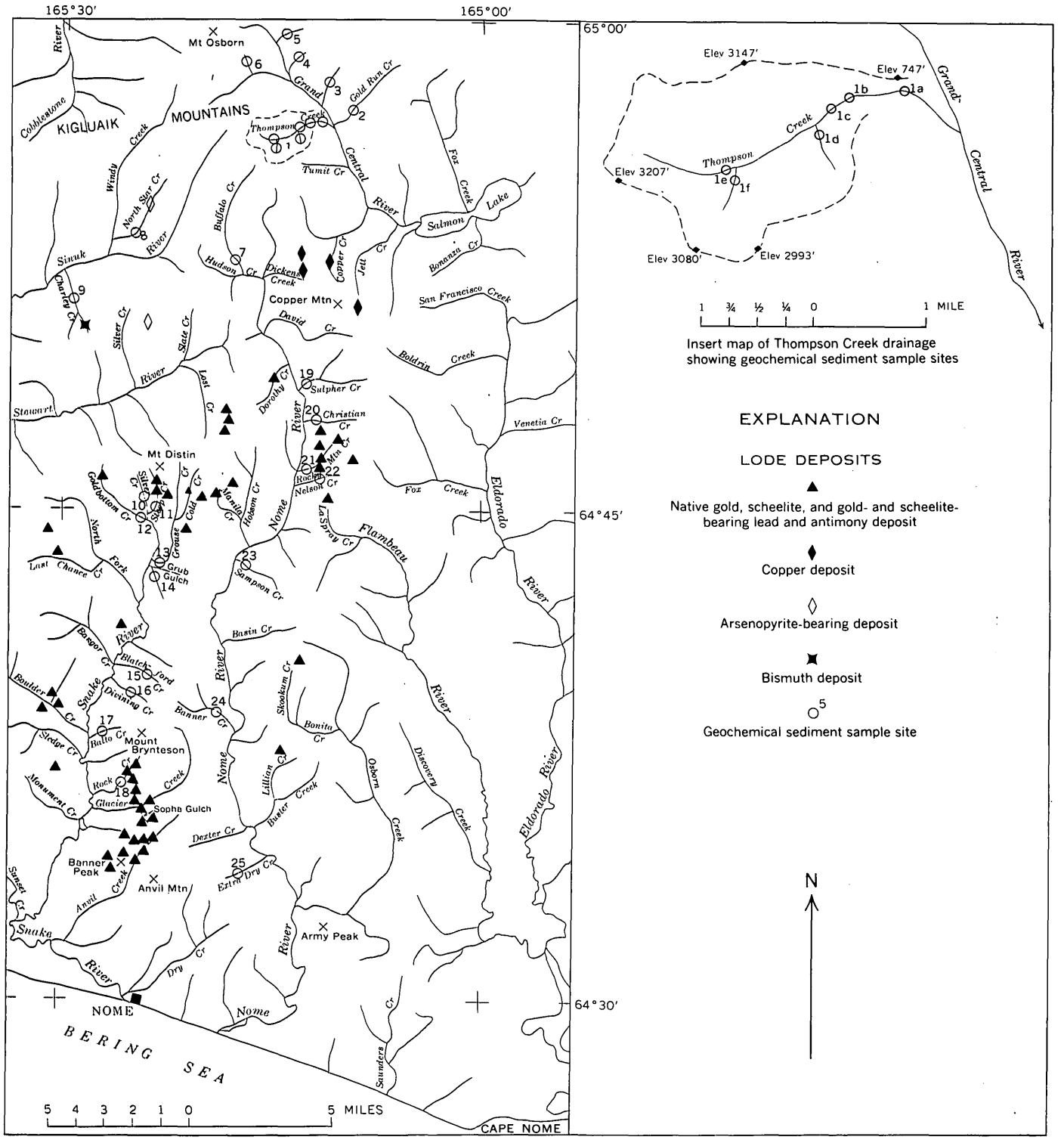

FIGURE 16.1.—Map showing location of lode deposits and geochemical sediment sample sites near Nome, Alaska.

tains and Bering Sea, in which the Nome goldfields lie (Moffit, 1913, p. 140). The bedrock of the goldfields is composed entirely of low grade schists and interbedded marble. Known lodes of the goldfields, of the type from which the gold of the alluvial and beach placers of the goldfields was derived, are for the most part filling-type deposits in shattered quartz masses (fig. 16.1). Scheelite and native gold are the dominant non-gangue constituents in a few deposits but base metal sulfides predominate in most of them. Except

for a single deposit in which native bismuth and bismuthinite occur and several copper sulfide deposits, most of the lodes are composed of lead and antimony sulfides with minor amounts of scheelite and gold.

The Nome goldfields are bounded on the north by the Kigluaik Mountains. The bedrock of the mountains is composed entirely of very high grade metamorphic rocks into which have been intruded many relatively small sills and dikes of silicic and mafic igneous rocks and granite pegmatites. Although the igneous rocks are thought to be genetically related to the mineral deposits of the goldfields, the only direct evidence of hydrothermal mineralization in the Kigluaik Mountains consists of a single lode on North Star Creek in which arsenopyrite was the only metallic mineral which was recognized.

The results obtained from geochemical sediment samples collected in the Nome goldfields closely reflect the presence or absence, and the composition and proximity to sample sites, of the known lode deposits in the drainage basins of the streams from which the sediments were collected (table 16.1). As might have been expected, most of the samples from the goldfields contained greater quantities of antimony and arsenic. However, in specific cases, anomalously high amounts of other metals were obtained from samples collected from drainage basins where lodes containing those metals crop out, such as lead in sample 11 from Steep Creek and bismuth in sample 9 from Charley Creek.

In marked contrast with the results obtained from sediment samples from the Nome goldfields were those obtained from samples collected from streams in the Kigluaik Mountains. In the absence of known metalliferous lodes, no anomalous quantities of the metals determined could be expected. In general, none were obtained; samples 2 through 8, collected from widely separated localities throughout the part of the Kigluaik Mountains included in the area of this report, had consistently small amounts of all the metals determined and thus provided a basis for estimating the quantities of these metals in sediments derived from the high grade metamorphic rocks. The only exceptions to these general results were some obtained from sediment samples collected from Thompson Creek a western tributary of the Grand Central River. The first sample (1A) was collected by the authors in 1957; other samples of the series (1B–1E) were collected at the request of the authors by D. M. Hopkins in 1959 on the basis of the geochemical results obtained from sample 1A.

Samples from Thompson Creek contained more copper, zinc, molybdenum, and bismuth than those from any other part of the area. The resulting anomalies of these metals were two to six times greater than the background content estimated from samples 2 to 8. Because no lode material has been found in the Thompson Creek drainage, the difference between the results obtained from there and those obtained from drainages with known lode deposits is significant. For example, the Thompson Creek samples contained more bismuth than samples 9 from Charley Creek although a lode containing native bismuth and bismuthinite crops out about half a mile above the sample site and both minerals are present in placer deposits at least as far downstream as the sample site. Similarly, although sphalerite is abundant in a lode cropping out at the head of Steep Creek, a headwater tributary of the Snake River, the quantity of zinc in a sample collected about a mile downstream did not exceed its background content. Individually, the Cu, Zn, Mo, and Bi geochemical anomalies are strong indicators of undiscovered metal-

TABLE 16.1.—*Content (in ppm) of several metals in sediment samples from streams near Nome, Alaska*

[Analysts: W. L. Jones, H. H. Mehnert, H. M. Nakagawa, H. Neiman, L. E. Patten]

Locality	Sample	Pb	Cu	Zn	As	W	Mo	Bi	Sb
Thompson Creek	1A	<20	120	400	<10	<20	10	<5	2
	1B	25	150	600	<10	<20	8	35	1
	1C	25	100	400	10	<20	12	45	2
	1D	25	75	125	10	<20	4	10	1
	1E	25	75	225	<10	<20	4	50	1
	1F	25	100	225	<10	<20	12	10	2
Kigluaik Mountains	2	<20	30	80	<10	<20	10	<5	2
	3	<20	30	100	<10	<20	4	5	2
	4	<20	30	100	10	<20	2	<5	2
	5	<20	30	100	<10	<20	4	<5	1
	6	<20	30	100	<10	<20	2	<5	2
	7	<20	30	100	30	<20	6	10	1
	8	<20	30	100	<10	<20	10	<5	2
Nome goldfields	9	<20	30	80	300	<20	2	20	6
	10	<25	20	50	150	<20	<4	<5	10
	11	50	30	75	60	<20	<4	<5	30
	12	<25	20	100	150	<20	<4	5	8
	13	<25	30	100	150	<20	<4	<5	10
	14	<25	30	125	60	<20	<4	<5	8
	15	<25	20	75	40	<20	<4	5	4
	16	<25	20	75	30	<20	<4	<5	4
	17	<25	20	75	80	<20	<4	<5	6
	18	<25	20	75	300	<20	<4	5	6
	19	<25	20	75	20	<20	<4	<5	4
	20	<25	30	75	60	<20	<4	<5	6
	21	25	30	100	150	<20	<4	<5	10
	22	<25	30	100	150	<20	<4	<5	4
	23	<25	30	75	80	<20	<4	<5	10
	24	<25	20	75	20	<20	<4	<5	4
	25	<20	30	100	10	<20	2	<5	2

liferous lodes in the Thompson Creek drainage. Taken together, they indicate that the Kigluaik Mountains, and perhaps other areas in which high-grade metamorphic rocks occur on the Seward Peninsula, contain hydrothermal deposits of base metals, even though they lack the gold-bearing lodes and placer deposits that characterize the Nome goldfields.

Briefly summarized, the conclusions of this report are:

1. Meaningful geochemical results were obtained from stream sediments in the mineralized metamorphic terrane of the Seward Peninsula.
2. The greatest quantities of copper, zinc, bismuth, and molybdenum in all of the sediment samples occurred in those collected from Thompson Creek in the Kigluaik Mountains and strongly indicate the presence of lode deposits containing these metals in the Thompson Creek drainage basin.
3. The indication of metalliferous lodes near Thompson Creek suggests that hydrothermal deposits may occur in the high-grade metamorphic rocks elsewhere in the Kigluaik Mountains and, perhaps, in those exposed at other places on the Seward Peninsula.

REFERENCE

Moffit, F. H., 1913, Geology of the Nome and Grand Central quadrangles, Alaska: U.S. Geol. Survey Bull. 533, p. 140.

17. STRUCTURAL GEOLOGY AND STRUCTURAL CONTROL OF MINERAL DEPOSITS NEAR NOME, ALASKA

By C. L. Hummel, Menlo Park, Calif.

Structures belonging to systems of two ages have been identified and mapped in the bedrock of an area near Nome, Alaska (fig. 17.1). The lode and placer deposits of the Nome goldfields are closely associated with some of the structures of the younger system.

Structures of the older system developed during a period of deep-seated deformation, probably in the Mesozoic era, at which time all the bedrock of the area was regionally metamorphosed. The major structures of this system once formed a series of nearly northward trending folds which may have extended northward for 100 miles across the middle of the Seward Peninsula. Other structures include numerous minor folds of various sizes and several types of axial lineation; all these features are more or less parallel to the major folds. The major folds were greatly modified by later orogenic activity, so that only deformed remnants of two of them are now recognizable in the area—a broad, open syncline about 25 miles wide in the eastern part of the area and a somewhat tighter but still open anticline in the western part.

Structures of the younger system are thought to be related to the eastward-trending uplift, probably of Tertiary age, from which the present Kigluaik mountain range developed. This uplift transected the older northward-trending folds about at right angles, leaving within the area the truncated ends of the two folds mentioned above. Structural features of the uplift are clearly expressed by the present topography. Not only does the range have the same trend as the uplift, but the uplift is bounded by steeply dipping normal faults, one of which marks the northern limit of the range and the other almost coincides with the southern limit. The highest mountains of the range lie along the axis of an arch, formed during the elevation of the uplift, that plunges eastward and westward from Mount Osborn, the highest peak in the range. Because of the arcuate pattern of the faults that bound it, the uplift is also widest through Mount Osborn. The southern boundary fault marks the contact between the high-grade metamorphic rocks which crop out only in the uplift and those of much lower metamorphic grade which form the bedrock throughout the area to the south. On the basis of this difference of metamorphic grade and on stratigraphic evidence, it is estimated that at least 30,000 feet of vertical movement has taken place in the center of the uplift.

Other structures of the younger system, present only in the area south of the Kigluaik Mountains, are thought to be subsidiary effects of the uplift. These include two folds of considerable size and three sets of faults. The folds, both of them just south of the uplift, are an eastward-plunging syncline in the west-central part of the area and a southwestward-plunging syncline in the northeastern part, superposed upon the eastern and western limbs of the older north-trending syncline. The three sets of faults strike to the north, northeast, and east, respectively. Only the east-west

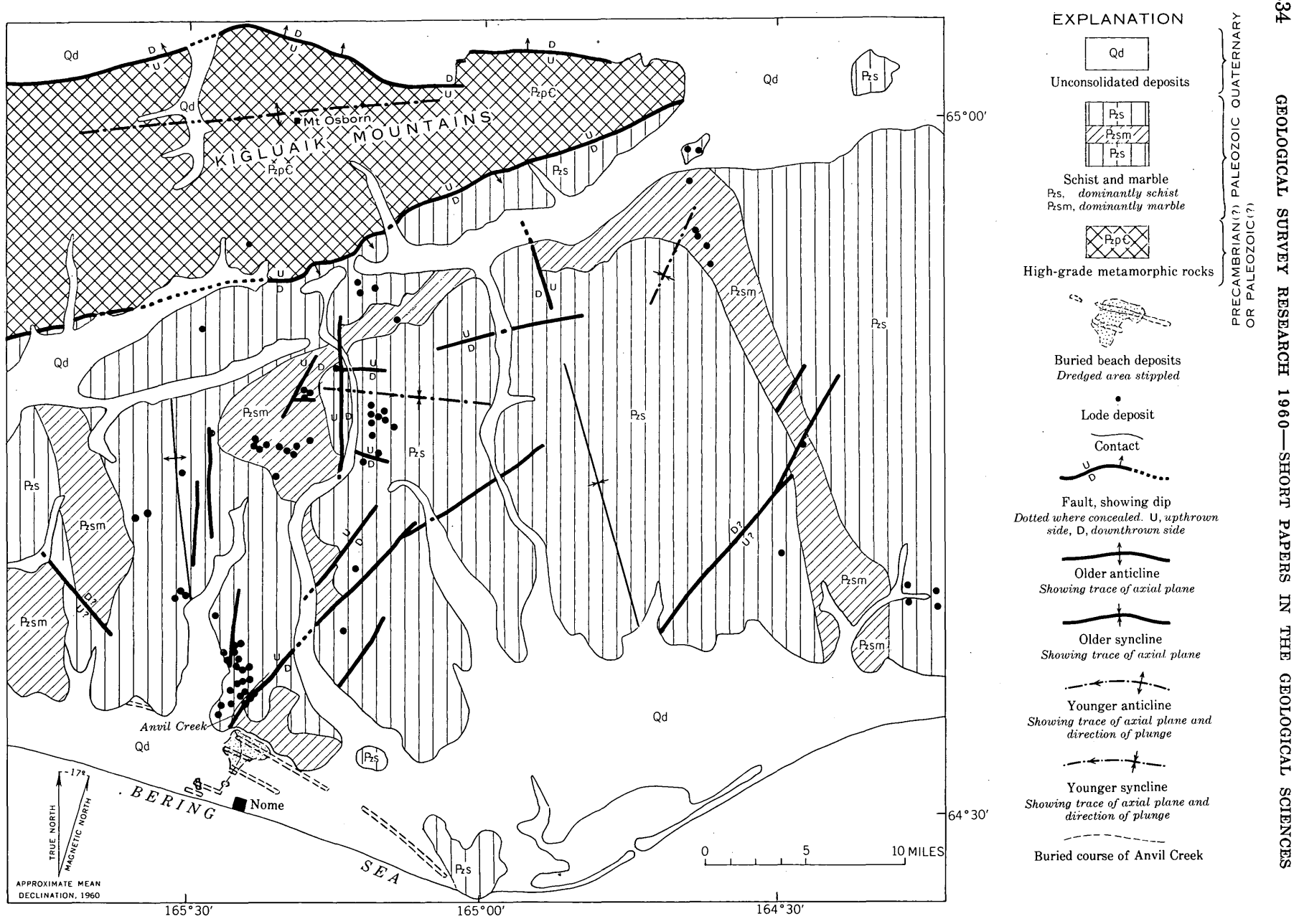

FIGURE 17.1.—Structures and mineral deposits near Nome, Alaska.

faults are obviously related to the uplift; they strike about parallel to the boundary faults, and the north sides of most of them are strongly upthrown.

The lode and placer deposits of the Nome goldfields are closely associated with the younger folds and faults south of the Kigluaik Mountains. The lode deposits, most of which are filling-type deposits composed of varying proportions of base-metal sulfides, scheelite, and native gold in shattered quartz, occur in three areas; two of these extend along the two younger synclines just south of the Kigluaik Mountains, and the third lies between a northward- and a northeastward-striking fault just north of Nome. Within each of these areas the lodes have been further localized along minor faults and disturbed joints.

The areal distribution of the placer deposits is generally related to that of the lodes and thus is indirectly controlled by structure. This indirect control is of particular interest and importance in the case of the northeastward-striking fault which reaches the coastal plain just north of Nome. Numerous lode deposits occur in and near the fault zone where it is exposed in the valley of Anvil Creek, which marks the southwestern end of the fault. Similar lodes in eroded portions of the fault and bedrock were the sources of the gold in the alluvial placer deposits on Anvil Creek, the richest in the goldfields, and of the gold in the richest parts of several buried beaches which have been formed along the ancestral course of Anvil Creek under deposits of the coastal plain.

18. STRUCTURAL CONTROL IN FIVE QUICKSILVER DEPOSITS IN SOUTHWESTERN ALASKA

By C. L. Sainsbury and E. M. MacKevett, Jr., Menlo Park, Calif.

Most of Alaska's known quicksilver deposits are in the southwestern part of the State. Five of them—the Red Devil, Red Top, Kagati Lake, White Mountain, and Willis—illustrate different types of structural control (fig. 18.1). These deposits were studied during 1958 and 1959 as a part of the U.S. Geological Survey's investigation of quicksilver deposits in southwestern Alaska.

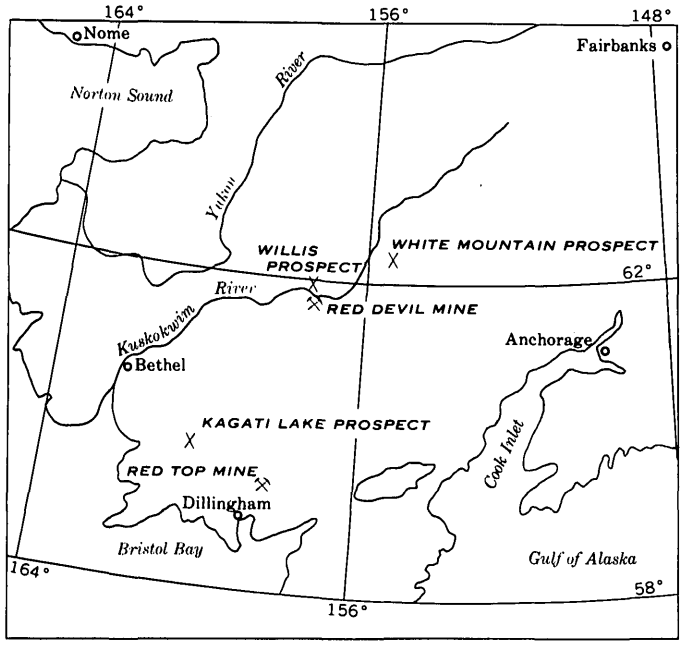

FIGURE 18.1.—Index map showing location of five quicksilver deposits in southwestern Alaska.

The quicksilver deposits, which are probably of Tertiary age, are alike in having been mainly formed by the deposition of cinnabar in open factures in competent rocks, but in detail each deposit has its individual structural control. The cinnabar is commonly accompanied by stibnite, but it also occurs alone, or less extensively with realgar and orpiment. The common gangue minerals are quartz, dolomite, and calcite.

The Red Devil mine, Alaska's largest quicksilver producer, has produced more than 20,000 flasks. The mine is in graywacke and argillaceous rock of the Cretaceous Kuskokwim group, which strike N. 30°–45° W. and dip 45°–60° SW, and in altered dikes that cut these rocks. The ore bodies were formed at and near intersections between northeast-trending dikes that dip 40°–60° SE. and northwest-trending faults that are essentially parallel to the bedding (fig. 18.2). This structural control was first recognized by J. D. Murphy, former manager and resident geologist at the mine. Typical ore bodies are pencil-shaped and plunge about 40° S. The northwest-striking faults have right-lateral displacements that range from a few inches to about 40 feet, and the cumulative right-lateral displacement of the faults is several hundred feet. The mineralized intersections are in a zone that is at least 600 feet wide and 1,500 feet long.

The Kagati Lake prospect is in a strongly fractured quartz monzonite and granodiorite stock, probably of Tertiary age (fig. 18.3). The quicksilver deposits are localized along favorable faults and joints, commonly in irregular quartz veins and pods. Most of the well-defined ore bodies are only a few inches wide and are traceable for less than 10 feet along their strikes. Most of the deposits lie in what is called the "main shear zone," which consists of many steep closely spaced fractures that strike about N. 20° W., but some are in subparallel fractures west of it. Minor amounts of ore occur in fractures that trend more nearly due northwest.

The Red Top mine has had a small production. The ore occurs along a steep fault zone where it intersects minor folds that plunge southward. The general strike of the fault zone is N. 70° W., parallel to the regional attitude of the graywackes and siltstones of the Gemuk group, of Carboniferous to Cretaceous age (J. M. Hoare, oral communication, 1960). The differing structures on opposite sides of the fault zone are illustrated in figure 18.4*A*. On the north side the beds along the line of section are essentially homoclinal, dipping steeply southwestward; on the south side they form small folds that plunge southward. Abundant breccia, shear zones, and divergent fractures occur where the fault intersects the plunging folds. Most of the ore consists of cinnabar in a dolomite gangue that is localized in breccia zones and veinlets along the divergent fractures. The competent graywacke fractured readily and is crossed by wide breccia zones and open fractures, whereas the fractures in the siltstone are tight, contain abundant gouge, and commonly lack ore. The minette dike that is shown in figure 18.4*A* is unaltered and apparently unrelated to the formation of the ore. The dump at the lower adit contains some

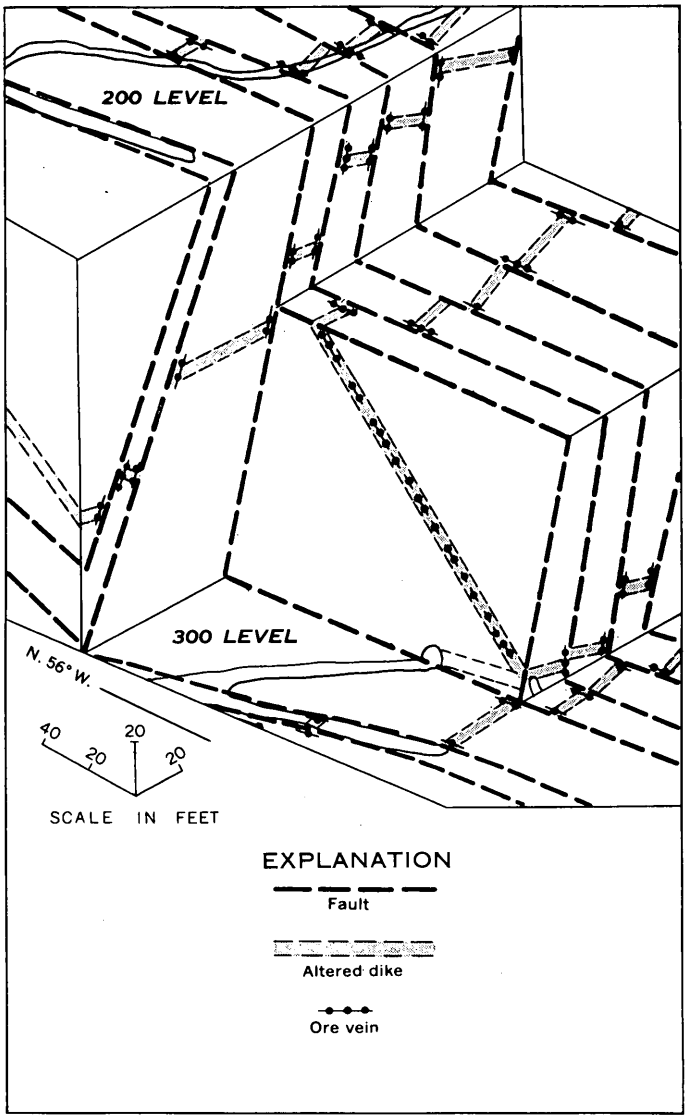

FIGURE 18.2.—Generalized isometric block diagram of part of the Red Devil mine. The dikes and veins cut graywacke and shale of the Kuskokwim group.

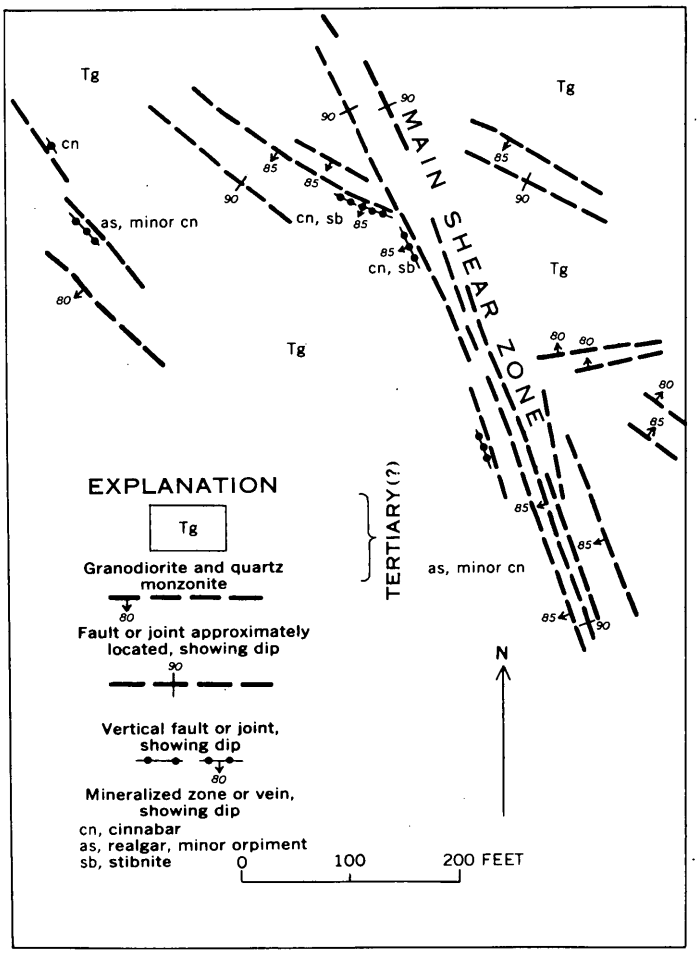

FIGURE 18.3.—Geologic sketch map of the Kagati Lake prospect.

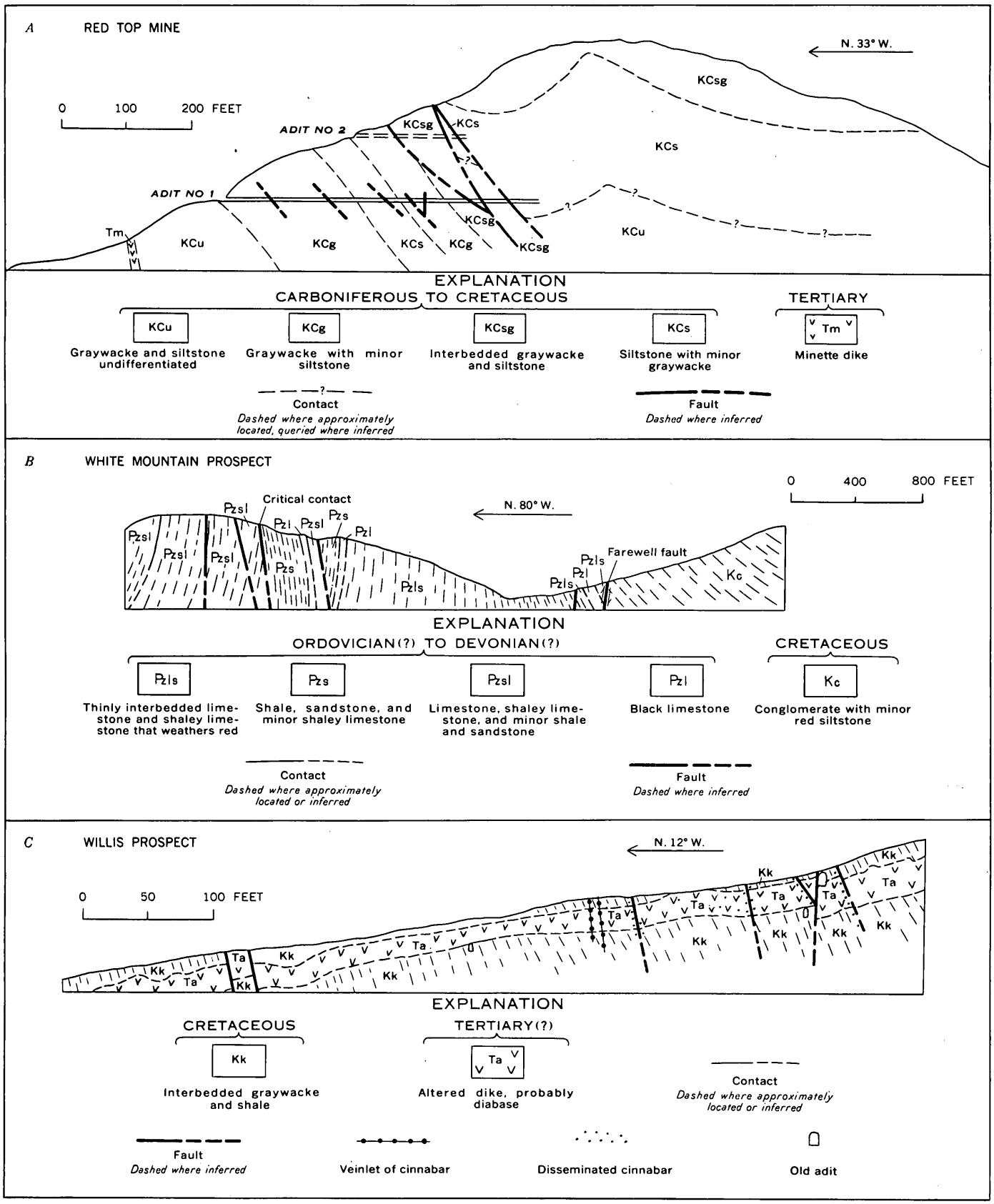

FIGURE 18.4.—Structure sections of *A*, Red Top mine; *B*, White Mountain prospect; *C*, Willis prospect.

ore averaging 1.1 percent of mercury obtained from a development drift in massive graywacke; the limits of the mineralized graywacke are not delineated by existing openings.

At the White Mountain prospect, illustrated by figure 18.4 *B*, the quicksilver deposits are northwest of a regional fault, the Farewell fault, which separates Paleozoic limestone and shale (Holitna group) on the northwest from Cretaceous (?) quartz conglomerate on the southeast. The main ore controls are steep faults, essentially parallel to bedding planes, that separate calcareous rocks from the only dominantly shaly unit in the section. One such fault is shown in figure 18.4 *B*, where it is labeled "critical contact". Cinnabar occurs in pods of brecciated, silicified, and dolomitized limestone adjacent to the faults. The ore in the White Mountain prospects unlike that in most cinnabar deposits in southwestern Alaska, is not closely associated with altered dikes. Altered dikes of unknown original composition and fresh diabase dikes are exposed, however, about a mile and a half west of the prospect. Possibly the ore-forming fluids migrated at depth from the neighborhood of the altered dikes and ascended the steep faults along barriers of impervious shale.

The geologic setting at the Willis prospect is similar to that at the nearby Red Devil mine. The host rocks are graywackes and shales of the Kuskokwim group, and altered dikes. The sedimentary rocks strike northwest and dip steeply southwest, but the altered dikes are nearly horizontal. Ore bodies occur at and near intersections between the altered dikes and northwest-trending faults that commonly strike parallel to the bedding. Although structural control is similar to that at Red Devil, the ore bodies are elongate horizontally and dip southward (fig. 18.4 *C*).

19. THREE AREAS OF POSSIBLE MINERAL RESOURCE POTENTIAL IN SOUTHEASTERN ALASKA

By Henry C. Berg, Menlo Park, Calif.

Reconnaissance geological mapping of Admiralty Island and the Chilkat Range (fig. 19.1) has disclosed three heretofore undescribed areas of higher mineral-resource potential than the surrounding terrain.

About 100 square miles of the central part of Admiralty Island (1, fig. 19.1) is underlain by intrusive, contact-metamorphic, and migmatitic rocks. The area comprises most of the high mountains west and northwest of Hasselborg Lake, and includes the southern end of the lake. It contains numerous outcrops of orange, dark-red, and dark-brown gossan, whose areas range from less than 100 to several thousand square feet. Field and laboratory (chemical, X-ray) studies indicate local concentrations of oxide and sulfide minerals, chiefly rutile, pyrite, pyrrhotite, and chalcopyrite, which contain traces to significant amounts of copper, zinc, titanium, and niobium.

Yttrium, zirconium, niobium, thorium(?), and the rare-earth elements lanthanum, cerium, praseodymium, and neodymium were detected by X-ray spectroscopic analysis of heavy minerals from pegmatite veins on Admiralty Island 5 miles west-southwest of the head of Seymour Canal (2, fig. 19.1). The pegmatite veins are associated with granite, migmatite, and contact-metamorphic rocks, which underlie an area of 50 square miles.

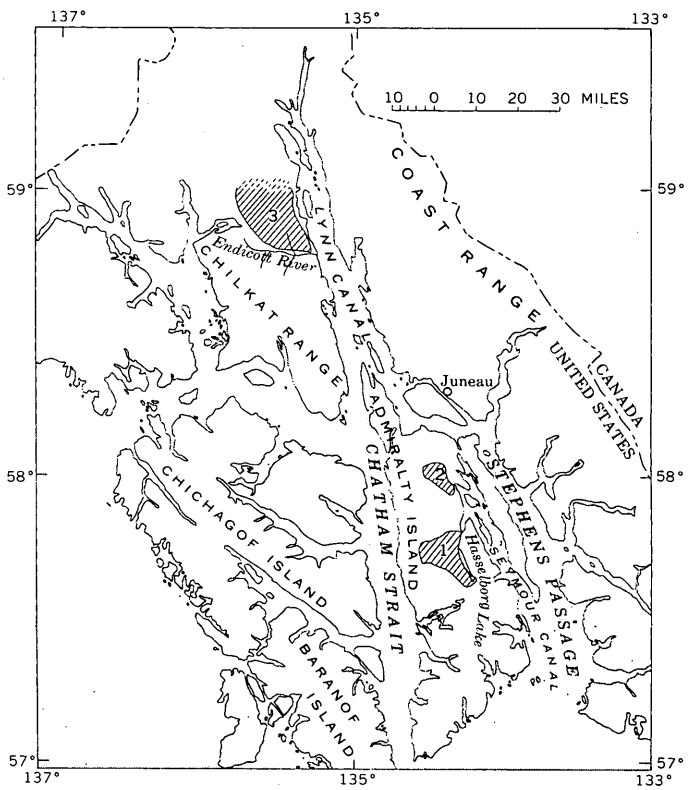

FIGURE 19.1.—Index map of part of southeastern Alaska showing three acres of possible mineral resource potential.

The part of the Chilkat Range north of the Endicott River (3, fig. 19.1) was found to be richer in sulfide minerals than the part south of the river. Orange, red, and brown gossan is widely distributed in the igneous, metamorphic, and volcanic rocks, which underlie an area of more than 200 square miles. The largest outcrops of gossan are several thousand square feet in area, but in general the gossan masses are not so common or extensive here as in central Admiralty Island. Sulfide minerals occur in local concentrations consisting chiefly of veinlets and disseminations of pyrite, pyrrhotite, and chalcopyrite. These minerals contain traces to major amounts of cobalt, copper, zinc, and lead. Magnetite and ilmenite commonly occur in disseminated particles, and in films coating shear surfaces in the rocks. In some places the oxides contain trace quantities of chromium. Small deposits of secondary copper salts are not uncommon; malachite, azurite, and chrysocolla form stringers and stained patches in the country rocks near some of the sulfide deposits.

The areas have been prospected superficially over a period of many years and several groups recently made reconnaissance mineral surveys of the general region with helicopter support. Little trenching, test pitting, or other physical exploration has been undertaken however, and few claims have been staked. No mineral production has been reported. Thick soil, glacial deposits, and dense vegetation cover much of the areas under consideration; hence geochemical and geophysical techniques, coupled with physical exploration, probably will be necessary to test fully the mineral potential.

20. A STUDY OF RHENIUM AND MOLYBDENUM IN URANIUM ORE FROM THE RUNGE MINE, FALL RIVER COUNTY, SOUTH DAKOTA, BY MEANS OF A SPECTROGRAPHIC AND CONCENTRATION METHOD

By A. T. Myers, J. C. Hamilton, and V. R. Wilmarth, Denver, Colo.

Work done in cooperation with the U.S. Atomic Energy Commission

GEOLOGY

The Runge mine is in an elongate lenslike northwest-trending uranium deposit extending along the intersection of an older and a younger Cretaceous stream channel, both filled with sandstone. The ore consists principally of uraninite, coffinite, häggite, and montroseite, with minor quantities of one or both of the blue molybdenum minerals ilsemannite and jordisite, in a gangue of pyrite, calcite, and hematite. It forms elongate irregular bodies in sandstone and along fractures.

Most of the ore is in a calcite-cemented sandstone that contains abundant pyrite; nearly everywhere in the mine this forms the basal unit in the younger channel. The bottom of the younger sandstone is locally marked by a discontinuous rubble bed made up of angular to rounded shale fragments in a sandstone matrix, but throughout the central part of the deposit the calcite-cemented sandstone is overlain by a red hematite-rich sandstone that grades upward to a gray pyrite-rich sandstone. In the northeastern, southeastern, and southwestern parts of the deposit, the calcite-cemented sandstone is generally overlain by a sandstone, characterized by irregular narrow black-brown stripes, that has gradational contacts with the red and gray sandstones. Heavily mineralized fractures cut all the sandstone units.

The average grade of the ore produced from the mine is 0.2 percent uranium and 0.5 percent vanadium. The average ratio of vanadium to uranium in ore samples from the fractures and black-striped sandstone is about 0.65; in samples from the other sandstones this ratio ranges from 1.3 to 1.7, being highest in the calcite-cemented sandstone.

METHOD OF ANALYSIS

Following the work of Peterson and others (1959), we have made a geochemical study of an occurrence of rhenium in uranium ore from the Runge mine. The principal new feature of this study is the application of a simple water extraction and concentration technique prior to spectrographic analysis.

The amount of rhenium in ore of this kind has commonly been estimated by a spectrochemical method of semiquantitative analyses. This is a total-energy method, based on the use of synthetic standards and a visual matching technique. Its limit of detection for rhenium is 50 ppm; and so, in an effort to measure smaller amounts, we used extraction with distilled water

to concentrate rhenium in the water-soluble fraction. This procedure does not necessarily give the total rhenium in the sample, but it does allow one to estimate the minimum quantity of rhenium present in soluble salts. This technique lowers the limit of detection by 25 to 500 times, making it possible to study the distribution of rhenium—or at least of water-soluble rhenium—in ore bodies of this type.

A 50-gram portion of the ground sample was added to 500 ml of distilled water. After heating to about 100° C for 1 hour the leachate was filtered and evaporated to dryness on a steam bath. A weighed amount of powdered pure quartz, about one-fourth the weight of the dried leachate, was added and the mixture thoroughly ground. The spectrographic analysis was made on 10 mg of the mixture.

GEOCHEMICAL RESULTS

Table 20.1 shows the results of analysis for molybdenum, uranium, vanadium, and rhenium. Of the 27 original samples, only 6 contain rhenium in amounts detectable by conventional methods, but when these same 27 samples were leached with distilled water and the dried leached-out material analyzed, 16 of them were found to contain rhenium.

In table 20.1 the samples are arranged as nearly as possible in order of decreasing molybdenum content. Our results indicate that the samples higher in molybdenum tend to be higher in rhenium, and this is also true, in general, of the soluble material leached from the samples.

The results of our analyses (table 20.1) show that molybdenum and rhenium are most abundant in samples from the black-striped sandstone and the mineralized fractures. The highest values are 0.007 percent rhenium and 0.7 percent molybdenum.

The ore minerals most abundant in the calcite-rich and pyrite-rich sandstones, and locally in the hematite-rich sandstones, are crystalline uraninite, coffinite, and montroseite, which are the low-valence oxides and silicates of uranium and vanadium. Oxidation of the ore minerals resulted in formation of paramontroseite, häggite and amorphous uraninite, with a little carnotite in the black-striped sandstone and along fractures. Analyses of the material leached from samples of these sandstones (tables 20.1) indicate that rhenium and

TABLE 20.1.—*Semiquantitative spectrographic determination of 4 elements in 27 samples from the Runge mine, Fall River County, S. Dak.*

[Add 260000 to sample numbers to obtain laboratory serial numbers. The series of numbers used for reporting—7, 3, 1.5, 0.7, 0.3 etc.—represent midpoints of group data on a geometric scale. Other symbols are: M=major constituent (greater than 10 percent); *d*=barely detected and concentration uncertain; 0=looked for but not found; <with number=below number shown; leaders indicate not looked for. Approximate detection limits in percent: Mo, 0.0005; U, 0.05; V, 0.001; Re, 0.005.]

Sample	Original samples				Processed samples (dried leachate plus added quartz; sample leaches by 500 ml of distilled water)						Sample location
	Percent—				Weight [1] of dried leachate (grams)	Added quartz (grams)	Percent—				
	Mo	U	V	Re			Mo	U	V	Re	
2310	0.7	0.07	0.015	0.007	1.13	0.275	7.	0.3	0.15	0.15	Black-striped sandstone.
2310	-------	------	-------	-------	[2].820	.200	7.	.3	.3	.3	Do.
2313	.3	.07	.015	d	[3].425	.100	7.	.7	.3	.3	Do.
2314	.3	.15	.015	d	.496	.126	1.5	.7	.07	.15	Do.
2314	-------	------	-------	-------	[4].335	.075	7.	1.5	.7	.3	Do.
4397	.3	0	.015	d	[3].400	.325	7.	0	1.5	.7	Do.
4397	.3	0	.015	d	.345	.300	7.	.7	1.5	.3	Do.
6550X	.07	.15	.07	.007	.652	.150	.15	.7	.3	.15	Do.
2309	.015	3	7.	<.007	1.056	.260	.0015	.3	.7	.15	Do.
3648	.015	1.5	.07	.007	[5].330	.075	.007	.07	.0015	.3	Mineralized fracture.
2302	.007	.07	.07	0	.112	.028	.3	.3	.7	.07	Calcite-cemented sandstone.
2311	.007	0	.07	0	.191	.049	.03	.3	.3	.015	Black-striped sandstone.
2312	.003	.03	.15	0	.220	.055	.007	.3	.15	.015	Do.
2315	.003	.15	.03	0	.080	.020	.3	0	.3	.007	Pyrite-rich sandstone.
2318	.003	0	.015	0	.284	.071	.015	.3	.3	.007	Do.
2320	.003	0	.03	0	1.488	.371	.007	0	.15	0	Do.
3650	.003	.3	.7	0	.690	.795	.15	.7	.7	.015	Mineralized fracture.
6546X	.003	1.5	3.	0	1.950	.500	0	.15	.3	.003	Calcite-cemented sandstone.
6548X	.003	.3	1.5	0	.360	.100	.07	0	7.	.15	Hematite-rich sandstone.
2307	.0015	.07	.7	0	1.345	.336	.0015	.15	.7	0	Mineralized fracture.
2321	.0015	0	.015	0	.070	.017	.15	.3	.07	0	Hematite-rich sandstone.
2316	.0015	3.	7.	0	.413	.102	.003	1.5	1.5	.007	Do.
2319	.0015	0	.07	0	.341	.085	.007	.15	.07	0	Pyrite-rich sandstone.
2303	.001	3.	7.	0	1.178	.300	.0015	0	M	0	Calcite-cemented sandstone.
2304	<.001	7.	7.	0	.498	.125	.003	1.5	.7	0	Pyrite-rich sandstone.
2305	<.001	3.	3.	0	1.820	.055	.007	0	1.5	0	Calcite-cemented sandstone.
2306	<.001	3.	7.	0	1.814	.446	.0007	0	3.	0	Rubble bed.
2308	<.001	3.	.3	0	.287	.071	.007	0	3.	0	Calcite-cemented sandstone.
2317	.0003	.7	3.	0	1.607	.402	0	.07	.3	0	Pyrite-rich sandstone.
6547X	0	1.5	1.5	0	.206	.050	.015	0	7.	0	Calcite-cemented sandstone.

[1] Amount of sample leached is 50 grams except where indicated: [2] 48 g; [3] 45 g; [4] 44 g; [5] 40 g.

molybdenum are associated with the ore minerals. Rhenium and molybdenum were concentrated along with amorphous uraninite, paramontroseite, and häggite.

REFERENCE

Peterson, R. G., Hamilton, J. C., and Myers, A. T., 1959, An occurrence of rhenium associated with uraninite in Coconino County, Arizona: Econ. Geology, v. 54, p. 254–267.

21. A STUDY OF URANIUM MIGRATION IN SANDSTONE-TYPE ORE DEPOSITS

By JOHN N. ROSHOLT, JR., Washington, D.C.

Work done in cooperation with the U.S. Atomic Energy Commission

Radiochemical studies have been made on most of the large areas in the western United States in which uranium ore is produced from sandstone-type deposits. Analyses for Pa^{231}, Th^{230}, Ra^{226}, Rn^{222}, and Pb^{210} were made, according to the methods described by Rosholt (1954, 1957) and Rosholt and Dooley (in press), on a total of approximately 300 samples.

The study of radioactive daughter product distribution uses natural tracers to deduce the mode of the migration of uranium. Apparent minimum and maximum dates for the introduction or redistribution of uranium based on the Pa^{231}/Th^{230} ratio in each sample have provided the best means for presenting the data. The primary assumption is that protactinium and thorium do not migrate in measurable quantities from the place where they are produced by decay of the parent uranium isotopes. This assumption is in many cases justified by the chemical properties of these two elements in natural geochemical environments. Because of the 34,300 year half life of Pa^{231}, and the 80,000 year half life of Th^{230}, involved in the age calculation, the practical limit of age determination by migration studies has been set at 250,000 years. Any ore, therefore, whose maximum age is greater than 250,000 years could be of any greater age.

Samples from the following uranium-producing areas were studied: South Riley Pass area (Harding County), S. Dak.; Hulett Creek area (Crook County), Shirley Basin (Carbon County), Gas Hills area and Crooks Gap area (Fremont County), Wyo.; Happy Jack mine and MiVida mine (San Juan County), Utah; Cougar mine (San Miguel County), Colo.; Ambrosia Lake district (McKinley County), N. Mex.; Karnes County and Palangana Salt mine (Duvall County), Tex.

The interpretation of the analytical results and calculations for the various deposits indicate that there are four basically different types of uranium migration or accumulation in sandstones. These could be defined as (a) migration from oxidized deposits with redeposition in carbonaceous materials, or as relatively insoluble sexivalent uranium minerals; (b) outward dissemination from high-grade ore bodies; (c) downward movements nearly simultaneous with lowering of water table, through sandstones containing little or no relatively old ore; and (d) accumulation well below the groundwater saturation level.

Many examples of the first type, which leads to the deposition of sexivalent uranium minerals in carbonaceous rocks, are described in the paper concerning the Colorado Plateau uranium ore compiled by Garrels and Larsen (1959). C. S. Robinson and I, in our study of the Hulett Creek area, have found carnotite and tyuyamunite minerals both in situ with primary uranium minerals and redeposited at some distance from the primary source. Results from this area indicate that oxidation and formation of secondary minerals occurred perhaps intermittently, during the interval from 10,000 and 80,000 years ago. Similar redistribution processes are recorded in many of the deposits studied, where oxidized uranium has moved downward or downdip and enrichment has subsequently occurred in carbonaceous zones. Secondary accumulation in carbonaceous matter is evident in the Happy Jack mine, the Gas Hills area, the South Riley Pass area, and the Ambrosia Lake district.

The second type is that in which uranium migrates from a primary ore body of any age and progressively contaminates the surrounding host rocks; the total uranium content of the source is meanwhile diminishing. Much of the disseminated uranium is not tightly bound in minerals but is leached out. Nearly all relatively unoxidized deposits at or above the water table demonstrate this type; it is predominant at the Mi

557753 O—60——4

Vida mine, in parts of the Happy Jack mine and the Ambrosia Lake deposits, and in the Karnes County deposits. The main differencee between the two types is that the first represents a redistribution of uranium at some definite time, and the uranium is fixed in a more permanent environment, whereas in the second type uranium is in the process of passing outward from the high-grade source through the host sandstone. The apparent age relationships therefore provide an estimate of the time over which the dissemination process has been operating, rather than of the time during which the present species of uranium and its daughter products have remained in the rock represented by the sample.

The third type, where a close correlation exists between lowering of water table and movement of uranium, is represented by ore bodies in the Gas Hills area. Very little of the ore resulting from this kind of migration is believed to be more than a few million years old, and most of it is probably much younger. The correlation is quite apparent at some locations in the Lucky Mac openpit (Rosholt, 1958) and in the Wintz mine, eastern Gas Hills. Much of the uranium that is not firmly bound to carbonaceous matter probably is fugitive and in the process of moving toward the water table.

The fourth type provides evidence used to introduce the concept of recent and present-day accumulation of uranium at favorable locations well below the water table. The very consistent relations between uranium, Pa^{231}, Th^{230}, and Ra^{226} in samples representing a large tonnage of ore from the Hauber mine in the Hulett Creek area, Crook County, Wyo., indicate that the deposit has had a simpler geochemical history than most deposits. The results of analyses indicate that the major part of the deposition of uranium started between 40,000 and 130,000 years ago, and that the rate of deposition has been increasing up to the present time. Somewhat similar occurrences are represented by the ground-water-saturated deposits in the Crooks Gap area, in the Shirley Basin, and in the Palangana Salt mine. In these places, however, the apparent age relations are not quite as consistent as in the Hauber mine.

This study has provided much evidence regarding the differing stability of uranium deposits in sandstone-type environments. As long as conditions at a given locality remain favorable for fixation of uranium in the sandstone, the uranium content in that locality will increase. As soon as these conditions are removed the uranium concentration will be progressively depleted by outward movement of uranium into the surrounding sandstone.

REFERENCES

Garrels, R. M., and Larsen, E. S., 3d, compilers, 1959, Geochemistry and mineralogy of the Colorado Plateau uranium ores: U.S. Geol. Survey Prof. Paper 320, 236 p.

Rosholt, J. N., Jr., 1954, Quantitative radiochemical method for the determination of major sources of natural radioactivity in ores and minerals: Anal. Chemistry, v. 26, p. 1307–1311.

——— 1957, Quantitative radiochemical methods for the determination of the sources of natural radioactivity: Anal. Chemistry, v. 29, p. 1398–1408.

——— 1958, Radioactive disequilibrium studies as an aid in understanding the natural migration of uranium and its decay products: United Nations Second Internat. Conf. on the Peaceful Uses of Atomic Energy, 2d., Geneva, 1958, Proc., v. 2, p. 230–236.

Rosholt, J. N., Jr., and Dooley, J. R., Jr., Automatic measurements and computations for radiochemical analyses: Anal. Chemistry (in press).

22. DISTRIBUTION AND LITHOLOGIC CHARACTERISTICS OF SANDSTONE BEDS THAT CONTAIN DEPOSITS OF COPPER, VANADIUM, AND URANIUM

By R. P. Fischer and J. H. Stewart, Denver, Colo., and Menlo Park, Calif.

Work done in cooperation with the U.S. Atomic Energy Commission

Sandstone deposits containing conspicuous accumulations of either copper, vanadium, or uranium, of both copper and uranium, or of both vanadium and uranium, are numerous and widespread in the western part of the United States, and a few occur in the Eastern States. The vanadium and uranium deposits have been the principal domestic source of these metals; the copper deposits have not been very productive but are well known geologically as the "red-beds" type (Finch, 1933).

The ore minerals below the zone of oxidation are sulfides of copper and low-valence oxides and silicates

of vanadium and uranium, in which these metals do not combine with one another. Pyrite and marcasite are common accessories but are generally not abundant. In the zone of oxidation many secondary minerals form, some of which contain two of these metals. The ore minerals mainly fill pores in the sandstones. Introduced gangue minerals other than those that commonly cement sandstone are inconspicuous or absent. The typical ore bodies are lenticular or tabular and nearly parallel to bedding.

The host sandstones are chiefly nonmarine; most of them accumulated by stream action, but a few by wind, or under lake or shoreline conditions. The copper deposits are mainly in first-cycle arkosic sandstones derived from granitic rocks; the vanadium deposits, with or without much uranium, are dominantly in second-cycle sandstones derived from sedimentary rocks; and the uranium deposits with little or no vanadium or copper are in either first- or second-cycle sandstones, commonly associated with beds containing altered volcanic debris. The geologic and geographic distribution of the principal host rocks and their characteristics are tabulated and described below; deposits in beds of Triassic age, where relations are somewhat complex and confusing, are discussed separately.

"Red-beds" copper deposits, some containing uranium and some a trace of vanadium, are most abundant in the Permian sandstones of Oklahoma, Texas, and New Mexico. The host rocks are coarse-grained arkosic beds containing fresh feldspar grains; they are first-cycle sediments, derived directly from areas of granitic rocks and deposited by streams.

Vanadium-uranium deposits are abundant in the Salt Wash member of the Morrison formation, which is of Jurassic age, in western Colorado and eastern Utah. Similar deposits, though with less vanadium, occur in the Inyan Kara group, of Cretaceous age, in the Black Hills area of South Dakota and Wyoming. The ore-bearing sandstones in both the Salt Wash (Craig and others, 1955) and the Inyan Kara (Bergenback and others, 1957) are stream-laid, fine to medium grained, and rich in quartz; they were derived mainly from pre-existing sediments, though from different source areas. Beds containing some altered volcanic ash are associated with the ore-bearing sandstones in both units. There are a few large vanadium deposits, containing only a little uranium, in the Entrada sandstone of Jurassic age and the Navajo(?) sandstone, of Jurassic and Jurassic(?) age, in western Colorado. These sandstones are composed of well-sorted quartz grains; they were probably derived from older sandstones and accumulated by wind action.

Large uranium deposits that contain little or no vanadium or copper occur in the Westwater Canyon and Brushy Basin members of the Morrison formation in New Mexico (Hilpert and Moench, 1958), in several Tertiary formations in Wyoming (Grutt, 1956), and in the Jackson formation (Eargle and Snider, 1957) and Goliad sand, both of Tertiary age, in Texas. The deposits in New Mexico are near the southern edge of Morrison accumulation, in arkosic sandstones that were laid down by streams and derived, at least in part, from igneous rocks. Associated with these beds are mudstones rich in altered volcanic ash. The ore-bear-

Distribution and characteristics of the sandstones that are hosts to deposits of copper, vanadium, and uranium

[Plus sign indicates wholly or dominantly of the class shown; minus sign indicates subordinate part; question mark indicates uncertainty]

Metal class	System	Dominant location, lithology, and environment of deposition	Genetic classification		Abundance of deposits	Other remarks
			First cycle	Second cycle		
Cu and Cu-U	Triassic	Utah, N. Mex.; sandstone, conglomerate; stream.	−?	+?	moderate	
	Permian	Okla., Texas, N. Mex.; arkosic sandstone; stream.	+	--------	many	
	Devonian	Penna.; graywacke; stream	+	--------	few	
V-U	Cretaceous	S. Dak., Wyo., N. Mex.; sandstone; stream	--------	+	many	Adjoining beds are somewhat tuffaceous
	Jurassic	Colo., Utah, Ariz.; sandstone; stream	--------	+	many	
	Triassic	Utah, Ariz.; conglomerate, sandstone; stream	−?	+?	few	
U	Tertiary	Wyo., Colo., Texas; arkosic sandstone; stream	+	−	many	Adjoining beds are commonly tuffaceous
	Cretaceous	N. Mex.; Ariz.; Colo.; sandstone; stream	−	+	few	
	Jurassic	N. Mex.; arkosic sandstone; stream	+	−	moderate	
	Triassic	Utah, Ariz., N. Mex ; conglomeratic sandstone; stream.	−?	+?	many	

ing Tertiary sandstones in Wyoming were laid down by streams in intermontane basins bordered by upland masses in which granitic rocks were exposed. They are for the most part conspicuously arkosic, and some beds are tuffaceous. The host beds in Texas are stream and shoreline deposits consisting chiefly of sands and muds derived from sedimentary rocks, but they contain some tuff and bentonite.

Copper deposits, some with uranium, occur in the Shinarump member of the Triassic Chinle formation in southeastern Utah, in the Agua Zarca sandstone member of the Chinle in northwestern New Mexico, and in some beds of the equivalent Dockum group in northeastern New Mexico. These host rocks were probably derived in part from granitic and metamorphic rocks of the Ancestral Rocky Mountains, though they are not conspicuously arkosic. The Shinarump also contains vanadium-uranium and uranium deposits in Arizona and southern Utah, but this part of the Shinarump was derived from sedimentary, volcanic, and perhaps granitic rocks to the south. Other members of the Chinle formation contain vanadium-uranium and uranium deposits in Arizona and Utah, and these units also were derived from areas lying south of them. All the Triassic ore-bearing units are stream deposits. Altered volcanic debris is abundant in some of the associated beds (Stewart and others, 1958).

Although many geologists believe that these copper, vanadium, and uranium deposits represent a particular type having a similar origin, no single genetic hypothesis is generally accepted. The geochemical habits of these metals may supply an explanation of their distribution in the deposits that contain them, and continued study may ultimately lead to a better understanding of the origin of the deposits.

All three metals are dispersed in igneous rocks, but not in close association. Copper and uranium enter the hydrothermal environment, but there is scant record of vanadium in hydrothermal solutions and veins (Fischer, 1959). Some of the uranium and most of the copper minerals in igneous rocks and veins oxidize readily, and the metals then go into surface- and ground-water solutions, where they are available to circulate in first-cycle sediments. Much of the vanadium in igneous rocks goes into clay minerals formed by weathering; diagenetic reactions and a second cycle of weathering may be required to mobilize this metal. All three metals may be precipitated from solutions in the presence of a reducing agent, such as the carbonaceous material or associated sulfide and ferrous ions commonly found in the host rocks of the deposits containing them. Perhaps the oxidation or devitrification of volcanic ash may contribute uranium to ground waters (and to either first- or second-cycle sediments), as does the weathering of igneous rocks.

REFERENCES

Bergenback, R. E., Chisholm, W. A., and Mapel, W. J., 1957, Petrology of some sandstone beds in the Inyan Kara group and associated rocks, *in* Geologic investigations of radioactive deposits, semiannual progress report, Dec. 1, 1956, to May 31, 1957: U.S. Geol. Survey TEI–690, p. 398–413, issued by U.S. Atomic Energy Comm. Tech. Inf. Service Extension, Oak Ridge, Tenn.

Craig, L. C., and others, 1955, Stratigraphy of the Morrison and related formations, Colorado Plateau region, a preliminary report: U.S. Geol. Survey Bull. 1009–E, p. 125–168.

Eargle, D. H., and Snider, J. L., 1957, A preliminary report on the stratigraphy of the uranium-bearing rocks of the Karnes County area, south-central Texas; Univ. Texas Bur. Econ. Geology, Rept. Inv. 30, 30 p.

Finch, J. W., 1933, Sedimentary copper deposits of the Western States, *in* Ore deposits of the Western States (Lindgren volume): New York, Am. Inst. Mining Metall. Engineers, p. 481–487.

Fischer, R. P., 1959, Vanadium and uranium in rocks and ore deposits: U.S. Geol. Survey Prof. Paper 320, pt. 20, p. 219–230.

Grutt, E. W., Jr., 1956, Uranium deposits in Tertiary sedimentary rocks in Wyoming and northern Colorado: U.S. Geol. Survey Prof. Paper 300, p. 361–370.

Hilpert, L. S., and Moench, R. H., 1958, Uranium deposits of the southern part of the San Juan Basin, New Mexico: Proceedings of the Second United Nations International Conference on the peaceful uses of atomic energy, v. 2, p. 527–538, United Nations, Geneva.

Stewart, J. H., Poole, F. G., and Wilson, R. F., 1958, Triassic studies, *in* Geologic investigations of radioactive deposits, semiannual progress report, Dec. 1, 1957, to May 31, 1958: U.S. Geol. Survey TEI–740, p. 130–139, issued by U.S. Atomic Energy Comm. Tech. Inf. Service Extension, Oak Ridge, Tenn.

23. LEAD-ISOTOPE AGE STUDIES IN CARBON COUNTY, PENNSYLVANIA

By T. W. Stern, L. R. Stieff, Harry Klemic, and M. H. Delevaux, Washington, D.C.

Work done in cooperation with the U.S. Atomic Energy Commission

Uranium minerals in sandstones have been known for years in Carbon County, Pennsylvania (Genth, 1875; Wherry, 1912; Klemic and Baker, 1954), but their geologic age has never been studied. Recently we made lead-isotope age determinations on two samples of uranium-bearing sandstone (nos. 346, 538) from the Mount Pisgah deposit in the basal sandstone and conglomerate member of the Mauch Chunk-Pottsville transition zone, in the Mauch Chunk formation (Mississippian) near Jim Thorpe, Pa. We also studied two well-cemented sandstone samples containing disseminated uraninite (403, 586) and a sample of clausthalite (512) from an uranium occurrence in the upper part of the Catskill formation (Devonian) near Penn Haven Junction. In addition, specimens of galena collected at Nesquehoning from post-Pottsville rock of Pennsylvanian age (584) and from tension fractures in the Trimmers Rock sandstone of Willard, 1935, of Devonian age (529) near Walcksville have been analyzed. The data obtained are given in table 23.1.

TABLE 23.1.—*Analytical data on galena, clausthalite, and uranium-bearing samples from Carbon County, Pa.*

Sample	Pb [1] (percent)	U [1] (percent)	Atom ratios of lead isotopes [2]		
			N_{204}/N_{208}	N_{207}/N_{206}	N_{207}/N_{208}
340 [3]	0.65	14.4	$0.029 \pm .003$	$0.0568_1 \pm .0003$	$10.5_4 \pm .05$
538 [3]	.21	4.34	$.027 \pm .001$	$.0564 \pm .0003$	$11.1_5 \pm .04$
586 [3]	3.30	12.4	$.0260_5 \pm .0001$	$.412_7 \pm .0009$	$.438_7 \pm .0002$
403 [3]	.055	50	$.0259_5 \pm .0002$	$.344_4 \pm .0015$	$.450_7 \pm .0018$
512 [4]	48.6	4.0	$.0262_7 \pm .0002$	$.783_7 \pm .002$	$.409_9 \pm .0008$
529 [4]	83.9	.0007	$.0260_6 \pm .0002$	$.846_4 \pm .0015$	$.409_2 \pm .0013$
584 [4]	79.3	.003	$.0263_6 \pm .00007$	$.827_3 \pm .0003$	$.408_3 \pm .0003$

[1] Analysts, Grafton J. Daniels and J. J. Warr.
[2] Limits of uncertainty are the range of averages of repeated ratio measurement of the Pb+ and Pb1+ spectra.
[3] Precision of colorimetric lead and uranium determination is approximately one percent and the accuracy of these methods is 5 and 2 percent respectively.
[4] Gravimetric lead methods are reproducible to better than 1 percent and are believed accurate to within 2 percent.

The "trial" lead-uranium and lead-lead ages of the uranium-bearing samples from Mount Pisgah and Penn Haven Junction obtained by the conventional methods of age calculation are discordant (table 23.2) and present three distinct problems: (a) The two Penn Haven Junction Pb^{207}/Pb^{206} ages disagree; (b) The two discordant Penn Haven Junction age sequences ($Pb^{206}/U^{238} < Pb^{207}/U^{235} \ll Pb^{207}/Pb^{206}$ and $Pb^{206}/U^{238} > Pb^{207}/U^{235} \gg Pb^{207}/Pb^{206}$) are reversed; and (c) The Pb^{207}/Pb^{206} ages of the uranium ores in Mississippian-Pennsylvanian rocks from Mount Pisgah are impossibly old.

TABLE 23.2.—*Calculated "trial" ages, in millions of years* [1]

Number	Locality	Age of enclosing rocks (millions of years)	Pb^{206}/U^{238}	Pb^{207}/U^{235}	Pb^{207}/Pb^{206}
346	Mount Pisgah	Mississippian-Pennsylvanian	314	325	413
538	do	330 [2]	300	312	402
403	Penn Haven Junction	Devonian	220	245	305
586	do	410–355 [2] / 400–350 [3]	438	428	368

[1] "Trial" ages obtained using Nesquehoning galena (584), Pb^{208} as the common lead index, and age calculation tables (Stieff and others, 1959).
[2] Kulp (1959).
[3] Holmes (1960).

The discrepancy between the two Penn Haven Junction Pb^{207}/Pb^{206} ages may be a result of past alteration, of original contamination at the time of mineral deposition by an older generation of radiogenic Pb^{207} and Pb^{206}, or of mass spectrometric errors. As radon loss cannot account for the age sequence of samples 586 or for the Pb^{207}/Pb^{206} ratio of the associated clausthalite (sample 512), it seems unlikely that this process is responsible for the discordant age sequence of sample 403 in view of the field and mineralogic relations. If mass spectrometric errors are averaged, the slope of the line passing through the measured N_{207}/N_{208} and N_{206}/N_{208} ratios of samples 584, 512, 586, and 403 (fig. 23.1) is equal to a N_{207}/N_{206} ratio of 0.0524 and a Pb^{207}/Pb^{206} age of 315 million years (Stieff and others, 1959). This average lead-lead age is somewhat low for a syngenetic Devonian deposit. If the bulk of the mass spectrometric errors are assigned to the measurement of the Pb^{207}/Pb^{208} ratio of sample 403 (table 23.1), the Pb^{207}/Pb^{206} ages of 403 and 586 are both approximately 370 million years.

Acceptance of the mass spectrometric data, on the other hand, leads to one of two conclusions. First, the alteration of the ore occurred at some time in the past history of the ore and the "true" age of the ore is in

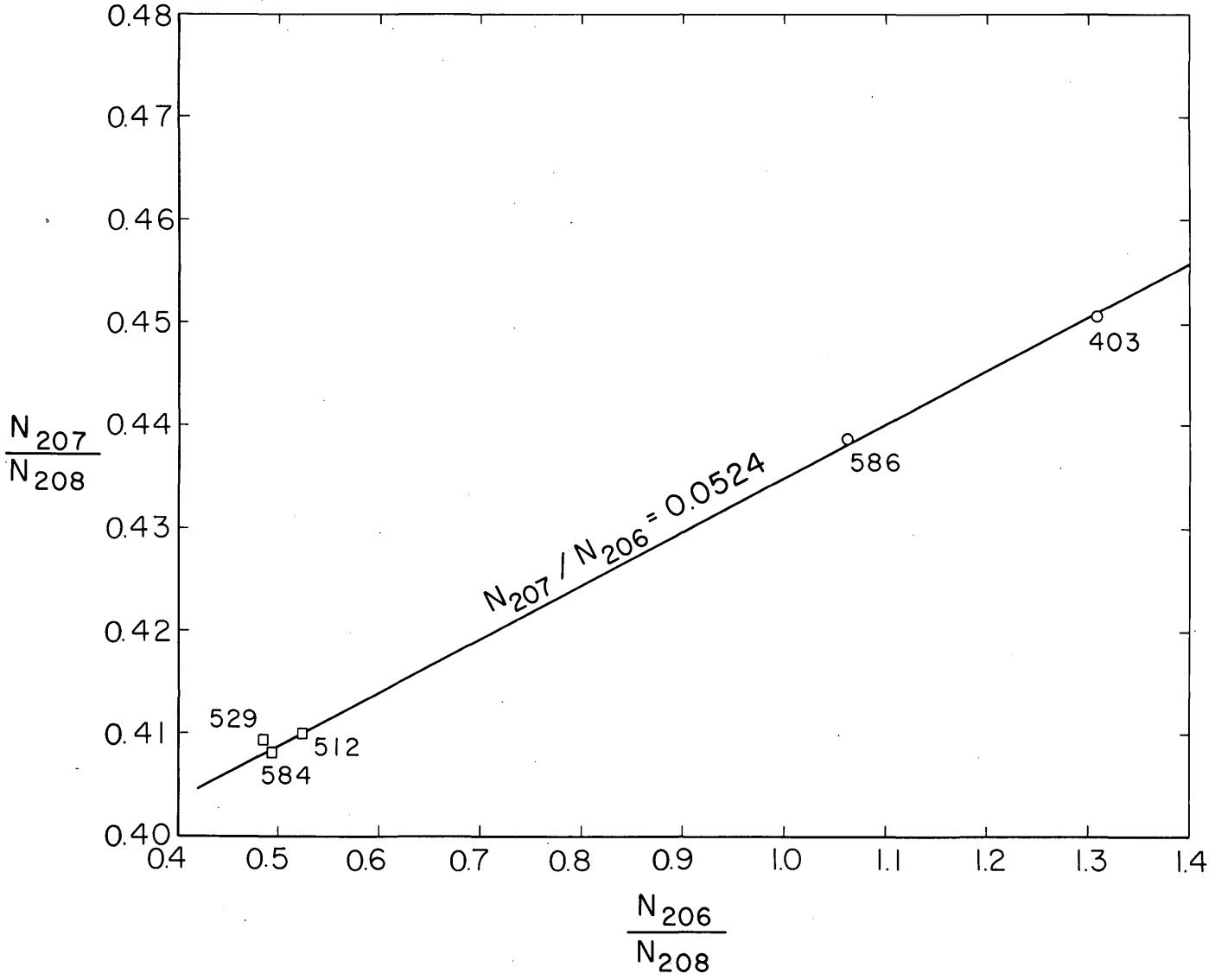

FIGURE 23.1.—Plot of N_{207}/N_{208} versus N_{206}/N_{208} lead isotope ratio of the samples from Penn Haven Junction, Walcksville, and Nesquehoning.

excess of 370 million years. Alternately, contamination of the ore at the time of deposition, not only by common lead but also by an older generation of radiogenic lead, would require that the Penn Haven Junction deposit be epigenetic and less than 200 million years old.

Whether the assumed alteration was recent or old, the reversal of the Penn Haven Junction age sequences implies that within the same small outcrop sample 403 lost lead or gained uranium, while sample 586 gained lead or lost uranium. The extensive alteration implicit in the magnitude of these discordant age sequences is difficult to reconcile with the absence of secondary minerals at the outcrop and the fresh appearance of the tightly cemented sandstone host rock. However, the single geologic process—contamination of old radiogenic lead at the time of deposition—is compatible with the discordant age sequences, the observed field relationships, and the occurrence of the radiogenically enriched clausthalite (sample 512).

The most perplexing aspect of the Mount Pisgah age data is the presence of radiogenic lead with a maximum corrected Pb^{207}/Pb^{206} age of approximately 415 million years—impossibly old for Mississippian and Pennsylvanian sedimentary rocks. The common lead contamination for the Mount Pisgah samples is so small that any reasonable choice for the isotopic composition of the contaminating common lead will not significantly affect the corrected Pb^{207}/Pb^{206} age of the ores. Although secondary uranium minerals are abundant at Mount Pisgah, the older Pb^{207}/Pb^{206} ages of the ores cannot be explained by recent lead loss, and past alteration would only make the age anomaly greater. The

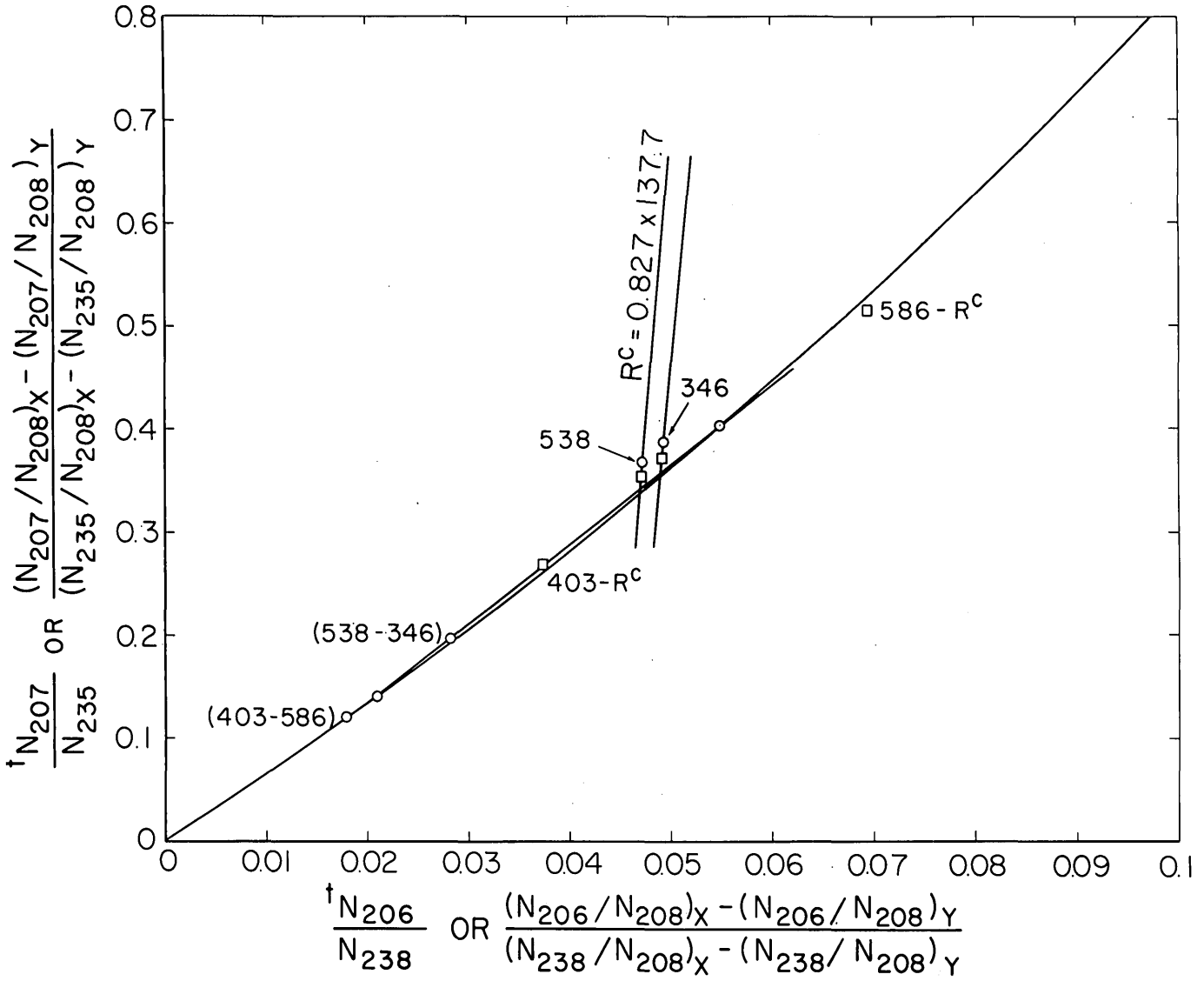

FIGURE 23.2.—Plots of the total $^{t}N_{207}/N_{235}$ versus $^{t}N_{206}/N_{238}$ and normalized difference ratios.

remaining alternatives are additions of old radiogenic lead or radon loss. In the latter instance, the essential identity of the Pb^{207}/Pb^{206} ages of samples 346 and 538, coupled with the threefold difference in uranium concentration, strongly suggests that radon loss, predominantly a diffusion process, is not the significant factor in the age discrepancies.

The graphical analysis of the discordant Carbon County ages in terms of old radiogenic lead contamination is shown in figure 23.2. The normalized difference ratios for the sample pairs from Penn Haven Junction and Mount Pisgah are represented by the points (403–586) and (538–346) respectively; the index isotope Pb^{208} being used to normalize the data. The points whose coordinates are equivalent to discordant trial lead-uranium ages of table 23.2 are plotted using square symbols. A detailed treatment of this new graphical procedure has been described by Stieff and Stern (in press).

To make the graphical analysis shown in figure 23.2, it is necessary to assume that (a) there was only one period of mineralization for each deposit; (b) the mineralizing solutions for each deposit were contaminated by a single common lead and a single generation of an older radiogenic lead; and (c) they have not been recently altered. These assumptions appear to be geologically reasonable.

Accepting assumptions (a) through (c), it is now possible to obtain one concordant ($Pb^{206}/U^{238} = Pb^{207}/U^{235}$) age for both deposits by passing a line through the points (403–586) and 538–346) and noting the intersection with the concordant age curve. This inter-

section has N_{207}/N_{235} and N_{206}/N_{238} ratios of approximately 0.127 and 0.0190, respectively, and is equivalent to the concordant age of 123 million years. Assuming an isotopic composition of the contaminating common lead similar to the Nesquehoning galena plus original radiogenic lead, concordant ages of 115 and 135 million years are obtained for Penn Haven Junction and Mount Pisgah, respectively. Maximum ages of source rock providing the old radiogenic lead range from approximately 350 to 475 million years.

The limitations imposed both by the number of samples available and the analytical data do not justify any emphasis on an exact age solution. However, the conclusion that both Carbon County uranium occurrences were formed near the end of the Jurassic or early in the Cretaceous would appear to be mathematically and geologically sound.

REFERENCES

Genth, F. A., 1875, Preliminary report on the mineralogy of Pennsylvania: Pennsylvania Geol. Survey, 2d, B, p. 144.

Holmes, Arthur, 1960, A revised geological time-scale: Edinburgh Geol. Soc. Trans., v. 17, p. 183–216.

Klemic, Harry, and Baker, R. C., 1954, Occurrences of uranium in Carbon County, Pennsylvania: U.S. Geol. Survey Circ. 350, 8 p.

Kulp, J. L., 1959, Geological time scale (abs.): Geol. Soc. America Bull., v. 70, p. 1634.

Stieff, L. R., and Stern, T. W., Graphic and algebraic solutions of the discordant lead-uranium age problem: Geochim. et Cosmochim. Acta (in press).

Stieff, L. R., Stern, T. W., Oshiro, Seiki, and Senftle, F. E., 1959, Tables for the calculation of lead isotope ages: U.S. Geol. Survey Prof. Paper 334–A, 40 p.

Wherry, E. T., 1912, A new occurrence of carnotite: Am. Jour. Sci., 4th ser., v. 33, p. 574–580.

Willard, B., 1935, Portage group in Pennsylvania: Geol. Soc. America Bull., v. 46, p. 1195–1218.

24. URANIUM AT PALANGANA SALT DOME, DUVAL COUNTY, TEXAS

By Alice D. Weeks and D. Hoyle Eargle, Washington, D.C., and Austin, Tex.

Work done in cooperation with the U.S. Atomic Energy Commission

One of the most unusual uranium deposits discovered in recent years is in Pliocene sediments above the caprock of Palangana salt dome, in Duval County, Texas. Palangana is in the Coastal Plain, about 70 miles west of the Gulf of Mexico and 100 miles north of the Rio Grande. The salt dome was discovered in 1916; sulfur was produced from the caprock in the 1920's and early 1930's, and during the same period a few thousand barrels of oil was produced from shallow sands above the caprock (Barton, 1925). At present brine is being produced by the Columbia Southern Chemical Company, and it was this company that discovered the uranium by gamma-ray logging of holes drilled in a search for potassium.

The surface expression of Palangana salt dome is a shallow basin in a brush-covered plain that slopes eastward about 20 feet per mile and is capped with a nearly continuous layer of caliche. The dome is covered by the Goliad sand (Pliocene), which dips 25 to 40 feet per mile east-southeastward and overlaps middle Tertiary rocks (Sayre, 1937) (fig. 24.1). The Goliad sand overlaps unconformably on the Lagarto clay (Miocene?), which is dominantly an impervious clay with a few sand lenses, on the Oakville sandstone (Miocene) a massive sand with some gravel, clay balls and ashy clay, and on the Catahoula tuff (Miocene?), which contains highly tuffaceous sand and clay and volcanic conglomerate (Sayre, 1937), and on the Frio clay (Oligocene?), which is dominantly clay and relatively impermeable.

Most of the Tertiary sediments, but especially the Catahoula tuff, contain large quantities of volcanic detritus, pebbles, sand grains of igneous minerals, and shards of glass. The most abundant rock types are chiefly andesite, trachyandesite, and soda trachyte (Bailey, 1926). The outcropping rocks of the Catahoula are slightly to considerably altered by alkaline ground water, which caused the development of a caliche cover, opal, and chalcedony cements, and formation of zeolites. The most likely sources of the Catahoula sediments appear to be the igneous rocks of Mexico, 100 miles or more to the west, or those of the Big Bend country, 300 miles northwest. Recent analyses of a suite of the Big Bend rocks indicate they contain more than average quantities of uranium (David Gottfried, written communication, 1959).

The salt of the Palangana dome is 850 to 1,000 feet below the surface (fig. 24.1). It is capped by anhydrite, gypsum, sulfur, and carbonate rock several hun-

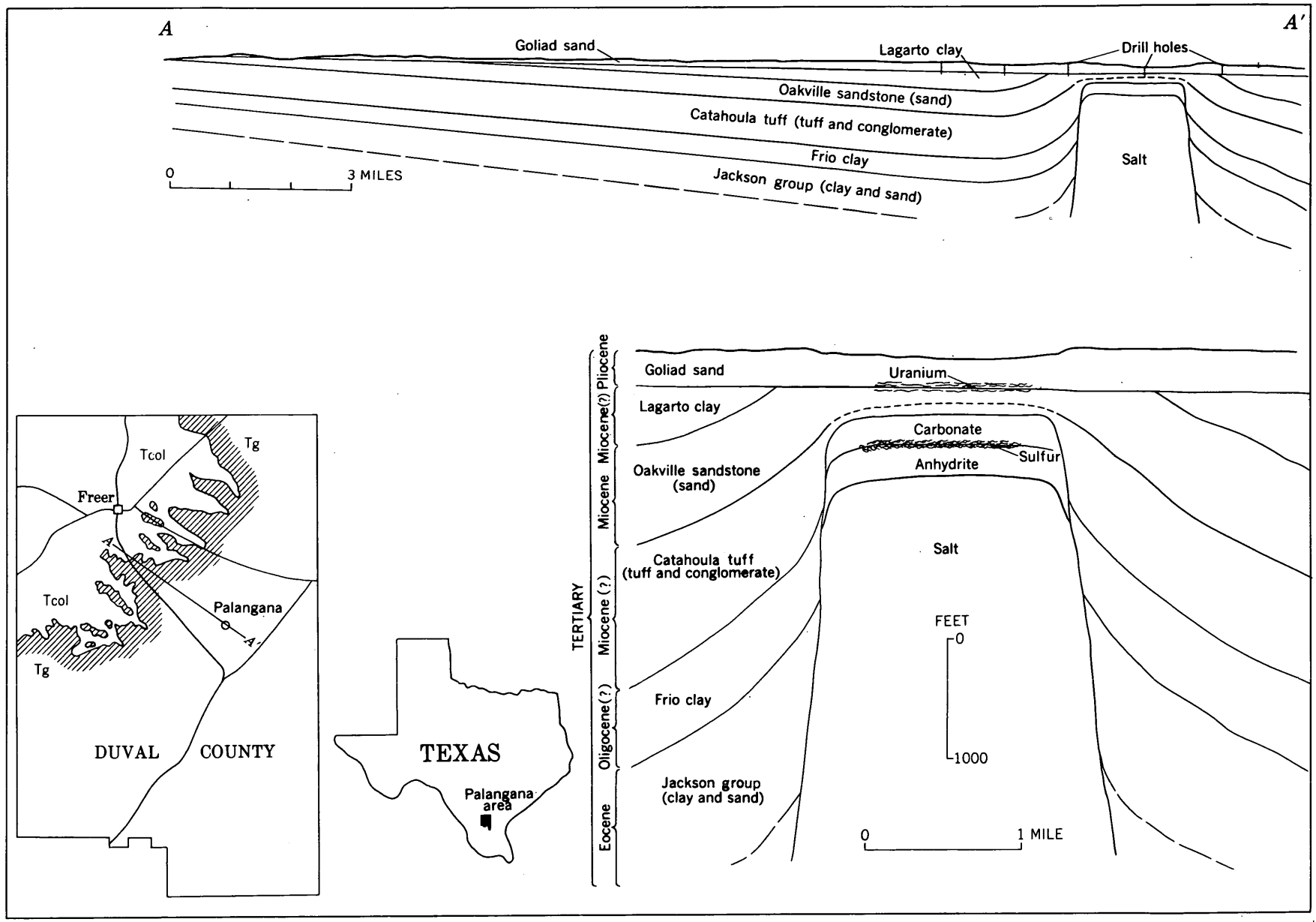

FIGURE 24.1.—Diagrammatic cross sections of Palangana salt dome and of the area between Freer and Palangana, Duval County, Tex.

dred feet in total thickness. The uranium ore, chiefly very fine divided sooty pitchblende, occurs at a depth of about 325 feet, more than 100 feet above the caprock. It is in highly calcareous clay-ball conglomerate interbedded with friable fine- to medium-grained sand locally impregnated with a little oil. Only a few beds are firmly cemented. The conglomerate contains black chert pebbles, nodular authigenic chalcedony, a little partly silicified fossil wood, and a few vertebrate fossils. Several horse teeth and a dog tooth found by company personnel and by us were identified by Prof. J. A. Wilson, of the University of Texas, as belonging to the fauna of the basal member of the Goliad sand.

The electric and the lithologic logs of drill holes on the dome have been correlated with those of drill holes a few miles northwest of the dome. The logs were correlated by means of clay-ball conglomerate at the base of the Goliad. The deepest core which we examined was 460 feet deep and on the dome. The sediments above the conglomerate show minor variations, but they consist mainly of moderately to very fine grained silty sandstone or sandy clay and are all at least slightly calcareous. The differences between the cores are in the rocks below the conglomerate and in the color of the ore zone. Over the salt dome between depths of about 276 and 460 feet the rocks within the ore zone as well as those in the first 50 feet above it and those below it are greenish gray, whereas off the dome correlative rocks are pinkish to yellowish gray. This color and the fine-grained disseminated pyrite in the ore zone and under it are due to the reducing environment of the H_2S emanating from the caprock. The sand under the ore zone contains reworked foraminifera and is believed to be Oakville sandstone. The Lagarto clay is not present on or close to the dome.

In March 1959 a suite of samples was collected along

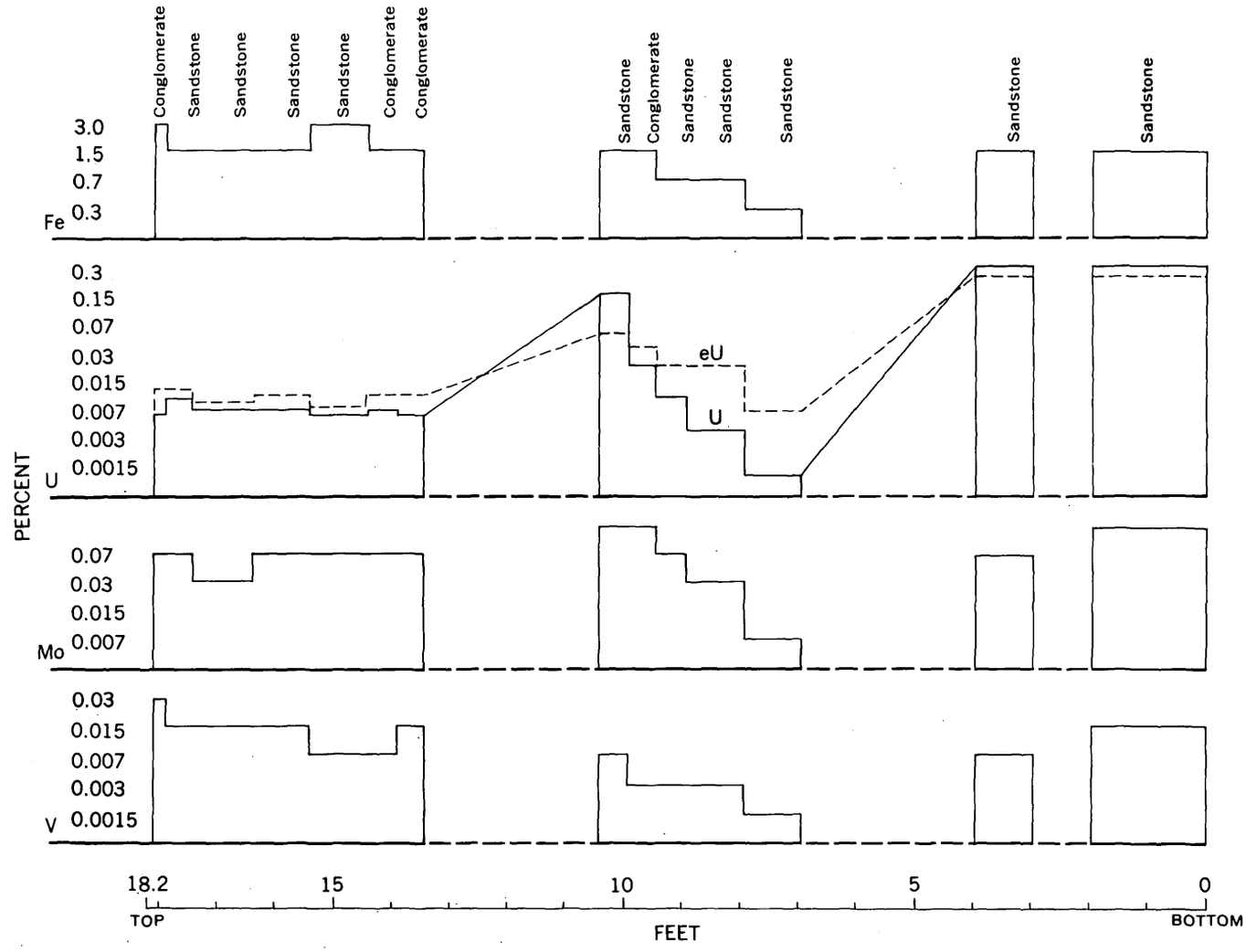

FIGURE 24.2.—Graph of selected data from radiometric, chemical, and semiquantitative spectrographic analyses of suite of samples through the ore zone at Palangana.

a vertical section through the ore zone in the small prospect mine. The rocks contain much water, are at a temperature of about 90° to 100° F, and give off considerable H_2S. Spectrographic and chemical analyses of the samples show that concentrations of the easily oxidizable and reducible elements iron, uranium, molybdenum, and vanadium are directly correlated (fig. 24.2). The ore zone contains several hundred times as much uranium as average sandstone, about 75 times as much molybdenum, and about 5 times as much vanadium. Molybdenum and vanadium though much less abundant than uranium are present in amounts that are significant when one considers that these elements commonly accompany uranium in the Colorado Plateau (Garrels and others, 1957). The carbonate content (percentage of acid-soluble fraction) ranges from 17 to 37 percent; the highest is in the firmly cemented sandstone 12 feet from the bottom in this suite.

The equivalent uranium of these samples differs considerably from the actual uranium content. Radiochemical analyses by J. R. Rosholt, Jr., show the nature of the disequilibrium (fig. 24.3). If the uranium and its daughter products were in perfect equilibrium, all the ratios would be 1 and would be represented by a horizontal line. The graph shows, however, that the three samples of ore grade are all low in radioactivity, and the six samples below ore grade high in radioactivity, as compared with uranium content determined chemically. The amount of radium in these samples is quite variable, and it is uncertain whether radium was added or uranium extracted from any particular sample. Migration is obviously taking place in this

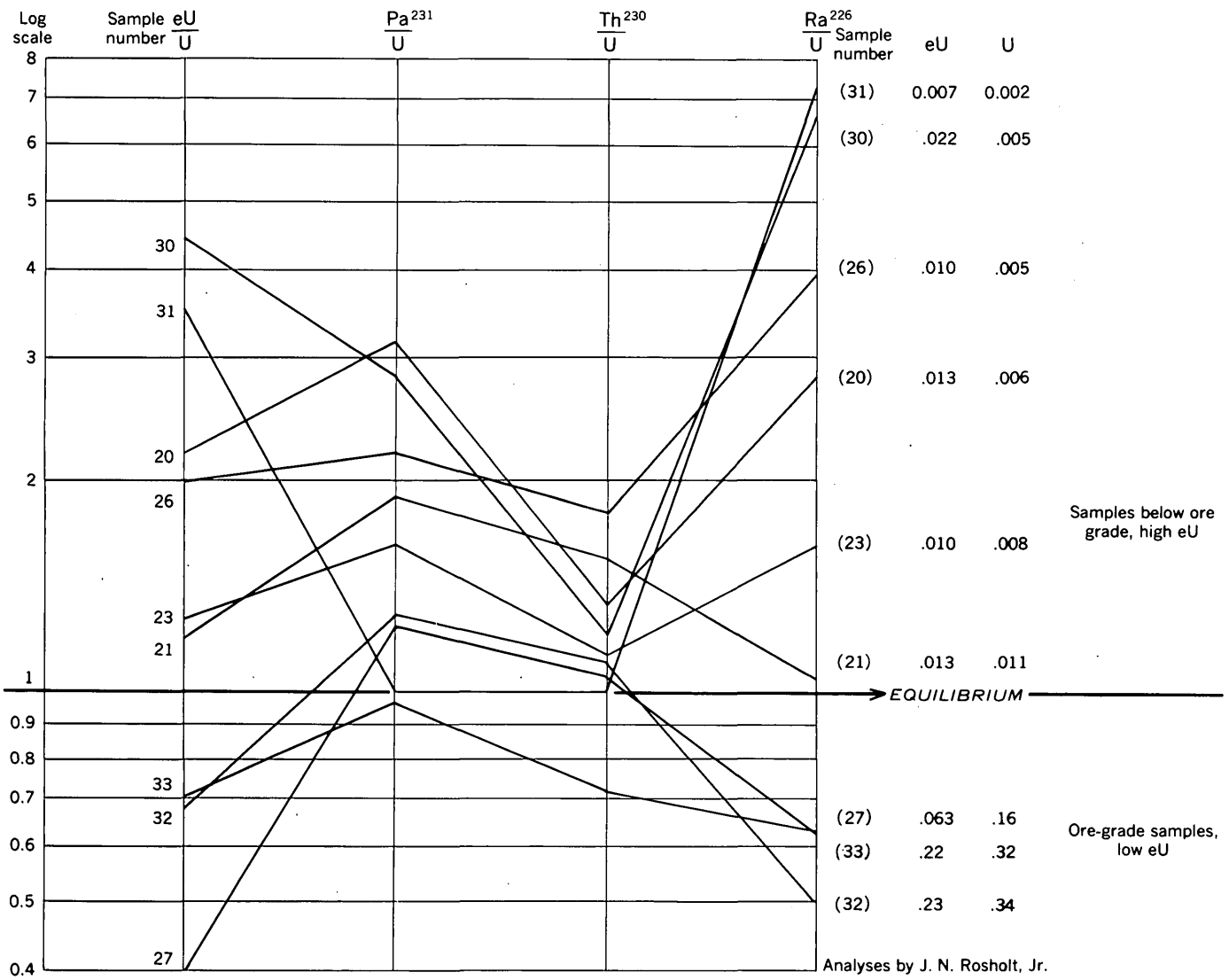

FIGURE 24.3.—Graph of ratios of uranium daughter products to uranium, showing nature of radioactive disequilibrium for suite of samples at Palangana (same suite as in fig. 24.2).

deposit, and in spite of moderately reducing conditions the uranium is not very firmly fixed.

We believe that uranium was leached by alkaline carbonate water from the volcanic material in the Tertiary sediments, chiefly from the Catahoula tuff but possibly in part from other rocks that contain a smaller proportion of volcanic debris. This is highly reasonable because (a) of the large volume of volcanic detritus that contains above average uranium, (b) the sediments consisted of highly reactive or unstable material in a terrestrial deposit, (c) the climate was hot, and so dry that leached products would remain in more concentrated solution than in humid climates. A consistent geochemical environment is indicated by the extensive caliche cap, the presence of highly mineralized ground water, the widespread occurrence of opal and chalcedony, the presence of many small concentrations of uranium in surface outcrops of the tuffaceous rocks, and by the zeolitic alteration of those rocks. Some of the uranyl carbonate in solution probably migrated downdip in permeable beds confined between less permeable clay beds until it reached the reducing environment of the salt dome. The precipitated uranium is very fine grained and disseminated; this fact as well as the radiochemical relationships indicates that the deposit is very young and unstable, and that it probably is still in the process of formation or modification.

REFERENCES

Bailey, T. L., 1926, The Gueydan, a new middle Tertiary formation from the southwestern coastal plain of Texas: Univ. Texas Bull. 2645, 187 p.

Barton, D. C., 1925, Salt domes of South Texas: Am. Assoc. Petroleum Geologists Bull., v. 9, p. 536–589.

Garrels, R. M., Hostetler, P. B., Christ, C. L., and Weeks, A. D., 1957, Stability of uranium, vanadium, copper, and molybdenum minerals in natural waters at low temperatures and pressures [abs.]: Geol. Soc. America Bull., v. 70, p. 1127–1184.

Sayre, A. N., 1937, Geology and ground-water resources of Duval County, Texas: U.S. Geol. Survey Water-Supply Paper 776, 116 p.

25. PARAGENESIS OF URANIUM ORES IN TODILTO LIMESTONE NEAR GRANTS, NEW MEXICO

By Alfred H. Truesdell and Alice D. Weeks, Washington, D.C.

Work done in cooperation with the U.S. Atomic Energy Commission

The Todilto limestone is locally replaced by minerals of uranium and vanadium, and to a lesser extent by minerals of fluorine, iron, lead, manganese, molybdenum, and selenium. The replacement started along grain boundaries, especially where the grains were dissimilar—for instance, along the borders of detrital quartz or feldspar, between coarse- and fine-grained calcite, or around carbonaceous masses. The uraninite was initially deposited as colloform coatings from which it expanded in rounded shapes into adjoining fine-grained calcite. The colloform bodies tended to coalesce, and in places they replaced the rock almost completely, leaving only relict quartz grains.

The ore can be loosely classified into three types: uranium ore, uranium-fluorine ore, and uranium-vanadium ore (fig. 25.1).

The simplest type is uranium ore containing no appreciable quantity of vanadium or fluorine. This occurs partly in separate deposits and partly within deposits containing irregularly distributed vanadium minerals. Polished sections show that some pyrite was formed before uraninite and coffinite and was strongly corroded by those minerals. Colloform uraninite replaced the limestone, starting along grain boundaries and finally replacing the grains themselves. Detrital grains commonly served as nucleating centers, as did boundaries between coarsely crystallized light-colored calcite and their finer grained limestone matrix; ore formed on these boundaries commonly extends into and replaces the limestone.

Later, coffinite coated the uraninite and filled shrinkage cracks that developed within it. The last-deposited uranium was in a fine-grained intergrowth of calcite and uraninite. Euhedral galena crystals were deposited at the same time as the uraninite and coffinite and have been partially replaced by calcite. In a few specimens the ore has been shattered and the fractures filled with late calcite. Late pyrite is also found in some polished sections; it replaces detrital grains, starting along their boundaries, and may surround the uraninite border of a grain.

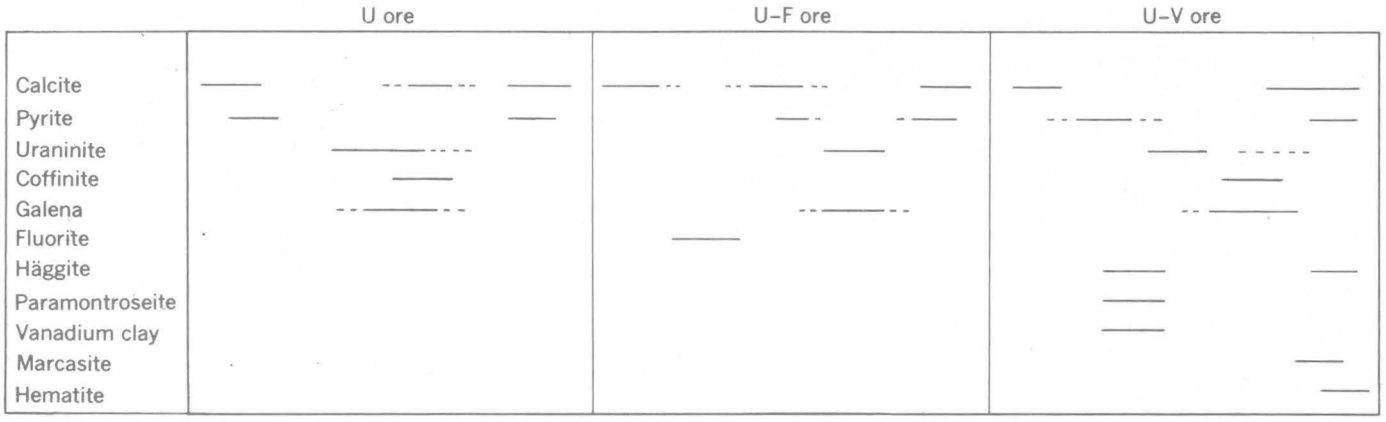

FIGURE 25.1—Paragenesis diagram of three types of uranium ore in Todilto limestone.

The fluorite-bearing uranium ore is scarcer than the other types. The limestone has been recrystallized and partly replaced by purple fluorite; certain favorable layers were completely replaced, and irregular masses above and below them partly replaced. The fluorite seems to have been introduced after partial recrystallization of the rock but before the uranium mineralization (fig. 25.1). Some ostracod shells were partly filled with fluorite, but most are filled with recrystallized calcite even if completely surrounded with fluorite. This indicates that some recrystallization preceded the introduction of fluorite. Later, coarse calcite cut the fluorite, and then both of these were replaced dendritically by uraninite and pyrite (fig. 25.2). Most of the uraninite is in interstitial replacements in the fine-grained calcite adjacent to the fluorite. Some of the pyrite was replaced by uraninite and galena, but most of it is later than these minerals. Cracks in the late pyrite are filled with fine-grained calcite, which also corrodes and partly replaces galena.

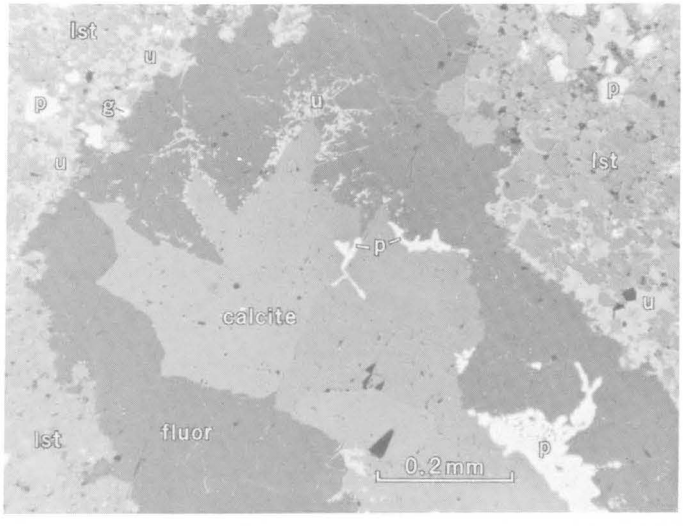

FIGURE 25.2.—Uranium-fluorine ore. Fluorite (dark-gray, *fluor*) has replaced fine-grained limestone (medium-gray, *lst*) and has been itself replaced by coarse calcite (medium-gray, *calcite*). The calcite and fluorite are replaced dendritically and along grain boundaries by uraninite (light-gray, *u*) and pyrite (white, *p*). Uraninite, pyrite, and galena (white, *g*) have also precipitated at the boundary between limestone and fluorite. Polished section. Manol pit, sec. 30, T. 13 N., R. 9 W., McKinley County, N. Mex.

No evidence of uraninite-fluorite intergrowth was noted in the polished sections, nor of a genetic connection between these minerals in time and space. Both the uraninite and the fluorite occur alone as commonly (or more commonly) as they do together.

Although the average vanadium-uranium ratio of the Todilto ores is in general less than 1:1, the vanadium is spottily distributed both areally and in detail. The minerals in relatively unoxidized uranium-vanadium ore are uraninite, coffinite, häggite, paramontroseite, vanadium clay, barite, pyrite, galena, specular hematite, and calcite.

In polished sections it can be seen that some recrystallization of calcite preceded and some accompanied the deposition of the ore minerals. Precipitation of ore minerals generally began along grain boundaries and then gradually replaced the grains themselves. Some open spaces, probably solution cavities, became lined with ore minerals and were later filled with coarse calcite. Early pyrite became severely corroded and replaced by the ore minerals. Most of the vanadium minerals were deposited before the uraninite (fig. 25.1). Häggite (color bronze in polished section, with strong blue, yellow, and orange polarization colors) was partly deposited in blades at the margins of solution channels, partly in fine fibers replacing limestone along grain boundaries (fig. 25.3), and partly intergrown with paramontroseite in rosettes between generations of recrystallized calcite. Some häggite has replaced montroseite (?) to form multiple crystals which together form a blade. In some places the häggite was preceded by a vanadium clay that formed nearly spherical aggregates enclosing pyrite or organic matter (fig. 25.3). The

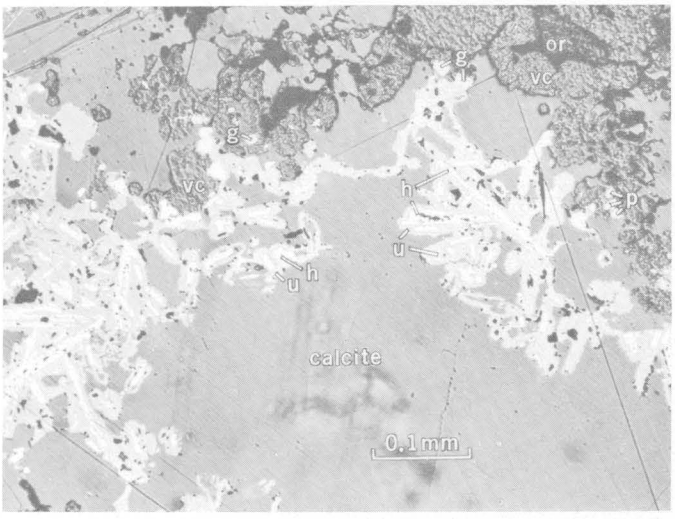

FIGURE 25.3.—Uranium-vanadium ore. A solution opening has been filled with vanadium clay (rubbly appearance, *vc*), pyrite (white, *p*), galena (white, *g*), häggite (very light gray, *h*), and coarse calcite (medium gray, *calcite*). The vanadium clay coats organic matter (black, *or*) and the häggite has been coated and partially replaced by uraninite (light gray, *u*). Polished section. F 33 mine, sec. 33, T. 12 N., R. 9 W., Valencia County, N. Mex.

borders of detrital grains of quartz and feldspar were favorable sites for deposition of this clay, which has slightly to almost completely replaced them.

Häggite was followed by colloform uraninite, which coated the häggite blades and rosettes and has characteristic shrinkage cracks. The uraninite was partly or wholly replaced by coffinite, which reflects a little less light in polished section. The coffinite spread inward along the shrinkage cracks in the uraninite and grew along boundaries between uraninite and häggite. The deposition of coffinite may indicate that the replacement of detrital grains by earlier ore minerals had released enough silica to saturate the solution with respect to uranium silicate. Some blades of häggite are almost completely replaced by calcite, leaving a ring of uranium minerals. Galena was deposited during and after the deposition of the uranium minerals, and it replaced early pyrite and häggite. The galena nearly always forms cubes; where it is irregular, it is usually in a cubic hole that indicates its original cubic form. The pyrite very seldom forms euhedral grains. The last uranium was precipitated as intimate intergrowths of uraninite and calcite, which in the highest grade samples have almost completely replaced calcite grains. Some late häggite was formed in spaces between blades of earlier häggite ringed with uraninite.

The solution openings were filled with coarse calcite, often enclosing irregular areas of vanadium clay and ghost crystals of pyrite and marcasite. In a few places vanadium clay is ringed with specular hematite. Where solution cavities were absent, late pyrite or marcasite appears to have replaced uraninite-ringed quartz without replacing the uraninite (fig. 25.4).

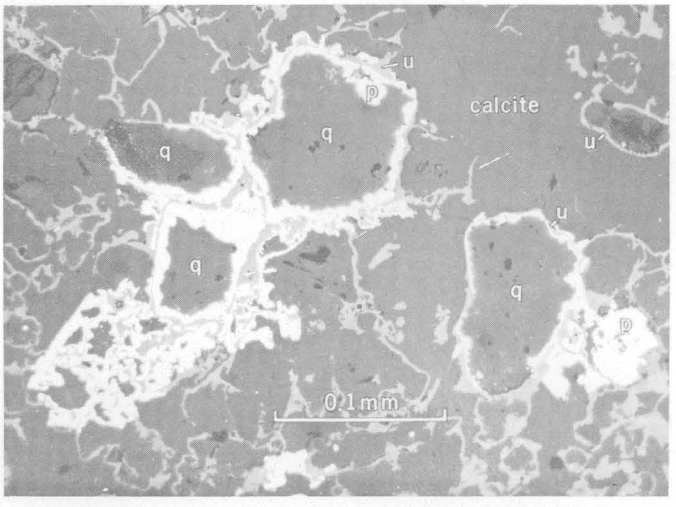

FIGURE 25.4.—Uraninite (light-gray, *u*) along grain boundaries of quartz (dark gray, *q*). Late pyrite (white, *p*) seems to replace quartz grains along boundaries without replacing uraninite. Polished section. Faith mine, sec. 29, T. 13 N., R. 9 W., McKinley County, N. Mex.

26. PITCHBLENDE IDENTIFIED IN A SANDSTONE-TYPE URANIUM DEPOSIT IN THE CENTRAL PART OF THE AMBROSIA LAKE DISTRICT, NEW MEXICO

By HARRY C. GRANGER, Denver, Colo.

The Ambrosia Lake district, in McKinley County, N. Mex., contains the largest known reserves of uranium in the United States. Its ore deposits are being intensively studied by the U.S. Geological Survey.

Most of the uranium in the district occurs in the form of coffinite in deposits in the Westwater Canyon member of the Morrison formation. Recently, however, a small amount of pitchblende (uraninite) was identified

in the Kermac Sec. 22 mine. This is the first pitchblende reported from the central part of the district.

The occurrence was reported by David Smouse, geologist at the Kermac mine, and was later sampled by me. Identification was verified from X-ray powder pattern by Edward Young, U.S. Geological Survey. The pattern was somewhat diffuse, indicating either extremely small grain size or poor crystallinity.

The pitchblende occurred on the 6,450-level, about 100 feet below the premining water table, in a vug extending along a northwest-trending fracture. Most of it formed a hard, black, vitreous, botryoidal crust less than 2 mm thick and having an area not more than 2 feet in diameter, on the walls of the fracture and vug. The remainder of the vug was filled with calcite, and the adjacent rock contained much disseminated pyrite.

Although this occurrence was below the ground-water table, hematite and limonite derived from oxidized pyrite also occur extensively on the same level of the mine. It appears likely that the pitchblende was deposited from ground-water solutions that acquired uranium by oxidizing nearby coffinite.

Pitchblende has also been identified from other sandstone-type deposits near the edges of the district, but these were partly oxidized deposits, near the outcrop and well above the ground-water table. To date, no pitchblende has been recognized in any deposit that is not either above the water table or near oxidized rock below the water table.

27. METAMORPHIC GRADE AND THE ABUNDANCE OF ThO_2 IN MONAZITE

By William C. Overstreet, Beltsville, Md.

Work done in cooperation with the U.S. Atomic Energy Commission

Monazite, an anhydrous phosphate of the cerium earths, commonly contains a small amount of thorium. Thorium for industry has been obtained from monazite since the 1880's. Before that period only a few specimens of monazite had been analyzed, to satisfy the curiosity of scientists, but after industrial needs arose, hundreds of samples of monazite from many districts were analyzed to determine whether they could serve as commercial sources of thorium. The results of these analyses are scattered in the literature, and until recently many obscurely published analyses were virtually lost. It is now possible, however, with the help of the extensive bibliographic card file of uranium and thorium compiled by Miss Margaret Cooper and her co-workers in the U.S. Geological Survey and U.S. Atomic Energy Commission, to review the world literature in a practicable length of time. During the past year I have examined about 800 of some 1,200 references to monazite published before 1959. From this unfinished review a pattern emerges that I interpret as evidence that monazite goes through a previously unrecognized geologic cycle. The chief features of the cycle, in appropriate rocks, are these: Detrital monazite is unstable in early stages of regional metamorphism, but as the metamorphic grade of its host rises, monazite becomes increasingly abundant and also richer in ThO_2.

GEOLOGIC DISTRIBUTION OF MONAZITE

Accessory monazite is widely distributed in metamorphic rocks of intermediate and high rank derived from pelitic sediments. It is especially common in schists, gneisses, and migmatites of the higher rank subfacies of the amphibolite and granulite facies. It may occur in plutonic rocks ranging in composition from diorite to muscovite granite, and in associated pegmatite, greisen, and vein quartz. In this group it is most often observed in biotite-quartz monzonite, two-mica granite, and cassiterite granite. Monazite is very rarely found in syenites, but it does occur locally in syenite pegmatites and carbonatites. It is not known to occur in lavas, and it has not been observed in plutonic mafic rocks or their metamorphic equivalents.

Erosion of its host rocks releases monazite for transport, during which it tends to settle and form placers along streams, lakes, and ocean beaches. Fossil placers are preserved in lithified sediments of many ages, and accessory detrital monazite has been found in sedimentary rocks of all ages from Precambrian to Recent.

RELATION OF MONAZITE TO GRADE OF METAMORPHISM

The opinion has long been current that particles of monazite in paraschists and paragneisses are remnants of detrital grains. If this were true, the abundance of monazite in the paraschists and paragneisses would be controlled by its abundance in the sediments from which the metamorphic rocks were derived, and there would be no relation between the abundance of monazite and the metamorphic facies of the host. The many hundreds of references in the literature to the sources of monazite show, however, that such a relation is clearly marked in metamorphosed pelitic rocks. Accessory monazite is exceedingly rare in the greenschist facies, rare to sparse in the epidote-amphibolite facies, sparse to common in the amphibolite facies, and common to abundant in the granulite facies.

I interpret this distribution of monazite among the facies as follows: Detrital monazite in pelitic sediments is unstable, so that at the onset of regional metamorphism it breaks down and shares its components with other minerals; detrital monazite as such disappears, and for a while not much of it is recrystallized. This accounts for its great rarity in the greenschist facies and sparseness in the epidote-amphibolite facies. As the grade of metamorphism increases, an environment is reached at which monazite is again stable, and metamorphic monazite begins to form at a few centers of crystallization, which multiply with increasing grade of metamorphism. The paragneisses, formed at very high metamorphic grades, contain more monazite, on the average, than their sedimentary counterparts, for more monazite in them has crystallized than was contained in the detrital grains of the original sediment. The components of this added monazite apparently come from trace amounts of thorium, the rare earths, and phosphorus in some of the other original detrital constituents of the sediment. One of the results of increasing metamorphism of pelite is thus the previously unrecognized generation of metamorphic monazite.

GEOLOGIC RELATIONS OF ThO_2 IN MONAZITE

The results of 181 analyses of monazite are grouped in table 27.1 according to geologic environment. They show that in metamorphosed pelites the proportion of thorium in monazite, despite a wide range and certain inconsistencies, increases on the average from 0.5 percent ThO_2 in phyllites of the greenschist facies to as much as 10 or 12 percent in rocks of the granulite facies.

Monazite in metamorphosed limestones and other calcareous rocks (Rose, Blade, and Ross, 1958, p. 996) is poor in thorium.

TABLE 27.1.—*Abundance of ThO_2 in monazite as related to geologic environment in Africa, Asia (exclusive of the U.S.S.R.), Australia, and South America*

Source of monazite	ThO_2 (in percent)		
	Least	Greatest	Average
Metamorphosed pelitic sediments:			
Greenschist facies, 2 samples, Brazil	0.00	1.09	0.54
Amphibolite facies:			
Middle and upper subfacies, 1 sample, New Zealand			5.32
Upper subfacies, 1 sample, New Zealand			5.47
Upper subfacies and granulite facies, 6 samples, Madagascar, Sierra Leone, and Travancore	9.0	12.6	10.2
Granulite facies, 6 samples, Ceylon and India	4.96	10.75	8.3
Metamorphosed calcareous sediments:			
Amphibolite facies, 2 samples, Madagascar and Brazil	.05	1.05	.55
Metamorphosed pelitic sediments associated with granitic rocks:			
Greenschist facies(?), 1 sample from diorite in slate, Australia			6.6
Amphibolite facies:			
Lower subfacies intruded by pegmatite, 2 samples from pegmatite, Australia	10.7	19.4	15.05
Lower and middle subfacies intruded by granite, 7 samples, Taiwan and Australia	3.20	6.79	5.23
Middle subfacies intruded by granite, 1 sample, Ghana			6.5
Middle subfacies intruded by pegmatite, 8 samples from pegmatite, Japan, Australia, and Brazil	4.0	8.0	5.2
Middle and upper subfacies intruded by granite, 18 samples, Brazil	5.0	11.5	5.8
Upper subfacies intruded by granite, 24 samples, Nigeria, Korea, Australia, and Brazil	2.3	10.0	6.3
Upper subfacies intruded by pegmatite, 17 samples from pegmatite, Madagascar, Union of South Africa, Japan, India, Bolivia, and Brazil	1.5	20.2	7.9
Granulite facies:			
Upper amphibolite subfacies to granulite facies intruded by granite, 18 samples, India	6.57	9.24	8.41
Upper amphibolite subfacies to granulite facies intruded by pegmatite, 1 sample from pegmatite, India			31.50
Granulite facies intruded by pegmatite, 11 samples from pegmatite, Madagascar, Ceylon, and India	6.00	28.20	10.72
Granites and pegmatites:			
Unclassified granite, 5 samples, Burma, Korea, and Brazil	1.99	9.49	7.14
Cassiterite-bearing granites, 31 samples, Indonesia, Malaya, and Australia	.00	9.41	3.46
Cassiterite-bearing pegmatites, 7 samples, Australia and Thailand	3.80	5.93	5.01
Carbonatites, 5 samples, Kenya, Northern Rhodesia, and Nyasaland	.00	<1.0	<1.0
Veins:			
Low-temperature, 6 samples, Belgian Congo, Union of South Africa, Australia, and Bolivia	.00	2.50	.74
High-temperature(?), 1 sample, Union of South Africa			8.01

The abundance of thorium in monazite from igneous and hydrothermal rocks is also evidently subject to geologic controls. Monazite is less abundant and poorer in thorium in granites that crystallized at shallow depths than it is in plutonic granites. Monazite from cassiterite granites intruded into sandstone, shale, phyllite, and limestone is devoid of thorium, but monazite from gneissic cassiterite granites intruded into rocks of the amphibolite facies contains as much as 9 percent of ThO_2. Monazite found in low-temperature veins, in vugs where it forms open growths, and in carbonatites contains little or no thorium, whereas monazite from high-temperature veins is thorium-rich.

The abundance of thorium in monazite appears to be partly determined by pressure and temperature of crystallization, but the chemical composition of the enclosing rock is also involved.

Estimates of the intrinsic ages of monazite from plutonic rocks should recognize that even such monazite may be of metamorphic origin.

REFERENCE

Rose, H. J., Jr., Blade, L. V., and Ross, Malcolm, 1958, Earthy monazite at Magnet Cove, Arkansas: Am. Mineralogist, v. 43, nos. 9–10, p. 995–997.

GEOLOGY OF LIGHT METALS AND INDUSTRIAL MINERALS

28. CONCENTRATIONS OF "ILMENITE" IN THE MIOCENE AND POST-MIOCENE FORMATIONS NEAR TRENTON, NEW JERSEY

By James P. Owens, James P. Minard, Donald R. Wiesnet, Washington, D.C., and Frank J. Markewicz, New Jersey Geological Survey, Trenton, N.J.

An intensive search for economic concentrations of "ilmenite" [1], followed the initial discovery of large low-grade deposits in the New Jersey coastal plain. The most difficult problem to solve in this search has been the relation of these deposits to the known "ilmenite"-bearing formations which include the Kirkwood formation of middle Miocene age, the Cohansey sand of the late Miocene(?) or Pliocene(?) age and the deposits (principally the Cape May formation) of Quarternary age. It was concluded from detailed mapping in the Browns Mills quadrangle and an analysis of the data supplied by the New Jersey State Bureau of Geology and Topography, that the highest concentrations occur in the Kirkwood and Cape May formations.

KIRKWOOD FORMATION

Moderate concentrations of fine-grained (mostly −60 to 200 mesh) heavy minerals were found in the Kirkwood formation (fig. 28.1 and table 28.1). This formation is primarily a massive-bedded marine quartz sand consisting of a lower dark-colored clayey sand and an upper light-colored sand (probably an eluviated bed). The heavy mineral concentrations apparently have the same distribution in both units (table 28.1).

"Ilmenite," generally fine to very fine grained and platy, constitutes between 60 and 80 percent of the heavy mineral fraction. Most of the grains have a black metallic appearance although a small percentage have an overall brown cast.

CAPE MAY FORMATION

The Cape May formation, a fluvial deposit in this region, is characterized by high concentrations of

[1] "Ilmenite" in these formations has been shown by X-ray analyses to be a mixture of ilmenite and ferric and titanium oxides. It has fixed chemical composition as shown by the analyses cited by Markewicz, Parrillo, and Johnson (1958, p. 8).

TABLE 28.1.—*Selected heavy-mineral analyses from the New Jersey coastal plain, Ocean and Burlington Counties*

Quadrangle	Field No.	Depth of boring		Heavy mineral content (percent)	Formation
		Feet	*In.*		
Cassville	259	9		14.4	Not recorded.
	236	6		3.9	Do.
	235	7		1.8	Do.
	237	15		2.3	Do.
	66	5		6.2	Do.
	7	5½		8.9	Do.
	18	3	5	2.4	Do.
	33	11	4	1.6	Do.
	38	7	2	2.4	Do.
	220	8		2.1	Do.
	48	15		1.0	Do.
	198	8		3.5	Do.
New Egypt	Ne 96	--------		3.89	Kirkwood (light).
	Do.	--------		1.13	Cohansey.
	Ne 97	5–10		0.93	Do.
	Do.	10–15		0.78	Do.
	Do.	15–20		1.63	Do.
	Ne 103	5		2.87	Kirkwood (light).
	Ne 107	--------		1.54	Cohansey.
	Ne 108	--------		1.06	Do.
	Ne 113	--------		3.22	Kirkwood (light).
	Ne 115	--------		2.43	Do.
	Do.	--------		1.49	Cohansey.
Browns Mills.	Bm 6	8–13		3.91	Kirkwood (light).
	Bm 9	22–24		1.80	Kirkwood (dark).
	Bm 15	16–18		6.58	Do.
	Do.	26–28		2.15	Do.
	Bm 16	8–12		7.04	Cape May.
	Do.	12–18		5.46	Do.
	Do.	18–28		.88	Cohansey.
	Do.	28–33		.43	Do.
	Bm 41	38		1.00	Cape May.
	Bm 40	0–18		11.14	Do.
	Do.	18–38		1.90	Cohansey.

557753 O—60——5

TABLE 28.1.—*Selected heavy-mineral analyses from the New Jersey coastal plain, Ocean and Burlington Counties*—Cont.

Quadrangle	Field No.	Depth of boring		Heavy mineral content (percent)	Formation
		Feet	*In.*		
Browns Mills—Cont.	Bm 42	0–38		3. 00	Cape May and Cohansey.
	Bm 48	0–28		4. 60	Cape May and Cohansey.
	Bm 29	7–18		1. 35	Cohansey.
Lakehurst	152			4. 1	
	154			7. 4	
	160			3. 0	
	88			5. 9	
	84			4. 8	
	86			4. 6	
	132a			2. 2	
	168			4. 0	
	172			2. 9	

heavy minerals (table 28.1) in small discontinuous deposits.

Most of the heavy minerals in these deposits are probably reconcentrations from the Cohansey sand. The heavy mineral suites are very similar mineralogically to those of both the Kirkwood and Cohansey formations but the grain-size distribution closely resembles the deposits in the Cohansey. A study of a small closed basin in the Browns Mills quadrangle, which is underlain only by the Kirkwood and Cohansey sediments, showed the high "ilmenite" concentrations in the Cape May formation to be of the Cohansey type.

COHANSEY SAND

The Cohansey sand is generally coarser grained than the underlying Kirkwood formation. It has essentially the same heavy mineral suite as the Kirkwood, although the minerals are commonly of medium sand size (−16 to 60 mesh primarily), and the concentra-

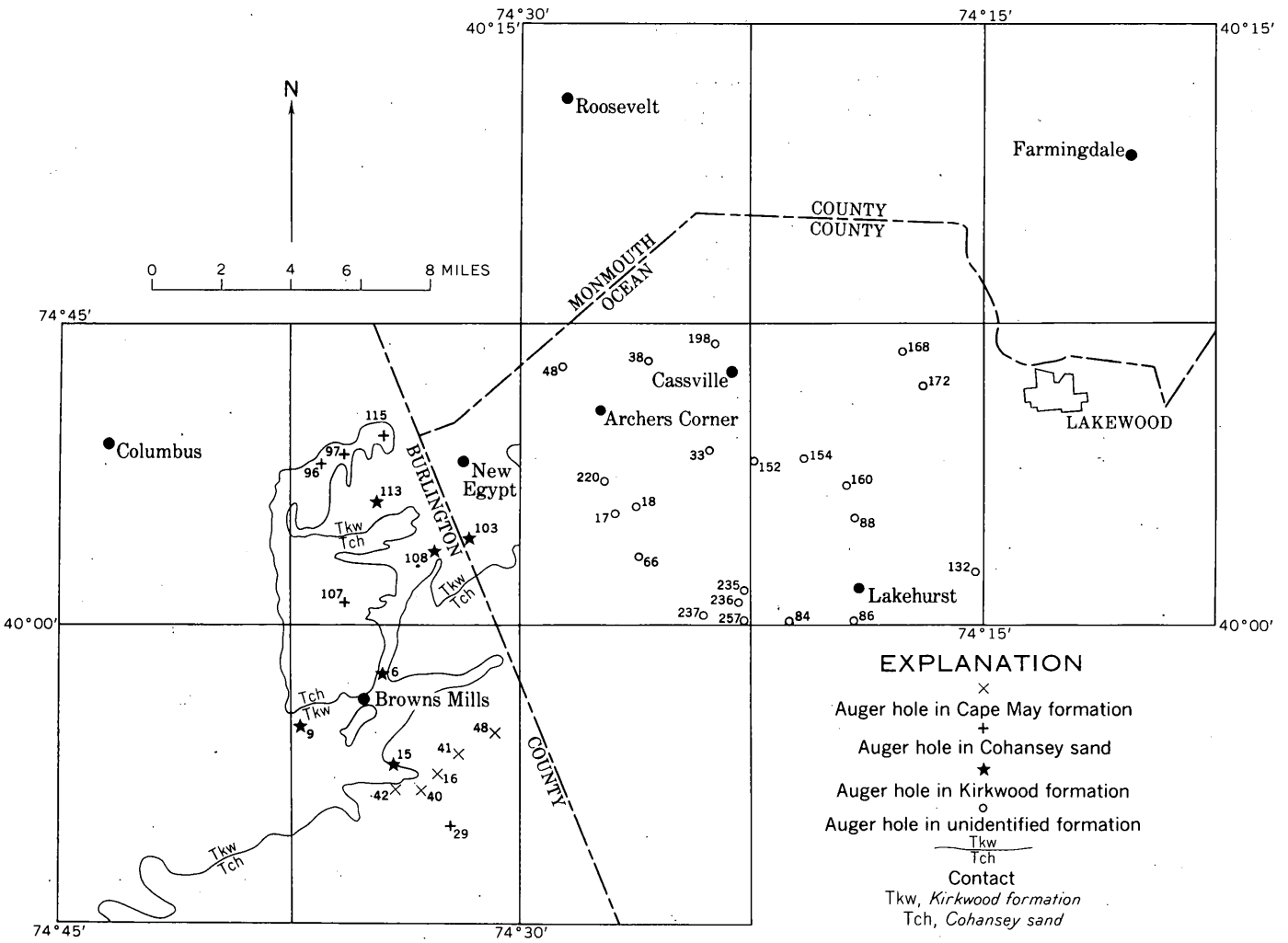

FIGURE 28.1.—Location of auger holes listed in table 28.1.

tions are leaner. A high incidence of brown (altered?) grains was noted among the "ilmenite" fractions.

Local concentrations of heavy minerals occur in this unit but are for the most part too small to be economically important.

SUMMARY

It seems from the data presented that two potentially economic sources of "ilmenite" occur near Trenton, N.J. These are:

1. The Kirkwood formation, which generally contains only 1 to 2 percent "ilmenite." The total available tonnage of "ilmenite" however is large because of the great volume of the deposit. The fine to very fine grained character of the "ilmenite" might be a problem in recovery operations.
2. The Cape May formation, which contains small deposits of relatively high-grade ore. These deposits are difficult to find, however, because of their fluvial origin. From a study of this formation, it appears that the heavy minerals tend to accumulate in narrow valleys into which the Cohansey sediments are carried. The best concentrations apparently occur where the "ilmenite" in the Cohansey sand was above average (about 1 percent).

REFERENCE

Markwicz, F. J., Parrillo, D. G., and Johnson, M. E., 1958, The titanium sand of southern New Jersey: New York, Am. Inst. Mining Metall. Engineers meeting (preprint No. 5818A5), Feb. 1958.

29. BLOATING CLAY IN MIOCENE STRATA OF MARYLAND, NEW JERSEY, AND VIRGINIA

By MAXWELL M. KNECHTEL and JOHN W. HOSTERMAN, Washington, D.C., and Beltsville, Md.

Work done in cooperation with Maryland Department of Geology, Mines and Water Resources and U.S. Bureau of Mines

The problem of locating supplies of expandable raw material for manufacture of lightweight aggregate has received attention in the course of a reconnaissance study of clay deposits in Maryland that the Geological Survey has been conducting since 1957. This paper includes information from an interim report (Knechtel, Hosterman, and Hamlin, 1959) on promising deposits of bloating clay in southern Maryland, and announces discoveries of such material, heretofore unreported, at two places in Virginia (fig. 29.1).

Samples were tested for bloating at the Electrotechnical Experiment Station, U.S. Bureau of Mines, Norris, Tenn. The tests, performed by Howard P. Hamlin, Supervising Ceramic Engineer, assisted by George Templin, involved drying, crushing, screening, and firing for 15 minutes at 1900°, 2000°, 2100°, 2200°, and 2300°F in a small electrically heated kiln, and also determination of unit weight, water absorption, and color of any fired products that showed sufficient expansion to warrant investigation of their suitability for use as lightweight aggregate.

The clue that led to the discoveries in Maryland and Virginia was a reported occurrence of expandable clay in strata of Miocene age in Salem County, N.J. (Lodding, 1956, p. 115). As this suggested that similar material might be present in sedimentary formations of that age elsewhere on the Atlantic Coastal Plain, we collected representative samples of argillaceous material in Maryland from the Calvert Cliffs, which extend along the Chesapeake Bay shore between Annapolis and the mouth of the Patuxent River. Samples from the Choptank formation and the underlying Calvert formation failed to bloat, but a sample of olive-gray silty clay obtained near Cove Point from the St. Marys formation, which rests on the Choptank, bloated satisfactorily. Additional samples of expandable clay were taken from outcrops in Calvert and St. Marys Counties, from holes bored with a truck-mounted 5-inch auger in St. Marys County, and from outcrops at two places in Virginia (fig. 29.1).

As the surface of southern Maryland is relatively hilly, sites at which open-pit mining would be feasible are here more numerous than in areas of lower relief more typical of the Atlantic Coastal Plain. Raw or finished material could possibly be shipped by low-cost water transport from some sites to markets in Washington, Baltimore, and Norfolk, and perhaps even to ports at greater distances.

There are many sites deserving consideration as potential sources of raw material for lightweight aggre-

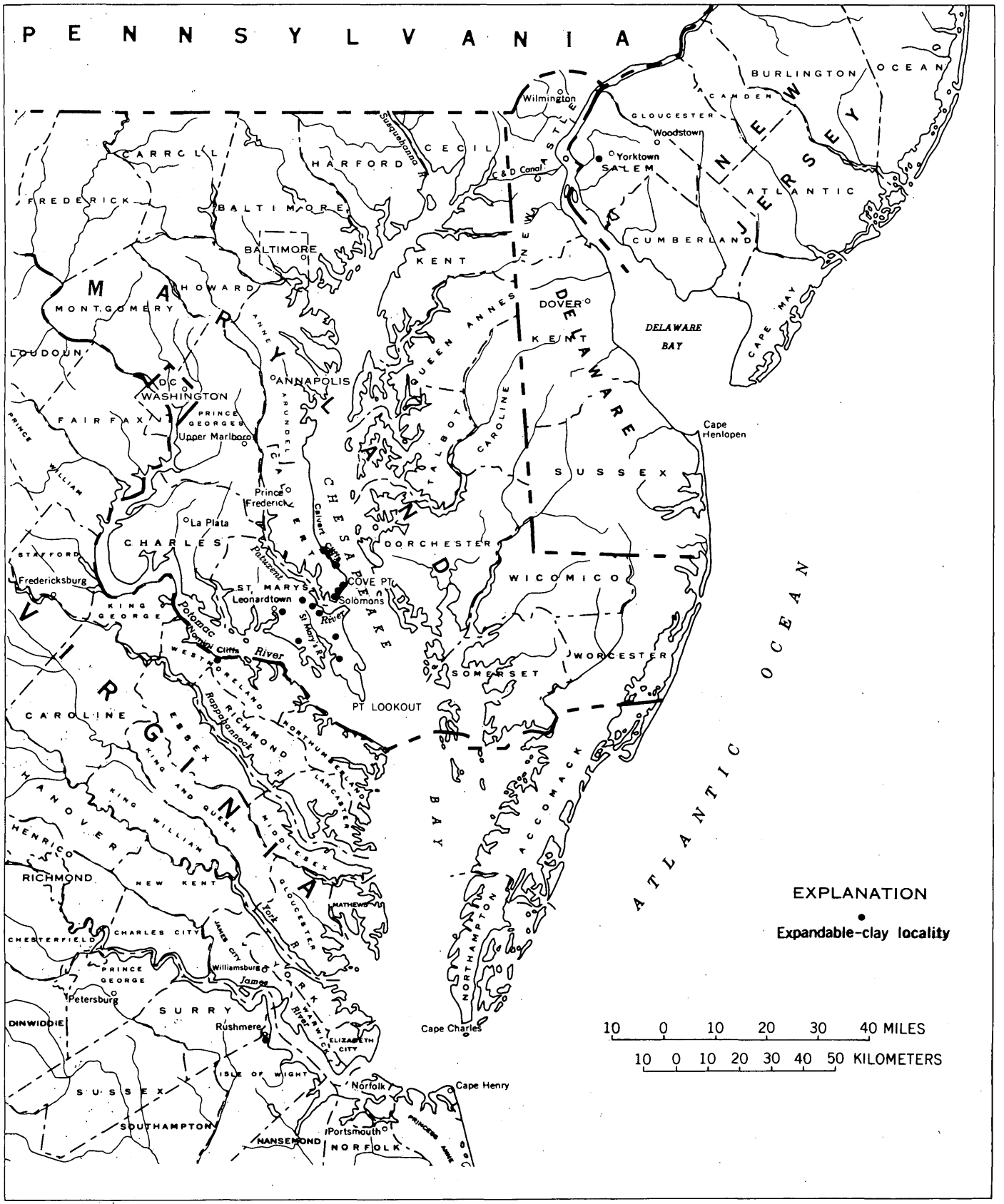

FIGURE 29.1.—Map showing localities in Maryland, New Jersey, and Virginia at which expandable clay is known to occur in strata of Miocene age.

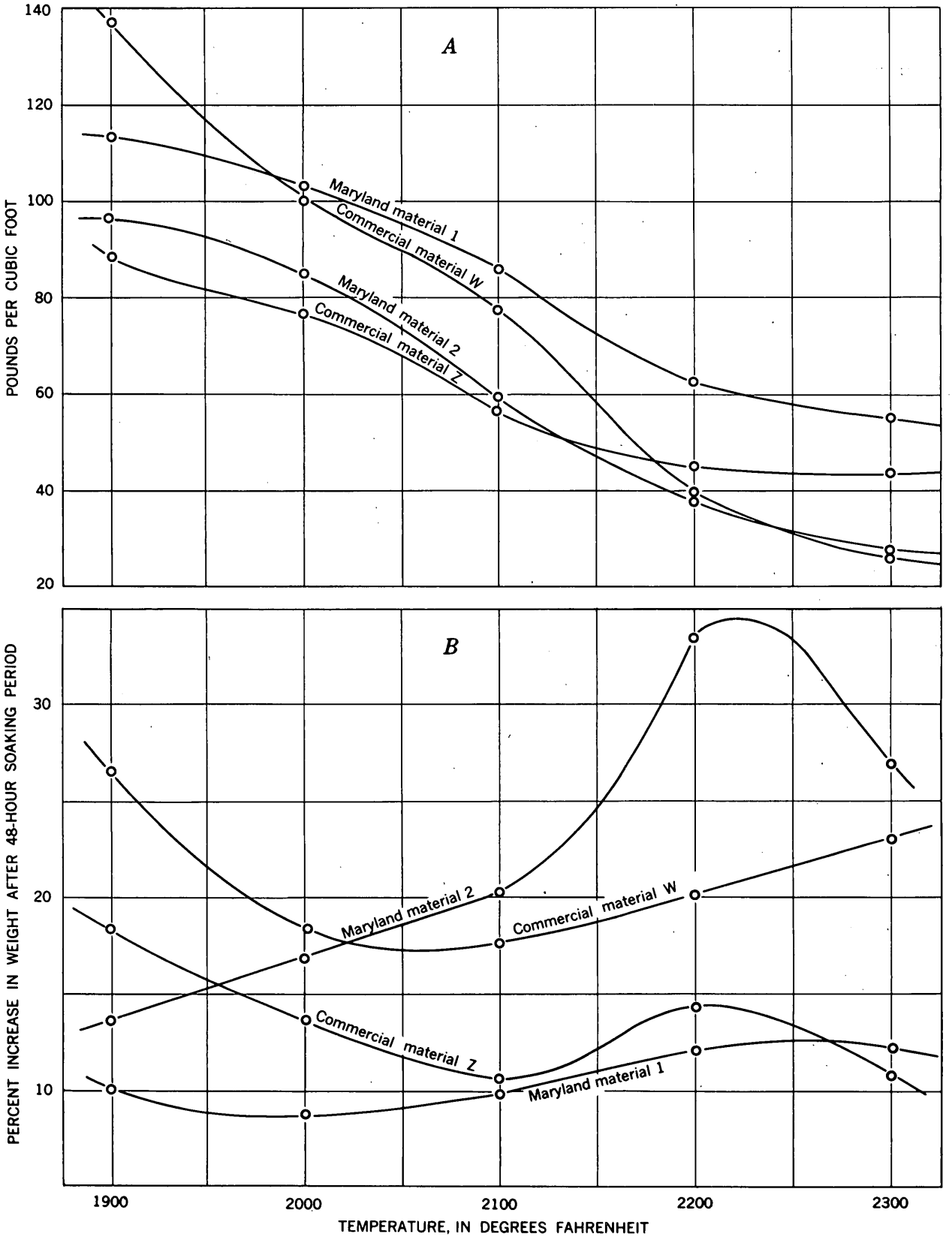

FIGURE 29.2.—Results of 15-minute bloating tests by U.S. Bureau of Mines of 2 sampled materials from southern Maryland, plotted together with comparable data on 2 commercial lightweight aggregate raw materials: *A*, unit weight (lb/ft^3) of fired products; *B*, percentages by weight of water absorbed by fired products in 48 hours.

gate where the St. Marys formation crops out in the Calvert Cliffs. The clay exposed here occurs in a layer that is generally more than 20 feet thick. Its thickness and its capacity for expansion vary, however, from place to place, and the clay is overlain by thick deposits of silt, sand, and gravel.

Samples of expandable materials have also been obtained from an exposure of the St. Marys formation in the Nomini Cliffs, along the south shore of the Potomac River two miles northeast of Stratford Hall, Westmoreland County, Va., and from the next younger unit, the Yorktown formation (Miocene), in cliffs on the west shore of the James River 1,000 feet south of Fergussons Wharf, Isle of Wight County, Va. According to Lodding (oral communication, 1958) the above-noted expandable clay from New Jersey came from an exposure of the Kirkwood formation (Miocene) in a brickyard west of the Alloway-Woodstown road, 1.3 miles south-southwest of Fenwick Salem County.

Some of the bloated materials formed at temperatures between 2000° and 2200° F are comparable in lightness and low water-absorption capacity to many of the best commercial aggregates produced in the United States. Unit-weight and water-absorption data for two clays from the St. Marys formation of Maryland are compared on figure 29.2 with two commercial materials from other parts of the country. Maryland material 1 is olive-gray silty clay from the bottom of an auger hole 100 feet deep near the west side of State Highway 5, southwest of its junction with Villa Road, in St. Marys County. Maryland material 2 represents olive-gray clayey silt approximately 20 feet thick exposed in the Calvert Cliffs, 5 miles northwest of Cove Point; the base of this material is about 23 feet above high tide.

Small concrete cubes of bloated material formed in firing one of the Maryland samples at 2100° F were prepared for tests of unit weight and compression strength. The unit weight, 86.3 pounds per cubic foot, proved to be less than that of much concrete made from domestic lightweight aggregates; the compression strength, 3,500 pounds per square inch, surpassed the requirements of most specifications for lightweight concrete. The 48-hour water-absorption capacity, 21.3 percent, is higher than that of most such concrete, but this percentage would probably have been lower if the aggregate had been fired in a rotary kiln.

The clay-minerals in the expandable material are montmorillonite, "illite", and subordinate amounts of kaolinite. These are intermixed with abundant silt- and sand-sized grains of quartz, and with smaller quantities of muscovite and of many kinds of heavy minerals. The clay mineralogy of the expandable material is similar to that of many sampled materials that gave negative results when tested for expansion. It is hoped that further laboratory study will result in satisfactory explanations for the differences in firing behavior among the materials tested. More testing is needed to determine how sampled raw materials that bloated satisfactorily in the small electric kiln will behave at comparable temperatures in large rotary kilns. If such testing confirms the results at hand, and if removal of the heavy overburden that is nearly everywhere present would not be too costly, the resources of expandable clay available for mining in southern Maryland should be adequate, both in quantity and quality, to satisfy much of the demand for lightweight aggregate here and in adjacent populous areas.

The proven occurrence of bloating clay of Miocene age at localities as much as 200 miles apart (fig. 29.1), and the known presence of formations of that age in all the States bordering the eastern seacoast from New Jersey southward, suggest the existence of vast potential resources. The increasing market for expanded aggregate in the east coast region warrants comprehensive studies of their distribution and possible commercial value.

REFERENCES

Knechtel, M. M., Hosterman, J. W., and Hamlin, H. P., 1959, Bloating clay deposits in southern Maryland: U.S. Geol. Survey open-file report.

Lodding, William, 1956, Raw materials for lightweight aggregate production in New Jersey: Rutgers Univ., Bur. Mineral Research Bull 7.

30. SIGNIFICANCE OF UNUSUAL MINERAL OCCURRENCE AT HICKS DOME, HARDIN COUNTY, ILLINOIS

By Robert D. Trace, Beltsville, Md.

Hicks Dome in the northern part of the Illinois-Kentucky fluorspar-zinc-lead district is a tectonic feature affecting rocks of Devonian, Mississippian, and Pennsylvanian age. It covers about 100 square miles centered in the western half of Hardin County, Ill. The core of the dome, where the rocks dip 10–15 degrees, includes nearly 2 square miles of limestone, chert, and black shale of Devonian age in which there are a few tabular and possibly oval-shaped pipelike masses of breccia, some radioactive areas, and an altered mafic dike (Bradbury and others, 1955, p. 1–3).

Hicks Dome has been described by Brown and others (1954, p. 895–897) as an incipient cryptovolcanic structure. This interpretation is in part based upon data from a 2,944-foot test well in the approximate center of the dome. Most of the sedimentary rocks in the lower half of the hole are brecciated, but the lateral extent and shape of the brecciated mass are not known. According to Brown and others (1954, p. 897–902), the breccia contains thorium, fluorite, barite, calcite, quartz, pyrite, sphalerite, and galena. The thorium and fluorite seem to be closely associated.

No igneous or metamorphic rocks have been identified in the breccia from the center of the dome, although plugs of explosion breccia containing igneous and metamorphosed rocks are known about 7 miles to the northeast and 1.5 and 7 miles to the south (Clegg and Bradbury, 1956, p. 17). The depth to Precambrian rocks at the center of the dome is at least 7,500 feet as shown by data from the M. D. Davis No. 1 test well near Tolu, Ky. (unpublished data, 1956, Shell Oil Company Information Release, mimeographed), about 11 miles to the southeast of the dome.

One of the surface radioactive localities (Bradbury and others, 1955, fig. 1, sample 72) was explored in 1955–56 (under a Defense Minerals Exploration Administration contract) by shallow diamond drilling and trenching in cherty residuum overlying Devonian limestone. The exploration showed two areas of breccia, but most of the radioactivity is concentrated in one—a tabular mass about 10 feet wide that extends N. 24° W. for at least 260 feet, is over 100 feet deep, and dips 85° NE. The highest radioactivity (about 0.1 percent eU) occurs in the central 1 to 2 feet of this tabular body.

A surface sample of the most radioactive material was found by semiquantitative spectrographic analysis to contain a high concentration of rare earths and thorium (table 30.1). The radioactive mineral in the sample was isolated and identified tentatively as monazite. Florencite, a cerium-aluminum phosphate, was found in association with the monazite.

The monazite is in small, soft, earthy, round to subround, brownish-yellow grains about 0.1 to 0.2 mm in diameter. Preliminary X-ray diffraction study shows that the mineral has monazite structure, but its cell size appears to be slightly smaller than that of monazite from other localities. Spectrographic analysis of the hand-picked material shows it to be a thorium-bearing rare-earth phosphate (table 30.1) that differs slightly in composition from most other monazite in that it is relatively rich in yttrium and lean in total rare earths. The abundance of yttrium may account for the small cell size. The relatively low content of cerium and lanthanum and abundance of yttrium suggest that the monazite is relatively unfractionated, or primitive, as described by Murata and others (1953, p. 296–297; 1957, p. 148–150).

Florencite is in small, soft, earthy, round to subround, pale-orange grains about 0.3 to 0.4 mm across. The florencite was identified from X-ray diffraction traces, and confirmed as a cerium-bearing mineral by X-ray fluorescence study (analyst: Richard Larson, 1959).

The narrow surface zone of radioactivity that was sampled is about 200 feet west of the deep test well and dips 85° NE. toward the well. Semiquantitative spectrographic analysis of 8 samples (tables 30.1 and 30.2) obtained by J. W. Hill of the U.S. Geological Survey from the test well and described by Brown and others (1954, p. 899), disclose above-normal quantities of thorium, the rare earths, niobium, zirconium, and beryllium. According to Warner and others (1959, p. 25–28), the BeO content of sedimentary rocks may be as much as 0.004 percent, although generally it is less than 0.001 percent. In the test well, the Be content is as high as 0.06 percent (table 30.2). In general, the greater the radioactivity, the more the Be, rare earths, Nb, and Zr.

The mineralogic and chemical data presented here provide new evidence for the existence of deep-seated

TABLE 30.1.—*Analyses of samples from Hicks Dome, Hardin County, Illinois*

Chemical and semiquantitative spectrographic analysis (weight percent) of surface sample RDT-6 [1]

Width (inches)	0.089–0.099	0.008	N.D.	>10	5–10	1–5	0.5–1	0.1–0.5	0.05–0.1	0.01–0.05	0.005–0.01	0.001–0.005	0.0005–0.001	0.0001–0005
16	eU	U	CaF_2	Si	Fe	Al	Ce, La, K, P	V, Ba, Ti, Nd, Ca, Mg, Th	Sr, Pb, Pr, Mn	B, V, Er, Nb, Tb, Na, Zn	Cu, Gd, Yb, Sm, Dy, Ni, Zr	Eu, Sn, Ga, Co, Lu, Cr, Sc	Be, Mo	Ag

Quantitative spectrographic analysis (weight percent) of monazite hand picked from sample RDT-6 [2]

Ce_2O_3	La_2O_3	Nd_2O_3	Sm_2O_3	Gd_2O_3	Pr_2O_3	Dy_2O_3	Y_2O_3	ThO_2	P_2O_5	SiO_2	Al_2O_3	MgO	CaO	Fe_2O_3	TiO_2	Total
16	11	6	2	1.5	2.5	1.5	4.2	4.4	29	4.4	2.2	0.2	3.8	6.6	2.7	98

Semiquantitative spectrographic analysis (weight percent) of test-well samples [3]

Sample no.	Depth (feet)	XX.	X.+	X.	X.-	0.X+	0.X	0.X-	0.0X+	0.0X	0.0X-	0.00X+	0.00X	0.00X-	0.000X+	Tr
1	1725–1750	Ca	Si	Mg	Al, Fe	K, Ba	Ti	Th, Y, Na	Mn, Sr	Pb, Zn	La, Dy, Sc, V	Yb	Cr, Cu	Bi, Ni	----------	Ga
2	1785–1815	Ca	Si	Mg	Al, Fe	K	Ti	Th, Y, Na	Mn, Sr	Pb, Zn Ba	La, Dy, Sc, V	Yb	Cr, Cu	Bi, Ni	----------	Ga
3	1975–2000	Ca	Mg	Si	---------	Al, Fe, Ba	K	Na	Mn	Ti	Sr	Pb, V Y	----------	Sc	Cr, Cu, Ni, Yb	
4	2150–2175	Ca	Si, Mg	---------	---------	Al, Fe	Ti	Y, Ba	Th, Na, Mn	Sr	Dy, V	Yb	Pb, Sc	Cr, Cu	Ni	Bi, La
5	2370–2400	Ca	Si	Fe, Mg	Al, K	---------	Ti	Mn, Na	Ce, Th, Y, Ba, Sr	La	Dy, Nd V	Sc	Cr, Cu Yb	Co, Ni	----------	Pb
6	2425–2450	Ca	Si, Mg	Al, Fe, K	---------	Ti	Mn, P, Na	----------	Ce, Ba, Sr	La	Nd, Se, V, Y	Cr	Ni, Pb, Yb	Co, Cu	----------	Dy, Ga, Th
7	2450–2475	Ca	Si, Mg	---------	Fe	Al, K	Ti	Ba, Na, Mn	----------	Sr	La, Pb	V, Y	Cr, Cu, Sc	Ni, Yb	Co	Ce, Dy, Ga, Th
8	2900–2925	Ca	Mg	---------	---------	Fe, K	Al, Ba	----------	Mn, Na	Ti	Pb, Sr	Y	Cu, V	Cr, Ni, Sc	Yb	

[1] Analysts, Katherine E. Valentine, C. Johnson, and G. Daniels. Sample RDT-6 analyzed for D. M. E. A. contract.
[2] Analyst, Harry J. Rose, Jr., 1960. Analysis on 15 mg. Sample diluted in graphite.
[3] Analyst, G. W. Beyes, Jr., 1953. Be, Nb, and Zr not shown, see later analysis in table 30.2.

igneous activity in the region of the Illinois-Kentucky fluorspar-zinc-lead district, but by themselves may neither confirm nor deny the existence of a connection between the igneous activity and the mineralization of the district.

TABLE 30.2.—*Analysis of samples from Hicks Dome, Hardin County, Illinois*

[Chemical and semiquantitative spectrographic analysis (weight percent) of additional constituents in test well samples [1]]

Sample	Depth (feet)	eU	U	CaF_2	Be	Nb	Zr
1	1725–1750	0.029	0.001	6.4	0.06	0.15	0.03
2	1785–1815	.024	.001	9.6	.06	.15	.03
3	1975–2000	.001	----------	1.3	.007	.03	.005
4	2150–2175	.016	.001	7.9	.06	.08	.02
5	2370–2400	.011	.001	10.8	.01	.10	.01
6	2425–2450	.008	.001	6.6	.006	.10	.02
7	2450–2475	.004	----------	4.6	.003	.03	.01
8	2900–2925	.001	----------	2.8	.005	.01	.006

[1] Analysts, Pauline J. Dunton, Ferman W. Montjoy, and P. Stuch.

REFERENCES

Bradbury, J. C., Ostrom, M. E., and McVicker, L. D., 1955, Preliminary report on uranium in Hardin County, Illinois: Illinois Geol. Survey Circ. 200, 21 p.

Brown, J. S., Emery, J. A., and Meyer, P. A., Jr., 1954, Explosion pipe in test well on Hicks Dome, Hardin County, Illinois: Econ. Geology, v. 49, no. 8, p. 891–902.

Clegg, K. E., and Bradbury, J. C., 1956, Igneous intrusive rocks in Illinois and their economic significance: Illinois Geol. Survey Rept. Inv. 197.

Murata, K. J., Rose, H. J., Jr., and Carron, M. K., 1953, Systematic variation of rare earths in monazite: Geochim. et Cosmochim, Acta, v. 4, p. 292–300.

Murata, K. J., Rose, H. J., Jr., Carron, M. K., and Glass, J. J., 1957, Systematic variation of rare-earth elements in cerium-earth minerals: Geochim. et Cosmochim. Acta, v. 11, p. 141–161.

Warner, L. A., Holser, W. T., Wilmarth, V. R., and Cameron, E. N., 1959, Occurrence of nonpegmatite beryllium in the United States: U.S. Geol. Survey Prof. Paper 318.

31. PHOSPHATE AND ASSOCIATED RESOURCES IN PERMIAN ROCKS OF SOUTHWESTERN MONTANA

By Roger W. Swanson, Spokane, Wash.

Work done in cooperation with the U.S. Bureau of Reclamation and the U.S. Atomic Energy Commission

The phosphate rock in southwestern Montana occurs in two phosphatic shale members of the Permian Phosphoria formation (McKelvey and others, 1959). The lower, or Meade Peak, phosphatic shale member is mostly less than 15 feet thick; it tongues out to the north and east and has not been recognized in the Melrose and Madison Range districts (fig. 31.1). The upper, or Retort, phosphatic shale member ranges up to 75 feet in thickness and is much more extensive, though it tongues out to the northeast. It contains phosphate of minable quality and thickness in all the districts shown in figure 31.1. No reserves are computed for the Permian rocks in the vicinity of Three Forks, because all the phosphorite in them is of poor quality or in thin beds.

Several potentially valuable elements occur in the phosphorite, but at present nothing but phosphorus is being recovered from rock mined in Montana. Fluorine maintains a fairly constant ratio of 1 percent F to 10 percent P_2O_5. It will soon be recovered from phosphorite mined in Idaho and treated in Utah (Anonymous, 1958). Uranium, vanadium, chromium, nickel, molybdenum, and rare earths are other elements that are notably concentrated in the phosphorite, but they generally make up only a few tenths to a few thousandths of 1 percent of the rock. Vanadium has been recovered from acid-grade phosphorite mined at Conda, Idaho (Caro, 1949). The ferrophosphorus produced in the electric furnace contains 1 to several percent of vanadium, chromium, and nickel (Banning and Rasmussen, 1951). Oil shale is also present in the Retort member over much of southwestern Montana.

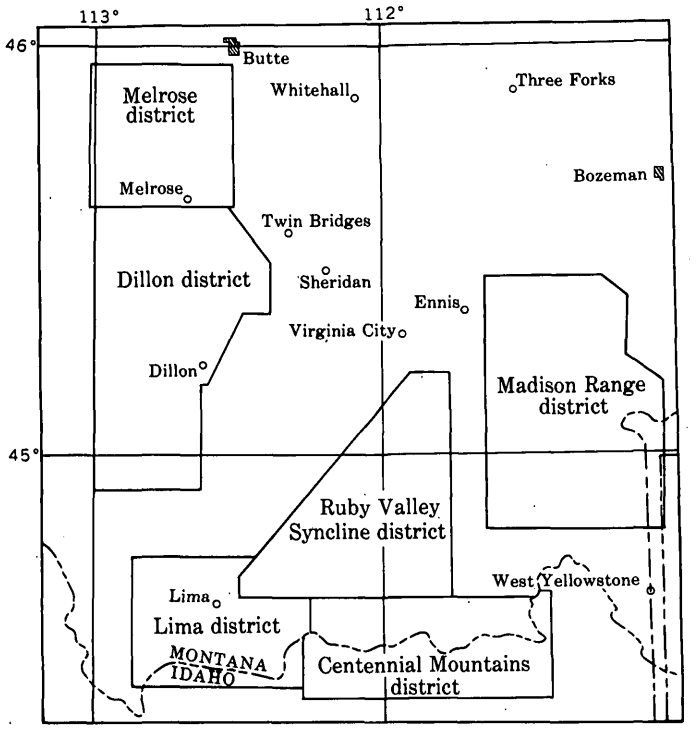

FIGURE 31.1.—Districts in southwestern Montana for which phosphate and uranium reserves in Permian rocks are estimated.

Most of the phosphorite coming from the western field is mined by surface methods, and most of the rock mined underground is above entry level. Reserve estimates of phosphorite are presented in table 31.1 for rock above entry level, rock within 100 feet vertically below that level, and total reserves in the block regardless of depth. Reserves of rock that can be mined by surface methods have not been computed separately. Estimates are also presented for grade cutoffs of 31 and 24 percent P_2O_5 (acid and furnace grades respectively) and for 18 percent rock that might be utilized after beneficiation or by blending.

The two phosphatic shale members contain more than 10 billion tons of P_2O_5, 80 percent of which is in the Retort member. More than 6 billion tons of rock, almost equally divided between the two members, occurs in beds at least 3 feet thick that contain 24 percent or more of P_2O_5, but only about 370 million tons is above entry level or within 100 feet below it; 450 million tons, mostly in the Retort member, occurs in beds at least 3 feet thick that contain more than 31 percent P_2O_5, and 50 million tons of this is above entry level or not more than 100 feet below it.

Uranium is present in all the phosphorite, though in small amounts. Reserve estimates (table 31.2) indicate that there is more than 400,000 tons of uranium in rock containing 24 percent or more P_2O_5, and that

nearly 25,000 tons of this is in rock that lies above entry level or not more than 100 feet below it. The acid-grade phosphorite is estimated to contain 35,000 tons of uranium, 20 percent of it above entry level or not more than 100 feet lower.

Most of the phosphorite likely to be mined within the next few decades lies within those limits. Most of the rock at lower levels need not be considered at present in extraction programs and short-term resource appraisals, though some of it is likely to be minable in the future.

REFERENCES

Banning, L. H., and Rasmussen, P. T. C., 1951, Processes for recovering vanadium from western phosphates: U.S. Bur. Mines Rept. Inv. 4822.

Caro, R. J., 1949, Anaconda phosphate plant, beneficiation and treatment of low-grade Idaho phosphate rock: Am. Inst. Mining Metall. Engineers Trans., v. 184, p. 282–284.

Anonymous, 1958, Cryolite: Chemical Week, v. 82, no. 8, p. 34, Feb. 22, 1958.

McKelvey, V. E., and others, 1959, Phosphoria, Park City, and Shedhorn formations in the western phosphate field: U.S. Geol. Survey Prof. Paper 313A, p. 1–44.

TABLE 31.1.—*Phosphate reserves in Permian rocks of southwestern Montana, in millions of short tons*

Reserve block	Basic data			Reserve of rock containing more than 31 percent P_2O_5					Reserve of rock containing more than 24 percent P_2O_5 [1]					Reserve of rock containing more than 18 percent P_2O_5 [1]				
	Average member thickness (feet)	Average grade (percent P_2O_5)	Total tons P_2O_5 in block	Thickness (feet)	Grade (percent P_2O_5)	Tonnage above entry level	Tonnage in first 100 feet below entry level	Total tons of rock in block	Thickness (feet)	Grade (percent P_2O_5)	Tonnage above entry level	Tonnage in first 100 feet below entry level	Total tons of rock in block	Thickness (feet)	Grade (percent P_2O_5)	Tonnage above entry level	Tonnage in first 100 feet below entry level	Total tons of rock in block
Retort phosphatic shale member (Phosphoria formation):																		
Melrose district	23.3	16.2	900	3.4	31.0	8	6	300	7.2	25.5	100	25	1,000	12.4	21.7	250	50	2,500
Dillon district	52.6	10.6	2,000	------	------	------	------	------	3.3	27.6	25	8	450	12.4	19.6	150	50	4,000
Lima district	76.7	9.0	900	------	------	------	------	------	------	------	------	------	------	6.0	21.0	50	15	650
Ruby Valley Syncline district	49.6	8.4	4,000	------	------	------	------	------	3.2	29.0	3	1	150	5.6	19.9	150	30	5,500
Centennial Mountains district	6.0	16.0	60	------	------	------	------	------	------	------	------	------	------	4.0	20.0	55	5	250
Madison Range district	10.6	9.8	650	------	------	------	------	------	3.2	25.7	20	3	1,000	4.0	20.3	100	30	2,500
Totals and averages	47.1	9.9	8,510	3.4	31.0	8	6	300	4.8	26.1	148	37	2,600	8.2	20.2	755	180	15,400
Meade Peak phosphatic shale member (Phosphoria formation):																		
Dillon district	4.3	10.0	15	------	------	------	------	------	3.0	25.0	1	1	5	3.5	22.0	1	1	6
Lima district	24.3	10.9	400	------	------	------	------	------	3.2	27.4	20	6	250	6.5	21.5	50	15	850
Ruby Valley Syncline district	9.5	16.4	1,500	------	------	------	------	------	4.7	26.6	75	20	3,000	5.9	19.6	100	30	6,000
Centennial Mountains district	13.7	19.4	100	3.5	32.9	35	4	150	5.5	28.0	55	5	250	8.5	23.2	80	8	400
Totals and averages	12.6	15.4	2,015	3.5	32.9	35	4	150	4.6	26.8	151	32	3,505	6.1	20.0	231	49	7,256
Grand totals	40.5	11.0	10,525	3.4	31.6	43	10	450	4.7	26.5	299	69	6,105	7.5	20.1	986	229	22,656

[1] Includes tonnages in columns to left.

TABLE 31.2.—*Uranium reserves in Permian phosphorite of southwestern Montana, in short tons*

	Uranium reserves in phosphorite containing > 31 percent P_2O_5				Uranium reserves in phosphorite containing > 24 percent P_2O_5 [1]				Uranium reserves in phosphorite containing > 18 percent P_2O_5 [1]			
	Grade (percent uranium)	Tonnage above entry level	Tonnage in first 100 feet below entry level	Total tonnage in block	Grade (percent uranium)	Tonnage above entry level	Tonnage in first 100 feet below entry level	Total tonnage in block	Grade (percent uranium)	Tonnage above entry level	Tonnage in first 100 feet below entry level	Total tonnage in block
Retort phosphatic shale member (Phosphoria formation):												
Melrose district	0.005	350	250	15,000	0.0049	5,500	1,000	55,000	0.0049	15,000	2,500	100,000
Dillon district	------	------	------	------	.0051	1,500	350	25,000	.0051	7,500	2,500	200,000
Lima district	------	------	------	------	------	------	------	------	.0043	1,500	600	30,000
Ruby Valley Syncline district	------	------	------	------	.0080	250	40	10,000	.0066	9,000	2,000	350,000
Centennial Mountains district	------	------	------	------	------	------	------	------	.005	2,500	250	15,000
Madison Range district	------	------	------	------	.0073	1,500	200	80,000	.0058	6,000	2,000	150,000
Totals and averages	0.005	350	250	15,000	0.0062	8,750	1,590	170,000	0.0058	41,500	9,850	845,000
Meade Peak phosphatic shale member (Phosphoria formation):												
Dillon district	------	------	------	------	.007	70	35	350	.006	65	35	350
Lima district	------	------	------	------	.0087	1,500	600	25,000	.0086	4,500	1,500	70,000
Ruby Valley Syncline district	------	------	------	------	.0061	5,000	1,000	200,000	.0060	6,000	1,500	300,000
Centennial Mountains district	.012	4,000	400	20,000	.010	5,500	500	25,000	.009	7,500	700	35,000
Totals and averages	0.012	4,000	400	20,000	0.0068	12,070	2,135	250,350	0.0068	18,065	3,735	402,350
Grand totals	0.0090	4,350	650	35,000	0.0066	20,820	3,725	420,350	0.0061	59,565	13,585	1,247,350

[1] Includes tonnages in columns to left.

32. HUGO PEGMATITE, KEYSTONE, SOUTH DAKOTA

By J. J. Norton, Denver, Colo.

The Hugo pegmatite, near Keystone, South Dakota, is a well exposed intrusive body, about whose crystallization history much can be inferred from detailed petrographic and structural study. This pegmatite consists of two segments, in large part separated from each other by a screen of schist. The larger of these, the south segment contains the seven zones and two replacement bodies shown in figure 32.1. The north segment

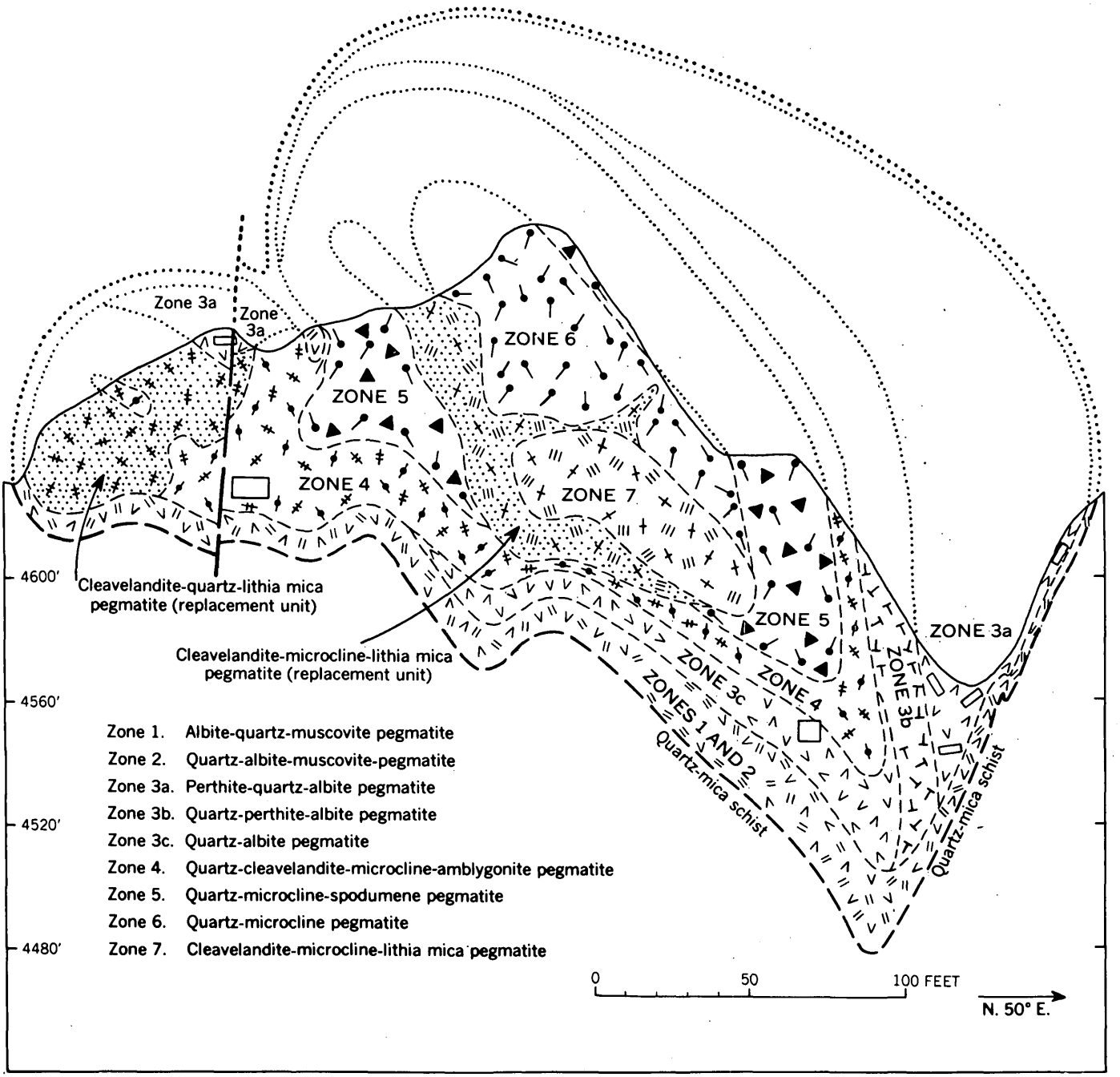

FIGURE 32.1.—Geologic section, Hugo pegmatite, Keystone, S. Dak.

TABLE 32.1.—*Estimated composition of the Hugo pegmatite, Keystone, S.D.*

Segment	Zone	Estimated tons of rock	Quartz	Albite (including cleavelandite	Mode (percent)[1]				Calculated chemical composition (percent)[2]				
					Perthite and microcline	Mica	Other[3] minerals	SiO_2	Al_2O_3	Na_2O	K_2O	H_2O+F	Other constituents
North	1 and 2	45,000	45	35	----------	15	T, 2.5	78.3	13.1	4.3	1.6	1.1	1.6
	3b	175,000	35	25	30	5	T, 2	76.3	13.5	4.0	4.2	.5	1.5
	3c	230,000	55	35	----------	7	----------	83.7	9.9	4.1	.9	.5	.9
	4	15,000	55	35	5	3	----------	85.3	9.0	4.2	1.2	.2	.1
South	1 and 2	165,000	40	30	----------	20	T, 7	73.5	15.3	3.9	2.1	1.5	3.7
	3a	200,000	15	10	75	----------	----------	69.8	16.9	3.5	8.9	.3	.6
	3b	340,000	35	25	30	5	Po, 4	73.8	12.8	3.9	4.1	.7	4.7
	3c	160,000	55	35	2	7	----------	83.3	10.0	4.1	1.0	.5	1.1
	4	165,000	50	35	8	2	Amb, 3	81.3	10.3	4.2	1.5	.4	2.3
	5	170,000	70	5	10	----------	S, 10 Amb, 4	86.6	7.3	.9	1.6	.4	3.2
	6	20,000	65	----------	35	----------	----------	87.0	6.8	.4	5.2	.1	.5
	7	11,000	15	35	25	25	----------	66.4	19.5	4.4	6.5	1.7	1.5
	Cleavelandite-microcline-lithia mica replacement unit.	19,000	15	40	25	20	----------	67.4	18.9	4.9	5.9	1.4	1.5
	Cleavelandite-quartz-lithia mica replacement unit.	15,000	15	70	4	10	----------	69.9	17.9	8.1	1.8	.8	1.5
	Composition of north segment	465,000	47	32	12	7	----------	80.5	11.5	4.1	2.2	.5	1.2
	Composition of south segment	1,265,000	41	24	24	6	----------	77.0	12.5	3.5	3.6	.6	2.8
	Composition of both segments	1,730,000	43	26	21	6	----------	77.9	12.2	3.7	3.2	.6	2.4

[1] Minerals forming less than 2 percent of a unit, based on visual estimates, are omitted from the modes, but they were used in calculating chemical composition.
[2] The modes were not converted from volume percent to weight percent in calculating chemical composition because the change would be too small to be significant.
[3] T, tourmaline; Po, iron-manganese phosphates; Amb, amblygonite; and S, spodumene.

contains only the four outer zones. By structural study of the pegmatite and estimates of the modes in the many available exposures, the approximate size and composition of the units in this pegmatite prior to erosion and mining have been calculated (table 32.1). About 50 percent of the north segment and 60 percent of the south segment lie between the lowest mine level and the surface, and thus are somewhat better known than the rest of the pegmatite, which has largely been extracted by open-pit mining but also includes material that has been removed by erosion or that lies beneath the lowest mine level.

About three-fourths of the rock in this pegmatite is in the outer three zones (zones 1 to 3 of table 32.1 and figs. 32.1 and 32.2), which consist almost entirely of quartz, feldspar, and muscovite. Albite is the predominant feldspar, but perthite is abundant in the upper part of zone 3. Zones 4 to 6 are highly silicic and contain abundant quartz; they also contain cleavelandite, microcline, spodumene, and amblygonite. Zone 7, the core of the pegmatite, is of quite different composition; it contains quartz, but its most abundant constituents are cleavelandite, microcline, and lithia mica. Small replacement units, resembling the core in their relatively high content of alumina and alkalies and low silica content, extend from the center of the pegmatite outward across the zones, and contain unreplaced remnants of the zones.

Textural relations, both megascopic and microscopic, indicate so much overlap in paragenesis of the minerals in each zone as to indicate that all the minerals in any one zone crystallized at virtually the same time. It appears reasonable to assume that as this pegmatite was crystallizing from the contact inward, there was at any given stage a fully crystallized outer part and an entirely fluid inner part, separated by a moderate thickness of material consisting of a crystal meshwork and an interstitial fluid. If this was so, one can regard the composition of the material inside any zonal contact as indicating, roughly, the composition of the fluid at that point in the crystallizing process; we may neglect the presumably small quantity of material that escaped to the wall rock in hydrothermal or pneumatolytic fluids.

Since about 94 percent of the material in the Hugo pegmatite consists of components of the system $KAlSi_3O_8$–$NaAlSi_3O_8$–SiO_2, the course of crystallization can be plotted on the triangular diagram in figure 32.2, which has these three compounds at its corners. The remaining 6 percent of the material includes about 3 percent alumina in excess of the amount required to form feldspar, and only very small quantities of other constituents. Whatever the effect of these minor constituents was, the diagram represents the natural system closely enough for use in discussing the course of crystallization in this pegmatite and for comparison with the results obtained by Tuttle and Bowen (1958) in their detailed studies of the pure system. The quartz-feldspar field boundary, as shown on this figure, is at P_{H_2O} of 4000 kg per cm^2, for this is the highest pressure at which the boundary was determined in the laboratory (Tuttle and Bowen, 1958, fig. 38) and is also the lowest pressure at which quartz and the two feldspars formed together in equilibrium. The diagram shows that: (a) the south segment contains more potassium and less sodium than the north segment; (b) the residual fluid became progressively richer in silica during most of the time the pegmatite was forming, but became higher in alumina and alkalies and lower

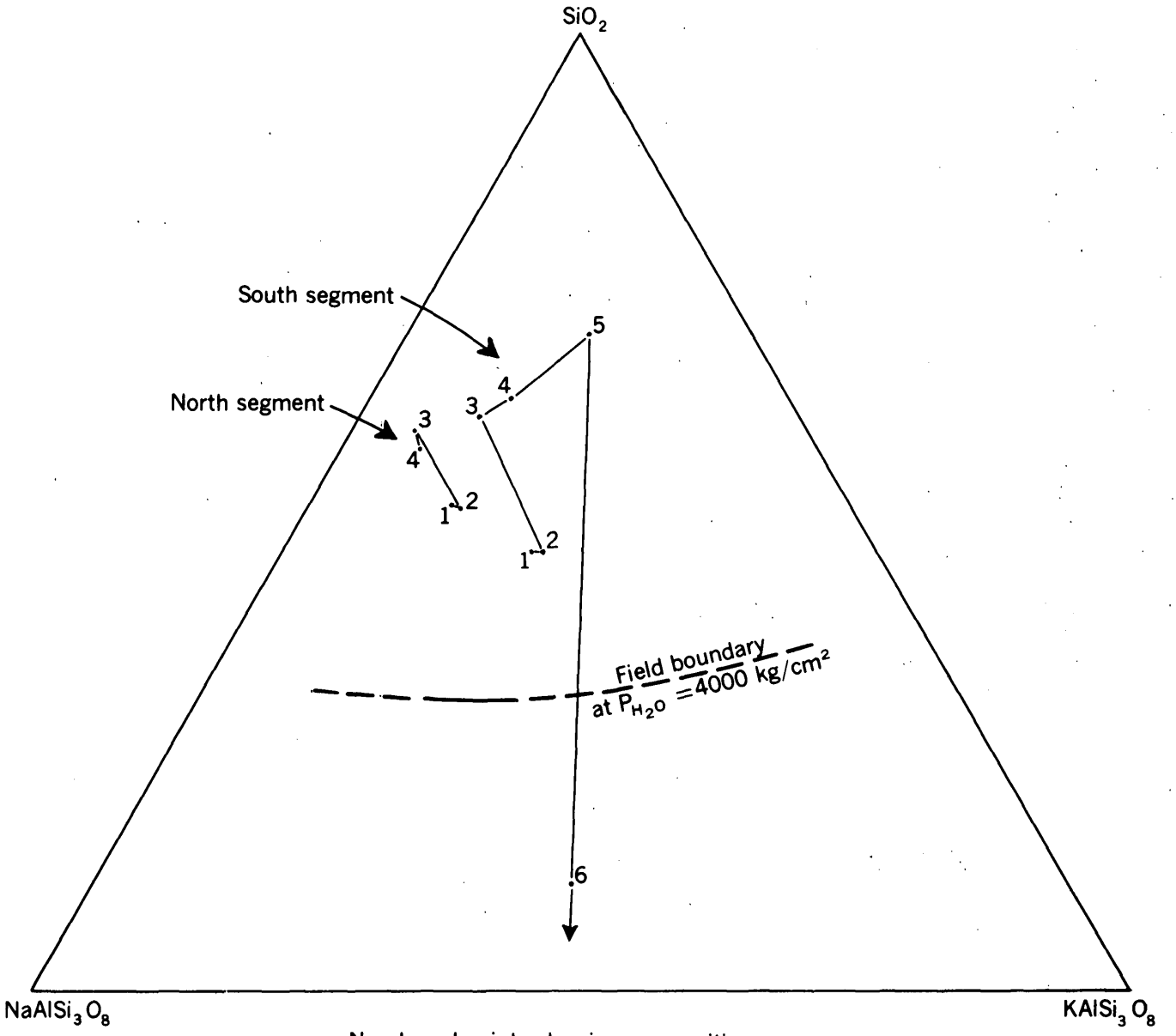

Numbered points showing compositions are:

1. Entire body
2. Units inside zones 1 and 2
3. Units inside zones 3a and 3b
4. Units inside zone 3c
5. Units inside zone 4
6. Units inside zone 5

The field boundary is from Tuttle and Bowen, 1958, fig. 38

FIGURE 32.2.—Inferred course of crystallization of the two segments of the Hugo pegmatite.

in silica at a late stage; and (c) the compositions at which quartz and feldspar crystallized together appear to have been much more silicic in the natural system (shown by points 1 to 5, fig. 32.2) than in the laboratory system (shown by the field boundary in fig. 32.2).

The south segment is at a higher altitude than the north segment, and the mechanism by which it obtained its high potassium content may be the same that caused perthite-rich hoods to form in the upper part of many zoned pegmatites. The narrow channel connecting the

two segments must have been sealed after the outer zones had crystallized, and thus the concentration of potassium in the south segment and sodium in the north segment must have taken place at a very early stage, probably by a physical mechanism. Potassium may have been carried upward through the liquid in a volatile phase before crystallization began.

The most marked feature of the course of crystallization as indicated in figure 32.2 is progressive enrichment in silica. The difference between points 1 to 5 (fig. 32.2) and the field boundary determined by Tuttle and Bowen (1958, fig. 38) suggests that excess of alumina and the minor constituents (such as lithium) in the natural system, at the high pressures that presumably prevailed when this pegmatite formed, caused the crystallizing fluid to become progressively richer in silica. The excess alumina surely affected the course of crystallization, because it gave rise to a significant amount of muscovite, but an extended discussion of its influence on the position of the field boundary will not be possible until more laboratory work has been done on systems containing mica, feldspar, and quartz.

The increase in silica content ended in zone 6, and the small amount of material that crystallized later, forming zone 7 and the replacement bodies, was low in silica and high in alumina, alkalies, water, and fluorine. The contrast in composition between this material and the rest of the pegmatite, coupled with the evidence for replacement of some previously solidified rock, suggests that a hydrothermal or pneumatolytic fluid separated from the silicate liquid. During the time that the outer zones were crystallizing, the content of water in the remaining liquid must have increased progressively until it had become as high as possible. Subsequently, a fluid phase rich in H_2O would have to separate, and dissolved materials would then be distributed between this and the remaining silicate liquid. This process could account for the concentration of alumina, alkalies, and volatiles in some places and of silica in others. At a very late stage the pressure of the fluid rich in H_2O must have increased until it exceeded the confining pressure, and this fluid then escaped outward and replaced previously crystallized rock.

REFERENCE

Tuttle, O. F., and Bowen, N. L., 1958, Origin of granite in the light of experimental studies in the system $NaAlSi_3O_8$—$KAlSi_3O_8$—SiO_2–H_2O: Geol. Soc. America Mem. 74.

33. A NEW BERYLLIUM DEPOSIT AT THE MOUNT WHEELER MINE, WHITE PINE COUNTY, NEVADA

(39)

By H. K. Stager, Menlo Park, Calif.

The recent discovery by Mt. Wheeler Mines, Inc. of a large beryllium deposit at the Mount Wheeler tungsten mine in Pole Canyon, on the west side of the Snake Range, White Pine County, Nev., has caused widespread interest among geologists and mining people. Because the principal beryllium minerals in this deposit—phenacite and bertrandite—are easily mistaken in hand specimens for ordinary quartz, this deposit had escaped the notice of the many geologists and engineers that had mapped the geology and explored the tungsten and other mineral deposits in the district. The geology of the deposit is described here to provide information on the mode of occurrence of this unusual ore that may be useful in searching for similar deposits elsewhere.

The rocks exposed in the Pole Canyon area are, from oldest to youngest, the Prospect Mountain quartzite, the Pioche shale, and the Pole Canyon limestone, all of Cambrian age (Drewes and Palmer, 1957). The beds strike northwest and dip 5° to 20° south.

About 400 feet of the Prospect Mountain quartzite is exposed in the mine area. The Pioche shale, which overlies the quartzite, is about 450 feet thick. It consists mainly of micaceous, siliceous, highly indurated shale, but includes several beds and lenses of limestone. The thickest of the limestone beds, known locally as the "Wheeler limestone", is about 50 feet above the quartzite contact and may be equivalent to the CM (Combined Metals) limestone at Pioche, Nev. Its average thickness is about 20 feet, but in places it is as much as 50 feet thick. At the outcrop in Pole Canyon it is pure white to gray, but in the mine workings, about 2,500 feet east of the outcrop, it is a black, carbonaceous limestone. In an area beginning about 3,800 feet east of the outcrop it is almost completely silicified, probably because of a nearby concealed granitic body. The lime-

stone is the host rock for the tungsten and beryllium deposit.

The sedimentary rocks are cut by three sets of faults. One set strikes north and dips steeply east or west, the second strikes east or northeast and dips steeply north, and the third strikes east and dips gently south nearly parallel with the bedding. These faults are commonly occupied by quartz veinlets from a few inches to as much as five feet wide.

Granitic rocks, ranging from quartz monzonite to granodiorite, are exposed about three miles north of the mine and crop out over an area of about 20 square miles (Drewes, 1958). The granitic body is believed to underlie the area at a shallow depth, perhaps less than 1,000 feet, and was possibly the source of the beryllium-bearing solutions that formed the deposit.

The Mount Wheeler tungsten deposit was discovered in 1950 and was explored by Mount Wheeler Mines, Inc., in cooperation with the Defense Minerals Exploration Administration, between 1952 and 1954. Beryl was first found to be present in the ore in 1951, but no significance was attached to the fact until 1959, when Mr. J. D. Williams, president of Mount Wheeler Mines, had the tungsten concentrates analyzed for beryllium. The analyses revealed more beryllium than could be accounted for by the small quantities of beryl that had been observed at the mine. Beryllium Resources, Inc., of Salt Lake City, Utah, then explored part of the beryllium deposit, and between September 1959 and March 1960 this company drove about 600 feet of new underground workings and did 10,000 feet of underground diamond-drilling.

The ore shoots are localized in the lower 15 feet of the "Wheeler limestone", along quartz veinlets in steeply dipping fault fissures that strike east or northeast. Exploration has shown that the beryllium minerals occur in a zone that extends for about 2,500 feet along the dip of the outcrop of the "Wheeler limestone" in Pole Canyon and extends eastward into the range along the strike for about 4,000 feet. The size and limits of the deposit have not yet been determined. The ore shoots within the explored area range from a few feet to more than 10 feet in width and from 15 to 20 feet in vertical extent, and one shoot has been traced for a strike length of about 1,500 feet. The average BeO content of the ore is about 1.0 percent.

Mineralogical studies by R. G. Coleman and others, U.S. Geological Survey, indicate that more than half the beryllium in the ores is contained in the mineral phenacite (Be_2SiO_4). The phenacite occurs in colorless, translucent, euhedral to subhedral crystals resembling quartz. It is found throughout the deposit but is most abundant in the western part, where it is associated with scheelite and pyrite. Bertrandite ($Be_4Si_2O_7(OH)_2$) is also an important ore mineral and in places accounts for nearly half the beryllium in the ore. It occurs in thin, bladed, translucent crystals and rosettes. It is most abundant in the eastern part of the deposit, where it is accompanied by fluorite and phenacite; it was probably derived from phenacite. The beryllium minerals are intimately associated with scheelite, fluorite, pyrite, sericite, and manganoan siderite. In places the ore contains a little galena and sphalerite. The beryl, which is pale blue, forms veinlets and small isolated euhedral crystals. It is most common in and near the thin quartz veinlets cutting the Pioche shale below the ore bodies, where it is associated with phyrite, calcite, sericite, fluorite, and rarely scheelite.

REFERENCES

Drewes, Harald, 1958, Structural geology of the southern Snake Range, Nevada: Geol. Soc. America Bull., v. 69, no. 2, p. 221–240.

Drewes, Harald, and Palmer, A. R., 1957, Cambrian rocks of the southern Snake Range, Nevada: Am. Assoc. Petroleum Geologists Bull., v. 41, p. 104–120.

34. PRE-MINERALIZATION FAULTING IN THE LAKE GEORGE AREA, PARK COUNTY, COLORADO

By C. C. Hawley, W. N. Sharp and W. R. Griffitts, Denver, Colo.

The Lake George beryllium area in Park County, Colo., is underlain mainly by Precambrian rocks. The area is traversed by large-scale lineaments trending north-northwest, which coincide at least in part with faults that are older than the mineralization. The rocks in the southwestern part of the area are mainly schists and gneisses, cut by many granite pegmatites of simple composition and by small granitic bodies. The

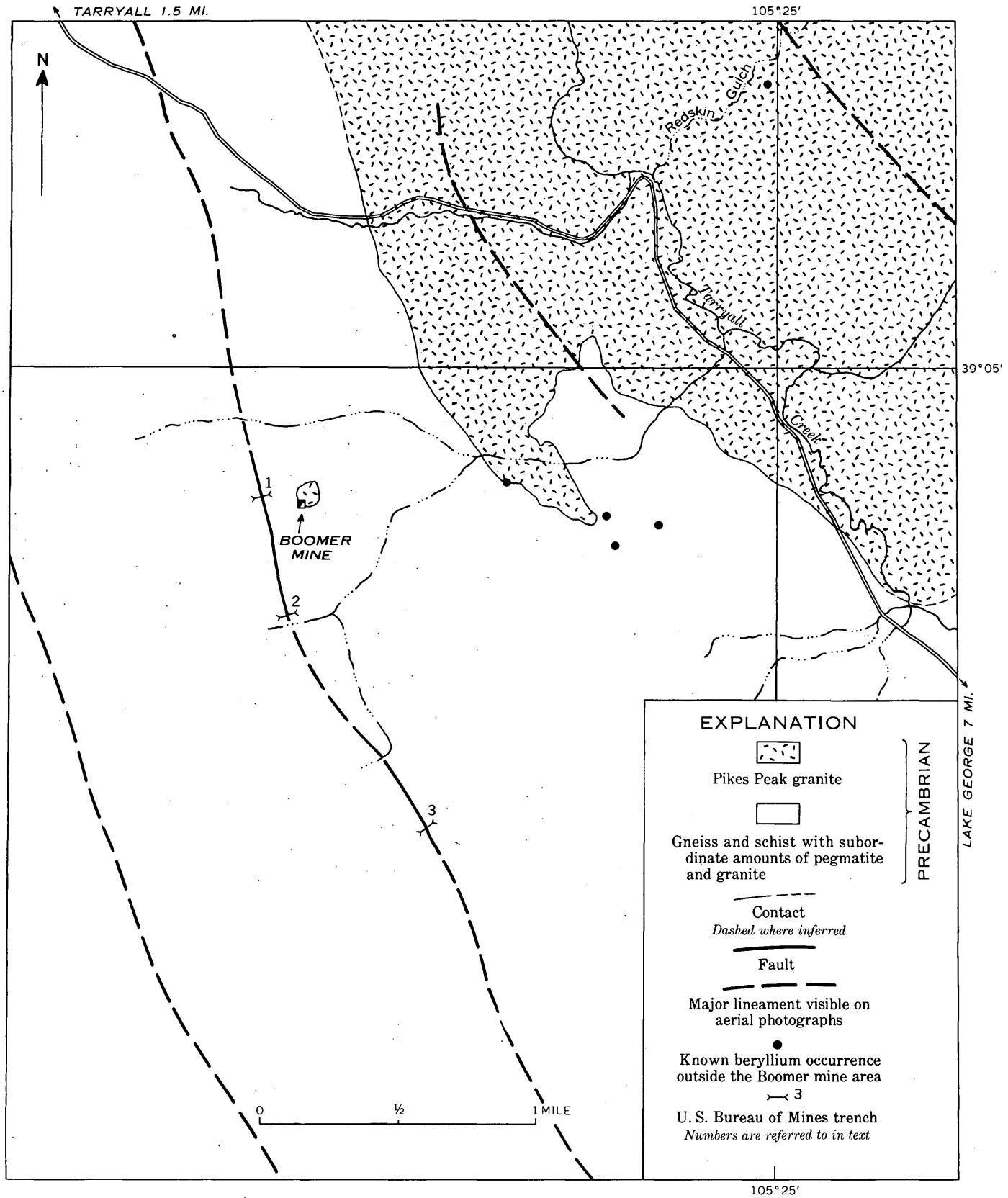

FIGURE 34.1.—Generalized geologic map of the Lake George beryllium area, Park County, Colo.

northeastern part of the area is underlain by the Pikes Peak granite, which is younger than all the other Precambrian rocks (fig. 34.1).

The beryllium deposits of the area are small replacement veins and pipes localized by fractures and rock contacts. The Boomer mine develops the most important deposits, which are in part extensively greisenized zones in the Pikes Peak granite and at its contact with the metamorphic rocks, and in part veins that cross that contact. Other deposits are associated with greisenized zones within the Pikes Peak batholith or along its contact.

The lineaments are most evident on areial photographs (fig. 34.1). Detailed mapping near the Boomer mine has shown that there at least these lineaments are faults. The faulting is probably older than the mineralization, for the rocks along the faults are locally greisenized and the greisens contain very small yet significant amounts of beryllium. The fault just west of the Boomer mine is exposed only in three trenches excavated by the U.S. Bureau of Mines on sites chosen in the light of our mapping. In trenches 1 and 2 (fig. 34.1) the fault is indicated by highly sheared rocks, which in trench 2 are partly greisenized. In trench 3, cut at the site of a beryllium geochemical anomaly, the fault zone is about 15 feet wide and is composed of about 12 feet of soft, sheared, fluorite-bearing rock and a 3-foot vein of iron-stained greisen.

The age of these faults that appear to have caused the lineaments is not known; most likely they were formed in several periods of movement. The parallelism of some lineaments in the metamorphic rocks with the main granite contact, particularly in the northern part of the area, suggests that they existed prior to the intrusion of granite and guided its emplacement. On the other hand, the granite batholith is cut by lineaments of similar trend, which indicate post-granite movement.

The relation of the faults to the beryllium mineralization is at this time highly speculative. The principal beryllium deposits of the Lake George area are not closely associated with the major lineaments, and further study may prove that there is no direct relation between them. The major lineaments, however, are not well prospected, and may be significantly mineralized in some places where they have not been examined. Furthermore, movement on the major faults may have caused smaller and less obvious subsidiary fractures along which localized mineralization occurred. A possible result of subsidiary fracturing is the vein and dike zone exposed in the J&S mine between the Boomer mine and the known fault.

Since there is good correlation of known deposits with beryllium soil anomalies, systematic soil sampling might be the most efficient way of prospecting the large faults.

35. BERTRANDITE-BEARING GREISEN, A NEW BERYLLIUM ORE, IN THE LAKE GEORGE DISTRICT, COLORADO

By W. N. Sharp and C. C. Hawley, Denver, Colo.

The Lake George beryllium district, in Park County, Colo., has produced most of the beryllium ore mined in recent years in the United States. The ore has consisted largely of beryl, but in 1959 bertrandite ($Be_4(OH)_2Si_2O_7$ [47 percent BeO]) was discovered in mica-quartz greisen associated with beryl ore. Some of the bertrandite-bearing greisen has proved to be richer in beryllium than the beryl ore, and it is considerably easier to mine. Visual determination of the grade of bertrandite-bearing rock is difficult, but selection of ore-grade rock has been made possible by use of a beryllium-detecting device similar in principle to the one described by Vaughn and others (1960).

The Lake George district is at the western edge of the Pikes Peak granite batholith. In the district a number of pipelike bodies and irregular masses of greisen and greisenized rock as much as 20 feet across are present within the main granite mass, and also in small outlying bodies of granite and along contacts of granite with the older metamorphic rocks. The Boomer mine, from which most of the ore has been produced, is in a zone of irregularly greisenized rock along the contact of a small granite stock. Both granite and metamorphic rock are intensely altered locally to mica-quartz greisen; related high-temperature veins consisting largely of quartz, muscovite, and beryl are enclosed in greisenized rock and cut adjacent granite and metamorphic rock.

The greisen in the Lake George district is generally a gray granular rock consisting of muscovite that is predominantly dark gray but locally yellow, dispersed as

557753 O—60——6

single crystals or clots of crystals in granular quartz. The relative amounts of quartz and muscovite in the normal greisen vary, but the granular texture and spangled gray color of the rock make it conspicuous wherever it is exposed. Fluorite is present in almost all of the greisen, and topaz is abundant locally. The greisen contains pyrite, sphalerite, molybdenite, wolframite, galena, chalcopyrite, arsenopyrite, sooty pitchblende, and bertrandite, but these are generally scarce and irregularly distributed; locally, however, one or more of them constitutes several percent of the rock.

The high-temperature veinlike deposits, generally beryl bearing, are not uniform in appearance or composition. They range in character from poorly defined, highly altered complex veins within strongly greisenized zones to small simple quartz-beryl veins in unaltered granite or metamorphic rock. Most of the beryl ore produced from the mine has come from the veinlike deposits in greisen, near contacts between granite and metamorphic rocks. The beryl ore consists largely of intergrown green and white beryl crystals with interstitial quartz and muscovite. Locally the beryl-bearing rock has been highly altered, and contains bertrandite, and possibly some hitherto unidentified beryllium minerals, in association with abundant yellow muscovite.

Bertrandite-bearing greisen is a local variant of normal greisen in the Lake George district, and in at least one place it is sufficiently abundant to be ore. This is at the Boomer mine, in a small granite stock, and such rock occurs in at least one of several pipes in Redskin Gulch in the main Pikes Peak granite batholith, several miles to the east.

Bertrandite in greisen is an inconspicuous mineral, hard to distinguish from feldspar or stained quartz in hand specimens, and much of the bertrandite-bearing greisen closely resembles normal greisen. At the Boomer mine, however, the bertrandite-bearing greisen appears to contain more fine-grained yellow muscovite than normal greisen, and locally at least it can be distinguished by its lighter color. The contact between the darker gray and the paler yellowish greisen is commonly sharp but irregular. But yellow muscovite cannot be used as a general criterion for bertrandite-bearing greisen, for it is a minor but widespread constituent of barren greisen as well. The bertrandite in the greisen forms pale flesh-colored crystalline aggregates and rounded grains evenly distributed through the rock; it is about equal in abundance to quartz and to muscovite. Fluorite appears to be more abundant in the bertrandite-bearing greisen at the Boomer mine than in the normal greisen. The bertrandite-bearing greisen in the Redskin Gulch pipe appears, from a brief preliminary study, to be similar to that at the Boomer deposit.

Bertrandite appears to be an original component of the greisen in which it occurs. Quartz and bertrandite form subhedral crystals and granular aggregates that show no replacement relations.

Greisen is associated with many granitic intrusive masses throughout the world. It is particularly common in Australia and Russia; other well-known occurrences are in England, France, China, and Egypt. In most of the major localities, greisen and associated high-temperature veins contain significant amounts of tin, tungsten, and molybdenum, which in places are sufficiently abundant to make the rock an ore. Beryl has been reported in many areas of greisenized rocks, and beryllium may be a more common constituent of these rocks than has heretofore been recognized, for beryllium was not given much attention before its recent increase in economic importance, and was rarely included in analyses. Beryl itself may occur in greisen in areas other than the Lake George district without having been recognized, and the same thing is even more likely to be true of the rarer mineral bertrandite.

Since known occurrences of bertrandite-bearing greisen in the Lake George district are associated with the Pikes Peak granite batholith, either in its peripheral zone or in an outlying stock, other, undiscovered areas of greisenized rock probably occur along the periphery, and perhaps deeper within the batholith. A general reconnaissance of the Pikes Peak granite and adjacent rocks might therefore reveal other beryllium deposits.

REFERENCE

Vaughn, W. W., Wilson, E. E., and Ohm, J. M., 1960, Instrument for quantitative determination of beryllium by activation analysis: U.S. Geol. Survey Circ. 427.

GEOLOGY OF FUELS

36. REGIONAL AEROMAGNETIC SURVEYS OF POSSIBLE PETROLEUM PROVINCES IN ALASKA

By Isidore Zietz, G. E. Andreasen, and Arthur Grantz, Washington, D.C., Washington, D.C., and Menlo Park, Calif.

The U.S. Geological Survey has conducted numerous regional aeromagnetic surveys to help evaluate some of the possible petroleum provinces in Alaska. Figure 36.1 shows the areas which have been surveyed for this purpose. Because most of the work was of a reconnaissance nature the results have been compiled in the form of "nested" profiles except for the Copper River basin, Kvichak Bay lowland, and on the Arctic slope, where close flight spacing permitted contouring of the data. The aeromagnetic data on which the interpretation discussed in this report is based have been placed on open-file or published (Andreasen, Dempsey, and Henderson, 1958a, 1958b; Andreasen, Dempsey, and Vargo, 1958; Andreasen, 1960; Dempsey and others, 1957; Keller and Henderson, 1947; Meuschke and others, 1957; Zietz and others, 1959).

Surveys were flown in areas known to be underlain by sedimentary rocks to provide information about the thickness of these rocks and their extent into unmapped or covered areas. Tracts of low, flat terrain covered by surficial deposits or water, where there is little geologic information, were also investigated to determine if they are underlain by significant thicknesses of nonmagnetic (possibly sedimentary) rocks.

The geologic structure of most areas in Alaska is complex, with much folding and faulting. In many places magnetic igneous rocks, both intrusive and extrusive, occur within the sedimentary rocks. As a consequence, the interpretation of aeromagnetic data is difficult and must be considered in terms of detailed local geologic information. Where the sedimentary rocks rest on nonmagnetic basement rocks, interpretations based upon the aeromagnetic data are ambiguous.

In many of the areas of flat terrain, magnetic rocks were found to be near the surface. Such areas include the Yukon and Susitna flats, Galena, Middle and Upper Tanana, and Selawik lowlands, the northern half of the Copper River Basin, and Norton Sound. It is believed that these areas are underlain at shallow depths by rocks similar to the partly magnetic formations that crop out in adjacent areas.

Evaluation of geologic and aeromagnetic data indicate that significant thicknesses of sedimentary rocks occur in several areas. For example, large areas of Cook Inlet and the Kenai lowland are underlain by sedimentary rocks 3 to 4 miles thick, and a thick sedimentary section is indicated in the Kvichak Bay and Kandik areas.

Analysis of magnetic data suggests that much of the southern Copper River basin is underlain by a thick section of nonmagnetic, possibly sedimentary rock. Thick masses of sedimentary rocks underlie the Yukon-Kuskokwim delta; these are overlain in places by lavas of late Cenozoic age.

A sedimentary basin has been outlined in the Koyukuk area east of the Seward Peninsula and west of Koyukuk Flats (Zietz and others, 1959). The basin is elliptical in shape, extends in a northeasterly direction and is about 80 miles wide. The basin is bounded on the east by the Yukon and Koyukuk Rivers, on the west and north by the edge of the exposed volcanic rocks, and it extends at least as far south as 64°30′ N. Depths to magnetic basement range from 3 to 5 miles.

In the Arctic slope area, magnetic basement deepens to the south from Point Barrow about to the Colville River, where depths of more than 5 miles are indicated. However, at several places along the Colville River, depths become much shallower (2 to 3 miles). Magnetic basement is also relatively shallow (2 to 3 miles) to the east in the neighborhood of the Anaktuvuk and Kuparuk Rivers between the latitudes of 69° N. and 70° N.

REFERENCES

Andreasen, G. E., 1960, Total intensity aeromagnetic profiles for parts of the Kobuk and Minchumina areas, Alaska: U.S. Geol. Survey open-file reports, 8 sheets.

Andreasen, G. E., Dempsey, W. J., Henderson, J. R., and Gilchrist, F. P., 1958a, Aeromagnetic map of the Copper River basin, Alaska: U.S. Geol. Survey Geophys. Inv. Map GP–156.

Andreasen, G. E., Dempsey, W. J., and Henderson, J. R., 1958b, Aeromagnetic map of part of the Dillingham quadrangle, Alaska: U.S. Geol. Survey open-file report, 1 map.

Andreasen, G. E., Dempsey, W. J., and Vargo, J. L., 1958, Aeromagnetic map of parts of the Ugashik, Karluk, and Naknek quadrangles, Alaska: U.S. Geol. Survey open-file report, 2 maps.

Dempsey, W. J., Meuschke, J. L., and Andreasen, G. E., 1957, Total intensity aeromagnetic profiles of Bethel Basin, Hogatza uplift, West Hogatza, Koyukuk, Alaska: U.S. Geol. Survey open-file reports, 7 sheets.

Keller, F., and Henderson, J. R., 1947, Aeromagnetic survey of Naval Petroleum Reserve No. 4 and adjacent areas, Alaska: U.S. Geol. Survey open-file report, 16 p., 1 map, 11 figs.

Meuschke, J. L., Henderson, J. R., and Dempsey, W. J., 1957, Total intensity aeromagnetic profiles of Cook Inlet, Alaska: U.S. Geol. Survey open-file report, 2 sheets.

Zietz, Isidore, Patton, W. W., and Dempsey, W. J., 1959 Preliminary interpretation of total intensity aeromagnetic profiles of the Koyukuk area, Alaska: U.S. Geol. Survey open-file report, 6 p., 7 figs.

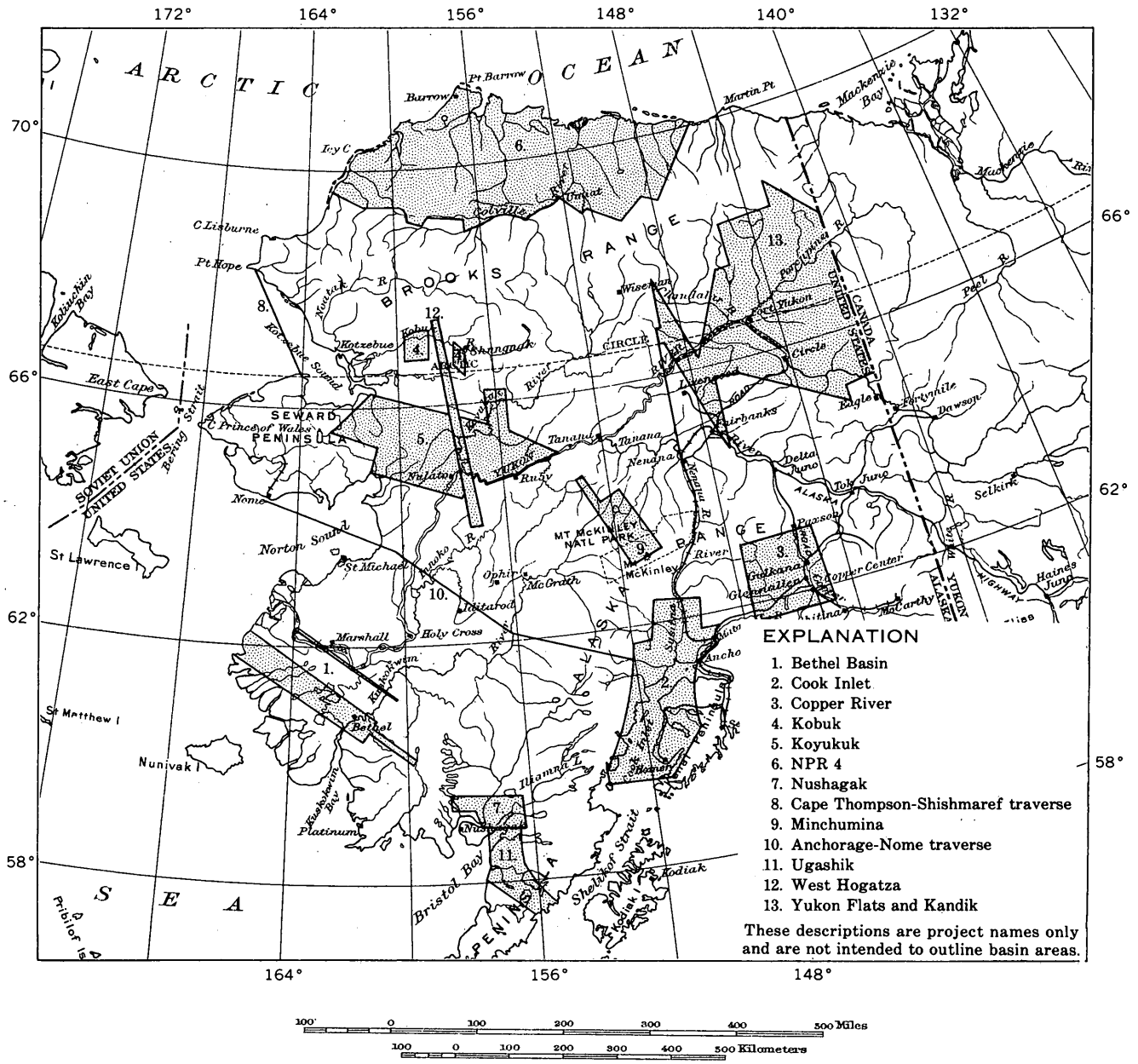

FIGURE 36.1.—Index map of Alaska showing location of aeromagnetic surveys over some possible petroleum provinces.

37. STUDIES OF HELIUM AND ASSOCIATED NATURAL GASES

By ARTHUR P. PIERCE, Denver, Colo.

Work done in cooperation with the U.S. Atomic Energy Commission

Few geologic studies have been made of helium in natural gases since that of Rogers (1921). Since then, a large body of analytical data has accumulated regarding the helium content of natural gases in the United States as the result of the helium surveys made by the U.S. Bureau of Mines (Anderson and Hinson, 1951; Boone, 1958). These data show that some helium is present in all gas fields. Also, the helium content of the gas fields tends to increase systematically with the geologic age of the reservoir rock (fig. 37.1), as would be expected if the helium were derived from slow decay of uranium and thorium inherent in rocks. Calculations, however, show that the reservoir rocks of the average gas field would have to contain about 0.03 percent uranium in order to generate the helium that is present in them. This is about one hundred times the uranium content of most sedimentary rocks and raises a serious question as to the origin of the helium.

As the hydrocarbons in natural gas fields are almost certainly derived from surrounding sedimentary source rocks, it is probable that at least part of the helium was derived from decay of uranium and thorium in the same rocks. In general such source rocks are saturated with water and are at structurally lower elevations than the gas fields they supply. If it is assumed that the radiogenic helium in these rocks can migrate into a gas field at a rate that is rapid enough to maintain an equilibrium concentration, then the partial pressure of helium in the gas reservoirs can be calculated from Henry's Law:

$$P_{He}=Kx$$

where P_{He} is the partial pressure of helium in the gas field, K is an equilibrium constant, and x is the mole fraction of helium in the pore waters of the source rock. x can be computed from radioactivity laws and rock properties. Doing this, the entire expression becomes:

$$P_{He}=KUf\left[8(e^{lt}-l)+7R'(e^{l't}-l)+6R''(e^{l''t}-l)\right]\frac{d}{w}$$

where U is the uranium content of the source rock in moles per gram of rock; f is the fraction of radiogenic helium escaping into the effective porosity; l, l' and l'' are the decay rates of U-238, U-236, and Th-232, respectively: R' is the present ratio of U-235 to U-238; R'' is the present ratio of Th-232 to U-238 in the rock; d is the rock density; t is the age of the rock; and w is the water content in moles per cubic centimeter of rock as calculated from the rock porosity (water saturated). For water at the temperatures in the usual sedimentary rock K is about 1.9×10^6 psia.

From the above expression we can calculate the partial pressure of helium as a function of the age of the rock. On the conservative assumptions that the average gas source rock has a uranium content of 3 ppm, a thorium to uranium ratio of 3.6, a density of 2.4 g/cc, 13 percent porosity, and retains 50 percent of its radiogenic helium as estimated by Hurley (1954), the helium partial pressure in a gas field in typical sedimentary rocks will increase at a rate of about 0.9 psi every 100 million years. As actual gas fields do not retain all the helium migrating into them, this estimate represents an upper limit. Even the most retentive gas fields will lose some helium due to diffusion. The available data on diffusion of helium, however, suggest that its diffusivity through impermeable rocks, such as the cap rocks of a gas field, is at least an order of magnitude less than its diffusivity through water. This would allow the helium partial pressures in gas fields with impermeable cap rocks to become quite close to those calculated from Henry's Law. Thus, gas fields in rocks of Tertiary age (1 to 60 million years) should have up to about 0.5 psi helium, gases in rocks of Mesozoic age (60 to 200 million years) should contain up to about 2 psi, and gases in rocks of Paleozoic age (200 to 600 million years) should contain up to about 5 psi helium. Comparison of these estimates with observed helium partial pressures in gas fields of different ages (fig. 37.1) indicates that the helium present in most gas fields has probably been derived from decay of trace amounts of uranium and thorium in the surrounding rocks.

Although the explanation just given will account for the helium present in most gas fields, there are some significant exceptions. Cambrian and Ordovician gas fields of the Central Kansas uplift contain from 10 to 60 psi helium. Most of these gas fields occur in folded rocks underlying a major unconformity. Rocks of Devonian and Mississippian age, including the uranif-

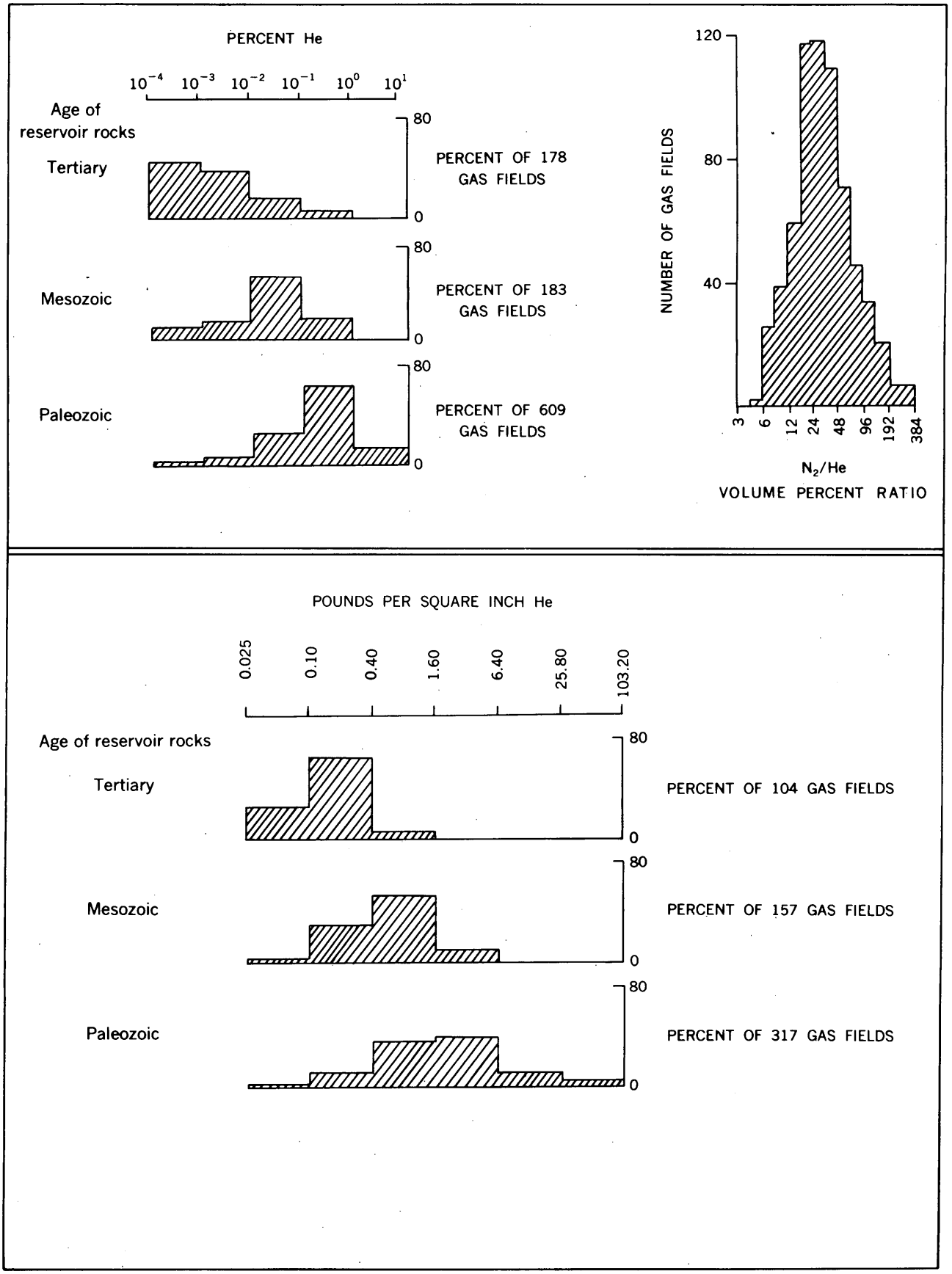

FIGURE 37.1.—Helium percentages, partial pressures, and nitrogen to helium ratios in gas fields of the United States.

erous Chattanooga shale, have been removed and truncated by erosion, and cap rocks of Pennsylvanian age were deposited over the top of the uplift. At least two possible sources exist for the helium in this area: (a) the underlying basement rocks, which should have a large helium content because of their great age; and (b) the truncated uraniferous Chattanooga shale from which the helium could have migrated laterally into the gas fields.

Other gas fields in which high helium partial pressures may be related to source rocks that are enriched in uranium are the Panhandle field, Texas, and the Harley Dome, Utah. In the Panhandle field reservoir rocks containing the highest partial pressures of helium (about 9 psi) are faulted against possible helium source rocks that are unusually radioactive and contain uraniferous asphaltite over large areas. In the Harley Dome, gases with an abnormal helium partial pressure (11 psi) occur in the Morrison formation, which is a significant host-rock for uranium deposits in nearby areas.

The highest helium partial pressure (about 240 psi) among gas fields of the United States occurs in the Rattlesnake field, New Mexico. No satisfactory explanation is known for the origin of the helium in this field. The high partial pressure may be related to the occurrence of the gas field in an area of abnormal geothermal gradients.

Nitrogen is intimately associated with helium in natural gases and its origin has never been well understood. Unusually high concentrations of nitrogen that are present in gases from mineral springs and in some shallow gas fields evidently represent dissolved air from circulating ground waters. In other gases, particularly helium-rich gases, the amount of nitrogen tends to increase with the age of the reservoir rock at a rate similar to the increase in helium. Much of this nitrogen may originate from slow decomposition of nitrogenous organic compounds, such as chitin, porphyrins, and amino acids, present in sedimentary rocks. Studies by Abelson (1959) indicate that the decomposition rates of such nitrogenous compounds are extremely slow under natural conditions, and in the case of some amino acids, may be of the same order of magnitude as the decay rates of uranium and thorium. This suggests that the parallel enrichment of nitrogen with helium in natural gases could be related to its derivation from such substances. The mean ratio of nitrogen to helium in natural gases is about 30 (fig. 37.1), and if the two gases are assumed to be derived from a typical source rock (3 ppm U, 11 ppm Th) would require the decomposition of about 3 ppm organic nitrogen from the rock every 100 million years, or about 20 ppm since the beginning of Cambrian time. This is considerably less than the organic nitrogen content of modern marine sediments (about 0.04 percent organic nitrogen). Such a source of nitrogen is, therefore, feasible.

REFERENCES

Abelson, P. H., 1959, Researches in geochemistry: New York, John Wiley and Sons, Inc., 511 p.

Anderson, C. C., and Hinson, H. A., 1951, Helium-bearing natural gases of the United States: U.S. Bur. Mines Bull. 486.

Boone, W. J., Jr., 1958, Helium-bearing natural gases of the United States: U.S. Bur. Mines Bull. 576.

Hurley, P. M., 1954, The helium age method and the distribution and migration of helium in rocks, *in* Nuclear geology (Henry Faul, editor), New York, John Wiley & Sons, Inc., p. 301–328.

Rogers, G. S., 1921, Helium-bearing natural gas: U.S. Geol. Survey Prof. Paper 121, 113 p.

38. THE INTERPRETATION OF TERTIARY SWAMP TYPES IN BROWN COAL

By Gerhard O. W. Kremp and Anton J. Kovar, Denver, Colo., and Pennsylvania State University, University Park, Pa.

Intensive palynological investigations of brown coal of early Miocene age from the Lower Rhine Basin in Germany made it possible for Thomson (1950) to recognize nine different pollen florules, indicating nine different ancient swamp types, within a seam that reaches a thickness of 300 feet (see table below). This helped decisively in solving some of the problems relating to coal seam correlation in the area (Rein, 1952). Plant associations similar to those he recognized were later recognized in many other lignites, and the distinctions between various types of fossil swamps were applied to the study of bituminous coals. This line of thinking also led to a better understanding of the petrography of various substances found in coal seams

(Teichmüller, 1950; Teichmüller and Thomson, 1958) and aided in solving problems of fuel technology (Pflug, 1957).

Fossil swamp types of the Rheinische Brown Coal, and their dependence on frequency of flooding

[According to P. W. Thomson, 1956, p. 67, fig. 1]

Frequency of flooding	Light-colored sediment	Dark-colored sediment
Seldom flooded, mostly dry.	Coal of ombrogenous swamps.	Coal of stump horizons (cf. *Sequoia*) with fusinite (forest fires).
Periodically flooded.	Coal of ± oligotrophic forest swamps.	Coal of forest swamps with many pines and palms (cf. *Sabal*). Coal of forest swamps with many Myricaceae–Betulaceae.
	Coal of sedge swamps (cf. *Cyperaceae*), treeless, and at the base with secondary allochthony (the "light layers" of Wölk, 1935).	Coal of forest swamps with many Taxodiaceae (*Glyptostrobus*, etc.) and *Nyssa*.
Always under water.	Gyttja, rich in clay--	Dy-gyttja.

After an extensive survey of the literature, Thomson concluded that the modern plant associations most closely related to the nine swamp types that he recognized were to be found in the southeastern part of the United States, especially in Florida. Our own field studies in the swamps of this region, however, indicate that Thomson's comparisons should be altered in some respect for the following swamp types:

1. "Treeless sedge swamps." It would appear that the plant associations characterizing the light layers of the Rheinische Brown Coal, though usually compared with those in the Everglades of Florida (Teichmüller, 1958), are not yet completely understood.

   Weyland (1958, p. 530) remarks that to judge from the records, remains of Cyperaceae and Gramineae are strikingly scarce in the Brown Coal, and Neuy-Stolz (1958) states that Cyperaceae pollen has not been definitely identified, and that pollen which might belong to the Gramineae has very seldom been recorded. The lack of recorded occurrences of these pollen has been explained on the assumption that the pollen as well as the leaves of the Glumiflorae are not preserved. But we found pollen of Cyperaceae and Gramineae in appreciable amounts in the sediments of the Everglades. These types of pollen are also reported in abundance from many Pleistocene localities; we are unaware, however, of any record of their being found in abundance in lower and middle Tertiary sediments. Since most pollen is generally well preserved in the Brown Coal, it seems unlikely that just the pollen mentioned above should have been destroyed by fossilization processes. It is more probable that extensive sedge and grass swamps did not exist in middle Tertiary time.

   Furthermore, quercoid pollen, which is very rare in the Everglades, dominates the light layers of the Brown Coal—e.g. *Quercoidites microhenrici* (Potonié, 1931), *Quercuspollenites henrici* (Potonié, 1931). Thomson supposed that these pollen were blown into the Tertiary swamps of Germany from nearby forests. It is possible, however, that many oaklike species able to grow in swamps existed during the Tertiary. Oaks are actually growing today in the southeastern swamps of the United States—e.g. *Quercus michauxii* Nuttall.
2. "Forest swamps with many Myricaceae-Betulaceae." Although *Myrica* and also Betulaceae are found in Florida today, they do not form extensive swamp vegetation, whose occurrence in many lower and middle Tertiary coals has been recorded by palynologists. Current observations favor the conclusions of Gladkova (1956), who states that more species of *Myrica* must have existed throughout early Tertiary time than exist at present. This would mean that the Myricaceae-Betulaceae-forest swamp types of the Tertiary cannot be compared with modern equivalents, simply because most of the Tertiary species of *Myrica* are now probably extinct.
3. "Ombrogenous swamp types." The relative abundance of *Sphagnum* spores and Ericacea pollen in certain coal layers of the Rhine valley does not necessarily indicate a "humid-lusitanic" climate as Thomson (1952) has suggested. Swamp plant associations in which *Sphagnum* is important also exist in the Okefenokee Swamp and elsewhere in Florida. These swamps, however, do not represent highmoors or other ombrogenous swamp types.
4. The "forest swamp types with much pine or palm pollen" may represent only bordering zones of other swamp types in which a large percentage of the pine or palm pollen they contain is blown in from drier areas.

5. The "cf. Sequoia-forest swamp type" may to a certain degree be best compared with modern cypress heads and dense, swampy cypress forests.

REFERENCES

Gladkova, A. N., 1956, The pollen of some contemporary and fossilized species of the genus *Myrica* L. (in Russian): Akad. Nauk SSSR Doklady, v. 109, no. 1, p. 213–216, 3 figs.

Neuy-Stolz, G., 1958, Zur Flora der Niederrheinischen Bucht während der Hauptflözbildung unter besondere Berücksichtigung der Pollen und Pilzreste in den hellen Schichten: Fortschr. Geol. Rheinland u. Westfalen, v. 2, p. 503–525, 7 pls., 2 figs.

Pflug, Hans, 1957, Die Untersuchung von Flözprofilen aus dem Nordrevier der rheinischen Braunkohle auf ihre Brikettiereigenschaften: Freiberger Forschungshefte, v. A 64, p. 1–68, 35 figs.

Rein, U., 1952, Die palynologische Flözfeinstratigraphie im Braunkohlenbergbau: Internat. Geol. Cong., 19th, Algiers 1952, Comptes rendus, sec. 12, p. 143–171.

Thomson, P. W., 1950, Grundsätzliches zur tertiären Pollen- und Sporenmikrostratigraphie auf Grund einer Untersuchung des Hauptflözes der rheinischen Braunkohle in Liblar, Neurath, Fortuna, und Brühl: Geol. Jahrb., v. 65, p. 113–126. [1951].

Thomson, P. W., 1952, Ombrogene Moorbildungen in der rheinischen Braunkohle: Deutsche geol. Gesell. Zeitschr. Jahrg. 1952, v. 104, p. 159.

——— 1956, Die Braunkohlenmoore des jüngeren Tertiärs und ihre Ablagerungen: Geol. Rundschau, v. 45, no. 1, p. 62–70.

Teichmüller, Marlies, 1950, Zum petrographischen Aufbau und Werdegang der Weichbraunkohle (mit Berücksichtigung genetischer Fragen der Steinkohlenpetrographie): Geol. Jahrb., v. 64, p. 429–488, 6 pls., 1 tab., 5 text figs.

——— 1958, Rekonstruktionen verschiedener Moortypen des Hauptflözes der niederrheinischen Braunkohle: Fortschr. Geol. Rheinland u. Westfalen, v. 2, p. 599–612, 3 pls., 5 figs.

Teichmüller, Marlies, and Thomson, P. W., 1958, Vergleichende mikroskopische und chemische Untersuchung der wichtigsten Fazies-Typen im Hauptflöz der niederrheinischen Braunkohle: Fortschr. Geol. Rheinland u. Westfalen, v. 2, p. 573–598, 4 pls., 3 figs., 5 tab.

Weyland, H., 1958, Die Monocotylen des "Hauptflözes" der Ville: Fortschr. Geol. Rheinland u. Westfalen, v. 2, p. 527–538.

Wölk, E., 1935, Mächtigkeit, Gliederung und Entstehung des niederrheinischen Hauptbraunkohlenflözes: Ber über die Vers. d. Niederrhein. Geol. Vereinigung, v. 28, p. 81–163, Bonn.

39. COAL RESERVES OF THE UNITED STATES, JANUARY 1, 1960

By Paul Averitt, Denver, Colo.

The coal reserves of the United States remaining in the ground on January 1, 1960, totaled 1,660,290 million tons, as shown in the accompanying table. The recoverable reserves totaled 830,145 million tons, based on the assumption that half of the coal in the ground will be lost in mining and half will be recovered.

The new totals are based on detailed, classified estimates in 14 States and provisional estimates in 5 States prepared since 1947 by the U.S. Geological Survey; on classified estimates in 7 States prepared by State geological surveys; and on older and incompletely documented estimates for the remaining States. The 26 States for which modern estimates have been prepared include about 90 percent of the total coal reserves of the United States as currently estimated.

The information in the table was taken from the following sources:

Averitt, Paul, Berryhill, L. R., and Taylor, D. A., 1953, Coal resources of the United States (A progress report, October 1, 1953): U.S. Geol. Survey Circ. 293, 49 p., [1954].

Barnes, F. F., Alaska coal reserves, written communication, 1959.

Brant, R. A., and DeLong, R. M., Coal resources of Ohio: Ohio Div. Geol. Survey Bull. 58 (in press).

Culbertson, W. C., Coal resources of Alabama, written communication, 1960.

Haley, B. R., 1960, Coal resources of Arkansas: U.S. Geol. Survey Bull. 1072–P.

Huddle, J. W., and others, Coal resources of eastern Kentucky, written communication, 1960.

Landis, E. R., 1959, Coal resources of Colorado: U.S. Geol. Survey Bull. 1072–C, p. 131–232.

Luther, E. T., 1959, The coal reserves of Tennessee: Tennessee Div. Geology Bull. 63, 294 p.

Mason, R. S., and Erwin, M. I., 1955, Coal resources of Oregon: U.S. Geol. Survey Circ. 362, 7 p.

Perkins, J. M., and Lonsdale, J. T., 1955, Mineral resources of the Texas coastal plain, a report for Bureau of Reclamation, Dept. of the Interior: Texas Univ., Bur. of Econ. Geology, p. 28–36.

Trumbull, J. V. A., 1957, Coal resources of Oklahoma: U.S. Geol. Survey Bull. 1042–J, p. 307–382.

TABLE 39.1.—*Coal reserves of the United States, Jan. 1, 1960, by States*

(In millions of short tons)

State	Date of publication of estimate	Estimated original reserves				Total	Reserves depleted to Jan. 1, 1960		Remaining reserves Jan. 1, 1960	Recoverable reserves, Jan. 1, 1960, assuming 50 percent recovery
		Bituminous coal	Subbituminous coal	Lignite	Anthracite and semi-anthracite		Production [1]	Production plus loss in mining [2]		
ALABAMA [3]	(4)	[5] 13,754		20		[5] 13,774	[6] 23	[6] 46	13,728	6,864
ALASKA	(7)	21,401	[8] 71,136	([8])	2,101	94,638	13	26	94,612	47,306
ARKANSAS	(4)	1,816		350	456	2,622	99	198	2,424	1,212
COLORADO	1959	63,203	18,492		90	81,785	506	1,012	80,773	40,387
GEORGIA	1953	100				100	12	24	76	38
ILLINOIS	1953	[9] 137,329				[9] 137,329	[10] 474	[10] 948	136,381	68,190
INDIANA	1953	37,293				37,293	1,148	2,296	34,997	17,499
Iowa [11]	1909	29,160				29,160	357	714	28,446	14,223
KANSAS	B-1951 L-1952	[9] 20,774		([12])		[9] 20,774	[10] 13	[10] 26	20,748	10,374
KENTUCKY	(4)	72,318				72,318	2,646	5,292	67,026	33,513
MARYLAND	1953	[9] 1,200				[9] 1,200	[10] 6	[10] 12	1,188	594
MICHIGAN	1950	297				297	46	92	205	102
Missouri	1913	79,362				79,362	287	574	78,788	39,394
MONTANA	1949	2,363	132,151	87,533		222,047	171	342	221,705	110,853
NEW MEXICO	1950	10,948	50,801		6	61,755	125	250	61,505	30,753
NORTH CAROLINA	1955	112				112	1	2	110	55
NORTH DAKOTA	1953			350,910		350,910	96	192	350,718	175,359
OHIO	(4)	46,488				46,488	2,052	4,104	42,384	21,192
OKLAHOMA	1957	3,673		([12])		3,673	180	360	3,313	1,656
OREGON	1955	20	180			200	3	6	194	97
PENNSYLVANIA	B-1928 A-1945	75,093			22,805	97,898	13,508	27,016	70,882	35,441
SOUTH DAKOTA	1952			2,033		2,033	1	2	2,031	1,015
TENNESSEE	1959	[13] 1,912				[13] 1,912	[14] 6	[14] 12	1,900	950
Texas [15]	B-1909 L-1955	8,000		7,070		15,070	95	190	14,880	7,440
UTAH	(7)	28,222	156			28,378	260	520	27,858	13,929
VIRGINIA	1952	11,696			355	12,051	782	1,564	10,487	5,244
Washington	1929	11,413	[8] 52,442	([8])	23	63,878	149	298	63,580	31,790
WEST VIRGINIA	1940	116,618				116,618	6,369	12,738	103,880	51,940
WYOMING	1950	13,235	[8] 108,319	([8])		121,554	402	804	120,750	60,375
Other States		[16] 620	[17] 4,065	[18] 50		4,735	7	14	4,721	2,360
Total		808,420	437,742	447,966	25,836	1,719,964	[19] 29,837	59,674	1,660,290	830,145

[1] Production, 1800 through 1885, from "The first century and a quarter of American coal industry," by H. N. Eavenson, privately printed, Pittsburgh, 1942; production, 1886 through 1923, from U.S. Geol. Survey Mineral Resources, annual volumes; production, 1924 through 1957, from U.S. Bureau of Mines Mineral Resources (1924–31) and Minerals Yearbook (1932–57), annual volumes, augmented for some States by records of State mine inspectors; production, 1958, from U.S. Bureau of Mines, Mineral Market Summary No. 2974, Sept. 9, 1959; production, 1959, from U.S. Bureau of Mines weekly coal reports and partly estimated.

[2] Assuming past losses equal past production.

[3] Reserve estimates of States in capital letters supersede estimates prepared by or under the direction of M. R. Campbell prior to 1928.

[4] New estimate from report in preparation or in press. See text.

[5] Remaining reserves, Jan. 1, 1958.

[6] Production 1958 and 1959 only.

[7] New estimate presented for first time in this report.

[8] Small reserves and production of lignite included under subbituminous coal.

[9] Remaining reserves, Jan. 1, 1950.

[10] Production 1950 through 1959.

[11] Reserve estimates of States in lower case letters were prepared by or under the direction of M. R. Campbell prior to 1928.

[12] Small reserves of lignite in beds generally less than 30 inches thick.

[13] Remaining reserves, Jan. 1, 1959.

[14] Estimated production 1959 only.

[15] New estimate of lignite reserves; Campbell estimate of bituminous coal reserves.

[16] ARIZONA, CALIFORNIA, Idaho, Nebraska, and Nevada.

[17] ARIZONA, CALIFORNIA, and Idaho.

[18] CALIFORNIA, Idaho, Louisiana, and Nevada.

[19] Less than total recorded production of about 34.8 billion tons. See footnotes 5, 6, 9, 10, 13, and 14.

40. RELATION OF THE MINOR ELEMENT CONTENT OF COAL TO POSSIBLE SOURCE ROCKS

By PETER ZUBOVIC, TAISIA STADNICHENKO, and NOLA B. SHEFFEY, Washington, D.C.

As denudation of an area proceeds, progressively older and more deep-seated rocks become exposed. It was therefore thought possible, since the coals of the Eastern Interior region represent a long period of sedimentation, that the minor-element content of specimens of these coals would reflect differences in the rocks that were being eroded at successive periods while the coal was being formed.

It is reasonable to assume that during the weathering of rocks, the material transported to the depositional sites reflects changes in the character of the rocks being weathered, and that during the periods when coal was being formed, the amounts of minor elements accumulated by the coal would depend upon the amounts of these elements being brought into the swamp. It is also reasonable to assume that the amounts of the elements in solution that form stable organic complexes would depend upon the amounts of those elements being brought into the swamp, and that the elements would be almost completely extracted by the coal from the

TABLE 40.1.—*Distribution of 46 bed samples of coal*

[Beds are arranged in their stratigraphic order]

Group	Beds	Illinois	Indiana	Kentucky	Total
McLeansboro	No. 7 (Ill.)=VI (Ind.)	2	1		3
	No. 14 (Ky.)			2	2
Carbondale	No. 6 (Ill.)=VI (Ind.)=No. 11 (Ky.)	7	2	1	10
	No. 5 (Ill.)=V (Ind.)=No. 9 (Ky.)	8	1	9	18
	No. 2 (Ill.)	2			2
Tradewater	III (Ind.)		1		1
	DeKoven (Ill.)	1			1
	Davis (Ill.)=No. 6 (Ky.)	1		1	2
	No. 1=(Murphysboro(?)) (Ill.)=Minshall (Ind.)	4		1	5
	L. Willis (Ill.)=L. Block (Ind.)	1	1		2
Totals		26	6	14	46

solutions entering the swamp. Most of the 15 elements looked for in these coals do form organic complexes having various degrees of solubility and stability.

The stratigraphic divisions in which the coals are grouped, and the correlation of the beds, are those used by Wanless and Siever (1956). The bed samples averaged for this comparison comprise 5 from the McLeansboro group, 30 from the Carbondale group, and 11 from the Tradewater group, a total of 46 bed samples representing 10 different coal beds. The distribution of the sampled coal among the different beds is shown in table 40.1.

Detailed analytical and geologic data will be published in a later report.

DISCUSSION OF THE DATA

During the differentiation of an igneous magma, certain elements, such as V, Cr, Co, Ni, and Cu, are generally associated with the earlier, more mafic differentiates. Later and more silicic differentiates are generally enriched in such elements as Be, B, Ga, Ge, Mo, Y, and La. The minerals consisting largely of the mafic elements are less stable and usually weather more rapidly than those consisting mainly of the silicic elements. Recycled sedimentary rocks, therefore, should contain smaller amounts of mafic elements released by weathering than sediments derived directly from the weathering and erosion of igneous materials. This is especially true of sediments of early pre-Paleozoic age. As boron is very high in these samples, only one-tenth of the boron is actually used in the summation in table 40.2, where the group Be+B/10+Ga+Ge+Mo+La+Y comprises the silicic elements and the group V+Cr+Co+Ni+Cu the mafic elements.

TABLE 40.2—*Average minor element content of the coals from three groups of the Pennsylvanian series of the Eastern Interior region*

[Parts per million in coal]

Group	Be	B	Tl	V	Cr	Co	Ni	Cu	Zn	Ga	Ge	Mo	Sn	Y	La
McLeansboro	3.2	112	510	33	23	5.4	18	10	14	5.2	12	3.9	5.3	9.4	3.1
Carbondale	2.0	107	440	39	20	2.7	14	12	56	3.9	13	4.8	1.1	6.3	3.5
Tradewater	3.2	66	400	22	16	6.3	15	9.3	28	3.7	11	2.3	.6	8.7	10.5

A summation of the figures in table 40.2 gives:

Group	Silicic elements (ppm in coal)	Mafic elements (ppm in coal)	Ratios (mafic to silicic)
McLeansboro	48	89.4	1.9
Carbondale	44.2	87.7	2.0
Tradewater	46	68.6	1.5

This summation shows that the quantity of silicic elements in the coal is nearly the same in the three groups. There is, however, an appreciable difference in the mafic elements, which are much less abundant in the Tradewater group than in the others. The ratios of mafic to silicic elements in the three groups are also significantly different. According to the theory of changing source rocks expressed above, the ratio in

the Carbondale coals should lie between those in the McLeansboro and the Tradewater coals, but in fact it is the highest of the three. The apparent discrepancy, however, is mainly due to the abnormally high vanadium content of some of the coals of bed 9 of western Kentucky. Nine samples from this bed average 70 ppm of vanadium, whereas eight samples from the same bed in Illinois average 25 ppm. Most of the vanadium in bed No. 9, in the area where it is so abundant, is in the extreme upper part of the bed. There is evidence, however, that the deposition of this coal was terminated in this area by a marine invasion, and it therefore seems possible that the anomalous vanadium was accumulated by marine organisms and thus incorporated in the uppermost part of the bed. If that is true, it should not be considered in making comparisons with the other coals. The ratio of the mafic to silicic elements is 1.7 for bed No. 6 in Illinois, and 1.6 for its correlatives in the other two States. For bed No. 5 in Illinois and its correlatives elsewhere, the ratio is 2.3. If, however, vanadium is excluded from the mafic group, the ratios are 1.2 and 1.1 for beds Nos. 6 and 5, respectively. This shows a great deal of similarity between the two beds.

A further degree of similarity is expressed by Co, Ni, and Cu, and by Y and La. The ratios of Co:Ni:Cu are 1:5.4:4.5 for bed No. 5, and 1:5.4:5 for bed No. 6. The ratio of Y to La is 1.6 for bed No. 5 and its correlatives; 1.7 for bed No. 6 and its correlatives. Not only are these ratios very close together, but the Be and Ge averages for the two beds are identical, and Ti, Cr, Mo, Y, and La differ by less than 25 percent. The differences are slightly higher for B, Co, Ni, Cu, and Ga.

From the above observations and discussions it may be seen that there is a similarity between the minor element content of beds Nos. 5 and 6 and that of their correlatives. It is also true that if the anomalous vanadium of bed No. 5 is discounted, the ratio for that bed (about 1.6) corresponds closely to that for bed No. 6 (about 1.7). With such a ratio for bed No. 5, the Carbondale group of beds bear out the assumption that the ratio of mafic to silicic elements should increase upward.

It is therefore almost certain that the changing minor element content of these coals reflects the progressive exposure and erosion of deeper seated rocks as Pennsylvanian sedimentation progressed. This conclusion accords with one expressed by Potter and Glass (1958, p. 52–53). They believe that in the earlier sedimentary history of the Eastern Interior basin, sedimentary rocks formed by repeated reworking of detritus from parental igneous rocks contributed most of the detritus to the basin, but that as Pennsylvanian sedimentation in the basin proceeded, crystalline rocks contributed an increasing proportion of detritus.

REFERENCES

Potter, P. E., and Glass, H. D., 1958, Petrology and sedimentation of the Pennsylvanian sediments in southern Illinois; a vertical profile: Illinois Geol. Survey Rept. Inv. no. 204, 60 p.

Wanless, H. R., and Siever, Raymond, 1956, Classification of the Pennsylvanian rocks of Illinois as of 1956: Illinois Geol. Survey circ. no. 217. 14 p.

41. THE ASSOCIATION OF SOME MINOR ELEMENTS WITH ORGANIC AND INORGANIC PHASES OF COAL

By Peter Zubovic, Taisia Stadnichenko, and Nola B. Sheffey, Washington, D.C.

In studying the minor elements contained in coal, it is worth while to estimate the degree to which each of the elements is associated with the organic and inorganic substances in the coal. Complete separation of organic and inorganic material is impossible, but a fair degree of separation can be achieved by relatively simple flotation procedures. Although most of the fractions in these separations consist predominantly of organic matter, there is less organic and more inorganic matter (ash) in the fractions of higher specific gravity. In the two-fraction separations, the float fractions contain about 2 to 4 percent inorganic matter (ash) and 96 to 98 percent organic matter, while the sink fractions contain about 20 to 30 percent ash and 70 to 80 percent organic matter. In multiple-fraction separations, the inorganic matter is more than 50 percent in the sink fractions, and the organic matter less than 50 percent. By comparing the recovery of each of the elements against the recovery of organic and inorganic matter in each of the fractions, it is possible to calculate the degree of association of the elements with either the organic or inorganic matter of the coal. In making

the calculation the organic matter is considered to be ashless and all the ash content of each of the separated fractions is included in the inorganic matter of that fraction. This procedure introduces a small error which can be ignored. A procedure similar to this was used by Horton and Aubrey (1950).

Thirteen samples of coal, 12 having a specific gravity of 1.32 and 1 a specific gravity of 1.36, were separated into float and sink fractions. Two samples were separated into 5 fractions and 1 sample into 3 fractions. The coals represent several different beds, and blocks taken from different parts of the beds. The recoveries of coal in the float fractions ranged from 10.6 percent to 92.7 percent. Figure 41.1 illustrates the method by which the degree of association with the organic phase of the coal was plotted for each of the 13 samples. This figure shows that 60 percent of the organic and 23 percent of the inorganic matter of the sample was recovered in the float fractions, while 90 percent of the organic and 77 percent of the inorganic matter was recovered in the sink fraction. Over 60 percent of the Be, B, Ge, and V was found in the float fraction, and less than 40 percent in the sink fraction. There is thus a correlation between these four elements and the organic matter. A similar correlation was found between Zn and La and the inorganic matter. The other elements have various degrees of correlation with the organic and inorganic matter. The dashed lines indicate divisions of 25, 50, and 75 percent correlation.

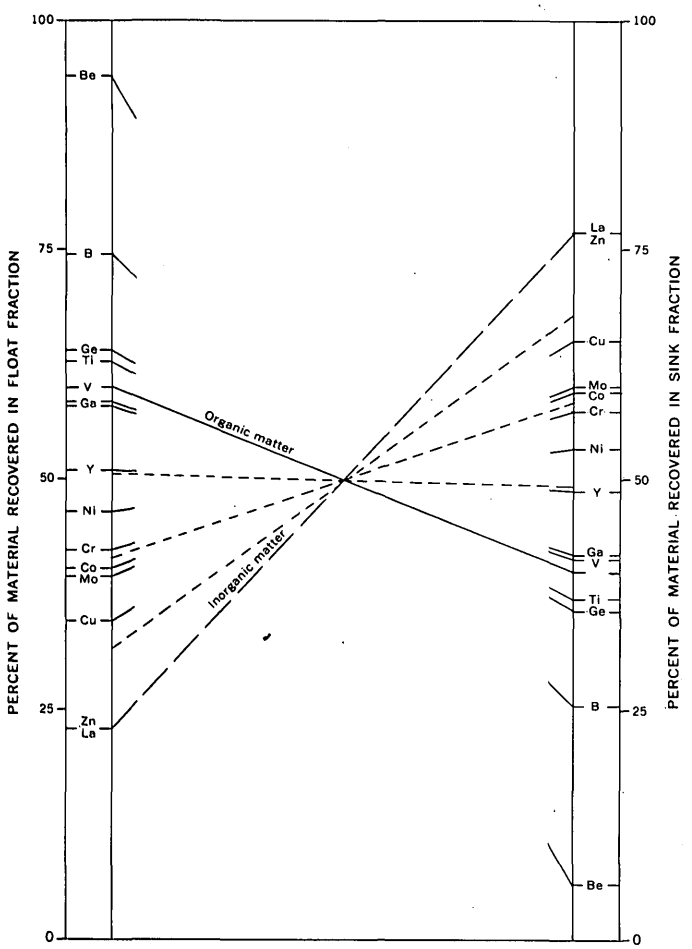

FIGURE 41.1.—Association of minor elements with the organic and inorganic fractions of coal; two-fraction separations. (Specific gravity of float media is 1.32.)

The data for the 13 samples are summarized in table 41.1. In several of the samples Zn, Sn, and La were below the limit of detection and could not be evaluated.

TABLE 41.1.—*Frequency of association of elements with the organic fractions*

[n.d.=not determined]

Element	Percent				Ranges for Horton and Aubrey (1950) (3 samples)
	100–75	75–50	50–25	25–0	
Be	8	3	1	1	75–100
B	8	2	2	1	75–100
Ti	8	3	1	1	>75–100
V	8	3	2	0	100
Cr	3	5	3	2	0–100
Co	2	5	5	1	>25–50
Ni	4	6	0	3	0–>75
Cu	1	3	3	6	25–50
Zn	0	0	0	7	0–<50
Ga	9	2	0	2	>75–100
Ge	10	2	0	1	100
Mo	1	5	3	4	50–75
Sn	1	1	1	6	0
Y	5	2	2	4	n.d.
La	0	0	0	10	n.d.

The order of decreasing association with organic matter as determined from the 13 two-fraction separations is: Ge, Ga, V, Be, Ti, B, Ni, Cr, Co, Y, Mo, Cu, Sn, Zn, and La. The first six of these elements are exactly the group of elements for which Horton and Aubrey (1950) showed the greatest degree of association with the organic matter of vitrains. The elements Cr, Ni, Zn, and Sn also show a correspondence to Horton and Aubrey's data. In their report, zinc and tin show a decided association with inorganic matter, and our results show that these two elements, and also lanthanum, are associated predominantly with the inorganic matter.

Curves were drawn for percentage recovery of organic and inorganic matter in each of the fractions of three multiple-fraction separations (fig. 41.2). Each element is treated as before, and the curves for the elements are compared with those for the organic and the inorganic matter. The degree of similarity between the curves for the elements and those for the organic or

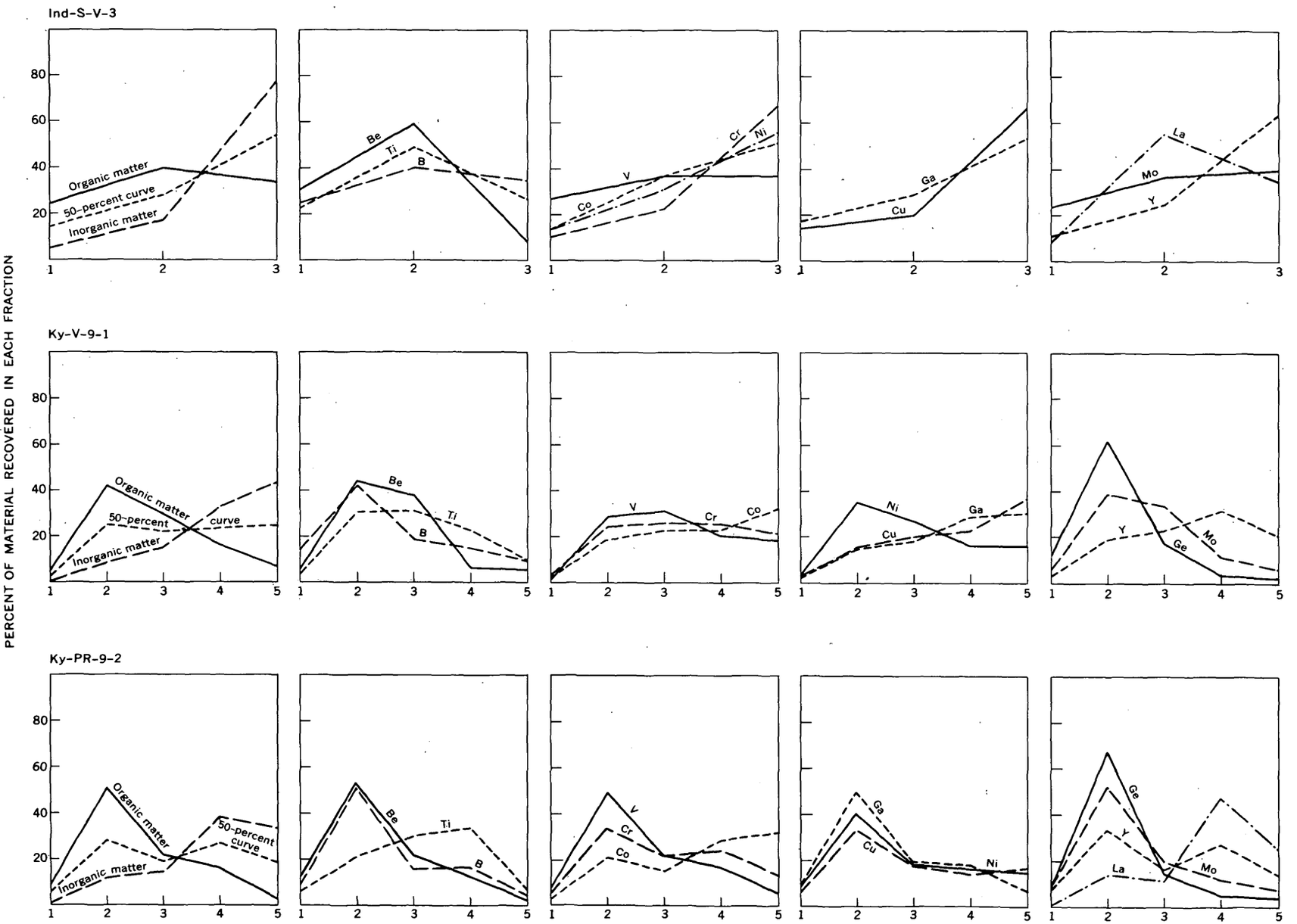

FIGURE 41.2.—Association of minor elements with the organic and inorganic fractions of coal: multiple-fraction separations. (In Ind–S–V–3, fractions 1, 2, and 3 are float on 1.24, 1.32, and sink on 1.32. In the other two samples, fractions 1, 2, 3, 4, and 5 are float on 1.28, 1.32, 1.36, 1.60, and sink on 1.60.)

inorganic fractions shows the degree of association of the element with either fraction.

In sample KY–PR–9–2 of figure 41.2, the elements Be, B, V, Ni, Ge, Mo, and Ga follow closely the patterns set by the distribution of the organic fraction, Ti, Co, Sn, and La have profiles similar to the inorganic fraction, while Cr, Cu, and Y are intermediate. In Ky–U–9–1, the elements Be, B, Ni, Ge, and Mo are predominantly associated with organic fraction, and Cu, Co, Ga, and Y with the inorganic, and Ti, V, and Cr are intermediate. In Ill–S–5–3, the elements Be, B, Ti, Mo, and La are associated with the organic fraction, Cr, Cu, Zn, and Y with the inorganic, while V, Ni, Co, Ga, and Sn are intermediate. These data indicate that certain elements are usually associated with either the organic or the inorganic matter; there are, however, some deviations from this general rule.

The data reveal several interesting relations between elements that are chemically similar, such as Ni and Co, V and Cr, and Y and La. Hirst and Nicholls (1958, p. 478–480) suggest an association of Ni and V with the nondetrital and of Co and Cr with the detrital portions of limestones. A similar association is shown by our data on coal: Ni and V are more closely associated with the organic or nondetrital fraction than Co and Cr, and Y shows a greater association with the organic fraction than La.

It is significant that the elements whose ions are small and highly charged are generally associated with the organic fractions. In this group are Be, B, Ti, V, and Ge, and to a lesser extent Ga. Elements, such as Zn, La, and Sn, consisting of large ions, are associated with the inorganic fraction of coal. We believe that Sn is reduced to the Sn^{+2} valence state in the reducing conditions of the coal swamp, thus putting it with the group consisting of large ions. Of the pairs of chemically similar elements, such as Co-Ni and Y-La, those with the smaller ions (Ni and Y) generally show a greater association with the organic fraction than those with larger ions (Co and La). It is generally known that large charge and a small ionic radius produce stable organic complexes.

Numerous other factors are involved in the accumulation of minor elements in coal; these include plant accumulation, the resistivity to weathering of certain minerals, post-depositional influences, and many others. One of the most important factors, however, is probably the formation of metallo-organic complexes, particularly at the time of coal deposition.

REFERENCES

Hirst, D. M., and Nicholls, G. D., 1958, Techniques in sedimentary geochemistry. (1) Separation of detrital and nondetrital fractions of limestones: Jour. Sed. Petrology, v. 28, no. 4, p. 468–482.

Horton, L., and Aubrey, K. V., 1950, The distribution of minor elements in vitrain: Three vitrains from the Barnsley seam: Soc. Chem. Industry Jour., v. 69, Supp. Issue 1, p. 541–548.

42. COMPARATIVE ABUNDANCE OF THE MINOR ELEMENTS IN COALS FROM DIFFERENT PARTS OF THE UNITED STATES

By Peter Zubovic, Taisia Stadnichenko, and Nola B. Sheffey, Washington, D.C.

This discussion is based on spectrographic analyses of 1,000 samples of ash from coals of the major coal-producing areas in the United States. The results of these analyses were first computed as averages of columnar samples of beds, and these bed averages were used to compute the averages for three great areas, the Northern Great Plains province, the Eastern Interior region, and the Appalachian region. (See table 42.1.)

The coals sampled range in age from Eocene to Pennsylvanian. The 46 bed samples from the Northern Great Plains province are of Eocene to Jurassic age, 35 being of Paleocene age, 6 of Eocene, 4 of Jurassic, and 1 of Cretaceous age. The 47 bed samples from the Eastern Interior region and the 65 bed samples of the Appalachian region are all of Pennsylvanian age.

The rank of the coals ranges from the lignite, subbituminous, and high-volatile bituminous coals of the Northern Great Plains province, through high-volatile bituminous coals of the Eastern Interior region, to high-, medium-, and low-volatile bituminous coals of the Appalachian region.

The averages shown in table 42.1 indicate that few of these minor elements are much more abundant in any one of the three great areas than in the others. The Northern Great Plains coal is highest in B, Ti, Zn, Ga, and La, and this area and the Appalachian region are

highest in Cu. The Eastern Interior region is highest in V, Cr, Ni, Ge, Mo, and shares the highest figure for Be with the Appalachian region. The Appalachian region is highest in Co and Y, one of the two highest in Be and Cu, and close to the highest in Ni, Ga, and La. It is strikingly poor in B and Zn, which have a much wider range of abundance than any of the other elements. This general similarity of abundance in regions whose coals differ widely in age suggests that the total amount of each inorganic element (except B and Zn) associated with the coal substance was in general fairly constant.

TABLE 42.1.—*Average content of each minor element in coals from three major coal producing areas of the United States*

[Parts per million in coal]

Elements	Northern Great Plains province (avg. of 46 bed samples)	Eastern Interior region (avg. of 47 bed samples)	Appalachian region (avg. of 65 bed samples)
Be	1.5	2.5	2.5
B	116	96	25
Ti	590	450	340
V	16	35	21
Cr	7	20	13
Co	2.7	3.8	5.1
Ni	7.2	15	14
Cu	15	11	15
Zn	59	44	7.6
Ga	5.5	4.1	4.9
Ge	1.6	13	5.8
Mo	1.7	4.3	3.5
Sn	.9	1.5	.4
Y	13	7.7	14
La	9.5	5.1	9.4

The element most uniformly distributed among the three main areas is gallium. Copper and beryllium are next in the uniformity of their distribution. The average for copper in the Eastern Interior region is surprisingly low; it is lower than in either of the other two areas, although there is copper mineralization north of the region, in areas from which some of the sediments in the basin were derived. The somewhat higher beryllium content of the Eastern Interior and the Appalachian coals can be related to the sedimentary sources of the two areas. This aspect is discussed in detail in a report by the authors now in preparation. Tin and zinc are not considered because they were found in only about 25 percent of the analyses. The metals for which the averages differ most widely among the three areas are germanium and boron. Nickel is in its expected order, and is highest in the Eastern Interior region. Cobalt averages highest in the Appalachian coals; in the northern part of that region the bed averages are about the same as in the Eastern Interior region, and in the southern part they are higher. Cobalt mineralization has occurred at many places in the southern Appalachians, and the high average for cobalt in the coal of that region may be related to this mineralization. We do not mean to imply that a high proportion of an element in coal is everywhere due to erosion of mineralized rocks; in some areas it may indicate that the coal is in a geochemical province in which the rocks contain that element in more than average abundance. In such areas the metal may have been freed by erosion of the common country rocks rather than of rocks or veins in which the metal has been concentrated by secondary processes.

The differences in germanium and molybdenum contents between the coals of the three areas cannot yet be explained. In all three areas, the content of boron and titanium is about inversely proportional to the rank of the coal, being lowest in the highest grade coals. Boron, which forms organic esters, could easily be lost as a result of the metamorphism of coals; whether the same is true for titanium is uncertain. The relatively high boron content of the coals in the Northern Great Plains province could be due to the character of the sedimentary rocks in that province. It is generally known that the Fort Union sediments are chiefly derived from volcanic rocks. Large amounts of bentonitic material are intercalated also with those sediments indicating contemporaneous volcanism, which might well have produced considerable quantities of volatile matter containing large amounts of boron, some of which could have become incorporated in the coal. Boron is also relatively abundant, on the average, in the coals of the Eastern Interior region, but its origin in this region is hard to explain.

The two chemically similar elements yttrium and lanthanum are twice as abundant in some areas as in others, but the ratio between them is remarkably constant; the highest average content being less than 7 percent above the lowest. It is about 1.5 and 1.4 in the coals, as compared with 1.6 in the earth's crust. These figures suggest that the two elements were weathered out, transported, and incorporated in the coal at nearly the same rate.

The distribution of minor elements taken collectively among the three areas is relatively uniform. Boron content and perhaps titanium content may depend on the degree of metamorphism of the coal. In general, however, the quantity of any minor element in a coal appears to have been controlled by the availability of that element to the swamp in which the coal was formed.

EXPLORATION AND MAPPING TECHNIQUES

43. FIELD APPLICATION OF ION-EXCHANGE RESINS IN HYDROGEOCHEMICAL PROSPECTING

By F. C. Canney and D. B. Hawkins, Denver, Colo.

The resin-collection technique developed by the Geological Survey for use in hydrogeochemical prospecting was first used successfully in northwestern Maine in 1958 to determine copper, lead, zinc, cobalt, and nickel in the barren surface waters, which usually contain only 25 to 50 parts per million total dissolved solids.

Conventional methods of conducting geochemical water surveys require either (a) that heavy and bulky water samples be collected and shipped to a laboratory for analysis, or (b) that the bulk water be analyzed directly in the field with a chemical kit. Procedure (a) is relatively inefficient, and may entail a loss of trace metals from solution before analysis. Procedure (b) is free from these disadvantages, but few of the available field methods of analysis are sufficiently sensitive for direct use. It is partly for these reasons that few geochemical water surveys have been made in recent years.

Synthetic ion-exchange resins became available shortly after World War II. Because of their ability to collect ions from very dilute aqueous solutions, coupled with the ease by which these ions can be released and concentrated in a small volume of eluant, many investigators have speculated on the possible usefulness of such resins in hydrogeochemical prospecting surveys. Kunin (1958, p. 262) suggested the feasibility of preparing resins in the form of cartridge columns which could be taken to the field and used to concentrate the ionic constituents in a water sample, and Riddell (in press) mentions the use of ion-exchange resins placed in waterways for fixed time intervals. The work of Nydahl (1950), who described the use of ion-exchange resins to collect elements of biological interest from lake water, was of considerable help to us in working out the technique described in this paper.

This technique consists, in brief, of using a plastic tube packed with a resin known commercially as IR–120 to collect the metals from a water sample, at the sample site, by allowing a known volume of water to percolate through the resin at a controlled rate. No apparatus other than this light and durable tube need be taken to the field or base laboratory, where the sorbed metals are easily eluted. The eluant, in which the metals of interest are much more highly concentrated than in the bulk water, can there be analyzed by conventional field or laboratory methods. The apparatus used for collecting and elution is shown in figure 43.1

Some of the more important factors in successful use of resins in geochemical water surveys are enumerated below. These remarks apply specifically to the collection of copper, lead, zinc, cobalt, and nickel. Any attempt to apply this technique to other elements should be preceded by experimental work on solutions of known metal content.

1. Purification of the IR–120 resin.—This is accomplished by alternately soaking the resin in 6N

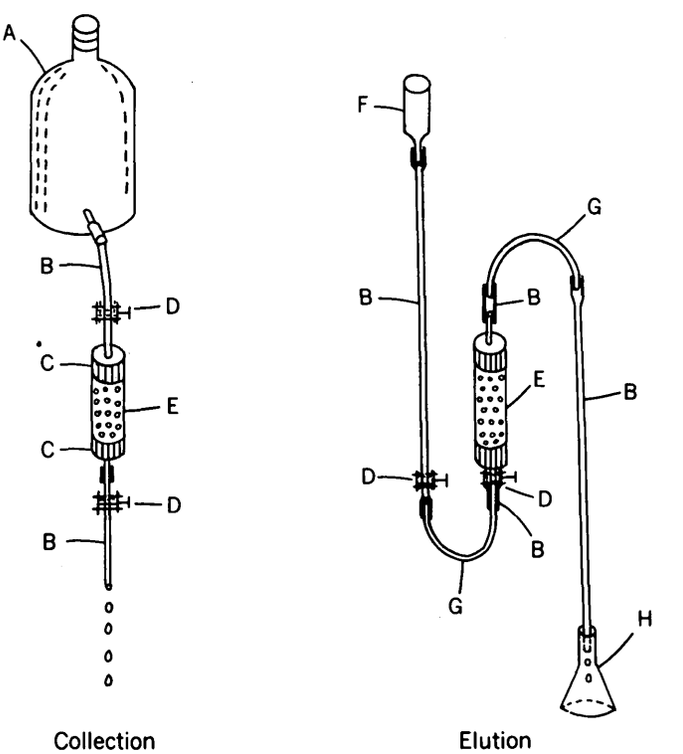

FIGURE 43.1.—Collection and elution apparatus. *A*, polyethylene bottle, 1-gallon size, for holding water sample; *B*, plastic tubing; *C*, glass wool plug, pyrex; *D*, screw-clamp; *E*, resin cartridge consisting of a 6-inch polyethylene drying tube (25 ml vol) packed with resin (IR–120, −20 to +50 mesh size); *F*, glass funnel; *G*, glass U-tube; *H*, volumetric flask, 100-ml capacity.

557753 O—60——7

hydrochloric acid and washing it in metal-free water until satisfactory blanks are obtained for iron and zinc. Zinc is the most difficult element to eliminate.

2. Preparation of the cartridge.—The resin cartridge is prepared by pouring a slurry of the purified resin onto a plug of glass wool in the bottom of the polyethylene tube; a similar plug is then placed over the resin. The resin should not be allowed to drain dry, for doing this will allow air bubbles to enter the cartridge and interfere in the collection step.

3. Collection.—The pH of the water sample should be checked, and then adjusted if necessary with hydrochloric acid or ammonium hydroxide until it is between 6.5 and 7.5. A flow rate through the column of about 100 ml per minute gives a recovery satisfactory for most geochemical prospecting investigations. After the water-sample bottle is attached to the cartridge, the top screw clamp should be opened first, and then the bottom clamp.

4. Elution.—The metals are eluted by passing 20 ml of 2N hydrochloric acid, and then 80 ml of demineralized water, through the column. An upflow technique should be used, as shown in figure 43.1, and the direction of flow through the resin cartridge should be opposite to that used in the collection step. A flow rate of 1 ml per minute is satisfactory. Precautions should be taken to prevent air bubbles entering the column when the elution process is started.

When 1-gallon samples are passed through the column an enrichment factor of 38 is obtained. If field colorimetric methods are used to analyze the eluant, their detection limits, expressed in terms of the concentration in bulk water, are about as follows:

Metal	*Concentration (micrograms per liter)*
Cu	0.2
Pb	1
Zn	1
Co	0.5
Ni	0.5

These detection limits can be lowered considerably by increasing the volume of the sample.

As a measure of the effectiveness of this technique to recover metals under field conditions, zinc was determined directly on 6 bulk waters, and the values compared with those obtained with the resin technique. That the agreement was satisfactory is shown by the following comparative data.

Zinc content, in micrograms per liter

Direct analysis	*Resin collection*
4	5
3	4
2	2
8	9
6	6
2	2

Major advantages of this resin-collection technique, which should appeal to investigators in the field of hydrogeochemical prospecting, are these: it is more sensitive than other methods; it eliminates the shipping of bulky water samples; and it prevents the loss of trace constituents from solution that may occur with other methods.

REFERENCES

Kunin, Robert, 1958, Ion exchange resins: New York, John Wiley and Sons, 466 p.

Nydahl, Folke, 1950, Sampling and analysis of lake waters by means of ion exchangers: Internat. Limnological Cong., 11th, Belgium 1950, Proceedings, p. 276–290.

Riddell, J. E., in press, A survey of geochemical exploration in eastern Canada: Internat. Geol. Cong., 20th, Mexico City 1956, Geochem. Symp.

44. GEOCHEMICAL PROSPECTING FOR BERYLLIUM

By Wallace R. Griffitts and U. Oda, Denver, Colo.

A major problem in prospecting for nonpegmatitic deposits of beryllium is to determine by some inexpensive reconnaissance method what districts are most worthy of further work. Random sampling or inspection of outcrops is time-consuming and is likely to be ineffective, for beryllium minerals in tactite, greisen, and granite generally have a spotty distribution, and veins containing beryl and bertrandite are commonly friable and readily broken down into fine rubble or soil.

Searching alluvium for traces of valuable minerals has long been an important technique in reconnaissance prospecting because a sample of alluvium from a small stream may roughly indicate the composition of the rocks exposed in the drainage basin. This technique

is very useful in seeking heavy minerals, such as gold, wolframite, or cassiterite, because they are concentrated in the alluvium. Unfortunately, however, the common beryllium minerals are too light to be concentrated readily and are difficult to recognize: their presence, therefore, must be inferred from the relatively high beryllium content of alluvium that contains them. The concentration of beryllium in most alluvium is less than 5 ppm (5 parts per million or 0.0005 percent), so that a few fragments of a beryllium mineral will increase the tenor of a sample by an amount readily detectable by rapid spectrographic or fluorimetric analyses.

We have made fairly thorough studies of alluvium in the beryllium districts near Lake George, Colo., at Iron Mountain, N. Mex., and in the Sheeprock Range, Utah; less thorough studies in other places confirm the conclusions reached in those three districts. V. Venkatesh and Y. G. K. Murty of the Geological Survey of India worked with us in the Lake George and Iron Mountain areas respectively.

Most of the beryl- and bertrandite-bearing veins in the Lake George area are in a broad intermontane valley underlain by schist and gneiss that are deeply covered with soils. The mountains at the eastern edge of the valley are underlain by granite of the Pikes Peak batholith. The soils and alluvium derived from the metamorphic rocks contain 2 to 3 ppm of Be; those derived from the granite may contain as much as 10 ppm. Near the beryllium-rich parts of veins, which weather readily, alluvium may contain as much as 20 ppm of Be. Figure 44.1 shows the increase in beryllium content of alluvial samples from a wash that flows eastward past the veins in and near the Boomer mine.

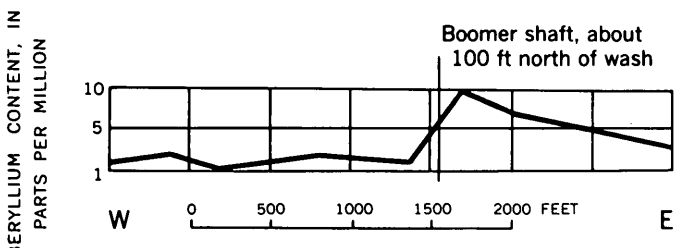

FIGURE 44.1.—Beryllium content of alluvium in wash south of Boomer mine.

In the Iron Mountain district, New Mexico, tactite has replaced limestone of the Magdalena group near intrusive masses of fine-grained monzonite, granite, and porphyritic rhyolite. Helvite occurs near the north end of the largest mass of tactite, but most of the known localities are in smaller masses west of the ridge crest. Samples of alluvium taken from washes and near the mountain front contain no more than 2 ppm of Be south of the area of figure 44.2. Nearer the mineralized rocks the beryllium content of similar alluvium samples is higher, reaching a maximum in the washes that drain the known helvite-bearing rocks in the NW quarter of section 2 (see figure 44.2). The low beryllium content of most alluvial samples taken east of the crest reflects the absence of known helvite occurrences in most of the large tactite mass. The two washes east of the ridge crest that yield the richest samples—with 30 and 100 ppm—drain the only known helvite-bearing rocks east of the divide. The two soil samples taken at the north end of the mountain indicate that the layer of tactite exposed there can account for the 30 ppm of Be found in the alluvium to the west. Samples of residual soil taken along several traverses in section 2 show anomalous beryllium content immediately above and downhill from metallized tactite layers.

The northwesterly-trending Sheeprock Range, near Eureka, Utah, is flanked by desert basins that contain Quaternary and older alluvium and volcanic rocks. The range consists mainly of Precambrian and Paleozoic sedimentary rocks, but a stock of granite extends about six miles along the range. Soils are poorly developed over this granite. Near the center of the stock clusters of blue beryl crystals are embedded in apparently unaltered granite. Beryl-free granite between the clusters of beryl crystals in this central area contains 10 to 15 ppm of Be, whereas granite from other parts of the stock generally contains less than 10 ppm. The coarser (over 200-mesh) fractions of alluvium contain more beryllium over the beryllium-rich granite than elsewhere, but the finer fraction contains a rather uniform 2 to 5 ppm in most places sampled over the stock.

Analysis of alluvium is an effective way to find districts in which beryllium-rich rocks crop out, and it is relatively economical, because taking and analyzing samples in a district of ordinary size requires about two man-weeks. In general, any district should be considered favorable if it yields samples containing 10 ppm or more of Be, but even values between 5 ppm and 10 ppm may be promising in samples taken from geologically favorable places. Analyses of residual soils can be used to find individual bodies of beryllium-rich rock, in the same way that float has long been used in finding veins.

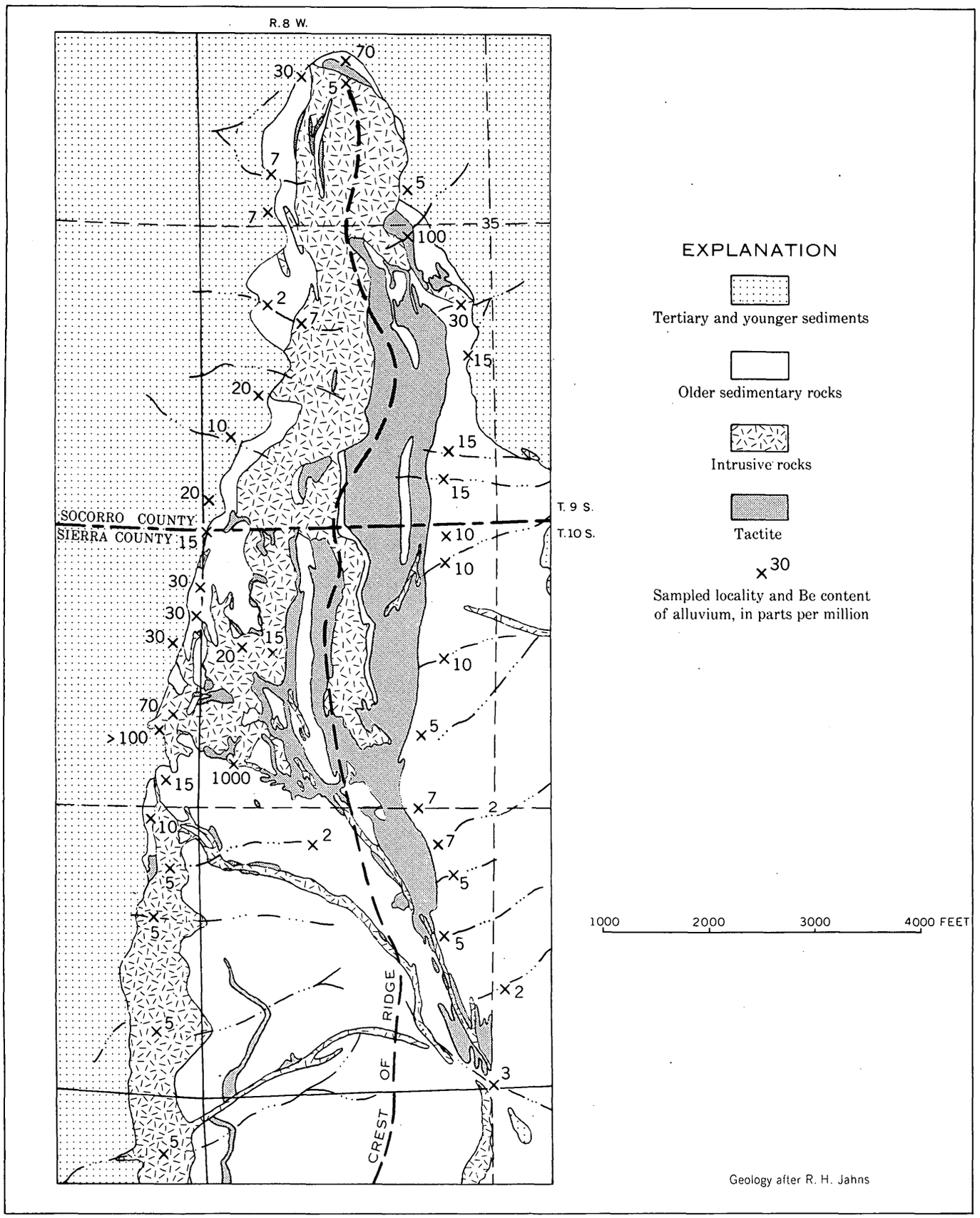

FIGURE 44.2.—Simplified geologic map of the Iron Mountain area, N. Mex., showing beryllium content of alluvium.

45. VARIATIONS IN BASE-METAL CONTENTS OF MONZONITIC INTRUSIVES

By WALLACE R. GRIFFITTS and H. M. NAKAGAWA, Denver, Colo.

Marked differences in the base-metal content of apparently unaltered igneous rocks from many mining districts in the Western United States cannot be ascribed entirely to magmatic, deuteric, or early postmagmatic processes. The metals were largely introduced into the rocks and were sorbed by the surfaces of dark minerals, without inducing any alteration that is recognizable either in outcrops or in thin sections. The metals can in large part be removed from the rocks with very dilute acid. In most districts the content of introduced metal increases toward major centers of mineralization, giving rise to broad hypogene geochemical anomalies that may extend as much as a mile from the center. Such anomalies are well developed in districts characterized by mesothermal ores containing dark sphalerite, pyrite, galena, copper sulfides, and carbonates, but are poorly developed in districts with epithermal-type gold or silver ores, even though they contain copper, zinc, and lead minerals. Zinc is particularly mobile, and forms anomalies that are larger than those of most other metals. Copper and manganese also form notable anomalies, but those of lead are slight and of small extent.

In some districts introduced metals are not most abundant near known centers of mineralization. In the Jamestown district of Colorado, for example, a prominent copper anomaly (fig. 45.1) and a nearly congruent zinc anomaly (not shown) have no apparent spatial relation to groups of fluorite, gold, or silver veins. The highest concentrations of metal are in monzonite along the western edge of the stock; they are not near any known ore deposits and presumably were due to deposition from solutions that moved along or near the contact. Most of the anomalous metal is affixed to augite, hornblende, biotite, and sphene; pyrite, which occurs in trace amounts in the monzonite, was altered to sulfides of zinc and copper in the metal-rich rocks.

The wide range in metal content within an individual stock, as shown at Jamestown, indicates that neither the average metal content of the monzonite nor its pre-mineralization metal content can be determined accurately from a small number of samples. Samples must be collected from sufficiently numerous and widely distributed localities to ensure that both metal-rich and metal-poor parts of the stock are adequately represented. In some districts the metal content of unmineralized or only slightly mineralized rocks varies widely (table 45.1). This suggests that some mineralized rocks were probably included in the table; if so, the averages are too high.

The high copper and zinc content of igneous rocks around ore deposits of those metals is probably due to leakage from the deposits during mineralization, rather than to an originally high metal content of the parent magma. The total metal contents therefore tell little about the relationship between magmas and ores. Some metallogenic provinces, however, may be related to large bodies of monzonite whose original base-metal content was exceptionally high.

TABLE 45.1.—*Metal contents of monzonitic rocks from Western United States.*

[Colorimetric analyses by H. M. Nakagawa, A. P. Marranzino, and H. L. Neiman except where there is an asterisk (*) after the district name. Asterisks indicate spectrographic analyses by U. Oda and E. F. Cooley. ? indicates uncertainty in mean, usually because there were many samples in which the metal was not detected. Feldspar proportions of all the rocks correspond to those of monzonites or quartz monzonites; rock names in parentheses were applied by other workers.]

Source of sample	Metal content, in parts per million									Number of samples
	Copper			Lead			Zinc			
	Minimum	Mean	Maximum	Minimum	Mean	Maximum	Minimum	Mean	Maximum	
Colorado:										
Jamestown district	13	46	80	11	17	28	20	71	95	27
Ward area	5	9	12	24	34	50	65	95	110	15
Albion stock	5	28	85	10	16	36	26	70	110	19
Caribou district	8	17	48	13	17	24	50	79	120	12
Empire district	6	10	15	13	35	70	60	120	190	15
Montezuma stock	4	16	50	15	17	24	10	37	80	19
Breckenridge district:										
Swan Mountain	4	9	24	10	31	65	28	61	130	50
Bald Mountain	7	14	110	8	22	50	65	110	190	24

TABLE 45.1.—*Metal contents of monzonitic rocks from Western United States*—Continued

Source of sample	Metal content, in parts per million									Number of samples
	Copper			Lead			Zinc			
	Minimum	Mean	Maximum	Minimum	Mean	Maximum	Minimum	Mean	Maximum	
New Mexico:										
Cook Mountain	22	26	30	12	15	20	65	74	85	5
Santa Rita (granodiorite)	5	8	14	17	28	36	65	109	220	5
Hanover (granodiorite)	5	26	55	6	9	14	28	58	120	8
Black Range	13	20	30	7	11	14	65	83	95	6
Iron Mountain*	<5	5	10	15	33	100	------	------	<200	9
Arizona:										
Cochise County:										
Schieffelin granodiorite	18	25	42	11	13	16	44	53	70	5
Uncle Sam porphyry	5	10	42	7	16	20	48	54	80	22
Cochise Peak quartz monzonite	14	15	19	14	17	20	32	37	40	3
Gleason quartz monzonite	5	7	10	7	13	28	10	29	60	8
Bagdad district, stocks	5	22	40	8	18	60	10	54	130	8
Bagdad district, dikes	7	18	55	5	22	120	10	77	130	19
Christmas district	60	70	80	6	10	11	16	30	48	5
Superior district	6	15	20	8	9	12	70	80	85	4
Utah:										
Frisco district, Estelle area	20	36	70	12	16	22	55	68	90	13
Frisco district, Copper Canyon area*	50	75	100	<10	<10	20	------	------	<200	5
Stockton area*	3	26	75	<10	19	50	------	------	<200	7
Deep Creek Range (granite)	<1	1?	3	20	27	34	22	42	60	11
Gold Hill district	6	25	34	14	29	42	38	54	75	7
West Tintic district	3	9	14	16	19	20	40	55	80	5
Sheeprock Range (granite)	<1	3	10	19	29	90	14	32	85	64
Desert Mountain	<1	2?	12	24	26	28	6	33	60	8
Mineral Range	<1	<1	<1	16	19	22	22	31	50	3
Cedar City district, Stoddard Mountain	8	37	70	18	24	38	65	75	130	53
Nevada:										
Cortez quadrangle, stock	<2	7	22	15	25	34	12	36	60	25
Carlin quadrangle*	30	80	150	10	10	10	------	------	<200	3
Austin area	4	7	20	19	25	40	10	47	70	26
Gabbs area*	<1	13	50	10	11	75	------	------	<200	5
Unionville quadrangle, Rocky Canyon area	5	8	10	20	26	36	16	41	60	7
Average	------	24	------	------	19	------	------	63	------	------

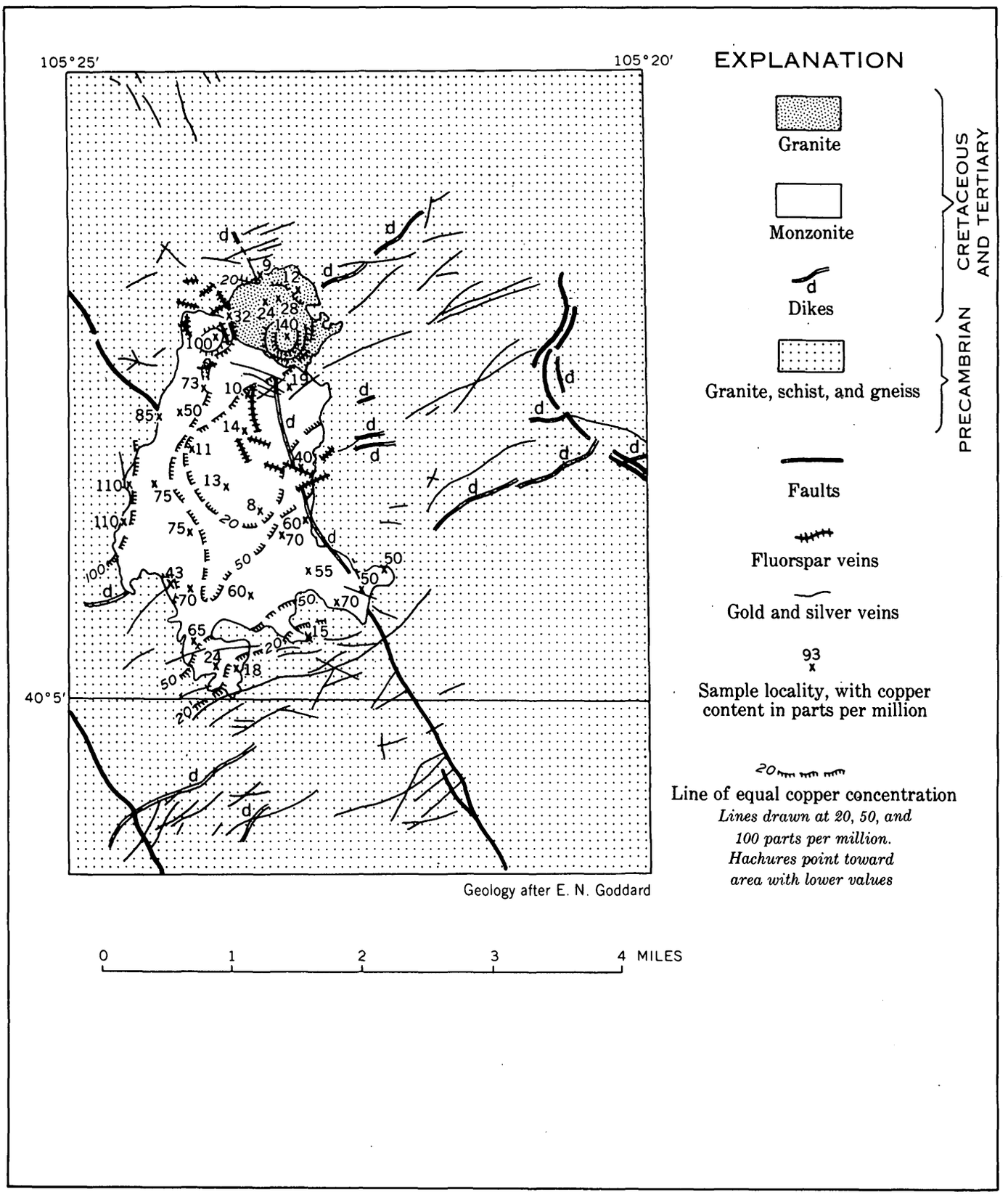

FIGURE 45.1.—Geochemical map of the Jamestown district, Colorado.

46. GEOCHEMISTRY OF SANDSTONES AND RELATED VEGETATION IN THE YELLOW CAT AREA OF THE THOMPSON DISTRICT, GRAND COUNTY, UTAH

By HELEN L. CANNON, Denver, Colo.

Work done in cooperation with U.S. Atomic Energy Commission

Oxidized ore bodies and the surrounding sandstone in the Yellow Cat area of the Thompson district were studied to establish what other elements are concentrated with uranium and vanadium in the ore deposits, to determine the geochemical behavior of these elements during weathering, and to decide whether selenium, molybdenum, or some other metal could be used as a pathfinder element in prospecting for uranium-vanadium deposits.

GEOCHEMISTRY OF HOST ROCKS

The distribution of metals in the Salt Wash sandstone member of the Morrison formation, in which the ores of the Yellow Cat area occur, is shown in table 46.1. The mean percentages of metals given in columns 2–5 were computed from analyses of channel samples taken for this purpose through 13 ore bodies and the surrounding sandstones. The samples were divided into unmineralized, mineralized, and ore categories according to grade cutoffs commonly used for Colorado Plateau ores. The contents of sulfur, selenium, arsenic, and molybdenum were found to be more than 10 times greater in the uranium-vanadium ore bodies than in the enclosing sandstones and these elements were assumed to be an intrinsic part of the ore. The same elements were also distinctly more abundant in the sandstones surrounding the ore bodies (columns 3 and 4) than Newman (1957) and Shoemaker and others (1959) later found them to be in more distant country rock (column 1). In other words, each ore body is enveloped by a geochemical halo of these metals, which enlarges the target for prospecting.

TABLE 46.1.—*Distribution of selected elements (parts per million) in sandstones of the Salt Wash member of the Morrison formation*

1	Colorado Plateau	Yellow Cat area			
	2	3	4	5	6
Element	Unmineralized rocks [1] (<40 U)	Unmineralized rocks (<40 U)	Mineralized rocks (40–84 U)	Ores (>84 U)	Ratio ore/unmineralized rocks
U	2	13	183	3, 800	292
S	—	430	1, 400	7, 300	17
V	18	578	1, 280	9, 510	16
Se	<0. 5–8	<14	51	190	>13. 5
As	<15	32	100	417	13
Mo	<7	<8	41	100	>12. 5
Ni	<. 7	<5	23	35	>7
Co	7	<8	45	59	>6. 5
Pb	<2	<12	11	52	>4. 5
Cu	20	7	9	23	3. 3
Ag	~. 5	<1	<. 6	3. 5	>3. 5
Zn	<30	<89	<71	228	>2. 6
Fe	3, 000	15, 000	19, 000	28, 000	1. 8
Cr	9	73	76	107	1. 4
Mn	380	496	338	292	. 59
$CaCO_3$	180, 000	71, 000	46, 000	30, 700	. 4

[1] Arithmetic means compiled from data presented by Newman (1957) and by Shoemaker and others (1959).

Special studies were made of an open pit where ore occurred at a depth of 44 feet. Selenium and molybdenum were found to be concentrated to a greater degree in the partially mineralized sandstone just above the ore than in the ore itself, and anomalous values of uranium, arsenic, and vanadium were also found in the sandstones and mudstones for varying distances above the ore. All these elements, therefore, were considered potentially useful in prospecting by plant analysis.

PROSPECTING BY PLANT ANALYSIS

Because surface waters and residual soil cover are lacking in the Yellow Cat area, its vegetation was investigated as a prospecting medium. Differences in absorption of uranium, vanadium, and molybdenum by three classes of vegetation are shown in table 46.2. All species of plants rooted in mineralized ground were found to contain concentrations of uranium, vanadium, selenium, and molybdenum sufficiently high to be useful in prospecting. The ratio of uranium, however, in plants growing on mineralized ground (m) to that in plants growing on unmineralized ground (unm) was greater than for any other element. As the uranium content in the leaves and end branches of trees and deep-rooted perennial shrubs was found to be consistent, several hundred samples of juniper and shadscale (*Atriplex confertifolia*) were collected and analyzed fluorimetrically; the limit of sensitivity of the method is 0.3 ppm uranium in the ash. On unmineralized

TABLE 46.2.—*Uranium, vanadium, and molybdenum content in vegetation of the Yellow Cat area*

Classes of vegetation	Uranium		Vanadium		Molybdenum	
	Mean (ppm)	ratio m/unm	mean (ppm)	ratio m/unm	mean (ppm)	ratio m/unm
Grasses	------	6. 1	------	3. 3	------	1. 3
On unmineralized ground	5. 7	------	40	------	25	------
On mineralized ground	35. 0	------	135	------	32	------
Other herbs (including Se indicators)	------	11. 0	------	5. 3	------	3. 7
On unmineralized ground	1. 9	------	36	------	42	------
On mineralized ground	21. 0	------	191	------	155	------
Trees and shrubs	------	9. 8	------	2. 6	------	3. 6
On unmineralized ground	. 9	------	19. 8	------	14. 2	------
On mineralized ground	8. 7	------	51	------	36. 5	------

ground the content was generally around 0.5 ppm, whereas on mineralized ground it was commonly greater than 2 ppm. Both juniper and shadscale contained anomalous amounts of uranium where the ore was less than 35 feet beneath the surface; where the ore lay at greater depths the water-loving juniper continued to be an effective guide but the shallow-rooted xerophytic shadscale failed to indicate any mineralization. Ore has since been mined from areas outlined by analysis of both juniper and shadscale.

PROSPECTING BY INDICATOR PLANTS

Near the uranium deposits there is an excess of metals, increased radioactivity, and a local change in pH, and the environment is consequently favorable for the growth of certain indicator plants listed in table 46.3. The selenium indicator plants starred in that table were selected as being the best mappable indicators of ore deposits. It was found that *Astragalus pattersoni*, a white-flowered poisonvetch, and *Astragalus preussi*, a purple species, are accumulators not only of selenium as they were long known to be, but of uranium, vanadium, and molybdenum as well, and that their distribution correlates more consistently than that of any of the other plants listed with mineralized ground.

TABLE *46.3.—Plants favored by mineralized ground in Yellow Cat area*

[Asterisk = selenium-indicator plants]

Grasses:	**Oryzopsis hymenoides* (ricegrass)
	Stipa comata (needleandthread)
Lily family:	*Calochortus nutalli* (Sego lily)
	Allium acuminatum (onion)
	Zigadenus gramineus (deathcamas)
Buckwheat family:	*Eriogonum inflatum* (deserttrumpet)
Legume family:	**Astragalus pattersoni* (Patterson loco)
	**Astragalus preussi* (Preuss loco)
	**Astragalus thompsonae* (Thompson loco)
	**Astragalus confertiflorus* (blue loco)
Borage family:	*Cryptantha flava* (cryptanthe)
Sunflower family:	*Grindelia squarrosa* (gumweed)
	**Townsendia incana* (townsendia)
	Aplopappus armeriodes (goldenweed)
	Senecio longilobus (groundsel)
	**Aster venustus* (woody aster)

By comparison of the indicator plant data with drilling results in the Yellow Cat area, it was found that plant mapping indicated 81 percent of the mineralized ground less than 32 feet below the surface, and 42 percent of the mineralized ground lying at depths between 32 and 170 feet. For mineralized ground at depths exceeding 170 feet, the ratio dropped abruptly to 16 percent, or about the same as on barren ground. Several ore bodies were found by means of plants in areas that had been believed from geologic evidence to be unfavorable for finding ore.

REFERENCES

Newman, W. L., 1957, Distribution of elements, *in* Geologic investigations of radioactive deposits—Semi-annual progress report, Dec. 1, 1956 to May 31, 1957: U.S. Geol. Survey TEI 690, book 2, p. 480, issued by U.S. Atomic Energy Comm. Tech. Inf. Service, Oak Ridge, Tenn.

Shoemaker, E. M., and others, 1959, Elemental composition of the sandstone-type deposits, *in* Garrels, R. M., and Larsen, E. S. 3d, Geochemistry and mineralogy of the Colorado Plateau uranium ores: U.S. Geol. Survey Prof. Paper 320, p. 25–31.

47. GEOCHEMICAL PROSPECTING FOR COPPER IN THE ROCKY RANGE, BEAVER COUNTY, UTAH

By R. L. Erickson and A. P. Marranzino, Denver, Colo.

The distribution of copper in transported alluvium on a pediment of the Rocky Range, Beaver County, Utah, was studied to determine whether known copper deposits in bedrock concealed by alluvium could be detected by geochemical methods. The principal problem in these studies is to distinguish between metal anomalies caused by detrital minerals, washed downslope from mineralized outcrops, and anomalies caused by metals carried upward in solution from underlying rock and precipitated in the alluvium. The part of the Rocky Range pediment investigated in this study is in sec. 22, T. 27 S., R. 11 W., northwest of the Old Hickory copper mine, and separates the southern tip of the range from its main body. The rocks exposed upslope from this pediment include quartzite, marble, hornfels, and skarn that are intruded by medium- to coarse-grained quartz monzonite; they strike about N. 45° W., dip steeply northeastward, and can be projected across the pediment to similar outcrops in the southern tip of the range.

Most of the copper deposits in the Rocky Range are tabular replacement pods composed of magnetite, chalcopyrite, garnet, and diopside, that occur in skarn near the contact with quartz monzonite. The concealed copper deposit in the mapped area occurs at depths ranging from 20 to 225 feet in a skarn zone that dips steeply northeast. The thickness of the alluvium over the deposit ranges from 6 to 72 feet.

The area was mapped on a scale of 1:1,200 to show the distribution of copper in alluvium in relation to topography, drainage, geology, and location of core holes in mineralized rock. Samples of alluvium were collected on the pediment on approximately 100-foot centers and at a depth of 8 to 12 inches. At this depth cobbles and pebbles in the alluvium are coated with caliche. The term "caliche" as here used is restricted to calcareous material precipitated in the zone of weathering, probably by evaporation of water.

The copper content of the minus-80-mesh fraction of the alluvial soil, determined by adding 2-2′ biquinoline in an isoamyl alcohol extract to the solution obtained by fusing the sample with potassium pyrosulfate, powdering the melt, and leaching the melt with dilute HCl (Almond, 1955), is highest in samples from the drainage systems in the eastern and western parts of the mapped area, and has no apparent spatial relation to the core holes in mineralized rock (fig. 47.1). These copper "highs" are caused by the concentration of detrital copper minerals that have been washed from old prospect pits and mines downslope into the drainage. The small "highs" near the center of the mapped area may come from accumulations of detrital copper minerals derived from the underlying mineralized skarn.

In an attempt to distinguish between the copper contributed by detrital minerals and the copper transported in solution, the white to light-gray and the light-grayish-brown caliché coatings on pebbles and cobbles in the alluvium were removed and analyzed for copper. If caliche is a chemical precipitate formed by evaporation of water, the composition of caliche must closely reflect the composition of the water from which the caliche was precipitated. Copper was determined by adding 2-2′ biquinoline, in an isoamyl alcohol extract, to the solution obtained by leaching powdered caliche with hot 6N HCl. Figure 47.2 shows that the largest "highs" of copper in caliche, as thus determined, occur near the known concealed copper deposit, whereas the "highs" that can be ascribed to detrital copper are comparatively small.

Within the area having the highest concentration of copper in caliche, the caliche coatings contain more copper than the alluvium, whereas in most of the remainder of the mapped area the alluvial soil contains more copper than the caliche (fig. 47.3). The most significant features shown on this map are these: (a) all the core holes in mineralized rock occur within the area in which the ratio of copper in caliche to copper in alluvium is one or greater, and (b) the strong detrital-copper "highs" (fig. 47.1) are eliminated. This suggests that the copper in caliche and ratio "highs" were not derived from detrital copper minerals, but from upward moving water that leached copper from a restricted bedrock source below the pediment. This source is probably the known copper deposit that underlies the caliche that is comparatively rich in copper.

REFERENCE

Almond, Hy, 1955, Rapid field and laboratory method for the determination of copper in soil and rocks: U.S. Geol. Survey Bull. 1036–A, p. 1–8.

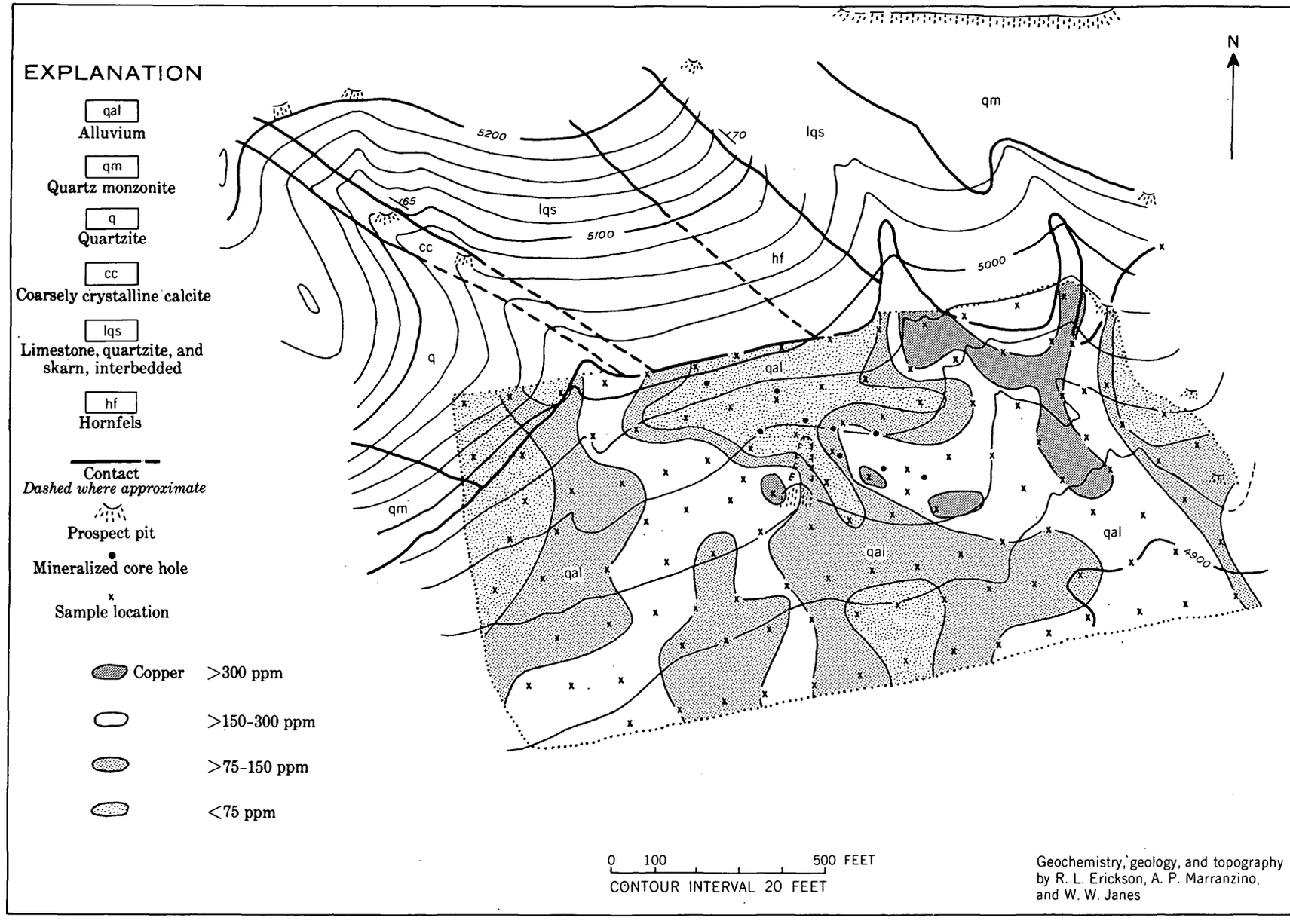

FIGURE 47.1.—Map showing copper content of alluvial soil on a pediment in the Rocky Range, Beaver County, Utah.

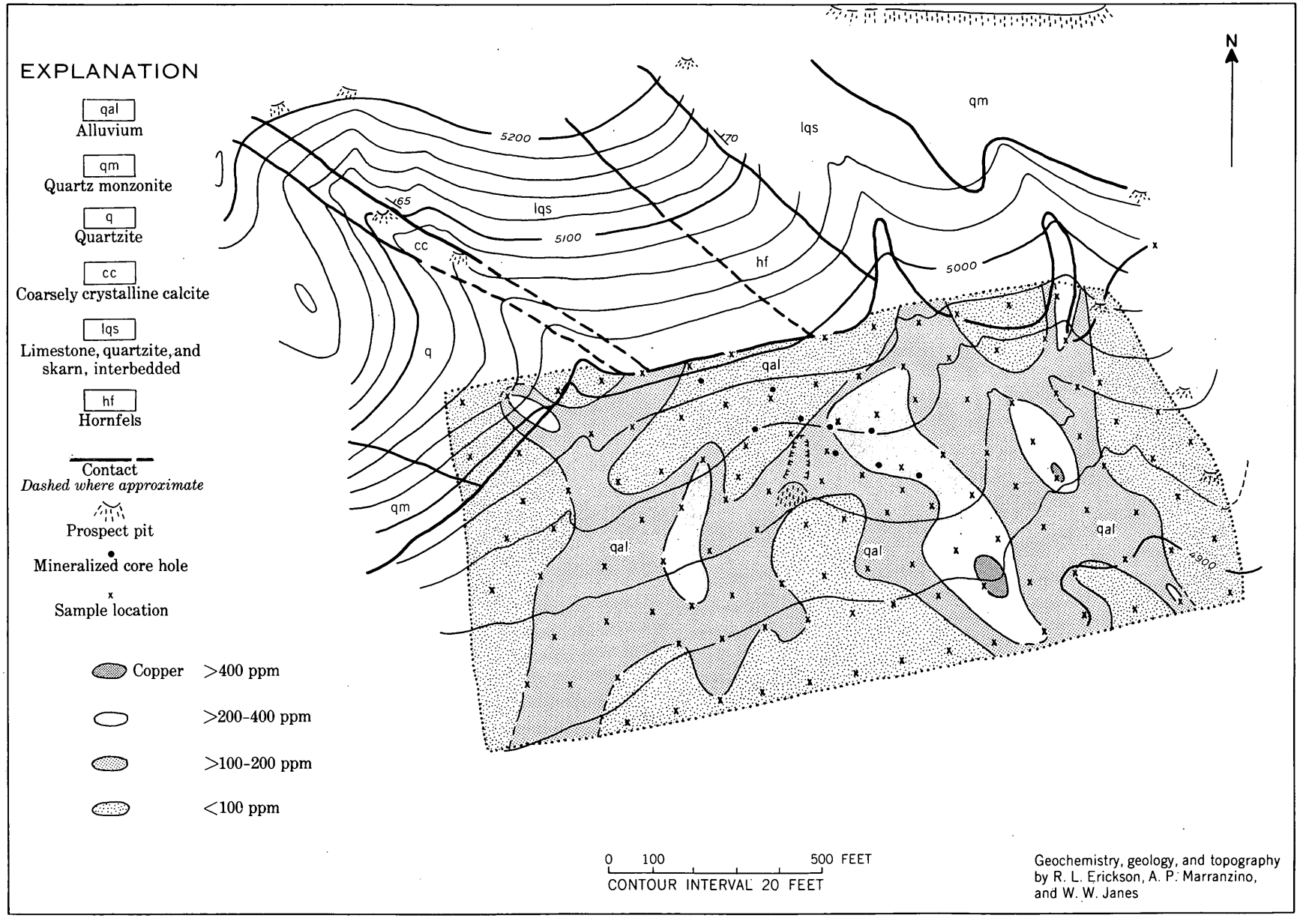

FIGURE 47.2.—Map showing copper content of caliche coatings on cobbles and pebbles in alluvium on a pediment in the Rocky Range, Beaver County, Utah.

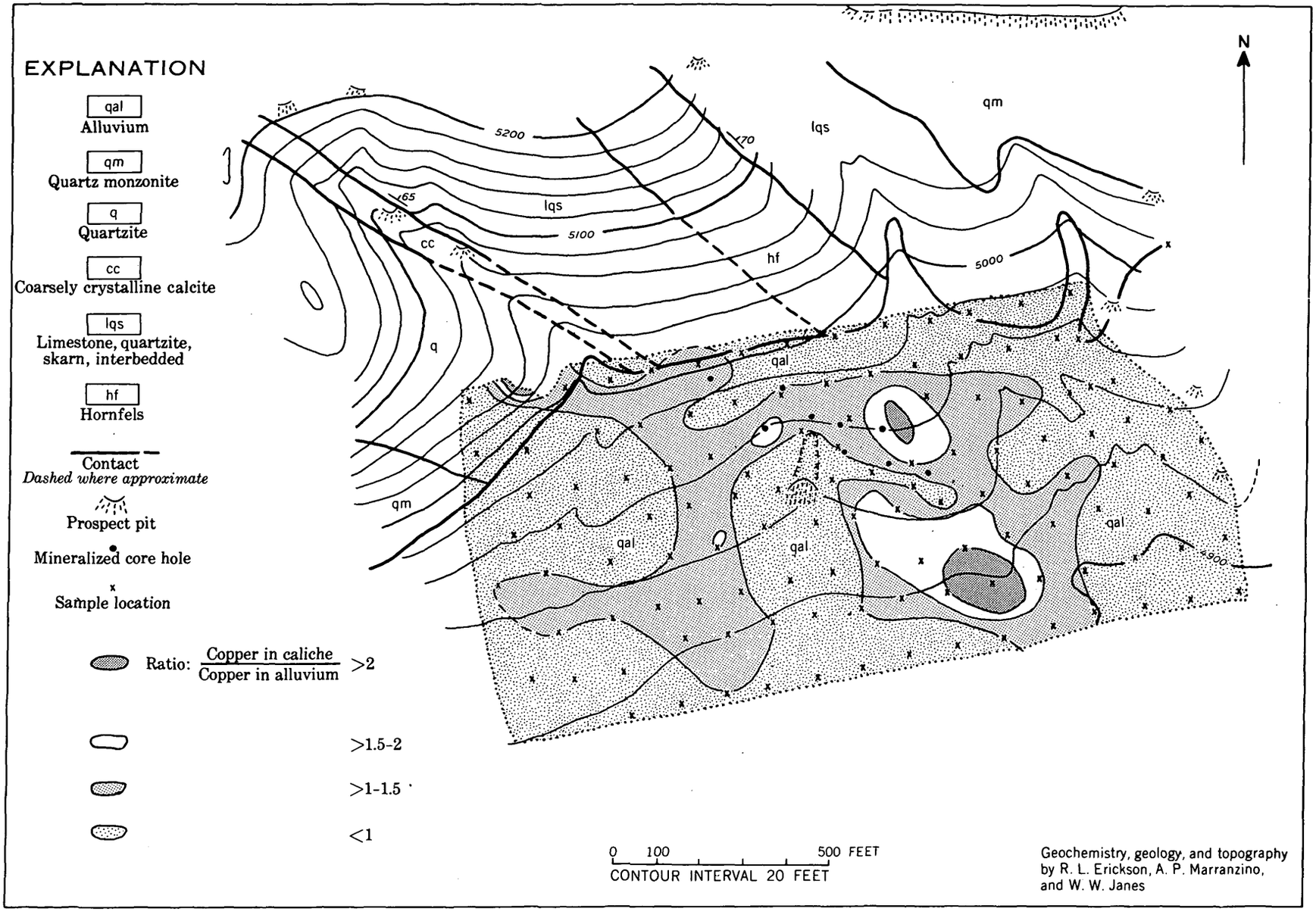

FIGURE 47.3.—Map showing ratio of copper in caliche to copper in alluvium on a pediment in the Rocky Range, Beaver County, Utah.

48. SOIL AND PLANT SAMPLING AT THE MAHONEY CREEK LEAD-ZINC DEPOSIT, REVILLAGIGEDO ISLAND, SOUTHEASTERN ALASKA

By HANSFORD T. SHACKLETTE, Georgetown, Ky.

The Mahoney Creek deposit is a vein of sphalerite and galena in black slate. The vein and country rock are covered with talus, soil, and vegetation, but the vein is exposed at the surface in a number of exploration pits. A base line was established along and parallel to the vein, and five traverse lines were laid out to cross the base line at or near the exploration pits (fig. 48.1). Sample sites on the traverses were spaced 30 to 40 feet apart; soil and plant samples were collected at each site and analyzed for lead and zinc content. Most of the soil samples were taken from the upper part of the C Horizon, which consists of finely divided inorganic material lying on the talus blocks; where this material was absent, the gley portion of the lowest part of the B Horizon was collected.

For the purpose of making comparisons the samples were divided into three groups: (a) those collected on or near the base line, which approximated the vein subcrop, designated "vein" samples; (b) those collected at sites on either side of the vein samples, designated "halo" samples; and (c) those collected from sites more remote from the vein than the "halo" samples, designated "background" samples. Mean percentages of lead and zinc with their standard deviation and standard error were computed for each plant species in each of the three sample groups. These values are presented in table 48.1, in addition to mean values for all Alaskan samples of these same plant species for the two elements. Table 48 2 presents a comparison of mean lead and zinc percentages in all plant species sampled and in all soil samples in the Mahoney Creek area.

It is apparent that a close correlation exists between the relative "background," "halo," and "vein" values of corresponding plant and soil samples, and that both classes of samples accurately reflect the known location of the mineral vein. If anomalous values are held to be those approximately twice background values, most of the plant species show "plus" anomalous concentrations of both lead and zinc over the vein. Two species of plants (western hemlock and salal) show "minus" anomalous concentrations in lead over the vein. This may indicate that the maximum toxicity tolerance of these two species for this element has been exceeded by the very high lead concentration in the soil over the vein, or that other chemical or physical differences associated with the vein have caused the amount of lead accumulated in the stems to be less than that in the

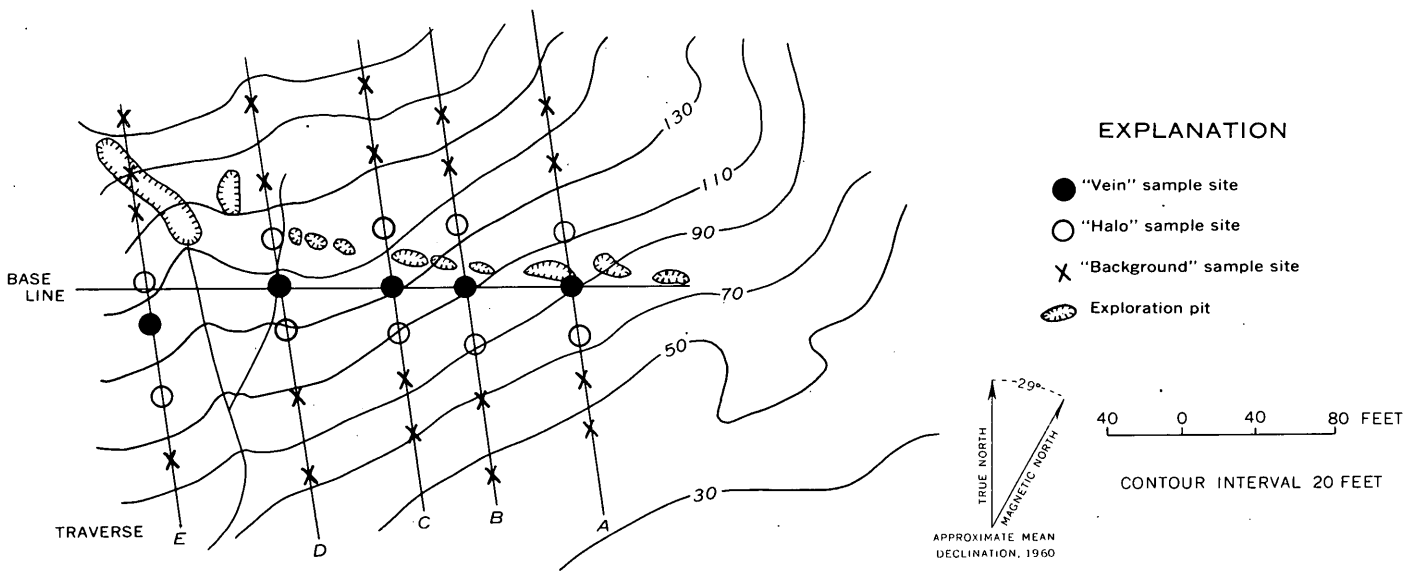

FIGURE 48.1.—Sketch map showing locations of geochemical sampling sites and exploration pits of the Mahoney Creek lead-zinc deposit, George Inlet, Revillagigedo Island, Ketchikan district (modified from map by W. S. Twenhofel, U.S. Geol. Survey Bull. 998–C, p. 80).

TABLE 48.1.—*Mean background and anomalous percentages of lead and zinc in plant ash*

Plant species, and tissue analyzed	Mean values, Mahoney Creek plant samples [1] (number of samples in parentheses)						Mean values, all Alaskan specimens [2] (number of samples in parentheses)	
	Lead			Zinc			Lead	Zinc
	Background	Halo	Vein	Background	Halo	Vein		
Menziesia (*M. ferruginosa*), stems 8 in. long excluding new growth.	(20) 0. 014±0. 001	(10) 0. 016±0. 002	(5) 0. 035±0. 006	(20) 0. 26±0. 02	(10) 0. 39±0. 06	(5) 0. 57±0. 06	(76) 0. 019	(76) 0. 26
Menziesia, leaves and new stem growth.	(20) . 004± . 001	(10) . 006± . 002	(5) . 011± . 003	(20) . 15± . 01	(10) . 20± . 02	(5) . 23± . 03	(61) . 008	(61) . 16
Early blueberry (*Vaccinium ovalifolium*), stems 10–12 in. long, with leaves.	(20) . 004± . 001	(10) . 006± . 002	(5) . 010± . 003	(20) . 14± . 02	(10) . 17± . 03	(5) . 19± . 04	(45) . 007	(45) . 15
Western hemlock (*Tsuga heterophylla*), stems 10–12 in. long, with needles.	(18) . 016± . 001	(9) . 016± . 002	(5) . 014± . 004	(18) . 08± . 01	(9) . 13± . 02	(5) . 20± . 05	(39) . 015	(39) . 11
Salal (*Gaultheria Shallon*), stems 10–12 in. long, with leaves.	(15) . 005± . 001	(8) . 017± . 012	(4) . 011± . 004	(15) . 08± . 01	(8) . 15± . 04	(4) . 16± . 04	(27) . 009	(27) . 11
Red huckleberry (*Vaccinium parvifolium*), stems 8–12 in. long, with leaves.	(4) . 005± . 001	(4) . 004± . 001	(2) . 018± . 010	(4) . 11± . 02	(4) . 18± . 01	(2) . 25± . 05	(10) . 004	(10) . 16
Sitka spruce (*Picea sitchensis*), stems 8–10 in. long, with needles.	(1) . 005	(1) . 005	(2) . 015	(1) . 15	(1) . 25	(2) . 28	(59) . 012	(59) . 13

[1] D. R. Marx, analyst.
[2] Analyses by staff, U.S. Geological Survey laboratory.

TABLE 48.2.—*Comparison of mean lead and zinc percentages in soils and plants sampled at Mahoney Creek, Revillagigedo Island, Alaska*

[D. R. Marx, analyst.]

	Lead			Zinc		
	Background	Halo	Vein	Background	Halo	Vein
Mean percentage in ash of all plant species sampled	0. 0090±0. 001	0. 011±0. 002	0. 016±0. 002	0. 14±0. 01	0. 21±0. 02	0. 27±0. 03
Mean percentage of all soil samples	. 002 ± . 001	. 011 ± . 004	. 130 ± . 069	. 003±. 001	. 008±. 003	. 087±. 046

"halo" samples. If "minus" anomalies can be shown to be consistent for a particular plant species and a specific element they can be useful in biogeochemical prospecting.

The averages of all Alaskan specimens of these species correspond well with the Mahoney Creek background values, being slightly higher because anomalous as well as background values were included in the computations.

The validity of differences between "background," "halo", and "vein" values of a certain species for each metal may be judged by the standard error included in the percentages table 48.1. If a difference between two values is as great or greater than twice its standard error, it is held to be a significant difference—not a sampling error (Standard Error of a Difference $=\sqrt{(\text{S.E.}_1)^2+(\text{S.E.}_2)^2}$). On this basis, minimum threshold values may be established which are significantly less than the commonly accepted standard of twice background values for soils. The physiological processes of primary salt absorption and ion exchange are operative in these plants, whereas the movement of

the metals through soils from their areas of concentration involves less complex processes. This "sensitivity" of plants to their substratum may make plant samples more accurate than soil samples as indicators of anomalous metal occurrence, particularly in "halo" value ranges.

49. GEOCHEMICAL EXPLORATION IN ALASKA

By Robert M. Chapman and Hansford T. Shacklette, Denver, Colo., and Georgetown, Ky.

Field and laboratory studies of the applicability in Alaska of presently known methods of geochemical exploration were begun in 1956; soils, plants, stream sediments, and stream waters were sampled in several regions of Alaska. Although most of the samples were taken over and near known mineral deposits, some were collected in areas that do not contain known deposits. Soil and plant sampling were concentrated in the areas shown on figure 49.1.

Thirty-eight different species of plants were used in evaluating methods of biogeochemical prospecting. Plant samples were collected at soil sample sites in order to relate the amount of metals in the plants to the amount in the soil where they were growing.

Analysis of the data is not fully completed and in some areas more samples are needed, but the following evaluations can be made:

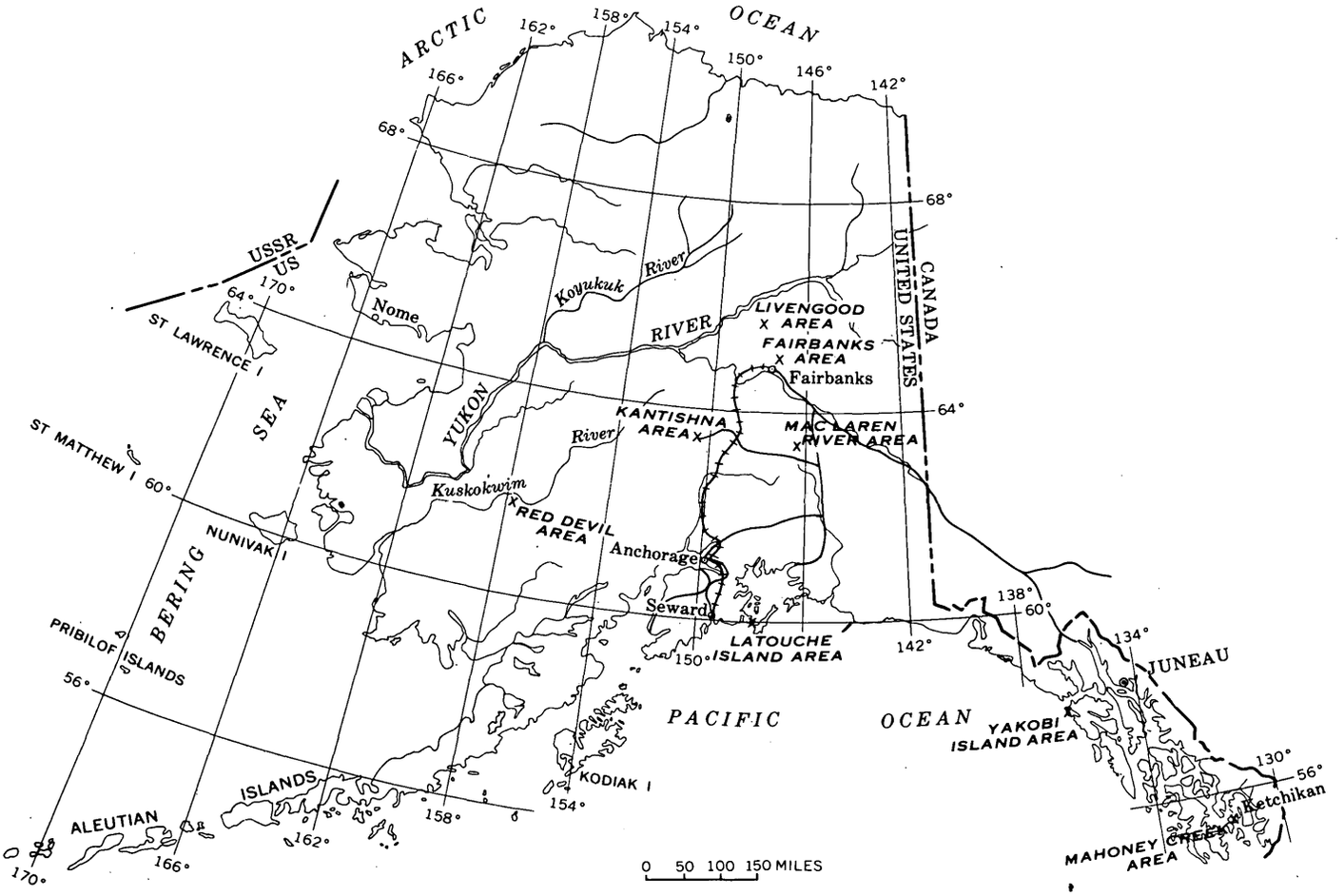

FIGURE 49.1.—Map of Alaska showing areas of detailed geochemical sampling.

1. Soil samples generally give anomaly patterns that assist in locating most of the deposits that were tested. Lead-zinc deposits at Mahoney Creek; lead-, zinc-, copper-, antimony-, and arsenic-bearing deposits in the Kantishna area; and silver-lead and tungsten deposits in the Fairbanks area showed clear-cut anomalies. Less distinct, but at least in part definitive, anomalies were obtained from samples taken over copper-nickel deposits on Yakobi Island, copper-bearing pyrite deposits on Latouche Island, mercury deposits at Red Devil, a copper deposit along the upper Maclaren River, and several sulfide-mineral deposits and a serpentine body near Livengood (table 49.1).
2. In general, samples from the C soil horizon near bedrock give the most reliable and useful sample and the largest metal content. Many of the A horizon samples show lower anomaly values and do not always reflect anomalies that are present in the underlying C horizon or bedrock and, owing to the humus content, are more difficult to process chemically.
3. Many plant and soil analyses show close correlation in the upper range of anomalous metal content, whereas the relationship is often obscure in the lower range of values.
4. On some sampling traverses the high metal values in plant ash do not occur at the sample site having

TABLE 49.1.—*Metal content, in parts per million, of soils in several areas of Alaska, based on approximately 1,060 samples*

[Analyses of −80 mesh material by rapid wet chemical field tests by staff of Geochemical Exploration Section laboratory. Soil C horizon may in places include some B horizon.]

Area	Rock type	Soil A_1 horizon											
		Background (ppm)						Anomalous (ppm)					
		Pb	Zn	Cu	Ni	As	Sb	Pb	Zn	Cu	Ni	As	Sb
Mahoney Creek	Slate												
Yakobi Island	Amphibole schist			<20	<20								
Yakobi Island	Gabbro and some diorite			<20–20	<20–20					>100–400	>50–400		
Yakobi Island	Norite			20–100	20–50					>100–400	>50–400		
Latouche Island	Graywacke and slate	<20–50	10–80+	10–50				100–1,250	100–200	>50–200			
Red Devil	Graywacke and shale												
Kantishna	Quartz-mica schist	<20–100(?)	<20–100(?)	10–50(?)		10–150(?)	?	>100–1,000 or 2,000	120(?)–180	60–100		200–1,200	?
Maclaren River	Basaltic rocks			30–70						>70–400			
Livengood	Ultramafic and mafic rocks.												
Livengood	Chert and metasedimentary rocks.												
Fairbanks	Quartz-mica schist and some granitic rocks.	<20–40	20–100			<10–20(?)		50–80	>100–180				

Area	Rock type	Soil C horizon												
		Background (ppm)							Anomalous (ppm)					
		Pb	Zn	Cu	Ni	As	Sb	Hg	Pb	Zn	Cu	Ni	As	Sb	Hg
Mahoney Creek	Slate	<20–50	<20–50	80–100(?)					>50–>3,000	>50–2,000	>100–300				
Yakobi Island	Amphibole schist			<20	<20										
Yakobi Island	Gabbro and some diorite.			50–70	20–50						100–1,500	100–600			
Yakobi Island	Norite			20–100	20–70						>100–1,500	100–600			
Latouche Island	Graywacke and slate	10–50	10–80+	10–50					80–200	100(?)–4,000	80–800				
Red Devil	Graywacke and shale					<10–150(?)	<1–6(?)	<2.5–6.5					>150–3,600	>6–900	9–160+
Kantishna	Quartz-mica schist	<20–100(?)	<20–100(?)	10–100(?)		<10–200(?)	1–10(?)		>100–4,000	>100–3,000	>100–300		>200–2,400 or 4,000	>10–1,100	
Maclaren River	Basaltic rocks			40–200							>200–1,200				
Livengood	Ultramafic and mafic rocks.	<20–50	25–120	20–80	50–400			<2.5–3(?)							
Livengood	Chert and metasedimentary rocks.	<20–20	20–120(?)	10–80	<25–100(?)			<2.5–(?)							>6(?)–15(?)
Fairbanks	Quartz-mica schist and some granitic rocks.	<20–40	20–150(?)	10–(?)			<1–4		50–8,000	>150(?)–7,000					

high soil values, but at an adjacent site. The direction of root growth of the plant in response to other soil factors having a physiological effect may cause this displacement.

5. Plant roots do not extend to great depths in Alaska, owing to (a) the general abundance of water in the upper soil horizons, (b) the thin soil mantle that usually overlies bedrock, and (c) the occurrence of permafrost or late-thawing cold subsoil which limits downward root growth. This growth characteristic restricts the usefulness of plants in indicating deeply buried metal deposits.
6. The ability of plants to indicate anomalous metal occurrence in the substratum on which they are growing varies with the species of plant and kind of metal. A species that accurately indicates anomalous amounts of one metal may be useless for indicating another metal.
7. The average metal content of all species for all areas studied varied with the different metals, and ranked in descending order as follows: zinc, iron, nickel, copper, lead, and molybdenum (table 49.2). High, low, and median values for these elements are also given.

TABLE 49.2.—*Mean metal content of 38 species of Alaskan plants, based on 5,126 analyses. Values expressed as percent in ash*

[Analyses by rapid wet chemical field tests by staff of U.S. Geological Survey laboratory]

Value	Metal content in number of analyses indicated					
	Lead (1,439)	Copper (1,502)	Zinc (1,439)	Nickel (396)	Iron (338)	Molybdenum (12)
High	0.500	0.300	4.00	0.600	7.50	0.003
Low	.002	.001	.02	.002	.04	.001
Mean	.012	.027	.32	.034	.28	.001
Median	.010	.022	.15	.015	.25	.001

8. There is commonly a great variation in amounts of a particular metal absorbed by different species of plants growing at the same site. This may represent the inherent limitations of the species in their range of metal absorption. Some species show a ratio of high to low metal content as great as 200:1, whereas others cover a range of only 5:1 to 10:1. Ratios of high to low percentages of several plants, which are considered to be representative of the total species analyzed, are given in table 49.3. Plants with high ratios have the capacity to indicate anomalous metal concentrations, whereas species with low ratios may be limited in this respect. These ratios may vary within a species, depending on the metal.
9. No definite geobotanical indicator species of flowering plants were observed in Alaska, although some of the species found on soil derived in part from serpentine may be included in this category. Several species of mosses and liverworts, however, were found which are generally recognized as occurring only on metal-rich substrata. The Alaskan specimens were found only on substrata containing, or presumed to contain, anomalous metal concentrations.

TABLE 49.3.—*Ratios of high to low content of metals in selected species of Alaskan plants*

[Analyses by rapid wet chemical field tests by staff of U.S. Geological Survey laboratory]

	Ratio of high to low metal content (number of analyses in parentheses)				
	Lead	Copper	Zinc	Nickel	Iron
Alder (*Alnus crispa* (Ait.) Pursh.)	(122)	(122)	(122)	(17)	----
	200:1	20:1	14:1	5:1	----
Crowberry (*Empetrum nigrum* L.)	(38)	(65)	(38)	(7)	(14)
	40:1	8:1	3:1	30:1	8:1
Deer cabbage (*Fauria Cristagalli* (Menz.) Makino)	(73)	(73)	(73)	(17)	(56)
	15:1	10:1	10:1	10:1	7:1
Dwarf blueberry (*Vaccinium uliginosum* L.)	(166)	(195)	(166)	(40)	(14)
	20:1	40:1	25:1	150:1	3:1
False hellebore (*Veratrum Eschscholtzii* A. Gray)	(44)	(44)	(44)	(21)	(23)
	10:1	100:1	10:1	50:1	5:1
Menziesia (*Menziesia ferruginea* Smith)	(76)	(76)	(76)	(15)	(26)
	60:1	20:1	8:1	25:1	16:1
Mountain hemlock (*Tsuga Mertensiana* (Bong.) Sarg.)	(66)	(66)	(66)	(7)	(56)
	200:1	20:1	2:1	20:1	8:1
White birch (*Betula resinifera* Britton)	(51)	(51)	(51)	(47)	----
	200:1	15:1	27:1	32:1	----

10. Stream sediments that were collected from 0.5 mile to as much as 2 or 3 miles downstream from deposits bearing one or more metals other than gold, generally showed an anomalous content of at least one metal (table 49.4). Lead, zinc, copper, antimony, arsenic, nickel, and chromium all give identifiable anomalies. Tests for tungsten, cobalt, molybdenum, titanium, manganese, and several other metals did not appear to be as useful, although these metals were not tested as extensively as the former group of metals.
11. Stream sediment derived chiefly or entirely from loessial mantle generally gives no clue to mineral deposits in the watershed.
12. Stream sediment sampling failed to detect placer deposits that lie beneath a relatively thick muck and gravel cover, which in most localities in interior Alaska is frozen. Apparently such deposits do not yield detrital or dissolved metal to the surficial stream sediment.
13. Stream water samples do not consistently give reliable leads to metalliferous deposits in the drain-

TABLE 49.4.—*Metal content of stream sediments in several areas of Alaska, based on approximately 455 samples*

[Analyses of −80 mesh material, after grinding it to −200 mesh, by rapid wet chemical field tests, by staff of U.S. Geological Survey laboratory]

Area and rock types	Background metal content (in ppm)								Anomalous metal content (in ppm)							
	Pb	Zn	Cu	Ni	Cr	As	Sb	W	Pb	Zn	Cu	Ni	Cr	As	Sb	W
Southeastern Alaska Many rock types.	<20-40(?)	<20-80(?)	<10-50(?)	<20-80(?)	20-150 (?)		<1-4 (?)		50(?)-4,000+	80(?)-4,000	>50(?)-400	>80(?)-1,200	>150(?)-1,500		5(?)-15	
Yakobi Island. Gabbro, norite, diorites and schist			30-50(?)	20-80(?)							60(?)-400	100(?)-400				
Latouche Island. Graywacke and slate	<10-40(?)	50-100(?)	10-60(?)			10-80(?)	3-10(?)									
Interior Alaska. Many rock types	<20-60(?)	<20-100(?)	<10-50(?)			<10-120(?)	<1-5(?)	<20(?)	>60(?)-300(?)	120(?)-700	60(?)-80			>120(?)-300	6(?)-45	20-40
Kantishna. Quartz-mica and chlorite schist	10-80(?)	20-120(?)	20-50(?)			<10-120(?)	1-12(?)		>80(?)-1,500	>120(?)-2,500	>50(?)-150			>120(?)-3,200	>12(?)-600	

age basins. Some base metal deposits were detected by anomalously high amounts of copper, lead, or zinc in water 0.5 mile downstream. Although this condition seemed to be detectable for as much as 3 miles downstream, it diminished to indefiniteness at that distance. In contrast, some other streams draining areas having similar deposits showed only normal metal content.

14. Apparently no useful correlation can be made between pH and metal content of stream waters, or between sulfide deposits and the sulfate content of waters draining from such deposits.

The analytical values given in tables 49.1 through 49.4 were determined by rapid wet chemical field tests that have a precision of −50 to +100 percent. Due consideration should also be given to the distance of the sample from the source deposit and to the rock type from which the sample material is derived. Thus, it is impossible to give an exact figure that divides background from anomalous values.

50. THERMOLUMINESCENCE AND POROSITY OF HOST ROCKS AT THE EAGLE MINE, GILMAN, COLO.

By CARL H. ROACH, Denver, Colo.

Preliminary results of a study of the base-metal replacement deposits in the Eagle mine, Gilman, Colo., indicate that thermoluminescence and porosity of host rocks adjacent to some ore bodies may be related to distance from ore and to alteration associated with ore.

The number 3 Lower Chimney ore body is enclosed by a large mass of dark aphanitic Leadville dolomite (Mississippian) that has been altered to "sanded dolomite" near the ore body (Lovering and Tweto, 1944). A few small patches of sanded dolomite occur at greater distances from the ore body. The sanding process changed the dark aphanitic dolomite to a coarse grained incoherent mass of light-gray dolomite sand. Generally, samples of sanded dolomite have less thermoluminescence than unaltered aphanitic dolomite and the amount of thermoluminescence of aphanitic dolomite increases with distance from the ore body (fig. 50.1). Exceptions are samples 49 through 52, which are slightly sanded and represent a rock type similar to the sanded dolomite near the chimney.

The porosity of the host rock near the number 3 Lower Chimney ore body is also related to intensity of alteration and to distance from ore (fig. 50.2). The porosity of sanded dolomite near ore ranges from 16 to 25 percent, whereas all dolomite samples more distant from ore than the mass of sanded dolomite have porosities of about 6 percent or less. An exception is sample number 38, which has a porosity between the two groups of samples. Sample 38 is very close to the mapped contact of sanded dolomite, and has probably been affected slightly by the sanding process even though this is not megascopically apparent. It is noteworthy that the porosity of samples 49 through 52 is not high with respect to the porosity of adjacent samples of aphanitic dolomite, even though these samples are slightly sanded.

The thermoluminescence of samples 49 through 52

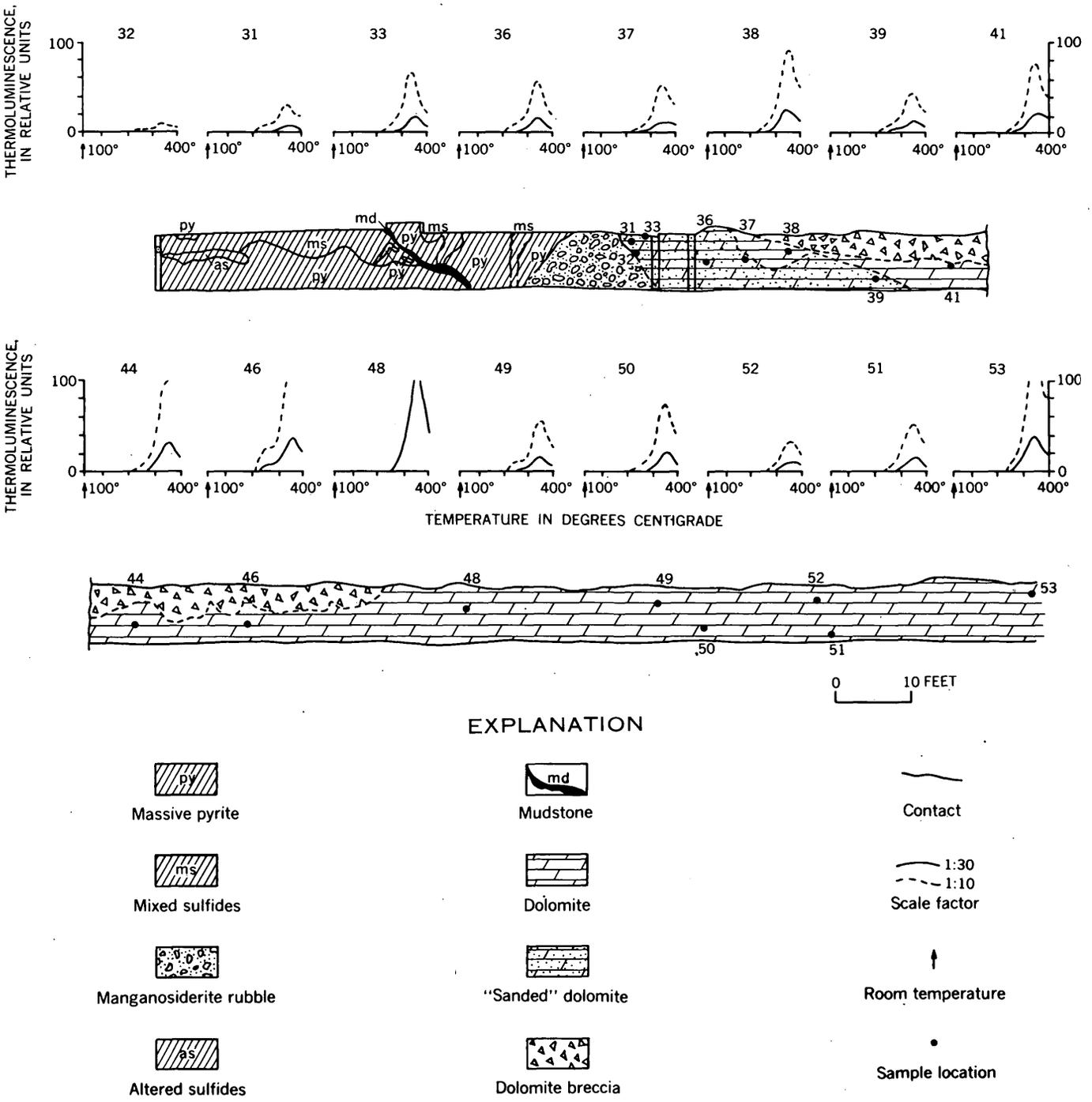

FIGURE 50.1.—Variations in thermoluminescence of the Leadville dolomite adjacent to the number 3 Lower Chimney ore body, Eagle Mine, Gilman, Colo.

was found to be similar to that of the sanded dolomite near the ore body (fig. 50.1). These relations suggest that porosity and thermoluminescence measurements might be useful in locating ore bodies. Porosity measurements might make it possible to differentiate between masses of intensely altered sanded dolomite near large ore bodies and small, less intensely altered masses of sanded dolomite that are far removed from ore. The porosity of sanded dolomite seems to be related to the intensity of alteration, which in turn seems to be related to nearness to ore bodies.

The Dyer dolomite member of the Chaffee formation (Upper Devonian) adjacent to the 18–35 chimney does not appear megascopically to have been intensely altered by sanding as is apparent near the ore body in the overlying Leadville dolomite. However, measure-

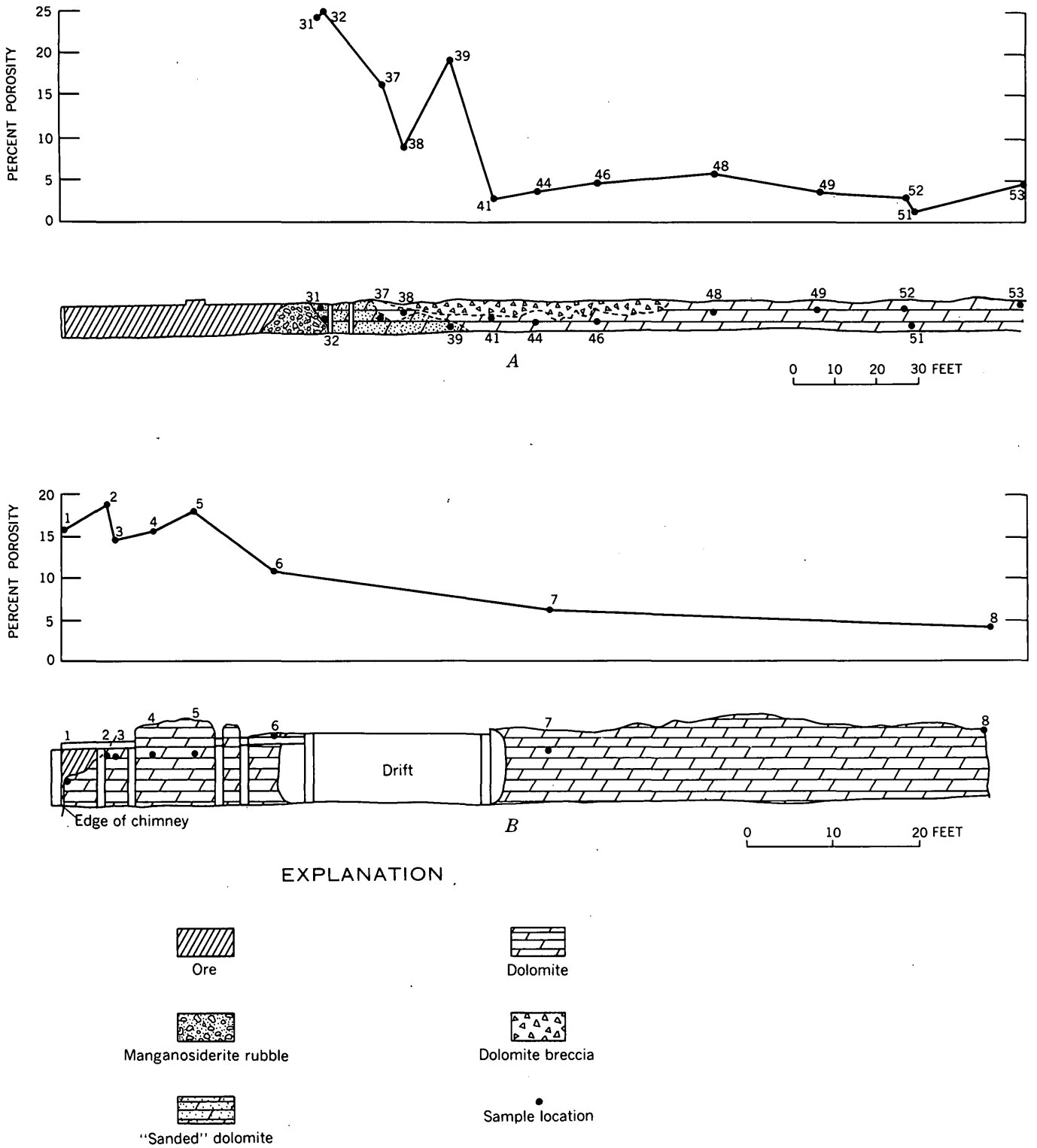

FIGURE 50.2.—Variations in porosity of (*A*) the Leadville dolomite adjacent to the number 3 Lower Chimney ore body, and (*B*) the Dyer dolomite member of the Chaffee formation adjacent to the 18–35 chimney ore body, Eagle Mine, Gilman, Colo.

ments show that the porosity of the Dyer dolomite member is high (15 to 20 percent) near ore and decreases with distance from ore (fig. 50.2*B*), indicating that alteration may have been more effective than is apparent megascopically. Dolomite more distant from ore than sample 8 may have lower porosity.

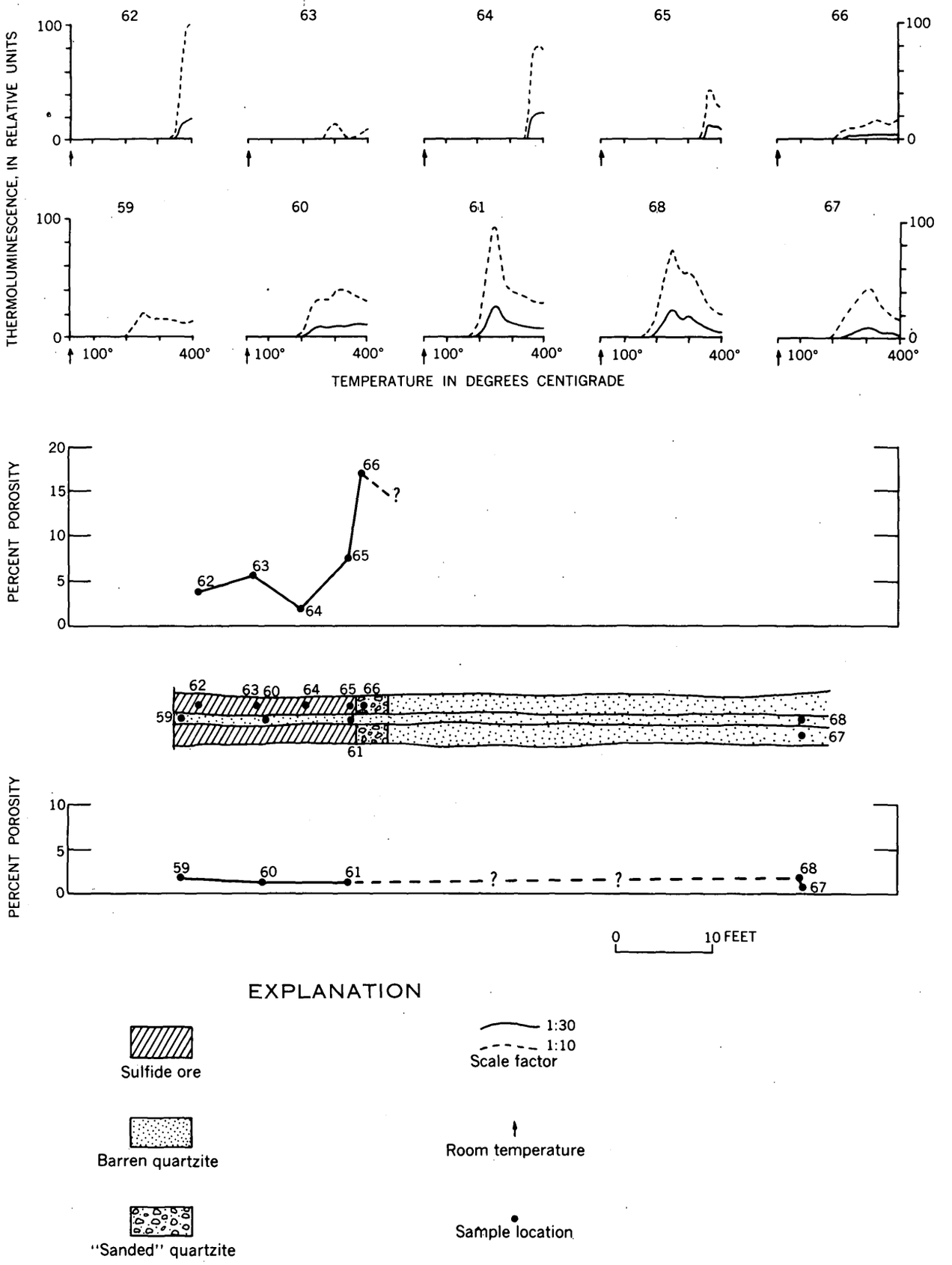

FIGURE 50.3.—Variations in thermoluminescence and porosity in and adjacent to a sulfide ore body in the Sawatch quartzite, Eagle Mine, Gilman, Colo.

It seems that alteration associated with the ore bodies has greatly increased the porosity of both the Leadville dolomite and the Dyer dolomite member of the Chaffee formation adjacent to ore (figs. 50.2*A* and 50.2*B*). The increased porosity associated with alteration in the Leadville dolomite is seemingly restricted to distances no greater than 50 feet from ore and terminates abruptly, whereas alteration in the Dyer dolomite member seems to have been more pervasive and to decrease gradually with distance from ore. These relations suggest that a unique porosity variation with distance from ore may be characteristic of each carbonate unit. These different variations taken together may be useful as a guide to ore.

Sulfide ore bodies also occur in the Sawatch quartzite (Upper Cambrian) in the deepest workings of the Eagle mine. One of these ore bodies consists of two layers of sulfide ore separated by a thin layer of quartzite (fig. 50.3) and is bisected by a vertical silver-bearing galena vein. Quartzite at the lateral edges of the two ore layers has been sanded. The thermoluminescence of the quartzite in the thin bed between the ore layers seems to be related to distance of the samples from the vein (fig. 50.3); the sanded quartzite has much less thermoluminescence than adjacent samples of unaltered quartzite.

The ore and altered quartzite have higher porosity than the barren unaltered quartzite (fig. 50.3). The sanded host rock has a much higher porosity than unaltered quartzite, but unlike sanded dolomite near ore in the Leadville, the sanded quartzite is limited to a very narrow zone at the edges of the ore body.

REFERENCE

Lovering, T. S., and Tweto, Ogden, 1944, Preliminary report on geology and ore deposits of the Minturn quadrangle, Colorado: U.S. Geol. Survey open-file report.

51. USEFULNESS OF THE EMANATION METHOD IN GEOLOGIC EXPLORATION

By Allen B. Tanner, Salt Lake City, Utah

[0] *Work done in cooperation with the U.S. Atomic Energy Commission*

Exploration for radioactive materials or geologic features by measurement of one or more of the emanation isotopes, radon, thoron, and actinon, contained in soil gas near the surface of the earth, is called the emanation method. The basic concept is that the emanation isotopes, being gaseous, may migrate by diffusion and transport for a distance from their source through soil overburden greater than the distance effectively penetrated by gamma rays from the same source. Because the techniques for emanation measurement are also more sensitive and more specific than field gamma-ray measurements, emanation surveying—particularly that using radon-222 measurement—has been practiced occasionally for about forty years (Ambronn, 1928). In the United States it has not won recognition or general acceptance as a practical method because of contradictory results of field testing. The principal matter of dispute has been the depth of penetration of the method, estimates of which—based on apparent field success—have ranged from several inches to hundreds of feet.

The theoretical approach has been fruitful and has been presented by Grammakov (1936), who showed the extent of emanation migration through permeable material to be a sharply decreasing hyperbolic function of distance. From various theoretical and laboratory results it may be estimated that the emanation method is accurate and effective to a maximum depth of about 30 feet in dry, coarse, nonradioactive overburden. Soil moisture content of more than about 6 percent reduces the effective depth many-fold, and moist clay layers practically prevent radon migration.

It is becoming apparent that most of the "radon" anomalies described in the literature probably occur not because of the migration of the gaseous but short-lived radon, but because of migration of radium and other intermediate decay products of uranium in solution. Rosholt (1959) has shown that the radioactive disequilibrium that would accompany such migration in solution is the rule, rather than the exception, in uranium ores. In Karnes County, Tex., a radon anomaly over a uranium ore body covered by 1 to 10 feet of overburden was due to migration of radium and other intermediate decay products of uranium; radon migration was virtually nil. Such anomalies tend to be displaced in the direction of ground-water move-

ment and therefore to be inaccurate in locating geologic features unless the features are large compared with the thickness of overburden.

REFERENCES

Ambronn, Richard, 1928, Elements of geophysics, translated by Margaret C. Cobb: New York, McGraw-Hill Book Co. (Chap. IV).

Grammakov, A. G., 1936, O vliyanii nekotorykh faktorov na rasprostraneniye radioaktivnykh emanatsiy v prirodnykh usloviyakh (On the influence of certain factors on the spreading of radioactive emanations under natural conditions) : Zhurnal Geofiziki, v. 6, no. 2–3, p. 123–148.

Rosholt, J. N., Jr., 1959, Natural radioactive disequilibrium of the uranium series: U.S. Geol. Survey Bull. 1084–A, p. 1–30.

52. POLAR CHARTS FOR EVALUATING MAGNETIC ANOMALIES OF THREE-DIMENSIONAL BODIES

By Roland G. Henderson, Washington, D.C.

CHART DEVELOPMENT

In the indirect approach to the interpretation of total-magnetic intensity anomalies, one makes an intelligent guess concerning the depth, size, shape, and magnetization of the disturbing body, and checks his hypothesis by calculations. For three-dimensional bodies (that is bodies with both horizontal dimensions not large in relation to the depth of burial) the calculations are quite difficult; accordingly, graphical methods are indicated. In this report we present a new and simple polar chart method for the rapid computation of the magnetic effect of any magnetic body.

The charts are based on the formula for the magnetic effect of an elemental solid sector cut from a buried hollow vertical cylinder of infinite depth extent.

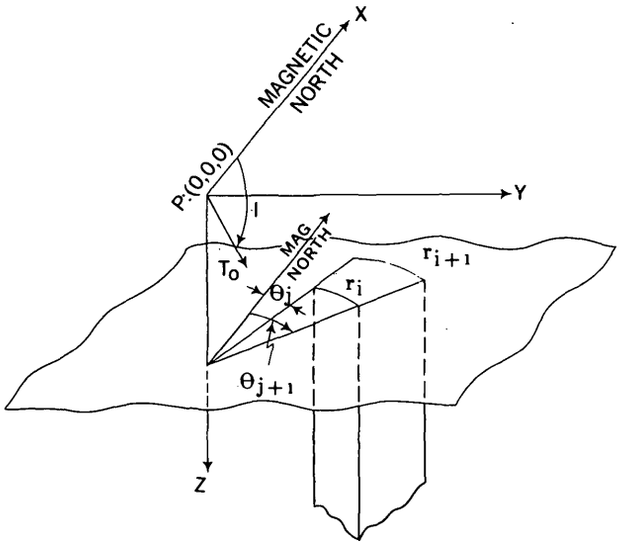

FIGURE 52.1.—Geometrical basis for effect at P due to elemental semi-infinite vertical cylinder magnetized by induction in a field, T_o.

In figure 52.1, let P: (0,0,0) be a point in the xy-plane on which the observations are presumed to have been made, and let the upper face of the cylinder terminate in a plane which is one depth unit below the xy-plane. Let r_i and r_{i+1} be the radii of the elemental hollow cylinder and let θ_j and θ_{j+1} be azimuths of the radial line boundaries of the sector. At P, the total magnetic intensity anomaly per unit magnetization produced by the elemental column is given by

$$\left(\frac{\Delta T}{kT_o}\right)_{i,j} = \int_{r_i}^{r_{i+1}} \int_{\theta_j}^{\theta_{j+1}} \left\{ \frac{\cos^2 I}{r}\left(\frac{1}{\sqrt{r^2_{+1}}}-1\right)(1-2\cos^2\theta) - \frac{r\cos^2 I\cos^2\theta}{(r^2+1)^{3/2}} + \frac{2r^2\sin I\cos I\cos\theta}{(r^2+1)^{3/2}} + \frac{r\sin^2 I}{(r^2+1)^{3/2}} \right\} dr d\theta \quad \ldots\ldots\ldots\ldots (1)$$

where k is the magnetic susceptibility, T_o the magnitude of the earth's normal magnetic field and I its inclination. For a given I, the infinite half-space anomaly per unit magnetization at P is, $\left(\frac{\Delta T}{kT_o}\right)$ ½-space= $\pi(2\sin^2 I-\cos^2 I)$ By integrating (1) from $\theta_j=0$ to $\theta_{j+1}=2\pi$, we obtain the anomaly at P due to the i-th ring cylinder of radii r_i and r_{i+1}. We use this formula to divide the half-space into a family of consecutive concentric cylinders each having an arbitrarily prescribed percent of the half-space magnetic intensity value. Next we find for each ring cylinder, in turn, the various azimuths θ_j, which divide the ring into sectors each having the same effect at P. A facsimile of the polar chart constructed for I=75° is shown in figure 52.2. Each non-numbered sector has the effect of 0.005652 gammas per unit magnetization at the center

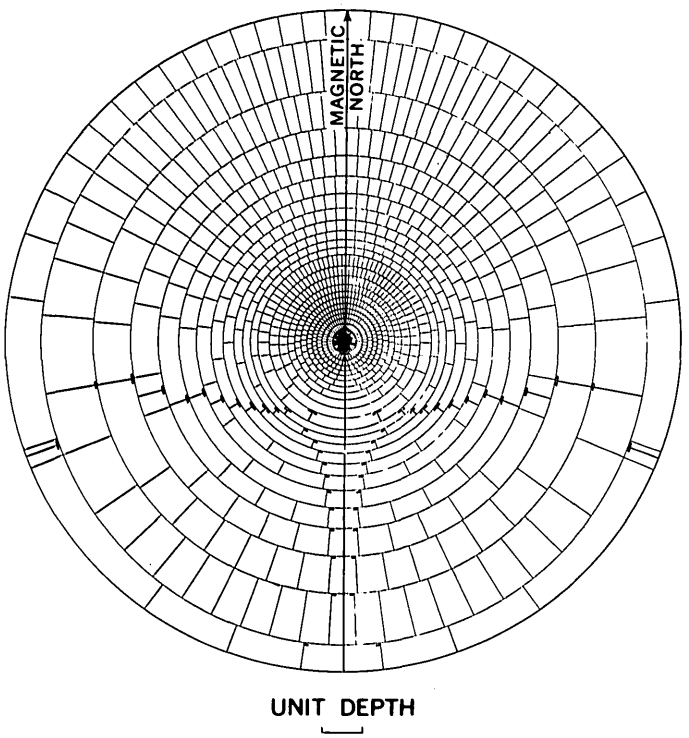

FIGURE 52.2.—Polar chart for computing the magnetic anomaly of three-dimensional bodies magnetized in a field of inclination I=75°.

of the chart. The sectors in the lower portion of the chart set off by heavy radial lines are negatives. Numbers indicate the partial value (in percent) for incomplete sectors. Similar polar charts have been constructed for inclinations I=90°, 75°, and 45°. Charts for I=30°, 20°, and 0° will be constructed. The computation of the charts is being carried out by Alphonso Wilson of the U.S. Geological Survey.

USE OF CHARTS

For desk use, film positives of the charts are reproduced at a scale one-half inch equals a depth of burial. In a three-dimensional computation the body is subdivided into horizontal layers represented by contours. Through each point to be computed on the plane of observations, a line is drawn in the direction of magnetic north. Because the depth of every level is different the scale at each level must be adjusted to agree with that of the chart. This scale reduction can be done either photographically or optically on a projector. The center of the chart is placed at the point to be computed, the axis being alined with magnetic north. The chart elements or portions thereof covering the area inside the contour are counted. At each level counts for the bottom contour of the overlying layer are prefixed with a negative sign, and counts for the top contour of the lower layer are prefixed with a positive sign. The counts for all levels are added algebraically to obtain the anomaly of the body at a given point on the surface. Tests show that the charts yield accurate results.

The method, although still developmental, is being used by J. W. Allingham and Montgomery Higgins of the U.S. Geological Survey to interpret anomalies caused by topography in southeast Missouri. Their computations for Bald Knob are illustrated in figure 52.3, which shows the generalized elevation contours, and in figure 52.4, which shows both a vertical section along *A–B* and the computed (solid line) together with the observed (broken line) magnetic profiles. The misfit on the north limb of figure 52.4 is attributed to the influence of adjacent magnetic material not included in the calculation.

The charts have a wide variety of applications. Since at a radius of 20 depth units the charts cover 95 percent of the half-space anomaly, they also can be used on bodies traditionally computed by two-dimensional methods. Vertical contacts, horsts, grabens, dikes, plugs, pipes, etc., are examples of bodies rapidly computed in this way.

REMANENT MAGNETIZATION CALCULATIONS

Remanent magnetization, invariably neglected in calculations, may sometimes be many times greater than the induced magnetization. In view of the in-

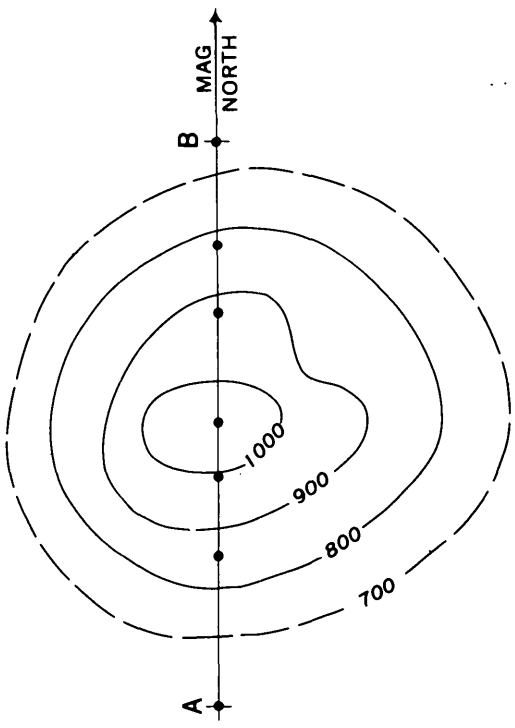

FIGURE 52.3.—Generalized topography of Bald Knob, southeast Missouri, showing location of section *A–B*.

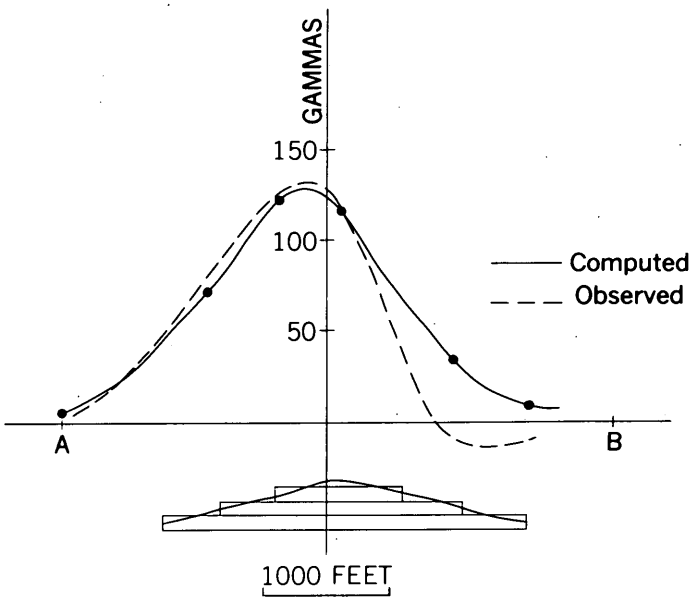

FIGURE 52.4.—Vertical section of Bald Knob taken along *A–B* and magnetic profile computed for three-dimensional topographic relief.

creasing volume of data on remanent magnetization, methods must be developed for making total magnetic intensity calculations when some knowledge of the remanent moment and shape of the body is available. Polar charts constructed for $\triangle Z$ and $\triangle H$ for various inclinations are required for these calculations. One excursion over the body must be made with each chart. The $\triangle Z$ charts also would be of much value to those conducting vertical component surveys.

CHARTS FOR OPTICAL ANALOGUE COMPUTER

Use of a chart involves a counting of the covering chart elements. This is an operation which can be performed on a commercially available optical analogue computer designed for gravity calculations. To adapt this equipment for magnetic applications we have devised charts equipped with a uniform number of light apertures per sector. The transmitted light is proportional to the anomaly and as it falls upon a photoelectric cell is measured in a potentiometer circuit. In a recent test the anomaly of a vertical cylinder was computed with an error of less than two percent. Methods of improving the sensitivity and drift characteristics of the equipment are being studied. This adaptation of the computer may be a major breakthrough in calculations for magnetic interpretation.

53. MAGNETIC EVIDENCE FOR THE ATTITUDE OF A BURIED MAGNETIC MASS

By GORDON E. ANDREASEN and ISIDORE ZIETZ, Washington, D.C.

It has long been recognized that one of the shortcomings in the analysis of magnetic and gravity data is the inability to determine a unique configuration for a rock mass that is assumed to produce an anomaly. The purpose of this paper is to show that despite this ambiguity, the dip of a dikelike mass at known depth can be confidently ascertained within narrow limits, irrespective of the thickness of the mass.

To illustrate the interpretive procedure, a typical linear aeromagnetic anomaly was selected for analysis.

A total-intensity aeromagnetic map of east-central Indiana (Henderson and Zietz, 1958, plate 4) shows a two-dimensional anomaly extending from Fayette County across Wayne County and into Randolph County (fig. 53.1). This anomaly trends northeast and has a magnetic relief ranging from 200 to 400 gammas. Magnetic profiles were flown, approximately 1,000 feet above the ground, along north-south lines one mile apart. Others were flown at the same altitude but crossing the feature at right angles to its trend (fig. 53.1). All these profiles are very similar in shape but differ in amplitude. From these, profile C was selected to represent the essentially two-dimensional feature producing the anomaly (fig. 53.2).

GEOLOGY

The area is underlain at depth by sedimentary rocks of Precambrian and Paleozoic age up to and including the Pennsylvanian, and the Pennsylvanian rocks are overlain by Quaternary sediments. There are three drill holes in the area. Two of these are on the east and west flanks of the anomaly (fig. 53.1), and reach Precambrian rocks at depths of 2,478 and 2,617 feet below mean sea level respectively. The third, in Jay County immediately north of Randolph County, reaches Precambrian rocks at a depth of 2,471 feet below mean sea level. Hence it is reasonable to assume that the relief of the Precambrian surface in the area

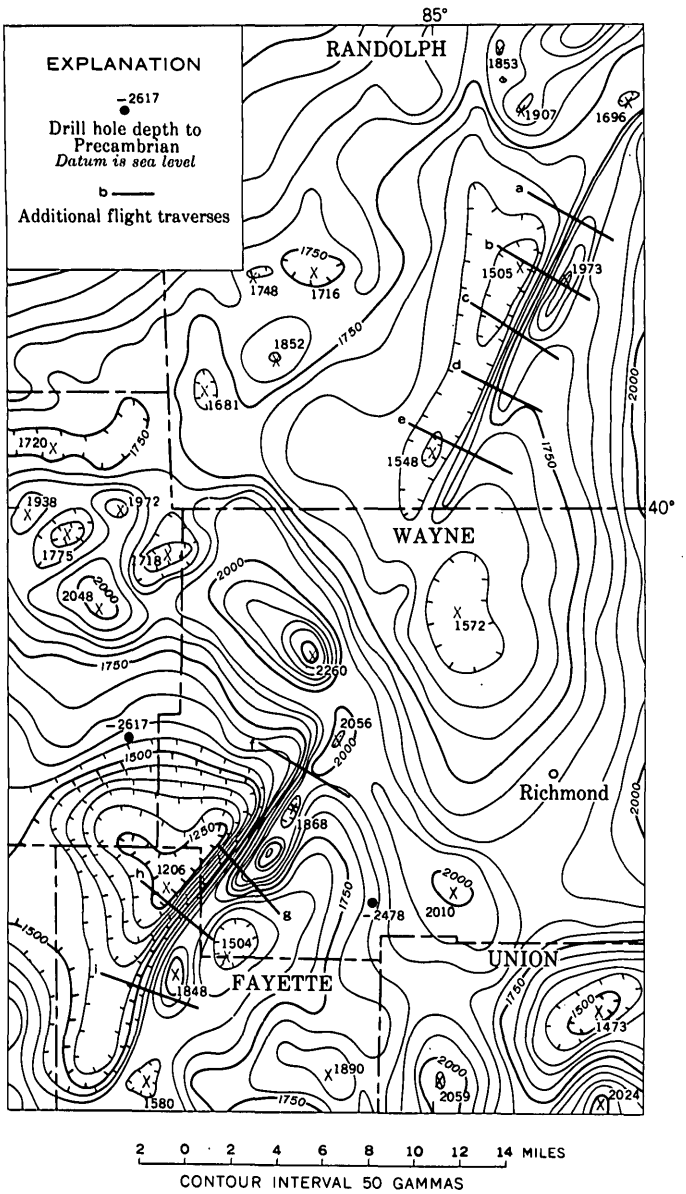

FIGURE 53.1.—Total intensity aeromagnetic map of part of Indiana (from Henderson and Zietz, 1958, pl. 4).

considered is at most only a few hundred feet. The magnetic anomaly could be due to igneous rock intruded into the sedimentary rocks, but no intrusive rocks are now known to be exposed in Indiana.

ASSUMPTIONS AND PROCEDURE

It is assumed that the upper surface of the anomaly-producing rock mass coincides with the surface of the Precambrian and that it is flat-topped, for topographic relief of several hundred feet at this depth would contribute little, if at all, to the magnetic anomaly. Experience has shown, also, that the magnetic susceptibility of the sedimentary rocks may be considered negligible.

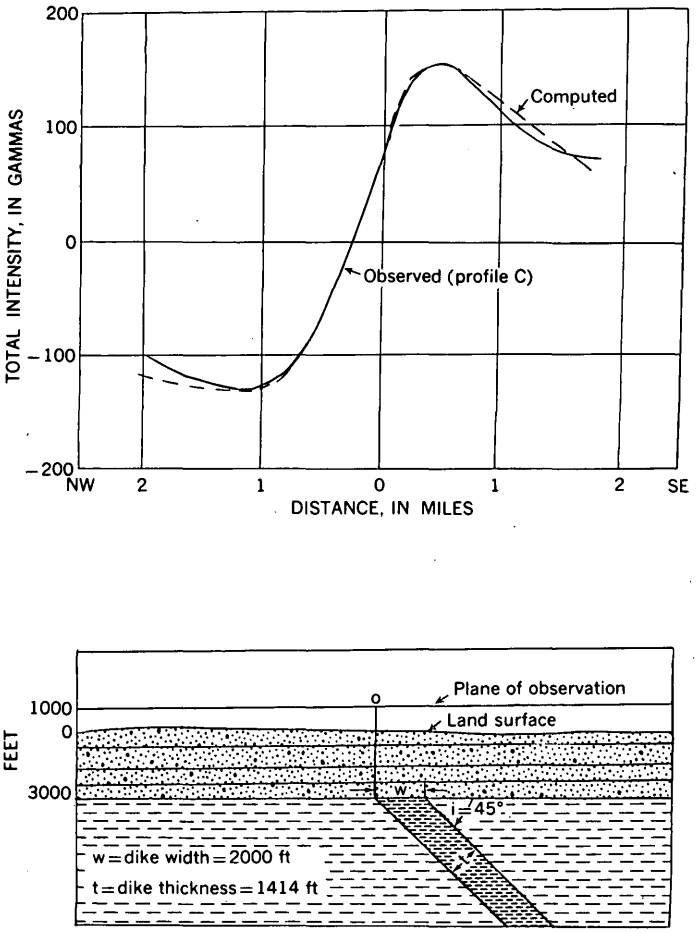

FIGURE 53.2.—Observed and computed magnetic profiles over an assumed dike of infinite depth extent.

Because of the linearity of the magnetic feature, it was believed that the anomaly might be produced by the juxtaposition of two rock masses of different magnetic properties within the Precambrian complex. One possible cause of such a juxtaposition would be faulting in the Precambrian basement, but computed magnetic profiles based on this assumption did not closely resemble the observed profile. Excellent agreement was obtained, however, by assuming a dikelike mass dipping to the southeast as shown in figure 53.2. It was also assumed that the rock mass was magnetized by induction in the earth's field, and that remanent magnetization, if present, was also in the same direction or was negligible.

Geophysical evidence thus indicated the probable existence of a dikelike mass whose top is at the surface of the Precambrian rocks. It remained to determine the numerous possible combinations of dike width and dip for which the profiles computed from the above-stated assumptions will provide reasonable fits to the observed anomaly.

GOODNESS OF FIT

As a help in making a quantitative estimate of the "goodness of fit," the symbol "G" was introduced. This represents a quantity that corresponds to the Chi-square of least-square theory and is the sum of the square of the differences between observed and computed values at equally spaced intervals (fig. 53.3) and is expressed

$$G=\sum_{j=1}^{j=n}(\Delta T_{j(\mathrm{obs})}-\Delta T_{j(\mathrm{comp})})^2.$$

For dike widths of multiples of 1,000 feet and dip angles to the southeast corresponding to values of 15°, 30°, 37½°, 45°, 52½°, 60°, 67½°, 75°, and 90°, the value of "G" was computed and contoured as shown in figure 53.4. For example, a dike with a thickness of 2,600 feet (horizontal width of 3,000 feet) and a dip angle of 60° produced a magnetic profile whose index of fit is 40.

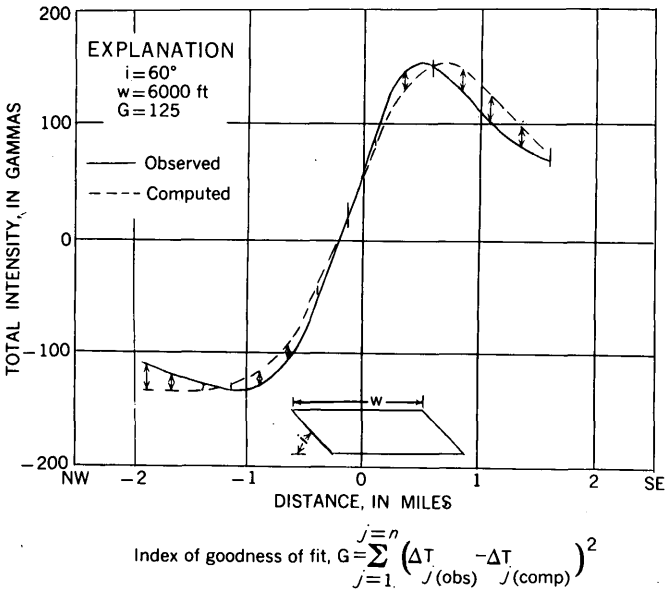

FIGURE 53.3.—Method of computing index of goodness of fit.

Figure 53.4 may be used to provide limits on dike thickness and dike width. According to theory the best fits are obtained for small values of "G," and comparison between the observed computed profiles indicates that all values of "G" less than 100 provide satisfactory fits. Furthermore, limits for both dip and thickness may be obtained by noting the values at which

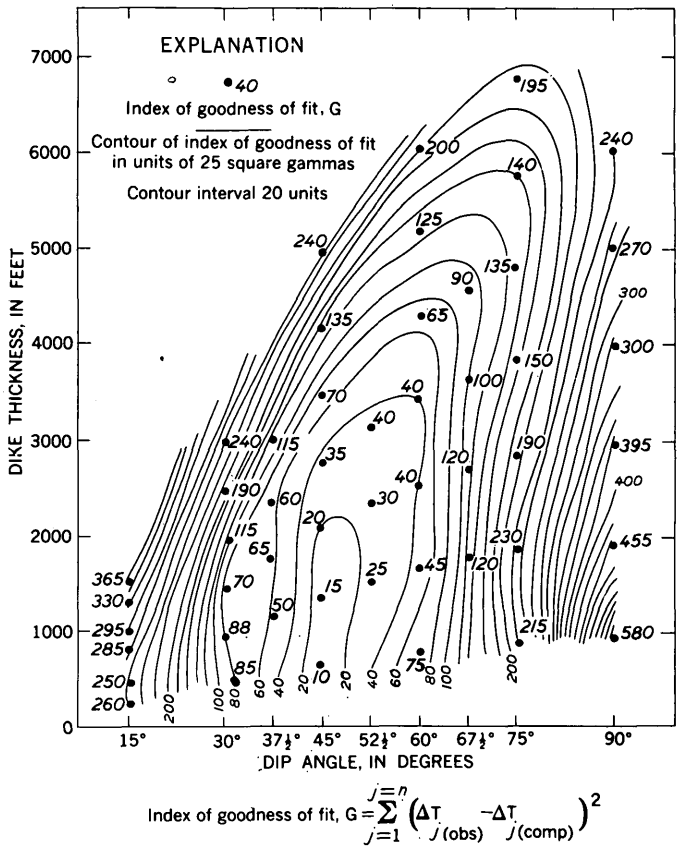

FIGURE 53.4.—Contour plot of goodness of fit for various dike thicknesses and dip angles.

sharp changes occur in the gradient of the contours. Specifically, it may be seen that between 30° and 60° a small change of dip angle results in a large change in the "G" factor. From these considerations, limits on dike width may be inferred to range from less than 1,000 feet to 5,000 feet or more. Limits on the dip of the dike, however, are restricted within the narrow range of 30° to 60°.

It may be concluded that, in spite of the ambiguity which is always present in the interpretation of magnetic data, it is possible in this case to infer the presence of a dikelike mass of intrusive rock in the Precambrian basement, dipping to the southeast at an angle that is almost certainly between 30° and 60° and probably not far from 45°.

REFERENCE

Henderson, J. R., Jr., and Zietz, Isidore, 1958, Interpretation of an aeromagnetic survey of Indiana: U.S. Geol. Survey Prof. Paper 316–B, p. 19–37.

54. USE OF AEROMAGNETIC DATA TO DETERMINE GEOLOGIC STRUCTURE IN NORTHERN MAINE

By JOHN W. ALLINGHAM, Washington, D.C.

Many geologic problems in northern Maine, such as correlating certain geologic units and determining their structural relations, can be solved by the application of geophysical methods. Three geophysical methods, aeromagnetic, electromagnetic (Frischknecht and Ekren, Art. 56), and gravity, have been applied successfully to specific geologic problems in areas of glacial cover. The aeromagnetic method is used in Maine to trace magnetic units, and thus to determine regional geologic structures, in areas of thin glacial cover.

Aeromagnetic surveys in northern Maine cover about 12,000 square miles. Most of these surveys were flown with ¼-mile spacing between flight lines and at an altitude of about 500 feet above the ground. A compilation of geologic and aeromagnetic data from northern Maine by Boucot and others (1960) contributes much new information on this area. Their maps provide a basis for planning detailed geologic and geophysical studies in areas considered favorable for mineral investigations. The magnetic patterns on these maps show (a) the orientation, attitude, and continuity of narrow belts of volcanic rocks, mafic intrusive rocks, and contact-metamorphic rocks; (b) a general northeasterly structural grain; (c) magnetically contrasting differentiates within felsic intrusives; and (d) the outlines of granitic plutons that have hornfels rims.

Several periods of sedimentation and volcanism, orogeny, and intrusion are represented in northern Maine. Large areas of sedimentary rocks, containing Ordovician fossils and interbedded with volcanic and pyroclastic rocks, were folded during a Late Ordovician orogeny and later intruded by granite, diorite, and gabbro. All these rocks are overlain unconformably by a second sedimentary sequence of Silurian and Lower Devonian strata, which contain widespread beds of slate and are associated with rhyolite, diabase, greenstone, and pyroclastic rocks. An Early or Middle Devonian orogeny affected the entire area and produced the largest structural feature in the region, the Moose River synclinorium, which trends northeastward from Eustice to Mount Katahdin. Structural relations northeast of Mount Katahdin are more complex and less well known than those to the southwest. This orogeny was followed by intrusion of Middle Devonian plutonic rocks, around most of which there are rims of hornfels.

The magnetic properties of these rocks, as determined by laboratory measurements, are very helpful in working out geologic structure. One of these properties, magnetic susceptibility, can be used to divide the rocks into three groups: (a) argillite, slate, and sandstone, which have negligible susceptibility; (b) granite, rhyolite, and pyrrhotitic slate, which have low susceptibility—usually less than 1×10^{-3} cgs; and (c) diorite, diabase, greenstone, gabbro, and serpentine, which have moderate susceptibility—greater than 1×10^{-3} cgs. Magnetic anomalies associated with felsic intrusive and hypabyssal rocks and some volcanic rocks range from 50 to 300 gammas, and those associated with diorite, gabbro, greenstone, and serpentinized ultramafic bodies range from 200 to 1500 gammas.

In the Aroostook area, interbedded volcanic flows, pyroclastic rocks, teschenite dikes, and manganiferous iron formation can be traced along their trend by characteristic aeromagnetic patterns. A 100- to 200-foot diabase dike has been traced for more than 25 miles in the Danforth area, indicating a possible extensive northeasterly zone of fracture. Not only can geologic units be traced across areas of sparse outcrop by use of aeromagnetic data, but interpretation of these data can be used in areas of intrusive rocks to study the form and attitude of instructive bodies. For example,

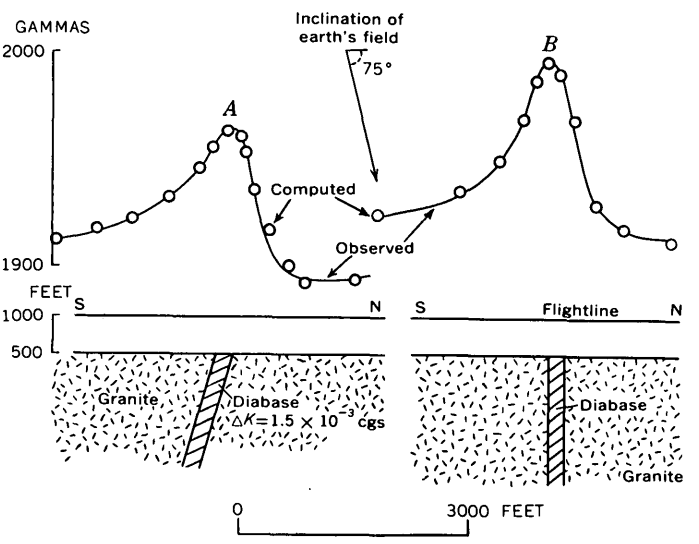

FIGURE 54.1.—Attitude of diabase dike, near Danforth, deduced from aeromagnetic profiles *A* and *B*. Bedrock geology by D. M. Larrabee.

fitting computed magnetic data to the aeromagnetic profiles observed over the diabase dike shown in figure 54.1 suggests that the dip of the dike changes from nearly vertical to about 75 degrees southeast where the dike is in the granite, but is less steep where the dike is in sedimentary rocks.

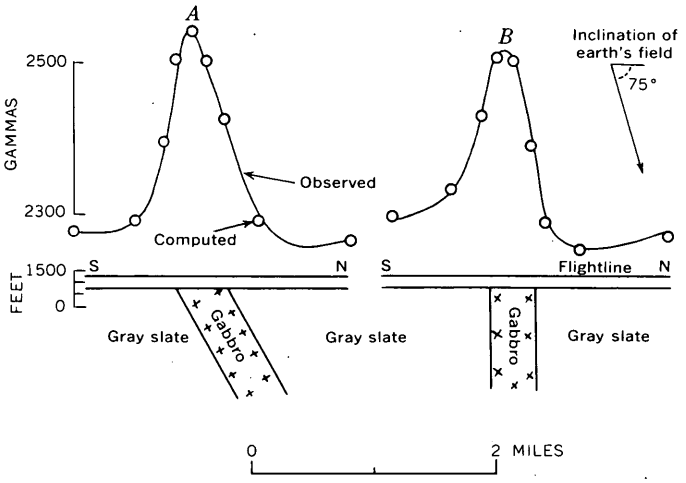

FIGURE 54.2.—Attitude of the gabbro near Moxie Pond as determined from aeromagnetic profiles *A* and *B*.

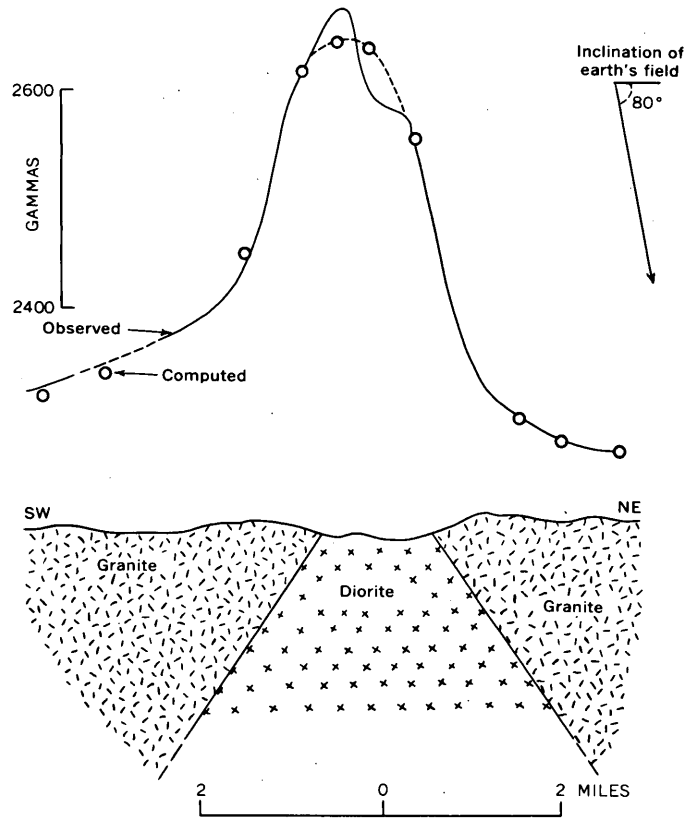

FIGURE 54.3.—Shape of diorite body in granite, near Mount Katahdin, as determined from aeromagnetic profile. Bedrock geology by A. Griscom.

From an examination of several profiles the dips of other linear sheetlike bodies, such as the gabbro near Moxie Pond (fig. 54.2), can be determined within 15 degrees. Locally the dip of this gabbro sheet changes abruptly from nearly vertical to about 60 degrees northwestward. This change in dip may indicate a significant structural dislocation in the rocks of this area.

Isolated magnetic anomalies within a felsic intrusive body may indicate mafic differentiates, separate intrusions, or large inclusions within the intrusive body, such as the diorite body in the granite near Mount Katahdin (fig. 54.3). A simple two-dimensional analysis (Pirson, 1940) of the aeromagnetic information (Balsley and others, 1957) gives a rapid estimate of the attitude of the contacts, and therefore determines the shape of the body. Irregularities in the profile near its peak indicate inhomogeneities in the diorite but do not materially affect the interpretation.

Magnetic slate containing pyrite and pyrrhotite is interbedded near Bingham with calcareous slate. The attitude of the slate, obtained by fitting computed data

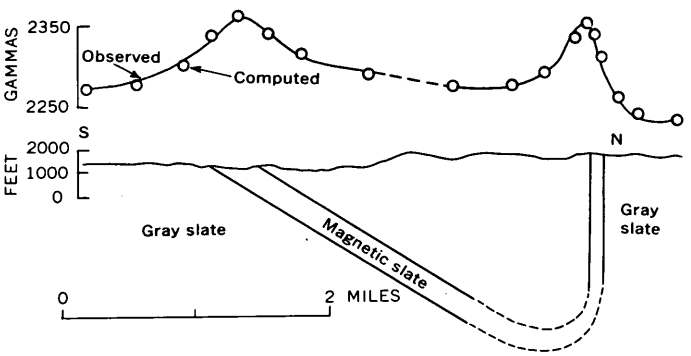

FIGURE 54.4.—Attitude of magnetic slate as determined from aeromagnetic profile.

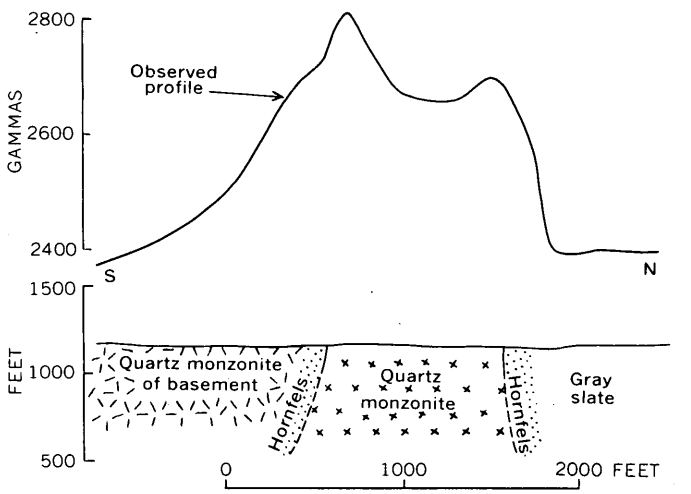

FIGURE 54.5.—Aeromagnetic profile over quartz monzonite. Bedrock geology by A. A. Albee.

to observed profiles, possibly indicates a significant fold, which may be either an asymetric syncline or an overturned anticline (fig. 54.4).

Some plutons, such as the intrusive quartz monzonite on Hog Island (fig. 54.5), are outlined by a more magnetic rim of hornfels, whereas other plutons, such as the granite at Bald Mountain, are not shown by the magnetic data, because they are not rimmed with magnetic metamorphosed rock. Bodies of gabbro and diorite commonly have a border more magnetic than the interior. Interpretation of magnetic profiles is sometimes complicated by these magnetic borders or by rims of hornfels; in such cases, however, much structural information, particularly the attitude of contacts, can be obtained by analysis of selected aeromagnetic data.

REFERENCES

Balsley, J. R., Blanchett, Jean, and Kirby, J. R., 1957, Aeromagnetic map of Harrington Lake quadrangle, Piscataquis County, Maine: U.S. Geol. Survey, Geophys. Inv. Map GP 155.

Boucot, A. F., Griscom, Andrew, Allingham, J. W., and Dempsey, W. J., 1960, Geologic and aeromagnetic map of northern Maine: U.S. Geol. Survey open-file report.

Pirson, S. J., 1940, Polar charts for interpreting magnetic anomalies: Am. Inst. Mining Metall. Engineers Trans., v. 138, p. 173–192.

55. CORRELATION OF AERORADIOACTIVITY DATA AND AREAL GEOLOGY

By Robert B. Guillou and Robert G. Schmidt, Washington, D.C.

Work done in cooperation with the U.S. Atomic Energy Commission

The correlation of aeroradioactivity data and areal geology in several areas of the United States is being investigated by the U.S. Geological Survey. Study of aeroradioactivity profiles obtained using equipment and surveying techniques developed in the search for deposits of radioactive materials indicates that aeroradioactivity surveying can be an important adjunct to a geological mapping program.

Aeroradioactivity surveys are flown at 500 feet above the ground on parallel flight lines oriented normal to geologic trends. A flight-line spacing of a quarter of a mile is used for detailed surveying and a spacing of 1 or 2 miles is used for reconnaissance surveys. The scintillation detection equipment used in the surveys, which utilizes six thallium-activated sodium iodide crystals (4 inches in diameter, 2 inches thick), has been described by Davis and Reinhardt (1957). Gamma radiation emanating from the top six inches or so of surficial material of a strip about 1,000 feet wide is recorded in counts per second (cps) as a continuous profile. The cosmic background component is removed and the data are compensated for deviations from the nominal 500 foot surveying altitude.

Correlation of aeroradioactivity data and areal geology is similar to subsurface correlation using gamma-ray logs of drill holes. Radiation units are delineated by connecting similar radioactivity features on adjacent profiles. The contact between radioactivity units is assumed to be the point where a reading halfway between two levels is recorded (fig. 55.1). Each unit is considered to represent an area on the ground that has a particular content of gamma emitters in the surfi-

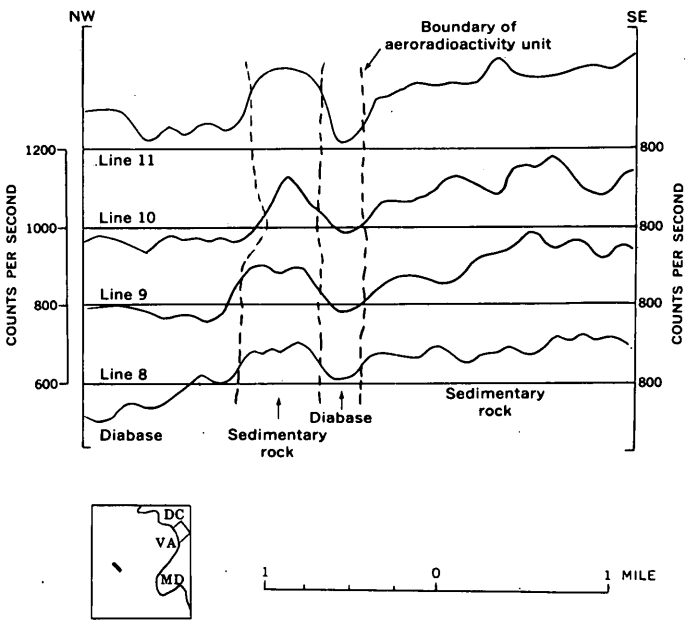

FIGURE 55.1.—Aeroradioactivity profiles in the Bealeton area, Virginia.

cial material. Where bedrock and residual soil are the surficial material, the major and minor aeroradioactivity features match the trends, and, in many places, the boundaries of geologic units. In areas of alluvium and eolian deposits, the radioactivity units are not related to bedrock but reflect the distribution of the transported material. Water is an effective radiation shield, a few inches being sufficient to mask the radioactivity of the ground.

The areal distribution of Triassic diabase and sedimentary rocks in an area near Bealeton, Virginia, can be determined from aeroradioactivity data recorded on flight lines spaced a quarter of a mile apart. The three contacts between aeroradioactivity units shown in figure 55.1 are within a few hundred feet of the lithologic contacts. The width of the diabase unit (about 1,300 feet) approaches the minimum width of a broad source (Sakakura, 1957). Narrower units can be detected easily but their boundaries cannot be picked accurately.

A comparison of areal geology and gamma aeroradioactivity has been made in the Savannah River area, South Carolina and Georgia (fig. 55.2, index map). In the Piedmont part of the area most of the granite has a high aeroradioactivity level (generally 1,000 to 1,500 cps), the slate is generally low (usually below 600 cps), and the metamorphic complex includes

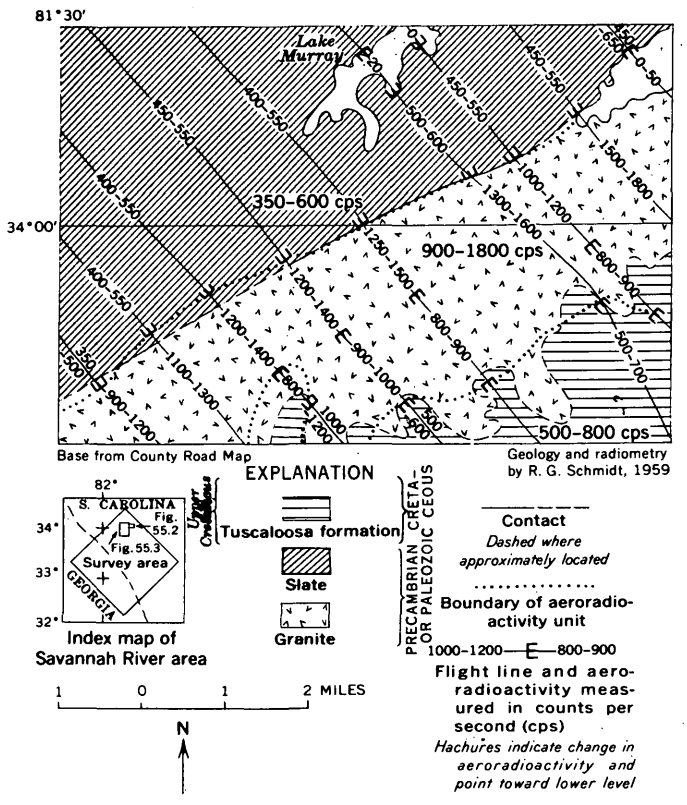

FIGURE 55.2.—Geology and aeroradioactivity of an area in Lexington County, S.C.

areas of high and low aeroradioactivity. In the Coastal Plain part of the area, the aeroradioactivity of the Upper Cretaceous and Eocene rocks ranges from low to high and the Oligocene and younger formations are generally low in aeroradioactivity.

The change in aeroradioactivity level can be used to locate geologic contacts at several places in the Piedmont part of the area, irrespective of the deep weathering of the rocks. The contact between granite and slate in an area in Lexington County, South Carolina (fig. 55.2) is marked by a change in level of about 500 cps. The sinuous contact between the granite and the overlapping Tuscaloosa formation could not be delineated with data from flight lines spaced one mile apart but on many profiles a good break in radioactivity level appears where the contact is crossed.

Approximately parallel aeroradioactivity units in Saluda County, South Carolina (fig. 55.3), indicate a zoning in the slate that could not be found in the field. The two distinct levels of aeroradioactivity are present for more than 35 miles. Areas of Piedmont rocks exposed in valleys in the Coastal Plain are, in many places, clearly indicated by the radioactivity data.

The highest aeroradioactivity levels in the surveyed part of the Coastal Plain are in Lexington and northeast Aiken Counties (in part shown on fig. 55.3). Monazite is probably the radioactive mineral in these irregular areas that occur in residual soil derived from Upper Cretaceous and Eocene strata. Monazite and other heavy minerals were mined until recently in Horse Creek near Aiken, South Carolina, from a large placer that probably developed by the reworking of Coastal Plain sedimentary rocks. The Coastal Plain rocks near Horse Creek are much less radioactive than those in Lexington and northeastern Aiken Counties, which suggests that the valleys of streams draining the more radioactive areas may be favorable sites for placer mineral deposits. Alluvium and water shielded the placers themselves from detection in this airborne survey.

The radioactivity of the flood plains of the larger streams in the Coastal Plain is related to the geology of their headwater areas. The flood plains of rivers having headwaters in the Piedmont or older Coastal Plain formations (the Savannah, Edisto, and Ogeechee Rivers) are more radioactive than the adjacent uplands. The flood plains of rivers that drain only the younger Coastal Plain formations (the Salkehatchie and Coosawhatchee Rivers) are equally or less radioactive than the adjacent formations.

The correlations between aeroradioactivity data and areal geology that have been made in several parts of the United States indicate that this technique is a use-

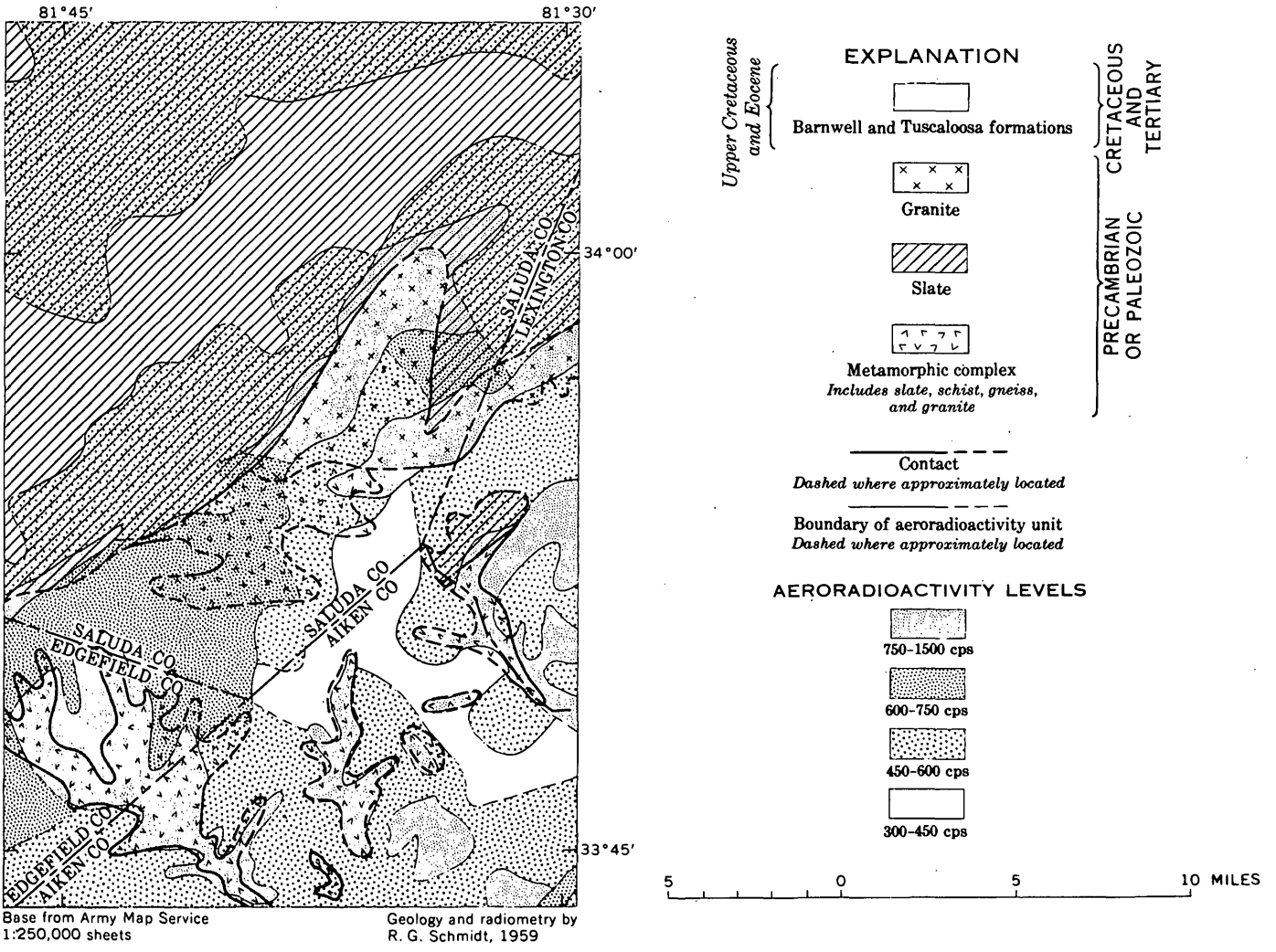

FIGURE 55.3.—Geology and generalized aeroradioactivity of an area near Batesburg, S.C.

ful mapping tool. It is of most value in areas of low to moderate topographic relief, residual soil, and poor outcrop, such as the Piedmont. These are the areas, of course, in which it is most difficult to determine the distribution and continuity of lithologic units by ordinary field methods.

REFERENCES

Davis, F. J., and Reinhardt, P. W., 1957, Instrumentation in aircraft for radiation measurements: Nuclear Science and Engineering, v. 2, no. 6, p. 713–727.

Sakakura, A. Y., 1957, Scattered gamma-rays from thick uranium sources: U.S. Geol. Survey Bull. 1052–A, p. 1–50.

56. MAPPING CONDUCTIVE STRATA BY ELECTROMAGNETIC METHODS

By F. C. FRISCHKNECHT and E. B. EKREN, Denver, Colo.

Since 1957 the U.S. Geological Survey has been studying the use of electromagnetic methods in tracing conductive strata beneath glacial drift in Minnesota, Wisconsin, and Maine. The objectives are to develop techniques that can be used in mapping bedrock geology in areas of extensive glacial drift or thick residual soil.

557753 O—60——9

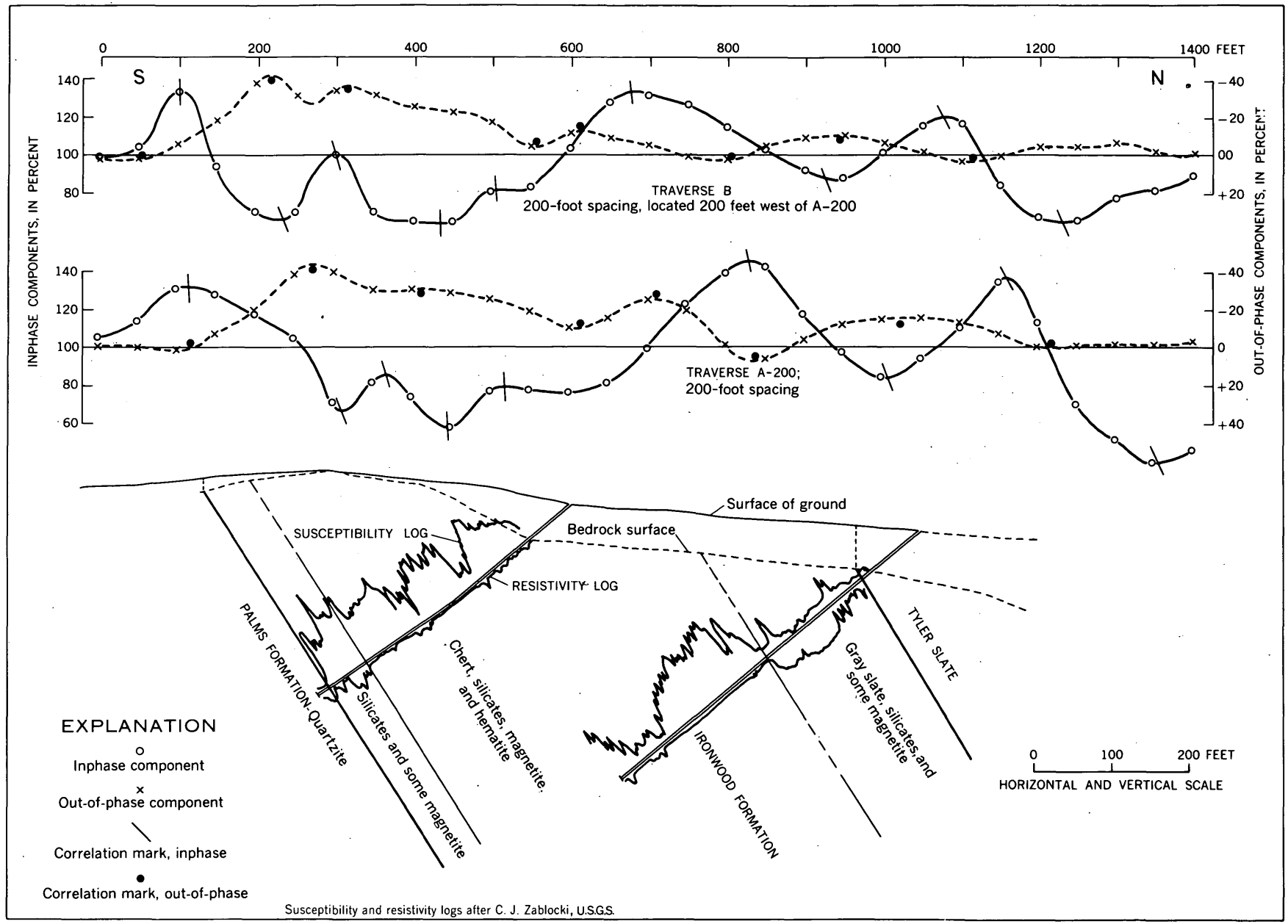

FIGURE 56.1.—Slingram profiles over iron formation, Gogebic range, Wisconsin.

DESCRIPTION OF METHOD

In most of these studies the slingram method (Frischknecht, 1959) was used. The apparatus consists of a battery-powered source of alternating current, a transmitting coil, a receiving coil, and a ratiometer. The ratiometer compares the signal picked up by the receiving coil with a reference signal transmitted by wire from the power source to the ratiometer. The signal picked up by the receiving coil varies in magnitude and phase with the electrical conductivity and magnetic susceptibility of the earth. The coils are moved together at a fixed separation which is usually between 100 and 300 feet. Measurements can be made rapidly, and because of the compactness and portability of the equipment, the method is well suited for reconnaissance work, even in heavy forest and brush.

CONDUCTORS

Electromagnetic conductors in metamorphic terranes of Minnesota, Wisconsin, and Maine commonly contain such metallic minerals as magnetic, specular hematite, and various sulphides, or graphite and carbon. This study is concerned with lithologic units that contain concentrations of conductive minerals. Conductive beds comprise only a small part of the total volume of metasedimentary rocks in the areas studied but they are sufficiently numerous and continuous to be used in tracing bedrock geology.

For a rock to have high conductivity, conductive minerals in the rock must be in the form of connected chains or bands. Some magnetic taconites containing abundant magnetite have low conductivity because individual magnetite grains are insulated from each other. Similarly, pyrite crystals in many black slates are disseminated and add little to the overall conductivity of the slate.

Most igneous rocks as well as quartzite, graywacke, and light-colored slate have low conductivity and give little electromagnetic response. Glacial drift masks bedrock anomalies only where it is thick or conductive.

MINNESOTA AND WISCONSIN

Studies were made over iron formations containing both oxidized and unoxidized iron ores in Minnesota and Wisconsin. Oxidized iron ores beneath thick deposits of glacial drift on the Cuyuna range in Minnesota could not be detected by the slingram measurements, but graphitic or other carbonaceous beds associated with the hanging-wall formation were readily located. Electromagnetic methods should prove useful in mapping new areas on the Cuyuna and Mesabi ranges because conductive beds commonly occur in the hanging-wall formations.

The magnetic taconite rocks of the eastern Mesabi and western Gogebic ranges were found to be sufficiently conductive over large areas to be traced easily, even under considerable thicknesses of glacial drift. The contact between the footwall and the iron formation was readily located. However, anomalies from the conductive graphitic strata, which occur in the basal part of the hanging-wall formation, make it difficult to distinguish between the iron formation and the hanging-wall formation (fig. 56.1). The various peaks and troughs on the slingram profiles can be correlated from traverse to traverse. If the stratigraphy is known on one traverse by drill-hole information or by surface exposures, it should be possible to trace a lithologic unit laterally for considerable distances by means of electromagnetic measurements.

MAINE

The most common electromagnetic conductors in Maine are 1) graphitic or carbonaceous beds associated with black pyritic slates and schists, and 2) massive

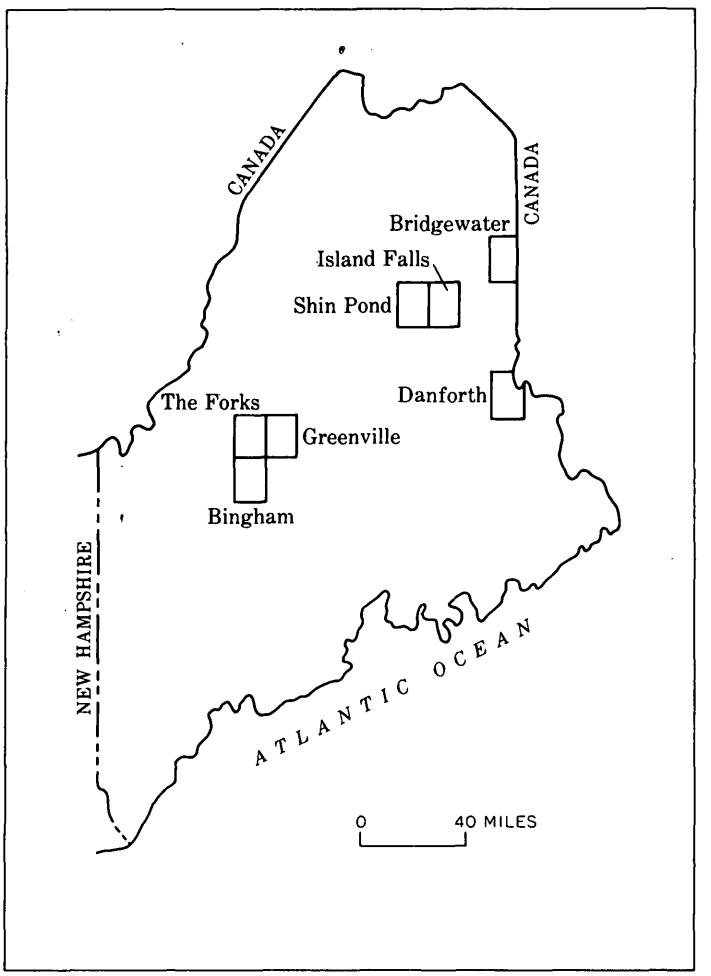

FIGURE 56.2.—Index map of Maine showing areas of study.

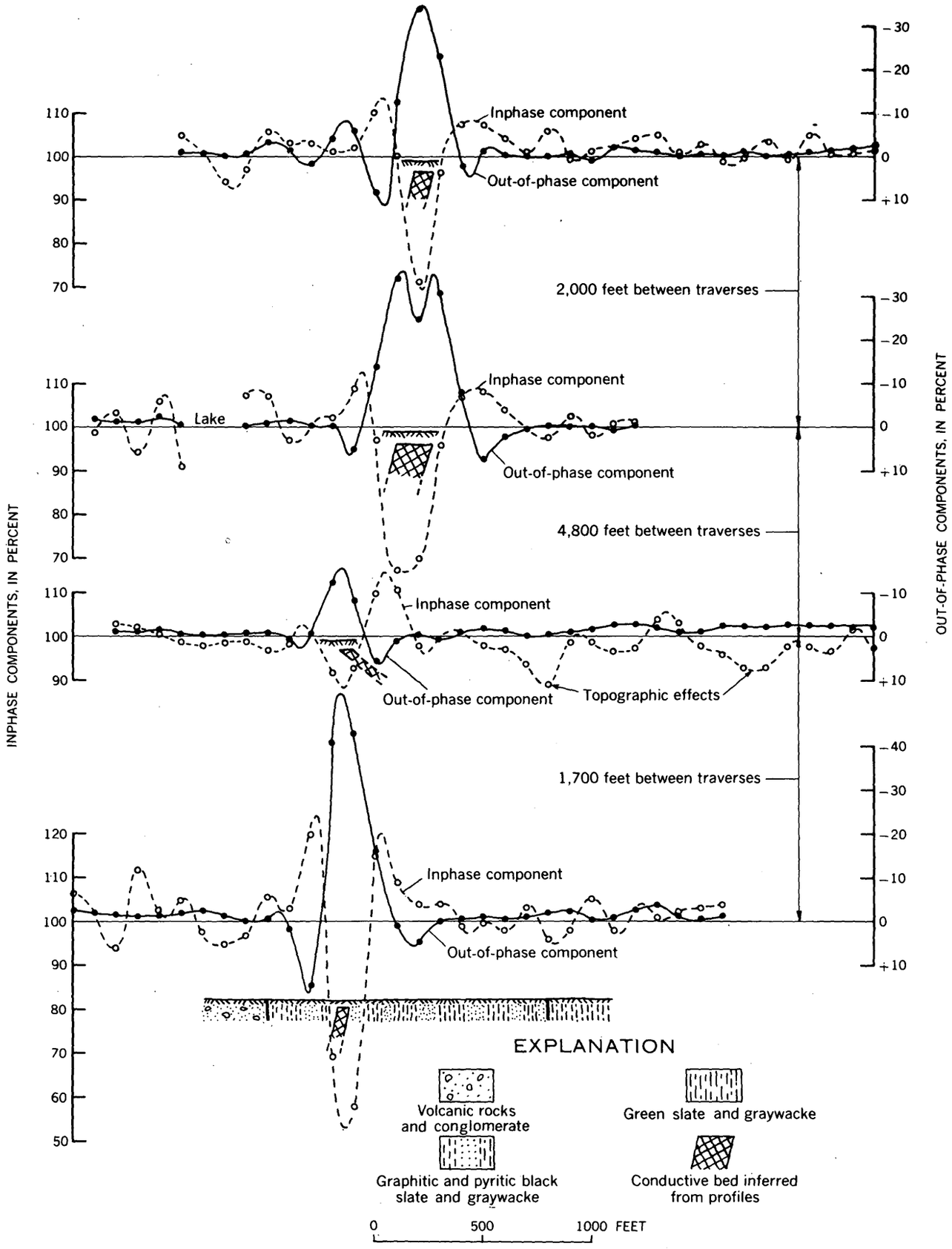

FIGURE 56.3.—Slingram profiles from Shin Pond quadrangle, Maine.

sulfide deposits occurring in mafic intrusive igneous masses.

Conductors were found in traversing over belts of steeply dipping black slate and contiguous rocks in the Bridgewater, Shin Pond, Bingham, Greenville, Island Falls, and The Forks quadrangles (fig. 56.2). A black graptolite-bearing chert associated with volcanic rocks in the Danforth quadrangle was found to be conductive.

In the Shin Pond quadrangle, from east to west, the traverses crossed green slate and graywacke; black, pyritic slate and graywacke; volcanic rocks; and a coarse conglomerate (fig. 56.3). The black slate belt is about a quarter of a mile wide but the conductive bed is commonly less than 200 feet wide. Similar conditions are found to prevail in nearly every area studied and it is concluded that the presence of black slate is no guarantee that a conductor is also present.

The Shin Pond conductor was traced for several miles by 15 traverses, four of which are shown in figure 56.3. The anomalies over this conductor are very distinct from "background" variations in the profiles; most of the small features in the inphase component are caused by steep topography and can be discounted in the field. Consequently, there is little difficulty in correlating traverses spaced half a mile to one mile apart. In other areas such as the Danforth quadrangle, the width and amplitude of the anomalies varies greatly along the strike of the conducting bed and it is then necessary to space the traverses more closely.

REFERENCES

Frischknecht, F. C., 1959, Scandinavian electromagnetic prospecting: Am. Inst. Mining Metall. Engineers Trans., v. 214, p. 932–937.

Zablocki, C. J., and Keller, G. V., 1957, Borehole geophysical logging methods in the Lake Superior district, *in* Drilling Symposium, 7th annual, exploration drilling: Minneapolis, Minnesota Univ. Center for Continuation Study, p. 15–24.

57. ELECTRICAL PROPERTIES OF SULFIDE ORES IN IGNEOUS AND METAMORPHIC ROCKS NEAR EAST UNION, MAINE

By L. A. Anderson, Denver, Colo.

Electrical properties of rocks in and around a large sulfide deposit near East Union, Maine, were measured using in-hole logging methods, which included resistivity, self-potential, and induced polarization. In addition, laboratory measurements were made for resistivity, induced polarization, grain density, and porosity on core samples taken at two-foot intervals from a drill hole that penetrated representative rocks in the area.

The sulfide minerals occur in a peridotite body that trends S. 20° W. and plunges gently to the south under quartz-biotite schist. The peridotite is intruded by pegmatites that are generally associated with mineralized areas. Pyrrhotite is the most abundant sulfide mineral. Pentlandite occurs along the borders of the most massive pyrrhotite-bearing zones, and chalcopyrite is found as irregular interstitial grains between pyrrhotite crystals and as veinlets along the borders of pyrrhotite crystals and the silicate minerals. Magnetite has formed as an alteration product between grains of olivine and pyrrhotite.

The negative potentials (fig. 57.1) in sections having concentrations of sulfide minerals indicate that the sulfides are being oxidized. Water samples collected below 30 feet revealed an oxygen content of less than one part per million, so the rate of oxidation may be slow. The low oxidation rate is further suggested by the lack of secondary oxidized minerals in the ore zone. The self-potential is more negative in the sulfide concentrations toward the top of the drill hole, suggesting a greater rate of oxidation owing to oxygen-charged surface waters.

The resistivity ranges from nearly zero to about 3,000 ohm-meters; the highest values occur in gabbro and the lowest occur in the zone of major sulfide concentration and in the graphitic schist below the sulfide zone. Where sulfide minerals occur in excess of 5 percent by weight, the individual grains are in physical contact with one another, forming continuous conductors. Therefore, any deviation from the 5 percent sulfide content will result in resistivity measurements that are either extremely low or are near the true resistivity of the host rock.

The resistivity log of a drill hole near that shown in figure 57.1 shows four major zones of extremely low resistivity (fig. 57.2). The low resistivity and high

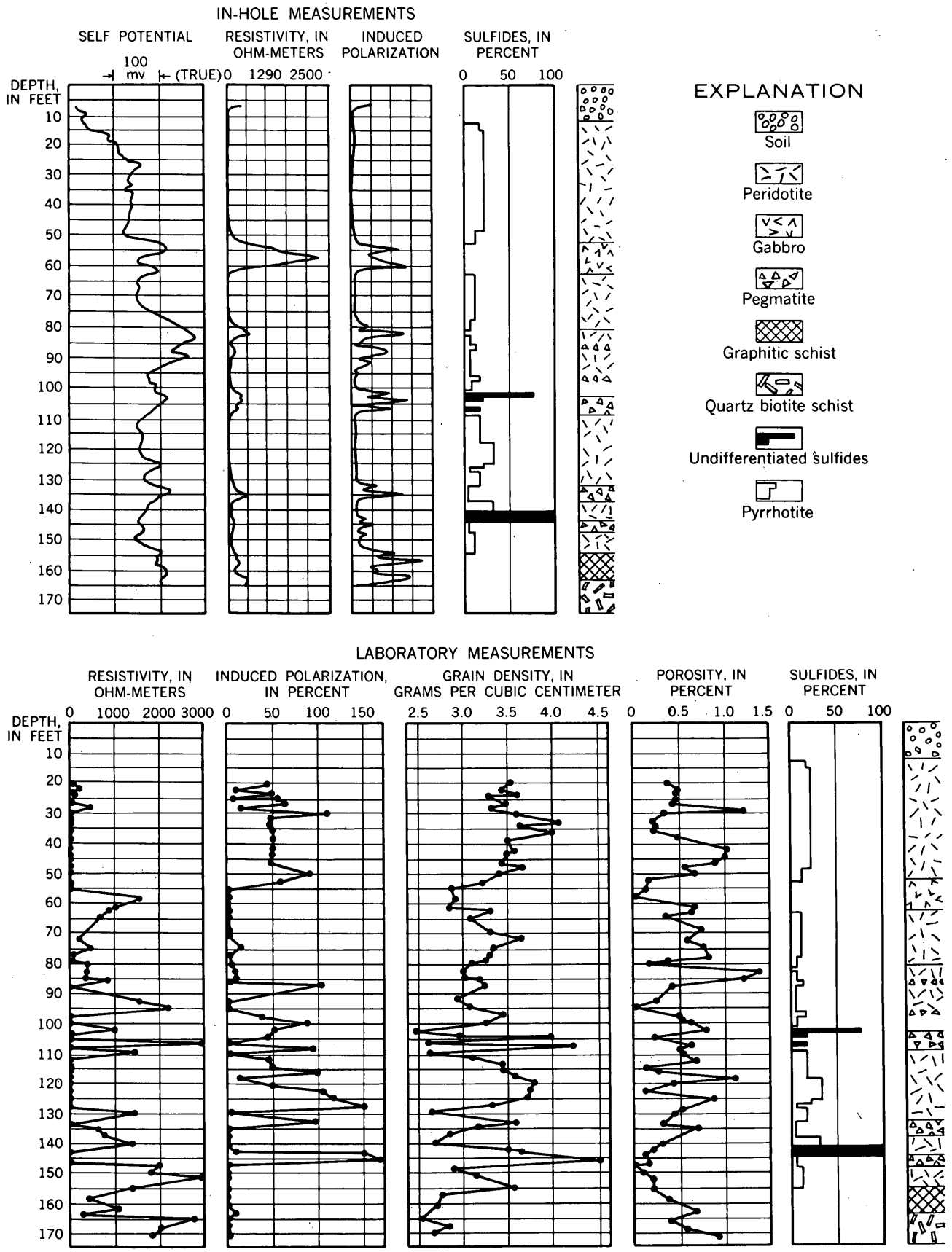

FIGURE 57.1.—In-hole and laboratory results of electrical and physical property measurements of a drill hole and core specimens from East Union, Maine.

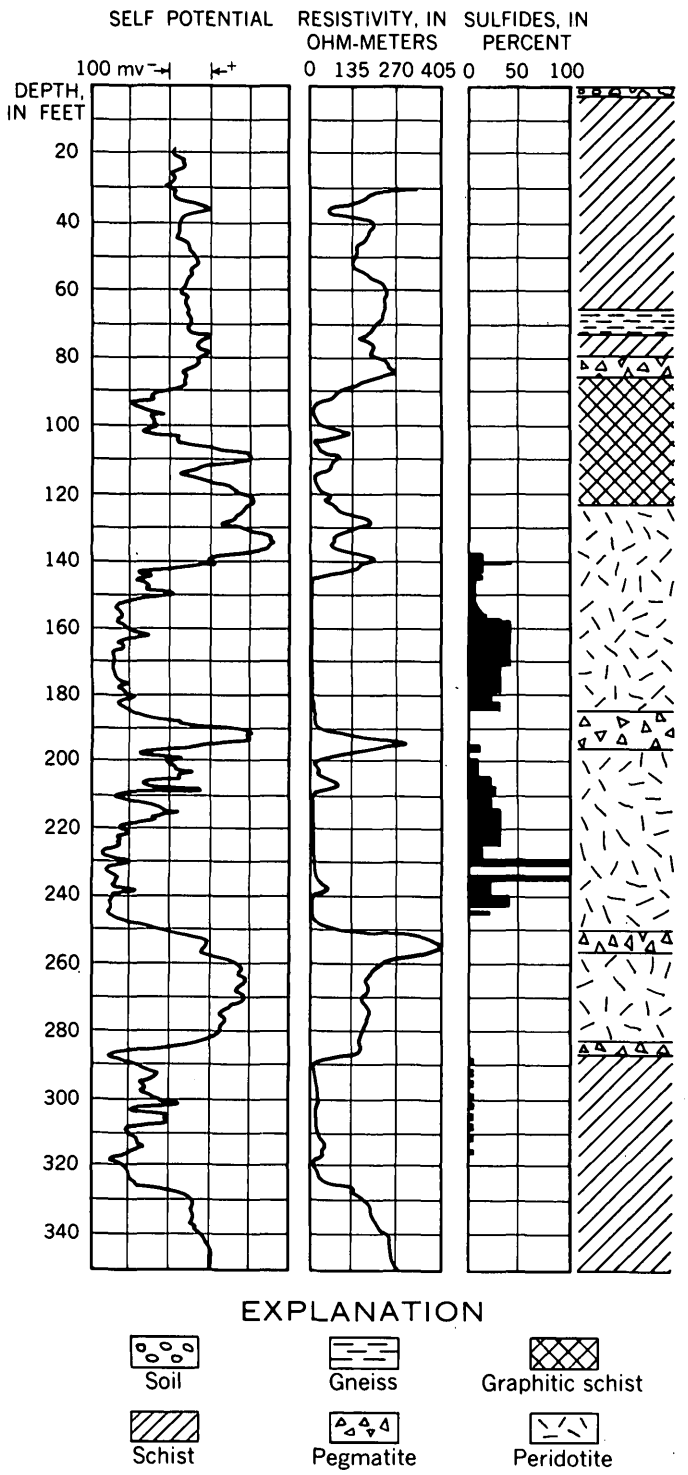

FIGURE 57.2.—Self-potential, resistivity, and lithologic logs from a drill hole near East Union, Maine.

negative self-potential values at depths of 140 to 185 feet and 195 to 245 feet suggest the presence of sulfide minerals undergoing oxidation. The upper and lower conducting zones at depths of 85 to 105 feet and 285 to 322 feet, respectively, on the resistivity log do not clearly define continuous conductors. In the lower zone, the self-potential has a high negative value suggesting the presence of sulfides, whereas the more positive self-potential values of the uppermost zone indicate graphite. The concentration of graphite in the schist (fig. 57.1) at a depth of 105 to 115 feet is thought to be too low or perhaps too localized to generate a significant potential. The induced-polarization measurements on core samples from the graphite zone show very little response, suggesting a low graphite content within the schist.

Induced polarization occurs at a metal-solution interface when it is exposed to a flow of current. The energy barrier at the interface acts as a resistance in association with a capacitance. During a flow of current, the capacitance stores a charge, and upon termination of the current flow, the charge will decay at a rate determined by the time constant of the simulated resistance-capacitance network at the interface. The discharge voltage is therefore a measure of the polarization that can be induced in a particular rock. Rocks containing disseminated sulfides, and therefore numerous energy barriers, are good polarizers, whereas rocks containing sulfides in the form of continuous conductors are poor polarizers.

The in-hole induced-polarization log (fig. 57.1) does not contribute significant data owing to the apparent continuity of the sulfides in the mineralized zones. The instrumentation relies upon a constant applied voltage, but in highly conductive rocks it becomes impossible to generate a potential field because the power supply is virtually shorted. The induced polarization log therefore closely follows the resistivity, reflecting the inability of the system to operate in very conductive rock.

Good correlation exists between the in-hole and laboratory resistivity measurements. Minor discrepancies between the in-hole and laboratory resistivity measurements are due to local variations within the rock. These variations are significant in the core samples but could not be detected in the massive rock.

The induced-polarization measurements made on the core samples give an accurate indication of the content and distribution of the sulfides within the mineralized zones. The dense barren rocks such as the gabbro show negligible polarization effects, and the sulfide-bearing peridotite has a polarization response proportional to the sulfide content and to its degree of dissemination.

Porosity and grain density of the core samples were correlated with the electrical-property measurements. The grain density reflects the sulfide content of the peri-

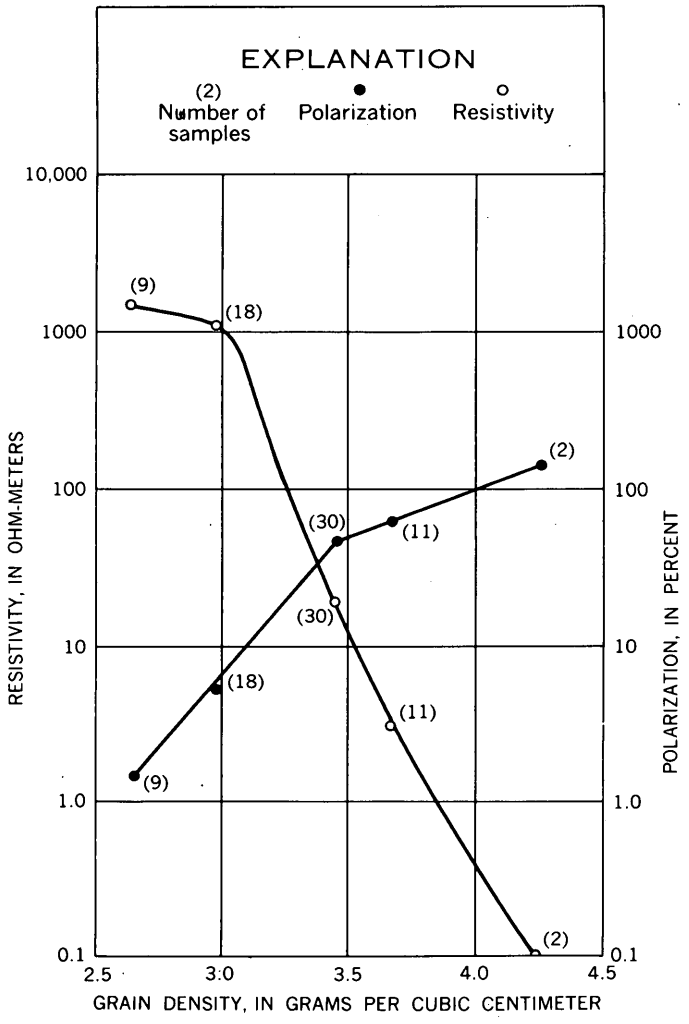

FIGURE 57.3.—Resistivity and polarization as a function of grain density for mineralized core samples.

dotite, and as would be expected, the zones of massive sulfides have the highest grain-density values. Low porosity values are indicative of the fine-grained texture of the representative rocks in this area.

Polarization and resistivity were plotted with respect to the grain density (fig. 57.3). As the grain density increases, the resistivity falls rapidly (fig. 57.3) indicating that a small increase in the sulfide concentration will cause a significant decrease in the resistivity. The polarization response increases with increasing grain density indicating that the sulfide concentration is not truly massive but that sulfide minerals are probably distributed in veins that yield high local polarization values.

The in-hole logging measurements show conductive zones that may be attributed to sulfide content or to the presence of graphite. The resistivity response to sulfide percentage could not be related quantitatively because of the apparent continuity of sulfide grains where the content is in excess of approximately five percent by weight. The self-potential log can, in some cases, be used to distinguish between sulfides that exist in quantities greater than a few percent by their more negative self-potentials as compared to the self-potentials measured in the graphitic zones.

The laboratory measurements show that induced polarization is an excellent method for estimating the relative sulfide concentration.

The author wishes to express his gratitude to the Roland F. Beers Company for allowing access to the drill holes and providing core samples and lithologic logs.

58. ELECTRICAL PROPERTIES OF ZINC-BEARING ROCKS IN JEFFERSON COUNTY, TENNESSEE

By G. V. KELLER, Denver, Colo.

An important belt of zinc ore low in iron occurs in the Knox group, of Cambrian and Ordovician age, in the area between the towns of Mascot and Jefferson City, in Knox and Jefferson Counties, Tennessee. The American Zinc Company drilled several dozen exploration holes north of the town of Strawberry Plains in 1957 as part of a Defense Minerals Exploration Administration project. Electric logs were run in 11 of these drill holes to determine whether anomalous electrical properties were associated with sphalerite mineralization and might serve as a guide for geophysical exploration.

The stratigraphy of the Mascot-Jefferson City zinc district has been described by Oder and Miller (1945) and by Bridge (1956). Sphalerite occurs in replacement deposits in the Kingsport limestone of the Knox group, which is of Ordovician age. The deposits conform roughly to the bedding in coarsely crystalline dolomitized limestone, and are accompanied by breccia filling in associated fine-grained primary dolomite.

The Kingsport limestone consists of 350 to 400 feet of limestone and dolomite, and the main ore horizons are in the lower two-thirds of this unit. Sphalerite is the only ore mineral, and the gangue mostly consists of white crystalline dolomite.

Drill holes in the Strawberry Plains drilling project ranged in depth from 900 to 2,700 feet. They penetrated several formations overlying the Kingsport limestone of the Knox group, including the Mascot dolomite of the Knox group, Lenoir limestone (including the Mosheim member), the Holston marble, and, in the deeper holes, the Ottosee formation. All of these are of Ordovician age.

The resistivity log from a hole in the Lenoir limestone including the Mosheim member, the Mascot dolomite, and the Kingsport limestone (fig. 58.1), indicates that the resistivity of most of the rock ranges from 7,000 to over 30,000 ohm-meters, but that in a mineralized zone between 900 and 1,000 feet, it is only 500 to 6,000 ohm-meters. The assay log for this zone shows only a few percent of iron between 950 and 1,000 feet. This indicates that there is only a little pyrite in the rock, and as sphalerite is not conductive the higher conductivity in the mineralized zone must be due to increased porosity rather than to solid conduction. When the resistivity log in the ore zone is com-

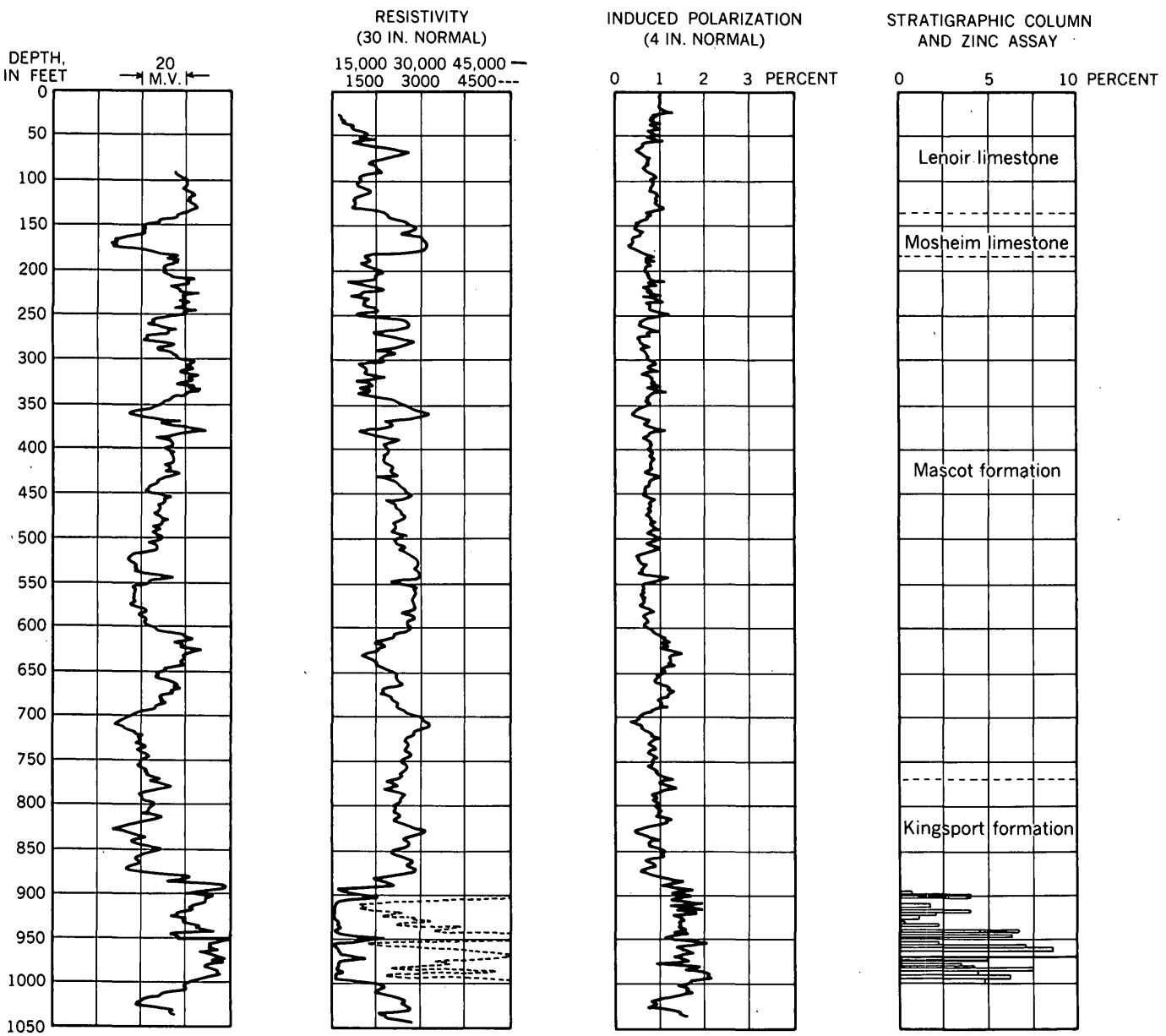

FIGURE 58.1.—Electrical and induced polarization logs from a drill hole penetrating sphalerite-bearing dolomite in eastern Tennessee.

pared in detail with the assay log it is found that there is no quantitative relation between resistivity and ore grade.

Neither the self-potential nor the induced-polarization logs show as striking a change in the ore zone as the resistivity log. The self-potential log opposite the ore deflects approximately 30 millivolts in a positive direction; why it does so is not known. Induced-polarization response in the ore zone is about 50 percent greater than in adjacent beds, but it is still low. It is therefore unlikely that either the self-potential method or the induced-polarization method would be of any use in exploring for ore such as is penetrated by this drill hole.

The large resistivity contrast between ore and barren rock does offer some hope that galvanic or inductive resistivity methods can be used. To determine the limiting conditions, such as depth of burial, for which electrical methods might work, average resistivities for the ore and overlying rocks were calculated (table 58.1) using Kalenov's method (1957).

The probable results of resistivity depth soundings may be calculated on the basis of the data in table 58.1. The low coefficient of macro-anisotropy for the rocks overlying the ore zone reflects the electrical uniformity of these rocks and provides ideal conditions for resistivity depth soundings. The large coefficient of anisotropy for the ore zone is also a favorable condition. In the case illustrated in figure 58.1, for example, the conducting zone would appear on a depth-sounding curve as 177 feet thick, rather than 100. Using charts prepared by Mooney and Wetzel (1956), depth-sounding curves were drawn that would be obtained at the location of the drill hole in figure 58.1 for various depths of burial (fig. 58.2). On these curves the effect of the ore horizon could easily be seen even when the depth of burial was 700 feet. The theoretical curves are based, however, on the assumption that the lateral extent of the conducting zone is infinite, and if it is less than several thousand feet the effect on the sounding curves will be reduced.

TABLE 58.1.—*Average electrical resistivities from the log shown in figure 58.1*

Rock unit	Average Transverse resistivity (ohm-meters)	Average Longitudinal resistivity (ohm-meters)	Coefficient of macro-anisotropy
Lenoir limestone (excluding Mosheim member)	7,550	5,800	1.14
Mosheim member of Lenoir limestone	15,500	14,700	1.04
Mascot dolomite	12,700	11,300	1.07
Kingsport limestone (barren)	13,800	13,400	1.01
Kingsport limestone (mineralized)	820	260	1.77

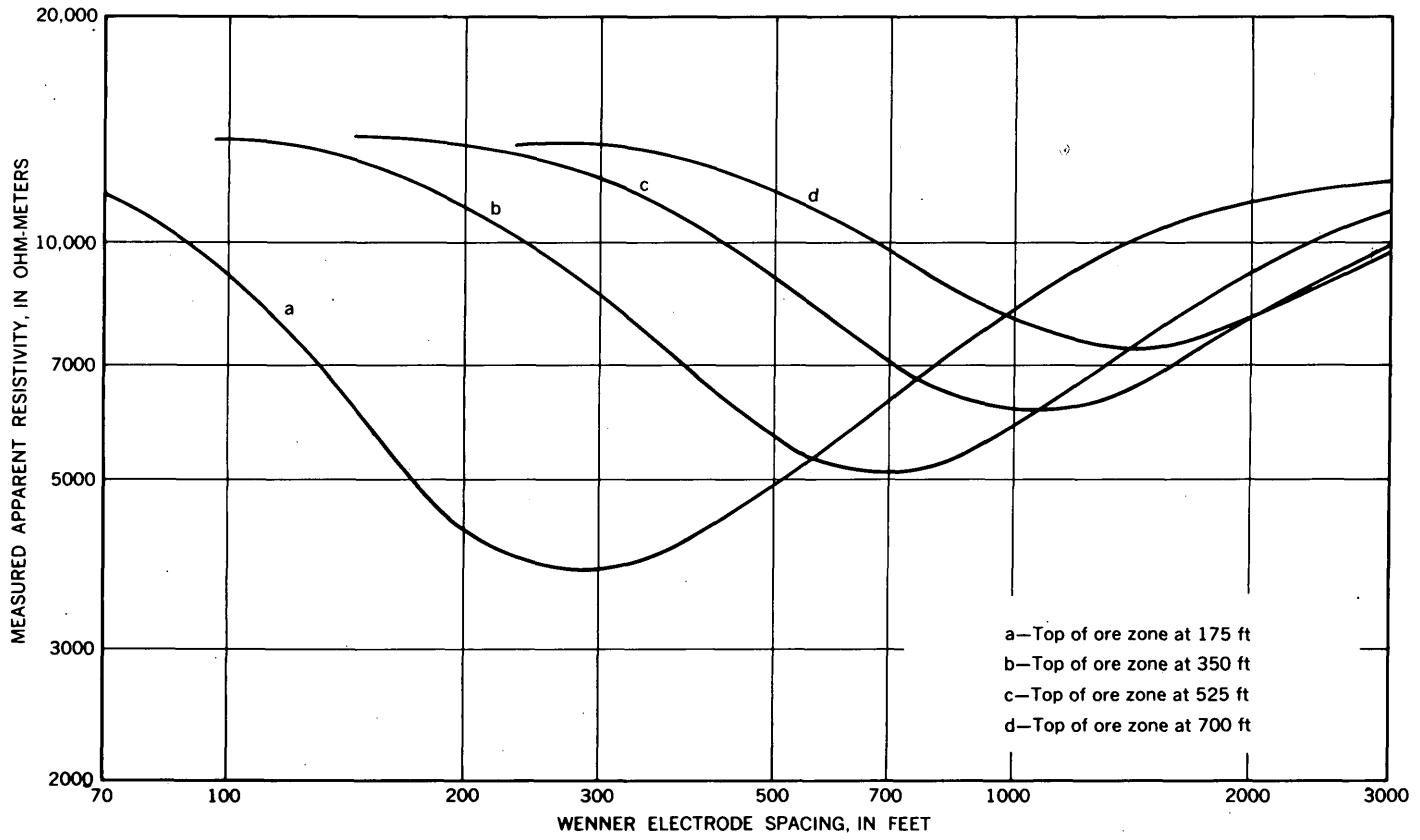

FIGURE 58.2.—Theoretical resistivity sounding curves for a bed 175 feet thick imbedded in beds with resistivity 20 times larger.

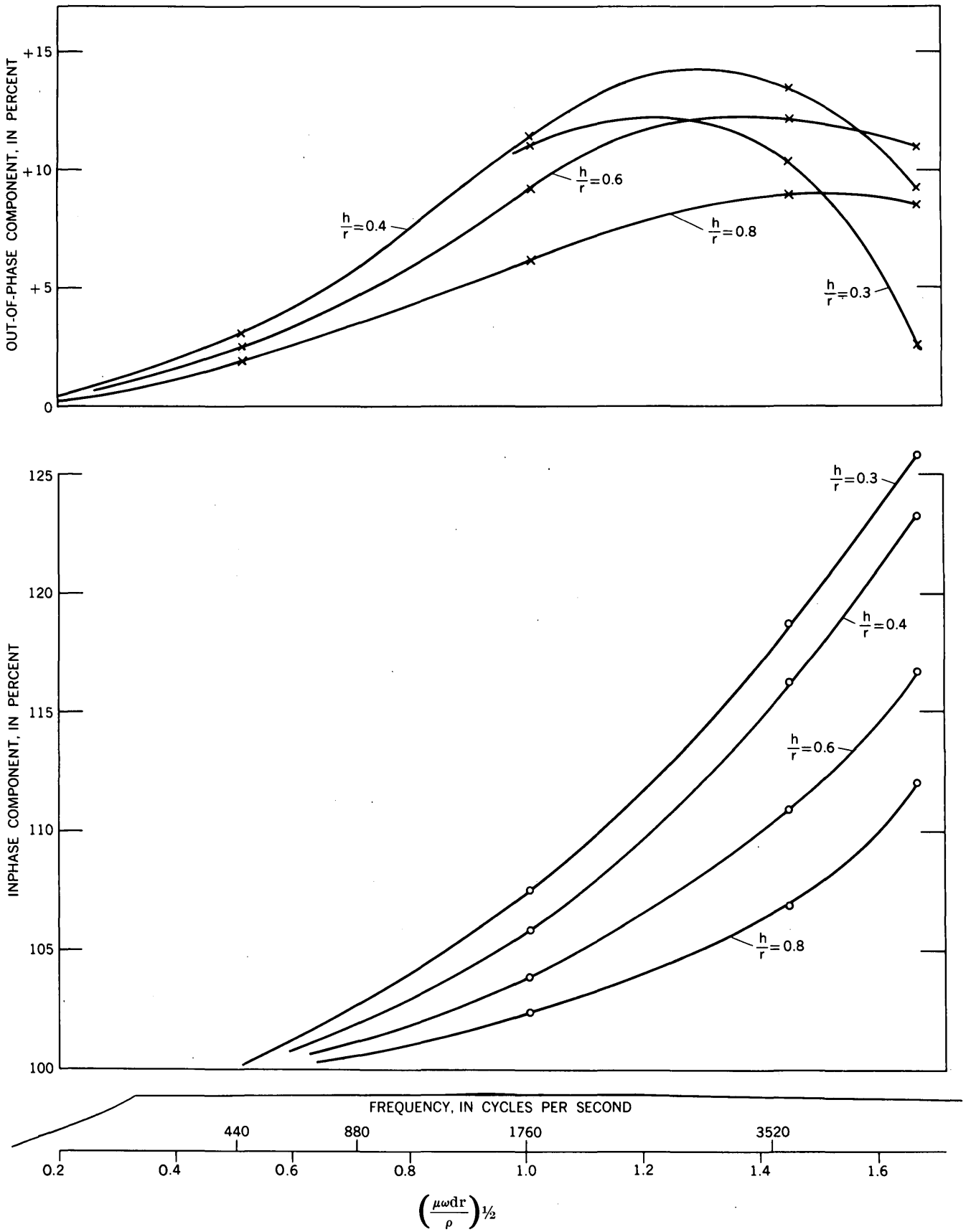

FIGURE 58.3.—Mutual impedance ratio between loops above a thin conducting sheet from model data.

It is also likely that the conducting zone might be detected by using electromagnetic methods (EM) for measuring conductivity. Mutual coupling curves were obtained for the case presented in table 58.1 for several depths of burial of the conducting zone, using an EM model (F. C. Frischknecht, oral communication). In-phase and out-of-phase components of the mutual impedance ratio for loops raised in air above a thin conducting sheet are shown in figure 58.3. The symbols used are: μ for magnetic permeability of free space ($4\ \pi x10^{-7}$ cgs), u for the angular frequency, ρ for the thickness of the conducting sheet and r for the separation between loops, and h is the height of the loops above the sheet.

At a frequency of 5 kilocycles per second, for example, the affect of overburden would be small: the response from a thick overburden having a resistivity of 10,000 ohm-meters would be less than 6 percent in the out-of-phase component and less than 3 percent in the in-phase component. At lower frequencies the response from the overburden would be even less. It is evident that the conducting zone could be readily located with EM methods even if deeply buried. If the conducting zone were buried at a depth of 1,000 feet, and if a coil separation of 2,000 feet were used, the in-phase component would be 112 percent and the out-of-phase component would be +13 percent, representing anomalies of 12 and 13 percent respectively (fig. 58.3).

ACKNOWLEDGMENTS

I am grateful to the American Zinc Company, and particularly to C. R. L. Oder, for providing me with core logs and assay data.

REFERENCES

Bridge, Josiah, 1956, Stratigraphy of the Mascot-Jefferson City zinc district, Tennessee: U.S. Geol. Survey Prof. Paper 277.

Kalenov, E. N., 1957, Interpretatsiya krivykh vertikal'nogo elektricheskogo zondirovaniya: Gostoptekizdat, Moscow, 468 p.

Mooney, H. M., and Wetzel, W. W., 1956, The potentials about a point electrode and apparent resistivity curves for a two-, three-, and four-layer earth: Minnesota Univ. Press, Minneapolis, 146 p.

Oder, C. R. L., and Miller, H. W., 1945, Stratigraphy of the Mascot-Jefferson City zinc district: Am. Inst. Mining Metall. Engineers, Tech. Pub. no. 1818, 9 p.

59. TERRAIN CORRECTIONS USING AN ELECTRONIC DIGITAL COMPUTER

By Martin F. Kane, Washington, D.C.

Computation of terrain corrections for gravity stations in irregular or mountainous terrain is the most time consuming part of the reduction of gravity data. Because of the variable nature of terrain, a correction is usually made by dividing the area around a station into a series of zones and compartments, and computing the terrain effect of each compartment. The effect of any compartment is a function of its elevation, size, and position relative to the gravity station. The sum of the effects of all the compartments is the terrain correction.

In conventional methods, the computation is made by first dividing the area into a series of circular zones concentric about the station, and then subdividing each zone into compartments of equal area. The gravity attraction of a circular zone on a point at its center is readily calculated, and the attraction of a compartment is a simple fraction of the attraction of the whole zone. The final correction usually includes an area within a 5- to 15-mile radius of the station, so that for surveys with a station-spacing of a few miles or less, considerable overlap occurs between the compartments about adjacent stations. Because of the relationship between the correction formula and the concentric arrangement of the compartments, however, the elevation data assembled for one station are not applicable to another. In gravity surveys with a dense station network, it is necessary to consider the same topography many times over.

A method that makes use of electronic computers has been developed to expedite the computation of these terrain corrections. In this method the topography of the entire survey area is converted to digital form by dividing the terrain into kilometer squares and tabulating the average elevations of the terrain within the squares. The average elevations are punched on cards and stored in the computer memory. They are not sufficiently precise for the area close to the station where

small changes in topography cause large terrain effects; and they are unnecessarily precise for distant areas where large changes in terrain contribute little, if any, terrain effect. The computer correction therefore, is limited to an area 40 by 40 kilometers square with the station at the center, and excludes a central area 2 by 2 kilometers square. The terrain beyond 40 kilometers can be safely ignored in most places, and the terrain within 2 kilometers of the station can be easily calculated by conventional methods.

The electronic-computer method was programed and tested on the U.S. Geological Survey's Datatron 205 for gravity stations in a moderately mountainous area in southern Nevada. The results were compared with conventional calculations for 10 stations and showed a maximum difference of 0.1 milligal. The electronic computer method is considerably faster and is internally more consistent because it uses identical field data for all corrections. The cost is presently about twice that of conventional methods, but this will be reduced by a factor of four when the program is completed for the newer and faster Datatron 220. The cost depends, to a great extent, on the station spacing, and the greatest savings are realized in surveys with a relatively dense network of stations. In surveys where the stations are widely spaced the method is more expensive, but its increased speed and improved internal consistency may justify the additional cost.

60. APPLICATION OF GRAVITY SURVEYS TO CHROMITE EXPLORATION IN CAMAGÜEY PROVINCE, CUBA

By W. E. Davis, W. H. Jackson, and D. H. Richter, Washington, D.C., Denver, Colo., and Hawaiian Volcano Observatory, Hawaii

Work done in cooperation with the General Services Administration

Chromite deposits in the Camagüey district, Cuba (fig. 60.1), occur in an ultramafic complex that consists principally of a lower serpentinized peridotite and dunite member and an upper feldspathic member. The complex was intruded into a series of metamorphic rocks as a nearly stratiform mass, and is unconformably overlain by Upper Cretaceous volcanic rocks interbedded with limestone and chert. Folding, probably concurrent with overthrusting from the north during early Tertiary time, has formed a number of long arcuate structures. Subsequent uplift was followed by erosion that has removed most of the overlying volcanic and feldspathic rocks except in deep synclinal areas. The deposits are irregular tabular bodies ranging in size from small pods to masses several hundred feet long that contain 200,000 tons or more, and occur in the upper part of the serpentinized rocks within half a mile of the feldspathic member.

Detailed gravity surveys made in this district between August 1954 and April 1956 successfully delineated bodies of high-density materials and, combined with evidence revealed by geologic mapping, helped guide exploration for chromite by drilling. The methods and principal results of this survey have already been published in a geophysical journal (Davis and others, 1957), but some of the results are repeated here to call wider attention to the potential use of gravity methods in the exploration of ultramafic complexes.

The difference in density between the chromite contained in commercial deposits of the district and the serpentinized peridotite and dunite is about 1.5 grams per cubic centimeter. This difference is sufficient for chromite masses lying at commercially exploitable depths to cause positive gravity anomalies of more than 0.5 gravity unit (0.05 milligal). Feldspathic rocks in the serpentinized peridotite and dunite range in density from 2.4 to 3.0 g per cu cm. Some of these rocks are dense enough to cause anomalies of much the same lateral extent and magnitude as the chromite. Similar anomalies are also created by density contrasts between different parts of the serpentinized masses, which vary in density from 2.2 to 2.8 g per cu cm.

During a 20-month exploration program in nine areas embracing about 12 square miles (fig. 60.1), a large number of anomalies with a gravity relief of 0.5 gravity unit or more were found and evaluated according to geology, areal extent, and gravity relief. Those

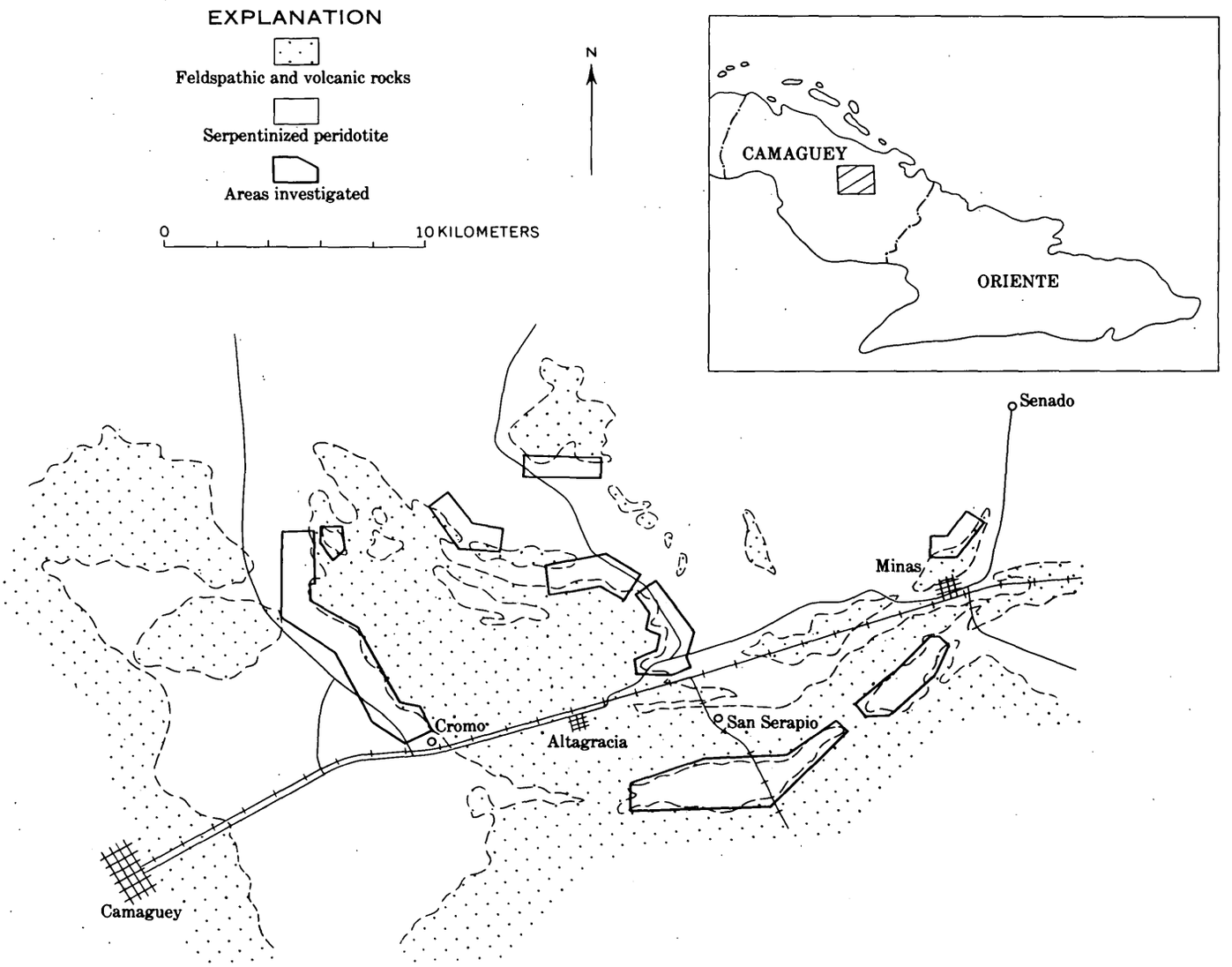

FIGURE 60.1.—Index map showing location of areas investigated by the U.S. Geological Survey in the Camagüey chromite district, Cuba.

not obviously associated with feldspathic rocks were selected for drilling. To guide the drilling, depths to the top and center of hypothetical bodies that would cause anomalies of similar magnitude were computed in terms of chromite and feldspathic rock.

Test holes from 27 to 375 feet in depth were drilled on 106 gravity anomalies, which constituted probably less than a third of the total number found. These holes revealed that 10 anomalies were over deposits of chromite, 47 over feldspathic rock, 40 over dense parts of the serpentinized rocks, 2 over deposits of magnesite-talc-quartz rock, and 7 over serpentinized rocks, cored samples of which did not indicate sufficient density to cause variations in gravity. Drilling on five of the chromite deposits revealed about 236,000 tons of chromite, of which 19,000 tons was disseminated ore. It was estimated that 6,000 tons of shipping-grade chromite and 6,000 tons of disseminated chromite was contained in three other deposits that were not blocked out. No estimate was made of the tonnage in two small chromite deposits.

A residual gravity anomaly associated with a deposit containing 115,000 tons of chromite is shown in figure 60.2. The anomaly is prominent and of a regular shape, involves 12 stations, and has a gravity relief of 1.6 gravity units. It delineates the chromite deposit fairly accurately. The chromite body comes within 10 feet of the surface (fig. 60.3), and dips steeply toward the southwest. Most of the ore lies below 75 feet, and the bottom of the deposit is between 224 and 250 feet deep.

The investigation revealed that in the Camagüey chromite district detailed gravity surveys combined

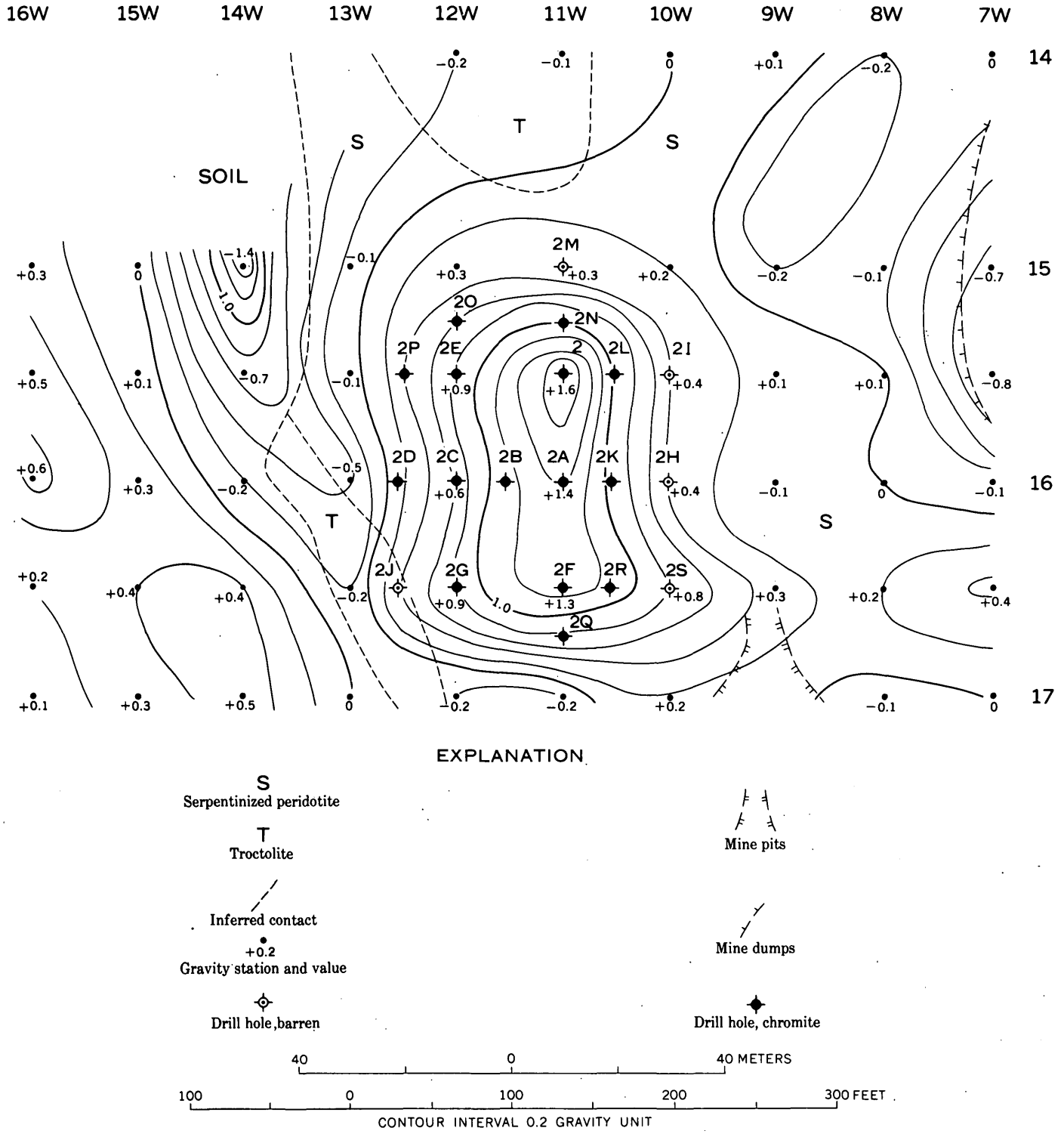

FIGURE 60.2.—Residual gravity anomaly over a chromite deposit containing 115,000 tons.

with geological mapping can be used to delineate areas in which chromite may be found, and to obtain data for locating and determining depths of drill holes. Evaluation of the anomalies on the basis of geology, areal extent, and gravity relief is helpful in limiting drilling, but does not serve to distinguish anomalies caused by chromite from those caused by unexposed masses of high-density rocks. The accuracy required in measuring small gravity differences that are significant in exploration can be attained by using gravimeters having

low scale constants, by exercising normal care in handling and reading the meters, and by frequently re-observing base stations and a limited number of intermediate stations to check the instrumental drift.

REFERENCE

Davis, W. E., Jackson, W. H., and Richter, D. H., 1957, Gravity prospecting for chromite deposits in Camagüey Province, Cuba : Geophysics, v. 22, p. 848–869.

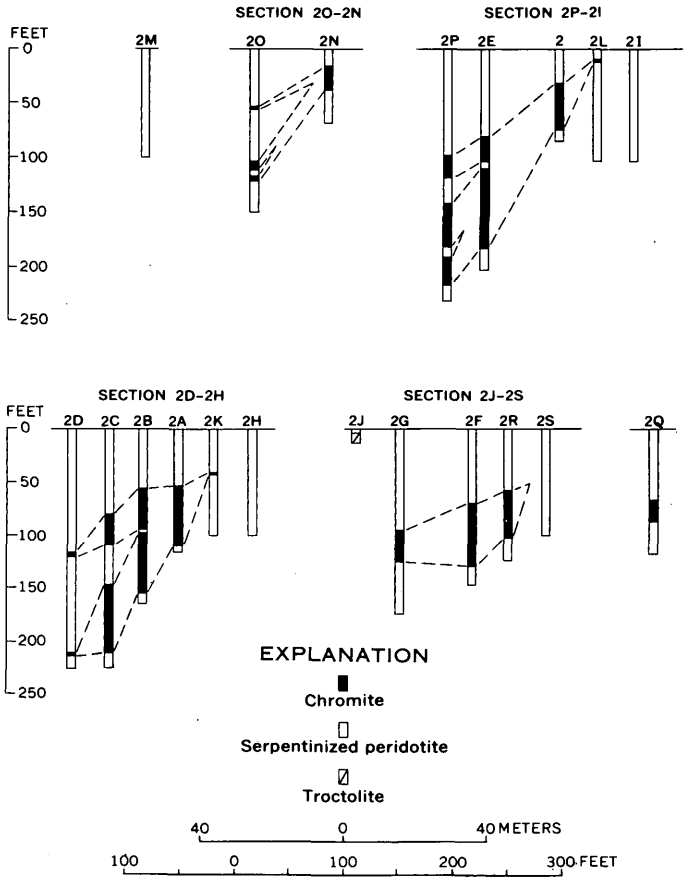

FIGURE 60.3.—Drill-hole sections through the chromite deposit illustrated in figure 60.2.

61. SPECTRAL REFLECTANCE MEASUREMENTS AS A BASIS FOR FILM-FILTER SELECTION FOR PHOTOGRAPHIC DIFFERENTIATION OF ROCK UNITS

By WILLIAM A. FISCHER, Washington, D.C.

Measurements of the reflectance spectra of several specimens of differently colored rocks collected near Corona, N. Mex., suggest that certain rocks may be more readily distinguishable on aerial photographs that record only selected wave lengths of light than on conventional aerial photographs. Figure 61.1 shows spectral reflectance curves, determined in the laboratory for samples of a light-brown sandstone (A), a gray limestone (B), a red shaly siltstone (C), and a gray sandstone (D). The determinations were made with a Bausch and Lomb Spectronic 20 colorimeter with color analyzer reflectance attachment.

Reflectance curves for A, B, and D are close together at the short (blue) end of the spectrum; these rocks reflect more blue light and will photograph lighter in tone than C, when only the short end of the spectrum is re-

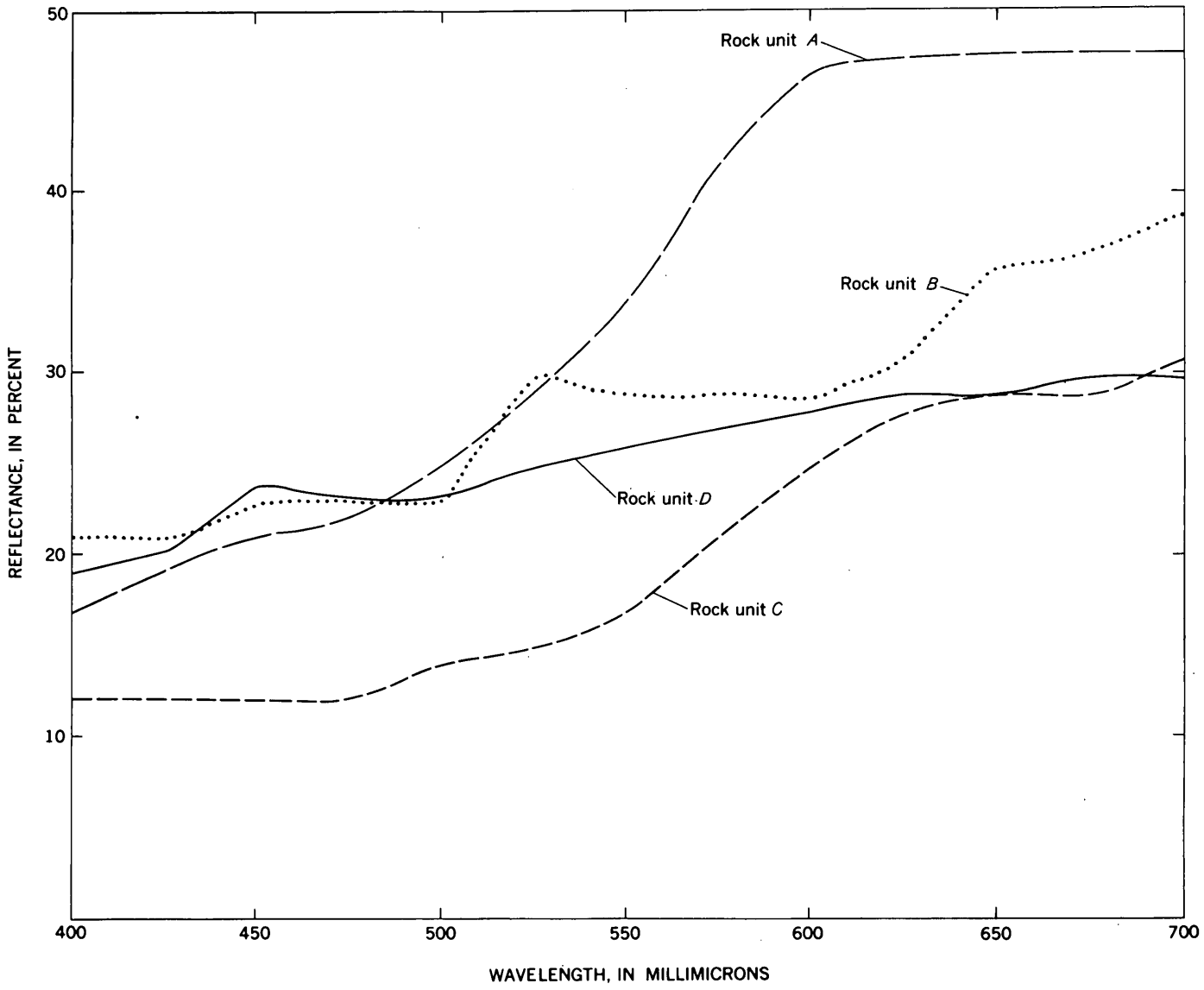

FIGURE 61.1.—Spectral reflectance curves of fresh samples of light-brown sandstone *A*, gray limestone *B*, red shaly siltstone *C*, and gray sandstone *D*.

corded (see fig. 61.2). If, on the other hand, only the long end of the spectrum is recorded, *B*, *C*, and *D* will photograph darker than *A* (see fig. 61.3).

On conventional aerial photographs there is usually but little tonal distinction between the various rocks, because light-reflectance differences are largely balanced out. Figures 61.2 and 61.3 suggest that for rocks in the area tested, film-filter systems could be designed that would make it easier than it is now to distinguish the different rocks on aerial photographs. Figure 61.2 was taken with a combination of No. 8 and 47B Wratten filters and records only reflected light less than 500 millimicrons in wave length. Figure 61.3 was taken with a No. 25 Wratten filter and records only reflected light more than 685 millimicrons in wave length.

557753 O—60——10

No aerial photographs taken through selected filters have, as yet, been obtained, but experimental rephotographing of aerial color photographs through selected filters has shown that tonal differences not readily seen on conventional aerial photographs are accentuated on photographs that record only selected wave lengths of light. This is seen by comparing figures 61.4 and 61.5. Figure 61.4 is a conventional aerial photograph; Figure 61.5 depicts approximately the same area on a photograph of an ecktachrome transparency rephotographed through a No. 47 Wratten filter on panchromatic film. Increased tonal contrast may be seen at *a* on figure 61.5, where it marks the contact between two different surficial materials. Filter selection in rephotographing the color transparency was based on spectral transmission measurements made on a densitometer.

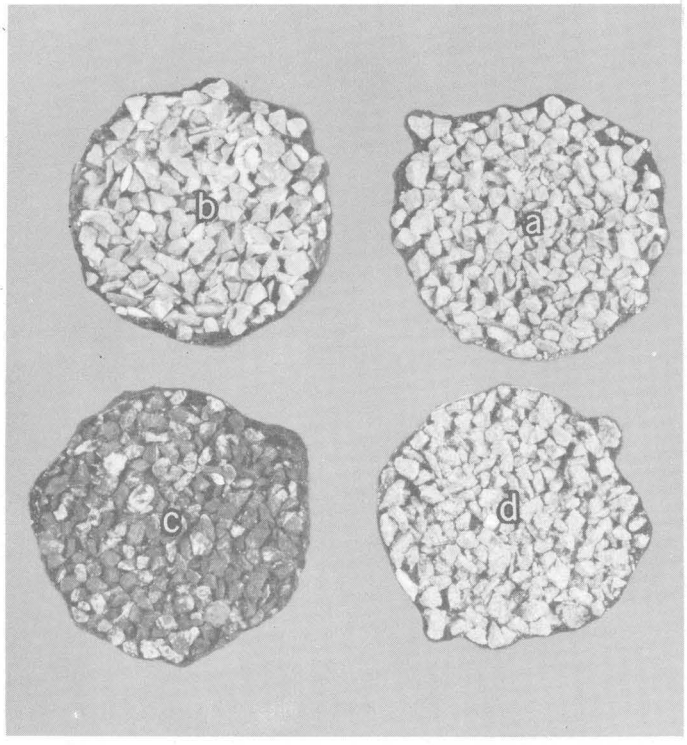

FIGURE 61.2.—Photograph of fresh samples of light-brown sandstone (*a*), gray limestone (*b*), red shaly siltstone (*c*), and gray sandstone (*d*), taken through a combination of No. 8 and 47B Wratten filters on panchromatic film. Note that samples *a*, *b*, and *d* appear lighter in tone than *c*.

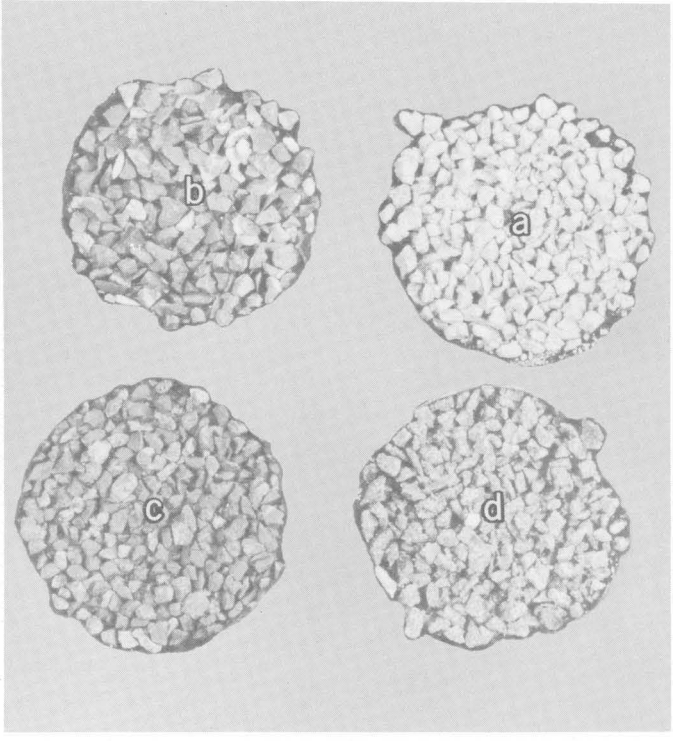

FIGURE 61.3.—Photograph of fresh samples of light-brown sandstone (*a*), gray limestone (*b*), red shaly siltstone (*c*), and gray sandstone (d) taken through a No. 25 Wratten filter on panchromatic film. Note that *b*, *c*, and *d* appear darker in tone than *a*.

FIGURE 61.4.—Part of a conventional aerial photograph showing several rock types and surficial materials of contrasting colors.

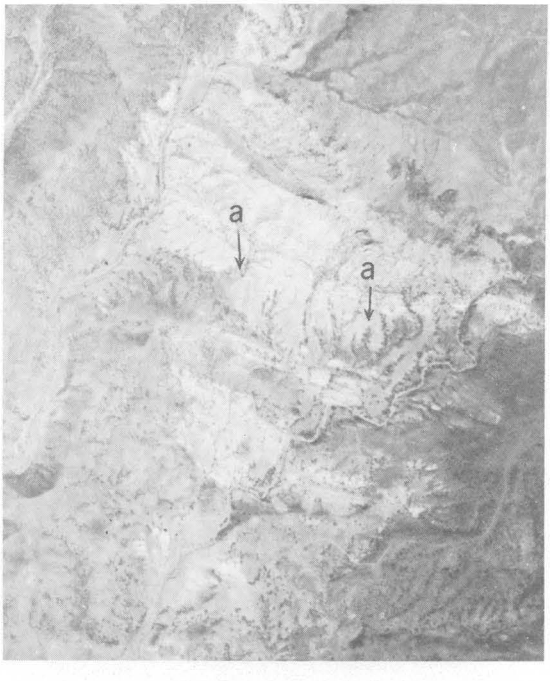

FIGURE 61.5.—Part of an ektachrome transparency photographed through a No. 47 Wratten filter showing same area as figure 61.4. The strengthening of tonal contrasts between different rocks is especially well seen at *a*.

62. TECHNIQUE FOR VIEWING MOON PHOTOGRAPHS STEREOSCOPICALLY

By Robert J. Hackman, Washington, D.C.

Work done in cooperation with the U.S. Army Corps of Engineers

The U.S. Geological Survey is engaged in a terrain study of the moon. Much of this work is being accomplished by a stereoscopic study of lunar photographs.

To the viewer on the earth, the moon has an apparent oscillation, known as libration. Because of this, a zone along the moon's perimeter is visible in one libration position but not in another. Photographs of the moon taken at different libration positions have an angular difference in view permitting a three-dimensional picture when viewed stereoscopically. The maximum angular difference is about 20°. Were it not for the libration, the maximum angular difference of view—from opposite sides of the earth—would be only ¾°, much too small for useful stereoscopic vision.

Figure 62.1*A* shows the moon at two different librations with respect to an earth station (A and A′), Photographs of the moon taken from this station would be the same as if photographs of the moon were taken simultaneously from two different stations in space about 50,000 miles apart (fig. 62.1*B*). The angular difference of view would be 12°.

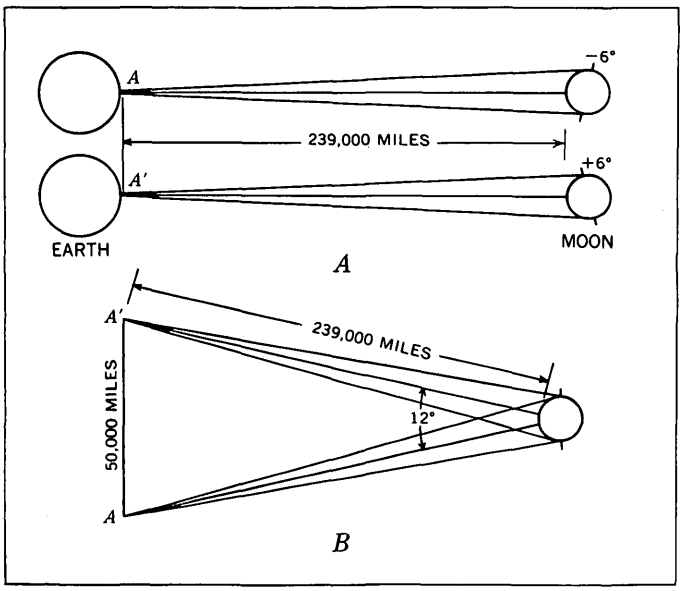

FIGURE 62.1.—*A*, Diagram showing moon at 2 different librations; *B*, diagram showing how photographs of moon at the 2 librations are the same as though they were taken simultaneously from 2 different points in space.

For best stereoscopic viewing, two lunar photographs should have the same scale, include the same area, be taken at different librations, and have image shadows that fall in the same direction. Although such photographs can be approximately positioned under the stereoscope by a trial and error method, a systematic method of orientation is best. A procedure for properly alining two moon photographs for stereoscopic viewing is as follows:

1. Locate on each picture the geometric center of curvature. (See fig. 62.2, points A and B.) This can be done by geometric construction or by use of a circular template.
2. Identify the conjugate image point of A on the photograph to the right (at point A′) and conversely the conjugate image point of B on the photograph to the left (at point B′).
3. Draw a straight line through the center and conjugate center of each photograph.
4. Position the photographs under the stereoscope so that all four points fall in a straight line (called the x-direction, fig. 62.2*CD*) and are in the following order: A, B′, A′ and B. Adjust the separation of the two photographs and the stereoscopic model is ready for viewing.

If several moon pictures taken at different librations are to be viewed stereoscopically, the following procedure for orienting the photographs may be preferable. Locate only the geometric center on each photograph. Flip one photograph up and down over the other so that image points appear to approximately coincide; determine the alinement of the two geometric centers. Note which geometric center is to the right and which is to the left in respect to the alinement. This will determine the right and left members of the stereoscopic pair. Maintaining approximate coincidence of image points, position the photographs so that alinement of the two centers is in the x-direction of the stereoscope. Adjust for proper separation, and the photographs are ready for stereoscopic viewing.

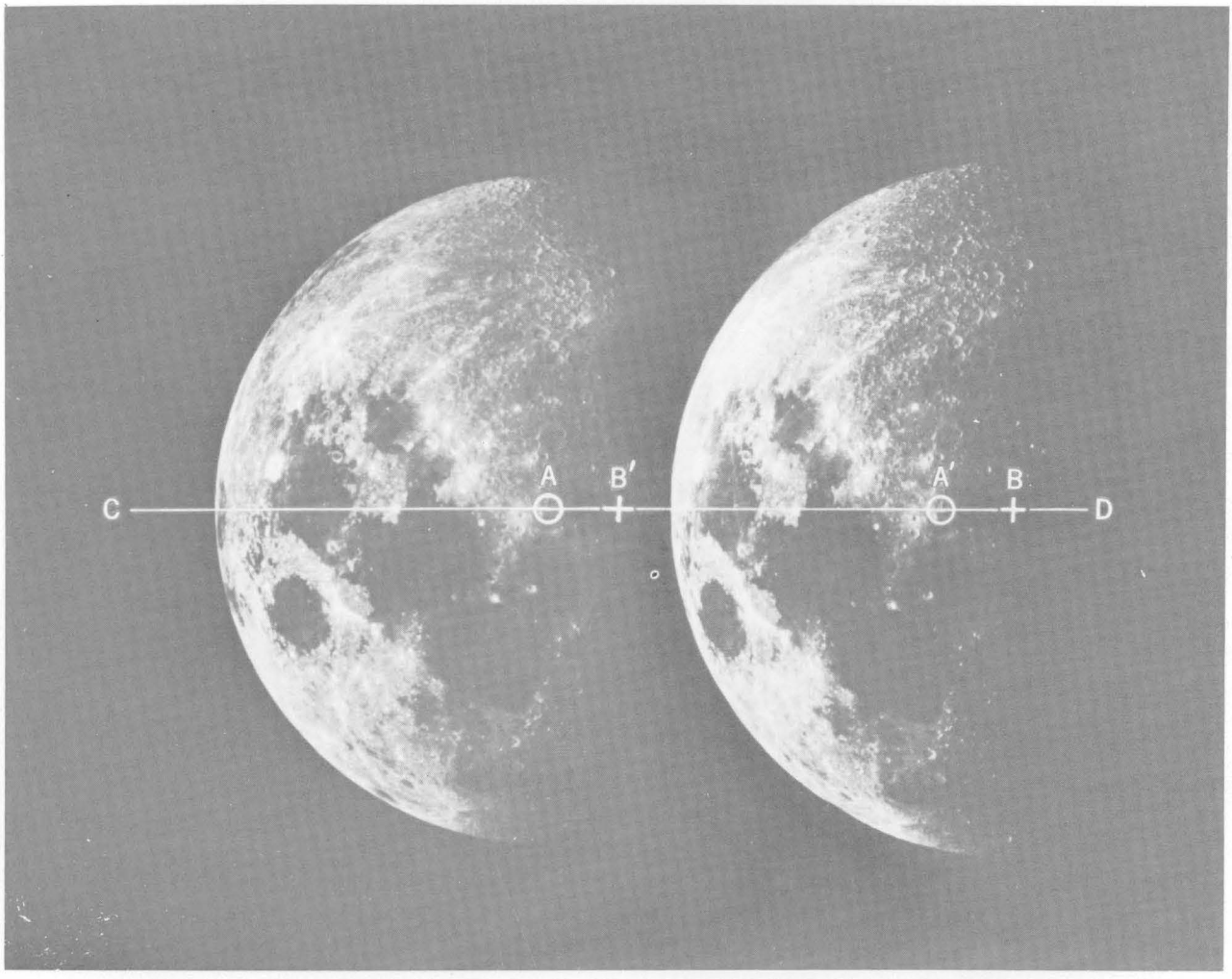

FIGURE 62.2.—Two moon photographs of different libration oriented for stereoscopic viewing with a lens or pocket stereoscope.

Enlarged photographs, approximate scale 1:4,270,000 (moon diameter 32″), are more suitable for a detailed study of lunar features than the smaller scale contact photographs, approximate scale 1:17,100,000 (moon diameter 8″). The enlargements, however, cannot be successfully handled under the desk-type mirror or prism stereoscope and must be cut into smaller sections. When enlarged sections of lunar photographs are prepared for stereoscopic viewing, allowance must be made for the fact that the image position of the geographic center of the moon (except at zero libration) can be in any direction from the geometric center of the photograph. A hexagonal format of enlarged sections was selected since it seemed most useful in accommodating the different orientations. Figure 62.3 is an example of a hexagonal pattern used on a series of enlarged moon photographs. Before the moon photograph is cut into sections, the geometric center, E, is located. A reference point, F, is then selected near the mean libration or geographic center; the crater Blagg in Sinus Media is near this center and will be satisfactory for this purpose. An additional reference point is located, preferably near the center of each hexagon (examples: F′, F″, etc. of fig. 62.3). The distance and bearing of the approximate geographic center, F, to the geometric center, E, is then plotted on each hexagon with respect to the reference point previously selected (examples: E′F′, E″F″, etc.).

The hexagons are indexed and cut apart. The process is repeated on a second moon enlargement of different libration. The geometric center is located and reference points F, F′, etc., of the first enlargement are transferred to the second photograph. The image points at the apices of each hexagonal section of the first photograph are used to identify conjugate image points on each new photograph. (The new six-sided

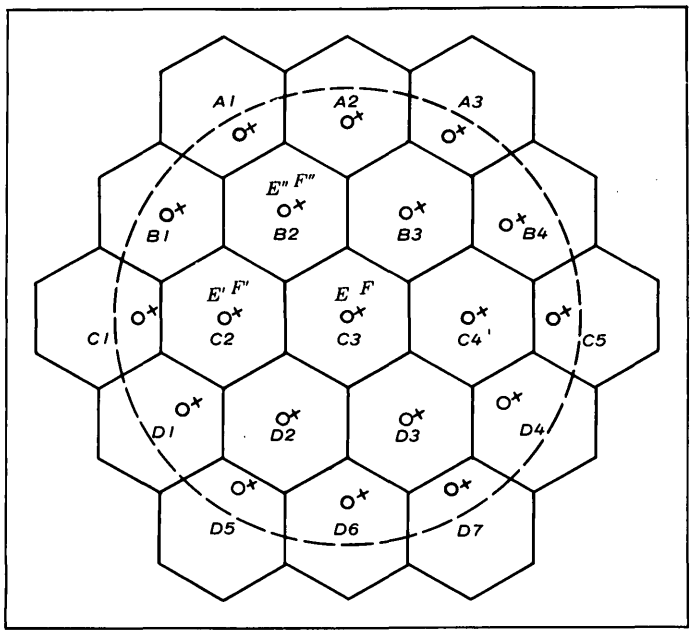

FIGURE 62.3.—Diagram showing how enlarged moon photographs are subdivided for viewing with a desk-type mirror or prism stereoscope.

figures will not be true hexagons. Some will be squeezed and others stretched, depending on the amount of inherent libration. However, each will cover the identical area.) The distance and bearing of the approximate geographic center, F, to the geometric center of the second photograph, is then plotted on each new hexagonal section with respect to the reference points F, F′, etc., transferred from the first photograph. The same index is used and the enlargement is cut into sections. Additional moon enlargements are prepared in a similar manner. Any pair of hexagonal sections having the same index number and not having opposing image shadows can be viewed stereoscopically using the same procedure for alinement described earlier in this paper.

Because many features of the moon show up better on one photograph than another, depending on the phase and libration of the moon at the time the photograph was taken, stereoscopic viewing of different pairs of such photographs permit the viewer to see many more features than would be visible on any single photograph.

⚒

GEOLOGY APPLIED TO ENGINEERING AND PUBLIC HEALTH

63. SOME THERMAL EFFECTS OF A ROADWAY ON PERMAFROST

By GORDON W. GREENE, ARTHUR H. LACHENBRUCH, and MAX C. BREWER, Menlo Park, Calif.

Work done in cooperation with the Bureau of Public Roads, Office of Naval Research, Air Force Cambridge Research Center, and the Bureau of Yards and Docks

The effects of a roadway on the thermal regime of the ground constitute one of the more important problems in permafrost engineering. A sizeable portion of the highway maintenance effort in permafrost terrain is directed toward repairing the results of differential settling and heaving in the subgrade materials. These thermal problems have been under study for several years by the U.S. Geological Survey in various places in Alaska.

The most conspicuous thermal effect of building a roadway is probably the increase in variability of ground temperature, that is, the increased sensitivity of ground temperature to changes in air temperature and surface radiation from summer to winter and from year to year. The effect is illustrated with data from the Richardson Highway in figure 63.1. It is seen that the total range of temperature from summer to winter at each depth is much greater beneath the roadway than beneath the nearby undisturbed ground. In the summer roadways are generally warmer than surrounding ground because of greater net absorption of radiation by their dark unshaded surfaces, and the absence of the cooling effect of evaporating moisture. In the winter roadways are generally cooler than the surrounding ground because snow, which serves as an insulator, is removed by plows or wind, or the insulating quality is destroyed by compaction under vehicular traffic. A larger seasonal range of temperature at the surface

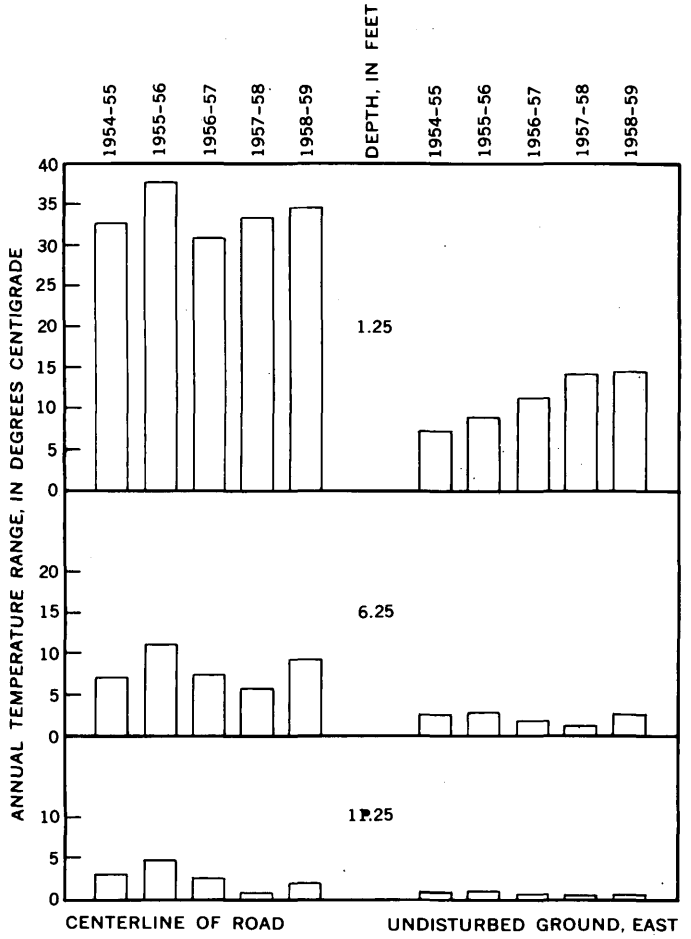

FIGURE 63.1.—Comparison of annual temperature ranges at selected depths beneath the surface of the roadway and nearby undisturbed ground, for the period July 1954 to June 1959, mile 130, Richardson Highway, Alaska.

generally results in a proportionally larger range at depth. Where coarse fill materials are used beneath the road the effect is accentuated as thermal changes are propagated downward with less attenuation in such high-diffusivity, low-moisture-content materials.

Almost as important as the seasonal range of temperature is the change in mean annual temperature beneath a roadway. Inasmuch as a roadway causes increased summer temperatures and decreases winter temperatures its effect on the mean is not obvious. Mean annual temperatures (for years beginning July 1) beneath the roadway and undisturbed ground are compared in figures 63.2 and 63.3. Shown also is the mean annual air temperature as recorded by the Weather Bureau at Gulkana Airfield, approximately 12 miles away. The changes in air temperature from year to year are followed by similar changes beneath the ground surface. Again the roadway shows a greater sensitivity to changing surface conditions. In both environments the temperature changes are attenuated with increasing depth.

Now consider the depth of thaw as illustrated in figure 63.4. We first notice that the thaw depth is consistently greater beneath the centerline of the roadway than at peripheral installations. This is the expected effect of the increased amplitude discussed above. It is interesting to note (figs. 63.2 and 63.3) that during the first three years the more deeply thawing centerline had lower mean temperatures than the undisturbed ground. This illustrates the independent roles played by amplitude and mean.

A striking feature of figure 63.4 is the sudden increase in maximum thaw depth beneath the centerline during the summer of 1957, and the persistence of this deep thawing in subsequent years. Inasmuch as the road was surfaced with asphalt late in the summer of 1956 it seems reasonable to suspect that the deep thawing was caused by an increase in the net radiation absorption by the dark surface during subsequent summers. If this were so, however, we should expect the cumulative thawing index beneath the surface to show an increase commensurate with the increased thaw depth. That it does not is shown by the data presented in table 63.1. The thawing index (maximum cumulative degree centigrade-days above freezing) at a depth of 5 feet is a rough measure of the quantity of heat available to thaw the material below 5 feet. The unusually warm summer of 1957 is associated with a large thawing index at 5 feet (487 degree centigrade-days) and an increase in active layer thickness from 6.9 feet to 10.5 feet. It is significant that roughly the same amount of thawing was accomplished in 1958 with only about half as much heat (258 degree centigrade-days) and in 1959 with less than one-fourth as much (104 degree centigrade-days). Clearly, the deep thawing in 1957, 1958, and 1959 is not the result of sustained increase in summer heat input due to surfacing the road, but the result of a progressive reduction in the amount of heat required to thaw to 10+ feet; that is, a reduction in moisture content. This conclusion is supported by the observation that thawing proceeds rapidly in ground previously thawed, and much more slowly at the degrading permafrost surface.

The effects can now be summarized in fairly general terms as follows. The presence of the road increases

TABLE 63.1—*Thawing index measured at 5 ft below surface of road at the centerline compared with depth of thawing beneath road.*

Year (July–June)	Thawing index, degree centigrade-days	Depth of thaw (feet)
1954–55	108	6.1
1955–56	140	6.5
1956–57	172	6.9
1957–58	487	10.5
1958–59	258	10.7
1959–60	104	10.2

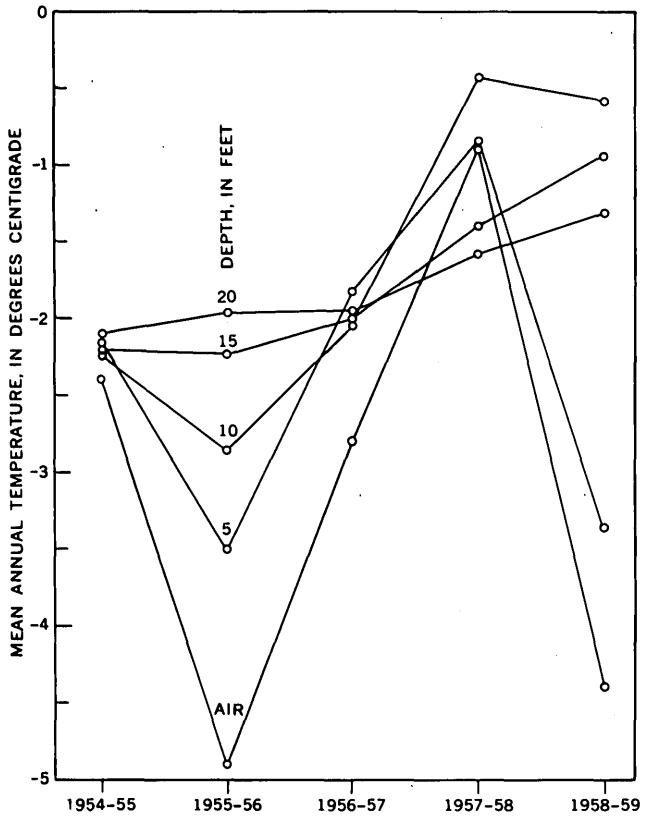

FIGURE 63.2.—Mean annual temperatures, centerline, mile 130, Richardson Highway, Alaska.

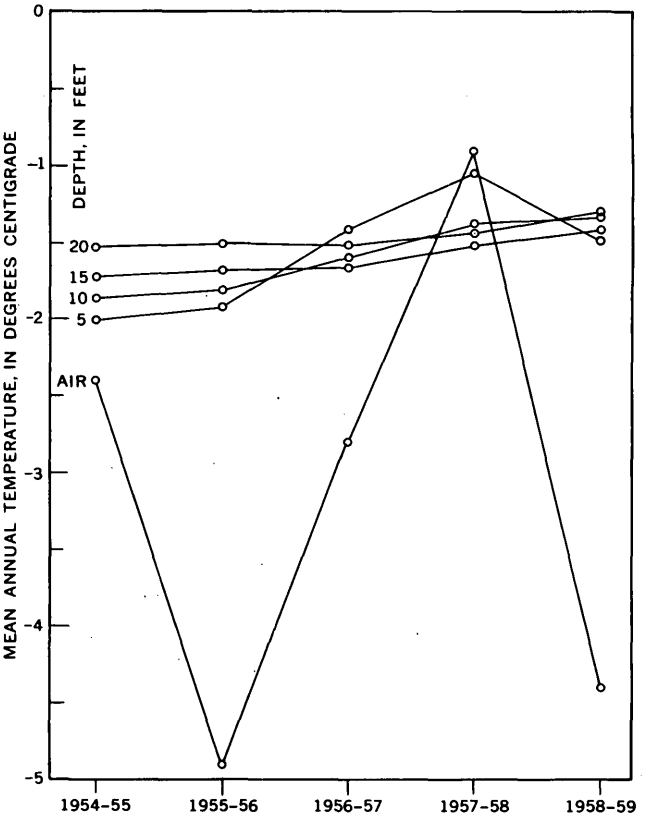

FIGURE 63.3.—Mean annual temperatures, undisturbed ground, east, mile 130, Richardson Highway, Alaska.

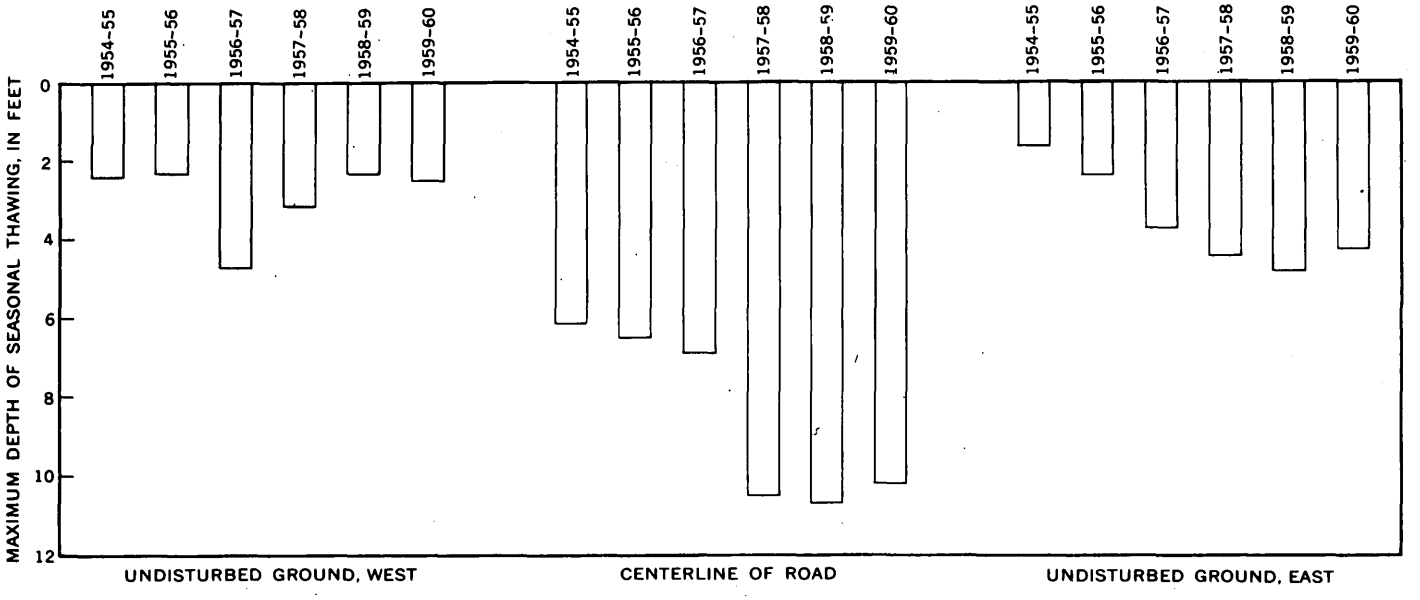

FIGURE 63.4.—Maximum depths of seasonal thawing at mile 130, Richardson Highway, Alaska.

the seasonal range of temperature (fig. 63.1) and hence increases the seasonal depth of thaw, causing the active layer to encroach on permafrost. The roadway is more sensitive to random climatic variation from year to year (figs. 63.2 and 63.3) and hence the deep thaw is accentuated during an anomalously warm season. If the excess water formed by melting ice in the surficial permafrost layers can drain off, the thickened active

layer will be drier and more easily thawed in subsequent years.

This, of course, will result in a settling of the roadway at the point where this progressive deep thawing occurs. The water would be expected to migrate in the thawed trough beneath the roadway until it is trapped in a basin, or escapes by exterior drainage. When it is trapped in a basin, as when the road crosses a swale or a large culvert, the water is ultimately refrozen and some heaving might be expected. In the case illustrated in figure 63.4, these effects were probably accentuated by the presence of a 3-foot sand layer known to occur between the depths of 8 and 11 feet. When the thaw depth exceeded 8 feet it is likely that water drained off through this permeable horizon. Transport of heat by the moving water probably aided the thawing process.

The continuing study of the thermal budget of the subgrade is expected to lead to a more detailed elaboration of the thermal and mechanical processes responsible for highway problems in permafrost. A regular unbroken series of field measurements, such as that now being obtained through the cooperation of the Bureau of Public Roads, will permit a more satisfactory quantitative treatment of the problem.

64. TENTATIVE CORRELATION BETWEEN COAL BUMPS AND ORIENTATION OF MINE WORKINGS IN THE SUNNYSIDE NO. 1 MINE, UTAH

By Frank W. Osterwald and Harold Brodsky, Denver, Colo.

Work done in cooperation with the U.S. Bureau of Mines

Violent, spontaneous destruction of coal faces, in what are commonly called bumps, endangers and at times destroys life and property in mines of the Book Cliffs coal field, Carbon County, Utah. The geometric arrangement of pillars, and redistribution of stress, causes many bumps, but other bumps, at least in the Sunnyside mines, occur at long distances from pillar workings (Peperakis, 1958). Much of the Sunnyside coal is under marked stress, and while being mined it shatters continuously (Clark, 1928, p. 80) and falls from the face. Mapping in the Sunnyside No. 1 mine to date supports the view that stress is released violently in workings that diverge at large angles from the orientation of predominant fractures within the coal. Recent mining operations in the Sunnyside mines also show that, in areas subject to violent bumps, some workings nearly parallel to a major fracture direction are less subject to bumps and require less roof support than nearby workings that intersect major fracture directions at large angles. This behavior may vary, and the theory here proposed to explain it may later have to be modified; it needs to be verified by mapping in other parts of this mine and in other mines, by measuring stress distribution in this and other mines, and by further testing of triaxial strength of the coal.

Fracture zones trending west and north to northwest (fig. 64.1) are common throughout the mine, and they, together with other structures, may directly influence the distribution and violence of bumps. The fracture zones are nearly tabular and consist of steeply dipping fractures; individual fractures within a zone vary slightly in strike and dip, and most of them are not parallel to the trend of the zone. A few of the fracture zones are parallel to mine workings and may have been formed after the workings were opened, but those that strike west and north-northwest are a part of the structural pattern of the district and are clearly older than the workings.

In the Sunnyside No. 1 mine, some headings were diverted from the normal N. 30° W., and N. 60° E. directions to take advantage of changes in strike or to make mining easy. Fracture zones at motor road parting (fig. 64.1) commonly trend about N. 70° W.; other zones trending about north-south are common but are narrower, less extensive, and less well marked than those trending N. 70° W. Where mine workings extend nearly parallel to fracture zones trending N. 70° W., rib failures occur frequently, indicating that stresses do not accumulate long before being relieved. Individual fractures in the zones are rotated inward toward the workings. The rotation is aided in part by failure of the ribs along new breaks that parallel the

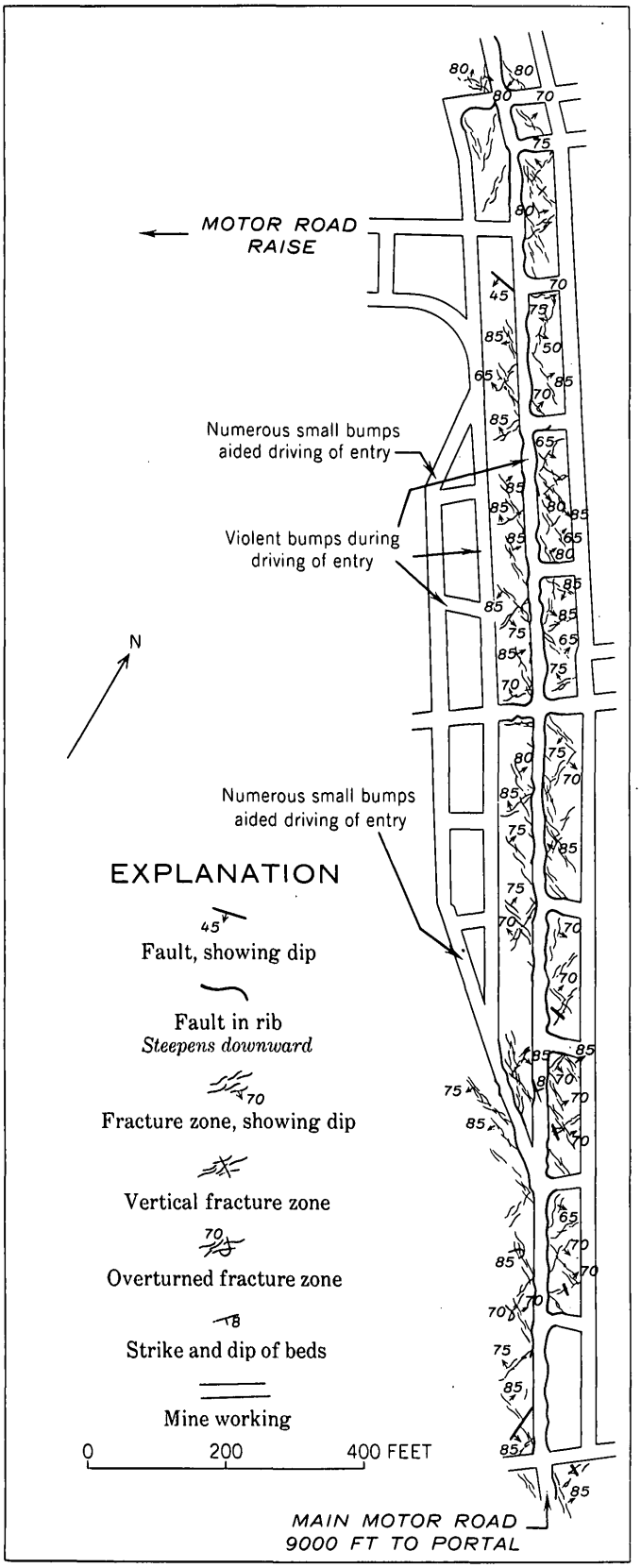

FIGURE 64.1.—Underground map of parting for motor road raise, Sunnyside No. 1 mine, Utah.

bedding near the roof but curve downward into steeply dipping fracture zones in the rib. Ribs that nearly coincide in direction with major fractures are strongly rock-bolted, and covered with heavy steel mesh, to prevent falls of coal.

Rib failures occur at much longer time intervals along workings that intersect the major fracture direction at large angles than they do in workings that intersect them at small angles (fig. 64.1). Miners report, moreover, that severe bumps, some of them powerful enough to overturn mine cars loaded with sand, have occurred during the driving of those headings in the parting that intersect the major fractures at large angles (fig. 64.1), whereas the bumps that attended the driving of headings nearly parallel to the major fracture zones were frequent, but so small that they helped to make mining easy.

The correlation here tentatively proposed of bumps with the angle between mine workings and fracture zones can be explained theoretically. The theory applies to all fractures, and may explain the observed relation between bumps and faults at Sunnyside (Watts, 1918; Peperakis, 1958). Bumps originate when strain energy stored in coal or in rock is released along a fracture; they can be regarded as small earthquakes of very shallow focus (Richter, 1958, p. 156–157). The fracture may form during the bump, or it may be older than the bump. Where only small amounts of stored energy are released, bumps are an aid to mining, but when the amounts are large they are a serious hazard.

While a heading is being driven, abnormal stresses are concentrated around it. The decrease of these concentrations away from the face is inversely proportional to the cube of the distance ahead of the face, but inversely proportional to the square of the distance into the rib (Isaacson, 1958, p. 119). The highest stress concentrations occur in a mass of coal whose long axis extends into the face at an angle of about 70° with the direction of the heading (fig. 64.2) (Isaacson, 1958, p. 78). Where the heading is near a fault or fracture, the volume of highly stressed coal becomes larger than where there is no fault nearby (Isaacson, 1958, p. 78). If a heading approaches a fault or fracture that is oriented at a large angle to its trend, stress is distributed uniformly over much of the face, and is not concentrated in a small volume of coal (fig. 64.2a). A violent bump may then occur over much of the face as soon as the accumulated stress exceeds the strength of the coal. If, on the other hand, the heading approaches a fault or fracture that is oriented at a small angle to its trend, stress is concentrated behind a small area of the face and causes only small bumps (fig. 64.2b).

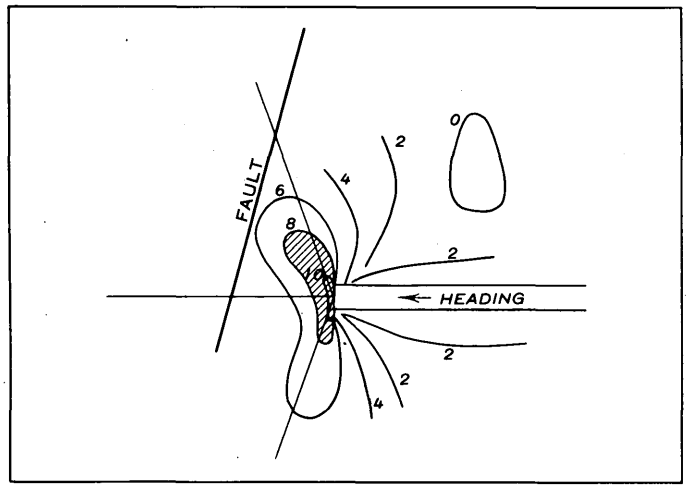

A HYPOTHETICAL SHEAR-STRESS CONTOURS (ARBITRARY UNITS) AROUND HEADING APPROACHING FAULT AT LARGE ANGLE

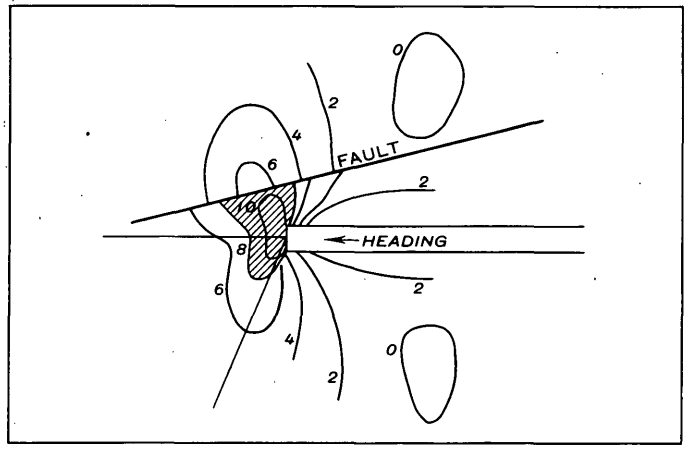

B SHEAR-STRESS CONCENTRATION (ARBITRARY UNITS) AROUND HEADING APPROACHING FAULT AT SMALL ANGLE

FIGURE 64.2.—Stress concentrations around a heading driven toward a fault.

Small bumps originating at the upper corner of a heading approaching an oblique fault were observed in the Sunnyside No. 2 mine in 1958.

When forces generated in mining cause renewed motion along a fault or fracture in a pillar, stress should be mainly concentrated in the coal near the ends of the fracture and about 70° to the right or left of its trend because the highest stress around a crack (Williams, 1957; 1959, p. 203–204) or a fault (St. Amand, 1956, p. 43–44) is ahead of and 70° to the right or left of its head. If, therefore, a fracture nearly parallel to a mine rib is reactivated, stress will be concentrated in a small volume of coal between the fracture and the rib, and bumping will occur before a large amount of stress can accumulate; but if the fracture makes a large angle with the rib, more strain energy will be stored in more coal, and failure will be more violent.

Finally, if the principal lateral stress in a pillar intersects a fault or fracture at a large angle, there is little slipping along the break. Laboratory tests have shown that smooth preexisting fractures in test cylinders of rock subjected to stress are most likely to slip when the angle between the fracture and the principal stress direction is between 15° and 33° (Jaeger, 1959). If, therefore, one of the principal stress directions in a pillar intersects a fault or fracture at a small angle, slippage will occur before much stress can accumulate; but if one of the principal stress directions intersects a fault or fracture at large angle, a large stress concentration and a violent bump may result.

REFERENCES

Clark, F. R., 1928, Economic geology of the Castlegate, Wellington, and Sunnyside quadrangles, Carbon County, Utah: U.S. Geol. Survey Bull. 793, 165 p.

Isaacson, E. de St. Q., 1958, Rock pressure in mines: London, Mining Publications Ltd., 212 p.

Jaeger, J. C., 1959, The frictional properties of joints in rocks: Geofisica pura e applicata, v. 43, p. 148–158.

Peperakis, John, 1958, Mountain bumps at the Sunnyside mines: Mining Eng., v. 10, p. 982–986.

Richter, C. F., 1958, Elementary seismology: San Francisco, W. H. Freeman & Co., 768 p.

St. Amand, Pierre, 1956, Two proposed measures of seismicity: Seismol. Soc. America Bull., v. 46, p. 41–46.

Watts, A. C., 1918, An unusual "bounce" condition: Coal Age, v. 14, p. 1028–1030.

Williams, M. L., 1957, On the stress distribution at the base of a stationary crack: Jour. Applied Mechanics, v. 24, p. 109–114.

——— 1959, The stresses around a fault or crack in dissimilar media: Seismol. Soc. America Bull., v. 49, p. 199–204.

65. REVIEW OF THE CAUSES OF SUBSIDENCE

By ALICE S. ALLEN, Washington, D.C.

Subsidence is the sagging or collapse of the ground surface. The area may be large or small; the movement may be abrupt or barely perceptible. The need to understand this phenomenon is increasing with the growing number and variety of engineering problems that are related to contemporary subsidence. Because subsidence problems have been encountered in many diverse fields, the Geological Survey has felt it desirable to search the literature of the various disciplines in an effort to inventory knowledge of the occurrences and causes of subsidence. Some of the results of this search are summarized here.

Presently recognized causes of subsidence include compaction of soil and subsurface materials, progressive readjustment around cavities, geochemical changes, melting, lateral migration of subsurface material, and contemporary tectonic disturbance. Rarely is it found that subsidence can be attributed without question to a single cause. Though evidence may show that one cause predominates, the exclusion of other possible causes is not easy because evidence of subsurface processes is largely circumstantial.

Compaction is the most frequently cited contributor to the subsidence cases being studied today. Much new evidence is becoming available in those areas where compaction is accelerated by the withdrawal of large quantities of artesian water, oil, or gas from subsuface formations. A significant new approach is the measurement of the differential compaction that takes place in different segments of the subsurface column. In subsiding areas in the San Joaquin Valley, Calif. (Inter-Agency Committee on Land Subsidence in the San Joaquin Valley, 1958, p. 97–106; 155–156), and in Mexico City (Zeevaert, 1957), subsurface bench marks have been installed at several stratigraphic horizons for measuring rates of differential compaction. Ground-water hydrology and petroleum reservoir engineering techniques are furnishing valuable quantitative data on two pertinent factors in compaction—pore space and fluid pressures. A check on compaction theories is provided by periodic measurements of fluid pressure changes in the producing zones, coordinated with subsidence measurements as rates of pumping increase or decrease. The most spectacular development in the control of subsidence is the injection under pressure of large quantities of sea water into the oil-producing zones of the Wilmington oil field, California (Stormont, 1959 a, b, and c), to halt subsidence and increase oil recovery.

Subsidence over cavities created by mining has been studied for more than a century, and papers that describe cases or analyze the mechanics of mine subsidence form the bulk of subsidence literature. Furthermore, research on many other mining problems, such as strength of roof and pillars, mine drainage, and intentional caving, has application to subsidence. Most promising is the modern resurgence of interest in subsidence as a part of the total picture of rock mechanics (Colorado School of Mines, 1956, 1957, 1959; European Congress on Ground Movement, 1957–1959; International Strata Control Congress, 1958).

Several chemical and physico-chemical processes are also causes of subsidence. The karst topography and thick layers of residuum found in humid climates show that subsidence takes place as the result of the solution of carbonate rocks, salines, and under some conditions, even igneous rocks. Although a new sinkhole may form suddenly by collapse of unconsolidated materials over a cavern, subsidence caused by solution generally proceeds too slowly to affect engineering works. Volume changes in clays stemming from changes in their state of hydration are being investigated in connection with foundation engineering. Oxidation of peat, with its extreme reduction in volume, accounts for large areas of subsidence. The subsidence of peat soils reclaimed by drainage has been studied in the San Joaquin delta, California, (Weir, 1950) and the Florida Everglades (Stephens, 1956). Subsidence due to melting of large ice masses in permafrost often follows changes in the thermal regime at the ground surface, and contributes to the destruction of roadways and structural foundations in Alaska and elsewhere.

Lateral migration of subsurface material includes squeezing of plastic clay and salt under load, and movement of molten lava beneath the surface. Ground-surface movements in response to underground movement of lava have been measured at Kilauea Volcano in Hawaii by high-precision survey methods (Wilson, 1935), and are being studied currently by the Geological Survey (K. J. Murata, 1959, written communication). Subsidence occurs at the summit and on the flanks of active volcanoes as the result of stoping, melting, and the withdrawal of lava, forming summit calderas, pit

craters, sector grabens, and trenches over lava tubes. Internal landsliding enlarges these features and other volcanic craters (such as the crater of Vesuvius following the "gas phase" of the 1906 eruption). Much larger scale subsidence takes place in response to paroxysmal explosions of ash, as occurred at Crater Lake in prehistoric times, at Krakatau in 1888, at Katmai in 1912, and in 1955 at Bezymianny in Kamchatka.

Appraisal of the role of tectonic movements in subsidence is difficult because most suspect areas are also areas where compaction is known to be a large factor. From the field of seismology, records of tilt, earthquake shocks, and ground-movement observations may provide data that can be correlated with subsidence. Evaluation of tectonic movements versus other factors causing subsidence has been attempted for the Wilmington area in California (Gilluly and Grant, 1949); the Mississippi Delta (Kolb and Van Lopik, 1958); and the coastal Netherlands (Symposium on Quaternary changes in Level, especially in the Netherlands, 1954). Part of the problem in coastal areas is to judge how much of the apparent subsidence of the coast actually represents sea-level rise. This problem has been approached from the analyses of tide-gage records and oceanographic studies of eustatic sea-level changes.

Whatever the local cause or causes of a particular case of subsidence may be, all subsidence investigations have two common requirements. First, and continuing through all stages of any subsidence study, is the need for a reliable datum, and for high-precision, repeated surveys of the same points, tied into that datum. In the United States the Coast and Geodetic Survey's first-order level net, plus special surveys connecting individual subsiding areas, furnish vertical control (Small, 1959). Secondly, for those reference points that are installed on some sort of manmade structure, the possibility that the individual structure may be settling on its own foundation must be evaluated. Soil mechanics techniques for studying soil consolidation provide a basis for judging whether subsidence rates recorded at individual stations are representative of the surrounding area.

REFERENCES

Colorado School of Mines, 1956, Symposium on rock mechanics: Colorado School Mines Quart., v. 51, no. 3.

——— 1957, Second annual symposium on rock mechanics: Colorado School Mines Quart., v. 52, no. 3.

——— 1959, Third symposium on rock mechanics: Colorado School Mines Quart., v. 54, no. 3.

European Congress on Ground Movement, 1957–1959, 19 papers published separately in various issues of Colliery Engineering, v. 34, 35, and 36 [London].

Gilluly, James, and Grant, U. S., 1949, Subsidence in the Long Beach Harbor area, California: Geol. Soc. America Bull., v. 60, no. 3, p. 461–529.

Inter-Agency Committee on Land Subsidence in the San Joaquin Valley, 1958, Progress report on land-subsidence investigations in the San Joaquin Valley, California, through 1957: Sacramento, Calif.

International Strata Control Congress, Leipzig, 1958, (Deutsche Akad. der Wiss. zu Berlin, Sektion für Bergbau), 319 p. 140 pl.

Kolb, C. R., and Van Lopik, J. R., 1958, Geology of the Mississippi River deltaic plain, southeastern Louisiana: U.S. Army Eng. Waterways Expt. Sta., [Vicksburg] Tech. Rept. no. 3–483.

Small, J. B., 1959, Settlement investigations in the vicinity of Galveston-Houston, Texas, and San Joaquin Valley, California: Jour. Geophys. Research, v. 64, no. 8, p. 1124–1125.

Stephens, J. C., 1956, Subsidence of organic soils in the Florida Everglades: Soil Sci. Soc. America, Proc., v. 20, no. 1, p. 77–80.

Stormont, D. H., 1959a, Speed is watchword at Wilmington: Oil and Gas Jour. v. 57, no. 31, p. 106–107.

——— 1959b, World's biggest water flood: Oil and Gas Jour., v. 57, no. 36, p. 55–60.

——— 1959c, New plants boost Wilmington's water-injection capacity: Oil and Gas Jour., v. 57, no. 52, p. 66–69.

Symposium on Quaternary changes in level, especially in the Netherlands, 1954, Geol. en Mijnb., new ser., v. 16, no. 6, p. 148–267.

Weir, W. W., 1950, Subsidence of peat lands of the Sacramento-San Joaquin Delta, California: Hilgardia, v. 20, p. 37–56.

Wilson, R. M., 1935, Ground surface movements at Kilauea Volcano, Hawaii: Hawaii Univ. Research Pub., no. 10.

Zeevaert, L., 1957, Compensated friction-pile foundation to reduce the settlement of buildings on the highly compressible volcanic clay of Mexico City: Internat. Conf. on Soil Mechanics and Foundation Eng., 4th [London] Proc., v. 2, p. 81–86.

66. A SAMPLE OF CALIFORNIA COAST RANGE LANDSLIDES

By M. G. Bonilla, Menlo Park, Calif.

The landslides in the San Francisco South quadrangle, California, are probably a fair sample, in regard to character and frequency, of those that are likely to become increasingly troublesome throughout the California Coast Ranges as construction increases. This area is intermediate in climate between the more humid area to the north and the less humid area to the south; it contains exposures of most of the rocks common in the Coast Ranges; and it is affected by landslides of many kinds.

At least 132 landslides have occurred in the quadrangle—an average of 2.4 per square mile. These exemplify all but 3 of the 16 types in the Highway Research Board's classification (Varnes, 1958). Debris slides have been by far the most common. Other types of slides that have occurred here, named in approximate order of decreasing number, are earthflow, complex landslide, slump, sand run, mudflow, debris avalanche, block glide, sandflow, debris flow, soilfall, rockslide, and rockfall. The only types in the Highway Research Board's classification that have not been recognized are failure by lateral spreading, rock-fragment flow, and loess flow.

Complex landslides affect the greatest total area, followed in decreasing order by earthflows, slumps, and debris slides. About 70 percent of the landslides cover less than 2,500 square yards apiece, but a few cover more than 100,000 square yards apiece.

Many kinds of material are affected by the landslides. About one-third of the slides involve only slope debris, consisting mostly of stony clay. Landslides in slightly indurated sediments of the Merced formation are almost as common, but nearly all are in the steep sea cliffs cut in that formation. Other materials, named in decreasing order of susceptibility to slides, are: sandstone and shale of the Franciscan formation, artificial fill, sheared rocks, serpentine, greenstone and chert of the Franciscan formation, and clayey sand of the Colma formation. No slides are known to have occurred in metamorphic rocks of the Franciscan formation. Quaternary alluvium, beach deposits, sand dunes, marine terrace deposits, and bay mud are not involved in sliding in this quadrangle, probably because they are rarely exposed there in steep slopes.

Landslides occur on slopes ranging from 10° to 55°, but most are on moderate slopes; more than one-third are on slopes of 20° to 25°. About one-sixth occur on slopes of about 40°; a large proportion of these, however, are on a long sea cliff having approximately that inclination.

Most landslides are on slopes that face west or southwest; this is in contrast to areas east and north of Berkeley, Calif., where Beaty (1956) found that most of the shallow landslides were on slopes that face north or east.

REFERENCES

Beaty, C. B., 1956, Landslides and slope exposure: Jour. Geology, v. 64, no. 1, p. 70–74.

Varnes, D. J., 1958, Landslide types and processes, *in* Eckel, E. B., ed., Landslides and engineering practice: Highway Research Board, Spec. Rept. 29, p. 20–47.

67. ALTERATION OF TUFFS BY RAINIER UNDERGROUND NUCLEAR EXPLOSION, NEVADA TEST SITE, NYE COUNTY, NEVADA

By V. R. Wilmarth, Theodore Botinelly, and R. E. Wilcox, Denver, Colo.

Work done in cooperation with the U.S. Atomic Energy Commission

The Rainier explosion occurred at the Nevada Test Site on September 19, 1957. According to Johnson and others (1959, p. 1467–1468) it released 1.7 kilotons of energy, raised the temperature to 1,000,000°K and the pressure to 7,000,000 atmospheres within a few microseconds, and formed a cavity having a radius of 62 feet

within 80 milliseconds. Kennedy and Higgins (1958) concluded that before the cavity collapsed it was lined with a shell of radioactive molten glass about 10 cm thick, and that during the interval between 30 and 120 seconds after detonation the cavity was filled with steam at 40 atmospheres pressure and a temperature of 1,500°C. One year after the explosion, a temperature of 50°C was measured in a drill hole 60 feet below the explosion chamber (Diment and others, 1959, fig. 9–1).

The Rainier explosion occurred in bedded, indurated, porphyritic, rhyolitic to quartz-latitic tuffs in the Oak Spring formation, of Tertiary age. As determined from samples taken before the explosion and near its point of release, these tuffs have a high proportion of shards and lapilli, and a high content of water (table 67.1). The water is largely in a fine-grained mixture of zeolite, clay, beta-cristobalite, and amorphous material that has replaced almost anhydrous glass. The zeolite is mainly clinoptilolite, a close relative of heulandite, but containing more potassium and silica. It has been recently recognized as an important constituent of many tuffaceous sediments (for example Deffeyes, 1959; Mumpton, 1960; Mason and Sands, 1960). The clay appears to be mainly montmorillonite, and the beta-cristobalite and amorphous material are presumably components of opaline silica.

TABLE 67.1.—*Average composition of tuff close to Rainier explosion chamber*

Chemical composition, 47 samples (percent by weight)		Mineral composition, 52 samples (percent by volume)		
SiO_2	66. 9	Phenocrysts	17. 4	------
Al_2O_3	12. 4	Quartz	------	2. 6
Fe_2O_3	2. 3	Alkali feldspar	------	6. 1
FeO	. 23	Plagioclase	------	6. 8
MgO	1. 1	Biotite	------	1. 3
CaO	2. 4	Pyroxene and amphibole	------	. 2
Na_2O	1. 4	Magnetite	------	. 4
K_2O	2. 3	Xenoliths	6. 9	6. 9
H_2O+	5. 5	Shards and lapilli	68	------
H_2O-	5. 3	Zeolite: Clinoptilolite(?)	------	23
CO_2	. 6	Clay: Montmorillonite	------	12
		Beta-cristobalite	------	11
		Amorphous material	------	22
		Vesicles	7. 7	7. 7
		Total	100. 0	100. 0

The heat and pressure produced by the Rainier explosion formed a breccia around the explosion chamber and fused some of the tuff to radioactive glass (see Bunker, Wilmarth, and Diment, Art. 68). The glass is most abundant in the matrix of the breccia, where it forms irregular to rounded masses as much as 3 inches wide and 1.5 feet long. The glass is black, red, or gray, opaque to clear, compact to frothy, and has a vitreous to dull luster. Its contacts with adjacent tuff are commonly sharp, and the tuff is stained brick red for a distance of about 2 inches from the glass.

Small tuff samples from the breccia containing radioactive glass were disintegrated in water and the glassy particles examined under a binocular microscope. A few of the particles are smooth spheres, 0.1 to 0.5 mm in diameter, of clear glass containing bubbles and dark streaks, but most of the particles have grooved and crenulated surfaces to which tuffaceous material is attached. Many of the particles are fragments of stemlike and hairlike masses with longitudinal markings and elongate bubbles and dark streaks. Some masses as much as 5 mm in diameter roughly resemble hubs with spokes and blunt protuberances.

Indices of refraction in the glass range from 1.495 to 1.530, as in medium to silicic natural glass. They vary not only from one particle to another but also within the same particle: For instance, in one particle they range from 1.507 to 1.530, and in another from 1.510 to 1.528.

In thin sections the glass contains minor quantities of red to black opaque fragments, and numerous elongate bubbles a few millimeters across; many of the smaller particles are simply hollow spheres. The phenocrysts in the glass are principally quartz, feldspar, and biotite with diffuse boundaries. Samples from the outer edge of the breccia have minute rounded masses of pale-gray glass in the tuff matrix but show no alteration of the phenocrysts. Some of this glass is radioactive. These data suggest that fusion began in the tuff matrix, and proceeded in some places until only the phenocrysts remained; most of the glass is therefore presumed to have resulted from the melting of the zeolite and clay of the matrix.

Tuff samples from the outer edge of the breccia zone show noticeable changes in texture. They contain many dark-gray and brown fine-grained irregular veinlets as much as 6 inches wide, a few of which are more radioactive than the adjacent tuff. The mineral content of the veinlets, however, appears from X-ray diffractometer analysis to be similar to that of the enclosing tuffs, except for a locally greater proportion of noncrystalline material. The darker color of the veinlets is presumably due to comminution of the tuff during brecciation.

The principal changes outside of the breccia zone are textural. Microscopic study of tuff samples taken 70 to 75 feet from the explosion show a network of irregular anastomosing veinlets, 0.003 to 0.05 mm wide, filled with fine-grained opaque material. In many sections these veinlets have no preferred orientation, but in others

one direction is dominant. Autoradiographs made a year after the explosion indicate that the veinlets are not appreciably more radioactive than the intervening tuff. Between 75 and 130 feet from the explosion the veinlets decrease in size and abundance. At 130 feet the largest veinlet observed is 0.003 mm wide and 0.01 mm long, with tapered ends.

Index of refraction and optic angle determinations on biotite, pyroxene and amphibole phenocrysts indicate no systematic variation with distance from the explosion. Undulatory extinction in quartz grains appears to be about equally marked in samples taken before and after the explosion, except that it is especially marked in some of the remelted tuff. X-ray diffraction analyses of phenocrysts and their matrix show no changes of pattern that can be related to the explosion.

The change in cation-exchange capacity from the breccia zone outward was determined by ammonia distillation (H. C. Starkey, written communication). Samples of tuff taken 40 to 135 feet from the breccia zone have exchange capacities of 72 to 90 milliequivalents per 100 grams. Between 40 and 0 feet the capacity decreases sharply, the lowest value (50.2 milliequivalents) being obtained on a sample adjacent to the breccia. X-ray analysis of the minerals gave about the same results for samples having low and high exchange capacities. Morey (1958) has shown that the clinoptilolite in the tuff changes to plagioclase when heated to 500° C under 5,000 psi of steam for 3 hours, and Mumpton (1960) has shown that clinoptilolite when heated above 700° C in air decomposes to amorphous material. The decrease in cation-exchange capacity toward the breccia zone may therefore be related to alteration of the zeolite by heat from the explosion.

Differential thermal and thermobalance analyses of tuff samples taken before the explosion show that the main effect of heating in air to 700° C is loss of water; upon cooling, however, the tuff regains the water. Samples taken after the explosion, 5 to 10 feet outside the breccia zone, give similar results, indicating that the temperatures and pressures at these distances were not high enough to cause any drastic change in the mineral constituents.

Thermoluminescence curves of tuff matrix from samples 2 to 70 feet outside the breccia zone show only minor differences, which cannot be related directly to the explosion.

We are grateful to Dr. Barrie Bieler and the Dow Chemical Company, Rocky Flats, Colo., for providing facilities and for help in preparing thin sections of the radioactive glass, and to John R. Dooley of the Geological Survey for making autoradiographs.

REFERENCES

Deffeyes, K. S., 1959, Zeolites in sedimentary rocks: Jour. Sed. Petrology, v. 29, no. 4, p. 602–609.

Diment, W. H., Wilmarth, V. R., and others, 1959, Geologic effects of the Rainier underground nuclear explosion: U.S. Geol. Survey TEI–355 (preliminary draft), open-file report.

Johnson, G. W., and others, 1959, Underground nuclear detonations: Jour. Geophys. Research, v. 64, no. 10, p. 1457–1470.

Kennedy, G. C., and Higgins, G. H., 1958, Temperatures and pressures associated with the cavity produced by the Rainier event: Univ. California, Livermore, Radiation Laboratory, UCRL–5281.

Mason, Brian, and Sands, L. B., 1960, Clinoptilolite from Patagonia; the relationship between clinoptilolite and heulandite: Am. Mineralogist, v. 45, p. 341–350.

Morey, G. W., 1958, The action of heat and of superheated steam on the tuff of the Oak Spring formation: U.S. Geol. Survey TEI–729, open-file report.

Mumpton, F. A., 1960, Clinoptilolite redefined: Am Mineralogist, v. 45, p. 351–369.

68. DISTRIBUTION OF GAMMA RADIOACTIVITY, RADIOACTIVE GLASS, AND TEMPERATURE SURROUNDING THE SITE OF THE RAINIER UNDERGROUND NUCLEAR EXPLOSION, NEVADA

By C. M. Bunker, W. H. Diment, and V. R. Wilmarth, Denver, Colo.

Work done in cooperation with the U.S. Atomic Energy Commission

The distribution of anomalous gamma radioactivity and temperature produced by the Rainier explosion of September 19, 1957, was determined in drill holes and in tunnels driven through the zone disturbed by the explosion. The 1.7 kiloton nuclear explosion was 900 feet vertically below the surface of the ground, in

bedded tuff of the Oak Spring formation. The pore space of the tuff (about 30 percent by volume) was saturated with water (Keller and Robertson, 1959).

DISTRIBUTION OF RADIOACTIVITY

Gamma radioactivity was determined with scintillation and Geiger-Mueller sensing elements from September 1958 to February 1960 (Bunker, 1959).

Most of the anomalous gamma-radioactivity is concentrated below the explosion point (fig. 68.1), and most of it is contained in glass formed by the explosion. The distribution of radioactivity supports the theory developed by Johnson and others (1959) that the explosion formed a cavity, lined with radioactive glass, the upper part of which collapsed shortly after the explosion. Most of the radioactive glass is therefore concentrated in the form of a bowl below the explosion point. In this region the outer limit of the anomalous radioactivity corresponds closely with the outer limit of the breccia produced by the explosion. The breccia consists of blocks and smaller fragments of rock that were crushed and disoriented by the explosion. Fracturing without disorientation of blocks extends outward from the breccia (Wilmarth, 1959).

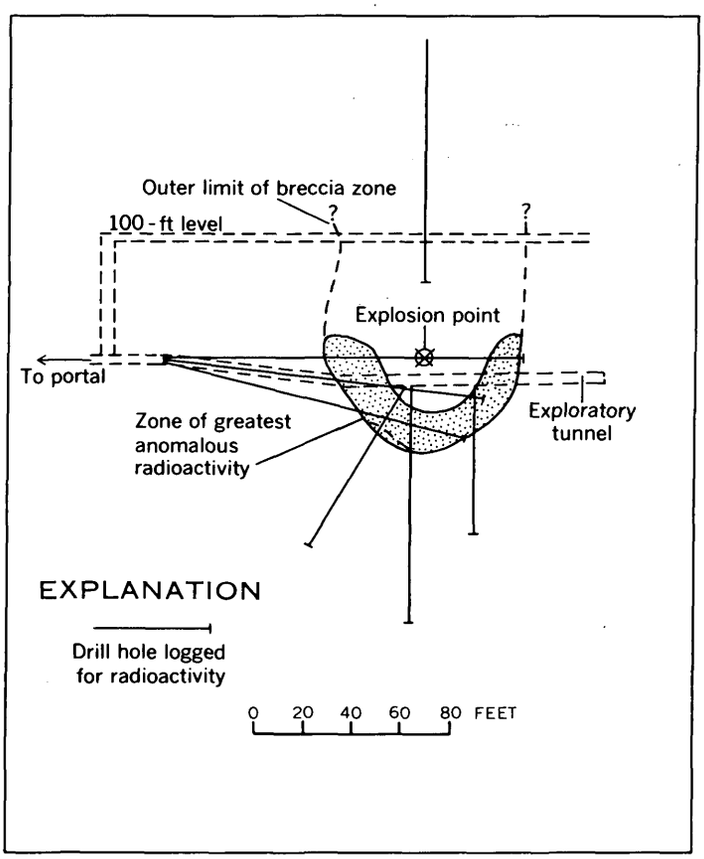

FIGURE 68.1.—Generalized vertical section through the Rainier explosion point showing generalized distribution of gamma radioactivity greater than about 1 mr per hr.

The outer limit of radioactivity as shown in figure 68.1 is the line bounding the region of clearly anomalous radioactivity as measured in drill holes. This is about one milliroentgen per hour (mr per hr), as compared with a pre-explosion background of about 0.03 mr per hr. Anomalous radioactivity undoubtedly extends beyond this limit, but the distance is difficult to establish because of the contamination that occurred in the drill holes and in the exploratory tunnel while they were being driven. Fission products having gaseous precursors were found to be relatively scarce in the radioactive glass (Johnson and others, 1959), and it is assumed that they moved considerably outside of the zone of obvious radioactivity. Krypton–85, a gaseous fission product, was found in a cavity of 385 feet above the explosion point about 6 weeks after the explosion (Johnson and others, 1958). No anomalous radioactivity was detected in the part of the original tunnel that was accessible after the explosion (radial distances greater than 200 feet from the explosion).

Gamma-radioactivity logs in the tunnel and in some drill holes (fig. 68.2) illustrate the uneven distribution of the radioactivity. The log for drill hole D shows that radioactivity was small directly above the explosion point but was concentrated toward the edges of the bowl. This concentration is particularly well shown by the measurements made in the exploratory tunnel.

RADIOACTIVE GLASS

Radiometric examination of tunnel workings and correlation of sample and gamma-radioactivity logs indicates that most of the radioactivity is contained in explosion-produced glass. Not all of it, however, is in the glass. Fine fractions (less than 0.01 mm) of the breccia contain some radioactive materials, and so do the solids in suspension in water samples from the exploratory tunnel (A. Clebsch, 1959, written communication), but it is not certain whether the radioactivity is in finely divided glass or not.

The appearance of the glass varies widely (Wilcox and Wilmarth, 1959). It may be black, gray, or red, opaque or clear, and compact or frothy. Most of the black and clear glass is compact and has a vitreous luster, whereas the gray glass is frothy and has a dull luster. Some of the frothy gray glass contains discrete schlieren-like masses of black glass. In some places cores consisting of brown clayey material and red compact glass are enclosed in shells of black glass.

Measurements of the radioactivity of glass specimens of approximately the same size, made in the exploratory tunnel, indicate that in general the black,

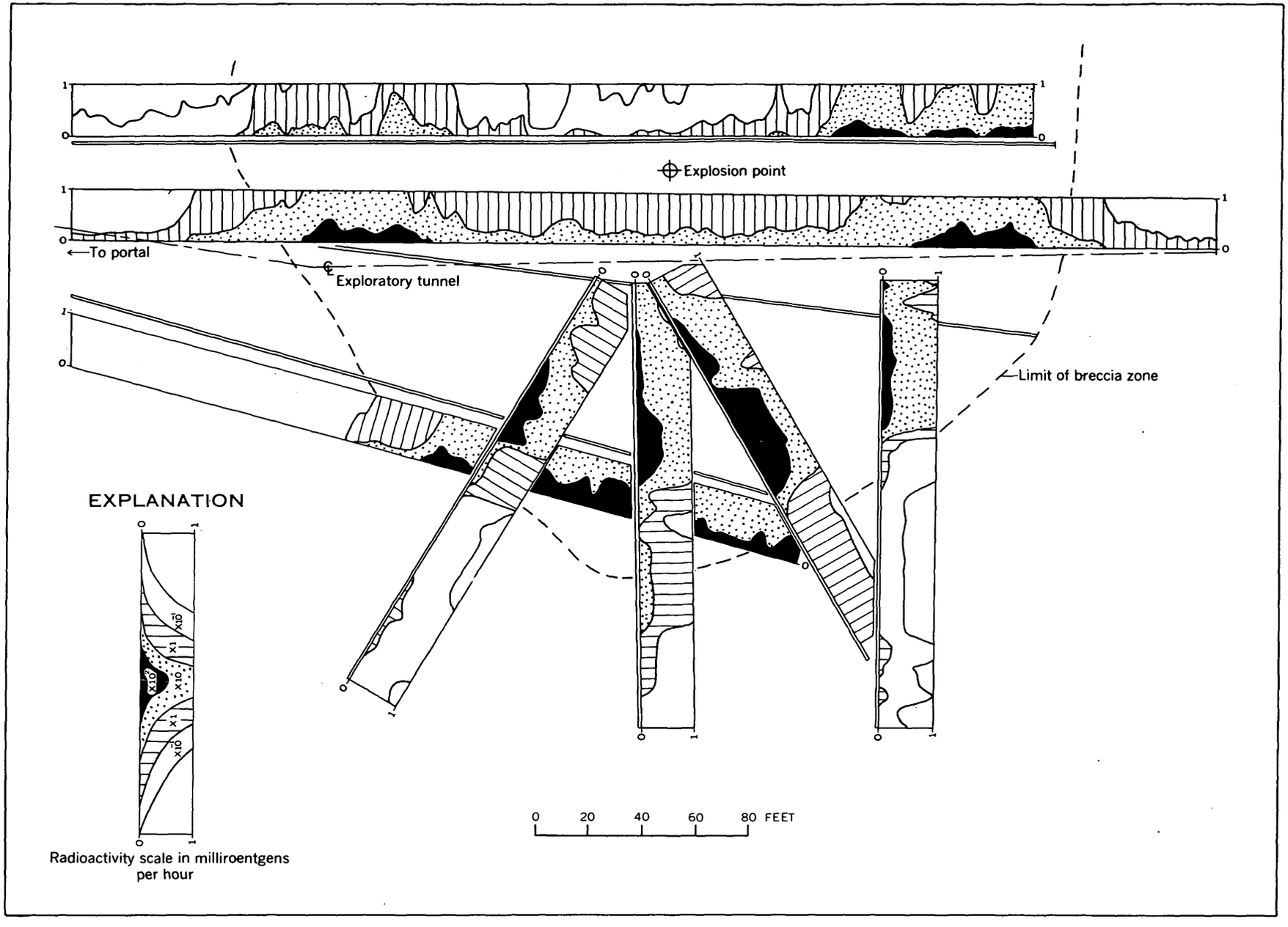

FIGURE 68.2.—Gamma-radioactivity logs from tunnel and drill holes illustrating variability of radioactivity.

557753 O—60——11

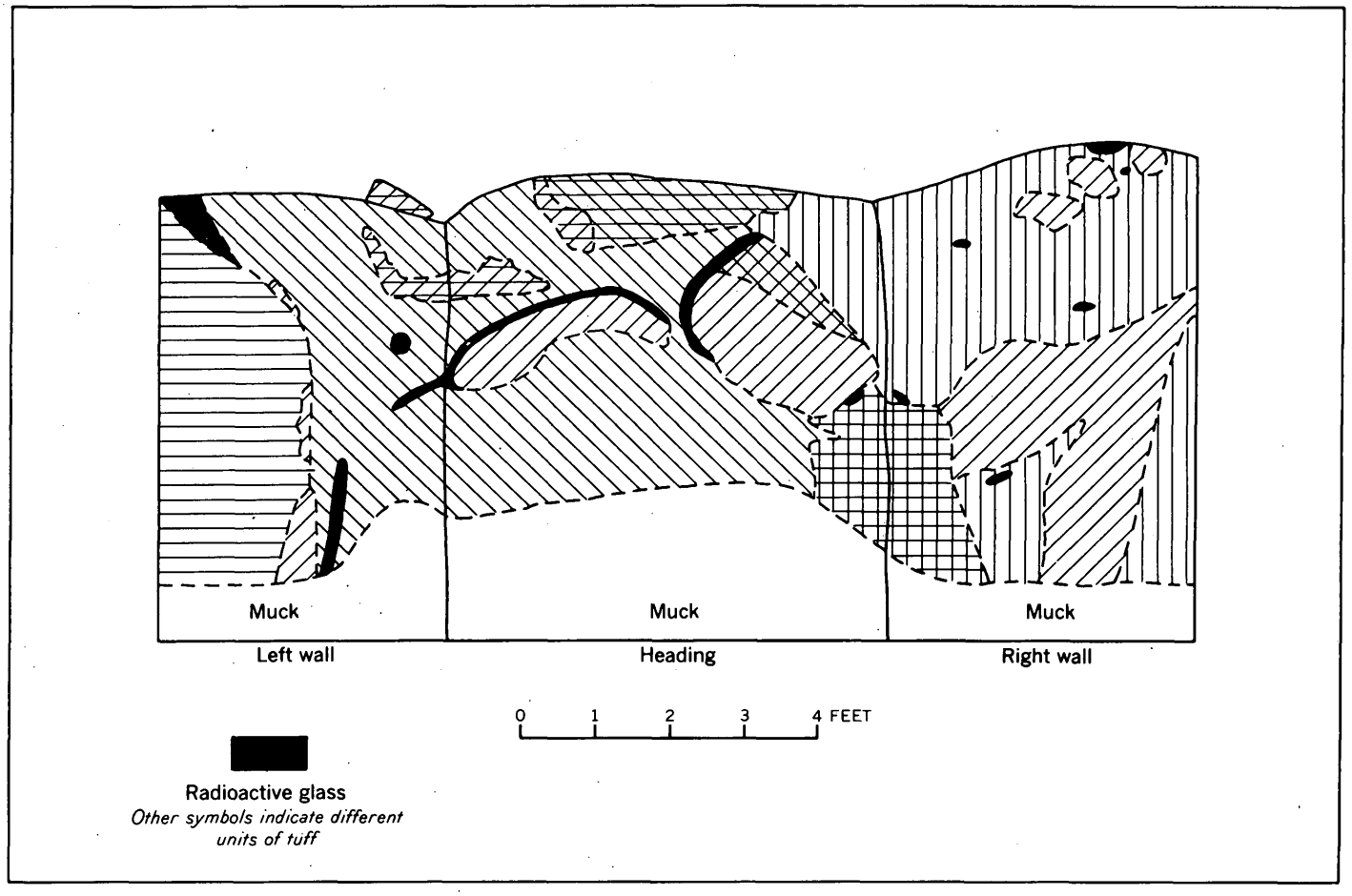

FIGURE 68.3.—Sketch map of part of the exploratory tunnel showing distribution of radioactive glass.

compact glass is the most radioactive and the gray frothy glass the least radioactive.

The distribution of the glass within the breccia zone is far from uniform. Figure 68.3 shows how irregularly it is distributed in the walls of the exploratory tunnel at a distance of about 70 feet from the explosion point. Here the glass forms a thin rind on the surfaces of some of the larger blocks, but most of it forms irregular masses as much as 3 inches across in the finer grained material, and in some places the glass is concentrated along fractures and shear planes in the breccia.

DISTRIBUTION OF TEMPERATURE

Temperature measurements were made with bead thermistors in four drill holes that are approximately in a vertical plane passing through the explosion point (fig. 68.4). The measurements were made one year after the explosion (Roth and Diment, 1959). However, the temperature distribution was probably not greatly different one year after the explosion than it was a few weeks after the explosion. The rocks surrounding the explosion probably cooled rapidly to the boiling point of water because of transport of heat by steam through natural and explosion-produced fractures, but lost little heat thereafter.

The distribution of the anomalous temperatures is roughly similar to that of the radioactivity, as would be expected from the concept of a collapsing shell. The asymmetry of the temperature distribution below the explosion point may have been due to an open pre-explosion fault which was intersected in the original tunnel about 50 feet from the explosion point. Because of many other natural fractures as well as those produced by the explosion, it is likely that the actual temperature distribution is much more irregular than that shown in figure 68.4.

The outer limit of the increase of temperature due to the explosion is not known. Temperature anomalies less than 2° C could not be determined because of thermal disturbance caused by drilling and because of the limited time permitted for temperature measurements. It is likely that in some places where the rock is fractured, anomalous temperatures extend several times as far from the explosion point as those shown.

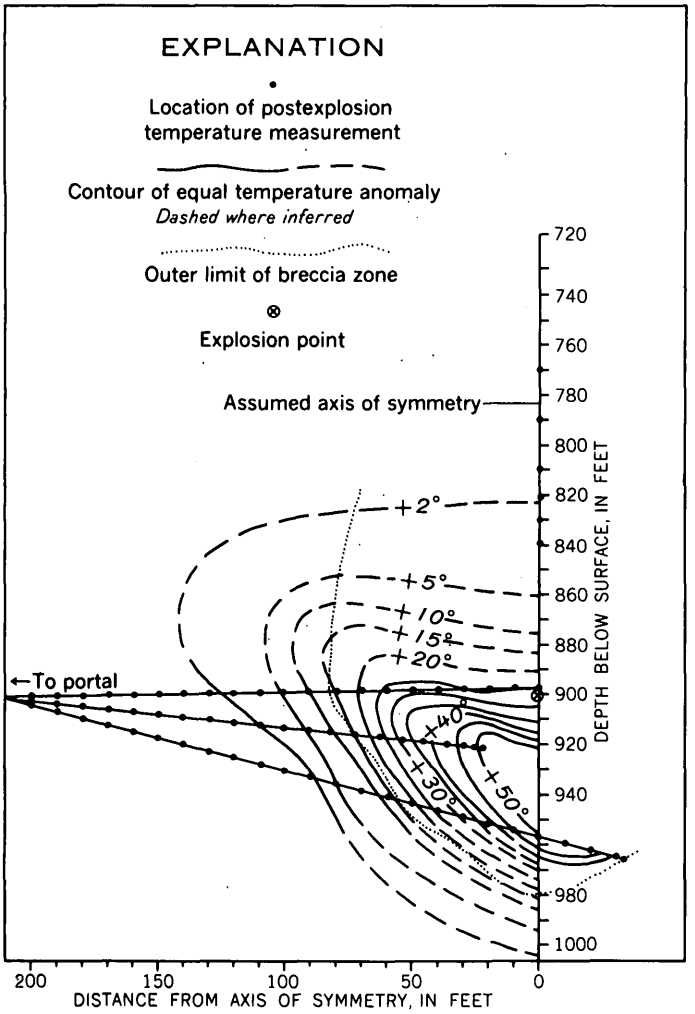

FIGURE 68.4.—Anomalous temperature distribution in vertical plane through Rainier explosion point. Anomalous temperatures are in °C and are the differences between the temperature observed before and after the explosion. Postexplosion temperature measurements were made 1 year after explosion. Preexplosion temperature at explosion point was 16.3° C and the gradient was 0.012° C per foot.

The amount of heat remaining in the rocks, as calculated on the assumption that the distribution of anomalous temperature is symmetrical about the vertical line shown in figure 68.4 and that the density and specific heat have uniform values of 1.8 g per cc and 0.29 cal per g deg., was 9×10^{11} calories. The total heat released by the Rainier explosion, according to Johnson and others (1959), was 1.7×10^{12} calories. The amount of heat remaining in the rocks surrounding the Rainier explosion after one year is therefore roughly equivalent to at least half of the total energy released by the explosion. This estimate is a minimum because: (a) Anomalous increases of temperature of less than 2° C were ignored for the reasons above stated. (b) Symmetry about the Ground Zero drill hole was assumed for the heat content computation, but the data suggest more heat in the half space to the right of the assumed axis of symmetry than in the half space containing the drill holes. (c) Water percolating downward from the surface and from drilling operations (over 60,000 gallons were lost in drilling) reduced the temperatures around the explosion point.

REFERENCES

Bunker, C. M., 1959, Distribution of explosion-produced gamma radioactivity, *in* Geologic effects of the Rainier underground explosion: U.S. Geol. Survey, TEI–355, open-file report, p. 6–1 to 6–5.

Johnson, G. W., Higgins, G. H., and Violet, C. E., 1959, Underground nuclear detonations: Jour. Geophys. Research, v. 64, p. 1457–1470.

Johnson, G. W., Pelsor, G. T., Preston, R. G., and Violet, C. E. 1958, The underground nuclear detonation of September 19, 1957—Rainier, Operation Plumbbob: UCRL–5124, 27 p.

Keller, G. V., and Robertson, E. C., 1959, Physical properties of units Tos_1 to Tos_8, *in* Geologic effects of the Rainier underground explosion: U.S. Geol. Survey, TEI–355, open-file report, p. 3–3 to 3–6.

Roth, E. F. and Diment, W. H., 1959, Thermal effects, *in* Geologic effects of the Rainier underground explosion: U.S. Geol. Survey, TEI–355, open-file report, p. 9–1 to 9–3.

Wilcox, R. E. and Wilmarth, V. R., 1959, Textural and chemical changes, *in* Geologic effects of the Rainier underground explosion: U.S. Geol. Survey, TEI–355, open-file report, p. 7–1 to 7–7.

Wilmarth, V. R., 1959, Structural changes, *in* Geologic effects of the Rainier underground explosion: U.S. Geol. Survey, TEI–355, open-file report, p. 4–1 to 4–12.

69. GRAVITY AND SEISMIC EXPLORATION AT THE NEVADA TEST SITE

By W. H. DIMENT, D. L. HEALEY, and J. C. ROLLER, Denver, Colo.

Work done in cooperation with the U.S. Atomic Energy Commission

Gravity and seismic refraction methods have been used in mapping the pre-Tertiary bedrock surface in parts of the Nevada Test Site (Diment, Healey, and Roller, 1959). The use of these methods is not unusual, but since little has been published about their use in such geologic environments as that of the Nevada Test Site (Mabey, 1956), an account of what was done with them there may be of interest as a case history.

F. E. Currey made most of the gravity observations. D. G. Murrey did the drilling and assisted in other field operations. J. D. Hendricks, C. H. Miller, E. D. Seals, and F. N. Valentine assisted in the field operations and in the reduction of data.

GENERAL GEOLOGY

The Nevada Test Site includes Yucca and Frenchman Valleys, together with surrounding ranges of Tertiary and younger volcanic rocks and of Paleozoic sedimentary and igneous rocks (fig. 69.1). The surface lies 3,100 to 7,700 feet above sea level, and its high relief and a scarcity of roads made field operations difficult.

The oldest rocks exposed in the area are Paleozoic sedimentary rocks of Early Cambrian to probable early Permian age. Their aggregate thickness is about 22,000 feet, of which more than 16,000 feet is limestone or dolomite (Johnson and Hibbard, 1957, p. 335). Except near intrusions they show only low-grade metamorphism. Their structure is exceedingly complex. Extrapolation of Paleozoic units under the cover of alluvium and tuff is difficult. The surface of the Paleozoic rocks is known to be irregular, with several thousand feet of relief. Although part of this relief is due to pre-Tertiary and pre-Quaternary erosion, a major part of it is the result of Tertiary and Quaternary faulting.

The volcanic rocks are in places over 2,000 feet thick. They are mostly bedded tuffs, welded tuffs, and felsic flows, but in parts of the section they are intercalated with beds of gravel and thin flows of basalt. Although the volcanic rocks are mainly Tertiary, they are in small part younger. The Tertiary volcanic rocks are extensively faulted.

Alluvial deposits, ranging from coarse bouldery gravels to the fine-grained silts on playas, cover large parts of the area and attain thicknesses of over 1,000 feet. A few fault scarps in the alluvium give evidence of recent tectonic activity.

DENSITY AND VELOCITY CONTRASTS

The density of the rocks and the velocity of seismic waves passing through them exhibit wide ranges; there are great differences in these properties among the three major groups (Paleozoic rocks, volcanic rocks, and alluvium), and also between different rocks within each group. Many measurements of density and velocity have been made, but it is difficult to give meaningful averages, because the complexity of the region makes each locality unique. The problem is illustrated, however, by the estimates of limits and averages given in the following table:

Rock type	Natural state density (g per cc)			Natural state velocity [1] (fps)		
	Lower limit	Average	Upper limit	Lower limit	Average	Upper limit
Alluvium	[2] 1.7	[2] 1.9	[2] 2.2	[3] 3,000	[3] 6,000	[3] 8,000 (?)
Tuff [4]	1.7	1.9+	[5] 2.3	6,000	8,000	13,000+
Pre-Tertiary	2.5 (?)	2.7	[6] 2.9	12,000	15,000	[6] 20,000

[1] Lower velocities within 100 feet of the surface have been excluded.
[2] Data from A. M. Piper (written communication, 1952) plus consideration of gravity anomalies over structures delineated by seismic methods and drilling.
[3] Data from Yucca Valley. Velocity increases with depth.
[4] From extensive measurements in a 2,000-foot section of tuff in the Rainier Mesa (Keller and Robertson, 1959).
[5] Welded tuff.
[6] Dolomite.

The average density of the tuff and the alluvium is about the same, therefore these rocks have been combined in the gravity analysis. Averages must be used with caution, especially for the volcanic rocks, which in some sections consist mainly of bedded tuff having an average density near 1.8 g per cc, whereas in other sections they consist mainly of welded tuff and flows having an average density near 2.2 g per cc.

The average velocities in the three major groups of rocks are significantly different, and it is sometimes possible to distinguish the groups with confidence on

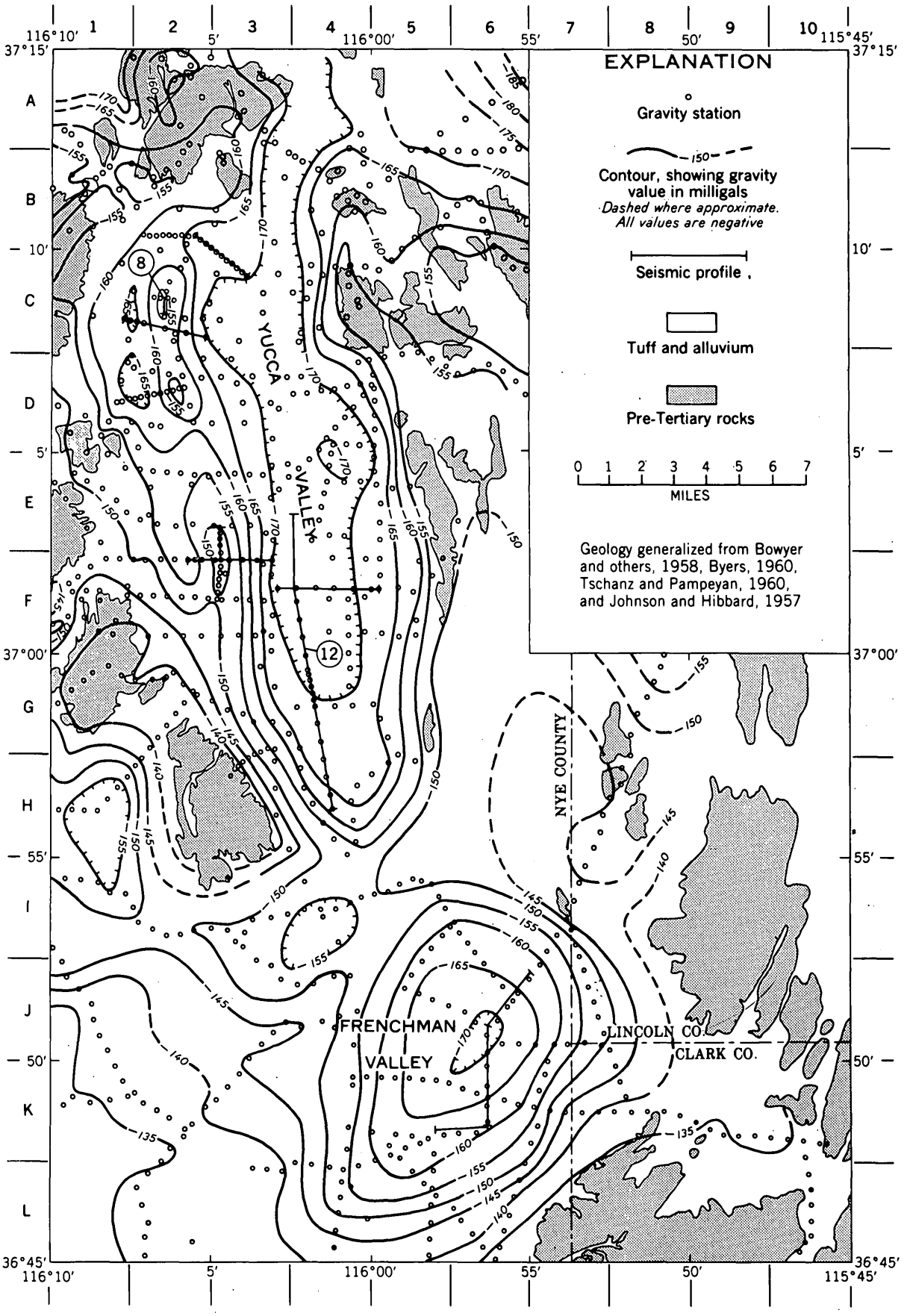

FIGURE 69.1.—Generalized Bouguer anomaly contour map of Yucca and Frenchman Valleys, Nevada Test Site.

the basis of time-distance graphs. Usually, however, it is difficult to do this, because the range of velocity in tuff overlaps that in each of the other two groups, and because the buried surfaces of the Paleozoic and volcanic rocks are very irregular.

METHODS

Standard gravity field methods and reduction techniques were used. Corrections for terrain were applied to a radial distance of 9 miles. Observed gravity was based on a value of 979,614.7 milligals at McCarran Field, Las Vegas, Nev. (Woollard, 1958).

Observed gravity values were reduced to sea level by using an elevation factor of 0.06 mgals per foot, which corresponds to a density of 2.67 g per cc. This means, as a first approximation, that variations in the Bouguer anomaly values are proportional to the thickness of the low-density tuff and alluvium overlying bedrock. Therefore, in areas that have strong topographic relief and are underlain by thick tuff deposits, the Bouguer anomaly contours show a marked correlation with topography. To remove this effect, and thus obtain a clearer picture of the configuration of the pre-Tertiary surface, the gravity values were reduced to a smoothly

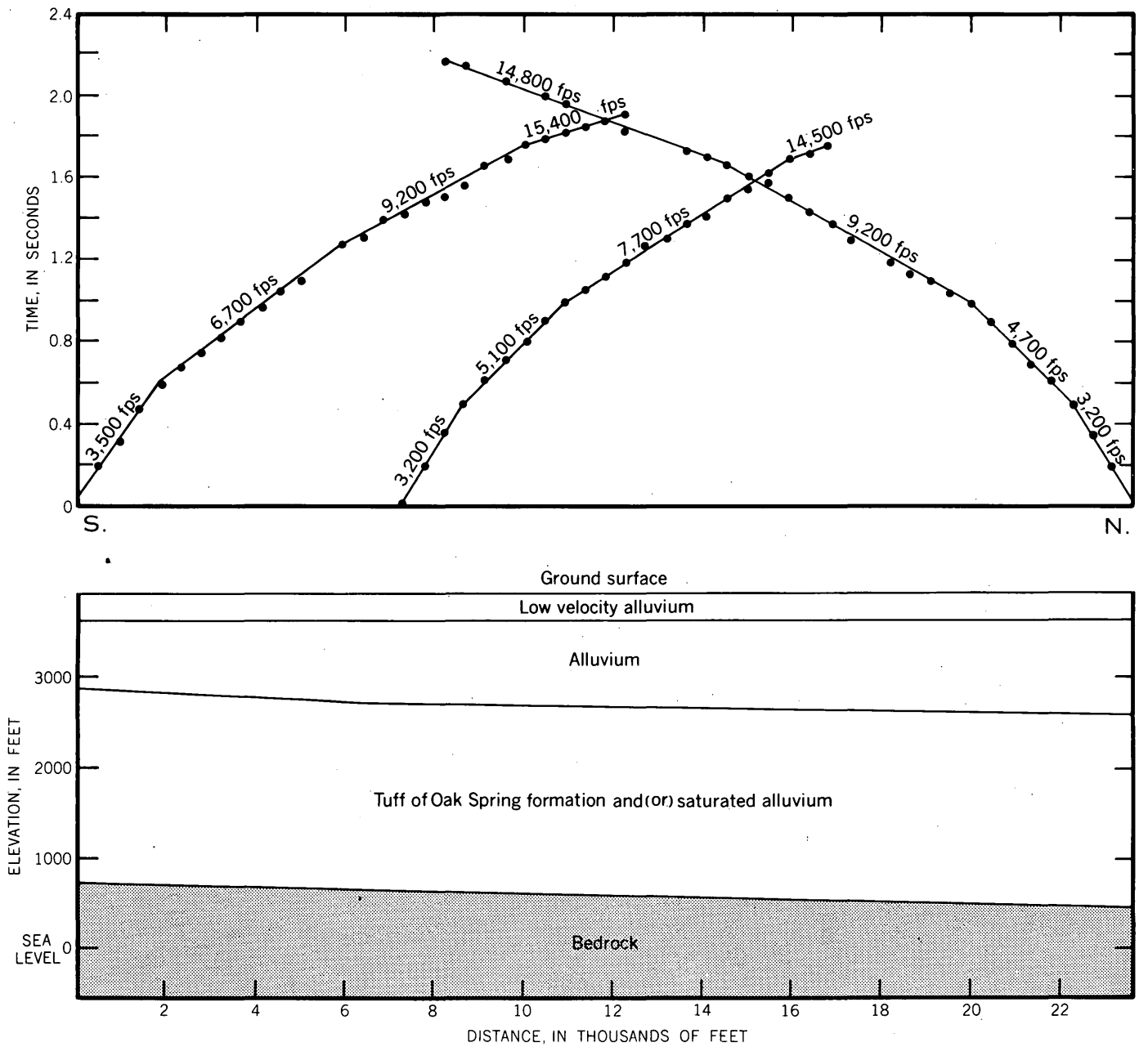

FIGURE 69.2.—Time-distance graphs and inferred geologic cross section along profile 12, Yucca Valley, Nevada Test Site.

varying datum using an elevation factor corresponding to the density of tuff. Between the variable datum and sea level a density of 2.67 g per cc was used for the reduction. This gives a map on which variations in Bouguer anomalies are proportional (as a first approximation) to the thickness of the low-density materials below the variable datum. It is necessary to recognize that the approximate proportionality between the Bouguer anomalies and the thickness of the low-density rocks holds good only when the low-density rocks have the form of a horizontal slab of infinite extent. Where the lower surface of these rocks has a steep dip, the approximation may be considerably in error.

The variable datum is at the topographic surface in areas where the pre-Tertiary rocks crop out, and it is at that surface, or very close to it, on the smooth bottoms of Yucca and Frenchman Valleys. In tuff-covered areas of high topographic relief the variable datum passes through or near the level of the principal stream channels, areas on the order of 10 square miles being considered. In most of the area covered by the map (fig. 69.1) the variable datum is nearly at the surface; the correction can be ignored in all but detailed consideration of the anomalies.

RESULTS

In figure 69.1 a generalized Bouguer anomaly map of part of the Nevada Test Site is superimposed on a generalized geologic map showing the outcrops of Paleozoic rocks. Faults are not shown.

By observing the variation of gravity among areas where the Paleozoic bedrock crops out, it can be seen that there is a regional gravity gradient of about one milligal per mile to the northeast. It is necessary to remove this gradient before depths to the bedrock can be computed, and hence it is desirable to have an adequate number of well-distributed stations on bedrock.

The marked gravity lows over Yucca and Frenchman Valleys indicate thick deposits of alluvium and tuff; the maximum thicknesses computed from a combined analysis of the gravity and seismic data are about 3,500 and 2,500+ feet, respectively, for the two areas. The gravity map of Yucca Valley shows that the deepest part of the valley is narrow, and this suggests that there are large faults along the sides of the valley.

The gravity contours are irregular, and they doubtless would be still more irregular if more stations were added. The close reflection of the irregularity of the pre-Tertiary surface by the gravity contours illustrates the usefulness of gravity methods in mapping such a surface. For example, the series of gravity highs in grids C2, D2, E3, and F3, which represent a pre-Tertiary ridge or series of knobs, were not suspected before the gravity survey. Seismic surveys and drilling have shown that the tops of two of the three buried knobs having gravity closures over them are less than 200 feet below the surface.

Two time-distance graphs illustrate the kinds of information that can be obtained from seismic refraction. The long profile (fig. 69.2) was designed to determine the depth to pre-Tertiary bedrock near the area where it lies deepest under Yucca Valley. The scatter of the data probably results mainly from the irregularity of the refracting surfaces, but partly from horizontal variations in velocity. This approach gives a generalized indication of subsurface conditions; much more detailed information would be required to improve the interpretation significantly.

The short profile (fig. 69.3) is typical of the refraction profiles over shallow bedrock. It passes near the

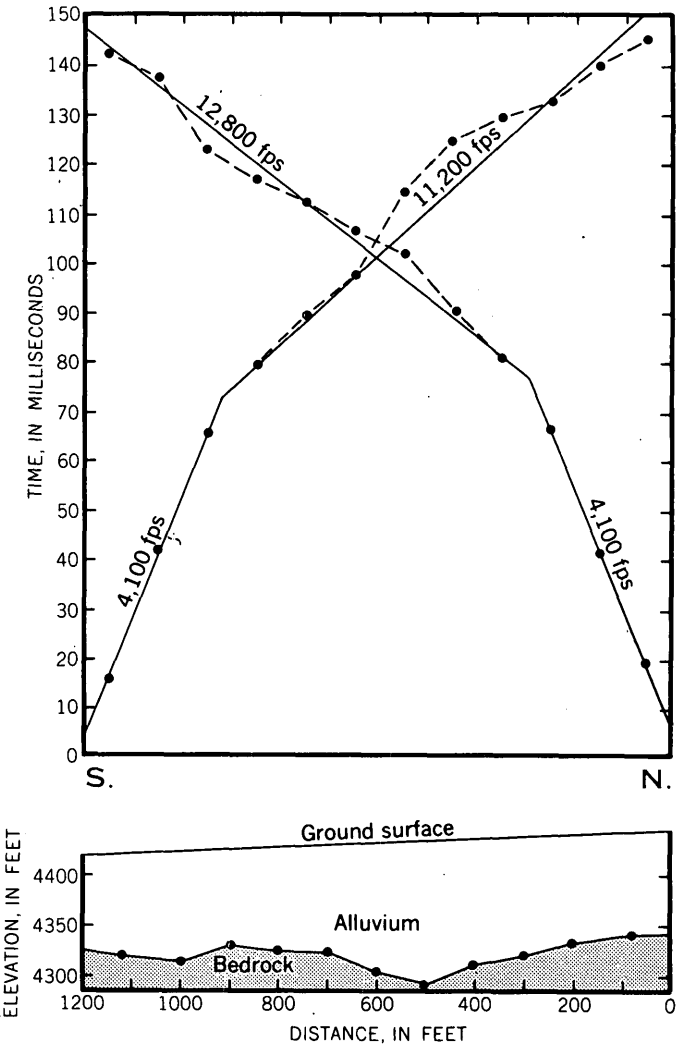

FIGURE 69.3.—Time-distance graphs and inferred geologic cross section along profile 8.

top of a bedrock knob (grid C2). The geologic cross-section has been constructed from the time-distance data according to a delay-time method described by Pakiser and Black (1957). As would be expected from inspection of bedrock outcrops, the buried bedrock surface is irregular. At the north end of profile 8, where the depth to bedrock computed from the refraction data was 105 feet, a drill hole penetrated a layer of cemented gravel at 97 feet and dolomite at 132 feet.

REFERENCES

Bowyer, Ben, Pampeyan, E. H., and Longwell, C. R., 1958, Geologic map of Clark County, Nevada: U.S. Geol. Survey Mineral Inv. Field Studies Map MF–138.

Diment, W. H., Healey, D. L., and Roller, J. C., 1959, Gravity and seismic exploration in Yucca Valley, Nevada Test Site—January–April, 1959: U.S. Geol. Survey, TEI–545, open-file report, 41 p.

Johnson, M. S., and Hibbard, C. E., 1957, Geology of the Atomic Energy Commission Nevada Proving Ground Area, Nevada: U.S. Geol. Survey Bull. 1021–K, p. 333–384.

Keller, G. C., and Robertson, E. C., 1959, Physical properties of units Tos_1 to Tos_8, *in* Geological effects of the Rainier underground nuclear explosion: U.S. Geol. Survey, TEI–355, open-file report, p. 3–3 to 3–6.

Mabey, D. R., 1956, Geophysical studies in the intermontane basins in southern California: Geophysics, v. 21, p. 839–853.

Pakiser, L. C., and Black, R. A., 1957, Exploring for ancient channels with the refraction seismograph: Geophysics, v. 22, p. 32–47.

Woollard, G. P., 1958, Results for a gravity control network at airports in the United States: Geophysics, v. 23, p. 520–535.

70. MAXIMUM GROUND ACCELERATIONS CAUSED BY NUCLEAR EXPLOSIONS AT DISTANCES OF 5 TO 300 KILOMETERS

By W. H. Diment, S. W. Stewart, and J. C. Roller, Denver, Colo.

Work done in cooperation with the U.S. Atomic Energy Commission

Seismic recordings were made of most of the nuclear explosions in the Plumbbob (1957) and Hardtack-Phase II (1958) series of nuclear tests (Stewart and others, 1959). The vertical, inline, and transverse components of motion were measured with instruments calibrated for velocity of ground motion in the frequency range 1 to 20 cycles per second.

For underground nuclear explosions in tuff, the following empirical scaling relation was developed between the maximum single component of acceleration (A, in units of gravity), yield (w, in kilotons), and distance (D, in kilometers):

$$A = 0.6W^{0.8}/D^2$$

Most of the data on which this relation is based were obtained in the distance range 20 to 70 kilometers, and they are supported by the remaining data, obtained in the range 5 to 300 kilometers. The standard deviation for the distance exponent and the standard deviation for the yield exponent (excluding pairs of explosions that have yield ratios less than ten) are both ± 0.2. The constant of proportionality varies between 0.13 and 1.9. These variations are due in part to differences in geologic conditions near the recording point. Maximum accelerations recorded on alluvium are several times as high as those recorded on tuff or bedrock. The better contained explosions appear to give higher acceleration than those that are less well contained.

The empirical form of the scaling relation must be stressed. Various arguments (Latter and others, 1959; Carder and others, 1960) imply that the frequency spectrum will become richer in low-frequency components as the size of the explosion increases. It would seem undesirable, therefore, to extrapolate from this formula to yields more than about ten times as large as that of the largest shot recorded, which was Blanca, with a yield of 19 kilotons. (See Johnson and others, 1959, for yields and placement of other underground explosions.)

The devices were exploded near the edge of a mesa composed mainly of bedded tuff and capped with welded tuff. The local topographic relief is several thousand feet. The points of explosion were within 600 to 1200 feet above crystalline dolomite. The results presented here have restricted application because of the unusual character of the bedded tuffs. This rock had the following properties before the explosions (Keller and Robertson, 1959; Johnson and others, 1959): The pore space in the rock was nearly filled with water; the wet bulk density was about 2.0 g per cc; the

porosity was about 30 percent; the velocity of the compressional wave was 8,000–10,000 ft per sec; and the compressional strength with uniaxial loading under a hydrostatic pressure of 1,000 psi was roughly 5×10^3 psi.

No scaling relation, similar to that for underground explosions, has been established for maximum accelerations from explosions in air. However, the exponent of the yield for explosions in air at identical heights above the ground is at least 0.6, when heights of 500, 750 and 1500 feet are considered. Explosions in air at heights of 500 to 750 feet above the alluvium of Yucca Valley cause maximum accelerations whose ratio to those caused by underground explosions of equal yield in tuff ranges from about 0.2 to 0.02, and averages about 0.1.

The frequency of the waves of maximum acceleration for underground explosions ranged from about 2 to 12 cycles per second. A poorly defined decrease in this frequency was noted in the range from 5 to a little less than 100 km from the explosions. Frequencies also depended on the material on which the seismometers were placed, higher frequencies being obtained with seismometers on bedrock and lower frequencies with seismometers on deep alluvium.

Maximum accelerations occurred in both body and surface waves, but more commonly they occurred only in the latter. Quantitative generalization concerning maximum accelerations is impossible, because the effects of local geologic conditions and the succession of mountain ranges and alluvium-filled valleys along the line of observations are unknown.

Observations within 60 km indicate that explosions in air above a nearly flat surface of alluvium more than 1,000 feet thick are better generators of surface waves than explosions in the tuff.

Seismograms from explosions in air at the same place are almost identical wave for wave, except for amplitude, which is dependent on yield. Seismograms from air explosions at the same horizontal position but at heights of 500, 750 and 1,500 feet exhibit strong similarities in detail. Seismograms from underground explosions separated by hundreds to a few thousand feet are different in detail, although their general character may be the same. Explosions in air where the horizontal positions differ by several thousand feet also exhibit differences in detail (see also Carder and Bailey, 1958).

REFERENCES

Carder, D. S., and Bailey, L. F., 1958, Seismic wave travel times from nuclear explosions: Seismol. Soc. America Bull., v. 48, p. 377–398.

Carder, D. S., Murphy, L. M., Cloud, W. K., and Pearce, T. H., 1960, Operation pre-Gnome, Seismic data from natural phenomena and high-explosive tests near Carlsbad, New Mexico; U.S. Coast and Geodetic Survey, 44 p.

Johnson, G. W., Higgins, G. H., and Violet, C. E., 1959, Underground nuclear detonations: Jour. Geophys. Research, v. 64, p. 1457–1470.

Keller, G. V., and Robertson, E. C., 1959, Physical properties of units Tos_1 to Tos_8, *in* Geologic effects of the Rainier underground explosion: U.S. Geol. Survey, TEI–355, open-file report, p. 3–3 to 3–6.

Latter, A. L., Martinelli, E. A., and Teller, E., 1959, Seismic scaling law for underground explosions: Phys. of Fluids, v. 2, p. 280–282.

Stewart, S. W., Roller, J. C., and Diment, W. H., 1959, Maximum accelerations caused by underground nuclear explosions in the Oak Spring formation in area 12 of the Nevada Test Site at distances of 5 to 300 kilometers, a preliminary summary: U.S. Geol. Survey, TEI–351, open-file report, 45 p.

71. CATION EXCHANGE WITH VERMICULITE

By Marian M. Schnepfe, Washington, D.C.

Work done in cooperation with the U.S. Atomic Energy Commission

Ion exchange of waste fission products by various minerals possessing high cation exchange capacities is one of the more favorably considered processes for use in disposing of radioactive wastes. One of the most hazardous fission products found in the wastes is cesium-137. Inasmuch as vermiculite has long been known to have a high cation exchange capacity (Grim, 1953) and is strongly selective in the sorption of the alkalis including cesium (Barshad, 1948) the rate of ion exchange with vermiculite was investigated as part of a more detailed study of the ion exchange properties of this mineral (Schnepfe, 1960). Experiments were

TABLE 71.1.—*Chemical analyses of vermiculite (percent)*

[Analysts, P. L. D. Elmore, I. H. Barlow, S. D. Botts, and G. W. Chloe. See table 71.2 for source of samples.]

	1	2	3	4	5	6	7	8	Average of 8 analyses	Range
SiO_2	36. 4	32. 8	29. 3	41. 3	43. 3	36. 7	38. 4	38. 4	37. 1	29. 3 –43. 3
Al_2O_3	12. 2	17. 7	10. 0	11. 0	12. 9	12. 2	9. 8	9. 4	11. 9	9. 4 –17. 7
Fe_2O_3	7. 3	14. 7	4. 5	5. 8	6. 5	8. 0	2. 6	4. 6	6. 8	2. 6 –14. 7
FeO	. 50	1. 9	. 22	. 72	1. 3	. 76	. 29	. 50	. 77	. 22– 1. 9
MgO	19. 7	10. 6	19. 0	20. 1	17. 9	20. 0	27. 2	26. 2	20. 1	10. 6 –27. 2
CaO	2. 1	1. 4	4. 2	1. 2	1. 3	1. 6	. 00	. 61	1. 6	. 00– 2. 1
Na_2O	. 14	. 10	. 18	. 18	. 27	. 14	. 04	. 06	. 14	. 04– . 27
K_2O	2. 0	2. 4	. 10	3. 4	5. 1	2. 5	. 04	4. 2	2. 5	. 04– 5. 1
H_2O	17. 4	15. 8	17. 7	11. 9	9. 3	16. 4	20. 9	12. 7	15. 3	9. 3 –20. 9
TiO_2	1. 0	2. 2	1. 3	1. 6	1. 7	1. 0	. 28	. 72	1. 2	. 28– 2. 2
P_2O_5	. 05	. 11	. 12	. 68	. 33	. 05	. 03	. 02	. 17	. 02– . 68
MnO	. 10	. 19	. 10	. 08	. 13	. 10	. 02	. 02	. 09	. 02– . 19
CO_2	. 2	. 1	2. 3	<. 1	. 11	. 1	. 1	. 9	. 48	<. 1 – 2. 3
$BaSO_4$			10. 0							

made with eight vermiculite samples, seven of which were supplied through the courtesy of the U.S. National Museum.

Vermiculite is seldom found in the pure state. The wide range in chemical composition of the vermiculites used in these studies is shown in table 71.1. The mineral content of these samples, as determined by X-ray analysis, is given in table 71.2.

The capacity of these samples for cesium was evaluated using sodium chloride saturating solution. Preliminary experiments indicated that the different vermiculite samples were saturated with sodium ions in varying degrees and at widely differing rates. Whereas one sample showed no increase in exchange capacity with treatment beyond one day, another sample required three weeks to become completely saturated under the prevailing conditions. It was desirable, therefore, to make a more systematic study of the time factor for saturating vermiculites.

Saturation of six 0.5-gram portions of each of eight vermiculites was started simultaneously. The rate of saturation was followed by determining the exchange capacity of one set of samples after 24 hours of treatment and then at weekly intervals withdrawing a set from the saturation procedure and determining the capacities. Table 71.3 gives the ion exchange capacities after specified saturation time. The data show the saturation time of a vermiculite may vary from 1 day to 3 weeks. Therefore, assessment of any vermiculite in regard to its use as an ion-exchanger must not be made before adequate time is allowed for complete saturation. That the ion-exchange rate may vary is an important consideration for those who propose to use vermiculite as a scavenger for cesium from radioactive wastes.

TABLE 71.2.—*Mineral composition of vermiculite samples as determined by X-ray analyses*

Sample	U.S. National Museum No.	Location	Minerals found by X-ray examination (identification by Daphne Ross)
1	92, 626	Libby, Mont	Vermiculite, vermiculite-montmorillonite mixed layer, mica-vermiculite mixed-layer, and calcite.
2	98, 359	Spruce Pine, N.C.	Vermiculite and mica-vermiculite mixed-layer.
3	107, 474	Hillside, Colo	Vermiculite and mica-vermiculite mixed-layer.
4	108, 799	Langford Station, S.C.	Mica-vermiculite mixed-layer and traces of quartz.
5		Travellers Rest, S.C.	Vermiculite, a montmorillonite mineral, mica-vermiculite mixed-layer, biotite, quartz, and possible amphibole.
6	97, 385	Libby, Mont	Mica-vermiculite mixed-layer, vermiculite and mica.
7	101, 933	Franklin, N.C	Possibly chlorite or dioctahedral vermiculite and mica-vermiculite mixed-layer.
8	106, 779	South Africa	Mica-vermiculite mixed-layer or chlorite-mica mixed-layer with a trace of chlorite.

PROCEDURE

The 100-mesh vermiculite sample (0.5000 to 1.0000 gram) is placed in a 15-ml glass-stoppered centrifuge tube and 15 ml of 5 *N* NaCl saturating solution are

TABLE 71.3.—*Cation exchange values, meq/100 grams*

Saturation time	Vermiculite sample number							
	1	2	3	4	5	6	7	8
1 day	143	102	139	100	69	137	159	110
1 week	159	121	143	139	93	159	160	147
2 weeks	163	123	143	147	107	159	163	167
3 weeks	165	125	143	150	119	161	163	171
4 weeks	163	128	143	150	121	161	163	172
5 weeks	163	127	143	150	120	163	161	173

added. The sample is agitated periodically and after 3 or 4 hours at 70° to 80° C is centrifuged and the supernatant liquid is discarded. Fresh portions of the saturating solution are added until saturation is complete. The sample is then washed with absolute methanol until a negative chloride test is obtained with acidified silver nitrate solution. The sodium saturated sample is then leached with a 15-ml portion of 2 *N* $NH_4C_2H_3O_2$ (pH7); during the leaching procedure the sample is agitated gently at intervals of time. After approximately 2 hours the sample is centrifuged and the supernatant liquid is filtered into a volumetric flask. Additional 15-ml portions of the leaching solution are used until leaching is complete. The sodium concentration of the combined leachings is determined by flame photometry.

REFERENCES

Barshad, Isaac, 1948, Vermiculite and its relation to biotite as revealed by base exchange reactions, differential thermal curves, and water content: Am. Mineralogist, v. 33, p. 655–678.

Grim, R. E., 1953, Clay mineralogy: New York, McGraw Hill Book Company, 384 p.

Schnepfe, M. M., 1960, A study of cation exchange with vermiculite: U.S. Geol. Survey open-file report, 40 p.

72. PREPARATION OF STABLE GELATIN-MONTMORILLONITE CLAY EXTRUSIONS

By IRVING MAY, Washington, D.C.

Work done in cooperation with the U.S. Atomic Energy Commission

THE PROBLEM

The relatively high cost and scarcity of nuclear reactor fuels require that fissionable elements be recovered by reprocessing. The waste solutions that result from this reprocessing are so highly radioactive that they cannot safely be discharged into the ground, rivers, or the sea. Because of this fact they are now retained in large storage tanks.

Fixation of the radioactive waste elements in stable solids would make their long-term storage safer and possibly cheaper. One fixation method that has been investigated by Hatch and his associates at the Brookhaven National Laboratory involves the exchange of radioactive waste elements on montmorillonite, followed by calcination to fix the exchange radioelements on the clay (Hatch and others, 1954). In this process the exchange column contains clay aggregates prepared from 100 parts of montmorillonite clay (Filtrol Corp. No. 101, dried at 110° C), 72 parts water, and 0.5 part of the soil conditioner Krilium. The resultant "crumbs" are extruded through a 0.03-inch orifice into a water-filled column; the extruded clay filament breaks into short lengths during the filling process.

It is very desirable to have the clay maintain a well-defined rod structure, because extensive swelling or disintegration of the rods reduces pore space and causes excessive resistance to the flow of solution through the column. A study was therefore made of the possibilities of producing clay extrusions that would be more resistant than the preparation then in use to mushing up during a run because of excessive swelling, and that could be dried and subsequently be resoaked without disaggregating.

EXPERIMENTS WITH CLAY MIXTURE

Various drying techniques were investigated first. No matter how the extruded clay rods were dried—air, oven, slow drying, displacement with acetone—the dried clay always promptly broke up when placed in water.

I then tried varying the composition of the clay extrusions. Preparations made with glycerol substituting for part of the water proved unsatisfactory. The addition of a polyethylene glycol compound was also found to be of no value. Gum arabic was then tried, and gave a product that only partially disaggregated

on soaking with water. This result prompted me to try gelatin.

Preparations containing 1 part of gelatin to 10 parts of clay give very stable rods. The extruded rods, after air-drying, can then be soaked in water for months without visible effect. Even after an hour's boiling with water, infrared tests by I. A. Breger and chemical tests indicated that little if any gelatin had washed out.

Since first preparing these clay-gelatin mixtures, I found that Ensminger and Gieseking (1941) had studied the effect of adsorbed proteins, including gelatin, on the base-exchange capacity of clays. From their work, one would expect no more than a 15-percent reduction in the base-exchange capacity of the gelatin-clay mixture in acid solutions, and none in alkaline solutions.

Samples of the dried gelatin-clay extrusions were sent to Brookhaven for evaluation. In tests with a solution used by them for comparing the performance of various clays in columns, this preparation withstood the passage of four to six times as much solution as the best of their clay preparations. There was no significant change in the base-exchange capacity of the preparation, whose capacity for cesium was determined by them to be 119 milli-equivalents per 100 grams.

PREPARATION OF GELATIN-CLAY EXTRUSIONS

Five grams of gelatin (Eastman Kodak No. 1099 calfskin gelatin) are dissolved in 50 grams of hot water. After cooling to room temperature, evaporated water (checked by weighing) was replenished. Fifty grams of clay (dried at 110° C), mixed with 0.25 gram of Krilium, was added to the gelatin solution while stirring. The sample was then extruded by means of a large screw-driven steel syringe. The coils of extruded clay were dried and then broken into short lengths.

REFERENCES

Ensminger, L. E., and Gieseking, 1941, The absorption of proteins by montmorillonitic clays and its effect on base-exchange capacity: Soil Sci., v. 51, p. 125–132.

Hatch, L. P., Martin J. J., and Ginell, W. S., 1954, Ultimate disposal of radioactive wastes: Brookhaven National Laboratory, BNL–1781, 31 p.

73. VARIATION OF ALUMINUM, SODIUM, AND MANGANESE IN COMMON ROCKS

By James R. Burns, Washington, D.C.

Work done in cooperation with Office, Chief of Engineers, and the Soil Conservation Service

Among the elements in soils and rocks that are most suceptible to neutron-induced radioactivity caused by the use of nuclear weapons or nuclear devices are aluminum, sodium, and manganese. This makes it desirable to estimate the degree to which these elements vary in abundance from place to place in different rocks, and to devise means for predicting their abundance in a given rock at a given place when direct sampling is impracticable.

As a first step, a statistical study was made of 450 rock analyses compiled from published literature and Geological Survey files. Analyses were selected to represent only rocks of wide occurrence, and rocks associated with ore deposits were avoided. Suitable and complete analyses, particularly with regard to manganese, are scarce for the common sedimentary rocks. This limited the total number of analyses regarded as suitable, because it was considered necessary to have the number of analyses representing each rock type roughly proportional to the abundance of that type on the earth's surface.

The rocks represented by the analyses used were separated into nine chemically distinct categories, found to differ significantly in their content of all three elements. Each category consists of several closely related rock types, and the number of analyses for each type is roughly proportional to the world-wide abundance of that type. Category I consists chiefly of granites, granodiorites, diorites, rhyolites, and andesites in almost equal proportions. Category II consists mainly of gabbros, diabases, and basalts; miscellaneous ultramafics make up less than 15 percent of this category. The seven other categories are explained in table 73.1. Average content of aluminum, sodium, and manganese was computed for each category, and

TABLE 73.1.—*Summary of observed variations of aluminum, sodium, and manganese in common rocks*

Rock category	Constituents (percent by weight)											
	Aluminum				Sodium				Manganese			
	Average	Median	Range [1]	Remarks [2]	Average	Median	Range [1]	Remarks [2]	Average	Median	Range [1]	Remarks [2]
I. Silicic and intermediate igneous rocks	8.17	7.4	6.8–9.5	A	2.80	2.6	1.8–4.0	A	0.12	0.10	0.04–0.26	B
II. Mafic and ultramafic igneous rocks	8.10	8.1	6.0–10.1	A	2.23	2.1	1.2–3.1	A	.18	.15	.08–.32	B
III. Siliceous sediments and metasediments (chiefly sandstones and quartzites)	5.34	5.7	1.05–8.5	C	1.58	1.7	.1–2.8	C	.09	.05	<.01–.24	E
a. Chert, highly pure sandstone and quartzite (SiO_2 > 90 percent)		[3] (1.0)	(.04–2.0)	(C)		(.1)	(.01–.28)	(D)				
b. Normal quartz sandstone and quartzite (SiO_2 75 percent–90 percent)		(4.0)	(2.0–6.0)	(A)		(1.5)	(.3–2.7)	(A)				
c. Clayey and arkosic sandstone and quartzite, arkose, graywacke		(7.5)	(4.0–10.0)	(A)		(2.0)	(1.2–4.0)	(A)				
IV. Argillaceous sediments and metasediments (chiefly shales and slates)	8.05	8.2	4.7–12	A	.92	.6	.13–2.0	D	.25	.09	.01–.38	E
a. Normal shale and slate		(9.0)	(6–14)	(A)								
b. Calcareous shale and slate		(8.5)	(4–14)	(A)								
c. Siliceous shale and slate		(4.0)	(.9–6)	(C)								
V. Calcareous sediments and metasediments (chiefly limestone, dolomite, and marble)	.50	.3	.05–1.3	D	.11	.06	.01–.26	E	.19	.10	.02–.5	E
VI. Gneiss and granulite	8.46	8.3	6.5–9.5	A	2.54	2.3	1.5–4.0	A	.07	.06	.02–.12	B
VII. Schist and phyllite	8.02	8.3	2.2–12.6	A	1.12	.9	.2–2.6	B	.23	.10	<.01–.25	D
VIII. Amphibolite and greenstone	7.75	8.2	4.4–10.0	A	1.30	1.3	.7–1.8	A	.18	.15	.08–.3	B
IX. Serpentinite	.82	.9	.25–1.2	A	.16	.12	.04–.37	B	.06	.06	.02–.14	B

[1] The most common range is established, for this presentation, by eliminating the highest 10 percent and the lowest 10 percent of values observed.

[2] Under "remarks", the variability is summarized as follows:

A. At least 80 percent of the values differ from the median by a factor of 2 or less (that is, fall between ½ median and 2 times median).

B. At least 80 percent of the values differ from the median by a factor of 3 or less.

C. At least 60 percent of the values differ from the median by a factor of 2 or less.

D. At least 60 percent of the actual values differ from the median by a factor of 3 or less.

E. At least 70 percent of the actual values differ from the median by a factor of 5 or less, and at least 50 percent differ by a factor of 3 or less.

[3] Data in parentheses have been estimated for subcategories by visual inspection of the data and by interpretation of lithologic properties from the chemical analyses; other data are based on actual frequency counts or computation.

other statistical data were obtained by frequency counts and construction of cumulative frequency curves.

Within certain categories, the content of sodium and aluminum showed a recognizable relationship to that of silicon or calcium, and on this basis it was possible to divide categories III and IV each into three subcategories, for which medians and ranges were estimated. These subcategories represent numerically about the following portions of categories III and IV: category III: subcategory a, 20 percent; b, 15 percent; and c, 65 percent; category IV: subcategory a, 85 percent; b, 10 percent; and c, 5 percent.

Selected results appear in the accompanying table. Summaries for each of the first seven categories are based on about 40 to 75 analyses. Eleven analyses were used for category VIII, and seven for category IX. Within most categories and subcategories the common range (60 percent to 80 percent of cases observed) is one-half M (median) to 2M for aluminum, ⅓M to 3M for sodium, and ⅕M to 5M for manganese. Medians of different groups generally differ less than the range within a single group.

These results are intended to provide a measure of the broad patterns of chemical variation within major groups of rocks. They cannot be directly compared with the numerous more refined computations of average composition made by other workers, because each rock category of the present study contains several diverse rock types, each weighted according to its abundance.

GEOLOGY OF EASTERN UNITED STATES

74. PRE-SILURIAN STRATIGRAPHY IN THE SHIN POND AND STACYVILLE QUADRANGLES, MAINE

By Robert B. Neuman, Washington, D.C.

Ordovician graptolites were found in slates associated with chert near the mouth of Wassataquoik Stream (A of fig. 74.1) by W. W. Dodge in 1881, and the trace fossil *Oldhamia* was discovered by E. S. C. Smith along the East Branch of the Penobscot River in 1928, leading him to conclude that beds there are Cambrian in age. These early workers, however, did not establish the geologic relations between these occurrences. The present mapping indicates that both are contained in the same anticlinorium, and that they are separated by a great thickness of Ordovician volcanic rocks.

The formation (Cg of fig. 74.1) containing *Oldhamia* was named Grand Falls formation by Ruedemann and Smith (1935, p. 354), but this name was preoccupied by the Grand Falls chert of Winslow (1894, p. 417–419). The *Oldhamia* occurs in maroon siltstone and slate both at Bowlin Falls (B of fig. 74.1) and at the type locality of the formation, which is indicated on the topographic map of the Shin Pond quadrangle as the Grand Pitch of the East Branch of the Penobscot River (C of fig. 74.1). Maroon rocks are a minor but conspicuous component of the formation; its more common constituents are gray to greenish-gray quartzite, and gray, greenish-gray, and dark-gray slate. Steep dips and tight folds characterize exposures of these rocks, and steeply dipping faults of unknown displacement can be identified at several places. Although the boundaries of the formation are fairly well established in the Shin Pond and Stacyville quadrangles, the tectonic pattern and stratigraphic succession within the formation are not yet understood.

Through most of this area the "Grand Falls" formation is overlain by greenstone (Ov of fig. 74.1). Volcanic conglomerate, graywacke, and fossiliferous tuffaceous sandstone (Ovt of fig. 74.1) intervene between them in the southwestern part of the synclinal belt that terminates on Sugarloaf Mountain. These sedimentary rocks are a thousand feet thick along Shin Brook; they may continue for a considerable distance to the northeast, but poor exposures hamper tracing them in that direction. Studies of the fossils from these rocks are not yet complete, but the assemblage of orthoid brachiopods, gastropods, cystid plates, bryozoans, and trilobites suggests an early Middle Ordovician age.

The greenstone and associated rocks have been intensely deformed. Although they have steep dips and strong cleavage, they are much less complex in structure than the sequence of interbedded quartzite and slate of the "Grand Falls" formation which underlies them. Some of this contrast may be due to differences in their tectonic competency in response to the Taconic and Acadian orogenies. Nevertheless, the abrupt lithic change, the structural contrast, and the presence in the volcanic conglomerate of pebbles of quartzite like that of the rocks below, all make it probable that the contact between these units is an angular unconformity, and that the quartzites and slates were folded before the deposition of the volcanic debris.

Greenstones immediately overlie the quartzite and slate units along a contact that follows the East Branch for almost ten miles and then swings northward around the southern flank of the anticlinorium. The chert and slate (Ovc of fig. 74.1), in which the graptolites were found, lie at the southeastern margin of these greenstones, apparently at their top. The present work has failed to uncover additional graptolite localities, although similar cherty rocks lie along the eastern border of the smaller body of volcanic rock that is probably a fault slice.

Ruedemann (Ruedemann and Smith, 1935, p. 353–354) identified the graptolites both in Dodge's collection and in one made by Smith at the same locality, and concluded that they were of Normanskill age. My own more recent collections, which contain conodonts as well as graptolites, do not alter this conclusion. If the volcanic rocks of the Sugarloaf-Roberts Mountain belt are of the same age as those to the southwest, the fossils at the base of the former and the top of the latter limit the time of their formation to the Middle Ordovician.

Intruding both the greenstones and the quartzite and slate is a porphyritic quartz diorite (Oqd of fig. 74.1) which contains fragments of greenstone and in one place forms the matrix of a greenstone breccia. There are two reasons for believing that this diorite is of Ordovician age: (a) the abundance of calcite in minute fractures pervading the diorite indicates that it is more altered than the Acadian intrusives in the region; and (b) cobbles of the diorite occur in conglomerate that overlies the greenstone on the east, and at one place graywacke associated with this conglomerate

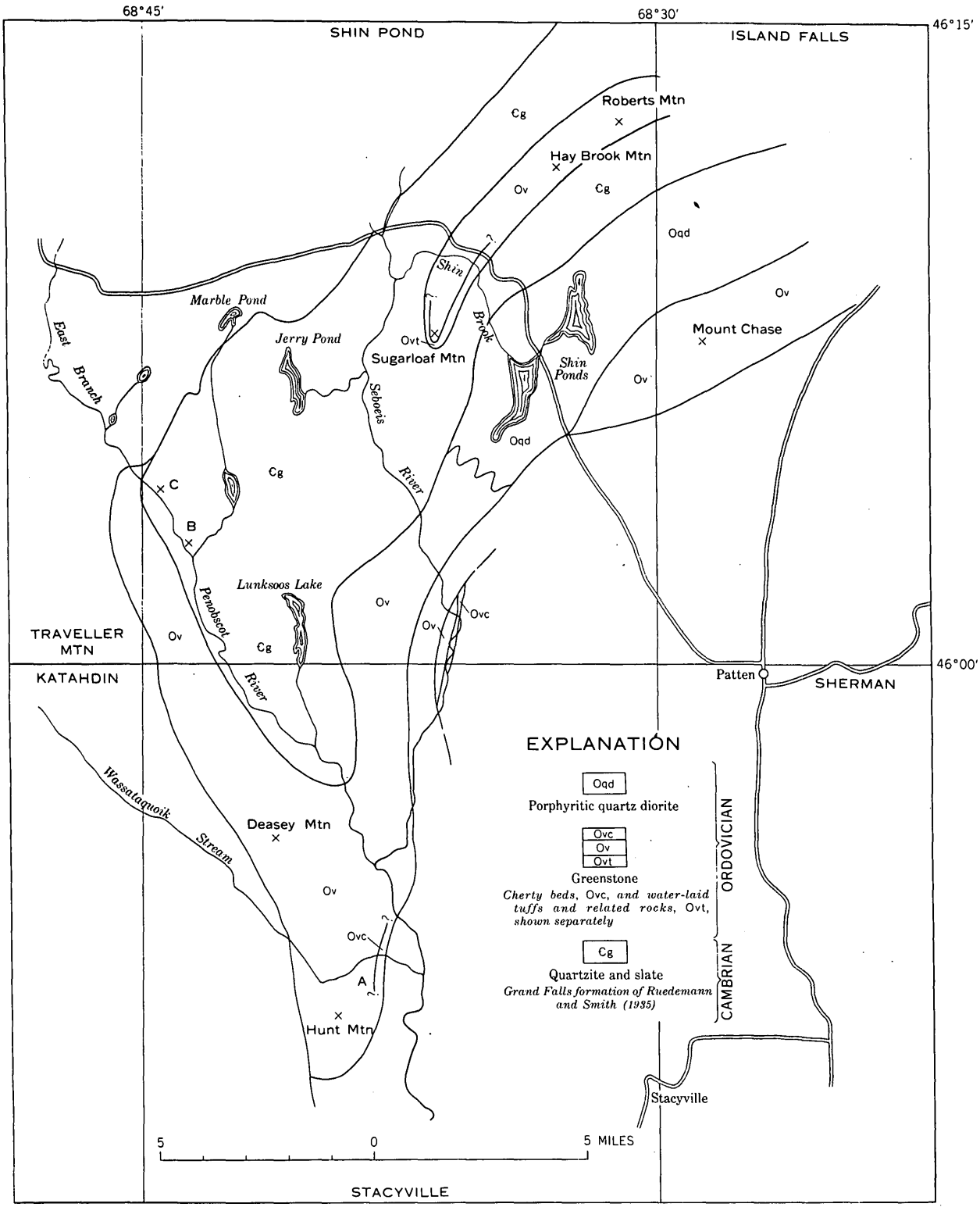

FIGURE 74.1.—Geologic map of the pre-Silurian rocks in the Shin Pond and Stacyville quadrangles, Maine. Localities referred to in text: *A*, Dodge's graptolite locality; *B*, Bowlin Falls, Smith's *Oldhamia* locality; *C*, Grand Pitch of the East Branch of the Penobscot River. Geologic mapping by R. B. Neuman, assisted by John Duane (1957), R. H. Raymond (1958), and H. H. Roepke (1959), supplemented by unpublished mapping in the Traveller Mountain quadrangle by D. W. Rankin (Vanderbilt University) and in the Island Falls quadrangle by E. B. Ekren (U.S. Geological Survey). Planimetry from U.S. Army Map Service Millinocket and Presque Isle 1:250,000 sheets, and place names from the U.S. Geological Survey topographic quadrangles indicated.

contains fragmentary fossils that are probably of Silurian age.

REFERENCES

Dodge, W. W., 1881, Lower Silurian fossils in northern Maine: Am. Jour. Sci., ser. 3, v. 22, p. 434–436.

Ruedemann, Rudolph, and Smith, E. S. C., 1935, The Ordovician in Maine: Am. Jour. Sci., ser. 5, v. 30, p. 353–355.

Smith, E. S. C., 1928, The Cambrian in northern Maine: Am. Jour. Sci., ser. 5, v. 15, p. 484–486.

Winslow, Arthur, 1894, Lead and zinc in Missouri: Missouri Geol. Survey, v. 7, sec. 2, p. 389–542.

75. A COMPARISON OF TWO ESTIMATES OF THE THORIUM CONTENT OF THE CONWAY GRANITE, NEW HAMPSHIRE

By F. J. Flanagan, W. L. Smith, and A. M. Sherwood, Washington, D.C., Batelle Memorial Institute, Columbus, Ohio, and Alexandria, Va.

Determining the distribution of uranium and thorium in the Conway granite of New Hampshire is part of a broader study of these elements in igneous rocks. The radioactivity of the red and green phases of the Conway granite from the quarry at Redstone, Carroll County, N.H., has been discussed by Smith and Flanagan (1956), who observed the differences in radioactivity of samples taken at closely spaced intervals. The differing amounts of the major contributors to the radioactivity in these samples might also prove valuable for future comparison with results obtained from samples taken over wide areas. Analyses of the two phases of the granite by W. H. Herdsman (Billings, 1928) indicate that potassium should also be classified as a major contributor to the radioactivity of the samples.

Uranium is present in igneous rocks approximately in the range 0.1 to 20 ppm and thorium from 1 to 100 ppm. The determination of these elements in igneous rocks, especially that of thorium, is time-consuming in spite of continuing improvements in analytical methods; potassium, on the other hand, can be determined rapidly by the methods of Shapiro and Brannock (1956), and the determination of radioactivity by beta-counting is a simple physical measurement.

Other investigators, for example Hurley (1956) and Adams and others (1958), have described methods for determining thorium in the parts-per-million range by gamma-scintillation spectroscopy and by alpha-counting methods. While thorium can be determined directly by gamma-scintillation spectroscopy, the method may require long counting periods, and the uranium content has to be known before the thorium content can be calculated from the alpha-counts. Although the technique described below probably cannot be used in the low (1 to 10 ppm) thorium range and is none too accurate for individual determinations, its less stringent requirements, such as short counting times (each sample in table 75.1 was counted for five minutes), and the use of an average potassium content of the rock under study, recommend its use in reconnaissance work where replicate samples are available. The useful range of the method covers only granites and some granodiorites and rocks abnormally enriched in thorium, but the method may be useful as an assay tool for low grade thorium ores.

Indirect estimates of the thorium content of uranium ores have been made for years by subtracting the uranium content of the ore from the radioactivity expressed as equivalent uranium, and then multiplying the remaining radioactivity by the specific counting rate ratio for U/Th. As the potassium contribution to the radioactivity of uranium ores is negligible, the correctness of these estimates depends on whether the uranium and thorium series are in equilibrium. When they are not in equilibrium the estimates are of little value.

If we are justified in assuming that radioactive equilibrium exists in the Conway granite, the indirect thorium values obtained by subtraction can be used in estimating the thorium content, despite the fact that both the radioactivity and the uranium and thorium content of the granite are two or three orders of magnitude lower than those of uranium ores. The correctness of these estimates, and hence the validity of the underlying assumption, can be tested by comparing them to values determined chemically.

INDIRECT THORIUM ESTIMATES

To determine if such indirect thorium estimates are valid, four samples were picked at random from each of the four groups (weathered and fresh, red and green) of samples of the Conway granite from the Red-

stone quarry (Smith and Flanagan, 1956). Uranium was then determined fluorimetrically, potassium by precipitation with tetraphenyl boron, and thorium colorimetrically with thoron as a reagent, after separation. Using the equation $eTh = R_1 [eU - (U + R_2K)]$, where R_1 is the U/Th counting-rate ratio for the counting system used, eU the radioactivity expressed as percent equivalent uranium, U the percent uranium, K the percent potassium, and R_2 the K/U counting-rate ratio, estimates of the thorium content can be calculated. These estimates and the determined values of eU, U, K, and Th are shown in table 75.1. The counting-rate ratios used were 4.0 for U/Th and 2,000 for U/K, in accord with the coaxial method of counting (Smith and Flanagan, 1956).

For comparing the value of the two methods—the chemical method and that proposed above—for estimating small amounts of thorium, several statistical methods are available, but the most attractive of these is the one that involves the pairing of observations and the use of Student's "t" test on the differences between pairs (Youden, 1951). For this test the variances of the two sets of data need not be homogeneous.

After one has noted the differences between the 16 pairs in column 6, table 75.1, the average difference, $\bar{d}(+1.5)$, and its standard deviation, $s_d(21.2)$, can be calculated. The hypothesis to be tested is that the average of the n differences, $\bar{d}$, is not significantly different from zero, or in other words that the averages of the two methods are virtually equal. Substitution in the equation $t = \frac{\bar{d}\sqrt{n}}{s_d}$ yields $t = 0.28$.

The 95-percent critical value for t with 15 degrees of freedom is ± 2.13. As the calculated value is much less than the critical value, it can be concluded that there is insufficient evidence for stating that the means of the two methods are significantly different. It is therefore justifiable to use the calculated thorium mean as an estimate of the mean of the chemical determinations. Inspection of these means (table 75.1) shows that the mean of the calculated values is about three percent greater than the average of the chemical determinations. Although three significant figures for potassium are reported in table 75.1, results obtained by rapid analysis (Shapiro and Brannock, 1956) would be adequate, for the second decimal place will not noticeably affect the calculated thorium values.

TABLE 75.1.—*Determinations of eU, U, K, and Th in samples of Conway granite*

Character	Sample	1	2	3	4	5	6
		eU (ppm)	U (ppm)	K (percent)	Th calculated (ppm)	Th determined (ppm)	Difference (4–5)
Weathered green.	137	46	7.6	4.64	61	62	−1
	142	44	7.5	4.85	49	53	−4
	143	47	8.6	4.64	61	52	9
	144	48	13.5	4.36	51	52	−1
Fresh green.	113	41	8.7	4.46	40	45	−5
	117	41	8.6	4.69	36	71	−35
	118	44	8.2	4.75	48	52	−4
	121	42	10.7	4.72	31	76	−45
Weathered red.	123	48	10.5	3.36	85	73	12
	128	55	12.1	4.25	87	65	22
	131	58	10.8	3.02	128	79	49
	134	51	10.1	3.29	98	83	15
Fresh red.	101	55	14.1	3.44	95	89	6
	103	60	16.6	3.90	96	98	−2
	109	57	17.8	4.18	73	74	−1
	111	63	16.5	3.90	108	99	9
Average		50.0	11.4	4.15	71.7	70.2	+1.5
Standard deviation		7.1	3.4	.60	28.7	16.9	21.2

When the average potassium contents of the red and green phases are used in place of the individual determinations in a phase, the average difference between the two methods is 0.25 ppm. Although this excellent agreement is undoubtedly fortuitous, it demonstrates that one need not use individual determinations if a reliable determination of average potassium content is available.

REFERENCES

Adams, J. A. S., Richardson, J. E., and Templeton, C. C., 1958, Determinations of thorium and uranium in sedimentary rocks by two independent methods: Geochim. et Cosmochim. Acta, v. 13, p. 270–279.

Billings, M. P., 1928, The petrology of the North Conway quadrangle in the White Mountains of New Hampshire: Am. Acad. Arts Sci. Proc., v. 63, p. 67–137.

Hurley, P. M., 1956, Direct radiometric measurement by gamma-ray scintillation spectrometer: Geol. Soc. America Bull., v. 67, p. 395–411.

Shapiro, Leonard, and Brannock, W. W., 1956, Rapid analysis of silicate rocks: U. S. Geol. Survey Bull. 1036–C, p. 19–56.

Smith, W. L., and Flanagan, F. J., 1956, Use of statistical methods to detect radioactivity change due to weathering of a granite: Am. Jour. Sci., v. 254, p. 316–324.

Youden, W. J., 1951, Statistical methods for chemists: New York, John Wiley and Sons, p. 28.

557753 O—60——12

76. POSSIBLE USE OF BORON, CHROMIUM, AND NICKEL CONTENT IN CORRELATING TRIASSIC IGNEOUS ROCKS IN CONNECTICUT

By P. M. HANSHAW and P. R. BARNETT, Boston, Mass., and Denver, Colo.

Work done in cooperation with Connecticut Geological and Natural History Survey

The general distribution, lithology, and structure of the Triassic rocks in Connecticut have been known for many years, and three layers of extrusive basalt, some of them consisting of more than one flow, are easily recognized where well exposed. In places, however, glacial deposits cover all bedrock except a few small outcrops of basalt, which are nearly indistinguishable by field and microscopic study, and therefore difficult to place in proper stratigraphic position. The intrusive rocks of different ages differ in character in some places; near Mount Carmel, for example, the porphyritic dikes are younger than both the nonporphyritic dikes and a large intrusive sheet (C. E. Fritts, written communication, November 17, 1959).

Quantitative spectrographic analyses of 37 random samples of Triassic basalt and diabase from the Connecticut Valley Lowland appear to show differences in boron, chromium, and nickel content which may possibly aid in correlating outcrops of these rocks, and thereby help in interpreting the geologic structure (fig. 76.1).

REGIONAL GEOLOGY

The Triassic rocks in Connecticut underlie the Connecticut Valley Lowland. They comprise a wedge of continental sedimentary rocks (red beds) dipping gently eastward, intercalated with three layers of basalt and cut by at least one intrusive sheet and many dikes of diabase. The three basalt layers from oldest to youngest, are called the Talcott basalt, the Holyoke basalt, and the Hampden basalt. The regional geology of Triassic rocks in Connecticut has been described by Percival (1842), Davis (1898), Longwell (1922), and Krynine (1950). A preliminary geologic map and description of bedrock units is contained in Rodgers and others (1959).

The set of northeast-trending faults, generally downthrown on the west, cuts the Triassic rocks in the lowland and is especially prominent in the area between Meriden and Hartford. Erosion along these faults has formed many subparallel northeast-trending ridges of basalt. As the sedimentary rocks stratigraphically below and above the basalt layers are covered by glacial deposits, and the basalts look alike both megascopically and microscopically, little evidence can be found for assigning any basalt outcrop to a particular stratigraphic position. It is necessary, however, to determine the stratigraphic positions of many outcrops of basalt before the structure of the Triassic in this area can be delineated and interpreted in detail.

DESCRIPTIONS OF BASALTS

The basalts are greenish to bluish gray, dense, and generally fine grained, but are coarse grained in places near the center of a flow. They are homogeneous in composition, being composed of augite, pigeonite, and labradorite with interstitial chloritic material and accessory magnetite(?). In central Connecticut, the Talcott basalt commonly has pillow structure and averages about 150 feet in thickness, the Holyoke basalt has well-developed columnar joints at many localities and is about 600 feet thick, and the Hampden basalt shows columnar joints in places and is about 160 feet thick. Locally each of these basalts consists of more than one flow, but where that is true the individual flows cannot be traced for more than a short distance, and their relative stratigraphic position within the basalt cannot be determined.

RESULTS OF SPECTROGRAPHIC ANALYSES

Samples were collected by C. E. Fritts, P. M. Hanshaw, R. W. Schnabel, and H. E. Simpson. The samples included (a) grab samples from various levels within each basalt layer, and (b) composite samples taken at regular intervals stratigraphically across one layer. Samples were also taken from intrusive masses. No mineralogic zoning of units was noted in the field.

The analyses indicate that the boron content of the Talcott and Hampden basalts is greater than that of the intrusive rocks. The boron content of the Holyoke basalt varies from place to place but averages higher

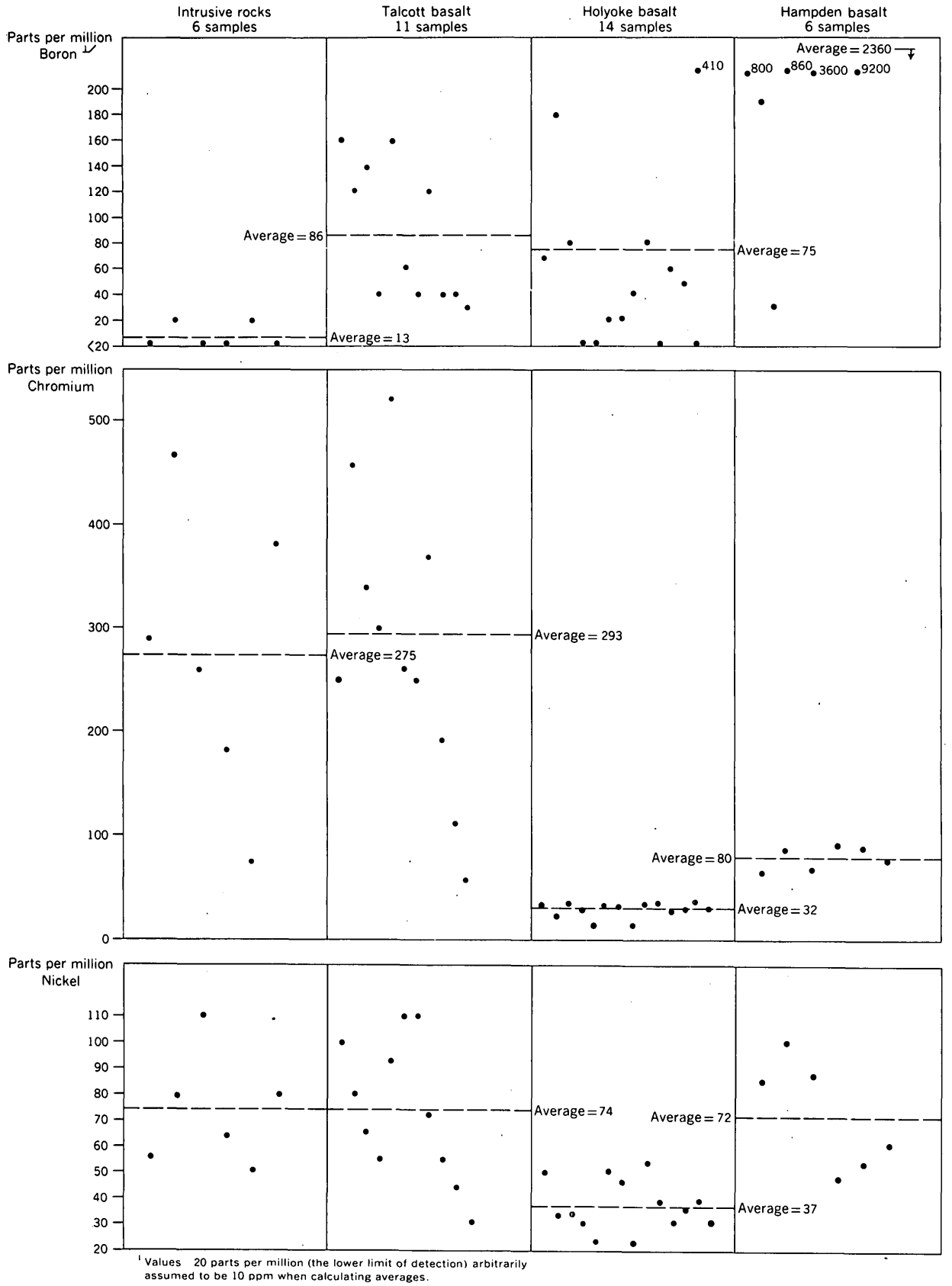

FIGURE 76.1.—Quantitative spectrographic analyses of boron, chromium, and nickel in 37 samples of Triassic igneous rocks from Connecticut. Analysts, P. R. Barnett and N. M. Conklin, U.S. Geological Survey.

than that of the intrusives. If the low boron content of the intrusives is substantiated by further analyses, it may be a useful criterion for determining the intrusive origin of a diabase body where field evidence of origin is lacking.

Analyses of the extrusive rocks indicate that the average chromium content of the Holyoke basalt is about one-half that of the Hampden basalt and about one-tenth that of the Talcott basalt. Several small outcrops of basalt in central Connecticut are inferred, on the basis of structural interpretations, to be Hampden, and the analyses made thus far have supported these inferences. These analyses are not shown in figure 76.1.

The nickel content of the Holyoke basalt appears to be about one-half that of other Triassic volcanic rocks in Connecticut. Low nickel content in conjunction with low chromium content might therefore permit correlating a basalt outcrop of unknown stratigraphic position with the Holyoke.

The analytical results summarized here are preliminary. Analyses of many additional samples, combined with field and petrographic study, will be needed to establish the trends indicated, their mineralogical relationships, and their geologic significance.

REFERENCES

Davis, W. M., 1898, The Triassic formation of Connecticut: U.S. Geol. Survey 18th Ann. Rept., pt. 2, p. 1–192.

Krynine, P. D., 1950, Petrology, stratigraphy, and origin of the Triassic sedimentary rocks of Connecticut: Connecticut Geol. and Nat. History Bull. 73.

Longwell, C. R., 1922, Notes on the structure of the Triassic rocks in southern Connecticut: Am. Jour. Sci., 5th ser., v. 4, p. 223–236.

Percival, J. G., 1842, Report on the geology of the State of Connecticut: New Haven.

Rodgers, John, Gates, R. M., and Rosenfeld, J. L., 1959, Explanatory text for Preliminary Geological Map of Connecticut, 1956: Connecticut Geol. and Nat. History Survey Bull. 84.

77. CORAL FAUNAS IN THE ONONDAGA LIMESTONE OF NEW YORK

By William A. Oliver, Jr., Washington, D.C.

Study of extensive collections of rugose corals from the Onondaga limestone in New York State has demonstrated the presence of two distinct coral assemblages, the upper one occupying a much greater stratigraphic thickness than the lower. The lower assemblage has not been described, and its recognition makes possible the correlation of the beds containing it over a large area.

The lower assemblage has been found in New York only in discontinuous beds, 2 to 4 feet thick, exposed at the base of the formation in the western part of the State. Characteristic and common rugose corals from these basal beds are *Acrophyllum oneidense*, *Aemulophyllum exiguum*, "*Cystiphyllum*" *sulcatum*, "*C.*" *squamosum*, *Kionelasma* sp., *Scenophyllum conigerum*, and *Syringaxon* sp. Several other, less common, species of corals are apparently limited to the lower assemblage. Associated forms include *Amphigenia* sp. cf. *A. curta*, *Centronella* sp., *Eodevonaria* sp. (identified by A. J. Boucot, oral communication, 1959) and several other brachiopods, platyceratid gastropods, and trilobites. The strata carrying the lower assemblage were designated by Oliver (1954, p. 626 and 632) as zone B (the *Amphigenia* zone) of the Edgecliff member.

The subdivisions of the Onondaga limestone in western New York are shown in figure 77.1 (after Oliver, 1954). The *Amphigenia* zone is lithologically as well as paleontologically distinct from the Edgecliff member and should no longer be included in it. The Edgecliff member is a distinctive coralline biostromal and biohermal limestone extending all the way across New York State and into Ontario. Paleontologically, it is characterized by a completely different group of rugose corals, here referred to as the upper coral assemblage. Among the common genera in this member are *Acinophyllum*, *Bethanyphyllum*, *Billingsastraea*, *Blothrophyllum*, *Cylindrophyllum*, *Cystiphylloides*, *Eridophyllum*, *Heliophyllum*, *Hexagonaria*, *Siphonophrentis*, and *Synaptophyllum* (see Oliver, 1954, p. 638–641, for lists of fossils occurring in all members). Although some genera occur in both the lower and upper assemblages, the rugose corals in the two are, as a whole, distinctive on a generic and even a family level.

The upper coral assemblage, broadly defined, is found throughout the Onondaga limestone of New York in the light-colored, coarser grained facies (Oliver, 1954, 1956), and similar corals (families, many genera

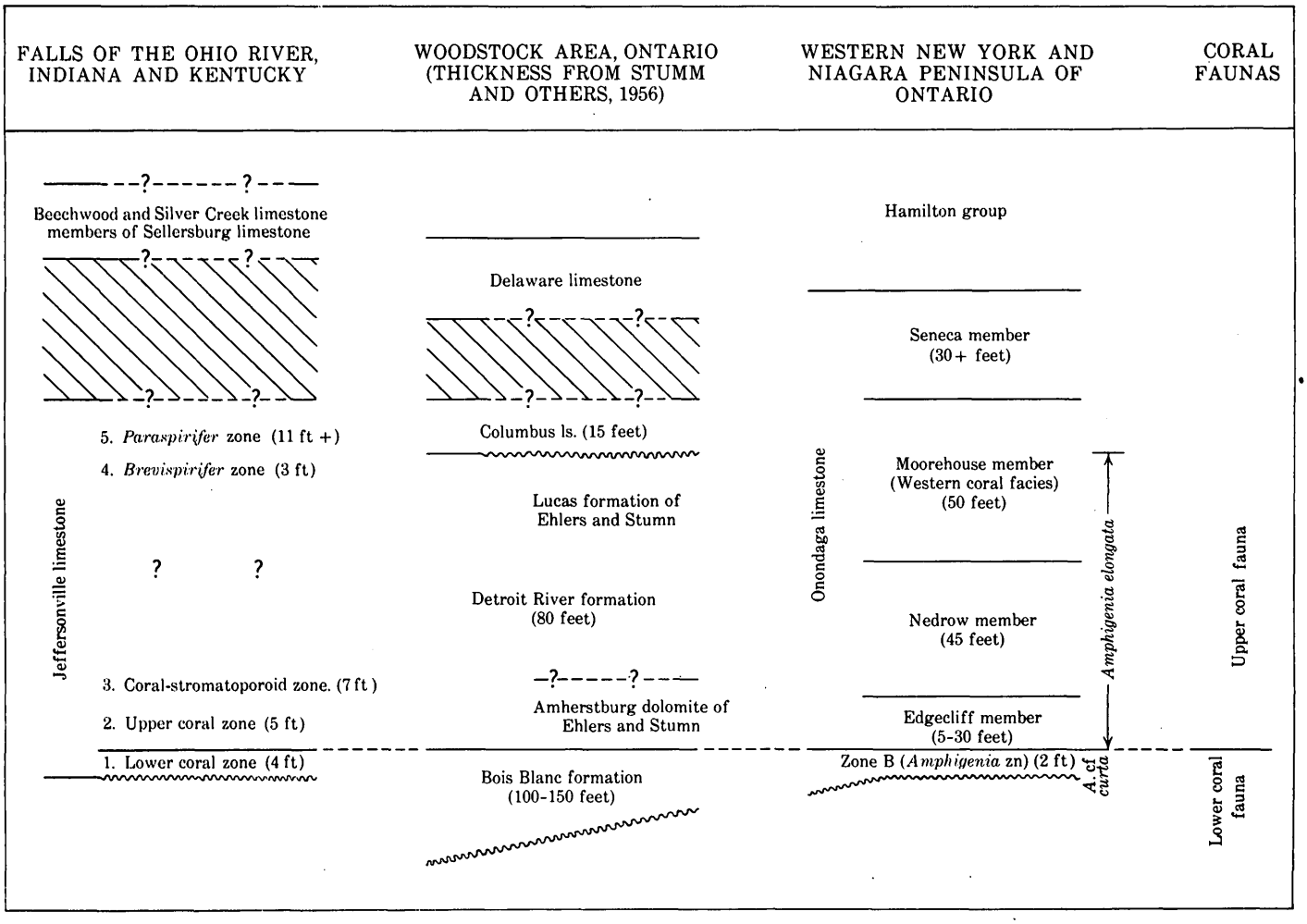

FIGURE 77.1.—Distribution of principal coral faunas in the Onondaga limestone and correlations with sections in Ontario and Indiana-Kentucky. The range of *Amphigenia* in western New York is shown on the right side of the New York column.

and some species) are found in the calcareous members of the overlying Hamilton group. Stratigraphic subdivision (zonation) of the strata carrying the upper assemblage is under study, but for present purposes the contrast of this assemblage with the lower one is its most significant feature.

The Onondaga formation has the same character in the Niagara Peninsula of Ontario. The *Amphigenia* zone thickens westward (lower brachiopod beds of Stauffer, 1915), but in other respects the lower members change only gradually and can be recognized as far as Hagarsville, 60 miles west of Buffalo.

Between Hagarsville and the Woodstock, Ontario area, 40 miles to the northwest, almost no outcrops are known. In the Woodstock area the rocks are completely different from what they are at Hagarsville, and Michigan stratigraphic terminology has been applied (section included in figure 77.1). The formations of the Woodstock area differ from the Onondaga limestone in facies and partly in age. At Innerkip, exposures of the lower 10 feet of the Bois Blanc formation carry the distinctive lower coral assemblage. The total thickness of the Bois Blanc is over 100 feet (Stumm and others, 1956); outcrops are few, but according to Best[1] most or all of this thickness carries the lower assemblage. The pre-Edgecliff *Amphigenia* zone, in western New York and adjacent Ontario, can be considered as the eastern feather edge of the Bois Blanc formation. Lateral discontinuity of the zone in western New York (Oliver, 1954), and possibly in the Niagara Peninsula of Ontario, suggests that the strata containing the upper assemblage may be separated from the *Amphigenia* zone by an unconformity.

The upper coral assemblage is found in the lower part of the Detroit River formation (Amherstburg dolomite of Ehlers and Stumm, 1951) in the Woodstock area,

[1] Best, E. W., 1953, Pre-Hamilton Devonian stratigraphy, southwestern Ontario, Canada: University of Wisconsin, unpublished Ph.D. thesis.

and also at Gorrie, farther north. The upper two-thirds of the Detroit River formation (Lucas formation of Ehlers and Stumm, 1951) contains a different coral assemblage, apparently reflecting environmental differences. The Detroit River formation correlates with most of the New York Onondaga. The overlying Columbus limestone is correlated with the upper part of the Moorehouse or Seneca on the presence of *Paraspirifer*. These general relationships are shown in figure 77.1

At the Falls of the Ohio River, near Louisville, Ky., several zones are recognized, partly on the basis of studies by Campbell (1942) and earlier workers (fig. 77.1). The lower coral zone (zone 1) carries the lower coral assemblage and is correlated with the Bois Blanc formation of Ontario and the pre-Edgecliff *Amphigenia* zone of western New York. Approximate correlations of zones 2 to 5, which carry the upper coral fauna, are shown in figure 77.1.

CONCLUSIONS

The corals of the upper assemblage of the Onondaga limestone are of distinctly Middle Devonian types. They are associated with nautiloid cephalopods of Middle Devonian age (R. H. Flower, oral communication, 1959), and with rare goniatites that are also of Middle Devonian age (M. R. House, oral communication, 1959). There is little doubt that the nearest faunal affinities of the corals and cephalopods from the Onondaga limestone of New York (exclusive of zone B) and its correlatives are with the Couvinian (early Middle Devonian) of Europe.

The corals of the lower assemblage are associated with brachiopods referred to the Schoharie fauna of Cooper and others (1942, p. 1780). The Schoharie grit underlies the Onondaga limestone in east-central New York and carries some at least of the corals occurring in the lower assemblage. Most of the arguments for regarding the Onondaga limestone as Early Devonian have been based on faunas (principally brachiopods) of units correlative with the Schoharie rather than with the Onondaga proper. The corals of the lower assemblage are more closely related to known Middle Devonian corals than to Early Devonian ones, but the species and many of the genera are not known to occur outside of northeastern North America and may be endemic to that area. The age of the pre-Edgecliff *Amphigenia* zone and its correlatives may be late Early Devonian (Emsian of Europe), but present knowledge of the lower corals neither proves nor disproves this.

REFERENCES

Campbell, Guy, 1942, Middle Devonian stratigraphy of Indiana: Geol. Soc. America Bull., v. 53, p. 1055–1072.

Cooper, G. A., and others, 1942, Correlation of the Devonian sedimentary formations of North America: Geol. Soc. America Bull., v. 53, p. 1729–1794.

Ehlers, G. M., and Stumm, E. C., 1951, Middle Devonian Columbus limestone near Ingersoll, Ontario, Canada: Am. Assoc. Petroleum Geologists Bull., v. 35, p. 1879–1888.

Oliver, W. A., Jr., 1954, Stratigraphy of the Onondaga limestone (Devonian) in central New York: Geol. Soc. America Bull., v. 65, p. 621–651.

———, 1956, Stratigraphy of the Onondaga limestone in eastern New York: Geol. Soc. America Bull., v. 67, p. 1441–1474.

Stauffer, C. R., 1915, The Devonian of southwestern Ontario: Canada Geol. Survey, Mem. 34, 341 p.

Stumm, E. C., and others, 1956, The Devonian strata of the London-Sarnia area, southwestern Ontario: Michigan Geol. Soc., Guidebook annual field trip, June 9–10, 1956, 21 p.

78. GEOPHYSICAL AND GEOLOGICAL INTERPRETATION OF A TRIASSIC STRUCTURE IN EASTERN PENNSYLVANIA

By Isidore Zietz and Carlyle Gray, Washington, D.C., and Bureau of Topographic and Geologic Survey, Harrisburg, Pa.

Work done in cooperation with the Bureau of Topographic and Geologic Survey, Commonwealth of Pennsylvania

GEOLOGY

The Triassic rocks of the Newark-Gettysburg basin are extensively exposed in Bucks County, eastern Pennsylvania (McLaughlin, 1959) (fig. 78.1). Here the basin contains three sedimentary formations; these are, in order of increasing age, the Stockton, Lockatong and Brunswick. The sequence is duplicated by faulting, and on Buckingham Mountain near the center of the

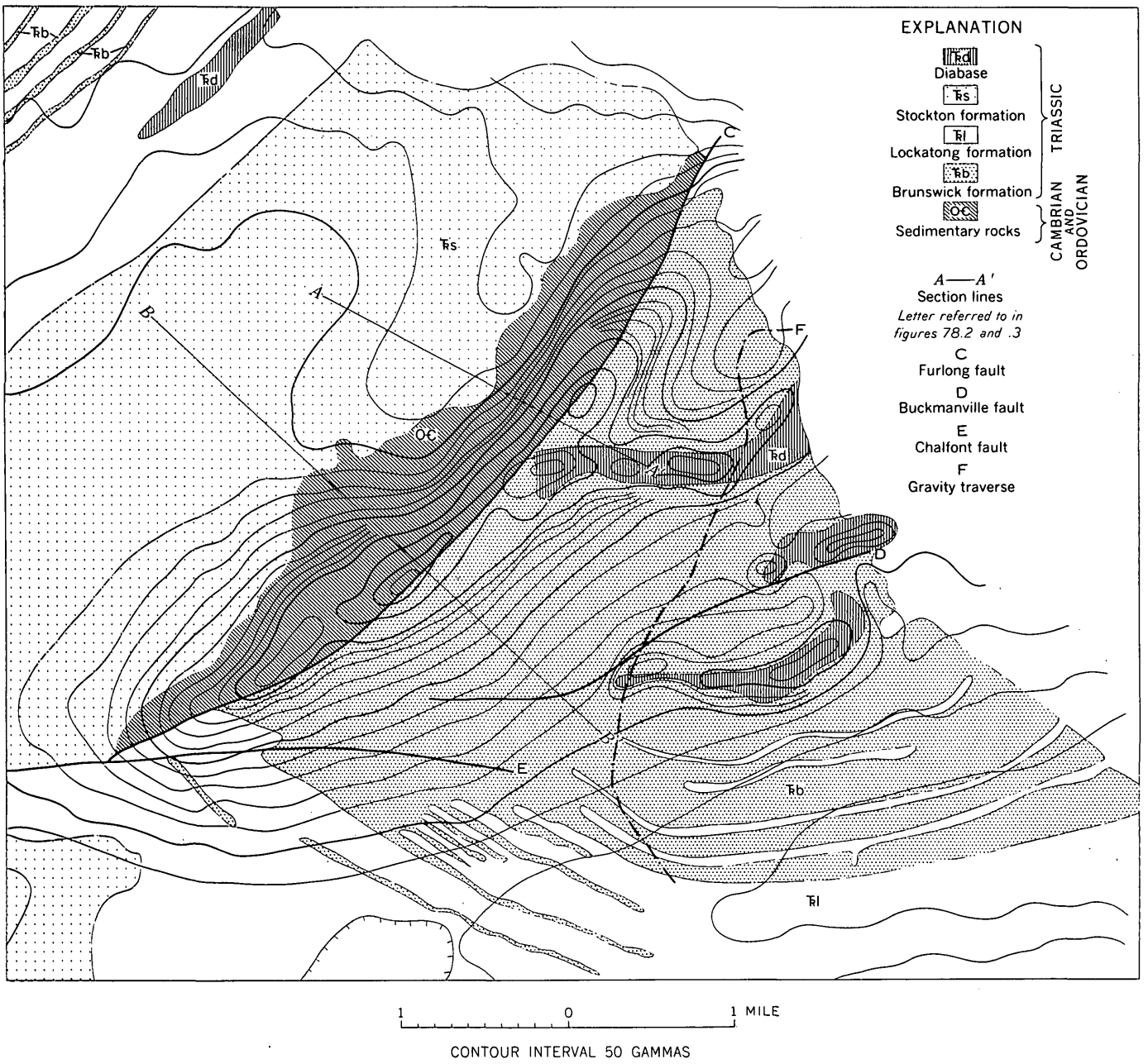

FIGURE 78.1.—Aeromagnetic map of the Buckingham Mountain area, Pennsylvania.

basin, the two areas of Triassic rocks are separated by a sizeable area of pre-Triassic rocks.

The pre-Triassic floor in the vicinity of Buckingham Mountain consists of Cambrian and Ordovician rocks. On the southeast side of the Buckingham Mountain area, the Furlong fault (*C*, fig. 78.1) brings Lower, Middle, and Upper Cambrian rocks in contact with the Brunswick formation. Northwest of the exposed Paleozoic rocks the Stockton formation lies unconformably on the Paleozoic sedimentary rocks. In one small area on Buckingham Mountain the presence of gneiss float blocks indicates that crystalline Precambrian basement rocks are actually exposed. The dip of the bedding in the Paleozoic sedimentary rocks is generally to the northwest.

At the southwest end of the inlier, the Furlong fault joins the Chalfont fault (*E*, fig. 78.1). McLaughlin (1959, p. 131) has estimated a maximum stratigraphic displacement of 10,000 feet on the Furlong fault and 6,500 feet on the Chalfont fault. The Chalfont fault extends east of its junction with the Furlong fault for about four miles and is then overlapped en echelon by

the Buckmanville fault (*D*, fig. 78.1), which extends the displacement to the Delaware River. The stratigraphic throw of these faults was computed from estimates of the total thickness of the Triassic sedimentary formations. It has long been recognized, however, that these formations may be in part equivalent to one another, and that in places the Brunswick formation lies on the pre-Triassic rocks. Such considerations indicate that the estimated stratigraphic throw on the faults may be only an approximation of the true throw.

The structure associated with the Furlong fault in the Buckingham area has magnetic expression, because the Precambrian basement rocks, which are much more magnetic than either the Triassic or the Paleozoic sedimentary rocks, are close to the surface on the northwest side of the fault.

INTERPRETATION

The most prominent feature on the areomagnetic map (fig. 78.1) is a large anomaly, striking northeast and having an amplitude of more than 1,000 gammas, that is centered over the Furlong fault. The map reveals differences between the countour features northeast and southwest of traverse *B*. The areomagnetic profile and the inferred geologic section along traverse *B*, which we regard as typical of the southwestern part of the Buckingham anomaly, is presented in figure

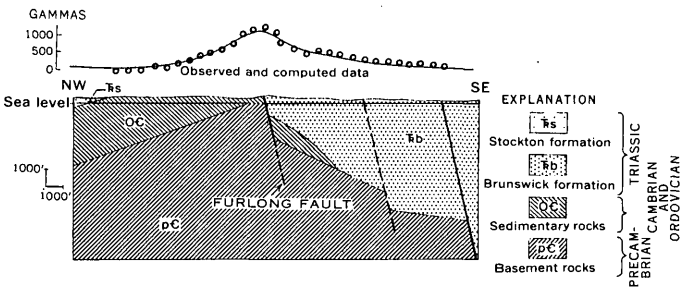

FIGURE 78.2.—Geologic section and aeromagnetic profile along traverse *B*.

78.2. The geologic section was constructed partly from surface mapping and stratigraphic considerations, and partly from calculations based on aeromagnetic data. Magnetic profiles for several hypothetical Precambrian surfaces were computed on the basis of a Pirson polar chart modified for total-intensity calculations (Pirson, 1940). The Precambrian surface shown in figure 78.2 is the one that produces the best fit to the observed profile. The circled points are computed data, based on the assumption that remanent magnetization is negligible and that the susceptibility of the Precambrian rocks exceeds that of the sedimentary rocks by 0.005 cgs units. The configuration and structure of the Precambrian surface as deduced from aeromagnetic data differ in two important respects from those based on geology alone: (a) The displacement along the Furlong fault is less than 3,000 feet, whereas stratigraphic data indicate that the total thickness of the sedimentary rocks, and therefore displacement, on this fault, is about 10,000 feet; (b) The Precambrian surface southeast of the Furlong fault dips southeastward, instead of northwestward as was expected from the surface structure of the Triassic rocks. Northeast of traverse *B* magnetic gradients are much steeper than they are southwest of it, and there is a broad minimum northwest of the Paleozoic rocks; and although the total Paleozoic sedimentary section is apparently thicker on the northeast side than on the southwest side, the amplitude of the anomalies and the magnetic gradients are higher on the southwest side.

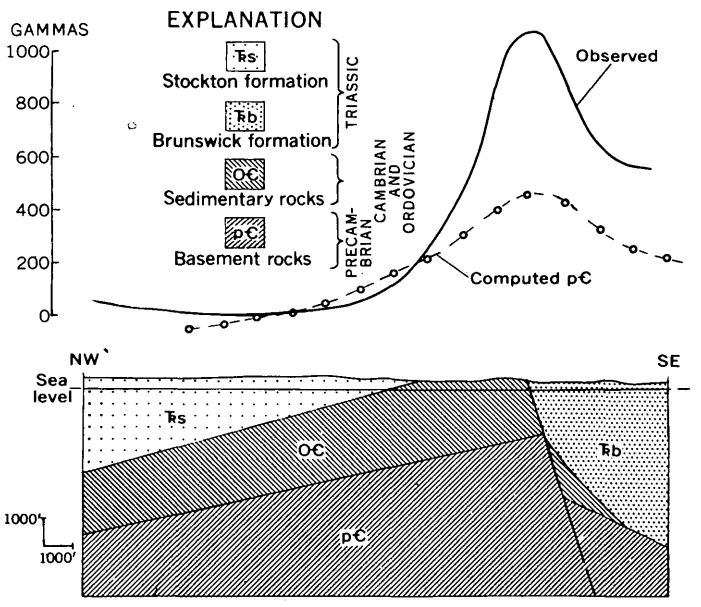

FIGURE 78.3.—Geologic section and aeromagnetic profile along traverse *A*.

Figure 78.3 shows an aeromagnetic profile, along traverse *A*, that we regard as typical of the northeastern half of the Buckingham anomaly. Superimposed on the observed profile is a magnetic profile computed from a structure section based on geological data and the computed section of traverse *B*. It is evident that in this province, if the susceptibility contrast is 0.005 cgs units as assumed in traverse *B*, the Precambrian structure does not contribute very much to the anomaly amplitude. Subtraction of the magnetic fields of the observed and computed profiles results in a residual magnetic profile shown in figure 78.4. This anomaly could be accounted for by assuming that a tabular

body, of small width but large vertical extent (fig. 78.4), cuts across the Paleozoic rocks, that its top is approximately 1,000 feet below the surface and 1,000 feet northwest of the Furlong fault, that this body is parallel to the Furlong fault and that its southwest end is near traverse *B*. Assuming that this body is 100 feet wide, its susceptibility is computed to be 0.09 cgs units, which corresponds to a magnetite content of over 25 percent by volume. If the body is only 50 feet wide, the magnetite content is over 50 percent.

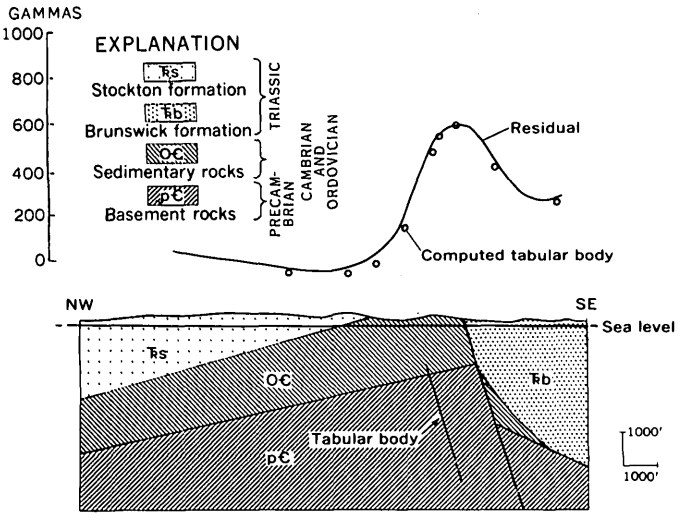

FIGURE 78.4.—Aeromagnetic profile across inferred dike.

In any curve-matching procedure involving magnetic data such as the one presented here, it is important to remember that a given observed profile could be satisfied by any one of many possible configurations; for example, the same anomaly might be produced by a shallow weakly magnetic body or a deep highly magnetic body. The dike postulated here is assumed to be of small mass and to lie at a depth of about 1,000 feet—the maximum depth at which a magetic source could yield the anomaly observed. The reason for assuming that the dike is small is that a large dense mass could be detected by gravity measurements if it lay near the surface; no such mass was indicated by a detailed gravity profile made in this vicinity under the direction of Martin Kane using a gravimeter with a sensitivity of 0.01 mgls per dial division.

Because of the geological setting, this thin tabular body might have economic importance.

Approximately 10 miles south of the intersection of the Furlong fault and traverse *A*, Precambrian rocks are exposed on the surface. They are described (Armstrong, 1941) as Baltimore gneiss ranging in composition from mafic to felsic. Magnetic anomalies in the vicinity of this exposure are numerous, and depth calculations based on the method described by Vacquier and others (1951) yield depths equal to the flight elevation. This partly confirms the belief that these methods are applicable in this area. Depths to the Precambrian surface approximately 3 miles north of this area are computed to be about 3,000 feet. Extrapolating linearly and using this depth and the points at the surface of the Precambrian as controls, we have computed that the depth near the south end of the profile in figure 78.2 is approximately 7,000 feet. This figure is in good agreement with the depth obtained by using the curve-matching procedures (see fig. 78.2), and confidence may be placed in figures that agree so closely though obtained by two entirely different methods of approach.

A cross section of the southern half of the Triassic basin is shown in figure 78.5. The configuration of the Precambrian surface is based entirely on interpretation

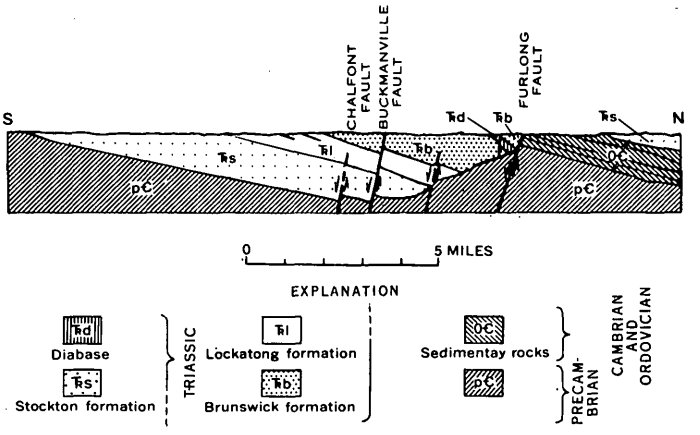

FIGURE 78.5.—A geologic section across the southern half of the Triassic basin, Bucks County, Pa.

of the magnetic data, and the stratigraphic column is based entirely on geologic mapping. Southeast of the Furlong fault, there are prominent magnetic anomalies over outcrops of diabase. These anomalies could be caused by strong magnetization of the rocks, either induced or remanent, or by the shape and attitude of the diabase mass. The simplest way to determine the configuration of the mass is by means of a gravity traverse at right angles to the strike of the diabase since there is a strong density contrast between it and the surrounding sedimentary rocks (approximately 0.4 g per cm^3). Toward this end, a gravity traverse (*F*), shown in figure 78.1, was made under the supervision of Martin Kane. The results show that the diabase is a sheet dipping to the northeast, nearly concordant with the bedding in the Triassic sedimentary rocks.

REFERENCES

Armstrong, Elizabeth, 1941, Mylonization of hybrid rocks near Philadelphia, Pennsylvania: Geol. Soc. America Bull., v. 52, no. 5, p. 667–694.

McLaughlin, D. B., 1959, Mesozic rocks, *in* Willard, Bradford, and others, Geology and Mineral Resources of Bucks County, Pennsylvania: Pennsylvania Geol. Survey, 4th ser., Bull. C–9.

Pirson, S. J., 1940, Polar charts for interpreting magnetic anomalies: Am. Inst. Mining Metall. Engineers Trans., v. 138, p. 179–192.

Vacquier, V., and others, 1951, Interpretation of aeromagnetic maps: Geol. Soc. America Mem. 47, 151 p.

76. PRELIMINARY INTERPRETATION OF AEROMAGNETIC DATA IN THE ALLENTOWN QUADRANGLE, PENNSYLVANIA

By Randolph W. Bromery, Washington, D.C.

Prepared in cooperation with the Bureau of Topographic and Geologic Survey, Commonwealth of Pennsylvania

The Allentown quadrangle was surveyed with the airborne magnetometer in 1956 as part of a detailed survey in southeastern Pennsylvania, to obtain geophysical data useful in areal geologic mapping and in searching for magnetic iron deposits. The flying was done at 500 feet above the ground surface, on traverses a quarter of a mile apart.

Precambrian metamorphic and igneous rocks of complex geologic structure form a continuous belt that trends northeast across the south-central part of the quadrangle, separating the Paleozoic sedimentary rocks in the northern half of the quadrangle from the Triassic sedimentary and igneous rocks in the southeastern part of the quadrangle (fig. 79.1).

The exposed Precambrian rocks are delineated in detail by a "bird's-eye maple" magnetic pattern. Some of this detail has been sacrificed in preparing figure 79.1, but the original magnetic contours (Bromery and others, 1959) have proved useful in mapping the areal extent of the underlying Precambrian rocks. The magnetic data indicate that some previously mapped faults are longer than was supposed, and that faulting may have occurred in some areas where it had not hitherto been recognized.

The Paleozoic sedimentary rocks in Saucon Valley are characterized by a uniform magnetic gradient leading to a magnetic low. This gradient extends northeastward along the northern edge of the valley beyond the head of the valley.

To show the possible configuration and depth of burial of magnetic rocks, three theoretical structure sections, *A*, *B*, and *C*, were graphically computed from the magnetic profiles across the Reading Prong. This analysis was performed by using a modified Pirson Polar Chart (Pirson, 1940). The calculations indicate that the Precambrian rock surface along the northern edge of Saucon Valley and its apparent northeast extension is nearly vertical. The buried surface of the magnetic rocks underlying Saucon Valley is approximately a mile deep. Low-amplitude magnetic anomalies observed along the southern edge of Saucon Valley are underlain by Precambrian rocks, and if a uniform magnetic susceptibility is assumed for these rocks the magnetic data along section *A* show that they are less than 1,000 feet thick. Magnetic anomalies of higher amplitude are observed along sections *B* and *C*, on strike with the low-amplitude anomalies, and calculations indicate that here the thickness of the underlying Precambrian rocks is far greater—4,000 feet. The Precambrian rock surface at the Triassic Border fault along sections *A* and *B* is nearly vertical, and there is no magnetic expression of buried Precambrian rocks over the Triassic Basin. Possibly this is because Precambrian rocks are deeply buried, so that any weak magnetic expression is masked by anomalies associated with Triassic diabase rocks, as for example at the southeast end of section *A*.

Along the northern edge of the Reading Prong, the magnetic profiles indicate that the Precambrian rocks were dropped 1,000 feet on the north side of a nearly vertical fault; and that the Precambrian surface north of the fault slopes northward beneath Paleozoic sedimentary rocks.

Along section *D*, magnetic computations indicate that an arching surface of Precambrian rocks four miles wide is buried a mile below the surface. An anticline in the overlying Paleozoic sedimentary rocks,

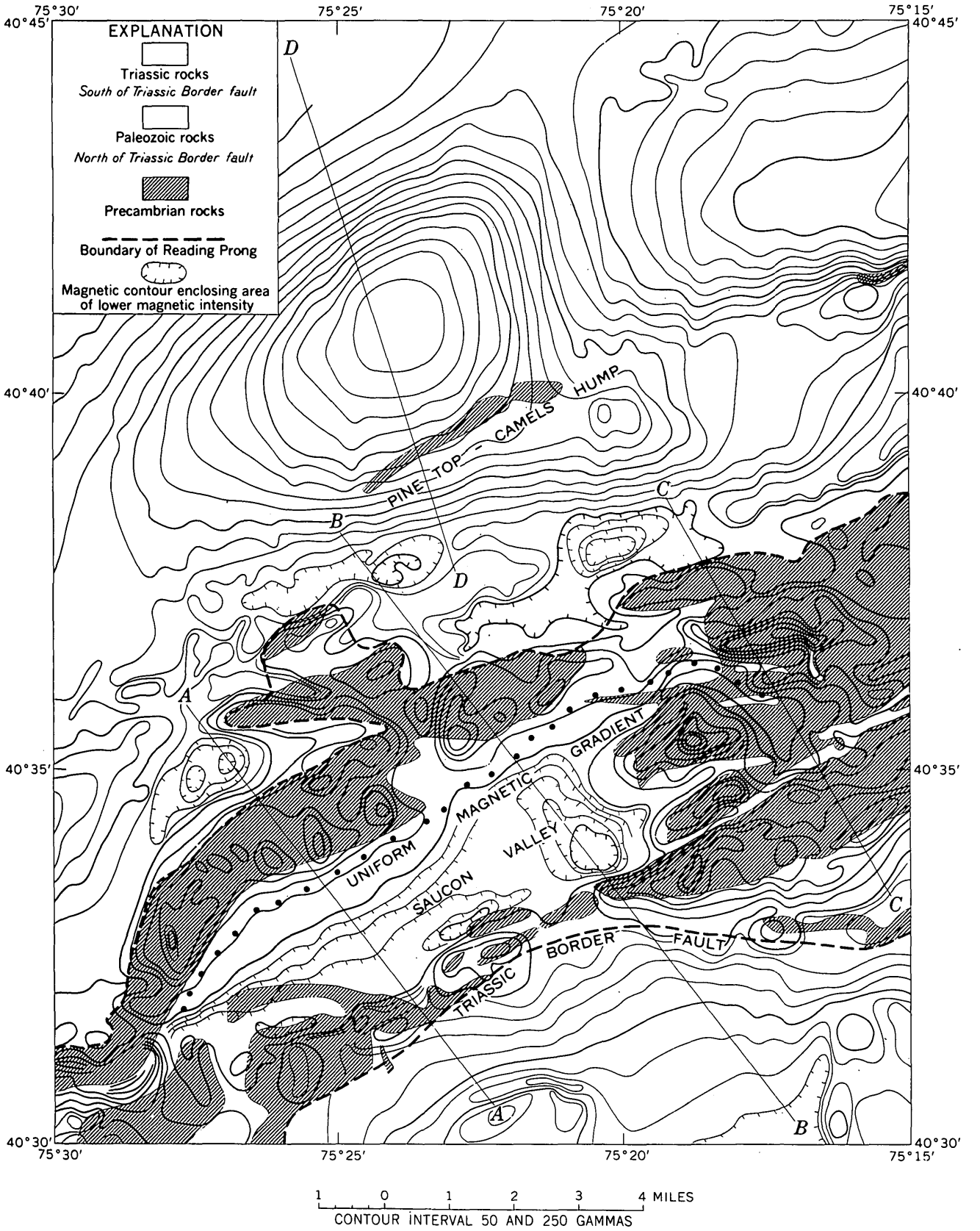

FIGURE 79.1.—Aeromagnetic and generalized geologic map of the Allentown quadrangle, Northampton, Lehigh, and Bucks Counties, Pa. Magnetic data from Bromery and others (1959).

shown on the new Pennsylvania State Geologic Map, is centered over this buried arch; the exposure of apparently non-magnetic Precambrian rocks on Pine Top and Camels Hump (fig. 79.1) extends along its southern edge. The magnetic anomaly associated with this buried structural feature extends to the northeast and increases in amplitude in the adjacent Easton quadrangle (Bromery and others, 1960), where it is underlain by exposed Precambrian rocks at Chestnut Hill. The exposed Precambrian rocks on Pine Top and Camels Hump are probably related to those at Chestnut Hill and to the buried magnetic mass along section *D*, but these relationships are not yet clear. Analysis of the magnetic data in the Allentown quadrangle and in the adjoining quadrangles indicates areas where Precambrian rocks may be relatively thin.

REFERENCES

Bromery, R. W., Bennett, B. L., and others, 1959, Aeromagnetic map of the Allentown quadrangle, Northampton, Lehigh, and Bucks Counties, Pennsylvania: U.S. Geol. Survey Geophys. Inv. Map GP–213.

Bromery, R. W., Henderson, J. R., Zandle, G. L., and others, 1960, Aeromagnetic map of part of the Easton quadrangle, Northampton County, Pennsylvania, and Warren County, New Jersey: U.S. Geol. Survey Geophys. Inv. Map GP–235.

Pirson, S. J., 1940, Polar charts for interpreting magnetic anomalies: Am. Inst. Mining Metall. Engineers Trans., v. 138, p. 179–192.

80. TACONIC AND POST-TACONIC FOLDS IN EASTERN PENNSYLVANIA AND WESTERN NEW JERSEY

By Avery A. Drake, Jr., Robert E. Davis, and Donald C. Alvord, Washington, D.C., Denver, Colo., and Denver, Colo.

Papers reviewing Appalachian structural geology and the chronology of Appalachian folding have recently been published by Spieker (1956) and by Woodward (1957a, 1957b, and 1958). Woodward agrees with some previous workers in believing that the folds in the Appalachians were produced in three similar but separate periods of deformation, rather than in a single period of disturbance at the close of the Paleozoic era. The purpose of this paper is to describe some of the structural relations along the Delaware River in eastern Pennsylvania and western New Jersey, and to state our present views regarding the relative intensity of the Taconic and post-Taconic orogenies.

The area considered here includes segments of the Reading Prong, Great Valley, and Folded Appalachians, and is underlain by rocks of Precambrian to Late Devonian age. It has long been recognized that an unconformity separates the Martinsburg shale, of Middle and Late Ordovician age, from the Shawangunk conglomerate of Silurian age, and that the pre-Silurian rocks were folded twice (Behre, 1925; Miller, 1926; and Stose, 1930). Stose thought that the pre-Silurian (Taconic) folding was less intense than the later (Appalachian) folding, whereas Behre and Miller thought that in eastern Pennsylvania the Taconic folding was almost if not quite as intense as the Appalachian. It is our thesis that in this area the Taconic folding was by far the stronger.

In the part of the Appalachians we have studied it has been difficult to relate the folds to specific periods of deformation, because there the structural trends are all nearly parallel. Detailed mapping and careful cataloguing of minor structural features has shown, however, that the folds in the pre-Silurian rocks are vastly different from those in the younger rocks.

The pre-Silurian sedimentary rocks—largely Cambrian and Ordovician carbonate rocks—and the Martinsburg shale are strongly folded. The folds, which range in amplitude from microscopic dimensions to at least 5 miles, are nearly all overturned to the northwest. Some are recumbent, and the axial planes of a few have been rotated past the horizontal. The traces of axial planes are hard to follow because of faulting and flowage, but major synclines and synclinoria have been mapped in the Musconetcong and Pohatcong Valleys, and also in the Great Valley north of Easton, Pa. The synclinorium in the Great Valley is the largest fold yet recognized in the area; its northwest limb extends even beyond the north boundary of the Bangor 7½-minute quadrangle. Its constituent folds are mostly recumbent. Their axes plunge, in places, gently east-northeast or west-southwest, but on the average they are probably almost horizontal.

Flow cleavage is present in all of the pre-Silurian rocks, and is by far the most prominent planar structure in the argillaceous Hershey limestone (Gray,

1952) and the Martinsburg shale. This cleavage is warped and folded, showing that subsequent stress was released along these planes rather than along bedding planes. Folds affecting the flow cleavage are superposed on preexisting folds in the argillaceous rocks, and slip cleavage has developed that is about parallel to the axial planes of the folds of the flow cleavage. Many of the thrust faults that can be recognized in outcrop are parallel to the slip cleavage, and these faults commonly extend along the crests of arches in the flow cleavage. These folds are certainly younger than the folds that affected the bedding, and it seems likely that they are post-Taconic.

The dips of the Silurian and Devonian beds, from their southernmost exposure at the Delaware Water Gap to the Pocono Plateau, are prevailingly northwestward. The regional dip is interrupted by several folds that are characterized by short southeast limbs. As one goes southeastward across these folds, one finds that the structural height of their successive crests increases, as if these folds were satellitic to a major anticline that once flanked them on the southeast. Linear elements in these rocks are nearly horizontal, but outcrop patterns indicate that the large folds in them plunge west-southwest. Folding becomes less intense toward the northwest, where the last mappable folds occur in the limestones of the Onondaga formation. There are asymmetric folds, too small to map, in the overlying Hamilton formation, but on the whole the rocks of this group are only gently flexed. The pre-Upper Devonian rocks have well-developed cleavage, which dip steeply southeastward and is nowhere rotated or folded.

Folds in the Silurian and Devonian rocks become tighter and even overturned along strike to the southwest, where they presumably pass into the structurally more complex terrane of the Wind Cap and Lehight Gap areas.

It can be seen from the above discussion that the rather simply folded Silurian and Devonian rocks overlie very complexly folded Ordovician rocks. Beerbower (1956), in describing the Ordovician-Silurian contact at the Delaware Water Gap, concluded that the Taconic disturbance was much less intense in this area than it was farther north and east. This conclusion, however, was based on the nearly parallel attitudes of the Shawangunk and Martinsburg formations in a single poor exposure. The fact is that the Martinsburg in this area was thrown into overturned and recumbent folds during the Taconic orogeny; in exposures both east and west of the contact described by Beerbower, beds have been rotated more than 180°, and Ordovician beds diverge at various angles from Silurian beds exposed nearby. The Ordovician-Silurian contact was folded after the deposition of the Devonian rocks, and the Martinsburg shale reaches the surface in several small anticlines along the southeastern slope of Kittatinny Mountain. The structural relations here are not yet fully understood, but as the Martinsburg farther south was sheared along its flow cleavage, the arches in this cleavage are probably parallel to anticlines in the beds of the Shawangunk formation.

In summary, the Taconic folding was very much stronger in this area than the post-Taconic folding, which was in fact rather gentle. During the later orogeny, pre-existing Taconic folds were deformed by folding that affected flow cleavage, and also by thrusting. The post-Taconic orogeny cannot be precisely dated, but it can probably be ascribed to the Appalachian disturbance.

REFERENCES

Beerbower, J. R., 1956, The Ordovician-Silurian contact, Delaware Water Gap, New Jersey: Pennsylvania Acad. Sci. Proc., v. 30, p. 146–149.

Behre, G. H., 1925, Taconic folding in the Martinsburg shales [abs.]: Geol. Soc. America Bull., v. 36, p. 157–158.

Gray, Carlyle, 1952, The high calcium limestones of the Annville belt in Lebanon and Berks Counties, Pennsylvania: Pennsylvania Geol. Survey, 4th ser., Progress Rept. 140, p. 4–5.

Miller, B. L., 1926, Taconic folding in Pennsylvania: Geol. Soc. America Bull., v. 37, p. 497–511.

Spieker, E. M., 1956, Mountain-building chronology and nature of geologic time scale: Am. Assoc. Petroleum Geologists Bull., v. 40, no. 8, p. 1769–1815.

Stose, G. W., 1930, Unconformity at the base of the Silurian in southeastern Pennsylvania: Geol. Soc. America Bull., v. 41, p. 629–658.

Woodward, H. P., 1957a, Structural elements of northeastern Appalachians: Am. Assoc. Petroleum Geologists Bull., v. 41, no. 7, p. 1429–1440.

——— 1957b, Chronology of Appalachian folding: Am. Assoc. Petroleum Geologists Bull., v. 41, no. 10, p. 2312–2327.

——— 1958, Ordovician and Silurian deformation at the northeast end of the Appalachian Basin [abs.]: Geol. Soc. America Bull., v. 69, no. 12, pt. 2, p. 1666.

81. LATE PALEOZOIC OROGENY IN EASTERN PENNSYLVANIA CONSISTS OF FIVE PROGRESSIVE STAGES

By HAROLD H. ARNDT and GORDON H. WOOD, JR., Washington, D.C.

Deformation during the late Paleozoic Appalachian orogeny is recorded by structural features in rocks of Cambrian to Pennsylvanian age in eastern Pennsylvania. The orogeny began after rocks of Pennsylvanian age were consolidated and prior to deposition of rocks of Late Triassic age. Moderately folded rocks are present in the Allegheny and Pocono plateaus. Strongly folded and faulted rocks occur in the Ridge and Valley province, and rocks in the Great Valley are even more complexly deformed. Although part of this complex deformation in the Great Valley is attributable to the Taconic disturbance of early Paleozoic age, it has been long recognized that the structural complexity of rocks effected by the Appalachian orogeny increases southeastward across these areas. The increase is most noticeable across the Anthracite region of eastern Pennsylvania which lies principally in the Ridge and Valley province, but also includes parts of the Allegheny and Pocono plateaus (fig. 81.1). Detailed studies in the Anthracite region and interpretation of data on the Great Valley (Gray, 1959) show that the structural features formed progressively in a sequence; this sequence is here classified on the basis of the increasing complexity of these features into five structural stages as follows:

1. Folding of horizontal strata into broad anticlines and synclines.
2. Low-angle thrusting and imbricate faulting, followed by formation of subsidiary folds on the larger folds to develop anticlinoria and synclinoria. Additional low-angle thrusting followed by high-angle thrusting accompanied the subsidiary folding.
3. Folding of low-angle and high-angle thrusts, and offsetting of pre-existing structural features by high-angle thrusts.
4. Development of overturned folds, and offsetting of overturned folds by tear faults and high-angle thrusts.
5. Development of recumbent folds and nappes. In this sequence it is obvious that an area with structural features of stage 5 had previously undergone deformation attendant with each of the preceding stages.

CONCEPT OF PROGRESSIVE DEFORMATION

Much speculation persists as to the relative times and the sequence of structural events during the Appalachian orogeny in eastern Pennsylvania. The authors believe that all structural features were formed during a single orogeny, and that orogenic forces were continuously transmitted through the Anthracite region from southeast to northwest with gradually increasing intensity so that the strata in the southeastern part of the region were deformed before those in the northwestern part. The simple folds of stage 1, therefore, probably formed in the southeastern part of the region before they did in the northwestern part. Further, the complicated folds and faults of stage 4 in the southeastern part of the region probably formed simultaneously with the simple folds of stage 1 in the northwestern part. Thus, deformation resulting from the Appalachian orogeny apparently was progressive both temporally and geographically.

AREAL DISTRIBUTION OF STRUCTURAL STAGES

From north to south the Anthracite region and Great Valley are divisible on the basis of increasing complexity of structural features into five geographic areas corresponding with the five stages.

The features in the northwestern part of the Anthracite region consists of large symmetrical open folds of stage 1 (fig. 81.1). In the north-central part of the region the principal features are anticlinoria and synclinoria composed of en echelon symmetric and asymmetric subsidiary folds that are commonly broken by folded low-angle and high-angle thrusts. Features of stage 2 are superimposed on folds of stage 1 in this part of the region.

Features indicative of stage 3 occur in the south-central part of the region. Here the folds and faults formed during the preceding two stages were further folded and offset by high-angle thrusts.

The overturned folds, tear faults, and high-angle thrusts of stage 4 are present in the southernmost part of the Anthracite region. Folds and faults that formed there during the preceding three stages were intensively deformed.

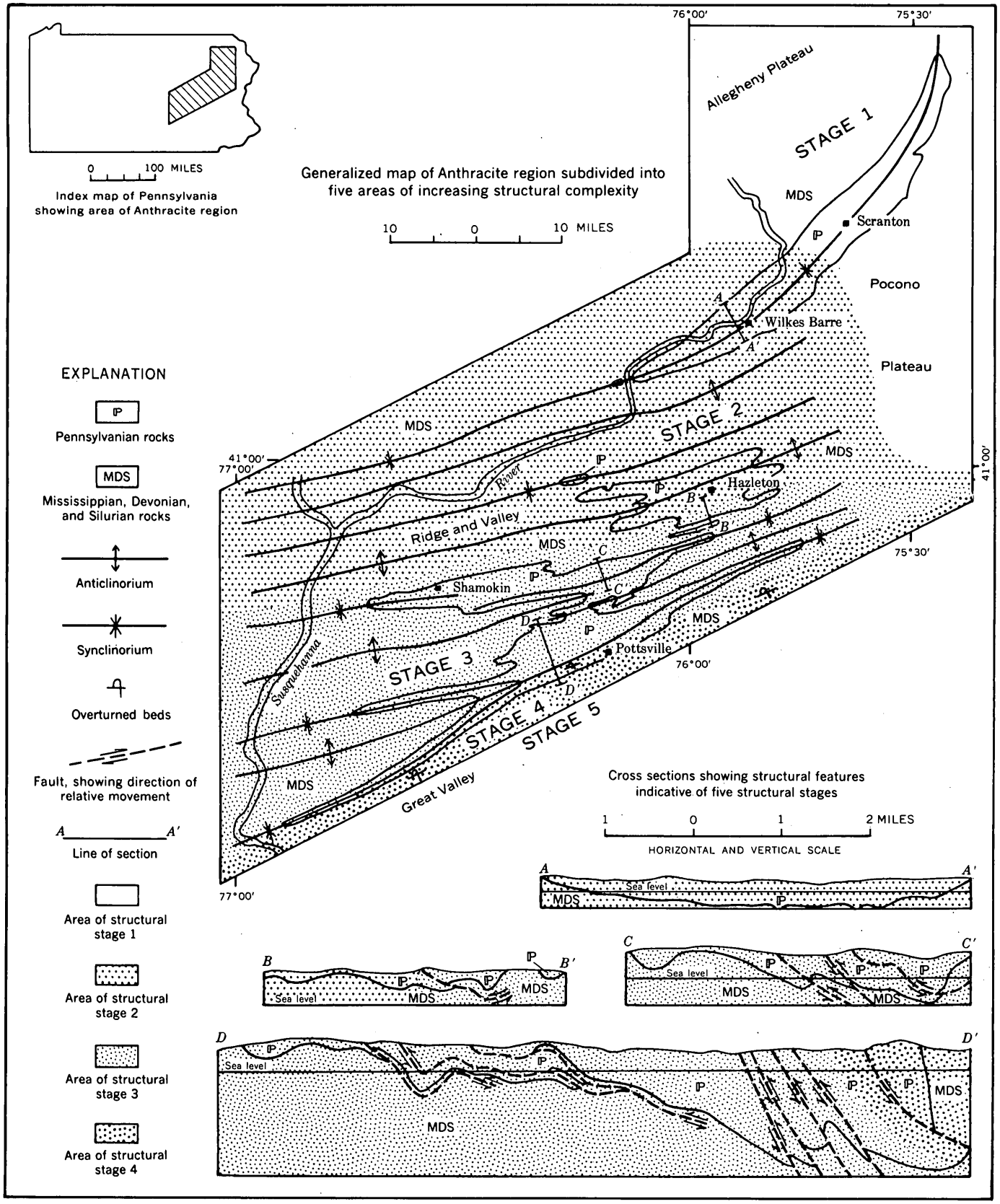

FIGURE 81.1.—Generalized map and cross sections of the Anthracite region, subdivided into five stages which are defined on the basis of structural complexity.

Small to large recumbent folds and nappes of stage 5 occur in the Great Valley, south of the Anthracite region. These structural features were probably superimposed on less complex features formed during the Taconic disturbance.

Some local areas did not undergo the stage of deformation that would be suggested by their geographic location, and others advanced beyond the stage indicated. These apparent discrepancies are explainable, however, because the varying structural competency of stratigraphic units and other stratigraphic and structural complications locally retarded or concentrated the stress, so that the resultant features were either less complicated or more complicated than normal for their geographic location.

CONCLUSIONS

The Appalachian orogeny in eastern Pennsylvania proceeded through a sequence of five structural stages. In the Anthracite region, the areas of most complex structures to the southeast underwent each of the first four stages of deformation, whereas the least intensively deformed area to the northwest was subjected only to the last orogenic force and contains features characteristic of only the first stage of deformation. The process of structural evolution appears to have been continuous and the result of a single orogeny that was not necessarily punctuated by pulsations.

REFERENCE

Gray, Carlyle, 1959, Nappe structures in Pennsylvania [abs.]: Geol. Soc. America Bull., v. 70, no. 12, pt. 2, p. 1611.

82. DIFFERENTIAL SUBSIDENCE OF THE SOUTHERN PART OF THE NEW JERSEY COASTAL PLAIN SINCE EARLY LATE CRETACEOUS TIME

By James P. Minard and James P. Owens, Washington, D.C.

Even the small-scale geologic map of the State of New Jersey reveals that there is a progressive easterly shift in strike of the successively younger formations of the coastal plain (fig. 82.1 and table 82.1). Recent detailed mapping in four 7½-minute quadrangles southeast of Trenton (fig. 82.1) corroborates this fact, and yet surprisingly, most workers have failed to recognize it or have passed it over without comment. Recognition of this shift, however, has a far-reaching effect on interpretation of the geology of this region,

Table 82.1.—*Average attitudes and contact relations of the Late Cretaceous to Pliocene(?) formations southeast of Trenton*

Age	Series or group	Formation	Symbol	Average strike (degrees)	Average dip (SE) in feet per mile	Basal contact relations
Tertiary	Pliocene(?)	Cohansey sand	Tch	N72E	10	Unconformable.
	Miocene(?)	Kirkwood	Tkw	N70E	18	Do.
	Rancocas	Manasquan	Tmq	N62E	25	Do.
		Vincentown	Tvt	N56E	30	Do.
		Hornerstown sand	Tht	N53E	45	Do.
Late Cretaceous	Monmouth	Red Bank	Krb	N47E	35	Conformable.
		Navesink	Kns	N47E	35	Unconformable.
		Mount Laurel sand	Kml	N47E	35	Do.
	Matawan	Wenonah	Kw	N46E	35	Conformable.
		Marshalltown	Kmt	N46E	35	Unconformable.
		Englishtown	Ket	N45E	38	Do.
		Woodbury clay	Kwb	N44E	40	Conformable.
		Merchantville	Kmv	N44E	40	Unconformable.
		Magothy	Km	N42E	42	Do.
		Raritan	Kr	N40E	60+	Do.

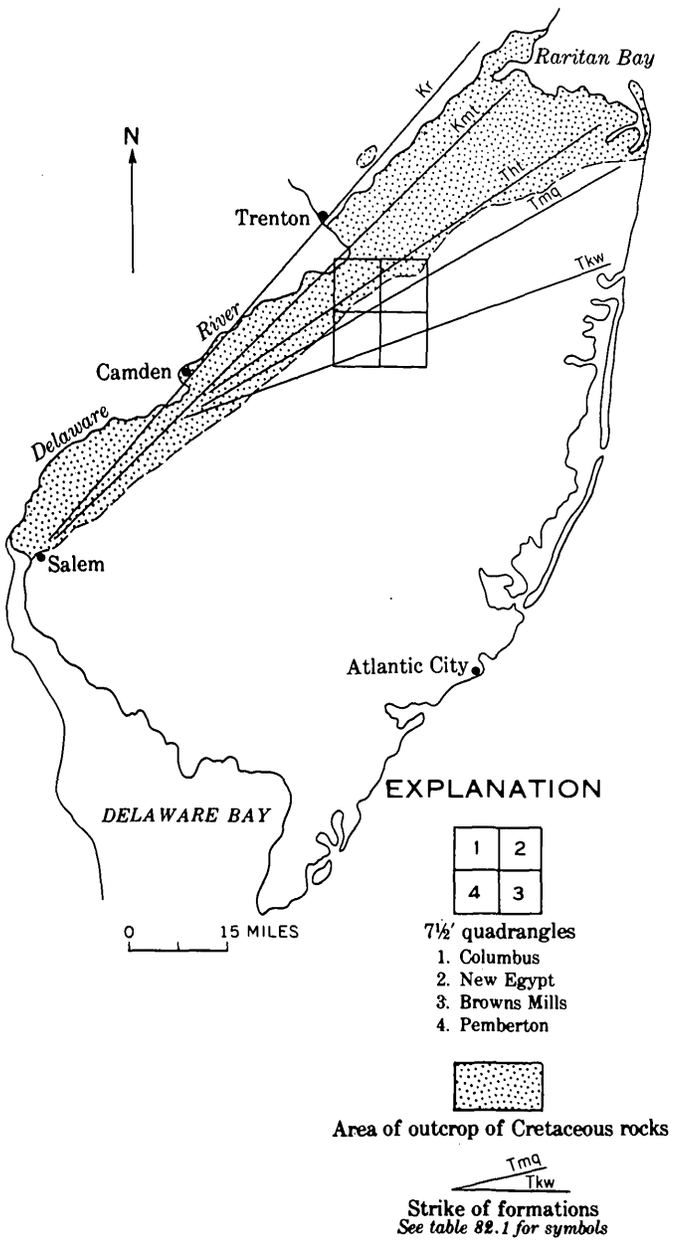

FIGURE 82.1.—Map of the coastal plain in New Jersey.

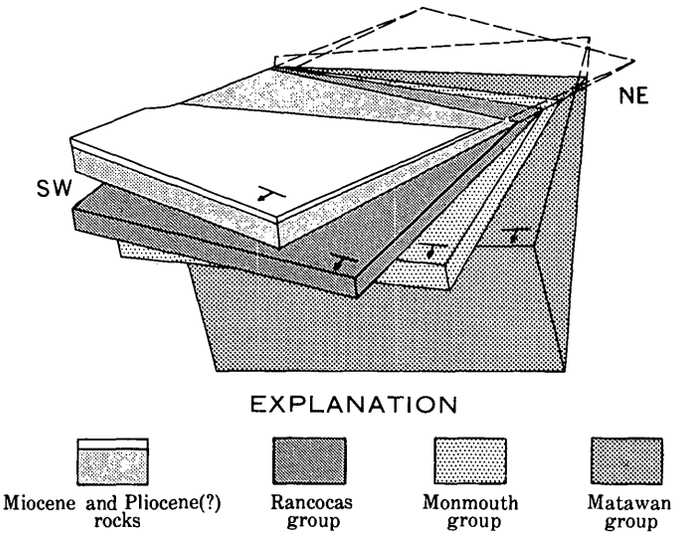

FIGURE 82.2.—Block diagram of several groups of formations in the New Jersey coastal plain. Thickening down dip is a result of subsidence during deposition. Erosion of the uplifted northeast part exposed thicker down dip facies or sections of the Cretaceous and early Tertiary formations in this region. Erosion exposed thicker down dip facies or sections of the two youngest formations in the southwest during Pleistocene uplift.

TABLE 82.2.—*Average thicknesses of formations in different parts of the New Jersey coastal plain*

Formation	Average outcrop thickness (feet) near Camden and Salem	Average outcrop thickness (feet) SE of Trenton	Average outcrop thickness (feet) at or near Raritan Bay	Direction in which formation thickens in outcrop	Downdip (SE) thickness compared with outcrop thickness
Cohansey	200±	200±	50±	SW	Nearly the same.
Kirkwood	120	60	30?	SW	Thicker.
Manasquan	15	40	60	NE	Do.
Vincentown	25	55	100	NE	Do.
Hornerstown sand.	20	30	30	NE	Do.
Tinton sand	0	0	20	NE	Do.
Red Bank	0	0–50	140	NE	Thinner?
Navesink	10	20	40	NE	(?).
Mount Laurel sand.	(?)	20	20	(?)	Thicker.
Wenonah	(?)	20	20	(?)	Do.
Marshalltown	35	35	35?	(?)	Do.
Englishtown	20	45	140	NE	Do.
Woodbury clay	50	50	50?	(?)	Do?.
Merchantville	48	60	60?	NE	Do.
Magothy	25	30	120	NE	Do.
Raritan	300?	300?	300?	(?)	Do.

being particularly helpful in assessing the role of facies changes both along strike and down dip. Our explanation of the shift is based on the following facts:

1. Nearly all the pre-Quaternary coastal plain formations thicken down dip or basinward, generally in a southeasterly direction (figure 82.2 and table 82.2), and the older formations generally dip progressively more steeply than the younger formations (table 82.2).
2. Most formations are thicker and wider in outcrop in the northeastern part of the coastal plain than in the southwestern part (fig. 82.1 and table 82.2).
3. More unconformities are present in the stratigraphic sequence than had been previously recognized (table 82.1).

557753 O—60——13

4. Marine planation was the dominant eroding agent throughout the area considered. This is suggested by the reworked sediments and marine fossils in the bases of the formations, and by the absence of subaerial weathering.

In the light of these facts, the simplest explanation for the progressive changes in strike is the presence of a large downwarp south of the New Jersey coastal plain, possibly near Delaware Bay, accompanied by differential uplift in the northern part of the coastal plain.

Downwarping while deposition was going on explains the sediments' thickening basinward—to the south and southeast. Subsequent marine planation, especially in the northeastern part of the coastal plain, eroded the nearshore facies of the sediments, exposing the thicker offshore facies or section.

Repeated cycles of deposition and marine planation during Late Cretaceous and early Tertiary time are indicated by the fact that most of the contacts between formations are unconformable. Throughout this time the locus of downwarping migrated westward, and therefore each younger formation was laid down on a surface that sloped more nearly southward than the surface underlying the next older formation, and the strike of each younger formation is more easterly than that of the formation beneath it.

The direction of downwarping was reversed at some time in the Pleistocene, and in the western and southwestern parts of the coastal plain, the Kirkwood and Cohansey formations were much eroded. The thicker offshore facies, particularly of the Kirkwood, were exposed, and outcrops of this formation consequently show a thickening toward the southwest.

Recognition of the progressively more eastward strike of the younger formations, and of the basinward thickening along outcrops, helps to explain the changes in the lithology of the formations along their strike. The glauconite and quartz sand of the Marshalltown formation near Camden is probably a nearshore facies, whereas the clay in the formation near Raritan Bay is probably an offshore facies. Similarly the thick clay in the Kirkwood formation near Salem is probably an offshore facies, whereas the sand and small pebbles in the formation east of Trenton suggest a near-shore facies.

83. DROWNED VALLEY TOPOGRAPHY AT BEGINNING OF MIDDLE ORDOVICIAN DEPOSITION IN SOUTHWEST VIRGINIA AND NORTHERN TENNESSEE

By Leonard D. Harris, Washington, D.C.

A disconformity between the Lower Ordovician part of the Knox group and the overlying Middle Ordovician rocks in southwest Virginia and northern Tennessee is widely recognized. Several authors (Cooper and Prouty, 1943, p. 823; Rogers and Kent, 1948, p. 32; Miller and Fuller, 1954, p. 67; and Bridge, 1955, p. 727) reported as much as 200 feet of relief on this surface. Because of the subtle nature of the topography on this disconformable surface a regional paleogeomorphic pattern has not been generally recognized or described. This paper briefly discusses the regional pre-Middle Ordovician paleogeomorphology in Lee County, Va., and northern Claiborne and Hancock Counties, Tenn. (fig. 83.1). In these counties the Lower and Middle Ordovician rocks dip from 15° to 35°. The outcrops are thus restricted to narrow northeast-trending belts, and, consequently, only profiles parallel to the regional strike can be drawn. Control for construction of these profiles is based on measured sections and detailed field mapping of key beds between sections.

GENERAL GEOLOGY AND PALEOGEOMORPHOLOGY

Detailed mapping and section measuring of the rocks below and above the disconformity indicate that the Lower Ordovician rocks were relatively flat lying at the time of erosion of the disconformable surface. Key beds that are cut out where valleys were eroded into the Lower Ordovician rocks retain their same stratigraphic position under highs on that surface. In general, the bedding of the Middle Ordovician rocks is parallel to that of the underlying Knox group, but locally the lower beds of the Middle Ordovician are draped nearly parallel to the slopes, and dip away at a small angle.

Subaerial erosion of the surface on the Knox group was long enough to have removed a maximum of 170 feet of dolomite, and to have developed a residuum of

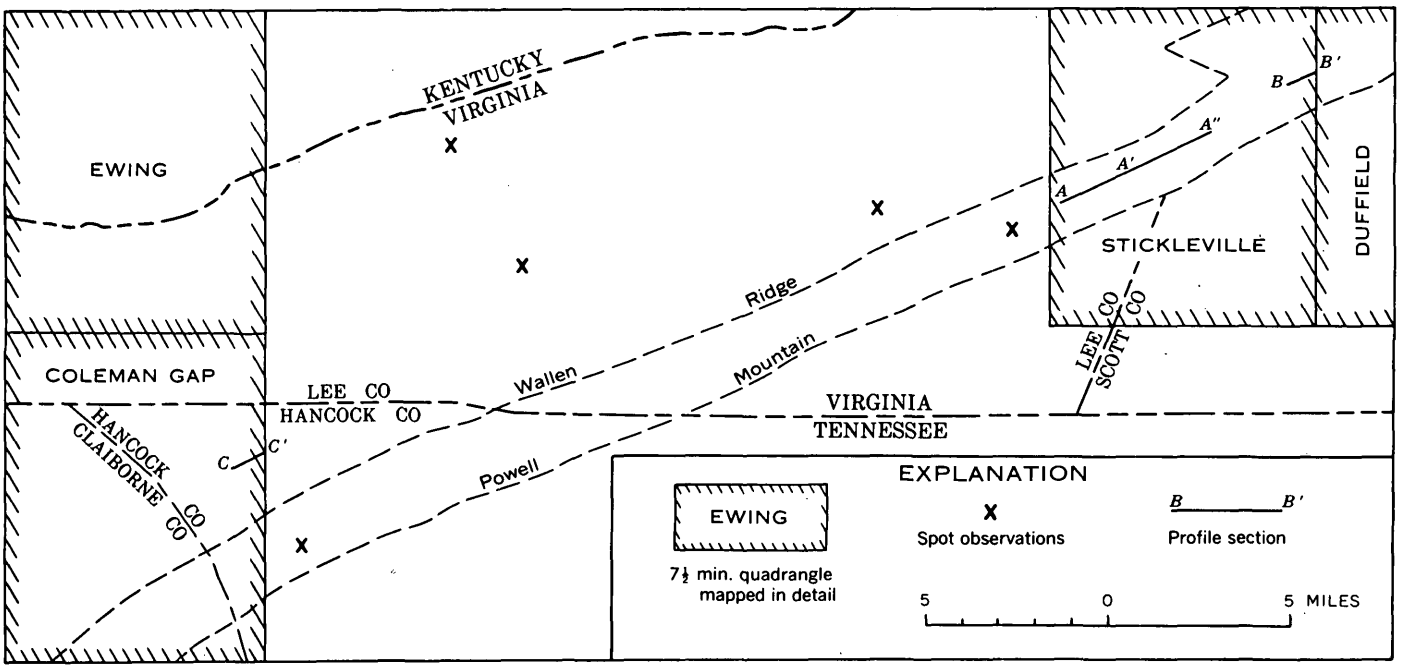

FIGURE 83.1.—Map of southwestern Virginia and northern Tennessee showing areas of detailed mapping, single points of observation, and location of profile sections.

unknown thickness. The residuum included the insoluble constituents in the dolomite, namely, clay, sand, and chert. There is some evidence to suggest that a soil profile was developed on the dolomite. This profile may have included an upper oxidized zone; at least the oldest deposits, which occur only in the lowest parts of the valleys, are invariably grayish-red dolomitic shale with some coarse clastic material. The very limited distribution of this grayish-red shale suggests that, upon submergence, red clay was the first sediment winnowed from the residuum.

The topography carved on top of the Lower Ordovician rocks is one of rolling hills and, in general, broad valleys (fig. 83.2). Relief ranges from about 100 feet to a maximum of 170 feet. Locally, some slopes are relatively steep; as shown in profile section *C–C'* (fig. 83.2), in the southwest part of the area, the west side of one valley was a nearly vertical cliff 110 feet high.

The ancient topography resembles a nearly mature coastal plain very near sea level. If this plain bordered on old land of greater relief, the area of investigation must have been far removed from the old land, because the first deposits above the disconformity were locally derived from the residuum developed on top of the Lower Ordovician rocks. These basal deposits, which range from 1 to 40 feet in thickness, include clay, small amounts of sand, and abundant fragments of chert and dolomite. Limestone, about 1,500 feet thick, overlies this reworked residuum.

During Middle Ordovician time, as this gently rolling plain was inundated by the sea, the coastline must have been quite irregular, and its appearance was that of a submerged coastal plain with many drowned valleys. The submergence probably was relatively constant and rapid, but not rapid enough to keep wave action from winnowing the residuum developed on the erosion surface. Winnowing separated the clay and small amounts of fine chert fragments and sand from the hill tops and partly filled the intervening valleys. The coarser pieces of chert and dolomite were concentrated as a lag deposit on the hill slopes and tops. Wave action was not intense enough to round the larger pieces (fig. 83.3) or to materially modify the topography.

REFERENCES

Bridge, Josiah, 1955, Disconformity between Lower and Middle Ordovician series at Douglas Lake, Tennessee: Geol. Soc. America Bull., v. 66, p. 725–730.

Cooper, B. N., and Prouty, C. E., 1943, Stratigraphy of the Lower Middle Ordovician of Tazewell County, Virginia: Geol. Soc. America Bull., v. 54, p. 819–886.

Miller, R. L., and Fuller, J. O., 1954, Geology and oil resources of the Rose Hill district—the fenster area of the Cumberland overthrust block—Lee County, Virginia: Virginia Geol. Survey Bull. 71, 283 p.

Rogers, John, and Kent, D. F., 1948, Stratigraphic section at Lee Valley, Hawkins County, Tennessee: Tennessee Div. Geol. Bull. 55, 47 p.

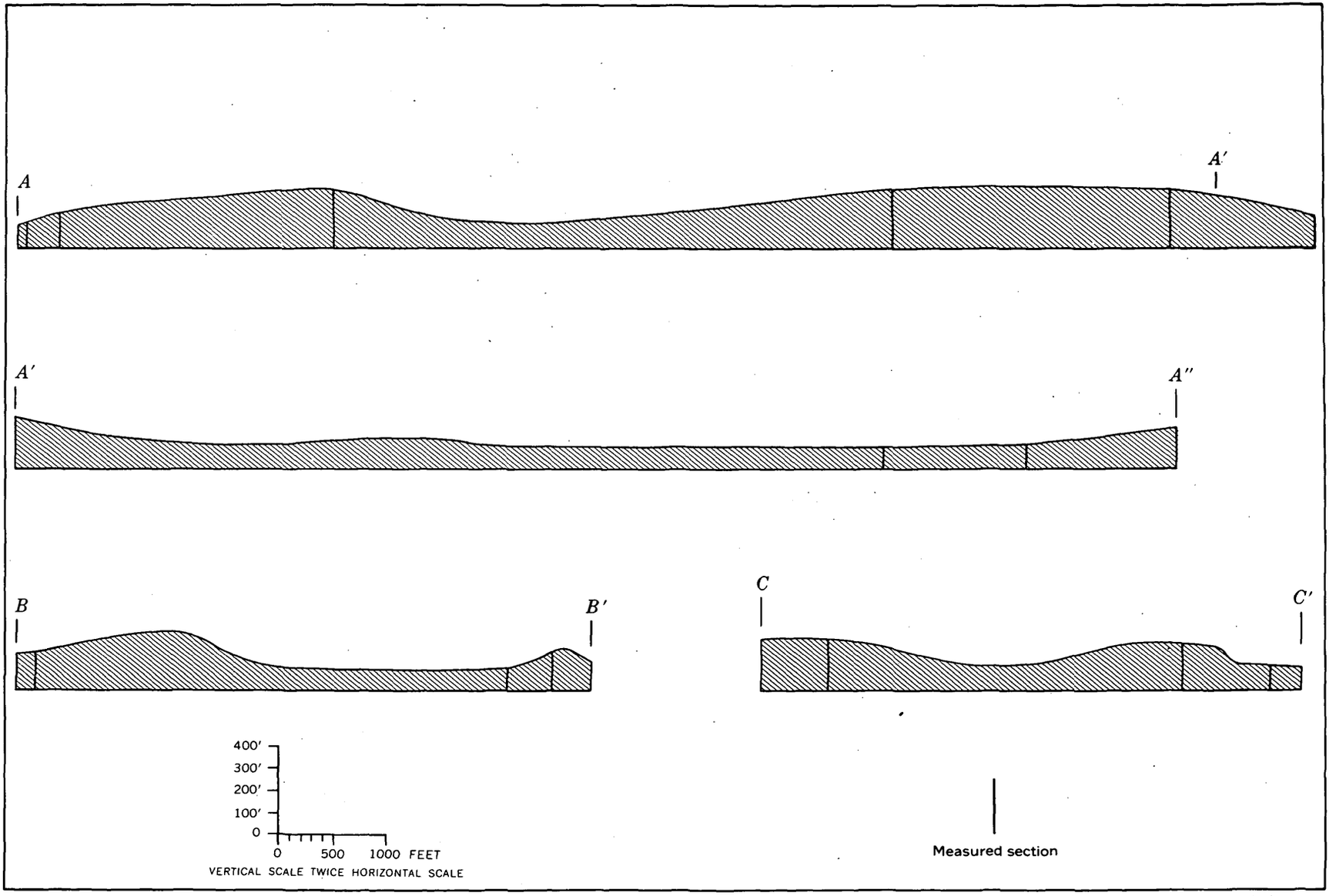

FIGURE 83.2.—Profiles of the disconformity on the top of Lower Ordovician rocks in southwestern Virginia and northern Tennessee. Control based on measured sections and detailed mapping of key beds between sections.

FIGURE 83.3.—Middle Ordovician conglomerate just above disconformity at the top of the Lower Ordovician. Most of the conglomerate is angular but a few pieces are subrounded. Scale is indicated by pencil in upper right of photograph.

84. A SYNTHESIS OF GEOLOGIC WORK IN THE CONCORD AREA, NORTH CAROLINA

By HENRY BELL III, Beltsville, Md.

Geochemical and heavy-mineral reconnaissance (Overstreet and Bell, 1960; Bell and Overstreet, 1960) in deeply weathered crystalline rocks of the Piedmont Plateau near Concord, N.C., has shown a more extensive distribution of gold, scheelite, and possibly base metals than had previously been recognized. The results of the reconnaissance, combined with geologic mapping, aeromagnetic surveys, and interpretation of soil maps, indicate that this distribution can be related to several geologic events in the Concord area that are common to the Piedmont as a whole.

The Concord area is partly in the region of fractured, sheared, and intruded plutonic rocks that P. B. King (1955, p. 346–350) named the Charlotte belt, and partly in the northeast-trending sedimentary and volcanic rocks of the Carolina slate belt, which lies to the east (fig. 84.1).

In the Concord area the rocks of the Charlotte belt consist of granitic and granodioritic gneisses, massive, and foliated dioritic and mafic rocks, and small bodies of granite. Some of the granite bodies are coarse grained, and one pluton of circular outline which extends into the northern part of the area consists of porphyritic granite. These rocks are cut by many dikes mostly of andesite, pyroxenite, granite, pegmatite, syenite, and lamprophyres. The largest dikes, which consist of light-colored coarse-grained augite syenite, form a partial ring structure near the center of the area. The ring structure is not so complete as it was thought to be by LeGrand and Mundorff (1952). Closely associated with the syenite is a large mass of coarse-grained hornblende gabbro.

Gold has been mined from placers and veins in this region since 1799 (Pardee and Park, 1948, p. 27–29). Vein deposits containing gold, scheelite, and base metals have recently been explored (Jones and Peyton, 1950) around the Furniss mine. These deposits are near the contact of the sedimentary and volcanic rocks of the Carolina slate belt with massive and foliated dioritic and mafic rocks of the Charlotte belt. In the Concord

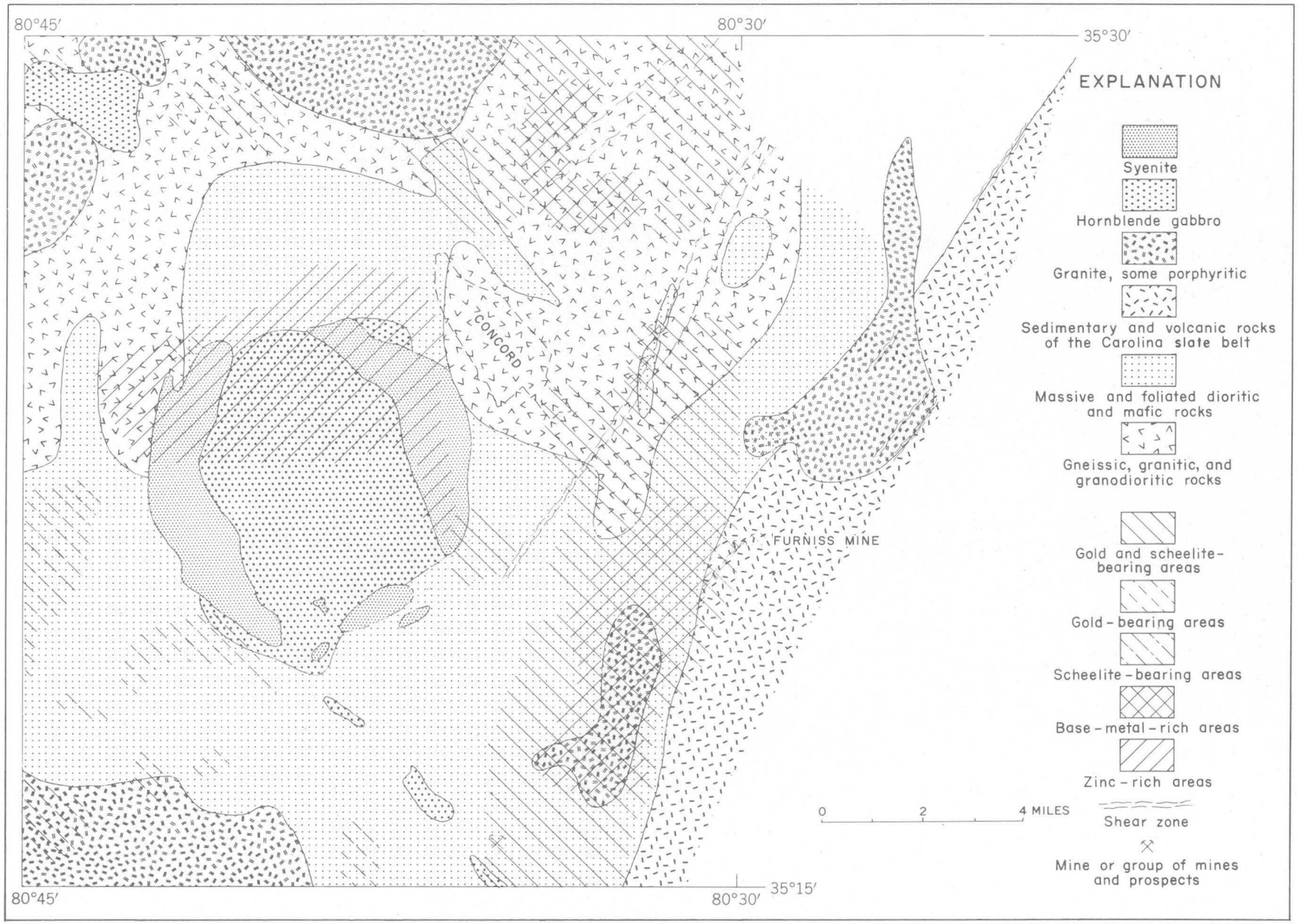

FIGURE 84.1.—Geologic map showing results of geochemical and heavy-mineral reconnaissance in the Concord area, N.C.

area there are several zones of shearing near this contact and in the Gold Hill district about 15 miles northeast the contact between the slates and plutonic rocks is a fault (Laney, 1910, p. 68–71).

Results of the heavy-mineral and geochemical reconnaissance are superimposed on the geologic map in figure 84.1 as patterns showing the distribution of gold, scheelite, and base metals. Gold and scheelite were recognized visually in 87 heavy-mineral concentrates panned from alluvium collected in streams having drainage areas of 0.1 to 1.5 square miles. Amounts of copper, lead, zinc, and molybdenum in samples of alluvial clay and silt, collected at essentially the same localities as the concentrates, were determined in the Geochemical Exploration laboratory by rapid methods (Lakin, Almond, and Ward, 1952). Only those areas are shown in figure 84.1 in which the base metals show closely grouped values of at least 0.006 percent more Cu, 0.002 percent Pb, and 0.005 percent Zn. The distribution of base metals and scheelite in the southwest 7½′ quadrangle and eastern third of the area is not known.

Geochemical and heavy-mineral reconnaissance in the Concord area has shown that the gold, scheelite, and rocks containing base metals are not restricted to the vicinity of the contact between the Charlotte belt and the Carolina slate belt, or even to the zones of shearing now recognized. Gold and scheelite are widely distributed in areas underlain by granitic and granodioritic gneisses, massive and foliated dioritic and mafic rocks, and the volcanic and sedimentary rocks of the Carolina slate belt where they are cut by intrusive rocks. Gold and scheelite have not been found in alluvium from streams that drain areas underlain only by the syenite-gabbro complex.

A large area in which samples of alluvium show high values for zinc alone coincides closely with the outcrop of a complex of coarse-grained augite syenite and hornblende gabbro. This complex is probably younger than the granite, and no granite dikes are known to cut it (Bell and Overstreet, 1959, map). Aeromagnetic surveys indicate that the complex is a steep-sided intrusive body (R. W. Johnson, oral communication, 1959). The base-metal content of magnetite separated from heavy-mineral concentrates panned from alluvium in streams draining the complex was examined and analyzed by P. K. Theobald, Jr., and C. E. Thompson of the Geological Survey, who found comparatively high values for zinc in concentrates from the areas where higher than average values for zinc occur in alluvial clay and silt. In other areas the base-metal content of magnetite is characteristically different and apparently does not show a close relationship with that in the alluvium. It may thus be possible, in places where the alluvium is found to be rich in zinc, to determine by analysis of the magnetite whether the zinc was derived from syenite or from granite.

The results of geochemical and heavy-mineral reconnaissance in the Concord area suggest that two periods of metallization have occurred there, resulting in different concentrations of metals and associated with different rocks. The earlier and more widespread metallization is characterized by gold, tungsten, and base metals, perhaps derived from veins related to small granite plutons. The second, characterized by zinc, seems to be closely related to the syenite-gabbro complex. No syenite-gabbro complexes have been found elsewhere in North Carolina, but there may be one or more in South Carolina near the Georgia border (Overstreet and Bell, Art. 87).

REFERENCES

Bell, Henry 3d, and Overstreet, W. C., 1959, Relations among some dikes in Cabarrus County, North Carolina: South Carolina State Devel. Board, Div. Geology, Geol. Notes, v. 3, no. 2, p. 1–4.

——— 1960, Geochemical and heavy-mineral reconnaissance of the Concord quadrangle, Cabarrus County, North Carolina: U.S. Geol. Survey Mineral Inv. Field Studies Map MF 234.

Jones, J. O., and Peyton, A. L., 1950, Investigation of Furniss tungsten deposits, Cabarrus County, North Carolina: U.S. Bur. Mines Rept. Inv. 4724, p. 1–14.

King, P. B., 1955, A geologic section across the southern Appalachians—an outline of the geology in the segment in Tennessee, North Carolina, and South Carolina, *in* Russell, R. J., ed., Guides to southeastern geology: Geol. Soc. America, p. 332–373.

Lakin, H. W., Almond, Hy, and Ward, F. N., 1952, Compilation of field methods used in geochemical prospecting by the U.S. Geological Survey: U.S. Geol. Survey Circ. 161, p. 1–34.

Laney, F. B., 1910, The Gold Hill mining district of North Carolina: North Carolina Geol. Survey Bull. 21, 137 p.

LeGrand, H. E., and Mundorff, M. J., 1952, Geology and groundwater in Charlotte area, North Carolina: North Carolina Dept. of Conserv. and Devel. Bull. 63, 88 p.

Overstreet, W. C., and Bell, Henry 3d, 1960, Geochemical and heavy-mineral reconnaissance of the Concord SE quadrangle, Cabarrus County, North Carolina: U.S. Geol. Survey Mineral Inv. Field Studies Map MF 235.

Pardee, J. T., and Park, C. F., Jr., 1948, Gold deposits of the southern Piedmont: U.S. Geol. Survey Prof. Paper 213, 156 p.

85. AEROMAGNETIC AND AERORADIOACTIVITY SURVEY OF THE CONCORD QUADRANGLE, NORTH CAROLINA

By Robert W. Johnson, Jr. and Robert G. Bates, Knoxville, Tenn. and Washington D.C.

An airborne magnetic and radioactivity survey has been made of the Concord quadrangle, North Carolina, which, together with a small adjacent area to the east, lies in the Piedmont of central North Carolina. Complex geologic patterns are here obscured by extensive development of saprolite, and although various kinds of rocks are usually identifiable in the saprolite their areal distribution and relations are largely indeterminable. They give rise, however, to well-defined aeromagnetic and aeroradioactivity features, which help guide the geologic work now in progress.

The magnetic data are shown in figure 85.1 and the radioactive areas in figure 85.2. These areas were delineated by connecting the points of half-maximum value of the anomalous radioactivity appearing on three or more adjacent profiles.

The Concord quadrangle is partly in the Charlotte belt as defined by King (1955, p. 346–350) and partly in the Carolina slate belt (King, 1955, p. 343–346). In this quadrangle the principal rocks of the Charlotte belt are gneisses, massive and foliated mafic rocks, and small bodies of granite. All these rocks are cut by numerous dikes of several kinds of rock; the most extensive dikes consist of augite-syenite. The syenite bodies form a discontinuous ring structure roughly six miles in diameter, with a large body of gabbro in the center. The two largest syenite bodies, approximately 5 to 6 miles long, form the east and west sides of the structure. The southeast corner of the quadrangle is underlain by volcanic and sedimentary rocks of the Carolina slate belt. In the Gold Hill district, a few miles northeast of the Concord quadrangle, these rocks are in fault contact with the rocks of the Charlotte belt (Laney, 1910, p. 68–71).

The dominant magnetic feature of the quadrangle is a large and complex group of anomalies that approximately coincides with the area of the ring structure. The most extensive of these anomalies lie just within the gabbro at its contact with the syenite. At the south end of the main structure, several magnetic peaks over 3000 gammas in amplitude occur at the contacts of the central gabbro body with small discontinuous bodies of syenite. The central mass of gabbro is less magnetic than the contacts, as is shown by the pronounced magnetic depression at the center of the ring structure. The anomalies ringing the gabbro mass are probably caused by concentrations of magentite along the contacts between the gabbro and the syenite. More intense though much less extensive, anomalies lie just within the mapped outlines of the syenite. Some of these, at the north end of the western syenite body, may be due to an interfingering of the syenite and gabbro. The interfingering is probably similar to that indicated by the radioactivity data, though it seems more intricate. Two well-defined areas of high radioactivity are in good general agreement with the mapped outlines of the syenite, although the one farther east suggests that the form of the eastern syenite body is somewhat different from that indicated by preliminary geologic mapping (fig. 85.2). The large magnetic unit related to the ring structure has a southeastward extension that is underlain by coarse-grained hornblende gabbro not previously reported.

The area of high radioactivity north of the eastern syenite body coincides in part with a strong magnetic low. This relation suggests the presence of a rock mass not previously recognized.

A small area of high-intensity magnetic anomalies in the extreme northwest corner of the quadrangle has not been investigated. The most intense of these anomalies appears to be on or near the contact between a small mass of gabbro and the enclosing granite and gneiss. No anomalous radioactivity was found over the two small granite bodies in this area.

A narrow discontinuous magnetic trend composed mainly of 2000- and 2500-gamma closed contours extends from the northeast corner to the southwest corner of the quadrangle, where it terminates in a small but intense peak; this passes south of the ring structure anomaly. Siliceous metasedimentary rocks, including ferruginous quartzite and epidotized quartz-mica schist, have been found at several places along this trend.

The radioactivity data indicate four areas of high radioactivity along the eastern edge of the quadrangle. The northern one is between two shear zones and overlies gneissic granitic and granodioritic rocks. The other anomalous radioactive areas are not closely associated with any of the rock masses shown in figure 85.2, but may be related to shear zones or to the contact between the Charlotte belt and the Carolina slate belt. The eastern edge of the southern area closely follows this contact, and the other two are between the contact and a prominent shear zone. One of these radioactive areas has a pronounced arcuate outline, and so do the two

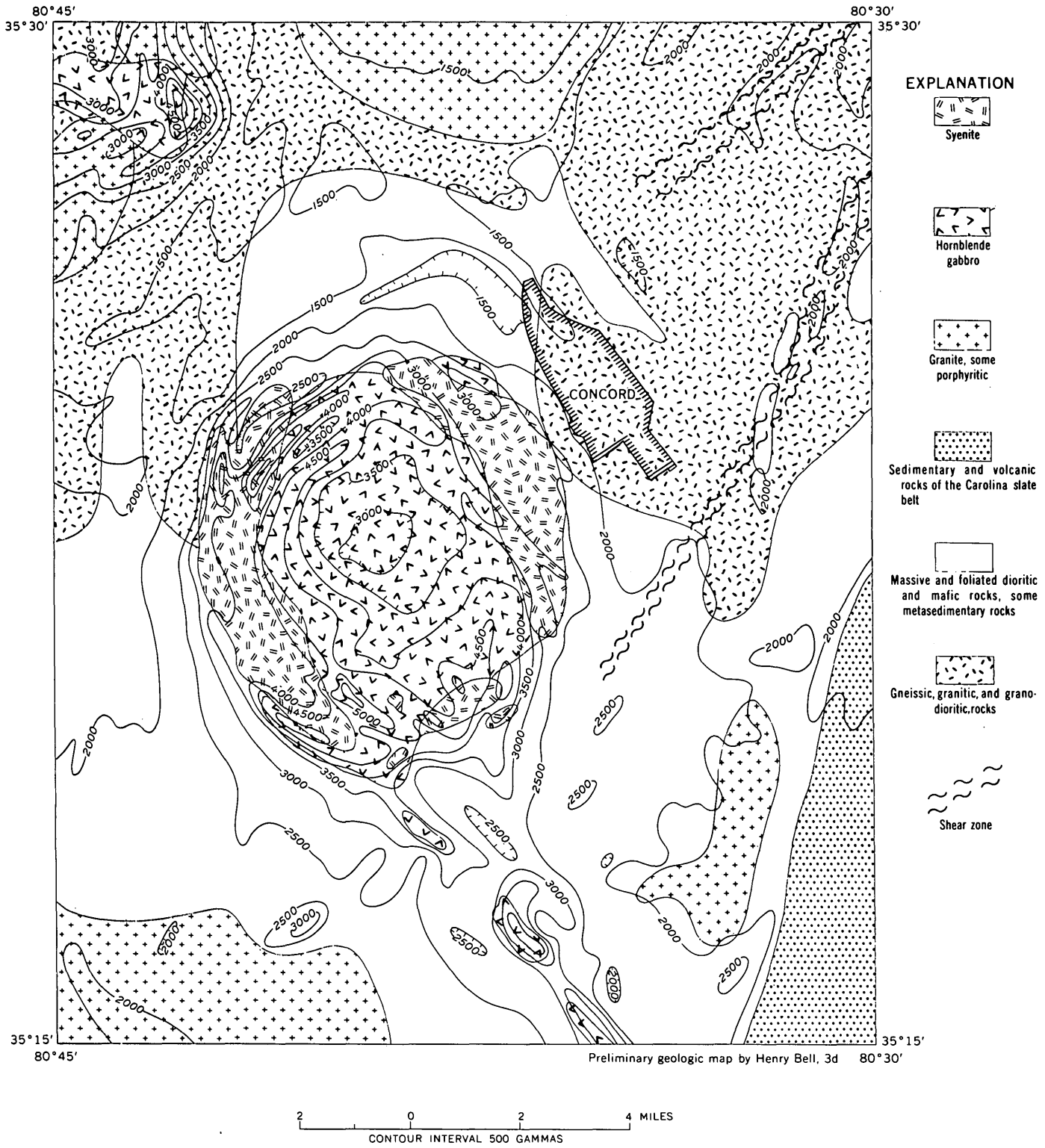

FIGURE 85.1.—Aeromagnetic and geologic map of the Concord quadrangle, North Carolina.

others taken together. These arcuate patterns suggest the possibility of ring fracturing or intersecting sets of fractures, though these have not yet been recognized in the field. Along the eastern edge of the area the similarity between the distribution of radioactivity and that of base metals and heavy minerals as determined by geochemical studies (Bell, Art. 84, fig. 84.1), indicate that these may be related.

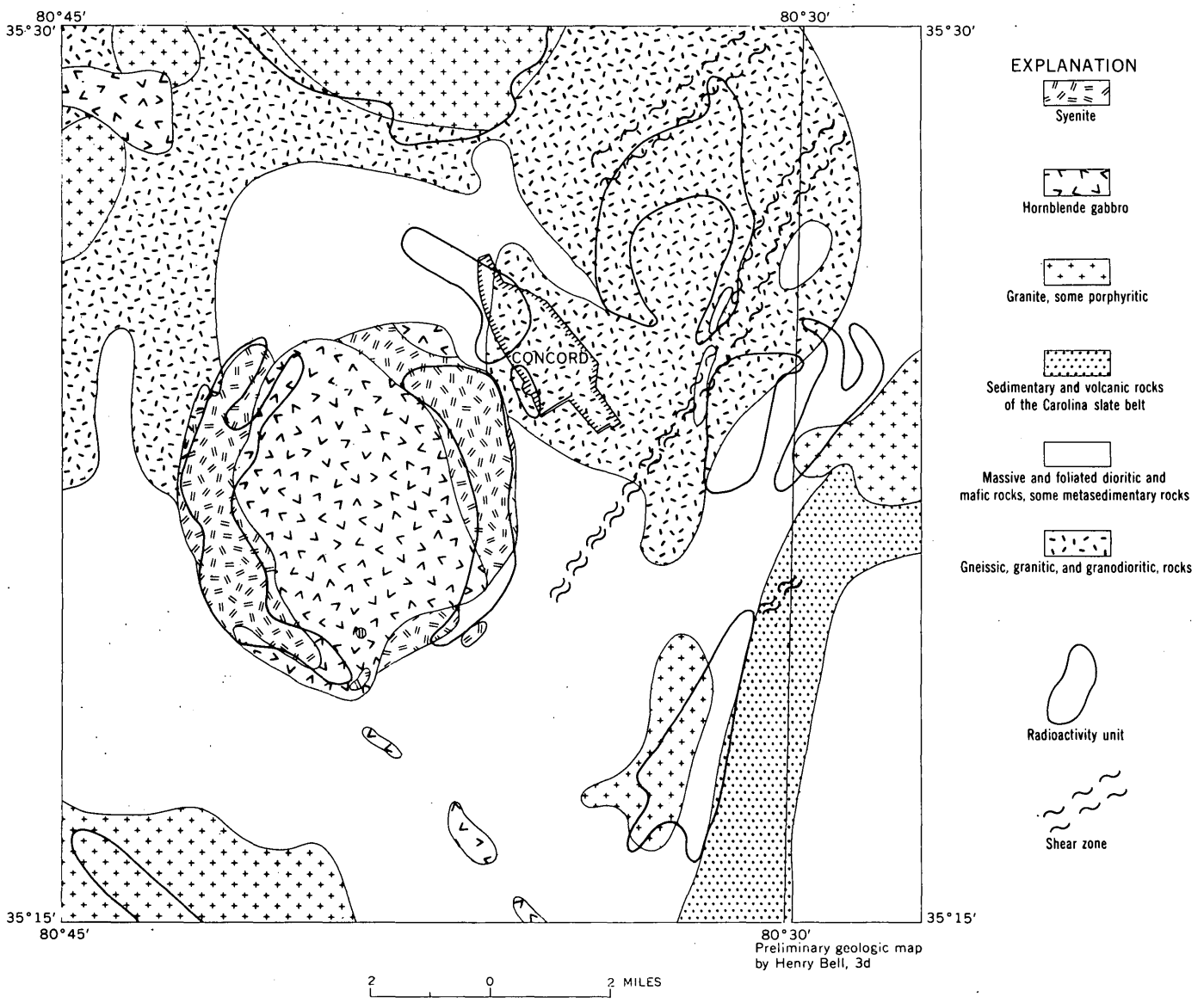

FIGURE 85.2.—Aeroradioactivity and geologic map, Concord area, North Carolina.

The borders of the radioactive area associated with the porphyritic granite along the northern edge of the quadrangle agree remarkably well with the mapped boundaries of the granite. The radioactivity level of this area is lower than that of those along the eastern edge of the quadrangle.

There is a small area of moderately intense radioactivity over the granite in the southwest corner of the quadrangle, but as this area is considerably less extensive than the mapped area of the granite it may represent local concentrations of radioactive minerals. The 2000-gamma magnetic contour line (fig. 85.1) coincides almost exactly with the outline of the radioactivity. This may be only coincidental, but it may indicate a change of lithology within the granite body, which has no distinctive geophysical expression at any other place where it has been mapped.

Our results may be summarized as follows: The radioactivity data are in excellent agreement with the mapped boundary of the porphyritic granite across the northern edge of the quadrangle. They are also in general agreement with the mapped outlines of the syenite bodies of the central ring structure. Both magnetism and radioactivity indicate possible interfingering of the syenite and gabbro at the northern end of the western syenite body. Most of the magnetic highs associated with the ring structure lie within the gabbro adjacent to the syenite-gabbro contact, which indicates that the magnetite causing the anomalies is localized along the contact. The areas of high radioactivity

along the eastern edge of the quadrangle do not appear to be associated with any particular type of rock; they may be related to prominent shear zones, or to base-metal and heavy-mineral concentrations along those zones, or to both.

REFERENCES

Bell, Henry, 3d, and Overstreet, W. C., 1959, Relations among some dikes in Cabarrus County, North Carolina: South Carolina Devel. Board, Div. Geology, Geol. Notes, v. 3, no. 2, p. 1–4.

King, P. B., 1955, A geologic section across the southern Appalachians—an outline of the geology in the segment in Tennessee, North Carolina, and South Carolina, *in* Russell, R. J., ed., Guides to southeastern geology: Geol. Soc. America, p. 332–373.

Laney, F. B., 1910, The Gold Hill mining district of North Carolina: North Carolina Geol. Survey Bull. 21, 137 p.

86. A MAJOR TOPOGRAPHIC LINEAMENT IN WESTERN NORTH CAROLINA AND ITS POSSIBLE STRUCTURAL SIGNIFICANCE

By JOHN C. REED, JR., and BRUCE H. BRYANT, Denver, Colo.

The Brevard belt is a narrow "dejective zone" (King, 1955) containing low-grade phyllites and schists and layers and lenses of recrystallized limestone (fig. 86.1). The belt has been traced for over 300 miles, from near Asheville, N.C., to its disappearance beneath Coastal Plain deposits in east-central Alabama. Keith (1905) interpreted these rocks as an infold of younger, less metamorphosed rocks, whereas Jonas (1932) interpreted them as retrogressively metamorphosed basement rocks. As mapped by Keith (1905), the belt turns north and fingers out a few miles southwest of the Grandfather Mountain window. Hamilton (1957) has shown, however, that what Keith mapped east of Asheville as fingers of Brevard belt rocks consist mainly of polymetamorphic schists formed by retrogressive metamorphism of adjacent higher grade rocks.

From a point southwest of Brevard to one 10 miles southeast of Asheville, the Brevard belt follows a pronounced topographic lineament which extends northeastward beyond the end of the belt as mapped by Keith; it passes northwest of Marion and just southeast of the Grandfather Mountain window, and extends down the valley of the Yakdin River at least as far as Elkin. Along the southeast side of the lineament, near Marion, lenses of marble resembling the crystalline limestone in the Brevard belt farther southwest have recently been found by Conrad (1959, and oral communication). East of Elkin, along the projected strike of the topographic lineament, is an area of quartzite, quartz schist, and marble about which little is known (Stuckey and Conrad, 1959). These are unusual rock types in the Piedmont, and their occurrence here may be related in some way to a structure expressed by the lineament.

In the course of mapping the Table Rock 15-minute quadrangle, the rocks along the lineament have been studied for about 16 miles northeastward along its course from a point north of Marion. Topographically the lineament is not as well defined in this segment as it is to the northeast and southwest, chiefly because no major stream flows along it. A zone of blastomylonites (first recognized by Stose and Stose, 1951) and other highly cataclastic rocks extends along the lineament continuously across the quadrangle. The blastomylonite zone has a slightly sinuous trace, and lies 0.8 mile to 1.5 miles southeast of the overthrust along the southeast side of the Grandfather Mountain window.

The rocks of the Inner Piedmont southeast of the blastomylonite zone are fine-grained well-layered biotite gneisses interlayered with biotite-muscovite schists, amphibole gneisses, and amphibolites. These rocks are all of amphibolite grade, but they clearly show polymetamorphic effects. They are intruded by concordant sill-like bodies of biotite-quartz monzonite of at least two types. Cleavage and layering are parallel in the metamorphic rocks; both strike northeast and dip 40° to 60° southeast, except for local reversals in the noses of tightly appressed isoclinal folds. Fold axes and an intense cataclastic lineation trend northeast-southwest, with low plunges in either direction.

The rocks between the blastomylonite zone and the Grandfather Mountain window are similar to those to the southeast, except that they show even more intense cataclastic effects and have undergone partial retrogressive metamorphism to the greenschist facies. Their cleavage is parallel to the axial planes of tight sheared-out isoclines in the layering, which generally strike northeast and dip 30° to 70° southeast. In places the

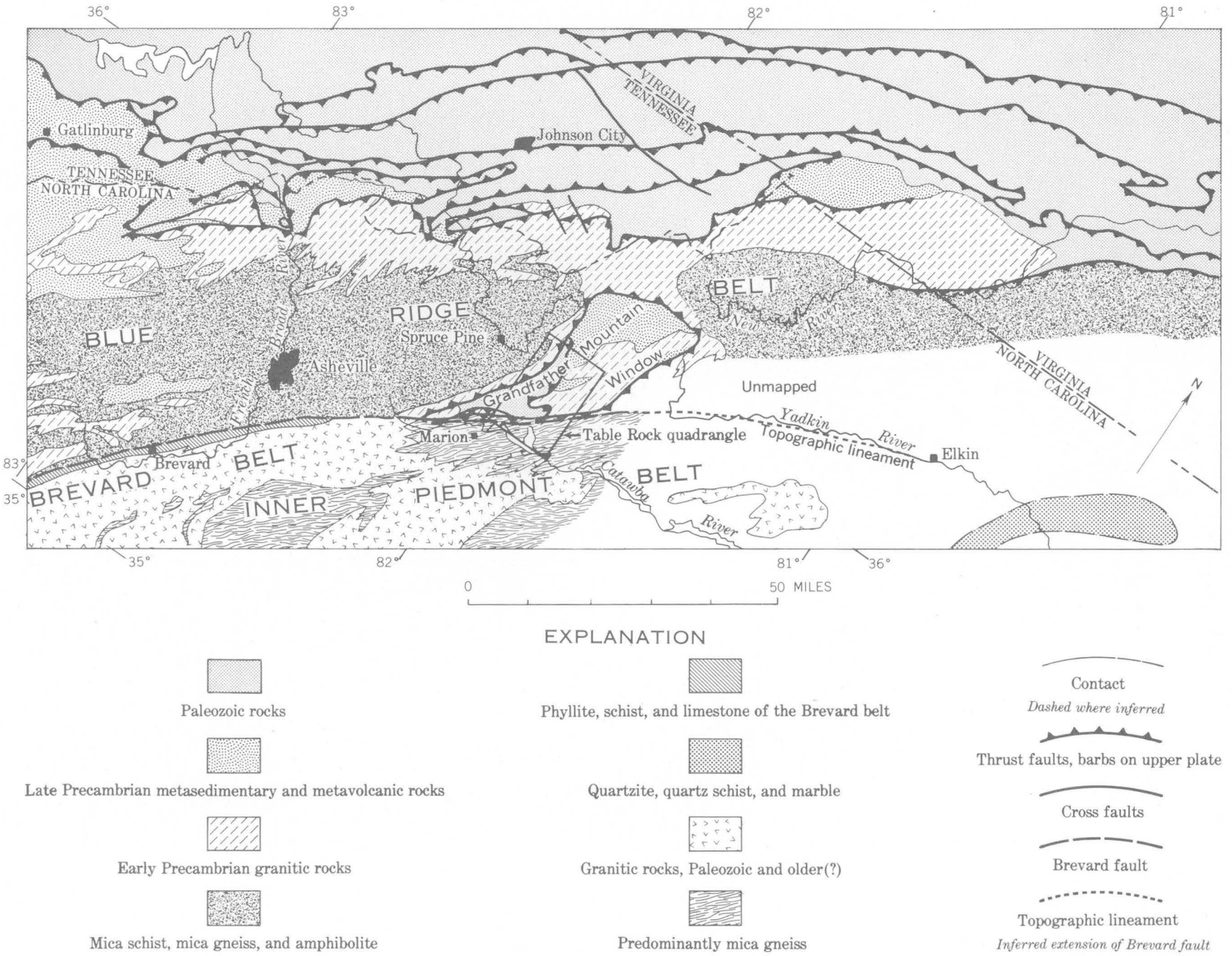

FIGURE 86.1.—Generalized geologic map of western North Carolina and adjacent parts of Virginia and Tennessee, showing location of the Brevard belt and its northeastern extension. Modified from King (1955), Geologic map of Virginia, 1928, Geologic map of North Carolina, 1958, and other sources.

cleavage and the limbs of the isoclines have been refolded, producing extremely complex structural patterns.

The lineament belt marks a rather abrupt change in the regional lineation pattern. Within the Grandfather Mountain window and in the rocks to the north and west a strong cataclastic "a" lineation trending northwest predominates. Near the southeastern boundary of the window this lineation swings to a north-south trend; the swing continues across the lineament belt to its southeastern edge, marked by the blastomylonite zone, where the lineation trends northeast, parallel to the regional lineation in the rocks of the Inner Piedmont.

The rocks of the Blue Ridge north and west of the Grandfather Mountain window are mica schists and gneisses, amphibolites, and amphibole gneisses, containing extensive areas of migmatitic granitic gneisses and massive granitic rocks. They differ from the Inner Piedmont rocks southeast of the lineament belt in the higher proportion of mica schist and amphibolite, in the more migmatitic aspect of many of the gneisses, in the character and structural habit of the granitic rocks, and in the composition of their pegmatites.

Strong lithologic differences between rocks on the two sides of the Brevard belt are indicated on Keith's map of the Pisgah quadrangle (1907), and to a lesser extent on his map of the Mount Mitchell quadrangle (1905), although his description of the rocks does not make these differences clear.

The Brevard belt and its northeastward extension constitute a major tectonic feature that separates the Blue Ridge belt from the Inner Piedmont belt. The differences between the rocks of these two belts, together with the occurrence of blastomylonites and retrogressive rocks along the lineament in the Table Rock quadrangle and the abrupt change in the lineation pattern described above, suggests that the belt marks a fault of considerable magnitude. Whether the fault is an overthrust, as believed by Jonas (1932), or a strike-slip fault is not yet established. It seems unlikely that the lineament marks a normal fault as believed by White (1950).

The relation of the retrogressed rocks and mylonites along the lineament in the Table Rock quadrangle to the Brevard schist mapped by Keith (1905, 1907) farther southwest is not yet understood.

REFERENCES

Conrad, S. G., 1959, New occurrence of crystalline limestone in McDowell County, N.C. [abs.]: Geol. Soc. America Bull., v. 70, p. 1760.

Hamilton, W. G., 1957, Polymetamorphic rocks of the Blue Ridge front near Old Fort, N.C.: Am. Jour. Sci., v. 255, p. 568–573.

Jonas, A. I., 1932, Structure of the metamorphic belt of the southern Appalachians: Am. Jour. Sci., 5th ser., v. 24, p. 228–243.

Keith, Arthur, 1905, Description of the Mount Mitchell quadrangle [North Carolina-Tennessee]: U.S. Geol. Survey Geol. Atlas, Folio 124.

——— 1907, Pisgah Folio, U.S. Geol. Survey Geol. Atlas, Folio 147.

King, P. B., 1955, A geologic section across the southern Appalachians—an outline of the geology in the segment in Tennessee, North Carolina, and South Carolina, *in* Russell, R. J., ed., Guides to southeastern geology: Geol. Soc. America, p. 332–373.

Stose, G. W., and Stose, A. J., 1951, Blue Ridge Front—a fault scarp: Geol. Soc. America Bull., v. 62, p. 1371–1373.

Stuckey, J. L., and Conrad, S. G., 1959, Metasedimentary rocks in Stokes, Surry, Yadkin, and Forsyth Counties, North Carolina [abs.]: Geol. Soc. America Bull., v. 70, p. 1770.

White, W. A., 1950, Blue Ridge Front—a fault scarp: Geol. Soc. America Bull., v. 61, p. 1309–1364.

87. GEOLOGIC RELATIONS INFERRED FROM THE PROVISIONAL GEOLOGIC MAP OF THE CRYSTALLINE ROCKS OF SOUTH CAROLINA

By William C. Overstreet and Henry Bell III, Beltsville, Md.

A provisional geologic map, showing the crystalline rocks and the overlapping edge of the coastal plain sediments in South Carolina, has been compiled on a scale of 1:250,000. Few geologic studies have been made in this area, but we have found from field reconnaissance in South Carolina and from detailed studies in North Carolina that the main bedrock types can be inferred from the county soil maps and reports of the U.S. Department of Agriculture; these county soil maps and reports are the main source of the data shown on the provisional geologic map.

Figure 87.1 shows the portion of the state covered by the map and some conspicuous geologic features. Though the absolute ages of the map units are un-

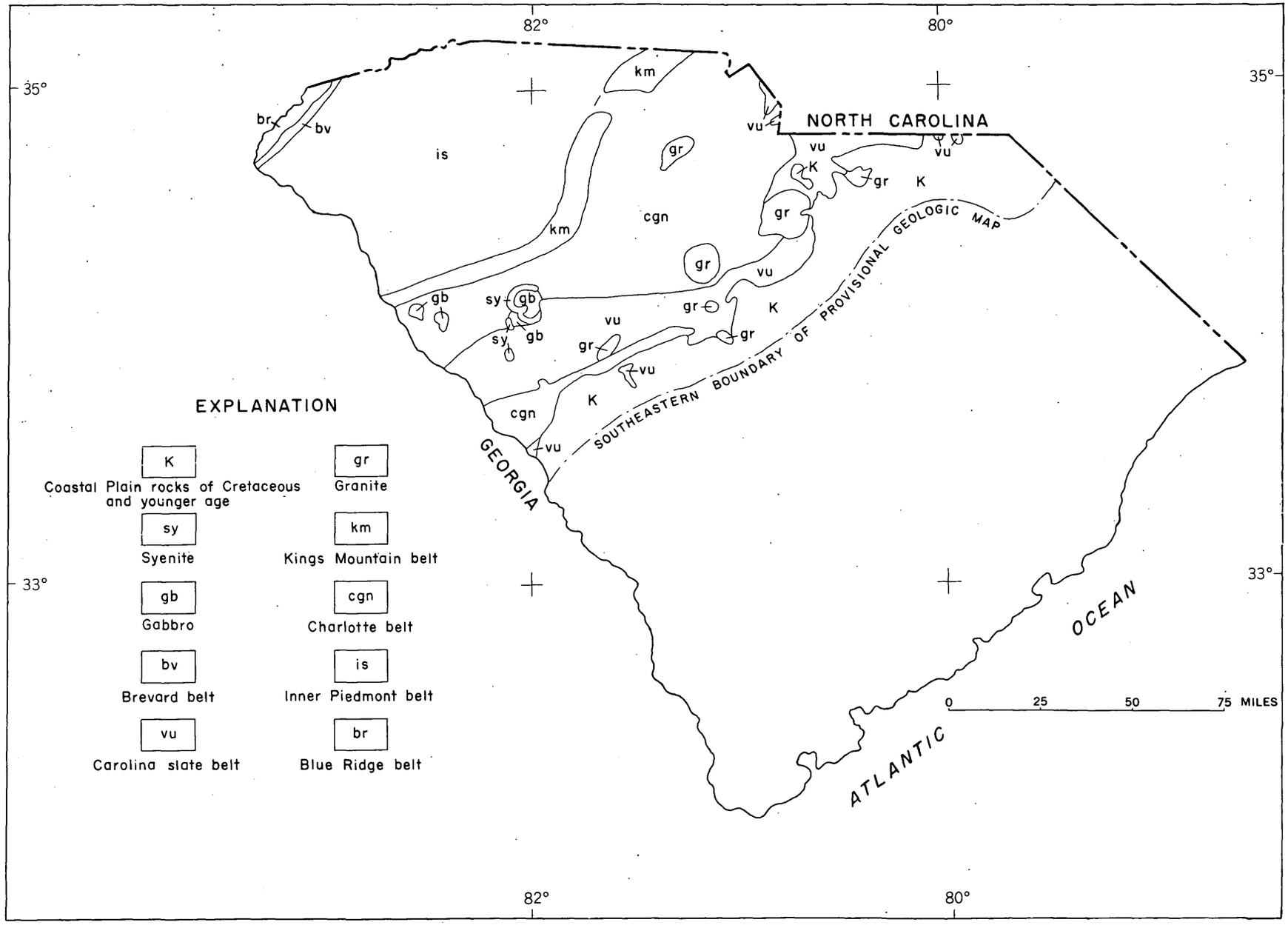

FIGURE 87.1.—Index map of South Carolina showing areas of provisional geologic map and prominent geologic features.

known, the map shows that a narrow belt of low-rank metasedimentary and metavolcanic rocks (fig. 87.1, unit km) extends southwestward across the central piedmont of South Carolina. The rocks at the northern end of this belt have been described by Arthur Keith and D. B. Sterrett (1931, p. 4–6) and by T. L. Kesler (1944, p. 758–759). The northern part of the belt, including its extension in North Carolina, has been called by P. B. King (1955, p. 350–352) the Kings Mountain belt, and we have extended this designation for the belt to the part crossing South Carolina. Where the Kings Mountain belt enters Georgia, its northwestern edge coincides with the most northwesterly exposure of the Little River series, shown by Stose and Smith (1939) on the geologic map of Georgia. Inasmuch as the eastern part of the Little River series is coextensive with rocks known farther northeastward in South Carolina, North Carolina, and Virginia as the "Carolina slate belt" (fig. 87.1, unit vu) Keith and Sterrett (1931, p. 4–5) and Kesler (1936, p. 34) have postulated that the rocks in the Kings Mountain belt and "Carolina slate belt" are possible stratigraphic equivalents. We suggest that this possibility may be demonstrated in Georgia.

The Brevard belt (King, 1955, p. 356–358) (fig. 87.1, unit bv) which consists of low-rank metamorphic rocks, is shown to extend across the northwest corner of South Carolina, separating the sillimanitic gneisses of the Inner Piedmont belt (King, 1955, p. 352–356) (fig. 87.1, unit is) from the kyanitic schists and gneisses of the Blue Ridge belt (King, 1955, p. 358–363) (fig. 87.1, unit br). Although the rocks of the Brevard belt resemble in many ways the rocks in the Kings Mountain belt, no other evidence for correlation has been found.

East of the Kings Mountain belt and mostly west of the Carolina slate belt is a group of plutonic rocks, largely gneisses, called by King (1955, p. 346–350) the Charlotte belt (fig. 87.1, unit cgn); this belt thins southwestward. The map shows for the first time circular and ring-shaped areas of syenite and gabbro within the Charlotte belt near the Georgia border. The map also discloses that several granitic bodies in the eastern Piedmont are small plutons, quite unlike the northeastward elongate batholiths that are generally supposed to exist in the area (Stose and Ljungstedt, 1932). The age of the plutons is not known, but some of them cut the Carolina slate belt, and we think they are slightly older than the syenite.

REFERENCES

Keith, Arthur, and Sterrett, D. B., 1931, Description of the Gaffney and Kings Mountain quadrangles: U.S. Geol. Survey Geol. Atlas, Folio 222, p. 1–13.

Kesler, T. L., 1936, Granitic injection processes in the Columbia quadrangle, South Carolina: Jour. Geology, v. 44, no. 1, p. 32–42.

——— 1944, Correlation of some metamorphic rocks in the central Carolina Piedmont: Geol. Soc. America Bull., v. 55, no 6, p. 755–782.

King, P. B., 1955, A geologic section across the southern Appalachians—an outline of the geology in the segment in Tennessee, North Carolina, and South Carolina, *in* Russell, R. J., ed., Guides to southeastern geology: Geol. Soc. America, p. 332–373.

Stose, G. W., and Ljungstedt, O. A., 1932, Geologic map of the United States: U.S. Geol. Survey.

Stose, G. W., and Smith, R. W., 1939, Geologic map of Georgia: Georgia Dept. Nat. Resources, Div. Mines, Mining and Geology.

88. DETERMINATION OF STRUCTURE IN THE APPALACHIAN BASIN BY GEOPHYSICAL METHODS

By Elizabeth R. King and Isidore Zietz, Washington, D.C.

The Geological Survey's geophysical data in the Appalachian Mountains and the plateau areas to the west have been brought together in an attempt to delineate trends and major lithologic units in the crystalline basement and to estimate the thickness of the overlying sedimentary rocks in various places. The data consist mainly of long aeromagnetic profiles flown by the Survey at various times over a period of more than ten years, but include a minor amount of gravity data.

The region studied lies west of the Blue Ridge province and extends from Alabama to New York State. It includes parts of the Valley and Ridge province and the Appalachian Plateau, and the portion of the Interior Low Plateaus that lies in Tennessee, Kentucky, and Ohio. In this region Paleozoic sedimentary rocks were deposited in a broad basin. Although many holes have been drilled in these rocks, very few have reached the crystalline basement, and in much of this

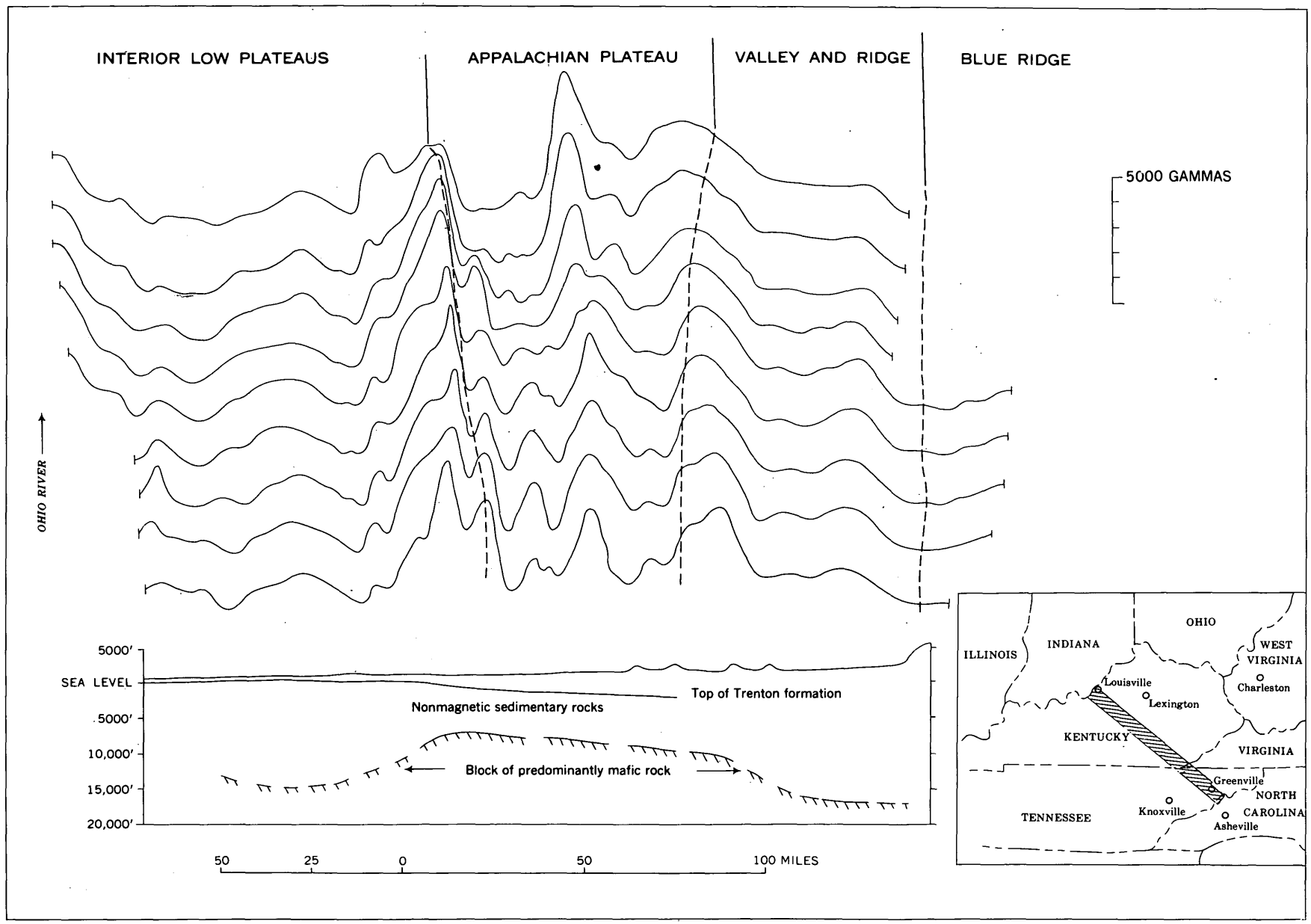

FIGURE 88.1.—Nine aeromagnetic profiles across the Appalachian basin, accompanied by a geologic cross section showing depth to crystalline basement rocks as calculated from the magnetic data.

area the total thickness of the Paleozoic rocks is not known.

The regional structures may be assigned to three major subdivisions of the area: (a) a central stable region, (b) a foreland, and (c) the Paleozoic basin (King, 1951). The first coincides roughly with the Interior Low Plateaus; it is bordered on the southeast by a series of structurally high areas, including the Nashville dome, the Cincinnati arch, and the Findlay arch, which are alined along the northwest side of a zone of downwarping. In this stable region the Paleozoic rocks are relatively thin except in local basins. The foreland lies east of the zone of downwarping; its structure consists of the broad Allegheny synclinorium, which underlies the Appalachian Plateau. The third sub-division is in the Valley and Ridge province or folded Appalachians, and forms part of the main basin of deposition of the Appalachian geosyncline.

Little is known about the Precambrian rocks beneath the Paleozoic sedimentary rocks. Precambrian rocks are exposed at the surface in the Blue Ridge to the east, where intrusion and metamorphism have produced a crystalline complex. Some of the later Precambrian sedimentary rocks, such as those of the Ocoee series and the Talladega series, do not differ greatly from the Paleozoic rocks except for their lack of fossils. Since magnetic anomalies are generally caused by igneous and metamorphic rocks and not by unmetamorphosed sedimentary rocks, depths to magnetic rocks calculated from the magnetic anomalies will not distinguish between an all-Paleozoic section and one that includes both Paleozoic and unmetamorphosed Precambrian rocks.

Our preliminary interpretations are mostly based on nine aeromagnetic profiles extending from a part of the Blue Ridge just north of Asheville, N.C., to the Ohio River at Louisville, Ky. The profiles intersect the prevailing structural trend at right angles, and cover a strip about 20 miles wide and 250 miles long across the southern Appalachian Mountains and the part of the plateau region that adjoins it on the west (fig. 88.1).

The individual magnetic anomalies have a pronounced northeasterly trend, parallel to the regional tectonic trend of the Appalachian Mountains. Their dominant feature is a group of exceptionally large anomalies which delineate a block of strongly magnetic rock, approximately 100 miles wide, under the Appalachian Plateau. The few gravity data available along this same strip (G. P. Woollard, written communication, 1960), show a marked resemblence to the over all magnetic pattern; a positive gravity anomaly, having a maximum Bouguer value of +30 milligals, coincides with the group of large magnetic anomalies. These magnetic and gravity anomalies probably indicate a large mass of predominently mafic igneous rock. Both the magnetic and gravity anomalies may be augmented by topography, for the crystalline rocks lie much deeper on both sides of this block (fig. 88.1). But topography alone cannot explain the large magnetic anomalies, for if they are projected even two miles upward, by the method of Henderson and Zietz (1949), they are still much larger than those observed in adjacent areas. A lithologic contrast is also indicated by the fact that where positive gravity anomalies of such amplitude occur over continental rocks, they are usually associated with dense, mafic rocks.

Depth to magnetic rock has been estimated from many of the individual magnetic anomalies. The results were generally consistent, and they indicate that in this part of the Appalachian Plateau province there are 8,000 to 10,000 feet of sedimentary rocks (fig. 88.1). These thicknesses are less than those predicted from stratigraphic evidence, but are supported by data from recently drilled wells that reach the basement.

How far this block of magnetic rock extends to the north and south is not clearly shown by the other magnetic profiles now available. The group of large anomalies is equally prominent on profiles between Knoxville and Nashville, Tennessee, but it is much less distinct and of smaller amplitude farther south, and is not observed on a profile across Alabama west of Birmingham. It is present, but much subdued, on a profile between Charleston, W. Va., and Lexington, Ky., and is not seen on profiles across southern Ohio.

In the Valley and Ridge province, depths to magnetic rocks calculated from anomalies on the nine profiles across southern Kentucky indicate that the thickness of the Paleozoic section averages about 17,000 feet but increases southeastward (fig. 88.1), as if the basement surface plunged in that direction. West of the Appalachian Plateau, over the Cincinnati arch, depths of about 15,000 feet were obtained—depths not only much greater than under the Plateau itself, but much greater than had previously been estimated for Paleozoic rocks of the central stable region. One possible explanation is that the arch is underlain by a great thickness of Precambrian sediments or other nonmagnetic rocks. In eastern Indiana, also, near the crest of the Cincinnati arch, the state-wide aeromagnetic survey revealed broad low-amplitude magnetic anomalies in Jay, Blackford, and Delaware Counties that suggest the presence of relatively nonmagnetic rock. This was confirmed in

557753 O—60——14

Jay County where a drill hole penetrated Precambrian dolomite (Henderson and Zietz, 1958, p. 22).

In the region northeast of Kentucky northeasterly magnetic trends appear to be indicated by sets of profiles across Ohio, West Virginia, and Pennsylvania. The magnetic data indicate also a much greater thickness of sedimentary rocks in the northern part of the Appalachian Plateau province. The Hope well, 15 miles east of Parkersburg, W. Va., reached basement at 13,310 feet. As a depth of over 10,000 feet was calculated from magnetic data obtained just west of Parkersburg, the deepest part of the basin may lie still farther east. The thickness also increases northeast of Parkersburg, on the Allegheny Plateau in central Pennsylvania, where depths of 19,000 to 22,000 feet were calculated from an aeromagnetic survey of Clearfield County (Joesting and others, 1949).

REFERENCES

Henderson, J. R., Jr., and Zeitz, Isidore, 1958, Interpretation of an aeromagnetic survey of Indiana: U.S. Geol. Survey Prof. Paper 316–B, p. 19–37.

Henderson, R. G., and Zeitz, Isidore, 1949. The upward continuation of anomalies in total magnetic intensity fields: Geophysics, v. 14, p. 517–534.

Joesting, H. R., Keller, Fred, and King, E. R., 1949, Geologic implications of aeromagnetic survey of Clearfield-Philipsburg area, central Pennsylvania: Am. Assoc. Petroleum Geologists Bull., v. 33, p. 1747–1766.

King, P. B., 1951, The tectonics of Middle North America: Princeton, New Jersey, Princeton University Press, 203 p.

89. RESIDUAL ORIGIN OF THE "PLEISTOCENE" SAND MANTLE IN CENTRAL FLORIDA UPLANDS AND ITS BEARING ON MARINE TERRACES AND CENOZOIC UPLIFT

By Z. S. Altschuler and E. J. Young, Washington, D.C.

The sedimentology of the quartz sands blanketing the Land Pebble phosphate field in west-central Florida was studied in relation to the lateritic weathering that affected the underlying Pliocene phosphorite (Altschuler and others, 1956). The sands are generally 3 to 8 feet thick. They are usually mapped as Pleistocene and are regarded as a succession of transgressive marine terraces, extensive, subparallel along the strike, and separated by scarps. The presumed terraces are mapped on the basis of altitude accordance, thus presupposing the absence of post-depositional differential uplift. Three aspects of the prevailing viewpoint will therefore be critically examined: (a) that the sands are transgressive deposits of Pleistocene age; (b) that the blanketed area is structurally stable; (c) that the sands are differentiated in a pattern, and at altitudes consistent with the terrace hypothesis.

The area studied begins about 20 miles east of the Tampa Bay region. It is generally very flat except for a low north-south ridge of karst topography that divides the Alafia and Peace River drainages and rises to over 250 feet (figs. 89.1 and 89.2). The central Florida region has many such long north-south ridges, which are the locales of the many sinkhole lakes. Off the ridge the prevailing altitude is 100 to 130 feet. According to Cooke (1945) the Sunderland and Coharie shorelines would be present at 170 feet and 215 feet. In MacNeil's (1950) modification, the Okefenokee shoreline would be present at 150 feet, but higher terraces would be absent in this area.

The contact between the sand mantle and the underlying clayey sands of the Pliocene Bone Valley formation is irregular and gradational in detail. Patches of clayey sand occur in the sand mantle above the "contact" and nests of eluviated loose quartz sand occur in the clayey sand beneath it. Size analyses and heavy mineral analyses of closely spaced samples through several vertical sections reveal that the sand blanket is essentially identical to the sand fraction of the subjacent Pliocene Bone Valley formation (fig. 89.2). Where observed along extensive plains, the sand mantle thins with corresponding thinning in the zone of lateritically altered clayey sand beneath it. These facts indicate that the quartz sand blanket is mainly an insoluble residue of the lateritic alteration of the Bone Valley formation, and not a transgressive Pleistocene deposit. Sellards (1915) and Ketner and McGreevey (1959) have also interpreted the sands to be residual. A few channel and dune deposits of Pleistocene to Recent age, and a thin veneer of wind-reworked material represent the principal nonresidual deposits.

The differentiation of the sand blanket (originally a clayey sand) was studied in terms of the size, sorting, and skewness properties of over 100 samples distributed

mainly across 9 townships (fig. 89.1a). Samples were taken from a zone 8 inches to 3 feet below the surface after numerous tests of the entire profile revealed essential identity throughout. However, most of the samples came from close to the surface. When the size data are plotted by sample location and contoured a definite relation to present-day topography is revealed. As seen in figure 89.1b, the coarser sands mantle the ridge, and the coarsest deposits form barlike accumulations on the ridge flanks. The finer sands are lowland deposits, flooring the valleys and straddling the lower parts of the ridge. Transitions between fine and coarse deposits are gradual except near the "bars." Despite this general relation of median size to topography (exhibited also by quartile, skewness, and sorting data) the sand differentiation is discordant to any of the proposed Pleistocene shorelines and to absolute altitudes. Note that the 160 foot contour outlining the ridge cuts directly across both the coarsest and finest deposits. In other words, the grade size distribution of the body of sand is completely independent of the previously proposed Coharie (215 feet), Sunderland (170 feet), or Okefenokee (150 feet) terraces. It reflects the size differentiation of Bone Valley time and suggests that the modern ridge existed as a shallow submerged ridge during Bone Valley time. (The phosphate pebble zone comprising the lower two-thirds of the Bone Valley formation is conglomeratic in the ridge and considerably finer in the adjoining low areas.)

It is known from a great volume of drilling data that the Bone Valley formation is continuous across the Land Pebble field. From this continuity and the structural relation of the formation to the central north-south ridge (fig. 89.3), it is evident that the formation has been considerably bowed up since deposition. This follows from the fact that a maximum altitude difference of the formation exceeds 100 feet, whereas the formation is generally only about 30 to 40 feet thick, although quite widespread over the region. Thus, uplift initiated in Pliocene or late pre-Pliocene time resulted in the development of shallow water facies in the Bone Valley formation, yielding a conglomeratic lower zone, and winnowed, barlike deposits in the clayey sands. Lateritic weathering has created a residual sand plain over the region, which preserves the original sediment differentiation. The larger ridges of the present landscape in the Land Pebble field result from the renewal or continuation of uplift rather than sand accumulations of presumed Pleistocene shorelines. The thickening of the deposits in some ridge areas is related to the influence of the uplift in localizing coarse detrital accumulation.

The derivation of the linear ridges by uplift dating back to pre-Pliocene offers a key to the pronounced concentration of simple and compound sinkhole lakes within the narrow uplifts. In contrast to the numerous shallow lakes and swamps of the surrounding flatlands, the lake basins of the ridges are deep, steep walled, often lacking in external drainage, and connected to a cavernous underground drainage network (Stewart, 1959). Many ridge basins have a present-day record of renewed, sudden deepening indicated by stepped profiles, soil movements and slanting trees, and dramatic historic accounts. Clusters of round sinkhole lakes occur as well where the ridges extend below presumed terrace altitudes, although MacNeil (1950, p. 101) asserted their general absence below 150 feet, and attributed this supposed absence to filling by the Okefenokee sea. (MacNeil's paper predates much of the topographic mapping in this region). Studies of the bottom configuration and stratigraphy of some of the lake sediments indicate a record of existence and renewal of collapse dating back, like the ridge uplifts, at least to pre-Pliocene. It seems clear, therefore, that the lakes in the ridges represent a renewal and intensification of karst development, generated by uplift. Such uplift initiates readjustments in the cavernous drainage network of the basement limestones, reactivating solutional downcutting and additional collapse in older sinks, and furthers the generation of new sinks. Sinkholes outside of the ridges are less numerous, generally less youthful, and more frequently plugged or filled. Such collapse is also evident in faulting within the Bone Valley formation in the Lakeland ridge.

The linearity and alinement of the ridges, the alinement of lake chains and sink holes within them, and our knowledge of major fault systems in peninsular Florida (Vernon, 1951) suggest that the uplift is caused by major faulting in deeper rock.

REFERENCES

Altschuler, Z. S., Jaffe, E. R., and Cuttitta, Frank, 1956, The aluminum phosphate zone of the Bone Valley formation, Florida, and its uranium deposits: U.S. Geol. Survey Prof. Paper 300, p. 495–504.

Cooke, C. W., 1945, Geology of Florida: Florida Geol. Survey Bull. 29.

Ketner, K. B., and McGreevey, L. J., 1959, Stratigraphy of the area between Herando and Hardee Counties, Florida: U.S. Geol. Survey Bull. 1074–C, p. 49–124.

MacNeil, F. S., 1950, Pleistocene shore lines in Florida and Georgia: U.S. Geol. Survey Prof. Paper 221–F, p. 95–107 [1951].

Sellards, E. H., 1915, The pebble phosphates of Florida: Florida Geol. Survey, 7th Ann. Rept., p. 25–117.

Stewart, H. G., 1959, Interim report on the geology and ground-Water resources of northwestern Polk County, Florida: Florida Geol. Survey Information Circ. No. 23.

Vernon, R. O., 1951, Geology of Citrus and Levy Counties, Florida: Florida Geol. Survey Bull. 33.

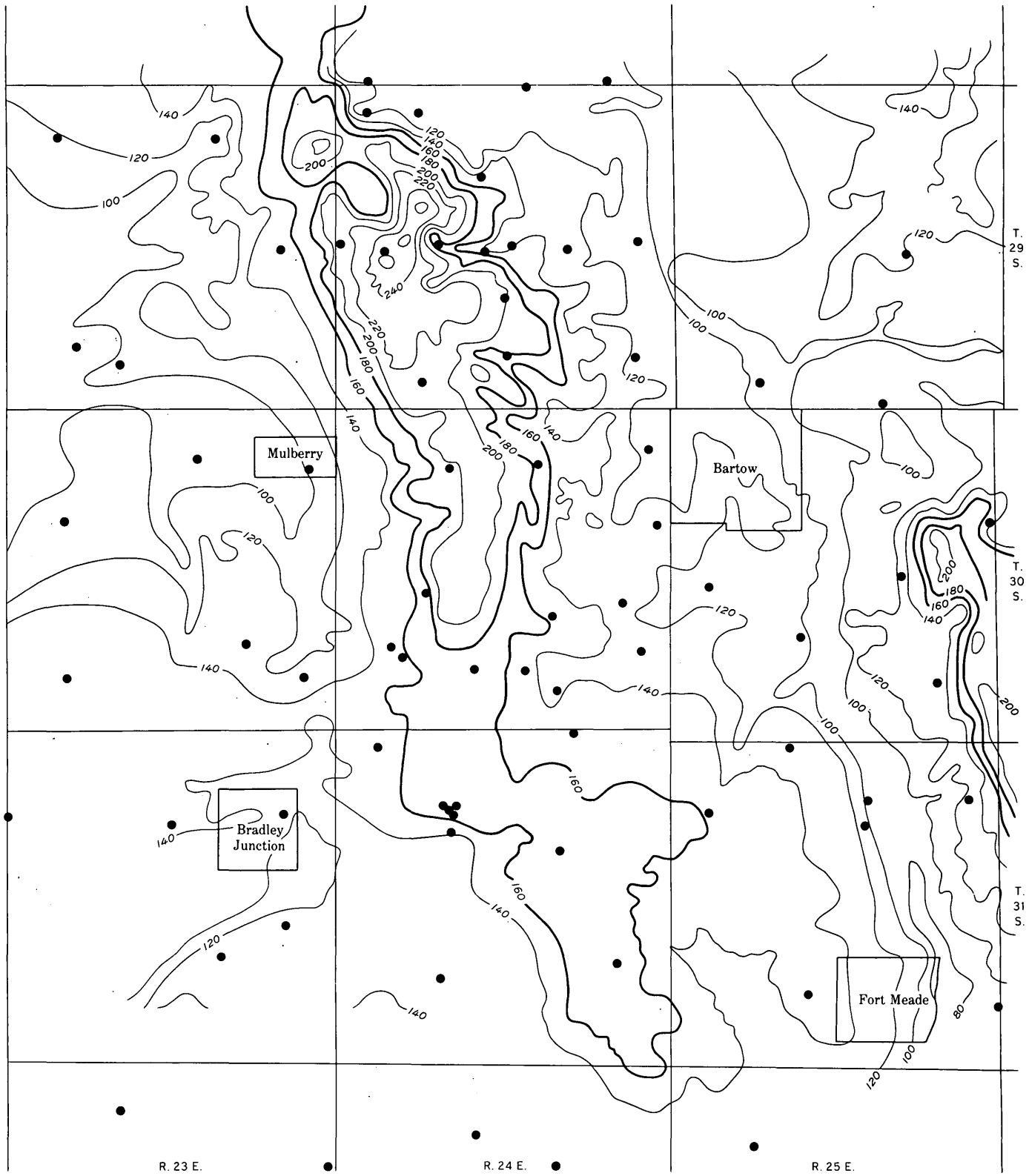

FIGURE 89.1.—Topographic map of parts of Hillsborough and Polk Counties, Fla. Black dots are sample locations. Contour interval=20 feet.

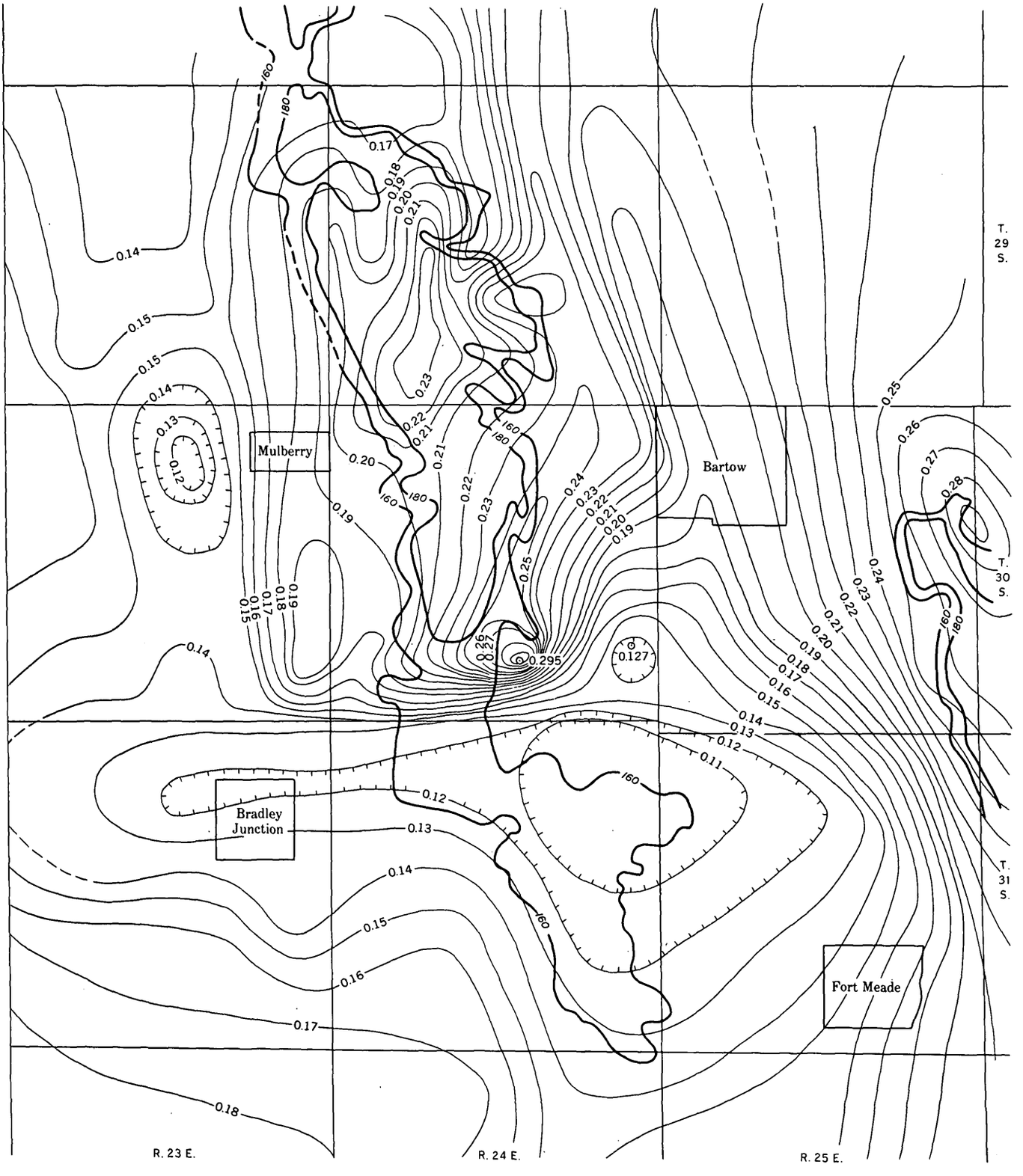

FIGURE 89.2.—Median size distribution of sand in surface mantle in parts of Polk and Hillsborough Counties, Fla. Data obtained from cumulative frequency curves. Isograde contour interval=0.01 mm. Heavy lines are the 160- and 180-foot topographic contours.

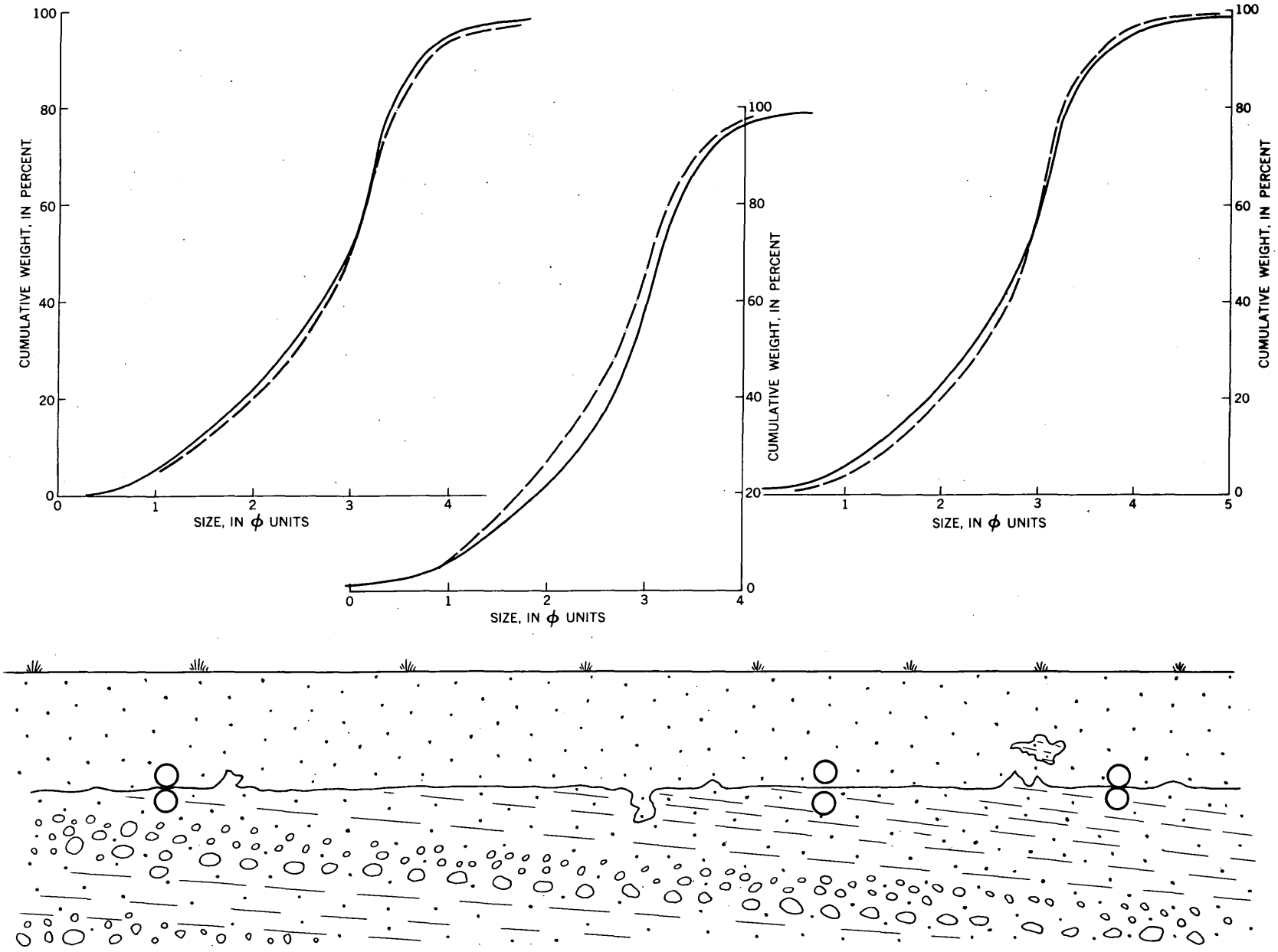

FIGURE 89.3.—Contact and grain-size relations of sand mantle and underlying clayey sand at Homeland, Fla. Cross section is 1,000 feet long and 12 feet thick. It illustrates relations of apparently transgressive sand over gently dipping sequence of graded bedded phosphorite and clayey sand, both of which have been lateritically altered to aluminum phosphate (Altschuler and others, 1956). Paired circles mark the sample locations for the paired size analyses shown above. The dashed curve is the size analysis of the sand fraction of the clayey sand; the solid line is that of the quartz sand above the contact.

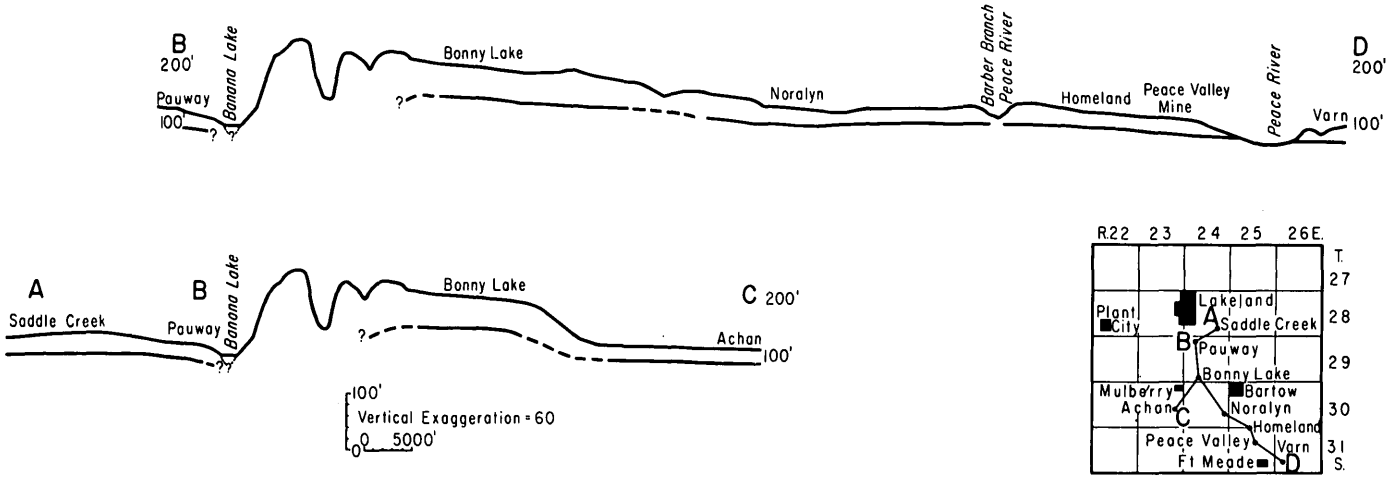

FIGURE 89.4.—Relation of Bone Valley formation to topography in Land Pebble phosphate field, Florida. Upper profile is surface topography. Lower profile is basal Bone Valley contact. Lower profile is not drawn in area of pronounced sinkhole collapsing.

90. A TROPICAL SEA IN CENTRAL GEORGIA IN LATE OLIGOCENE TIME

By ESTHER R. APPLIN, Jackson, Miss.

The discovery of many well preserved specimens of the foraminiferal genus *Miogypsina* in samples from a well in Coffee County, Ga., leads to the inference that a sea extended into central Georgia in late Oligocene time (figs. 90.1 and 90.2). The nearest previously known occurrence of the genus was in test well 3 at Port St. Joe, Gulf County, Fla. (Cole, 1938, p. 8–19); there is no published record of its having been found in any well or in any outcrop of Oligocene rocks between Gulf County, Fla., and Coffee County, Ga., which are about 200 miles apart (fig. 1). The genus *Miogypsina*, which lived in warm, clear, shallow seas, has been found, however, in sediments of late Oligocene age in the Panama Canal Zone (Cole, 1957) and in Puerto Rico (Sachs, 1959). The geographic distribution of the genus in the central and eastern Gulf Coast was described by Akers and Drooger (1957).

Numerous detailed studies of the effects of environmental conditions on various groups of living organisms indicate that closely similar fossil genera probably grew in similar environments. It therefore seems likely that sediments containing the miogypsinids found in Georgia were deposited in one of the marginal overlaps of the sea which oscillated back and forth over the inner Continental Shelf in late Oligocene time, when the waters of the Atlantic Ocean were still warm and equable. The temperature of this sea is believed to have been appreciably lowered in Miocene time by an influx of Arctic waters. Although the Oligocene sea in Georgia, like other seas of Oligocene time, was probably an inner neritic, fluctuating sea, it covered the area long enough to deposit about 600 feet of fine-textured, impure calcium-carbonate sediments, and long enough to allow the periodic introduction of several microfaunas, which appeared in the same sequence here as in the Panamanian region. The miogypsinid zone is the youngest faunal zone represented in this sequence.

Miogypsinids are particularly significant because of their very limited time-range, and because of their wide geographic distribution in the Gulf of Mexico, Caribbean, and Mediterranean areas. They are therefore useful in helping to solve interregional correlation problems, and since little had been published regarding the Oligocene rocks of the Atlantic Coastal Plain, the discovery of a moderately thick body of Oligocene sediments, identified by their containing *Myogypsina* and other characteristic Oligocene micro-fossils, in eastern Georgia, adds greatly to our knowledge of the Teritiary geology of that region.

In a report on the geology of the Coastal Plain in the central Atlantic States, Spangler and Peterson (1950, p. 97) wrote, "Uplift followed Eocene deposition and

during Oligocene and part of lower Miocene erosion took place." According to Spangler (1950, p. 131) "No Oligocene has been identified either in outcrop or from well samples in North Carolina." Swain (1951, p. 6, 7), however, assigned a questionable Oligocene age to a part of the sections in Hatteras Light well No. 1, and the North Carolina Esso well No. 2, both in North Carolina. Very little information has been published regarding sediments of Oligocene age in the eastern part of the Florida peninsula. Cole (1944, p. 23–24) identified five feet of Oligocene beds in a well in Nassau County, Fla., and the occurrence of 20 feet of Oligocene rocks penetrated in a well in Duval County is described in an unpublished report of my own. No miogypsinids were found, however, in either of these Florida wells, and none were found in the North Carolina wells.

REFERENCES

Akers, W. H., and Drooger, C. W., 1957, Miogypsinids, planktonic Foraminifera, and Gulf Coast Oligocene-Miocene correlations: Am. Assoc. Petroleum Geologists Bull., v. 41, p. 656–678.

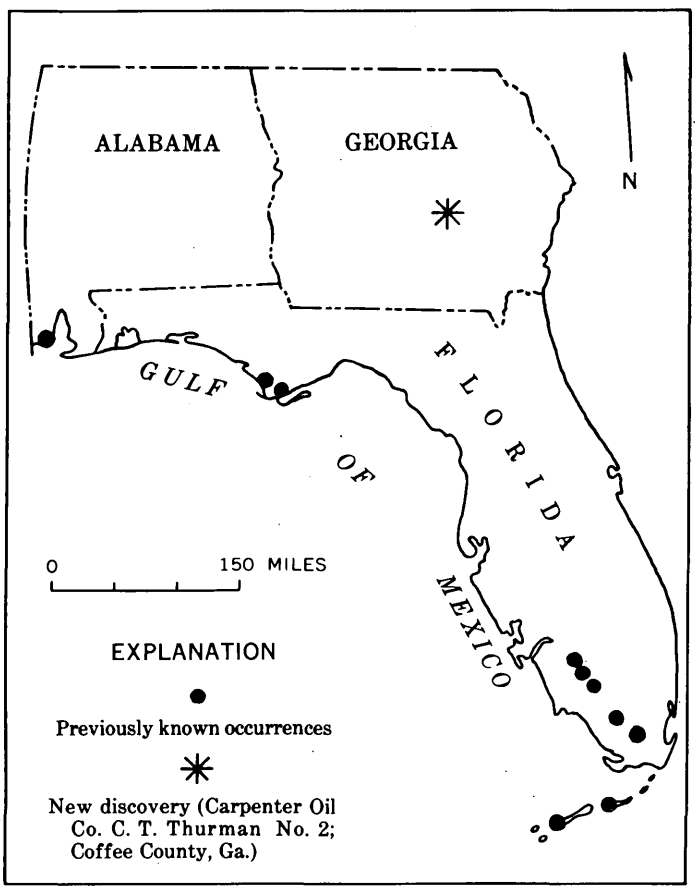

FIGURE 90.1.—Geographic distribution of Miogypsinadae in central and eastern Gulf Coast. (Adapted from Akers and Drooger, 1957, fig. 2).

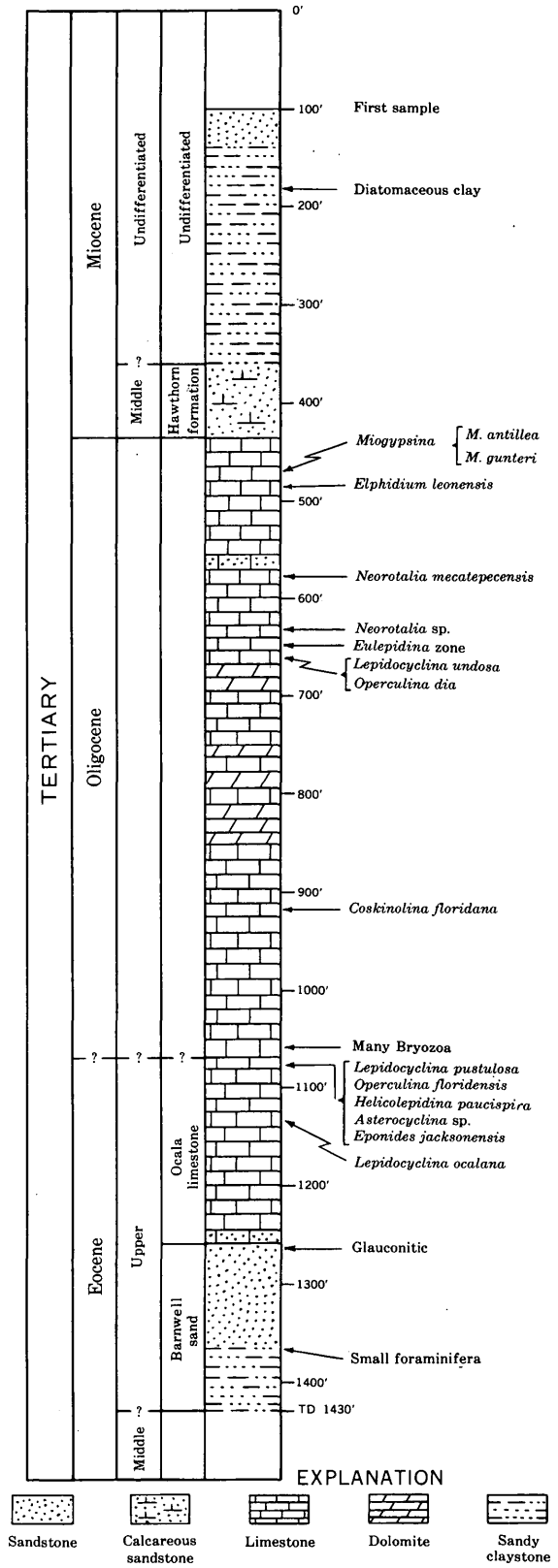

FIGURE 90.2.—Log prepared from samples from the upper part of the Carpenter Oil Co., C. T. Thurman No. 2, Coffee County, Ga. (Specific determinations of "larger Foraminifera" made by W. Storrs Cole.)

Cole, W. S., 1938, Port St. Joe Test Wells 3 and 4: Florida Geol. Survey Bull. 16, p. 8–19.

——— 1944, St. Mary's Oil Corp., Hilliard Turpentine Co. No. 1 well: Florida Geol. Survey Bull. 26, p. 18–100.

——— 1957, Late Oligocene larger Foraminifera from Barro Colorado Island, Panama Canal Zone: Am. Paleontology Bull., v. 37, no. 163, p. 313–338.

Sachs, K. N., Jr., 1958, Puerto Rican upper Oligocene larger Foraminifera: Am. Paleontology Bull., v. 39, no. 183, p. 399–413.

Spangler, W. B., 1950, Subsurface geology of Atlantic Coastal Plain of North Carolina: Am. Assoc. Petroleum Geologists Bull., v. 34, p. 100–132.

Spangler, W. B., and Peterson, J. J., 1950, Geology of Atlantic Coastal Plain of New Jersey, Delaware, Maryland, and Virginia: Am. Assoc. Petroleum Geologists Bull., v. 34, p. 1–100.

Swain, F. M., 1951, Ostracoda from wells in North Carolina, Part 1, Cenozoic Ostracods: U.S. Geol. Survey Prof. Paper 234–A, p. 1–53.

91. SIGNIFICANCE OF CHANGES IN THICKNESS AND LITHOFACIES OF THE SUNNILAND LIMESTONE, COLLIER COUNTY, FLA.

By Paul L. Applin, Jackson, Miss.

The Sunniland limestone, of Trinity (Comanche) age, was penetrated in about 60 deep test wells in central and southern Florida. This Lower Cretaceous limestone contains the reservoir rock of the Sunniland oil field (fig. 91.1), Florida's only producing field. In the short-lived (1954–55) Forty Mile Bend field (fig. 91.1), in Dade County, two wells produced a small quantity of oil from the Sunniland limestone; and showings of oil have been observed in the limestone in scattered wildcat test wells in southern Florida.

The term "Sunniland," as applied to a rock unit, was first published by Pressler (1947, p. 1859 and fig. 3), who referred to the "Sunniland zone," the "Sunniland limestone," and "the formation." Although neither Pressler nor later writers defined the unit or described a type section in a published article, common usage has established the name "Sunniland limestone" in the geologic nomenclature of Florida. It is here used to designate a subsurface unit (fig. 91.2) of middle Trinity (Comanche) age in southern Florida. The Sunniland is composed chiefly of limestone, dolomite, and shale. It overlies the so-called "thick anhydrite" or "lower anhydrite" unit, and underlies the so-called "upper anhydrite" unit, both of Trinity age.

The Sunniland limestone is about 100 feet thick in several wells in central Florida, but appears to thin northeastward and pinch out on the southwest flank of the Peninsular arch (fig. 91.1). It gradually thickens southwestward from the wells in central Florida, and is 200 to 275 feet thick in wells in southern Florida between Punta Gorda on the west coast and Key Largo on the east coast. The Sunniland limestone (fig. 91.2) is 250 to 275 feet thick in wells in and near the Sunniland field; but about 25 miles southwestward, in the Humble Oil & Refining Co's Collier Corp. well 1 in Collier County, it is only 69 feet thick (fig. 91.2).

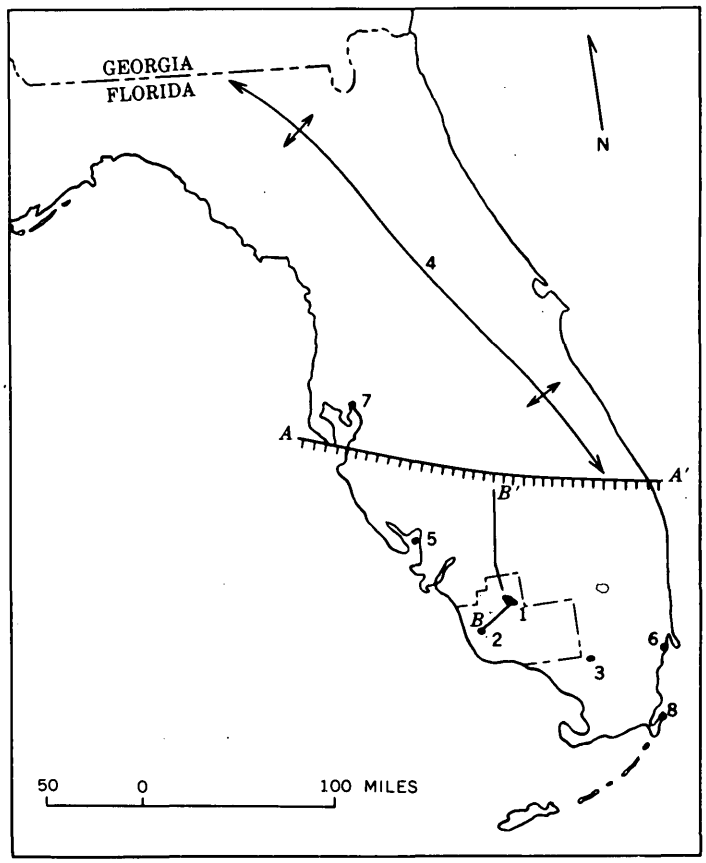

Figure 91.1.—Outline map of the Florida peninsula showing location of Collier County; 1, Sunniland oil field; 2, Collier Corporation well; 3, Forty Mile Bend oil field; 4, axis of Peninsular arch; 5, Punta Gorda; 6, Miami; 7, Tampa; 8, Key Largo; approximate northern limit of Sunniland limestone (*A–A'*); line of cross section, figure 91.2 (*B–B'*).

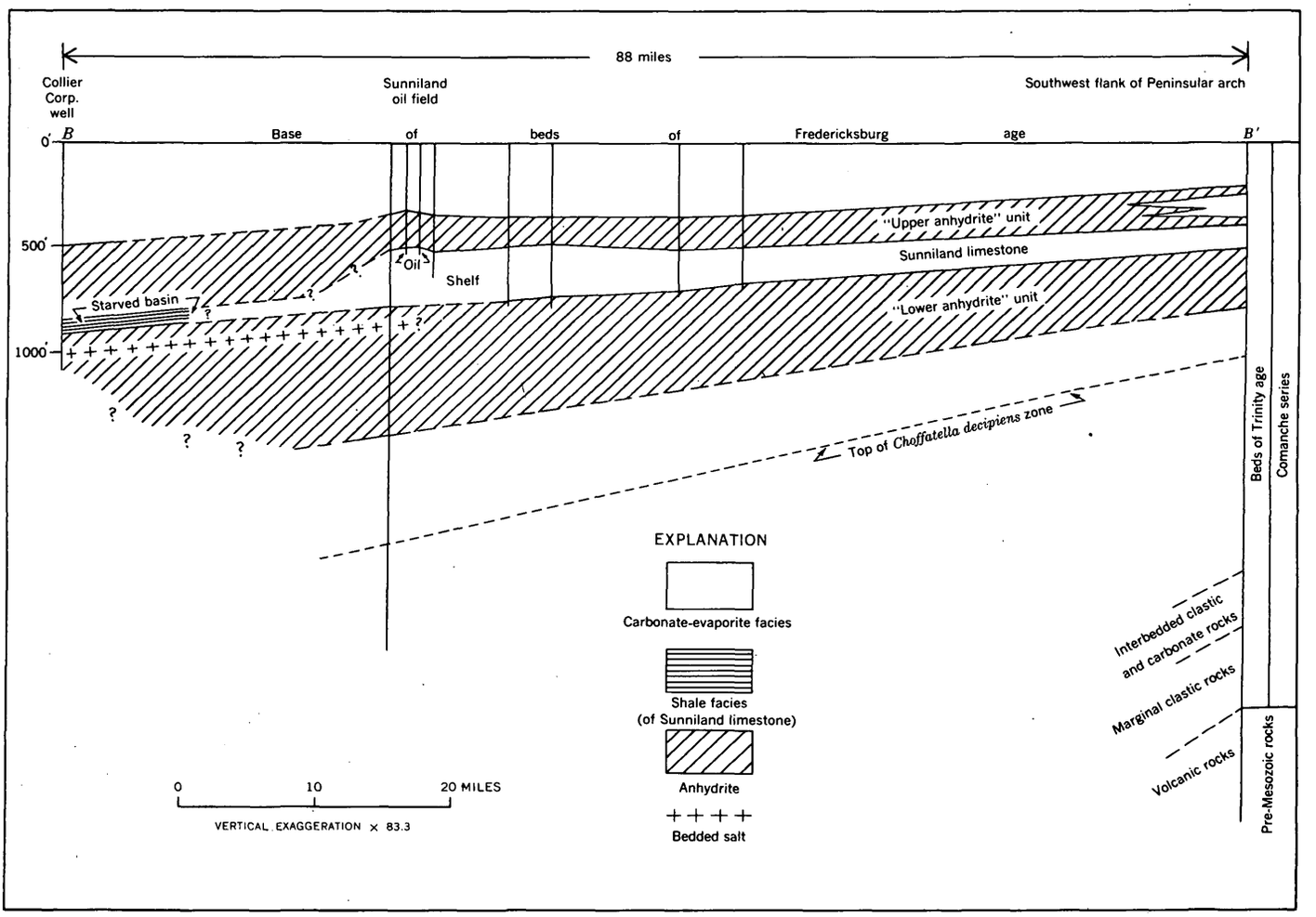

FIGURE 91.2.—Stratigraphic cross section of beds of Trinity (Comanche) age penetrated in wells from Collier County to Highlands County, Fla. Cross section shows changes in thickness and lithofacies of the Sunniland limestone. Section along *B–B'* of figure 91.1.

The Sunniland limestone is composed in general of dark dense argillaceous limestone and light-tan chalky limestone, interbedded with lenses of fine- to very fine-grained brown dolomite and dark-gray shale. Near the base of the unit in some wells, thin lenses of anhydrite alternate with lenses of limestone, dolomite, and shale that contain fossils characteristic of the Sunniland. Several wells also penetrated a few thin lenses of anhydrite near the top of the unit. Stylolites are common in the Sunniland limestone, but these, unlike the stylolites in other units of Comanche age, are generally filled with bituminous residue. The unit contains irregularly spaced lenses of bioclastic limestone, some of which are composed of broken shell fragments and others of algal debris. In the Sunniland field the uppermost 36 to 40 feet (Pressler, 1947, p. 1859) of the Sunniland limestone forms the reservoir rock, which consists mainly of interbedded hard, dense to porous limestone and hard, dense dolomite.

In contrast to the prevailing carbonate lithofacies of the Sunniland limestone, the stratigraphically equivalent unit in the Collier Corp. well southwest of the Sunniland field consists chiefly of dark-gray to black thinly laminated calcareous shale that has a strong odor of sulfur and contains free sulfur in the shale partings. Interbedded with the shale are thin lenses of dark argillaceous limestone, which is fossiliferous and somewhat stained with oil.

The variations in thickness of the Sunniland limestone, and the marked changes in lithologic facies indicated by samples from wells in Collier County, suggest that during Sunniland time the site of the Sunniland oil field was near the margin of a shelf that bordered the northeastern rim of a rapidly subsiding basin. The changes in thickness and lithofacies of this unit from the Sunniland field southwestward to the Collier Corp. well are analogous, in general, to changes in the Pennsylvanian rocks of west Texas described by Adams and

others (1951) as originating in "unfilled basins * * * surrounded by broad sediment-hoarding epicontinental shelves." These basins, in which the rate of subsidence was materially greater than the rate of deposition, were termed "starved basins."

The available subsurface data indicate that a starved basin existed in southern Florida during Sunniland time. The greatly thickened "upper anhydrite" unit that overlies the thin Sunniland limestone in the Collier Corp. well apparently filled the basin after the deposition of the Sunniland limestone. Since the Collier Corp. well provides the only evidence of a starved basin environment, data from additional deep test wells are needed to confirm the interpretation, to define the areal extent of the basin, and to determine the relation of the basin to relatively thick sections of the Sunniland limestone in other parts of southern Florida.

REFERENCES

Adams, J. E., Frenzel, H. N., Rhodes, M. L., and Johnson, D. P., 1951, Starved Pennsylvanian Midland basin: Am. Assoc. Petroleum Geologists Bull., v. 35, p. 2600–2607.

Pressler, E. D., 1947, Geology and occurrence of oil in Florida: Am. Assoc. Petroleum Geologists Bull., v. 31, p. 1851–1862.

92. SIGNIFICANCE OF LOESS DEPOSITS ALONG THE OHIO RIVER VALLEY

By Louis L. Ray, Washington, D.C.

A stratigraphic succession of four loess deposits of Quaternary age occurs along the valley of the Ohio River between Louisville, Ky., and its mouth. The oldest, of Kansan age, is exposed in only two outcrops, one near Yankeetown, Ind., and the other near Cairo, Ill. At each of these places the Kansan loess overlies materials that were deeply altered by weathering during the pre-Kansan (Aftonian) interglacial age. The loess deposited on this weathered surface was, in turn, deeply weathered during the succeeding post-Kansan (Yarmouth) interglacial age. Overlying the weathered Kansan loess at each outcrop is a sequence of three distinct loess deposits that are well exposed at many points along the Ohio River valley. They are: the Loveland loess, of Illinoian age, on which a characteristic profile of weathering was developed during the Sangamon interglacial age, and the distinctive Farmdale and Peorian loesses, both of Wisconsin age. The physical properties of these three loesses indicate remarkable regional uniformity.

The well-recognized relationship of loess to valley trains, from which the loessial silts were derived by wind deflation, leads inescapably to the conclusion that four valley trains, each of the same age as one of the four loess deposits, were developed within the valley of the Ohio River. The older valley trains, developed by the aggrading river during glacial invasion of its drainage basin, were in part removed by degradation during succeeding interglacial intervals, and their remnants were buried by later valley trains. The surfaces of only the last two valley trains, of Wisconsin age, are now observable as terrace remnants along the river. The surface of the higher terrace, of Tazewell age, marks the maximum Quaternary alluviation of the valley below Louisville; the lower terrace represents the modified surface of the youngest valley train, of Cary age.

The exposure near Cairo, Ill., in which all four of the loess deposits crop out, is adjacent to the ancient abandoned valley of the Ohio River, to which the three older loesses are closely related. As the present courses of both the Mississippi and Ohio Rivers in this area are believed to have been established during the Wisconsin age, the youngest loess, the Peorian, may be in large part more closely related to the valley trains of the Mississippi than to those of the more distant Ohio River.

Glacial drifts of Kansan, Illinoian, and Wisconsin ages are recognized along and adjacent to the valley of the Ohio above Louisville, but thus far no drift assignable to the Farmdale substage of the Wisconsin has been reported, although its existence is implied by the presence of the Farmdale loess. In all loess sequences examined, no loess deposit has been observed between the weathered surface of the Loveland and the base of the overlying Farmdale loess. There is thus no evidence to support the idea, suggested by some geologists, that an ice sheet advanced into the drainage basin of the Ohio during the interval between the deposition of the Loveland and that of the overlying Farmdale loess. If such a glaciation had occurred, a valley train contemporaneous with it should have been developed by the Ohio River, and a correlative loess deposit should occur in the outcrops adjacent to the river valley.

93. MAGNETIZATION OF VOLCANIC ROCKS IN THE LAKE SUPERIOR GEOSYNCLINE

By Gordon D. Bath, Menlo Park, Calif.

The magnetization of the huge mass of Keweenawan lava flows in the Lake Superior geosyncline is of fundamental importance in the interpretation of magnetic surveys in nearby areas. Unexpected magnetic anomalies were found in the area of the Duluth gabbro of northern Minnesota, and it is difficult to distinguish the magnetic effect of the gabbro and associated rocks from the wide-spread lateral effect produced by the large mass of lava flows. One of the constants needed for calculating the magnitude and extent of this lateral effect is the magnetization of the lava.

The purpose of this paper is to explain the magnetization by an indirect method, which consists of comparing the aeromagnetic anomalies found over the lava with the computed anomaly for the rock mass. The dominant factor in the calculations is the configuration of the rock mass. Fortunately the general structure of the lavas of the geosyncline is well known from geological studies that have been made over the past 75 years, and from recent gravity surveys by Thiel (1956).

The lava flows on the northwest limb of the geosyncline dip about 10° southeastward, and those on the southeast limb dip 35° to nearly 90° northwestward. The axial part of the structure is occupied by upper Keweenawan sedimentary rocks (fig. 93.1). In the area of the aeromagnetic traverses, the lavas are disrupted on the north limb by the Douglas fault, and on the south limb by a similar fault which was indicated only by the gravity data.

The lower part of figure 93.2, which shows the volcanic rock mass as a large block of simple form, is a reasonable representation of the general structure. The general character of Thiel's gravity profile, section A–A', suggests a nearly symmetrical distribution of anomalous density in this mass. Thiel computed a maximum lava thickness of 33,000 feet along the profile, assuming densities of 2.90 g per cm^3 for the lavas and 2.67 g cm^3 for the sedimentary rocks.

The areomagnetic profiles B–B' and C–C' show a remarkable similarity for profiles 10 miles apart. The flight elevation was 1,000 feet above the ground surface, and small anomalies were found over places where the volcanic rocks are near the surface. The anomaly for the structure reaches about 700 gammas over the axial part of the geosyncline, which is an area of nonmagnetic sandstone, arkose, and shale. If these sediments were replaced by an equal volume of volcanic rock, the magnetic field here would be as great as 1,000 gammas.

The theoretical anomalies of figure 93.2 were computed for several directions of magnetization, following the general procedure of Press and Ewing (1952). The magnetized rock mass was assumed to have a uniform cross section and uniform magnetization, and an average magnetic susceptibility of 0.003 cgs. Mooney (Mooney and Bleifuss, 1953) found a mean value of 0.004 cgs for 16 small rock samples measured in the

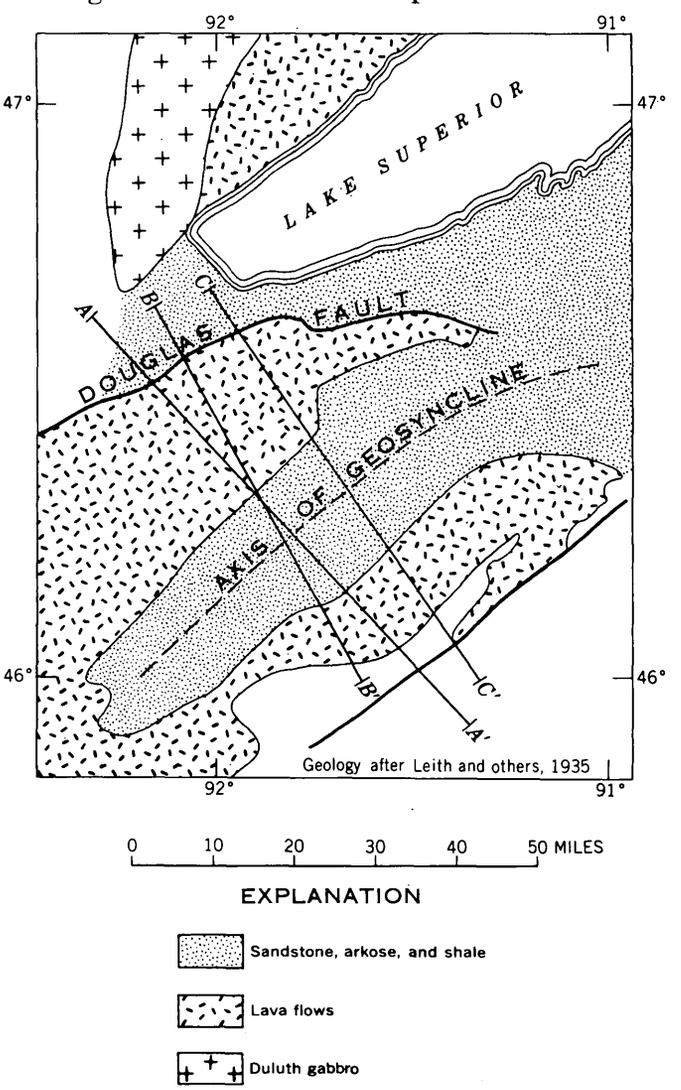

FIGURE 93.1.—Geologic map of part of the Lake Superior geosyncline, showing locations of gravity profile A–A', and areomagnetic profiles B–B' and C–C'.

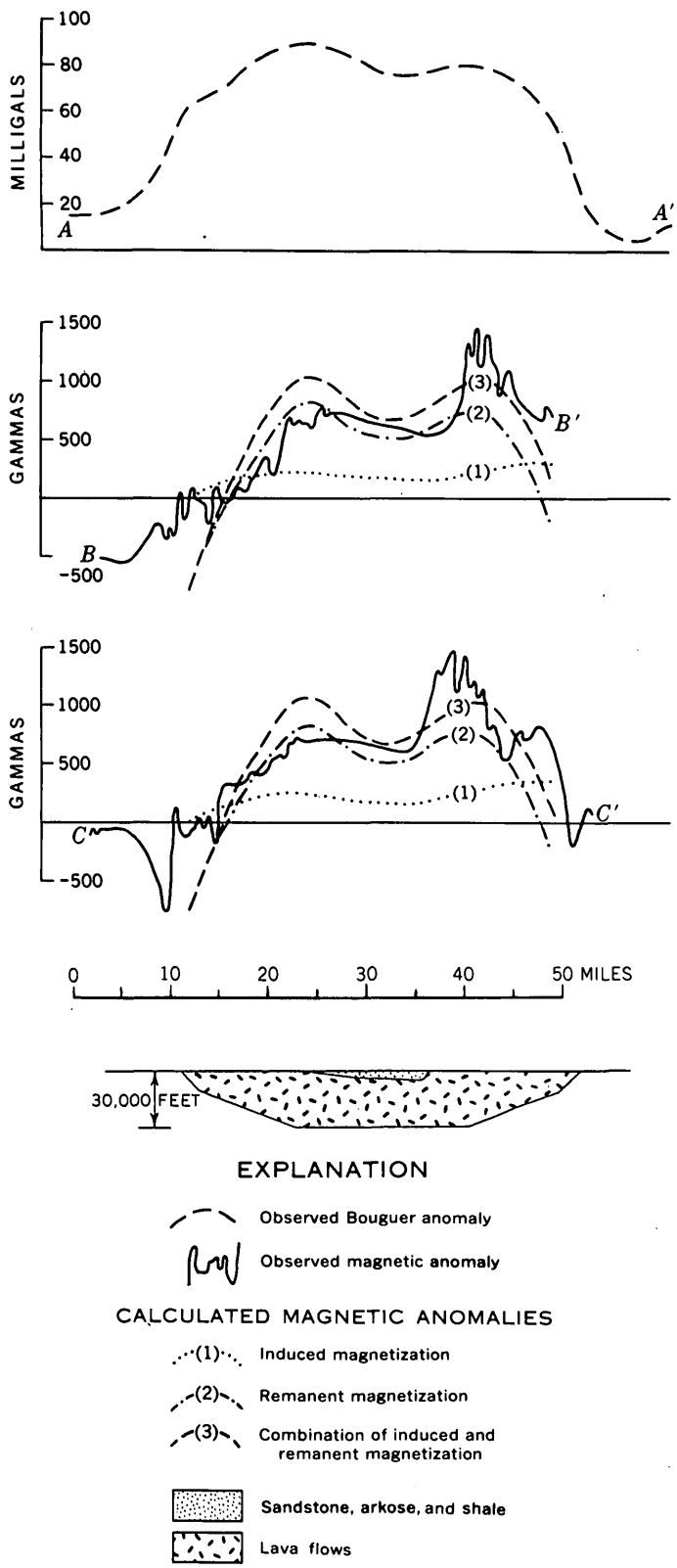

FIGURE 93.2.—Observed gravity profile and observed and calculated magnetic profiles over an idealized section of the Lake Superior geosyncline.

laboratory, and 0.003 cgs for 37 large samples measured at the outcrop site. The direction of magnetization is measured in a vertical plane normal to the axis of the syncline shown in figure 93.1.

Assuming that there was only induced magnetization and that the general structure is as shown in figure 93.2, a 1,000-gamma high over the axial part of the syncline would require a magnetization of 0.008 gauss and a magnetic susceptibility of 0.013 cgs. These values are about four times the values found by Mooney. A magnetic susceptibility of 0.003 cgs gives the small anomaly (1) of figure 93.2.

A closer correlation between observed and calculated anomaly is obtained by assuming that the rock mass has a remanent magnetization in addition to its induced magnetization. Twenty rock samples of basalt collected by the U.S. Geological Survey from the north limb have an average remanent intensity of 0.01 gauss and a remanent direction normal to the axis of about 40° for flows dipping 20° to the southeast. DuBois (1955) found that samples of lava from the south limb have a similar direction after correcting for the angle of dip. The lavas are not metamorphosed, and the remanent magnetization was probably acquired when the rocks solidified and cooled through the Curie temperature. Subsequent change in attitude would therefore give a corresponding change in direction of magnetization. This would be expected to differ in the two limbs because of the great difference in the average dip of the flows. The calculated anomaly (2) in figure 93.2 shows the effect of a remanent magnetization of 0.01 gauss for nearly horizontal flows on the north limb, and for flows with an average dip of 60° on the south limb.

Calculated profile (3) shows the combined effect of a 0.002-gauss induced magnetization and a 0.01-gauss remanent magnetization. Profile (3) is so similar to observed profiles *B–B′* and *C–C′* as to establish the order of magnitude of the magnetization of the large rock mass. The aeromagnetic anomalies produced by the bulk magnetic effect of the Keweenawan lava flows can thus be explained by combining the induced magnetization with a remanent magnetization of about 0.01 gauss.

REFERENCES

DuBois, P. M., 1955, Paleomagnetic measurements of the Keweenawan: Nature, v. 176, p. 506.

Leith, C. K., Lund, R. J., and Leith, Andrew, 1935, Precambrian rocks of the Lake Superior region, a review of newly discovered geologic features, with a revised geologic map: U.S. Geol. Survey Prof. Paper 184.

Mooney, H. M., and Bleifuss, Rodney, 1953, Magnetic susceptibility measurements in Minnesota, Part II: Analysis of field results: Geophysics, v. 28, no. 2, p. 383–392.

Press, Frank, and Ewing, Maurice, 1952, Magnetic anomalies over oceanic structures: Am. Geophys. Union Trans., v. 33, no. 3, p. 349–355.

Thiel, Edward, 1956, Correlation of gravity anomalies with the Keweenawan geology of Wisconsin and Minnesota: Geol. Soc. America Bull., v. 67, no. 8, p. 1079–1100.

GEOLOGY OF WESTERN CONTERMINOUS UNITED STATES

94. MEASUREMENTS OF ELECTRICAL PROPERTIES OF ROCKS IN SOUTHEAST MISSOURI

By C. J. Zablocki, Denver, Colo.

Electrical-property measurements were made of the rocks penetrated by 6 drill holes in southeast Missouri using inhole logging methods. The properties studied included self-potential, resistivity, induced polarization, and magnetic susceptibility. The holes ranged from 2,000 to 3,000 feet in depth and penetrated sedimentary rocks of Late Cambrian age underlain by a Precambrian complex of metavolcanic and intrusive rocks. The Precambrian rocks, about 1,500 feet from the surface, contain large amounts of magnetite, and in places, traces of sulfides.

The wide range in electrical properties on all the logs (fig. 94.1) are similar to those of many Precambrian rocks logged in other areas (Zablocki and Keller, 1957). The self-potential log, which for the most part is a "mirror image" of the resistivity log, shows variations as large as one-half volt. The mechanism of self-potentials developed in hard rocks is not fully understood; thus an interpretation is of little value at this time.

The Lamotte sandstone of Late Cambrian age has a resistivity of 800 to 1,000 ohm-meters, which corresponds to a porosity of about 6 percent. The top of the Precambrian, a weathered pink-gray quartz porphyry, has a slightly lower resistivity, probably because of a higher porosity developed by weathering. The reddish-gray quartz porphyry has a fairly high resistivity of 14,000 ohm-meters because of the low porosity. The magnetic susceptibility of this section is low, indicating that most of any original magnetite has been altered to hematite. (See table 94.1.)

The rock below 1,500 feet is mainly reddish to gray quartz monzonite that contains introduced magnetite up to about 15 percent by volume, and sulfides. Variations in the magnetic susceptibility log correspond to a striking degree with the color of the quartz monzonite as given in the detailed core log—that is, reddish zones have low susceptibility, gray zones have high susceptibility.

TABLE 94.1.—*Average values of the properties measured for the major rock types encountered*

Geologic unit	Lithology	Resistivity (ohm-meters)	Induced polarization (Percent)	Magnetic susceptibility ($\times 10^{-6}$ cgs)
Upper Cambrian:		$\times 10^3$		$\times 10^3$
Elvins group	Shale, dolomite	0.300–1.3	3	nil
Bonneterre dolomite.	Dolomite	6.2	3	nil
Lamotte sandstone.	Sandstone	.800–1	3	nil
Precambrian:				
Intrusive rocks	Weathered pink-gray quartz porphyry.	.400–1	3	nil
	Reddish-gray quartz porphyry.	14	3	nil
	Red quartz monzonite.	14	3	nil
	Reddish-gray monzonite.	1–16	5	5–18
	Gray quartz monzonite.	.0001–16	10	15–40
	Dark basic dike	14		2
	Pink granite	32	1	nil
Volcanic rocks	Andesite porphyry	37	3	25
	Welded agglommerate.	28	3	10–20
	Reddish rhyolite porphyry.	14		10–60

The magnetic susceptibility log also indicates that most of the zones of low resistivity are caused by higher concentrations of magnetite. The zones of pink granite are identified readily by their high resistivity and low magnetic susceptibility. Zones of abundant sulfide minerals indicated on the log as good traces, have low resistivity owing to the combined presence of the magnetite and sulfides. In sections of minor sulfide concentration, the resistivity is fairly high.

An anomalous zone with resistivity of nearly zero exists between 1,580 and 1,610 feet. A resistivity as low as this almost always indicates that the primary

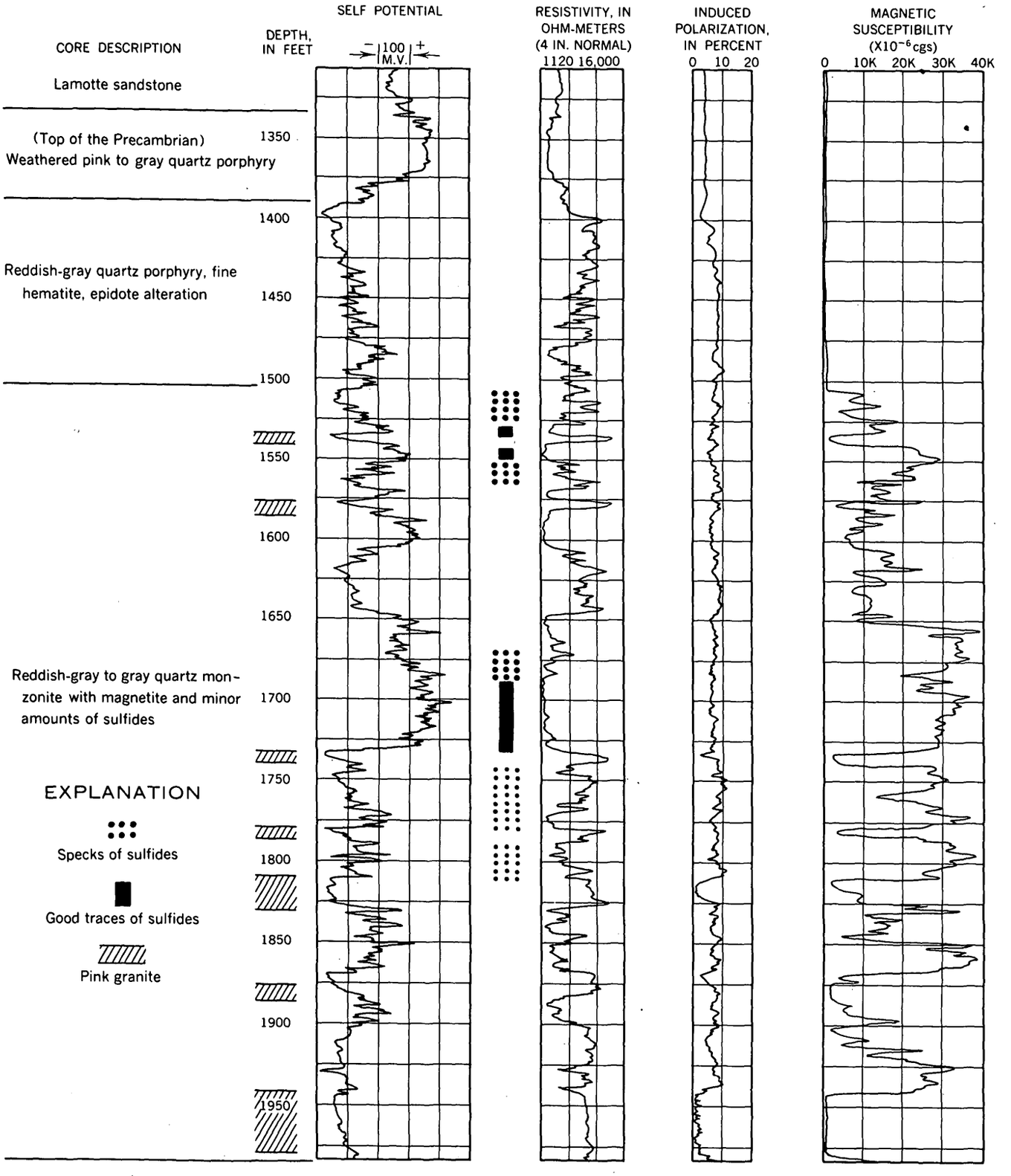

FIGURE 94.1.—Electric logs from a drill hole in southeast Missouri.

mode of conduction is through metallic grains rather than pore waters. The magnetic susceptibility, which is also low in this interval, indicates only that the amount of magnetite is small. Three possible explanations for the extremely low resistivity are:

1. A small amount of continuously connected grains of magnetite.
2. The presence of specular hematite (metallic), or
3. An abundant amount of sulfide minerals not indicated on the core log.

The Lamotte sandstone has an induced polarization response of about 5 percent. The response of the quartz monzonite is moderately high (about 8 percent) because of the presence of magnetite and sulfides. The pink granite has virtually no response, and the sulfide mineralized zones are indistinguishable from the magnetite-bearing sections.

REFERENCE

Zablocki, C. J., and Keller, G. V., 1957, Borehole geophysical logging methods in the Lake Superior district, *in* Drilling Symposium, 7th annual, exploration drilling: Minneapolis, Minnesota Univ. Center for Continuation Study, p. 15–24.

95. INTERPRETATION OF AEROMAGNETIC ANOMALIES IN SOUTHEAST MISSOURI

By John W. Allingham, Washington, D.C.

Work done in cooperation with the Missouri Geological Survey and Water Resources

The Ozark uplift, the major structural feature in the Paleozoic rocks of southeastern Missouri, is a gentle arch of low structural relief surrounded by shallow basins and terminated on the north end by the St. Genevieve fault zone. Exposed in a part of the uplift is the top of a granite batholith, which was intruded into volcanic rock and encloses small bodies of granophyre and roof pendants of resistant extrusive rock. These rocks are part of the basement on which Paleozoic strata were deposited.

The major faults and dominant fracture patterns trend northeast, northwest, and west. Faulting and tilting of the basement rocks, prior to sedimentation, provided sufficient local relief for the development of a maturely dissected landscape of ridges and rounded knobs. The fault zones are believed to be channelways or permeable zones in which mineral-bearing fluids migrated upward (Brown, 1958). This migration was partly controlled by the pinchout line of sandy beds around the knobs, and by peripheral fractures developed in the Paleozoic rocks. In early Paleozoic time the dissected, hilly, partly faulted, platformlike borders of the basins of sedimentation formed an archipelago environment, characterized by sand ridges, wave-cut benches, reef structures, and slide breccias. These sedimentary features and their controlling topography localized later deposits of lead (James, 1952; Ohle and Brown, 1954; Snyder and Odell, 1958). Much of the region surrounding the mountainous or hilly core of Precambrian rock is characterized by a flat landscape, with flat-lying Cambrian sedimentary carbonate formations that lap up against or bury ridges and knobs of Precambrian rock.

As most of the magnetic patterns are caused by Precambrian igneous rocks, interpretation of regional aeromagnetic maps of southeast Missouri permits us to separate areas underlain by granite from those underlain by volcanic rocks, to locate and define some basement ridges and hills, to determine the extent and depth of shallow Paleozoic basins, to outline basin areas underlain by granite, and to trace faults that may partly control basement topography.

Figure 95.1 shows an aeromagnetic map covering an area of buried Precambrian igneous rock. This area can be divided into two parts of different magnetic character: (a) a magnetically flat basin underlain by granite of low susceptibility (shown at right), and (b) a magnetically complex area underlain by older volcanic rocks of high susceptibility that form near-surface features (shown at left). The magnetic pattern associated with the border of the basin results mainly from the contrasting magnetic character of granite and volcanic rock. The map shows several types of anomalies: (a) broad high-amplitude anomalies (as much as 2,500 gammas) partly caused by magnetite-bearing volcanic rock and partly by magnetite-rich iron deposits of economic importance, such as the one causing the Pea Ridge anomaly (near point shown as 5,175); (b) broad ano-

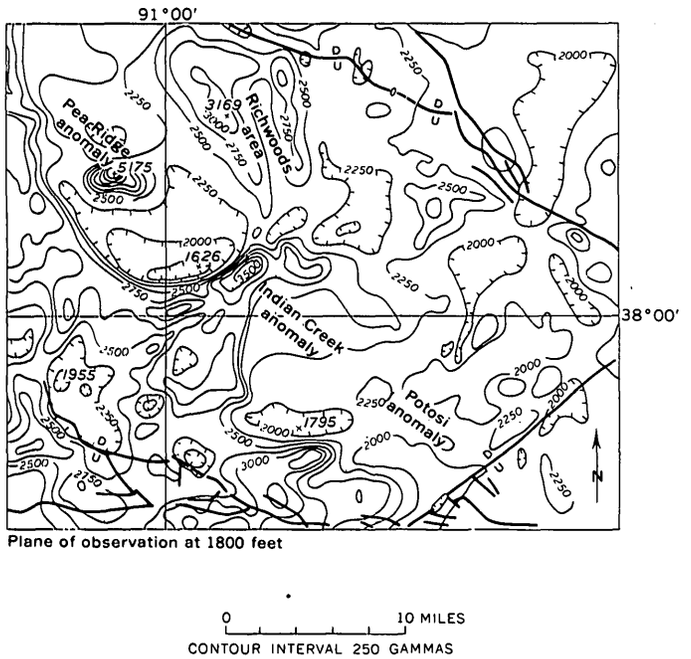

FIGURE 95.1.—Total-intensity aeromagnetic map of part of southeast Missouri.

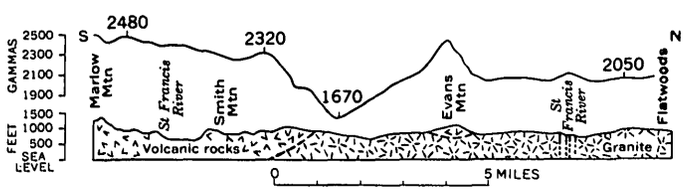

FIGURE 95.2.—Profile showing correlation of aeromagnetic data with geology.

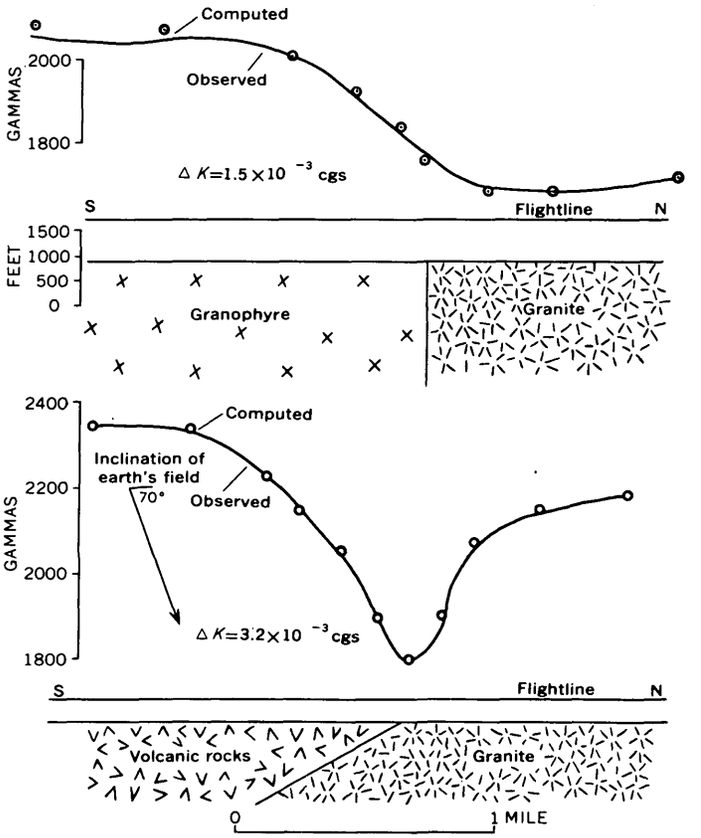

FIGURE 95.3.—Aeromagnetic profile over a contact between granite and volcanic rock or granophyre.

malies of relatively low amplitude (less than 600 gammas), such as the one in the Richwoods area (3,169), due to a roof pendant of volcanic rock in granite; (c) small, low amplitude anomalies (less than 300 gammas), such as the one over a buried knob at Potosi, east of 1,795. The low-amplitude anomalies (less than 150 gammas) are commonly caused by topographic relief, and to a lesser degree by lithologic differences, altered zones at intrusive contacts, or local concentration of magnetic minerals in the Precambrain rocks. The magnitude of magnetic anomalies associated with knobs of volcanic rock is generally twice as large as that of anomalies over comparable surfaces of granite. The distinctive magnetically flat pattern associated with the granite outlines partly rounded structural basins containing Paleozoic carbonate strata, and shows a distinct gradient sloping southwest. This gradient is interpreted as indicating that the faulted granite blocks are tilted southwestward. The presence of small bodies of granophyre and isolated pendants of volcanic rock complicates the magnetic pattern in areas of relatively low magnetic relief.

Aeromagnetic profiles are used to deduce plausible geometric relations as an aid in mapping areal geology. These relations are verified by fitting computed profiles to observed data by two- or three-dimensional analyses of the suggested geometry (Pirson, 1940; Henderson and Zietz, 1956, 1957; Henderson, see Art. 52). A section from Marlow Mountain to Flatwoods (fig. 95.2) shows that the magnetic intensity is about 650 gammas higher over volcanic rock than over granite. The shape and magnitude of the anomaly over the southward-dipping contact between granite and volcanic rock consequently differs from that over a vertical contact (fig. 95.3). In this area the attitude of intrusive contacts can be determined from magnetic data. The anomaly over Evans Mountain is greater than that over a comparable hill on volcanic rocks. The 50-gamma anomaly at the St. Francis River north of Evans Mountain is caused by a swarm of diabase dikes of easterly trend. The magnetic profile over the granite north of Evans Mountain is uniformly flat.

Many anomalies of 150 to 300 gammas amplitude correlate with erosionally resistant roof pendants of volcanic rock in the granite; an example of this correlation occurs at Evans Mountain (fig. 95.4). Isolated bodies

557753 O—60——15

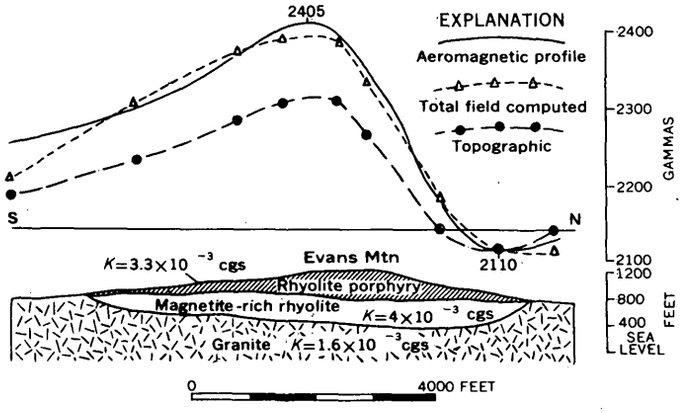

FIGURE 95.4.—Magnetic expression of a roof pendant of volcanic rock in granite.

of volcanic rocks forming roof pendants have an increased magnetite content near the granite contacts, and the same is true of masses of intrusive felsite.

Some ridges of volcanic rock, such as the one at Indian Creek, can be represented by prisms of infinite depth (fig. 95.5). The contacts there seems to be nearly vertical. The magnetic contribution of the topographic relief of the ridge to the total intensity field is comparatively small. The magnitude of the anomaly indicates a rock of high susceptibility containing an abnormally high concentration of magnetite.

Recognition of faulting from the magnetic pattern is important in mineral exploration. Generally the anomalies observed over fault zones are small. Major fault zones, where magnetic minerals have been altered, can be detected from a series of closed lows on contour maps (fig. 95.1) or by inflections or dips in magnetic profiles (fig. 95.6).

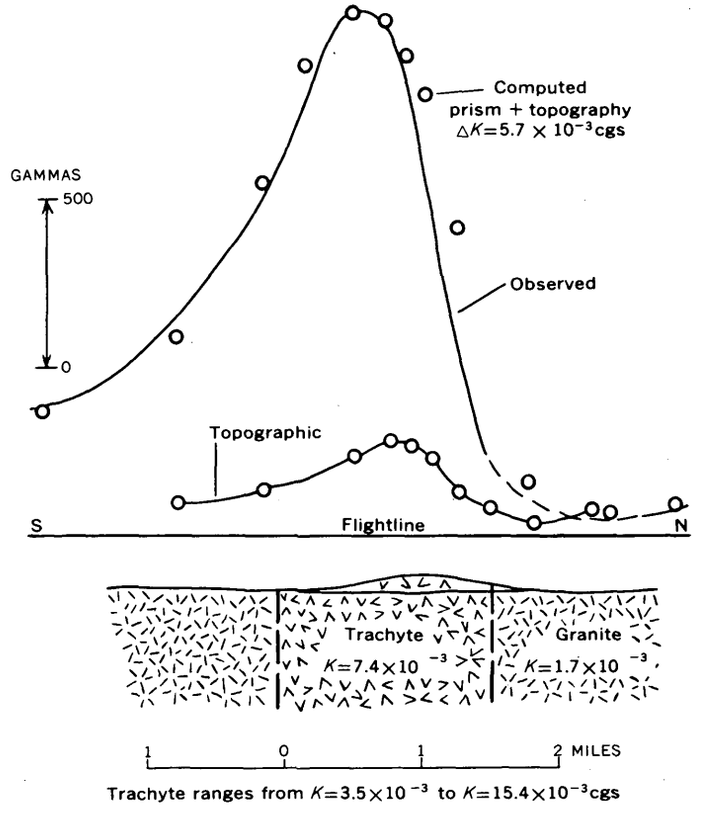

FIGURE 95.5.—Aeromagnetic profile over a ridge of trachyte of high susceptibility near Indian Creek. Susceptibility of trachyte ranges from 3.5×10^{-3} to 15.4×10^{-3} cgs. Subsurface data supplied by St. Joseph Lead Co.

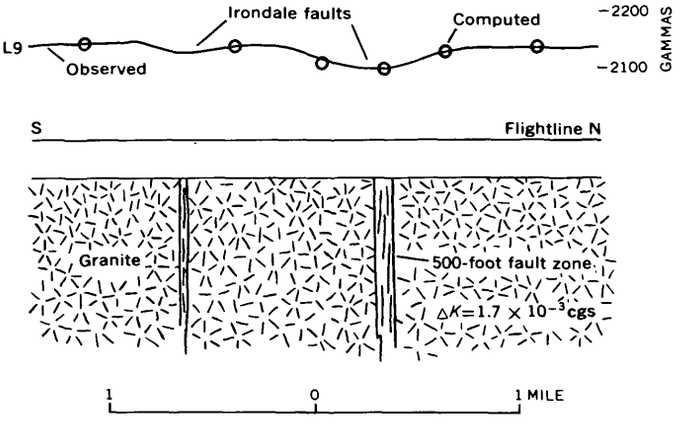

FIGURE 95.6.—Aeromagnetic profile over the Irondale fault zone.

Profiles computed from two-dimensional models for the interpretation of flat-lying flows and pyroclastic rocks show the characteristic edge effects exhibited by the magnetic field associated with this type of geometry. A profile computed from a slab model shows that the Criswell anomaly results mainly from the effect of topographic relief (fig. 95.7).

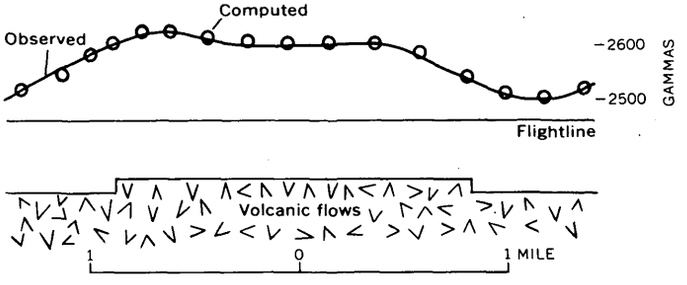

FIGURE 95.7.—Aeromagnetic profile over a volcanic flow near Criswell, Mo.

Magnetic relief of low-amplitude aeromagnetic anomalies can be exaggerated by second-vertical derivative or continuation downward of the total intensity magnetic field (Henderson and Zietz, 1949; Henderson, 1960). Contour maps of these intensified fields resemble the basement topography. Use of these fields in areas where anomalies are caused by irregularities on the buried Precambrian surface can eliminate the need for

some conventional ground magnetic surveys. As buried hills of granite and volcanic rock control the sedimentary and structural environment of some lead deposits, the total-intensity aeromagnetic field over one knob of rhyolite was continued downward to a level corresponding to the surface of the basement rocks and correlated with second-vertical derivative maps of these fields (fig. 95.8).

The zero contour of the second-derivative of the observed field corresponds to the outer extremities of mine workings in a nearby lead deposit. The 250-gamma contour of the second-derivative of the continued field corresponds to the pinch-out line of the Lamotte sandstone. The relative steepness of the continued field and vertical derivatives seem to indicate the absence or presence of the pinch-out line of the sand and may be a useful guide in delineating more favorable areas for exploration.

Aeromagnetic information in southeast Missouri is useful in distinguishing (a) areas having potential economic deposits of magnetite, (b) borders of basins having possible archipelago environments, (c) knobs and ridges having suitable sedimentary structures for localizing deposits of galena, (d) areas of faulting, and (e) the attitude of contacts.

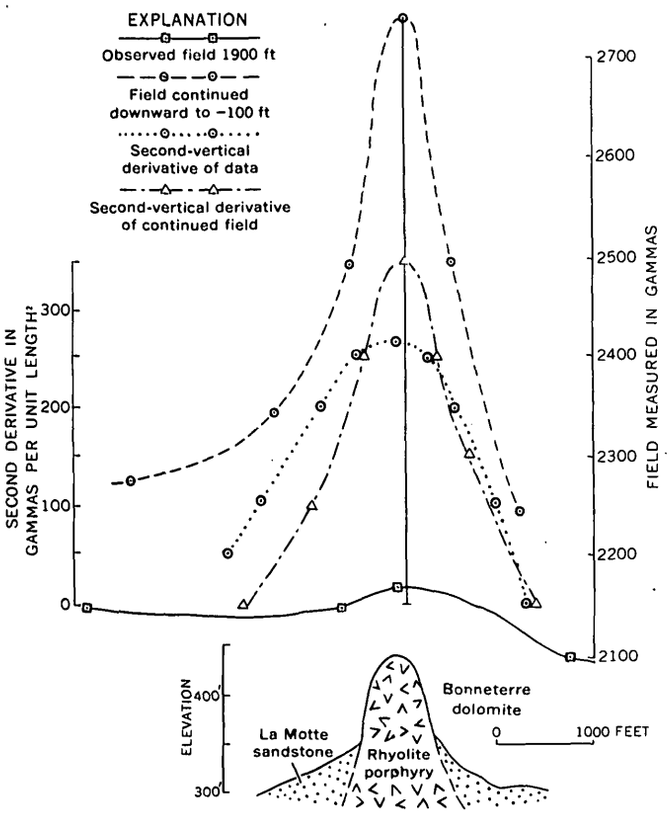

FIGURE 95.8.—Profiles of derived magnetic fields over a knob of rhyolite. Subsurface data supplied by the St. Joseph Lead Co.

REFERENCES

Brown, J. S., 1958, Southeast Missouri lead belt *in* Geol. Soc. America Guidebook, St. Louis meeting, 1958: p. 1–7.

Henderson, R. G., 1960, A comprehensive system of automatic computation in magnetic and gravity interpretation: Geophysics, v. 25, no. 3, p. 569–585.

Henderson, R. G., and Zietz, Isidore, 1949, The computation of second vertical derivatives of geomagnetic fields: Geophysics, v. 14, no. 4, p. 508–516.

——— 1956, A preliminary report of model studies of magnetic anomalies of three-dimensional bodies: Geophysics, v. 21, no. 3, p. 794–814.

——— 1957, Graphical calculation of total-intensity anomalies of three-dimensional bodies: Geophysics, v. 22, no. 4, p. 887–904.

James, J. A., 1952, Structural environments of the lead deposits in the Southeastern Missouri mining district: Econ. Geology, v. 47, no. 6, p. 650–660.

Ohle, E. L., and Brown, J. S., 1954, Geologic problems in the southeast Missouri lead district: Geol. Soc. America Bull., v. 65, no. 3, p. 201–222, no. 9, p. 935–936.

Pirson, S. J., 1940, Polar charts for interpreting magnetic anomalies: Am. Inst. Mining Metall. Engineers Trans., v. 138, p. 173–192.

Snyder, F. G., and Odell, J. W., 1958, Sedimentary breccias in the Southeast Missouri lead district: Geol. Soc. America Bull., v. 69, no. 7, p. 899–926.

96. SOME AFTERSHOCKS OF THE HEBGEN LAKE, MONTANA, EARTHQUAKE OF AUGUST 1959

By S. W. STEWART, R. B. HOFMANN, and W. H. DIMENT, Denver, Colo.

Prepared in cooperation with the U.S. Atomic Energy Commission

Two portable seismographs were operated intermittently at three stations from 1800h August 21 to 0900h August 24, 1959 G.c.t. (Greenwich civil time), to record aftershocks of the Hebgen Lage, Mont., earthquake of August 18, 1959 G.c.t. This was done because of current interest in determining possible differences

between ground motion caused by earthquakes and that caused by underground nuclear explosions. The seismographs used were identical with those previously used to record nuclear explosions at the Nevada Test Site (Stewart and others, 1959). In order to make the comparison it was necessary to learn, by study of seismograms, the approximate epicentral locations and magnitudes of the more clearly recorded aftershocks of the Montana earthquake. It is the purpose of this note to summarize some of this information, but not to make any general comparison between the effects of nuclear explosions and earthquakes.

Two three-component seismographs were operated intermittently at three locations from 3.5 to 6.1 days after the main shock of August 18, 1959, 06h 37m 15.0s G.c.t. (Seismological Society of America, 1959, p. 419). Moving-coil seismometers having a damped natural frequency of about 3 cycles per second were used. The seismic system was calibrated in the range 1 to 20 cycles per second. WWV timing signals or chronometer relay closure marks were recorded on the seismograms. Locations for the three seismograph stations were as follows:

Station	Latitude	Longitude	Elevation (feet)
Keg Spring, Idaho	44°31.21′N	111°37.14′W	7, 620
Victor 1, Idaho	43°36.64′N	110°5.36′W	6, 250
Victor 2, Idaho	43°38.41′N	111°10.25′W	6, 000

The Keg Spring and Victor stations were respectively about 40 km southwest and 130 km south of Hebgen Lake, which is near the center of the aftershock activity.

At the Keg Spring station 604 aftershocks were recorded with sufficient amplitude to permit calculation of their approximate magnitudes by the method of Richter (1958, p. 338–345). Recording with different magnifications for various intervals of time made it possible to determine a wide range of magnitudes. By weighting the observed frequency of occurrence of aftershocks with respect to magnification, an estimate was made of the numbers of aftershocks that would have been observed in the recording interval of about 22 hours if the seismograph had always operated at its maximum magnification (fig. 96.1). The data were not weighted below magnitude 1.15 because of the small sample size below this magnitude.

The weighted values of the numbers of shocks indicate increasing numbers of aftershocks for decreasing magnitudes from 3.7 to 1.2 (fig. 96.1). The smallest shock recorded at the Keg Spring station had a magnitude of 0.4. Richter and Nordquist (1948, p. 260), in a

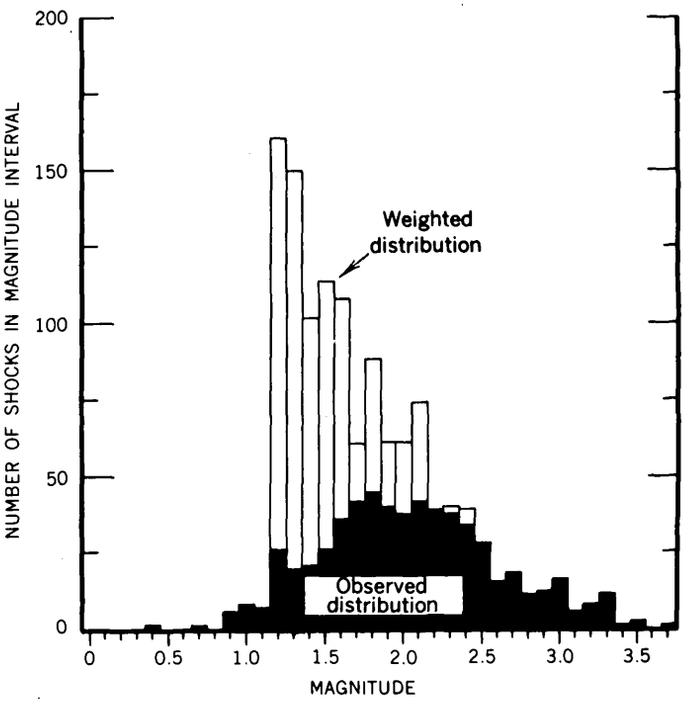

FIGURE 96.1.—Observed and weighted frequency of occurrence of aftershocks versus magnitude recorded at Keg Spring, Idaho, seismic station, August 22–24, 1959 G.c.t. Sample below magnitude 1.15 is too small to be meaningful.

study of aftershocks recorded in southern California, observed that the number of aftershocks increased regularly down to a magnitude of 0.4. Asada and others (1958, p. 23) have reported magnitudes as low as −2, and have indicated that the numbers of aftershocks of magnitudes ranging from 5 to −1 increase regularly with a decrease in magnitude. Many more low-magnitude aftershocks would probably have been recorded if a seismograph had been located in the midst of the aftershock activity, instead of 30 to 60 kilometers from it, because the lower limit of the magnitude of recordable earthquakes is apparently less than −2.

Thirty aftershocks were sufficiently well recorded at two stations to determine the approximate locations of their epicenters (fig. 96.2). Although the location of a shock cannot be determined precisely from recordings at two stations, approximate locations can be determined by making the following assumptions: The focus of the aftershock is at a depth of 10 km and to the northeast of the line connecting the Keg Spring and Victor 1 stations; the velocity of compressional waves in the crust is 6 km per second; and Poisson's ratio for crustal material is 0.25.

The epicenters were determined from the time interval between the onset of the direct P and S waves at the two stations, and the difference between the times of onset of the direct P-wave at both stations. These two

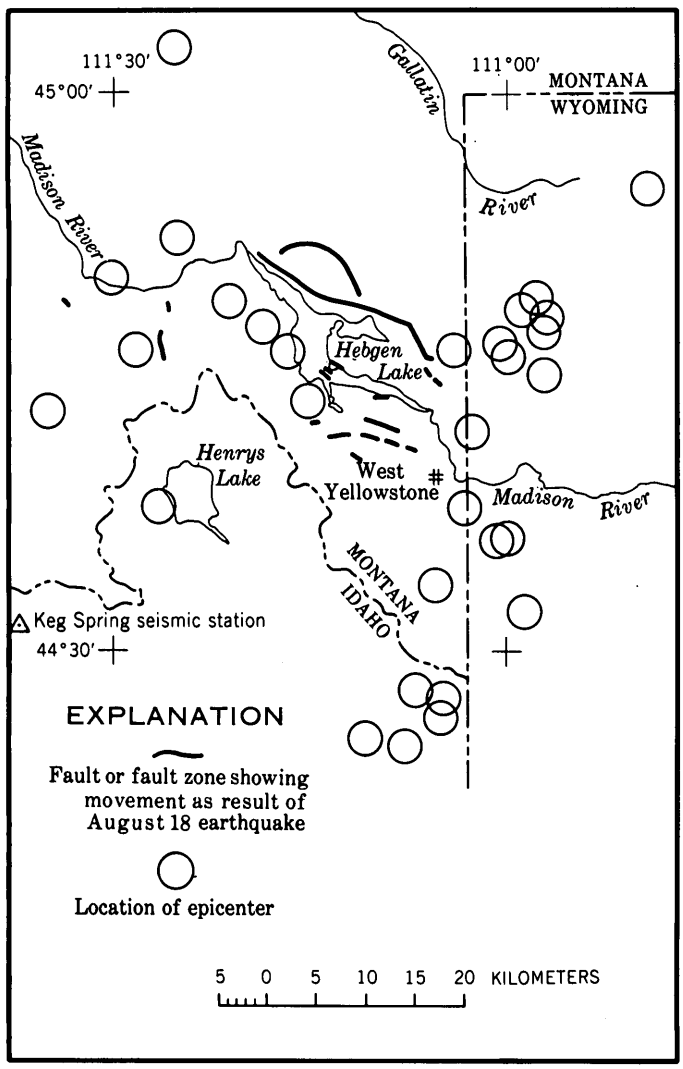

FIGURE 96.2.—Approximate locations of epicenters of 30 aftershocks of the Hebgen Lake, Montana, earthquake of August 18, 1959 G.c.t., recorded August 22–24, 1959 G.c.t.

methods give a "triangle of closure" that gives, on the assumptions above stated, an estimate of the error in locating the epicenters. For the epicenters in figure 96.2 the longest sides of the triangles range from 0 to 13 kilometers and have an average length of 5 kilometers.

In estimating the size of the area in which the aftershocks occurred, it is necessary to remember that the range of perceptibility of the small shocks is rather limited. There may, for example, have been some undetected activity north and east of Hebgen Lake. It is noteworthy, however, that no shocks were detected south of the area covered by the map, and if any shocks comparable to those recorded in this area had occurred father south they would probably have been detected at both stations.

A group of epicenters in the eastern part of the map suggests a zone of activity trending slightly east of north. This alinement does not correlate with any known surface effects of the earthquake or with any known geologic trends. It occurs in an area covered with volcanic rocks and alluvium of Cenozoic age. Most of the remaining epicenters are in the area where the surface was deformed by the earthquake.

ACKNOWLEDGEMENTS

W. H. Jackson, C. H. Miller, and R. E. Warrick assisted in the field work, and F. M. Valentine made many of the office compilations. W. B. Myers and G. D. Fraser provided geologic information and gave the locations of the fault zones associated with the main shock as shown in figure 96.2 of this report.

REFERENCES

Asada, T., Suyehiro, S., and Akamatu, K., 1958, Observation of near-by microearthquakes with ultra-sensitive seismometers at Matsushiro, Japan: Jour, Physics of Earth (Tokyo), v. 6, no. 1, p. 23–33.

Richter, C. F., 1958, Elementary seismology: San Francisco, W. H. Freeman and Company, 768 p.

Richter, C. F., and Nordquist, J. M., 1948, Minimal recorded earthquakes: Seismol. Soc. America Bull., v. 38, no. 4, p. 257–261.

Seismological Society of America, 1959, Seismological notes: Seismol. Soc. America Bull., v. 49, no. 4, p. 415–421.

Stewart, S. W., Roller, J. C., and Diment, W. H., 1959, Maximum accelerations caused by underground nuclear explosions in the Oak Spring formation in area 12 of the Nevada Test Site at distances of 5 to 300 kilometers, a preliminary summary: U.S. Geol. Survey TEI–351, open-file report, 45 p.

97. DEPTH SOUNDINGS IN HEBGEN LAKE, MONTANA, AFTER THE EARTHQUAKE OF AUGUST 17, 1959

By W. H. JACKSON, Denver, Colo.

The major surface effects of the Montana earthquake of August 17, 1959, in the area bordering Hebgen Lake, Montana, included reactivation of the Hebgen fault with the exposure of new scarps as high as 20 feet, tilting and warping of the Hebgen Lake basin, and alteration of Hebgen Lake shoreline by landslides. Because

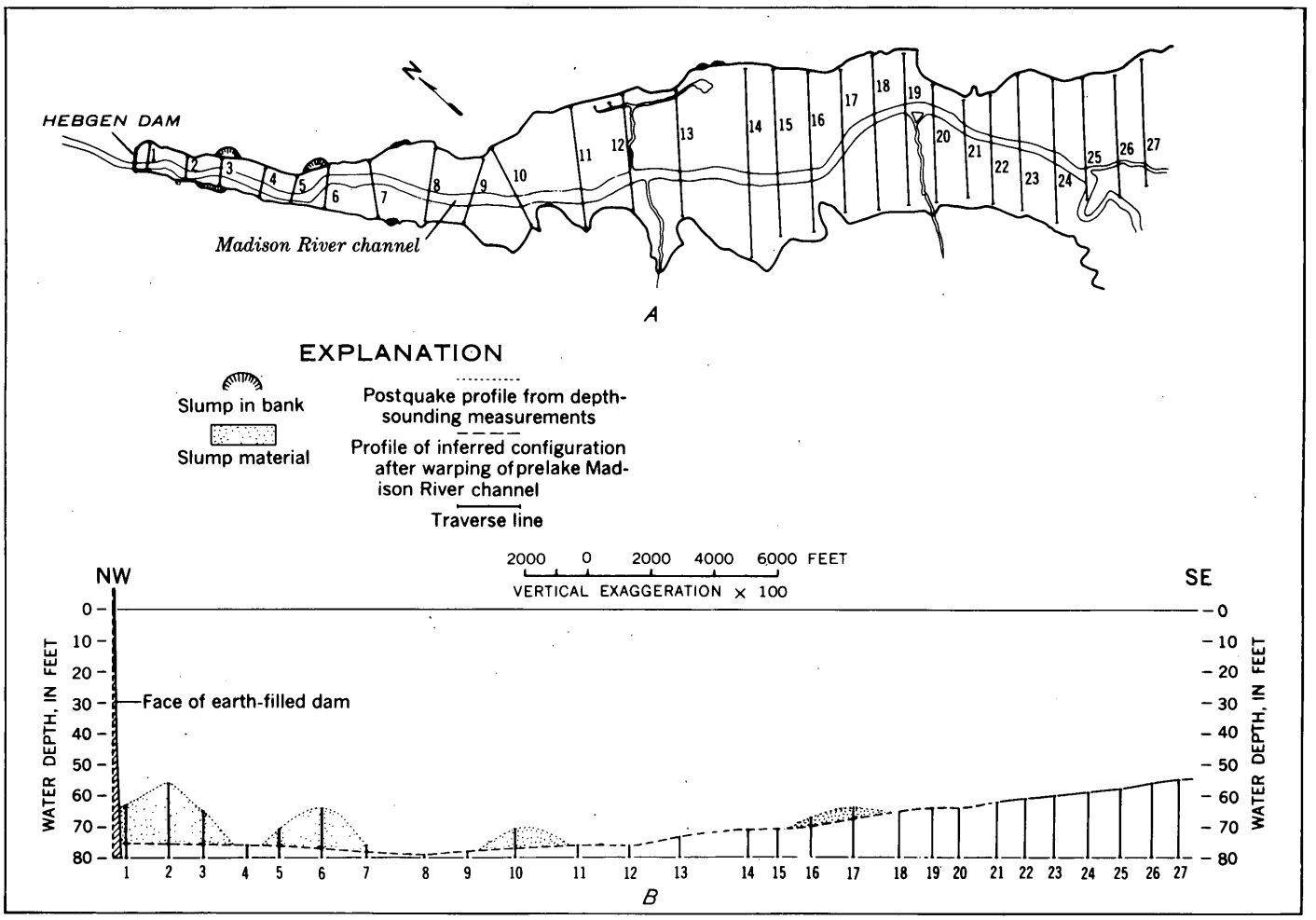

FIGURE 97.1.—*A*, Map of northwest arm of Hebgen Lake showing location of depth-sounding traverses; *B*, profile of lake bottom along Madison River channel.

of the possibility that similar changes may have occurred in the submerged banks and floor of Hebgen Lake, depth soundings were made throughout the lake to determine the extent of any changes.

The lake was traversed from shore to shore and measurements were made with an acoustic echo-sounder that emitted pulses having a frequency of 37.5 kilocycles per second, a length of 6 milliseconds, and a peak power of 150 watts. Soundings were made at the rate of 550 per minute, and echoes from the bottom were recorded on moving paper to produce, in effect, a continuous profile of the lake floor along the traverse lines. Because of the sharp attenuation of the high frequency energy in bottom sediments, sonic penetration is limited to the upper few feet of unconsolidated material, mainly slurries of fine clays, and the records do not reveal subbottom layering or structure.

A vertical profile of the northwestern arm of Hebgen Lake along the deepest part of the Madison River channel shows a uniform gradient of 6 feet per mile between traverses 27 and 12 (fig. 97.1) and a slight decrease in gradient between traverses 12 and 8. Between traverse 8 and the dam, the channel has been partly covered with landslide debris and control points cannot be determined readily; however, the depth of the channel at the dam, according to construction data, is now 4 feet less than at traverse 8 (fig. 97.1). The present gradient determined by the channel depth at the dam, and at traverses 4 and 8 is about 2 feet per mile *upstream*. This reversal in gradient suggests warping of the lake floor and a relative vertical movement of the dam with respect to the floor at traverse 8. If the original stream gradient between traverse 8 and the dam were 3 feet per mile, a vertical displacement of the dam of 10 feet would be required to place the dam in its present position. This agrees approximately with measurements of the lake basin deformation determined by W. B. Myers (written communication).

Assuming a uniform channel gradient between trav-

erse 8 and the dam (fig. 97.1), the depth of debris covering the channel at traverse 2 is about 20 feet and at traverse 6 it is about 13 feet. The debris is undoubtedly part of the several hundred thousand cubic yards of material removed by landslides from the banks along the northeast shore of the lake (J. B. Hadley, written communication).

Evidence of tilting was observed in other parts of the lake, but the soundings gave no indications of major faulting of the lake bottom.

98. CORRELATION OF ALPINE AND CONTINENTAL GLACIAL DEPOSITS OF GLACIER NATIONAL PARK AND ADJACENT HIGH PLAINS, MONTANA

By Gerald M. Richmond, Denver, Colo.

Study of the east slope of Glacier National Park and the adjacent High Plains of the Blackfeet Indian Reservation has revealed new information on the relation of alpine to continental glaciation in this region. In the mountains, an upland erosion surface lying between 7,500 and 8,500 feet and about 1,000 feet below peaks along the Continental Divide, is believed to be of Pliocene age. On the plains, the highest erosion surface, which slopes northeast from an altitude of about 7,000 feet at the mountain front, was probably cut in late Pliocene or early Pleistocene time. The oldest alpine glacial deposits, probably of early Pleistocene age, lie on this surface. Deposits of a second early or middle Pleistocene glaciation lie on broad valley surfaces cut some 200 to 300 feet below the highest plains surface and, like that surface, drain northeast.

Subsequent to the second glaciation, the St. Mary River cut headward along the east flank of the mountains from the north, capturing the northeast-flowing drainage in the northern part of the area. At the same time, Two Medicine Creek cut headward along the mountain front from the southeast to capture most of the northeast-flowing drainage in the southern part of the area. Extensive canyons, about 1,000 feet deep, were cut along these two new drainage systems, whereas only 200 to 300 feet of erosion took place along the beheaded former northeast-flowing drainage on the plains.

Subsequently, ice of a third alpine glaciation, of probable middle Pleistocene age, not only filled the canyons but overflowed into the old northeast-trending drainage. The main body of the ice, however, flowed north into Canada where its outwash is probably included in the Saskatchewan gravel of southern Alberta.

The tills of these three ancient glaciations are all included in the Kennedy Drift of Horberg (1954) and their related outwash deposits extend at least as far east as the Cypress Hills. They have no continental counterparts in this region, but are correlated with the Nebraskan, Kansan, and Illinoian tills of the central interior.

Deposits of two late Pleistocene alpine glaciations are correlated with the Bull Lake and Pinedale glaciations of Wyoming. The older, or Bull Lake glaciation, consists of two distinct advances separated by a major recession. Its two sets of moraines can be traced northeast from the mountain front for 18 miles to a point where the younger overlaps the older and merges with continental drift of the same age. The boundary of this continental drift has been traced by the writer and R. W. Lemke, with A. McS. Stalker of the Canadian Geological Survey, northeast through Canada, back into the United States near Cutbank, and by way of reentrants up Two Medicine Creek and Birch Creek as far west as longitude 112°30′, through Choteau to Great Falls, Montana. The drift is correlated with the "Basal till" of Horberg (1952) and with the Iowan Till of Iowa, which has been dated as >29,000 to >37,000 years (Ruhe and Scholtes, 1959). It is then probably older than the Farmdale loess of Illinois, dated as between 22,900±900 years to 26,100±600 years (Frye and Willman, 1960).

The younger, or Pinedale glaciation, consists of three advances separated by minor recessions. These are correlated with the advances of classical Wisconsin glaciation of Illinois. The till of the early advance merges with an equivalent continental till about 9 miles northeast of the mountain front. Farther out, it is either overlain by that till or lies on uplands above deposits of it on the valley floors. The outer limit of this continental drift, called "Outer Continental drift" by Horberg (1954) has been traced like the continental drift of Bull Lake age as far south as Choteau, Mont. Northwest of Cutbank it lies immediately back of that older drift border, but to the south is 10 to 15 miles from it.

End moraines of the intermediate advance of Pinedale glaciation lie at the mouths of canyons along the

mountain front, and are correlated with the continental drift of the "Lethbridge moraine" and the "Lower till" of Horberg (1952). End moraines of the last advance of Pinedale glaciation lie 3 to 7 miles upstream from those of the intermediate advance, and are tentatively correlated with the Valders advance of the continental ice.

Moraines of two small postaltithermal advances of the ice in the cirques are correlated with those of the Temple Lake and historic advances of the ice in the Wind River Mountains of Wyoming.

REFERENCES

Frye, J. C., and Willman, H. B., 1960, Classification of the Wisconsinian stage in the Lake Michigan glacial lobe: Illinois State Geol. Survey Circ. 285, 16 p.

Horberg, Leland, 1952, Pleistocene drift sheets in the Lethbridge region, Alberta, Canada: Jour. Geology, v. 60, p. 303–330.

——— 1954, Rocky Mountain and continental Pleistocene deposits in the Waterton region, Alberta, Canada: Geol. Soc. America Bull., v. 65, p. 1093–1150.

Ruhe, R. V., and Scholtes, W. H., 1959, Important elements in the classification of the Wisconsin glacial stage: Jour. Geology, v. 67, p. 585–593.

99. THE LATE QUATERNARY AGE OF OBSIDIAN-RHYOLITE FLOWS IN THE WESTERN PART OF YELLOWSTONE NATIONAL PARK, WYOMING

By Gerald M. Richmond and Warren Hamilton, Denver, Colo.

While participating in a reconnaissance study of the Hebgen Lake earthquake, we found that some of the obsidian-rhyolite flows of the Madison Plateau are of late Quaternary age. Near the headwaters of the

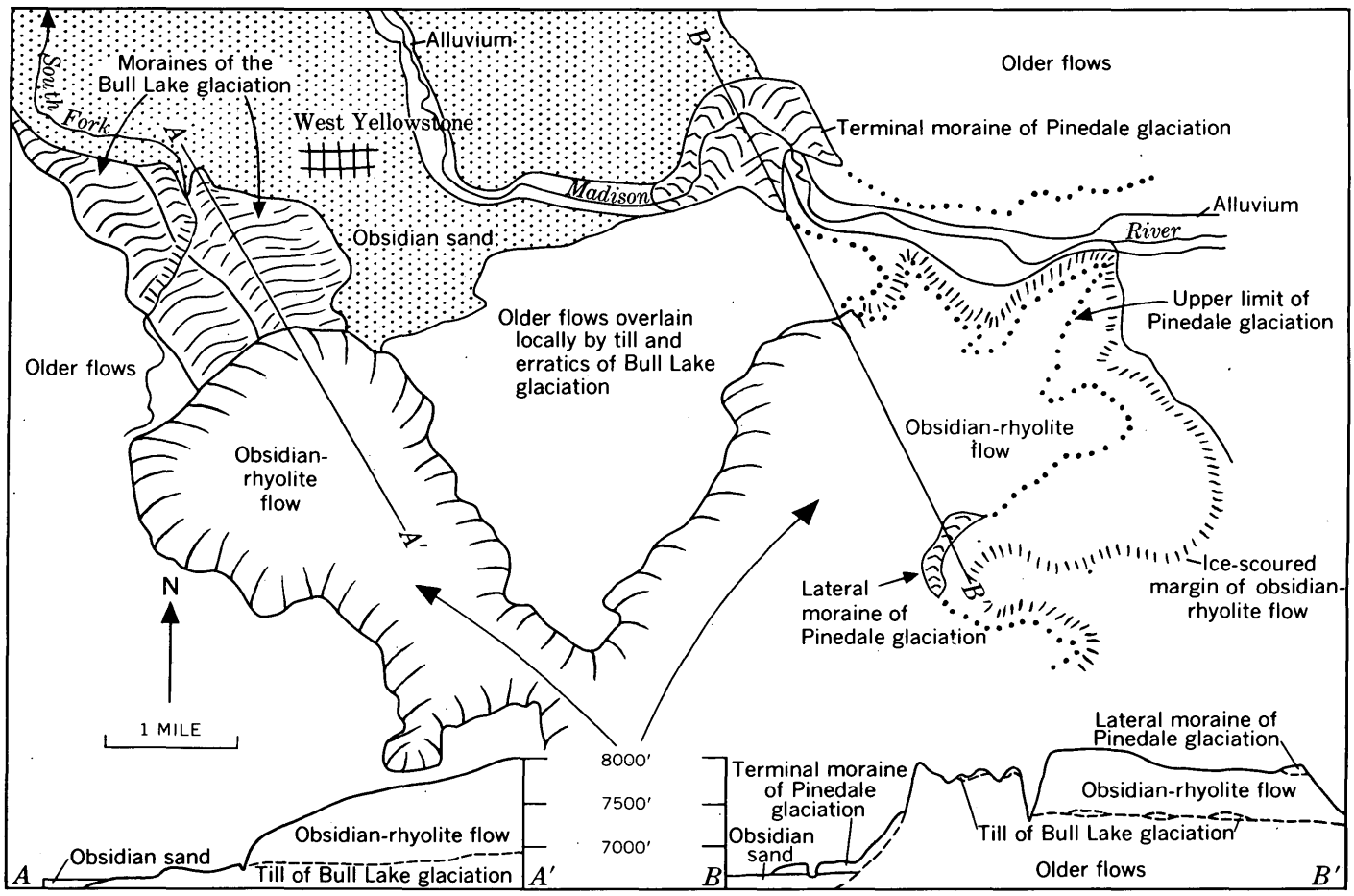

FIGURE 99.1.—Sketch map and sections showing relations of obsidian-rhyolite flow to moraines of the Bull Lake and Pinedale glaciations.

South Fork of the Madison River one of these flows, about 500 feet thick, overlaps large lateral moraines of the late Quaternary Bull Lake glaciation (fig. 99.1). A layer of obsidian sand 40 to 100 feet thick, derived from the lava flow, overlies glacial lake beds retained by the moraines. The moraines, the obsidian sand, and a loess capping the flow are all mantled with a similar maturely developed zonal soil.

The outermost terminal moraine of the subsequent Pinedale glaciation overlaps the obsidian sand at the mouth of the Madison Canyon east of West Yellowstone, and the lateral moraines of the Pinedale glaciation overlap the flow west of the Lower Geyser Basin in Yellowstone National Park. The deposits of the Pinedale glaciation bear a submature zonal soil, which commonly contains a layer of volcanic ash and is quite distinct from the mature zonal soil on deposits of the Bull Lake glaciation.

The obsidian-rhyolite flow must therefore have been extruded between the Bull Lake and the Pinedale glaciations and before the period in which post-Bull Lake—pre-Pinedale soil formation reached a maximum.

100. DISTRIBUTION OF CORALS IN THE MADISON GROUP AND CORRELATIVE STRATA IN MONTANA, WESTERN WYOMING, AND NORTHEASTERN UTAH

By William J. Sando, Washington, D.C.

Preliminary studies of corals collected from sections of the Madison group and correlative rocks of Mississippian age in the northern Cordilleran region (fig. 100.1) suggest the following tentative zonation (figs. 100.2, 100.3).

Zone A comprises the lower 10 to 50 feet of the Lodgepole limestone and equivalent beds in the Hannan limestone. It is characterized by a few species of small corals, including "*Metriophyllum*" cf. "*M.*" *deminutivum* Easton, *Cyathaxonia* cf. *C. tantilla* (Miller), and species of *Permia*?, *Zaphrentites*, and "*Amplexus*."

Zone B includes beds in the lower part of the Lodgepole limestone, and equivalent beds in the Hannan limestone, that are characterized by a few amplexoid corals and *Cyathaxonia*.

Zone C includes the middle and upper parts of the Lodgepole limestone, the lower parts of the Mission Canyon, Brazer, and Charles formations, and equivalent strata in the middle and upper parts of the Hannan limestone. This zone contains a distinctive coral assemblage characterized by species of *Homalopyllites*, *Vesiculophyllum*, and *Zaphrentites*. Its lower part, designated C_1, also contains species of *Rylstonia*, *Michelinia*, *Cleistopora*, and *Lithostrotionella*. In its upper part, designated C_2, *Lithostrotionella* and *Rystonia* are rare and *Michelinia* and *Cleistopora* are absent. The boundary between C_1 and C_2 cannot be precisely established on present information, but it is now placed arbitrarily at the top of the Lodgepole limestone. The C_1 index corals occur at various levels below this boundary but not above it. More detailed work, par-

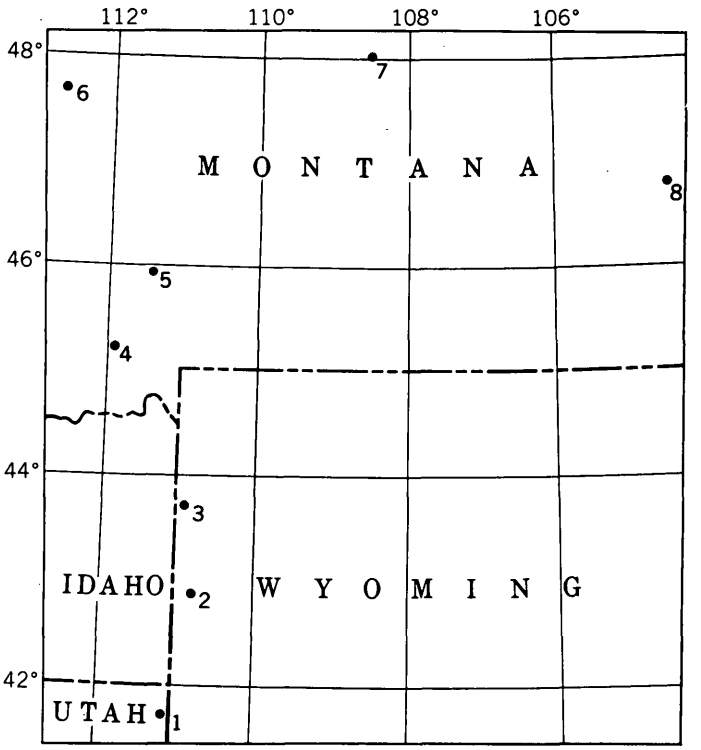

FIGURE 100.1.—Index map showing location of sections studied.

1. Type section of Brazer dolomite, Brazer Canyon, Rich County, Utah.
2. Southeast of Haystack Peak along north tributary of Strawberry Creek, Lincoln County, Wyo.
3. Darby Canyon, Teton County, Wyo.
4. Baldy Mountain, Madison County, Mont.
5. Type section of Madison group, north of Logan, Gallatin County, Mont.
6. Gibson Reservoir on Sun River, Teton County, Mont.
7. Type section of Lodgepole limestone, along Lodgepole Creek, Blaine County, Mont.
8. Shell Oil Co. Pine Unit No. 1 well, Wibaux County, Mont.

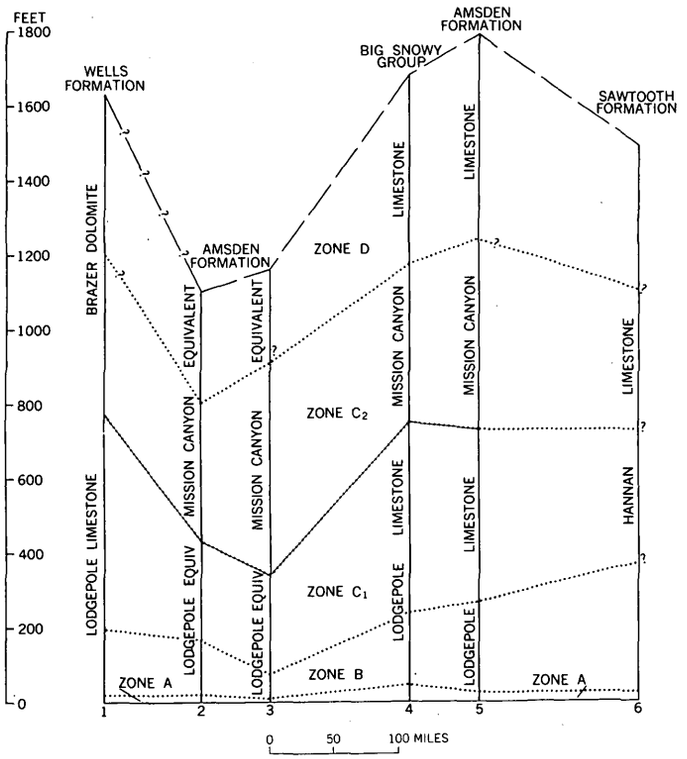

FIGURE 100.2.—Stratigraphic sections from northeastern Utah to northwestern Montana, showing distribution of coral zones in formations of the Madison group and their equivalents.

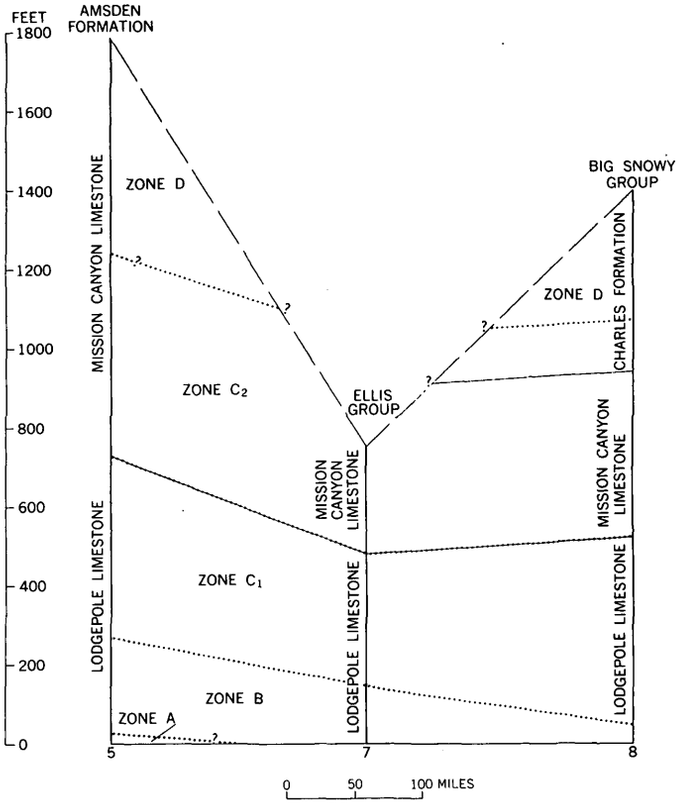

FIGURE 100.3.—Stratigraphic sections from southwestern Montana to northeastern Montana, showing distribution of coral zones in the Madison group.

ticularly on the distribution of species, may provide a more satisfactory basis for subdivision of Zone C.

Zone D includes the upper parts of the Brazer, Mission Canyon, and Charles formations, and equivalent strata in the upper part of the Hannan limestone. This zone is characterized by species of *Vesiculophyllum*, *Faberophyllum*, and fasciculate lithostrotionoids, chiefly belonging to *Siphonodendron* and *Diphyphyllum*. A distinctive new horn coral genus also occurs in the upper part of the Brazer and upper part of the Hannan.

Coral genera other than those mentioned occur in all the zones. Many of these are rare, and details of the taxonomy of some are yet to be worked out. Species of *Syringopora* are abundant throughout the sequence, but these are not considered important at present because of the difficulty of recognizing stratigraphically useful species.

Correlations cannot be made with equal confidence between all the sections studied, because several depositional provinces appear to be represented. As corals are rather sensitive to environmental changes, different lithic facies tend to contain different assemblages of corals. The scarcity of fossils in the Brazer may be related to the predominance of dolomite in that unit. The lower part of the Brazer contains the critical elements of the C_2 fauna, whereas only one, or possibly two, of the corals of Zone D have been found in the upper part, most of which is unfossiliferous, and whose late Mission Canyon age is therefore not well established. The coral assemblages of sections 2, 3, 4, and 5 are very similar, except that the Zone D assemblage is poorly represented in sections 3 and 5. The five zones can all be identified in the Hannan limestone, but the positions of most of their boundaries are uncertain. The Hannan may be more similar in faunal content and lithic succession to the Mississippian sequence in the Canadian Rockies than it is to the sections south of it.

In each of the western sections (1 through 6), the thicknesses of all the zones are roughly proportional to the total thicknesses of the formations. Thickening and thinning thus appear to depend mainly on varying rates of deposition. Erosion at the top of the Mission Canyon limestone and its equivalents has not appreciably altered the general pattern of thickness variation in these sections. In central Montana (section 7), however, beds included in Zone D and part of Zone C have been removed by post-Mission Canyon erosion.

In central and eastern Montana (sections 7 and 8), the Zone A assemblage was not identified, and rocks containing the Zone B assemblage appear to thin eastward. This suggests that Zone A may not be present in these sections. Zone A and part of Zone B may be represented in the Little Chief Canyon member of the Lodgepole limestone of central Montana and the Bakken formation of the Williston basin. Zones C_1, C_2, and D are readily identified in cores drilled in the Williston basin (section 8). Cores from the Charles formation contain C_2 and D assemblages, suggesting correlation with the upper part of the Mission Canyon as exposed at the surface.

Coral faunas of the Madison group and its correlatives do not provide a satisfactory basis for detailed correlation with the type Mississippian of the Mid-Continent region, because their sensitivity to depositional conditions appears to have given rise to different assemblages and distribution patterns in rocks believed to be nearly contemporaneous. Preliminary studies by J. T. Dutro, Jr., of brachiopods associated with the coral assemblages suggests the following tentative correlations with the type Mississippian: Zone A appears to be entirely of Kinderhook age. Beds equivalent to part of Kinderhook may be present in Zone B, and they possibly extend into C_1. Osage equivalents are found in C_1, C_2, and D, but part of Zone D is probably of Meramec age. These correlations are confirmed, in general, by the distribution patterns of coral genera common to the Madison and the type Mississippian sequences.

101. MIDDLE TERTIARY UNCONFORMITY IN SOUTHWESTERN MONTANA

By G. D. Robinson, Denver, Colo.

Since the earliest paleontologic work by Douglass (1899 and several later papers), geologists have suspected that there was a regional middle Tertiary unconformity in the Cenozoic basins of southwestern Montana (see fig. 101.1). In several basins, Douglass found many early Oligocene and many late Miocene vertebrates but few of intervening age, and this has been the experience of all later workers. The existence of an unconformity thus became increasingly certain, and the nature and duration of the unconformity are gradually being demonstrated by detailed mapping combined with intensive fossil collecting. In the southern part of the Townsend basin, the unconformity has been mapped as an erosional one separating lower Oligocene from upper Miocene or lower Pliocene strata. (For southeastern part, see H. D. Klemme, unpublished Ph. D. thesis, Princeton University, 1949; and for southwestern part, see Freeman, Ruppel, and Klepper, 1958.)

Recent detailed mapping of the Toston 15-minute quadrangle (see fig. 101.1) has shown that in the southeastern part of the Townsend basin middle as well as lower Oligocene rocks are preserved beneath the unconformity; inconclusive structural evidence suggests that during the hiatus these rocks were probably folded and faulted as well as deeply eroded. The unconformity has been traced southward throughout the Clarkston basin, where the youngest rocks beneath it are lower Oligocene; in this basin also, the existence of an angular unconformity is probable but not certain. Reconnaissance observations make it seem likely that the hiatus

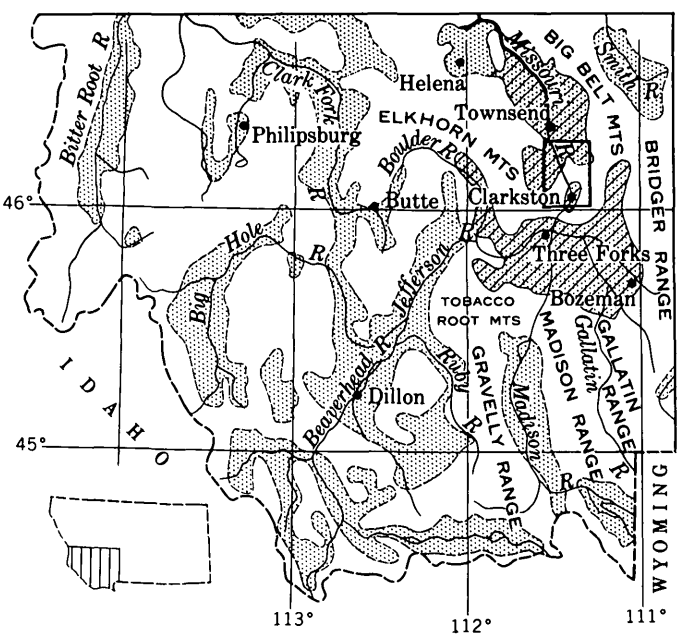

FIGURE 101.1.—Index map of southwestern Montana. Cenozoic basins stippled. Townsend, Clarkston, and Three Forks basins diagonally ruled. Toston quadrangle heavily outlined.

can be mapped northward at least throughout the Townsend basin and southward throughout the Three Forks basin; these basins contain an area of more than 1,500 square miles of Tertiary rocks. The present flood plain of the Missouri River and that of its main headwater tributary, the Madison, are remarkably close to the trace of the unconformity. In the three basins studied, most of the Tertiary rocks exposed west of these rivers are Oligocene or older; most of those east of the rivers are Miocene or younger.

These basins were being eroded by through-flowing streams during most of late Oligocene to middle Miocene time. In some places, however, a little alluvium was deposited and is still partly preserved.

The Tertiary rocks above and below the unconformity have much in common—they are rich in contemporaneous volcanic ash, and are of complex origin, having been deposited in streams, lakes, and bolsons—yet they show persistent differences, apparent in the field, that make it possible to distinguish the older assemblage from the younger. The most useful of these involves waterlaid glass shards. In the older rocks most of them are so much devitrified as to appear cloudy and dull in hand specimens; in the younger rocks almost all are notably clear and bright. But this criterion applies only to rocks deposited in water, for unaltered glass is abundant in much of the Tertiary tuff deposited on dry land irrespective of age. Tuffaceous rocks that contain intimately mixed rounded grains of terrigenous sand must have been deposited in water, and in practice the test is used only on visibly polygenetic sandstone, thin beds of which are common both in the rocks above the hiatus and in those below.

Why the shards in the older and younger waterlaid beds are so differently altered is unknown. The older glass is not more altered simply because it is older or because it was deeply weathered during the erosion interval, for if either age or weathering were decisive the glass of the older tuffs deposited on dry land would be as much altered as that in water laid tuffs. Undeciphered differences in depositional or diagenetic environment are probably responsible.

Certain differences between pre- and post-hiatus conglomerates are also helpful. Conglomerate is a minor component of the Oligocene section, even near basin edges. The few beds are usually thin, the stones are rarely larger than small cobbles, and consolidation is generally only poor to fair. In the Miocene and Pliocene formations, on the other hand, conglomerate is a major constituent. Here, moreover, the beds are very thick, cobble and boulder sizes are abundant, and the conglomerates are firmly cemented with calcite and clay. These differences reflect rather low relief and equable climate in early Oligocene time, as opposed to high relief and semiarid climate in late Miocene and early Pliocene time.

It must be emphasized, however, that the conglomerates are helpful only in distinguishing Oligocene from younger strata. Eocene rocks in the Three Forks basin (Robinson and others, 1957) and Eocene and Paleocene rocks in other basins of southwestern Montana (Peale, 1896; Lowell and Klepper, 1953) also include much coarse conglomerate, in thick beds, with calcite cement.

The validity of the contacts mapped with the aid of these crude lithologic guides is confirmed by paleontologic evidence. Nearly every sizable body of rocks in southeastern Townsend Valley and in Clarkston Valley that was assigned to the early Tertiary on lithologic grounds has yielded diagnostic middle Oligocene or older vertebrate fossils; and almost every large mass mapped as late Tertiary has yielded diagnostic Miocene or younger fossils. (I am indebted to Edward Lewis for identifying the collections, some of which were made by others, notably H. Morton Sperry of Townsend.)

It remains for future study to delimit the areas within which the unconformity can be confidently mapped on lithologic grounds, even where diagnostic fossils may be lacking.

REFERENCES

Douglass, Earl, 1899, The Neocene lake beds of western Montana and descriptions of some new vertebrates from the Loup Fork: Master's thesis, Montana University (published by the University).

Freeman, V. L., Ruppel, E. T., and Klepper, M. R., 1958, Geology of part of the Townsend Valley, Broadwater and Jefferson Counties, Montana: U.S. Geol. Survey Bull. 1042–N, p. 481–556.

Lowell, W.R., and Klepper, M.R., 1953, Beaverhead formation, a Laramide deposit in Beaverhead County, Montana: Geol. Soc. America Bull., v. 64, no. 2, p. 235–243.

Peale, A. C., 1896, Description of the Three Forks sheet, Montana: U.S. Geol. Survey, Geol. Atlas Folio 24.

Robinson, G. D., Lewis, Edward, and Taylor, D. W., 1957, Eocene continental deposits in Three Forks Basin, Mont. (abs.): Geol. Soc. America Bull., v. 68, no. 12, pt. 2, p. 1786.

102. CONFIGURATION OF THE 10N PLUTON, THREE FORKS, MONTANA

By Isidore Zietz, Washington, D.C.

In the summer of 1959, the U.S. Geological Survey made a detailed aeromagnetic survey in the Three Forks area, Montana, to determine the approximate shape of the 10N pluton (named for U.S. Highway 10N, which crosses it) and its relation to the Lombard thrust, which crops out about a mile to the east.

The pluton has been described by G. D. Robinson of the U.S. Geological Survey in a report now in preparation, as an igneous mass made up of a wide variety of rock types but consisting chiefly of light-colored pinkish quartz monzonite. It intrudes Paleozoic and younger sedimentary rocks and has a surface extent of more than three miles east-west and more than a mile north-south (fig. 102.1).

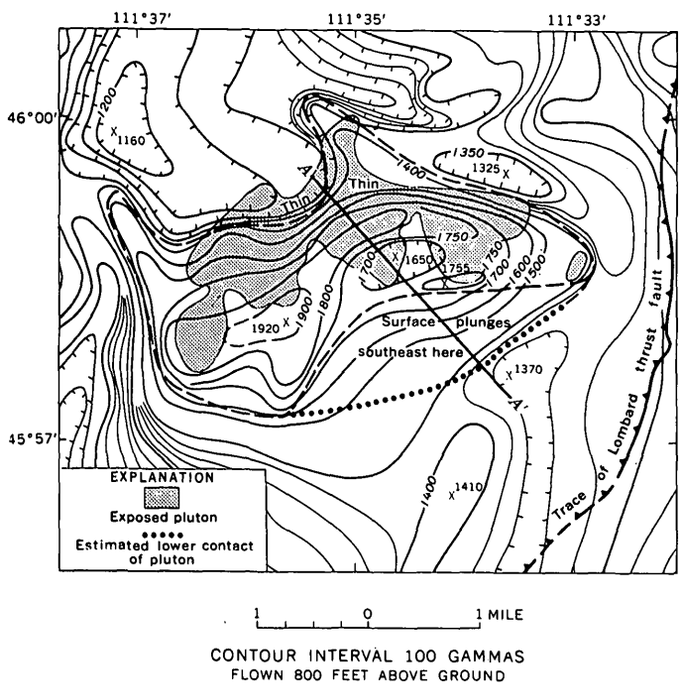

Figure 102.1.—Aeromagnetic map of Three Forks area, Montana.

The aeromagnetic survey, which was made at Robinson's request, was flown north-south at an elevation of approximately 800 feet above the ground and with a flight separation of a quarter of a mile. The upper surface of the pluton is well defined by the magnetic contours, and is interpreted to have the boundary indicated by the dashed line in figure 102.1. The contours also suggest the presence of two spurs at the north edge of the pluton. To the north, west, and southwest of the pluton, the gradients are sharp and the amplitude large, indicating that the pluton extends downward for several thousand feet. To the southeast, the gradient is flatter and the amplitude smaller, indicating that the pluton is buried beneath a sedimentary cover and thins to the southeast. In other parts of the area, especially to the north, the aeromagnetic data imply local thinning, as is indicated on the map.

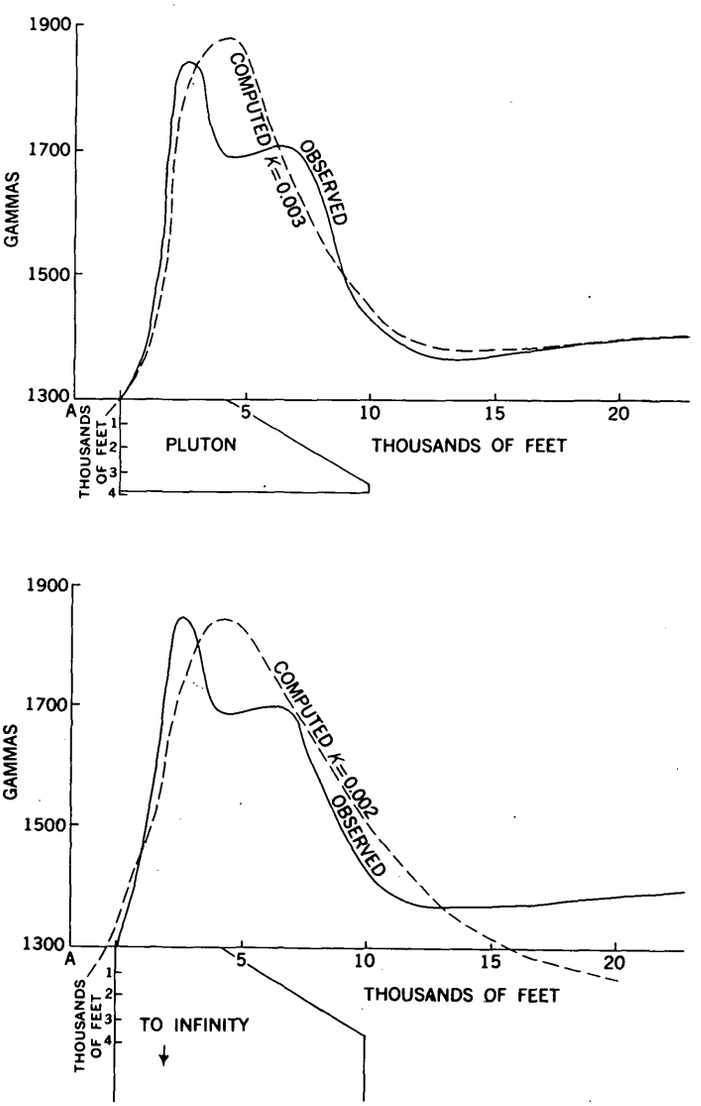

Figure 102.2.—Magnetic profiles across the 10N pluton, Three Forks area, Montana.

To determine the approximate shape of the pluton, and especially its vertical extent, a magnetic profile, *A–B*, at right angles to the main magnetic trend, was analyzed (figs. 102.1 and 102.2). The magnetic anomalies of two possible geologic cross sections were then computed (fig. 102.2) and compared with the observed profile A–B. On both cross sections the upper surface dips to the southeast at an angle of 30°, corresponding to the dip of the overlying sedimentary rocks. In the upper figure the pluton is assumed to have a bottom 3,800 feet below the surface, and in the lower figure it is assumed to extend indefinitely downward. At the northwest edge there is good agreement for both configurations. At the southeast, however, the fit for the bottomed pluton is much better than for the other. The magnetic susceptibilities calculated for both masses, $K=0.003$ cgs and $K=0.002$ cgs, are reasonable for quartz monzonite.

Because of the ambiguity inherent in magnetic calculations, there are a large number of masses with different shapes that could produce reasonable fits to the observed magnetic profile, and for this reason the available evidence for the configuration of the pluton is not conclusive. The calculations strongly suggest, however, that the pluton is bottomed at a depth of several thousand feet. This would imply that the thrusting may be younger than the intrusive and that the 10N pluton may be cut off by the Lombard thrust.

103. METAMORPHISM AND THRUST FAULTING IN THE RIGGINS QUADRANGLE, IDAHO

By Warren Hamilton, Denver, Colo.

In the Riggins quadrangle, Idaho, metamorphosed volcanic rocks of the andesite-keratophyre kindred, and associated metasedimentary rocks dominantly of volcanic origin, increase in metamorphic grade eastward toward a broad complex of intrusive and metamorphic gneisses marginal to the Idaho batholith of Cretaceous age. The rocks to be considered here (which have not yet been given a geologic name) pass eastward from, for example, greenstone through green phyllite, greenschist, and hornblende schist to amphibolite. Isograds have been drawn through the westernmost points at which each of the following minerals appears: aluminian prochlorite, biotite, clinozoisite, garnet, oligoclase, andesine, and, in calc-silicate rocks only, clinopyroxene (fig. 103.1). Black hornblende appears first near the garnet isograd. Neither staurolite, kyanite, nor sillimanite is anywhere present.

Although the upper grade limit of ferroan prochlorite is at about the garnet isograd, that of aluminian prochlorite is near the andesine isograd. Aluminian prochlorite, muscovite, garnet, and oligoclase occur in apparently equilibrium assemblages in some specimens.

In the western part of the quadrangle, a postmetamorphic, west-directed overthrust fault trending north-northeast has pushed the rocks here considered over the low-grade rocks of the Seven Devils volcanics and associated formations (Permian and Triassic) on the west. Within the quadrangle, all the isograds in the upper plate from aluminian prochlorite to andesine are truncated by the fault and brought against rocks of the ferroan-prochlorite zone in the lower plate (fig. 103.1). In the northern part of the quadrangle, the fault is hidden by Miocene basalt. Where it emerges from the basalt cover the fault is folded, and a few miles farther north the upper plate is cut off by a sheet of intrusive quartz diorite gneiss.

Above this overthrust is another, subparallel to it but converging with it southward; the average distance between the two is about a mile (fig. 103.1). Amphibolite and trondhjemite were shoved westward over middle-grade schists on this upper fault, which is marked by a thick zone of phyllonites and flaser gneisses. The total displacement on the two thrust faults is about 10 miles. Toward the north the upper fault dies out and a greater proportion of the total displacement is taken up by the lower one.

Thrusting east of the Idaho batholith is mostly directed eastward. If the west-directed thrust faulting west of the batholith is of regional extent, tectonic symmetry on a grand scale exists that may be genetically related to the batholith.

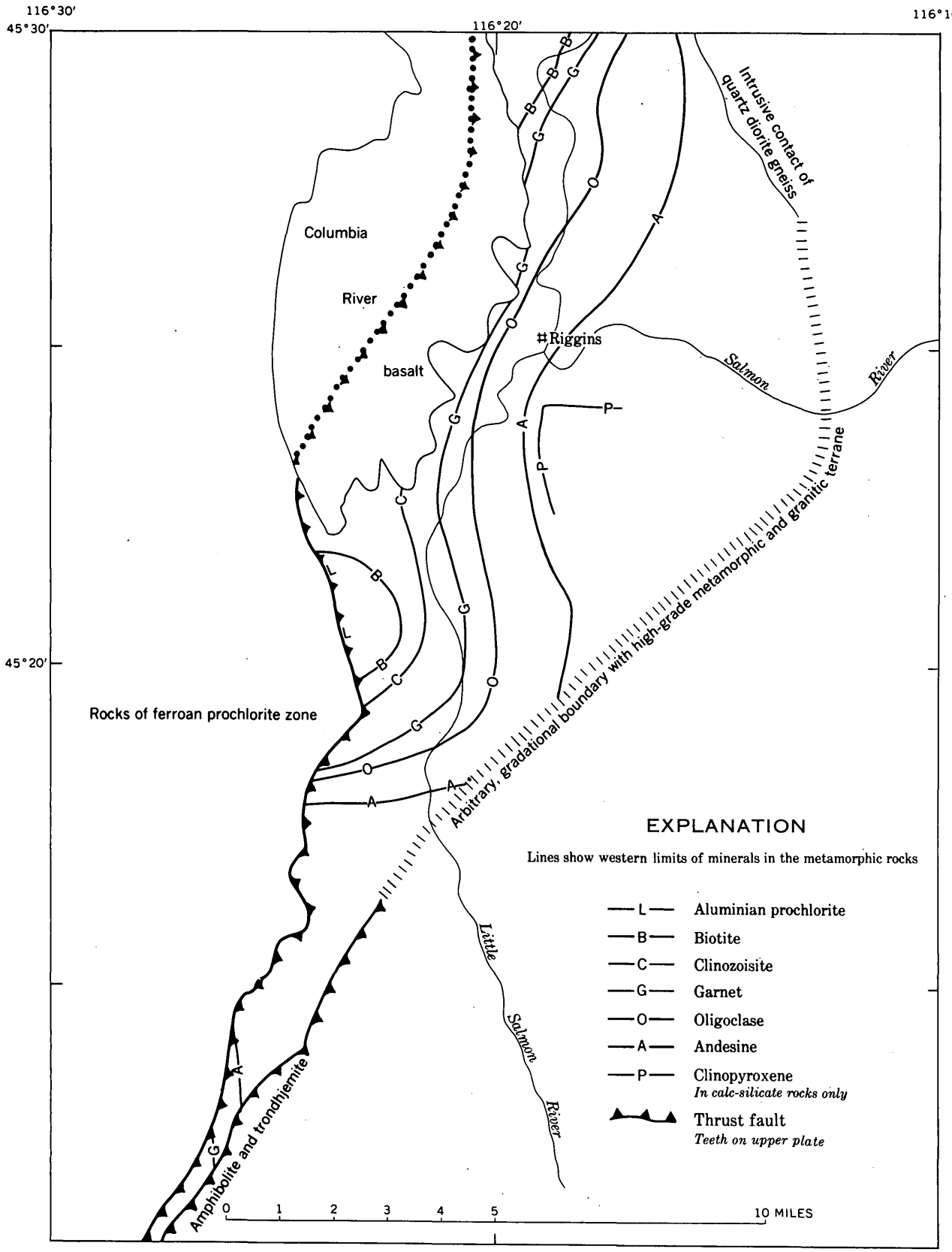

FIGURE 103.1.—Thrust faults and isograds in metamorphic rocks of northwest part of Riggins quadrangle, Idaho.

104. DIVERSE INTERFINGERING CARBONIFEROUS STRATA IN THE MACKAY QUADRANGLE, IDAHO

By Clyde P. Ross, Denver, Colo.

Throughout the limited area in central Idaho, north of the Snake River Plain, in which Paleozoic sedimentary rocks occur, those rocks vary in composition and stratigraphic relations within short distances. This is particularly true of the post-Devonian part of the sequence. Exposures of late Paleozoic strata in the Mackay quadrangle furnish essential clues to the reasons for the stratigraphic variation in the surrounding region.

The region contains the Milligen formation (Mississippian and Devonian?), the Brazer limestone (mainly Mississippian), and the Wood River formation (Pennsylvanian and Permian). The Milligen formation in its type locality (Umpleby and others, 1930, p. 25–29), which is west of the Mackay quadrangle, is very heterogeneous, but its distinguishing feature is the presence of abundant black, carbonaceous argillite. The formation contains some graphitic coal. The Milligen formation may be over 7,000 feet thick (Kiilsgaard, 1950). In this locality the formation was deposited close to the western shore of the Paleozoic sea, perhaps mainly in estuaries and other relatively stagnant bodies of water. It contains hardly any diagnostic fossils, but its relations to other formations indicate that the formation may represent all of Mississippian time and may possibly range downward into the Devonian. Rocks assigned to the Milligen, largely because of their carbon content, have been mapped over a wide region in the southeastern part of central Idaho. In the mountain range east and northeast of the principal exposures of the Carboniferous rocks of the Mackay quadrangle the Milligen formation attains a maximum thickness of at least 1,000 feet and is clearly of Early Mississippian age, for it is underlain by fossiliferous rocks of very late Devonian age and overlain by fossiliferous limestone of Late Mississippian age that belongs to the Brazer limestone as that term is applied locally.

The Wood River formation where exposed west of the Mackay quadrangle (Umpleby, Westgate, and Ross, 1930, p. 24–34) is lithologically diverse, but is characterized by abundant sandy beds and, especially near the base, by abundant conglomerate, part of it coarse and in thick layers. The formation must have been deposited close to the shore; the conglomerate in it may be at least in part of fluviatile origin. The Wood River formation has been regarded as of Pennsylvanian age (Umpleby, Westgate, and Ross, 1930, p. 32–34), but microfossils (Bostwick, 1955), discovered since the formation was defined, have shown that large thicknesses of beds assigned to it by Bostwick are of Permian age. These beds have nowhere been separately mapped. The Wood River formation west of the Mackay quadrangle is probably at least 8,000 feet thick, and may be much thicker if the beds containing Permian fossils are included in it. Beds definitely assignable to the Wood River formation are not known to occur east of the western part of the Mackay quadrangle, but the name has been used tentatively as far east as the Montana boundary (Scholten, 1957a, p. 165; Scholten, 1957b).

Rocks commonly called Brazer limestone are widespread from an interrupted zone trending nearly north through the middle of the Mackay quadrangle well to the north and eastward into Montana, and of large but variable thickness. In the Mackay quadrangle itself their thickness exceeds 8,000 feet. They consist mainly of limestone but include some quartzite and conglomerate of Mississippian age. As originally used in central Idaho (Ross, 1934, fig. 2, p. 977–985) the Brazer limestone is of Late Mississippian age, but in localities far to the northeast of the Mackay quadrangle, limestone that has not yet been mapped separately from the Brazer limestone has yielded fossils of Pennsylvanian and Permian age. In that part of Idaho the Brazer limestone together with these younger, associated beds may have an aggregate thickness of more than 10,000 feet. In the Mackay quadrangle, rocks that were mapped in the field as Brazer limestone are now known on paleontologic evidence to be largely of late Early to Late Mississippian age, and in several outcrops they even include rocks of Pennsylvanian age (Dutro, J. T., Jr., oral communication, 1959; Douglass, R. C., and Yochelson, E. L., 1958, written communication), but the Pennsylvanian limestone cannot be distinguished in mapping from the limestone of Mississippian age without far more refined work than it has been practicable to do in making the present map of that quadrangle. In the northern part of the Mackay quadrangle the Pennsylvanian limestone is intercalated with clastic beds of nearshore origin (Skipp, 1958).

The Mackay quadrangle contains a stratigraphic unit, not previously recognized anywhere else in Idaho, that includes lithologic equivalents of nearly all the components of the three formations briefly described

above, but these rocks are so intermingled that they cannot be mapped separately. They include much quartzite, siltstone, argillite, and conglomerate, but in most places little or no limestone. This unit, at least 5,000 feet thick where mapped, constitutes a formation that interfingers with the local representatives of the Milligen and Wood River formations and the Brazer limestone. Relations to these three formations demonstrate that this unit ranges in age from Early Mississippian well into the Pennsylvanian. No fossils of Permian age are known in the Mackay quadrangle, and structural relations make it improbable that any beds of that age are exposed there. It is reasonable to surmise, however, that somewhere, presumably south or southwest of the Mackay quadrangle, the newly recognized unit includes beds of Permian age.

This unit is known only in the western part of a geosynclinal lobe that extends into central Idaho from the south. It constitutes a mingling of beds of diverse but largely clastic character that were laid down near shore in late Paleozoic time. Farther east, in the middle part of that lobe, carbonate rocks predominate. Northeast of the boundary between Idaho and Montana beds of late Paleozoic age were deposited on a broad shelf. In that region the stratigraphy is drastically different from that outlined here. The lobe in central Idaho is the northern part of the large geosynclinal mass that is widespread in southeastern Idaho and regions farther south.

REFERENCES

Bostwick, D. A., 1955, Stratigraphy of the Wood River formation, south-central Idaho: Jour. Paleontology, v. 29, p. 941–951.

Kiilsgaard, T. H., 1950, The Geology and ore deposits of the Triumph-Parker mine mineral belt: Part II *in* Anderson, A. L., Kiilsgaard, T. H., and Fryklund, V. C., Jr., Detailed geology of certain areas in the Mineral Hill and Warm Springs mining districts: Idaho Bur. Mines and Geology Pamph. 90, p. 39–62.

Ross, C. P., 1934, Correlation and interpretation of Paleozoic stratigraphy in south-central Idaho: Geol. Soc. America Bull., v. 45, p. 937–1000.

Scholten, Robert, 1957a, Paleozoic evolution of the geosynclinal margin north of the Snake River Plain, Idaho-Montana: Geol. Soc. America Bull., v. 68, no. 2, p. 151–170.

——— 1957b, Preliminary interpretation of Permo-Carboniferous stratigraphy in east-central Idaho [abs.]: Geol. Soc. America Bull., v. 68, no. 12, pt. 2, p. 1794.

Skipp, B. A. L., 1958, Significant sedimentary features in Mississippian rocks in Custer County, Idaho [abs.]: Geol. Soc. America Bull., v. 69, no. 12, pt. 2, p. 1744.

Umpleby, J. B., Westgate, L. C., and Ross, C. P., 1930, Geology and ore deposits of the Wood River regions: U.S. Geol. Survey Bull. 814.

105. PROGRESSIVE GROWTH OF ANTICLINES DURING LATE CRETACEOUS AND PALEOCENE TIME IN CENTRAL WYOMING

By William R. Keefer, Laramie, Wyo.

The progressive growth of some anticlines during Late Cretaceous and early Tertiary time can be demonstrated in the Wind River Basin, central Wyoming. This information helps in local and regional correlation of stratigraphic units and in the interpretation of geophysical data and well records. The stratigraphic and structural relations have especial importance in the Wind River Basin, because the rocks involved contain oil and gas in some parts of the basin, and an understanding of the history of folding and sedimentation may lead to the discovery of traps in other parts.

The geology of two areas, Shotgun Butte and Alkali Butte, illustrate progressive growth of anticlines. Basic data were obtained by measuring sections in detail and mapping individual beds or groups of beds in the field. A multiplex stereo-plotter was used to complete the mapping, and compilation was made on topographic base maps. Ages of the rocks were determined by fossil vertebrates, leaves, and pollen.

557753 O—60——16

SHOTGUN BUTTE

Figure 105.1 shows changes in thickness of the Meeteetse, Lance, and Fort Union formations in outcrops extending southward from the vicinity of Shotgun Butte (Troyer and Keefer, 1955; Keefer and Troyer, 1956). The line of section crosses a series of southeast-plunging anticlines and synclines, the Shotgun Butte syncline, an extension of one of the major structural troughs of the Wind River Basin, being at its north end and the Little Dome anticline at its south end (inset, fig. 105.1).

The relations shown in figure 105.1 indicate that several folds began to form during deposition of the Meeteetse formation, and that moderate deformation

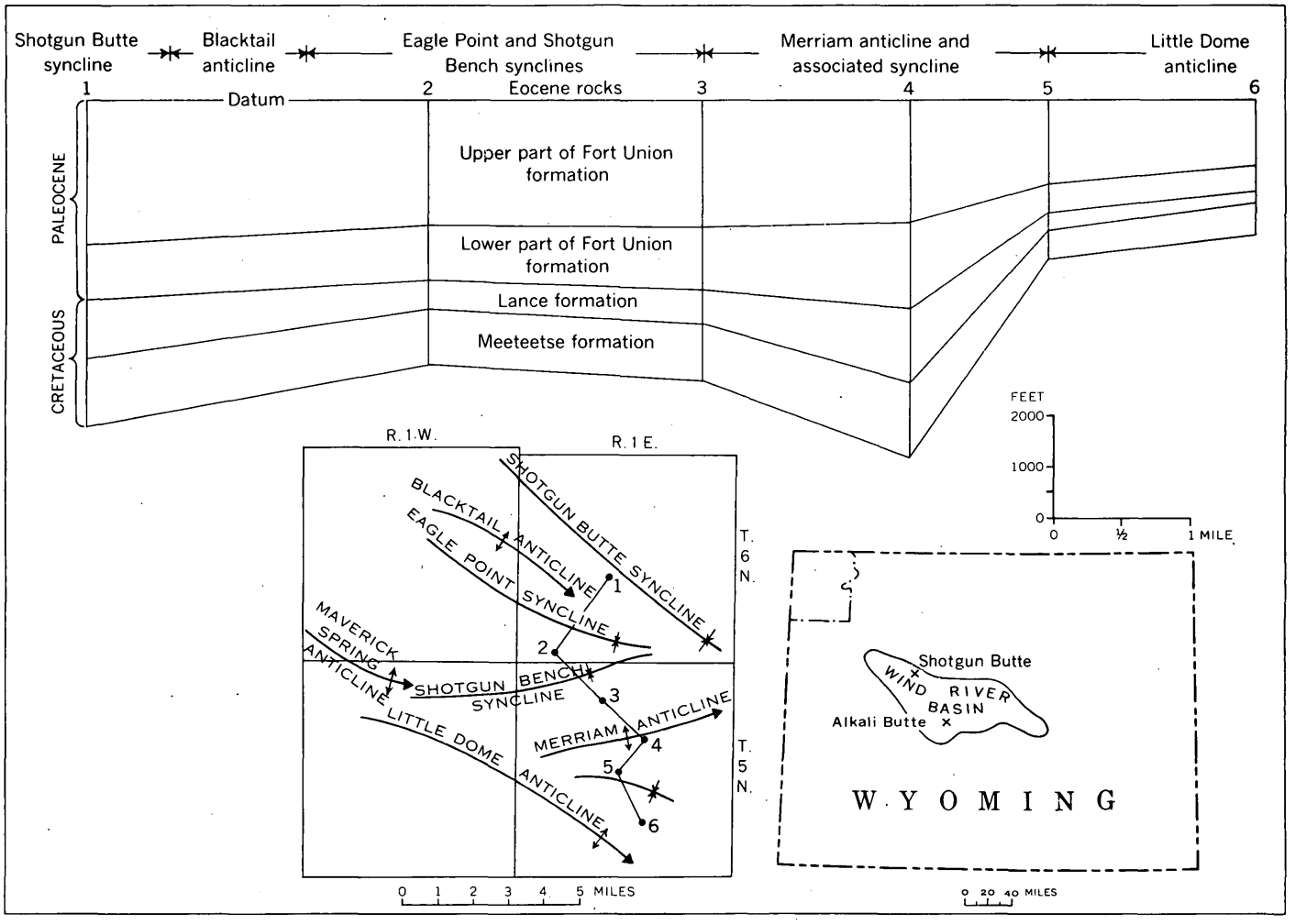

FIGURE 105.1.—Stratigraphic relations of uppermost Cretaceous and Paleocene rocks in vicinity of Shotgun Butte and Little Dome anticline. Inset map shows location of Alkali Butte and Shotgun Butte with reference to Wind River basin.

was generally continuous through latest Cretaceous and Paleocene time. During this time sediments accumulated in thick conformable sequences in certain rough areas, whereas the sediments on the crest and along the north flank of Little Dome anticline are much thinner and are broken by unconformities. As a result of continuous downwarping, the trough areas in this region contain some of the thickest and most complete sections of Upper Cretaceous and Paleocene rocks exposed in central Wyoming. Paleontologic studies of numerous plant and vertebrate fossils also indicate that sedimentation in these troughs was continuous.

At some places the upwarps and downwarps which began to form in Late Cretaceous time continued to develop along the same structural trends throughout the later and major phases of the Laramide orogeny, in latest Paleocene and early Eocene times. The present sites of the Little Dome anticline and the Shotgun Butte syncline, for example, coincide closely with the features ancestral to them. The Merriam anticline and the Shotgun Bench syncline, on the other hand, were probably the sites of a trough and an upfold, respectively, during Late Cretaceous and Paleocene time. Murphy and others (1956) and Troyer and Keefer (1955), basing their conclusions largely on structural data, have pointed out that neither the Merriam anticline nor the Shotgun Bench syncline was formed until late early Eocene time, and that they trend east-west whereas the older folds trend northwest (inset, fig. 105.1). The stratigraphic relations tend to confirm these views as to the time of folding of the older structural features. Thinning of Upper Cretaceous and Paleocene sediments toward the present site of the Shotgun Bench syncline was probably caused by the initial folding of the Maverick Spring anticline, which lies directly northwest of the Little Dome anticline in the southwestern part of T. 6 N., and the northwestern part of T. 5 N., R. 1 W. (fig. 105.1). The thickening of

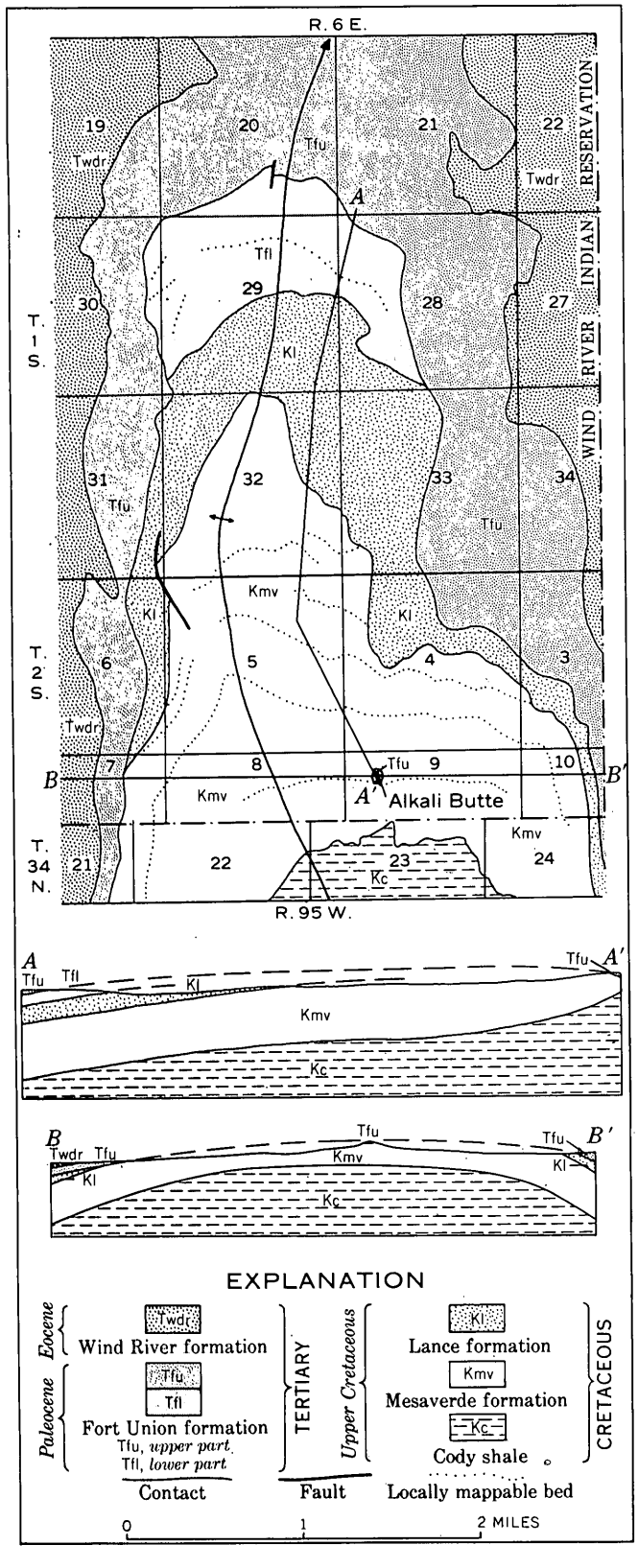

FIGURE 105.2.—Geologic map and structure sections of Alkali Butte anticline (mapping partly adapted from Thompson and White, 1954).

strata toward the present site of the Merriam anticline may be a reflection of the ancestral syncline between Maverick Spring and Little Dome anticlines.

ALKALI BUTTE

The Alkali Butte anticline (fig. 105.2) is an elongate north-plunging fold in Late Cretaceous and early Tertiary rocks. As shown by the areal distribution of the geologic units on figure 105.2, unconformities are present on the flanks of the anticline at the base of the Lance formation, at the base of arkosic conglomerate beds believed to form the upper part of the Fort Union formation, and at the base of the Wind River formation. The same unconformable relationships exist along the axis of the anticline, but are less apparent than on the flanks (compare sections *A–A′* and *B–B′*, figure 105.2).

These unconformities were produced by intermittent arching of the anticline during late Cretaceous and Paleocene time. Of particular significance is the conspicuous overlap of the upper beds in the Fort Union formation. These rocks form the upper few feet of Alkali Butte, where they rest with an angular discordance of about 20° on strata in the lower part of the Mesaverde formation (fig. 105.2). The Wind River formation has been tilted about 5° along both flanks of the fold, indicating that the final minor movements occurred later than early Eocene time.

The main outcrop belt of Upper Cretaceous and Paleocene rocks along the southern margin of the Wind River Basin extends nearly eastward from Alkali Butte for about 25 miles (Love and others, 1955). In this belt the surfaces of unconformity maintain relatively constant stratigraphic positions, indicating a regional northward tilting of the south margin of the basin, presumably caused by orogenic pulsations in the Granite Mountains to the south. The only appreciable deviations in this pattern of unconformity occur on such features as the Alkali Butte anticline, in outcrops that extend farther north or south than the main belt of exposures. These facts imply that the degree of discordance between any two formations in the Upper Cretaceous and Paleocene sequence decreases progressively toward the center of the Wind River Basin, in much the same manner as may now be observed from south to north along the crest of Alkali Butte anticline.

REFERENCES

Keefer, W. R., and Troyer, M. L., 1956, Stratigraphy of the Upper Cretaceous and Lower Tertiary rocks of the Shotgun Butte area, Fremont County, Wyoming: U.S. Geol. Survey Oil and Gas Inv. Chart OC–56.

Love, J. D., Weitz, J. L., and Hose, R. K., 1955, Geologic map of Wyoming: U.S. Geol. Survey.

Murphy, J. F., Privrasky, N. C., and Moerlein, G. A., 1956, Geology of the Sheldon-Little Dome area, Fremont County, Wyoming: U.S. Geol. Survey Oil and Gas Inv. Map OM–181.

Thompson, R. M., and White, V. L., 1954, Geology of the Riverton area, Central Wyoming: U.S. Geol. Survey Oil and Gas Inv. Map OM–127.

Troyer, M. L., and Keefer, W. R., 1955, Geology of the Shotgun Butte area, Fremont County, Wyoming: U.S. Geol. Survey Oil and Gas Inv. Map OM–172.

106. THE "BREAK-AWAY" POINT OF THE HEART MOUNTAIN DETACHMENT FAULT IN NORTHWESTERN WYOMING

By William G. Pierce, Menlo Park, Calif.

The Heart Mountain detachment fault, or "overthrust" as it was originally called, extends southeastward from the northeast corner of Yellowstone Park. I had previously described this fault as the result of

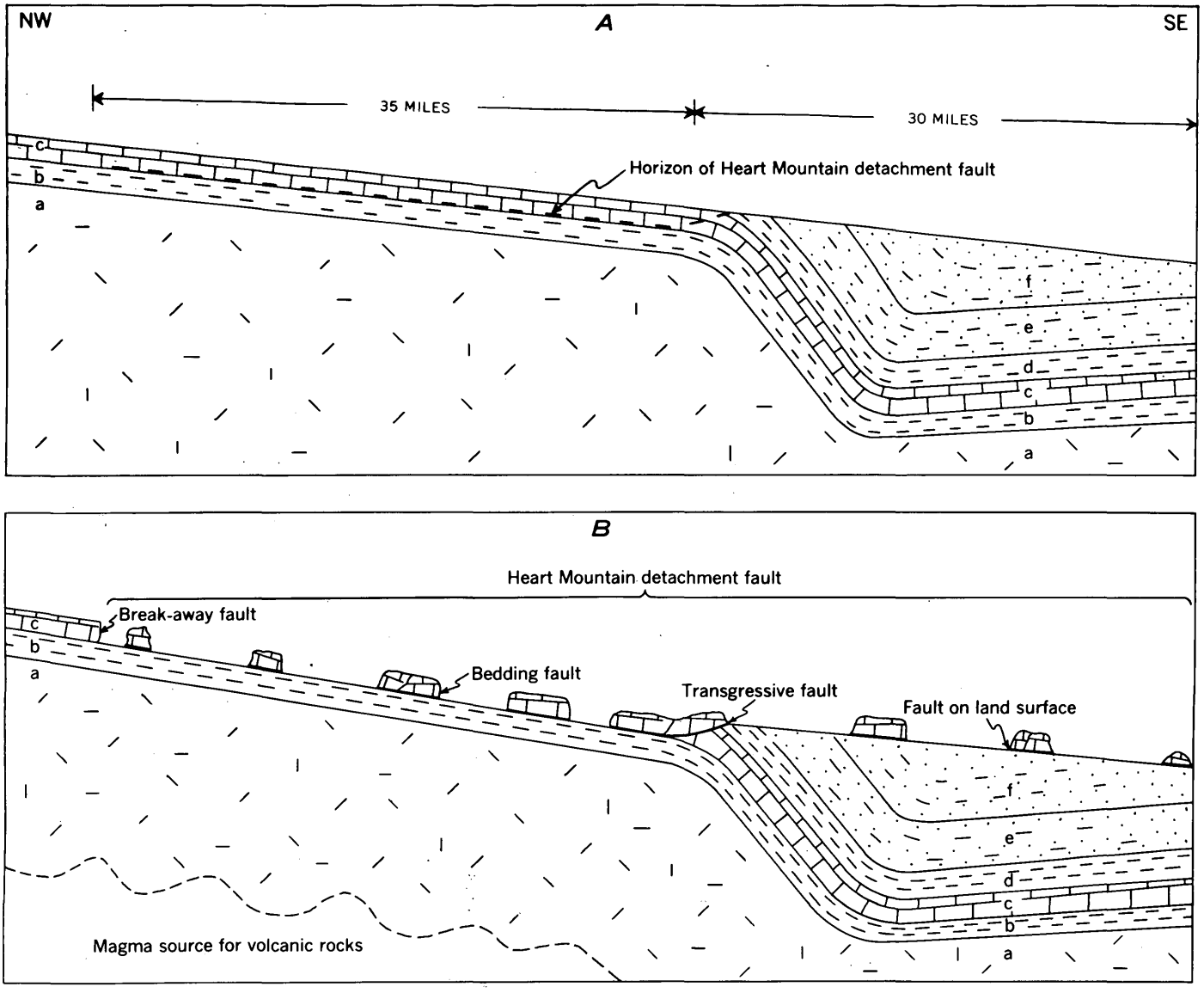

FIGURE 106.1.—Diagrammatic cross sections illustrating formation of Heart Mountain detachment fault. Diagram *A*, before faulting: *B*, after last movement showing "break-away". *a*, Precambrian; *b*, Cambrian; *c*, Ordovician, Devonian, and Mississippian; *d*, Pennsylvanian, Permian, Triassic, and Jurassic; *e*, Cretaceous; *f*, Tertiary.

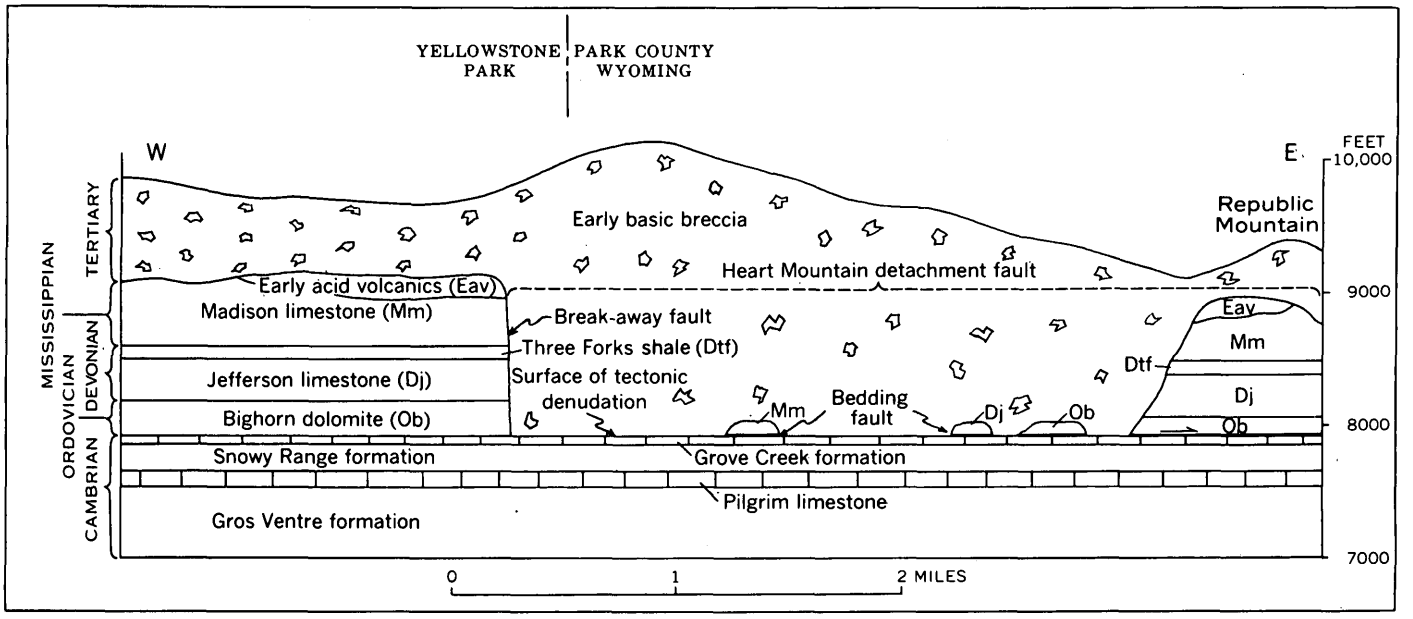

FIGURE 106.2.—Diagrammatic section showing relation of Heart Mountain detachment fault to break-away fault. The early basic breccia postdates the faulting.

faulting of three types: (a) a bedding fault, (b) transgressive faulting (called shear faulting in a previous paper) where the fault passes upward from a bedding-plane fault across younger beds until it reaches the surface, and (c) a fault in which the displaced blocks move over the land surface (Pierce, 1957, p. 597). To these there can now be added a fourth type of fault, which occurred at the place where the detached mass broke away from unfaulted beds (see fig. 106.1B). This will be referred to by the simple descriptive term of "break-away fault". Although these four types of faults are only phases of one large detachment fault, it is important to distinguish them because their strongly contrasting field characteristics may erroneously suggest unrelated faults.

The "break-away" of the Heart Mountain fault was observed at the northeastern corner of Yellowstone Park, only a few hundred feet west of the Park boundary, this being possibly the first time that such a feature has been recognized. The stratigraphic and structural relations at this place are shown in figure 106.2. The rocks at the left side of the figure are unfaulted and are in the normal sequence of Paleozoic rocks in this area. Beginning at the break-away fault, the rocks from the Bighorn dolomite up to and including the early acid volcanics have moved to the right, or eastward, along the Heart Mountain detachment plane, which is at the base of the massive Bighorn dolomite. A large open space was created immediately to the east of the break-away fault, and the top of the Grove Creek limestone became exposed on what could be called a surface of tectonic denudation. Some smaller blocks toppled off the larger ones as they moved laterally, and came to rest on the bedding-fault surface.

The break-away fault is nearly vertical and trends almost due north. Reconnaissance mapping indicates that it has an observable length of 6 miles; it is concealed beneath volcanic rocks on the south, and its trace has been removed by erosion to the north. Some indication of brecciation along the break-away fault suggests the possibility that there may have been some slight lateral movement parallel to this fault before the main lateral movement to the east took place. The fault blocks were immediately engulfed by the great mass of early basic breccia, and a record of the sequence in which the events took place was thus preserved intact until exposed by Recent erosion.

REFERENCE

Pierce, W. G., 1957, Heart Mountain and South Fork detachment thrusts of Wyoming: Am. Assoc. Petroleum Geologists Bull., v. 41, no. 4, p. 591–626.

107. REGIONAL GEOLOGICAL INTERPRETATION OF AEROMAGNETIC AND GRAVITY DATA FOR THE ROWE-MORA AREA, NEW MEXICO

By Gordon E. Andreasen, Martin F. Kane, and Isidore Zietz, Washington, D.C.

The Rowe-Mora area of northeastern New Mexico is characterized by high plateaus in the north, lower plains in the south, and by the lower ranges of the eastern Sangre de Cristo Mountains on the west. The plateaus and plains consist of flat-lying Triassic and Cretaceous strata with numerous volcanic features surmounting the northern Plateaus (Harley, 1940). Pennsylvanian clastic sedimentary rocks and an undivided complex of Precambrian gneisses, schists, and intrusive rocks crop out in the core of the Sangre de Cristo Mountains. Deep drill holes in the plains-plateau area east of the foothills penetrate essentially flat-lying Mesozoic and Paleozoic sedimentary rocks up to several thousand feet thick, and bottom in Precambrian crystalline rocks similar to those exposed in the mountains to the west. Igneous rocks intrude the Paleozoic and Mesozoic strata in western Mora County, in an area south of Raton, and possibly in central Mora County.

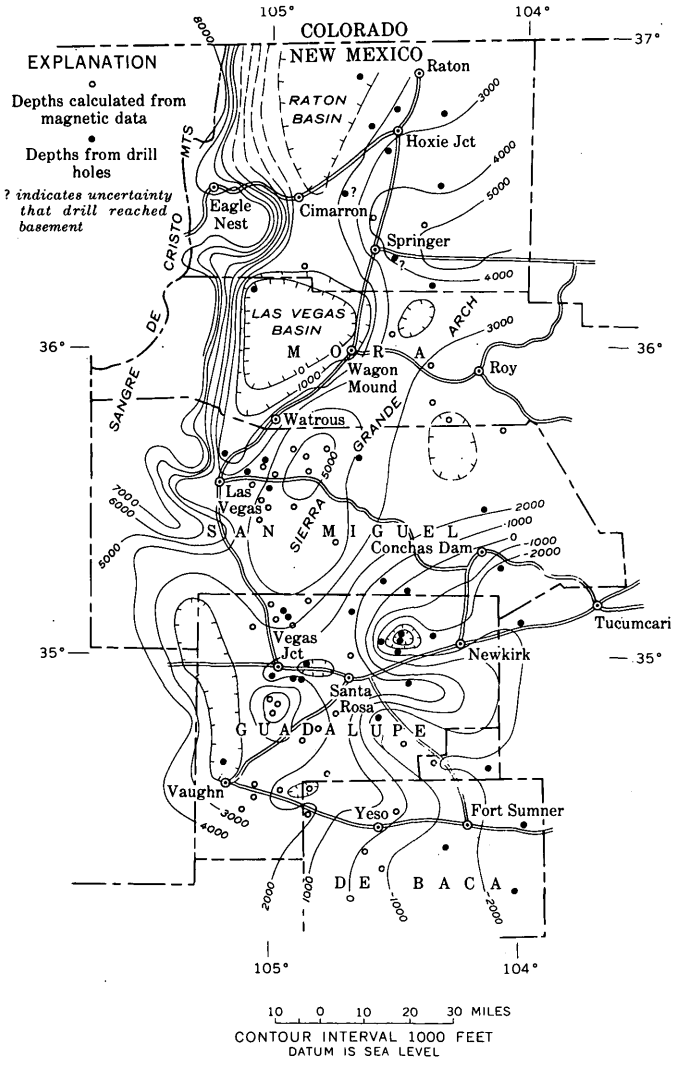

FIGURE 107.1.—Contour map of the Precambrian surface, Rowe-Mora area, New Mexico.

A contour map of the Precambrian surface (fig. 107.1) was prepared using 40 depths computed from aeromagnetic anomalies, 45 depths from drill holes, and exposures of Precambrian rocks along the east edge of the Sangre de Cristo Mountains. Only a few depths were computed in the northern part of the area because the magnetic anomalies caused by the Precambrian rocks are partly obscured by the magnetic expression due to the widespread instrusive and extrusive rocks of younger age. In the southern part of the area, where good depth control is available, a close correlation was found between gravity anomalies and basement relief. The regional gravity data, therefore, provide a basis for contouring the Precambrian surface in areas of meager depth control, especially in the north, where the younger igneous rocks are present.

The major feature of the contour map is the Sierra Grande arch, a basement highland trending northeast across the area. The highland stands 3,000 to 7,000 feet above the nearby basins and is separated into two parts by a saddle northeast of Wagon Mound. Major depressions are outlined west of Vegas Junction, northeast of Santa Rosa, and west of Wagon Mound. The largest of these, Las Vegas basin, is more than 7,000 feet in depth and more than 1,000 square miles in area. Its thick section of sedimentary rocks marks it as a favorable prospect for petroleum exploration. The gravity data indicate that the east edge of the basin may be formed by a fault in the Precambrian basement. A gravity low trending northward from the vicinity of Las Vegas to Cimarron indicates that Las Vegas basin extends to Cimarron and probably connects with the Raton basin of northeastern New Mexico and southeastern Colorado (Johnson and Wood, 1956) through a low saddle. In the southern part of the Rowe-Mora area, steep basement surfaces suggest the presence of faults near Newkirk and Vegas Junction.

REFERENCES

Harley, G. T., 1940, The geology and ore deposits of northeastern New Mexico (exclusive of Colfax County): New Mexico School of Mines, State Bur. Mines and Mineral Resources Bull. 15.

Johnson, R. B., and Wood, G. H., 1956, Stratography of Upper Cretaceous and Tertiary rocks of Raton basin, Colorado and New Mexico: Am. Assoc. Petroleum Geologists Bull., v. 40, no. 4, p. 707.

108. SOUTHWESTERN EDGE OF LATE PALEOZOIC LANDMASS IN NEW MEXICO

By George O. Bachman, Denver, Colo.

At many localities in central New Mexico, Permian strata lie directly on Precambrian rocks. The surface on the Precambrian rocks is highly irregular, being locally diversified with hills, ridges, and even mountains. Thompson (1942) said that "these pre-Cambrian rocks probably represent the buried remnants of a large land area of the Ancestral Rocky Mountains," and he named this positive element the Pedernal landmass. It is difficult, if not impossible, to determine the exact extent of the Pedernal landmass; in many parts of New Mexico evidence on this point can be obtained only from widely spaced outcrops and drill holes. It has been shown, however, that during parts of Pennsylvanian and Permian time this landmass extended north-south at least 150 miles in central New Mexico.

The remarkable influence of the Pedernal landmass on Pennsylvanian and Permian sedimentation has been discussed by other workers (Read and Wood, 1947; Cline, 1959; Otte, 1959).

During reconnaissance geologic mapping in 1954, R. L. Sutton and I discovered exposures in northern Otero County, N. Mex., where the Abo formation of Permian age lies on rocks of Precambrian age (Bachman, 1954; Dane and Bachman, 1958). These exposures are near Bent, which is about 12 miles northeast of Tularosa, in secs. 25 and 26, T. 13 S., R. 11 E., and sec. 30, T. 13 S., R. 12 E. The outcrops are on the east flank of a small dome, here called Bent dome. I have since mapped these exposures in more detail (fig. 108.1). They are the southernmost exposures in New Mexico, so far as I know, in which this relation may be observed at the surface, and they are of particular interest because in the Sacramento Mountains, about 20 miles to the south of Bent dome, pre-Permian Paleozoic rocks attain a thickness of about 5,500 feet (Pray, 1959, p. 88).

The Precambrian rocks on Bent dome consist chiefly of light-gray quartzite. At one small exposure (sec. 25, T. 13 S., R. 11 E.) the quartzite appears to be intruded by coarsely crystalline granite, which closely resembles that forming cobbles and pebbles in the Abo formation on Bent dome and in areas to the west. The Abo formation contains cobbles and pebbles of quartzite that resembles Precambrian quartzite in texture but not in color, being generally dark gray, maroon, or purple whereas the quartzite of the Precambrian exposures is light gray.

Diorite exposed on the west side of Bent dome (sec. 26, T. 13 S., R. 11 E.) may also be of Precambrian age (Foster, 1959, p. 143), but its age is uncertain. This diorite is very similar to Tertiary diorite found elsewhere in the region; and, moreover, it is not intricately jointed as are the rocks known to be Precambrian, and no pebbles of diorite like that on Bent dome have been identified in the Abo formation.

On the west side of Bent dome, and also in the vicinity of the Virginia Mine and at a locality on U.S. Highway 70 one mile east of Bent, there are exposures of light-gray, medium-grained, well-sorted sandstone beds thought to be of Pennsylvanian age. The Abo formation overlies these beds unconformably. The supposedly Pennsylvanian beds are estimated to be about 200 feet thick near the Virginia Mine, but they are absent on the east side of the dome and are presumed to wedge out eastward from the mine. The high degree of sorting indicates that these beds may have been deposited before major uplift of the Pedernal landmass.

The Abo formation on Bent dome consists of poorly consolidated dark-red shale, arkose, and conglomerate. Cobbles of granite and quartzite as much as 10 inches in diameter have been observed at the base of the formation, and also some pebbles of a distinctive brownish-red rhyolite porphyry. The formation is 220 feet thick on

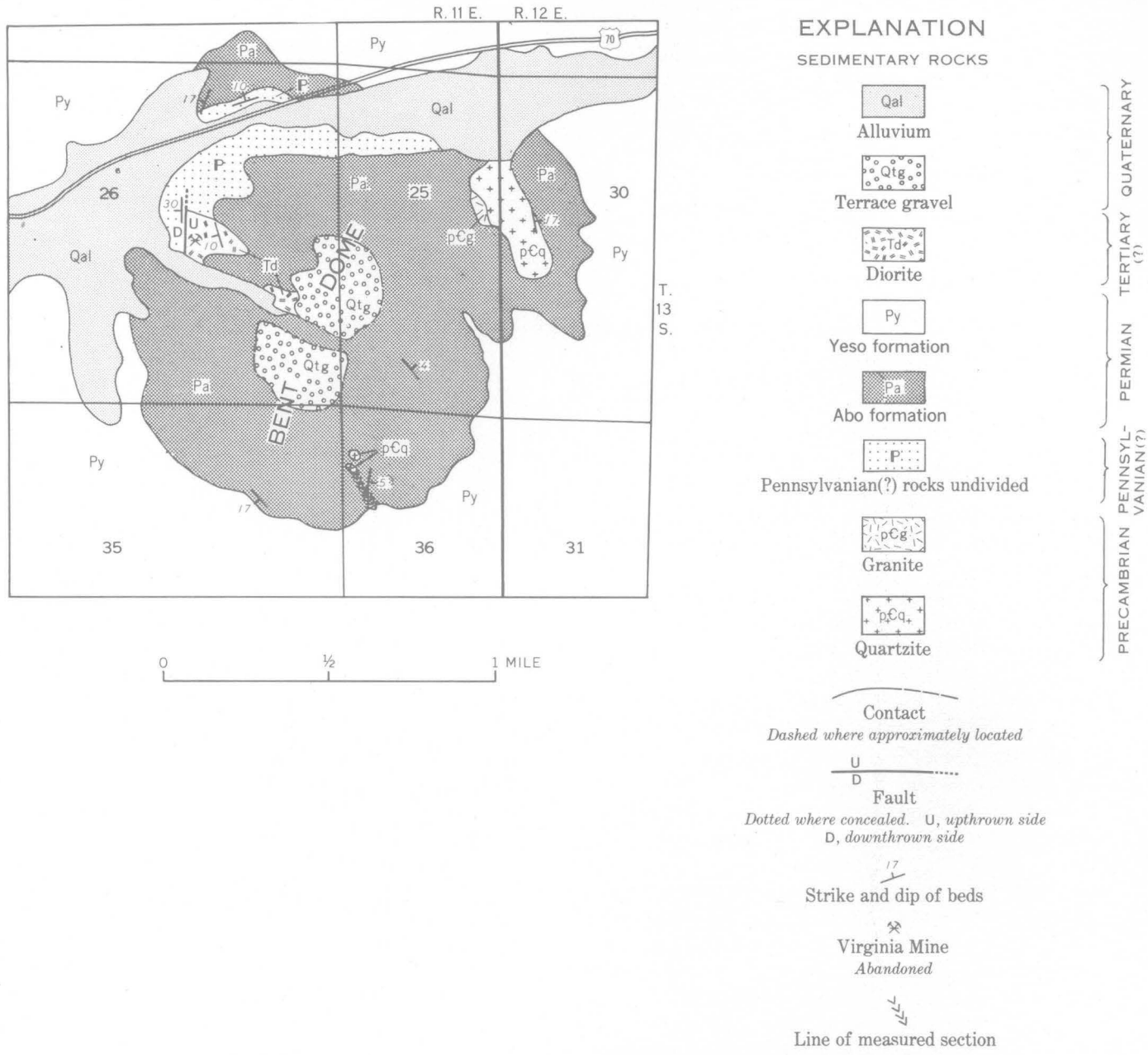

FIGURE 108.1.—Geologic map of Bent dome, Otero County, N. Mex.

the southeastern part of the dome (fig. 108.2). On the eastern flank of the dome the Abo is apparently thinner and it may be no more than 100 feet thick where it overlies the highest points on the surface of Precambrian rocks (NW¼SW¼ sec. 30, T. 13 S., R. 12 E.). About 6 miles west of Bent dome the Abo formation is about 1,400 feet thick (Pray, 1959, p. 118) and rests on rocks of Late Pennsylvanian and early Permian age.

The unconformity at the base of the Abo sandstone and the onlap of the Abo on pre-Permian rocks of various ages in the Sacramento Mountains have long been known (Pray, 1949, p. 1914–1915). Early Permian folding and faulting are indicated throughout the length of the Sacramento Mountains and are directly related to uplift of the Pedernal landmass. The exposures at Bent dome provide a point of geographic control for the southwestern part of the landmass and probably represent a part of the early Permian tectonic system of the Sacramento Mountains.

REFERENCES

Bachman, G. O., 1954, Reconnaissance map of an area southeast of Sierra Blanca in Lincoln, Otero, and Chaves Counties, New Mexico, *in* New Mexico Geol. Soc. Guidebook, 5th Field Conf., 1954: p. 94b.

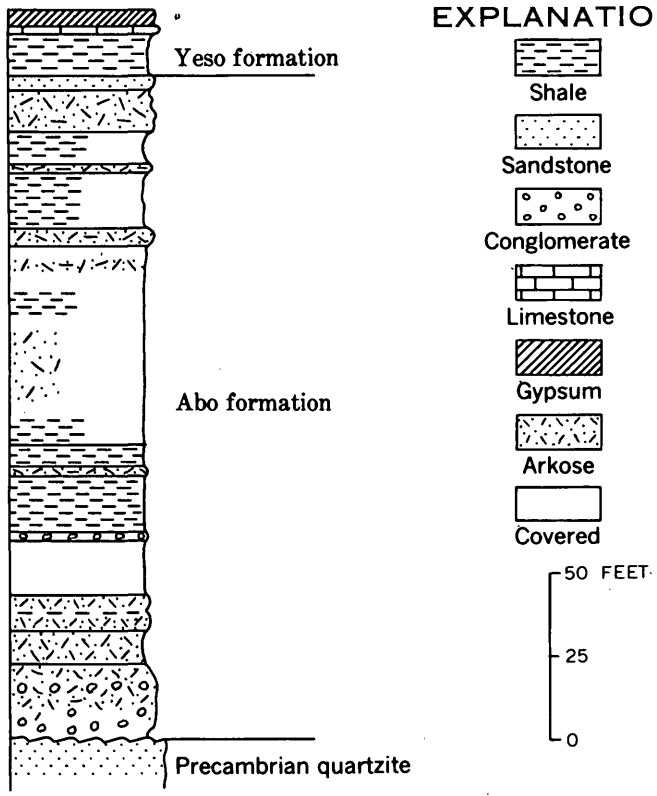

FIGURE 108.2.—Graphic section of Abo formation and adjacent rocks at Bent dome (NW¼ sec. 36, T. 13 S., R. 11 E.).

Cline, L. M., 1959, Preliminary studies of the cyclical sedimentation and paleontology of upper Virgil strata of the La Luz area, *in* Permian Basin Sec. Soc. Econ. Paleontologists and Mineralogists and Roswell Geol. Soc. Guidebook, Sacramento Mtns., 1959: p. 172–185.

Dane, C. H., and Bachman, G. O., 1958, Preliminary geologic map of the southeastern part of New Mexico: U.S. Geol. Survey Misc. Geol. Inv. Map I–256.

Foster, R. W., 1959, Precambrian rocks of the Sacramento Mountains and vicinity, *in* Permian Basin Sec. Soc. Econ. Paleontologists and Mineralogists and Roswell Geol. Soc. Guidebook, Sacramento Mtns., 1959: p. 137–153.

Otte, Carel, Jr., 1959, Late Pennsylvanian and early Permian stratigraphy of the northern Sacramento Mountains, Otero County, New Mexico: New Mexico Inst. Mining Technology, State Bur. Mines and Mineral Resources Bull. 50, p. 21–58.

Pray, L. C., 1949, Pre-Abo deformation in the Sacramento Mountains, New Mexico [abs.]: Geol. Soc. America Bull., v. 60, no. 12, p. 1914–1915.

———, 1959, Stratigraphy and structure of the Sacramento Mountains, *in* Permian Basin Sec. Soc. Econ. Paleontologists and Mineralogists and Roswell Geol. Soc. Guidebook, Sacramento Mtns., 1959: p. 86–130.

Read, C. B., and Wood, G. H., Jr., 1947, Distribution and correlation of Pennsylvanian rocks in late Paleozoic sedimentary basins in northern New Mexico: Jour. Geology, v. 55, no. 3, p. 220–236.

Thompson, M. L., 1942, Pennsylvania System in New Mexico: New Mexico School Mines, State Bur. Mines and Mineral Resources Bull. 17, p. 12–13.

109. NEW INFORMATION ON THE AREAL EXTENT OF SOME UPPER CRETACEOUS UNITS IN NORTHWESTERN NEW MEXICO

By CARLE H. DANE, Washington, D.C.

Stratigraphic studies of Upper Cretaceous rocks in parts of northwestern New Mexico, made in connection with the compilation of a new geologic map of New Mexico by Carle H. Dane and George O. Bachman, have recently been supplemented by paleontologic studies by W. A. Cobban. Although incomplete, these combined studies give a new picture of the distribution of several of the rock units of Late Cretaceous age (fig. 109.1).

The Tres Hermanos sandstone member of the Mancos shale of early Greenhorn age (fig. 109.1, *A*), including the sandstones probably equivalent to it, is believed to have a much greater extent than previously recognized. This interpretation is based in part on indications that equivalents of the somewhat older Dakota sandstone are missing in southwestern New Mexico. The Dakota is locally absent south and southwest of Santa Fe (Stearns, 1953, p. 964–966); it is inferred to be absent east of Socorro, where shales lie at the base of the Upper Cretaceous (Wilpolt and Wanek, 1951, sections on sheet No. 2); and it is locally absent northwest of Socorro (Gadway, 1959, p. 18). In all of these areas, the Tres Hermanos sandstone is thick and extensive. Furthermore, fossils of the oldest Late Cretaceous faunal zones are not known in southwestern New Mexico. Therefore, some of the upper parts of the Beartooth quartzite and the Sarten sandstone of southwestern New Mexico, and the so-called Dakota sandstone of south-central New Mexico may be equivalent to the Tres Hermanos sandstone member. This interpretation is consistent with paleontologic data now available. The Tres Her-

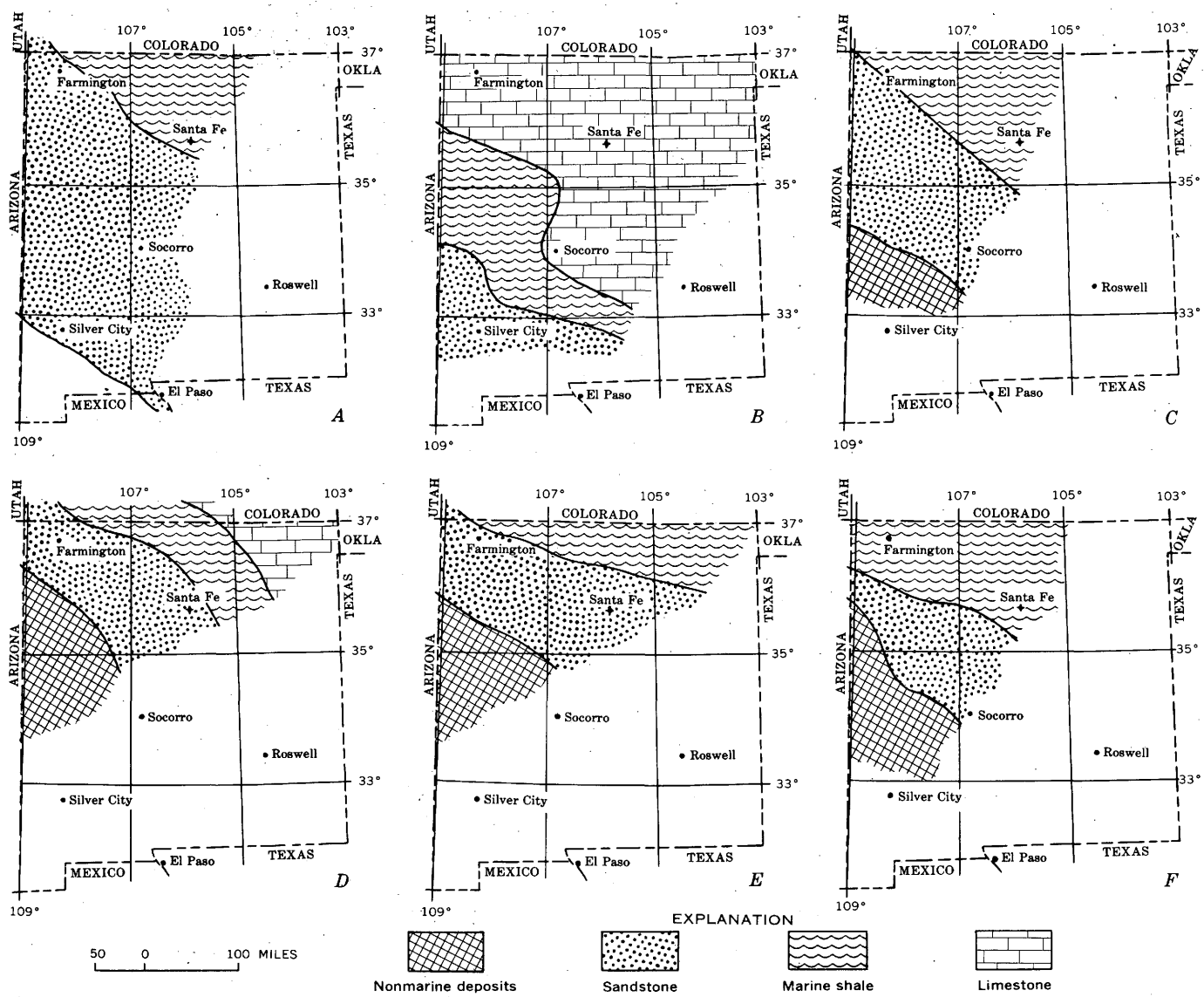

FIGURE 109.1.—Sketch maps showing part of the inferred original extent of some of the principal named sandstone units of Late Cretaceous age and rocks equivalent to them in western and northern New Mexico. *A*, the Tres Hermanos sandstone member of the Mancos shale, and sandstones of probably about the same early Greenhorn age in southwestern New Mexico; *B*, sandstone of latest Greenhorn age in southwestern New Mexico, and the Greenhorn limestone member of the Mancos shale, also of latest Greenhorn age, in northern and eastern New Mexico; *C*, upper part of the Gallup sandstone, including the Gallego sandstone member and equivalent sandstone beds of latest Carlile and earliest Niobrara age; *D*, the "stray" sandstone of Sears, Hunt, and Hendricks (1941) and approximately equivalent sandstone beds of early Niobrara age, and the partly equivalent Fort Hays limestone member of the Niobrara formation; *E*, Dalton sandstone member of the Crevasse Canyon formation, early middle Niobrara age; *F*, Hosta tongue of the Point Lookout sandstone, middle Niobrara age.

manos sandstone member wedges out to the northeast in marine shale in the San Juan Basin, roughly along a line extending between Santa Fe and Farmington.

The Greenhorn limestone member of the Mancos shale (fig. 109.1, *B*) has a rather sharply defined reverse S-shaped southern boundary; it is present east of Socorro, but is absent above the Tres Hermanos sandstone member northwest of Socorro. The Greenhorn limestone member grades southwestward into marine shale, which in turn grades into sandstone that has been included in the basal part of the Mesaverde formation in south-central New Mexico (Kelly and Silver, 1952, p. 112). The basal part of this sandstone carries the *Inoceramus labiatus* fauna of latest Greenhorn age (J. B. Reeside, Jr., written communication, April 2, 1956).

Areal limits of the upper part of the Gallup sandstone (fig. 109.1, *C*), which is the oldest sandstone formation of the Mesaverde group here shown, have not been greatly revised from those previously recognized (Pike, 1947, fig. 7, p. 95). However, the next younger sandstone of the group, the "stray" sandstone of Sears, Hunt, and Hendricks (1941, p. 112) seems to be represented by laterally discontinuous sandstone units over a much larger area than previously recognized (fig. 109.1, *D*). These glauconitic, generally coarser grained sandstone units are regarded as probably equivalent to and contemporaneous with the "stray" sandstone, and lie above an unconformity representing the latter part of Carlile time (Dane, 1960). The northern arcuate boundary of these discontinuous sandstones is convex to the north; this boundary is about 60 miles southwest of, but approximately parallel to, the southern limit of the Fort Hays limestone member of the Niobrara formation, which is of nearly the same age.

About 200 to 300 feet higher in the section is the Dalton sandstone member of the Crevasse Canyon formation, which also extends farther north and east than previously recognized (fig. 109.1, *E*). The thin sandstone in northeastern New Mexico at about the stratigraphic position of the Dalton has previously been suggested as a correlative of the Gallup sandstone (Dane, Bachman, and Reeside, 1957, p. 113).

The youngest unit shown is the Hosta sandstone (fig. 109.1, *F*), a lower tongue of the Point Lookout sandstone of the Mesaverde group. The Point Lookout sandstone extends far to the north and northeast of the area shown on the accompanying maps but the Hosta sandstone tongue terminates well to the south of the feather edges of the "stray" sandstone and Dalton sandstone member.

The stratigraphic relations and the patterns of distribution of the sandstone units suggest that all these sandstones were derived from a southwestern source and were deposited on a marine shelf lateral to the main body of the Late Cretaceous sea to the east.

REFERENCES

Dane, C. H., 1960, The boundary between rocks of Carlile and Niobrara age in San Juan Basin, New Mexico and Colorado: Am. Jour. Sci., v. 258–A, p. 46–56.

Dane, C. H., Bachman, G. O., and Reeside, J. B., Jr., 1957, The Gallup sandstone, its age and stratigraphic relationships south and east of the type locality, *in* Four Corners Geol. Soc. Guidebook, Geology of southwestern San Juan Basin 1957: p. 99–113.

Gadway, K. L., 1959, Cretaceous sediments of the North Plains and adjacent areas, McKinley, Valencia and Catron Counties, New Mexico, *in* New Mexico Geol. Soc. Guidebook 10th Ann. Field Conf., West Central New Mexico, 1959: p. 81–84.

Kelley, V. C., and Silver, Caswell, 1952, Geology of the Caballo Mountains, New Mexico: New Mexico Univ. Pub., Geology, no. 4, 282 p.

Pike, W. S., 1947, Intertonguing marine and non-marine Upper Cretaceous deposits of New Mexico, Arizona, and southwestern Colorado: Geol. Soc. America Mem. 24, p. 1–103.

Sears, J. D., Hunt, C. B., and Hendricks, T. A., 1941, Transgressive and regressive Cretaceous deposits in southern San Juan Basin, New Mexico: U.S. Geol. Survey Prof. Paper 193–F, p. 101–121.

Stearns, C. E., 1953, Upper Cretaceous rocks of the Galisteo-Tonque area, north-central New Mexico: Am. Assoc. Petroleum Geologists Bull., v. 27, p. 961–974.

Wilpolt, R. H., and Wanek, A. A., 1951, Geology of the region from Socorro and San Antonio east to Chupadera Mesa, Socorro County, New Mexico: U.S. Geol. Survey Oil and Gas Inv. Map OM–121.

110. LITHOLOGIC SUBDIVISIONS OF THE REDWALL LIMESTONE IN NORTHERN ARIZONA—THEIR PALEOGEOGRAPHIC AND ECONOMIC SIGNIFICANCE

By Edwin D. McKee, Denver, Colo.

The Redwall limestone of Mississippian age extends across most of northern Arizona with relatively little change from one place to another either in lithologic sequence or in relative proportions of rock types. Although the formation ranges in thickness from a thin edge in the eastern part of the State to slightly more

than 800 feet in northwestern Arizona, the four members into which it is divided persist throughout most of the area and show only very gradual changes in thickness.

The four members of the Redwall limestone are tentatively designated as: (a) member *A*—the basal thick-bedded unit, 70 to 130 feet thick in Grand Canyon, consisting of limestone in the western part but of dolomite in the eastern part; (b) member *B*—65 to 105 feet thick, composed of alternating beds of chert and carbonate rock 1 to 6 inches thick and which form a conspicuous banded cliff in most places; (c) member *C*—a very thick-bedded, massive, cliff-forming unit, 200 to 400 feet thick, composed of both aphanitic limestone and coarse-grained, largely crinoidal limestone; and (d) member *D*—40 to 100 feet thick, thin-bedded, mostly aphanitic limestone, with some chert beds.

The change from thick to thin bedding from member *A* to member *B*, and a similar change from member *C* to member *D*, probably resulted from significant changes in base level during deposition. Development of a relatively shallow base level with consequent interruptions in sedimentation is indicated by a change to thin-bedded deposits. Deposition of these thin beds in the upper part of each sequence terminated with general bevelling of the surface. Thus, the thin strata probably represent deposits of sea regression, whereas the underlying thick beds indicate an advancing sea and maximum rate of water deepening. The formation, therefore, is believed to be the result of sedimentation during two major cycles of advance and retreat of the sea across a relatively flat area.

Delineation of the four subdivisions of the Redwall limestone makes possible the recognition of significant regional trends that are otherwise obscure. For example, thinning of the formation toward the Defiance uplift area in northeastern Arizona is the result, at least in part, or onlap of sediments against a positive element, for immediately west of the Defiance area the lower two members are absent and the upper ones rest upon Devonian strata. Another trend of the formation as a whole is its thinning southward across the area adjacent to its margin in central Arizona. This trend is the result of post-Redwall stripping of uppermost units in that area; originally the formation thickened southward, as illustrated by the thickness-trends of lower members which have not been reduced by erosion (fig. 110.1, *A* and *B*).

The major paleogeographic elements that existed in northern Arizona during Early Mississippian time have been determined on the basis of regional trends of individual members in the Redwall. The Defiance up-

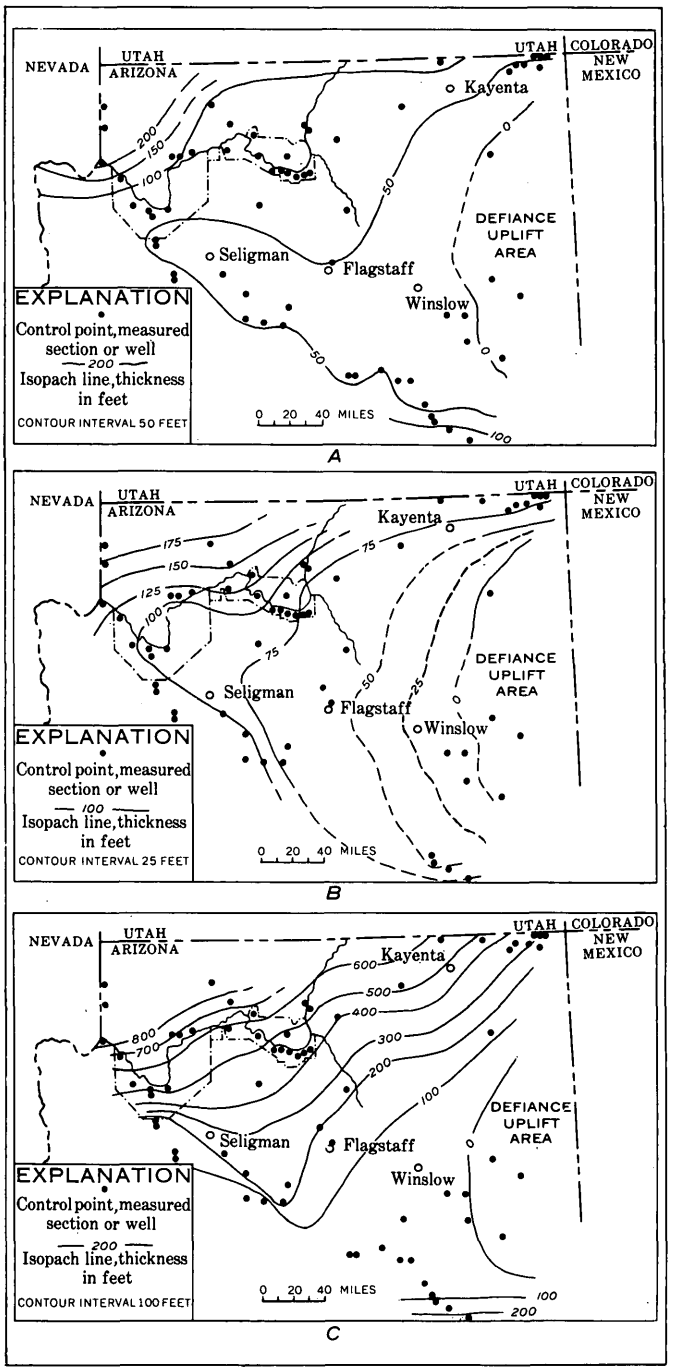

FIGURE 110.1.—Isopach maps of Redwall limestone in northern Arizona; *A*, member A; *B*, member B; *C*, total Redwall. Isopach lines dashed where approximate.

lift in northeastern Arizona was a positive element and stood above sea level. Westward from it a prong or submarine ridge marked the boundary between an even-surfaced, northwest-sloping shelf, and a shelf that sloped southwestward into central Arizona. The shelf areas seem to have been very even and flat—one extending to the edge or hinge of the Cordilleran geosyncline

to the northwest, and the other forming the northern rim of a basin in which the thick Escabrosa limestone of southern Arizona was formed.

The importance of differentiating the members of the Redwall limestone and of determining lithologic and thickness trends of these members has become apparent with the recent discovery of oil and gas in rocks of Early Mississippian age of the region. Production is reported from member *B* in at least two localities and also from member *C* in one locality. Careful tracing of these units in the subsurface already has proven of considerable economic value.

111. PLIOCENE SEDIMENTS NEAR SALIDA, CHAFFEE COUNTY, COLORADO

By Ralph E. Van Alstine and G. Edward Lewis, Washington, D.C., and Denver, Colo.

Work done in cooperation with Colorado State Metal Mining Fund Board

Geologic mapping in the Poncha Springs quadrangle, Chaffee County, Colo., has shown the presence of probable lower Pliocene sediments. The sediments are dated from vertebrate fossils collected at two localities between 7 and 11 miles north-northwest of Salida, near the junction of U.S. Highway 285 with Colorado Highway 291: at locality D296, fragments of fossil camel bones were found, and at locality D298, an antilocaprid bone and fragments of fossil horse teeth were found.

The sediments consist of gray, yellow, brown, pink, and red interbedded clays, silts, sands, and gravels. They are poorly consolidated, with the exception of some well-cemented calcareous lenses of gravel and sand and an argillaceous siltstone that has a blocky fracture. The gravels and sands are locally arkosic and cross-bedded. Well-rounded pebbles, cobbles, and boulders in the gravels are derived chiefly from the nearby Precambrian igneous and metamorphic rocks and Tertiary volcanic rocks. The Pliocene sediments dip generally less than 10° in various directions, rest unconformably on the Precambrian rocks and Tertiary volcanic rocks, and are overlain locally by glacial outwash. A section of the beds about 500 feet thick is exposed in the area northwest of Salida.

Tentative identifications of the fossils are:

?*Pliauchenia* sp.; USGS fossil vertebrate locality D296, SW¼ SW¼ sec. 34. T. 51 N., R. 8 E., Chaffee Co., Colo.; 22 fragments of a metapodial.

?*Neohipparion* sp.; USGS fossil vertebrate locality D298, NW¼ SE¼ sec. 16, T. 51 N., R. 8 E., Chaffee Co., Colo.; 2 fragments of an upper cheek tooth and an incomplete lower cheek tooth.

Antilocaprid, gen. and sp. indet.; also from locality D298; incomplete astragalus.

These identified specimens are elements of a fauna that is probably of early Pliocene age, comparable to the fauna from the lower part of the Ogallala of Nebraska, and possibly comparable in age to that of the horse identified by Gazin (in Stark and others, 1949, p. 69) from the Wagontongue formation of South Park, Colo. *Pliohippus leidyanus* Osborn was identified by Romer from a molar tooth found "near Salida" (in Powers, 1935, p. 189); this is a species characteristic of the upper part of the Ogallala of Nebraska. The presence of *Pliohippus leidyanus* would indicate that the sediments near Salida may be in part of younger age than those that yielded the ?*Neohipparion* sp. identified in this report.

REFERENCES

Powers, W. E., 1935, Physiographic history of the upper Arkansas River Valley and the Royal Gorge, Colorado: Jour. Geology, v. 43, p. 184–199.

Stark, J. T., and others, 1949, Geology and origin of South Park, Colorado: Geol. Soc. America Mem. 33, 188p.

112. SOME LATE CRETACEOUS STRAND LINES IN NORTHWESTERN COLORADO AND NORTHEASTERN UTAH

By A. D. Zapp and W. A. Cobban, Denver, Colo.

The eastward withdrawal of the Late Cretaceous sea from northeastern Utah and northwestern Colorado was interrupted by many partial readvances of the sea, as recorded by superposition of tongues of marine strata on tongues of nonmarine strata. This paper describes some of the regressive-transgressive cycles recorded in strata of late Campanian and Maestrichtian age.

This is a brief progress report on a field investigation begun in 1958. The work thus far has not included subsurface studies. For a full summary and discussion of intertonguing sedimentary facies in part of the area the reader is referred to Spieker (1949). Weimer (1960) has summarized the major Cretaceous regressive-transgressive cycles over a broad area.

THICKNESS AND FACIES

The rocks here considered are thickest—about 6,000 feet—in the northeastern part of the area and thin markedly southwestward toward two ancient positive features, the Uncompahgre uplift and the Douglas Creek arch (fig. 112.1). The variation in thickness is attributed to differential subsidence in an area of continuous sedimentation.

The rocks have been divided broadly into marine and nonmarine facies, with two subfacies distinguished in each category. The geographic and stratigraphic distribution of these facies are summarized in figure 112.2, which shows that many of the facies boundaries do not coincide with formational boundaries.

Most of the nonmarine rocks are grouped as an undifferentiated assemblage of lenticular sandstone, siltstone, shale, and coal, characterized as a whole by irregular bedding, discontinuity of beds, and relatively poor sorting. Coal typically occurs near the seaward margins of the nonmarine assemblage, commonly associated with beds of brackish-water origin.

The correlative nonmarine Castlegate and Rimrock sandstones (columns 1 and 10, fig. 112.2) are notable exceptions to the general discontinuity of nonmarine rock units, though bedding is irregular and individual beds are lenticular. The sandstone is somewhat coarser than in the other facies here considered, much of it being medium to coarse grained. Spieker (1949, p. 70–73) has shown that the Castlegate sandstone resulted from an orogenic pulse in the source area. Young (1955, p. 188) has shown that the Castlegate sandstone

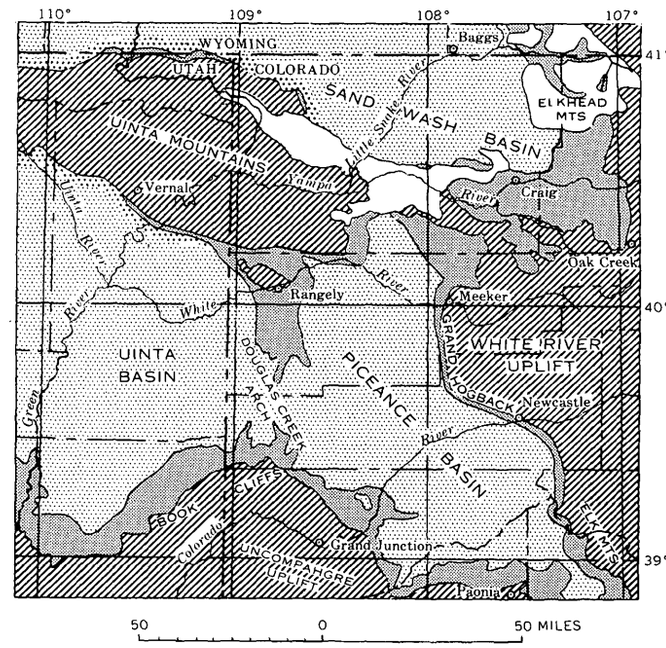

FIGURE 112.1.—Generalized geologic map of part of northwestern Colorado, northeastern Utah, and southwestern Wyoming, showing principal areas of outcrop of:

1. Mesaverde formation or group and younger Upper Cretaceous rocks (dense stippling).
2. Rocks older than Mesaverde (diagonal ruling).
3. Older Tertiary rocks (light stippling where concordant with Upper Cretaceous rocks; coarse dots where discordant).
4. Late Tertiary rocks (white) that rest discordantly on older rocks.

of the type area is replaced eastward by coal-bearing sediments (undifferentiated nonmarine rocks of this paper), which are in turn replaced farther east by the marine Castlegate sandstone. The Rimrock sandstone shows similar lateral relations. The Ericson sandstone of the area north of the Uinta Mountains (fig. 112.1) is similar in lithology and stratigraphic position to the nonmarine Castlegate and Rimrock sandstones.

The rocks of the marine facies are characterized by regular, parallel bedding, excellent sorting, and wide persistence of beds. Thick-bedded to massive fine-grained light-gray sandstone, generally containing casts of *Halymenites major*, characteristically occurs at and near the landward margins of the marine rocks; dark-gray siltstone and shale characterize the more seaward sediments.

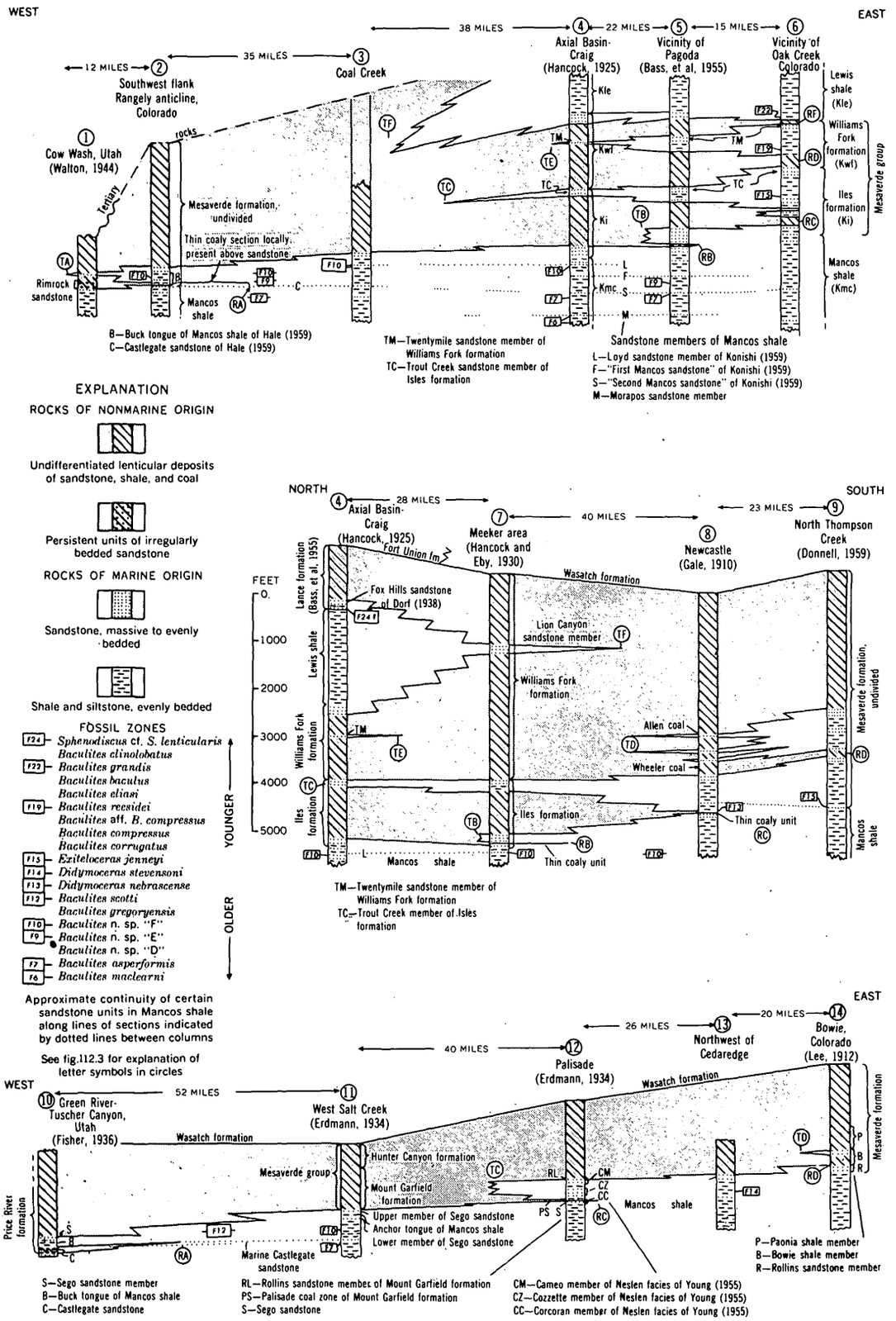

FIGURE 112.2.—Generalized columnar sections of uppermost Cretaceous rocks in northwestern Colorado and northeastern Utah, showing distribution of facies and correlation of named stratigraphic units. For location of sections see figure 112.3. Sections are modified after the authors cited.

REGRESSIVE-TRANSGRESSIVE CYCLES

Regressive movements of the sea are recorded by superposition of nonmarine upon marine strata; transgressive movements are recorded by reversal of that succession. The wedge-edge of a tongue of marine rocks penetrating nonmarine rocks, or of nonmarine rocks penetrating marine rocks, marks the position of an ancient strand line. A large number of regressive-transgressive cycles are recorded by interfingered marine and nonmarine Upper Cretaceous rocks in this area, but only cycles that involve at least 300 feet of strata are enumerated here.

In the northeastern part of the area, the transgressive marine tongues include considerable shale and siltstone. Regressive marine sandstone is invariably at the top of the shaly tongues, and transgressive marine sandstone commonly occurs at the base. Sandstone may be the only marine facies present toward the landward tips of the tongues. In the thinner sections along the Book Cliffs to the south, marine shale and siltstone are subordinate in the tongues, and transgressive sandstones have not been observed.

Regressive pulses may be reflected for variable distances seaward from the strand line by tongues of marine sandstone penetrating the shale-siltstone facies. The Morapos sandstone member of the Mancos shale (columns 4 and 5, fig. 112.2) may thus reflect a regressive movement older than those here enumerated, for fossil evidence (fig. 112.2) shows the Morapos to be older than the marine Castlegate sandstone.

The several nonmarine and marine tongues that have been recognized are identified on figure 112.2 and the general positions of corresponding strand lines, as inferred from the results of lateral tracing of those tongues and from paleontologic evidence, are shown in figure 112.3. Hale (1959, p. 64–65) has previously depicted the TA strand line, and Weimer (1960, p. 16) has shown the TF strand line. The following relates to data not evident in figure 112.2.

1. The lower Iles cycle (RB and TB, figs. 112.2 and 112.3) has not been identified along the Book Cliffs. Possibly it is reflected in the lower Sego sandstone-Anchor tongue marine sequence near the Colorado-Utah line (column 11, fig. 112.2), in which case the corresponding nonmarine-marine cycle may be present somewhere farther west. If so, the southwestward extension of lines RB and TB (fig. 112.3) must swing to a west-southwesterly direction. That the sea lingered relatively longer in eastern Utah is also suggested by marine fossils as young as the basal part of the *Baculites scotti* zone in the Sego sandstone of that area (fig. 112.2).

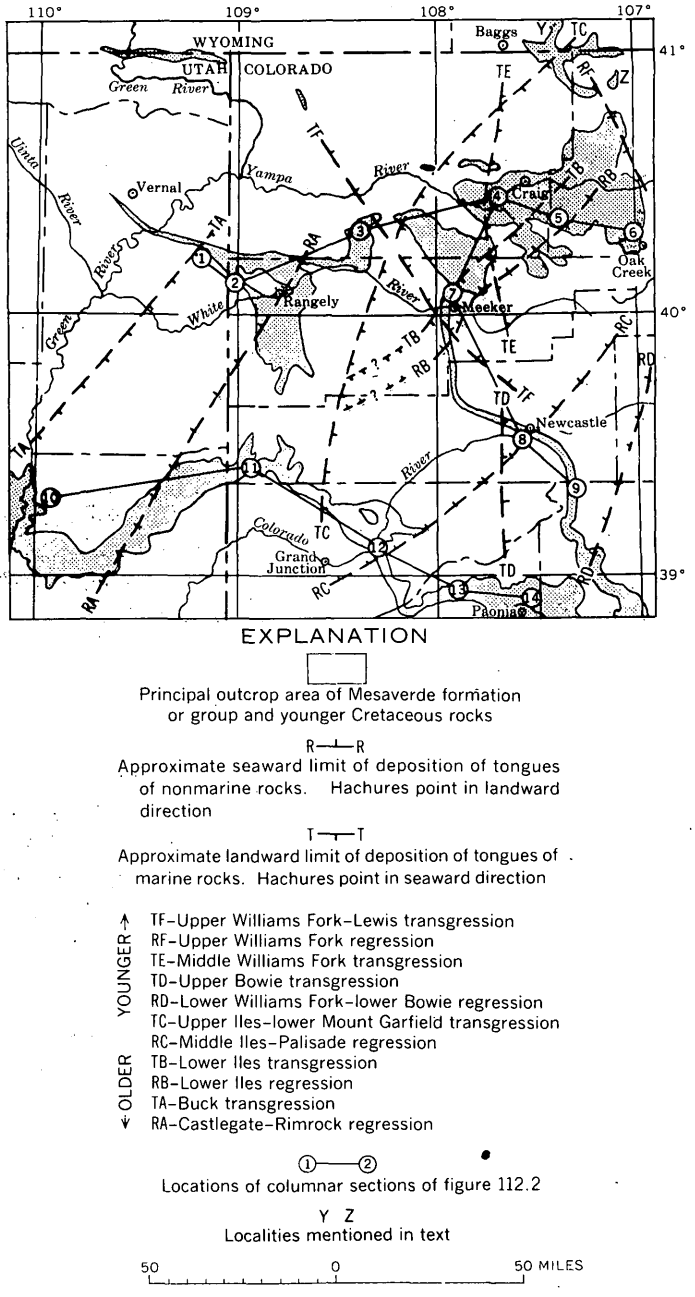

FIGURE 112.3.—Map showing location of sections in figure 112.2 and general location and trend of certain regressive and transgressive strand lines during Late Cretaceous time, as inferred from outcrop studies.

2. A marine intercalation correlated with the TC tongue on the basis of stratigraphic position occurs southeast of Baggs, Wyo. at locality Z (fig. 112.3) but was not found at locality Y (fig. 112.3). Another marine intercalation similarly correlated with the TE tongue occurs at locality Y (fig. 112.3) but is absent about ten miles northwest.
3. The RC and RD nonmarine tongues, though thinning rapidly, are still present in the easternmost

exposures near Oak Creek (column 6, fig. 112.2) but equivalent rocks are entirely marine in the next exposed section about 25 miles to the east.

4. The exact correlation of the transgressive tongues above the RD tongue in columns 14, 8, and 5 (fig. 112.2), is not known. The upper tongue of the Bowie shale member of column 14 undoubtedly correlates with one of the two prominent tongues below the Allen coal of column 8; in either case, there must have been a strand line in the general position of TD (fig. 112.3). The TE strand line (fig. 112.3) represents the known extent of the Twentymile sandstone member and associated marine rocks. It may be represented by the uppermost marine tongue of column 8.
5. The position of the upper Williams Fork regressive strand line (RF, fig. 112.3) is poorly known. The basal part of the Lewis shale overlying the greatly thinned RF tongue near Oak Creek (column 6, fig. 112.3) has yielded fossils indicative of the zone of *Baculites grandis*. The basal Lewis at locality Z (fig. 112.3) has yielded the older *Baculites eliasi*, indicating that the RF tongue is replaced by marine rocks in the intervening area.

REFERENCES

Bass, N. W., Eby, J. B., and Campbell, M. R., 1955, Geology and mineral fuels of parts of Routt and Moffat Counties, Colorado: U.S. Geol. Survey Bull. 1027–D, p. 143–250.

Donnell, J. R., 1959, Mesaverde stratigraphy in the Carbondale area, northwestern Colorado, *in* Rocky Mtn. Assoc. Geologists, Guidebook 11th Ann. Field Conf., Washakie, Sand Wash, and Piceance Basins, 1959: p. 76–77.

Dorf, Erling, 1938, Upper Cretaceous floras of the Rocky Mountain region; 1, Stratigraphy and paleontology of the Fox Hills and lower Medicine Bow formations of southern Wyoming and northwestern Colorado: Carnegie Inst. Washington Pub. 508, p. 1–78 [1942].

Erdmann, C. E., 1934, The Book Cliffs coal field in Garfield and Mesa Counties, Colorado: U.S. Geol. Survey Bull. 851, and Mesa Counties, Colorado: U.S. Geol. Survey Bull. 851,

Fisher, D. J., 1936, The Book Cliffs coal field in Emery and Grand Counties, Utah: U.S. Geol. Survey Bull. 852, 104 p.

Gale, H. S., 1910, Coal fields of northwestern Colorado and northeastern Utah: U.S Geol.. Survey Bull. 415, 265 p.

Hale, L. A., 1959, Intertonguing Upper Cretaceous sediments of northeastern Utah—northwestern Colorado, *in* Rocky Mtn. Assoc. Geologists, Guidebook 11th Ann. Field Conf., Washakie, Sand Wash. and Piceance Basins, 1959: p. 55–56.

Hancock, E. T., 1925, Geology and coal resources of the Axial and Monument Butte quadrangles, Moffat County, Colorado: U.S. Geol. Survey Bull. 757, 134 p.

Hancock, E. T., and Eby, J. B., 1930, Geology and coal resources of the Meeker quadrangle, Moffat and Rio Blanco Counties, Colorado: U.S. Geol. Survey Bull. 812–C, p. 191–242.

Konishi, Kenji, 1959, Upper Cretaceous surface stratigraphy, Axial Basin and Williams Fork area, Moffat and Routt Counties, Colorado, *in* Rocky Mtn. Assoc. Geologists, Guidebook 11th Ann. Field Conf., Washakie, Sand Wash, and Piceance Basins, 1959: p. 67–73.

Lee, W. T., 1912, Coal fields of Grand Mesa and the west Elk Mountains, Colorado: U.S. Geol. Survey Bull. 510, 237 p.

Spieker, E. M., 1949, Sedimentary facies and associated diastrophism in the Upper Cretaceous of central and eastern Utah, *in* Sedimentary facies in geologic history: Geol. Soc. America Mem. 39, p. 55–82.

Walton, P. T., 1944, Geology of the Cretaceous of the Uinta Basin, Utah: Geol. Soc. America Bull., v. 55, no. 1, p. 91–130.

Weimer, R. J., 1960, Upper Cretaceous stratigraphy, Rocky Mountain area: Am. Assoc. Petroleum Geologists Bull., v. 44, no. 1, p. 1–20.

Young, R. G., 1955, Sedimentary facies and intertonguing in the Upper Cretaceous of the Book Cliffs, Utah-Colorado: Geol. Soc. America Bull., v. 66, no. 2, p. 177–202.

113. STRATIGRAPHY AND STRUCTURE OF THE PRECAMBRIAN METAMORPHIC ROCKS IN THE TENMILE RANGE, COLORADO

By A. H. Koschmann and M. H. Bergendahl, Denver, Colo.

Work done in cooperation with the Colorado State Metal Mining Fund Board

The Tenmile Range lies in north-central Colorado, in the southern part of Summit County, about 80 miles west-southwest of Denver (fig. 113.1). Exposed along the crest and upper slopes of the range is a complex of Precambrian contorted metasedimentary granulite, gneiss, and migmatite, which have been intruded by Precambrian granite and Tertiary granodiorite. On the geologic map of Colorado (Burbank and others, 1935) this complex is included in a much larger mass of Precambrian rocks that extends northwestward into the Gore Range and southward into the Mosquito Range. These rocks can be subdivided into four dis-

557753 O—60——17

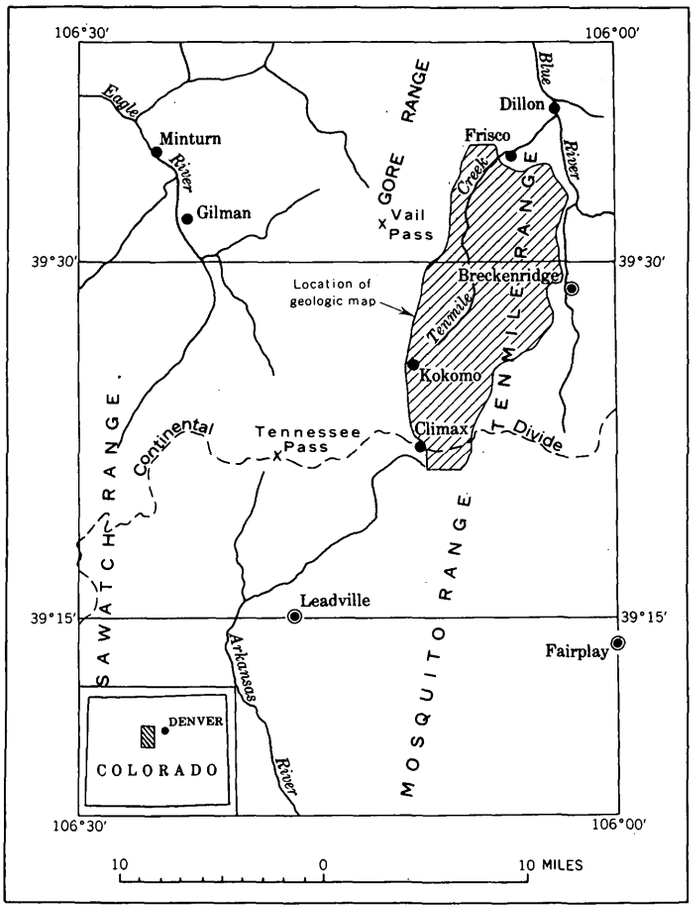

FIGURE 113.1.—Index map showing location of the Tenmile Range, Colo.

crete and persistent stratigraphic units, whose relative age can be determined by their order of superposition in areas where their layering and foliation have relatively flat dips. These units consist, in ascending order, of granulite, banded gneiss, migmatite, and pink quartz-biotite-plagioclase gneiss. The high metamorphic grade of these rocks is indicated by the presence of hornblende, pyroxene, garnet, and sillimanite, chiefly in the banded gneiss and migmatite (see fig. 113.2). The major structure in the area is a syncline that trends eastward and southeastward and is flanked by anticlines.

LITHOLOGY

GRANULITE

The granulite of the Tenmile Range is a high-grade metamorphic rock of granoblastic texture, consisting essentially of quartz, white oligoclase-andesine, and white microcline; its chief accessories are biotite and muscovite. The proportions of these components vary locally, producing dominantly quartzose facies at some localities and a feldspathic facies at others. Much of the rock displays gneissic foliation, imparted by oriented flakes of mica and lenticles of quartz and feldspar, but in some places foliation is very faint or absent. The use of the term granulite accords with that of Harker (1939, p. 246–248).

The granulite is exposed only along the axes of the anticlines, and no exposure shows its base; hence its true thickness cannot be determined. An approximate minimum thickness is about 6,500 feet.

BANDED GNEISS

Overlying the granulite is a banded rock made up of alternate layers of amphibolite and granulite that range in thickness from about a sixteenth of an inch to several feet. The total thickness of the banded gneiss ranges from 20 feet to 1,600 feet. Locally, probably through tectonic processes, this unit is absent. The amphibolite layers in the gneiss are traceable in places for more than 100 feet, but more commonly they are fractured at short intervals, or broken into strings of boudins. The granulite layers were the more plastic, having flowed locally; the amphibolite layers were more competent and yielded by fracture. Near the contact of the banded gneiss with the underlying granulite, the rock layers of the banded gneiss are usually thicker than elsewhere. The upper third of the gneiss is composed of thinner layers, and the mafic layers there contain variable amounts of biotite in addition to hornblende. The contact of the banded gneiss with the overlying migmatite is gradational through as much as 200 feet.

MIGMATITE

The most widespread rock unit in the area is a migmatite, composed mainly of quartz-biotite-plagioclase gneiss and schist interlayered with subparallel lenses and stringers of a quartz-feldspar rock of granitoid to pegmatitic texture. In some places the unit contains lenses and layers rich in sillimanite, garnet, calcite, and lime silicates. The layering is usually wavy and contorted, and much less regular than that of the banded gneiss. As this unit is exposed only along axes of synclines, its true thickness cannot be ascertained; it is estimated, however, to be at least 15,000 feet.

PINK GNEISS

Exposed along the western margin of the area, immediately west of a large north-south fault, is a gneiss that consists mainly of quartz, biotite, and a characteristic pink plagioclase but that locally contains lenses of lime-silicate gneiss. This rock apparently overlies the migmatite (fig. 113.2), but the exact relations are not clear. No complete section of this rock unit is exposed in the mapped area and its thickness is not known.

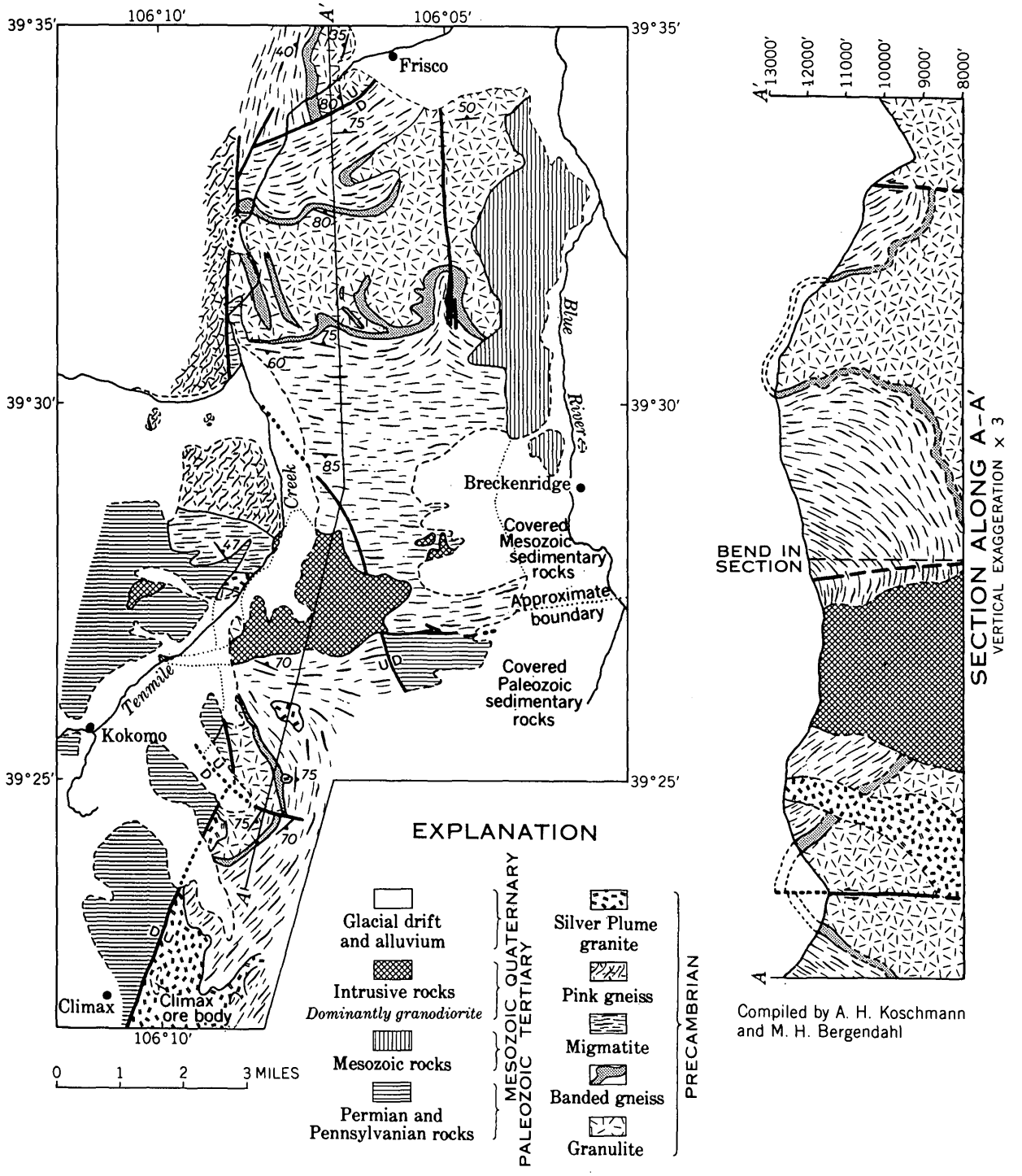

FIGURE 113.2—Generalized geologic map and cross section of the Tenmile Range, Colo.

STRATIGRAPHIC SUCCESSION

The stratigraphic sequence of the metamorphic rocks had to be determined by means of structural evidence, for they contain few relict sedimentary structures and those that were found were too poorly preserved to be useful. In the northern and southern parts of the area, where the dips of the layers and foliation range from 35° to 60°, the stratigraphic relations are everywhere the same; the granulite is overlain by banded gneiss, which is overlain by migmatite. In some areas where the dips are steeper (fig. 113.2), an overturned limb of a fold may suggest that the migmatite is oldest, but this relation is always very local and was never observed where the dips of foliation are relatively flat. The persistent stratigraphic sequence in areas of low dips also makes it unlikely that there has been any recumbent folding, for if such folding had occurred for considerable distances along an inverted limb—and it has never been seen to do so—the migmatite would somewhere underlie the granulite. Furthermore, no Alpine-type folding is known to exist elsewhere in the central Rocky Mountains.

The relation of the pink gneiss to the other gneisses is not clearly revealed. The pink gneiss is exposed only in the northwestern part of the area, and there it seems to overlie the migmatite. For this reason it is considered younger than the migmatite.

STRUCTURE

The metamorphic rocks have been thrown into a series of isoclinal folds and cut by faults.

FOLDS

The principal fold in the area is a syncline trending eastward or southeastward, flanked on the south by a southeastward-plunging anticlinal nose and on the north by an anticline trending east-west (fig. 113.2). On the limbs of the northern anticline there are minor folds, some due to drag and others due to local flowage of the felsic rock layers. In the extreme northern part of the area, west of Frisco, only the west limb of a northward-trending anticline or the truncated nose of an anticline is exposed. It is separated from the structures to the south by a fault and their mutual relations are not revealed.

FAULTS

The Precambrian rocks in the Tenmile Range are cut by several large high-angle faults, marked by shatter zones that range in width from a few tens of feet to several hundred feet (fig. 113.2). Most of the shattered rock in these zones has been cemented by silica, and they are interlaced with quartz veins carrying variable amounts of sulfides. The north-south fault fissure southeast of Frisco contains potassium feldspar. Numerous slickensides in the sheared rocks indicate recurrent movements in various directions.

REFERENCES

Burbank, W. S., Lovering, T. S., Goddard, E. N., and Eckel, E. B., 1935, Geologic map of Colorado: U.S. Geol. Survey.

Harker, Alfred, 1939, Metamorphism, 2d ed. rev.: London. Methuen and Co., Ltd.

114. SALT ANTICLINES AND DEEP-SEATED STRUCTURES IN THE PARADOX BASIN, COLORADO AND UTAH

By H. R. Joesting and J. E. Case, Washington, D.C., and Berkeley, Calif.

Work done partly in cooperation with the U.S. Atomic Energy Commission

The salt anticlines of the Paradox basin (fig. 114.1) were formed by plastic flow of evaporites of Pennsylvanian age, which were originally more than 6,000 feet thick in the deepest parts of the basin. Some of the anticlines are as much as 75 miles long, and their salt cores are something like 2 miles high and 2 to 4 miles long. The cores of the larger anticlines were exposed during much of their growth, so that sediments deposited during that period pinch out against their flanks. Thick deposits of limestone and clastic rocks of late Paleozoic and Mesozoic age now cover the evaporites, except over the axes of the anticlines.

All of the larger salt antinclines are in the deeper, northeastern part of the Paradox basin, where the Precambrian basement may in some places be as much as 17,000 feet beneath the surface. The anticlines all strike northwestward, parallel to the axis of the basin and to the structural front of the uplifted Uncom-

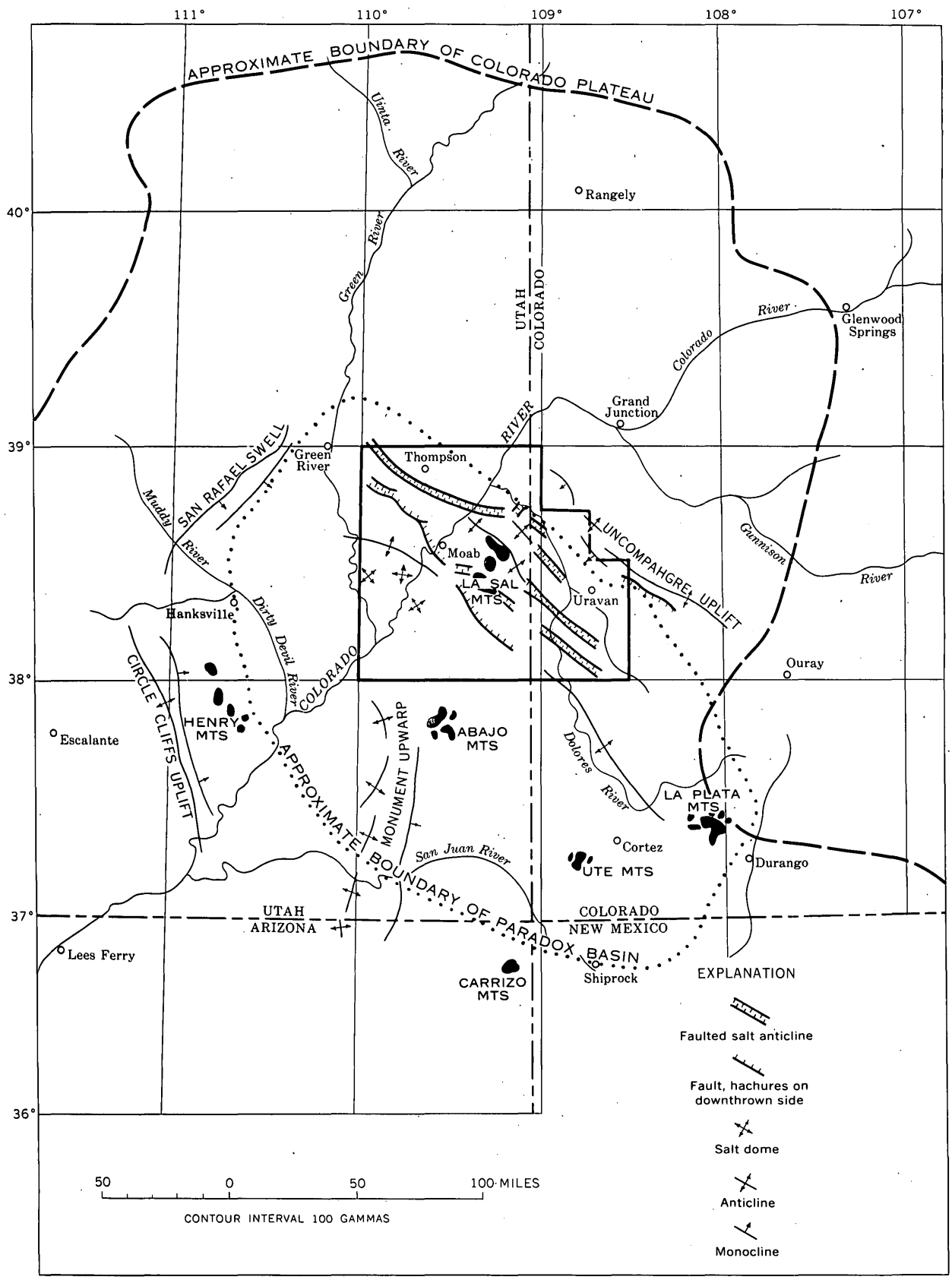

FIGURE 114.1.—Sketch map of northern Colorado Plateau, showing Paradox basin and area discussed.

pahgre Plateau (fig. 114.1). This fact suggests a relation between the anticlines and deep-seated regional structures, but if such a relation exists direct geologic evidence for it is buried beneath thick deposits of Permian and Mesozoic rocks.

The tectonics of the Paradox basin, the nature and history of the salt structures, and the causes of salt flow, have been studied by many investigators. Selected bibliographies accompany publications by Shoemaker, Case, and Elston (1958); Joesting and Byerly (1958); and Jones (1959). Jones thinks it probable that the salt anticlines were formed solely as a result of differential loading of the evaporites, rather than by compressional folding or deep-seated faulting as believed by some of the earlier investigators. In this paper we are concerned only with the magnetic and gravity evidence bearing on the configuration and structure of the Precambrian basement in the salt anticline area of the Paradox basin, and on the association of deep-seated structures with the salt anticlines.

ACKNOWLEDGMENTS

Associated with us during most of the investigations were P. Edward Byerly and Donald Plouff of the Geological Survey, who conducted much of the gravity work and made many of the interpretations based upon it. The aeromagnetic surveys were made under the direction of J. L. Meuschke and R. W. Bromery of the Geological Survey.

SIGNIFICANCE OF THE MAGNETIC AND GRAVITY MAPS

Preliminary aeromagnetic and gravity maps of the area are shown in figures 114.2 and 114.3. They are based on procedures described by Joesting and Byerly (1958) and Byerly and Joesting (1959). Because of the small scale and large contour intervals of the maps, they show only the more prominent anomalies.

Magnetic and gravity highs are associated with the uplifted Uncompahgre Plateau and its buried northwestern extension, where the generally magnetic and dense rocks of the Precambrian complex are closer to the surface than in the adjoining basin. Others are associated with the diorite porphyry laccoliths of the La Sal Mountains, which are denser and more magnetic than the enclosing sedimentary rocks. Large gravity lows, on the other hand, are associated with the larger salt anticlines, because the density of the thickened salt masses is only about 2.2 g per cm^3, compared with about 2.55 g per cm^3 for the adjoining rocks (Joesting and Byerly, 1958, p. 14–15). The evaporites and other sedimentary rocks are virtually nonmagnetic.

Ridges or upwarps of Precambrian basement rocks, some of them having a vertical relief of several thousand feet, are indicated by the magnetic highs bordering Gypsum Valley on the southwest and Moab Valley on the south and southwest (Joesting and Byerly, 1958, p. 10; Joesting and Plouff, 1958, p. 89). These basement highs apparently form the southwestern boundaries of the deeper parts of the Paradox salt basin. Estimates of depths to these sources of the magnetic highs were based on the methods of Vacquier and others (1951), and on methods described by Heiland (1940).

The magnetic evidence for basement highs is supported by regional gravity gradients along parts of Gypsum and Moab Valleys. These gradients indicate that the basement is denser or nearer the surface to the southwest and south, but the gradients are also partly due to the thinning of salt. The evidence for basement highs is partly confirmed by recently drilled holes that penetrated rocks of Mississippian age; the locations of some of these holes are shown in figure 114.2. Estimates of the thickness of the underlying sedimentary rocks were made from the isopach maps of Cooper (1955), Baars (1958), and Neff and Brown (1958). In some localities these estimates may be in error because of irregularities on the Precambrian surface, and because we know little about the stratigraphy and structure of the older Paleozoic rocks. Estimates of depths from magnetic data may, of course, also be in error.

The magnetic and gravity evidence also suggests comparatively shallow depths to the basement just north and also southwest of Lisbon Valley salt anticline (Byerly and Joesting, 1959, p. 44–45). This evidence is partly confirmed by recent drilling, which penetrated rocks of Mississippian age. Southwest of Lisbon Valley, however, the depth indicated by drilling is much greater than that estimated from the magnetic data. Gravity evidence (Byerly and Joesting, 1959, p. 46) also indicates that the basement lies deeper northeast of Lisbon Valley anticline, but the effects of changes in density and depth cannot be separated.

The gravity and magnetic data further indicate that the La Sal Mountains and a large area to the southeast rest on a broad basement platform. The northeastern boundary of this platform is apparently defined by a continuation of the Paradox Valley regional gravity and magnetic gradients past the La Sal Mountains, the southeastern boundary by a southwest-trending gravity gradient extending from Paradox Valley to the northwest end of Gypsum Valley, and the northwestern boundary by a gravity gradient that bounds the La Sal Mountains on the northwest. These inferred boundaries are shown on figures 114.2 and 114.3.

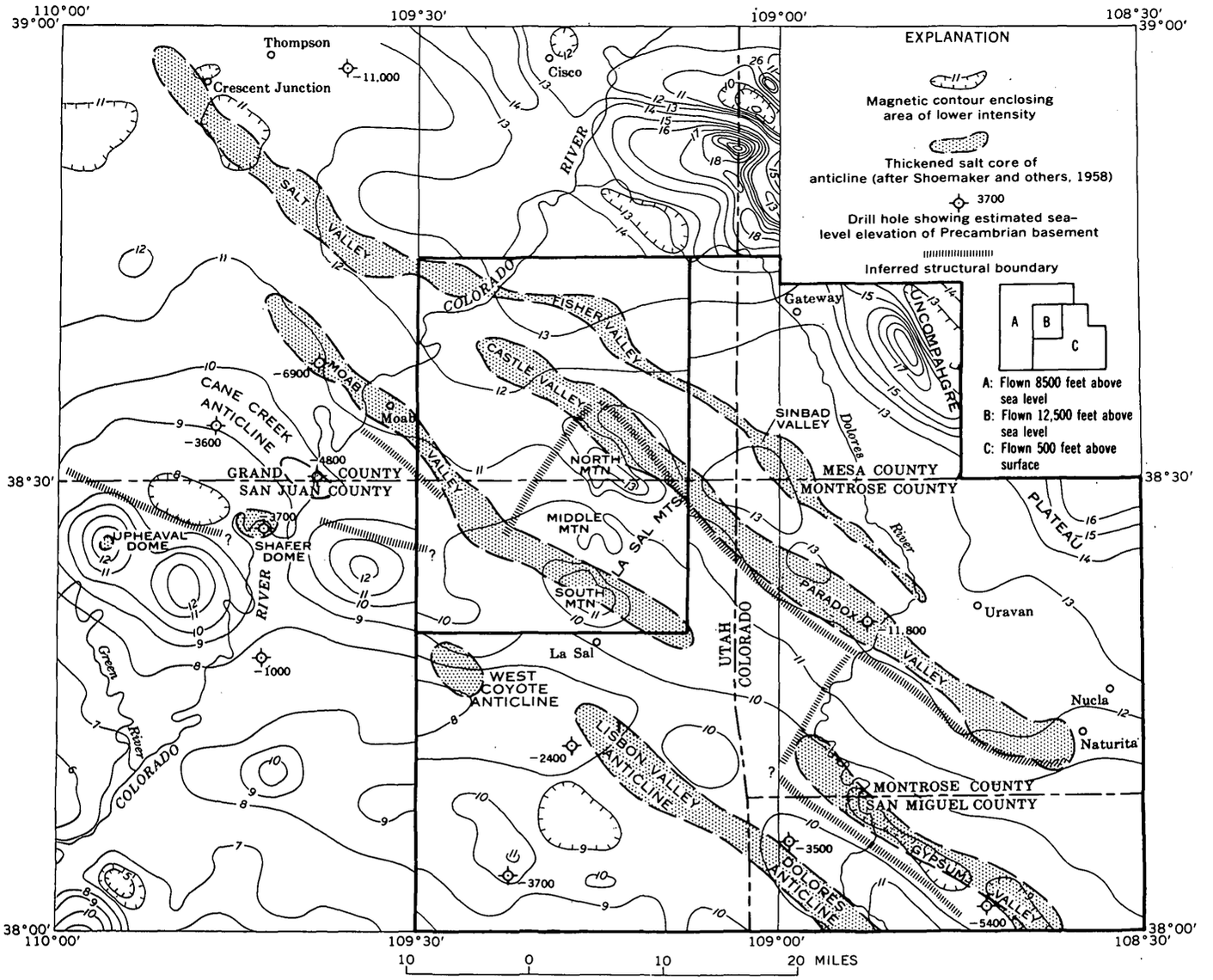

FIGURE 114.2.—Preliminary aeromagnetic map of salt anticline area of Paradox basin, Colorado and Utah.

The gravity anomalies along the inferred boundaries of the platform are probably caused in part by thinning of salt; for example, from Moab and Castle Valleys southeastward toward the La Sal Mountains, and from Gypsum and Paradox Valleys northwestward. Their main causes, however, are differences in the density or depth of the basement rocks. Magnetic evidence indicates comparatively shallow depth to basement at the northwestern end of Paradox Valley, and it therefore seems likely that the regional anomalies may be due in part to relief on the surface of the Precambrian basement.

REFERENCES

Baars, D. L., 1958, Cambrian stratigraphy of the Paradox basin region, *in* Intermountain Assoc. Petroleum Geologists Guidebook 9th Ann. Field Conf., Guidebook to the geology of the Paradox basin, 1958: p. 93–101.

Byerly, P. E., and Joesting, H. R., 1959, Regional geophysical investigations of the Lisbon Valley area, Utah and Colorado: U.S. Geol. Survey Prof. Paper 316–C.

Cooper, J. C., 1955, Cambrian, Devonian, and Mississippian rocks of the Four Corners area: Four Corners Geol. Soc. Field Conf. Guidebook, p. 59–65.

Heiland, C. A., 1940, Geophysical exploration: New York, Prentice-Hall, Inc.

Joesting, H. R., and Byerly, P. E., 1958, Regional geophysical investigations of the Uravan area, Colorado: U.S. Geol. Survey Prof. Paper 316–A.

Joesting, H. R., and Plouff, Donald, 1958, Geophysical studies of the Upheaval Dome area, San Juan County, Utah, *in* Intermountain Assoc. Petroleum Geologists Guidebook 9th Ann. Field Conf., Guidebook to the geology of the Paradox basin, 1958: p. 86–92.

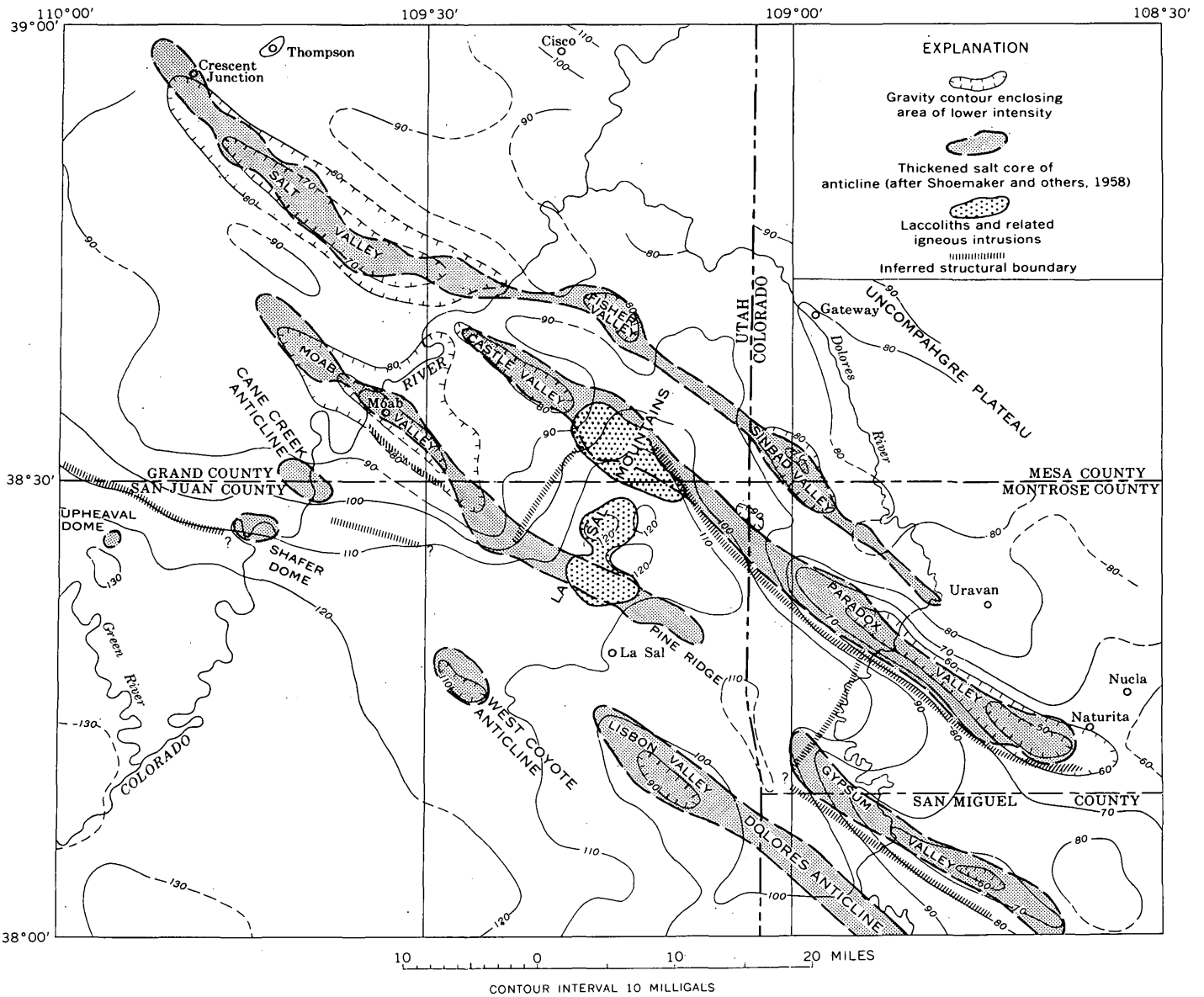

FIGURE 114.3.—Preliminary gravity map of salt anticline area of Paradox basin, Colorado and Utah.

Jones, R. W., 1959, Origin of salt anticlines of Paradox basin: Am. Assoc. Petroleum Geologists Bull., v. 43, no. 8, p. 1869–1895.

Neff, A. W., and Brown, S. C., 1958, Ordovician-Mississippian rocks of the Paradox basin, *in* Intermountain Assoc. Petroleum Geologists Guidebook 9th Ann. Field Conf., Guidebook to the geology of the Paradox basin, 1958: p. 102–108.

Shoemaker, E. M., Case, J. E., and Elston, D. P., 1958, Salt anticlines of the Paradox basin, *in* Intermountain Assoc. Petroleum Geologists Guidebook 9th Ann. Field Conf., Guidebook to the geology of the Paradox basin, 1958: p. 86–92.

Vacquier, Victor, and others, 1951, Interpretation of aeromagnetic maps: Geol. Soc. America Mem. 47, 151 p.

115. DISTRIBUTION AND PHYSIOGRAPHIC SIGNIFICANCE OF THE BROWNS PARK FORMATION, FLAMING GORGE AND RED CANYON AREAS, UTAH-COLORADO

By WALLACE R. HANSEN, DOUGLAS M. KINNEY, AND JOHN M. GOOD, Denver, Colo., Washington, D.C., and U.S. National Park Service, Washington, D.C.

The Browns Park formation (Miocene?), named by Powell (1876, p. 44 and 168), is typically exposed in the valley of Browns Park, in the Uinta Mountains, which lies astride the Utah-Colorado State line. From its type area the formation extends eastward as an unbroken blanket almost to Craig, Colorado (Sears, 1924a, pl. 35; 1924b, fig. 1), a distance of about 85 miles; from Craig it extends discontinuously northward to and beyond Saratoga, Wyoming (Love, Weitz, and Hose, 1955). Its outcrop belt marks the course of an ancestral stream that probably flowed eastward toward the Mississippi drainage system (Bradley, 1936, p. 188). Recently discovered remnants of the Browns Park formation extend discontinuously westward from the type area for another 25 miles or so, in and alongside Red Canyon of the Green River. On the south slope of the Uinta Mountains, the formation is represented by blanketlike deposits that cover broad areas north of Vernal, Utah (fig. 115.1).

In its type area the Browns Park formation is widely and well exposed. Along the north side of the valley, its boundary is rather well defined by faulting, flexing, and erosion that occurred after its deposition. Along the south side of the valley, however, the formation has an irregular depositional boundary, because it extends partway up tributary valleys that had previously been cut into the Uinta Mountain group (Precambrian).

Long tongue-shaped remnants of the Browns Park formation that have a different history occur in the headward parts of most of these tributary valleys, including the valleys of Crouse Creek, Sears Creek, Warren Draw, Jackson Creek, Gorge Creek, and Cart Creek. These remnants, never previously mapped, are scattered over a maturely dissected terrain along the main divide of the Uinta range, and fill valleys cut by streams that originally flowed southward. They have been separated from the main body of the formation by subsequent erosion, and near their mouths the streams mentioned above have stripped off the Browns Park deposits or cut through them into the underlying Uinta Mountain group. Each tributary valley now has a precipitous inner canyon near its mouth, cut into the Uinta Mountain group. Farther south the tonguelike remnants merge into a blanket that fills Summit Valley and tops Diamond Mountain, north of Vernal (Kinney, Hansen, and Good, 1959, p. 1630). The formation must once have extended across the eastern end of the Uinta range as a continuous blanket, above which only the higher peaks and ridges protruded.

The configuration of the hard-rock floor of the axial portion of Browns Park Valley is unknown. Along the margins of the valley, however—particularly the south margin—the floor is highly irregular. In many places windows, spurs, and salients of Precambrian rock protrude through the Browns Park formation; the most notable of these is Kings Point, through which Swallow Canyon has been cut by the Green River in a classic example of superposition.

Westward from the type area, discontinuous remnants of the Browns Park formation become progressively smaller, thinner, and more widely separated. They consist of interbedded fanglomerates, sandstones, tuffs, and tuffaceous sandstones, lithologically similar to equivalent deposits in the type area. Thick and rather extensive remnants at Little Hole reach from the river, which here is about 5,500 feet above sea level, to an altitude of more than 7,000 feet. The formation was deposited here on the walls and floor of a deep, irregular canyon. Smaller remnants along Red Canyon west of Little Hole (fig. 115.1) have similar physiographic relations but do not reach river level; the surface on which they rest slopes upward toward the west.

As remnants of the Browns Park formation in the Red Canyon area lie well below the Bear Mountain erosion surface, they must be a good deal younger than that surface. Eastward the Bear Mountain erosion surface appears to project into the air above Browns Park, rather than beneath it as Bradley supposed (1936, p. 163 and 180), and to merge into the remnants of the Gilbert Peak erosion surface that are preserved north of Browns Park on Goslin, Mountain Home, Head of Cottonwood, Bender, O-Wi-Yu-Kuts, and Cold Spring Mountains. Discordances in altitude between remnants of the Bear Mountain surface in the Red Canyon area and remnants of the Gilbert Peak surface on adjacent Goslin Mountain are attributed to faulting and warping that occurred before, during, and after the deposition of the Browns Park formation.

A cycle of valley cutting intervened between development of the Bear Mountain erosion surface and the deposition of the Browns Park formation. The shift

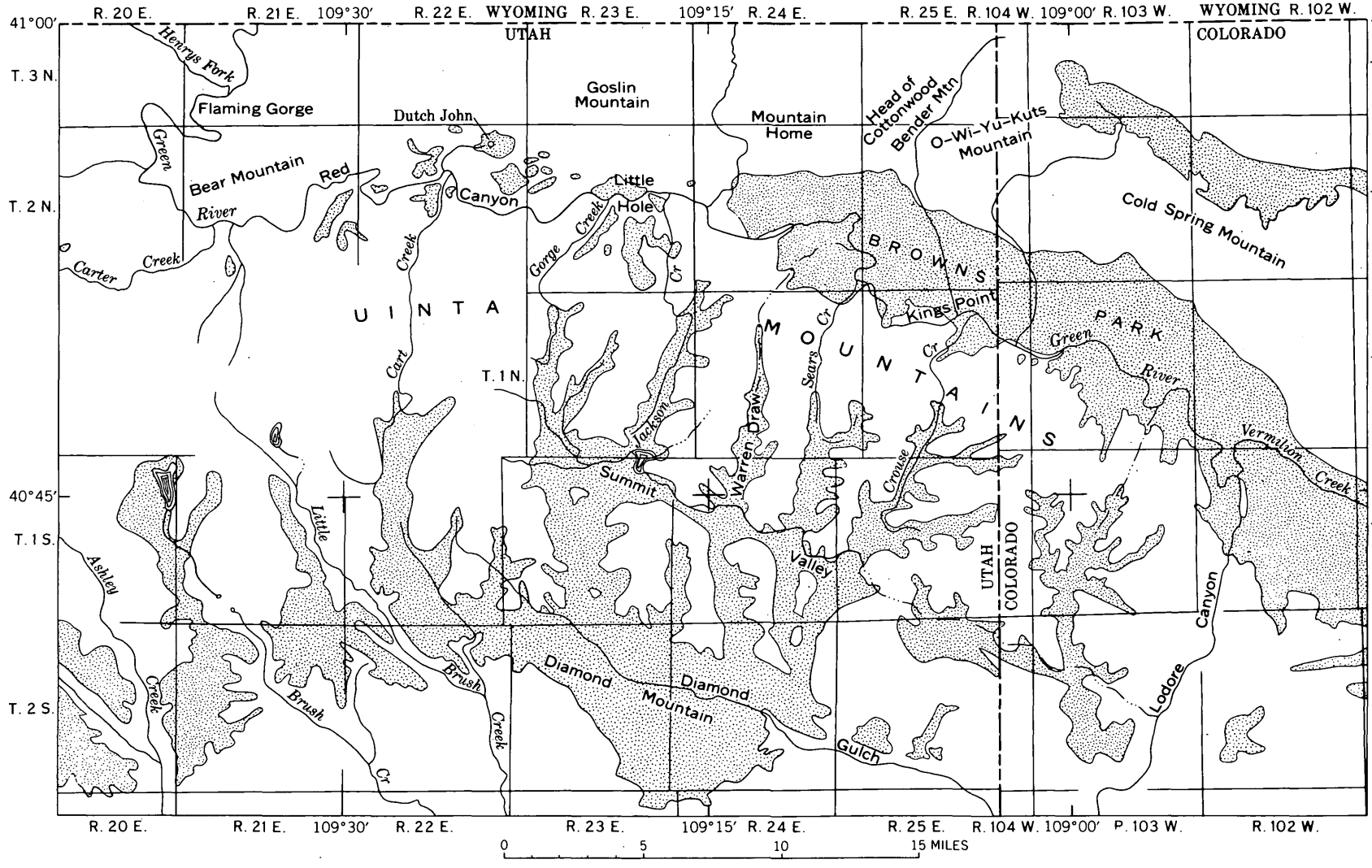

FIGURE 115.1.—Sketch map showing general distribution of Browns Park formation (stippled) in part of eastern Uinta Mountains, Utah-Colorado. Based on detailed mapping on north slope by Hansen and on south slope by Kinney, and on reconnaissance and photogeology along crestal area.

from degradation to aggradation may have been caused by heavy falls of volcanic ash, that mantled hillsides and clogged valleys and that were preceded and accompanied by tectonic adjustments, rather than a climatic change. The Browns Park formation thus has a haphazard relation to earlier topography; it caps a pediment remnant here, fills a valley there, or overtops a hillock somewhere else. In the Red Canyon area it filled an old canyon, overtopped the rims, and spread out onto the Bear Mountain surface. Subsequent rejuvenation entrenched the present Green River, which then carved Red Canyon by cutting through the Browns Park formation and into the Uinta Mountain group.

REFERENCES

Bradley, W. H., 1936, Geomorphology of the north flank of the Uinta Mountains: U.S. Geol. Survey Prof. Paper 185–I, p. 163–199.

Kinney, D. M., Hansen, W. R., and Good, J. M., 1959, Distribution of Browns Park formation in eastern Uinta Mountains, northeastern Utah and northwestern Colorado [abs.]: Geol. Soc. America Bull., v. 70, no. 12, pt. 2, p. 1630.

Love, J. D., Weitz, J. L., and Hose, R. K., 1955, Geologic map of Wyoming: U.S. Geol. Survey.

Powell, J. W., 1876, Report on the geology of the eastern portion of the Uinta Mountains: U.S. Geol. and Geog. Survey Terr., 218 p.

Sears, J. D., 1924a, Geology and oil and gas prospects of part of Moffat County, Colorado, and southern Sweetwater County, Wyoming: U.S. Geol. Survey Bull. 751, p. 269–319.

——— 1924b, Relations of the Browns Park formation and the Bishop conglomerate and their role in the origin of Green and Yampa Rivers: Geol. Soc. America Bull., v. 35, p. 279–304.

116. PROBABLE LATE MIOCENE AGE OF THE NORTH PARK FORMATION IN THE NORTH PARK AREA, COLORADO

By W. J. Hail, Jr., and G. Edward Lewis, Denver, Colo.

The discovery of fragments of fossil vertebrates of probable late Miocene age in the North Park formation in its type area in North Park, Colo., permits tentative dating of the formation, and supports correlation with rocks of late Miocene age (Montagne and Barnes, 1957, p. 59) mapped as the North Park formation in the Saratoga basin of northern Colorado and southern Wyoming, and in other nearby areas.

Beekly's (1915, p. 66) redefinition of the North Park formation has generally been followed by subsequent workers. In the type area south of Walden in central Jackson County, Colo., the formation is at least 2,000 feet thick, and at different places lies on the White River formation of Oligocene age and on the Coalmont formation of Paleocene and Eocene age. Oligocene rocks underlying part of the North Park formation were recognized by Montagne (Montagne and Barnes, 1957, p. 56). The North Park formation of the type area is not continuous with rocks mapped as the North Park formation 20 to 30 miles farther north in the Saratoga basin of northern Colorado and southern Wyoming (McGrew, 1951, p. 54–57; 1953, p. 63–64; and Montagne and Barnes, 1957, p. 55–60). In the Saratoga basin area, the North Park formation lies on rocks as old as Precambrian.

The North Park formation both in its type area and to the north in Colorado and adjacent parts of southern Wyoming consists mostly of calcareous sandstone, with abundant conglomerate, conglomeratic sandstone, and limestone, and lesser amounts of shale, bentonitic clay, volcanic ash, and tuff. Volcanic detritus composes much of the formation.

Vertebrate fossils were collected at three localities. Locality D437 is in the type area southwest of Walden, Colo., and localities D146 and D272 are in the southern Saratoga basin, Colorado and Wyoming. At locality D437 two weathered fragments of a fossil horse tooth were found in a bed of light-gray fine-grained calcareous sandstone about 900 feet above the base of the formation. In this area, the North Park formation lies unconformably on the Coalmont formation of Paleocene and Eocene age, and is about 1,100 feet thick; younger beds of the North Park have been eroded away. At locality D146 fragments of fossil horse teeth were found in beds of light-brown fine-grained calcareous sandstone that are estimated to be several hundred feet above the base of the formation. The formation in this area lies on Precambrian metamorphic rocks. At locality D272, fragments of an oreodont jaw were found in a bed of light-gray fine-grained calcareous sandstone 200 to 300 feet above the base of the formation. At this locality the North Park also lies on Precambrian metamorphic rocks. Tentative identification of the specimens and the localities from which they came are as follows:

Merychippus sp.; USGS fossil vertebrate loc. D437, NW¾ SW¼ sec. 17, T. 8 N., R. 80 W., Jackson County, Colo.; two fragments of an upper cheek tooth.

Merychippus sp.; USGS fossil vertebrate loc. D146, SW¼ sec. 7, T. 12 N., R. 80 W., Carbon County, Wyo.; four fragments of upper cheek teeth.

?Brachycrus sp.; USGS fossil vertebrate loc. D272, NE¼ NE¼ sec. 7, T. 11 N., R. 80 W., Jackson County, Colo.; fragment of right ramus with one incomplete lower molar, and fragment of left ramus with lower molar and incomplete lower molars 1 and 3.

These identified forms are elements of a fauna, probably of late Miocene age, comparable to the fauna in the upper part of the Hemingford group of Nebraska which Lugn (1939, p. 1253–1258, 1264, table 2) believes to be of latest Miocene age. Many authorities believe that this fauna may be as old as early late Miocene, somewhat older than Lugn believed it to be (Wood and others, 1941, pl. 1).

REFERENCES

Beekly, A. L., 1915, Geology and coal resources of North Park, Colorado: U.S. Geol. Survey Bull. 596, 121 p.

Lugn, A. L., 1939, Classification of the Tertiary system in Nebraska: Geol. Soc. America Bull., v. 50, p. 1245–1276.

McGrew, P. O., 1951, Tertiary stratigraphy and paleontology of south-central Wyoming, *in* Wyoming Geol. Assoc. Guidebook 6th Ann. Field Conf., south-central Wyoming, 1951: p 54–57.

——— 1953, Tertiary deposits of southeastern Wyoming, *in* Wyoming Geol. Assoc. Guidebook 8th Ann. Field Conf., Laramie Basin, Wyoming, and North Park, Colorado, 1953; p. 61–64.

Montagne, John De la, and Barnes, W. C., 1957, Stratigraphy of the North Park formation in the North Park area, Colorado, *in* Rocky Mountain Assoc. of Geologists, Guidebook to the geology of North and Middle Park Basins, Colorado: p. 55–60.

Wood, H. E., 2d, and others, 1941, Nomenclature and correlation of the North American continental Tertiary: Geol. Soc. America Bull., v. 52, p. 1–48.

117. PALEOCENE AND EOCENE AGE OF THE COALMONT FORMATION, NORTH PARK, COLORADO

By W. J. Hail, Jr., and Estella B. Leopold, Denver, Colo.

Study of pollen and spore assemblages from the Coalmont formation of the North Park basin, Jackson County, Colo., indicates an Eocene age for the upper part of the formation instead of a Paleocene age as was previously thought. The Coalmont formation has an aggregate thickness of as much as 9,000 feet in parts of North Park. It unconformably overlies rocks mostly of Cretaceous age, and is unconformably overlain locally by the White River formation of Oligocene age and by the North Park formation of late Miocene age. The Coalmont formation forms the surface rock for much of the North Park basin.

The Coalmont formation has been correlated in earlier studies entirely or in part with the Fort Union formation of Paleocene age in the western interior basin (Beekly, 1915, p. 62–63; Brown, 1949). This correlation was based on fossil leaves collected by A. L. Beekly and studied by F. H. Knowlton (Beekly, 1915, p. 61–66), and on fossil leaves collected and studied by R. W. Brown. More recently, however, R. W. Brown (written communication, 1958) suggested that a collection of fragmentary leaves from a bed of shaly sandstone in the upper part of the formation might be younger than Paleocene.

A sample of carbonaceous shale for pollen and spore study was collected at USGS paleobotanical loc. D1369, about 5 miles southwest of Walden (NW¼ sec. 8, T. 8 N., R. 80 W.), from a bed at least 900 feet stratigraphically below the horizon of the fragmentary leaf collection examined by Brown (written communication, 1958) but at least 2,000 feet stratigraphically above any of Beekly's leaf collections in western North Park (Beekly, 1915, p. 64–66). This sample contains five pollen and spore species common to Paleocene and Eocene rocks of Wyoming; but, significantly, the sample also contains pollen of *Platycarya*. The genus *Platycarya*, a member of the walnut family, has only one living species, which is now restricted to forests of northern China and Japan. To date, *Platycarya* pollen is known in the New World only from rocks of Eocene age; it is present in the Knight, Wasatch, and Green River formations in Wyoming, and the Clarno formation in Oregon (E. B. Leopold and R. A. Scott, unpublished data).

Many additional samples for pollen and spore studies were collected in the Pole Mountain-Coalmont area, the type area of the Coalmont formation in southwestern Jackson County. This area is about 14 miles southwest of Walden. The stratigraphically highest sample (USGS paleobotanical loc. D1359, NE ¼ sec. 21, T. 7 N., R. 80 W.) collected in the Pole Mountain-Coalmont area was from a bed of carbonaceous shale

about 3,500 feet below the top of the formation. This sample contains eight pollen and spore forms regionally common to Paleocene and Eocene rocks, as well as abundant pollen of *Platycarya* and Gramineae. Pollen similar to modern Gramineae (grass) pollen is not yet known from rocks older than Eocene. Gramineae pollen has been found in Wyoming in the Green River formation of early and middle Eocene age, and in rocks younger than Green River.

A suite of abundantly fossiliferous samples was collected at USGS paleobotanical loc. D1408 (SW ¼ sec. 4, T. 6 N., R. 81 W.) and D1409 (NW ¼ sec. 4, T. 6 N., R. 81 W.) from an 800-foot-thick carbonaceous shale sequence which lies about 2,800 feet stratigraphically below loc. D1359. Ten samples yielded 38 species of pollen and spores, of which the dominant form in most of the samples is pollen of *Platycarya*. Also present is pollen of Tiliaceae (linden family), here assigned to *Tilia crassipites* Wodehouse; *Tilia crassipites* pollen is known in Wyoming and Colorado from rocks of early Eocene through Oligocene age, but is lacking in rocks of Paleocene age. All but 2 of the 38 species occur in the Wasatch formation of early Eocene age, near Sheridan, Wyo. The other two species are found in the Green River formation of early and middle Eocene age in southwestern Wyoming.

A local unconformity in the Coalmont formation in the Pole Mountain-Coalmont area separates the 800-foot-thick carbonaceous shale sequence from the lower part of the formation; in this area the part below the unconformity has a minimum thickness of about 1,500 feet. Carbonaceous shale samples from several localities in this lower part of the formation yielded only six pollen species, none of which is an exclusively Eocene form, but all of which are common in early Tertiary rocks of the Western United States.

The authors conclude that the lower part of the Coalmont formation is of Paleocene age, based on the presence of Paleocene leaves; and that the upper part of the Coalmont is of Eocene age, perhaps early Eocene, based on the presence of pollen of *Platycarya*, Gramineae, and *Tilia crassipites*.

REFERENCES

Beekly, A. L., 1915, Geology and coal resources of North Park, Colorado: U.S. Geol. Survey Bull. 596, 121 p.

Brown, R. W., 1949, Paleocene deposits of the Rocky Mountains and Plains: U.S. Geol. Survey map.

118. PRE-CUTLER UNCONFORMITIES AND EARLY GROWTH OF THE PARADOX VALLEY AND GYPSUM VALLEY SALT ANTICLINES, COLORADO

D. P. Elston and E. R. Landis, Denver, Colo.

Work done in cooperation with the U.S. Atomic Energy Commission

The salt anticline region of the Colorado Plateau occupies the deep, axial part of the Paradox basin in western Colorado and eastern Utah. The five major northwest-trending salt anticlines (inset, fig. 118.1), which are 30 to 70 miles long, have structurally complex central parts 2 to 6 miles wide, and salt cores 4,100 to 13,700 feet thick. Southwest of these, the salt-bearing unit of the Paradox member of the Hermosa formation (Middle Pennsylvanian) ranges from 0 to about 3,000 feet in thickness, whereas its original thickness in the deep part of the basin may have been about 7,000 feet.

Rocks of the Paradox member, consisting of gypsum, generally fine-grained clastics, and carbonates, crop out locally in several valleys eroded along the axes of the salt anticlines, together with some broken beds of clayey gypsum, that appear to be residual from leached salt beds. These rocks are about 400 to 1,300 feet thick. They overlie the salt and are unconformably overlapped by Paleozoic beds that consist of marine limestone and shale and of marine and continental siltstone, arkosic sandstone, and conglomerate. The aggregate thickness of the younger Paleozoic beds is only a few hundred feet over parts of the salt structures, but is more than 5,000 feet in areas between the salt structures.

PARADOX VALLEY

Unconformities have been found at several places in Paradox Valley beneath thinned sequences of the upper member of the Hermosa formation (Middle Pennsylvanian), the Rico formation (Middle and Late Pennsylvanian in the Gypsum Valley and Paradox Valley areas), and the Cutler formation (Permian).

The upper member of the Hermosa formation is commonly less than 50 feet thick in scattered outcrops, and in the northwest part of Paradox Valley it is separated from the Cutler formation by about 150 feet of interbedded limestone and arkosic sandstone of the Rico formation, both of whose contacts are unconformable. Both the upper member of the Hermosa formation and the Rico formation are about 3,000 feet thick on the south flank of the Paradox Valley salt anticline.

There is a marked unconformity beneath the Cutler formation (fig. 118.1). The basal beds (units Pca, Pcb and Pcc) consist of about 100 feet of gray, platybedded to indistinctly bedded, marine (?) sandstone and conglomerate, which grade upward into fluviatile red beds typical of the Cutler (unit Pcd). The lowest unit of the Cutler (Pca), which is about 50 feet thick in the eastern part of the map area and contains scattered pebbles derived from underlying rocks, was deposited in fold troughs on an irregular erosion surface. Although this unit (Pca) pinches out locally to the west, an outlier rests unconformably on the Paradox member of the Hermosa formation about 900 feet to the south of the pinch-out. In the western part of the map area, the next younger unit (Pcb) unconformably overlies the upper member of the Hermosa formation, which apparently truncates a part of the Paradox member.

GYPSUM VALLEY

Unconformities are seen in Gypsum Valley beneath the Cutler and Rico formations and beneath the upper member of the Hermosa formation in the map area of figure 118.2, and also two unconformities within that member. The upper member of the Hermosa formation and the Rico formation rest unconformably on several different units of the Paradox member.

The upper member of the Hermosa formation, which pinches out over the anticline in the central part of the map area but which is about 100 feet thick on its flanks, consists chiefly of gray dolomite and limestone. Its lowermost persistent unit is a bed of resistant dolomite, about 5 feet thick. West of the topographic saddle near the crest of the anticline, this dolomite overlies black shale of the Paradox member with sharp angular discordance, and also truncates an isolated dolomite bed of the upper member of the Hermosa that is sharply folded into the black shale. About 300 feet south of the anticline, the persistent dolomite overlies a gypsum unit of the Paradox member. On the southwest side of the saddle, about 50 feet of thin-bedded dolomite in the upper member of the Hermosa is truncated in a distance of about 150 feet beneath a breccia-rubble that contains pebbles, cobbles, and boulders of limestone and sandstone. An overlying dolomite is truncated in turn by the Rico formation.

The Rico formation, which is about 100 feet in maximum thickness but pinches out over the salt structure, consists of irregularly bedded grayish-red siltstone, sandstone, limestone, and dolomite. Some of the carbonate beds in the upper half of the formation are clastic and consist of angular carbonate fragments in carbonate cement, indicating unsettled conditions of deposition. In the northeast part of the map area the Rico formation is unconformably overlain by a thin wedge of purplish arkosic to conglomeratic sandstone, typical of the Cutler formation.

CONCLUSIONS

The facts outlined above show that the cores of the Paradox Valley and Gypsum Valley salt anticlines are overlain by thin post-Paradox formations of Pennsylvanian and Permian age, pinching out over the anticlines and separated by unconformities. These facts indicate that the growth of the salt cores in both anticlines began in Middle Pennsylvanian time, not later than sometime during the deposition of the upper member of the Hermosa formation, that the tops of the salt structures generally stayed near local base level, and that the unconformities within, and separating, the thinned late Paleozoic formations record pulses of vertical movement in the salt cores.

Because of the relatively thin cover of rocks above the salt prior to growth of the cores, it is thought that growth of the salt core was initiated by tectonic activity. Such activity is recorded at some places by the arkosic debris, shed from the ancestral Uncompahgre Range, that is interbedded with evaporite and carbonate rocks in the Hermosa and Rico formations. Repeated tectonic pulses may have caused continual growth, or at least intermittent growth, in Pennsylvanian time, during which more sedimentation took place alongside the growing salt structures than on their tops. After the uplift of the Uncompahgre Range, however, the continued growth of the salt cores during much of Permian time probably resulted from differential loading.

The widely held concept that a great thickness of late Paleozoic beds was pierced by intrusive salt masses during inception of the salt anticlines is not compatible with the field evidence. This, however, does not preclude later intrusion into beds of the Cutler formation that may have covered the salt structures in Permian time.

REFERENCES

Cater, F. W., Jr., 1955a, The salt anticlines of southwestern Colorado and southeastern Utah, *in* Four Corners Geol. Soc.

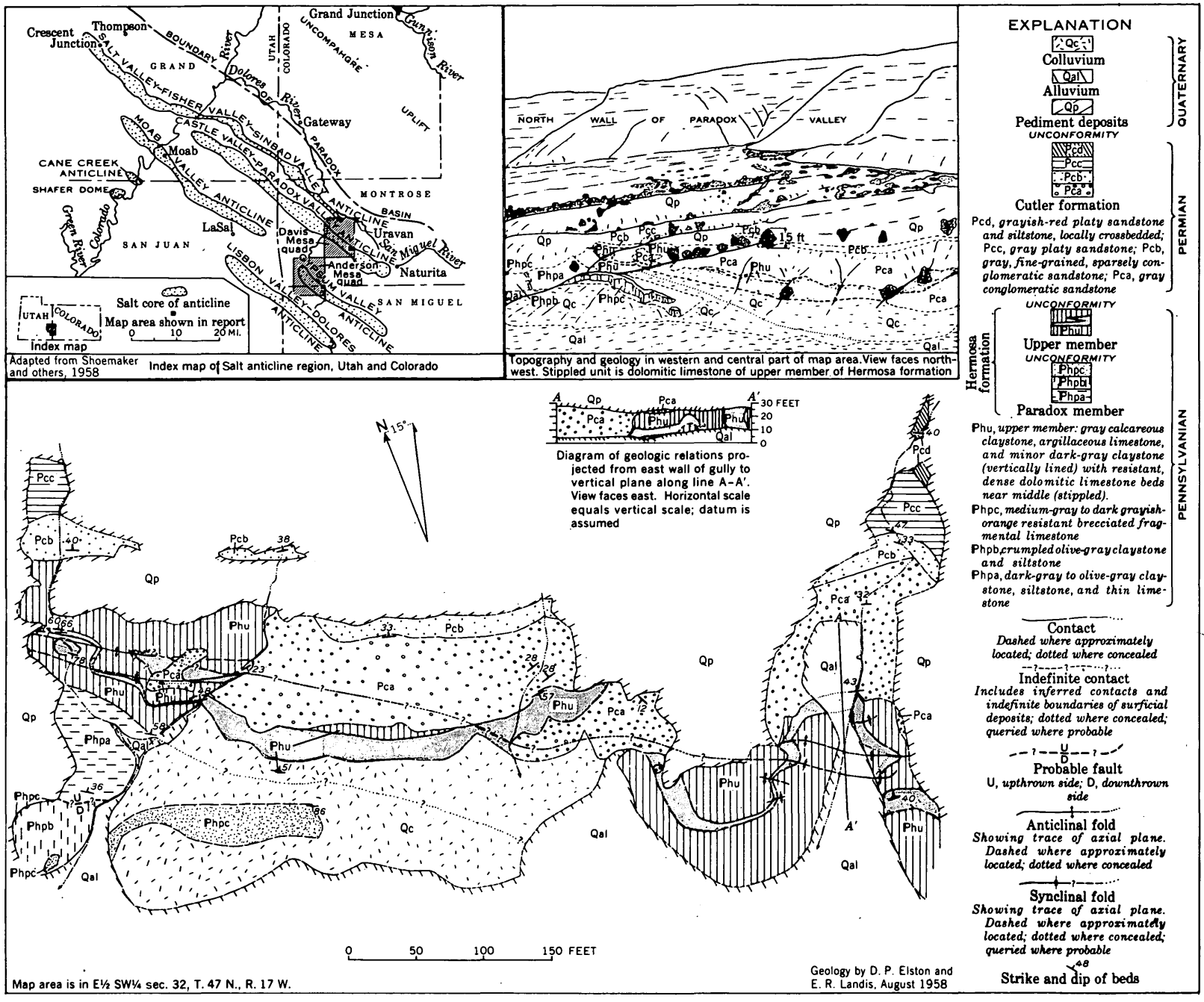

FIGURE 118.1.—Geologic map of part of Paradox Valley, Colo.

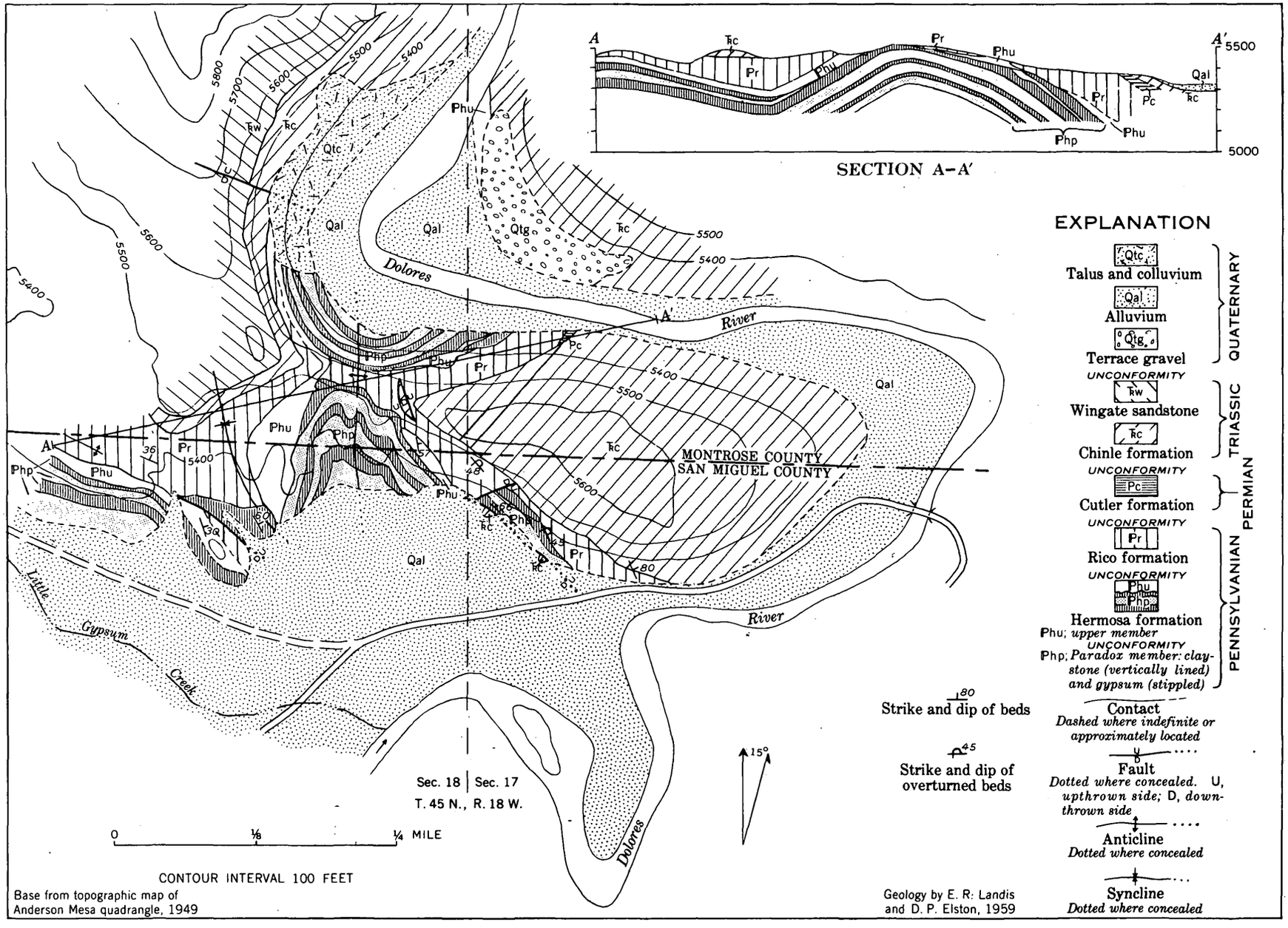

FIGURE 118.2.—Geologic map of part of Little Gypsum Valley, Colo.

Guidebook Field Conf. No. 1, Geology of parts of Paradox, Black Mesa, and San Juan Basins, 1955: p. 125–131.

——— 1955b, Geology of the Davis Mesa quadrangle, Colorado: U.S. Geol. Survey Geol. Quad. Map GQ–71.

——— 1955c, Geology of the Anderson Mesa quadrangle, Colorado: U.S. Geol. Survey Geol. Quad. Map GQ–77.

Herman, George, and Barkell, C. A., 1957, Paradox salt basin: Am. Assoc. Petroleum Geologists Bull., v. 41, no. 5, p. 861–881.

Jones, R. W., 1959, Origin of salt anticlines of Paradox Basin: Am. Assoc. Petroleum Geologists Bull., v. 43, no. 8, p. 1869–1895.

Prommel, H. W. C., and Crum, H. E., 1927, Salt domes of Permian and Pennsylvanian age in southeastern Utah and their influence on oil accumulation: Am. Assoc. Petroleum Geologists Bull., v. 11, no. 4, p. 373–393.

Shoemaker, E. M., 1954, Structural features of southeastern Utah and adjacent parts of Colorado, New Mexico, and Arizona, *in* Utah Geol. Soc., Guidebook to the geology of Utah, No. 9, 1954: p. 48–69.

Shoemaker, E. M., Case, J. E., and Elston, D. P., 1958, Salt anticlines of the Paradox basin, *in* Intermountain Assoc. Petroleum Geologists Guidebook 9th Ann. Field Conf., Guidebook to the geology of the Paradox basin, 1958: p. 39–59.

Stokes, W. L., 1948, Geology of the Utah-Colorado salt dome region with emphasis on Gypsum Valley, Colorado: Utah Geol. Soc., Guidebook to the geology of Utah, No. 3, 50 p.

——— 1956, Nature and origin of Paradox basin salt structures, *in* Intermountain Assoc. Petroleum Geologists Guidebook 7th Ann. Field Conf., Geology and economic deposits of east central Utah, 1956: p. 42–47.

Stokes, W. L., and Phoenix, D. A., 1948, Geology of the Egnar-Gypsum Valley area, San Miguel and Montrose Counties, Colorado: U.S. Geol. Survey Oil and Gas Inv. Prelim. Map 93.

Wengerd, S. A., and Matheny, M. L., 1958, Pennsylvanian system of Four Corners region: Am. Assoc. Petroleum Geologists Bull., v. 42, no. 9, p. 2048–2106.

Wengerd, S. A., and Strickland, J. W., 1954, Pennsylvanian stratigraphy of Paradox salt basin, Four Corners region, Colorado and Utah: Am. Assoc. Petroleum Geologists Bull., v. 38, no. 10, p. 2157–2199.

119. STRUCTURE OF PALEOZOIC AND EARLY MESOZOIC ROCKS IN THE NORTHERN PART OF THE SHOSHONE RANGE, NEVADA

By JAMES GILLULY, Denver, Colo.

Work done in cooperation with the Nevada Bureau of Mines

Structural analysis of the area has revealed structures that rival those of the Alps in complexity. The Roberts thrust has moved sheets many thousands of feet thick, composed of siliceous Ordovician, Silurian, and Devonian rocks, over carbonate rocks of Cambrian, Ordovician, Silurian, and Devonian age. Not only is the Roberts thrust itself folded into a tight overturned anticline, but the numerous thrust slices composing its upper plate have been folded into isoclinal folds, some of them several thousand feet across. Some of these folds are recumbent, others upright, but all ride on the Roberts thrust. They are cut by a vertical fault about 10 miles long, almost normal to their trend, on either side of which very diverse structures have been developed simultaneously. All these structures are probably of Early Mississippian age.

Superimposed on, and doubtless to some extent modifying, the Paleozoic structures are thrust sheets involving rocks of Ordovician, Pennsylvanian, Permian, and probable Triassic age. These sheets, though warped, are much less complexly folded than those below. Their transection of the underlying thrust sheets, as well as their simpler structure and differing facies, prove them to be younger, but the absence of any dated rocks between Triassic and Miocene in the area makes it impossible to assign a precise date to this orogeny.

557753 O—60——18

120. STRUCTURAL FEATURES OF PYROCLASTIC ROCKS OF THE OAK SPRING FORMATION AT THE NEVADA TEST SITE, NYE COUNTY, NEVADA, AS RELATED TO THE TOPOGRAPHY OF THE UNDERLYING SURFACE

By F. N. Houser and F. G. Poole, Denver, Colo.

Based on work done in cooperation with the U.S. Atomic Energy Commission

All the contained underground nuclear explosions of the past few years at the Nevada Test Site have been in tuff of the Oak Spring formation, of Tertiary age. For a complete understanding of the regional Tertiary geologic history and the local geology of the underground test sites, it is necessary to decipher the local structure—particularly the anticlines and synclines that were mainly formed by deposition on the hilly erosion surface underlying the Oak Spring formation—and to distinguish them from similar structures of tectonic origin. These anticlines and synclines (termed primary for purposes of this report) are moulded on pre-existing ridges and valleys, to which they roughly conform, and delimit the areas of relatively thin and thick tuff. The initial dips assumed by the beds have been modified to an unknown extent by differential compaction. Ray E. Wilcox (1958) and W. R. Hansen and R. W. Lemke (written communication, 1958) were among the first to attribute these anticlines and synclines to the causes above outlined.

The primary anticlines and synclines in the pyroclastic rocks at the Nevada Test Site have been modified by tectonic tilting, folding, and normal faulting. In the mapped area (fig. 120.1), known faulting has been taken into account in analyzing the structure. This area may have been tilted or folded as a whole, though evidence for this is lacking.

In the northern part of the Test Site the Oak Spring formation is as much as 2,300 feet thick and consists of very thick to thin layers of welded and nonwelded tuff and thick-bedded to laminated fluvial, lacustrine, and possibly eolian tuffaceous deposits. The tuffs were initially deposited, as ash falls or ash flows, on an irregular surface of considerable relief, and were subsequently reworked in large part by water and wind to form tuffaceous sedimentary rocks.

The width, length, amplitude, and location of the primary folds in the Oak Spring formation depend directly on the local relief of the underlying surface and the thickness and character of the deposit—ash-fall tuffs, ash-flow tuffs, or tuffaceous sediments.

Detailed study has shown that the local relief on the erosion surface under the Oak Spring formation is of the same order of magnitude as the relief on the present topography of nearby surfaces carved from Paleozoic rocks and not covered by pyroclastics (fig. 120.1). The maximum local relief on the old surface ranges from 400 to 1,600 feet in horizontal distances of 1,200 to 19,000 feet. The rocks on which this surface is cut are structurally complex Paleozoic argillites, quartzites, and carbonates, and an igneous stock of Mesozoic or early Tertiary age. In some localities the present stream valleys and ridges developed in these rocks are in part alined with those in the surface underlying the Oak Spring formation.

The variations in the thickness and structure of the Oak Spring formation in the mapped area reflect the underlying topography. Because it was deposited on a highly irregular surface, the Oak Spring formation has a range in thickness of at least 1,200 feet. But although the thicker parts overlie the old hollows they never completely filled them; and volcanic rocks only partly filled the valleys and draped themselves, in smaller thickness, over buried ridges. The bedding in the basal part of the formation is generally subparallel to the underlying surface. Dips of about 30° are most common, but locally, adjacent to steep slopes or cliffs on the old surface, dips of as much as 40° were observed. Farther from this surface the dips have become progressively lower, because the topographic relief was gradually subdued by continued deposition, erosion and redistribution of volcanic material.

Figure 120.1 shows the close relationship of primary anticlines and synclines to the configuration of the underlying surface. The mapping of the major drainage and contours on that surface is based on study of outcrops. The primary structural axes are taken from structure contours drawn on the base of a persistent welded tuff.

The closeness with which the old topography is expressed by the primary structures differs for the three different types of deposits—lacustrine and fluvial tuffaceous sediments, ash flows, and ash falls.

The tuffaceous sediments were deposited in valleys and are generally in horizontal or gently dipping beds, depending on the slope of the underlying surface, and they generally form lenticular bodies.

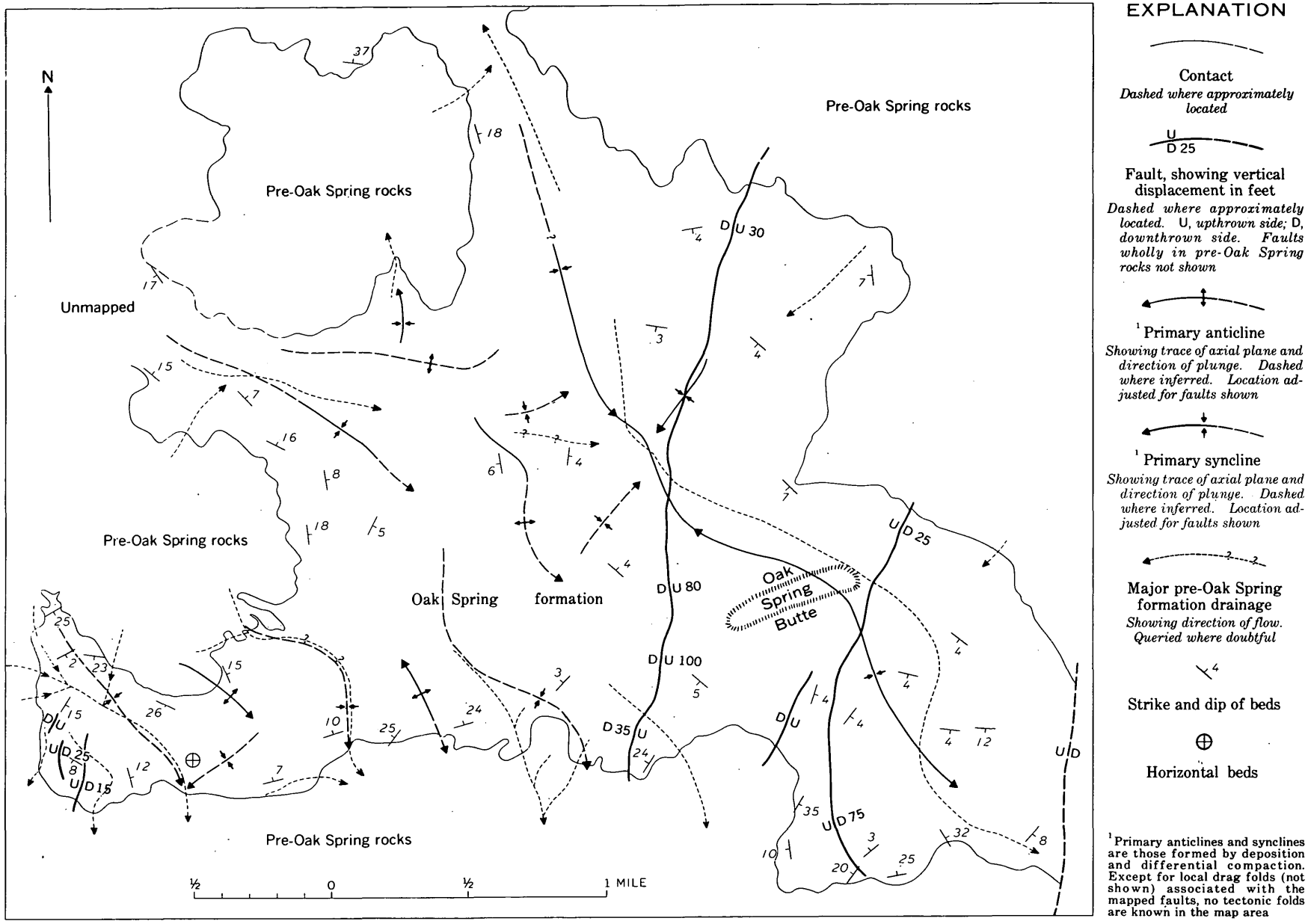

FIGURE 120.1.—Map of the Oak Spring Butte area, Nye County, Nev., showing t he relations between the general structure of a welded tuff marker unit in the middle of the Oak Spring formation (Tertiary) to the former drainage on the underlying surface.

In the ash flows, at least in the welded flows, most of the layering is horizontal or gently dipping. The initial dips measured in the welded-tuff marker unit (fig. 120.1) are mostly between 3° and 6° and average about 4°; the highest dip measured in them was 7°. Some tuff units in the lower part of the Oak Spring formation that exhibit characteristics of ash flows are restricted to the old valleys. These units thicken in the lower parts of the valleys and generally have a flat or slightly concave upper surface and an uneven or convex base. They are structureless, very thick bedded, and poorly sorted, and in places they show a poorly developed columnar structure.

The ash falls are blanketlike and conform most closely to the old topography. It is in these deposits that high primary dips are found. At one locality in the southwestern part of the mapped area, where both ash-fall and ash-flow tuffs were deposited against a buried hill, the primary dips about 150 feet from the old erosion surface are 25° in the ash fall but only 7° in the ash flow.

Many other primary structures, including contorted strata, cross-bedding, ripple marks, erosional unconformities, graded bedding, and faults of small offset associated with slump structures, characterize parts of the tuffaceous sediments and the nonwelded tuffs. These features appear to be commonest in the deposits that lie in the medial parts of the old valleys or extend along steep slopes. Although their total effect is small as compared with the volume of the rocks affected by them within the map area, they indicate that deposition of tuff was locally interrupted for long enough periods to permit redistribution of some material by slumping and by fluvial and possibly eolian transport.

REFERENCE

Wilcox, R. E., 1958, Petrography and chemistry of the Oak Spring formation, Chapter 2, in Diment, W. H., and others, Properties of the Oak Spring formation in Area 12 at the Nevada Test Site: U.S. Geol. Survey TEI–672 (preliminary draft), open-file report.

121. ORIGIN OF THE AMARGOSA THRUST FAULT, DEATH VALLEY AREA, CALIFORNIA: A RESULT OF STRIKE-SLIP FAULTING IN TERTIARY TIME

By Harald Drewes, Denver, Colo.

BLACK MOUNTAINS FAULT BLOCK

The Black Mountains block is a lozenge-shaped structural block 70 miles long and 25 miles wide just east of Death Valley. It is bounded on the northeast and southwest by faults that appear to be strike-slip faults, and is probably bounded on the east and west by similar faults buried beneath Death Valley and Amargosa Valley. The strike-slip fault on the southwest (Noble and Wright, 1954, pl. 7) branches from the Garlock strike-slip fault where it swings southward to join the Soda-Avawatz strike-slip fault.

Precambrian metamorphic and sedimentary rocks are unconformably overlain in this region by Paleozoic carbonate and clastic rocks about 4 miles thick, and are intruded by monzonitic stocks of Mesozoic or Tertiary age. These rocks are unconformably overlain in most places by thin continental sedimentary deposits and by volcanic rocks, collectively of middle and late Tertiary age. The rocks are broken into large, tilted structural blocks bounded, at least in part, by faults presumably typical of the Basin and Range province. Thick Quaternary deposits fill parts of the fault-controlled valleys.

In the Black Mountains block the only Paleozoic rocks remaining are in small masses chaotically scattered between the underlying Amargosa thrust fault and the overlying volcanic rocks. The block also contains monzonitic rocks of early or middle Tertiary age (Drewes, 1959, p. 1500). Fanglomerate of middle Tertiary age, consisting of fragments eroded from the Black Mountains block before the extrusion of the volcanics, lies high on the mountains northeast of the block. At least two small basins on the block are filled with sediments about 2 miles thick, deposited during late Tertiary time.

The block was unusually mobile during Tertiary time. During middle Tertiary time and before extrusion of rhyolitic lavas, it was raised several miles and most of the Paleozoic rocks were removed, some to be deposited as the fanglomerate to the northeast. Before late Tertiary time the lavas were much faulted and tilted, and at least two parts of the block subsided to

form basins in which sediments several miles thick were deposited. One of these basins lies adjacent to the fanglomerate to the northeast; hence displacement of the block was reversed. The rate of uplift of the Black Mountains with respect to Death Valley has increased from middle Tertiary to Recent time, judging from the disproportionately large displacement of the younger rocks, as compared with the older rocks, along the front fault. Such large recurrent and reversible movements support the inference that the faults do bound the block and do extend beneath the adjacent valleys to enclose the Black Mountains block as a large horse in a strike-slip fault zone.

AMARGOSA THRUST FAULT

The Amargosa thrust fault is restricted to the Black Mountains block; it is extensively exposed in the southern part of the block, largely eroded from the central part, and either eroded away or buried in the northern part. Sedimentary rocks of younger Precambrian and older Paleozoic ages are chaotically broken into blocks hundreds to thousands of feet long, which are separated from each other and from the underlying rocks by gouge sheets a few inches to a few feet thick. This assemblage is the Amargosa Chaos of Noble (1941). The blocks comprise small parts of many formations that are locally imbricated in a normal, but foreshortened, stratigraphic sequence (Noble, 1941, p. 966). The chaotic blocks are surrounded by gouge, and are less shattered and more heterogeneous than those in the megabreccias common in many younger formations of the region, and they are not interbedded in fanglomerates as the megabreccias are. The net displacement on the Amargosa thrust fault is small, for most of the adjacent ranges contain undisturbed Paleozoic rocks or rocks with less-broken plates between bedding-plane thrust faults; yet the total movement was considerable, judging from the many thousands of feet of missing strata. The Amargosa thrust fault is younger than the stocks, for unaltered Paleozoic rocks are thrust over coarse-grained monzonitic rocks, and monzonitic rock is included with the chaotic blocks; but it is older than the volcanics, for lavas lie unconformably on chaotic blocks, and feeders to the lavas cut the blocks.

Three hypotheses of the origin of the Amargosa thrust fault, as illustrated in figure 121.1, involve (a) a rooted thrust fault branching near the surface, (b) landsliding, and (c) jostling within a large block in a strike-slip fault. A rooted structure does not explain the areal restriction of the Amargosa fault, and the short distance of movement available to such a fault does not explain the absence of so much of the Paleozoic sequence. A landslide origin fails to explain either

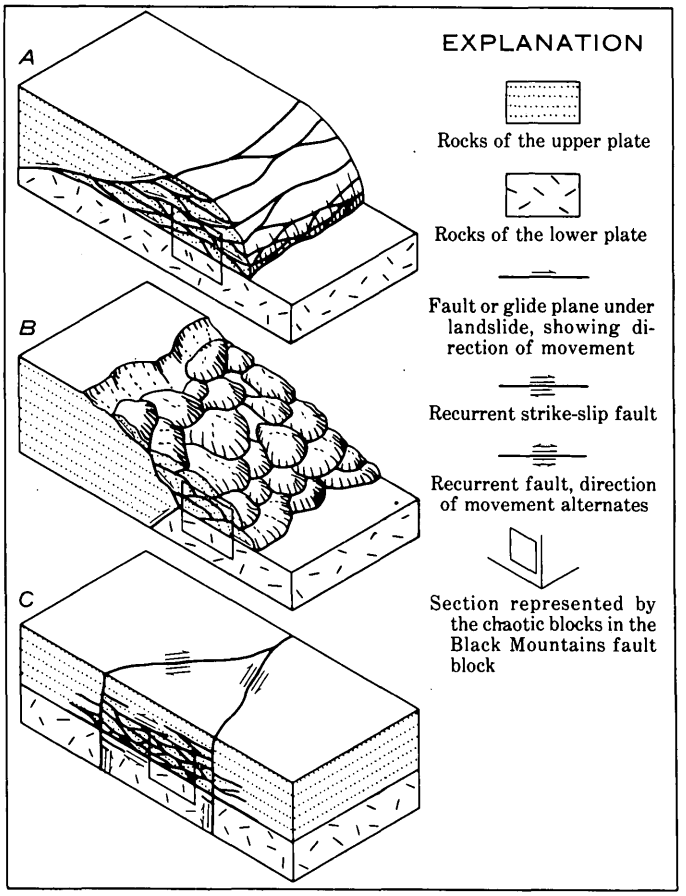

FIGURE 121.1.—Block diagrams illustrating three basic hypotheses of the origin of the Amargosa thrust fault. *A*, local thrust fault branching near the surface. *B*, shingled landslides from raised area. *C*, jostling within a large block in a recurrently shifting strike-slip fault.

the normal stratigraphic sequence or the missing strata. It also fails to explain the relatively unshattered blocks surrounded by gouge, which differ markedly from those in the magabreccia deposits demonstrably of landslide origin. The hypothesis that I favor ascribes the Amargosa thrust fault to jostling within a large fault block as a result of recurrent movement on the bounding strike-slip faults. It explains the localization of the fault and the fact that the rocks in parts of the block are in the normal stratigraphic sequence. It also provides much movement with little displacement, which could have ground up the missing rocks. How the ground-up rock was removed is not clear, but that process is not fully explained by the other hypotheses either.

Noble and Wright (1954, p. 152) explain the origin of the fault by a squeezing and arching of the Black Mountains block that produced landsliding off the crests of the arches or possibly caused bedding-plane rupture along their limbs. The age of the folds, how-

ever, is probably Precambrian, for some of the younger Precambrian rocks in the region are not folded. Some of the difficulties of the first hypothesis (a) are also inherent in their explanation. The explanations offered by Sears (1953, p. 182–186) and Bucher (1956, p. 1311) also involve gravity sliding plus other modifications.

IMPLICATION TO REGIONAL STRUCTURE

The Riggs Chaos in the Silurian Hills, 40 miles southeast of the Amargosa Chaos, is thrust along nearly the same horizons as the Amargosa Chaos (Kupfer, 1960); it also lies adjacent to a large strike-slip fault, and according to Kupfer (1960, p. 205) it did not originate by landsliding. I suspect that this is another structure formed by thrust faults resulting from recurrent movement along a strike-slip fault.

Bedding-plane thrust faults along which younger rocks are moved over older ones are common in eastern Nevada and western Utah. Perhaps some of them are neither rooted thrust faults nor gravity-slid plates, but are formed, like the Amargosa thrust fault, as a rupture within blocks adjacent to recurrently and complexly moving faults. Thrust faults along the same stratigraphic horizons on opposite sides of a strike-slip fault need not have been continuous. The amount of movement along thrust faults should diminish away from widely spaced strike-slip faults.

REFERENCES

Bucher, W. H., 1956, Role of gravity in orogenesis: Geol. Soc. America Bull., v. 67, no. 10, p. 1295–1318.

Drewes, Harald, 1959, Turtleback faults of Death Valley, California; a reinterpretation: Geol. Soc. America Bull., v. 70, no. 12, pt. 1, p. 1497–1508.

Kupfer, D. H., 1960, Thrust faulting and chaos structure, Silurian Hills, San Bernardino County, California: Geol Soc. America Bull., v. 71, no. 2, p. 181–214.

Noble, Levi, 1941, Structural features of the Virgin Spring area, Death Valley, California: Geol. Soc. America Bull., v. 52, no. 7, p. 941–1000.

Noble, Levi, and Wright, L. A., 1954, Geology of the central and southern Death Valley region, California, pt. 10 *in* chap. 2 *of* Jahns, R. H. ed., Geology of southern California: California Div. Mines Bull. 170, p. 143–160.

Sears, D. H., 1953, Origin of Amargosa chaos, Virgin Spring Area, Death Valley, California: Jour. Geology, v. 61, no. 2, p. 182–186.

122. BEDDING-PLANE THRUST FAULTS EAST OF CONNORS PASS, SCHELL CREEK RANGE, EASTERN NEVADA

By Harald Drewes, Denver, Colo.

Connors Pass, in which U.S. Highways 6 and 93 cross the Schell Creek Range, lies about 20 miles southeast of Ely, Nev. Geologic mapping east of the pass (fig. 122.1) confirms Misch and Easton's (1954) recognition of thrust faults in a Paleozoic section, but it has led to a different interpretation of the stratigraphy and structure. Whereas Misch and Easton believed that an inverted Devonian and Mississippian sequence had overridden the Prospect Mountain quartzite and remnants of Cambrian limestone, I regard the overriding rocks as a sequence of Cambrian to Permian formations in normal order but tectonically thinned along thrust faults that are near bedding planes. The largest thrust fault has cut out all the many thousands of feet of rocks of Middle Ordovician to Pennsylvanian age, with the exception of two small blocks of Middle Devonian age.

The rocks of the lower major plate are similar to those in the southern part of the Snake Range, across Spring Valley (Drewes and Palmer, 1957). They include parts of the Prospect Mountain quartzite, Pioche shale, Pole Canyon limestone, Lincoln Peak formation, and Windfall formation-Pogonip group undifferentiated (essentially the Pogonip limestone of Hague). The Pole Canyon limestone is recrystallized, and near its top it is much sheared. It is alternately thickened and thinned northward by an overlying minor thrust fault that cuts its beds at varying angles. The Lincoln Peak formation, which provisionally includes beds a little younger than the youngest in the type section, generally consists of shale and shaly limestone with a few thin limestone beds, but here the shale is metamorphosed to phyllite and slate, though the interbedded limestone is little changed. This formation has commonly been correlated with the Pilot shale, of Devonian and Mississippian age, but it is continuous with less metamorphosed and abundantly fossiliferous Cambrian shale eight miles farther north. The overlying thin, strongly sheared limestone is a klippe of the Pogonip group, three units of which have been traced

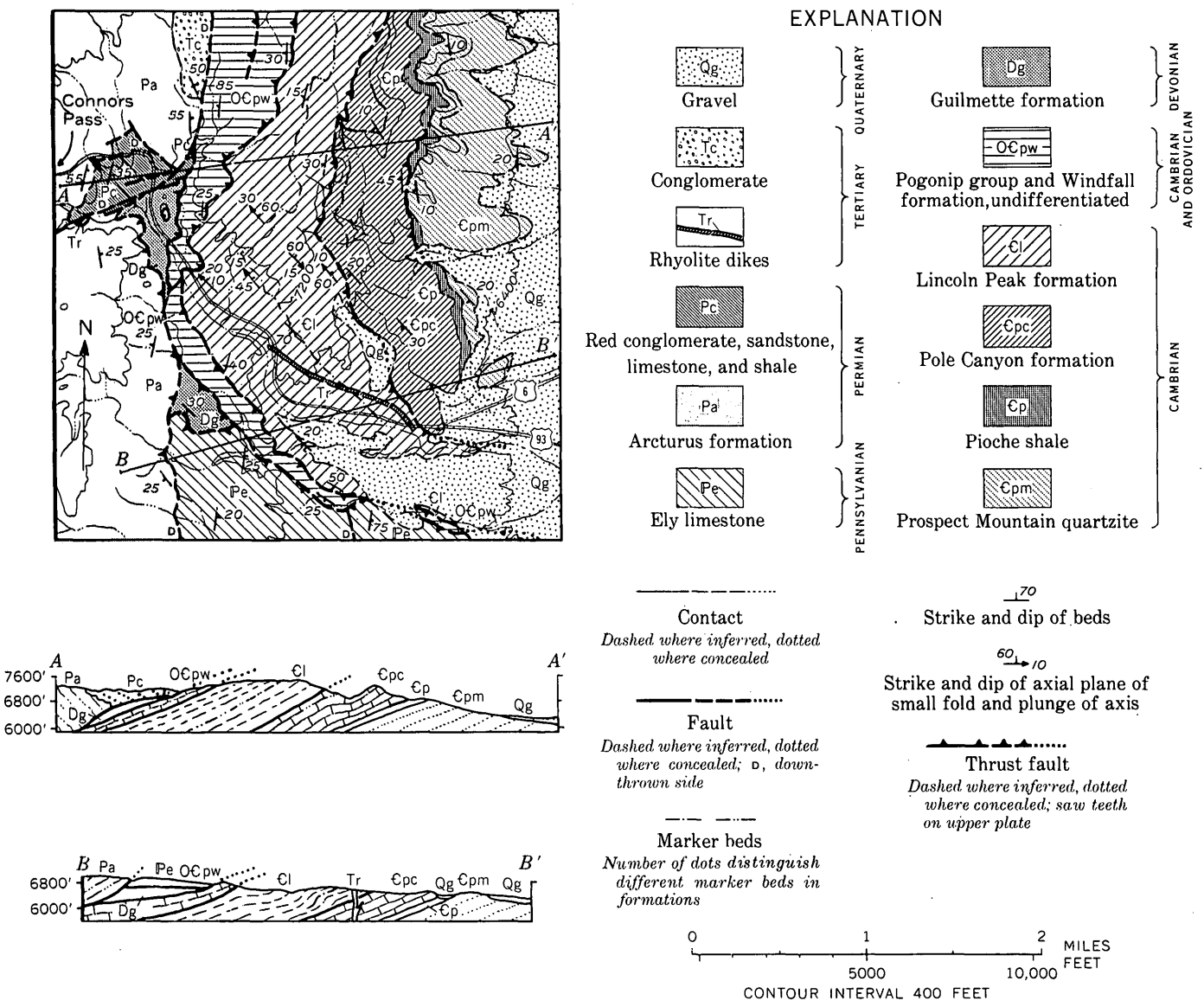

FIGURE 122.1.—Map and structure sections of an area east of Connors Pass, Schell Creek Range, Nev.

northward to fossiliferous rocks. The basal few hundred feet of the group, though present to the north, are missing here, and at the top of the group several thousand feet of beds are progressively sheared out southward, so that south of the junction of Highways 6 and 93 scarcely 100 feet of the group remains beneath the rocks of the upper major plate.

The rocks of the upper major plate include much limy siltstone, sandstone, and limestone of the Arcturus formation, together with a large wedge of Ely limestone and two small blocks of limestone and dolomite of the Guilmette formation. The Arcturus formation is unconformably overlain by red conglomerate interbedded with a little limestone and associated with black shale and tuff. The conglomerate contains pebbles of chert and quartzite foreign to the area. The Arcturus formation beneath the red conglomerate contains fusulinids of Wolfcamp age or slightly older; the limestone in the conglomerate, according to J. T. Dutro, Jr., contains the brachiopods *Heteralosia* sp., *Phricodothyris?* sp., and an aulostegid brachiopod of a new genus, probably of Wolfcamp or Leonard age. These rocks closely bracket an orogenic episode that probably occurred in Wolfcamp time. The Guilmette formation (Devonian) and the Ely limestone (Pennsylvanian) are also fossiliferous and their ages were verified locally.

The relations between the red conglomerate and small patch of black shale and tuffaceous sandstone exposed only along the highway is uncertain; the shale may be surrounded by faults. Plant remains collected

from the shale by F. E. Digert and Neal Smith were identified by D. I. Axelrod as possibly of Late Cretaceous or early Paleocene age (Van Houten, 1956, p. 2808, and F. E. Digert, written communication). For the present, however, the shale is mapped with the Permian conglomerate until more plant remains are collected and the local structure is clarified.

Poorly consolidated conglomerate with locally derived cobbles, and tuffaceous sandstone, similar to rocks beneath the volcanics to the north, are probably of Tertiary age. The other rocks in this area include two rhyolitic dikes and some younger gravels.

Structurally, the area is chiefly characterized by thrust faults that nearly follow bedding planes and it contains a few normal faults. Most of the thrust faults have cut out only a few tens or a few hundreds of feet of beds, but one fault has cut out many thousands of feet. The thrust faults of large stratigraphic throw are generally traceable for longer distances than those of smaller throw. Rocks along the thrust faults, especially the larger ones, are sheared, and locally the beds on both sides of the fault dip into the fault. Folds, commonly less than 20 feet in amplitude, are abundant in phyllitic rocks of the Lincoln Peak formation just northeast of the highway. Their axes trend northwestward, and most of their axial planes dip steeply northeastward, or about normal to the thrust plane.

Some of the normal faults adjacent to the red conglomerate end at the thrust fault and are therefore contemporaneous with it, or older; others bend northward and follow a large thrust fault a few miles and therefore must be younger than it is. The Tertiary conglomerate may thus be downfaulted on a normal fault localized by the thrust fault. Further mapping of the Tertiary rocks to the northwest, which appear to be in similar relations to the thrust fault, may clarify this point.

Since the present interpretation of the structure east of Connors Pass does not assume that an overturned stratigraphic section was thrust over the Prospect Mountain quartzite, it requires fewer major thrust faults than the concept of Misch and Easton (1954). It is consistent, moreover, with the structures mapped along 15 miles of the east flank of the Schell Creek Range, and also with those in the southern part of the Snake Range (Drewes, 1958). Some thrust faults follow the same weak formations in both ranges, but this does not make it possible to correlate individual faults from range to range. Neither the amount of movement nor the amount of displacement on any of the thrust faults is known; but both of these probably exceed the stratigraphic throw.

REFERENCES

Drewes, Harald, 1958, Structural geology of the southern Snake Range, Nevada: Geol. Soc. America Bull., v. 69, no. 2, p. 221–240.

Drewes, Harald, and Palmer, A. R., 1957, Cambrian rocks of the southern Snake Range, Nevada: Am. Assoc. Petroleum Geologists Bull., v. 41, no. 1, p. 104–120.

Misch, Peter, and Easton, W. H., 1954, Large overthrusts near Connors Pass in the southern Schell Creek Range, White Pine County, Eastern Nevada [abs.]: Geol. Soc. America Bull., v. 65, no. 12, pt. 2, p. 1347.

Van Houten, F. B., 1956, Reconnaissance of Cenozoic sedimentary rocks of Nevada: Am. Assoc. Petroleum Geologists Bull., v. 40, no. 12, p. 2801–2825.

123. POSSIBLE INTERBASIN CIRCULATION OF GROUND WATER IN THE SOUTHERN PART OF THE GREAT BASIN

By Charles B. Hunt and T. W. Robinson, Denver, Colo., and Water Resources Division, Menlo Park, Calif.

Large springs on both sides of the north end of the Death Valley salt pan, California, have catchment areas that seem too small to supply the quantity of water that is being discharged from them. As these springs are on fault zones, the water may have flowed to them underground along fault fissures that reached higher basins nearby. This hypothesis is supported by geochemical studies of the water. Water from springs on the northwest side of the salt pan is chemically similar to that from springs on Mesquite Flat, in the next basin to the northwest; water from springs on the east side of the salt pan is like that from springs at Ash Meadows, in the Amargosa Desert, Nevada, in the next basin to the east. This evidence is forceful because the water on the two sides of the salt pan is very different (fig. 123.1). The water on the east side is a bicarbonate-sulfate water high in calcium and fluoride, whereas water on the west side is chloride-sulfate water low in calcium and fluoride but containing some arsenic (fig. 123.2); and there are corresponding differences between the waters from the adjacent higher basins.

The hypothesis here advanced, if it could be verified by tracers, would have considerable importance. If the water is moving for long distances along faults, it may be moving in open conduits through the thick Paleozoic carbonate formations, and therefore at much faster rates than ground water ordinarily does. This would affect estimates of water resources in the Great Basin and opinions about the suitability of certain areas for underground storage of radioactive wastes.

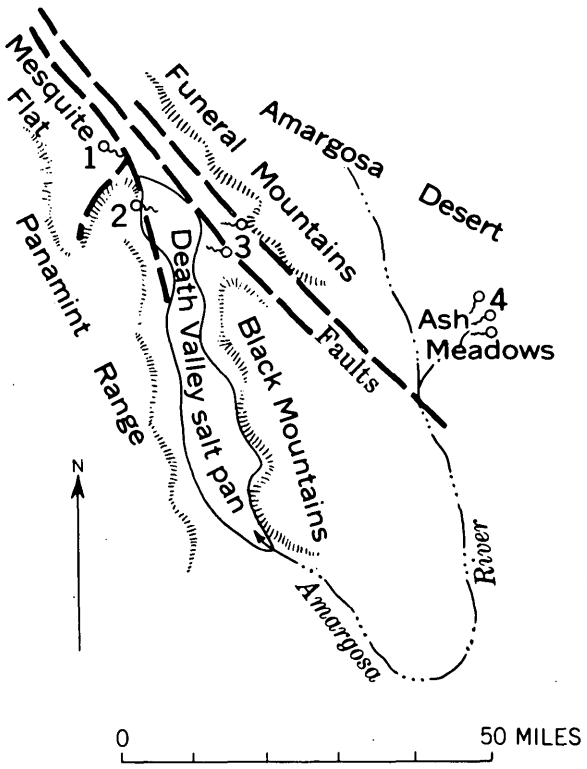

Figure 123.1.—Index map of the area in the vicinity of the Death Valley salt pan, showing location of major faults and springs from which samples were taken.

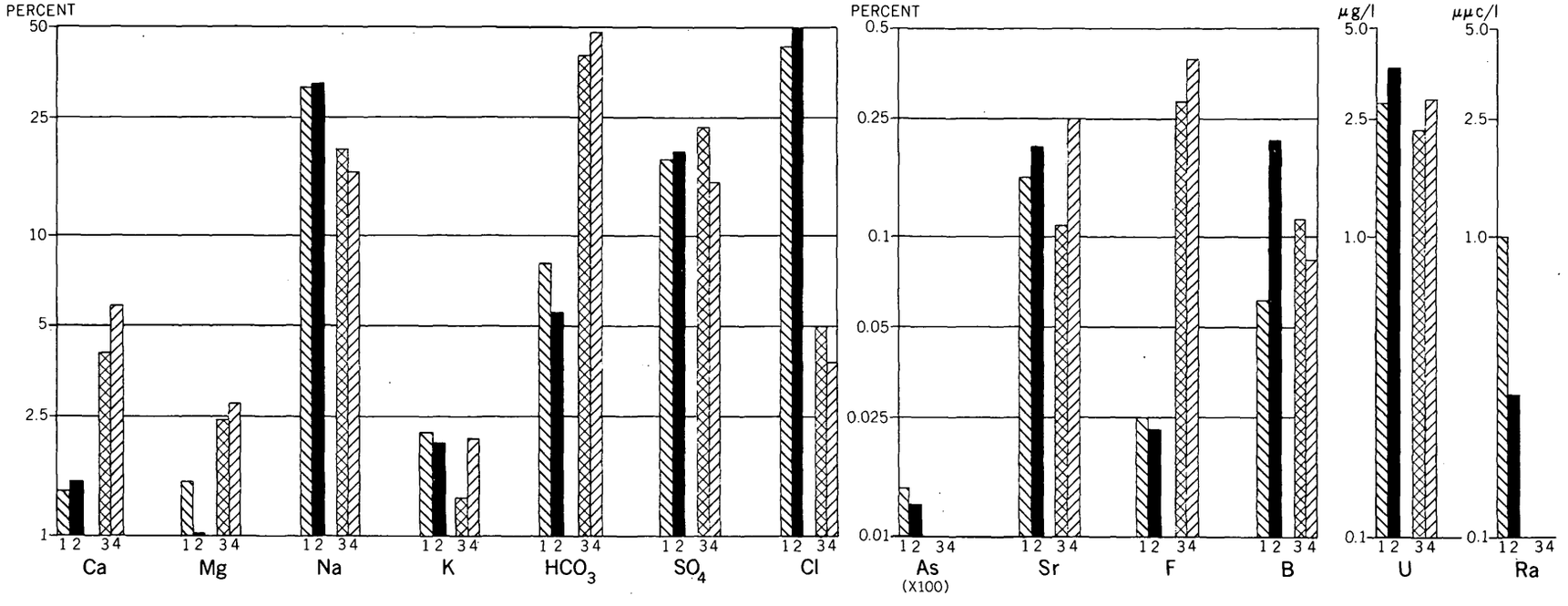

FIGURE 123.2.—Bar graphs showing compositions of waters from four different areas of springs. Water entering the west side of Death Valley (sample 2) is chemically like the water at Mesquite Flat (sample 1) northwest of the salt pan. Water entering the east side of Death Valley (sample 3) is like water at Ash Meadows in the Amargosa Desert east of Death Valley (sample 4). Water from the two directions is very different. That from the west is chloride-sulfate water low in calcium and fluoride but containing some arsenic; that from the east is bicarbonate-sulfate water high in calcium and fluoride and containing no arsenic. Each bar represents the average of several analyses.

124. OBSERVATIONS OF CURRENT TILTING OF THE EARTH'S SURFACE IN THE DEATH VALLEY, CALIFORNIA, AREA

By Gordon W. Greene and Charles B. Hunt, Menlo Park, Calif., and Denver, Colo.

Archeological and geological studies in Death Valley, Calif., indicate that the valley floor has been tilted 20 feet over a distance of about 3 miles during the last 2,000 years. The eastern shoreline of a shallow lake, which flooded the floor just prior to introduction of the bow and arrow, is now 20 feet lower than the western shoreline. Part of the tilt can be explained by the presence of a recent fault scarp with 10 feet of vertical displacement at the foot of the Black Mountains; the balance appears to be the result of slow surface deformation.

Whether earth movements occur in episodes, followed by relatively long periods of stability, or whether the earth's surface is subject to slow continuous movement, is a fundamental problem in the study of earth mechanics and seismology. To explore this problem in the Death Valley area, seven tiltmeter stations were established across the valley (fig. 124.1) during 1958 and 1959.

INSTRUMENTATION

Each tiltmeter station consists of three machined brass hubs placed in concrete upon rock outcrops. The hubs are positioned to form a nearly equilateral triangle with sides 30 to 50 m long. Hub tops are established within ± 0.5 cm of a level plane. The portable tiltmeter used in the Death Valley study was developed by U. S. Geological Survey personnel at the Hawaii Volcano Observatory under the direction of Jerry P. Eaton, and used successfully to observe tilting of the ground associated with subsurface magma movement at Kilauea.

The tiltmeter consists of two closed cylindrical water pots connected by two tubes. When the pots are partly filled with water, one tube provides a continuous water connection, while the second tube connects the vapor phase of each pot. A sharp point on a micrometer screw extends through the bottom of each pot. The micrometer point is viewed through a lens and adjusted to just touch the water surface. This serves to measure the relative height of water in each pot. By reversing the water pots and repeating the procedure, the elevation difference between the two hubs may be measured with an error of less than three microns. If the hubs are spaced 30 m apart a sensitivity of one part in 10 million is realized.

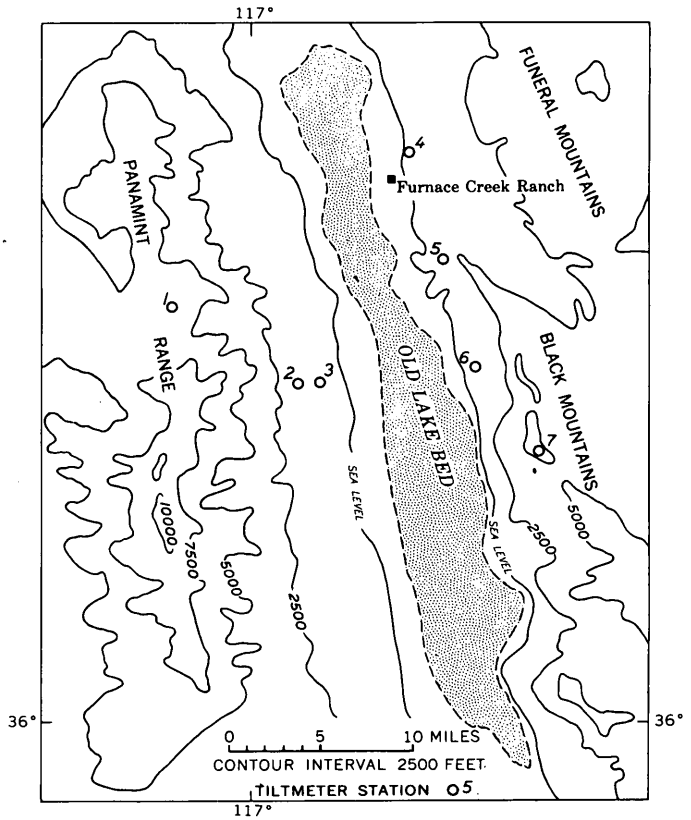

FIGURE 124.1.—Map of Death Valley showing extent of old lake bed (broken line) that has been tilted eastward and the locations of tiltmeter stations (numbered).

Because the system is sensitive to temperature changes, it cannot be used where solar radiation, or rapid changes in air temperature, are present. Therefore, it is necessary to use the tiltmeter at night. Best results are obtained with an overcast sky to reduce radiation losses and with a slight wind blowing to assist in maintaining a constant temperature in the system.

A detailed description of the tiltmeter and how it is used is given by Eaton (1959).

The precision of the measurements may be checked by adding the measured elevation differences for the three sides of the triangle. The closure error, which should be less than 10 microns for valid readings, is then distributed around the circuit.

RESULTS

There appears to be good evidence of tilting occurring at the present time in the Death Valley area. The

TABLE 124.1.—*Summary of tilting observed at selected locations in Death Valley, California*

No.	Station	Observed		Number of observations	Component of tilting in micro-radians toward—	
		From—	To—		North	East
1	Aguereberry Point	May 1958	April 1960	5	[1] 36	12
2	Trail Canyon	April 1959	April 1960	2	1	2
3	Trail Canyon Fan	Oct. 1959	April 1960	2	[2] −1	1
4	East Coleman Hills	Oct. 1959	April 1960	2	[3] 2	----------
5	Gower Gulch	Oct. 1959	April 1960	2	[4] 1	----------
6	Artists Drive	Jan. 1959	April 1960	4	−4	−3
7	Dantes View	Jan. 1959	Oct. 1959	2	−2	1

[1] Maximum tilting, observed in October 1959, was 35×10^{-6} radians northward and 25×10^{-6} radians eastward.
[2] A negative value indicates tilting toward the south or west.
[3] Tilting measured in an adit lying N 2° W.
[4] Tilting measured in an adit lying N 19° E.

amount and direction of observed tilting is different from one station to another, and the rate of tilting at a given station varies from time to time. Table 124.1 summarizes the data from each of the seven stations.

Usually the amount of tilting occurring between successive observations is so small as to be of the same order of magnitude as probable instrument error. However, as readings are accumulated over a longer period of time, the total observed tilting becomes several times larger than probable instrument errors.

In general, geologic studies have shown that the area is broken into a number of distinct blocks, most of which have been tilted toward the east since the time they were formed. It is significant that the direction and amount of tilting measured thus far agree with the known geologic structure and movements in the recent geologic past.

The structural relationships in Death Valley are very similar to those at Hebgen Lake, near West Yellowstone, scene of the August 1959 earthquake. This earthquake resulted from faulting along one side of the valley and tilting of the valley floor toward the faulted side. The amount of displacement and tilting are about the same as at Death Valley. It is planned to apply the methods now being used in Death Valley to the area of Hebgen Lake.

REFERENCE

Eaton, J. P., 1959, A portable water-tube tiltmeter: Seismol. Soc. America Bull., v. 49, no. 4, p. 301–316.

125. PLIOCENE(?) SEDIMENTS OF SALT WATER ORIGIN NEAR BLYTHE, SOUTHEASTERN CALIFORNIA

By WARREN HAMILTON, Denver, Colo.

Sediments of late Cenozoic age carrying abundant fossils, dominantly of marine types, occur in the southeastern part of the Big Maria Mountains, west of the Colorado River and about 75 miles north of the Mexican border. The oldest and most widely distributed of these sediments are "lime caps," similar in part to the beachrock of tropical shores. "Lime caps" are found at altitudes of at least 800 feet. (The present altitude of the Colorado River here is about 290 feet.) They form the tops of many hills of pre-Tertiary rocks and encircle others. The caps consist of pure, hard travertine, and of talus, crossbedded gravel, and coquina, all firmly cemented by dense calcite. They contain abundant algae, barnacles, and pelecypods. Some of the caps are richly manganiferous, and contain large and possibly commercial quantities of soft manganese oxide interlayered in their lower portions, particularly in valley bottoms and low on the hillsides.

Unconsolidated beds of clay, silt, sand, and gravel overlie the "lime caps." These sediments are generally thin but are locally several hundred feet thick. Remnants of them occur as much as 650 feet above sea level.

They contain abundant Foraminifera and ostracods and sparse pelecypods.

The fossils were identified by W. P. Woodring, Patsy B. Smith, I. G. Sohn, and Richard Rezak, who believe that they grew either in sea water or marinelike brackish water. (The present Colorado River carries more sulfate than chloride.)

Either the Gulf of California previously extended into this area, or else a huge saline lake existed here. Such a lake might have been dammed by the rising of the Chocolate Mountains, 50 miles to the south, across the Colorado River, but if so, the mountains have since been lowered by subsidence as well as by erosion.

The salt water sediments were largely buried during early Pleistocene time by fan gravels and river alluvium.

126. STRUCTURE IN THE BIG MARIA MOUNTAINS OF SOUTHEASTERN CALIFORNIA

By Warren Hamilton, Denver, Colo.

In the arid Big Maria Mountains, north of Blythe in southeastern California, there are almost continuous exposures of a sequence of thin distinctive sedimentary formations probably of Paleozoic age. These have been metamorphosed and extremely deformed, probably during late Mesozoic time. The metasedimentary rocks are underlain by a complex of granitic and gneissic rocks, over which they slid along a surface at or near their base. Both the metasedimentary and the basement rocks were invaded, after being metamorphosed, by hornblende gabbro and by leucocratic quartz monzonite.

The most pervasive structures in the metasedimentary rocks are shears and isoclinal folds subparallel to the bedding (fig. 126.1*A*). The limbs of the isoclinal folds are mostly between 5 and 200 feet in length, and the same is true of the lenses bounded by shear planes. The structure is particularly well displayed in a thin formation consisting of marble interlayered with chert. The total thickness of this unit commonly ranges between 50 and 100 feet, but reaches a maximum of 500 feet; the variations are due primarily to thinning and thickening by shear. The formation now consists of a parallel bundle of isoclines and limbs of isoclines sheared apart along planes nearly parallel to the bedding; but the shears have nowhere displaced the formation as a whole, and it crops out as a continuous band for many miles. The rocks of each formation are isoclinally interfolded along both upper and lower contacts with those of the adjacent formations but the zones of interfolding are generally less than 20 feet thick. The isoclinal folds must have been formed by a rolling progression of drag folds due to shear along the bedding, so that they were isoclinal at all times.

Superimposed upon these small-scale structures are some on a larger scale. Figure 126.1*B* illustrates comparatively large isoclines, and 126.1*C* a thrust fault; the rocks of each formation in these structures are complexly deformed by bedding-plane isoclines too small to be shown in the drawings. Many of the thrust faults have themselves been folded almost isoclinally (fig. 126.1*D*). Most of the structures are directed northeastward; the dips are low and in all directions.

The plutonic rocks were variably sheared and retrogressively reconstituted near the decollement surface, and were broken by thrust faults subparallel to it at lower levels, but they are surprisingly little deformed and metamorphosed in view of the complexity of structure in the metasedimentary rocks above.

The latest deformation consisted of normal faulting, which affected all the rocks, including the intrusives.

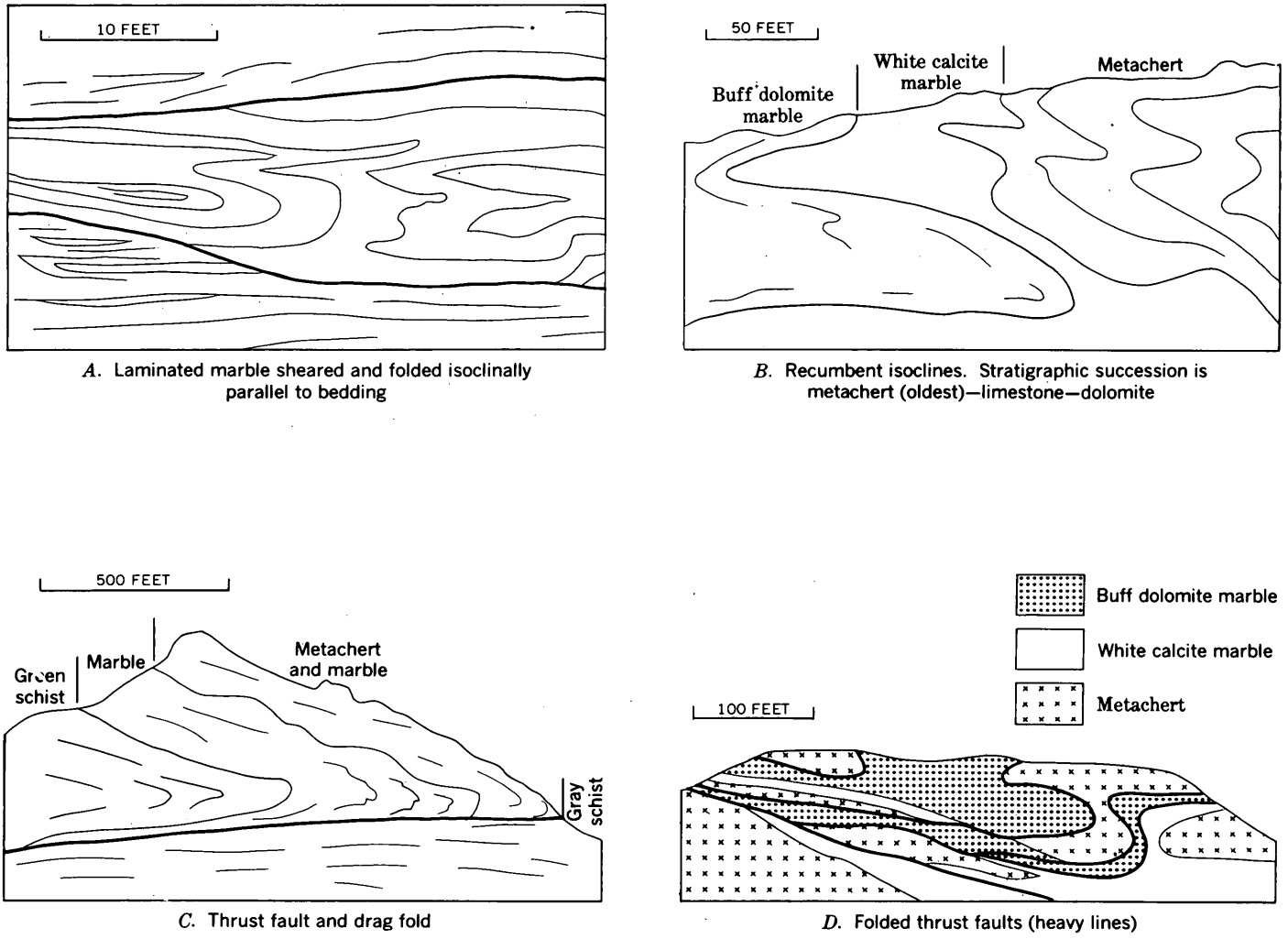

FIGURE 126.1.—Field sketches of structures exposed in cliffs in the Big Maria Mountains.

127. FOSSIL FORAMINIFERA FROM THE SOUTHEASTERN CALIFORNIA DESERTS

By PATSY BECKSTEAD SMITH, Menlo Park, Calif.

Fossil Foraminifera have been found in flat-lying upper Cenozoic sediments over an extensive area of desert in southeastern California. At all localities except Panamint dry lake, the Foraminifera are associated with gastropods, barnacles, and ostracodes that indicate brackish water or lagoonal conditions (W. P. Woodring, written communication, 1953).

The fossils have been found along the Colorado River between Earp, Calif., and the Palo Verde Mountains, 25 miles south of Blythe, at elevations of 300 to 650 feet above sea level. They are also found in cores from Danby and Cadiz dry lakes (Bassett and others, 1959), located 50 and 60 miles west of Earp, in southeast-trending depressions now separated from the Colorado River by low passes. Foraminifera occur also in cores from Panamint dry lake (Smith and Pratt, 1957), which is about 200 miles northwest of Earp and is separated from the other localities by numerous high ranges. The foraminiferal faunas from all these localities except Panamint dry lake are very similar to one

another, and also to the lagoonal faunas of the Gulf of California (Bandy, 1960). The Foraminifera are *Streblus beccarii* (Linné), *Elphidium* cf. *E. poeyanum* (d'Orbigny), and a few other rare species.

In the cores from Danby dry lake, whose surface is 541 feet above sea level, Foraminifera are found within two stratigraphic intervals, 396 to 439 feet, and 648 to 845 feet. The fossil-bearing sediments are green clay. The specimens are large and regular except at 648 feet, where they are small and stunted; their relative abundance is as follows:

[A=abundant, C=common, R=rare]

	Depth (feet)			
	396-439	648-680	688-732	738-845
Streblus beccarii	A	A	A	A
Elphidium cf. *E. poeyanum*	C	C	C	C
Bolivina cf. *B. brevior*			R	

In the cores from Cadiz dry lake, whose surface is 612 feet in elevation, Foraminifera are found in green clay at depths of 267 to 271 feet. Only *Streblus beccarii* is present here.

Core Panamint 1, from Panamint dry lake, contains Foraminifera at depths of 134 to 137 feet. They are all of one species, *Elphidium* cf. *E. poeyanum*, which is abundant. Specimens are large and regular. As in the other cores, the fossil-bearing sediments are green clay.

Fossiliferous sediments are exposed in a road-cut along the west side of the highway between Earp, California, and Parker, Arizona; they consist of 10 to 20 feet of cross-bedded gravels and coarse to fine sands. The section appears to be interbedded with river gravels, but their relations are obscure. Foraminifera (*S. beccarii*) are abundant in the finer grained beds, but they are dwarfed.

Several hundred feet of well-bedded fossiliferous clay and fine sand crop out in the Big Maria Mountains at elevations from a few feet to 350 feet above the present level of the Colorado River (Hamilton, see Art. 125). These sediments contain Foraminifera belonging to the following species:

Streblus beccarii—Abundant
Elphidium cf. *E. poeyanum*—Common
Elphidiella sp.—Rare

The specimens throughout the part of the section examined are consistently large and well formed, which probably indicates a uniform and favorable environment.

A statistical study is now being made of the morphological variation in *Streblus beccarii* from these thick fossiliferous sections to determine whether or not they indicate environmental changes. Laboratory studies on living *S. beccarii* (Bradshaw, 1957) indicate that the species will grow and reproduce normally in a salinity range of 2 to 4 percent. Lower salinities result in a larger number of chambers before reproduction (and death); growth and reproduction cease below a salinity of 0.7 percent.

The significance and relative ages of these widely scattered fossiliferous sections are problematical. The thick fossiliferous sections of the Cadiz and Danby dry lakes and along the Colorado River are characterized by quite uniform and similar faunas; they all might represent either a shallow marine invasion, one large saline lake, or several isolated saline lakes. Although the method of introducing these faunas into lakes is a serious problem, Panamint Lake could not have been connected with the sea at the time the fossiliferous sediments were deposited, and the existence of even a limited foraminiferal fauna in this distant body of water forces consideration of the saline lakes environments.

REFERENCES

Bandy, O. L., 1960, Foraminiferal ecology of the Gulf of California (abs.): Geol. Soc. America, Cordilleran Section meeting, Vancouver, B.C., program, p. 13–14.

Bradshaw, J. S., 1957, Laboratory studies on the rate of growth of the Foraminifer, "*Streblus beccarii* (Linné) var. *tepida* (Cushman)": Jour. Paleontology, v. 31, p. 1138–1147.

Bassett, A. M., Kupfer, D. H., and Barstow, F. C., 1959, Core logs from Bristol, Cadiz, and Danby dry lakes, San Bernardino County, California: U.S. Geol. Survey Bull. 1045–D.

Smith, G. I., and Pratt, W. P., 1957, Core logs from Owens, China, Searles, and Panamint Basins, California: U.S. Geol. Survey Bull. 1045–A.

128. TIME OF THE LAST DISPLACEMENT ON THE MIDDLE PART OF THE GARLOCK FAULT, CALIFORNIA

By GEORGE I. SMITH, Menlo Park, Calif.

Work done in cooperation with the California Division of Mines

Throughout the southern half of the Searles Lake basin, in California, there are numerous deposits of tufa. From their position within the basin, and from their internal structures, it is evident that these deposits were formed at or below the surface of the water in Searles Lake, which stood at levels as high as its spillway (at an elevation of 2,250 feet) in Pleistocene time. One of them, at an elevation of about 2,200 feet, in SW¼NW¼ sec. 12, T. 28 S., R. 43 E., rests on a well-preserved north-sloping scarp, 40 feet high, of the strike-slip Garlock fault. The tufa was clearly formed later than this scarp, and it is almost certain that the scarp was formed during the most recent displacement along this segment of the fault that resulted in appreciable uplift; in this area, the Garlock fault is expressed physiographically by a single line of scarps and lineaments, and it is highly improbable that the traces of successive displacements on strike-slip faults would precisely coincide. Where the highest shoreline crosses the fault scarp, it does not appear to have been offset. This does not prove conclusively that there has been no later movement whatever on the fault here inasmuch as the angle between the fault and the shoreline is too small to allow the detection of minor horizontal displacements; it does support the conclusion, however, that there has not been considerable movement since the shoreline and the tufa were formed.

Surface and subsurface evidence obtained from Searles Lake and related basins indicates that the lake has not stood as high as 2,200 feet since the time that immediately followed its last period of overflow; this overflow occurred during the latter part of the Pleistocene pluvial stage that is correlated with the Tahoe glacial stage of Blackwelder (1931) in the Sierra Nevada. In Searles Lake core L–W–D (Smith and Pratt, 1957), the sediments regarded as contemporaneous with this last period of overflow lie at a depth of about 140 feet, about 20 feet below the top of the muds correlated with the Tahoe glacial deposits. A carbon-14 date of 46,350 ± 1,500 years B. P. has been obtained on a sample collected from about 10 feet below the top of these muds (Flint and Gale, 1958, p. 704). As sedimentation rates of 1,000 years or more per foot are indicated for muds of this type (Flint and Gale, 1958, p. 706), the sediments deposited during the last period of overflow are probably at least 10,000 years older than this carbon-14 date, and may therefore be between 55,000 and 60,000 years old. It appears quite safe to say that they are at least 50,000 years old, and that the tufa described above is about the same age.

The above evidence contradicts the widely held belief, based on the existence of well-perserved scarps such as the one here described, that the Garlock fault was active in Recent time.

REFERENCES

Blackwelder, Eliot, 1931, Pleistocene glaciation in the Sierra Nevada and Basin Ranges: Geol. Soc. America Bull., v. 42, no. 4, p. 865–922.

Flint, R. F., and Gale, W. A., 1958, Stratigraphy and radiocarbon dates at Searles Lake, California: Am. Jour. Sci., v. 256, p. 689–714.

Smith, G. I., and Pratt, W. P., 1957, Core logs from Owens, China, Searles, and Panamint basins, California: U.S. Geol. Survey Bull. 1045–A, p. 1–62.

129. WELDED TUFFS IN THE NORTHERN TOIYABE RANGE, NEVADA

By HAROLD MASURSKY, Denver, Colo.

Work done in cooperation with the Nevada Bureau of Mines

In central Nevada, near the place where the north end of the Toiyabe Range abuts against the Cortez and Shoshone Ranges (fig. 129.1), a thick sequence of welded tuffs occupies a trough about 50 miles long and 10 miles wide. Described here is an area about 6 miles on a side at the east end of this trough, mapped by James Gilluly and me in 1957–59. In this area the tuffs, deeply dissected and well exposed, are bounded by high-angle faults on the north and south and by alluvium on the east and west.

STRATIGRAPHY

The volcanic sequence, about 8,000 feet thick, consists of pinkish-gray to light-gray vitric crystal tuff interbedded with water-laid tuff with pebble conglomerates eroded from Paleozoic rocks. The sequence contains many lenticular layered ash-flow units (a term proposed by R. L. Smith, written communication) as much as 1,200 feet thick and 2 miles long (table 129.1).

The beautifully developed vitroclastic texture, characterized by deformed and agglutinated glass fragments, demonstrates that the tuffs are welded, that they are ash flows emplaced when they were so hot that the glass fragments stuck together (Fenner, 1923; Marshall, 1935). The xenoliths of chert, mostly scattered through the ash rather than in discrete layers, indicate that the ash flows moved in a very turbulent fashion. The few interbedded layers of gravel are mainly pebble conglomerates with red silt matrix. The pebbles are of chert, quartzite, argillite, and limestone from nearby Paleozoic rocks. Near the northern boundary there are giant boulder conglomerates containing blocks of chert and quartzite more than 100 feet long; toward the center of the volcanic area the gravel beds are thinner and finer grained.

The phenocryst composition together with the bulk chemical composition shown by eight analyses, to be published elsewhere, match very closely Nockolds' (1954) rhyolite plus rhyolite obsidian.

GEOLOGIC RELATIONS AND AGE

The welded tuffs lie unconformably on lower and middle Paleozoic rocks that were complexly faulted in late Paleozoic time (Roberts and others, 1958), and into which a quartz monzonite stock was intruded in Tertiary time. (See fig. 129.1.) On the west, the welded tuffs are partly overlapped by, and partly in fault contact with, a thick sequence of gravel, sand, fresh-water limestone, and vitric tuff that has yielded remains of early and late Pliocene horses (Edward Lewis, written communication) and middle Pliocene snails (D. W. Taylor, written communication).

Scanty fossil evidence indicates that the welded tuffs are of early Tertiary age. Interbedded water-laid tuffs have yielded scraps of vertebrates that, though of unidentifiable species, are surely Tertiary, and also Tertiary pollens that are Miocene or older (Estella B. Leopold, written communication). Regional evidence indicates that the tuffs are pre-Miocene, possibly Oligocene. As they seem to be older than the basalt 30 miles to the northeast in the Cortez Range, whose age

TABLE 129.1.—*Sequence of rock types in an ash-flow unit*

Lithology [1]	Consolidation	Thickness (feet)
Top		
Pale red-purple to medium-gray vitric crystal tuff containing numerous fragments of white devitrified pumice.	Partially welded.	150 to 500.
Pale red-purple vitric crystal tuff; crude layering due to schlieren and blebs of deformed glass, mostly devitrified.	Thoroughly welded.	200 to 800.
Black vitrophyre interbedded with medium light-gray vitric crystal tuff; commonly two vitrophyre layers.	Thoroughly welded.	Vitrophyre layers 10 to 50 each; total of unit 50 to 200.
Pinkish-gray vitric crystal tuff.	Not welded	0 to 20.
Base		

[1] In the unit as a whole, phenocrysts average about 25 percent; they are mainly sanidine and quartz, with subordinate oligoclase and a little biotite and magnetite. Pumice, in places devitrified, is scattered throughout, increasing in abundance upward. Pebbles of black chert and, rarely, of quartzite are scattered throughout but are most abundant at the base.

557753 O—60——19

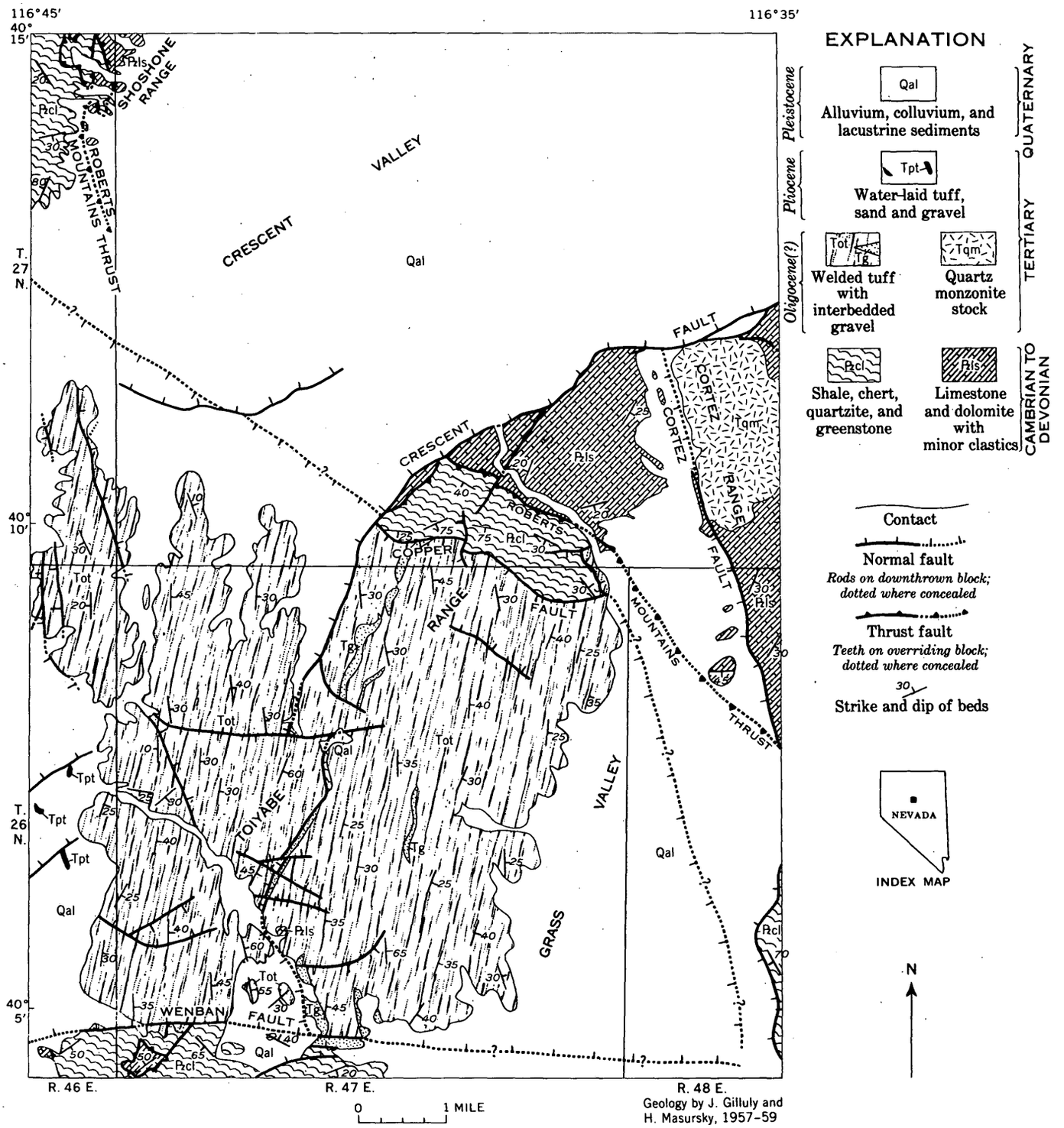

FIGURE 129.1.—Sketch map showing geology in the northern Toiyabe Range, Nev.

is regarded on vertebrate fossil evidence as pre-late Miocene (Jerome Regnier, written communication), they are very likely of about the same age as similar rocks in eastern Nevada that E. F. Cook (oral communication), on the basis of a biotite age of 37 million years, has dated as Oligocene.

STRUCTURE

The east-trending high-angle Wenban fault, which forms the south boundary of the volcanic area, crosses the Toiyabe Range and continues west across the Shoshone Range. The Copper fault, which bounds the area on the north, separates the volcanic rocks from

the Paleozoic rocks, continues westward across the range, and is offset by the Crescent fault; still farther west, it crosses the Shoshone Range at Wilson Pass. The outcrops of Paleozoic rocks at the head of Grass Valley, on the projected trace of the Copper fault, show that a fault must be concealed there beneath the alluvium, for the thick body of volcanics all disappears within a mile and a half. Gravity surveys by the Geological Survey in this place also indicate a major break. Since the volcanics are missing on the upthrown sides of both the Wenban fault and the Copper fault, the throw of each of these faults must have been more than 8,000 feet.

The Crescent fault cuts and repeats the entire volcanic sequence, crosses Grass Valley, and marks the northwest boundary of the Cortez Range. Gravity measurements and displacement of basalt sheets in the Shoshone and Cortez Ranges indicate that it has a throw of more than 10,000 feet along a 60 degree dipping surface. The accordance of the range front with the Crescent fault and the many scarplets in the alluvium show that this fault and a branch of it, the Cortez fault, are still active.

The interbedded gravels that pinch out and become finer grained away from the faults are probably fans deposited at the feet of active scarps. The east-trending Wenban and Copper faults thus appear to have bounded a linear trough, or volcano-tectonic depression (Williams, 1941, p. 246), that was actively sinking during the deposition of the volcanics, probably in Oligocene time.

The extreme lenticularity of the individual units in the welded tuff here described, and their extraordinary total thickness and absence from the surrounding area, are evidence of their having been deposited originally in a local basin. That is, they are not remnants of a formerly extensive cover preserved in a graben. Other deposits of welded tuff in eastern Nevada and western Utah (Cook, 1957; Mackin, 1960) are very thin and very widespread, and they must have been deposited in a manner analogous to flood or plateau basalts in contrast to the local tectonic basin fills described here. Much later, probably during Pliocene and Pleistocene time, the Crescent and Cortez faults blocked out the present basin ranges almost at right angles to the earlier fault system.

REFERENCES

Cook, E. F., 1957, Geology of the Pine Valley Mountains, Utah: Utah Geol. Mineralog. Survey Bull. 58, 111 p.

Fenner, C. N., 1923, The origin and mode of emplacement of the great tuff deposit in the Valley of Ten Thousand Smokes: Natl. Geog. Soc. Contr. Techn. Papers, Katmai ser., no. 1, 74 p.

Mackin, J. H., 1960, Structural significance of Tertiary volcanic rocks in southwestern Utah: Am. Jour. Sci., v. 258, no. 2, p. 81–131.

Marshall, P., 1935, Acid rocks of the Taupo-Rotorua volcanic district: Royal Soc. New Zealand Trans., v. 64, p. 323–366.

Nockolds, S. R., 1954, Average chemical compositions of some igneous rocks: Geol. Soc. America Bull., v. 65, no. 10, p. 1007–1032.

Roberts, R. J., Hotz, P. E., Gilluly, James, and Ferguson, H. G., 1958, Paleozoic rocks of north-central Nevada: Am. Assoc. Petroleum Geologists Bull., v. 42, no. 12, p. 2813–2857.

Williams, Howel, 1941, Calderas and their origin: California Univ. Dept. Geol. Sci. Bull., v. 25, no. 6, p. 239–346.

130. REGIONAL GRAVITY SURVEY OF PART OF THE BASIN AND RANGE PROVINCE

By Don R. Mabey, Menlo Park, Calif.

For several years the U.S. Geological Survey has been conducting gravity studies in the Basin and Range province in Utah, Nevada, and California. Gravity measurements have been made to determine local structure in several areas where geologic mapping was going on; these surveys, however, cover only a small part of the total area. In the areas not covered by the local surveys, gravity observations have been made at bench marks, at triangulation stations, and along major highways. All the gravity data collected by the Survey have been tied to a common datum through a network of base stations. This network is referred to four airport base stations established by Woollard (1958).

The data thus collected have been useful in studying the structural geology in the basins and in parts of some of the mountain ranges. Over most of the region the dominant local Bouguer gravity anomalies are produced by the density contrast between the pre-Tertiary rocks and the generally less dense younger volcanic and sedimentary rocks. These local anomalies, which have amplitudes up to 60 milligals, are usually

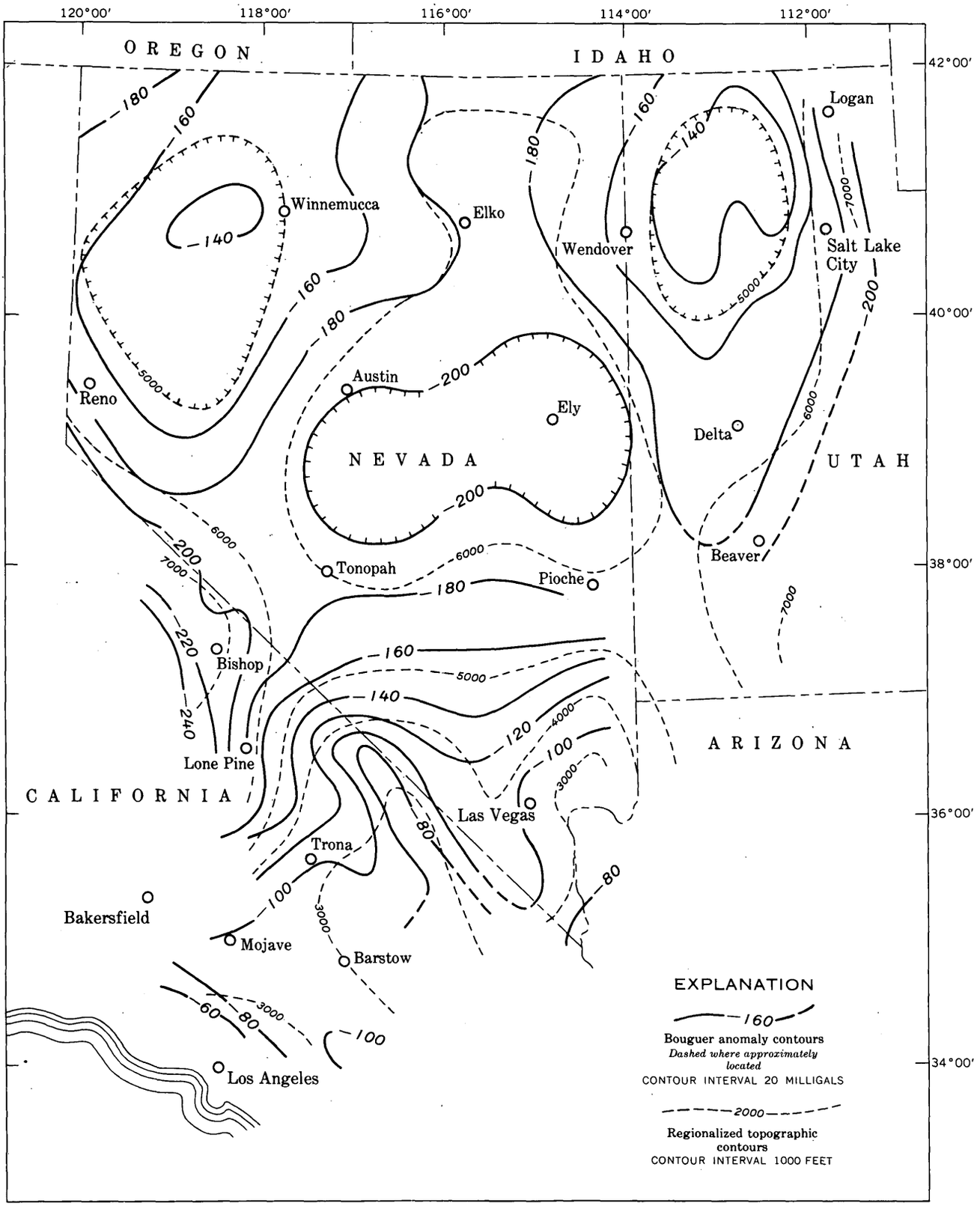

FIGURE 130.1.—Regionalized Bouguer anomaly and topographic map of part of the Basin and Range province. The gravity contours are based on representative stations in the ranges. The topography is averaged over circles 128 km in diameter. The gravity data are from surveys made under the supervision of K. L. Cook, R. W. Decker, D. L. Healey, M. F. Kane, D. R. Mabey, L. C. Pakiser, S. W. Stewart, and G. A. Thompson.

located in basin areas underlain by thick accumulations of Tertiary rocks and valley fill. They can be interpreted in terms of the thickness of the low-density rocks and the configuration of the basins in which they occur. The local anomalies associated with density contrasts within the pre-Tertiary rocks are generally of smaller amplitude, but significant local anomalies associated with bedrock features have been observed.

A knowledge of the broad regional variations in Bouguer anomaly values is of great use in the study of the large-scale variations in the thickness and composition of the crust. It is also helpful in isolating the local gravity anomalies superimposed on the regional variations. In the Basin and Range province the preparation of a contour map to illustrate the regional gravity anomalies is complicated by numerous local anomalies of large amplitude. The anomaly value for an individual gravity station may not be even approximately representative of the anomaly values over an area of even a few square miles, particularly if the station is near the margin of a basin underlain by several thousand feet of low density Cenozoic rocks. To prepare an anomaly map that will show the regional gravity anomalies some method of averaging values or selecting stations must be used. The map in figure 130.1 was prepared by contouring the anomaly values for representative stations located in the ranges.

The regional Bouguer anomaly values range from about −60 milligals to −240 milligals, and show an inverse correlation with the regional topography. The highest anomaly values are at the southwest edge of the map. Here the anomaly values rise abruptly where the regional elevation decreases toward the Pacific Ocean. Over the western Mojave Desert, where the surface relief is small, the regional gravity relief is small. North of the western Mojave Desert the anomaly values decrease as the surface rises to a high over the Sierra Nevada and White Mountains. Relatively high anomaly values occur in topographically low areas around Death Valley and the Colorado River. Northward from these areas the general level of the surface rises and the anomaly values decrease. In east-central Nevada the surface is higher, and the Bouguer anomaly values are lower than in any other part of the State.

Along the west-central border of Nevada the anomaly values decrease as the surface rises toward the Sierra Nevada. In northwestern Nevada the main gravity feature is a high, which is in the topographic low containing the Smoke Creek and Black Rock Deserts, Desert Valley, the lower Humboldt River valley, and the Carson Sink. Northwest of this area the anomaly values decrease over a topographic highland. A strip in which gravity is low and the surface is high extends northward from the Ely area to the Idaho-Nevada State line. East of this low trend there is a gravity high in the Lake Bonneville basin. East of the Lake Bonneville basin the anomaly values are lower over the Wasatch Range.

The correlation between low Bouguer anomaly values and high regional topography clearly shows that there is a relative mass deficiency under the regional highlands. Although the gravity data do not indicate the nature of the mass deficiency, which can occur anywhere within the crust or in the upper mantle, the correlation with topography suggests that some form of regional isostatic compensation exists.

REFERENCE

Woollard, G. P., 1958, Results for a gravity control network at airports in the United States: Geophysics, v. 23, no. 3, p. 520–536.

131. MESOZOIC AGE OF ROOF PENDANTS IN WEST-CENTRAL NEVADA

By James G. Moore, Menlo Park, Calif.

Work done in cooperation with the Nevada Bureau of Mines

In an area of roughly 3,000 square miles in the western Great Basin, lying mainly in Lyon, Douglas, and Ormsby Counties, Nev. (fig. 131.1), about 430 square miles are underlain by Cretaceous(?) intrusive rocks, largely granitic, related to the Sierra Nevada batholith, and about 180 square miles by partly metamorphosed rocks older than the batholith. The metamorphic rocks occur in irregular roof pendants and septa, which have

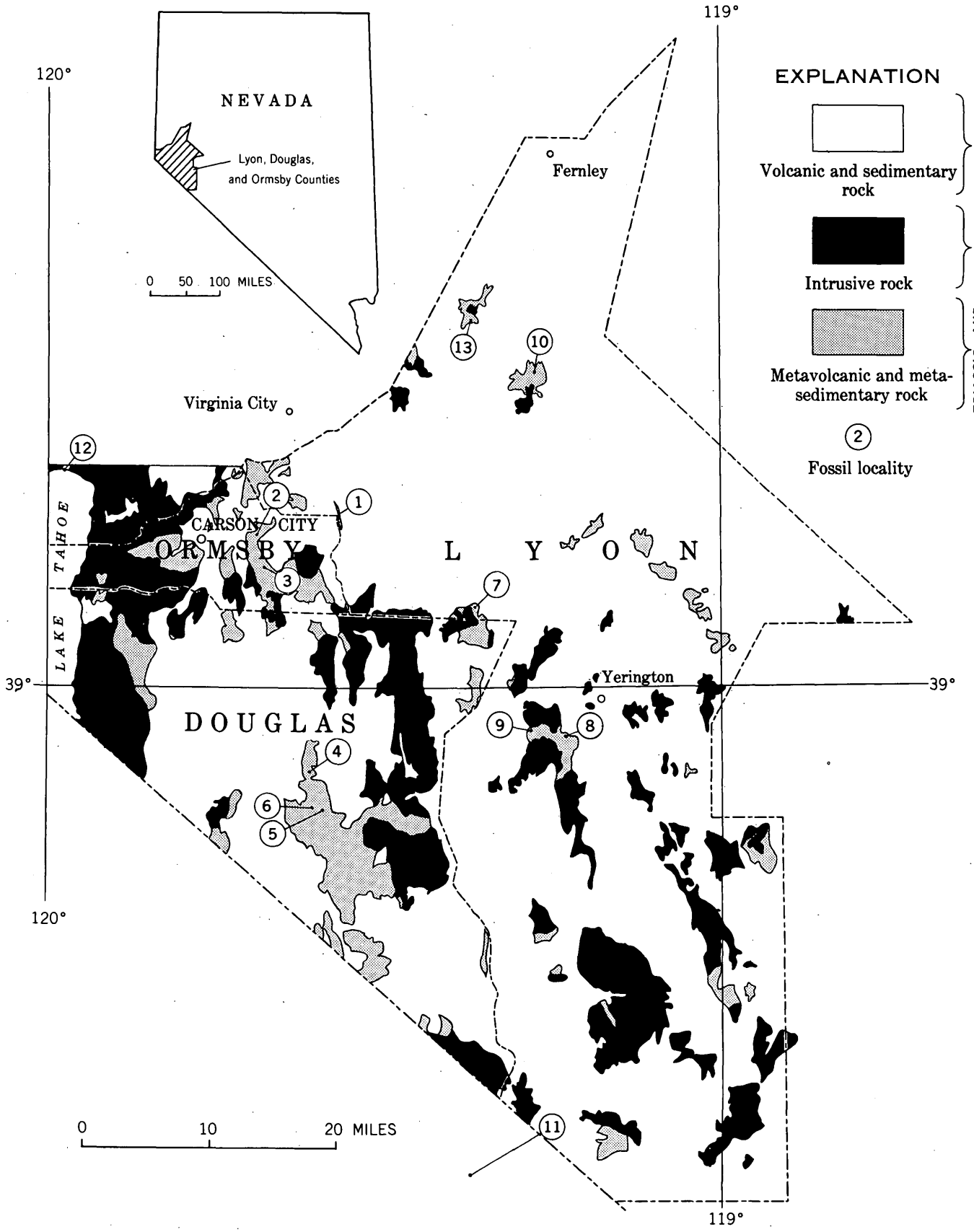

FIGURE 131.1.—Generalized geologic map of Lyon, Douglas, and Ormsby Counties, Nev.

been deformed, intruded, and recrystallized by the granitic rocks. The rest of the area is underlain by Cenozoic volcanic and sedimentary deposits. The area is considered to be within the borders of the batholith, because granitic rocks are more than twice as abundant as the older rocks.

In the prebatholithic sequence, metavolcanic rocks are somewhat more abundant than metasedimentary rocks, which were themselves largely derived from volcanic detritus. The metavolcanic rocks are dominantly meta-andesite and meta-dacite, mostly in the form of volcanic breccia, but also include much metabasalt and metarhyolite. The metavolcanic rocks are interbedded with marine sedimentary rocks and are at least in part of submarine origin. The rarity of pillow lava, however, and the association of volcanic rocks with gypsum deposits, suggest that part of the volcanic rock was formed in a terrestrial or near-shore environment.

The metasedimentary rocks originally consisted mainly of shale, siltstone (commonly tuffaceous), and limestone, but these are interbedded with sandstone, graywacke, dolomite, gypsum, and small amounts of chert. Intercalated with them, also, are conglomerate and sedimentary breccia that may have originated as submarine mud flows.

In general the metasedimentary rocks underlie the metavolcanic rocks. This is so in the area north of Carson City, in the Sweetwater Range, and in the Virginia City quadrangle, which lies just north of the tri-county area (Thompson, 1956, p. 48). But at Yerington the metasedimentary rocks mostly overlie the metavolcanic rocks (Knopf, 1918, p. 13), and in all areas much of the sedimentary rock contains volcanic material. In many places, however, the stratigraphy and structure of these rocks are not well understood and the relations of the sedimentary and volcanic units are uncertain.

Fossils have been collected from the metasedimentary rocks at 13 localities in the tri-county area (table 131.1

TABLE 131.1.—*Mesozoic fossils from Lyon, Douglas, and Ormsby Counties and adjacent areas*

No. on fig. 131.1	Mountain range	Locality	Fossils	Age	Reference
1a	Pine Nut	Eldorado Canyon, 4 miles southeast of Dayton. Bottom of canyon on east side of creek, sec. 6, T. 15 N., R. 22 E.	*Monotis subcircularis* Gabb.	Late Triassic (late Norian).	Gianella, 1936, p. 37. Identified by S.W. Muller.
1b	do	do	Arietitid ammonites	Early Jurassic, probably Sinemurian (late early Early Jurassic).	This report. Identified by N. J. Silberling.
2	do	Brunswick site. Ridge crest 500 feet west of bridge across Carson River at site of Brunswick. Two miles east of New Empire.	Spherical and crescentic cavities suggest the globose ammonite *Arcestes*.	If these are not inorganic they indicate a Late Triassic age.	Do.
3	do	Sand Canyon, a southern tributary of Brunswick Canyon. West side of road at the boundary between secs. 19 and 30, T. 15 N., R. 21 E.	*Monotis subcircularis* Gabb.	Late Late Triassic (middle or late Norian).	Do.
4	do	South of Pine Nut Creek in sec. 15, T. 12 N., R. 21 E.	*Spiriferina*	Early Mesozoic, probably Late Triassic.	Collected and identified by E. R. Larson, written communication, 1958.
5	do	Southwest of ridge crest ½ mile west of Alpine Mill on Pine Nut Creek: NE¼NE¼ sec. 35, T. 12 N., R. 21 E.	*Monotis subcircularis* Gabb. *Hetarastridium* sp. *Placites* sp. *Rhabdoceras* sp. *Sandlingiles*? sp. *Halorites*? sp. Choristoceratid.	Late Late Triassic (middle or late Norian).	This report. Identified by N. J. Silberling.

TABLE 131.1.—*Mesozoic fossils from Lyon, Douglas, and Ormsby Counties and adjacent areas*—Continued

No. on fig. 131.1	Mountain range	Locality	Fossils	Age	Reference
6	do	One and one-half miles west of Albine Mill on Pine Nut Creek NW¼NW¼ sec. 35, T. 12 N., R. 21 E.	*Pinna* sp. Indeterminate pectenoid. Indeterminate gastropods. Fragments of large concentrically ribbed pelecypod.	The large pelecypods with concentric ribbing indicate a Mesozoic age.	This report. Identified by N. J. Silberling.
7	Buckskin	Northeast part of Buckskin Range, near intersection of Churchill Canyon and road from Lincoln Flat: NW¼NE¼ sec. 12, T. 14 N., R. 23 E.	"*Pecten*" aff. "*P.*" *valoniensis*. *Pteria* sp. Nuculid? pelecypods.	Early Mesozoic	Do.
8a	Singatse	Yerington district; on the south side of road near Malachite mine. Near SE¼SE¼ sec. 31, T. 13 N., R. 25 E.	*Daonella* sp. *Halobia*.	Triassic	Knopf, 1918, p. 13. Identified by T. W. Stanton.
8b	do	do	*Halobia* sp.	Late Triassic	This report. Identified by N. J. Silberling.
9	do	Ludwig mine	Not specified	Triassic	Jones, 1912, p. 400.
10	Churchill Butte.	Northeast side of butte in SE¼ sec. 3, T. 17 N., R. 24 E.	*Arietites*	Early Jurassic	Collected and identified by V. P. Gianella, written communication, 1958.
11	Sweetwater	Lobdel Lake district	Ammonite either a *Caloceras*? or a *Arnioceras*?	do	Halsey,[1] 1953, p. 28. Identified by S. W. Muller.
12	Sierra Nevada.	Beach pebble at northern end of Lake Tahoe.	Ammonoid cephalopod.	Mesozoic	Larson and Gianella, 1951.
13	Virginia Range.	North-central sec. 23, T. 18 N., R. 23 E. Churchill Butte 15-minute quadrangle.	Arietitid ammonite	Early Jurassic	Collected by V. P. Gianella and D.I. Axelrod, 1959. Identified by N. J. Silberling.

[1] Halsey, J. H., 1953, Geology of parts of the Bridgeport, Calif., and Wellington, Nev., quadrangles. University of California Ph. D. thesis, 498 pages. Halsey also mentions (p. 27) that poorly preserved ammonites and *Halobia* probably of Triassic age have been collected "in the hills surrounding Topaz Lake and in Risue Canyon." Both localities are on the west side of the Sweetwater Range.

and fig. 131.1). During the course of recent reconnaissance mapping, 5 new fossil localities were found, and enlarged collections were made from 2 previously known localities. In addition, this note lists the fossils in 4 collections by others of which no descriptions had previously been published. All 13 collections consist of Mesozoic fossils; in 5 of them, the fossils are Triassic (mostly Late Triassic) and in 3 they are Early Jurassic. No Paleozoic rocks have been recognized in the mapped area, though the extensive faulting and folding of the prebatholithic rocks should have caused them to be exposed if they were present.

REFERENCES

Gianella, V. P., 1936, Geology of the Silver City district and the southern portion of the Comstock Lode, Nevada: University of Nevada Bull., v. 30, no. 9, 108 p.

Jones, J. C., 1912, The origin of the anhydrite at the Ludwig mine, Lyon County, Nev.: Econ. Geology, v. 7, p. 400–402.

Knopf, Adolph, 1918, Geology and ore deposits of the Yerington district, Nevada: U.S. Geol. Survey Prof. Paper 114, 68 p.

Larson, E. R., and Gianella, V. P., 1951, Ammonoid from Lake Tahoe, Nevado (abs.): Geol. Soc. America Bull., v. 62, p. 1522.

Thompson, G. A., 1956, Geology of the Virginia City quadrangle, Nevada: U.S. Geol. Survey Bull. 1042–C, p. 45–75.

132. IDENTIFICATION OF THE DUNDERBERG SHALE OF LATE CAMBRIAN AGE IN THE EASTERN GREAT BASIN

By Allison R. Palmer, Washington, D.C.

Previous to 1958 the Dunderberg shale, or a supposedly equivalent unit, had been identified at many places in the eastern half of the Great Basin where it had been regarded as an important regional stratigraphic marker (Palmer, 1956). Bentley (1958) has described what he called the "Dunderberg shale" as occurring at many localities in western Utah, and has shown that it is a shaly westward extension of the Worm Creek quartzite member of the St. Charles formation of the northern Wasatch Range. He has also shown that the trilobite fauna of the "Dunderberg shale" in western Utah is entirely that of the *Elvinia* zone. It has now been established, however, by detailed examination of the Dunderberg shale at its type locality in the Eureka district, Nevada, that trilobites of the *Elvinia* zone are confined to limestones in the upper 50 feet of the formation. The lower 200 feet, which includes most of the shale in the formation, contains abundant representatives of the *Dunderbergia* zone (Palmer, 1960). Bentley's "Dunderberg shale," therefore, is younger than almost all of the Dunderberg shale at its type locality.

In the Eureka district the contact of the Dunderberg shale with the underlying Hamburg dolomite is a zone of shearing (Nolan, Merriam, and Williams, 1956, p. 18), but until recently only a few feet of beds was believed to be missing. New evidence now indicates that as much as 200 to 300 feet of the lower part of the Dunderberg shale may be faulted out at Eureka. An essentially unfaulted exposure of Dunderberg shale, 600 feet thick, has now been recognized near Cherry Creek, about 65 miles northeast of Eureka. In this section the upper 350 feet of beds contains trilobites of both the *Elvinia* and *Dunderbergia* zones, similar to those found at Eureka. The lower 250 feet contains different trilobites, belonging to the *Aphelaspis* zone. Below these beds, and above another shaly unit containing *Eldoradia*, there is about 1,000 feet of thick-bedded limestone which has not been named. As *Eldoradia* is found in the upper beds of the Secret Canyon shale, which lies just beneath the Hamburg dolomite at Eureka, the unnamed limestone near Cherry Creek should probably be correlated with the Hamburg dolomite. The estimated thickness of 1,000 feet for the Hamburg dolomite (Nolan, Merriam, and Williams, 1956, p. 17) is approximately the same as that of the unnamed limestone unit, and the thickness of the *Dunderbergia* zone is also about the same in the two areas. There is thus no indication of significant stratigraphic thinning between Cherry Creek and Eureka and it seems likely that the absence of the lower part of the Dunderberg at Eureka is due to faulting.

The Hicks formation, exposed in the Deep Creek Range about 55 miles east of Cherry Creek, consists of units of interbedded shale and thin-bedded limestone alternating with units of medium- to thick-bedded dolomite (fig. 132.1). A 30-foot unit of interbedded limestone and shale at the top of the formation contains trilobites of the *Elvinia* zone. This unit was identified by Bentley as the "Dunderberg shale" and separated from the underlying Hicks formation. A shaly unit in the middle of the Hicks formation, separated from Bentley's "Dunderberg shale" by 120 feet of dolomite, contains trilobites of the *Dunderbergia* zone in its upper part and trilobites of the *Aphelaspis* zone in its lower part. This unit correlates with the lower part of the Dunderberg shale as exposed near Cherry Creek. Therefore, the unit that has been called the "Dunderberg shale" by Bentley and by those who have studied it at many localities in western Utah is not equivalent to the whole of the Dunderberg shale exposed near Eureka and Cherry Creek, Nev.

The stratigraphic evidence presented above indicates that the name "Dunderberg shale" should no longer be used for a thin unit of interbedded limestones and shales occurring in western Utah and containing *Elvinia* zone trilobites. This unit is better named the Corset Spring shale. Bentley has pointed out correctly that the Corset Spring shale, which occurs in the Snake Range just west of the Nevada-Utah line, is equivalent to his "Dunderberg shale" (Bentley, 1958, p. 21).

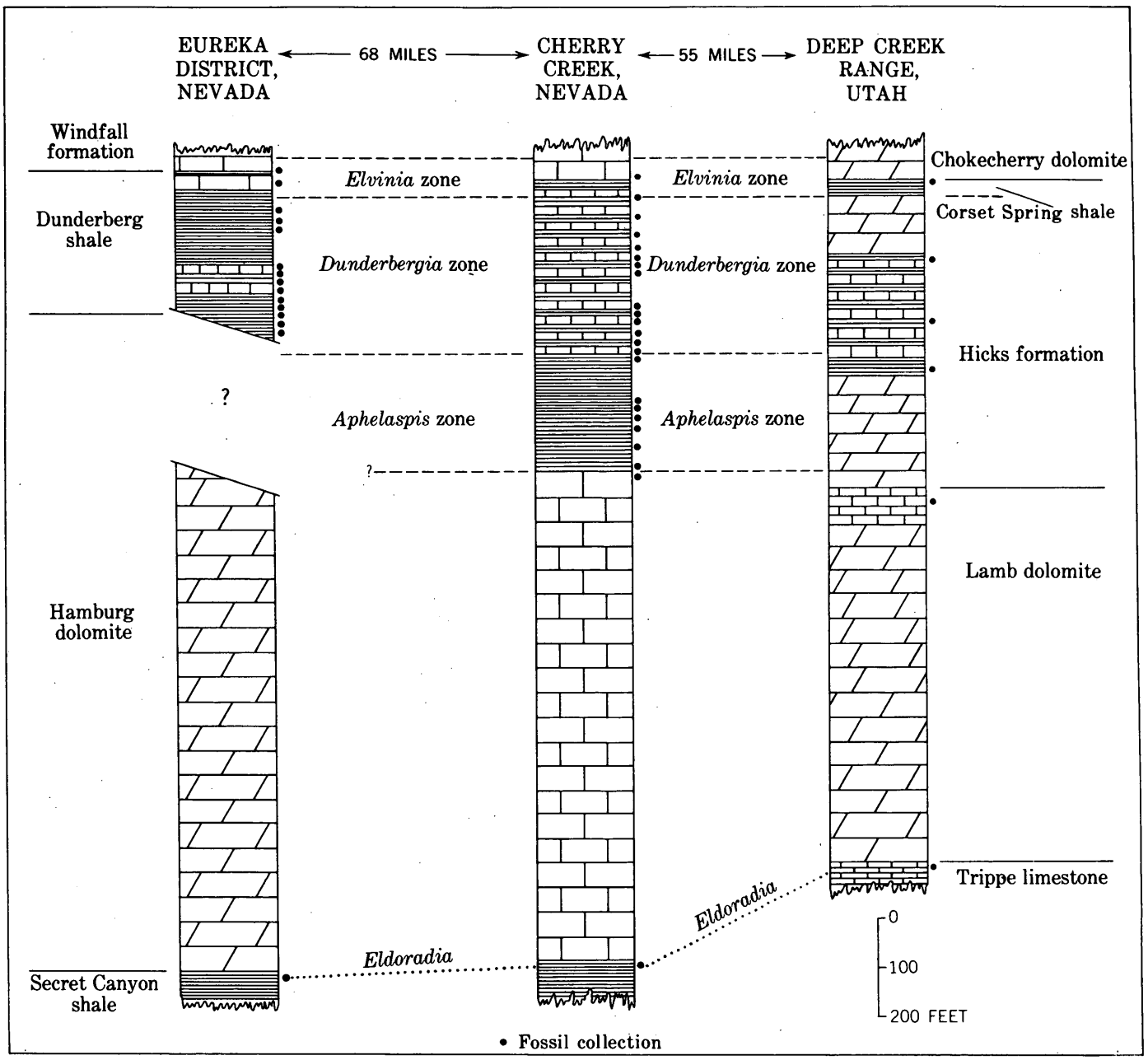

FIGURE 132.1.—Correlation of lower parts of Upper Cambrian sections at Eureka and Cherry Creek, Nev., and in the Deep Creek Range, Utah.

REFERENCES

Bentley, C. B., 1958, Upper Cambrian stratigraphy of western Utah: Brigham Young Univ. Research Studies, Geol. Ser., v. 5, no. 6, 70 p., 5 pl., 7 fig.

Nolan, T. B., Merriam, C. W., and Williams, J. S., 1956, The stratigraphic section in the vicinity of Eureka, Nevada: U.S. Geol. Survey Prof. Paper 276, 77 p.

Palmer, A. R., 1956, The Cambrian system of the Great Basin in western United States: *in* El Sistema Cambrico, su paleogeografia y el problema de su base, XX Internat. Geol. Congress symposium, v. 2, part 2, p. 663–681.

———1960, Trilobites of the Upper Cambrian Dunderberg shale, Eureka district, Nevada: U.S. Geol. Survey Prof. Paper 334–C, p. 53–109.

133. INTRUSIVE ROCKS OF PERMIAN AND TRIASSIC AGE IN THE HUMBOLDT RANGE, NEVADA

By Robert E. Wallace, Donald B. Tatlock, and Norman J. Silberling, Menlo Park, Calif.

Work done in cooperation with the Nevada Bureau of Mines

Numerous bodies of rhyolite porphyry and leucogranite in the Humboldt Range, Nev. (fig. 133.1) have been found to represent feeders for, or intrusive relatives of, the volcanic rocks of the Koipato group, which are of Permian(?) and Triassic age. This relationship had not previously been recognized, although the volcanic rocks of the Koipato group had long been known (King, 1878, p. 270; Knopf, 1924, p. 13).

Volcanic rocks of the Koipato group having a total thickness of more than 12,000 feet are exposed in the Humboldt Range. They are divisible into three units. The oldest unit of Permian(?) and Early Triassic(?) age is the Limerick greenstone (Limerick keratophyre of Jenney, 1935, p. 19), the exposed part of which consists of about 4,000 feet of greenstone; this grades upward into a heterogeneous assortment of tuffs, breccias, and flows of the Rochester rhyolite (Rochester trachyte of Knopf, 1924, p. 14) of Permian(?) and Early Triassic(?) age. The uppermost unit of Permian(?) and Early Triassic age, the Weaver rhyolite (Knopf, 1924, p. 26), is characterized by flows of porphyritic rhyolite and of felsite, and by rhyolitic tuffs.

Numerous dikes, sills, and stocks of leucogranite, rhyolite porphyry, and quartz monzonite were intruded into this thick pile of extrusive rocks. The quartz monzonite, which cuts Triassic rocks and is probably of late Mesozoic or Tertiary age, is not included in the following discussion.

The leucogranite is a fine- to medium-grained, light-colored granite containing quartz and both potassic and sodic feldspars; it contains very little mafic minerals and much tourmaline. Much of this rock could appropriately be termed aplite. Stocks of leucogranite, one of which underlies an area of more than four square miles, are exposed near the axes of major anticlines. Some of these cut the lower part of the Koipato group, but none is known to have penetrated as high as the Weaver rhyolite.

The rhyolite porphyry contains small (< 2 mm) phenocrysts of quartz and larger (1 to 5 mm) phenocrysts of K-feldspar, embedded in a vitreous-appearing groundmass so fine grained that much of it can hardly be resolved under the microscope. Rhyolite porphyry dikes intrude the leucogranite as well as all units of the Koipato group below the Weaver rhyolite. Some irregular swarms of dikes and sills of porphyry are clustered near the stocks of leucogranite, and a group of large elongate stocks of rhyolite porphyry, one of them over a mile long and nearly half a mile wide, are distributed in a belt along the east side of the Humboldt Range.

The Weaver rhyolite appears to be genetically related to both the rhyolite porphyry and the leucogranite; the rhyolite porphyry bodies probably represent, in part, direct feeders for the Weaver rhyolite, but the leucogranite is less closely related to the rhyolite. Chemical, microscopic, and X-ray analyses of the Weaver rhyolite and the intrusive rhyolite porphyry are so similar as to be almost indistinguishable. In many places only field relations, such as cross-cutting contacts or the presence of tuffs interbedded with the rhyolite, enable one to distinguish between intrusive and volcanic rocks. Although the rhyolite porphyry cuts the Koipato group, it has nowhere been found to cut the rocks of the Star Peak group, which is of Middle and Late Triassic age and overlies the Koipato group with slight angular unconformity. At a few places, indeed, field relations suggest that rocks of the Star Peak group overlie the rhyolite porphyry in sedimentary contact. The largest rhyolite porphyry stock, about a mile and a half southwest of Unionville, is in contact with rocks of the Star Peak group, but all the contacts between the two units are believed to be faults.

Two samples of rhyolite porphyry from the stock southwest of Unionville gave lead-alpha ages of 230 ±40 and 290±45 million years (Thomas W. Stern, 1960, written communication). This, according to Kulp, would indicate that the porphyry is of late Paleozoic age, for he has estimated on the basis of isotopic age measurements, that the Mesozoic era began 220 million years ago (Kulp, 1959, p. 1634). Early Early Triassic ammonoids are found in tuffs immediately overlying, or perhaps in part interbedded with, the Weaver rhyolite, and one specimen of "*Helicoprion*" reported from the Rochester by Wheeler (1939, p. 109) is probably pre-Mesozoic (David H. Dunkle, 1957, written communication). The lead-alpha ages obtained for

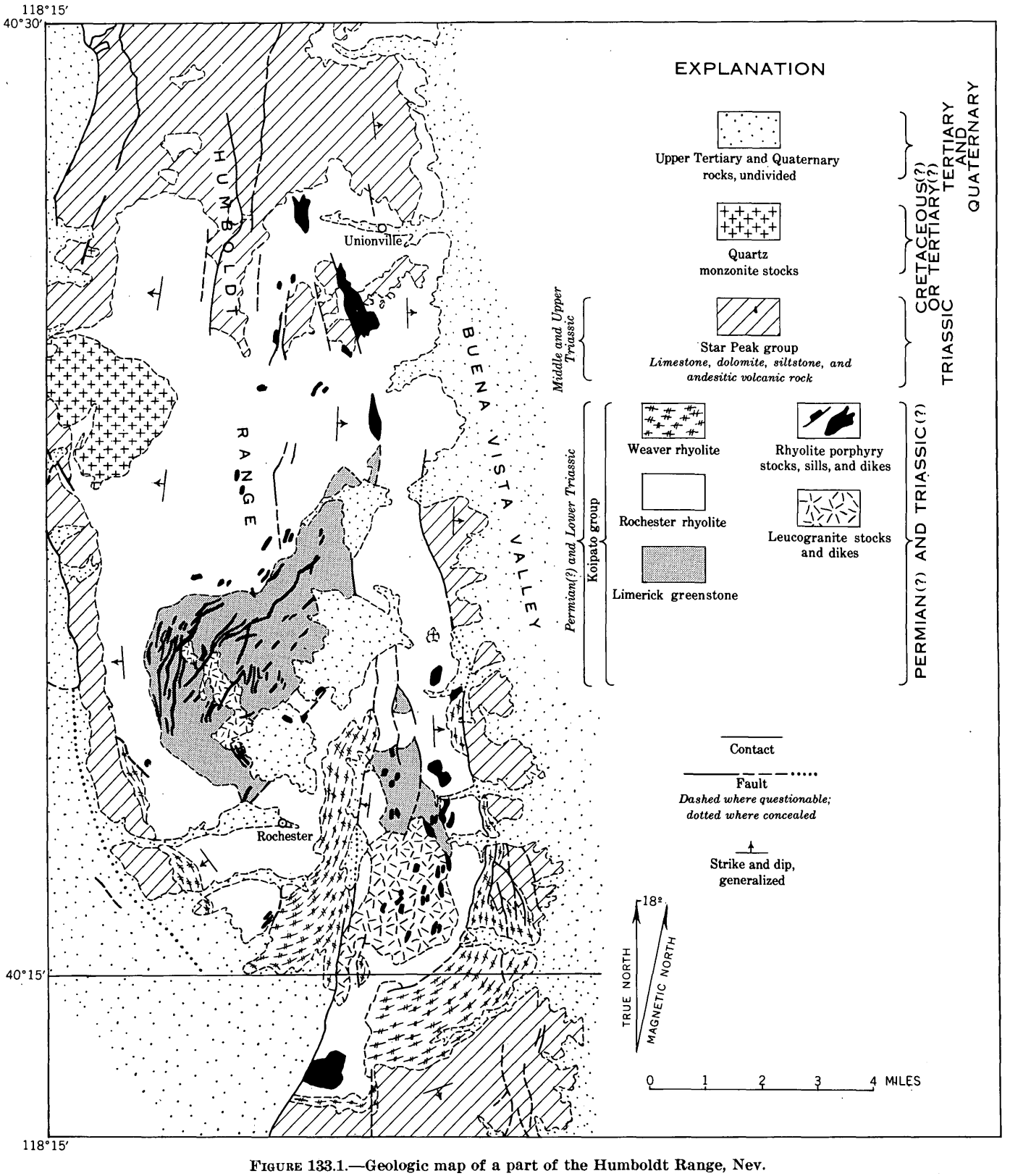

FIGURE 133.1.—Geologic map of a part of the Humboldt Range, Nev.

the rhyolite porphyry thus appear to be consistent with the paleontologic evidence for the ages of the Weaver and Rochester rhyolites.

Although the rhyolite porphyry cuts the leucogranite, contacts between the two are in places clearly gradational, as though the leucogranite had not been

completely solidified when the rhyolite porphyry dikes were intruded. The leucogranite cuts the Rochester rhyolite, but does not extend high enough into the pile of volcanic rocks to reach the Weaver rhyolite. The time of mobilization of the leucogranite must therefore have been only slightly earlier than, or even partly contemporaneous with, the mobilization of the rhyolite porphyry and its extrusive eqiuvalent, the Weaver rhyolite. Since the rhyolite, the rhyolite porphyry, and the leucogranite are so nearly of the same age and so much alike in chemical and mineralogic composition, they are probably differentiates of the same magma.

This evidence, taken as a whole, shows that both the leucogranite and rhyolite porphyry bodies must have been emplaced very near the beginning of the Mesozoic era.

REFERENCES

Jenney, C. P., 1935, Geology of the central Humboldt Range, Nevada: Univ. Nevada Bull., v. 29, no. 6, p. 1–73.

King, Clarence, 1878, Systematic geology: U.S. Geol. Explor. of the Fortieth Parallel, v. 1, p. 270.

Knopf, Adolph, 1924, Geology and ore deposits of the Rochester district, Nev.: U.S. Geol. Survey Bull. 762, 78 p.

Kulp, J. L., 1959, Geologic time scale: Geol. Soc. America Bull., v. 70, no. 12, pt. 2, p. 1634.

Wheeler, H. E., 1939, Helicoprion in the Anthracolithic (Late Paleozoic) of Nevada and California, and its stratigraphic significance: Jour. Paleontology, v. 13, no. 1, p. 103–114.

134. REGIONAL SIGNIFICANCE OF SOME LACUSTRINE LIMESTONES IN LINCOLN COUNTY, NEVADA, RECENTLY DATED AS MIOCENE

By CHARLES M. TSCHANZ, Menlo Park, Calif.

Recent independent fossil and radioactive dating of lacustrine limestones from many widely separated localities in Lincoln and Clark Counties, Nev., has clarified certain stratigraphic relationships, and has consequently advanced the understanding of the structural history of southeastern Nevada and southwestern Utah. These limestones have all been assigned a Miocene age, chiefly on the basis of pollen studies, but a lacustrine limestone unit in the Horse Spring formation, which was previously thought to be Cretaceous or early Tertiary, has now been assigned to the Miocene on the basis of a potassium-argon (K–Ar) date of biotite from an interbedded tuff. Similar limestones of Miocene(?) age occur in the Oak Spring formation, which crops out in Nye County, Nev., and in southwestern Utah.

Lacustrine limestone from nine localities (fig. 134.1) was studied by G. O. W. Kremp, who identified 31 pollen species in six samples that also contain abundant algal fragments and some fungispores. A complete list of these fossils will be published in a subsequent report. Five samples from Lincoln County (1–5) were dated as Miocene or possibly younger by *Compositae* pollen. Samples 6, 8, and 9 did not contain pollen, and sample 7 contained only 2 grains of pollen of possible Miocene(?) age. G. O. W. Kremp (1960, written communications) says:

> The pollen association found in the [first] four samples is practically the same. The flora shows a dominance of pine-like pollen * * * associated with other coniferous pollen * * * The relative high frequency of *Compositae* pollen is remarkable. * * * pollen of the *Compositae* appear first in sediments of late Oligocene age; these pollen become common in the Rocky Mountain area beginning with Miocene. This would date your samples as Miocene or possibly younger. * * * only very few of the 31 species * * * are identical with the upper Oligocene pollen and spore from the Florissant lake beds, Colorado. This * * * makes me somewhat more confident about my Miocene age determination * * *.

The pollen-bearing limestone in Lincoln County is correlated with limestone of the Horse Spring formation in Clark County, which is interbedded with tuff containing biotite that was determined to have a K-Ar age of less than 24 million years (middle Miocene) (G. H. Curtis and J. F. Everden, K-Ar laboratory, University of California, as orally reported to Dr. C. R. Longwell). Pollen was not found in the limestone near the tuff (sample 9). The Horse Spring formation was previously assigned to the Cretaceous or early Tertiary on the basis of plants, ostracods, and snails, which, however, were too poorly preserved to be identified generically.

The upper part of the basal limestone of the Oak Spring formation in Nye County (locality A, fig. 134.1) contains a fossil fish, *Fundulus*, that according to Miller (1955) is restricted to the Pliocene and Quaternary (David Dunkle, 1956, written communication). The fish occurs 150 feet above the base of the exposed sequence (A. B. Gibbons, 1958, written communication). The lower part of this limestone, however, is similar

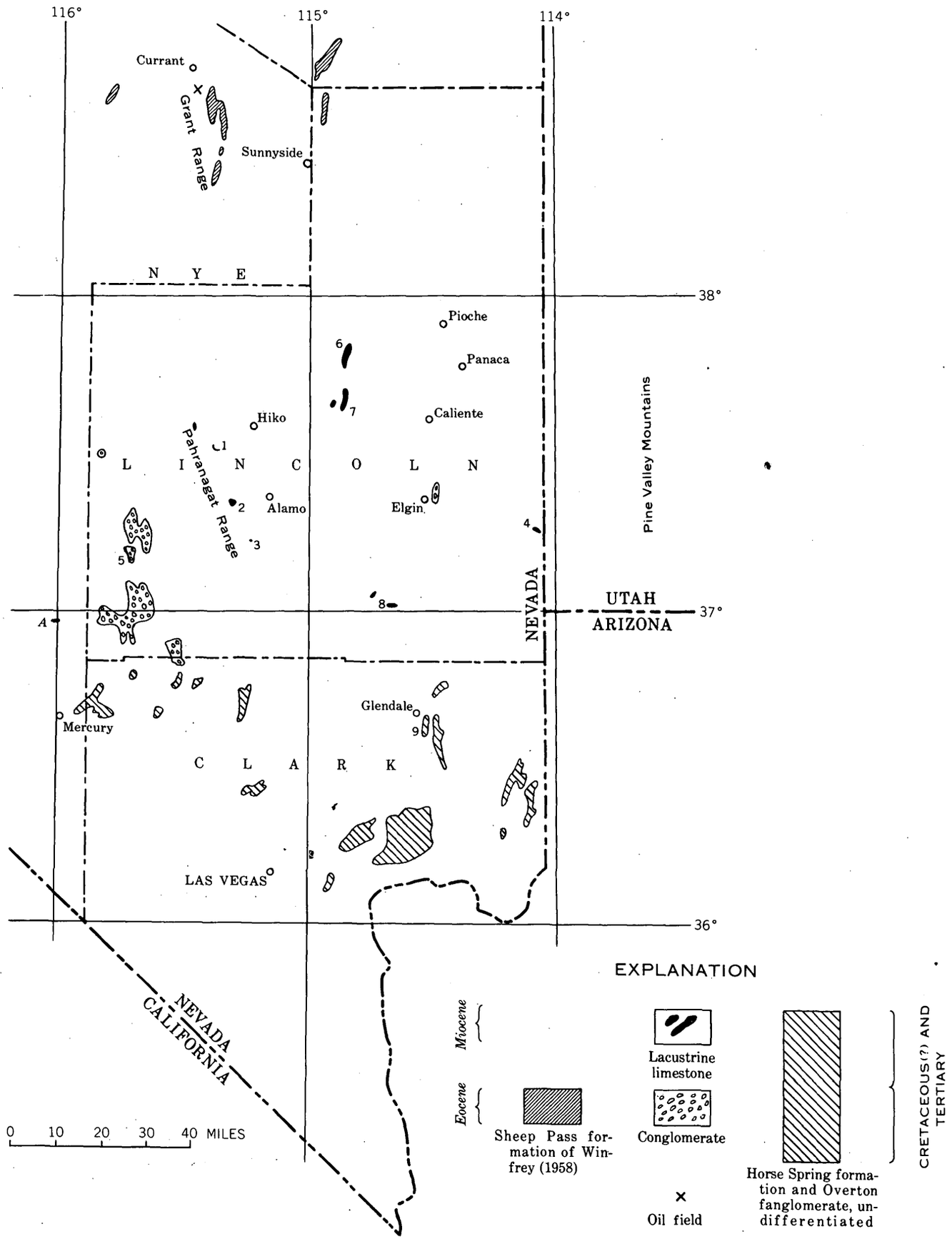

FIGURE 134.1.—Map showing sample locations and outcrops of Tertiary and Cretaceous(?) rocks in southeastern Nevada.

to Miocene limestone in Lincoln County and contains poorly preserved gastropods which Teng Chien Yen has dated as late Tertiary, possibly Miocene, (Johnson and Hibbard, 1957, p. 369). This suggests that the limestone of the Oak Spring may be partly Miocene and partly Pliocene, and that the lower part is correlative with the widespread Miocene limestone in Lincoln and Clark Counties.

The Miocene limestones in Nevada are equivalent to lacustrine limestone and conglomerate near the base of the Rencher and the overlying Grass Valley formation of Cook (1957, p. 16) in the Pine Valley Mountains, Utah. These formations overlie the Quichapa formation of Mackin (1960), whose lowest member has a lead-alpha age of 28 million years (early Miocene) (Mackin, 1960, p. 98). This member in turn lies on lacustrine limestone of the Claron formation. Cook correlates a biotite ignimbrite unit, part of the Needles Range formation of Mackin (1960, p. 100-102), interbedded with limestone in the upper part of the Claron, with one in the Grant Range, Nev., which has a K-A age of 34 million years (middle Oligocene) (Winfrey, 1958, p. 77–82). These facts indicate that the lacustrine limestone near the top of the Claron is Oligocene or earliest Miocene, instead of Eocene as formerly believed.

All the lacustrine limestones discussed here were deposited in local basins on an extensive land surface of low relief that formed during a long period of erosion following Laramide orogeny. These limestones lie unconformably on truncated folds or thrust faults in pre-Jurassic rocks, or on thick orogenic clastic rocks composed chiefly of well-rounded pebbles of Paleozoic rocks. These clastic rocks include the conglomerate in the lower Claron and Wasatch formations, the Overton fanglomerate, and an unnamed conglomerate in southwest Lincoln County (fig. 134.1). They may range in age from Late Cretaceous to Oligocene. In a few places the limestone rests on volcanic rocks.

The limestones are generally overlain by thick volcanic rocks of Miocene and Pliocene age. After the volcanic activity had almost ceased, basin-and-range faulting occurred, most of it in late Miocene and Early Pliocene time.

It is economically important to distinguish the Miocene lacustrine rocks discussed in the paper from the similar rocks of Eocene age. The borate deposits formerly mined from the Horse Spring formation, in Clark County, occur, like the other major borate deposits in California and Nevada, in Miocene or younger rocks, whereas the similar Eocene rocks, such as the Sheep Pass formation of Winfrey (fig. 134.1), contain petroleum.

REFERENCES

Cook, E. F., 1957, Geology of the Pine Valley Mountains, Utah: Utah Geol. and Mineralog. Survey Bull. 58, 111 p.

Johnson, M. S., and Hibbard, D. E., 1957, Geology of the Atomic Energy Commission Nevada Proving Grounds Area, Nevada: U.S. Geol. Survey Bull. 1021–K, p. 333–384.

Mackin, J. H., 1960, Structural significance of Tertiary volcanic rocks in southwestern Utah: Am. Jour. Sci., v. 258, p. 81–131.

Winfrey, W. M., Jr., 1958, Stratigraphy, correlation, and oil potential of the Sheep Pass formation, east-central Nevada: Am. Assoc. Petroleum Geologists, 1958 Geol. Record, Rocky Mountain Section, p. 77–82.

135. EVIDENCE IN THE SNAKE RIVER PLAIN, IDAHO, OF A CATASTROPHIC FLOOD FROM PLEISTOCENE LAKE BONNEVILLE

By Harold E. Malde, Denver, Colo.

When G. K. Gilbert discovered that Lake Bonneville had overflowed at Red Rock Pass, near Preston, Idaho, and had rapidly discharged a vast amount of water northward into the Snake River, he looked downstream for effects of the sudden outflow. Near McCammon, 22 miles downstream from Red Rock Pass, he found (1890, p. 177) a lava flow whose upper surface "is fluted and polished, and pitted with pot-holes after the manner of a riverbed." The present paper is a summary of the effects of the Lake Bonneville outflow found farther downstream along the Snake River.

The Lake Bonneville outflow from Red Rock Pass joined the Portneuf River valley near McCammon and flowed northwestward to the Snake River Plain at Pocatello. At the mouth of the Portneuf River, in the area known as Michaud Flats, the overflow deposited a fan-shaped body of gravel about 50 feet thick whose upper surface is diversified by ridges as much as 20

feet high and a mile long and by irregular closed depressions of similar dimensions. Dissected remnants of the gravel extend 20 miles southwestward, almost to American Falls. Current studies by D. E. Trimble and W. J. Carr, U.S. Geological Survey, show that the gravel was deposited in a shallow lake that was impounded by a lava dam a few miles downstream from American Falls (see also Stearns and Isotoff, 1956, p. 27–28). A rapid downstream decrease in the coarseness of the gravel supports this interpretation. Boulders as much as 8 feet in diameter are abundant at Pocatello, but the gravel 10 miles southwest contains nothing larger than small pebbles, and at Aberdeen, 20 miles west of Pocatello, equivalent deposits near the opposite shore of the former lake consist only of sand and silt.

Spectacular erosion across the lava dam downstream from American Falls is attributed by Trimble and Carr to the Lake Bonneville outflow. Southwest of American Falls, on the upland northwest of the Snake River canyon, there is a strip of scabland 10 miles long and 1 to 4 miles broad, which was a spillway from the former lake. It is bounded downstream by abandoned cataracts, one of which is at the head of Lake Channel, a vertical-walled coulee 6 miles long, half a mile broad, and 100 feet deep (see map in Stearns and others, 1938, pl. 6). Other abandoned cataracts at the heads of alcoves and channels demonstrate that 8 miles of the Snake River canyon in this reach was formed by cataract recession. At the mouths of the alcoves and channels are gravel bars that contain basalt boulders as much as 20 feet in diameter.

Erosion by Lake Bonneville outflow took place on a grand scale near Twin Falls, where the Snake River canyon is half a mile wide, 40 miles long, and as much as 500 feet deep. H. A. Powers, of the U.S. Geological Survey, has shown that at least 24 miles of this canyon was cut by cataract recession contemporaneous with deposition of boulder gravel, most of which accumulated farther downstream. The northern canyon wall near Twin Falls is indented by a series of large cataract alcoves that probably represent successive stages of canyon recession; the three most conspicuous are known as Blue Lake alcove, Devils Corral, and Devils Washbowl. (See map in Stearns and others, 1938, pl. 5.) These cataracts were thought by Russell (1902, p. 127–130) and Stearns (1936) to have been formed by springs, but they, like the alcoves and side channels near American Falls, resemble the abandoned cataracts in the channeled scabland of eastern Washington (Bretz and others, 1956). Deposits of boulder gravel dating from the period when canyon cutting was in progress near Twin Falls form bars more than 100 feet high on the canyon floor. Deposits containing boulders as much as 5 feet in diameter can be seen on the upland north of the canyon along State Highway 25 about 11 miles east-northeast of Twin Falls, and along U.S. Highway 93 about 5 miles north of Twin Falls.

Boulder gravel is especially abundant within the Snake River canyon along a stretch beginning 20 miles downstream from Twin Falls and extending nearly to the Oregon State line. The gravel displays various features that indicate deposition in rapidly moving deep water. The boulders average 3 feet in diameter, and some are as much as 10 feet in diameter. The gravel occurs mainly in wide segments of the canyon, where it forms huge bars and boulder terraces that partly fill the canyon to a depth as great as 300 feet. The gravel bars block the mouths of tributary valleys, and at most places they are separated from the canyon walls by marginal troughs as much as 150 feet deep. Because the boulder gravel commonly occurs downstream from basalt outcrops, Stearns (1936, p. 441–442) mistakenly attributed the boulders to erosion at the toes of successive intracanyon lava flows, not realizing that all the boulder deposits are contemporaneous and that their source rocks are mostly older than the present canyon.

Backwater deposits in tributary valleys, together with internal features of the boulder gravel, indicate that the gravel was deposited in temporary lakes upstream from canyon constrictions. The gravel varies in texture but consists mainly of boulders and sand, both derived almost entirely from the local basalt. Although the boulders are ordinarily distributed at random, some lie in inclined layers, alternating with layers of sand. The inclined layers resemble deltaic foreset beds arranged in courses as much as 50 feet thick between horizontal crossbeds. Such bedding indicates deposition in ponded water. The surfaces of the gravel bars and terraces are conspicuously strewn with lag boulders that seem to indicate reworking during subsidence of the ponded water. In all these respects, the boulder gravel of the Snake River canyon is similar to the gravel bars in the channeled scabland of eastern Washington (Bretz and others, 1956), and like the scabland bars it can be accounted for by the passage of a catastrophic flood.

REFERENCES

Bretz, J H., Smith, H. T. U., and Neff, G. E., 1956, Channeled scabland of Washington; new data and interpretations: Geol. Soc. America Bull., v. 67, no. 8, p. 957–1050.

Gilbert, G. K., 1890, Lake Bonneville: U.S. Geol. Survey Mon. 1, 438 p.

Russell, I. C., 1902, Geology and water resources of the Snake River Plains of Idaho: U. S. Geol. Survey Bull. 199, 192 p.

Stearns, H. T., 1936, Origin of the large springs and their alcoves along the Snake River in southern Idaho: Jour. Geology, v. 44, no. 4, p. 429–450.

Stearns, H. T., Crandall, Lynn, and Steward, W. G., 1938, Geology and ground-water resources of the Snake River Plain in southeastern Idaho: U. S. Geol. Survey Water-Supply Paper 774, 268 p.

Stearns, H. T., and Isotoff, Andrei, 1956, Stratigraphic sequence in the Eagle Rock volcanic area near American Falls, Idaho: Geol. Soc. America Bull., v. 67, no. 1, p. 19–34.

136. ALKALIC LAVA FLOW, WITH FLUIDITY OF BASALT, IN THE SNAKE RIVER PLAIN, IDAHO

By Howard A. Powers, Denver, Colo.

Fine-grained alkalic lava of middle Pleistocene age occupies an area about 10 miles long and 1 mile wide near King Hill, Idaho. Three separate sheets of the molten rock, each less than 30 feet thick, flowed down a gentle slope, the gradient of which decreases from 80 feet per mile to 25 feet per mile. The distribution and thickness of the flow units indicate that the fluid lava had as great mobility as that of the common basalt in the area, which contains labradorite plagioclase.

The upper parts of the flow units are black and are aphanitic to glassy; their vesicular texture resembles that of Swiss cheese. The internal and basal parts are holocrystalline but very fine grained. Olivine and plagioclase are the only minerals visible in the hand sample, mostly as microphenocrysts less than 1 mm in greatest dimension. Rare tablets of plagioclase, only a millimeter thick but as much as 2 cm long by 2 cm wide, are characteristic of one flow unit.

The microscopic texture is dominated by stubby tablets of plagioclase, commonly in jackstraw pattern, but locally oriented in flow pattern. Interstitial spaces are occupied by euhedral to subhedral crystals of clinopyroxene, olivine, magnetite, ilmenite, and apatite, and by patches of anhedral alkali feldspar. The plagioclase is sodic andesine, about An_{35}. The olivine ranges from Fo_{40} to Fo_{25} as determined by powder X-ray diffraction pattern (Yoder and Sahama, 1957, p. 484). The clinopyroxene is iron rich and probably also titanium rich because there is not enough visible ilmenite to account for all of the TiO_2 found by chemical analysis.

The rock is too fine grained for modal analysis, but the computed norm has been adjusted to approximate the mineral content, as shown in the table below. Some *ab* was combined with the *or* in orthoclase, and most of the TiO_2 was allotted to pyroxene. The olivine was computed to agree with the composition indicated by X-ray analysis.

Lava of the composition shown by these analyses does not fall within the range of basalt adopted by Green and Poldervaart (1955), because it is too low in lime and magnesia, and too high in potassia and phosphate. Nor does the composition match that of any igneous rock average in the compilation of Nockolds (1954). The ratio of lime to alkalies in the King Hill Rock approximates that of Nockolds' average alkali doreite, but the King Hill rock is lower in total feldspar, and higher in iron, titania, and phosphate. In content of silica and alumina, the King Hill rock compares reasonably with the average alkali andesite. It is significantly higher than average alkali andesite, however, in titania, total iron, potassia and phosphate and it is much lower in magnesia and lime.

TABLE 136.1.—*Chemical and approximate mineral composition of lava near King Hill, Idaho, as determined from five analyses*

[D. F. Powers, U.S. Geological Survey, analyst]

	Results of 5 analyses			Approximate mineral composition	
	Average	Range	Norm		
SiO_2	49.45	47.17–51.23	Q .15		
Al_2O_3	13.71	13.34–14.45	or 14.7	Alkali feldspar	16
TiO_2	3.32	4.15– 2.90	ab 28.8	Plagioclase An_{35}	42
Fe_2O_3	3.07		an 14.6		
		15.45–13.27		Clinopyroxene	31
FeO	11.28		wo 4.1		
				Olivine	2
MnO	.22	.24– .20	fs 13.2		
MgO	3.68	4.42– 3.33	en 9.2		
CaO	6.77	7.68– 6.36	il 6.2	Ilmenite	.5
Na_2O	3.39	3.18– 3.54	mt 4.4	Magnetite	4.4
K_2O	2.43	2.00– 2.60	ap 3.4	Apatite	3.4
P_2O_5	1.40	2.05– .90			
H_2O	.80	.41– 1.09			

REFERENCES

Green, Jack, and Poldervaart, Arie, 1955, Some basaltic provinces: Geochim. et Cosmochim. Acta, v. 7, p. 177–188.

Nockolds, S. R., 1954, Chemical compositions of igneous rocks: Geol. Soc. America Bull., v. 65, no. 10, p. 1007–1032.

Yoder, H. S., Jr., and Sahama, Th. G., 1957, Olivine X-ray determinative curve: Am. Mineralogist, v. 42, p. 475–491.

557753 O—60——20

137. A DISTINCTIVE CHEMICAL CHARACTERISTIC OF SNAKE RIVER BASALTS OF IDAHO

By Howard A. Powers, Denver, Colo.

The basaltic rocks, of Pliocene to Recent age, from the Snake River valley in southern Idaho are shown by chemical analyses to have a high degree of consanguinity. These basalts may constitute a *clan* in the sense proposed by Tyrrell (1926, p. 136)—that is a group of rocks with the highest degree of consanguinity within a *kindred*.

Preliminary comparisons have shown, also, that the Snake River basalts differ significantly from other basalts of the northwestern United States. One prominent difference is portrayed in figure 137.1, a three-component plot of the ratios between silica, magnesia, and total iron plus manganese in chemical analyses. The diagram shows these ratios for all available analyses of Snake River basalts (except one of a nepheline basalt and a few that contain less than four percent by weight of magnesia) together with all the available analyses of Columbia River basalts, as compiled by A. C. Waters (1960). To represent the basalts of the Cascades, two sample groups of analyses containing more than three percent magnesia were arbitrarily chosen; one sample group was from near Mount Lassen and the other from near Mount Hood.

The rocks from the Snake River valley are all lower in silica than those from other areas. In the Snake River clan, moreover, the silica generally decreases as the ratio of iron to magnesia increases, whereas the opposite is true of the other rocks. The reasons for these and other differences may become apparent as more data are accumulated.

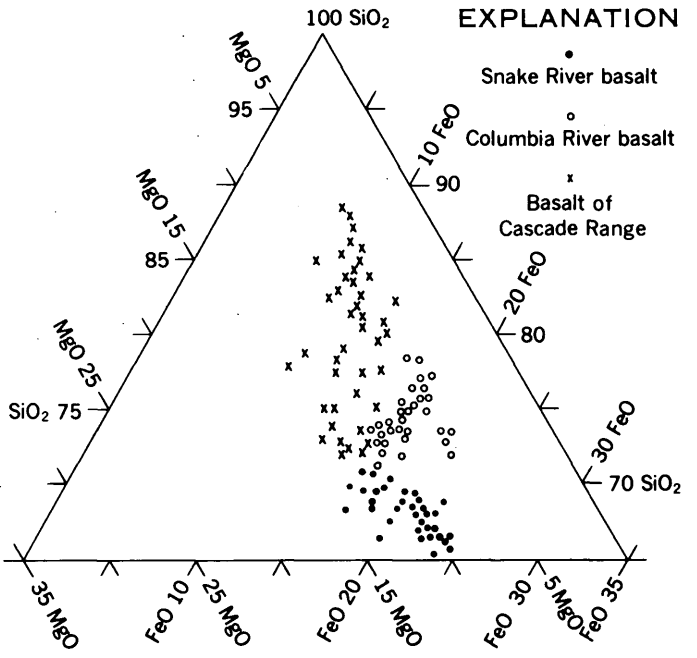

FIGURE 137.1.—Ratios between SiO_2, MgO, and total iron plus manganese in some basalts of the northwestern United States. Data plotted are weight percent of SiO_2, MgO, and sum of $FeO+0.9Fe_2O_3+MnO$ computed to 100 percent.

REFERENCES

Tyrrell, F. W., 1926, The principles of petrology: London, Methuen & Co., Ltd.

Waters, A. C., 1960, Stratigraphic and lithologic variations in the Columbia River basalt: Am. Jour. Sci. (in press)

138. AGE AND CORRELATION OF SOME UNNAMED VOLCANIC ROCKS IN SOUTH-CENTRAL OREGON

By George W. Walker, Menlo Park, Calif.

Fragmentary collections of vertebrate fossils from several newly discovered localities in southeastern Lake County, Oreg., (fig. 138.1) indicate that the enclosing rocks are of approximately the same age as certain Miocene volcanic rocks of central Oregon and adjacent parts of Nevada and California.

The fossils, consisting principally of bone fragments and teeth that have weathered out of tuffaceous beds, apparently represent a single fauna including *Merychippus*, Camelidae, *Dromomeryx* sp. (tentative identifications by G. E. Lewis, 1959), and other mammalian genera. According to Lewis, this fauna is comparable

to that of the Mascall formation of Grant, Crook, and Jefferson Counties, Oreg., (Downs, 1956); it also resembles the mammalian faunas from Beatty and Corral Buttes, Oregon (Wallace, 1946), and Virgin Valley, Nevada (Merriam, 1910), all of which are considered to be of late middle to early late Miocene age.

Andesitic and rhyodacitic volcanic rocks of comparable age, mapped by Russell (1928) as the upper part of the Cedarville series, are exposed in northeastern California and northwestern Nevada. The age assignment of these rocks and their correlation with the Mascall formation is based on studies of fossil floras by Chaney (*in* Russell, 1928) and LaMotte (1936).

The vertebrate-bearing strata of southeastern Lake County are in a section several hundred feet thick largely composed of fine-grained poorly bedded silicic tuff and tuffaceous sedimentary rocks that range in color from pale yellowish-orange to tan, yellow, and light gray. These strata were probably deposited for the most part on dry land, but to a minor extent in shallow lakes. Near major volcanic centers of south-central Oregon some of the fine-grained tuffaceous rocks grade laterally into coarse pumice lapilli tuffs, and interstratified layers of sintered or welded tuff become more abundant. These pyroclastic rocks rest with angular discordance on an extensive series of basalt flows locally more than 1,000 feet thick. Flows near the top of the series consist of ophitic to subophitic diktytaxitic, locally olivine-bearing, basalt that contains little mafic glass; in some of these flows plagioclase pheno-

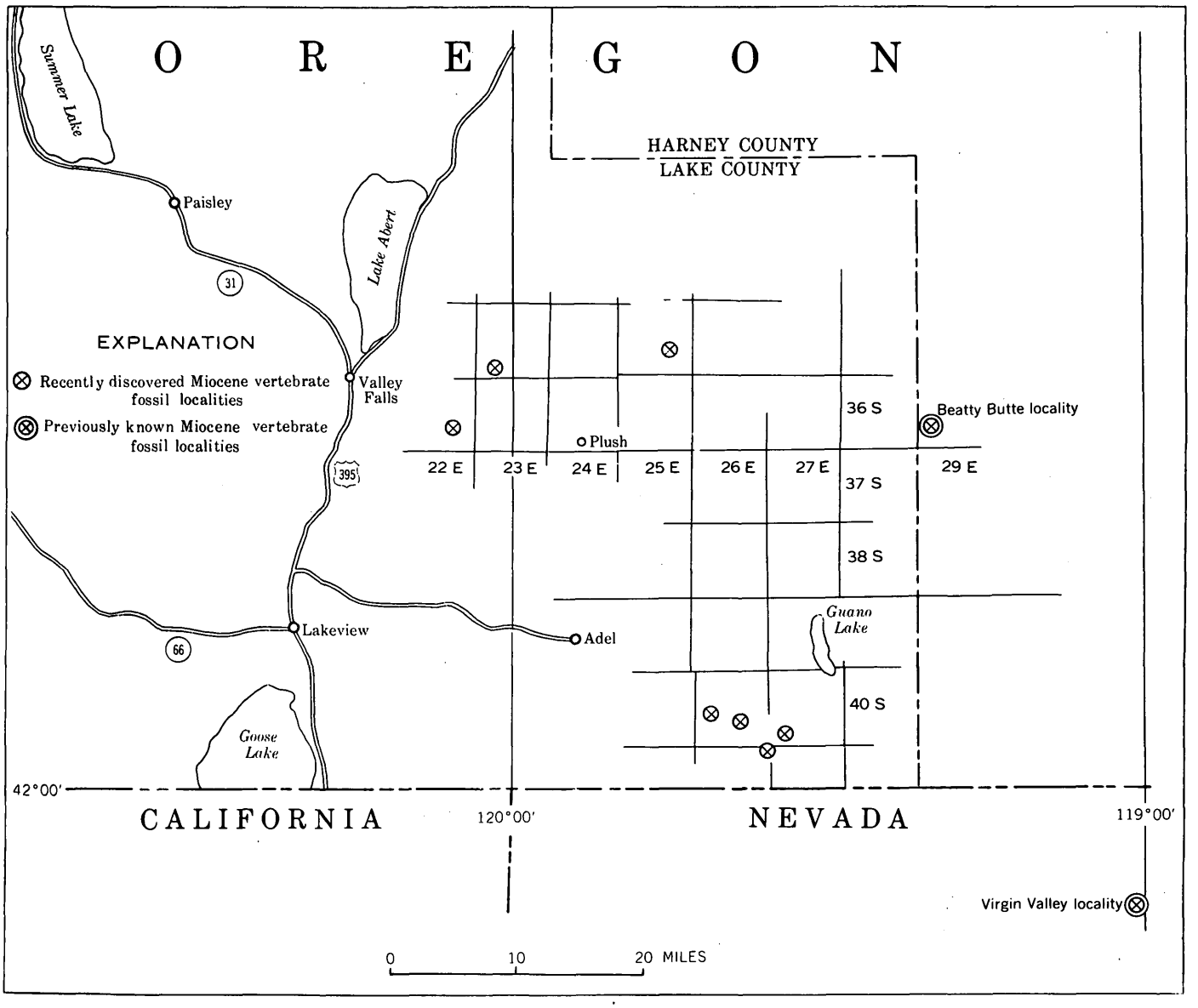

FIGURE 138.1.—Index map showing distribution of Miocene vertebrate fossil localities.

crysts are abundant. These flows are fresh; the constituent minerals reveal only slight evidence of alteration. Other flows, chiefly in the lower part of the basalt series, contain altered phenocrystic and groundmass olivine, altered mafic glass, and zeolites. Dustlike grains of hematite appear on plagioclase cleavage surfaces and surfaces of discontinuity between crystals. Beneath the basalts are silicic pyroclastic rocks lithologically similar to, and probably correlative with, pyroclastic rocks exposed several tens of miles to the west; the latter have been dated as of lower Miocene or John Day age on the basis of a *Diceratherium* tooth, or possibly of middle Miocene (Hemingfordian) age on the basis of fossil plants collected from the same beds that contained the tooth (Peterson, 1959). These rocks in turn are underlain discordantly, south and southeast of Paisley, by andesitic volcanic rocks presumably of pre-Miocene age.

The general sequence of Miocene and older volcanic rocks in southern Lake County is similar to that which comprises the Clarno, John Day, Columbia River, and Mascall formations of central Oregon, but differs from it in some details, particularly in the mineralogy and physical characteristics of the mafic flow units. The late middle to early late Miocene silicic tuff and tuffaceous sedimentary rocks of southeastern Lake County are roughly similar in bulk lithology to rocks of comparable age in Virgin Valley, Nev. Although both these units are apparently of the same age as the upper part of the Cedarville series, exposed in northeastern California and northwestern Nevada, similarities in bulk lithology between the two sections are not obvious.

REFERENCES

Downs, Theodore, 1956, The Mascall fauna from the Miocene of Oregon: California Univ. Dept. Geol. Sci. Bull., v. 31, p. 199–354.

LaMotte, R. S., 1936, The Upper Cedarville flora of northwestern Nevada and adjacent California: Carnegie Inst. Washington Pub. 455, p. 57–142.

Merriam, J. C., 1910, Tertiary mammal beds of Virgin Valley and Thousand Creek in northwestern Nevada: California Univ. Dept. Geol. Sci. Bull., v. 6, p. 21–53.

Peterson, N. V., 1959, Preliminary geology of the Lakeview uranium area, Oregon: Oregon State Dept. of Geology and Mineral Industries, The Ore.-Bin, v. 21, p. 11–16.

Russell, R. J., 1928, Basin Range structure and stratigraphy of the Warner Range, northeastern California: California Univ. Dept. Geol. Sci. Bull., v. 17, p. 387–496.

Wallace, R. E., 1946, A Miocene mammalian fauna from Beatty Buttes, Oregon: Carnegie Inst. Washington Pub. 551, p. 113–134.

139. UPPER TRIASSIC GRAYWACKES AND ASSOCIATED ROCKS IN THE ALDRICH MOUNTAINS, OREGON

By T. P. Thayer and C. E. Brown, Washington, D.C.

Upper Triassic rocks aggregating 40,000 to 50,000 feet in maximum thickness occupy a triangular area about 35 miles from east to west and 16 to 18 miles from north to south in the Aldrich Mountains, Oregon. These rocks are mainly volcanic graywackes and shales, andesitic tuffs, basaltic lavas, and conglomerates that include boulders and fragments of Upper Triassic sedimentary rocks. Slide breccias consisting largely or entirely of basement rocks characterize parts of the section, and the graywackes are in large part turbidites. Although most individual beds or corresponding volcanic units are lenticular and of relatively small extent, angular unconformities and differences in lithology make it possible to recognize three major stratigraphic divisions.

The oldest of these comprises three members (fig. 139.1). The lowest member, exposed near the western edge of the area, west of the fault which crosses Murderers and Deer Creeks, is at least 8,000 feet thick; it is dominantly conglomeratic but includes some basalt flows near the base. The middle member, which occupies the northwestern part of the map area between Fields and Riley Creeks, is 17,000 to 18,000 feet thick. The lowest 5,000 feet of this member is characterized by slide breccias and volcanic flows and breccias interlayered with mudstone and shale, the middle part by mudstones, shale, and graywackes, and the upper 3,000 to 8,500 feet by massive tuff. The upper member is a wedge of interbedded tuff, graywacke, and shale which lies with its thin edge at Riley Creek Butte, near the center of the map, and thickens to 10,000 or 11,000 feet near Fall Mountain, 8 miles to the east.

The middle division is a relatively uniform sheet, 1,000 to 2,000 feet thick, which forms the only stratigraphic unit that can confidently be traced across the map area. It contains no volcanic rocks, and consists

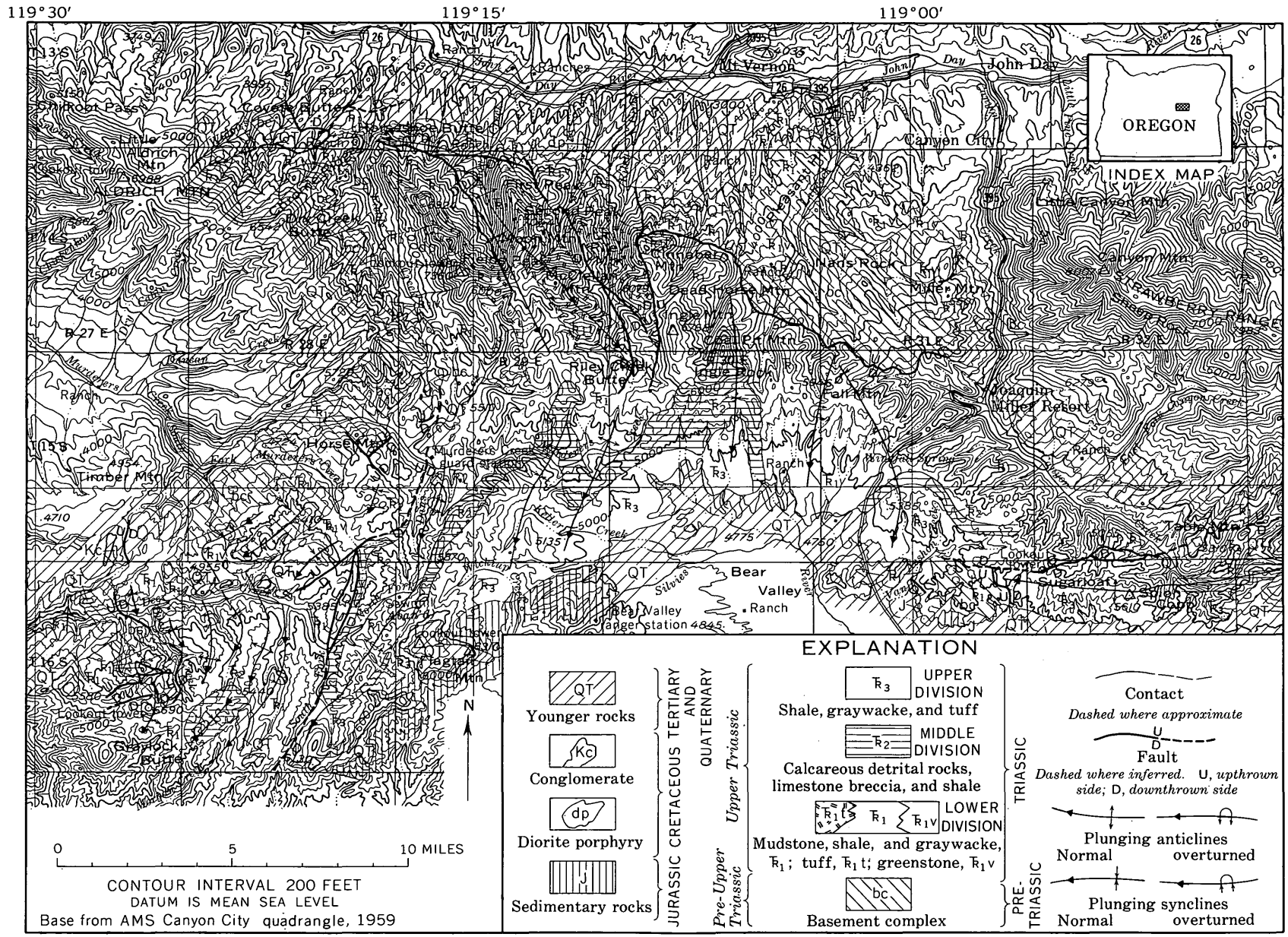

FIGURE 139.1—Geologic map of the Upper Triassic rocks in the Aldrich Mountains, Oreg.

mainly of well-bedded coarse- to fine-grained graywacke and shale in which the matrix is mostly carbonate. Its basal part contains lenticular masses of limestone breccia and conglomerate as much as 75 feet thick and 1,200 feet long associated with beds of detrital limestone.

The upper division consists mainly of graywacke and shale whose total thickness is between 5,000 and 7,000 feet. It contains only a few thin layers of tuff. In the valley of the South Fork of Deer Creek the lower part of this unit contains at least a thousand feet of cobbly mudstone in which many of the cobbles are of Paleozoic limestone. This division is overlain unconformably by Lower Jurassic beds.

The area mapped is believed to cover the northwestern corner of a large basin of deposition. Along the western margin of the basin the Triassic rocks lie on a basement of Paleozoic metavolcanic rocks and serpentine. The present northern border of the basin, where not concealed under younger rocks, is a steep north-dipping reverse fault, along which Paleozoic rocks, serpentine, and Triassic rocks believed to be part of the lower member of the lower division lie against overturned Upper Triassic beds. The successive divisions and members overlap eastward and southward on angular unconformities. The middle member of the lower division lies across tight folds of northeasterly trend that involve the lower member. The upper member in turn lies across folds of northwesterly trend in the middle member, and changes abruptly in thickness across faults related to the folds. The middle and upper divisions together lie partly conformably, partly unconformably, across the lower unit, and in places they are themselves separated by erosional unconformities.

Strong and almost continuous deformation while the rocks were accumulating is recorded by the nature of the sediments and by numerous unconformities. The abrupt thickening in the beds of the upper member of the lower division where they cross folds and faults in the middle member can be explained only by contemporaneous fault movements of 3,000 to 4,000 feet. Several lines of evidence indicate recurrent movement totaling many thousands of feet along the northern border fault; this movement began at least as early as the deposition of the middle member of the lower division, and it involved beds of the upper division. The northeast-trending folds in the middle and upper division differ in strike by 60 to 70 degrees from the older northwest-trending major folds in the middle member of the lower division, and tight cross-folding has been found only in the lower member of the lower division. The prevalence of materials deposited by mass transport, such as slide breccias, cobbly mudstones, massive graywackes, and graded graywackes, shows that conditions around the margins of the basin were unstable, and the abundance of reworked Upper Triassic debris in the conglomerates and breccias shows extensive "cannibalism" of the rocks soon after their deposition. Diagnostic fossils and unconformable relations with overlying Jurassic formations indicate that all the rocks here described were probably deposited during the later half of Late Triassic (Norian) time, and were deformed as shown in figure 139.1 before Early Jurassic (Sinemurian) time.

Although even the upper division has been tightly folded and overturned in places, none of the rocks are foliated. Much of the coarser tuff and graywacke is extensively altered to laumontite, prehnite, albite, and chlorite, and pumpellyite is common in the lavas. Except for local development of actinolite, mica, and pyroxene near contacts with later intrusives, the rocks are in the zeolite metamorphic facies described by Coombs and others (1959).

REFERENCE

Coombs, D. C., Ellis, A. J., Fyfe, W. S., and Taylor, A. M., 1959, The zeolite facies, with comments on the interpretation of hydrothermal syntheses: Geochm. et Cosmochim. Acta, v. 17, p. 53–107.

140. THE JOHN DAY FORMATION IN THE MONUMENT QUADRANGLE, OREGON

By Richard V. Fisher and Ray E. Wilcox, Denver, Colo.

The Monument quadrangle, located in Grant County, Oreg., 30 miles northwest of the town of John Day, includes the Clarno formation of Eocene age, the John Day formation of late Oligocene and early Miocene age, the Columbia River basalt of Miocene age, and the Rattlesnake formation of Pliocene and Pleistocene age. The John Day formation is exposed mainly in the southern part of the quadrangle. It has an aggregate

thickness of about 950 feet, and consists of primary and reworked pyroclastic material that fell on dry land. The lower part, which is dominantly deep red, grades upward through lighter red, green, and buff beds into the light-gray and buff material that forms the upper part. We have tentatively divided the formation into three members, which do not strictly conform to those proposed by Merriam (1901) for the section at Picture Gorge:

	Monument quadrangle	Local measured thickness (feet)	Merriam (1901)
John Day formation	Upper member	346	Upper division.
	Middle member (welded tuff locally present in upper part).	530	Middle division.
	Lower member	67	Lower division.

LOWER MEMBER

The lower member consists of deep-red friable mudstones and siltstones, rich in montmorillonitic clays and locally containing black manganese- and barium-bearing nodules. It weathers to a clayey, silty red soil. A thickness of 67 feet of this member was measured in NE¼ sec. 30, T. 9 S., R. 28 E., but there its base is not exposed. Four miles away, near the town of Hamilton (sec. 3, T. 10 S., R. 28 E., Courtrock quadrangle), the member is 241 feet thick and lies upon weathered andesite of the Clarno formation. Its top is taken as the contact with a thin but distinctive layer of tuff containing fragments of green phyllite. No mammal or plant remains were found in this member in the Monument quadrangle.

MIDDLE MEMBER

The middle member may be divided into two parts, the lower dominantly reddish and the upper colored in light shades of red, yellow, gray, and green. Its composite thickness is 530 feet. Its rocks weather to a hard, cloddy soil that is distinct from the soils on the upper and lower members, and it erodes into a characteristic pinnacled badlands topography. It is found under the microscope to consist mainly of glass fragments, largely altered to a zeolite (clinoptilolite?), mixed with montmorillonite and opaline material. Although this member appears distinctly bedded when viewed from a distance, it has few sharply defined bedding planes. Some layers contain rounded and subangular aggregates up to an inch in diameter that have the same general constitution as the surrounding material. Vertebrate remains occur in this member, being most common in its upper part, but here as elsewhere in the formation they are usually disarticulated.

A layer of welded tuff, about 50 feet in maximum thickness, is locally present in the upper part of this member. In E½ sec. 13, T. 9 S., R. 27 E., where this tuff lies 140 feet below the top, a layer of tuff 13 feet below it contains a few fossil leaves, and apparently equivalent layers occur below the welded tuff in SW¼ sec. 6, T. 9 S., R. 28 E., and in SW¼ sec. 9, T. 9 S., R. 27 E. This welded tuff layer may be equivalent to a similar layer near Picture Gorge that Merriam (1901) regarded as the top of his "Middle division" of the John Day formation. At its contact with the upper member there is a marked change in color and soil type.

UPPER MEMBER

The upper member, which is 346 feet thick in SE¼ sec. 28, T. 9 S., R. 28 E., is characterized by light-gray or buff colors and weathers to silty powdery soil. It is found under the microscope to consist mainly of glass fragments partly altered to clay (montmorillonite?); both siliceous and basaltic glass shards are present, and the rock contains iddingsite pseudomorphs after olivine. Bedding is inconspicuous in the upper member, except where it is marked by local conglomeratic and sandy beds consisting of reworked John Day material. In many places at the base of the overlying Columbia River basalt, beds of reworked basaltic pyroclastics occur, and these perhaps are more appropriately regarded as part of the Columbia River basalt.

Structures within the John Day formation are relatively simple, with dips generally less than 25°. The apparent folds (regarding which more will be said presently) form a branching rather than a parallel pattern, and they plunge in various directions. Dips are usually gentler in the upper member than in the middle member. The formation is cut by fractures and by feeder dikes of the Columbia River basalt, both trending north-northwest, and the beds are locally disturbed by boss-like intrusions of basalt. A major normal fault near the southern edge of the quadrangle drops John Day beds on the north side against volcanics in the Clarno formation, and also cuts the Columbia River basalt.

ORIGIN

The preponderance of pyroclastic material in the John Day formation and the evidence that it could not have been deposited in lakes, as formerly presumed, was pointed out by Calkins (1902). In the Monument quadrangle the John Day formation was apparently deposited during a prolonged period of pyroclastic

volcanic activity in a nearby region. The pyroclastic debris in the lower member is mixed, however, with much red clay and silt, probably derived from saprolite developed on the Clarno formation. The smaller proportion of red material in the middle and upper members is presumably due to progressive mantling of the Clarno rocks by volcanic ash.

Some beds consisting almost exclusively of pyroclastic material may have been formed by thicker falls of ash that remained where it fell. The bulk of the material, however, appears to have been deposited in such small increments that it did not greatly interfere with the growth of animals and plants. This indicates that most of the material in the formation was carried in by the winds from weathered surfaces and loose primary pyroclastic deposits. The rounded and subangular aggregates found locally in some beds are ascribed to colluvial action.

The structures that simulate folds may be regarded as mainly due to initial dips in material mantling a ridge-and-valley topography which became progressively more subdued as deposition continued. The welded tuff at the top of the middle member represents an ash flow that followed the valleys. During diagenesis of the buried sediments, differential compaction locally increased the dips, especially in material that contained much clay, and intrusion by the feeders of the Columbia River basalt resulted in further local disturbances.

REFERENCES

Calkins, F. C., 1902, A contribution to the petrography of the John Day Basin: California Univ., Dept. Geol. Sci. Bull., v. 3, p. 109–172.

Merriam, J. C., 1901, A contribution to the geology of the John Day Basin, Oregon: California Univ., Dept. Geol. Sci. Bull., v. 2, p. 269–314.

141. THE REPUBLIC GRABEN, A MAJOR STRUCTURE IN NORTHEASTERN WASHINGTON

By Mortimer H. Staatz, Denver, Colo.

A large graben, named for the old gold-mining town of Republic, has been outlined in the central part of the Okanogan Highlands, and mapped in detail by R. L. Parker, J. A. Calkins, S. J. Muessig, and M. H. Staatz (fig. 141.1). The graben is about 4 to 10 miles wide and at least 52 miles long. It is bounded on the northwest by the branching faults that make up the Scatter Creek fault zone, and on the southeast by the Sherman fault. The bounding faults are either nearly vertical or dip toward the middle of the graben. The total vertical displacement on them is not known, but in the northern part of the Bald Knob quadrangle the middle of the graben is at least 7,000 feet lower structurally than the adjacent blocks.

Rocks formed before the graben faulting include metamorphosed sedimentary and igneous rocks, unmetamorphosed intrusive rocks in stocks and batholiths of Mesozoic and early Tertiary age, and intrusive porphyry and volcanic rocks that are probably Eocene. Rocks formed during and after the graben faulting are intrusive porphyry and volcanic extrusives. The volcanics are mainly rhyodacite flows but include some beds of tuff and breccia. Over 90 percent of them were formed after the graben started to subside.

The flows are the extrusive equivalents of the porphyry, and are closely similar to them in mineral and chemical composition. In the central part of the Bald Knob quadrangle a rhyodacite body showing intrusive relations along its west side has been traced eastward into extrusive rhyodacite with well-developed flow structure. Dikes and other small intrusions of porphyry are found both inside and outside the graben; the volcanic rocks, however, are now found only within the graben, having elsewhere been eroded away. Porphyry masses that probably solidified in volcanic vents occur at a number of places within the graben, but are most common along the marginal faults. The flows were likewise extruded mainly along the marginal faults although some rose along smaller breaks within the graben.

The Republic graben was formed in early or middle Tertiary time. It started to sink soon after the earliest volcanic rocks were erupted, and continued to sink while the succeeding thick flows and pyroclastic rocks were erupted. The sinking of this block was caused by the weight of the thick sequence of volcanic rocks deposited on its top, coupled with removal of the support that was given by the volcanic material before it was ex-

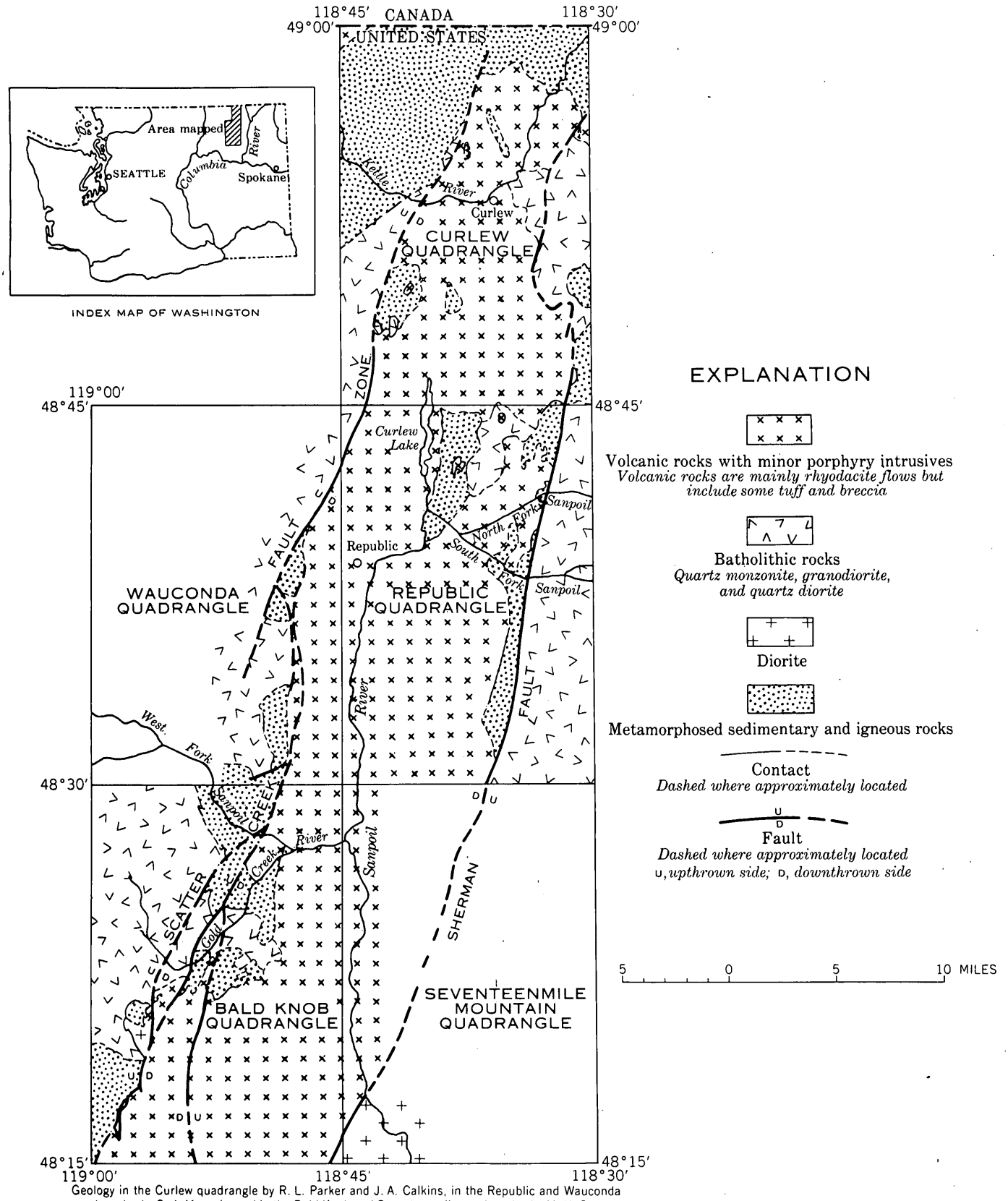

Geology in the Curlew quadrangle by R. L. Parker and J. A. Calkins, in the Republic and Wauconda quadrangles by S. J. Muessig, and in the Bald Knob and Seventeenmile quadrangles by M. H. Staatz

FIGURE 141.1.—Generalized geologic map of the Republic graben.

truded. Five angular unconformities that separate tuff beds in different parts of the graben indicate that the graben sank unevenly. The sinking was probably almost continuous but varied in direction and amount.

During and since the formation of the graben the rocks of this region were eroded, and any volcanic rocks that may have accumulated on the blocks adjacent to the graben were thus removed. Several small bodies of porphyry are found in the adjacent blocks, and some of these presumably fill vents from which flows were extruded. The volcanic rocks in the graben itself were protected from erosion because of their lower elevations.

The Republic graben has remarkably little topographic expression for so large a structural feature. The surrounding mountains have gently rounded tops, and in many places one observes little difference of relief in passing across the graben.

142. SUGGESTED SOURCE OF MIOCENE VOLCANIC DETRITUS FLANKING THE CENTRAL CASCADE RANGE, WASHINGTON

By Leonard M. Gard, Jr., Denver, Colo.

Poorly consolidated pumiceous fluvial and lacustrine sediments of late Miocene age, interbedded with ash layers and volcanic mudflows, have been recognized on the west flank of the Cascade Range in Washington (Mullineaux, Gard, and Crandell, 1959) (fig. 142.1). As these deposits contain fragments of hornblende, and of hornblende andesite that is markedly different from the earlier Tertiary pyroxene-rich volcanic rocks that predominate in the central Cascade Range, they may be products of an eruptive phase of the Snoqualmie granodiorite batholith.

These sediments are correlated in part, on the basis of lithologic similarity and age (Mullineaux, Gard, and Crandell, 1959, p. 695), with the Ellensburg formation (Miocene-Pliocene) which overlaps the east flank of the Cascades (fig. 142.1). The Ellensburg also is characterized by pumiceous volcanic mudflows and alluvial deposits rich in hornblende andesite debris, which according to Waters (1955, p. 673) was derived from a growing chain of explosive andesitic volcanoes to the west of the Yakima area. But although the volcanic materials in the Ellensburg must have been derived from vents in the Cascades, none of these vents have been recognized. Waters (1955, p. 664) states that extensive remnants of volcanoes of the requisite age are exposed in the present Cascade Mountains, but he does not specifically identify or locate any one of these remnants, and a search of the published literature has not revealed any reference to them.

The Snoqualmie granodiorite was intruded into earlier Tertiary rocks that now form much of the Cascade Range. The time of intrusion is inexactly known. Warren (1941, p. 797) indicated that it was intruded in Oligocene(?) time, whereas Smith and Calkins (1906) suggested a late Miocene age of intrusion. Coombs (1936, p. 167), as well as Smith and Calkins, pointed out that green hornblende and biotite are the predominant ferromagnesian minerals in the granodiorite. Fuller[1] suggested that the lack, in the Snoqualmie granodiorite, of both ore deposits and late differentiates was due to its having solidified prematurely because it lost a vast quantity of volatile constituents that broke through to the surface.

It is here suggested that the magma reached the surface and the volatile constituents were given off during explosive volcanism. This eruptive phase of the Snoqualmie produced the hornblende-bearing pumice, ash, and mudflow deposits of late Miocene age now preserved only on the flanks of the Cascades. If, as suggested here, the Snoqualmie is the source of this volcanic detritus, then at least some granodiorite must have been intruded in late Miocene time. Recently published information by Waters (1955, p. 664) and Cheney (1959, p. 122) indicates that the upper part of the Ellensburg formation is of early Pliocene age. The abundance of newly erupted volcanic material in the Ellensburg suggests that the extrusive phase of the Snoqualmie might have lasted into early Pliocene time. Snoqualmie volcanoes probably have been removed completely by erosion that has exposed the top of the batholith in many places (fig. 142.1). This idea, although partly anticipated some 35 years ago, has recently been reached independently and by way of different lines of evidence

[1] Fuller, R. E., 1925, The geology of the northeastern part of the Cedar Lake quadrangle, with special reference to the deroofed Snoqualmie batholith: Washington Univ. [Seattle], unpublished Master's thesis.

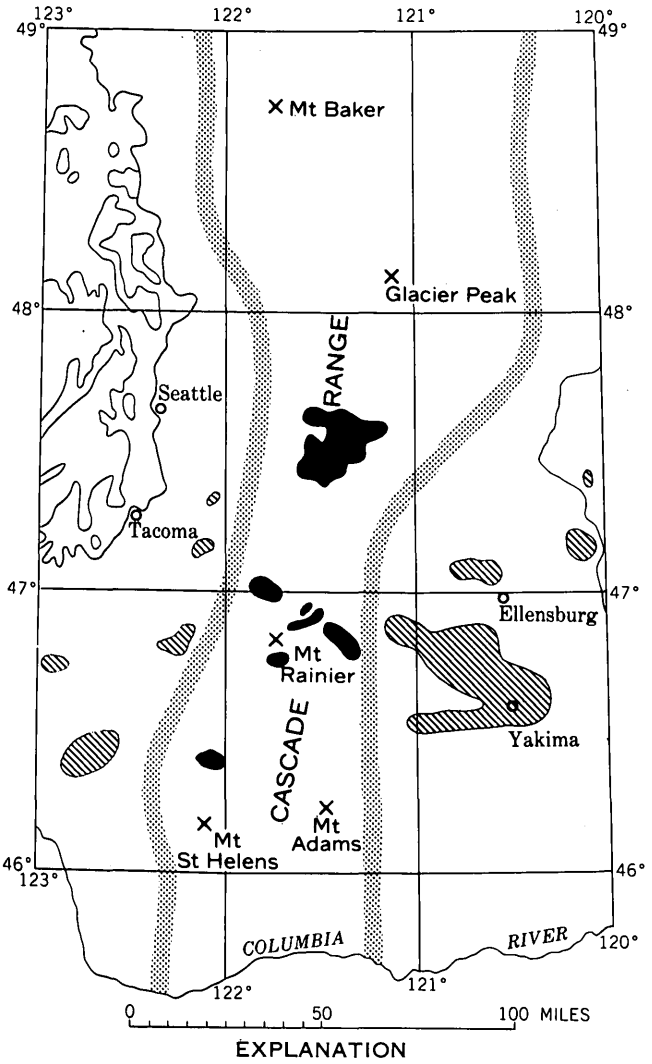

FIGURE 142.1.—Sketch map of Miocene intrusive rocks and related volcanic debris in and near the central Cascade Range, Wash.

by others working in the central Cascade Range. Therefore, more evidence on the problem will be forthcoming.

REFERENCES

Cheney, R. W., 1959, Miocene floras of the Columbia River Plateau: Carnegie Inst. of Washington Publ. 617, Part 1, 134 p.

Coombs, H. A., 1936, The geology of Mount Rainer National Park: Washington Univ. [Seattle] Pub. *in* Geology, v. 3, no. 2, p. 121–212.

Mullineaux, D. R., Gard, L. M., and Crandell, D. R., 1959, Continental sediments of Miocene age in the Puget Sound lowland, Washington: Am. Assoc. Petroleum Geologists Bull., v. 43, p. 688–696.

Roberts, A. E., 1958, Geology and coal resources of the Toledo-Castle Rock district, Cowlitz and Lewis Counties, Washington: U.S. Geol. Survey Bull. 1062, 71 p.

Smith, G. O., and Calkins, F. C., 1906, Description of the Snoqualmie quadrangle, Washington: U.S. Geol. Survey Geol. Atlas, Folio 139.

Snavely, P. D., Jr., Brown, R. D., Roberts, A. E., and Rau, W. W., 1958, Geology and coal resources of the Centralia-Chehalis district, Washington: U.S. Geol. Survey Bull. 1053, 159 p.

Washington Division of Geology, 1936, Preliminary geologic map, State of Washington: Washington State Dept. Conserv. and Devel., scale 1 : 500,000.

Warren, W. C., 1941, Relation of the Yakima basalt to the Keechelus andesitic series: Jour. Geology, v. 49, no. 8, p. 795–814.

Waters, A. C., 1955, Geomorphology of south-central Washington, illustrated by the Yakima East quadrangle: Geol. Soc. America Bull., v. 66, p. 663–684.

143. LATE RECENT AGE OF MOUNT ST. HELENS VOLCANO, WASHINGTON

By D. R. MULLINEAUX and D. R. CRANDELL, Denver, Colo.

Mount St. Helens is a high symmetrical stratovolcano on the western flank of the Cascade Range in southern Washington. The modern cone, composed of pyroxene andesite and olivine basalt, is built on an older cone of hornblende dacite and hornblende-hypersthene andesite (Verhoogen, 1937). From the time of the early geological exploration of the Pacific Northwest in the 19th century, the smooth slopes and lack of pronounced glacial features on Mount St. Helens have been interpreted as evidence that the volcano is young. Verhoogen believed that many flows from the mountain were no more than a few hundred years old, and he noted that actual eruptions were reported in 1842 and

1854. Because of the topographic evidence and the absence of olivine basalt stones in terrace deposits in the Toutle River valley northwest of the volcano, Verhoogen dated the modern volcano as Recent. He regarded the terrace deposits as glaciofluvial gravel derived from the older Mount St. Helens during Pleistocene time.

Our studies indicate that the terrace deposits in the Toutle River valley consist of interbedded debris flows and alluvium composed almost entirely of the older rocks from Mount St. Helens. These deposits are traceable downvalley for a distance of 55 miles. A fragment of a conifer stem and branch from within a debris flow in the terrace deposits at Silver Lake, 25 miles west of the volcano, has a radiocarbon age of 2,030±240 years (U.S. Geological Survey sample W–811, Meyer Rubin, written communication).

In the upper part of the debris flow that contained the wood is a soil about 12 inches thick, consisting of a humified zone and an oxidized zone, separated by a thin lighter colored layer that is interpreted as the bleached horizon of a podzolic soil. This soil is overlain by alluvial gravel, which is overlain in turn by two younger debris flows. None of these deposits contain stones of either the pyroxene andesite or the olivine basalt typical of the modern Mount St. Helens. The uppermost debris flow, which forms the top of the terrace here, is oxidized to an average depth of about 18 inches, but no bleached horizon has been seen under the 1- to 2-inch layer of organic material at the top. As environmental conditions during the formation of the two soil profiles were probably similar, the lower profile probably required at least as long a time to form as the upper profile. If so, the volcano must have continued to erupt only the hornblende dacite and hornblende-hypersthene andesite of the older Mount St. Helens for another thousand years after the dated wood was incorporated.

From the composition of the debris flows, the radiocarbon age of the wood sample, and the soil profiles within the flows, it is inferred that Mount St. Helens did not begin to erupt the olivine basalt and pyroxene andesite of the present cone until very late in Recent time, and that the modern cone may well be a product of the last thousand years.

REFERENCE

Verhoogen, Jean, 1937, Mount St. Helens, a recent Cascade volcano: California Univ. Dept. Geol. Sci. Bull., v. 24, p. 263–302.

144. CENOZOIC VOLCANISM IN THE OREGON CASCADES

By Dallas L. Peck, Menlo Park, Calif.

Work done in cooperation with the Oregon Department of Geology and Mineral Industries

The Cascade Range in Oregon comprises two major sequences of volcanic rocks of Cenozoic age (Callaghan, 1933). The older sequence, the volcanic rocks of the Western Cascades, makes up the western slope of the range, and consists of warped, faulted, and partially altered upper Eocene to upper Miocene flows and pyroclastic rocks, 12,000 feet thick on the average. The younger sequence, the volcanic rocks of the High Cascades, forms the crest and most of the eastern slope of the range, and consists predominantly of unaltered and undeformed Pliocene to Recent andesite[1] and basalt flows from relatively undissected shield and stratovolcanoes (Williams, 1942).

[1] The rock classification of Williams and others (1954) is followed in this report.

The age, lithology, and thickness of the major volcanic units of the Cascade Range are summarized in table 144.1.

The formations are dated on the basis of fossil plants from more than 50 localities. Marine strata that underlie and interfinger with the volcanic rocks along the western foothills have yielded fossil mollusks and Foraminifera of Eocene, Oligocene, and early Miocene age. Fossiliferous lacustrine and fluviatile tuffaceous strata of late Miocene and Pliocene age interfinger with the volcanic rocks along the eastern and western flanks of the range.

The rocks of the Cascades are calc-alkaline, similar chemically to Nockolds' (1954) average "central" basalt, andesite, dacite, rhyodacite, and dellinite. They have

TABLE 144.1.—*Summary of the major Cenozoic units in the Cascade Range in Oregon*

Age	Name	Lithology	Thickness (feet)
Pliocene and Quaternary.	Volcanic rocks of the High Cascades.	Flows and minor pyroclastic rocks of olivine andesite and olivine basalt, subordinate pyroxene andesite, and minor dacite. Flows are typically porous textured and sparsely porphyritic, and contain phenocrysts of olivine that are partially altered to iddingsite. Vents represented by line 5 in fig. 144.1.	0–73,000
		—Unconformity—	
Middle and late Miocene.	Unnamed volcanic formation.	Flows, tuff breccia, and tuff of hypersthene andesite and mafic hypersthene dacite, subordinate labradorite andesite, olivine andesite, augite andesite, and mafic dacite, and sparse felsic dacite and olivine basalt. Flows are typically platy and porphyritic, and contain phenocrysts of calcic plagioclase and prismatic black hypersthene. Massive beds of mudflow breccia are locally abundant. Vents represented by line 4 in fig. 144.1.	0–10,000, avg about 3,000.
Middle Miocene	Columbia River basalt.	Flows of tholeiitic basalt and basaltic andesite. Flows are typically columnar-jointed, and are composed of very fine-grained black basalt that contains abundant glass, intermediate plagioclase, augitic pyroxene, and chlorophaeite, but little or no olivine. Extruded from fissures that are outside the Cascade Range and not shown on fig. 144.1; present only locally within the range.	0–2, 500
		—Unconformity—	
Oligocene and early Miocene.	Unnamed volcanic series.	Dacitic and andesitic tuff and less abundant flows and breccia of olivine basalt, olivine andesite, and pyroxene andesite, dacitic and rhyodacitic flows and domes, and rhyodacitic tuff. Pumice lapilli vitric tuff in massive beds that were presumably deposited as glowing avalanches is the most abundant rock type. Basaltic flows typically contain sparse phenocrysts of pyroxene (salite) and altered olivine, as well as microphenocrysts of calcic plagioclase and pyroxene. The series contains internal disconformity east of Eugene. Vents represented by lines 1, 2, and 3 in fig. 144.1.	3, 000–15, 000
		—Local unconformity—	
Late Eocene	Colestin formation	Andesitic tuff, conglomerate tuffaceous siltstone and sandstone, and less abundant flows and breccia of olivine andesite and pyroxene andesite. Location of vents uncertain, questionably represented by line 1 on fig. 144.1.	0–3, 000

a total volume of about 30,000 cubic miles. Andesite that has a silica content of about 56 percent is the most abundant rock type; rocks containing 63 to 68 percent silica are sparse, and rocks that have about 70 percent silica are moderately abundant. The nature and relative abundance of phenocrysts in the volcanic rocks of different composition are shown in figure 144.1.

The Miocene and older volcanic rocks are partly altered. Throughout most of the Western Cascades volcanic glass in pyroclastic rocks and flows is replaced by fine-grained aggregates consisting chiefly of zeolite (mordenite or clinoptilolite) or alkalic feldspar, together with cristobalite or chalcedonic quartz and montmorillonitic clay. In restricted areas around former volcanic centers the rocks are propylitically altered and are intruded by small dioritic and granitic stocks, pipes, and dikes.

The regional alinement of successive series of vents of the volcanic rocks of the Cascade Range in Oregon is indicated in figure 144.2. Vents for the different volcanic units are apparently alined in northward trending belts that generally shifted progressively eastward during the Cenozoic. During the latter part of the Oligocene and the early Miocene groups of vents were alined in two separate belts; vents in the western belt yielded mostly flows of olivine basalt and olivine andesite whereas contemporaneous vents farther east yielded mostly dacitic and rhyodacitic pyroclastic rocks.

REFERENCES

Callaghan, Eugene, 1933, Some features of the volcanic sequence in the Cascade Range in Oregon: Am. Geophys. Union, Trans. 14th Ann. Mtg., p. 243–249.

Nockolds, S. R., 1954, Average chemical compositions of some igneous rocks: Geol. Soc. America Bull., v. 65, p. 1007–1032.

Williams, Howel, 1942, The geology of Crater Lake National Park, Oregon, with a reconnaissance of the Cascade Range southward to Mount Shasta: Carnegie Inst. Washington Pub. 540, 162 p.

———1954, in Williams, Howel, Turner, F. J., and Gilbert, C. M., Petrography—an introduction to the study of rocks in thin sections: San Francisco, W. H. Freeman and Co., 406 p.

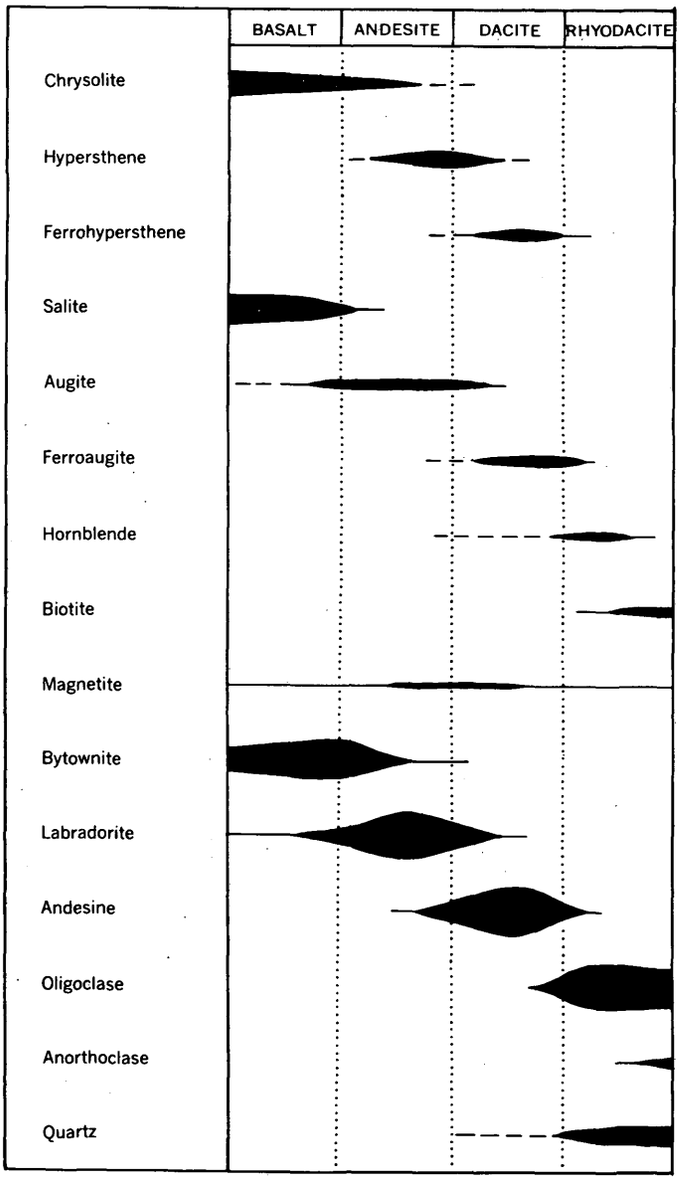

FIGURE 144.1.—Phenocrysts in volcanic rocks of the Cascade Range in Oregon.

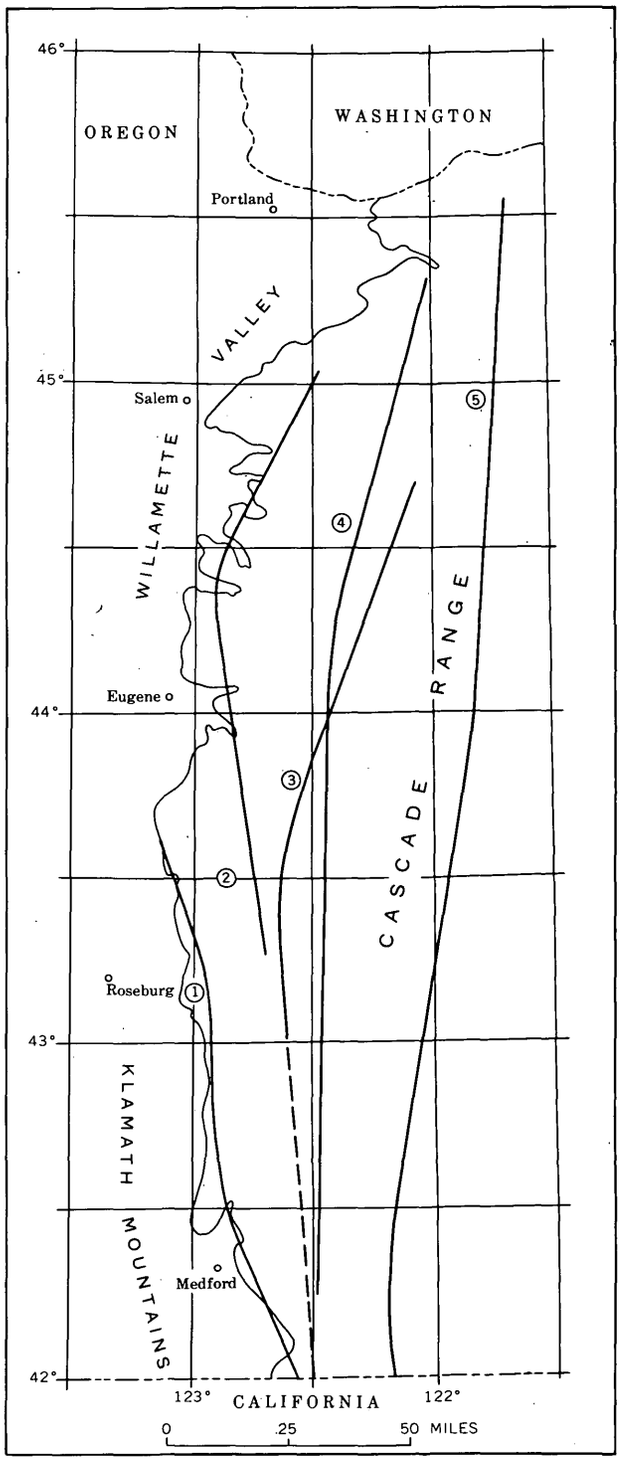

FIGURE 144.2.—Center lines of belts of vents of Cenozoic volcanic rocks in the Cascade Range in Oregon. 1, Vents of upper Eocene(?) and lower Oligocene andesitic volcanic rocks; 2, middle Oligocene to lower Miocene flows of basalt and basaltic andesite; 3, Oligocene and lower Miocene dacitic, andesitic, and rhyodacitic pyroclastic rocks; 4, middle and upper Miocene andesitic volcanic rocks; 5, Pliocene and Quaternary andesitic and basaltic volcanic rocks.

145. RODINGITE FROM ANGEL ISLAND, SAN FRANCISCO BAY, CALIFORNIA

By JULIUS SCHLOCKER, Menlo Park, Calif.

The calcium silicate-rich rock rodingite, found in serpentine thorughout the world, is also found in the serpentine of Angel Island, in San Francisco Bay, Calif. Rodingite at other localities is described as forming altered dikes of calcium-rich gabbro or diorite, though a rodingite in the Ural Mountains is said to form pyroxenite schlieren in serpentine (Baker, 1959, p. 33; Suzuki, 1953, p. 425; Miles, 1950, p. 126; Cater and Wells, 1953, p. 103, Wells, Hotz, and Cater, 1949, p. 12).

The serpentine that encloses the rodingite on Angel Island is a steep, tabular body, about 600 feet thick, squeezed into rocks of the Franciscan formation. The rodingite occurs, together with various clearly metamorphic rocks, in scattered, isolated fragments oriented at random in the serpentine. These are all "tectonic inclusions" as defined by Brothers (1954, p. 616). The inclusions of rodingite are round masses 1 to 4 feet in diameter. They are fine- to medium-grained, are very tough, and generally have a specific gravity well above 3.0. Their color ranges from light yellowish gray to dark greenish gray. The most conspicuous and abundant ones have light-colored cores and medium- to dark-gray rims 1 to 3 inches thick (fig. 145.1).

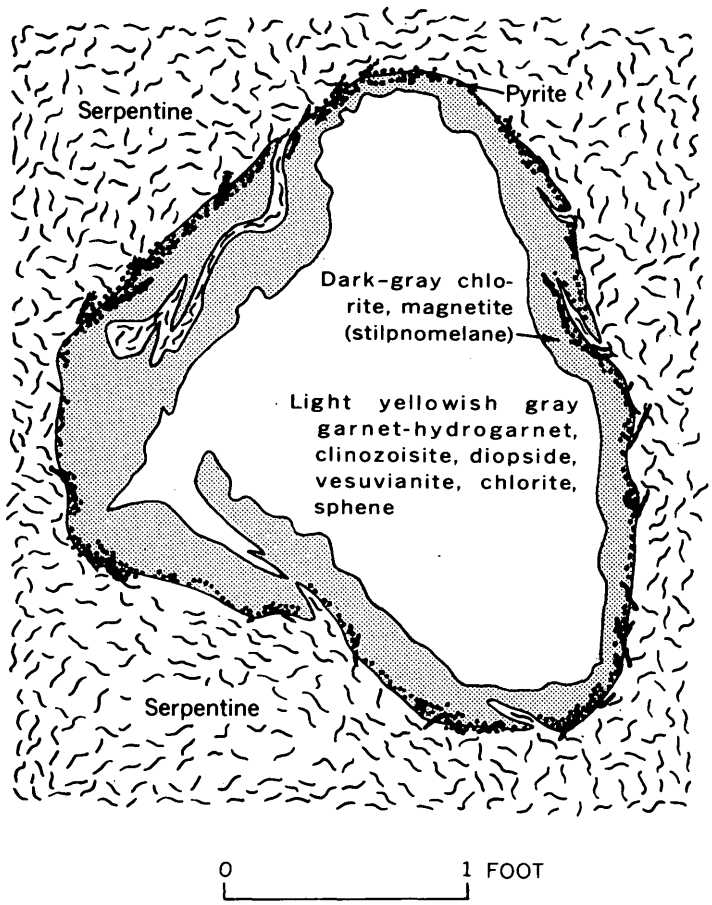

FIGURE 145.1.—Diagrammatic sketch of typical rodingite inclusion, Angel Island, San Francisco Bay, Calif.

MINERALOGY

The Angel Island rodingite consists mainly of calc-silicates and several species of chlorite. Several mineralogical types have been recognized: garnet-vesuvianite, garnet-chlorite-vesuvianite, clinozoisite-diopside-garnet-vesuvianite, chlorite-sphene-vesuvianite, and diopside-chlorite. Accessories are calcite, magnetite, ilmenite, pyrite, stilpnomelane, garnet, vesuvianite, sphene, and chlorite.

The composition of the garnets and garnet-like minerals, which are abundant in most of the Angel Island rodingite, was determined by measuring refractive indices and unit-cell edges. Graphs of Sriramadas (1957, p. 295–296) show that one specimen of garnet is approximately 45 percent grossularite and 45 percent andradite. More common are garnet-like minerals whose refractive index is too low and whose unit-cell edge is too large for garnet. These fall on Winchell and Winchell's (1951, p. 493) graph for minerals of the garnet-hydrogarnet (hibschite) series, which consist of the following four components: grossularite ($Ca_3Al_2(SiO_4)_3$), andradite ($Ca_3Fe_2(SiO_4)_3$), $Ca_3Al_2O_6 \cdot 6H_2O$, and $Ca_3Fe_2O_6 \cdot 6H_2O$. The Angel Island garnet-hydrogarnets contain 40 to 70 percent grossularite, 30 to 60 percent andradite, and 1 to 1.2 moles H_2O. Hydrogrossular, a hydrogarnet high in grossularite containing 0.72 moles H_2O, was first identified in rodingite from New Zealand (Hutton, 1943, p. 174–180) and has been found in other rodingites (Miles, 1950, p. 128).

The dark rims found on most rodingite inclusions consist predominantly of chlorite and disseminated magnetite. Calc-silicates, similar to those in the rodingite cores, are generally present in small amount near the inner borders of the rims. Stilpnomelane veinlets occur in these rims, and also veinlets and masses of antigorite. A pyrite-rich zone is found on or near the borders of some rodingite inclusions.

ORIGIN OF ANGEL ISLAND RODINGITE

The origin of some of the rodingite is indicated by relict textures and minerals. Euhedral to subhedral crystals of diopsidic augite occur in what appear to be relicts of a porphyritic rock or a crystal tuff. Some of the rodingite, however, shows well-preserved textures of porphyritic basaltic glass or tachylite identical with those found in surficial volcanic rocks (greenstones) of the Franciscan formation of Angel Island (Schlocker and others, 1958). What appear to be relict vesicles and euhedral laths, probably once plagioclase, are now mostly represented by masses of colorless chlorite sharply outlined against a groundmass of cloudy garnet aggregates. The groundmass shows irregular, flat-sided and rounded masses identical in structure with those seen in tachylitic pyroclastic rocks and pillow greenstones of the Franciscan formation. Greenstone structures and textures are also represented in the dark rims of the rodingite fragments by layers consisting of tiny aggregates of magnetite, sphene, and garnet embedded in chlorite.

Rodingite of tachylite origin may be older than, or contemporaneous with, serpentine; other rodingite may be younger than serpentine. Veins of serpentine in rodingite merely show that the veining is younger than the rodingite. The high mobility of serpentine complicates the problem of deciding relative age on the basis of cross cutting, for crustal pressures may have mobilized the serpentine many times after it was first formed. Some of the Angel Island rodingite may have formed igneous dikes which cut an ultramafic rock but which were broken up and moved about during and after the serpentinization of that rock. Fragments of tachylitic greenstone may have become altered to rodingite either before or after they were caught up in the serpentine. Other masses of rodingite throughout the world are generally regarded as dikes cutting older serpentine; Baker (1959, p. 33), however, concluded that the Tasmanian rodingite formed before the serpentine intruded it.

Although no chemical analyses of the Angel Island rodingites are yet available, the mineral content of the rocks indicates that the conversion of greenstone to rodingite was accompanied by a considerable increase in calcium and loss of silica. A calculation was made on the assumption that the dark rims were originally greenstone and that the additional calcium in the cores was derived from them, but this calculation showed that the cores contained considerably more calcium than could have been obtained from the rims. Serpentinization of diallage, which was probably common in the original ultramafic rock, may have freed calcium that migrated to tectonic inclusions of rocks such as greenstone, which were probably the only other calcium-bearing materials in the ultramafic rock, and the calcium may have become bonded to other atoms in the inclusions to form calc-silicates. Such a concentration of calcium could have been accompanied by migration of silica from the inclusion to the surrounding silica-undersaturated ultramafic rock.

If tectonic inclusions of greenstone of the Franciscan formation were converted to rodingite, the same change may have operated on other rocks of the formation, similar in chemical composition, such as volcanic graywackes.

REFERENCES

Baker, George, 1959, Rodingite in nickeliferous serpentinite, near Beaconsfield, Northern Tasmania: Geol. Soc. Australia Jour., v. 6, pt. 1, p. 21–35.

Brothers, R. N., 1954, Glaucophane schist from the north Berkeley Hills, California: Am. Jour. Sci., v. 252, p. 614–626.

Cater, F. W., Jr., and Wells, F. G., 1953, Geology and mineral resources of the Gasquet quadrangle, California-Oregon: U. S. Geol. Survey Bull. 995–C, p. 79–133.

Hutton, C. O., 1943, Hydrogrossular, a new mineral of the garnet-hydrogarnet series: Royal Soc. New Zealand Trans., v. 73, p. 174–180.

Miles, K. R., 1950, Garnetized gabbros from the Eulaminna district, Mount Margaret Goldfield: Western Australia Geol. Survey Bull. 103, pt. 2, p. 108–130.

Schlocker, Julius, Bonilla, M. G., and Radbruch, D. H., 1958, Geology of the San Francisco North quadrangle, California: U.S. Geol. Survey Misc. Geol. Inv. Map I–272.

Sriramadas, A., 1957, Diagrams for the correlation of unit cell edges and refractive indices with the chemical composition of granites: Am. Mineralogist, v. 42, nos. 3–4, p. 294–298.

Suzuki, Jun, 1953, On the rodingitic rocks within the serpentinite masses of Hokkaido: Jour. Fac. Sci. Hokkaido Univ., ser. 4, v. 8, no. 4, p. 419–430.

Turner, F. J., and Verhoogen, Jean, 1951, Igneous and metamorphic petrology: New York, McGraw-Hill Book Co., Inc., 602 p.

Wells, F. G., Hotz, P. E., and Cater, F. W., Jr., 1949, Preliminary description of the Kerby quadrangle, Oregon: Oregon Dept. Geology and Mineral Industries Bull. 40, p. 1–23.

Winchell, A. N., and Winchell, Horace, 1951, Elements of optical mineralogy, 4th ed.: New York, John Wiley and Sons, 551 p.

146. GRAVITY ANOMALIES AT MOUNT WHITNEY, CALIFORNIA

By H. W. Oliver, Washington, D.C.

A gravity station on the top of Mount Whitney, California, was occupied with a Worden gravimeter on August 18, 1957, in connection with a regional gravity study of the southern half of the Sierra Nevada. The station was established by L. C. Pakiser and G. Turner relative to a gravity station at Whitney Pass, which had previously been tied to U.S. Coast and Geodetic Survey pendulum stations at Independence and Waukena (Duerksen, 1949, p. 36) and to airport gravity bases at Merced and Fresno (Woollard, 1958, p. 532). The Mount Whitney station is now the highest gravity station in North America (14,496 feet above sea level) and provides important data for testing the principle of isostasy.

GRAVITY DATA

Gravity reductions were carried out for the station on Mount Whitney according to the methods described by Swick (1942) and Heiskanen (1938). A Bouguer reduction density of 2.67 g per cm^3 was used, and the corrections for topography and compensation for zones 10 to 1 were taken from the world reduction charts prepared by Niskanen and Kivioja (1951).

Table 146.1 lists the principal gravity data at Mount Whitney, and for comparison it includes similar data for Pikes Peak, in the Colorado Front Range. Figure 146.1 is a plot of the Mount Whitney data, showing the effect of different assumptions on the value of the gravity anomalies. The free-air anomaly is treated in the figure as a Hayford anomaly (Hayford and Bowie, 1912) for which the depth of compensation, D, is zero. The free-air anomaly is also treated as a Heiskanen anomaly (Heiskanen, 1938) for which the thickness of the normal crust, T, is zero relative to the earth's surface, which becomes a negative thickness relative to sea level. The Bouguer anomaly, likewise, may be considered as either a Hayford or a Heiskanen anomaly for which the depth of compensation or the normal crustal thickness, respectively, is infinite.

DISCUSSION OF RESULTS

It is seen from figure 146.1 that the gravity anomalies at Mount Whitney can be reduced to zero by assuming a Hayford isostatic system with $D=71$ km or a Heiskanen system with $T=17$ km. These values for D and T are somewhat smaller than the "best" values of $D=96$ km derived by Bowie from gravity data at stations in mountainous regions (1917, p. 133), and of $T=30$ km determined seismically as the normal sea-level thickness of the earth's crust in California (Press, 1957). Isostatic anomalies corresponding to these values are negative by about 30 mgals.

There are two possible interpretations of these data: (a) the Mount Whitney region is slightly overcompensated and will tend to approach isostatic equilibrium by further uplift of the mountain block, or (b) both the Heiskanen and Hayford systems are incorrect and do not adequately represent the true nature of isostatic compensation for the southern Sierra Nevada.

The first interpretation is supported by geologic evidence that the Sierra is still rising relative to the surrounding valleys, but there is some question regarding the absolute sense of the vertical displacements (Paul Bateman, 1960, written communication).

Table 1.—*Gravity data at Mount Whitney, California, and Pikes Peak, Colorado. All gravity values and anomalies are in milligals*

	Mount Whitney	Pikes Peak
Elevation (feet)	14, 496	[1] 14, 086
Observed gravity	978735	[1] 978959
Free-air anomaly	+217	[1] +203
Simple Bouguer anomaly	−278	−277
Terrain correction	76	[2] 57
Bouguer anomaly	−202	[1] −220
Isostatic anomalies		
Hayford, $D=56.9$ km	+18	[1] +45
$D=96$ km	−22	[1] +24
$D=113.7$ km	−34	[1] +18
$D=127.9$ km	−42	[3] +13
Heiskanen, $T=20$ km	−11	?
$T=30$ km	−31	[4] +17
$T=40$ km	−47	[5] +3
$T=60$ km	−72	[5] −7

[1] Duerksen (1949, p. 8).

[2] Rice, Donald (1960, oral communication).

[3] Bowie (1917, p. 103). Eleven mgals have been subtracted from Bowie's value of the Hayford anomaly corresponding to D=127.9 km, in order to bring it in line with Duerksen's more recent determination of Hayford anomalies corresponding to D=56.9, 96, and 113.7 km. This difference is due largely to a change in reference gravity from the Helmert formula of 1901 to the International Gravity Formula of 1930.

[4] Quresky, M. N., 1958, Gravity anomalies and computed variations in the thickness of the earth's crust in Colorado: Colorado School of Mines, Ph.D. thesis, pl. 3.

[5] Heiskanen (1939, p. 31). Five mgals have been subtracted from the cited values of Heiskanen anomalies corresponding to T=40 km and 60 km, in order to bring these data in line with Duerksen's more recent determination of the Bouguer anomaly.

557753 O—60——21

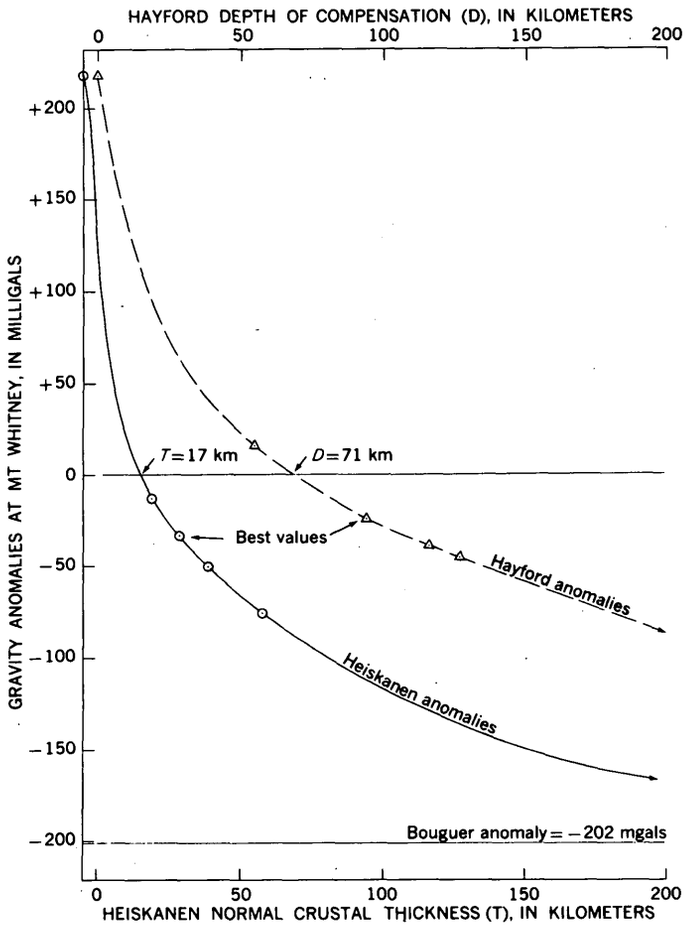

FIGURE 146.1.—Isostatic anomalies at Mount Whitney, Calif. The Hayford and Heiskanen anomaly curves approach the Bouguer anomaly value of −202 milligals as D and T, respectively, approach infinity.

The Airy-Heiskanen model of isostatic compensation is favored over the Pratt-Hayford model by seismic evidence of thickening of the earth's crust beneath the Sierra Nevada (Byerly, 1938; Gutenberg, 1943; Press, 1956). It has become increasingly apparent, however, that the Airy-Heiskanen model is only a first-order approximation to a very complex phenomenon. Press (1960) has recently shown that the earth's crust in the desert areas south of the Sierra Nevada is made up of at least two discrete layers, and that there are significant lateral variations in the velocity and presumably the density of the lower layer. Gravity gradients at the west edge of the Sierra Nevada indicate that part of the mass deficiency under the range is produced by a lateral variation in the density of rocks of the upper crustal layer. This conclusion is further supported by density measurements of surface samples, which show a systematic decrease from a value of about 2.8 g per cm^3 in the western foothills to about 2.6 g per cm^3 near the eastern crest of the Sierra Navada. A modification of Heiskanen's model by the introduction of mass deficiencies within the earth's crust tends to reduce the magnitude of the negative Heiskanen anomalies at Mount Whitney by bringing part of the compensating mass closer to the earth's surface.

COMPARISON OF CALIFORNIA AND COLORADO ANOMALIES

Table 146.1 shows that the isostatic anomalies at Pikes Peak are generally positive, in contrast to the negative anomalies observed at Mount Whitney. The algebraic differences average about 50 mgals.

The contrast in the geologic history of these two regions is also striking. The Nevadan orogeny in the Sierra Nevada is characterized by tight isoclinal folding, a high degree of metamorphism, and perhaps the complete transformation of older rocks to form the Sierra Nevada batholith. The Laramide orogeny, on the other hand, did not extensively alter the lithologic character of the Rocky Mountains in Colorado; upper Paleozoic and Mesozoic rocks were broadly folded, thrusted and uplifted without much lithologic transformation. This comparison suggests that there may possibly be a relation between isostatic anomalies and the extent of deformation and lithologic change.

CONCLUSION

Bouguer and isostatic anomalies at Mount Whitney show that there is a large mass deficiency below the Sierra Nevada, which is in general accordance with the principle of isostasy, and that the gravitational effect of this "defective" mass on Mount Whitney is approximated within 85 percent by Heiskanen and Hayford models that correspond to $T=30$ km and $D=96$ km, respectively. A better isostatic model for the Sierra Nevada would probably be a combination of the Hieskanen and Hayford models, the parameters for which cannot be determined uniquely except by the application of several geophysical methods. Isostatic anomalies based on present models are probably indicative in many cases of density changes within the earth's crust resulting from orogenic activity.

REFERENCES

Bowie, William, 1917, Investigations of gravity and isostasy: U.S. Coast and Geod. Survey, Spec. Pub. No. 40, 196 p.

Byerly, Perry, 1938, The Sierra Nevada in the light of isostasy: Geol. Soc. America Bull., v. 48, p. 2025–2031.

Duerksen, J. A., 1949, Pendulum gravity data in the United States: U.S. Coast and Geod. Survey, Spec. Pub. No. 244, 218 p.

Gutenberg, Beno, 1943, Seismological evidence for roots of mountains: Geol. Soc. America Bull., v. 54, p. 473–498.

Hayford, J. F., and Bowie, William, 1912, The effect of topography and isostatic compensation upon the intensity of gravity: U.S. Coast and Geod. Survey, Spec. Pub. No. 10, 132 p.

Heiskanen, W., 1938, New isostatic tables for the reduction of gravity values calculated on the basis of Airy's hypothesis: Internat. Assoc. of Geodesy, Isostatic Inst. Pub. No. 2, 42 p.

——— 1939, Catalogue of the isostatically reduced gravity stations: Internat. Assoc. of Geodesy, Isostatic Inst. Pub. No. 5, 139 p.

Niskanen, E., and Kivioja, L., 1951, Topographic-isostatic world maps of the effect of the Hayford zones 10 to 1 for the Airy-Heiskanen and Pratt-Hayford systems: Internat. Assoc. of Geodesy, Isostatic Inst. Pub. No. 27, 6 p.

Press, Frank, 1956, Determination of crustal structure from phase velocity of Rayleigh waves, Part I: Southern California: Geol. Soc. America Bull., v. 67, p. 1647–1658.

——— 1957, Determination of crustal structure from phase velocity of Rayleigh waves, Part II: San Francisco Bay region: Seismol. Soc. America Bull., v. 47, no. 2, p. 87–88.

——— 1960, Crustal structures in the California-Nevada region: Jour. Geophys. Research, v. 65, no. 3, p. 1039–1051.

Swick, C. H., 1942, Pendulum gravity measurements and isostatic reductions: U.S. Coast and Geod. Survey, Spec. Pub. No. 232, 82 p.

Woollard, G. P., 1958, Results for a gravity control network at airports in the United States: Geophysics, v. 23, no. 3, p. 520–535.

147. RELATIONS BETWEEN ABRAMS MICA SCHIST AND SALMON HORNBLENDE SCHIST IN WEAVERVILLE QUADRANGLE, CALIFORNIA

By William P. Irwin, Menlo Park, Calif.

Work done in cooperation with the California Division of Mines

Metamorphic rocks form an arcuate belt, 10 miles wide and trending nearly north-south for 90 miles, in the central part of the Klamath Mountains of California (fig. 147.1). A smaller area of similar rocks lies farther north, extending beyond the Oregon boundary. The metamorphic rocks midway along the belt were divided by Hershey (1901, p. 226–230) into the Abrams mica schist and the Salmon hornblende schist. These units can be recognized in at least the southern half of the belt, where detailed reconnaissance was done later by J. S. Diller and H. G. Ferguson (unpublished data, 1922) and by Hinds (1933). These early workers noted that the Abrams formation contained lenses of marble, but they attached no particular stratigraphic significance to them.

Hershey and Hinds regarded the amphibolitic Salmon formation as a thick layer of metamorphosed mafic volcanic rock that overlay the Abrams formation. Diller and Ferguson, on the other hand, believe that the Salmon formation probably consisted originally of diorite or gabbro that had been intruded into the Abrams formation; they noted, however, that there were irregularities in the contact between the two formations, and admitted that these might have resulted from interfingering of volcanic rock with sedimentary rock rather than from intrusion. It now appears certain that the Salmon is of volcanic origin. The age of all these rocks is generally regarded as pre-Silurian or Precambrian.

Geologic mapping in the Weaverville 15-minute quadrangle (fig. 147.1) indicates that (a) the structure of the metamorphic rocks included in that quadrangle is synclinorial, with the Abrams mica schist overlying the Salmon hornblende schist, (b) the Abrams is probably younger rather than older than the Salmon, and (c) the marble lenses are of stratigraphic significance in that they are chiefly in the lower part of the Abrams.

In the Weaverville 15-minute quadrangle the Abrams mica schist predominates in the central part of the belt. The Salmon hornblende schist crops out chiefly along the margins of the belt, but it is also exposed at a few places in the central part of the belt on the crests of minor anticlines. The marble lenses and the foliation and compositional banding in the Abrams are generally parallel to the contact between the two schists, and generally dip away from areas of the Salmon. The dominant structure appears to be an open synclinorium, although some of the minor folds are isoclinal. The Abrams occupies the trough of the synclinorium, and thus structurally overlies the Salmon.

The marble is chiefly in the lower part of the Abrams, near the contact with the Salmon. At a few places, however, the Salmon contains thin layers of marble

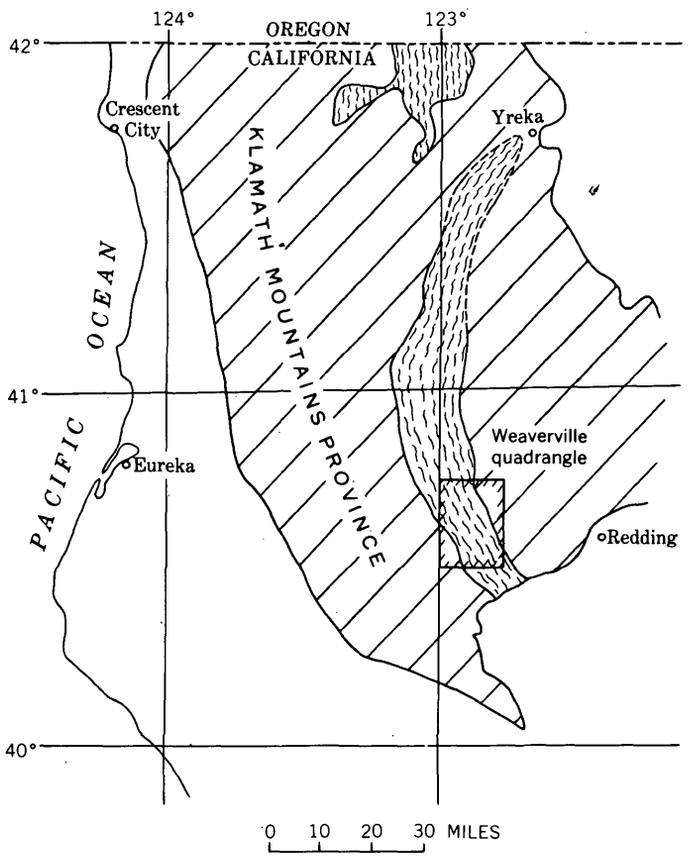

FIGURE 147.1.—Map of part of northwestern California showing the Klamath Mountains province (diagonal pattern) and Weaverville 15-minute quadrangle. The central belt of metamorphic rocks and area of related rocks are indicated by schist pattern.

near this contact. The marble occurs mostly in short lenses that are widely and unevenly spaced. Some of the discontinuity of the marble lenses has probably resulted from pinching off of limestone beds during deformation, but some of it may be a feature of original deposition. Along the east margin of the belt of metamorphic rocks, however, the marble is essentially continuous for more than 5 miles, and closely follows the contact between the Abrams and Salmon schists. At some places in the quadrangle several closely spaced layers of marble alternate with mica schist of the Abrams, and at these places it is uncertain whether the marble layers represent several original beds or a single bed repeated by isoclinal folding.

The early workers believed that the Salmon hornblende schist overlay the Abrams mica schist, but this view, based chiefly on reconnaissance, now seems to be erroneous, and so does the view, tentatively advanced by Diller and Ferguson, that the Salmon represents an intrusive body. The Abrams appears to overlie the Salmon in a large part of the Weaverville 15-minute quadrangle, and unless the normal stratigraphic sequence has been complicated by thrust faulting or overturning on a grand scale, no evidence of which has been recognized, the Abrams mica schist is the younger.

REFERENCES

Hershey, O. H., 1901, Metamorphic formations of northwestern California: Am. Geologist, v. 27, p. 225–245.

Hinds, N. E. A., 1933, Geologic formations of the Redding-Weaverville districts, northern California, *in* 29th report of the State Mineralogist: California Div. Mines, v. 29, nos. 1, 2, p. 77–122.

148. EVIDENCE FOR TWO STAGES OF DEFORMATION IN THE WESTERN SIERRA NEVADA METAMORPHIC BELT, CALIFORNIA

By LORIN D. CLARK, Menlo Park, Calif.

Work done in cooperation with the California Division of Mines

Structures in the metamorphosed sedimentary and volcanic rocks exposed in the western Sierra Nevada are related to two distinct stages of deformation. During the first stage, major folds having nearly horizontal axes and steeply dipping axial planes were formed. During the second, these folds were truncated by large faults (Clark, 1960) in the western part of the belt, and were modified by pervasive shearing and attendant development of steeply plunging b-lineations and minor folds in the eastern part of the region. Attitudes of sheer surfaces related to the second deformation make an angle of less than 30° in most places with the attitudes of axial planes of folds resulting from the first deformation, suggesting significant changes in the directions of the deforming pressures between the two stages. Had there been little change in pressure direc-

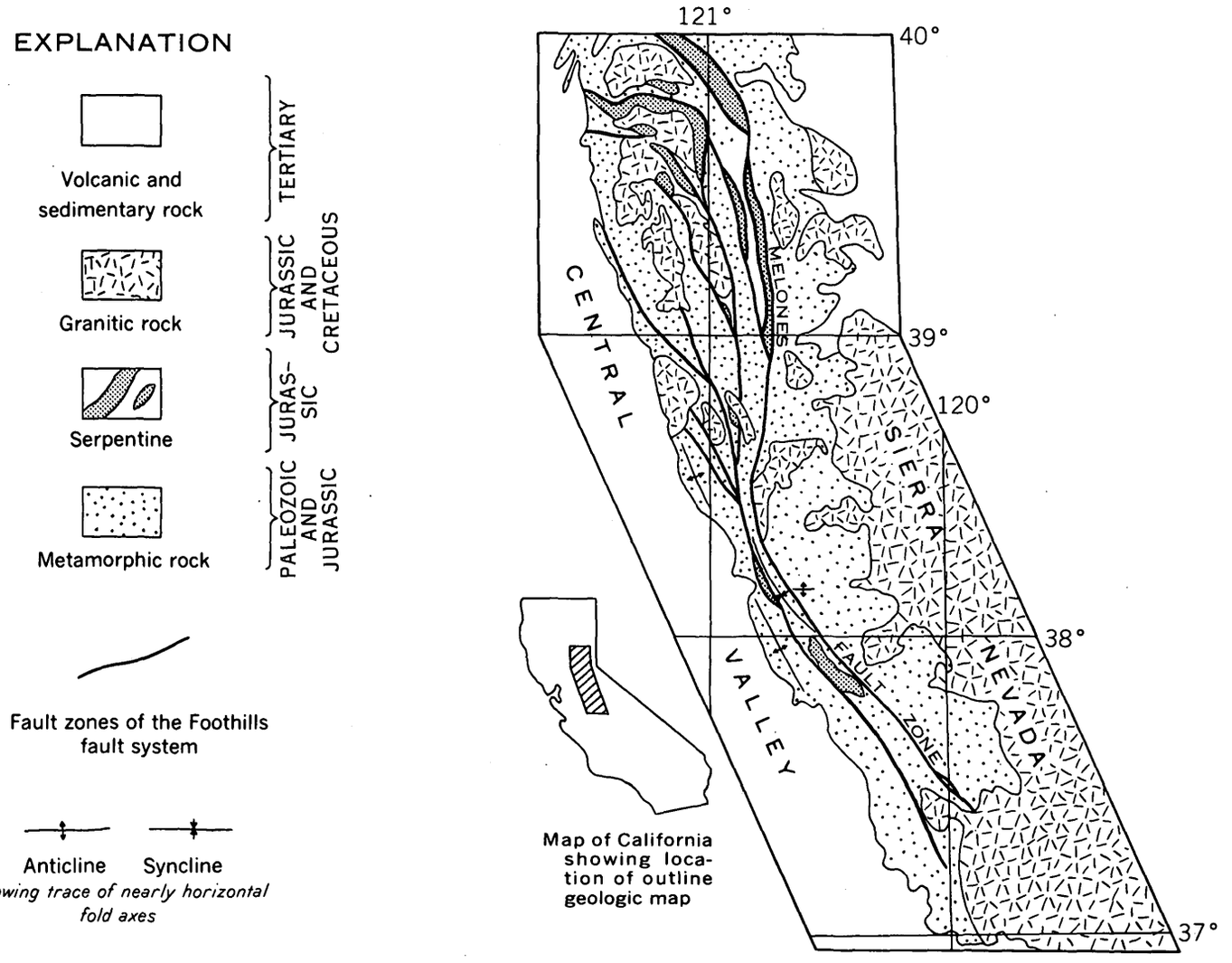

FIGURE 148.1.—Outline geologic map of the western Sierra Nevada metamorphic belt. Rock distribution adapted from tectonic map of the United States (King and others, 1944).

tions, the angle between these reference planes would be much more than 30°.

The present attitudes of the beds have resulted mainly from folding during the first stage of deformation. In the southern part of the region the formations strike about N. 30° W., and in the northern part they strike nearly due north. The outcrop belts of some formations are nearly straight for distances of more than 90 miles. In most places the beds dip steeply east or are vertical. The regional strike of the formations has resulted from folding on nearly horizontal axes. This is shown not only by the outcrop pattern of formations but by the attitudes of beds on the crests and troughs of major folds, by intersections of bedding and cleavage, and by attitudes of minor fold axes. West of the Melones fault zone (fig. 148.1) slaty cleavage is about parallel to the axial planes of the folds. East of it, axial-plane cleavage in some places and bedding-plane schistosity (fig. 148.2) elsewhere are related to the large folds having nearly horizontal axes. In small areas east of the Melones fault zone, lineations marked by elongate fragments in deformed conglomerates and tectonic breccias plunge at low angles and are also apparently related to the major folds.

Folds formed during the first stage of deformation are truncated by steeply dipping fault zones (fig. 148.1), some of which are several miles wide. In much of the area east of the Melones fault zone, the early structures are also complicated by slip cleavage (White, 1949, p. 589–590), steeply plunging *b*-lineations, and minor shear and flexure folds. The slip cleavage strikes north to northwest and dips steeply eastward or is vertical. In some places there has been little movement along

FIGURE 148.2.—Photograph showing slip cleavage cutting bedding-plane schistosity (dark streaks in light layers) and bedding in felsite tuff of Blue Canyon formation on bank of South Yuba River, 3½ miles east of Washington, Calif. Penny in upper right shows scale. Surface is normal to bedding and nearly normal to slip cleavage. Slip cleavage consists of microfaults in thin-bedded material and shear flexures in thicker light beds. Owing to refraction, it makes a larger angle with bedding in the coarser grained (light) thick layers than the finer grained thin layers. Photograph also illustrates incipent development of second-stage *b*-lineations of cataclastic origin. At this stage of development, the attitude of crude prisms resulting from segmentation of beds by movement along cleavage planes, depends upon the attitudes of bedding and schistosity, rather than direction of movement. At a later stage, prisms not normal to the direction of movement are divided by new cleavage surfaces into shorter elongate elements that are normal to the direction of movement.

slip-cleavage surfaces (fig. 148.2), but in others the bedding has been obliterated by shearing along those surfaces. The *b*-lineations rake nearly down the dip of the cleavage and plunge northeastward and southeastward.

Some of the *b*-lineations are marked by flat triaxial ellipsoids derived from fragments that are of pyroclastic, epiclastic, and cataclastic origin, others by elongate pods of chlorite and mica, by parallel amphibole crystals, or by flat slivers along intersecting slip cleavages. Lineation of minerals and of fragments are commonly associated. Wherever the lineations are associated with minor folds, they parallel the fold axes, indicating that they are parallel to *b*. No prevailing sense of regional movement has been established: in some places the steeply plunging minor folds are all sinistral, but elsewhere there are isolated dextral folds. Schistosity within the fault zones has resulted from shearing and recrystallization and is parallel to the fault zones. The *b*-lineations within the fault zones are of the kinds described above and plunge steeply northeast and southeast. Cleavage, lineation, and minor folds that are of different orientations than those grouped in the two sets described occur locally. The significance of these has not been established.

After the first stage of deformation was completed, Upper Jurassic granitic rocks were emplaced. The second stage began before this intrusive episode, but may have continued into the period of emplacement of the Sierra Nevada batholith, which occurred in middle Cretaceous time.

REFERENCES

Clark, L. D., 1960, The Foothills fault system, western Sierra Nevada, California: Geol. Soc. America Bull., v. 71, p. 483–496.

King, P. B., and others, 1944, Tectonic map of the United States: Am. Assoc. Petroleum Geologists, prepared under the direction of the Committee on Tectonics, Div. Geology and Geography, Natl. Research Council.

White, W. S., 1949, Cleavage in east-central Vermont: Am. Geophys. Union Trans., v. 30, p. 587–594.

149. EARLY CRETACEOUS FOSSILS IN SUBMARINE SLUMP DEPOSITS OF LATE CRETACEOUS AGE, NORTHERN SACRAMENTO VALLEY, CALIFORNIA

By ROBERT D. BROWN, JR., and ERNEST I. RICH, Menlo Park, Calif.

Several well-known northern California localities from which Early Cretaceous fossils have been collected are in the area between the town of Sites, northern Colusa County, and Logan Creek in southern Glenn County. There, a relatively abundant fauna, indicative of the Albian stage of the Early Cretaceous, has been found in lenses in the upper part of an unnamed siltstone sequence immediately beneath the ridge-forming Venado formation (Kirby, 1943). The presence of this fauna at this position is puzzling because the underlying rocks have yielded a sparse but distinctive Late Cretaceous (Cenomanian) fauna. Evidence

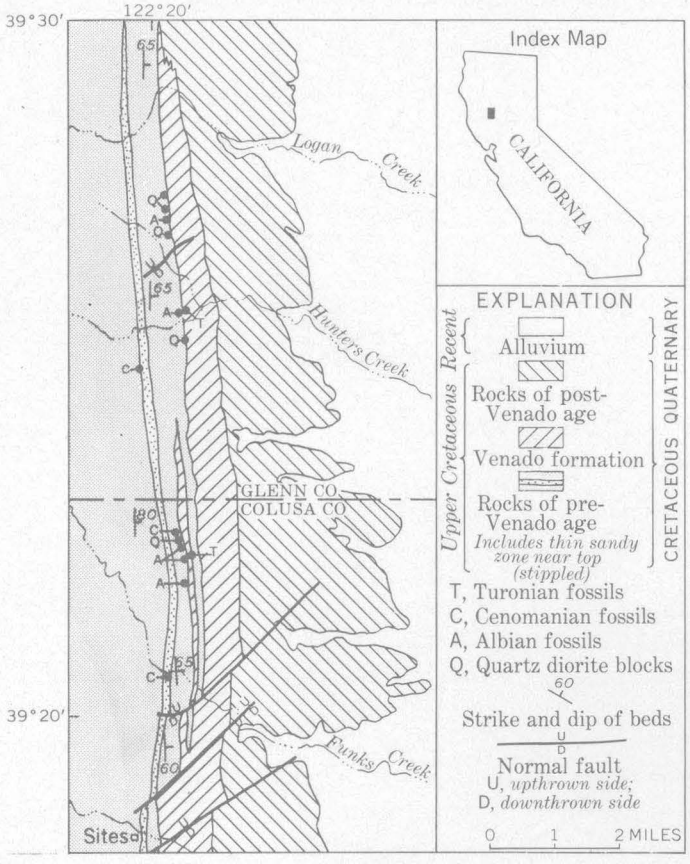

FIGURE 149.1.—Geologic sketch map showing exposed rocks of Late Cretaceous age and fossil localities along a part of the northwestern border of the Sacramento Valley, Calif.

gathered during detailed geologic mapping suggests that the anomalous fossils are derived from older rocks and have been redeposited by submarine slumping and sliding.

Sandstone, siltstone, and conglomerate of Cretaceous age crop out in a north-trending belt along the west side of the Sacramento Valley, and dip eastward beneath the valley alluvium. One of the units in these Cretaceous rocks is the Venada formation, a resistant fine- to medium-grained sandstone, which crops out for many miles in a series of low ridges near the western border of the Sacramento Valley. In most places the Venado formation is underlain conformably by a thick sequence of thin-bedded siltstone, and, in at least one locality, between Hunters Creek and Funks Creek (fig. 149.1), sandstone at the base of the Venado intertongues with the uppermost part of this siltstone. Mappable lithologic units in the Venado and in the underlying siltstone unit parallel each other and fossils from these two units indicate a normal stratigraphic succession without any appreciable hiatus. The siltstone unit contains, among other fossils, *Calycoceras* sp., and *Euomphaloceras* sp.[1], which are characteristic of the middle and late Cenomanian (Late Cretaceous) stage, and the base of the Venado has yielded *Inoceramus* cf. *I. labiatus* (Schlotheim), of the Turonian (Late Cretaceous) stage.

Fossils of Albian (Early Cretaceous) age have been found in a few outcrops of pebbly mudstone[2] directly below the basal contact of the Venado, but chiefly as float on hill slopes within about a hundred feet below the base of the Venado formation.

The fossils have been found in concretions within the blocks of sedimentary rocks, in transported and contorted resistant beds, and in transported concretions in a mudstone matrix. Most of the fossils are characteristic of the Albian stage, and typical forms are: *Desmoceras* (*Pseudouhligella*) cf. *D. dawsoni* Whiteaves, *Pachydesmoceras colusaense* (Anderson), *Mortoniceras* sp., and *Inoceramus* cf. *I. concentricus* Parkinson. A few fossils of Turonian age have also been collected in areas underlain by the pebbly mudstone lenses, but these probably are in talus from the overlying Venado formation.

The fossiliferous pebbly mudstone forms a series of elongate lenses which, in section, exhibit a channeled relation to the unnamed siltstone unit in which they occur (fig. 149.2). The largest lens, about 4 miles north of Sites, is a little more than a mile long and as much as 150 feet thick where it is exposed on a steep west-facing hillside. It is planoconvex when viewed in section, and its lower surface truncates bedding in the underlying siltstone. Its upper surface is apparently a nearly smooth plane and coincides with the base of the Venado. Other mudstone lenses farther to the north are smaller but similar in shape and in their relations to the enclosing strata.

The pebbly mudstone lenses consist of unsorted, unbedded debris that ranges in size from clay particles to blocks as much as 20 feet long. The mudstone may contain as much as 20 percent pebbles, which are generally rounded or subrounded, range from a fraction of an inch to several inches in maximum diameter, and are randomly distributed through the rock. The pebbles are predominantly volcanic rock of andesitic or more siliceous composition, but they also include sedimentary, metamorphic, and equigranular intrusive rocks.

Large blocks of sedimentary and plutonic rock are exposed at a few places in the pebbly mudstone lenses. In many of the larger blocks of sedimentary rock, the

[1] These and other paleontologic determinations listed in this report are by David L. Jones, U.S. Geological Survey.

[2] The term "mudstone" is used here for rocks that are generally unsorted and unstratified and exhibit a range in grain size from clay to sand.

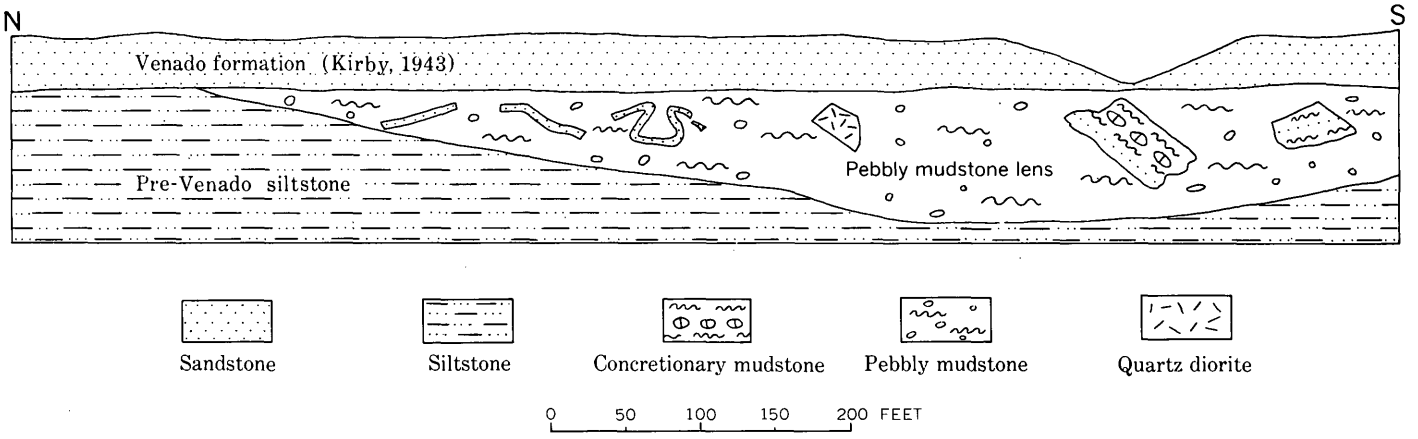

FIGURE 149.2.—Generalized geologic section of pebbly mudstone lens about 4 miles north of Sites, Calif., showing transported blocks of sedimentary and plutonic rock. Beds dip east about 60°, into the plane of the section.

bedding is uniform but is inclined at various angles to the bedding of other blocks and to the bedding of the adjacent rock units. At a few places thin contorted beds of fossiliferous sandstone, as much as 100 feet long and only 1 to 3 feet thick, are also enclosed in massive pebbly mudstone. Blocks of hornblende-quartz diorite have been noted in a few exposures of pebbly mudstone, but most of the blocks, some as much as 15 feet on a side, merely project from grass-covered slopes along the strike of the mudstone lenses.

The association of pebbly mudstone, exotic blocks of large size, and displaced faunas has been described from many areas and from strata of widely differing age (Crowell, 1957, p. 994). Such deposits generally have been interpreted as debris flows formed by submarine slumping, either in response to tectonic activity or as an indirect result of turbidity currents. The evidence of a similar origin for the mudstone lenses beneath the Venado formation is convincing: these lenses are enclosed in an otherwise unbroken sequence of marine sediments; they are channeled into the strata beneath them; their internal lithology and structure are typical of submarine landslide deposits, and they contain dislocated blocks of fossiliferous Lower Cretaceous rocks. The mechanism which caused the slumping cannot be determined from the evidence now available, but because of the uniform mineralogy and large size and the angular shape of the exotic blocks of quartz diorite, an origin in which tectonic activity played an important part is favored.

REFERENCES

Crowell, J. C., 1957, Origin of pebbly mudstones: Geol. Soc. America Bull., v. 68, p. 993–1010.

Kirby, J. M., 1943, Upper Cretaceous stratigraphy of west side of Sacramento Valley south of Willows, Glenn County, California: Am. Assoc. Petroleum Geologists Bull., v. 27, p. 287–289.

150. GRAVITY VARIATIONS AND THE GEOLOGY OF THE LOS ANGELES BASIN OF CALIFORNIA

By THANE H. MCCULLOH, Riverside, Calif.

Work done in cooperation with the University of California

The Los Angeles Basin is a topographic lowland and Cenozoic sedimentary basin adjoining the coast of southern California. It is bordered on the southeast by the Peninsular Ranges, on the north by the Transverse Ranges, and on the west by the submarine basins and ridges of the continental borderland.

Diverse types of plutonic igneous and metamorphic rocks crop out in the bordering hills and mountains and

constitute the basin floor, and in the basin they are unconformably overlain by Upper Cretaceous and Cenozoic sedimentary rocks. Sinking of the basin floor and consequent filling of the depression began in Late Cretaceous time, but ceased for a while before the end of the Cretaceous. Sedimentation was resumed early in the Cenozoic era in small areas, and by the beginning of late Miocene time it had spread throughout the basin. The maximum rate of subsidence and filling was reached during late Miocene time. Not less than 30,000 feet of predominantly marine micaceous siltstone, feldspathic sandstone, and polymictic conglomerate, mostly of Miocene, Pliocene, and Quaternary age, accumulated in the central part of the basin.

The present configuration of the floor of the basin (fig. 150.1) as deduced from surface geology, well data, and reflection seismic data, provides a graphic measure of the great structural relief of the basin and of its subsidence.

The Bouguer gravity map (fig. 150.2), though it has a strong general resemblance to the structure contour map of figure 150.1 shows that the gravitational effects of the local geology are superimposed on a steep basin-wide regional gravity gradient sloping downward toward the north-northeast. For this reason, Bouguer gravity values at stations near outcrops of pre-Cretaceous rocks are 100 milligals greater in the southwestern part of the basin than in the northeastern part. The exact nature and cause of this regional gradient are of considerable practical as well as theoretical interest.

Geologic information of the sort summarized in figure 150.1 combined with data concerning the water-saturated or "natural" bulk density of the rocks, can yield a density model from which we can compute the approximate gravitational effects of the geology. Laboratory measurements of bulk "natural" density of rocks have been criticized as being poor approximations of the actual bulk density of rocks in place (Hammer, 1950, p. 645), because of changes in the rock during or after the coring process, and there is no doubt that density given by such measurements is consistently lower than the actual density of rock in place. Investigations however, of compressibility of sandstone (Fatt, 1958, p. 1932) suggest that the errors produced by such changes in sandstone and siltstone, which constitute most of the fill of the Los Angeles Basin, are very small as compared with errors from other sources. Only in shale or claystone, and only after they have undergone mechanical changes resulting from dehydration followed by wetting, are the determinations of natural density seriously or unpredictably in error. These conclusions are substantiated by the accuracy with which commercial laboratories have estimated porosities of Los Angeles Basin rocks in place from bulk-density measurements of cores.

In order to correlate rock density with lithology, depth of burial, age, geographic location, and deformational history, the "natural" densities of more than 2,000 surface and subsurface rock samples from the Los Angeles Basin were measured. The results were combined with structural and stratigraphic information to yield a compartmentalized density model of the basin. The actual model consists of a series of seventeen level sections through the basin, each representing a rock layer 1,000, 2,000, or 5,000 feet thick, upon which isopycnic lines (lines of equal rock density) appropriate to the level were drawn. The complex and somewhat unpredictable manner in which the isopycnic lines transect formational boundaries is shown in vertical section by figure 150.3.

By means of this density model the gravitational effects were computed for 100 gravity stations. Considered in this computation are the rocks extending from sea level to minus 20,000 feet within a horizontal radius of 15 miles of each station, together with those extending from minus 20,000 to minus 30,000 feet within a horizontal radius of 25 miles.

Subtraction of the computed gravity value for each station from the observed gravity value, which was corrected for differences of latitude, elevation, and an approximation of the densities of the rocks above sea level, yields a regional residual gravity value. Figure 150.4 was prepared by plotting and contouring these values on a map.

The regional residual gravity variations result mainly from density variations below minus 30,000 feet, but to a limited degree from incorrect assumptions concerning rock density above 30,000 feet, and from errors introduced by the computational procedure. The residual variations thus provide an indirect means of determining the deep structure of the crust, and of deciphering the shallow structure and stratigraphy in local areas where geologic or density control is inadequate. The large positive residual anomaly in the southeastern part of the map area (fig. 150.4) can be explained by assuming that the unsampled "basement rocks" of that area include a vertical stock of gabbro of the sort that crops out in the Peninsular Ranges southeast of the basin. Similarly, the furrow of negative residual anomaly, peripheral to the positive residual anomaly, disappears if the densities assigned to rocks above minus 6,000 feet in that area are decreased on the average of 0.1 g per cu cm, a change consistent

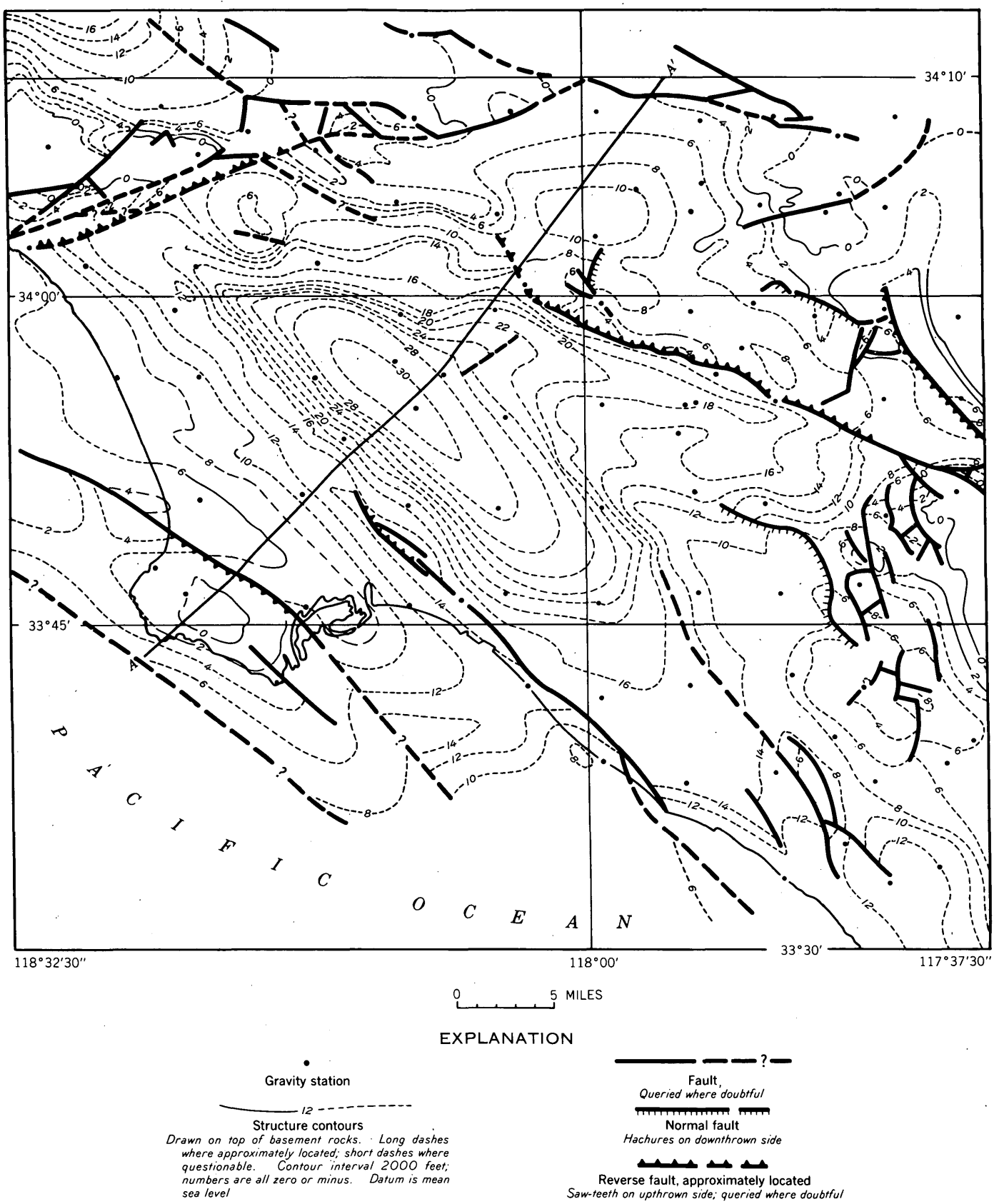

FIGURE 150.1.—Structure contour map on the top of the basement rocks in the Los Angeles Basin, Calif.

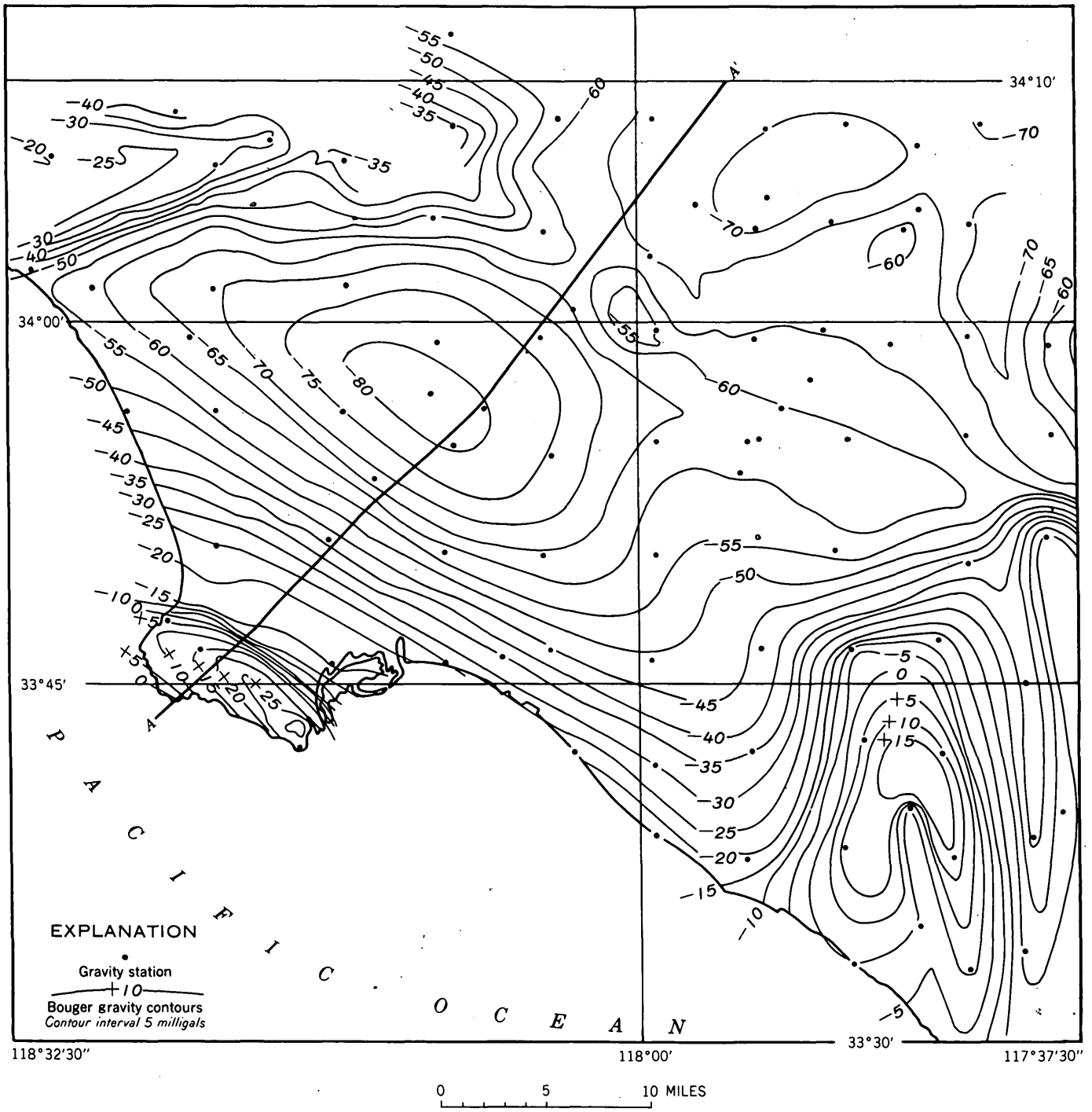

FIGURE 150.2.—Bouguer gravity map of the Los Angeles Basin, Calif.

with densities measured from samples obtained after the density model was constructed. Revision of the density model would eliminate these residual anomalies and others of the same kind. The model shows two other residual anomalies, however, that must arise from density variations below minus 30,000 feet. One of these is a slight downbowing near the middle of the residual gravity profile of figure 150.3. The only way in which this anomaly can readily be explained is by assuming that in a small area beneath the central part of the basin the bedrock floor is considerably deeper than minus 30,000 feet.

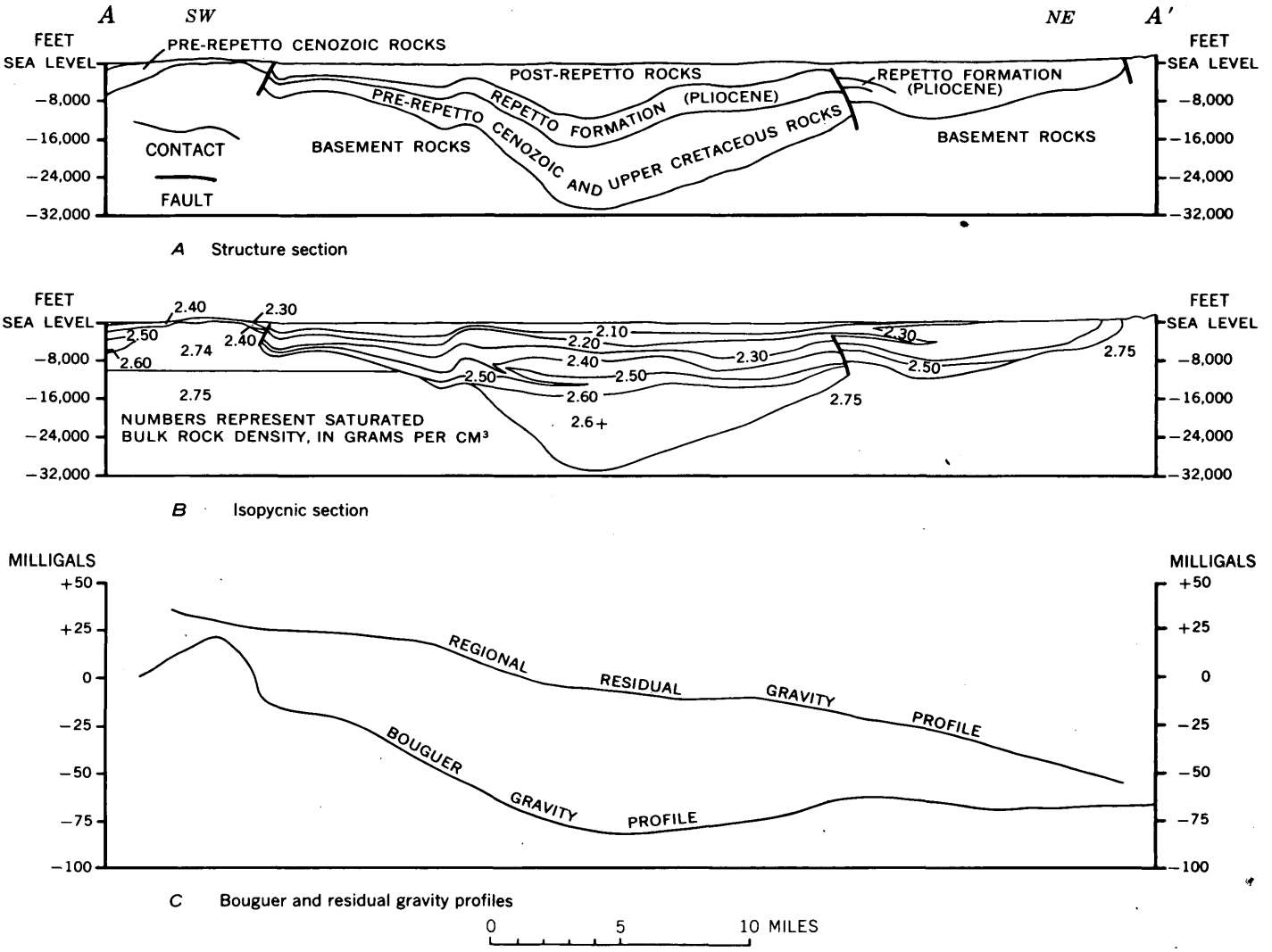

FIGURE 150.3.—*A*, Structure section; *B*, isopycnic section; and *C*, Bouguer gravity and residual gravity profiles through the Los Angeles Basin, Calif.

The regional residual gravity gradient persistently sloping to the northeast is clearly due to density variations below minus 30,000 feet, and could be the effect of landward thickening of the crust. If one assumes (a) that the Mohorovičić discontinuity slopes 15° N. 40° E. beneath the basin, (b) that a density contrast of 0.3 g per cu cm occurs at the discontinuity, (c) that the depth to the discontinuity beneath the center of the basin is 100,000 feet, and (d) that the slope of the discontinuity flattens both southwest of the basin beneath the deep channel immediately offshore and landward beneath the high mountains north of the basin, a theoretical profile may be computed that satisfactorily matches the residual regional gravity gradient of figure 150.4. Other possible profiles based upon different sets of assumptions do not fit as well.

REFERENCES

Fatt, Irving, 1958, Compressibility of sandstones at low to moderate pressures: Am. Assoc. Petroleum Geologists Bull., v. 42, no. 8, p. 1924–1957.

Hammer, Sigmund, 1950, Density determinations by underground gravity measurements: Geophysics, v. 15, no. 4, p. 637–652.

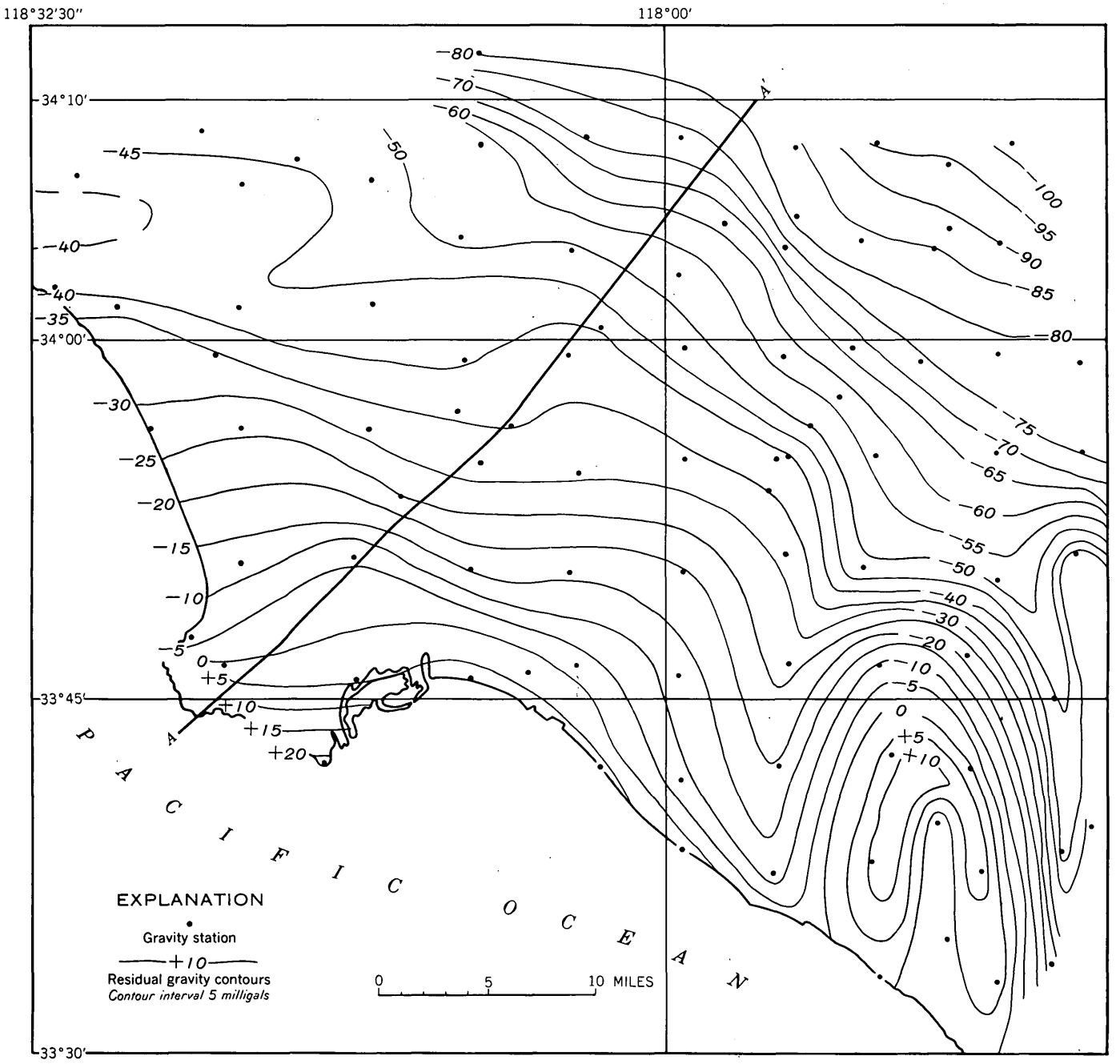

FIGURE 150.4.—Residual gravity map of the Los Angeles Basin, Calif.

151. PREVIOUSLY UNREPORTED PLIOCENE MOLLUSCA FROM THE SOUTHEASTERN LOS ANGELES BASIN

By J. G. Vedder, Menlo Park, Calif.

Sandstone and conglomerate beds in the lower part of the Niguel formation of Veddar and others (1957), which is exposed in the vicinity of San Juan Capistrano southeast of Los Angeles, have yielded relatively shallow water molluscan faunas that suggest correlation with similar depth assemblages from several localities in the Los Angeles basin and other depositional basins in southern California and Baja California. A deeper-water envirnoment is indicated by the fauna collected from silty fine-grained sandstone in the upper part of the unnamed sandstone, of Pliocene age, which is exposed in Upper Newport Bay about four miles northeast of Newport Beach (Vedder and others, 1957). The unnamed sandstone assemblage is best correlated with a fauna of comparable bathymetric distribution from strata in the city of Los Angeles.

The paleoecology and age of the faunas in the new collections are based on molluscan assemblages presumed to be large enough for reliable interpretation. Fossils of 124 species and subspecies have been identified in collections from the Niguel formation, and 114 species and subspecies from the unnamed sandstone. A combined total of 205 identified forms includes 26 species not hitherto recorded from Pliocene rocks of the Los Angeles basin, 16 species not previously reported from the Pliocene rocks of western North America, and five species whose occurrence in fossil form is not known to have been recorded (table 151.1).

TABLE 151.1.—*New Stratigraphic records of selected mollusks from the Niguel formation and the unnamed sandstone*

[U, collected from upper part of the unnamed sandstone; N, collected from the Niguel formation]

Species	Not previously reported in fossil form	Not previously reported from Pliocene strata in western North America	Not previously reported from Pliocene strata in the Los Angeles basin
Gastropods:			
Haliotis assimilis Dall?	U		
Puncturella galeata (Gould)		U	
Puncturella cf. *P. cooperi* Carpenter			U
"Tegula" montereyi (Fischer)		U	
Tegula regina (Stearns)	N		
"Turcicula" cf. *"T." bairdii* Dall		U	
Cidarina cidaris (Adams *in* Carpenter)			U
Solariella peramabilis Carpenter			U, N
Pupillaria aresta (Berry)		U	
Caecum californicum Dall		U	
Micranellum cf. *M. crebricinctum* Carpenter			U, N
Spiroglyphus lituellus (Mörchn)		U	
Bittium cf. *B. casmaliense* Bartsch			N
"Gyrineum" cf. *"G." elsmerense* English			N
"Gyrineum" cf. *"G." mediocre lewisii* Carson.			N
Turbonilla cf. *T. latifundia* Dall and Bartsch.		U	
Turbonilla cf. *L. halia* Dall and Bartsch		U	
Odostomia cf. *O. lastra* Dall and Bartsch	U		
Odostomia cf. *O. valdezi* Dall and Bartsch	U		
Opalia varicostata anomala Stearns			N
Maxwellia cf. *M. eldridgei* (Arnold)			N
Forreria wrighti Jordan and Hertlein			N
Neptunea cf. *N. smirnia* (Dall)	N		
Fulgoraria cf. *F. oregonensis* (Dall)			N
"Cancellaria" rapa Nomland			N
"Cancellaria" rapa perrini Carson			N
Crawfordina fugleri (Arnold)			U
Crassispira cf. *C. zizyphus* (Berry)		U	
Rectiplanes rotula (Dall)			U
Taranis aff. *T. strongi* (Arnold)			U
Microglyphus breviculus (Dall)		U	
Coleophysis cf. *C. harpa* (Dall)		U	
Cylichna cf. *C. attonsa* Carpenter			U
Scaphopods:			
Dentalium cf. *D. pretiosum* Nuttall			U
Dentalium cf. *D. semipolitum* Broderip and Sowerby.			N
Pelecypods:			
Huxleyia munita (Dall)		U	
Nuculana aff. *N. minuta* (Fabricius)		U	
Mytilus cf. *M. coalingensis* Arnold			N
Milneria cf. *M. kelseyi* Dall		U	
Crenella decussata (Montagu)			U
Aequipecten invalidus (Hanna)			N
Chlamys aff. *C. anapleus* Woodring		U	
Diplodonta parilis (Conrad)			N
Psephidia cf. *P. salmonea* (Carpenter)			U
Amiantis cf. *A. callosa* (Conrad)			N
Corbula cf. *C. gibbiformis* Grant and Gale.			N
Pandora filosa (Carpenter)			U
Cardiomya cf. *C. pectinata* (Carpenter)		U	

PALEOECOLOGY AND CORRELATION OF ASSEMBLAGES FROM THE NIGUEL FORMATION

The faunal composition of the bulk of the collections from the Niguel formation indicates an inner sublittoral depth facies (low water to 50± fathoms) (Hedgpeth, 1957, p. 18), with a few outer sublittoral (50± to 100± fathoms) and intertidal mollusks. Some of the living species that are also present in the collections are now found only farther south than the collection localities. This suggests that shallow-water temperatures off southern California may have been slightly higher during part of Pliocene time than they are today. Most of the species still living now inhabit sandy or rocky bottom that is subjected to little or no wave action.

The formation's content of diagnostic Pliocene mollusks is strikingly similar to that of assemblages from comparable depth facies in sediments at Santa Maria, in the eastern Ventura basin, and at San Diego (table

TABLE 151.2.—*Mollusks from the Niguel formation regarded as diagnostic Pliocene species in southern California, and their previously reported distribution in other areas in southern California and Baja California*

[Qualifications of identifications not shown]

Diagnostic forms from the Niguel formation	Santa Maria district	Eastern Ventura basin	Temescal Canyon, Santa Monica	Brea-Olinda area, Puente Hills	San Diego district	Turtle Bay and Cedros Island, Baja California
	Careaga sandstone and upper part of Foxen mudstone (Woodring *in* Woodring and Bramlette, 1950)	Upper part of Pico formation and lower part of Saugus formation (Woodring, 1930; Winterer, 1956)	"Pico" formation (Woodring *in* Hoots, 1931)	Upper part of Fernando formation (unpublished data)	San Diego formation at Pacific Beach (except as noted) (Hertlein and Grant, 1944; Woodring *in* Woodring and Bramlette, 1950; Hertlein, oral communication, 1960)	(Jordan and Hertlein, 1926; Hertlein, 1933)
Gastropods:						
Pomaulax gradatus (Grant and Gale)		×		×		
"Gyrineum" mediocre lewisii Carson	×	× [1]			× [2]	
Opalia varicostata Stearns	×	×	×		×	
Opalia varicostata anomala Stearns	×				×	
Forreria wrighti Jordan and Hertlein		×			×	×
Calicantharus humerosus (Gabb)		×		×		
Nassarius moranianus (Martin)	×	×		×	× [2]	
Fulgoraria oregonensis (Dall)	×	×				
"Cancellaria" rapa Nomland	×					
"Cancellaria" rapa perrini Carson	×	× [1]				
Ophiodermella graciosana (Arnold)	×	×			×	
Pelecypods:						
Anadara trilineata (Conrad)	×	×		×	×	
Anadara trilineata calcarea (Grant and Gale)					× [2]	
Mytilus coalingensis Arnold	×				× [2]	
Pecten hemphilli Dall	×	×	×		×	×
Aequipecten invalidus (Hanna)		×			×	×
Chlamys parmeleei (Dall)	×	×	×	×	×	
Patinopecten healeyi (Arnold)	×	×	×	×	×	×
Patinopecten dilleri (Dall)	×	×		×	× [2]	×
Lyropecten cerrosensis (Gabb)	×	×	×	×	×	×
Ostrea erici Hertlein	×			×	× [2]	×
Chione fernandoensis English		×		×	× [2]	
Corbula gibbiformis Grant and Gale		×				

[1] May have been collected from lower part of Pico formation.
[2] Stratigraphic position in the San Diego formation unknown.

151.2). If a two-fold division of the Pliocene of California is employed, the faunas from the stratigraphic units cited in table 151.2 would be regarded as of late Pliocene age. A late Pliocene age is assigned to the molluscan faunas from the Niguel formation primarily on the close resemblance of the entire assemblage to that of the Careaga sandstone in the Santa Maria district (Woodring *in* Woodring and Bramlette, 1950, p. 62–66, 102–107).

PALEOECOLOGY AND CORRELATION OF AN ASSEMBLAGE FROM THE UPPER PART OF THE UNNAMED SANDSTONE

A large molluscan assemblage collected from the upper part of the unnamed sandstone is interpreted as representing intermediate and deeper parts of the sublittoral zone (estimated depth about 20 to 100 fathoms) even though some of the living forms extend downward into bathyl depths. As several mollusks occur here that now live at these depths only north of southern California, the water may have been cooler throughout the estimated depth range during part of Pliocene time than it is now; or some of these mollusks may then have had a greater geographic range than they now have. Most of the species in this fauna suggest a sandy or muddy habitat.

The molluscan assemblage from the upper part of the unnamed sandstone is comparable to large faunas of similar or slightly shallower depth facies collected from upper Pliocene strata in downtown Los Angeles

TABLE 151.3.—*Mollusks from the upper part of the unnamed sandstone that presumably are stratigraphically restricted, and their previously reported distribution in upper Pliocene and Pleistocene strata in southern California*

[Qualifications of identifications not shown]

Species collected from the upper part of the unnamed sandstone	Previous records		
	Late Pliocene	Early Pleistocene	Late Pleistocene
Gastropods:			
Pupillaria aresta (Berry)		×	
Crepidula princeps Conrad	×	× (uncommon)	× (rare)
Trochita trochiformis (Born)	× [1]		
Bittium casmaliense Bartsch	×		
Opalia varicostata Stearns	× [2]		
Boreotrophon raymondi (Moody)	×	×	
"Cancellaria" angelana Hanna	× [2]		
Crawfordina fugleri (Arnold)	× [2]		
Crassispira zizyphus (Berry)		×	
Pelecypods:			
Pecten bellus Conrad	×	× (uncommon)	
Pecten stearnsii Dall	×	×	
Chlamys opuntia (Dall)	×	×	
Chlamys jordani (Arnold)	× [3]	×	
Chlamys anapleus Woodring		×	
Patinopecten caurinus (Gould)	× [4] (rare)	×	× (rare)
Cyclocardia californica (Dall)	×	(?)	

[1] Living south of Panama.
[2] Reported only from strata of late Pliocene age.
[3] Living in Puget Sound and north.
[4] Living north of Pt. Reyes, Calif.

(Soper and Grant, 1932, p. 1050–1067). Approximately 60 percent of the forms from the upper part of the unnamed sandstone are represented in the Los Angeles collections, which are generally considered to be of late Pliocene age. This is one reason for regarding the molluscan fauna from the upper part of the unnamed sandstone as late Pliocene, and another is that this unit has yielded several forms hitherto reported only from strata of this age (table 151.3). The high percentage of species still living, both in the collections from downtown Los Angeles and in those from the upper part of the unnamed sandstone, may indicate a slower rate of extinction in the deeper-water facies, although it could mean that the faunas are post-Pliocene.

REFERENCES

Hedgpeth, J. W., 1957, Classification of marine environments, *in* Hedgpeth, J. W., ed., Treatise on marine ecology and paleoecology: Geol. Soc. America Mem. 67, v. 1, 1296 p.

Hertlein, L. G., 1933, Additions to the Pliocene fauna of Turtle Bay, Lower California, with a note on the Miocene diatomite: Jour. Paleontology, v. 7, p. 438–441.

Hertlein, L. G., and Grant, U. S., IV, 1944, The geology and paleontology of the marine Pliocene of San Diego, California: San Diego Soc. Natural History Mem., v. 2, pt. 1, 72 p.

Hoots, H. W., 1931, Geology of the eastern part of the Santa Monica Mountains, Los Angeles County, California: U.S. Geol. Survey Prof. Paper 165–C, p. 83–134.

Jordan, E. K., and Hertlein, L. G., 1926, Contribution to the geology and paleontology of the Tertiary of Cedros Island and adjacent parts of Lower California: California Acad. Sci. Proc., 4th ser., v. 15, p. 409–464.

Soper, E. K., and Grant, U. S., IV, 1932, Geology and paleontology of a portion of Los Angeles, California: Geol. Soc. America Bull., v. 43, p. 1041–1068.

Vedder, J. G., Yerkes, R. F., and Schoellhamer, J. E., 1957, Geologic map of the San Joaquin Hills-San Juan Capistrano area, Orange County, California: U.S. Geol. Survey Oil and Gas Inv. Map OM–193.

Winterer, E. L., 1956, Geology of the southeastern Ventura basin, Los Angeles County, California: U.S. Geol. Survey open-file report, 164 p.

Woodring, W. P., 1930, Pliocene deposits north of Semi Valley, California: California Acad. Sci. Proc., 4th ser., v. 19, no. 6, p. 57–64.

Woodring, W. P., and Bramlette, M. N., 1950, Geology and paleontology of the Santa Maria district, California: U.S. Geol. Survey Prof. Paper 222, 185 p. [1951].

GEOLOGY OF ALASKA

152. CENOZOIC SEDIMENTS BENEATH THE CENTRAL YUKON FLATS, ALASKA

By JOHN R. WILLIAMS, Washington, D.C.

Work done in cooperation with the Office, Chief of Engineers

The log of a water well drilled near Fort Yukon by Alaska District, Corps of Engineers, U.S. Army, provides the first stratigraphic information on the upper 440 feet of sediment in the central part of the Yukon Flats Cenozoic Basin. The basin consists of the Yukon Flats, an alluvial plain of about 9,000 square miles, and the bordering marginal upland, an area of dissected high terraces and piedmont slopes flanking the surrounding highlands. Rocks of pre-Cenozoic age do not crop out in the Yukon Flats but are exposed in gullies in the marginal upland and in the 200- to 700-foot escarpment which separates the upland from the Yukon Flats. These rocks are overlain in most places by thin deposits of late Cenozoic gravel and loess and in one area by stratified rocks of early Cenozoic(?) age.

The Corps of Engineers well was drilled August 7 to October 1, 1954, on a stabilized dune approximately 460 feet above sea level and one-half mile east of Fort Yukon. The log of this well appears to contradict an earlier report (Mertie, 1937, p. 16) of bedrock of unspecified type at 237 feet beneath Fort Yukon. The 1954 well penetrated (a) 48 feet of light tan silty eolian sand of Pleistocene or Recent age, (b) 100 feet of gray alluvial sandy gravel of Pleistocene age, and (c) 292 feet of fine sediments (172 feet of blue silt, 70 feet of gray poorly consolidated silt, 35 feet of silty sand, and 15 feet of silt). The base of the fine-grained deposits was not encountered at a depth of 440 feet, the point at which the dry hole was abandoned. Permafrost was logged from 8 to 320 feet, and ice lenses were recorded in gray silt between 320 and 390 feet.

A sample collected from 393 feet by Professor George S. Tulloch of Brooklyn College was examined for pollen by W. S. Benninghoff and for microfossils by Harlan Bergquist of the Geological Survey. The sample lacks Foraminifera but contains pollen. Preliminary studies (Benninghoff, letter March 7, 1960) show that among the tree pollen pine, spruce, alder, birch, hemlock, and fir are abundant, and that hickory also occurs. Of these, pine, hemlock, fir, and hickory do not grow in the region today.

Information from a single well is insufficient to eliminate alternate hypotheses of origin and age of the fine-grained sediments at depth in the Fort Yukon well and to evaluate the significance of these sediments in terms of the origin and history of the Yukon Flats basin. The thickness and relatively uniform fine texture of these sediments and the topographic form of the basin suggest that they were deposited in a large lake, similar to that postulated by Spurr (1898), but in late Tertiary to early Quaternary time. The upper age limit is fixed by stratigraphic position of the deposits beneath late Quaternary alluvium. The lower limit is late Tertiary, for the incised meanders of the Fort Hamlin-Rampart Canyon which are cut across tilted Eocene rocks (Collier, 1903) are believed to have been inherited from the meandering channel of the lake outlet; and the sediments, lying below the altitude of the lowest known threshhold in the pre-Cenozoic rocks that rim the Yukon Flats, were probably deposited in a depression formed by subsidence of the Yukon Flats. Preliminary identification of pollen by Benninghoff (written communication) suggests the possibility of late Tertiary age for the deposits from 393 feet, assuming that the pollen had not been redeposited from older sediments.

REFERENCES

Collier, A. J., 1903, The coal resources of the Yukon, Alaska: U.S. Geol. Survey Bull. 218, 71 p.

Mertie, J. B., Jr., 1937, The Yukon-Tanana region, Alaska: U.S. Geol. Survey Bull. 872, 276 p.

Spurr, J. E., 1898, Geology of the Yukon gold district, Alaska: U.S. Geol. Survey 18th Ann. Rept., pt. III–b, p. 87–392.

557753 O—60——22

153. THE COOK INLET, ALASKA, GLACIAL RECORD AND QUATERNARY CLASSIFICATION

By THOR N. V. KARLSTROM, Washington, D.C.

Work done in cooperation with the Office, Chief of Engineers

Quaternary deposits in Cook Inlet, Alaska, record five major Pleistocene glaciations and several Recent glacial advances, all separated by intervals of retreat in which alpine glaciers were probably at least as contracted as they are today. Late Pleistocene and Recent glacial oscillations and related depositional changes are now closely dated by more than 50 radiocarbon-dated organic samples. Approximate dates for older events are obtained by extrapolations controlled by roughly quantitative geologic data. Each named glaciation and advance is here defined in terms of moraines and associated deposits, in accord with standard procedures based on Pleistocene type localities.

RECONSTRUCTED COOK INLET GLACIAL CURVES

The Cook Inlet chronology, as represented by the moraines deposited by the Tustumena glacier on the Kenai Lowland (fig. 153.1, *A* and *C*), is based on geologic information that will be discussed in detail in a manuscript report in preparation. The positions of most named glacial advances are plotted in figure 153.1 according to distance of end moraines from the existing glacier front. The record includes end moraines of Knik age; Naptowne end moraines of the Moosehorn, Killey, Skilak, and Tanya advances; and Alaskan end moraines of the Tustumena and Tunnel advances. Lateral moraines and high-level drift of Mount Susitna, Caribou Hills, and Eklutna age record more extensive glaciations, during which the Cook Inlet trough was filled with ice. No end moraines of these older glaciations were deposited in the region, and their curves are truncated approximately at the position of coalescence of the Tustumena glacier with the Cook Inlet trunk glacier.

The lower boundary of the Naptowne glaciation is dated between 46,000 and 37,000 B.C. (about 45,000 B.C.). This dating is based on an ionium-uranium ratio date of 46,000-31,000 B.C.[1] for marine sediments recording a major glacio-eustatic transgression of late Knik age, and on the radiocarbon date of 37,000 B.C. (Olson and Broecker, 1959) for wood collected from stratigraphically higher deposits of early Naptowne age. Organic samples from underlying deposits of Knik and Eklutna age are all too old to be finitely dated by the radiocarbon method. The upper boundary of the Naptowne glaciation is placed about 3,500 B.C., coincident with the dated culmination in late Tanya time of a marine transgression to a sea-level stand about 5 or 10 feet above present datum. As bracketed by the two dated higher sea-level stands, the Naptowne glaciation records a major glacial cycle of about 40,000 years.

Roughly estimated dates for the Knik, Eklutna, and Caribou Hills glacial maxima, respectively, are 50,000 to 65,000, 90,000 to 110,000, and 155,000 to 190,000 years ago. These dates are derived from statistical sampling of surface boulder concentrations in carefully selected sites by (a) assuming uniform rates of surface weathering and (b) assuming that the Naptowne maximum occurred 20,000 to 25,000 years ago. The Mount Sustina glaciation has not yet been dated by any direct means, but it probably occurred at least 200,000 or 250,000 years ago.

Subdivision and dating of post-Killey moraines of Skilak age or younger (fig. 153.1, *C*) are based on stratigraphic sections and moraine sequences that record regional depositional changes contemporaneous with glacial oscillations and are cross-dated by radiocarbon measurements. This closely dated part of the chronology expresses a systematic pattern of glacial oscillations, with major retreats occurring every 3,000 to 4,000 years (about 3,500 years) and important but subordinate retreats occurring every 1,000 to 1,200 years (about 1,100 years). Some smaller oscillations of glaciers and sea level that have been recorded are not represented on the reconstructed curve.

Schematic reconstruction of the pre-Skilak part of the Naptowne curve is based on the assumption that pre-Skilak glacial oscillations were produced by the same pulsatory climatic regimen that is recorded by the younger deposits. It gives the following extrapolated dates: about 13,500 B.C. for culmination of the Moosehorn retreat, about 17,000 B.C. for culmination of the retreat just prior to the Moosehorn maximum advance, and about 20,500 B.C., 24,000 B.C., and so on,

[1] Sackett, W. M., 1958, Ionium-uranium ratios in marine deposited calcium carbonates and related materials: Doctoral thesis, Washington University, St. Louis, Mo.

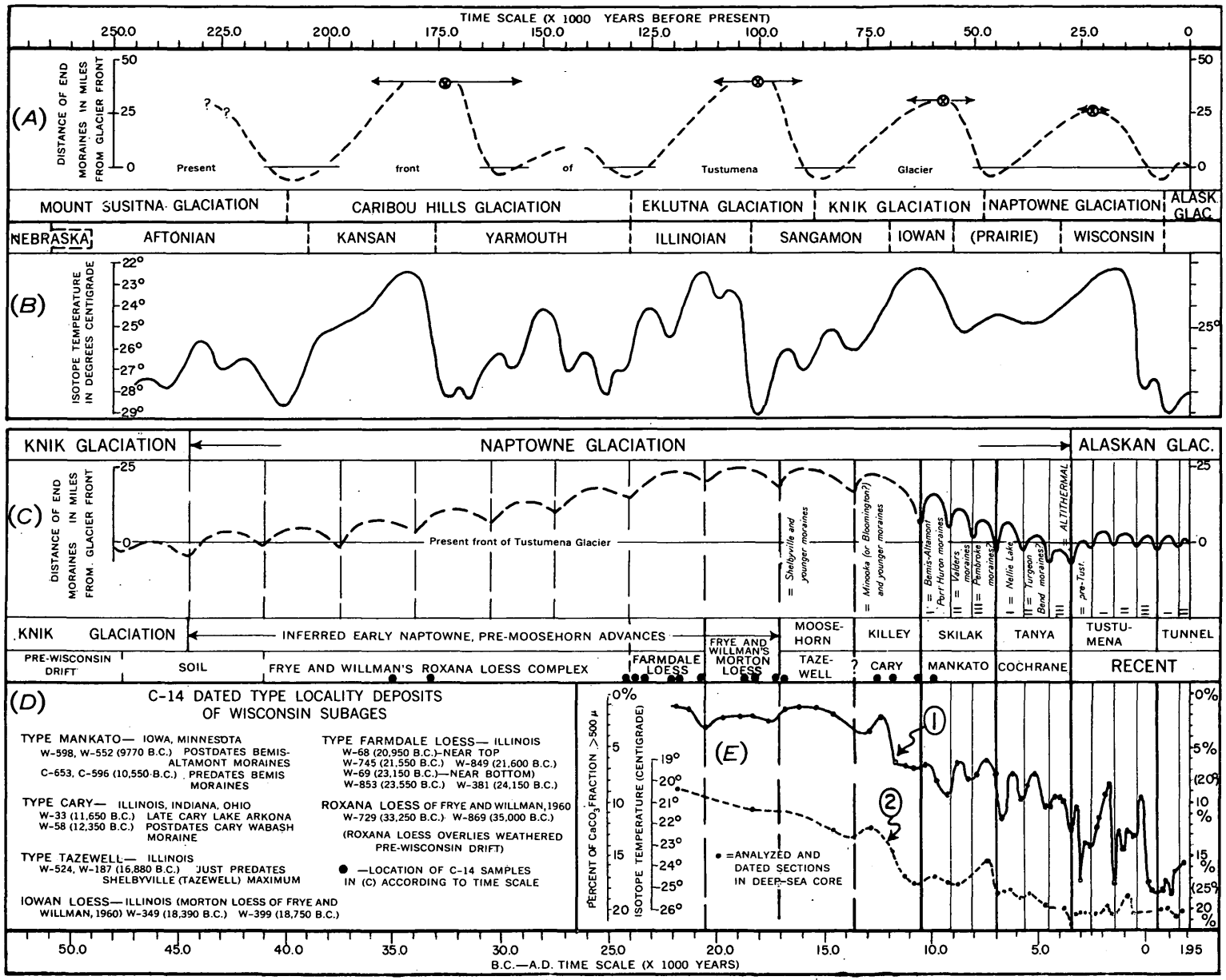

FIGURE 153.1.—Cook Inlet glacial curves and other Quaternary chronologies. *A*, Generalized curve of Cook Inlet glaciations (Karlstrom, 1955, 1957b). *B*, Generalized temperature curve for tropical surface waters correlated with midcontinent events (Emiliani and Geiss, 1957). *C*, Generalized, partly schematic, curve of glacial advances of Naptowne and Alaskan age with midcontinent correlations (Karlstrom 1956, 1957a, 1959). *D*, C–14 dating of type-locality deposits of Wisconsin substage events by Rubin and Libby from published radiocarbon date lists and from Frye and Willman (1960). *E*, Secondary temperature oscillations in an equatorial deep-sea core (Wiseman, 1958, 1959): Curve 1, percentage $CaCO_3$, fraction coarser than 500μ; curve 2, isotope temperatures of *Globigerinoides sacculifera*.

for the earlier intraglacial retreats which presumably interrupted the general advance of the Tustumena glacier to its maximum extension in Moosehorn time. Other Cook Inlet glaciers attained their Naptowne maxima during either pre-Moosehorn or post-Moosehorn advances; in this regard their glacial curves would differ from the reconstructed Tustumena glacier curve.

PLEISTOCENE CLASSIFICATION AND CORRELATIONS

The standard North American Pleistocene classification is subdivided on the basis of moraine boundaries, associated stratigraphy, and weathering relations as mapped in the midcontinent drift region. Named stage and substage events are defined in accordance with conventional geologic procedures, from drift deposits in selected areas (Leighton, 1958). Correlation of moraines and related Pliestocene deposits is based on the assumption that glaciers and other geologic processes responded almost immediately, and at about the same time, to widespread paleoclimatic changes.

Important elements of this classical approach to Pleistocene classifications and correlation have been questioned recently (by, among others, Miller, 1958; Frye and Willman, 1960). Some geologists question the use of radiocarbon-dated samples for correlation and dating (Antevs, 1957; Miller, 1958). Many of these criticisms, however, fail to take account of the striking agreement between the reconstructed Cook Inlet glacial sequence and the substage sequence of the midcontinent Wisconsin stage (when these substage events are directly dated from deposits within their defined type localities) (fig. 153.1, *D*), and of other independently dated and detailed Pleistocene chronologies (examples in fig. 153.1, *B* and *D*). These facts, taken together, substantially strengthen the case for: (a) widespread paleoclimatic and glacial synchronism, (b) utility of radiocarbon samples for dating and correlating, and (c) functional validity of the traditional approach to Pleistocene classification, based primarily on regional mapping of moraines and associated drift units in heavily glaciated areas. Climatic controls on depositional and erosional processes may, in most cases, be more directly inferred from such deposits than from bedded deposits in non-glaciated regions. I therefore believe that relatively minor, rather than drastic, revision of the standard North American Pleistocene classification and nomenclature is in order.

REFERENCES

Antevs, Ernst, 1957, Geologic tests of the varve and radiocarbon chronologies: Jour. Geology, v. 65, p. 129–148.

Emiliani, Cesare, and Geiss, J., 1957, On glaciations and their causes: Geol. Rundschau, v. 46, pt. 2, p. 576–601.

Frye, J. C., and Willman, H. B., 1960, Classification of the Wisconsin stage in the Lake Michigan glacial lobe: Illinois State Geol. Survey, Circ. 285, p. 1–15.

Karlstrom, T. N. V., 1955, Late Pleistocene and Recent glacial chronology of southcentral Alaska [abs.]: Geol. Soc. America Bull., v. 66, p. 1581–1582.

——— 1956, The problem of the Cochrane in late Pleistocene chronology: U. S. Geol. Survey Bull. 1021–J, p. 303–331.

——— 1957a, Tentative correlation of Alaskan glacial sequences: Science, v. 125, no. 3237, p. 73–74.

——— 1957b, Alaskan evidence in support of a post-Illinoian, pre-Wisconsin glaciation [abs.]: Geol. Soc. America Bull., v. 68, p. 1906.

——— 1959, Reassessment of radiocarbon dating and correlations of standard late Pleistocene chronologies [abs.]: Geol. Soc. America Bull., v. 70, no. 12, pt. 2, p. 1627.

Leighton, M. M., 1958, Important elements in the classification of the Wisconsin glacial stage: Jour. Geology, v. 66, no. 3, p. 288–309.

Miller, J. P., 1958, Problems of the Pleistocene in Cordilleran North America, as related to reconstruction of environmental changes that affected early man: Univ. Arizona Bull., v. 28, no. 4, p. 19–49.

Olson, E. A., and Broecker, W. S., 1959, Lamont natural radiocarbon measurements V.: Am. Jour. Sci., Radiocarbon Supplement, v. 1, p. 506.

Wiseman, J. D. H., 1958, La topographie et la géologie des profondeurs océaniques: Colloques Internationaux, Centre National de las Recherche Scientifique, v. 83, p. 193–208.

——— 1959, The relation between paleotemperatures and carbonate in an equatorial Atlantic pilot core: Jour. Geology, v. 67, no. 6, p. 685–690.

154. SURFICIAL DEPOSITS OF ALASKA

By THOR N. V. KARLSTROM, Washington, D.C.

Work done in cooperation with the Office, Chief of Engineers

The surficial deposits of Alaska map (compilation scale 1:1,584,000) provides for the first time a regional synthesis of geologic information on the surficial deposits of the State. A preliminary copy of the map, on open-file inspection at Washington, D.C., was exhibited by the U.S. Geological Survey at the First International Symposium on Arctic Geology, Calgary, Canada, January 1960. Final compilation is in progress.

The map, a product of over 50 years of geologic mapping in Alaska, incorporates field observations of numerous geologists, and was compiled in coordination with a Survey Committee appointed to compile a glacial map of Alaska. Principal collaborators in compilation are Henry W. Coulter, John R. Williams, Arthur T. Fernald, David M. Hopkins, Troy L. Péwé, and Harald Drewes.

MAP EXPLANATION

Density and quality of information on surficial deposits varies appreciably from region to region in Alaska; the map legend is designed to show available information at various levels of completeness. The deposits are classified, where possible, into genetic categories including glacial, glaciofluvial, glaciolacustrine, fluvial, eolian, volcanic, and coastal-type sediments. Where such distinctions are not possible, broader categories are used to show the deposits as sedimentary complexes associated with different types of mountainous and hilly terrain, and as undifferentiated units in unmapped parts of lowlands and broad upland valleys.

The glacial deposits are subdivided, largely on the basis of morainal sequence and morphology, into four map units ranging in age from early Pleistocene to Recent. The age ranges of the nonglacial surficial deposits are placed in reference to the glacial sequence. The moraine units represent the major subdivisions recognized in most regions. More refined subdivisions made in local areas are shown by lines representing significant moraine boundaries within the mapped units. The named glacial deposits of published chronologies included within each map unit are listed in a chart. The chart has been brought up to date by each geologist involved, and represents the latest judgments on correlations between the moraine sequences of Alaska.

In addition to an areal breakdown of deposits into 23 genetic and age categories, the map shows (a) distribution of present glaciers and ice fields; (b) location of significant stratigraphic sections, high-level glacial drifts, and erratics, with accompanying brief descriptions in an inset; (c) major faults along which surficial deposits have been displaced locally; (d) inferred boundaries of submarine glacial drift in coastal areas; and (e) regions compiled by each principal contributor (presented in an index map and accompanied by a list of principal sources of information).

SCIENTIFIC RESULTS

The pattern of surficial deposits in Alaska provides basic geologic information bearing primarily on the State's Quaternary history. As field mapping continues, refinements in the map and in geologic interpretations will follow.

In figure 154.1 the surficial deposits are generalized to show regional units which reflect the major geomorphic environments and dominant geologic processes that affected Quaternary deposition.

The major areas of coastal sediments are restricted to the Arctic coastal plain, the north coast of Seward Peninsula, and the large Bering Sea delta formed at the mouths of the Yukon and Kuskokwim Rivers. Elsewhere emerged coastal sediments are restricted to narrow discontinuous zones commonly interrupted by abrupt rocky shorelines. Where studied, the coastal deposits record complex sea level changes of both tectonic and eustatic origin. The present coastal deposits are much more restricted than in the past, when marine regressions accompanying Pleistocene glaciations exposed vast areas of shallow sea bottom, particularly in the Bering Sea.

Important areas of fluvial deposits occur in the unglaciated interior region where thick alluvium underlies the Yukon and other large valleys. Likewise the main areas of thick eolian deposits lie in unglaciated regions bordering heavily glaciated terrain or along major valleys of the interior. Deposits with high percentages of volcanic material are associated with vol-

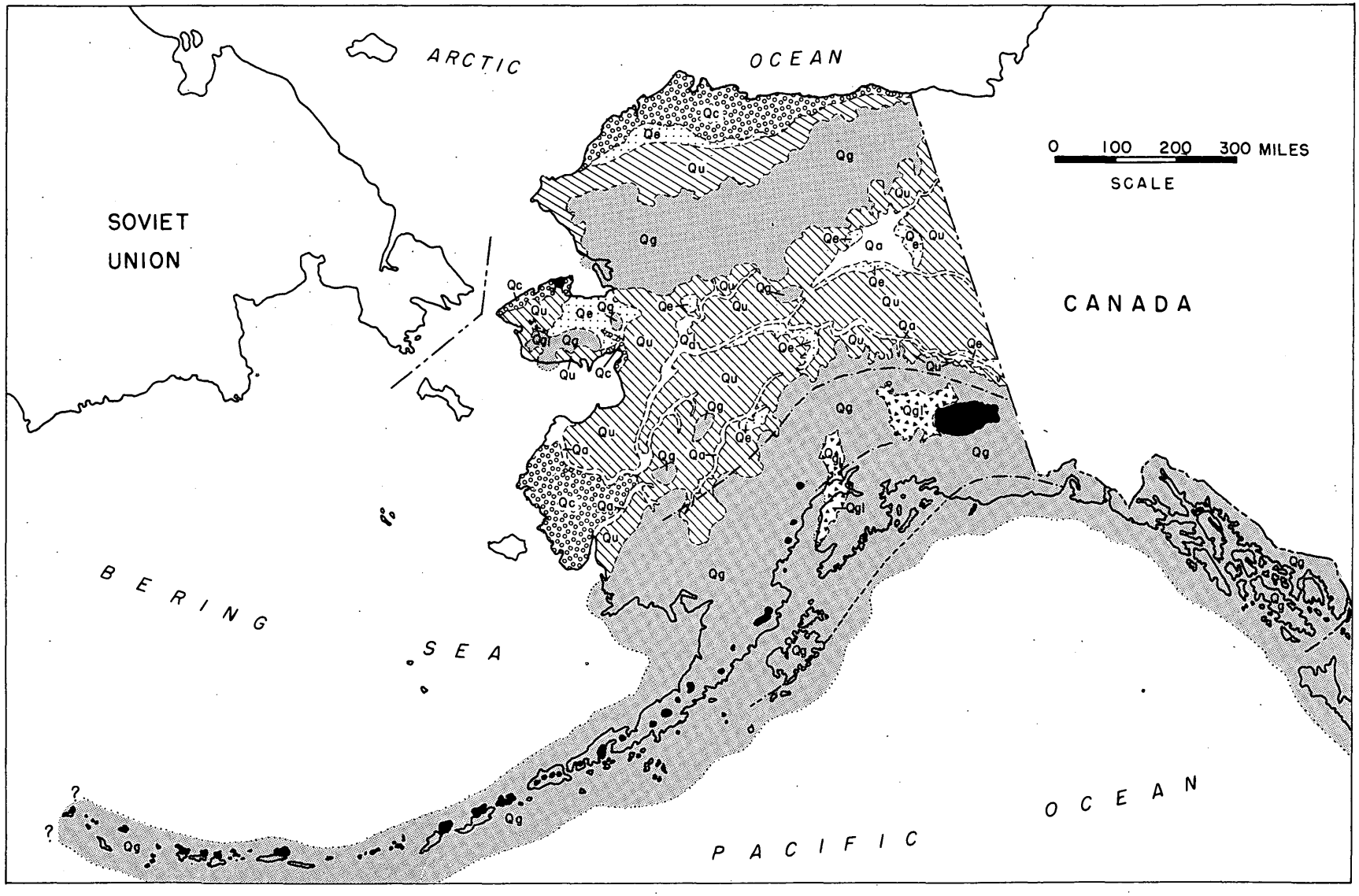

FIGURE 154.1.—Sketch map of major regional groups of surficial deposits in Alaska. Qg—glacial and other deposits associated with heavily glaciated alpine mountains; Ggl—glaciolacustrine deposits of larger Pleistocene proglacial lakes; Qu—undifferentiated deposits associated with generally unglaciated uplands and lowlands of the interior and North Slope; Qa—fluvial deposits; Qe—eolian deposits; and Qc—coastal deposits of interbedded marine and terrestrial sediments. Solid black areas—deposits associated with volcanic peaks and flows of Quaternary and Tertiary age. Heavy dot-dash lines—traces of major pre-Quaternary faults recording local Quaternary displacements (washed lines—inferred trace). Dotted lines—inferred, partly schematic, boundaries of submarine glacial deposits.

canic peaks of Quaternary and Tertiary age along the Aleutian chain and in the Wrangell Mountains, and with cones and flows of Quaternary age on Seward Peninsula. Thick proglacial lake deposits, including "till-like" stony silt, locally underlie basins and trunk valleys in or adjoining the glaciated regions, and record ice damming of regional drainage lines during one or more glaciations.

Quaternary faulting, recorded by minor offsets of surficial deposits, is concentrated along major arcuate pre-Quaternary fault zones cutting underlying bedrock, and assists in delineating these regional fault trends as important linear elements in the tectonic structure and history of the State. Greatest Quaternary movement seemingly was concentrated along the Chugach-St. Elias fault of southern coastal Alaska. Elevated strandlines and marine deposits along the coast south of the fault record notable tectonic displacements during late Quaternary time. In contrast, the evidence along the coast north of the fault indicates essential crustal stability over the same time interval.

The regional pattern of glacial deposits provides significant information on the nature of Quaternary climatic changes in Alaska. The deposits, recording separate, successively less extensive glaciations, form subparallel belts flanking the alpine mountain ranges. The regional distribution indicates that the Pleistocene glaciers: (a) fed from the same high areas which essentially comprise the modern alpine divides, (b) were largest near the Pacific coast and progressively smaller northward towards the Arctic coast, and (c) were more extensive on the south slopes than on the north slopes of all the alpine ranges. This regional glacial intensity pattern, repeated during each glaciation, conforms with the distribution of existing glaciers, with regional southward inclination of the modern climatic snowline, and with present climatic zonation orographically produced by predominant precipation supplies from the Pacific Ocean. The pattern reveals neither significant differential uplifts between the coastal mountains north of the Chugach-St. Elias fault and the Alaska and Brooks Ranges nor profound regional atmospheric circulation changes throughout the period of morainal record. The recorded shifts towards more glacial climate thus appear to have been produced primarily from increased precipitation rates resulting from intensification of atmospheric circulation patterns centered, as today, in the North Pacific.

155. RECENT EUSTATIC SEA-LEVEL FLUCTUATIONS RECORDED BY ARCTIC BEACH RIDGES

By G. W. Moore, Menlo Park, Calif.

Work done in cooperation with the U.S. Atomic Energy Commission

In the areas near Point Hope and Cape Krusenstern, on the northwestern coast of Alaska, extensive barrier bars composed of numerous beach ridges have been formed since the last major rise of sea level. These areas are about 300 km northwest of Bering Strait and about 190 km apart. The building of gravel beach ridges has prograded the shoreline (moved it seaward) approximately 2 km at Point Hope and 7 km at Cape Krusenstern. Sea level rose nearly to its present position in this area (and throughout the world) about 3000 B.C. (Hopkins, 1959), and the ridges were formed more recently. The age of many of the ridges can be closely estimated from archeological findings. The former inhabitants subsisted principally on marine mammals, and it is safe to assume that they lived close to the sea (Giddings, 1960); the present-day Eskimos build their houses about 100 m from the shoreline. The dated beach ridges thus provide evidence regarding former positions of sea level.

John Y. Cole, Jr., assisted in the geological work. The estimates of age were made possible by archeological studies, especially those of J. L. Giddings of Brown University, who made some of his results available to us before he had published them.

The barrier bars extend parallel to the shore for about 15 km at both Point Hope and Cape Krusenstern. The individual beach ridges in the barrier bars are remarkably persistent. The highest ridges stand about 3 m above sea level. The amplitudes between crests and swales may be as much as 2 m, and the

crests are, on the average, about 50 m apart. At both localities the broader parts of the barriers partly enclose large lagoons.

The beach ridges were evidently formed either during storms or during periods when persistent onshore winds caused a temporary rise in sea levels. There is some evidence that their growth was mainly due to persistent winds, for whereas the total range of ordinary astronomical tides in this area is only a few tenths of a meter, we have observed that sea level rises more than a meter during some onshore winds. But the beach ridges probably have a broader significance. As the number of beach ridges is only a small fraction of the number of violent storms and abnormally high wind tides that must have occurred while the ridges were being formed, the ridges may record minor worldwide eustatic changes of sea level, or may at least mark the limits of its fluctuations.

There are three reasons for regarding this region as an especially suitable place for finding evidence of former small eustatic changes of sea level: (a) The region was not glaciated during the Wisconsin stage, and therefore did not then undergo isostatic readjustments due to melting of ice; (b) it has not recently been subjected to rapid erosion or sedimentation that would cause isostatic uplift or downwarping; and (c) it does not contain epicenters of any recent earthquakes, which indicates that it is not tectonically active. There is no evidence that any crustal movements have occurred in the region during the last few thousand years. Apart from the minor irregularities associated with the beach ridges, the general altitude of beach sediments is remarkably uniform at both Point Hope and Cape Krusenstern.

In the Cape Krusenstern area, which contains the oldest ridges, the older beach deposits are slightly lower than the younger ones. The oldest dated beach ridge at Cape Krusenstern was formed earlier than 2500 B.C. (Giddings, 1960, p. 127). The highest part of this ridge is about 2 m above sea level, whereas comparable parts of more recent beach ridges in this area are 3 m above sea level. Beaches older than 2500 B. C. and that are farther from the shore and nearer the lagoon are lower; some are submerged in the lagoon behind the cape and are below present sea level, which is here at least 3 m higher than it was when the ridges were formed. The conditions at Cape Krusenstern may be interpreted as follows: Sea level was once considerably lower than it is at present, but rose at some time near 3000 B.C. until it was only about 3 m below its present position. Since then it has been slowly rising, probably at an uneven rate. The late submergence may con-

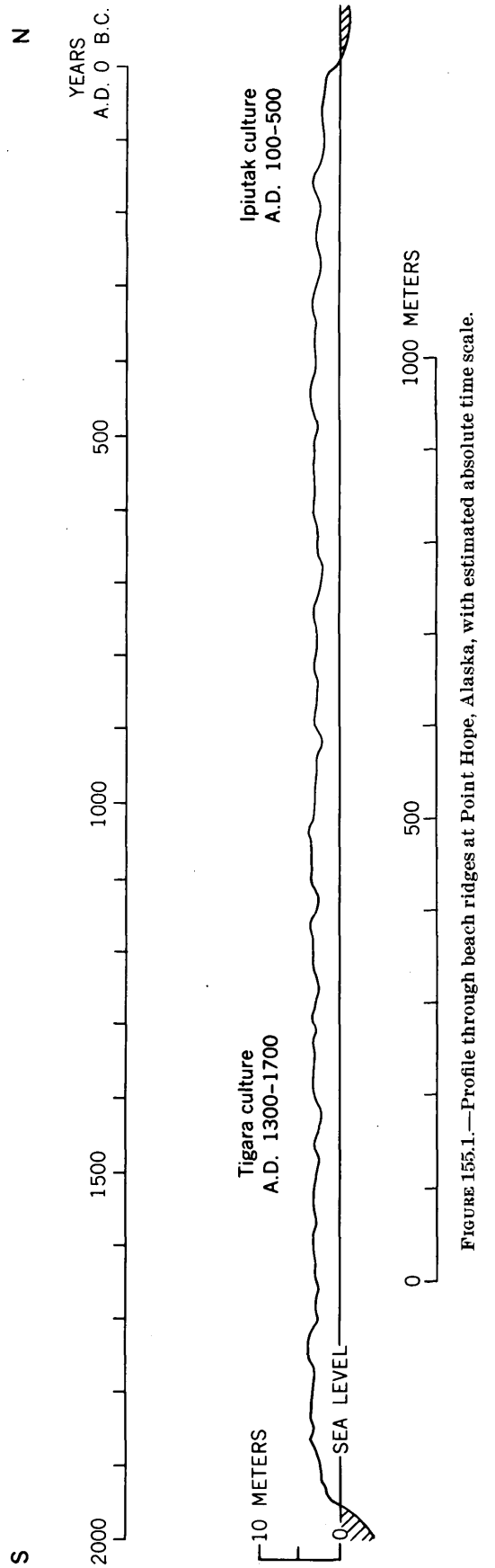

FIGURE 155.1.—Profile through beach ridges at Point Hope, Alaska, with estimated absolute time scale.

ceivably have been due to downwarping, but it appears far more likely, in view of the evidence for the general stability of the coast, that the submergence resulted from eustatic rise of sea level.

At Point Hope the youngest beach ridges have been related to an absolute time scale (fig. 155.1) by the Tigara culture (A. D. 1300–1700) and the Ipiutak culture (A.D. 100–500), which have both been dated by the radiocarbon method (Rainey and Ralph, 1959). The oldest beach ridges now preserved at Point Hope were formed about 200 B. C. Older ridges have been removed by wave erosion cutting inward from the opposite side of the point. The shoreline south of Point Hope is prograding at about 80 m a century, and new ridges have formed at average intervals of about 60 years. Two especially high beach ridges indicate that sea level may have been relatively high from A. D. 1000 to 1100 and from 1700 to 1850, and two especially low swales indicate that it may have been relatively low from 900 to 1000 and from 1400 to 1500.

Whether these fluctuations are general and accurately dated must remain uncertain until similar studies have been made in other stable parts of the world. As it stands, however, this evidence from Arctic beach ridges indicates that sea level rose about 3 m during the last 5,000 years, and that the rise was characterized by minor fluctuations with an amplitude of 1 to 2 m. The highest stand of sea level since the Wisconsin stage was attained in the 19th century.

REFERENCES

Giddings, J. L., 1960, The archeology of Bering Strait: Current Anthropology, v. 1, p. 121–138.

Hopkins, D. M., 1959, Cenozoic history of the Bering land bridge: Science, v. 129, p. 1519–1528.

Rainey, F., and Ralph, E., 1959, Radiocarbon dating in the Arctic: Am. Antiquity, v. 24, p. 365–374.

156. GENERALIZED STRATIGRAPHIC SECTION OF THE LISBURNE GROUP IN THE POINT HOPE A-2 QUADRANGLE, NORTHWESTERN ALASKA

By Russell H. Campbell, Menlo Park, Calif.

Work done in cooperation with the U.S. Atomic Energy Commission

During the summer of 1959 a stratigraphic section of rocks of the Lisburne group, of Early and Late Mississippian age, was measured along continuous sea-cliff exposures southeast of Point Hope, Alaska. Five distinctive lithologic units were recognized in the Lisburne group, which has a total thickness of more than 5,700 feet. The units have been tentatively designated, from oldest to youngest, Ml_1, Ml_2, Ml_3, Ml_4, and Ml_5.

UNIT Ml_1

Unit Ml_1 is about 165 feet thick where measured and is composed of interbedded dark-gray to grayish-black silt-clay shale, medium-gray to dark-gray bioclastic limestone, and grayish-black to black chert. The upper 45 feet consists predominantly of grayish-black shale in beds 0.1 foot to 5 feet thick, composed of fine quartz silt and clay (illite?) with generally minor amounts of disseminated very fine-grained calcite, but it includes a few interbeds of dark-gray limestone. The middle 35 feet consists of grayish-black chert and minor amounts of interbedded dark-gray bioclastic limestone in beds commonly about 0.5 foot thick. The lower part of the unit consists chiefly of medium-dark-gray mudstone, in beds 0.1 foot to 8 feet thick, composed of fine quartz silt, clay, and some disseminated fine calcite; but this is interbedded with minor amounts of partly dolomitized bioclastic limestone in beds commonly about 0.5 foot thick. The bioclasts are chiefly crinoid columnals and Bryozoa, but brachiopods and horn corals are locally abundant, and the unit contains a few colonial corals and gastropods.

The upper shaly zone locally intertongues with the overlying unit, Ml_2. The contact of Ml_1 with the sandstone-shale formation that underlies the Lisburne group is gradational.

UNIT Ml_2

Unit Ml_2 is about 225 feet thick. It consists wholly of light-gray to light olive-gray bioclastic limestone composed predominantly of sparry calcite fossil fragments ranging from fine sand to very fine pebbles in size, with generally minor amounts of very fine quartz

silt, cemented with sparry calcite and microcrystalline quartz in varying proportions. Microcrystalline quartz also commonly forms rims around fossil fragments and spongy intergrowths with calcite that preserve organic structures within the fragments. In some places fossil fragments have been partly dolomitized. The chief recognizable fossils are crinoid columnals and Bryozoa, but brachiopods and horn corals are also present.

The unit is very thick bedded, locally cropping out as a single thick bed with a few short, discontinuous, uneven bedding planes. Bedding is expressed internally by crinkly uneven laminae at generally regular intervals of 0.5 inch to 1 foot. The contact with the overlying unit Ml_3 is conformable.

UNIT Ml_3

Unit Ml_3 is about 1,650 feet thick and consists predominantly of interbedded dark-gray bioclastic limestone and grayish-black quartz-calcite siltstone. It contains relatively abundant well-preserved fossils. The limestone is composed chiefly of sparry calcite bioclasts of fine-sand to fine pebble size with variable amounts of fine quartz silt, sparry calcite cement, microcrystalline quartz cement, very finely crystalline dolomite cement, and, in a few beds, a small amount of clay (illite?). Replacement of fossils by microcrystalline quartz has occurred, and may be found in all stages from thin rims around bioclasts, through spongy intergrowths preserving organic structure, to complete replacement. The most abundant fossils are crinoid columnals and Bryozoa, but brachiopods, horn corals, and colonial corals are also locally common. Nodular limestone beds containing variable amounts of dark-gray to black chert are common at some horizons. Dark chert is locally abundant in several zones, chiefly as lenticular nodules and irregular angular masses in limestone. The basal 50 feet of unit Ml_3 contains several very thick beds of grayish-black quartz-clay-calcite siltstone containing sparsely scattered small pyrite concretions and a few pyritized fossils.

Rhythmic interbedding of limestone beds 0.2 to 1 foot thick with silt shale laminae 0.01 to 0.1 foot thick is characteristic of the unit. The bedding is generally regular and continuous, although the bedding surfaces are very slightly undulating to very uneven, the uneven surfaces being on nodular beds. The thickness of the silt shale interbeds and the abundance of shaly zones generally decrease upward. The contact between units Ml_3 and Ml_4 was arbitrarily placed at the base of the lowermost thick-bedded dolomitic limestone, but the units grade into each other.

UNIT Ml_4

Unit Ml_4 consists predominantly of light-gray to dark-gray very finely crystalline dolomitic limestone, interbedded with generally minor amounts of dark-gray partly dolomitized bioclastic limestone and a few interbeds and partings apparently consisting largely of calcareous quartz clay siltstone. The bioclastic limestone consists chiefly of sparry calcite fossil fragments ranging in size from fine sand grains to fine pebbles. In some beds the fragments are cemented and in places partly replaced by very finely crystalline dolomite; in other beds they are in a matrix of microcrystalline calcite or dolomite or both. Light-gray and dark-gray chert commonly forms nodules and continuous and discontinuous layers in some limestone beds. The chert content varies greatly from bed to bed, and also along the strike of individual beds. About 140 feet below the top of the unit is a zone of breccia about 400 feet thick, composed of very small to very large fragments of chert and dolomitic limestone in a microcrystalline matrix that is predominantly dolomite. Crinoid columnals and bryozoa predominate in the bioclastic limestone, but horn corals, colonial corals, brachiopods, and a blastoid (*Pentremites?*) were also found. A total of about 3,330 feet of strata was assigned to unit Ml_4 where the section was measured. An unknown thickness has been faulted out of the upper part by three high-angle faults, one of which forms the contact with the unit Ml_5.

Irregular interbedding of thin, medium, thick, and very thick beds is characteristic of the unit. Very thick beds, one as much as 140 feet thick, of crystalline dolomitic limestone are relatively abundant and commonly show internal horizontal and gently cross-stratified current lamination, brought out by low-contrast color banding. The bedding planes are commonly even but many are discontinuous.

The contact between units Ml_4 and Ml_5 is a high-angle fault where well exposed on the sea cliff, but probably only a few hundred feet of strata are missing.

UNIT Ml_5

Unit Ml_5, the youngest unit of the Lisburne group, is about 330 feet thick in the incomplete section measured. It consists of interbedded grayish-black chert, dark-gray to medium-dark-gray calcareous and noncalcareous siltstone and mudstone, dark-gray to light medium-gray very finely crystalline to microcrystalline calcitic limestone, and a smaller amount of greenish-black to dark-greenish-gray chert and noncalcareous argillite. Most of the chert is in beds 0.1 foot to

2 feet thick, with slightly uneven but generally continuous bedding surfaces. The limestone beds contain variable but generally small amounts of nodular chert. The siltstone and mudstone beds range from less than 0.1 foot to 3 feet in thickness. The limestone is commonly in beds 0.6 to 1 foot thick. The bedding is generally continuous, regular, and even. Fossils are very rare, but a few gastropods were collected from one siltstone bed.

The contact with the overlying Siksikpuk formation, of Permian(?) age, is a high-angle fault where the rocks are well exposed. Further inland, however, the configuration of the contact, together with the presence in unit Ml_5 of interbedded greenish-gray chert and argillite resembling rocks in the Siksikpuk formation, suggests that the Siksikpuk grades into the Lisburne group, and that the missing part of the measured section is not more than a few hundred feet thick.

157. A MARINE FAUNA PROBABLY OF LATE PLIOCENE AGE NEAR KIVALINA, ALASKA

By D. M. Hopkins and F. S. MacNeil, Menlo Park, Calif.

In 1957, the Rev. Milton Swan of Kivalina, Alaska, found a beautifully preserved shell of *Patinopecten* (*Fortipecten*) *hallae* (Dall) near Kivalina, Alaska, on the coast of Chukchi Sea about 200 miles north of Bering Strait (fig. 157.1). Because of the importance of the find (Hopkins, 1959, p. 1521) Hopkins visited the Kivalina locality briefly in 1959 to examine the stratigraphy and to collect additional fossils. This report summarizes the results of field observations by Hopkins, and studies of the mollusks by MacNeil, of the Foraminifera by Ruth Todd, and of the ostracodes by I. G. Sohn.

GEOLOGIC SETTING

The fossiliferous sediments lie at the inner edge of a coastal plain that fringes the Chukchi Sea coast from 30 miles to the northwest to 150 miles to the southeast of Kivalina. Northwest of Kivalina Lagoon, the coastal plain consists of a nearly horizontal surface less than 25 feet above sea level, terminated at its inner edge by a scarp (fig. 157.1), apparently carved in unconsolidated material, that is similar in appearance and altitude to the ancient wave-cut scarp of Second Beach, of Sangamon age, at Nome (MacNeil, Mertie, and Pilsbry, 1943; Hopkins, MacNeil, and Leopold, in press). Inland from this scarp a smooth surface slopes gently upward, but just north of Kivalina Lagoon and about 50 feet above sea level it is interrupted by a second row of scarps carved in bedrock. The marine fossils were obtained near the projected trend of the second row of scarps, in a small valley that enters the Kivalina River about 1.3 miles above Kivalina Lagoon. The second row of scarps probably represents a wave-cut cliff carved during the maximum landward transgression of Chukchi Sea during late Cenozoic time; it may represent the shoreline at the time that the fossiliferous sediments were deposited.

The marine fauna was obtained from black organic clay, pebbly clay, and silty sand, having a total thickness of 10–15 feet. The sediments rest upon limestone bedrock containing abundant corals of Mississippian age (Helen Duncan, written communication, 1960), and are overlain by 10 to 15 feet of light olive gray sand-free pebble gravel and sandy pebble gravel and 5 to 10 feet of windblown silt (fig. 157.2). The base of the marine clay lies 17.5 feet above the surface of the Kivalina River and probably about 20 feet above sea level; the top lies about 30 feet above the river. Scattered through the basal layers are poorly rounded cobbles and boulders as much as 3 feet across, some consisting of limestone perforated with pholad borings, and others of pebble conglomerate and basalt. The fauna obtained from the marine clay is listed in table 157.1.

The pebble gravel overlying the fossiliferous marine clay is considerably more extensive than the clay itself; it rests directly on the limestone bedrock along the north bank of the Kivalina River downstream from the creek in which the marine clay is exposed, and it may extend throughout the gently sloping area at the inner edge of the coastal plain north of Kivalina Lagoon. Although the gravel is only 10 to 15 feet thick where it overlies the marine clay, it is at least 30 feet thick nearer Kivalina Lagoon.

The gravel consists chiefly of pebbles of chert and limestone a quarter of an inch to an inch in diameter; the small pebbles are well rounded, but the large ones are subrounded to subangular. Limestone pebbles in

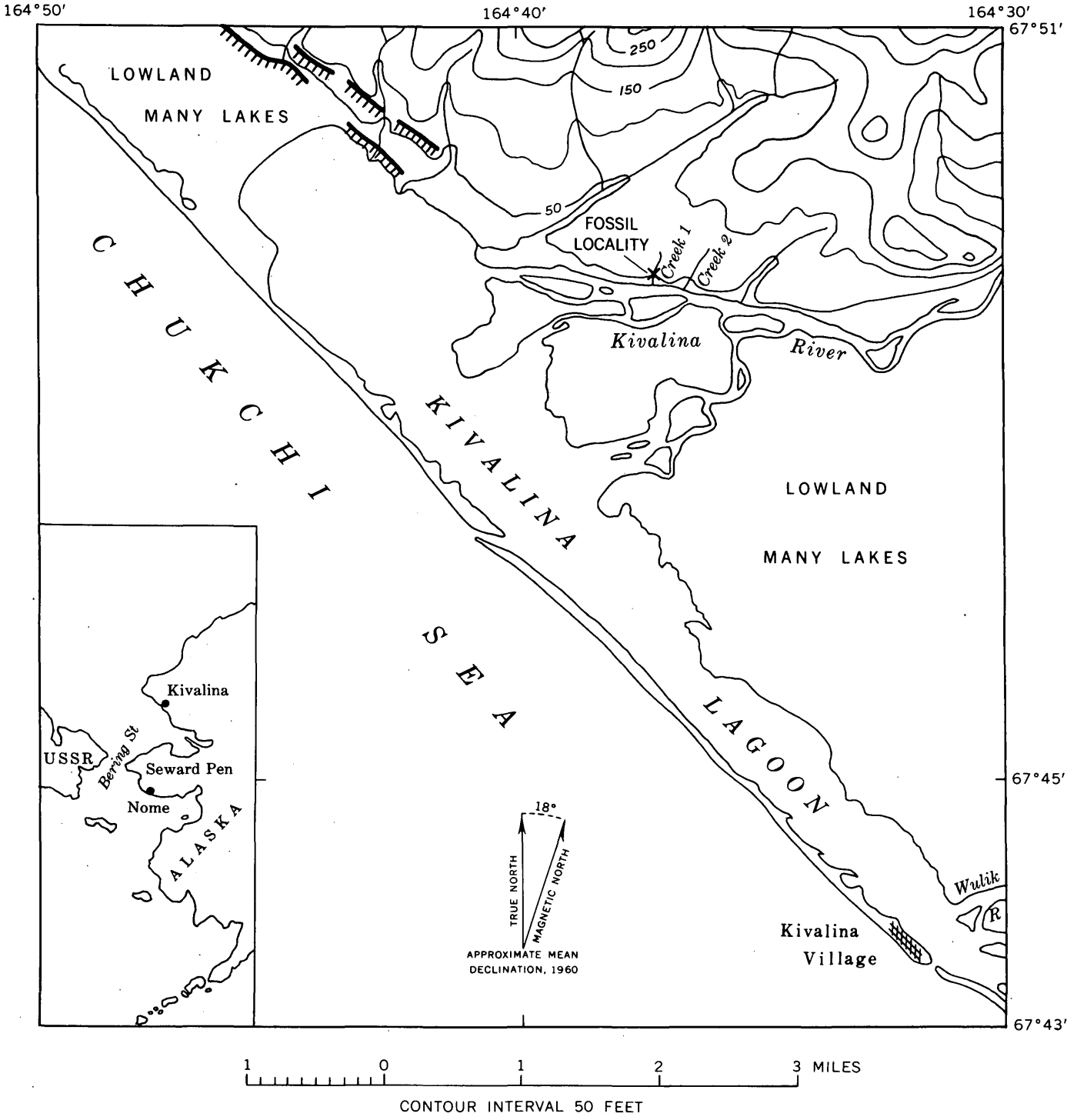

FIGURE 157.1.—Location of fauna probably of Pliocene age near Kivalina, Alaska. Hachures represent scarps believed to be ancient wave-cut cliffs. The lower scarp was probably formed during the last Pleistocene interglacial interval; the upper scarp (between the 50- and 100-foot contours) may have been formed during Pliocene time. Base map adapted from Coast and Geodetic Survey preliminary topographic sheets.

the gravel are strongly leached. Where the gravel rests directly on bedrock, the basal layers contain boulders of basalt and limestone one or two feet in diameter, some of which are riddled with pholad borings. No Cenozoic fossils have been found in the gravel. The fineness of the gravel, the lack of a sandy matrix in some layers, and the pholad-bored boulders in the basal layers suggest that the gravel is a marine sediment, but

TABLE 157.1.—*List of fossils from marine clay near Kivalina, Alaska, and their occurrence at Nome, Alaska, and in Bering and Chukchi Seas* [1]

	Submarine Beach	Third Beach-Int. Beach	Second Beach	Recent in Bering and Chukchi Seas
Pelecypoda:				
Patinopecten (Fortipecten) hallae (Dall)	?			
Astarte hemicymata Dall	×	×		
Astarte nortonensis MacNeil	×	×		
Cardita (Cyclocardia) subcrassidens MacNeil	×	×	×	×
Cardita (Cyclocardia) crebicostata (Krause)	×	×	×	×
Serripes groenlandicus (Brugière)	?	------	×	×
Mya sp. (*truncata* or *japonica*)	×	×	×	×
Saxicava arctica (Linnè)	×	×	×	×
Gastropoda:				
Admete or *Buccinum*	×	×	------	×
Neptunea aff. *N. ventricosa* (Gmelin)	------	------	------	×
Colus aff. *C. halibrectus* Dall	------	------	------	?
Boreotrophon sp. cf. *B. rotundatus* (Dall)	------	------	------	?
Polinices pallida Broderip and Sowerby	------	------	------	×
Foraminifera:				
Buccella inusitata Andersen	×	------	------	×
Elphidiella hannai (Cushman and Grant)	×			
Elphidiella nitida Cushman	×	×		
Elphidium clavatum Cushman	×	×	×	×
Elphidium orbiculare (Brady)	×	×		
Elphidium subarcticum Cushman	×	×	------	×
Quinqualoculina seminulum (Linnè)	------	------	------	×
Ostracoda:				
Clithrocytheridea sp	?	------	------	?
Haplocytheridea sp	------	------	------	?
Cytheridea? s.l. sp	------	------	------	?
Hemicytherura? sp	------	------	------	?
"*Cythereis*" s.l. sp	------	------	------	?
Gen. aff. *Trachyleberis* sp	------	------	------	?
Gen. aff. *Loxoconcha* sp	------	------	------	?

[1] Fossil occurrences at Nome from MacNeil, Mertie, and Pilsbry (1943) and Hopkins, MacNeil, and Leopold (in press). Recent occurrences in Bering and Chukchi Seas from those sources and from MacGinitie (1959), Loeblich and Tappan (1953), and Patsy Smith, table 3 *in* Scholl and Sainsbury (1960).

the relatively poor rounding of the larger pebbles suggests a fluvial origin.

AGE AND AFFINITIES OF THE FAUNA FROM THE MARINE CLAY

The fauna in the marine clay near Kivalina is probably of late Pliocene age but possibly of early Pleistocene age. It is closely similar to both the fauna of Submarine Beach (probably late Pliocene) and that of Third Beach-Intermediate Beach (middle Pleistocene) at Nome (table 157.1). The stratigraphic relations, however, suggest a correlation with Submarine Beach rather than with Third Beach-Intermediate Beach. The fauna is generally similar to Pliocene and Pleistocene molluscan faunas from the Gubik formation in northern Alaska described by MacNeil (1957), and quite different from Miocene and Pliocene molluscan and foraminiferal faunas from the Nuwok formation of Dall (1919) of northeastern Alaska described by MacNeil (1957) and Todd (1957). One of the ostracode species, *Clithrocytheridea* sp., is present in the Gubik formation, and the others are similar to undescribed species in the Gubik formation (I. G. Sohn, written communication, 1960).

Representatives of all of the mollusks except *Patinopecten (Fortipecten) hallae* and *Astarte hemicymata*, and of all of the Foraminifera except *Elphidiella hannai* and *Elphidiella nitida*, are found in Bering and Chukchi Seas today. *Patinopecten (Fortipecten) hallae* and *Astarte hemicymata* are extinct; *Elphidiella hannai* and *Elphidiella nitida* have been reported as living forms only from the North Pacific Ocean. The presence of *Fortipecten* in the Kivalina fauna constitutes strong evidence for regarding that fauna as Pliocene, because in Japan and Sakhalin that subgenus is confined to beds of Pliocene age (Yabe and Hatai, 1940; K. Kobayashi, written communication, 1959). However, *Fortipecten* could not have reached Kivalina until Bering Strait came into existence, and Hopkins (1959) presents evidence indicating that the first seaway through Bering Strait opened no earlier than late Pliocene time.

A minimum age for the marine clay is established by the stratigraphic relations between the overlying gravel and the windblown silt by which the gravel is itself overlain. Study of air photos suggests that the lowland southeast of the Kivalina River represents an outwash plain mantled within the area of figure 157.1 by marine sediments of Second Beach (Sangamon) age. This plain terminates to the east against moraines resembling those of the Nome River glaciation, of Illinoian age, at Nome. The gravel overlying the fossiliferous marine clay lies above the level of the presumed outwash plain and therefore is probably older. The windblown silt overlying the gravel is probably of the same age as the nearby outwash and therefore largely of Illinoian age. If this reasoning is correct, the marine clay can be no younger than middle Pleistocene.

The physical stratigraphy indicates that the marine clay is the correlative of either Submarine Beach or

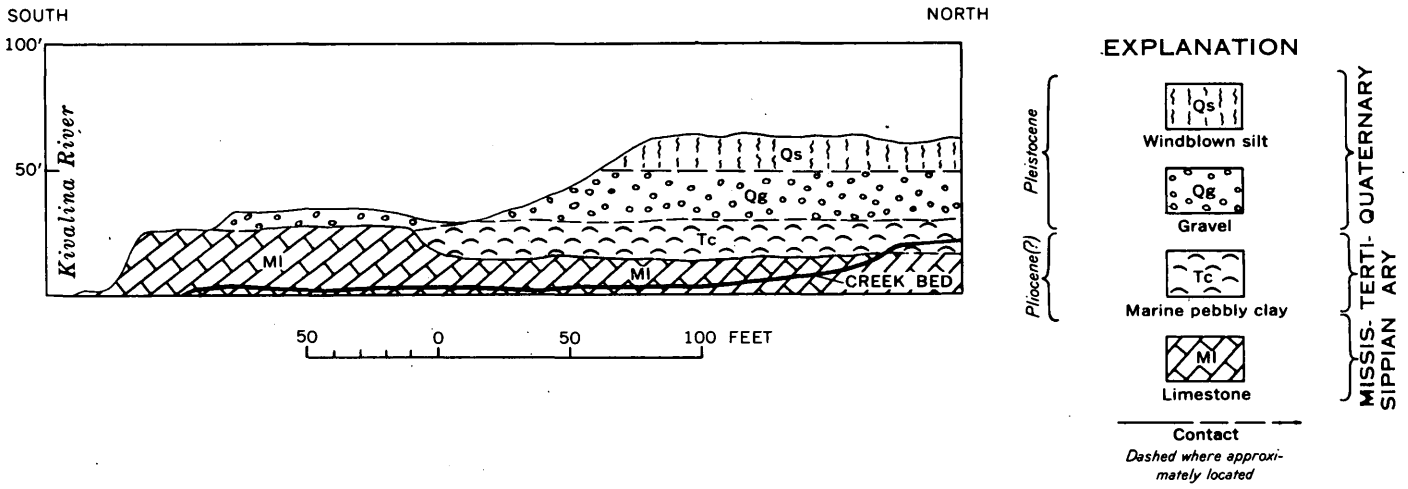

FIGURE 157.2.—Sediments exposed in valley of small tributary entering Kivalina River 1.3 miles above Kivalina Lagoon. Surface of Kivalina River at left is probably less than 5 feet above sea level.

Third Beach-Intermediate Beach at Nome (Hopkins, MacNeil, and Leopold, in press). The fauna is more closely similar to the fauna of Submarine Beach than to that of Third Beach-Intermediate Beach at Nome; and the presence of *Fortipecten* provides strong evidence for a late Pliocene age and for correlation with Submarine Beach at Nome.

REFERENCES

Dall, W. H., 1919, Mollusks, Recent and Pleistocene: Report of the Canadian Arctic Expedition, 1913–1918, v. 8, pt. A, Ottawa.

Hopkins, D. M., 1959, The Cenozoic history of the Bering land bridge: Science, v. 129, p. 1519–1528.

Hopkins, D. M., MacNeil, F. S., and Leopold, E. B., in press, The coastal plain at Nome, Alaska: a late Cenozoic type section for the Bering Strait region: Internat. Geol. Cong., 21st, Copenhagen, 1960.

Loeblich, A. R., Jr., and Tappan, Helen, 1953, Studies of Arctic Foraminifera: Smithsonian Pub. 4105, 150 p.

MacGinitie, Nettie, 1959, Marine mollusca of Point Barrow, Alaska: U.S. Natl. Museum Proc., v. 109, p. 59–208.

MacNeil, F. S., 1957, Cenozoic megafossils of northern Alaska: U.S. Geol. Survey Prof. Paper 294–C, p. 99–126.

MacNeil, F. S., Mertie, J. B., and Pilsbry, H. A., 1943, Marine invertebrate faunas of the buried beaches near Nome, Alaska: Jour. Paleontology, v. 17, p. 69–96.

Scholl, D. W., and Sainsbury, C. L., 1960, Marine geology and bathymetry of the nearshore shelf of the Chukchi Sea-Ogotoruk Creek area, northwest Alaska: U.S. Geol. Survey TEI—606, issued by U.S. Atomic Energy Comm. Tech. Inf. Service, Oak Ridge, Tenn.; also U.S. Geol. Survey open-file report.

Todd, Ruth, 1957, Foraminifera from Carter Creek, northeastern Alaska: U.S. Geol. Survey Prof. Paper 294–F, p. 223–234.

Yabe, Hisakatsu, and Hatai, K. M., 1940, A note on *Pecten* (*Fortipecten* subg. nov.) *takahashii* Yokoyama and its bearing on the Neogene deposits of Japan: Tohoku Imp. Univ. Sci. Rept., ser. 2 (Geology), v. 21, p. 147–160.

158. POSSIBLE SIGNIFICANCE OF BROAD MAGNETIC HIGHS OVER BELTS OF MODERATELY DEFORMED SEDIMENTARY ROCKS IN ALASKA AND CALIFORNIA

By ARTHUR GRANTZ and ISIDORE ZIETZ, Menlo Park, Calif., and Washington, D.C.

Regional aeromagnetic surveys over the Cook Inlet and Copper River Lowlands, Alaska, and the northern and central Great Valley, Calif., record broad total intensity magnetic highs over the belts of Jurassic and Cretaceous marine sedimentary rocks that underlie these areas. These highs are parallel to the major geologic features in each area, and are absent over parallel belts of more severely deformed sedimentary rocks of similar age, which occur in the bordering Chugach Mountains and Alaska Range in Alaska and the Coast Ranges in California. Available magnetic data over the Jurassic slate and greenstone belt in the foothills

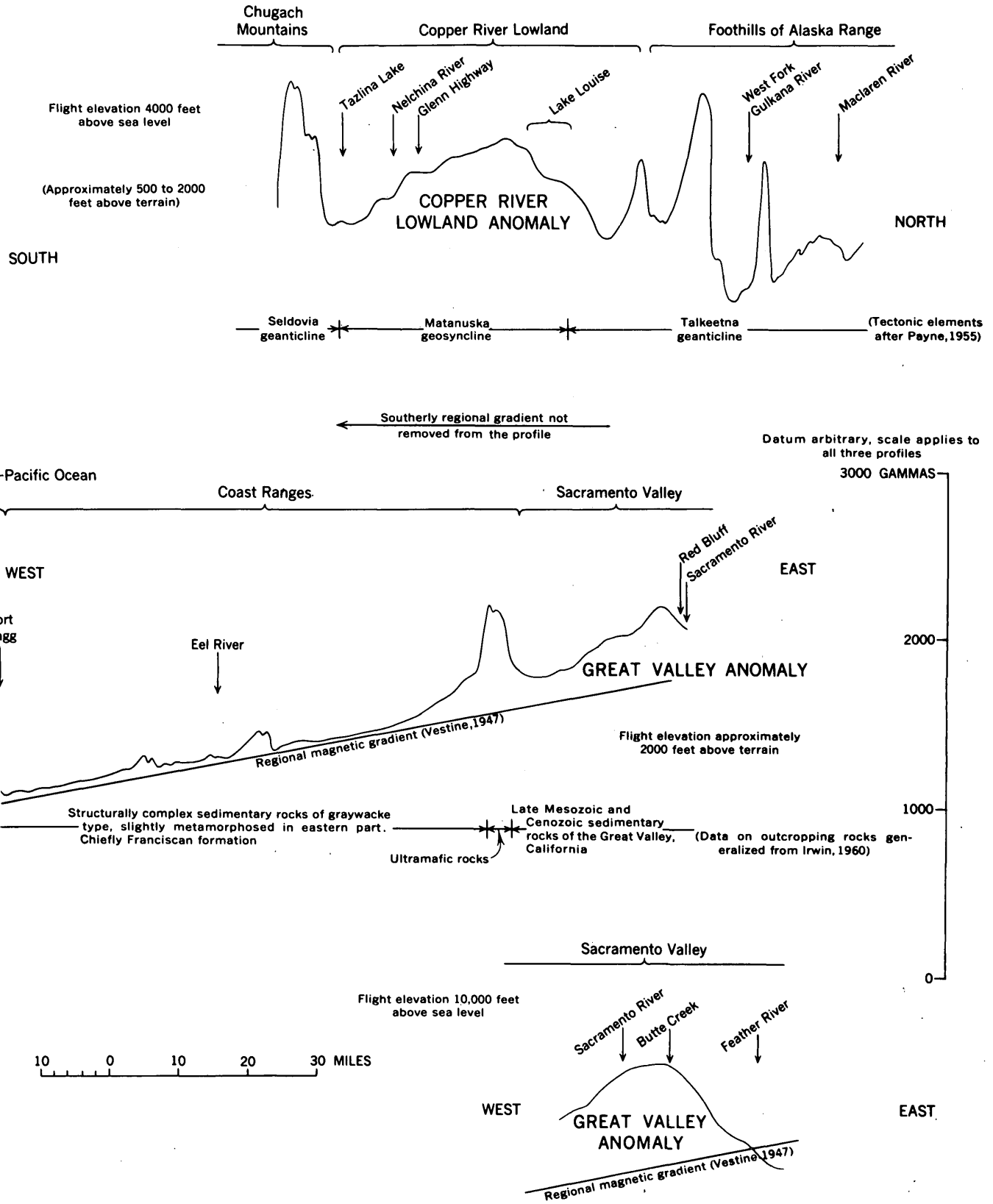

FIGURE 158.1.—Aeromagnetic profiles across Copper River Lowland, Alaska, and Great Valley and Coast Ranges, Calif.

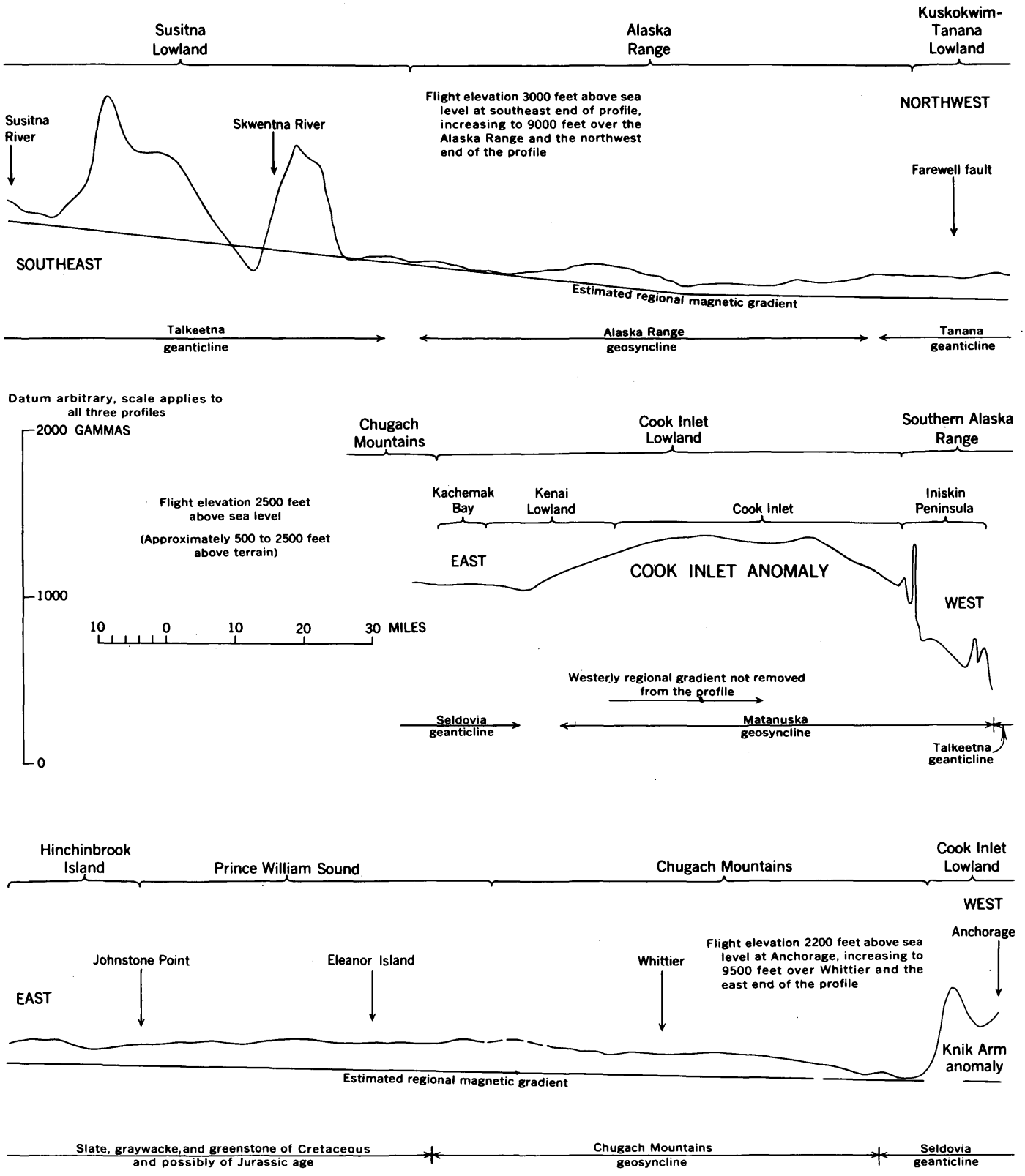

FIGURE 158.2.—Aeromagnetic profiles across Cook Inlet Lowland, Chugach Mountains, and Alaska Range, Alaska.

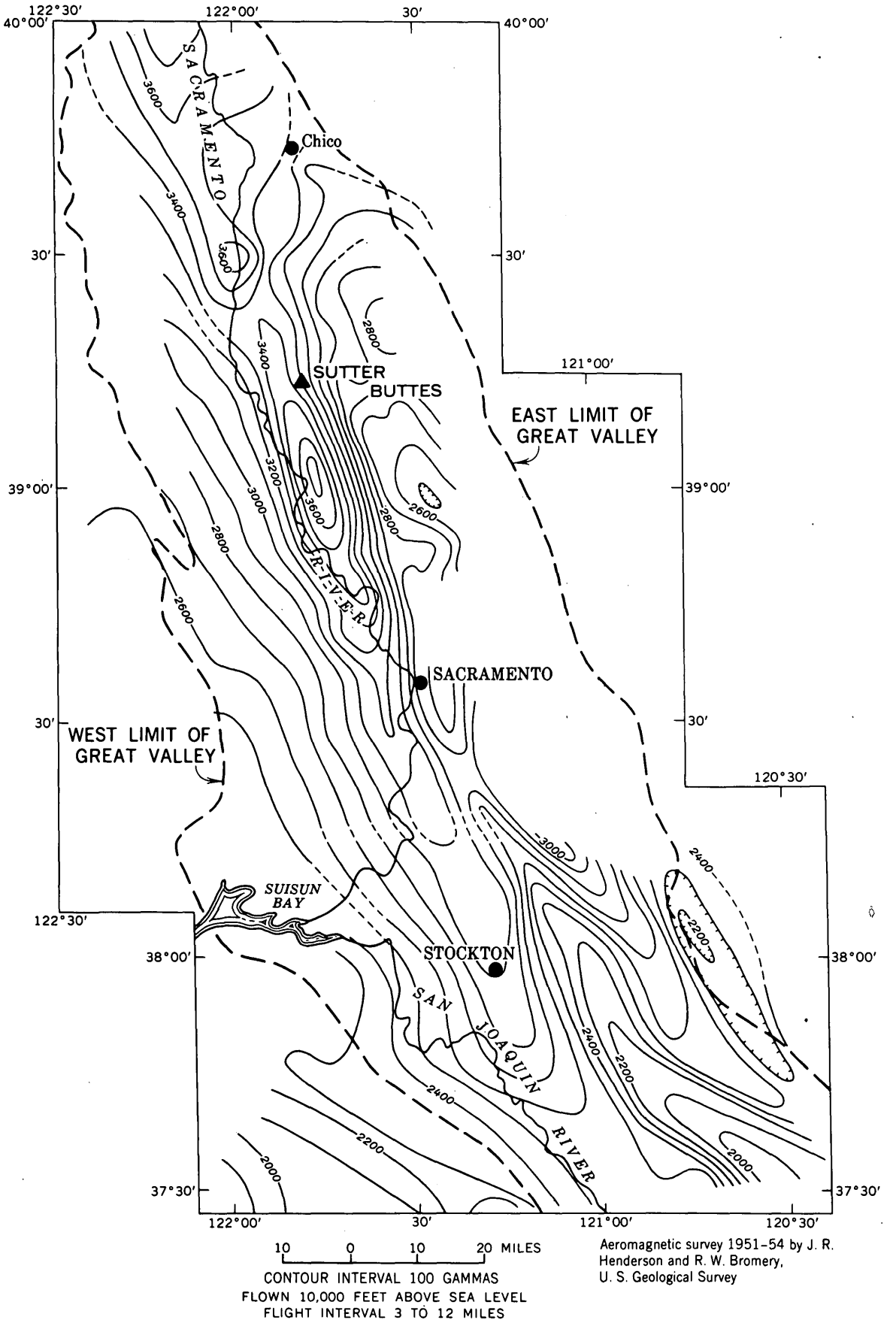

FIGURE 158.3.—Total intensity aeromagnetic map of part of the Great Valley, Calif., relative to arbitrary datum.

557753 O—60——23

of the Sierra Nevada, which borders the Great Valley on the east, record so many magnetic features of shallow origin that it is difficult to determine whether or not broad magnetic highs occur there.

Aeromagnetic profiles across the moderately deformed rocks of the lowland areas and the parallel belts of more severely deformed sedimentary rocks are shown in figures 158.1 and 158.2. The anomalies are seen more clearly if viewed with respect to the sloping regional magnetic gradient. An aeromagnetic map of the northern and central Great Valley is shown in figure 158.3.

The magnetic high over the Cook Inlet Lowland trends northeastward for at least 150 miles, is 50 to 75 miles wide, and has a maximum observed amplitude of about 500 gammas. The magnetic high over the southern Copper River Lowland trends eastward for at least 60 miles, is 35 to 40 miles wide, and has an amplitude of about 400 gammas. The anomaly over the northern and central Great Valley trends northwest along the valley for at least 180 miles, is about 30 miles wide, and ranges in amplitude from a few hundred to more than 1,000 gammas. A broad positive Bouguer gravity anomaly with about the position and width of the magnetic anomaly was found in the Great Valley between the latitudes of Sacramento and Sutter Buttes by George A. Thompson and Manik Talwani (oral communication, March 1960).

The size and gradients of the broad magnetic anomalies suggest that they are produced by areally extensive and thick rock masses that are more magnetic than the surrounding rocks. Depth estimates based on these gradients, patterned after the methods described by Vacquier and others (1951), indicate that a magnetic rock mass may lie 5 to 10 miles beneath Cook Inlet and perhaps as much as 10 miles beneath the southern Copper River Lowland. Depth estimates also indicate that the rocks producing the Great Valley anomaly are buried about 5 to 10 miles, but sharper, superimposed anomalies yield depths that approximate the base of the Mesozoic and Tertiary sedimentary rocks. Because they are magnetic and very large, the rock masses which produce the broad magnetic highs are thought to be igneous.

The Cook Inlet and Copper River Lowland anomalies occur over marine sedimentary rocks deposited in the Matanuska geosyncline (Payne, 1955), which at least in places was a narrow depositional trough. This geosyncline received a thick section of sedimentary rocks of Middle Jurassic to Late Cretaceous age and extended for at least 800 miles from the upper Chitina Valley near the Alaska-Yukon border to a point beyond Herendeen Bay near the tip of the Alaska Peninsula. The Great Valley anomaly occurs over a belt of marine sedimentary rocks of Late Jurassic to Late Cretaceous age. The crests of the magnetic highs lie several miles north and a few miles east, respectively, of the thickest part of the Mesozoic sedimentary prisms in the Copper River Lowland and the Great Valley, and are probably on the more stable side of the troughs in which the sediments were deposited.

The late Mesozoic sedimentary rocks in the Matanuska geosyncline and the Great Valley are characterized by sandstones that are gradational in lithology between wacke and arenite. They are generally somewhat better sorted than the sandstones in the parallel belts of slate or shale and graywacke in the Chugach Mountains and the Alaska Range in Alaska, and in the Franciscan formation in the Coast Ranges of California.

The sequences of slate or shale and graywacke are apparently very thick, for, although they are intensely folded and faulted, they are the only rocks that crop out over large tracts of mountainous terrain. Their apparent great thickness, poor sorting, and lenticularity, and the presence of interstratified volcanic rocks in some areas, suggest that they were deposited in unstable or tectonically active deep geosynclinal troughs with steep slopes. The sedimentary rocks of the Matanuska geosyncline and the Great Valley are better sorted, probably thinner, and lack interstratified volcanic rocks except thin beds of volcanic ash. They seem to have been deposited in more stable and shallower geosynclinal troughs than the sequences with graywacke.

Structural deformation of the sedimentary rocks of the Matanuska geosyncline and the Great Valley is characteristically gentle to moderate. In contrast, the parallel belts with graywacke are severely deformed. The marked difference in structural deformation between the belts of contrasting lithologic aspect indicates that the area of the Matanuska geosyncline and of the Great Valley continued to be tectonically more stable in latest Mesozoic and Cenozoic time than the belts containing slate or shale and graywacke.

There may be a casual relationship between the existence of the rocks that produce the broad magnetic highs and the structure and lithology of the sedimentary prisms that overlie them. This could be true if the magnetic rock masses are structurally more competent than the rocks under the severely deformed belts, where such broad magnetic highs were not observed. Large competent igneous masses beneath the Matanuska geosyncline and the Great Valley could explain the more stable late Mesozoic depositional environment of these areas and their subsequent greater structural stability.

The suggested contrasts in structural competence be-

tween the rocks underlying the moderately and the severely deformed belts of sedimentary rocks cannot be considered as established by the data at hand, and must be tested by other geophysical methods. For example, it is possible that large, nonmagnetic, structurally competent rock masses underlie the severely deformed belts. Magnetic studies of other areas with analogous structural and stratigraphic conditions are desirable to determine whether the association of the magnetic highs with the tectonically more stable sedimentary belts is more than a local coincidence.

REFERENCES

Irwin, W. P., 1960, Geologic reconnaissance of the northern Coast Ranges and Klamath Mountains, California: Calif. Div. Mines Bull. 179 (in press).

Payne, T. G., 1955, Mesozoic and Cenozoic tectonic elements of Alaska: U. S. Geol. Survey Misc. Geol. Inv. Map I–84.

Vacquier, Victor, Steenland, N.C., Henderson, R. G., and Zietz, Isidore, 1951, Interpretation of aeromagnetic maps: Geol. Soc. America Mem. 47.

Vestine, E. H., and others, 1947, Description of the earth's main magnetic field and its secular change, 1905–1945: Carnegie Inst. Washington Pub. 578.

159. STRATIGRAPHY AND AGE OF THE MATANUSKA FORMATION, SOUTH-CENTRAL ALASKA

By Arthur Grantz and David L. Jones, Menlo Park, Calif.

A thick sequence of dark-gray siltstones and shales and light-colored sandstones and conglomerates, all of marine origin, is well exposed in the narrow Matanuska Valley, which extends westward from the southwest Copper River lowland to the town of Palmer (see inset map, fig. 159.1). Martin and Katz (1912, p. 34–39) measured a section of these rocks and were the first to show that they were of Cretaceous age. Martin (1926, p. 317) stated that these rocks "* * * have a broad extent and attain a great thickness in the Matanuska Valley, but they apparently constitute only a single formation * * *", and he proposed that they be named the Matanuska formation.

Mapping by Grantz in the Nelchina area in 1952–57, followed by a stratigraphic reconnaissance by Grantz and Jones farther west in the Matanuska Valley in 1959, demonstrated that several lithologic units within the formation can be mapped in the Nelchina area, and that at least two units can be distinguished by reconnaissance methods in the structurally and stratigraphically complex Matanuska Valley. The difference in the number of units that can be distinguished in the two areas arises from the fact that the structure is simpler, and the exposures more complete, in the Nelchina area than in the Matanuska Valley. The units recognized in the Nelchina area are designated in the schematic columnar sections of figure 159.2. Many of these units are limited at the top by unconformities that record deep erosion. The number indicates that the Matanuska formation was deposited in an unstable seaway.

In the Nelchina area the Matanuska formation unconformably overlies beds of Sinemurian to Neocomian age and is succeeded by coal-bearing rocks of Paleocene or early Eocene age, but the contact at the top of the Matanuska has not been observed. In the Matanuska Valley the Matanuska formation probably rests directly on Lower Jurassic rocks in most places, and regional relations indicate that it is unconformably overlain by the Chickaloon formation, of Paleocene or early Eocene age. As it is here more indurated and more deformed than the Chickaloon formation, it was probably involved in tectonic events that occurred before the Chickaloon formation was deposited.

Study of the numerous collections of mollusks obtained from the formation, and determination of their ages, was begun by Ralph W. Imlay and completed by David L. Jones. These mollusks can be grouped into assemblages of Albian, Cenomanian, Turonian, Campanian, and Upper Campanian and Maestrichtian(?) ages. The critical fossils of these assemblages are listed in table 159.1. Their position in the lithogenetic units is shown in figure 159.2, and the locations of those collected in the Matanuska Valley are shown in figure 159.1.

Albian fossils occur in hard siltstones with sandstone interbeds along the north front of the Chugach Mountains from Palmer to Tazlina Lake, and in distinctly different soft coaly sandstone and abundantly fossiliferous claystone that crop out in the northern part of the Nelchina area. The difference between these rocks is due in part to structural deformation, which was ac-

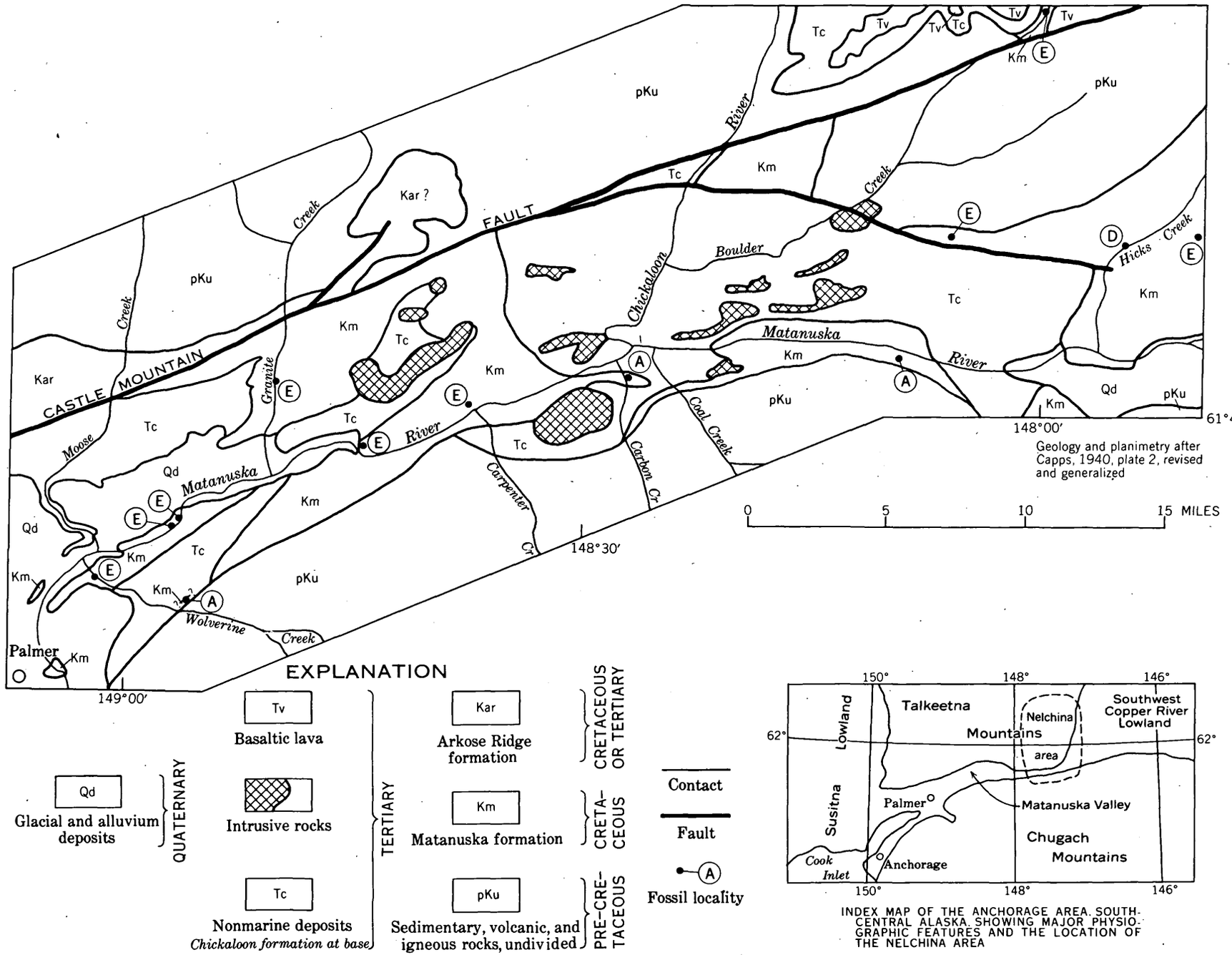

FIGURE 159.1.—Generalized geologic map of the Matanuska Valley, Alaska, showing Cretaceous fossil localities; these are indicated by letters which correspond with fossil assemblages listed in table 159.1.

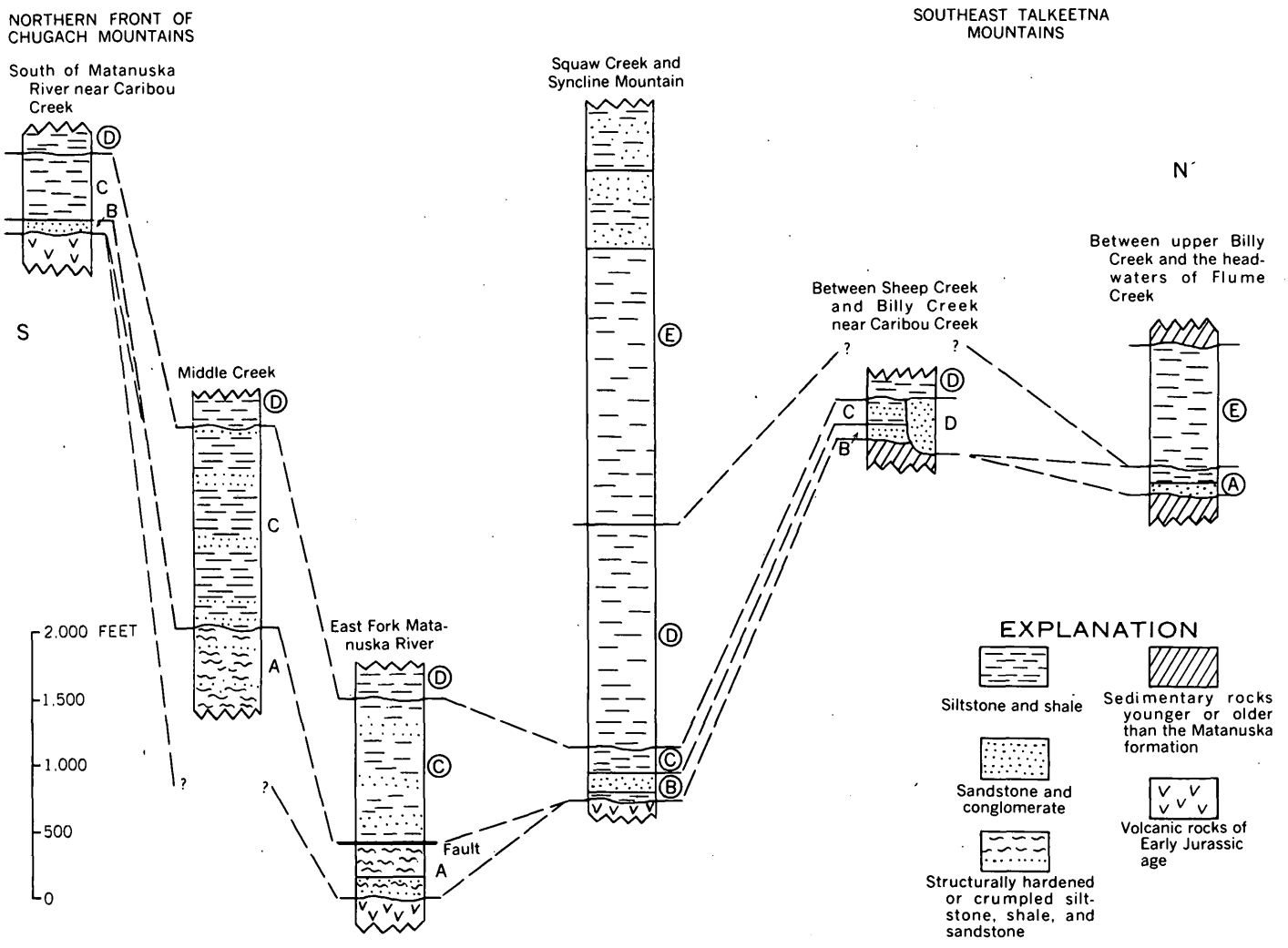

FIGURE 159.2.—Schematic columnar sections of the Matanuska formation, Nelchina area, Alaska. Letters correspond with fossil assemblages listed in table 159.1. Circled letters indicate lithogenetic units from which critical fossils were collected. Uncircled letters indicate lithogenetic units correlated on the basis of lithology.

tive along the Chugach Mountains but not in the northern Nelchina area. This deformation occurred before the overlying Cenomanian to Maestrichtian rocks were deposited.

The structural contrasts in the Albian sedimentary rocks, the rapid coarsening and other changes in the lithology of Cenomanian and Turonian sedimentary rocks in approaching the north front of the Chugach Mountains, and the absence of Bajocian to Valanginian beds in the south part of the Nelchina area suggest that during post-Valanginian Cretaceous time and much of Matanuska time the area of the northern Chugach Mountains was positive and contributed sediment to the Matanuska formation. A more important source of sediment, however, and probably a larger landmass, lay to the north of the Nelchina area.

TABLE 159.1.—*Fossil assemblages and critical fossils found in the Matanuska formation*

Lithologic unit	*Age and fossils*
E	Upper Campanian and Maestrichtian (?)
	Pachydiscus (*Neodesmoceras*) n. sp.
	Pachydiscus ootacodensis (Stoliczka)
	Pachydiscus n. sp.
	Pseudophyllites indra (Forbes)
	Baculites occidentalis Meek
	Baculites n. sp.
	Didymoceras hornbyense (Whiteaves)
	Diplomoceras notabile Whiteaves
	Inoceramus subundatus Meek
D	Campanian
	Inoceramus schmidti Michael
	Anapachydiscus sp.
	Helcion cf. *H. giganteus* Schmidt

TABLE 159.7.—*Fossil assemblages and critical fossils found in the Matanuska formation*—Continued

Lithologic unit	*Age and fossils*
C	Turonian
	Inoceramus aff. *I. corpulentus* McLearn
	Sciponoceras aff. *S. bohemicus* (Fritsch)
	Inoceramus woodsi Boehm (=*Inoceramus costellatus* Woods)
	Mesopuzosia indopacifica (Kossmat)
	Tetragonites aff. *T. glabrus* (Jimbo)
	Inoceramus aff. *I. cuvierii* Sowerby
	Otoscaphites puerculus (Yabe)
B	Cenomanian
	Calycoceras sp. indeter.
	Desmoceras (*Pseudouhligella*) *japonicum* Yabe
	Inoceramus n. sp. aff. *I. yabei* Nagao and Matsumoto
A	Albian
	Brewericeras hulenense (Anderson)
	Freboldiceras singulare Imlay
	Beudanticeras glabrum (Whiteaves)
	Lemuroceras sp.

Because of the northward coarsening in some units, the northward thinning and overlapping of others, and the beach deposits and coal in the basal Albian deposits of the northern Nelchina area, it seems likely that the north edge of the Matanuska seaway was not far beyond the present northern limit of the Matanuska formation in the Nelchina area.

The Matanuska formation underlies a part of the Cook Inlet lowland and much of the southern Copper River lowland. Since the formation is very thick (see fig. 159.2), consists predominantly of dark-gray marine siltstone and shale, and contains abundant mollusks, foraminifers, and radiolaria in many beds, it may be a source of petroleum in the Cook Inlet and Copper River lowlands. In the Nelchina area, however, preliminary tests of porosity and permeability based on a few samples collected at the surface suggest that reservoir rocks may not be abundant even among the beds of sandstone and conglomerate which occur in the formation there at many levels.

REFERENCES

Capps, S. R., 1940, Geology of the Alaska Railroad region: U.S. Geol. Survey Bull. 907, 201 p.

Martin, G. C., 1926, The Mesozoic stratigraphy of Alaska: U.S. Geol. Survey Bull. 776, 493 p.

Martin, G. C., and Katz, F. J., 1912, Geology and coal fields of the lower Matanuska Valley, Alaska: U.S. Geol. Survey Bull. 500, 98 p.

160. RADIOCARBON DATES RELATING TO THE GUBIK FORMATION, NORTHERN ALASKA

By HENRY W. COULTER, KEITH M. HUSSEY, and JOHN B O'SULLIVAN, Washington, D.C., Iowa State University, Ames, Iowa, and Iowa State University, Ames, Iowa

Radiocarbon dates indicate that deposition of the upper member of the Gubik formation near Barrow was initiated prior to 38,000 years B.P. and was terminated prior to 9,100 years B.P. In the eastern part of the Arctic coastal plain province the Quaternary Gubik formation, consisting of as much as 150 feet of unconsolidated marine and nonmarine gravel, sand, silt, and clay, unconformably overlies the Upper Cretaceous Colville group (Miller, Payne and Gryc, 1959, p. 106). Near Barrow the upper member of the formation comprises 15 to 25 feet of tan, fine-grained sand with cross-bedded gravel lenses and contains an extensive marine fauna.

A log (sample W–380) from the base of the upper member of the Gubik formation has been dated at greater than 38,000 years. Although not found in growth position the log showed no evidence of the degree of abrasion which would be expected if it had been successively buried, uncovered, and redeposited. Furthermore, the unweathered condition of the wood suggests that it did not remain long at the surface prior to burial. Consequently, the log cannot predate the enclosing deposits by more than a relatively short period and deposition of the basal sediments must have begun more than 38,000 years ago.

Bedded lacustrine silt, deposited in thaw-lake basins, overlies the upper member of the Gubik formation in many localities near Barrow. Pits dug in the bottom of an artificially drained lake basin 4 miles south of Barrow show two peat-bearing beds in lacustrine silt, one 12 inches and the other one 44 inches below the top of the lake deposits. Radiocarbon age determinations

on samples from these two beds give dates of 3,540±300 years (W–432) and 9,100±260 years (W–847) respectively. Therefore, the uppermost beds of the Gubik formation were deposited more than 9,100 years ago.

REFERENCE

Miller, D. J., Payne, T. G., and Gryc, George, 1959, Geology of possible petroleum provinces in Alaska: U.S. Geol. Survey Bull. 1094, 131 p.

161. METASEDIMENTARY ROCKS IN THE SOUTH-CENTRAL BROOKS RANGE, ALASKA

By WILLIAM P. BROSGÉ, Menlo Park, Calif.

Devonian and older metasedimentary rocks and post-Devonian mafic intrusive rocks form most of the southern Brooks Range in the John River-Wiseman area (fig. 161.1). The Lisburne group and Kayak shale of Mississippian age and the Kanayut conglomerate, in contact with the underlying sandstone of Late Devonian age, occur only near the crest of the range. The Kanayut conglomerate wedges out southward beneath Mississippian rocks. South of the crest a thick unit of black slate and phyllite lies beneath the Upper Devonian sandstone and rests with apparent conformity on the Skajit limestone and with apparent unconformity on Middle(?) Devonian and older chloritic to calcareous schists, chloritic phyllites, black siltstones and limestones.

Although the Skajit limestone has been referred to the Silurian (Schrader; Smith and Mertie), in the type area on the John River it seems related to limestone that is locally interbedded in the basal part of the black slate and phyllite unit and that contains fossils of Middle(?) Devonian age. Furthermore, fossils of Middle or Late Devonian age were collected by I. L. Tailleur (personal communication, 1955) in the Western Brooks Range from limestone which had been mapped as Skajit by Smith and Mertie (1930). The black slate–phyllite unit that overlies the Skajit limestone is correlated tentatively with black mica schist that overlies interbedded marble and calcareous schist in a belt south of the outcrop belt of typical Skajit limestone. A previously unmapped thick silty limestone may be the youngest unit beneath the unconformity.

The metamorphic grade of the rocks near the crest of the range increases southward, from slate to schist of the greenschist facies. Farther south the metamorphic grade decreases sharply to slate and phyllite in the south front of the range.

A belt of Jurassic(?) and Cretaceous graywacke, conglomerate, shale, chert, and mafic igneous rocks lies south of the range and pinches out eastward. Schist pebbles in the graywackes show pre-middle Cretaceous metamorphism.

Granite, granodiorite, and granite gneiss intrude the northern part of the schist belt in the Chandalar Lake area (fig. 161.1). Most of the known metal prospects and zones of silicification lie in the schist belt near the granite and along a line between the granite near Chandalar Lake and an uninvestigated granite on the Alatna River to the west. Lode gold occurs near Chandalar Lake, stibnite and some copper sulfides occur near Wiseman, and small amounts of copper sulfides are common in breccia beneath the Skajit limestone from Wild Lake to the John River.

In addition, copper sulfides occur on the West Fork of Chandalar River in mafic igneous bodies in the Mesozoic rocks. Analyses of stream sediments show a slight concentration of copper around the mafic intrusive rocks at Mount Doonerak and Boreal Mountain, and a marked concentration of zinc at Cladonia Creek.

Cymrite was identified by X-ray diffraction analysis in samples collected from a pyritized zone near the head of Bonanza Creek in the Wiseman quadrangle. This is the first known United States occurrence of that rare barium silicate mineral.

REFERENCES

Schrader, F. C., 1902, A reconnaissance in Northern Alaska: U.S. Geol. Survey Prof. Paper 20, 139 p.

Smith, P. S., and Mertie, J. B., Jr., 1930, Geology and mineral resources of northwestern Alaska: U.S. Geol. Survey Bull. 815, 351 p.

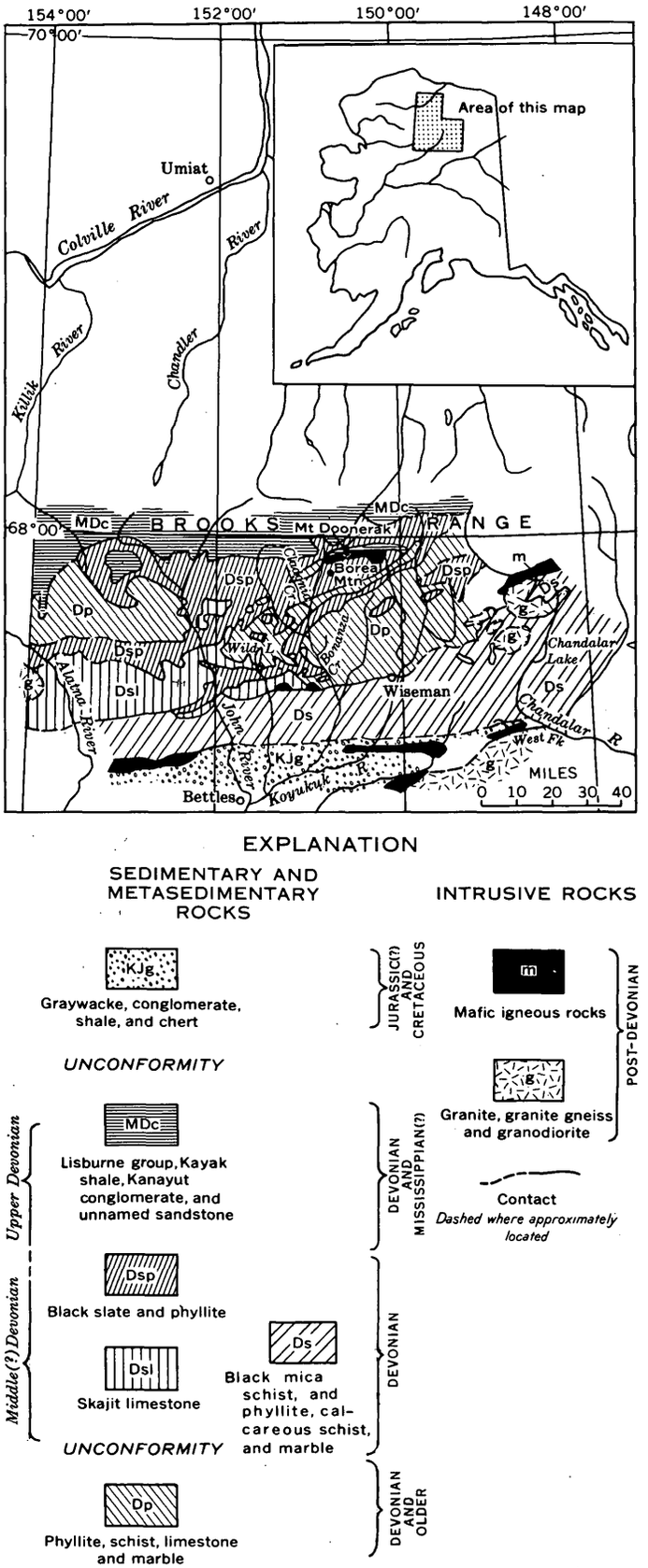

FIGURE 161.1.—Generalized geologic map of the south-central Brooks Range. Inset map shows location in Alaska.

162. SLUMP STRUCTURES IN PLEISTOCENE LAKE SEDIMENTS, COPPER RIVER BASIN, ALASKA

By DONALD R. NICHOLS, Washington, D.C.

Work done in cooperation with Office, Chief of Engineers

Various types of contorted bedding occur in horizontal zones in thin-bedded Pleistocene lake deposits in the Copper River Basin, Alaska. The zones are generally 1 to 5 feet thick and contain folded and sometimes faulted beds of sand, silt, clay, and locally one or more thin beds of volcanic ash that have been faulted and folded. A zone may persist throughout an exposure, but none can be identified in more than one exposure. Two types of contortion, described below, are attributed to slumping generated by earthquakes.

Highly deformed beds lying between undisturbed lake sediments are exposed on the east bank of the Tonsina River, 2 miles south of the Upper Tonsina bridge (fig. 162.1). Both disturbed and undisturbed beds consist mainly of finely laminated, rhythmically bedded sand, silt, and clay, and each bed includes thin layers of white volcanic ash. Intensity of deformation is uniform throughout any vertical section of the contorted zone, which has sharp upper and lower boundaries. Folds generally are tight, commonly are recumbent, and in places are fanshaped. Most of the faults are normal, but some are low-angle thrusts; displacement generally is along the axial plane of folds, which dip in random directions.

FIGURE 162.1.—Compacted strength of lake sediments and included white ash beds is shown by the excellent preservation of bedding after strong folding and faulting. Contorted zone lies between undisturbed varvelike beds.

The excellent preservation of bedding in the lake sediments at this locality indicates considerable compaction. Subsequent deformation either broke the beds into tabular fragments or crinkled them by plastic-fluid flow (fig. 162.1); graded bedding or other evidence of density currents in these materials is lacking. The abrupt termination of folds and faults at the base and top of the zone, together with a lack of soil horizons, excludes glacier overriding, iceberg drag, and frost action as causes of deformation. The contorted beds probably were not transported far; their character suggests that they had the same depositional environment as the undisturbed beds. It seems probable, from the character and composition of the contorted beds, that the deformation was caused by subaqueous sliding of a discrete upper zone of coherent sediment over a gently sloping bed of "fatty" clay that served as a lubricant.

Mendenhall (1905, pl. 9–B and p. 66) described laminated and folded lake silt exposed in a bluff on the Tazlina River, 1 mile above its mouth. He attributed these structures to drag of floating icebergs on the lake bottom or to overriding of glacier ice. The deformed silt and overlying deposits were observed by the author to terminate upstream in a newly exposed, nearly vertical contact with a mass of till. The till, which rises 60 feet above river level, probably formed a subaqueous or subaerial escarpment. The character of the contact suggests that the folds, which gradually diminish in intensity downward and downstream, were developed by subaqueous sliding generated by lateral compression of silt that was displaced when some of the till slumped to the base of the bluff—perhaps during an earthquake. Till blocks in the troughs of some of the folds were probably dislodged contemporaneously to form load casts.

Seismic activity presumably accompanied widespread volcanism to the east, which produced andesite flows, volcanic mud flows, and ash deposits interbedded with Pleistocene glacial and lacustrine deposits in the Copper

River Basin (summarized by Nichols and Yehle, 1960). Earthquakes as far distant as the Yakutat disturbance of July 1958 have caused bluff debris to cascade onto flood plains. Earthquakes provide an ideal mechanism for triggering subaqueous slides, and they probably were the cause of many types of slump structures.

REFERENCES

Mendenhall, W. C., 1905, Geology of the Copper River region, Alaska: U.S. Geol. Survey Prof. Paper 41, 133 p., 20 pls., 11 figs.

Nichols, D. R., and Yehle, L. A., 1960, Mud volcanoes in the Copper River Basin, Alaska: Proc. 1st Internat. Symposium on Arctic Geology, Calgary, Alberta. (in press)

GEOLOGY OF HAWAII, PUERTO RICO, PACIFIC ISLANDS, AND ANTARCTICA

163. PAHALA ASH—AN UNUSUAL DEPOSIT FROM KILAUEA VOLCANO, HAWAII

By GEORGE D. FRASER, Denver, Colo.

On three of the large volcanoes on the island of Hawaii—Kilauea, Mauna Loa, and Mauna Kea—older and younger volcanic series are separated by the Pahala ash. This is the only ash bed in the Hawaiian Islands that is thick and extensive enough to be used for stratigraphic correlation on more than one volcano. Because fire fountains, cinder cones, and associated local ash deposits near the vents are constant elements of the Hawaiian volcanic process, while regional ash blankets are not, the Pahala ash must be explained by a series of events not duplicated in historic time. These events were coneless phreatomagmatic explosions at Kilauea Volcano. There were many closely spaced explosions during a small part of Pleistocene time. Prior to Pahala time, as defined by the thickest ash on Mauna Loa and Kilauea, Kilauea exploded violently but at less frequent intervals so that no thick, regionally identifiable ash blanket could accumulate. Since Pahala time explosions at Kilauea have been much smaller, less frequent, and less numerous, but some of these were also phreatomagmatic blasts of unusual violence. As a stratigraphic unit, the Pahala ash is unique in the Hawaiian Islands; but large explosions, whose products are concealed by lava, eroded, or weathered beyond recognition, may have occurred infrequently at other volcanoes.

Throughout an area of 2,000 square miles on the southeast half of the island (fig. 163.1) the Pahala ash was originally at least 10 feet thick. In about half of this area its thickness exceeded 20 feet, and for miles downwind (south and southwest) from Kilauea Caldera it was about 100 feet thick. The present caldera is younger than the ash, but the presumed source includes the caldera area and may extend for a few miles along the southwest rift.

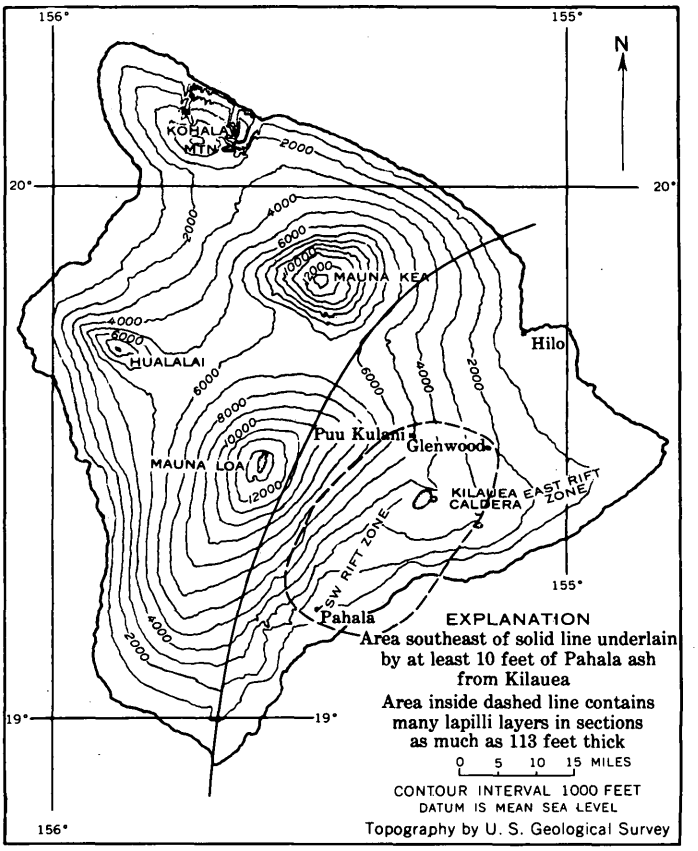

FIGURE 163.1.—Map of the Island of Hawaii, showing distribution and character of Pahala ash.

Because of lava intercalations and thick lava cover, reasonably complete sections of this ash can be seen only in places 6 miles or more from the caldera, beyond the range of fire fountains. Thickness figures and lithologic descriptions in this report are based on these sections.

The ash was deposited in distinct layers which lost their identity over a distance of 30 to 40 miles as coarse particles dropped out. Most of the grains are sideromelane shards, weathered to yellow palagonite in dry areas and to red lateritic materials in wet areas. A few layers of lithic dust are present nearly everywhere.

In sections 6 to 10 miles downwind from Kilauea Caldera about half of the layers contain conspicuous lithic fragments, pumice fragments, and olivine crystals, and have an average grain size greater than 1 mm. More than 20 distinct layers of lapilli, some a foot thick, and a few bomb and block layers, are interbedded with the coarse and fine ash layers. Some of the lapilli are dense, lithic, and angular, while others are pumiceous, vitric, and rounded; the two kinds are commonly in the same layer. Thinned remnants of lapilli layers are recognizable for 20 miles downwind and at least 10 miles upwind.

Index of refraction measurements and chemical analyses confirm the field evidence that Kilauea is the source for the Pahala ash on Kilauea and adjacent slopes of Mauna Loa. This same conclusion was reached by Stone in 1926, and though denied by others it was confirmed by Stearns and Macdonald in 1946.

On the wet southeast slope of Mauna Kea the extensive blanket of Pahala ash is so highly altered that index of refraction and chemical analysis cannot show what its source was. This ash has always been attributed to cinder cones on Mauna Kea, but field evidence now suggests that most of it came from Kilauea. Partial sections of ash 10 miles northeast of Kilauea Caldera contain lapilli layers, but nearly complete sections 12 miles farther from Kilauea and closer to the Mauna Kea cones do not. Coarse ash layers can be traced northward from Hilo for 11 miles. In this entire area the ash is a constant distance (about 20 miles) and bearing from the summit cones on Mauna Kea. In spite of this there is a systematic change in the deposit and that change occurs outward from Kilauea. The layers converge very gradually, the coarse grains get smaller, and the section gradually becomes thinner. The Pahala ash forms gradually changing layers of regional extent, which is not true of any other ash in the Hawaiian Islands. No deposits from summit and flank cones on any Hawaiian volcano, including Mauna Kea, can be traced more than 7 miles from their source.

In 1924, according to eyewitnesses, a series of coneless phreatic explosions at Kilauea scattered thin deposits of lithic dust all over the area underlain by Pahala ash, including the entire east slope of Mauna Kea; but these deposits can be identified now only in the immediate vicinity of Kilauea Caldera. By any criterion the Pahala explosions were much larger, and though they took place on Kilauea they readily account for 15 feet of ash on Mauna Kea. At about that distance downwind from Kilauea Caldera the ash is 55 feet thick.

It is concluded that Pahala ash on the lower, though not the upper, southeast slope of Mauna Kea came from Kilauea and not from the cones on Mauna Kea.

Most of the Pahala ash elsewhere on the island is less than 10 feet thick and is commonly overlain, underlain, or mixed with local cone-derived ash from Mauna Kea or one of the other volcanoes. Where local contributions dominate, the percentage of ash from Kilauea is indeterminate and the stratigraphic value of the formation is questionable.

Several lines of evidence indicate that the cause for the series of large phreatomagmatic explosions at Kilauea was massive foundering in the summit and southwest rift areas, followed by ingress of the ground water abundantly available near sea level in the Ghyben-Herzberg lens:

1. The presumed source area contains more large faults and is closer to sea level than similar areas on the other volcanoes. There is a lava-filled graben on the southwest rift.
2. Phreatic explosions in 1924 were accompanied by foundering in the summit area.
3. Lithic debris, so abundant in the Pahala ash near its source, is characteristic of modern phreatic and phreatomagmatic explosions at Kilauea.
4. Nonvesicular glass fragments (not shards) are present in the Pahala ash far from the sea, and this unique "black sand" forms today only where sea or ground water mixes with lava and explodes.
5. Kilauea has remained a primative volcano extruding tholeiitic basalt throughout its history, but Mauna Kea, with its many cones, has changed chemically. This change from tholeiitic to a somewhat more alkalic magma (Powers, 1955, p. 93) is very common throughout the islands and results in a mild increase in explosivity; but there appears to be no way to get large explosions in Hawaiian volcanoes except by extraneous water.

REFERENCES

Powers, H. A., 1955, Composition and origin of basaltic magma of the Hawaiian Islands: Geochim. et Cosmochim. Acta, v. 7, p. 77–107.

Stearns, H. T., and Macdonald, G. A., 1946, Geology and ground-water resources of the Island of Hawaii: Hawaii Div. Hydrography Bull. 9, 363 p.

Stone, J. B., 1926, The products and structure of Kilauea: Bernice P. Bishop Mus. Bull. 33, 59 p.

164. SINKHOLES AND TOWERS IN THE KARST AREA OF NORTH-CENTRAL PUERTO RICO

By WATSON H. MONROE, San Juan, P.R.

Work done in cooperation with the Department of Industrial Research, Puerto Rico Economic Development Administration

Limestone formations of Oligocene and Miocene age that dip gently northward have been eroded into a mature karst topography in a belt measuring about 18 km by 120 km along the northern coast of Puerto Rico west of San Juan. Detailed geological studies in an area measuring 25 km by 20 km, the eastern border of which is 14 km west of San Juan (fig. 164.1), show that the kinds of karst topography differ from one formation to another (figs. 164.2 and 164.3).

At the base of the Oligocene and Miocene sequence is the San Sebastián formation, which consists of 0 to 80 m of sand and laminated sand and clay, and contains local lenses of gravel and small cobbles. Near the top of the formation is a persistent layer of silty, finely glauconitic marl.

Overlying the San Sebastián is the Lares limestone, which at most places has a basal unit of coarse to very coarse, commonly glauconitic quartz sand and calcareous sandstone as much as 60 m thick. The sand unit is overlain by very pure to earthy, massive to thin-bedded limestone 10 to 140 m thick.

The Cibao formation, which overlies the Lares limestone, is a lenticular unit of marl, chalk, limestone, sand, and sandstone, 170 to 210 m thick.

Above the Cibao is the Aguada limestone, about 90 meters thick and consisting of somewhat earthy limestone interbedded with chalk and marl.

Overlying the Aguada limestone is the Aymamón limestone, which consists of more than 200 meters of very pure limestone, generally stratified to massive but locally consisting of breccia.

A large variety of Quaternary surficial deposits consisting of beach deposits, dunes, swamp deposits, marine and fluvial terrace deposits, alluvium, and locally landslide debris forms a discontinuous mantle over the Oligocene and Miocene formations.

Solution and erosion of the limestone formations have produced three distinct topographic forms: steep-sided generally deep cone sinks, very steep-sided towers, and low rounded hills. Some lines of sinks have coalesced into uvalas, and some uvalas and sinks have been partly filled by alluvium to form poljes. Figure 164.3 is an objective depiction of the sinkholes, uvalas, and poljes showing in black all areas surrounded by depression contours except those related to landslides. For each sink, uvala, and polje the depths from the highest depression contour to the lowest in each pit were tabulated to determine the maximum and median depth for each belt of sinkholes; the figures given below are conservative as they refer only to the depth of the present surface, whereas many of the sinks are considerably deeper to bedrock than measured because of an indeterminate thickness of alluvium.

The Lares limestone has been eroded at most places into a terrain of very steep-sided towers 75 to 150 m high, separated by long, narrow valleys consisting of connected sinkholes. A rather poorly defined alinement of the valleys and notches suggests that they follow a weak joint system. The median depth of sinkholes in the Lares is 8 m and the maximum depth is 40 m.

At most places the Cibao formation weathers to gently rolling hills; sinkholes occur only where limestone members are thicker than 20 m. The median depth of these sinkholes is 10 m and the maximum depth is 40 m.

Typical mature sinkhole karst, consisting of deep sinkholes separated one from another only by narrow ridges of limestone is developed on the Aguada limestone. The ridges and low hills between the sinkholes are characterized by rounded slopes in notable contrast to the steep-sided towers on the Lares and Aymamón limestones. The median depth of sinkholes in the Aguada is 16 m and the maximum is 60 m.

The Aymamón limestone at the top of the sequence weathers into steep-sided towers (fig. 164.4) and ridges parallel to the strike of the formation. Most of the towers are less than 50 m high. Sinkholes are common only in its lower part where the Aguada is just below the surface.

Preliminary studies indicate that closely spaced deep sinkholes form in rocks consisting of alternating hard and soft beds and that tower-karst develops on homogenerous medium to dense limestone.

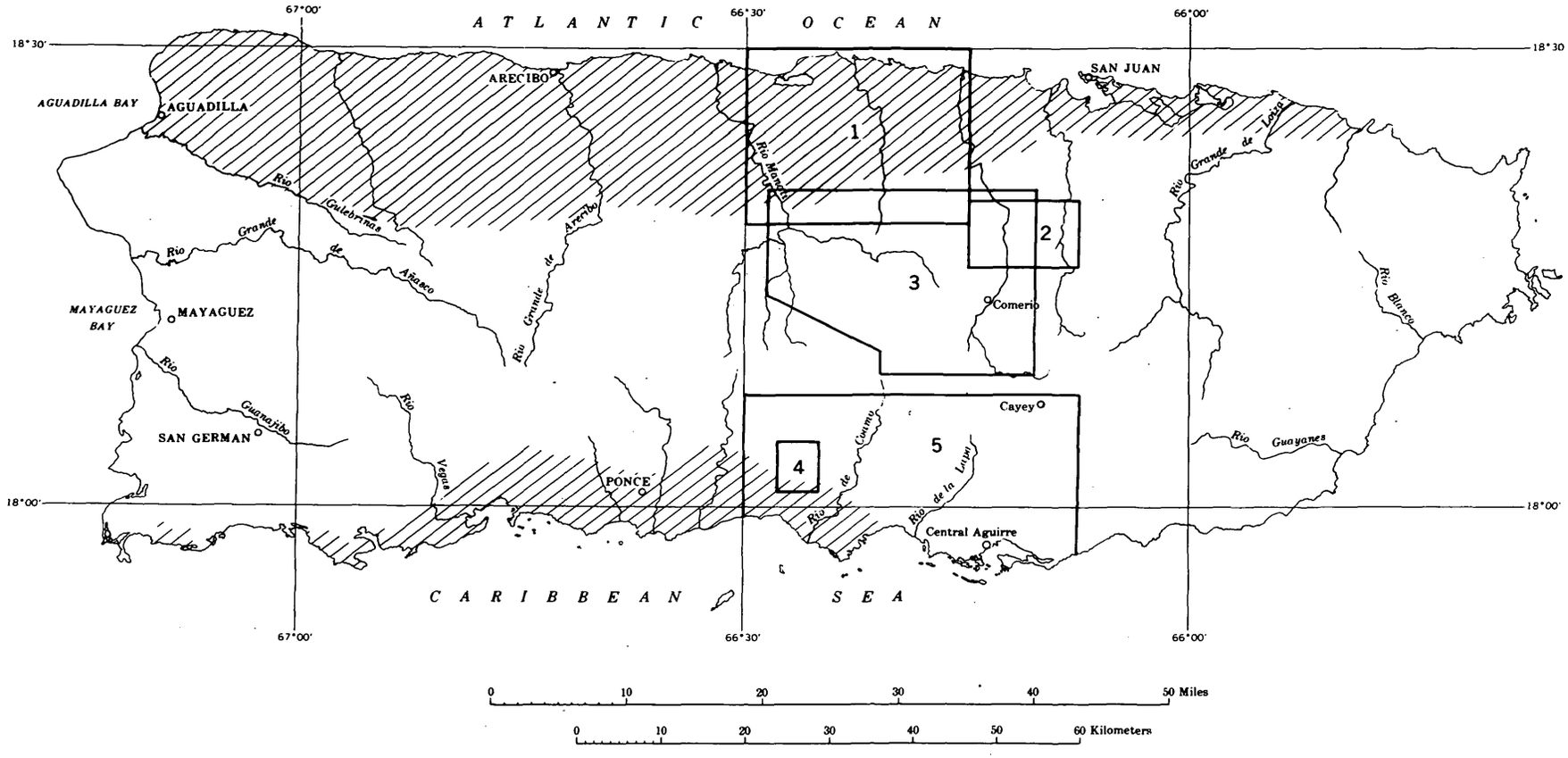

FIGURE 164.1.—Map of Puerto Rico showing extent of undifferentiated middle Tertiary limestones and Quaternary rocks (diagonal lines), and extent of undifferentiated early Tertiary and Cretaceous volcanic rocks and early Tertiary(?) plutonic intrusive rocks (unpatterned areas). Outlines of areas referred to in this and other papers in this volume on Puerto Rico are shown also, as follows: 1, This report; 2, Pease, p. B360–B363; 3. Briggs and Pease, p. B365–B366; 4, Glover and Mattson, p. B363–B365; and 5, Mattson and Glover, p. B367–B369.

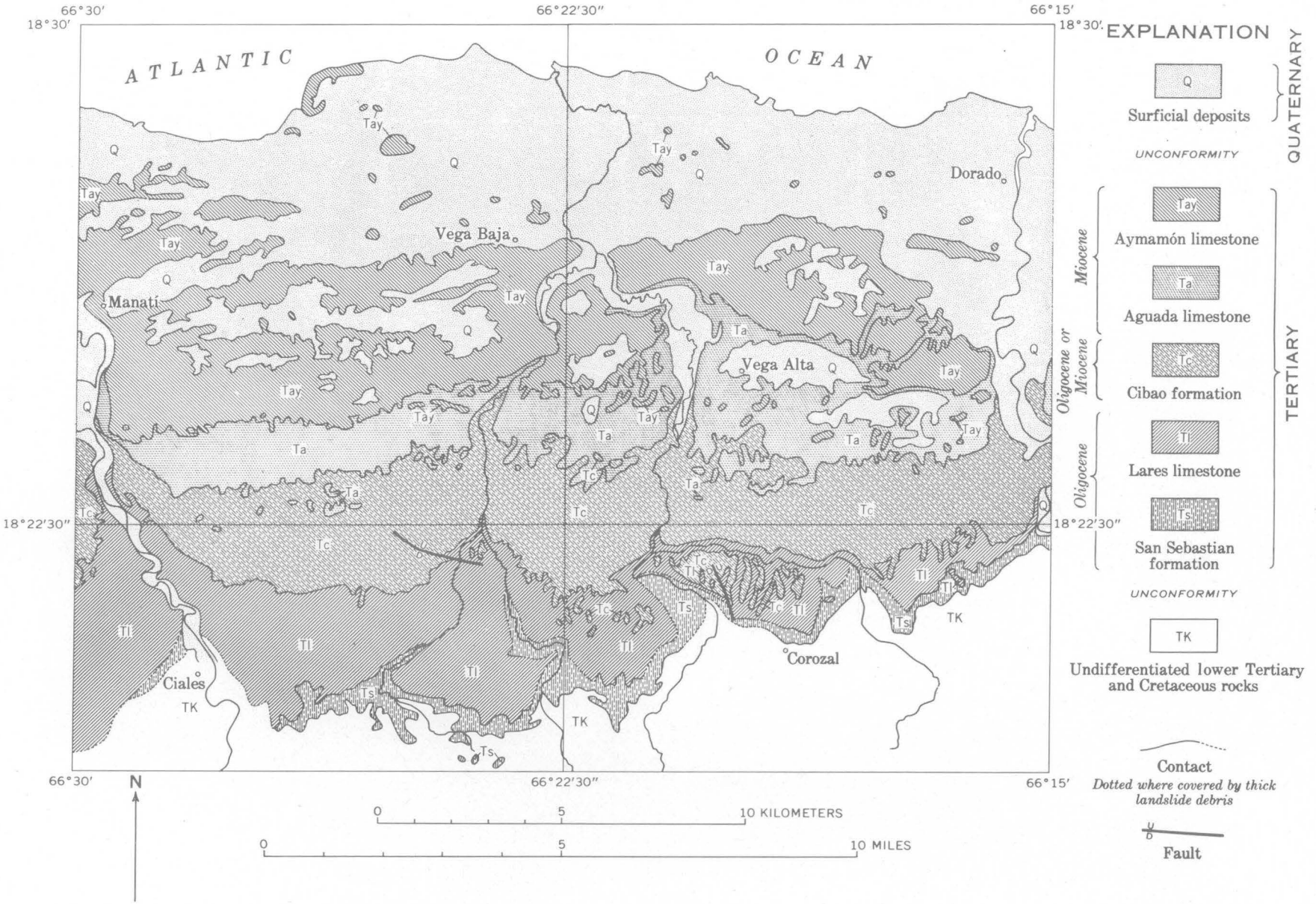

FIGURE 164.2.—Generalized geologic map of middle Tertiary and Quaternary rocks in the Ciales, Corozal, Manatí, and Vega Alta quadrangles. Only larger bodies of Quaternary deposits shown.

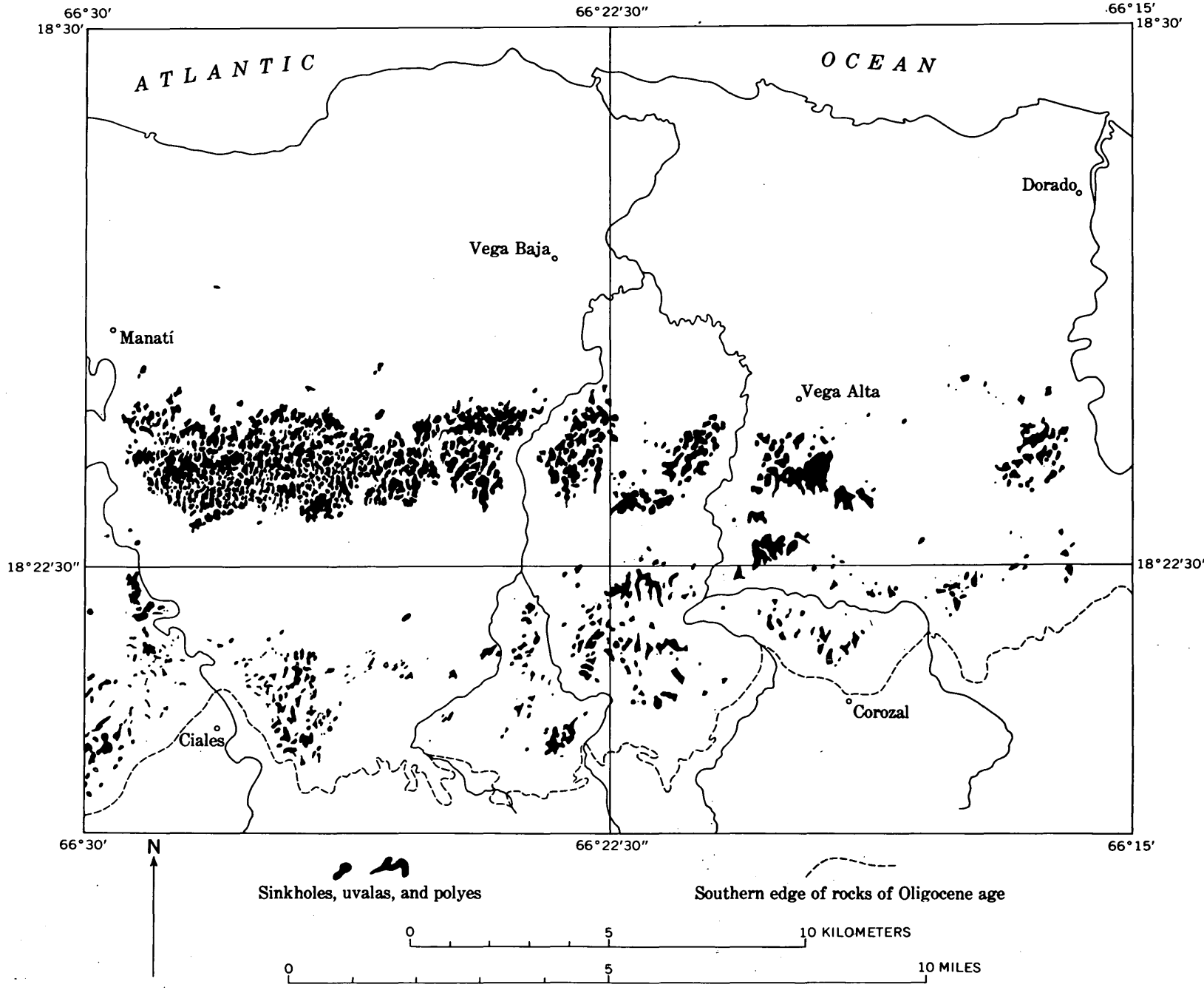

FIGURE 164.3.—Map of same area as figure 164.2 showing locations of sinkholes, uvalas, and poljes. The belt of closely spaced sinkholes across center of map corresponds to outcrop of Aguada limestone and lower part of Aymamón limestone. The sinkholes in the Lares limestone near southern border of map are interspersed with high towers.

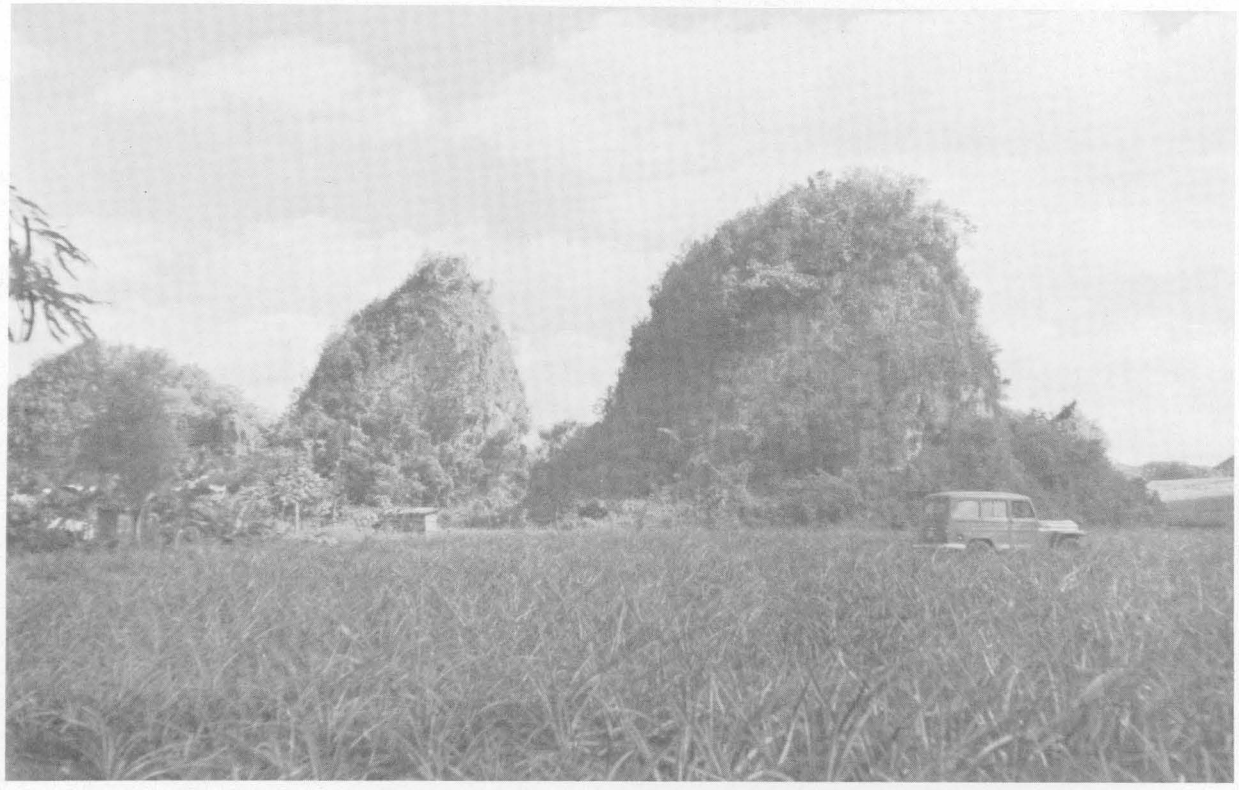

FIGURES 164.4.—Low towers of Aymamón limestone that rise above plain of Quaternary sandy clay.

165. STRUCTURAL CONTROL OF HYDROTHERMAL ALTERATION IN SOME VOLCANIC ROCKS IN PUERTO RICO

By M. H. PEASE, JR., San Juan, P.R.

Work done in cooperation with the Department of Industrial Research, Puerto Rico Economic Development Administration

Chloritized volcanic rocks of the Naranjito quadrangle, Puerto Rico (fig. 164.1), are partly or wholly silicified and sericitized in a broad belt trending about N. 80° W. across the center of the quadrangle, (fig. 165.1). The contacts of these silicified rocks are not sharply defined, but transcurrent faults trending west-northwest mark the general borders of the belt. Shearing is prominent along these faults, and they are cut in several places by right-lateral faults trending north-northwest and of small displacement.

Narrow discontinuous zones of hydrothermally altered rocks that trend about N. 80° W., parallel to the regional structure, occur locally in this belt. Their contacts are commonly marked by strong shears. In most outcrops the altered rocks seem to be homogeneous as a result of tropical weathering, but in the canyon of the Río Bayamón (fig. 165.2) exposures are sufficiently fresh to show a heterogeneity in the degree of alteration of the rocks. Exposures in the riverbed itself exhibit an intricate structural pattern that could not be detected in more weathered exposures of altered rock.

Five rock types have been mapped in the canyon of the Río Bayamón (fig. 165.2): (a) greenish-gray chloritized and finely pyritized volcanic rocks that lie outside the hydrothermally altered zone; (b) greenish-gray finely pyritized volcanic rocks within the altered zone in which finely disseminated hydrothermal quartz is ubiquitous—locally anastomosing veins of quartz with cubic pyrite trend east-northeast; (c) light-gray hard jasperoid rock, stained shades of yellowish brown and

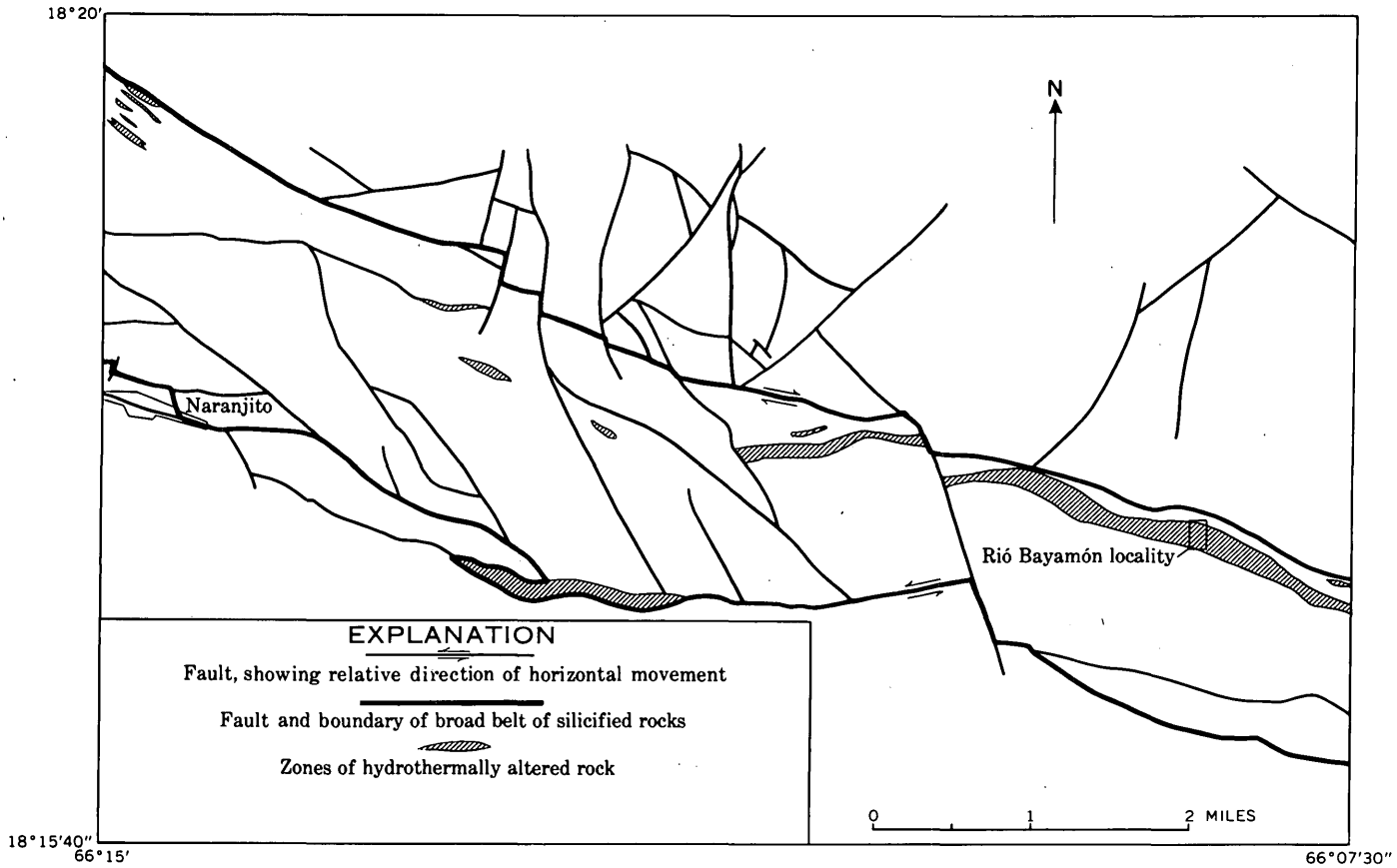

FIGURE 165.1.—Fault map of the central part of the Naranjito quadrangle showing the outline of the belt of silicified rocks, the zones of hydrothermally altered rock, and the area included in figure 165.2.

composed chiefly of quartz with pyrite and minor sericite; (d) light-gray soft sericitic rock, stained shades of yellowish brown and composed chiefly of sericite and clay with minor quartz and pyrite; (e) fine- to medium-grained dioritic dikes that are virtually unaltered except along their borders.

All the rocks in this canyon exposure are severely fractured except for the comparatively massive dioritic rocks. The boundaries of the zone of altered rock are gradational and are generalized on the geologic map (fig. 165.2). Although the volcanic rock types mapped within the hydrothermally altered zone are distinctive, their contacts are commonly either obscured or gradational, and where the rock is highly weathered, contacts could not be mapped.

Four significant directions of shear and (or) fracture have been noted in the major belt that contains the hydrothermally altered rock: (a) west-northwest-trending faults (fig. 165.1) and shears mark the regional trend of the structure and in particular the trend of the hydrothermally altered zones; (b) west-trending red hematite-bearing shears such as those shown in figure 165.2 are common throughout the belt; (c) fractures trending east-northeast as represented by the quartz-pyrite veins of figure 165.2 are prominent in the fresh Río Bayamón exposure but not elsewhere; (d) faults trending north-northwest with small left- and right-lateral displacements are very common in the area. They offset faults that trend west-northwest (fig. 165.1), and in the Río Bayamón exposure are the only fractures along which displacement is clear.

Movement took place along the two right-lateral faults that trend north-northwest (*A* and *B* in figure 165.2) before hydrothermal solutions invaded the rocks; quartz-pyrite veins are more abundant on the east sides of both faults *A* and *B* than on the west sides and some of these veins appear to turn northward along fault *A* or *B* before continuing westward. This evidence suggests that faults trending north-northwest acted as western barriers to the migration of these solutions and are therefore older. However, there is also evidence that the altered rocks have been displaced by movement on other faults that trend north-northwest, indicating that movement also took place along this fault system after invasion of the altering solutions.

Evidence derived from study of the detailed map of the Río Bayamón area and the regional geology of the

55773 O—60——24

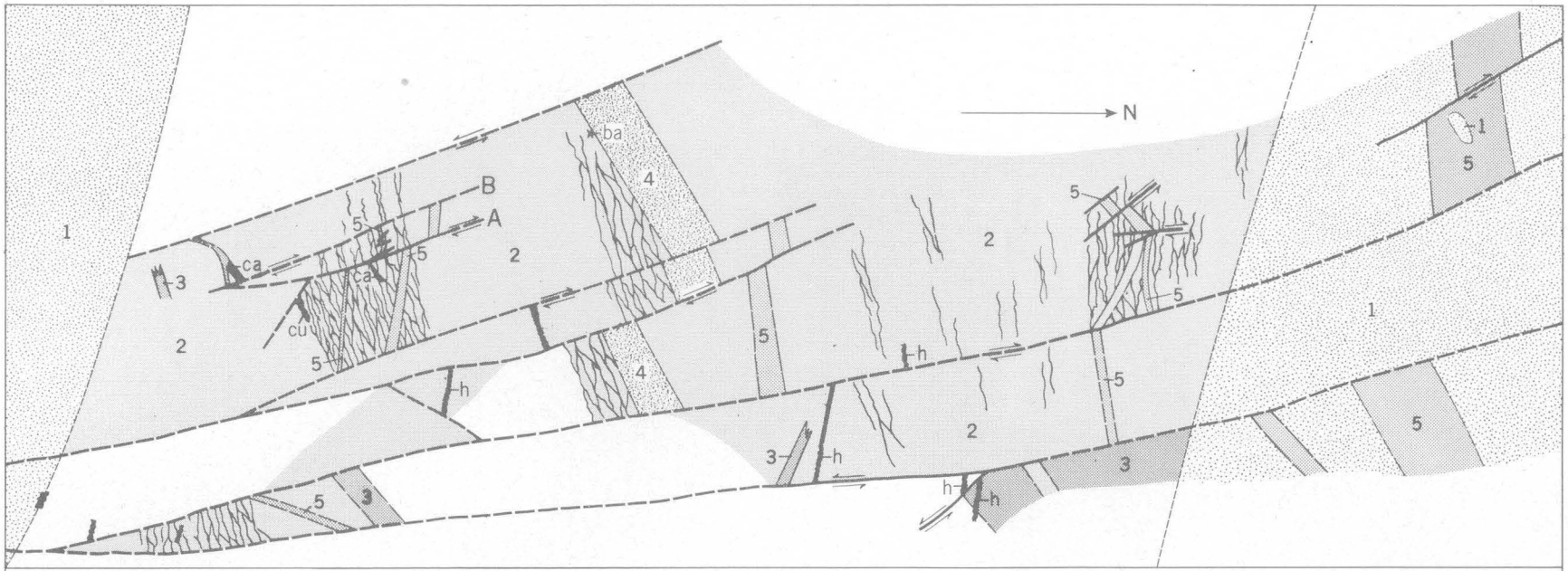

EXPLANATION

1 — Green volcanic rocks

2 — Green volcanic rocks, with interstitial secondary quartz and cut by many anastamosing veins of quartz with coarse cubic pyrite

3 — Light-gray, hard jasperoid rock

4 — Light-gray, soft sericitic rock

5 — Massive dioritic dikes

Fault
Dashed where uncertain or projected; arrows indicate direction of apparent movement

Contact
Dashed where uncertain or projected; short dashes indicate generalized border of hydrothermally altered zone

Strong shear zone or vein
h = *red hematitic coloration in shears*
cu = *copper mineralization in quartz vein*
ca = *calcite vein*
ba = *barite occurrence*

Where no pattern is shown, the geology cannot be interpreted because of heavy vegetation and rock debris

0 100 200 300 400 FEET

FIGURE 165.2.—Geologic map of the hydrothermally altered zone exposed in the canyon of the Río Bayamón.

Naranjito quadrangle suggests the following sequence of geologic events:

1. Volcanic rocks were chloritized and finely pyritized, possibly as a result of deuteric action or at a later date by regional metamorphism.
2. Compressive forces from the west-southwest and east-northeast developed shears trending west- and west-northwest and opened fractures trending east-northeast.
3. Diorite dikes were emplaced after the major fracturing had ended; these dikes are relatively unshattered and are altered only near their borders.
4. Later displacement along faults trending north-northwest offset the east-northeast fractures chiefly in a right-lateral direction; the hematite-bearing shears and the dikes were also displaced at this time.
5. Hydrothermal solutions emanating from depth disseminated silica throughout these highly fractured volcanic rocks, but altered only the borders of the more massive intrusive rocks. Quartz and coarse cubic pyrite were concentrated in the open fractures that trend east-northeast, which served as conduits for the passage of these solutions. Westward migration of these solutions was partially obstructed by earlier offset along the set of tight faults that trend north-northwest. Where concentration of the solutions was sufficiently great, however, volcanic rock in places was almost entirely transformed to quartz-sericite-pyrite or sericite-quartz-pyrite rock.
6. Further movement on the faults trending north-northwest offset these zones of hydrothermally altered rocks.

166. SUCCESSIVE THRUST AND TRANSCURRENT FAULTING DURING THE EARLY TERTIARY IN SOUTH-CENTRAL PUERTO RICO

By Lynn Glover III and Peter H. Mattson, Ponce, P.R.

Work done in cooperation with the Department of Industrial Research, Puerto Rico Economic Development Administration

Late Cretaceous and middle Eocene(?) (Pessagno, 1959) rocks, largely of volcanic origin, crop out in south-central Puerto Rico (fig. 164.1). Paleocene and early Eocene fossils have not been found and may be absent because of an unconformity in the sequence.

Folds in this sequence are generally asymmetrical with the axial plane inclined toward the southwest, and those wider than 1 kilometer trend N. 70°–80° W., parallel to the dominant direction of folding in Puerto Rico. Smaller folds are commonly isoclinal and do not parallel the regional structures so closely.

The thrust faults commonly have sinuous traces but are generally parallel to the trend of the folds. Thrust fault surfaces are uneven but probably have an average dip of 30° to the southwest. Detachment planes at shallow depth are indicated by small-scale isoclinal folds in the thin-bedded tuffaceous sandstone at several places in the northern part of the area shown in figure 166.1. Along a large thrust fault west of Poblado Río Cañas Arriba, breccia is as much as 60 meters thick and one breccia block is 60 meters thick, 900 meters long, and 500 meters wide.

In the southern part of the area shown in figure 166.1 a steeply southward-dipping fault trends N. 60°–70° W., and passes through Las Ollas. The fault appears to be normal in that the south side is down; regional considerations, however, suggest that it is primarily a left-lateral transcurrent fault. South of Las Ollas is the Esmeralda fault which also trends N. 70° W. over the 25-kilometer distance that it has been mapped within and outside the area of figure 166.1. The Esmeralda fault dips about 70° southward, and is a left-lateral transcurrent fault as shown by the drag effects in the southern block west of the Río Descalabrado. The transcurrent faults cut the folds in the area shown in figure 166.1 and, just east of the area, cut the thrusts. The transcurrent faults also commonly produce a graben and horst structure as shown in figure 166.1.

A few kilometers west of the mapped area the rocks and structures shown in figure 166.1 are overlapped by conglomerate of the Juana Díaz formation of middle Oligocene age.

Both folds and thrust faults probably were caused by compression in about a N. 20° E. direction, or possibly

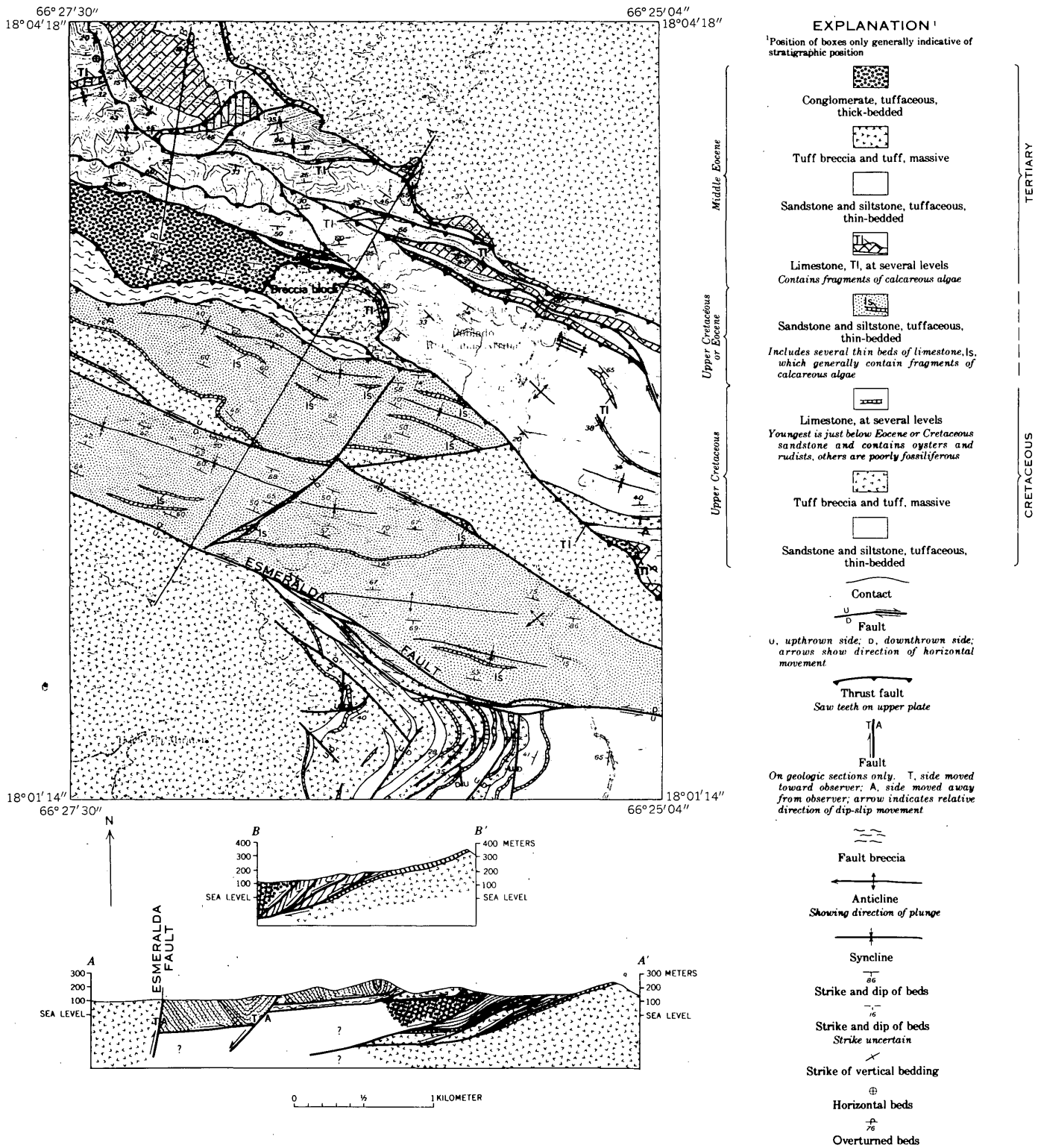

FIGURE 166.1.—Geologic map and sections of part of the Río Descalabrado quadrangle, Puerto Rico, between long. 66°25'04" and 66°27'30", and lat. 18°01'14" and 18°04'18".

by gravity sliding in that direction. The transcurrent faults indicate compression in a N. 80° E. direction later than the thrusting. Both events occurred after the middle Eocene and before the middle Oligocene.

REFERENCE

Pessagno, E. A., Jr., 1959, Preliminary note on the geology of the Ponce-Coamo area, Puerto Rico [abs.]: Caribbean Geol. Conf, 2d Mayaguez, P. R. Program, p. 25.

167. COMPRESSIONAL GRABEN AND HORST STRUCTURES IN EAST-CENTRAL PUERTO RICO

By R. P. Briggs and M. H. Pease, Jr., San Juan, P.R.

Work done in cooperation with the Department of Industrial Research, Puerto Rico Economic Development Administration

Grabens and horsts showing apparent stratigraphic displacements of as much as 2,000 meters are common features of the structural pattern in east-central Puerto Rico (fig. 167.1). Of these structures, only those in which stratigraphic displacement is large and in which the ratio of the width of the block to the apparent stratigraphic offset on either side approaches unity are discussed.

In the area studied two types of such grabens occur. The first is shown by graben G–1 and graben G–2 and its faulted extension G–2A (fig. 167.1). Southern boundary faults in this type of graben have greater apparent stratigraphic displacement than their northern boundary faults, and the boundary faults are vertical or dip away from the graben. The second type is shown by grabens G–3 and G–4 which are considered as highly deformed slivers or slices in the large fault zone that is east-central Puerto Rico.

Three types of horsts are present in this area. Horst H–1 is bounded on the north and south by faults that decrease in displacement eastward; the apparent stratigraphic displacement is greatest on its southern boundary fault. Horst H–2 is a block that seems to have been squeezed upward between two major faults, and the apparent displacement on its northern boundary fault is greater than on its southern boundary fault. Horst H–3 is a block tilted up to the northwest between a transcurrent fault that strikes northwest and a dip-slip fault striking generally north.

The fault system in which these features occur is dominated by transcurrent faults trending west to west-northwest, some of which have important dip-slip components, and by faults that trend northwest in which the dip-slip component of movement was locally greater than the strike-slip component. Left-lateral drag is evident at a number of places, but is best shown south of horst H–1 and north of graben G–1 (fig. 167.1), where the beds have been warped by movement along the fault zone in which H–1 and G–1 occur. Left-lateral displacement along this fault zone is at least 4 kilometers and may be as much as 15 kilometers in aggregate. Warping of beds northeast of horst H–3 also indicates possible left-lateral drag, despite the apparent right-lateral displacement of the rocks. This inconsistency is best explained by assuming a dip-slip component of movement considerably exceeding the strike-slip component along the northwest trending fault on the northeast side of H–3. Strong support for this assumption in relation to this fault is found along another fault that has a similar trend but along which the exposures are considerably better; this is the high-angle reverse fault that strikes northwest from Barranquitas and then curves westward parallel to the southern boundary fault of graben G–1. On the northwest-trending part of this fault, dip-slip displacement is dominant; no evidence of important strike-slip displacement was seen. However, along the west-trending section of the same fault, left-lateral transcurrent movement is apparently dominant over dip-slip movement.

Apparent right-lateral stratigraphic displacement is shown along a number of faults in figure 167.1, but evidences of right-lateral drag are lacking. Whether these occurrences represent real right-lateral movement or whether these relationships are principally due to dip-slip displacement is as yet not clear. Nevertheless, it is certain that regional compression, most likely resulting from opposing forces from the southwest and northeast, was the prime mover in forming the structural pattern in east-central Puerto Rico, and that the grabens and horsts were results of this compression.

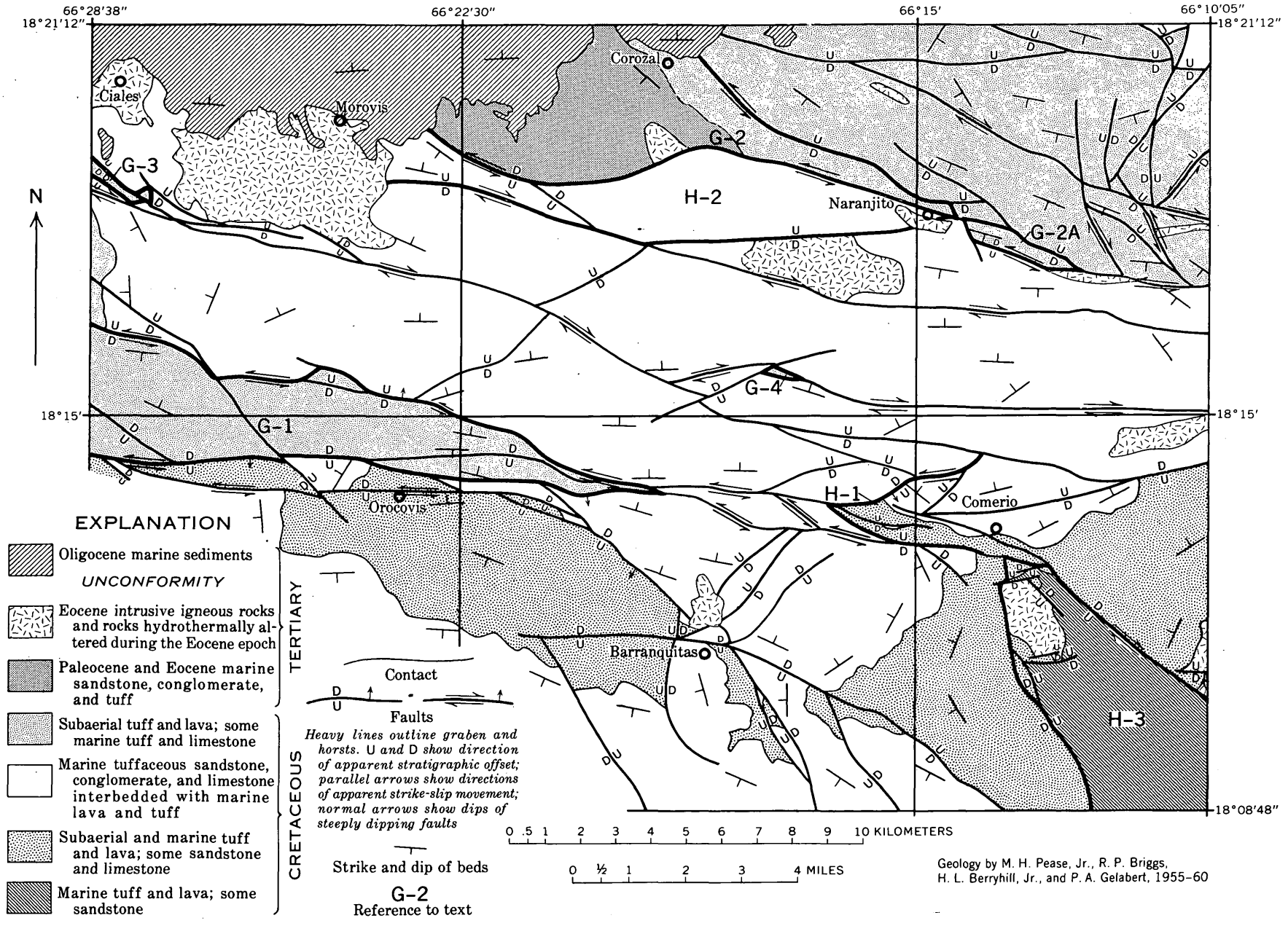

FIGURE 167.1.—Graben and horst structures in east-central Puerto Rico.

168. STRATIGRAPHIC DISTRIBUTION OF DETRITAL QUARTZ IN PRE-OLIGOCENE ROCKS IN SOUTH-CENTRAL PUERTO RICO

By PETER H. MATTSON and LYNN GLOVER III, Ponce, P.R.

Work done in cooperation with the Economic Development Administration, Commonwealth of Puerto Rico

The pre-Oligocene rocks of south-central Puerto Rico (fig. 164.1) are divided into six broad lithologic units (table 168.1) with a minimum composite thickness of about 7,000 meters. The oldest unit is either latest Early Cretaceous or earliest Late Cretaceous (Berryhill and others, 1960); the youngest unit is probably Eocene (Pessagno, in press). Detrital quartz is confined almost entirely to the three youngest units, which are latest Cretaceous and younger. These units have a minimum composite thickness of about 1,200 meters. Quartz forms as much as 10 percent of some beds in the uppermost Upper Cretaceous and Eocene(?) tuffaceous conglomerates, breccias, and sandstones, and is even more abundant in Eocene(?) sandstones and conglomerates.

TABLE 168.1.—*General sequence of pre-Oligocene rocks in south-central Puerto Rico*

Stratigraphic unit	Brief description	Detrital quartz	Age
Naranjo formation of Pessagno (in press).	Green and brown sandstone and siltstone; some green tuff, red conglomerate, and limestone.	Common	Eocene(?).
Unnamed	Hard white limestone chiefly composed of algal fragments.	Rare	Early Tertiary(?).
Coamo formation (Berryhill and others, 1960).	Tuff breccia, tuffaceous conglomerate, tuff; some sandstone, siltstone, and limestone.	Present	Late Cretaceous.
Cariblanco formation (Do.)	Alternating units of siltstone, sandstone, conglomerate; some limestone, tuff, and lava.	Not found	
Robles formation (Do.)	Thin-bedded sandstone, siltstone, lava; some limestone and breccia.	Not found	
Pre-Robles rocks (Do.)	Lava, flow breccia, and tuff breccia; some sandstone, conglomerate, and limestone.	(See text.)	Late Cretaceous or latest Early Cretaceous.

While the three lower units are generally quartz-free, a single locality has been found where a tuff previously thought to be of pre-Robles age (table 168.1) contains 10 percent quartz. This tuff, however, is possibly unconformable on the pre-Robles rocks nearby and thus younger. To correlate it on a lithologic basis is difficult because it has been slightly metamorphosed by a nearby igneous intrusion. If the tuff really is pre-Robles, it may have been derived from a local quartz-rich volcanic source. No other quartz-bearing sediments older than the Coamo formation have been found during several years of study by the U.S. Geological Survey.

The pre-Oligocene rocks of Puerto Rico consist mainly of primary and reworked volcanic debris but include minor amounts of limestone. No other source for the debris forming Puerto Rico, no old land mass for example, has yet been found or indicated. The appearance, therefore, of detrital quartz in the younger rocks probably shows progressive enrichment in silica in the magmas supplying the Late Cretaceous to Eocene(?) volcanoes. A volcanic or hypabyssal source for the silica is also indicated by the fact that some detrital quartz grains in the younger rocks have the hexagonal dipyramid crystal habit characteristic of beta or "high" quartz. The general upward increase in the ratio of pyroclastic to effusive material also may indicate an increase in silica content of the supplying magma.

REFERENCES

Berryhill, H. L., Jr., Briggs, R. P., and Glover, Lynn III, 1960, Stratigraphy, sedimentation, and structure of Late Cretaceous rocks in eastern Puerto Rico—Preliminary Report: Am. Assoc. Petroleum Geologists Bull., v. 44, no. 2, p. 137–155.

Pessagno, E. A., Jr., in press, A résumé of the geology of the Ponce-Coamo area: Caribbean Geol. Conf., 2d., Mayagüez, Puerto Rico 1959, Proc.

169. OCCURRENCES OF BAUXITIC CLAY IN THE KARST AREA OF NORTH-CENTRAL PUERTO RICO

By Fred A. Hildebrand, Denver, Colo.

Work done in cooperation with the Department of Industrial Research, Puerto Rico Economic Development Administration

Deposits of bauxitic clay in north-central Puerto Rico were discovered during a preliminary survey of the mineral resources of Puerto Rico. The clays are confined largely to sinkholes in a belt of pronounced karst topography developed in marine limestones of Tertiary age along the north coast of the island. The belt of limestones lies along the north flank of the east-trending Cordillera Central, a complexly faulted sequence of Cretaceous rocks of volcanic origin composing the backbone of the island (Zapp, Bergquist, and Thomas, 1948) (fig. 169.1). The rocks of the Cordillera Central consist principally of lavas, tuffs, tuff breccias, volcanic conglomerates and volcanic-derived siltstones and sandstones. The Tertiary limestones, which are of middle Oligocene to middle(?) Miocene age, dip about 6° north and lie unconformably on an irregular surface of Cretaceous rocks. The limestone belt is unconformably overlain by sandy and limy deposits of Quaternary age.

The Tertiary rocks have been subdivided into the San Sebastian formation, Lares limestone, Aguada limestone, and Aymamon limestone (Zapp and others, 1948). The San Sebastian, the basal formation, is a conglomerate containing fragments, pebbles, and boulders of the pre-middle Oligocene rocks. The Lares limestone is principally a massive, white reef-type rock. The Aguada and Aymamon limestones are chiefly dense to chalky and reddish gray.

The belt of karst limestone extends about 60 miles eastward from the west coast of Puerto Rico and varies in width as shown in figure 169.1. The most rugged karst development is generally in the southern part of the belt. The morphological forms are typical of mature karst topography; they consist of numerous conical hills resembling haystacks (mogotes) and cucumber-shaped (pepino) hills and connecting sinkholes.

Preliminary sampling across the karst belt south of Florida, Puerto Rico shows that the bauxitic clays are confined largely to the Lares limestone along a 3-mile-wide strip at the south edge of the karst belt. Other scattered samples collected farther east and west of the Florida area show that the bauxitic clay belt has a minimum length of at least 14 miles (fig. 169.1). Figure 169.2 shows the distribution of boehmitic samples in the Florida area. The belt probably extends east and west of the limits established by the preliminary sampling.

About 70 samples of surface soil were collected, mainly from sinkholes. Sampling was limited to white to dark-brown, nonsandy, nonlimy clays. Mineral determinations by X-ray powder diffraction methods were made of 42 of the 70 samples collected. Ferruginous minerals and organic substances detrimental to X-ray powder pattern interpretation were removed by preliminary treatment of the samples with 30 percent hydrogen peroxide and hydrochloric acid diluted 1:1. The total mineral assemblage shown by these 42 samples is: boehmite, quartz, goethite, hematite, kaolinite, halloysite, anatase, oligoclase, sanidine, unidentified feldspar minerals, and organic matter.

Of the 42 samples, 17 were found to contain boehmite. The boehmitic clays are buff to reddish brown. Some of them are clastic rocks containing small (less than ½ mm) angular and subrounded quartz grains and well-rounded, black, opaque grains—possibly ilmenite or anatase. The clays are tough when dry and plastic when wet. They have both a rough, hackly fracture and a smooth conchoidal fracture. From the 17 boehmitic samples, 8 containing the most boehmite were chemically analyzed. These analyses are shown in table 169.1. The analyses of the Puerto Rico bauxitic clays are similar to analyses of surface soil samples

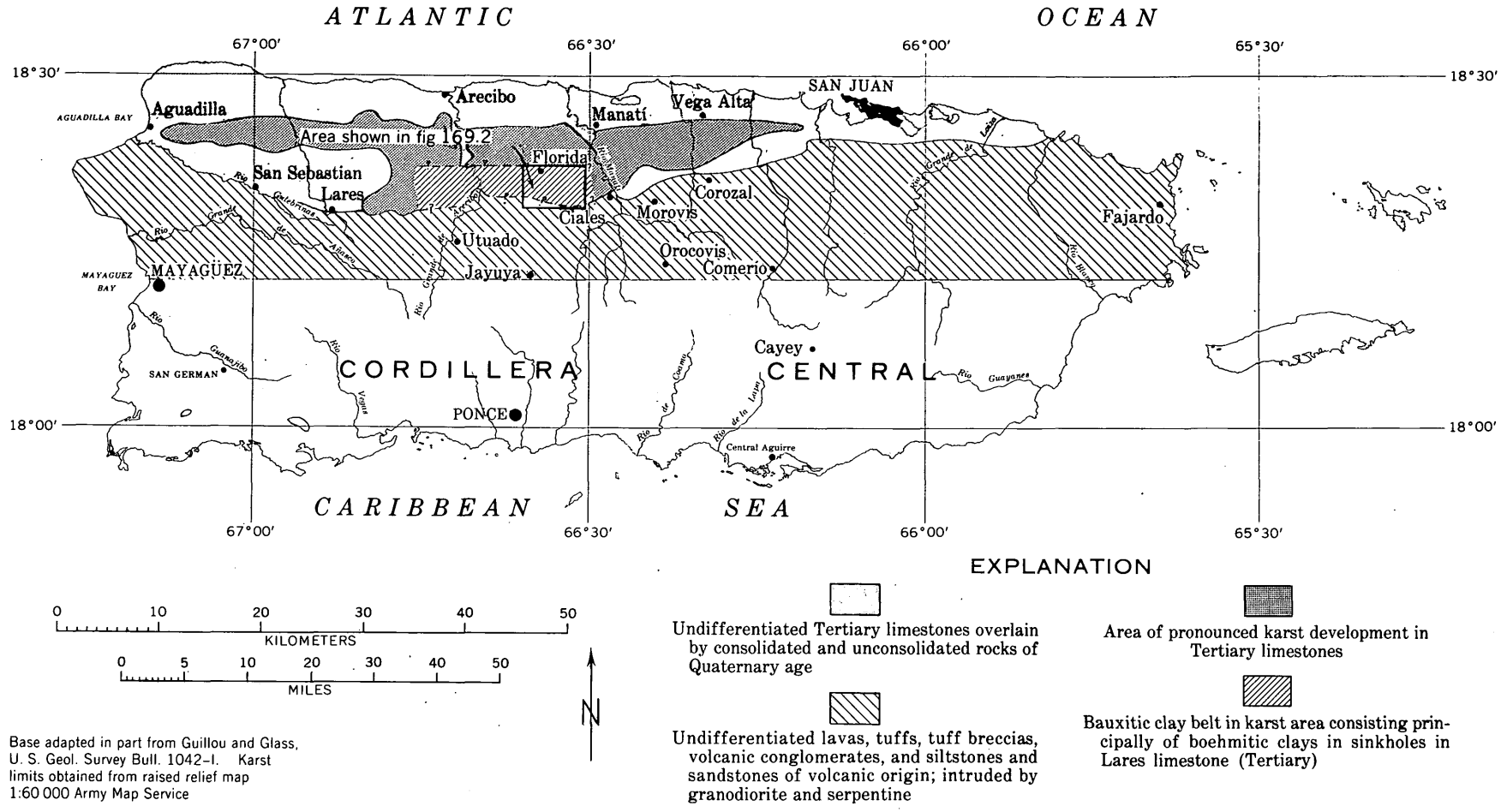

Base adapted in part from Guillou and Glass, U. S. Geol. Survey Bull. 1042–I. Karst limits obtained from raised relief map 1:60 000 Army Map Service

FIGURE 169.1.—Sketch map showing the Tertiary limestone belt, the bauxitic clay belt, and the area of principal karst development in Puerto Rico. The bauxitic clay belt probably extends farther east and west of the limits shown.

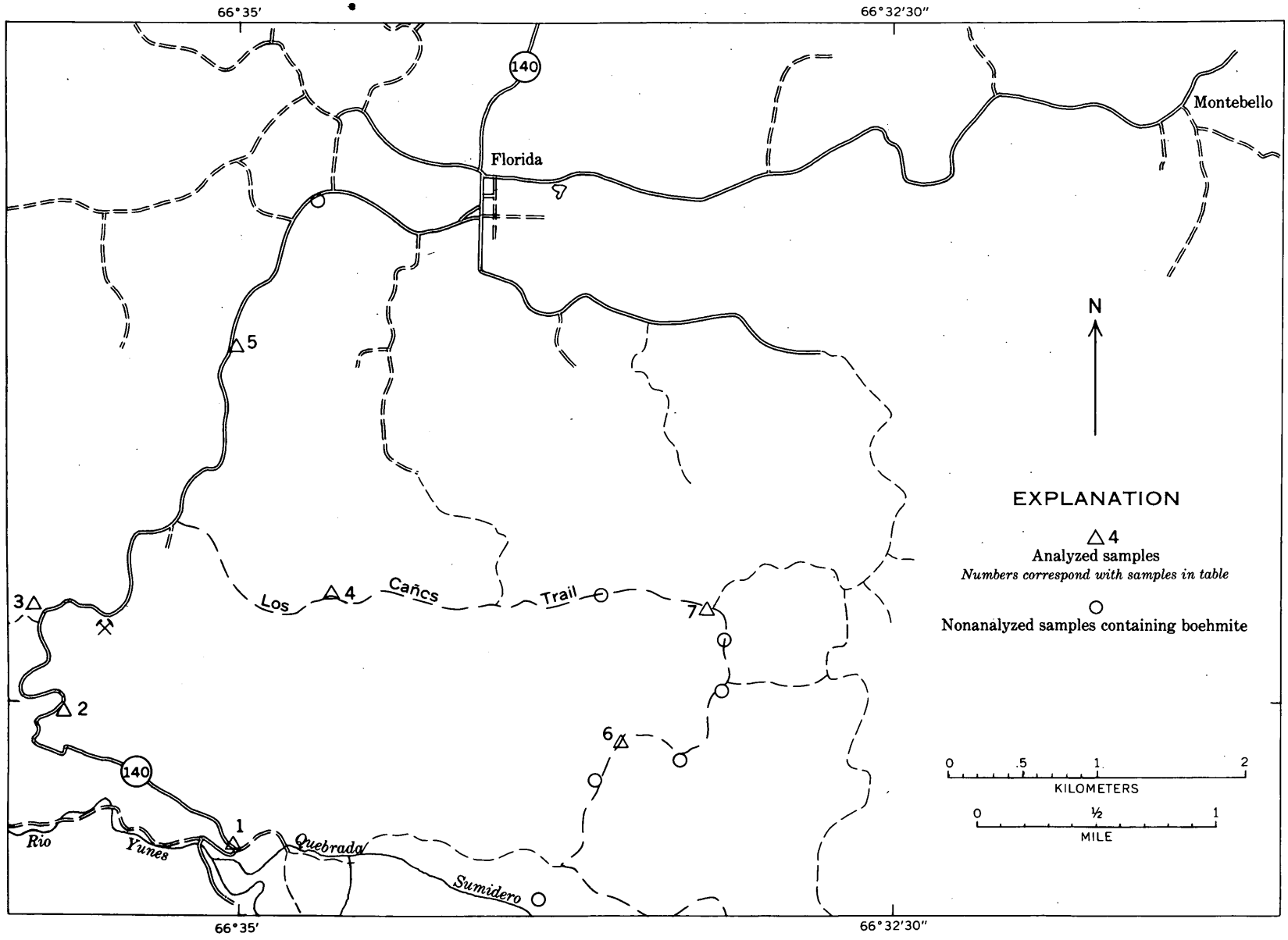

FIGURE 169.2.—Sketch map showing locations of analyzed and unanalyzed bauxitic clay samples in the area south of Florida, P.R. Three other bauxitic clay samples from the bauxitic clay belt are not shown. The location of the easternmost unanalyzed bauxitic clay sample is 15,600 feet east and 2,700 feet south of sample 6. Analyzed sample 5 is from the Utuado quadrangle 43,800 feet west and 500 feet north of sample 3. Another unanalyzed bauxitic clay sample is from a location 3,700 feet east and 600 feet south of sample 5.

TABLE 169.1.—*Chemical analyses of bauxitic clays*[1] *from the Florida and Utuado quadrangles, Puerto Rico*

[Analysts, Paul L. D. Elmore, Samuel D. Botts, and Marvin D. Mack. Samples were analyzed by rapid rock analysis methods similar to those described by Shapiro and Brannock (1956)]

	Locality and PR-FAH sample number							
	[2] 1	2	3	4	5	6	7	8
	1304	1318-C	1305	1361	1336	1353	1357	1339
SiO_2	18.7	22.5	23.0	29.7	29.0	26.3	30.2	36.9
Al_2O_3	40.7	38.2	36.0	32.6	32.5	31.6	27.2	23.2
Total iron [3] as Fe_2O_3	18.3	17.4	16.4	14.4	18.2	16.0	15.0	10.8
TiO_2	1.8	1.6	1.6	1.3	1.4	1.8	1.4	1.0
CaO	.26	.22	.62	.64	.24	.72	1.0	2.1
MgO	.26	.43	.45	.60	.48	.70	1.4	1.8
K_2O	.18	.22	.24	.27	.20	.40	.42	.37
Na_2O	.10	.06	.06	.08	.07	.07	.09	.32
P_2O_5	1.0	.66	2.5	.81	1.0	2.4	2.3	.68
CO_2	.08	.18	<.05	.30	.06	.12	.14	.18
MnO	.04	.06	.12	.04	.32	.46	.31	.37
H_2O+	16.0	15.8	15.5	14.4	14.7	13.8	14.2	13.4
H_2O-	1.5	2.0	1.7	2.7	1.5	2.7	3.0	3.9
Total	99	99	98	98	100	97	97	95

[1] Bauxitic clay, as used in this paper is not meant to imply that a major contribution of SiO_2 and Al_2O_3 to the analyses is attributable to kaolinite, halloysite, and feldspar. The mineralogical examinations show that most of the SiO_2 content is contributed by megascopically visible quartz grains and that nearly all of the Al_2O_3 content is contributed by boehmite. X-ray powder diffraction patterns of bulk samples from which the quartz grains have been removed by hand picking show that only traces of quartz occur in the fine-grained boehmitic matrix.

[2] At edge of karst area.

[3] Samples contained organic matter which precluded accurate determinations of FeO. The locations of these samples are shown in figure 169.2.

1. Florida quadrangle. Tan clay overlying weathered volcanic rocks in roadcut.
2. Florida quadrangle. Tan clay from 3 feet beneath surface in roadcut in sinkhole.
3. Florida quadrangle. Tan surface soil sample from plowed field in bottom of large, deep sinkhole.
4. Florida quadrangle. Tan surface soil sample from creek bank in large, circular sinkhole.
5. Florida quadrangle. Tan clay from base of shallow roadcut in saddle between sinkholes.
6. Florida quadrangle. Tan surface soil sample from bottom of deep, oval-shaped sinkhole.
7. Florida quadrangle. Tan surface soil sample from bottom of large, deep sinkhole.
8. Utuado quadrangle. Tan clay from base of roadcut.

from the Pedernales—El Fondo de Milla trail area of the Dominican Republic (Goldich and Bergquist, 1947, p. 72).

Quartz, anatase, and kaolinite were found in nearly all of the 42 samples. Kaolinite and halloysite were found in 37 samples. Seven samples collected from the Quaternary deposits north of the Florida area contain kaolinite as the dominant constituent. Six samples containing halloysite and 24 containing moderate amounts of kaolinite came from within the bauxitic clay belt. Four samples consisting almost wholly of oligoclase or sanidine came from the south edge of the karst area near the contact of the Tertiary and Cretaceous rocks. Small quantities of feldspars were found in about 13 samples from the belt, but no significant correlation could be made between their abundance and distribution in relation to the contact of the Cretaceous and Tertiary rocks.

The age and origin of the bauxitic clay deposits are uncertain. This investigation indicates that the bauxitic clay is a clastic fine-grained rock in which feldspars are widely distributed. It also shows that the clay is widely distributed in the southern part of the karst area as far north as the town of Florida. Water-well data in the Florida area (McGuinness, 1946) show that the clays overlie at least 350 feet of limestone. These observations suggest that the parent rock was not a limestone but a volcanic rock. According to Zans (in press) bauxite deposits in Jamaica developed (and may still be forming) in a mature karst area by bauxitization of an andesitic volcanic detritus carried into cavernous limestones when the basement rocks of the karst area are laid bare in upland areas. Zans believes that bauxitization of the volcanic detritus was aided by alkaline solutions from the limestone environment. The Puerto Rico deposits may have developed similarly or the bauxitic clay may have been transported into the karst from bauxitized andesitic rocks on highland surfaces to the south. The writer does not have sufficient evidence to determine if bauxitization processes are currently taking place in Puerto Rico.

REFERENCES

Goldich, S. S., and Bergquist, H. R., 1947, Aluminous lateritic soil of the Sierra de Bahoruco area, Dominican Republic, W. I.: U.S. Geol. Survey Bull. 953–C, p. 53–84.

McGuinness, C. L., 1946, Records of wells in Puerto Rico: San Juan, Puerto Rico Aqueduct and Sewer Service, 267 p.

Shapiro, Leonard, and Brannock, W. W., 1956, Rapid analysis of silicate rocks: U.S. Geol. Survey Bull. 1036–C, p. 19–56.

Zans, V. A., in press The origin of the bauxite deposits of Jamaica: Internat. Geol. Cong., 20th, Mexico City 1956 (in press).

Zapp, A. D., Bergquist, H. R., and Thomas, C. R., 1948, Tertiary geology of the coastal plains of Puerto Rico: U.S. Geol. Survey Oil and Gas Inv. Prelim. Map 85.

170. THE STRATIGRAPHY OF ISHIGAKI-SHIMA, RYŪKYŪ-RETTŌ

By Helen L. Foster, Washington, D.C.

(Work done in cooperation with Office, Chief of Engineers)

Ishigaki-shima is one of the southernmost islands of the Ryūkyū-rettō, an arcuate chain of islands which extends from southern Japan southwestward nearly to Taiwan. It lies about 275 miles southwest of Okinawa-jima and 150 miles east of Taiwan. It has an area of 86 square miles, and the highest summit on it is a little more than 1,700 feet above sea level. Most of the northern part of the island is mountainous and bordered by narrow marine terraces. The southern part consists largely of gently sloping marine terraces in various stages of dissection, but also is partly mountainous and hilly.

The foundation of Ishigaki-shima consists of low-grade metamorphic rocks, probably of Paleozoic age, which include green schist, glaucophane schist, phyllite, quartz-mica schist, chert, sandstone, and a little marble. These rocks have been folded, faulted, uplifted, and eroded. They have also been intruded by granitic, granodioritic, and dioritic rocks, probably of late Mesozoic or Tertiary age, which occupy an area of about 10 square miles. Granular intrusive rocks such as these are not known to occur elsewhere in the southern part of the Ryūkyū-rettō, though intrusive rhyolite porphyry, andesite porphyry, and hypersthene andesite occur on Okinawa-jima.

Upper Eocene (Tertiary *b*) limestone, sandstone, and conglomerate unconformably overlie the metamorphic rocks in scattered small patches totaling 1.5 square miles in area at elevations ranging from sea level to about 300 feet. These rocks are tilted and faulted, but not folded. Their age was determined from larger Foraminifera, and from calcareous algae which are exceptionally well preserved.

A major period of Tertiary submarine volcanic activity followed the deposition of the Eocene sediments, or possibly began before its close. The volcanic rocks—interbedded tuff, breccia, and lava—are chiefly andesitic, but partly dacitic and rhyolitic. They are at least 600 feet and probably more than 1,000 feet thick, and underlie an area of about 9 square miles.

Later Tertiary deposits have not been identified; most of the island's area was probably land throughout late Tertiary time.

The earliest Pleistocene deposit is a fossiliferous gray marine clay containing abundant larger and smaller Foraminifera, ostracodes, and mollusks, some corals, bryozoans, and pollen, and deer bones in one area. The clay is overlain in places by gravel deposits from a few feet to more than 70 feet thick. The youngest Pleistocene deposit is the Ryūkyū limestone, a raised reef limestone, which constitutes much of the southern part of the island and forms a discontinuous fringe along the coast on other parts of the island.

Recent deposits include sand and gravel on raised beaches, sand dunes, stream alluvium, and sand and gravel on the present beaches. Bones of pigs were found in a Recent terrace deposit.

171. FOSSIL MAMMALS FROM ISHIGAKI-SHIMA, RYŪKYŪ-RETTŌ

By Frank C. Whitmore, Jr., Washington, D.C.

A field party under the direction of Helen L. Foster has collected two suites of fossil mammal remains in the course of mapping the island of Ishigaki in the Ryūkyū-rettō, about 150 miles east of Taiwan. The Ryūkyūs comprise an island arc extending from Taiwan on the south to Kyūshū, the southernmost of the Japanese islands, on the north. The rocks exposed on the islands record a complex history of tectonic changes in

land levels during Tertiary and Quaternary time, accompanied in the Quaternary by eustatic changes in sea level. It is certain that the islands have been connected at one time or another and that land bridges at times connected the arc with the Asiatic mainland by way of Japan and Taiwan. The exact times when these connections existed are still, however, a matter of speculation. Study of fossil mammals from the island may help solve this paleogeographic problem.

The older suite of fossil mammals consists mainly of *Metacervulus astylodon* (Matsumoto), a small extinct deer related to the Muntjac now living in Southeast Asia; there is also a box turtle (cf. *Geoemyda*) similar to but larger than those now living in the Ryūkyūs, and a few small bones, as yet undetermined, which probably represent rodents. These bones are found in a gray marine clay below gravel. The age of both the clay and gravel is in doubt; the clay also contains invertebrates which seem to indicate a Pleistocene age.

Metacervulus has also been found on Okinawa and neighboring islets, where it is abundant, and on Miyako-jima, an island about 60 miles east of Ishigaki-shima. These finds differ from those of Ishigaki-shima in that the bones are found in fissure deposits rather than in clay beds. The Ishigaki bones therefore seem to be stratigraphically more significant than those found on the other islands. *Metacervulus astylodon* occurs in the middle Pliocene of North China. In the Ryūkyūs it is younger: probably Pleistocene, although possibly late Pliocene. The presence of these deer indicates a probable emergence of this area during the Pliocene so that mammals could have migrated through the southern Ryūkyūs. The three islands where *Metacervulus* is found are all south of the Watase Line or Tokara Strait, a deep channel between Yaku-shima and Amami-o-shima which divides the Ryūkyū-rettō into north and south halves. The absence of this deer in fossil fauna of islands north of Tokara Strait and of the Japanese islands implies that this strait existed during the Pleistocene and possibly in the late Pliocene, and that mammalian migration was from South China via Taiwan.

The younger of the two fossil suites consists entirely of bones of a pig, probably related to the Recent variety *Sus leucomystax riukiuanus* Kuroda. The bones, which are unmineralized, have been C^{14} dated by Meyer Rubin of the U.S. Geological Survey at 8,500±500 years. Because of the presence of inorganic carbonates in fossil bone, dates based on such material are probably inaccurate, and the actual age is almost certainly greater than the result of the C^{14} determination. The pig bones occur as a densely packed bone breccia, cemented by travertine, in terrace deposits laid down in a nip, or undercut shelter, which resulted from erosion of a limestone cliff at sea level. A peculiar feature of this collection is that almost all of the bones are of young individuals. Several explanations of this high proportion of young individuals are possible. One is that they were domestic stock, selectively killed by man. No artifacts have been found associated with the bones, however, although some chert flakes which occur in the deposit may have resulted from the sharpening of stone implements. No tool marks are found on the bones, and they have been so broken during burial that it is impossible to tell whether long bones were split as they would be to obtain marrow. Some of the bones are blackened by a carbonaceous residue, which may have resulted from cooking or from slow oxidation through time.

Further study of Recent and extinct pig species may indicate whether these pigs were introduced by man or migrated in the wild state. If they are shown to have been domesticated, it would be one of the earliest examples of pig domestication known.

The subfossil pig is intermediate in size between species of *Sus* found on the Asiatic mainland and that living on Ishigaki today. This is in keeping with the general rule that island species of mammals tend to be smaller than their mainland ancestors. Detailed morphological studies, such as consideration of the accessory conules of the molar teeth, may aid in establishing the mainland relatives of the Ishigaki pigs and also, perhaps, in establishing the length of time during which the island form was isolated. It is perhaps significant that the modern wild pigs of the Ryūkyūs are only found south of the Tokara Strait. This may mean that their ancestors either migrated or were introduced from the south.

Hanzawa (1935) has discussed the distribution in the Ryūkyūs of *Trimeresurus*, a viper locally known as the habu. This snake is not present on all islands of the group; it is Hanzawa's opinion (1935, p. 56–59) that the snakes migrated from Taiwan in post-Shimajiri (probably Pliocene) time over a land bridge. Subsequent rise in sea level, according to Hanzawa, divided the area into several large islands on each one of which a distinct species of *Trimeresurus* developed. Islands which do not have the habu were submerged at that time. This stage was succeeded by a period of submergence with limestone deposition. Then, in post-Naha (Pleistocene) time, an extensive deposition of clastic materials took place which again probably indicates an extensive land surface in the area of the archipelago. It is possible that the pigs could have reached

the area at this time; migration at an earlier date does not seem reasonable because the Ishigaki subfossil pigs seem to differ only in minor characteristics from those of the Asiatic mainland.

REFERENCE

Hanzawa, S., 1935, Topography and geology of the Riukiu Islands: Tokoku Imp. Univ., Sci. Repts, 2nd ser. (Geology), v. 18, p. 56–59.

172. DISTRIBUTION OF MOLLUSCAN FAUNAS IN THE PACIFIC ISLANDS DURING THE CENOZOIC

By Harry S. Ladd, Washington, D.C.

Studies of large collections of fossil mollusks from outcrops and drill holes in six island groups in the western Pacific suggest that the faunas were more abundant and diversified during parts of Tertiary time than they are in the same areas today.

As shown in figure 172.1, the islands form a broad belt spreading nearly 4,000 miles across the tropical latitudes of the western Pacific from Palau and the Marianas on the northwest to Fiji and the New Hebrides on the southeast. Most of the collections on which the study is based were obtained in the field by Geological Survey personnel; others have been loaned for study by museums. Four of the island groups—Palau, the Marianas, Fiji, and the New Hebrides—lie southwest of the andesite line in an area characterized by elevation in late Cenozoic time. The other two groups—the Marshall and Ellice Islands—lie to the northeast of the line in the Pacific Basin proper, an area characterized by deep subsidence. Collections from the elevated island groups are from outcrops; those from the submerged areas are from drill holes. Fossil mollusks and other organisms that are found above the sea to the west occur below the sea to the east.

Detailed studies of the molluscan faunas will not be completed for some time, but the work done thus far supports the hypothesis that many elements of the "Indo-Pacific fauna," generally believed to have spread from Indonesia, may have originated among the islands in the Pacific Basin in Cretaceous and Tertiary times. During these times there were more island "stepping stones" than now, many of them being located in the broad island-free area that now separates the Marshalls from Hawaii (Hamilton, 1956). Mollusks and other shallow water forms could have migrated from the islands toward Indonesia with the aid of favorable waves and currents such as those prevailing today (Ladd, 1960).

Most of the sediments from which fossil mollusks have been obtained represent deposits in shallow waters. Many of the limestones are reef limestones or clearly represent sediments that accumulated in lagoons not far removed from reefs (Emery and others, 1954; Ladd and Schlanger, 1960). A few mollusk-bearing limestones and some of the marls appear to represent off-reef deposits in somewhat deeper waters, but no deposits suggesting abyssal depths have been recognized.

The oldest mollusks found to date are Eocene but they are few in number and poorly preserved. Miocene mollusks are abundant and varied. Lagoonal sediments obtained from drill holes appear to be far richer in mollusks than any sediments dredged from existing lagoons in the same area. Younger mollusk faunas, presumably Pleistocene, contain mostly still-living species but they include a number that now have a more restricted distribution.

REFERENCES

Emery, K. O., Tracey, J. I., Jr., and Ladd, H. S., 1954, Geology of Bikini and nearby atolls: U.S. Geol. Survey Prof. Paper 260, pt. 1, chap. A, 265 p.

Hamilton, E. L., 1956, Sunken islands of the Mid-Pacific Mountains: Geol. Soc. America Mem. 64, 97 p.

Ladd, H. S., 1960, Origin of the Pacific island molluscan fauna: Am. Jour. Sci., v. 258–A, p. 137–150.

Ladd, H. S., and Schlanger, S. O., 1960, Drilling operations on Eniwetok Atoll: U.S. Geol. Survey Prof. Paper 260–Y. (In press.)

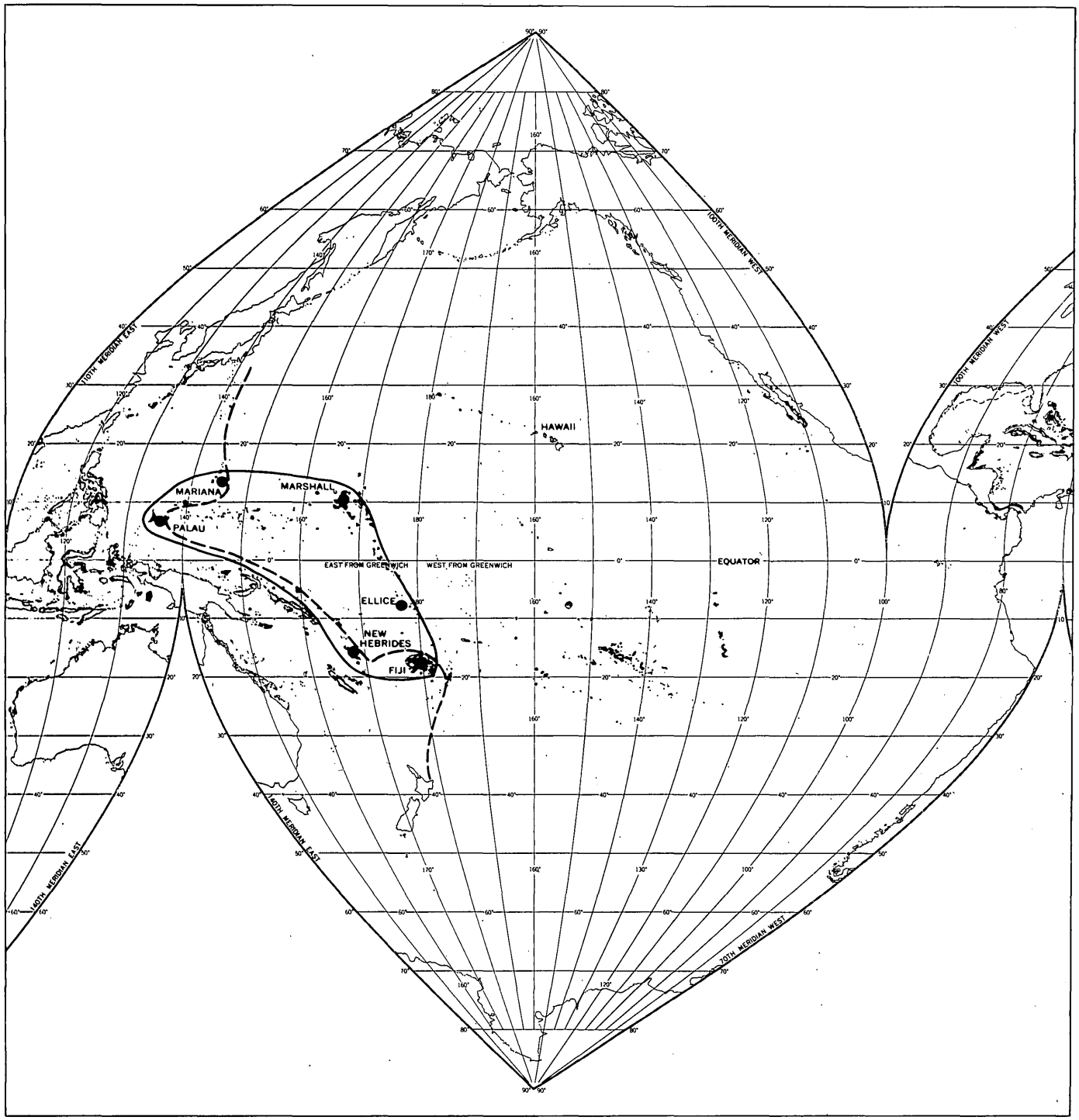

FIGURE 172.1.—Location of island area from which fossil mollusks have been obtained. Dashed line marks structural boundary of Pacific Basin (andesite line).

173. GEOLOGY OF TAYLOR GLACIER-TAYLOR DRY VALLEY REGION, SOUTH VICTORIA LAND, ANTARCTICA

By WARREN HAMILTON and PHILIP T. HAYES, Denver, Colo.

Work done in cooperation with National Science Foundation

During the southern summer 1958–9, the U.S. Geological Survey began field work west of McMurdo Sound, Antarctica, as part of the U.S. Antractic Research Program administered by the National Science Foundation. Field camps were established by U.S. Navy aircraft on the upper Taylor Glacier, at Bonney Lake and at Suess Glacier in Taylor Dry Valley, and in a previously unvisited dry valley north of lower Taylor Glacier. Geology was studied in a strip 50 miles long, extending most of the way through the mountains from McMurdo Sound to the interior ice plateau.

The coastal metamorphic belt, here 15 miles wide, consists of metasedimentary rocks, among which metapelitic rocks and calc-silicate schists and gneisses of probable late Precambrian and Early Cambrian age are dominant. The metasediments strike subparallel to the coast; they vary in dip but are nearly vertical near the batholith which intruded them from the west (fig. 173.1). The batholith is a composite mass of plutons of quartz diorite, granodiorite, quartz monzonite, and granite, varying to diorite, monzonite, and quartz syenite. Accessory minerals are hornblende or biotite or both and, in one mass of quartz diorite and diorite, minor augite is present. There is no orthopyroxene, such as is widespread in some parts of East Antarctica. Some of the plutons are separated by septa of para-amphibolite and calc-silicate gneisses.

Dikes of mafic, lamprophyric hornblende diorites and quartz latites cut these basement rocks, and are particularly abundant near the contact between the metasediments and the batholith. Prior to the deposition of the overlying Beacon sandstone (named by Ferrar, 1907, p. 39), the diked basement complex was intricately broken by minor faults (fig. 173.1).

The Beacon sandstone, known from other areas to have a stratigraphic range from Devonian to Permian, was deposited upon an essentially horizontal erosion surface on the basement rocks. The Beacon consists of coarse-grained, crossbedded sandstone, mostly quartz-rich but partly arkosic, and lesser amounts of siltstone peble conglomerate, and, high in the section, thin beds of coal (fig. 173.2). Its thickness is only about 3,000 feet, exclusive of diabase sills.

At least four great sills of quartz diabase, each 500 to 1,300 feet thick, were intruded within the Beacon sandstone (fig. 173.2). Another such sill lies at or near the contact between Beacon and basement, and another, probably continuous for scores of miles, follows exfoliation joints in the basement related to and 500 to 1,500 feet below the pre-Beacon erosion surface. The diabases are strongly differentiated, and contain abundant mafic and silicic granophyre and gabbro-pegmatite in their upper portions. Differentiation has been documented by 19 chemical analyses, which show the normal diabase to have 55 percent SiO_2. The quartz of most of the Beacon sandstone was recrystallized, and the coal was baked, by heat released from the sills.

Several normal faults trend parallel to the coast and offset the Beacon sandstone and the diabases about 1,000 feet, but the gross structure of the mountain system is anticlinal. There is no "Great Antarctic horst" here, although such a structure has long been assumed to be present.

Past glaciers filled the valleys 1,000 to 1,500 feet above present ice surfaces, but there has been very little change—possibly slight local advances of the ice—since the region was first visited in the early 1900's by British expeditions. Numerous small cinder cones and lava flows of mafic, alkaline basalts (SiO_2 42 to 48 percent by weight, Na_2O 3.7 to 4.7 percent, K_2O 1.5 to 1.8 percent, in four analyses) were erupted within Taylor Valley before, between, and since past episodes of glaciation.

REFERENCE

Ferrar, H. T., 1907, Report on the field-geology of the region explored during the "Discovery" Antarctic Expedition, 1901–4: Natl. Antarctic Exped., Natural History, v. 1, pt. 1, p. 1–100.

FIGURE 173.1.—Contact between metamorphic and granitic rocks. Calc-silicate hornfels, gneiss, and schist (left) are mostly light colored. Darker, gneissic border zone of batholith (right) consists of quartz monzonite-quartz diorite migmatite. Crosscutting dikes, mostly hornblende diorite, are offset along minor faults. Looking south across Taylor Dry Valley to north side of Kukri Hills. U.S. Navy photograph.

557753 O—60——25

FIGURE 173.2.—Sheets of quartz diabase in Beacon sandstone. The inclined sheet becomes a concordant sill just left of the summit. Layers of coal stripe the sandstone between the diabase sheets. The height of the cliff is nearly 3,000 feet. The photograph also shows Finger Mountain as viewed from the north, and the base of upper Taylor Glacier. The interior ice plateau is just out of the picture to the west (right), and McMurdo Sound is 50 miles to the east.

174. NEW INTERPRETATION OF ANTARCTIC TECTONICS

By WARREN HAMILTON, Denver, Colo.

Work done in cooperation with National Science Foundation

A continuous chain of high mountains, 2,500 miles long, crosses Antarctica near the South Pole and borders the Ross and Weddell Seas. It extends from south of New Zealand to south of West Africa. These mountains have long been assumed to be a great horst of rocks of an ancient Precambrian shield, but incomplete data suggest that they lie instead along a belt of crystalline rocks metamorphosed and intruded by batholiths during Cambrian time.[1]

The mountain chain is composed of varied crystalline rocks overlain unconformably by thin, slightly deformed sandstones, the stratigraphic range of which is Devonian to Permian, and by huge sills of diabase. The concept that the mountains form a "Great Antarctic horst" was based upon extrapolation from the inferred horst structure of the imposing Royal Society Range, which accounts for one-quarter of the width of the mountain system in the McMurdo Sound region. West of that range, the sandstones dip gently westward, beneath the interior ice plateau, broken only by relatively minor faults. At least at Granite Harbour, on the east side of the mountains north of the Royal Society Range, structures dip gently eastward toward the Ross Sea. The broad structure of the mountain system in the McMurdo Sound region is domical and similar structure probably characterizes the mountain system at least from Granite Harbour to the Beardmore Glacier. Analogy with other continents indicates that a vast mountain system such as this is far more likely to lie along an orogen than to be a crosscutting uplift.

That this is indeed the case for the Antarctic ranges is strongly suggested by the petrologic and structural continuity of the province at least from the Horlick Mountains to Terra Nova Bay, a distance of 1,100 miles. The dominant rocks of this part of the chain belong to a composite batholith of plutons of various types of granitic rocks, the characteristic type being coarse-grained pink quartz monzonite ranging to granite. The batholith is intrusive into nonvolcanic metasedimentary rocks of various types, among which metashales and calc-silicate rocks are particularly widespread. In the McMurdo Sound region, the metasedimentary rocks occur chiefly in a belt along the coast—that is, gross structures are subparallel to the mountain system.

Many granodiorites, quartz monzonites, and granites known from this Antarctic batholith are characterized by lightly colored potassic feldspar which is in well-shaped crystals but is not generally phenocrystic. Plagioclase is only obscurely zoned. As most other batholiths contain potassic feldspar that is more commonly white than colored and more commonly anhedral than not, and as plagioclase in most other batholiths is commonly zoned, these granitic rocks are distinctive. A striking feature of composite batholiths is that rock types within them repeat over distances of hundreds or even thousands of miles; the petrologic continuity in the Antarctic mountains suggests tectonic continuity also.

Cobbles and erratics containing Early Cambrian pleosponges, both metamorphosed and nonmetamorphosed, have been found in four places in or near the trans-Antarctic mountains, in positions consistent with derivation from ice-buried geosynclinal materials along the inland side of the mountains. Similar fossils characterize the Adelaide geosyncline of South Australia.

The Antarctic coast from 50° to 145° east longitude is characterized by charnockitic (orthopyroxene-bearing) granitic and gneissic rocks. The various age determinations made on these rocks indicate Precambrian ages (Starik, Ravich, Krylov, and Silin, 1959; 1960).

No similar rocks have been found in the trans-Antarctic mountains. A K/Ar analysis of biotite in gneiss indicates an age of 500 million years (Cameron, Goldich, and Hoffman, 1960) at Marble Point, and seven whole-rock K/Ar determinations in the same tectonic belt in Oates Land indicate an age of metamorphism and formation of granitic rocks of about 500 million years (Starik, Ravich, Krylov, and Silin, 1959[2]). This appears to confirm the Cambrian orogeny inferred on geologic grounds.

East Antarctica can thus be interpreted to be largely formed of a Precambrian shield, along whose Ross Sea-

[1] The following discussion is based upon published references too numerous to acknowledge in this note, upon unpublished information given by Jon Stephenson, W. E. Long, and others, and upon my field studies in the McMurdo Sound region and my petrographic studies of Antarctic and Australian granites.

[2] The actual measurements yielded calculated ages of 425–460 million years; but these must be increased by 20 or 30 percent to indicate true ages, because of the loss of argon from feldspars in the rocks, according to J. L. Kulp (oral communication).

Weddell Sea side a geosyncline was filled by early Cambrian and, presumably, late Precambrian sediments. The contents of this geosyncline were metamorphosed and intruded by batholiths during Cambrian time.

This inferred pattern is strikingly similar to that of Australia, where the Precambrian shield of western Australia gives way in South Australia to the Adelaide geosyncline of Lower Cambrian and upper Precambrian sediments, and that to a Cambrian batholith characterized by granitic rocks (for example, the Murray Bridge granite) which are remarkably similar to those of the trans-Antarctic mountains. (The younger Paleozoic granites of Australia are very different.)

Analogy with structures in Australia and New Zealand suggests that orogenic belts of middle and late Paleozoic age may be present in Antarctica. One may be in eastern Marie Byrd Land, between the trans-Antarctic mountains and the Andean-type ranges of the Palmer Peninsula and in the Cape Adare region of eastern Antarctica.

It may be significant that the position of the Cambrian(?) orogen of Antarctica accords with Du Toit's (1937) theoretical reassembly of the southern-hemisphere continents, and forms a bridge between the Cambrian batholiths of Australia and South Africa; Du Toit was not aware of the correlations between these granites, nor of their petrologic kinship. Many other features of Antarctic geology also fit well with Du Toit's reconstruction.

REFERENCES

Cameron, R. L., Goldich, S. S., and Hoffman, J. H., 1960, Radioactivity age of rocks from the Windmill Islands, Budd Coast, Antarctica: Stockholm Univ. Contribs. Geol., v. 6, p. 1–6.

Du Toit, A. L., 1937, Our wandering continents: Edinburgh, Oliver and Boyd, 366 p.

Starik, I. Ye., Ravich, M. G., Krylov, A. Ya., and Silin, Yu. I., 1959, Ob absolyutnom vozraste porod vostochna-Antarkticheskoi platformy: Akad. Nauk SSSR. Doklady, v. 126, no. 1, p. 144–146.

PALEONTOLOGY, GEOMORPHOLOGY, AND PLANT ECOLOGY

175. GIGANTOPTERIDACEAE IN PERMIAN FLORAS OF THE SOUTHWESTERN UNITED STATES

By Sergius H. Mamay, Washington, D.C.

The plant genus *Gigantopteris* is important as the Northern Hemisphere contemporary of *Glossopteris*, which dominated the Permian floras of Gondwanaland. In eastern Asia the gigantopterids had a broad geographic distribution, but in North America they are known in only a small province east of the Ancestral Rocky Mountains; there they occur in Leonard-equivalent rocks. Their most significant occurrences are in north-central Texas, where they show the longest stratigraphic range and greatest floristic differentiation.

Gigantopteris americana White is the oldest and only previously described American gigantopterid species. It apparently is limited to the Belle Plains and basal Clyde formations of the Wichita group, with questionable occurrences beneath the Talpa limestone member of the Clyde formation marking the upper limit of its stratigraphic range. Associated with it is the most diverse North American Permian flora known. This includes many coal-swamp types, some representing new taxa.

Above the Talpa limestone member, *G. americana* is succeeded by two new gigantopterid species. They both have approximately the same stratigraphic range, extending upward into the Vale formation of the Clear Fork group. Associated floras contain fewer coal-swamp types than the Belle Plains and Clyde floras, and in their highest known occurrence near the top of the Vale, the new gigantopterid species are associated with dominant conifers and other elements suggestive of increased aridity.

The Texas gigantopterids and some associated species strikingly resemble plants of the Permian Shihhotse series of central China and correlative strata of adjacent areas; still others resemble Permian plants from the Ural region of Russia. Plant migration between North America and Asia is thus suggested, with the southwestern United States a likely point of origin.

176. UPPER PALEOZOIC FLORAL ZONES OF THE UNITED STATES

By CHARLES B. READ and SERGIUS H. MAMAY, Albuquerque, N. Mex., Washington, D.C.

Much information has now accumulated regarding the stratigraphic and lateral distribution of upper Paleozoic megafossil floras in the United States. The ensuing account is to be regarded as a report of progress based on data that are admittedly incomplete and that very likely will continue to be incomplete for some decades.

Investigations of upper Paleozoic floras have been chiefly of the plants in or associated with coal, although a number of floras have been reported that do not seem to have grown in coal-forming swamps. Facies problems, therefore, exist in interpreting the sequences and distributions of floras.

At present, 15 floral zones are recognized in the Mississippian (Read, 1955), Pennsylvanian (Read, 1947), and Permian systems (Mamay and Read, 1954) in the United States (tables 176.1 and 176.2). Three of these are in the Mississippian, nine in the Pennsyl-

TABLE 176.1.—*Mississippian and Pennsylvanian floral zones*

Zone	Name	Appalachian region except for Southern anthracite field	Southern anthracite field	Midcontinent region
		Upper Pennsylvanian		
12	*Danaeites* spp	Upper part Monogahela formation.	Not known	Missouri and Virgil series.
11	*Lescuropteris* spp	Lower part Monogahela formation and upper part Conemaugh formation.	do	In Midcontinent region zones 11 and 12 are not separable and are together designated the zone of *Odonopteris* spp.
10	*Neuropteris flexuosa* and *Pecopteris* spp.	Lower part Conemaugh formation and upper part Allegheny formation.	Post-Pottsville rocks undifferentiated.	Upper part of the Des Moines series.
		Middle Pennsylvanian		
9	*N. rarinervis*	Lower part Allegheny formation.	Upper part Sharp Mountain conglomerate member, Pottsville formation.	Lower part of Des Moines series.
8	*N. tenuifolia*	Major part Kanawha formation.	Not known	Major portion of Atoka series.
7	*Megalopteris* spp	Base of Kanawha formation	do	Base of Atoka series.
		Lower Pennsylvanian		
6	*Mariopteris pygmaea and N. tennesseeana*	Upper part New River formation and upper part Lee formation.	Schuylkill conglomerate member, Pottsville formation.	Bloyd shale, Morrow series.
5	*Mariopteris pottsvillea* and *Aneimites* spp.	Lower part New River formation.	Lykens Valley No. 4 coal bed and adjacent strata of Tumbling Run conglomerate member, Pottsville formation.	Locally basal strata of Pennsylvanian system in Midcontinent region.
4	*N. pocahontas* and *Mariopteris eremopteroides.*	Pocahontas formation	Lykens Valley No. 5 and No. 6 coal beds and adjacent strata of Tumbling Run conglomerate member, Pottsville formation.	

TABLE 176.1.—*Mississippian and Pennsylvanian floral zones*—Continued

Zone	Name	Appalachian region except for Southern anthracite field	Southern anthracite field	Midcontinent region
		Mississippian		
3	*Cardiopteris* spp. and *Spenopteridium* spp.	Mauch Chunk formation	Mauch Chunk formation	Chester series (similar flora occur in Stanley shale).
		(No floras known)	(No floras known)	Meramec series (no floras known).
2	*Triphyllopteris* spp	Upper part of Pocono and Price formations.	Upper part of Pocono formation.	Osage series (no floras known).
1	*Adiantites* spp	Lower part of Pocono and Price formations.	Lower part of Pocono formation.	Kinderhook series (only spores and fossil wood known).

TABLE 176.2.—*Permian floral zones*

Zone	Name	Kansas	Oklahoma	North Texas	Arizona and New Mexico
15	Younger *Gigantopteris* flora.			Clear Fork group	
14	Zone of older *Gigantopteris* flora, *Glenopteris* flora; *Supaia* flora.	Summer group (*Glenopteris*).	Garber sandstone (older *Gigantopteris* flora).	Belle Plains formation (older *Gigantopteris* flora).	Upper part Abo formation; Hermit shale (*Supaia* flora).
13	*Callipteris* spp	Wolfcamp equivalents; highest occurrences in Chase group.	Wolfcamp equivalents; highest occurrences in Stratford formation.	Wolfcamp equivalents; highest occurrences in Moran formation.	Lower part of Abo formation.

vanian, and three in the Permian. Although each of the Mississippian and Pennsylvanian zones is reasonably consistent in its botanical makeup, the floristic zonation in the Permian is more complex. The floras of lowermost Permian maintain much similarity wherever found, but the succeeding floras display a striking provinciality that invites speculation as to the reasons therefor, in terms of evolving paleogeography, paleoedaphology, and other ecologic factors.

The upper Paleozoic floral zones (tables 176.1 and 176.2) are named for one or more especially characteristic plants. The following notes are intended to supplement briefly the tables and to report other common plant forms in the floral zones.

Zone 1. *Rhodea, Rhacopteris, Alcicornopteris, Lagenospermum, Calathiops, Girtya, Lepidodendropsis.*

Zone 2. *Rhodea*, early forms of *Cardiopteris.*

Zone 3. Appearance of *Sphenopteridium, Aneimites*-like *Adiantites.*

Zone 4. Diminutive, round-lobed *Sphenopteris;* early *Eremopteris.*

Zone 5. *Neuropteris smithsii, Sphenophyllum tenue*, early *Alethopteris.*

Zone 6. *Neuropteris smithsii, Diplothmema cheathami;* in Rocky Mountains, *Trichopitys.*

Zone 7. *Neriopteris lanceolata, Cardiocarpon phillipsi* group.

Zone 8. Appearance of *Neuropteris rarinervis, N. flexuosa, Pecopteris vestita.*

Zone 9. *Pecopteris restita, Mariopteris occidentalis, Neuropteris ovata, Linopteris rubella*, cyatheoid pecopterids.

Zone 10. *Neuropteris ovata*, cyatheoid pecopterids.

Zone 11. *Neuropteris ovata, Odontopteris* spp, cyatheoid pecopterids; the Midcontinent and the ancestral Rocky Mountains *Lebachia piniformis* sporadic.

Zone 12. Pecopterids of zones 10 and 11 abundant, *Lepidodendron* spp., *Sigillaria* spp. abundant.

Zones 11 and 12 (locally combined). These zones differentiated in Appalachians, not recognized farther west. Interval, characterized by *Odontopteris* spp., *Neuropteris lindahli*, cyatheoid pecopterids.

Zone 13. Many species common in zones 11 and 12. Conifers locally abundant.

Zone 14. Floras provincial, the distribution dependent on paleogeographic and paleoedaphic factors. The *Gigantopteris* spp. and *Glenopteris* spp. floras contain elements present in zones 11, 12, 13. The *Supaia* spp. flora has some elements that suggest relationships with contemporary austral plant associations.

Zone 15. Floras of this zone less diversified than in zone 14; contain elements of Permian Angara floras of Siberia.

REFERENCES

Mamay, S. H., and Read, C. B., 1954, Differentiation of Permian floras in the southwestern United States: Internat. Bot. Cong., 8th, Paris, 1954, Rept. and Commun., sec. 5, p. 157–158.

Read, C. B., 1947, Pennsylvanian floral zones and floral provinces: Jour. Geology, v. 55, no. 3, p. 271–279.

——— 1955, Floras of the Pocono formation and Price sandstone in parts of Pennsylcania, Maryland, West Virginia, and Virginia: U.S. Geol. Survey Prof. Paper 263, 32 p.

177. FOSSIL SPOOR AND THEIR ENVIRONMENTAL SIGNIFICANCE IN MORROW AND ATOKA SERIES, PENNSYLVANIAN, WASHINGTON COUNTY, ARKANSAS

By Lloyd G. Henbest, Washington, D.C.

The Morrow flora and fauna of northwestern Arkansas are widely recognized as a standard of reference for early Pennsylvanian stratigraphy (Mather, 1915; Purdue and Miser, 1916; Henbest, 1953). Though the overlying Atoka series is a standard of reference in the Mid-Continent for rocks of early Middle Pennsylvanian age, its fossils are less well known (Miller, Downs, and Henbest, 1948). Among the most abundant but least studied of the fossils of both series, however, are the spoor (that is, tracks, burrow marks, or other artifacts) of unknown animals. The spoor are commonly preserved in sandstone, siltstone, or claystone beds that are virtually barren of other fossils. The nature of such animals can be inferred only by the shape, position, and sedimentary environment of their artifacts compared with similar spoor of living forms. Such spoor have commonly been treated as oddities and, because of problematic origin, as unworthy of taxonomic nomenclature.

Many kinds of spoor, including several new and previously undescribed forms, compose the Morrow and Atoka assemblages. Six of the most typical are illustrated on figure 177.1. Arthrophycid and paleophycid burrows are particularly characteristic of sediments composed of thin, alternating, ripplemarked beds of sandstone and of clay or siltstone shale. *Conostichus* Lesquereux, 1876, and *Laevicyclus* Quenstedt also belong in this association. The bottom side of the sandstone sheets are commonly crowded with the paleophycid and arthrophycid burrows (fig. 177.1*F*). This is especially true of the Cane Hill member of the Hale formation (Henbest, 1953, p. 1938–9) and a phase of the cyclothems in the Atoka (unit 4 and 9—same bed but offset by fault) of Miller, Downs, and Henbest (1948, p. 674–5).

Taonurus colletti (Lesquereux), 1890, and *Scalarituba* Weller, 1899 (see unit 6 and 11 (same bed), idem) are commonly associated and overlap with a marine invertebrate zone. These marine invertebrate faunas include forms that are common in the marine phases of Illinois cyclothems and in cyclical sequences of the Pennsylvanian of Kansas. No evidence of abyssal origin for the cyclothems in Illinois, Kansas, or in the Atoka series in the Ozark region has been seen by this writer. On the contrary, evidence of shallow, near strand, and near sea level conditions is abundant. The *Taonurus* and *Scalarituba* assemblages are characteristic of the Atoka and higher Pennsylvanian rocks of the Ozark and Arkansas Valley provinces.

CONCLUSIONS

The assemblages characterized by *Taonurus* and those characterized by arthrophycids and paleophycids are regarded by some specialists as exclusively characteristic of flysch deposits and as indicators of abyssal environment. Without questioning the occurrence of similar spoor in abyssal environment or in flysch, it is evident that (a) these spoor in the Morrow and in the Atoka series are preserved in sediments that were laid down in shallow, well-circulated, or well-aerated marine and possibly estuarine waters, (b) the organisms were burrowing forms, (c) the environment supported a relatively meager fauna of shell-bearing invertebrates, and (d) of the few invertebrate shells preserved, some were probably detrital and exotic.

So far as identifiable, most of the Morrow and Atoka genera of spoor have a long stratigraphic range and are unreliable as indicators of age. Preliminary studies indicate that the fossil spoor in the Morrow and Atoka series are significant as indicators of environment and conditions of deposition and that they comprise valuable local aids in differentiating and tracing sedimentary facies or rock units in mapping. The use of such spoor as the arthrophycids for determining the original attitude of sedimentary rocks in complex structures in

the Ouachita Mountains is supported by these occurrences in the related but undisturbed rocks of the Ozark Highlands.

REFERENCES

Branson, C. C., 1959, Some problematical fossils: Oklahoma Geol. Notes, Oklahoma Geol. Survey, v. 19, p. 82–87.

Croneis, C. G., 1930, Geology of the Arkansas Paleozoic area with special reference to oil and gas possibilities: Arkansas Geol. Survey Bull., v. 3, 457 p., 30 figs., 45 pls., maps.

Henbest, L. G., 1953, Morrow group and lower Atoka formation of Arkansas: Am. Assoc. Petroleum Geologists Bull., v. 37, p. 1935–1953, 2 figs.

Mather, K. F., 1915, The fauna of the Morrow group of Arkansas and Oklahoma: Denison Univ. Sci. Lab. Bull., v. 18, p. 59–284, pls. 1–16.

Miller, A. K., Downs, R. H., and Henbest, L. G., 1948, A cephalopod fauna from the type section of the Pennsylvanian "Winslow formation" of Arkansas: Jour. Paleontology, v. 22, p. 672–680, pls. 101–103.

Purdue, A. H., and Miser, H. D., 1916, Geology of the Eureka Springs-Harrison quadrangles, Arkansas and Missouri, U.S. Geol. Survey, Geol. Atlas, Folio 202, 22 p., maps, illus.

Seilacher, A., 1953, Studien zur Palichnologie; I. Über die Methoden der Palichnologie: Neues Jahrb., Geologie u. Paläontologie, Stuttgart, v. 96, p. 421–452.

Explanation of figure 177.1

A–C, *Conostichus* sp. Specimen cut in half. *A*, top; *B*, sectional view; *C*, side. USNM 120231. Marine or estuarine shale above the Baldwin coal, Bloyd shale; Round Mountain, NW¼, sec. 14, T. 16 N., R. 29 W.

Conostichus Lesquereux, 1876 (see also Branson, 1959), originally thought to be a plant fossil, is here tentatively interpreted as the sand-filled spoor of a sedentary burrowing animal. Natural attitude, apex down. Some specimens show cone-in-cone vertical column, each cone flush with successive layers of sand and representing ascent with increment of sediment. Locally abundant in Cane Hill member, Hale formation, and in Atoka series.

D, Spoor of unknown animal. Casts on bottom side, slab 5–8 cm thick, fine-grained sandstone. Specimen collected and deposited in University of Arkansas Museum, by L. G. Henbest, 1923. Loose block probably from Cane Hill member, Hale formation; near center E½, sec. 24, T. 14 N., R. 32 W.

Although appearing to be vertebrate tracks, presence of six digits, irregular retracking, and absence of series of tracks for left legs suggest (but not conclusively) invertebrate origin, possibly the spoor of a side-walking crustacean. Sparsely scattered impressions of small crinoid columnals and brachiopod shells. Opposite side of sandstone slab bears oscillation ripple marks and trail of a gastropod.

E, *Laevicyclus* sp. Concentric marks on sandstone slab, Cane Hill member, Hale formation; cut, state highway 59, near center, south side, sec. 35, T. 13 N., R. 33 W. USNM 120232.

These concentric marks were probably made by the waving tentacles of a polychaete worm (see also Seilacher, 1953, p. 430). A peculiar feature of several is the diametral ridge through the center which has no apparent correlation with polychaetid morphology.

F, Spoor related to *Arthrophycus* Hall, 1852, and *Paleophycus* Hall, 1847. USNM 120233; abundant in Cane Hill member, Hale formation, at same source as *E*. Genera originally classed as algae. Now regarded by some as spoor of burrowing animal, an interpretation here adopted. Sand-filled, attached to bottom side of sandstone slab, and extending into underlying, somewhat organic, dark shale. "Claw" or digging marks present.

G, Weathered vertical joint face on cliff of typical "honeycombed", calcareous sandstone, Prairie Grove member, Hale formation. Source same as of specimens in *E* and *F*, but half a mile north. Not collected. Origin of this prominent and characteristic feature of the Prairie Grove member demonstrated at locality of *E* and *F* where cavities are directly traceable into arthrophycid spoor.

H (left side) *Taonurus colletti* Lesquereux, 1870. Roughly 150 feet above base, Atoka series, near center, south side, sec. 23, T. 13 N., R. 31 W. USNM 120234.

Originally thought to be plant impressions, now regarded by most paleontologists as marks of a burrowing sedentary animal.

H (right side) *Scalarituba* sp. These tubes with cone-in-cone septa are more or less horizontal, commonly hook- or U-shaped. Abundant in many sandstone beds of Atoka and later Pennsylvanian rocks of Boston Mountain and Arkansas Valley provinces. Also found in thin-bedded limestone, Early Mississippian age, New Mexico and Mississippi Valley. Here interpreted as spoor of sediment-eating, burrowing, worm-like animal in shallow marine and estuarine waters.

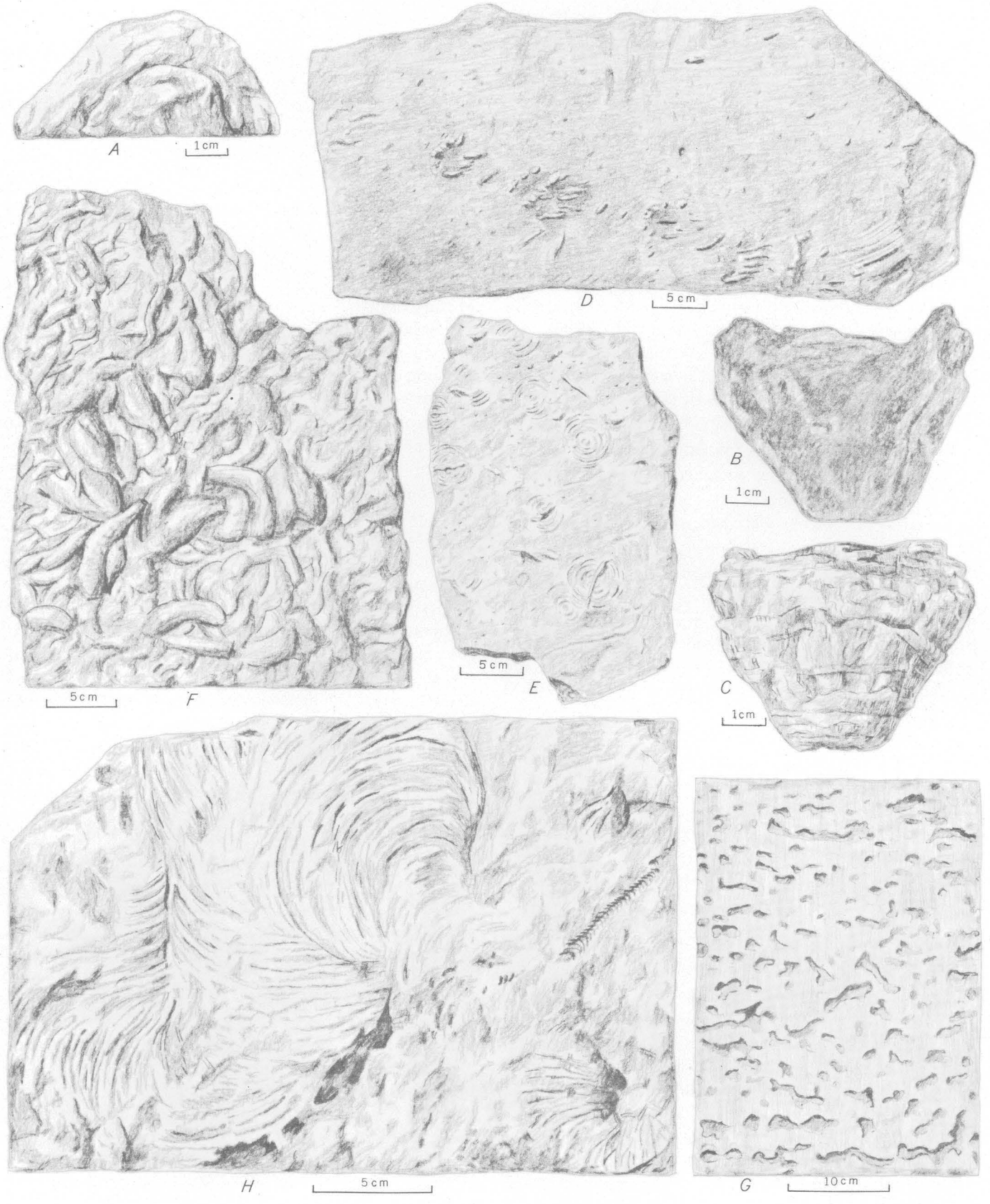

FIGURE 177.1.—Fossil spoor from Pennsylvanian rocks of Washington County, Ark.

178. PALEONTOLOGIC SIGNIFICANCE OF SHELL COMPOSITION AND DIAGENESIS OF CERTAIN LATE PALEOZOIC SEDENTARY FORAMINIFERA

By Lloyd G. Henbest, Washington, D.C.

Foraminfera that had tube-shaped tests and lived permanently attached to invertebrate shells and seaweed have been abundant in shelf seas since middle Paleozoic time. Their shells are widely distributed in most marine limestones, but their protean growth form together with striking similarities in external appearance between common but unrelated genera has confused efforts to classify them and has led to neglect. The neglect is disproportionate, however, to the potential value of these foraminifers in paleoecology, particularly for subsurface exploration for oil.

The sedentary, tubiform foraminifers are divided into two unrelated families primarily on shell composition. Those whose shells are composed of cemented aggregates of bottom detritus are classed with the Tolypamminidae and those with secreted carbonate shells are classed wtih Cornuspirinae, family Opthalmidiidae. These differences in shell composition provide a simple means of recognizing the family relations of living species, but diagenetic changes in shells as old as the late Paleozoic have introduced confusing alterations in both the tolypamminid and cornuspirid fossils.

Petrologic study of the shell material of *Serpulopsis* Girty, 1911, and of *Apterrinella* Cushman and Waters, 1928, respectively among the most typical and abundant genera of Tolypamminidae and Cornuspirinae in the late Paleozoic, together with a study of *Osagia* Twenhofel, 1919, an algal-foraminiferal commensal, has revealed information applicable for classifying related genera.

SHELL COMPOSITION AND CLASSIFICATION OF SERPULOPSIS GIRTY, 1911

Girty (1911, p. 124; 1915, p. 41) originally classed *Serpulopsis* as the shell of a sedentary, marine worm. In 1934, however, he suspected that *Serpulopsis* was a foraminifer and asked me to correct the error. The shell consists of a proloculus followed by a tight coil of one to two volutions. The coil is followed by linear or wandering growth conforming to the surface of the support. Beginning with the proloculus, the shell has a low profile in cross-section and its attachment to the support is broadly festooned—a characteristic of tubiform, sedentary foraminifers that live in shallow waters and therefore are subject to wave or current action and attrition or to capture by grazing animals.

Externally, the shells of Girty's types have an agglutinate appearance, being composed of quartz grains of clay and silt sizes up to 15 microns in diameter. Some of the grains have glittering faces, indicative of secondary enlargement. In collections from other localities, many serpulosid and related shells are covered with a distinct, euhedral quartz druse. These facts have been interpreted by some as positive evidence that the shell is a replacement, by quartz, of an original carbonate shell, and that such fossils belong to the cornuspirids instead of the tolypamminids. Others have claimed that the shells were actually agglutinate as they appear.

To test these counter claims, very thin sections of *Serpulopsis* shells were made from Girty's type material and were mounted in Hyrax—a cement of 1.71 refractive index. The sections reveal that: (a) the grains are poorly sorted, the largest being 15 microns in diameter, and are composed mostly of quartz; (b) the boundaries of adjacent grains are dissimilar and do not mesh; (c) the grains of the innermost zone are fitted and laid like masonry with the largest or flat faces toward the sarcode, forming a smooth inner surface; (d) the grains have random optical orientation; (e) the larger grains can be resolved in sufficient detail to reveal that some have simultaneous and some have wavy extinction. These conditions show that the grains were of different origins and that the shell was originally a cemented aggregate of detrital grains, at least a part of which were quartz. For these reasons *Serpulopsis* Girty, 1911, should be classed as a tolypamminid.

The same criteria may be applied to determine the origin for other supposedly agglutinate shells.

COMPOSITION AND DIAGENESIS OF CORNUSPIRID SHELLS

A perplexing feature of virtually all late Paleozoic foraminifer shells that appear externally to be cornuspirids is that in thin sections they prove to be composed of a dark, finely granular material which is unlike the shell material of most other foraminifers and invertebrates. Irregular parts of such shells resist digestion in very weak acid but no recognizable parts of the shells remain after digestion in 10 percent HCl. Preliminary X-ray analysis does not indicate the pres-

ence of dolomite in the dark shell material. Question arose whether such shell material was originally (a) a chitinoid or other organic secretion, (b) an extremely fine aggregate of detritus masked by metamorphosed cement, or (c) a diagenetic end product of a peculiar carbonate material.

A study of type material of *Apterrinella* Cushman and Waters, 1928, from a well core from the "Dothan limestone" of Permian age in Archer County, Texas, revealed preservations of very rare quality in which the shells have a "porcellaneous" or ivory luster externally and a slightly brownish hue and amorphous structure in section. At magnifications of ×1200, the shell material shows a vaguely granular appearance. These features characterize the shells of living species of Ophthalmidiidae (Wood, 1949, p. 235). A further indication of the quality of preservation is seen with polarized light. The submicroscopic crystals in the shells of living ophthalmids show little or no preferred orientation. In these rare preservations of *Apterrinella*, the crystal orientation remains partly random and such orientation as exists is related to the matrix rather than to the shell structure. Though apterrinellid and similar shells of the Paleozoic have long been accepted as originally "porcellaneous," these preservations comprise the first mineralogic proof known to me.

The significance of the Archer County preservations is extended by recent collections from the Ibex limestone of Cheney at Ibex, Shackelford County, Texas, in which numerous specimens of the same species of *Apterrinella* show, within single shells, the diagenetic stages from "porcellaneous" carbonate material to the dark, finely granular end product that heretofore has been so perplexing and confusing. The diagenetic reconstruction also resulted in a volume change and loss of all but the gross shell structures. The fact that a surface ornamentation consisting of deep, honeycomb-like pits, heretofore unrecognized, is preserved in the unaltered parts of these shells suggests that a more careful study of the Paleozoic sessile cornuspirids may reveal structures of unsuspected taxonomic value. A study of *Osagia* Twenhofel, 1919, and *Ottonosia* Twenhofel, 1919, of Pennsylvanian and Permian age (form genera composed of more or less concentric colonies of stony algae and sessile cornuspirid Foraminifera) indicates a similar diagenesis in both the algal and the foraminiferal shell material.

In a recent important paper on shell composition, Blackmon and Todd (1959, p. 4) determined that the shells of seven living species of Ophthalmidiidae from shallow water were composed of calcite that has the very high magnesian content of 14 to 18 mol percent. It is here proposed that the shells of the late Paleozoic Cornuspirinae and of *Osagia* and *Ottonosia* colonies were likewise composed of magnesian calcite and that their instability was a result of a high magnesian content. It is also suggested that the magnesian content of the ophthalmid shells is determined by the role of symbiotic, chlorophyll-bearing Algae in the internal economy of the animal.

Pseudovermiporella Elliott, 1958, late Permian of Asia Minor, was classed with some uncertainty by its author as Algae. Its peculiar, alveolar surface ornamentation is related to that possessed by the early Permian apterrinellids from Ibex, Texas. The ornamentation is usually obscured by diagenesis and heretofore has been unrecognized. *Pseudovermiporella* is here transferred from the Algae to the protozoan family Ophthalmidiidae.

REFERENCES

Blackmon, P. D., and Todd, Ruth, 1959, Mineralogy of some Foraminifera as related to their classification and ecology: Jour. Paleontology, v. 33, p. 1–15, 1 fig., 4 tables.

Girty, G. H., 1911, On some new genera and species of Pennsylvanian fossils from the Wewoka formation of Oklahoma: New York Acad. Sci., Annals v. 21, p. 119–156.

——— 1915, Fauna of the Wewoka formation of Oklahoma: U.S. Geol. Survey Bull. 544, 353 p., 35 pls.

Wood, A., 1949, The structure of the wall of the test in Foraminifera: its value in classification: Geol. Soc. London Quart. Jour., v. 104, p. 229–255.

179. RELATION OF SOLUTION FEATURES TO CHEMICAL CHARACTER OF WATER IN THE SHENANDOAH VALLEY, VIRGINIA

By JOHN T. HACK, Washington, D.C.

The Shenandoah Valley, Virginia (fig. 179.1), is an area about 130 miles long and 40 miles wide in the Appalachian Mountains. The valley floor is underlain by intensely deformed Cambrian and Ordovician limestone and dolomite. The valley is flanked on the southeast by the Blue Ridge, a highland area of resistant

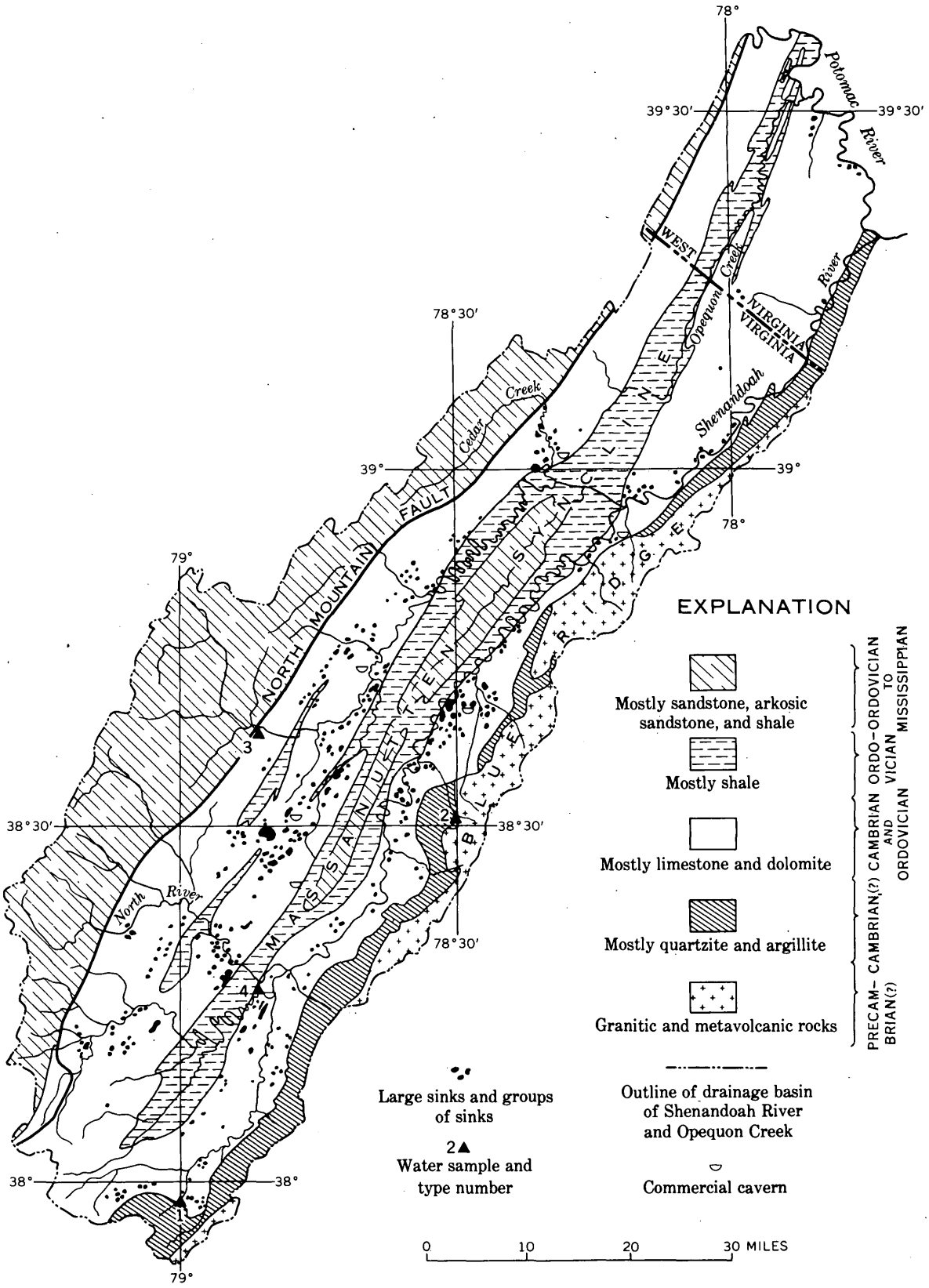

FIGURE 179.1.—Map of Shenandoah Valley, Virginia and West Virginia, showing the distribution of the principal kinds of rock and the location of sinks. Geology simplified from several sources, principally Butts (1933) and Edmundson (1945). Faults are not shown except for the North Mountain fault, on the northwest side of the valley.

Precambrian(?) igneous rocks and Cambrian(?) quartzite, graywacke, and argillite. On the northwest side of the valley, separated from the carbonate area by the North Mountain thrust fault, is another mountainous area, underlain by shale and sandstone of Ordovician to Mississippian age. The Massanutten syncline, a major structural feature in the center of the valley, brings Ordovician, Silurian, and Devonian rocks down to the present topographic surface.

The chemical quality of the water of each stream in this region, at periods of low or normal flow, depends on the kinds of rock in the drainage basin. The range in composition of the waters is illustrated by the examples shown in table 179.1, chosen from analyses of water at about 30 localities (Connor and Schroeder, 1957, Schroeder and Kapustka, 1957, and data collected by the writer). Water from quartzite basins in the Blue Ridge has an extremely low content of dissolved solids, low bicarbonate content, and a pH that is consistently below 7 and may go as low as 5.0 (type 1, table 179.1). The water of the few streams that drain areas of granitic and metavolcanic rock in the Blue Ridge is higher in sodium and potassium and higher in silica than that of other streams, but like type 1 it is relatively low in bicarbonate and its pH averages about 7.0 (type 2, table 179.1). A third class of streams drains areas of Mississippian to Ordovician sandstone and shale along the northwest side of the valley and on Massanutten Mountain. The water of these streams is intermediate in calcium and bicarbonate content between the waters from basins in quartzite and carbonate rocks. Its pH ranges from 6.8 to 7.8 (type 3, table 179.1). Water that drains areas of limestone and dolomite is high in calcium, magnesium, and bicarbonate. Its total content of dissolved solids is high, averaging about 200, and its pH ranges from about 7.6 to 8.2 (type 4, table 179.1). Many streams in the limestone area may be saturated in calcium carbonate at periods of low flow, during which travertine is deposited on the beds at many riffles. Though the sample of this kind of water shown in table 179.1 (type 4) is from a large stream, the quality of these waters is independent of the size of the drainage basin. Water from a certain small stream in carbonate rocks was found to have a similar composition, its bicarbonate content being 171 ppm. and its pH 8.1 (Bell Creek, drainage area 9 sq mi, Schroeder and Kapustka, 1957, p. 28).

TABLE 179.1.—*Analyses (in parts per million) of water of four streams typical of the Shenandoah Valley, Va.*

	Type 1 (quartzite area)	Type 2 (igneous rock area)	Type 3 (sandstone-shale area)	Type 4 (carbonate rock area)
Silica	7.2	14.0	5.9	4.4
Iron	.00	.00	.01	.01
Calcium	.8	4.8	13.0	50.0
Magnesium	1.4	2.2	3.5	19.0
Sodium and potassium	1.1	5.4	4.5	4.2
Bicarbonate	5.8	25.0	49.0	236.0
Sulfate	.6	9.2	8.2	7.7
Chloride	.4	1.0	2.5	3.0
Fluoride	.0	.2	.0	.1
Nitrate	.1	1.0	2.0	2.7
Total dissolved solids	14.0	50.0	63.	204
Alkalinity (as $CaCO_3$)	4.8	21.0	47.	203
pH (laboratory measurement)	6.4	6.8	7.6	8.1
pH (measured in field)	6.0	7.5	----	----

Type 1. Canada Run, Augusta Co., Va. Drainage area ½ square mile, whole in quartzite. Collected by J. T. Hack, April 8, 1959. pH measured in field. J. W. Barnhart and W. B. Hurlburt, analysts.

Type 2. East Fork, Stony Run, Page Co., Va. Drainage area 1 square mile, mostly in granodiorite. Collected by J. T. Hack, April 8, 1959. pH measured in field. J. W. Barnhart and W. B. Hurlburt, analysts.

Type 3. North Fork, Shenandoah River, at Cootes Store. Drainage area 215 square miles in sandstone, arkosic sandstone and shale (Data from Schroeder and Kapustka, 1957, p. 28).

Type 4. Middle River near Grottoes. Drainage area 360 square miles. Mostly in limestone but includes shale and some sandstone (Data from Schroeder and Kapustka, 1957, p. 27).

The solution cavities in the carbonate rocks of the Shenandoah Valley are distributed with relation to the streams in a way that suggests a relation to the source of the water. In figure 179.1 the distribution of all the sinks large enough to be enclosed by 20-foot contours and shown on the Geological Survey's topographic maps of the area are indicated. Sinks are abundant in carbonate rock areas flanked by highlands of clastic rocks from which waters of low alkalinity issue. The map shows that at either end of the valley, where there are large areas of carbonate rocks in which most of the drainage is local, sinks are rare and occur only near the large rivers. Sinks tend to be further localized along streams, such as Cedar Creek and the North River, that drain areas of clastic rock. The solution of carbonate rocks may be favored, therefore, by a large source of water of low alkalinity, in which the pH is less than 7.8 (Krumbein and Garrels, 1952, p. 8 and 24). Other factors, of course, contribute to the localization of sinks and must be at least as important as the original character of the water entering the carbonate rocks. These include various qualities of the rocks themselves, such as composition, permeability, and structural features like fractures and joints. Data on aerial photographs of the southern part of the valley show, for example, that the Ordovician carbonate rocks have, on the average, 4.25 sinks per square mile, whereas the Cambrian carbonate rocks have only 1.5 sinks per square mile. Solution features also appear to be especially numerous in areas where the rocks have low dips.

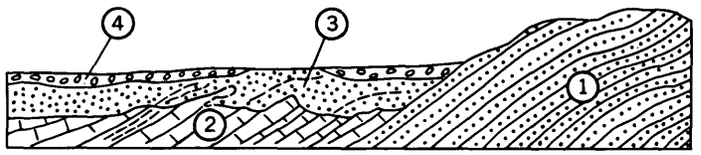

FIGURE 179.2.—Diagrammatic cross section showing inferred geologic conditions along the northwest foot of the Blue Ridge. 1, Quartzite in foothills of Blue Ridge; 2, dolomite and impure limestone of Cambrian age; 3, residuum of clay, silt, and sand; 4, quartzite gravel derived from (1) on terraces and flood plains.

Sinks filled with gravel are common along the northwest foot of the Blue Ridge, where impure Cambrian limestone and dolomite are overlain and almost completely blanketed by gravel derived from the quartzite areas in the mountains, as shown diagrammatically in figure 179.2. The waters issuing from the mountains at temperatures between 11° and 25° C have pH values ranging from 5 to 6.8 and Eh values ranging from +0.3 to +0.5 volts, as measured by the writer in the field. These waters infiltrate the gravelly and cobbly alluvium on entering the limestone area, then react with the carbonate bedrock and emerge with a high alkalinity and pH, which clearly shows that solution is taking place beneath the alluvial cover. As the insoluble residue of the carbonate rocks cannot escape because of the gravel cover, the fresh bedrock is overlain by silty and clayey residuum that is in many places over 100 feet thick. This process contributes to the formation of iron and manganese deposits, which occur in considerable numbers in the residuum. Whatever iron and manganese are present in the carbonate rocks is nearly insoluble in water having the pH and oxidation potential of the water of the Blue Ridge streams (Krauskopf, 1957). These elements, therefore, like the siliceous residues, accumulate beneath the alluvium as oxides and hydroxides, and in some places they are concentrated in deposits of minable grade.

REFERENCES

Butts, Charles, 1933, Geologic map of the Appalachian Valley of Virginia; scale 1:250,000: Virginia Geol. Survey.

Connor, J. G., and Schroeder, M. E., 1957, Chemical and physical character of surface waters of Virginia: Virginia, Dept. Conserv. and Devel., Div. Water Resources, Bull. 20, 107 p.

Edmundson, R. S., 1945, Industrial limestones and dolomites in Virginia; northern and central parts of the Shenandoah Valley: Virginia Geol. Survey Bull. 65, 195 p.

Krauskopf, K. B., 1957, Separation of manganese from iron in sedimentary processes: Geochim. et Cosmochim. Acta, v. 12, p. 61–84.

Krumbein, W. C., and Garrels, R. M., 1952, Origin and classification of chemical sediments in terms of pH and oxidation-reduction potentials: Jour. Geology, v. 60, p. 1–33.

Schroeder, M. E., and Kapustka, S. F., 1957, Chemical and physical character of surface waters of Virginia: Virginia, Dept. Conserv. and Devel., Div. Water Resources, Bull. 21, 199 p.

180. SOME EXAMPLES OF GEOLOGIC FACTORS IN PLANT DISTRIBUTION

By CHARLES B. HUNT, Denver, Colo.

In Death Valley, Calif., the area below about 1,000 feet above sea level supports three quite different floral assemblages, reflecting three equally different kinds of ground. The area lies entirely within the Lower Sonoran Zone, and its climate is essentially uniform. Annual rainfall is about 1.5 inches; evaporation is about 150 inches a year; average temperatures in July exceed 100°F; minimum temperatures in winter rarely reach freezing; ground temperatures in summer go as high as 190°F.

The gravel fans surrounding the salt pan consist mainly of permeable ground, in which the water table is scores to hundreds of feet below the surface. They support stands of xerophytes (fig. 180.1), plants that root in the zone of vadose water above the water table and that are capable of surviving protracted drought.

At the foot of the fans and at the edge of the salt pan, ground water comes near the surface, and the plants

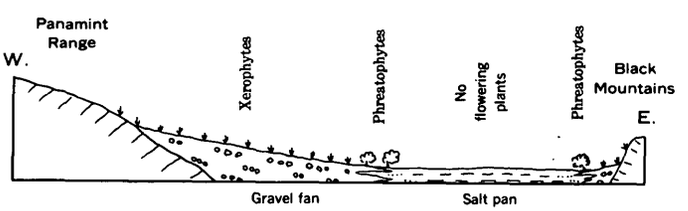

FIGURE 180.1.—Generalized section across Death Valley, Calif., showing distribution of plants. Xerophytes grow on gravel fans, phreatophytes grow at the foot of the fans where ground water is shallow. There are no flowering plants on the salt pans.

there are phreatophytes—plants that cannot live unless their roots reach the water table or the capillary fringe above it.

The salt pan, covering the lowest part of the valley, is without flowering plants, because the water in it is too saline to support them.

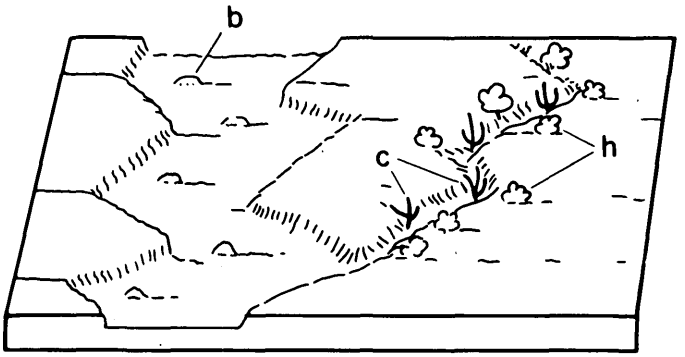

FIGURE 180.2.—Details of distribution of xerophytes on gravel fans in Death Valley. The main washes, which benefit by runoff from the mountains, support stands of burroweed (*b*). Tributary washes that collect runoff from benchlands on the fans have stands of creosote bush (*c*) flanked by stands of desert holly (*h*). Benchlands between the washes commonly have an impermeable surface of desert pavement and are bare.

The xerophytes are distributed in three principal zones (fig. 180.2). At the foot of the fans the commonest shrub is desert holly (*Atriplex hymenelytra*). Above this is a belt of creosote bush (*Larrea tridentata*). The highest parts of the fans have stands of burroweed (*Franseria dumosa*). The distribution of these shrubs, however, when looked at in detail, is controlled chiefly by differences in ground conditions; the climatic differences due to the differences in altitude are slight. For example, the most barren ground on the fans is gravel having an impermeable pavement of caliche at the surface, which favors very rapid runoff. This kind of ground is without flowering plants whether it is on the high or low parts of the fans. Ground around the foot of the fans, also, that contains more than 5 percent (by volume) of salts is bare.

Burroweed occupies those high parts of the fans that benefit by runoff from the mountains, where rainfall is much greater than it is on the fans. But because the runoff rapidly collects in washes floored with highly permeable gravel, it rarely extends far down on the fans. Vadose water on the middle and lower parts of the fans is replenished chiefly by the rainwater that falls there, and by the runoff from neighboring impermeable surfaces. Creosote bush grows where the catchment areas are moderately large; desert holly grows where the catchment areas are small. The distribution of each of the species is clearly a function of the availability of vadose water.

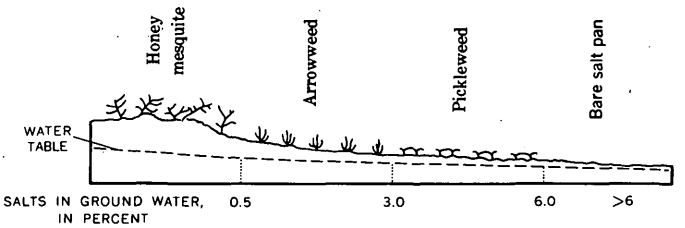

FIGURE 180.3.—Zoning of phreatophytes with respect to salinity of the ground water in Death Valley.

The phreatophytes in the belt of near-surface ground water at the foot of the fans are zoned in an orderly way with respect to the salinity of the ground water around their roots (fig. 180.3) Honey mesquite (*Prosopsis juliflora*) grows where the water contains less than 0.5 percent of salts. Arrowweed (*Pluchea sericea*) grows farther panward, to where the ground water contains 3 percent of salts. Pickleweed (*Allenrolfea occidentalis*), the most salt-tolerant plant, extends panward to where the ground water contains 6 percent of salts. The salinity of the ground water varies seasonally; the limits represent the maxima reached during dry seasons.

In the salt pan proper, where the brines contain more than 6 percent of salts, there are no flowering plants, and even thallophytes (algae, fungi, and bacteria) are few.

GEOPHYSICS

181. RATE OF MELTING AT THE BOTTOM OF FLOATING ICE

By DAVID F. BARNES and JOHN E. HOBBIE, Menlo Park, Calif., and Arctic Institute of North America, Bloomington, Ind.

Work done in cooperation with the Arctic Institute of North America, the Air Force Cambridge Research Center, and the Office of Naval Research

The ice sheets covering Arctic lakes and seas have an important influence on both the surficial geology and the climate of their environment. Yet the influence of the underlying water on the thickness and duration of these ice sheets has received little attention, although important effects are sometimes attributed to small changes in water temperature. Research on the thermal regimen and physical properties of a melting ice sheet at Lake Peters, Alaska, provided an opportunity to study the effect of a deep, current-free body of fresh water on an overlying sheet of ice.

At Lake Peters a nearly continuous record was maintained of the micrometeorological and limnological factors influencing ice melt. The study began early in May, when the temperature of the 6-foot-thick ice cover was still below freezing, and ended in the last week of July, when the last ice melted off the lake. The rate of melting at the bottom of the ice sheet was obtained by freezing translucent plastic horizon markers into the ice early in the season and measuring their distances from the top and bottom of the ice sheet at 4-day intervals during the melting season. Many of these markers were originally attached to white wooden poles, but these poles absorbed so much solar radiation that they became loose midway in the season. Another marker, however, attached to a white wire, persisted nearly throughout the melting season. Because of the loosening of the markers and the unevenness of the top and bottom ice surfaces, there is considerable scatter in the measurements. Nevertheless the data indicate that not more than a few centimeters melted from the bottom of the ice sheet during the entire melting season.

This small amount of melting is consistent with the thermal gradients measured in the water beneath the ice. Water temperatures at various depths in the lake were determined at frequent intervals with a small thermistor probe lowered into the lake. Four curves obtained at the middle of Lake Peters during the melting season are shown in figure 181.1. The three early-season curves show a well-mixed constant-temperature layer which grows warmer and thicker as the season progresses. The temperature gradient beneath the ice may be computed for the early part of the melting season, during which this constant-temperature layer is

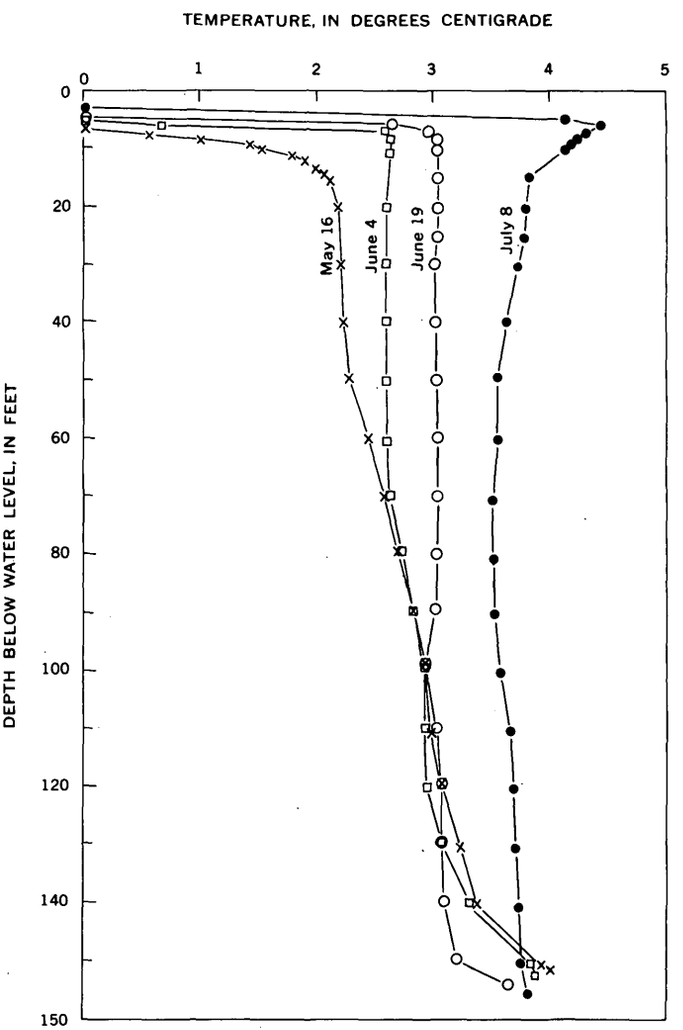

FIGURE 181.1.—Water temperature versus depth curves from Lake Peters, 1959.

developing, but the proposed theory does not give the gradient in the later part of the melting season.

The water temperature is below the maximum-density point, and the well-mixed layer can be created by warming the water just beneath the ice so that it sinks and creates convection. Solar radiation penetrating the ice is the major source of heat for the lake water before mid-June, when rivers begin to flow and a shoreline moat develops. The heat radiated into the well-mixed layer is transferred downward by convection. Above the well-mixed layer is a thin, stably stratified boundary layer where the absorbed radiant heat is transferred upward by conduction. This is the heat that causes melting at the bottom of the ice, and its source is solar radiation.

Because the convective processes in the well-mixed layer are very slow, we may assume that almost no heat is transferred from this layer to the boundary layer. The thermal processes in the stable boundary layer may then be expressed mathematically for steady-state conditions by the equation:

$$Lm=\mathrm{K}\frac{\partial v}{\partial x}\bigg|_{x=0}=I_0(1-e^{-\eta h}) \tag{1}$$

where L is the latent heat of ice, m the mass of ice melted per unit time and area, K the thermal-conductivity of water, v the temperature at depth x below the bottom of the ice, I_0 the solar radiation that enters the water, η the extinction coefficient of water, and l the thickness of the stable boundary layer. This equation does not take into account the heat transferred upward by a thermal gradient within the ice. Measurements reveal, however, that during the melting season such gradients are negligible. During the winter and before the melting condition is established the right-hand side of equation (1) gives the heat which is supplied to the ice by the water and which tends to reduce the amount of new ice formed by a thermal gradient in the ice. It thus furnishes a correction for Stefan's (1889) formula for ice growth.

Equation (1) shows that in the absence of currents the heat available for melting ice cannot exceed the radiation reaching the lake water. At Lake Peters the solar radiation at the top of the ice was about 700 cal per cm² per day, but less than 1/10 of this passed through the ice. In the following paragraphs we show that only about 1/5 of the radiation reaching the water was absorbed in the stable boundary layer and caused melting of the ice.

The thickness of the boundary layer, l, may be obtained by integrating

$$\frac{\partial^2 v}{\partial x^2}=-\frac{\eta I_0}{K}e^{-\eta x} \tag{2}$$

Using the boundary conditions $x=l$, $\frac{\partial v}{\partial x}=0$ and $x=0$, $v=0$ we get:

$$v=\frac{I_0}{\eta K}-\frac{I_0}{\eta K}e^{-\eta x}-\frac{I_0 x}{K}e^{-\eta l} \tag{3}$$

which gives the water temperature at any depth in the boundary layer. Since the temperature at the base of the boundary layer ($x=h$) is $v=T$, the temperature of the mixed layer, we get:

$$(1+\eta h)e^{-\eta l}=1-\frac{\eta KT}{I_0} \tag{4}$$

which defines ηl as a function of $\frac{\eta KT}{I_0}$. Figure 181.2 shows the relation between $\frac{\eta KT}{I_0}$ and both ηh and $(1-e^{-\eta h})$. The latter gives from equation (1) the proportion of radiation that goes into melting ice. The dashed line in figure 181.2 shows an approximation that leads to:

$$Lm\approx 1.4\sqrt{\eta KTI_0} \tag{5}$$

which shows that T, and I_0 all have an equal effect on the rate of melting. However, solar radiation and water transparency are more variable and cause greater variations in melting rate.

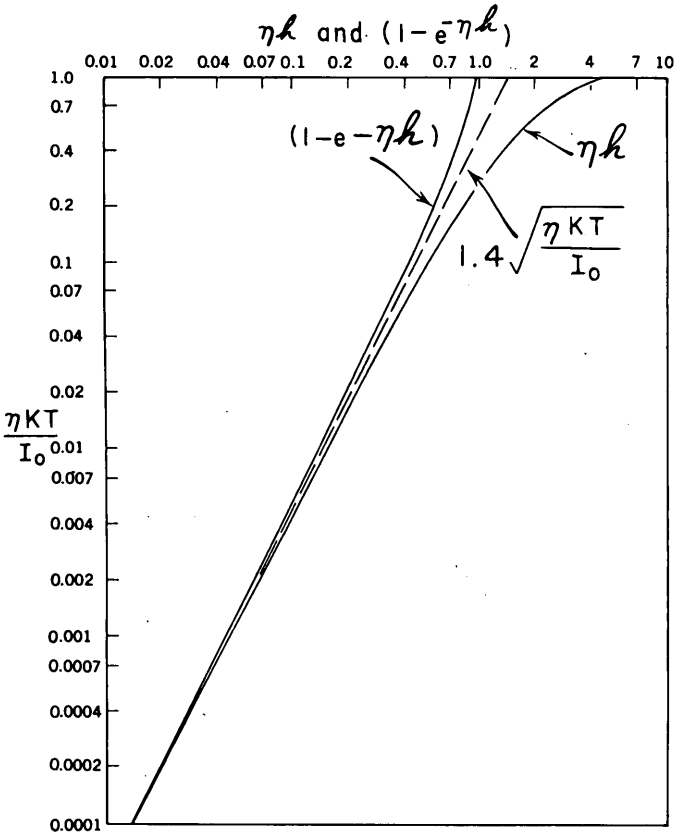

FIGURE 181. 2.—Relationship between $\frac{\eta KT}{I_0}$ and both ηh and $(1-e^{-\eta h})$.

Sufficient data were obtained at Lake Peters to check the reliability of these formulas. The values of L and K are well known; they are about 80 cal/gm and 0.0013 cal $°C^{-1}$ cm^{-1} sec^{-1} respectively. The values of T and h may be obtained by plotting water temperature against depth. The extinction coefficient η and solar radiation I_o were measured with a submarine photometer. Some uncertainty is involved in the photocell calibration, which depends on both the spectral distribution and the angular incidence of radiation at the point of measurement. However, an analysis of data obtained from Moon (1940), Lyons and Stoiber (1959), and the photocell manufacturer has provided a calibration factor which is also supported by computations of water-heat increments from the temperature-depth curves. The extinction coefficient varied from 0.002 cm^{-1} to 0.005 cm^{-1}, and we used an average value of 0.003 cm^{-1}.

In the early part of June the radiation penetrating the ice was about 63 cal/cm^2/day, or 0.0007 cal/cm^2/sec, and the temperature of the mixed layer was about 3° C. From figure 181.2 these values give a boundary-layer thickness of about 67 cm, which is very close to the measured value of a little more than 60 cm. The calculated heat flow to the overlying ice is about 10 cal per day, which implies an ablation rate of about one centimeter per week. This agrees well with the measured ablation data.

The variation of temperature with depth in the boundary layer may best be measured early in the season, when the boundary layer is thicker then it is later on when there is no snow cover to absorb radiation. The May 16 temperature curve in figure 181.1 was obtained under snow-covered ice, and figure 181.3 shows how well the data from the upper part of this curve agree with a theoretical curve obtained by using an I_0 of 0.00004 in equation (3). No radiation measurements were made on May 16, but a value of 0.00004 is consistent with a value measured a few days later.

These formulas seem to provide a reliable method for estimating the steady-state, under-ice thermal gradient during the freeze-up, winter, and early melting season. They do not take account of turbulent heat transfers resulting from water currents or ice drift. Later in the melting season (after mid-June at Lake Peters in 1959 when the ice was about four feet thick) such turbulent transfers may become important. Furthermore, when

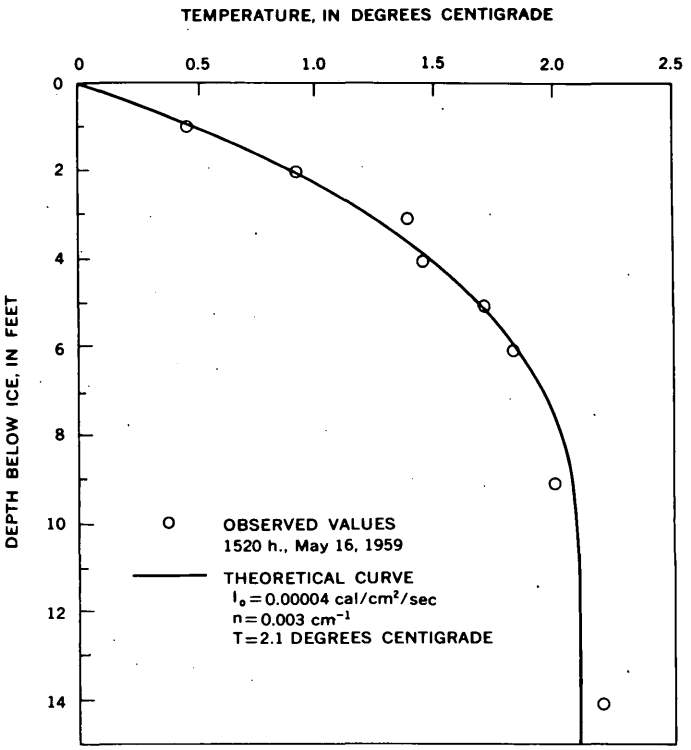

FIGURE 181.3.—Comparison of observed and theoretical water temperatures beneath Lake Peters ice on May 16, 1959.

the water temperature approaches the maximum density value of 4°C small variations in salinity become important, and layers of warmer, fresher water (Birge, 1910) may develop beneath the ice, as shown in the July 8 curve of figure 181.1. Analyses of the Lake Peters thermal data for this portion of the melting season are not complete, but the ablation-marker data show that the rate of melting at the bottom of the ice did not exceed 1 cm per week before the last week of the melting season.

REFERENCES

Birge, E. A., 1910, The apparent sinking of ice in lakes: Science, v. 32, p. 81–82.

Lyons, J. B., and Stoiber, R. E., 1959, The absorptivity of ice: A critical review: Scientific Report No. 3, Dartmouth College, Contract AF 19(604)–2159, Oct. 31, 1959, AFCRC–TN–59–656.

Moon, Parry, 1940, Proposed standard solar-radiation curves for engineering use: Jour. Franklin Inst., v. 230, no. 5, p. 583–618.

Stefan, Julius, 1889, Über die Theorien des Eisbildung insbesondere über die Eisbildung in Polarmeere: Wien Sitzungsber. Akad. Wiss., A, v. 42, pt. 2, p. 965–83.

182. INTERNAL FRICTION AND RIGIDITY MODULUS OF SOLENHOFEN LIMESTONE OVER A WIDE FREQUENCY RANGE

By L. Peselnick and W.F. Outerbridge, Washington, D.C.

Previous work on internal friction of fine-grained limestone (Peselnick and Zietz, 1959) has shown a linear dependence of the absorption coefficient with frequency in the range 3 to 10 megacycles per second, and no variation in the modulus of rigidity with frequency within 4 percent experimental precision.

A measurement of internal friction and rigidity was made for one of these samples, Solenhofen limestone, at 3.59 cycles per second using the torsion pendulum. The internal friction, expressed in terms of the logarithmic decrement and amplitude absorption coefficient, was obtained for maximum surface shear strains of the order of 10^{-5} cm per cm, and at a temperature of 25° C. The absolute error in this low frequency measurement of internal friction was estimated to be less than 7 percent. The rigidity or shear modulus μ was obtained to within an error of ± 1 percent and with a precision of one-half percent.

The rigidity modulus μ for the limestone at 3.59 cycles per second was found to be 2.29 x 10^{11} dynes per sq cm and was independent of the applied strains. This low frequency determination of μ agrees with the high frequency value of 2.2 x 10^{11} to 4 percent, which is within the experimental precision of the high frequency method. Therefore, the rigidity modulus for Solenhofen limestone is the same for either low or high frequencies within 4 percent.

Figure 182.1 shows the shear absorption coefficient for Solenhofen limestone plotted against frequency for the high frequency data of Peselnick and Zietz

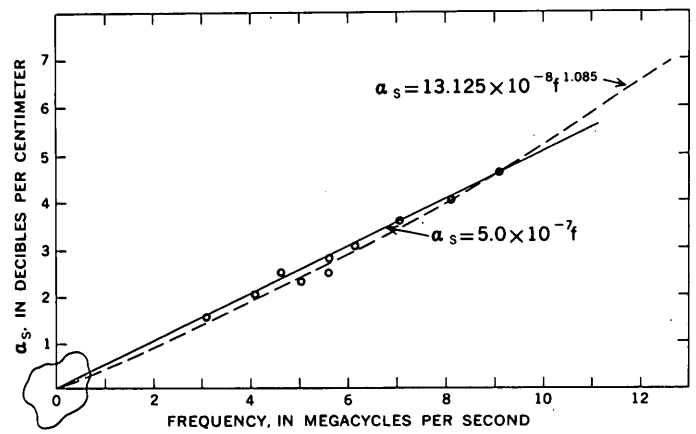

FIGURE 182.1.—Shear absorption coefficient α_s versus frequency for Solenhofen limestone.

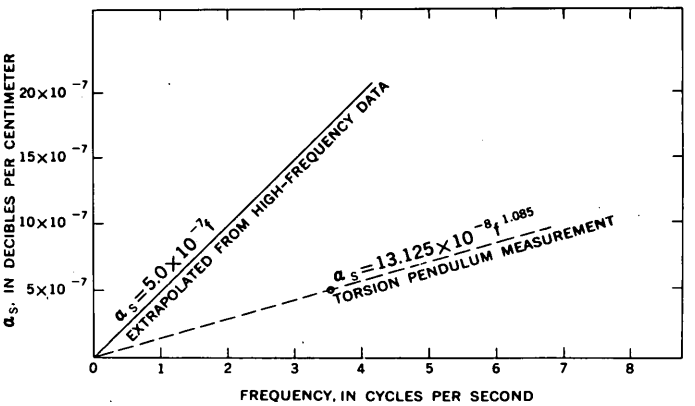

FIGURE 182.2.—Expanded section near origin of figure 182.1 for α_s versus frequency.

(1959). The graph is a straight line drawn through the origin, $\alpha_s = 5.0 \times 10^{-7}\ (f)$ db per cm, where f is in cycles per second.

Figure 182.2 is an enlarged drawing of the section near the origin of the graph of figure 182.1. The logarithmic decrement at 3.59 cycles per second was found to be 5.0 x 10^{-3}. The relation between the logarithmic decrement δ and the absorption coefficient α_s for shear vibration is (Peselnick and Zietz, 1959; Born, W.T., 1941)

$$\alpha_s = \frac{\delta f}{C} \frac{8.686}{} \text{db per cm} \qquad (1)$$

where f is the frequency of vibration in cycles per second and C is the shear velocity in cycles per second. The shear velocity, calculated from the measurements of density (2.59 grams per cc) and rigidity ($\mu = 2.29$ x 10^{11} dynes per sq cm) is $C = \sqrt{\mu \text{ per } \rho} = 2.97$ x 10^5 cycles per second. By substitution of the appropriate quantities into equation one, the shear absorption coefficient at 3.59 cycles per second is 5.25 x 10^{-7} db per cm: the extrapolated value of α_s at 3.59 cycles per second from the high frequency data is 18 x 10^{-7} (see fig. 182.2). Thus, the internal friction is a factor of 3.5 times lower than that obtained by linearly extrapolating the high frequency data to 3.59 cycles per second.

The factor of 3.5, representing the ratio of internal friction at the specified high and low frequencies, cannot be accounted for solely by experimental error. An immediate consequence of this is that the absorption coefficient is not a linear function of the frequency over

the extended frequency range of 3.59 cycles per second to 10 megacycles per second. Thus, the previously reported linear function for the shear absorption coefficient in Solenhofen limestone (Peselnick and Zietz, 1959), $\alpha_s = 5.0 \times 10^{-7}$ (f) db per cm, must be modified to express the dependence of internal friction for the extended frequency range. The exponential function, $\alpha_s = 13.125 \times 10^{-8}$ $(f)^{1.085}$ db per cm, was chosen, and the agreement is within experimental error (see figs. 182.1 and 182.2). It should be noted that the newer exponential function is very close to a linear function in the frequency range from 3 to 10 megacycles per second, the exponent being nearly equal to one.

More data are required to complete the spectrum; frequencies higher than 10^7 are required to show where scattering losses become predominant while lower frequencies are of interest to define carefully the loss function.

The shear velocity as calculated from the rigidity at 3.59 cycles per second is the same as the velocity determined in the megacycle frequency range within the experimental uncertainty of 4 percent, at 25° C and at atmospheric pressure. A relaxation process might have been suspected as a result of viscous behavior of the grain boundaries (Kê, 1947), since grain boundary losses were found to be prevalent in Solenhofen limestone (Peselnick and Zietz, 1959). Any difference between the relaxed and unrelaxed velocities would necessarily be less than 4 percent had such a process taken place between 3.59 cycles per second and 10 megacycles per second. If it is assumed that no relaxation mechanisms exist in this frequency range, it is reasonable that the elastic moduli at high and low frequencies should agree closely, because their magnitudes are related through intergranular and interatomic forces, both of which presumably do not change for small amplitude measurements.

REFERENCES

Born, W. T., 1941, The attenuation constant of earth materials: Geophysics, v. 6, p. 140.

Kê, T. S., 1947, Experimental evidence of the viscous behavior of grain boundaries in metals: Phys. Rev., v. 54, p. 293.

Peselnick, L., and Zietz, I., 1959, Internal friction of fine-grained limestones at ultrasonic frequencies: Geophysics, v. 24, p. 285–296.

183. PHYSICAL PROPERTIES OF TUFFS OF THE OAK SPRING FORMATION, NEVADA

By George V. Keller, Denver, Colo.

Work done in cooperation with the U.S. Atomic Energy Commission

The U.S. Geological Survey has made intensive physical properties studies in support of the Atomic Energy Commission's underground weapons test program at the Nevada Test Site. Most of the underground nuclear explosions in the 1 to 20 kiloton range have been detonated in the tuffs of the Oak Spring formation of Tertiary age. The underground test area is located in a mesa at the northwest corner of the Nevada Test Site, approximately 55 miles north of Mercury, Nev.

Near the test chambers, the tuffs are about 2,000 feet thick. All are rhyolitic to quartz latitic in composition (Wilcox, 1959). The tuffs may be subdivided into three groups on the basis of texture: bedded tuff, friable tuff, and welded tuff. The bedded tuffs are distinguishable from the friable tuffs by their greater coherency. The chemical difference between bedded and friable tuffs is small, except for a greater content of water in the bedded tuffs. In the friable tuffs, the conversion of glass fragments to zeolite is not so extensive as in the bedded tuffs, and only a thin rind of zeolite surrounds the glass fragments, so the rock is only weakly cemented and crumbles readily. The welded tuffs do not differ from the other units significantly in bulk chemical composition, and generally the lower parts of welded units grade into bedded and friable tuff.

Samples for testing were obtained from several core holes drilled near the test chambers and from underground workings. Properties studied included textural properties, such as porosity, density, permeability and water content; strength and elastic properties, including acoustic velocities; thermal properties, including conductivity, enthalpy and entropy; and electrical properties.

TABLE 183.1.—*Summary of physical properties of volcanic tuffs from the Oak Spring formation*

Textural subdivision	Porosity [1] (g per cm³)	Bulk density dry [1] (g per cm³)	Grain or powder density (g per cm³)	Permeability water [2] (millidarcys)		Permeability air [2] (millidarcys)	
				Average	Range	Average	Range
Bedded tuffs	0.388±0.070	1.50±0.16	2.44±0.11	0.040	0.00076–17	0.90	0.07 –39
Bedded tuffs (pumiceous)	.402± .126	1.37±0.30	2.28±0.12	11.5	3.7 –61	21	4.1 –75
Friable tuffs	.355± .138	1.50±0.35	2.33±0.24	1.4	0.084 –27	6.0	0.95 –41
Welded tuffs	.141± .089	2.18±0.23	2.55±0.09	.33	0.00092–58	0.66	0.022–58

[1] Ranges expressed are one standard deviation.
[2] Ranges expressed are the complete range of observed values.

TEXTURAL PROPERTIES

The porosities, densities and permeabilities measured on drill cores from the tuffs in the Oak Spring are summarized in table 183.1. Porosities were determined by measuring the volume of water required to saturate samples, so the values presented in table 183.1 represent interconnected pore volumes. Grain density measurements indicate that there is almost no "blind" or unsaturable porosity in the tuff.

The porosities are very high. Many hundreds of water-content determinations have been made on samples obtained in their natural state from the mine workings, and in almost every determination the rocks have been found to be almost completely saturated with water. Almost complete saturation with water is found in rocks several hundred feet above the permanent water table. The water is held by impermeable beds in perched water tables and by capillarity in fine pores in rock.

STRENGTH AND ELASTIC PROPERTIES

Tensile and compressive strengths were determined for several samples of bedded and welded tuffs at the Geological Survey laboratory, and by the Applied Physics Laboratory of the U.S. Bureau of Mines (Robertson, 1959). No samples of friable tuff were obtained for strength tests, because the strength was too low to permit coring of a long enough specimen. Average uniaxial tensile and compressive strengths under atmospheric confining pressure, are listed in table 183.2.

Values of compressive strength are about 25,000 pounds per square inch (psi) for the welded tuff and about 5,000 psi for the bedded tuff. As might be expected, the compressive strengths of both types of tuff are much higher than the tensile strengths. The tensile strength, under atmospheric confining pressure, is about 500 psi for welded tuff and about 200 psi for bedded tuff.

Elastic moduli given in table 183.2 were determined by the Bureau of Mines by measuring the resonant frequencies of 2-inch samples excited in longitudinal and torsional modes, and also from the slope of the stress-strain curves obtained during static load tests.

Shear and dilatational velocities given in table 183.2 were measured in small samples of tuff using an ultrasonic pulse technique at a frequency of 400 kilocycles per second (Peselnick, 1959). Dilatational velocities were also measured at confining pressures up to 450 psi and it was found that velocity of acoustic waves was increased 50 to 100 percent over the value at atmospheric confining pressure for friable tuffs, 10 to 20 percent for bedded tuffs, and not appreciably in welded samples.

A great amount of information was obtained concerning acoustic velocities in place by refraction seismic surveys in drill holes and in tunnels and by acoustic logging of drill holes. It is likely that the acoustic velocity of rock in place is determined to a large extent by fracturing in the rock and by the confining pressure. This is particularly well shown by the acoustic log in the right column of figure 183.1. A linear increase in velocity with depth is apparent, probably representing the effect of increasing overburden pressure. The rock between depths of 1,050 and 1,120 feet through which an exceptionally low velocity is recorded is welded tuff, which the laboratory measurements showed to haye a high inherent velocity. The low recorded velocity is apparently caused by dry fractures.

THERMAL PROPERTIES

The enthalpy, or heat required to melt the tuff of the Oak Spring formation and to raise the liquid to a temperature of 1,500°C, given in table 183.3, was calculated from modal analyses by F. C. Kracek (1959) of the Geological Survey. Variations in total enthalpy depend on the mineral composition, particularly the amount of water in the rock, because water absorbs the highest amount of energy per unit mass.

Thermal conductivities were measured at room temperatures on several hundred drill cores of tuff. The conventional divided-bar technique was used. Measurements were made both with the samples dry and saturated with water. The data (fig. 183.2) may be

TABLE 183.2.—*Summary of strengths and elastic properties for tuff of the Oak Spring formation*

[All measurements were made on dry samples. Velocity data for tuff in its natural state are best obtained from velocity logs (fig. 183.1).]

Test	Bedded tuff (psi)		Welded tuff (psi)	
	Avg.	Range	Avg.	Range
Uniaxial strength tests				
Tensile	120	85–165	330	165–480
Compressive	4.9×10^3	3.4–8.7	21.1×10^3	6.8–29.1
Dynamic tests				
Young's modulus	0.61×10^6	0.40–1.07	1.48×10^6	1.22–2.01
Rigidity modulus	0.30×10^6	0.20–0.49	0.59×10^6	0.40–0.77
Poisson's ratio	----------	0.06–0.09	----------	0.02–0.53
Static tension tests				
Young's modulus	0.71×10^6	0.40–1.60	1.69×10^6	0.86–1.75
Rigidity modulus	0.25×10^6	0.19–0.32	0.78×10^6	0.40–0.82
Poisson's ratio	0.03	0.02–0.04	0.08	0.05–0.15

Acoustic velocities

Test	Bedded tuff (fps)		Friable tuff (fps)		Welded tuff (fps)	
	Avg.	Range	Avg.	Range	Avg.	Range
Dilatational	5700	2750–10,500	5690	3250–8750	9750	9100–11,000
Shear	3300	2000–6200	2900	1700–5500	6360	5600–7150

TABLE 183.3.—*Modes and calculated enthalpy for tuff of the Oak Spring formation*

Constituent	Welded tuff		Bedded tuff	
	Percentage by weight	Enthalpy contribution (cal per g of rock)	Percentage by weight	Enthalpy contribution (cal per g of rock)
Quartz	35	141.9	19	77.0
Orthoclase	23	111.9	10	48.6
Albite	25	119.3	10	47.6
Anorthite	3	15.0	2	10.0
Zeolite	----------	----------	25	146.0
Montmorillonite	5	38.0	9	68.4
Nontronite	----------	----------	1	6.5
Micas	----------	----------	1	5.8
Magnetite	1	2.5	1	2.5
Water	8	115.0	20	288.0
Total	----------	543.6	----------	705.4

extrapolated to zero porosity to obtain an estimate of the conductivity of the mineral grains. Extrapolating the curve for measurements on dry samples gives a thermal conductivity of 2.67 cgs units, and for wet samples, 3.09 cgs units. The extrapolated value for dry samples is probably low because of the effects of boundaries between grains. Such boundary resistances should be less in wet samples. The thermal conductivity may be expressed in terms of porosity by an empirical equation:

$$\sigma_d = 2.67(1-\phi)^{1.84} \quad (1)$$

$$\sigma_w = 3.09(1-\phi)^{1.84} + \frac{0.088}{(1-\phi)4.8} \quad (2)$$

where σ_d and σ_w are the dry and wet conductivities, respectively, in millicalories per centimeter second degree, and ϕ is the pore fraction.

ELECTRICAL PROPERTIES

The electrical properties of the tuff in the Oak Spring formation were studied to determine water content of the rock in place. Direct determinations of water content are difficult because drilling water may contaminate drill-core samples, and tunnel-wall samples may be dried by circulating air. Water content may be estimated from electrical resistivity measurements, if the ground water resistivity is known. Measurements of electrical properties consisted of two types; in-place measurement of resistivities in drill holes and tunnels,

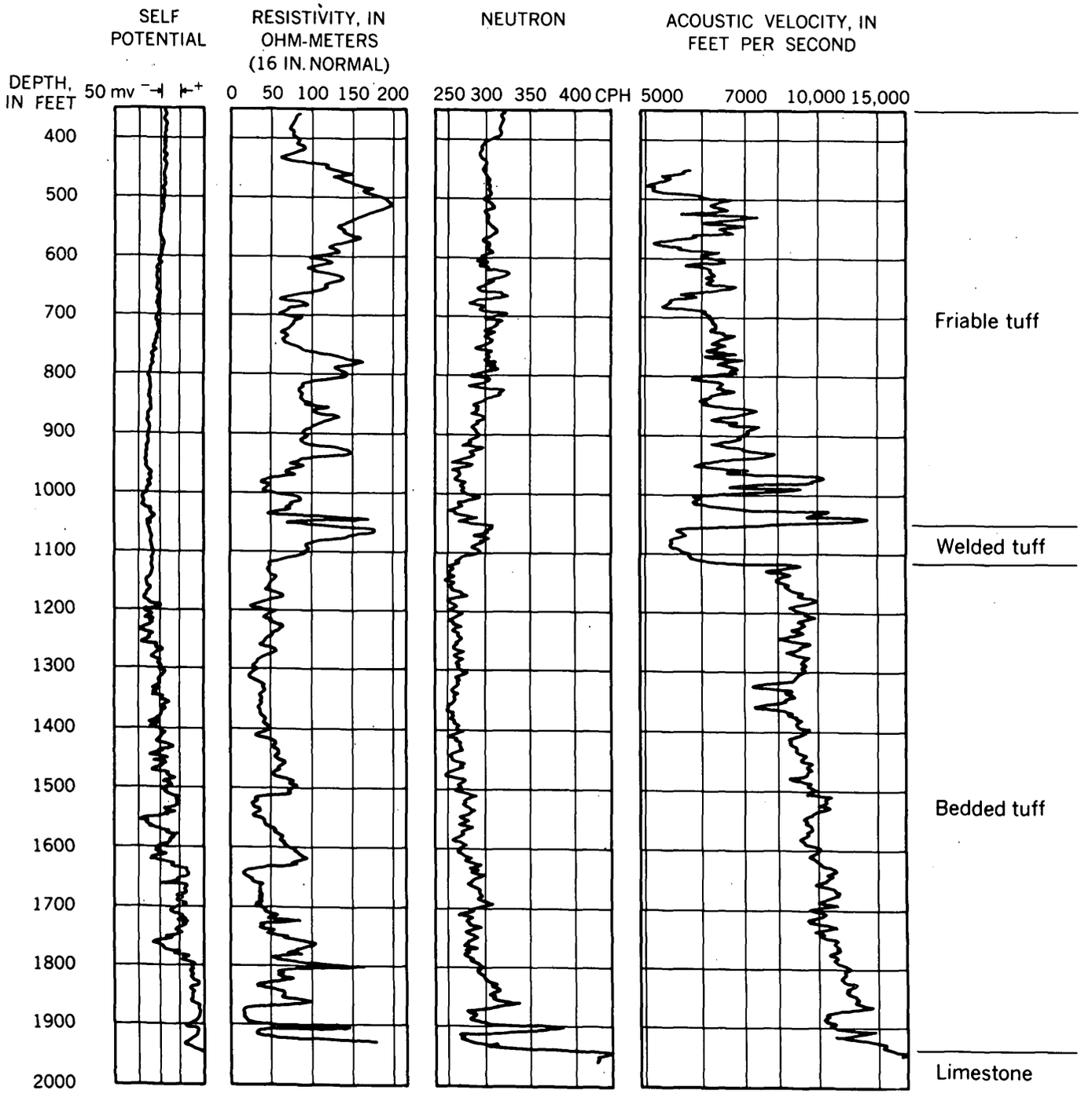

FIGURE 183.1.—Electric, neutron, and acoustic velocity logs of the Oak Spring formation in a drill hole near the underground test chamber.

and laboratory studies of the correlation between water content and electrical properties.

Resistivity measurements were made by routine methods on core samples resaturated in the laboratory with salt solutions of known concentrations (fig. 183.3). The relationship may be represented by an empirical equation:

$$\rho = 1.5\rho_w W^{-2.2} \qquad (3)$$

where ρ is the resistivity of the rock, in ohm-meters, ρ_w is the resistivity of the water saturating the rock and W is the volume fraction of water in the rock.

Rock resistivities were measured for about 100 samples of tuff obtained in the natural state by underground air drilling. These data were used with equation 3 to determine the resistivity of the pore water in the rock. The average value so determined was 1.6

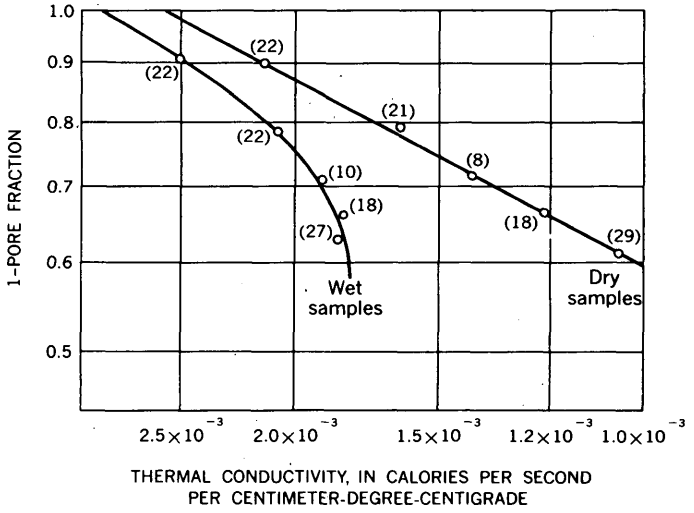

FIGURE 183.2.—Empirical correlation between average values of thermal conductivity and porosity for groups of tuff samples. The number of samples in each group is shown in parentheses.

ohm-meters, with a total range in measurements from 1.04 to 2.13 ohm-meters.

Interpretation of the in-place resistivity measurements on the basis of equation 3 shows that the tuff in the Oak Spring formation in the area of the underground tests is water-saturated at depths of more than 200 feet, but that fractures are not saturated, even at a depth of 900 feet.

SUMMARY

The amount of water in the rock was found to be the most important single factor in determining the physical properties of the tuff in Oak Spring formation. Variations in thermal conductivity, bulk density, enthalpy, and electrical properties of the tuff are all determined by the water content, directly or indirectly. Variations in strength and acoustic velocity are probably controlled by the fractures as well as by water content. The ability of the tuff to transmit fluids is probably more dependent upon fractures than upon permeability, because the permeability of unfractured samples is low.

ACKNOWLEDGMENTS

Much of the information in this report has been abstracted from unpublished reports by other Survey investigators. In particular, information about strengths was obtained from work by E. C. Robertson; about enthalpy, from F. C. Kracek; about acoustic velocities, from Louis Peselnick, and about mineralogy, from R. E. Wilcox.

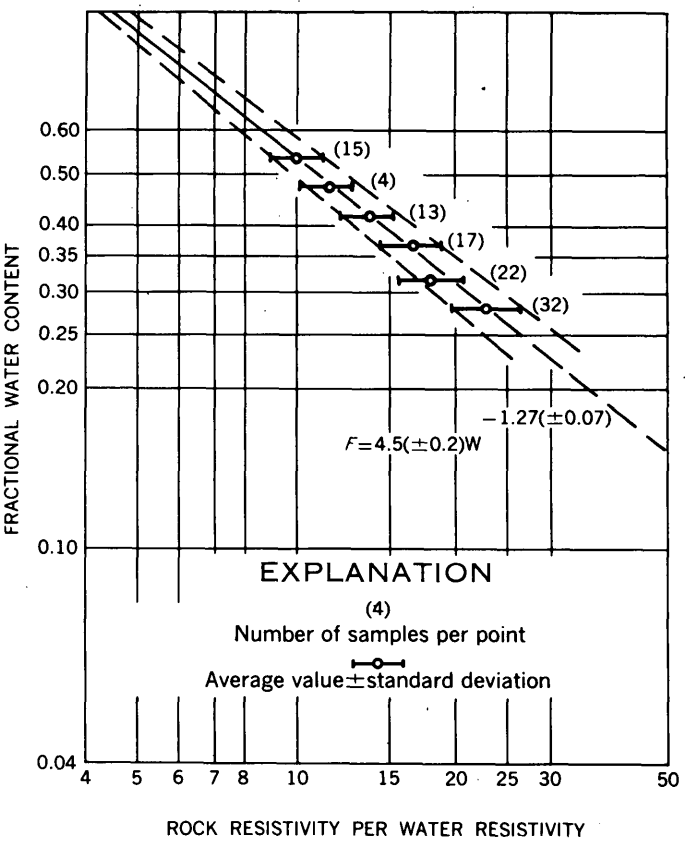

FIGURE 183.3—Correlation between average values of resistivity and porosity for samples of tuff.

REFERENCES

Keller, G. V., 1959, Chap. 6, Thermal conductivity of the Oak Spring tuff, *in* Diment, W. H., and others, Properties of Oak Spring formation in area 12 at the Nevada Test Site: U.S. Geol. Survey TEI–672, open-file report.

Kracek, F. C., 1959, Chap. 7, Heat required to melt Oak Spring tuff from Nevada Test Site, and to raise the liquid to 1500°C and 2000°C, *in* Diment, W. H., and others, Properties of Oak Spring formation in area 12 at the Nevada Test Site: U.S. Geol. Survey TEI–672, open-file report.

Peselnick, Louis, 1959, Chap. 9, Velocity measurements on samples of Oak Spring tuff, *in* Diment, W. H., and others, Properties of Oak Spring formation in area 12 at the Nevada Test Site: U.S. Geol. Survey TEI–672, open-file report.

Robertson, E. C., 1959, Chap. 10, Strength and elastic properties of Oak Spring tuff, *in* Diment, W. H., and others, Properties of Oak Spring formation in area 12 at the Nevada Test Site: U.S. Geol. Survey TEI–672, open-file report.

Wilcox, R. E., 1959, Chap. 2, Petrography and chemistry of the Oak Spring formation, *in* Diment, W. H., and others, Properties of Oak Spring formation in area 12 at the Nevada Test Site: U.S. Geol. Survey TEI–672, open-file report.

184. MAGNETIC SUSCEPTIBILITY AND THERMOLUMINESCENCE OF CALCITE

By Frank E. Senftle, Arthur Thorpe, and Francis J. Flanagan, Washington, D.C.

Work done in cooperation with the U.S. Atomic Energy Commission

It is well known that both magnetic susceptibility and thermoluminescence are related to trapped electrons in a crystal lattice. It is therefore of interest to examine the magnetic effects in crystals known to be thermoluminescent.

Thermoluminescent light is produced when a crystal is heated, thereby causing a release of trapped electrons from one excited state to some other lower energy state. Electrons displaced by ionizing radiation can be trapped by impurity centers or at so-called F-centers in the crystal. If an ionic crystal has impurity ions held interstitially, it is possible for such an ion to trap an electron in its field. On heating, the electron is released and moves to a region in which de-excitation can occur. The result is a drop in energy and the emission of light. Alternately, if an ionic crystal is irradiated, electrons are also released from the anions and diffuse through the crystal until they are trapped by an anion vacancy site. The trapped electron is known as an F-center and is capable of absorbing visible light of a given frequency, thus producing a characteristic color. When the crystal is subsequently heated, the electron will be released from the F-center and will certainly recombine with a neutral atom or a positive hole. As before, the recombination results in the emission of thermoluminescent light (Friedman and Glover, 1952).

Both of the above mechanisms of thermoluminescence involve electrons which may be unpaired with neighboring electrons, that is, these electrons will have a resultant spin and will thus contribute to the magnetic susceptibility of the crystal (Jensen, 1939; Heer and Rauch, 1953). Therefore if the number of electrons involved is large enough, there should be a noticeable change in the magnetic susceptibility of an irradiated crystal after heating. To determine whether the annealing of electron traps as observed in thermoluminescence phenomena would also cause perceptible changes in the magnetic susceptibilty, some exploratory experiments were made.

THEORY AND EXPERIMENTAL RESULTS

Let us consider the contribution of these crystal defects to the magnetic susceptibility. If an electron is trapped at such an impurity site or an F-center, the spin only will contribute to the magnetic susceptibility as the orbital angular momentum will be quenched by the interatomic forces in the lattice. The magnetic susceptibility per gram will be given by

$$\chi=\frac{n\beta^2}{3MKT}[4S(S+1)] \qquad (1)$$

where n is the number of defect centers, β is the unit Bohr magneton, K is Boltzmann's constant, T is absolute temperature, M is the molecular weight, and S is the spin quantum number. As pointed out by McClelland (1953), depending on whether the impurity is a doubly or singly charged ion or a neutral atom, the value of S may be 0, $\frac{1}{2}$, or 1. An F-center, of course, will have a spin of $\frac{1}{2}$.

For the preliminary experiments, a specimen of natural pink calcite was chosen. The pink color is due to manganese impurity and hence, if it is interstital, it will be a bivalent ion or a neutral atom. If it is a bivalent ion, the spin will be zero, and it will not contribute to the susceptibility; if it is a neutral atom, the spin will be 1. Thus the susceptibility of n such manganese atoms per gram can be shown from equation (1) to be

$$\chi=0.556\times10^{-28}n \qquad (2)$$

Assuming a manganese content of 8 percent, which is about the amount necessary to produce a light pink calcite, there would be some 8.7×10^{20} impurity centers per gram if they were all interstital. The susceptibility due to these would be 0.048×10^{-6} emu per gram from equation (2).

Medlin (1959) has shown that manganese produces thermoluminescent peaks at 77° C. and 197° C. in calcite. The low temperature peak will have been annealed out by normal earth temperatures, but the higher peak will remain. The specimen was therefore heated to several temperatures on either side of the 197° C. and the magnetic susceptibility measured after each heating cycle, using the quartz helical spring balance (Senftle and others, 1958). The results in table 184.1 indicate a substantial change in susceptibility and of the same order as predicted from the rough calculation, that is, 0.055×10^{-6} emu/gram.

In a second experiment, the blue and green portions of calcite from Las Cruces, New Mexico were separated

TABLE 184.1.—*Magnetic susceptibility of pink calcite*

Time and temperature	Magnetic susceptibility (emu/gram)
Unheated	0.19×10^{-6}
60°C for 30 min	$.19\times10^{-6}$
145°C for 60 min	$.178\times10^{-6}$ $\Delta X=0.055\times10^{-6}$
244°C for 60 min	$.135\times10^{-6}$

by hand-picking. The crystals were first heated to about 500° C. in an inert atmosphere to anneal out any naturally trapped electrons. They were then X-rayed for 10 minutes at 50 kv to refill the electron traps. The subsequent magnetic susceptibility data are shown in table 184.2. Why the susceptibility dropped in one case and not in the other is not obvious, but the reason may be related to the type of impurity content. Upon reheating to 500° C., the electron traps were again annealed out, and there was an accompanying drop in the magnetic susceptibility. Similar measurement on other calcite specimens generally showed analogous decreases after the thermoluminescent peaks were annealed out.

TABLE 184.2—*Magnetic susceptibility of calcite from Las Cruces, N. Mex.*

Treatment	Magnetic susceptibility (emu/gram)	
	Blue	Green
Unheated calcite	-0.41×10^{-6}	-0.31×10^{-6}
Heated to 500° C and X-rayed	-0.29×10^{-6}	-0.91×10^{-6}
Same sample, reheated to 500° C	-0.07×10^{-6}	Sample lost

To investigate the effect of F-centers on the magnetic susceptibility, a clear crystal of a natural sample of calcite was chosen. This specimen contained less impurities than the previous specimens and hence would have few trapped electrons associated with impurities. It was irradiated with X-rays until it was colored a deep purple due to F-center formation. The magnetic susceptibility before and after irradiation was almost identical. It is not clear why a change in the susceptibility did not occur. Although the crystal was purple due to X-radiation, it may not have had a sufficient number of F-centers formed to produce a measureable change. A barely perceptible coloration by the unaided eye is equivalent to about 10^{15} F-centers and from the density of coloration in the above crystals one would estimate a minimum of 10^{18} or 10^{19} centers. For a spin of ½, the magnetic susceptibility per gram due to F-center formation can be shown to be

$$\chi=0.209\times10^{-28}n \qquad (3)$$

Thus 10^{19} F-centers per gram would yield a magnetic susceptibility of 0.0002×10^{-6} emu/gram, a value too low to be detected.

To obtain additional data on the effect, the susceptibility of a relatively fresh nonmetamict zircon, distinctly purple in color, was measured. It was then heated to 600° C. in a helium atmosphere for one hour, after which the F-centers were completely bleached, leaving clear granular sugarlike crystals of zircon. There was, however, no difference between the magnetic susceptibility before and after heating.

CONCLUSIONS

These experiments indicate that natural crystals, such as calcite, which are thermoluminescent owing to impurity content, have enough electron traps to significantly affect the magnetic susceptibility. On the other hand, crystals colored by F-center formation will probably not have enough traps, unless they have received a large radiation dose to perceptibly alter the magnetic properties. While thermoluminescence "glow curves" are only qualitative, thermomagnetic curves can probably be determined for natural minerals from which the actual number of interstitial impurity atoms can be calculated. Comparison of the experimental curve with that calculated from a knowledge of the chemical impurity data might shed some light on the past thermal history of the mineral. Also as thermoluminescence is used for radiation dosimetry, it may also be useful to use magnetic susceptibility to measure radiation doses.

REFERENCES

Friedman, H., and Glover, C. P., 1952, Radiosensitivity of alkali halide crystals: Nucleonics, v. 10, p. 24–29.

Heer, C. V., and Rauch, J., 1953, Magnetic susceptibility of colored potassium chloride from 1°K to 300°K: Phys. Rev., v. 90, p. 530.

Jensen, P., 1939, Die magnetisch Suszeptibilität von Kalum Bromidkristallen mit Farbzentven: Ann. Physik, v. 34, p. 161.

McClelland, J. D., 1953, Effect of neutron bombardment upon the magnetic susceptibility of various oxides: U.S. Atomic Energy Commission, NAA–SR–263.

Medlin, W. L., 1959, Thermoluminescent properties of calcite: Jour. Chem. Physics, v. 30, p. 451–458.

Senftle, F. E., Lee, M. D., Monkewiez, A. A., Mayo, J. U., and Pankey, T., 1958, Quartz helix magnetic susceptibility balance using the Curie-Cheneveau principle: Rev. Sci. Instruments, v. 29, p. 429–432.

185. SALT FEATURES THAT SIMULATE GROUND PATTERNS FORMED IN COLD CLIMATES

By CHARLES B. HUNT and A. L. WASHBURN, Denver, Colo., and University of Canterbury, Christchurch, New Zealand

Polar, subpolar, and alpine regions are characterized by ground patterns consisting of circles, nets, polygons, steps, and stripes. The mechanisms that produce these ground patterns are not fully understood, but frost action is clearly a major factor. Very similar ground patterns have recently been studied in Death Valley, Calif., where freezing temperatures are seldom reached and the patterns must be attributed to deposition, solution, and cracking of salts.

Sorted polygons resembling those associated with frost action have developed where there is a layer of rock salt a few inches below the surface (fig. 185.1*A*). The salt, commonly about 6 inches thick, is cracked polygonally, and the positions of the cracks at the surface are marked by shallow troughs in which stones have collected.

Nonsorted polygonal patterns have formed also above some gypsum deposits, where a surface layer of loose grains of gypsum 1 to 6 inches thick is underlain by a firm layer of anhydrite 3 to 6 inches thick (fig. 185.1*B*). The anhydrite is broken by polygonal cracks, which widen into troughs at the surface.

Other nonsorted polygons in Death Valley, apparently due to desiccation or thermal cracking, are outlined by wedges of salt and resemble the ice-wedge polygons found in cold climates.

The gravel fans around the sides of Death Valley are terraced with sorted steps, each consisting of a lobate riser of stones and a tread of finer material (fig. 185.1*C*). These are very similar to the terracettes observed in cold climates. In Death Valley the fine-grained material of the treads contains up to 10 times more water-soluble salt (up to 5 percent by volume) than the stable ground around the steps, but we cannot be sure whether the steps developed because of the salt or the salt accumulated because of the steps. Rows of pegs across two steps show that no significant movement has occurred in three years, despite several soaking rains. These Death Valley terracettes appear to be fossil features that date from a past climatic condition, and that are developing very slowly if at all under the present climate.

Other kinds of ground patterns noted in Death Valley that resemble those in cold climates include sorted circles, sorted and nonsorted nets, and sorted stripes.

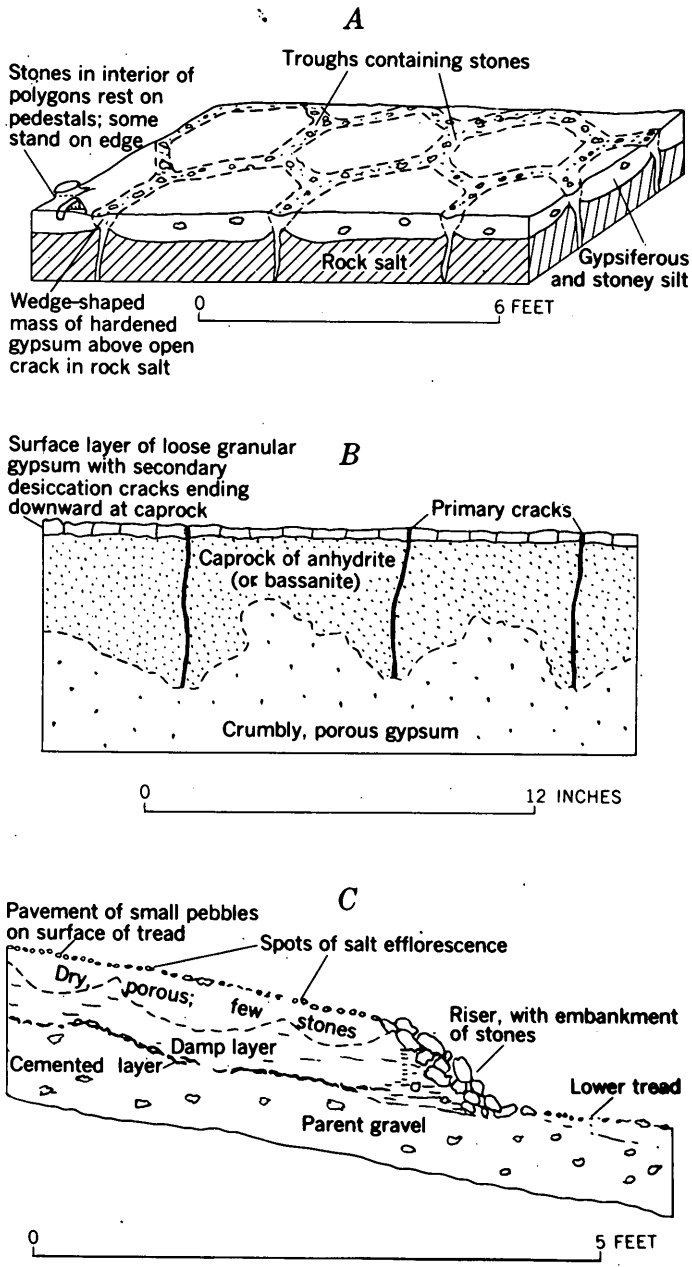

FIGURE 185.1.—Sketch and cross sections of ground patterns in Death Valley. *A*, Diagram of sorted polygons above layer of rock salt; *B*, cross section of nonsorted polygons in anhydrite caprock on gypsum; *C*, cross section of sorted step (terracette).

186. THERMAL CONTRACTION CRACKS AND ICE WEDGES IN PERMAFROST

By Arthur H. Lachenbruch, Menlo Park, Calif.

Ice wedges are relatively clear, vertical wedge-shaped masses of ice which taper downward into permafrost to depths of several meters (fig. 186.1). They intersect every 20 meters or so to produce a honeycomb of ice, the trace of which produces a polygonal pattern on the tundra surface.

Although ice wedges have been discussed widely by geologists for more than a century, and their differential thawing has long plagued engineers, their origin and significance are still imperfectly understood.

It is now generally accepted that ice wedges form in response to thermal tension set up in the frozen ground by its tendency to contract during the cold Artic winter (see, for example, Popov, 1955). Thermal contraction cracks, formed in winter, penetrate permafrost to depths as great as 5 to 10 meters (fig. 186.2A). They are sealed by the freezing of surface water which enters when the surface thaws in early summer. The resulting vertical ice vein (fig. 186.2B) is a zone of weakness subject to recurrent fracture and growth by repetition of the cycle in succeeding winters (fig. 186.2C). The thickened veins or "ice wedges," (fig. 186.2D) underlie the boundaries of the surface polygons and their differential thawing produces the shallow troughs by which ice-wedge polygons are usually delineated on the tundra surface.

The size and configuration of the polygons are controlled to a large measure by the depth and mode of propagation of the thermal contraction cracks, and these in turn depend upon the nature of the thermally induced volume change and the rheological properties of the permafrost. In an attempt to gain a better understanding of how these factors interrelate to control ice-wedge polygons, and the related phenomena of mud-crack polygons and basalt-joint polygons, a theoretical study was carried out. A qualitative summary of those findings pertinent to the evolution of a single crack is outlined below. In the companion article (187), multiple cracking and the evolution of polygonal form will be discussed. Numerical and analytical details of the study will be elaborated elsewhere.

RELATION BETWEEN TEMPERATURE AND STRESS IN THE UNFRACTURED MEDIUM

The stresses that lead to fracture of the frozen ground must be accounted for by a visco-elastic response to thermal contraction, not an elastic one; for a formal calculation shows that thermal stresses developed in an elastic medium under the thermal regime of permafrost would be too large by an order of magnitude to satisfy requirements of the frost-crack theory. A simple linear relation between rate of cooling and stress is also unsatisfactory for it predicts that the stress falls off too rapidly with depth to account for observed details of the fracture process.

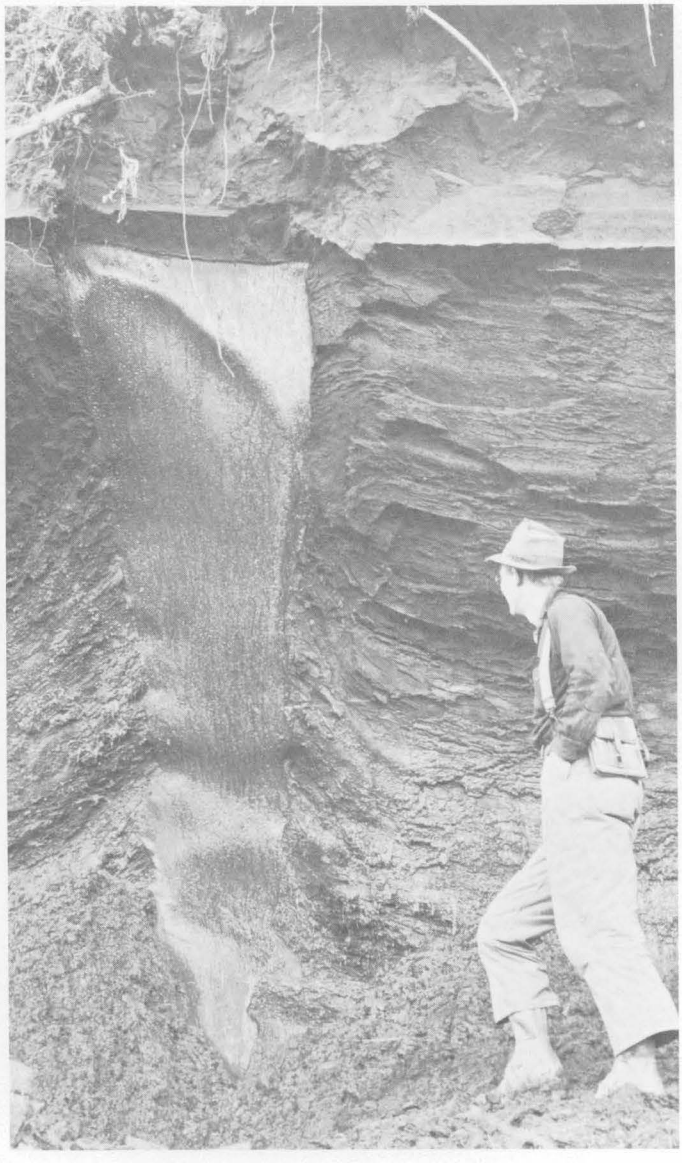

Figure 186.1—Ice wedge in permafrost (photo by Troy L. Péwé)

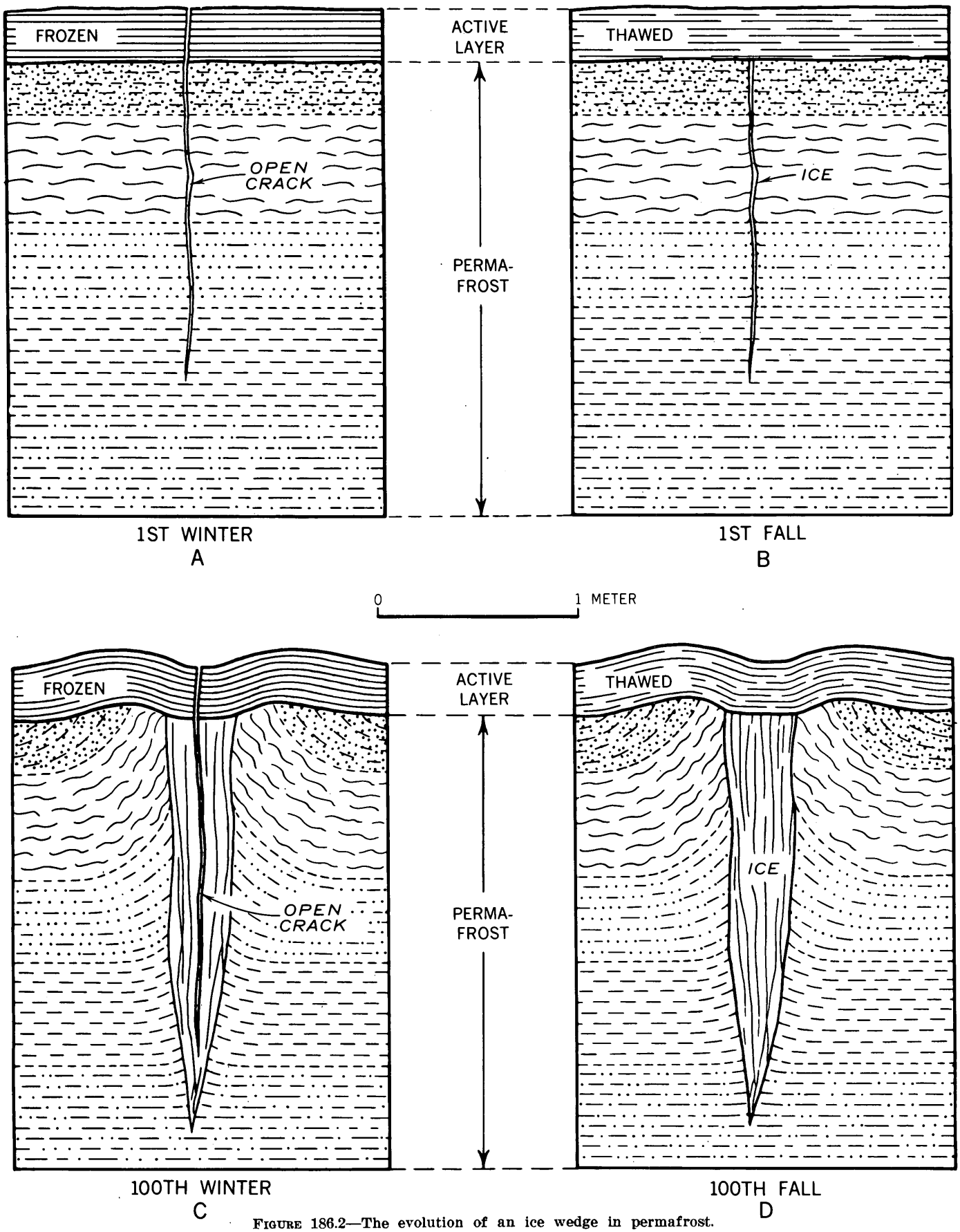

FIGURE 186.2—The evolution of an ice wedge in permafrost.

A nonlinear relation between the principal components of distortional stress (P_i) and distortional strain (E_i) of the form

$$\frac{1}{\bar{\eta}}P_i^n+\frac{dP_i}{dt}=\mu\frac{dE_i}{dt},\ i=1,2,3 \qquad (1)$$

yields stress distributions compatible with field inferences regarding the fracture process. Numerical values required for the exponent n, the elastic shear modulus μ, and the viscoelastic parameter $\bar{\eta}$ are consistent with pertinent laboratory results.

Assuming the nondistortional component of deformation to be elastic, horizontal stress $\tau\ (x, t)$ and ground temperature $\Theta\ (x, t)$ are given at any depth, x, and any time, t, by the nonlinear differential equation

$$\frac{d\tau}{dt}+\frac{Y}{1-\nu}\frac{1}{3n_{2\bar{\eta}}}\tau^n=\frac{-Y}{1-\nu}\frac{d\Theta}{dt} \qquad (2)$$

where Y and ν are Young's modulus and Poisson's ratio respectively. Application of (2) indicates that rapid cooling is as important as low temperature in producing the large stresses that crack frozen ground.

MECHANICS OF THE FRACTURE PROCESS AND PREDICTION OF CRACK DEPTH

When the tension near the surface is approaching the tensile strength, stresses at depths on the order of 10 feet and more are generally compressive owing to the combined effects of the time lag in the penetration of the seasonal thermal wave, and compression caused by the weight of overburden. When the tensile strength is exceeded near the surface, a tension crack forms and propagates downward. The depth at which it stops depends primarily upon the opposing effect of compression at depth, and the dissipation of strain energy by plastic deformation near the leading edge of the crack. Theoretical calculations show that if the medium is relatively nonplastic, the tension crack will penetrate deep into the compressional zone; if not, it will stop near the neutral horizon at the base of the surficial tensile zone. Judging from experimental results reported by Irwin (1958) for other materials, it is likely that initial crack depths in most solidly frozen earth materials can be approximated satisfactorily by neglecting the plastic dissipation. Thus it is probable that most contraction cracks in permafrost penetrate initially much deeper than the tension that produced them, with more than half of the crack lying in strata that were in compression at the time of cracking. Subsequent viscoelastic effects might be expected to produce a slow closing of part of the crack from the bottom.

The crack depth is dependent on the actual stress distribution at the time of cracking. Other things being equal, deeper cooling generally produces deeper tension and deeper cracks. The depth of a crack can, of course, change as the stress regime changes with the progressing season. Numerical calculations based upon temperatures measured in Alaskan permafrost, equation (2), and a mathematical formulation of the present considerations of fracture mechanics yield results consistent with the observed depth, frequency, and mode of cracking.

REFERENCES

Irwin, G. R., 1958, Fracture, *in* Handbuch der Physik; v. 6, Springer-Verlag, p. 551–590.

Popov, A. I., 1955, The origin and evolution of fossil ice: Inst. Merzlotovedeniya, Akad. Nauk SSSR, no. 2, p. 5–25.

187. CONTRACTION-CRACK POLYGONS

By Arthur H. Lachenbruch, Menlo Park, Calif.

"Contraction-crack polygons" is the name applied to a reticulate system of intersecting contraction cracks on the surface of a body. They form in response to tension resulting from decrease in volume, usually caused by cooling or dessication. They occur in diverse media on a variety of scales ranging from a few millimeters in cooling ceramic ware to 50 meters in permafrost. They include mud cracks, columnar-basalt joints and shrinkage cracks in concrete. Some mechanical considerations arising from a theoretical study of ice-wedge polygons are applied briefly to the general problem of contraction-crack polygons in the qualitative summary that follows.

THE "ZONE OF STRESS RELIEF" AND POLYGON DIAMETERS

When tension (τ_0), caused by dessication or thermal contraction exceeds the tensile strength at the surface

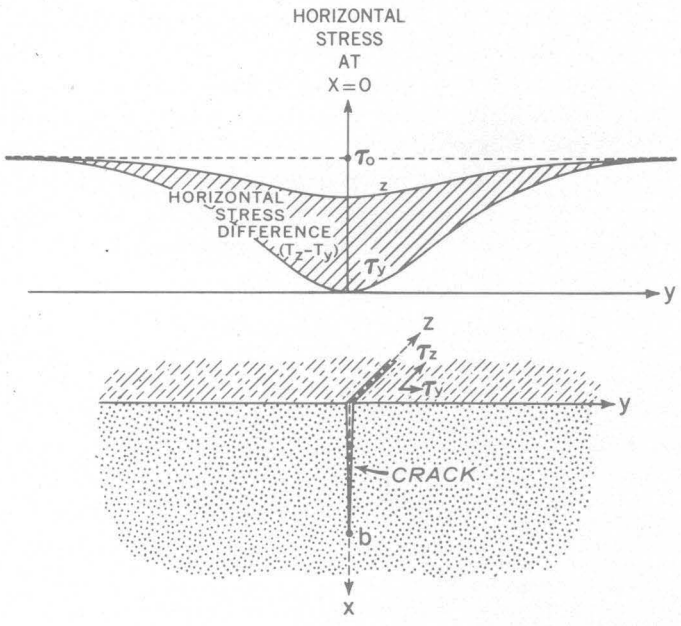

FIGURE 187.1.—Stress at ground surface near an isolated contraction crack.

τ_o=uniform horizontal tension before fracture.
τ_z=component of tension parallel to crack after fracture.
τ_y=component of tension perpendicular to crack after fracture.

(x=0), a crack forms and penetrates the medium to some finite depth (x=b), determined by factors discussed in the previous article. The horizontal component of stress, τ_y, in the direction normal to the crack vanishes at the crack walls (y=0), but it increases asymptotically to the precracking value (τ_o) at large horizontal distance from the crack (y>>b) (see fig. 187.1). Each crack is therefore surrounded by a band in which the cracking has caused appreciable reduction of horizontal tension: the "zone of stress-relief." The stress configuration in the zone of stress-relief depends primarily upon the stress distribution that would exist in the medium if it were not fractured, i.e. upon the thermal stress. It has been calculated approximately by applying Muskhelishvili's method of complex stress functions to the problem of a crack in a semi-infinite elastic medium with a nonuniform stress field. The thermal stress upon which this solution is superimposed is calculated from a visco-elastic relation (like equation 2, p. B406) and hence most inelastic effects are accounted for. (The problem of nonlinearity is handled separately.) In general, increased depth of thermal tension and (or) increased crack-depth results in wider zones of stress-relief, and hence more widely spaced cracks and larger polygons. Application of the theory to ice-wedge polygons yield numerical results compatible with observed polygon diameters.

MULTIPLE CRACKING AND EVOLUTION OF POLYGONAL FORM

The component of thermal tension (τ_z) at the ground surface in the direction parallel to the crack is relieved only slightly by the cracking, and hence large horizontal stress differences ($\tau_z-\tau_y$) occur within the zone of stress relief (fig. 187.1). A second crack entering this zone of stress relief tends to aline itself perpendicular to the greatest tension, τ_z, and hence tends to intersect the first crack at right angles. Conversely the occurrence of an orthogonal intersection generally implies that one of the cracks predated the other. This suggests a useful scheme for classifying contraction-crack polygons as follows:

ORTHOGONAL SYSTEMS

Orthogonal systems of polygons are those that have a preponderance of orthogonal intersections. They are evidently characteristic of somewhat inhomogeneous or plastic media in which the stress builds up gradually, with cracks forming first at loci of low strength or high stress concentration. With increasing thermal (or dessication) stress, polygons are subdivided by cracks initiating near polygon centers. The polygons attain such a size that zones of stress-relief of neighboring cracks are superimposed at the polygon centers in such a way as to keep the stress there below the tensile strength. The polygon size at any time depends upon the nature of the applied stress and configuration of the zones of stress relief of individual cracks. The cracks do not all form simultaneously and hence each

FIGURE 187.2.—Random orthogonal ice-wedge polygons in permafrost. 1 inch≈100 yards in foreground. (Photo by Gordon W. Greene.)

new crack tends to join existing ones at orthogonal intersections. Orthogonal systems can be conveniently divided into two subgroups:

a. Random orthogonal systems in which the cracks have no preferred directional orientation (fig. 187.2).

b. Oriented orthogonal systems in which the cracks have preferred directional orientation. Most oriented orthogonal systems in permafrost are probably caused by horizontal stress differences which are generated by horizontal thermal gradients near the edges of gradually receding bodies of water (for example, slowly draining lakes and shifting river channels). Under such conditions the induced polygonal system forms with one set of cracks parallel to the position of the water's edge and the second set normal to it (fig. 187.3). Oriented orthogonal systems can also result from topographic effects or from anisotropy of horizontal tensile strength as in steeply dipping shales.

NONORTHOGONAL SYSTEMS

Nonorthogonal systems of polygons are those that have a preponderance of tri-radial intersections, usually forming three obtuse angles of about 120°. It is suggested that they result from the uniform cooling of very homogeneous, relatively nonplastic media. Judging from experimental and theoretical results from the field of fracture mechanics, it is likely that under these conditions cracks propagate laterally until they reach a critical velocity (on the order of half that of elastic shear waves) and then branch at obtuse angles. The branches then accelerate to critical velocity and branch, and so on. Unlike in the orthogonal system, all elements of a nonorthogonal intersection are generated virtually simultaneously.

FIGURE 187.3.—Oriented orthogonal ice-wedge polygons in permafrost, Alaskan Arctic Coastal Plain. Pattern generated on slip-off slopes by thermomechanical effect of migrating meanders. 1 inch≈1,500 feet.

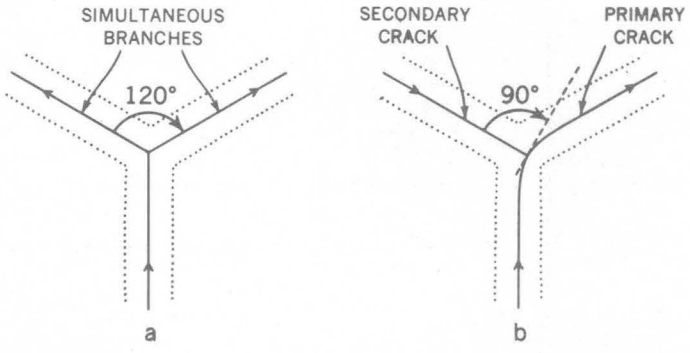

FIGURE 187.4.—Comparison of nonorthogonal intersection (*a*) and an orthogonal intersection (*b*) at a convex bend in a primary fracture. Arrows indicate direction of propagation. When crack trace widens (dotted lines), the two forms may be indistinguishable.

Although many ice-wedge intersections appear to be of the nonorthogonal type, the surface expression of a wedge is so wide that it is generally difficult to distinguish between a nonorthogonal intersection (fig. 187.4a) and an orthogonal intersection at a convexity in the primary fracture (fig. 187.4b). From mechanical considerations it can be shown that if a curve exists in a primary fracture, its convex side is favored as a site of (orthogonal) intersection by a secondary fracture. It is therefore difficult to determine with certainty whether any fracture systems in permafrost are nonorthogonal. It is worth noting, however, that ice-wedge polygons, which superficially at least seem to be nonorthogonal, occur commonly in the homogeneous sediments of rapidly drained lake basins. On the basis of the present point of view such an environment, thermally and mechanically uniform, would favor nonorthogonal systems.

THE CLASSIFICATION APPLIED TO OTHER TYPES OF CONTRACTION-CRACK POLYGONS

Inasmuch as this geometric classification seems to have genetic significance, at least for ice-wedge polygons, it might be useful when applied to contraction-crack polygons in general. Crackle-finish ceramic ware generally displays a random orthogonal pattern, except locally where topography of the object (ash tray, vase,

FIGURE 187.5.—Nonorthogonal contraction-crack polygons in basalt, Devils Post Pile National Monument, Calif. (Photo by Gordon W. Greene.)

etc.) may produce an oriented orthogonal system. This is consistent with the observed fact that ceramic polygons evolve gradually. The classic occurrences of columnar basalt joints described in the literature seem to be of the nonorthogonal type; consistent with the requirements of thermal and mechanical homogeneity and low plasticity (fig. 187.5).

Dessication polygons in mud and shrinkage polygons in concrete seem generally to be of the orthogonal type, although certain complications beyond the scope of this paper are introduced by their plastic behavior. Inasmuch as cracks in these media are often irregular, they have many "convexities" at which orthogonal intersections (fig. 187.4a) could be confused with nonorthogonal ones (fig. 187.4b) as the cracks widened. Laboratory experiments by the writer confirm that in general mudcracks propagate slowly, do not branch, and form orthogonal intersections. This is consistent with the present point of view which calls for high propagation velocities and branching to produce nonorthogonal intersections.

188. CURVATURE OF NORMAL FAULTS IN THE BASIN AND RANGE PROVINCE OF THE WESTERN UNITED STATES

By JAMES G. MOORE, Menlo Park, Calif.

Work done in cooperation with the Nevada Bureau of Mines

Recently many new data have become available on details of the topography of the Basin and Range province. The new series of Army Map Service topographic maps provides almost complete coverage of the province at a scale of 1:250,000 with a 200-foot contour interval. One of the most striking features that the maps show is the nonlinearity of the ranges. Many of the ranges are arcuate, the longer ranges being linked segments of arcs. The arcuate pattern of a range as a whole is believed to reflect the arcuate pattern of the main bounding fault.

Many of the individual ranges of the Basin and Range province are tilted Cenozoic fault blocks (Davis, 1925; Mackin, 1960; Osmond, 1960). The geology of many ranges is still little understood, but geologic mapping in recent years has yielded information on the direction of tilt of some of the ranges. The criteria by which the direction of Cenozoic tilt of ranges is determined are listed in order of decreasing reliability: (a) general direction of dip of Cenozoic sedimentary and volcanic rocks, (b) distribution of rocks of different ages within a range, (c) topographic asymmetry of a range, (d) dip of major Cenozoic normal faults, and (e) general dip and structure of pre-Tertiary strata. In addition, criteria which point to the asymmetry (and hence direction of tilt) of the intermontane basins also provide data on the Cenozoic tilt of adjacent ranges. These criteria include topographic shape of basin surface as well as the topography of the buried bedrock surface determined by geophysical measurements, chiefly gravity surveys.

An interesting relation appears to exist between the tilt of each range and its map plan. Many of the ranges exhibit an arcuate map pattern. Fairly simple tilted block mountains are made up of a single arc which is generally from 10 to 30 miles long with a radius of curvature of 20 to 40 miles, and the ranges are generally tilted toward the convex side of the arc.

557753 O—60——27

TABLE 188.1.—*Fault block ranges in the Basin and Range province showing direction of curvature and probable Cenozoic tilt. Fifty-five of better known ranges have been selected*

Range	Army Map Service sheet	East tilt			West tilt		
		Convex east	Convex west	Straight, irregular	Convex east	Convex west	Straight, irregular
Abert Rim	Klamath Falls		[1] ×				
Amargosa Range	Death Valley			×			
Argus Range	Death Valley			×			
Bare Mountain	Death Valley	×					
Belted Range	Goldfield	×					
Black Rock Range, south end	Vya	×					
Bristol Range	Lund	×					
Buckskin Range	Reno						×
Cedar Mountains	Tooele			×			
Cortez Mountains	Winnemucca	×					
Coso Range	Death Valley						×
Deep Creek Range	Delta				×		
Dove Creek Mountains	Brigham City					×	
East Humboldt Range	Winnemucca	[1] ×					
Egan Range, northern part	Ely					×	
Egan Range, southern part	Lund	×					
Eugene Mountains	Lovelock			×			
Fish Springs Range	Delta					×	
Fortification Range	Lund	×					
Grant Range	Lund			×			
House Range	Delta	×					
Inyo Range, south end	Death Valley					×	
Kawich Range	Goldfield	×					
Kingsley Range	Elko	×					
Kings River Range, southern part	Vya	×					
Klamath Lake, rim east of	Klamath Falls	[1] ×					
Last Chance Range	Goldfield	×					
Mineral Mountains	Richfield	×					
Monitor Range	Millett					[1] ×	
Newfoundland Mountains	Brigham City					×	
North Promontory Mountains	Brigham City	×					
Oquirrh Mountains	Tooele			×			
Osgood Mountains, southern part	McDermitt					×	
Pahrock Range (southern)	Caliente					×	
Panamint Range	Death Valley			×			
Poker Jim Ridge	Adel	×					
Reveille Range	Goldfield	×					
Ruby Mountains	Elko					×	
Seven Troughs Range	Lovelock					×	
Sheep Range	Caliente	×					
Shoshone Range, south part	Winnemucca	×					
Simpson Park Mountains	Millett	×					
Singatse Range	Reno						×
Spruce Mountain Ridge	Elko	×					
Stansbury Mountains	Tooele			×			
Steens Mountain	Adel					×	
Sulphur Springs Range	Millett					×	
Terrill Mountains	Reno					×	
Toiyabe Range	Millett					[1] ×	
Virginia Range							×
Wah Wah Mountains	Richfield	×					
Warner Mountains	Alturas					×	
West Humboldt Range	Lovelock	×					
West Tintic Mountains	Delta	×					
Winter Rim	Klamath Falls					×	
Total		25	1	8	1	16	4

[1] Refers to ranges composed of more than one linked arcuate segment.

For example, the north-trending House Range in western Utah is convex to the east in plan and is tilted to the east. The central Ruby Mountains of northeastern Nevada is convex to the west in plan and is tilted to the west. More complex ranges are made of several of these arcuate segments, as, for example, the Egan Range and the Toiyabe Range of central Nevada. Each segment must be considered rather than the range as a whole, and clearly defined arcs of the scale indicated above generally are convex toward the direction the range is tilted. Ranges that are nearly straight in plan are generally those which are more horstlike, that is, flanked on both sides by major faults.

Table 188.1 lists 55 ranges about which there is some data on the direction of tilting. Of 34 ranges tilted east, 25 are convex east, 1 is convex west, and 8 are rather straight or irregular in shape. Of 21 ranges tilted west, 16 are convex west, 1 is convex east, and 4 are straight or irregular in shape. This relation between the arcuate plan and sense of tilt of mountain blocks is not entirely consistent, but the pattern is repeated so frequently that it is considered to be an important feature of basin-range structure. The curvature of the fault block ranges reflects the curvature of the main bounding fault in plan; hence, the fault itself is believed to be convex toward the direction of tilt of the range, or concave toward the downthrown side of the fault (fig. 188.1).

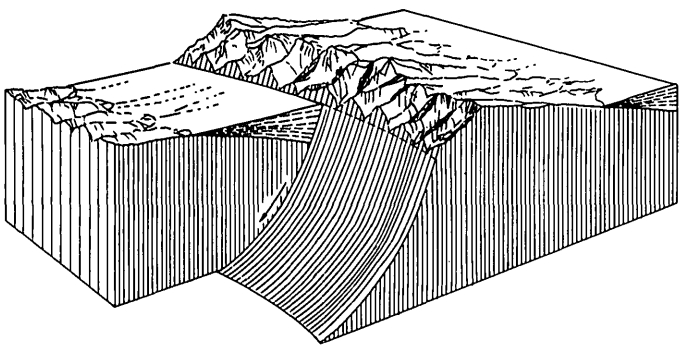

FIGURE 188.1.—Block diagram showing typical curvature and tilt of ranges in the Basin and Range province. The fault surface is believed to be doubly concave (spoon-shaped) toward the downthrown side.

There is evidence that the master normal faults which bound the ranges are also curved in section so that they dip less steeply with depth. Tilting and rotation of blocks is facilitated by a downward flattening of the fault surface (De Sitter, 1956, p. 155), and perhaps for this reason the main normal faults are shown in recent papers (Mackin, 1960, p. 112; and Osmond, 1960) to flatten with depth. Davis (1925) calls on a mathematical analysis and experiments to show that normal faults should flatten with depth. Longwell (1945) finds that many normal faults in southern Nevada flatten downwards.

The fact that many normal faults in the Basin and Range province are concave in plan toward the downthrown side, together with the evidence that many are concave in section upwards, indicates that many of the fault surfaces are probably doubly concave toward the downthrown side. This double concavity suggests that the fault surfaces are spoon-shaped in much the same way that the faults that bound many landslides are spoon-shaped surfaces (Eckel, 1958, p. 24).

REFERENCES

Davis, W. M., 1925, The Basin Range problem: Natl. Acad. Sci. Proc., v. 11, p. 387–392.

Eckel, E. B. (ed.), 1958, Landslides and engineering practice: Highway Research Board, Special Report 29, Washington, D.C., 232 p.

Longwell, C. R., 1945, Low-angle normal faults in the Basin and Range Province: Am. Geophys. Union Trans., v. 26, pt. 1, p. 107–118.

Mackin, J. H., 1960, Structural significance of Tertiary volcanic rocks in southwestern Utah: Am. Jour. Sci., v. 258, p. 81–131.

Osmond, J. C., 1960, Tectonic history of the Basin and Range province in Utah and Nevada: Mining Engineering, v. 12, no. 3, p. 251–265.

Sitter, L. U. de, 1956, Structural geology: New York, McGraw-Hill Book Company, Inc., 552 p.

189. VOLCANISM IN EASTERN CALIFORNIA—A PROPOSED ERUPTION MECHANISM

By L. C. PAKISER, Denver, Colo.

Geologic and geophysical evidence suggests that the volcanic rocks along the eastern front of the Sierra Nevada were erupted from regions of relative tension or stress relief in offsets of a major left-lateral en-echelon shear zone (fig. 189.1). This hypothesis was recently put forward for the volcanic activity in Owens

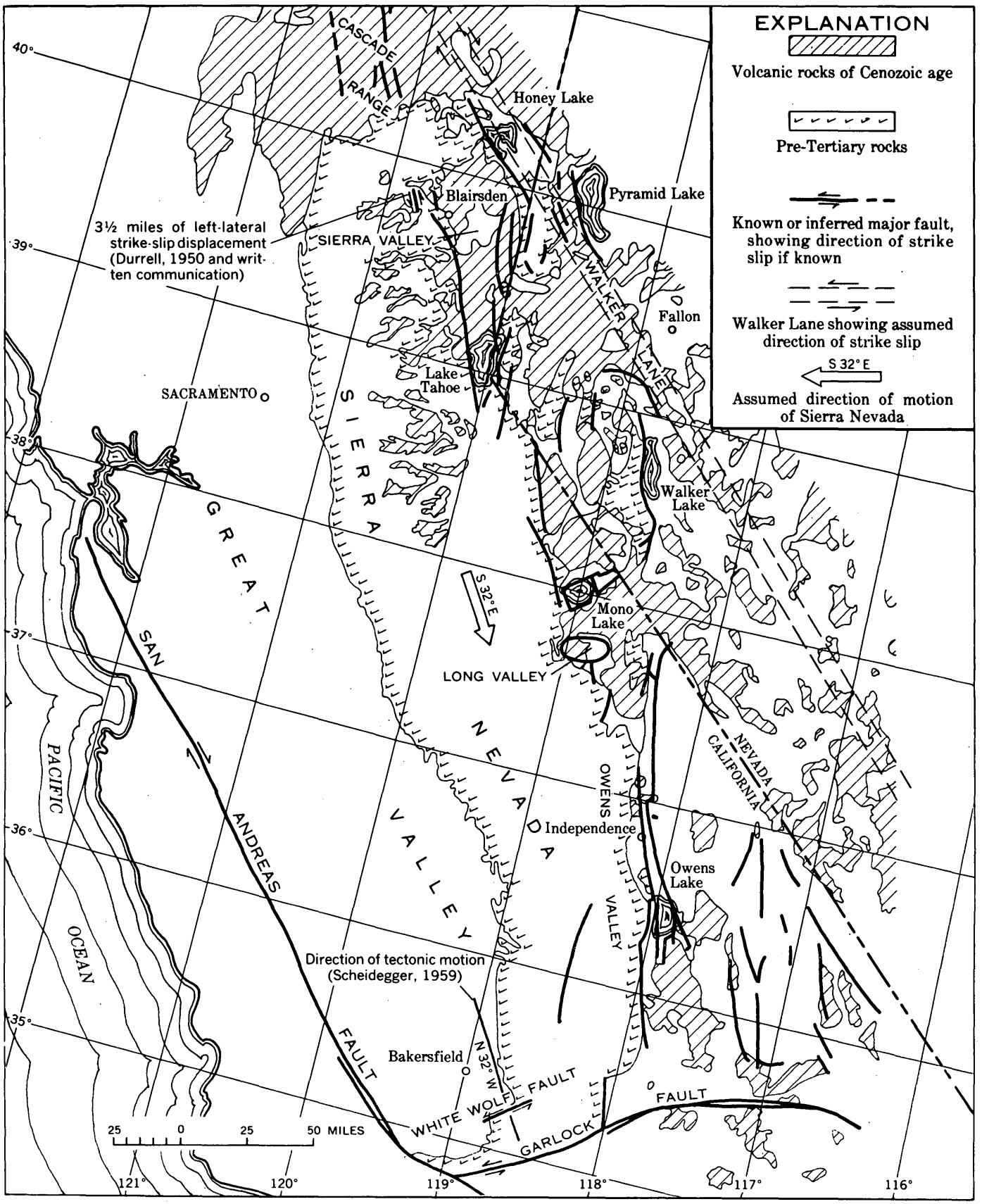

FIGURE 189.1—Tectonic pattern of eastern California and western Nevada.

Valley, which seems to have taken place near the ends of left-lateral faults where tension would be expected (Pakiser, 1960). It seems a reasonable explanation also for the Mono Basin and Long Valley subsidence structures. These have been identified as volcano-tectonic depressions (Pakiser, Press, and Kane, 1960) and they lie in a large offset in the eastern front of the Sierra Nevada. If the Sierra Nevada moved south with respect to the Great Basin, the crust in this offset would have been under tension; as a zone of weakness, the area might therefore have been susceptible to volcanic eruption.

Similar offsets of the eastern front of the Sierra Nevada are found farther north (fig. 189.1). One of these offsets, east of Blairsden, contains Sierra Valley. Gravity data and outcropping volcanic rocks suggest that this valley may be a volcano-tectonic depression similar to Mono Basin and Long Valley. Cordell Durrell (1950 and written communication) mapped a fault west of Blairsden (fig. 189.1) with 3½ miles of left-lateral strike-slip displacement. This fault is nearly parallel to Owens Valley and the strike-slip displacement is several times the dip-slip displacement.

In the Sierra Valley area, the Sierra Nevada block moved south with respect to the area to the east. The concept that the Sierra Nevada block moved southward along left-lateral strike-slip faults is also supported by the thrusting on the White Wolf fault and by Scheidegger's (1959) determination that the direction of tectonic motion for the aftershocks of the Arvin-Tehachapi earthquake of 1952 was N. 32° W. (fig. 189.1). Southward movement of the Sierra block is compatible with the right-lateral strike slip along the San Andreas fault and the Walker Lane (Longwell, 1950).

These facts and inferences suggest that the eastern front of the Sierra Nevada is an en-echelon shear zone along which left-lateral strike-slip movements (and in most places larger vertical movements) took place (fig. 189.2). Discontinuities or overlapping offsets in this shear zone would be regions of relative tension or stress relief in which volcanic eruptions would be facilitated by reduction of the confining pressure on magma chambers (fig. 189.3).

Gravity lows with residual relief of about −50 mgals were found in Mono Basin and Long Valley (Pakiser, Press, and Kane, 1960). These gravity lows represent low-density volcanic debris and sediments that fill the subsidence structures. In more general terms, the gravity lows express the mass deficiency that results when intermediate to silicic magma is erupted from a bounded magma chamber within the earth's sialic crust and is spread as lower density volcanic debris over an area large compared to that of the magma chamber.

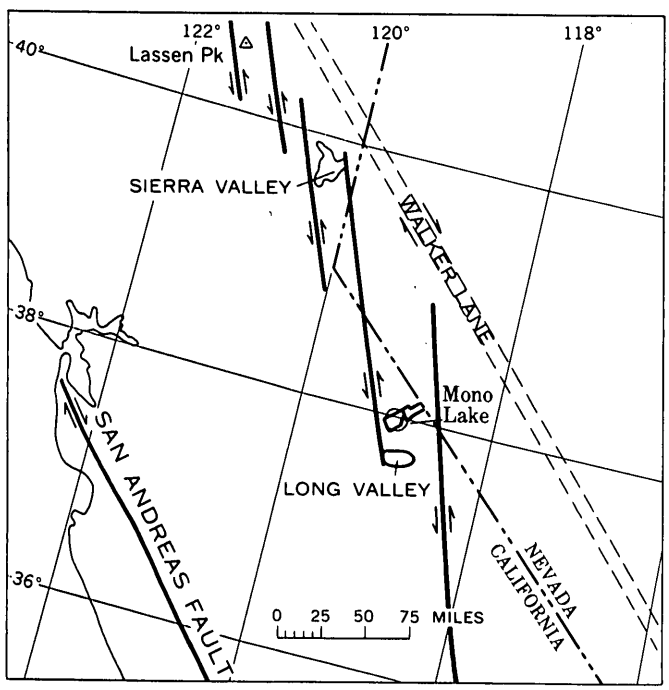

FIGURE 189.3.—Interpretation of strike-slip fault system of eastern California and western Nevada.

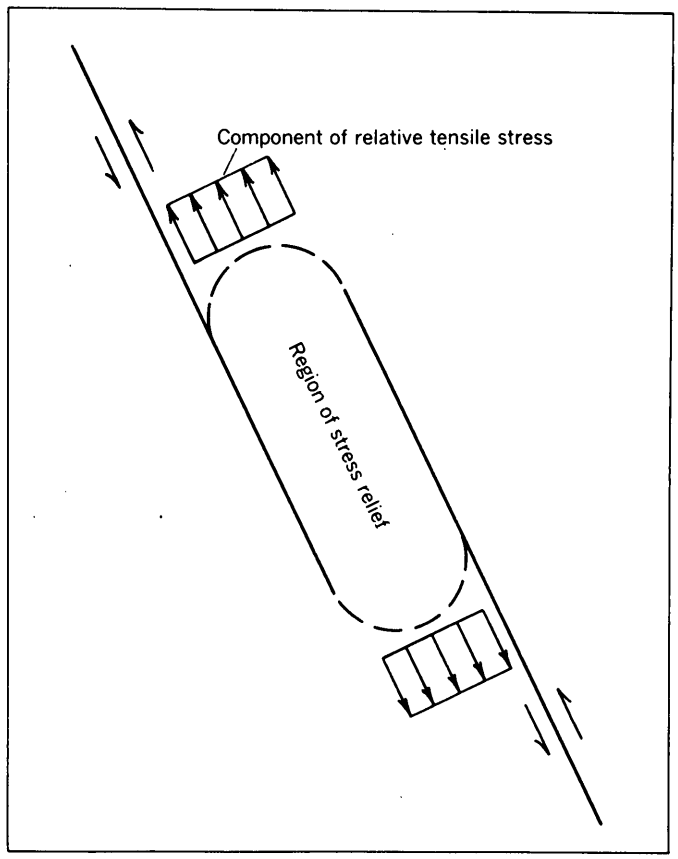

FIGURE 189.2.—Region of stress relief in an en-echelon shear zone.

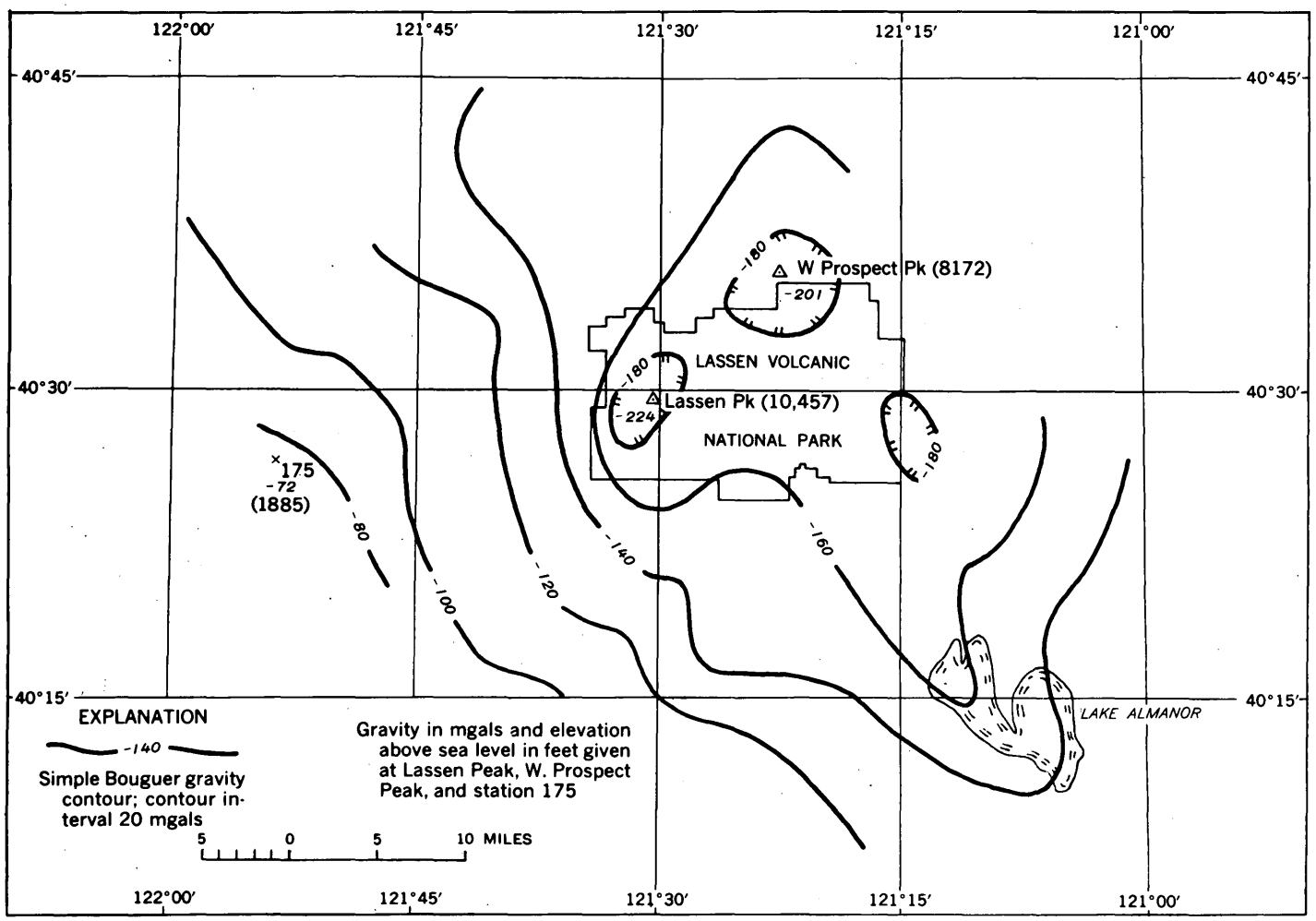

FIGURE 189.4.—Gravity in and around Lassen Volcanic National Park, Calif.

Field work in and around Lassen Volcanic National Park in 1958 and 1959 revealed a large gravity low (fig. 189.4) associated with the volcanic rocks there. The zone of steep gravity gradients directly west of Lassen Peak may express a northward continuation under volcanic cover into the southern Cascades of the en-echelon shear zone along the eastern front of the Sierra Nevada (fig. 189.2). If this interpretation is correct, the Lassen volcanic field lies in an offset of this shear zone similar to the one containing Mono Basin and Long Valley.

REFERENCES

American Association of Petroleum Geologists, 1944, Tectonic map of the United States: Tulsa, Oklahoma.

Durrell, Cordell, 1950, Strike-slip faulting in the eastern Sierra Nevada near Blairsden, California (abs.): Geol. Soc. America Bull., v. 61, p. 1522.

Longwell, C. R., 1950, Tectonic theory viewed from the Basin Ranges: Geol. Soc. America Bull., v. 61, p. 413–434.

Pakiser, L. C., 1960, Transcurrent faulting and volcanism in Owens Valley, California: Geol. Soc. America Bull., v. 71, p. 153–160.

Pakiser, L. C., Press, Frank, and Kane, M. F., 1960, Geophysical investigation of Mono Basin, California: Geol. Soc. America Bull., v. 71, p. 415–448.

Scheidegger, A. E., 1959, Note on the tectonics of Kern County, California, as evidenced by the 1952 earthquakes: Jour. Geophys. Res., v. 64, p. 1499–1501.

Stose, G. W., and Ljungstedt, O. A., 1932, Geologic map of the United States: U.S. Geological Survey.

190. SOME RELATIONS BETWEEN GEOLOGY AND EFFECTS OF UNDERGROUND NUCLEAR EXPLOSIONS AT NEVADA TEST SITE, NYE COUNTY, NEVADA

By F. A. McKeown and D. D. Dickey, Denver, Colo.

Work done in cooperation with the U.S. Atomic Energy Commission

The underground nuclear explosions, code named Logan and Blanca, with yields of 5 and 19 kilotons, respectively (Johnson and others, 1959, p. 1461), provide data for evaluating geologic control of fracturing within tunnels and at the surface.

The Logan explosion was detonated October 15, 1958, and Blanca was detonated October 30, 1958. Both explosions were detonated in tuff of the Oak Spring formation, of Tertiary age, in straight tunnels having a minimum depth over the explosion chambers of 830 and 835 feet, respectively.

One of the phenomena resulting from an underground explosion that must be considered when evaluating the effects on rock in tunnels or at the surface is the passage of high-velocity stress waves generated during the momentary confinement by the rock of an extremely high pressure system of gases and other explosion products. Part of the energy of a contained explosion is transmitted in a stress wave as kinetic energy. This energy is a function of the particle velocity of the wave. Particle velocity, however, is a function of the amplitude, shape, and propagation velocity of the wave. Changes in these variables per unit distance in rocks are determined primarily by fractures and beds or layers of rocks that differ in composition and physical properties. Since the number of fractures and the average compositions of beds differ in different directions, the attenuation of the energy of a stress wave during propagation away from an explosion likewise depends on the direction of the wave. For the

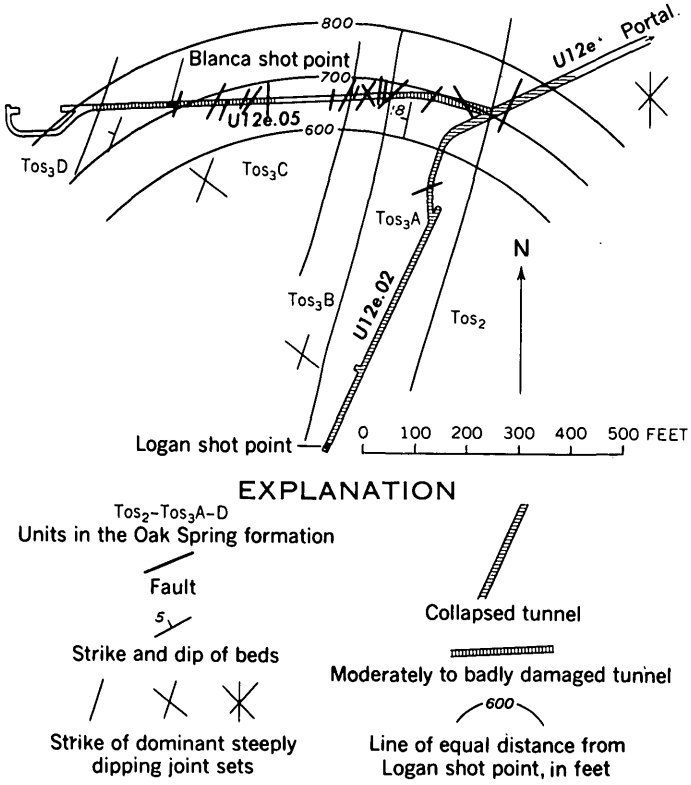

FIGURE 190.1.—Generalized geologic map showing U12e.02, U12e.05, and part of U12e tunnels and extent of collapse due to the Logan explosion.

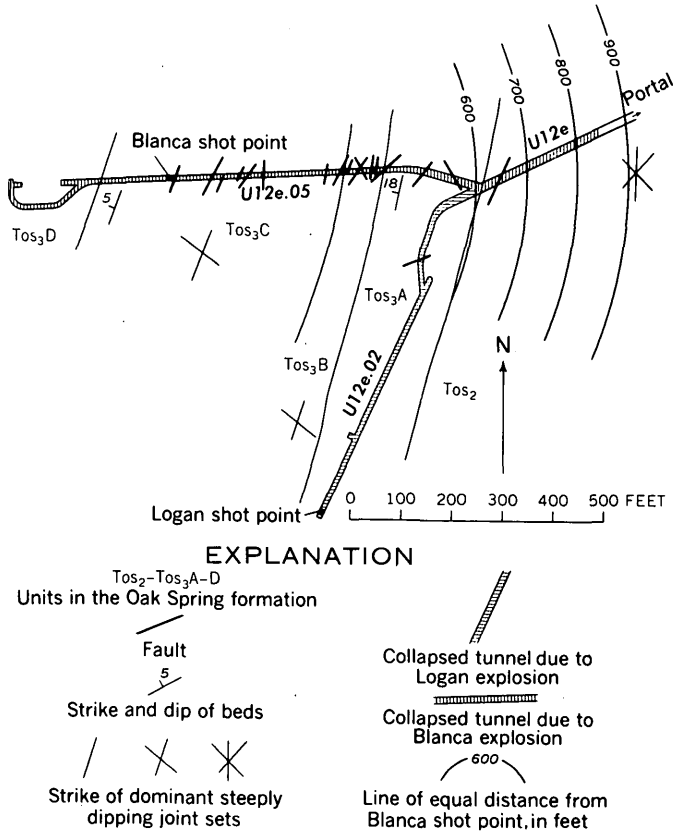

FIGURE 190.2.—Generalized geologic map showing U12e.02, U12e.05, and part of U12e tunnels and extent of collapse due to the Blanca explosion.

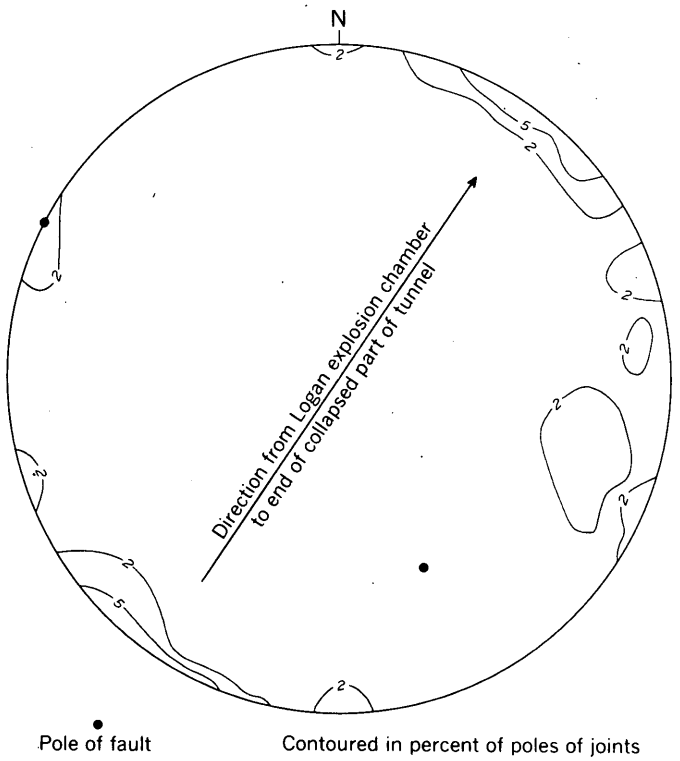

FIGURE 190.3.—Contour diagram of 287 poles of joints and plot of 2 faults mapped in U12e.02 and U12e tunnels from the explosion chamber to end of collapsed part of tunnel. Upper-hemisphere plot.

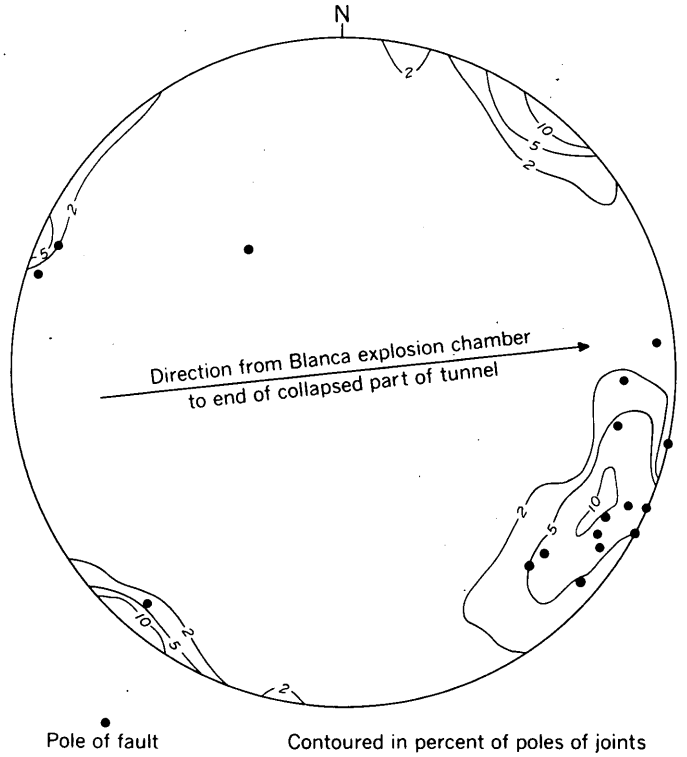

FIGURE 190.4.—Contour diagram of 324 poles of joints and plot of the poles of 17 faults mapped in U12e.05 and U12e tunnels from the explosion chamber to end of collapsed part of tunnel. Upper-hemisphere plot.

Logan and Blanca explosions these differences can be estimated only roughly.

Since the effectiveness of an explosion in breaking rock is approximately proportional to the cube root of the yield, the Blanca explosion should, if the two tunnels had had the same geologic environment, have collapsed its tunnel approximately 1.6 times as far from the explosion point as the much weaker Logan explosion.

$$\frac{19^{1/3}}{5^{1/3}} \cong 1.6$$

In fact, however, the tunnel collapse due to the Logan explosion extended for a radial distance of 820 feet from the shot point, and that due to the Blanca explosion for only 860 feet—a ratio of 1.05 (figs. 190.1 and 190.2). This disproportionate extent of damage could be due in part to the difference in the properties of the rocks traversed by the stress waves from the Logan explosion. This conjecture can be checked by comparing the properties of the rocks affected by the two explosions.

The parts of U12e and U12e.05 tunnels (fig. 190.1) most heavily damaged by the Logan explosion are in or near subunit *A* of Tos_3. (See fig. 190.2). The tuff in this subunit is harder than the other beds of tuff exposed in the tunnels. It contains three to five times as many phenocrysts, fewer vesicles, and less zeolite and clay minerals than the overlying tuff; and it has a density of 2.11±0.06 g per cc, a grain density of 2.6±0.016 g per cc, and a porosity of 30.6±3.2 percent, as compared to averages of 1.95 g per cc, 2.38 g per cc, and 32.9 percent, respectively, for adjacent units (F.M. Byers, Jr., written communication). It may be inferred from these data that stress waves have a higher acoustic velocity, and a lower rate of attenuation, in subunit *A* than in adjacent rocks. The kinetic energy of stress waves, at points equally distant from their source, would therefore be greater in subunit *A* than in adjacent rocks. The very close relation between amount of tunnel damage and character of rock in U12e.05 tunnel (fig. 190.1) seems to support this inference.

The attitudes and relative abundance of fractures in the tuffs may cause directional variations in attenuation of stress waves. Fractures produced by the Logan explosion, which was detonated before the Blanca explosion, are known to be relatively few in the rock several hundred feet from the explosion chambers and exposed by postexplosion tunneling. Attenuation due to these fractures is therefore probably local and relatively insignificant compared with natural fractures. Figures 190.3 shows that the direction of propagation of waves from the Logan explosion point to the collapsed tunnel is nearly parallel to one set of joints and

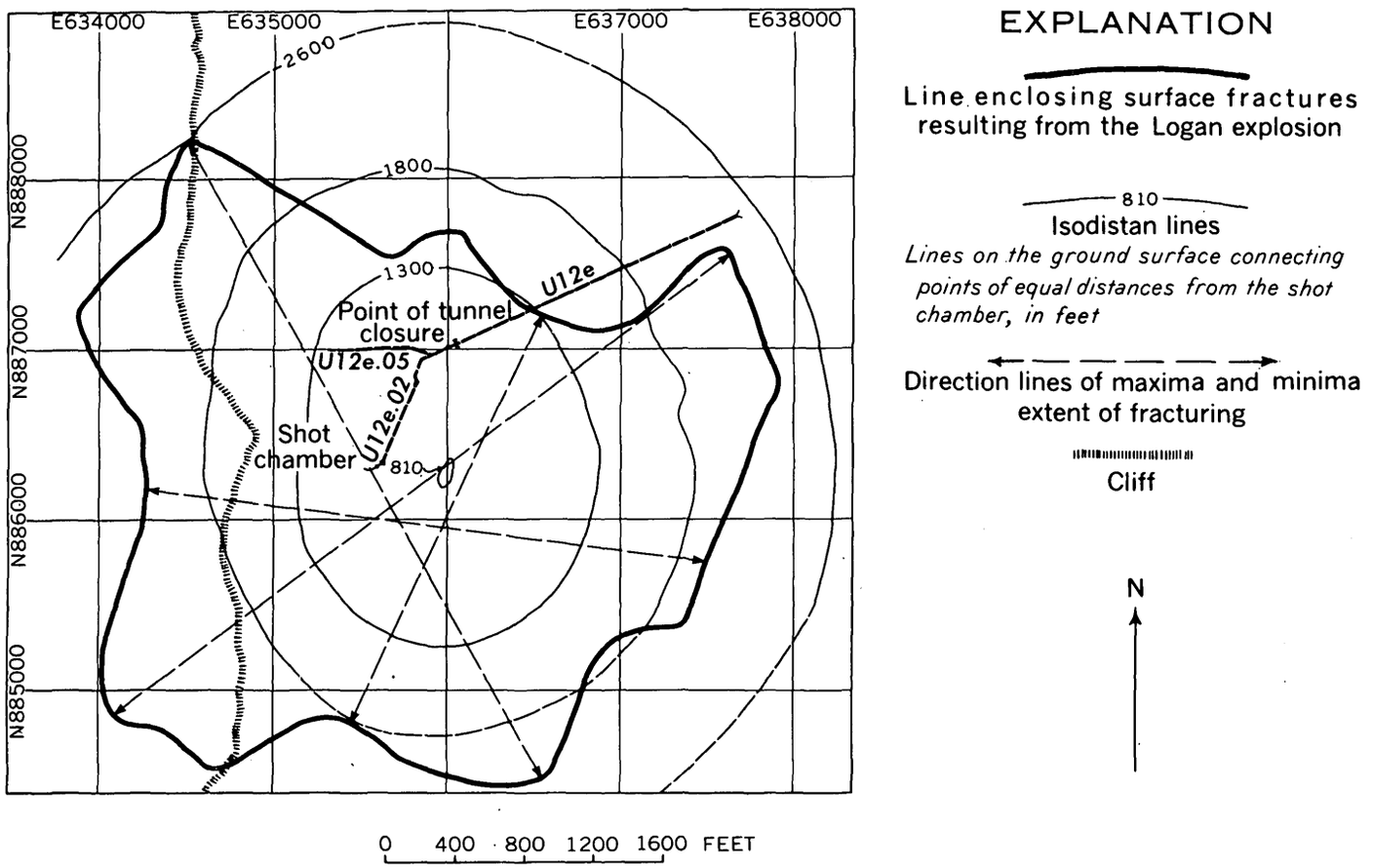

FIGURE 190.5.—Map showing extent of fracturing due to Logan explosion.

two faults, and perpendicular to another set of joints. The direction of propagation of waves from the Blanca explosion point to tunnel collapse, on the other hand, intersects two sets of fractures and 17 faults at about 45° (fig. 190.4).

The limits of fractured rock at the surface above the explosion sites are lobate (figs. 190.5 and 190.6), and the alinements of lobes about 180° apart coincide approximately with directions of sets of fractures.

Both the underground and the surface data show that explosion-produced fracturing extends farthest in the directions of sets of fractures. A corollary is that at equal distances from an explosion, the greatest fracturing may be expected to occur along radii parallel to a set of fractures.

In summary, the extent and intensity of fracturing in different directions, and consequently tunnel damage, may to a significant degree depend upon (a) the relations of beds of different chemical and physical properties to the direction of propagation of stress waves and (b) the angles between the direction of propagation and sets of fractures in the rock.

REFERENCES

Johnson, G. W., and others, 1959, Underground nuclear detonations: Jour. Geophys. Research, v. 64, no. 10, p. 1457–1470.

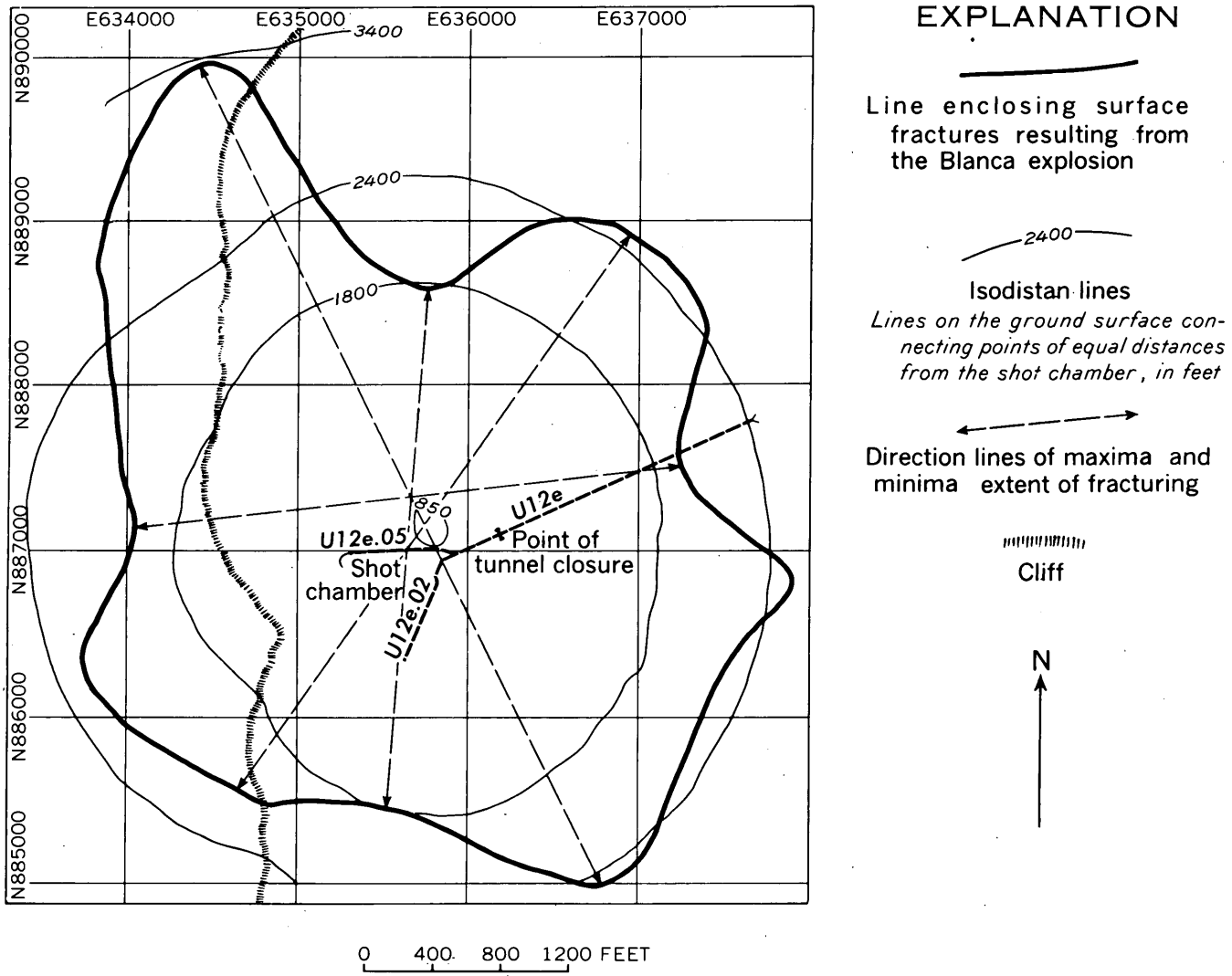

FIGURE 190.6.—Map showing extent of fracturing due to Blanca explosion.

191. STRUCTURAL EFFECTS OF RAINIER, LOGAN, AND BLANCA UNDERGROUND NUCLEAR EXPLOSIONS, NEVADA TEST SITE, NYE COUNTY, NEVADA

By V. R. WILMARTH and F. A. MCKEOWN, Denver, Colo.

Work done in cooperation with the U.S. Atomic Energy Commission

The Rainier, Logan, and Blanca contained nuclear explosions, with energy yields of 1.7, 5, and 19 kilotons (Johnson and others, 1959, p. 1461), were detonated at minimum distances below the nearest ground surface of 820, 830, and 835 feet respectively. The explosion chambers were at the ends of tunnels 2,000 to 3,000 feet long, driven from the steep east slope of Rainier Mesa in massive to well-bedded friable to compact tuffs of the Oak Spring formation (Tertiary). Rainier Mesa is capped with about 270 feet of cliff-forming welded tuff

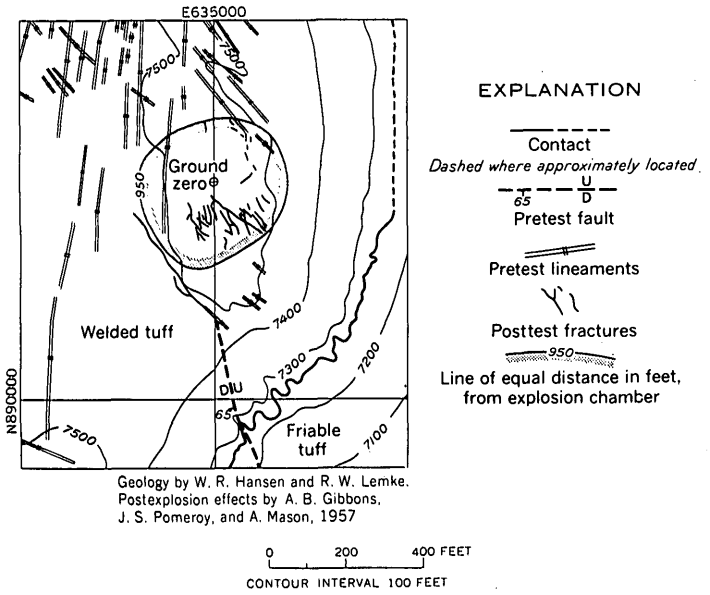

FIGURE 191.1.—Geologic map showing fractures caused by Rainier explosion, Nevada Test Site, Nye County, Nev.

of this formation, broken by many northeast- to northwest-trending fractures.

On the surface, the most obvious result of the explosions was to produce rockslides and rockfalls from the welded tuff. These extend discontinuously for 3,200 to 3,500 feet north and south of the ground zeros (Glasstone, 1957, p. 549), though the slides are notably more abundant and larger within 1,500 feet than at greater distances.

Nearly all the fractures produced by the Rainier, Logan, and Blanca explosions that have been mapped on the surface (figs. 191.1–191.3) are within the 1,000-, 2,600-, and 3,300-foot isodistan lines[1] respectively. These fractures are most numerous in the welded tuff and in the bedded compact tuffs east of the epicenters—the points on the surface nearest the shot chambers. The mesa area around the epicenters is immediately underlain by friable tuffs in which fractures are less nu-

[1] Lines on surface connecting points equidistant from the explosion chamber.

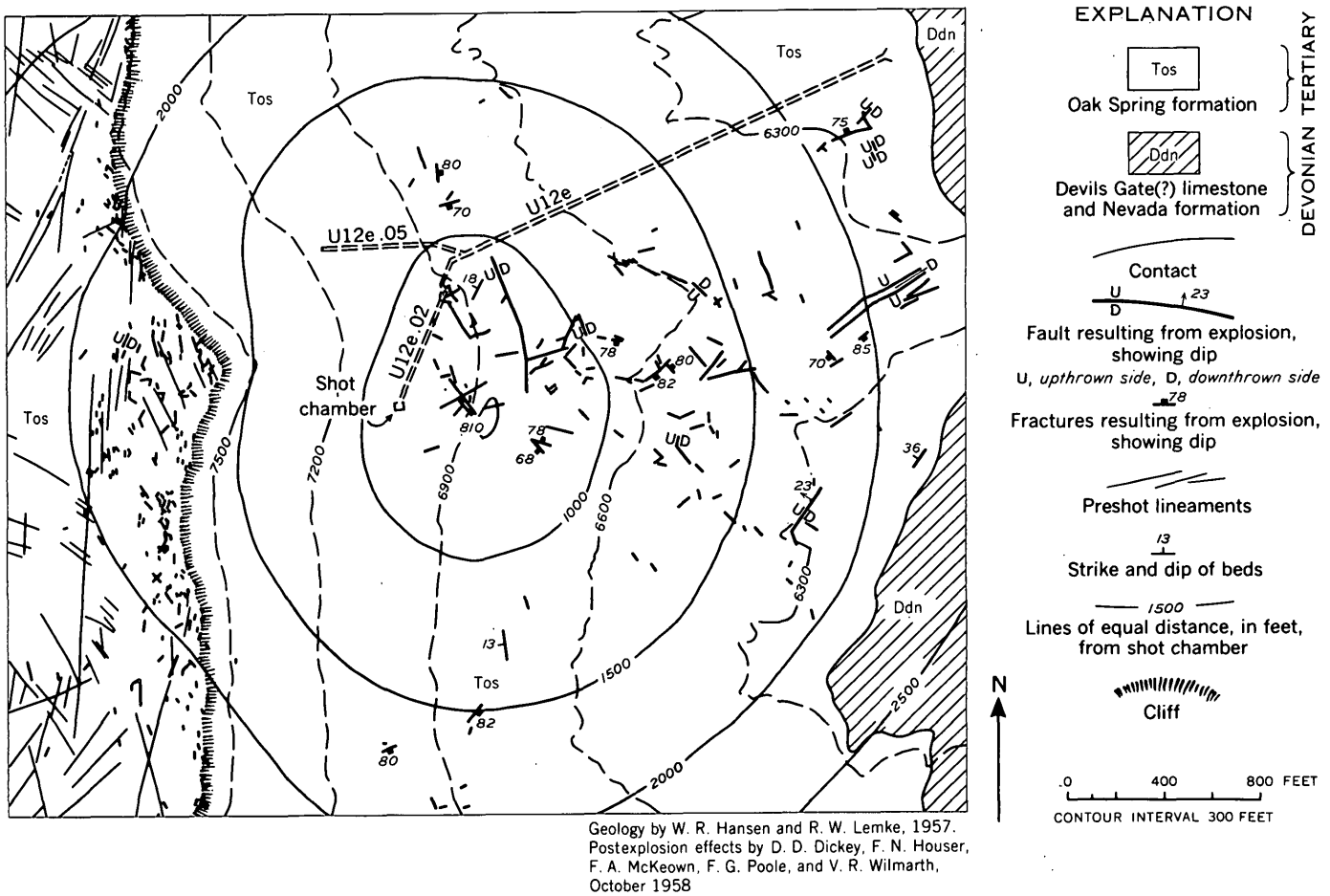

FIGURE 191.2.—Geologic map of the U12e tunnel area, showing fractures and faults caused by the Logan explosion, Nevada Test Site, Nye County, Nev.

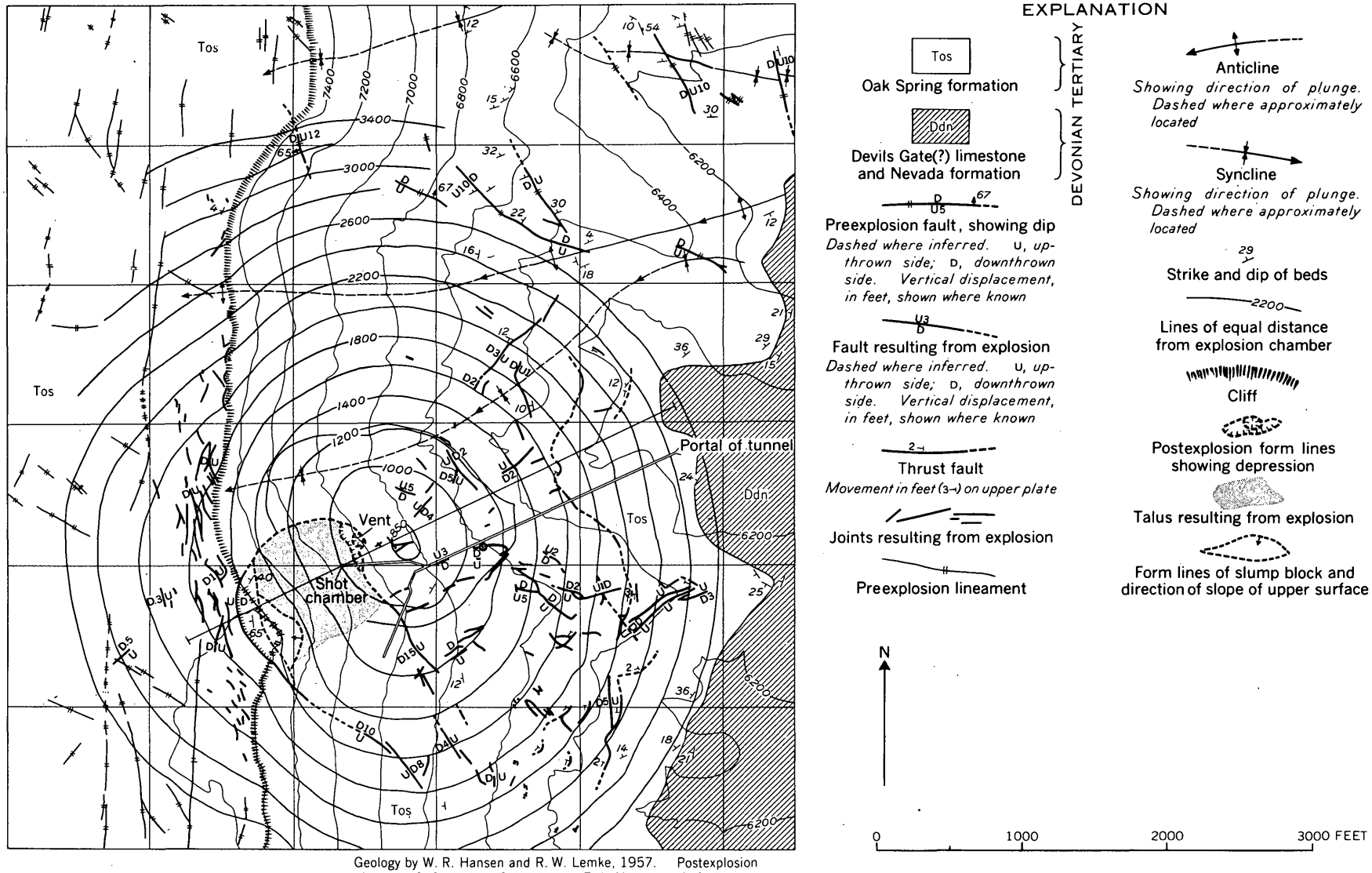

Geology by W. R. Hansen and R. W. Lemke, 1957. Postexplosion effects by D. D. Dickey, F. N. Houser, F. A. McKeown, F. G. Poole, and V. R. Wilmarth, November 1958 and January, March, and April 1959

FIGURE 191.3.—Geologic map of the U12e tunnel area showing joints and faults caused by the Blanca explosion, Nevada Test Site, Nye County, Nev.

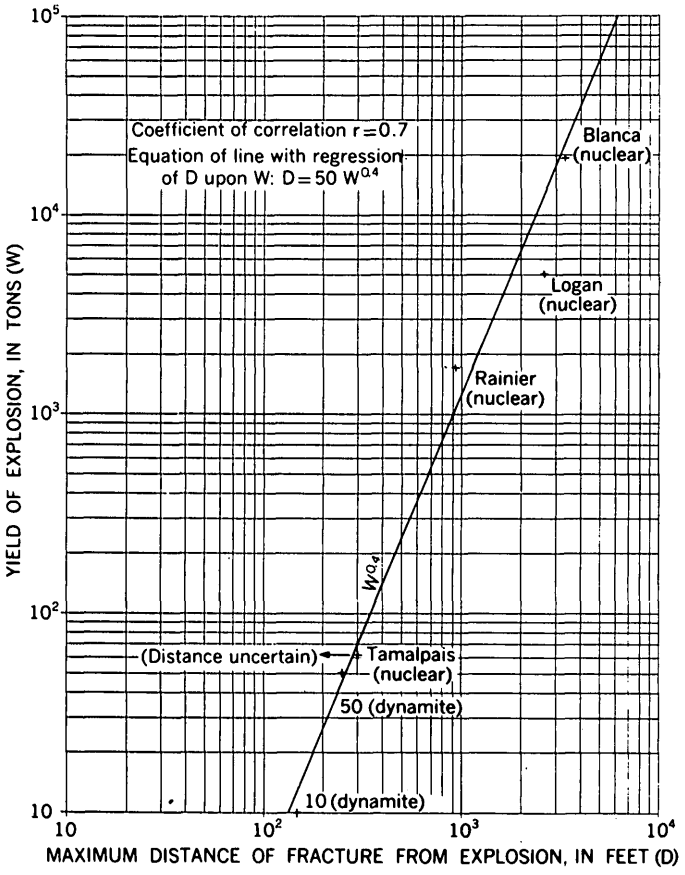

FIGURE 191.4.—Graph showing relation of yield of explosion to distance of fractures from explosion in tuff of Oak Spring formation.

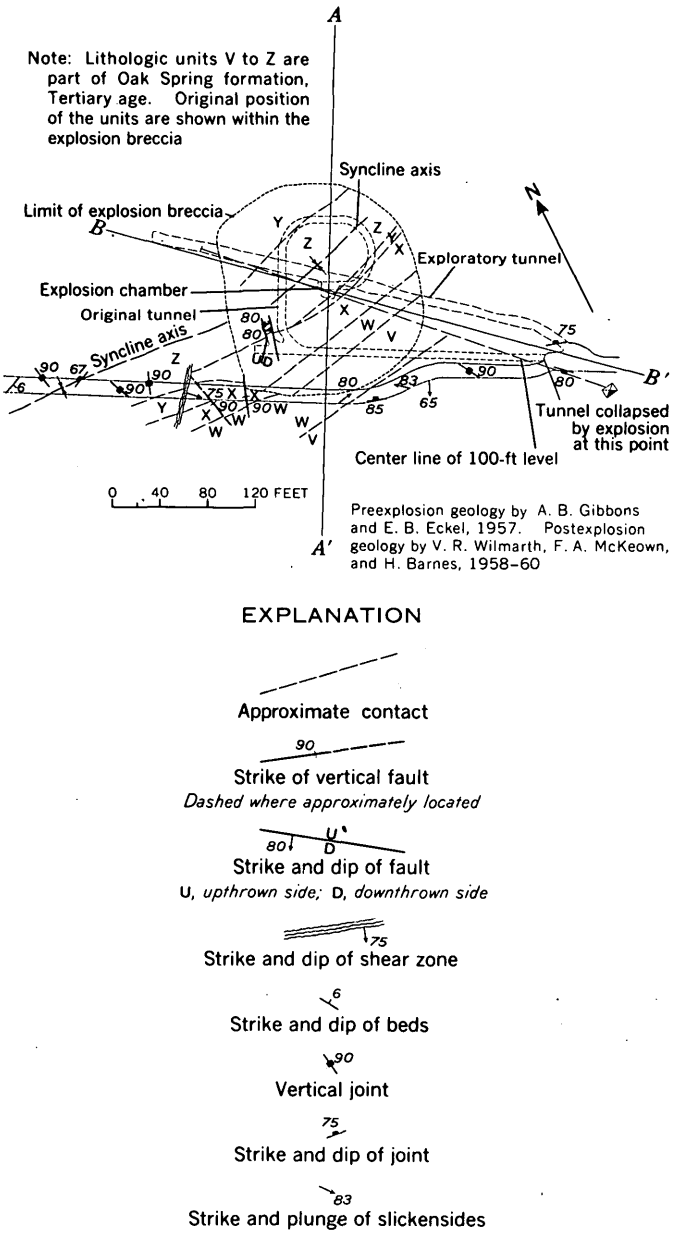

FIGURE 191.5.—Geologic map of Rainier tunnel showing effects of Rainier explosion.

merous than in the welded tuff and are poorly developed. Many of the postexplosion fractures coincide with or parallel the tectonic fractures, which are particularly numerous in the welded tuff. Most of the explosion-produced fractures (figs. 191.2 and 191.3) dip steeply; they range from 15 to 600 feet in length, and some are open as much as 3 feet in width. Some of the Blanca-produced fractures are open to depths of at least 40 feet below the surface, which is about as far down as one can see.

The nuclear explosions produced both overthrusts and normal faults. Gently dipping thrust faults are along or near bedding planes and are traceable along strike for a maximum of 2,200 feet (figs. 191.2 and 191.3). The hanging walls of the thrust faults have moved upward and away from the explosion chamber, in some places as much as 5 feet. Most of the thrust faults crop out more than 1,800 feet from the chamber (figs. 191.2 and 191.3), in areas where the bedding planes are nearly parallel to radii from the shot chamber. In contrast the steeply dipping normal faults trend predominantly northwest to northeast, parallel to tectonic fractures, and generally have strike lengths of less than 500 feet; the displacements on most of them range from 6 inches to 5 feet.

The maximum radial distance from the explosion chambers of fractures in tuffs of the Oak Spring formation scales empirically as the 0.4 power of the yield in tons of the explosion. This figure applies to both nuclear and high-explosive tests (fig. 191.4).

The largest structure formed at the surface by the Blanca test is a northwest-trending graben southwest of the epicenter (fig. 191.3). Vertical displacements

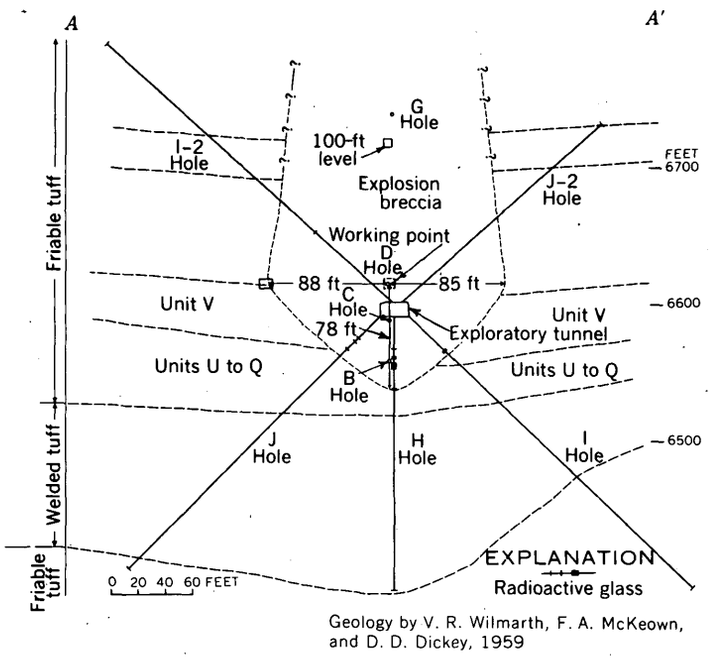

FIGURE 191.6.—Section *A–A'* through zone affected by Rainier explosion.

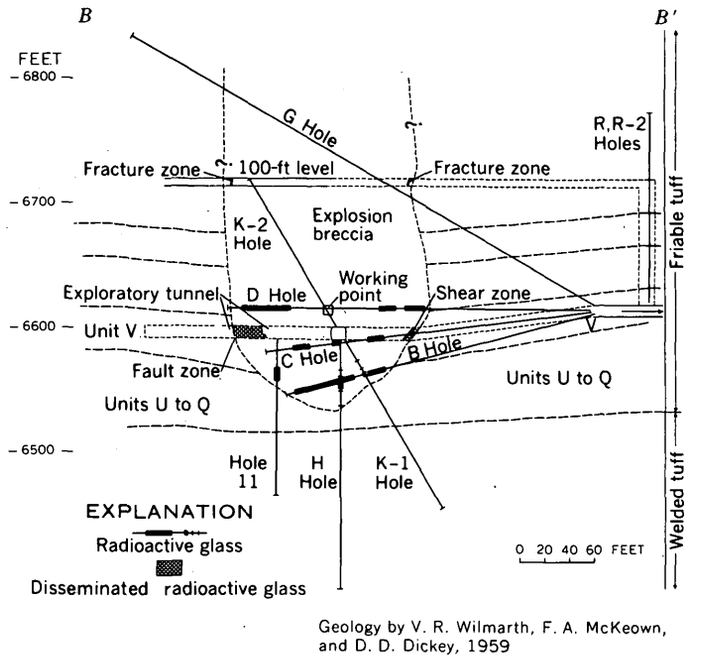

FIGURE 191.7.—Section *B–B'* through zone affected by Rainier explosion.

on the bounding faults are as much as 65 feet, but the movement here was not of the same sort as that on the small normal faults. The graben resulted primarily from collapse of a cavity, produced by explosion, though its large size is due in part to the extensive fracturing of the tuffs by the earlier Logan explosion.

In the tunnels, the amount of rock spalled from the walls increased from the portal inward to points where the tunnels were completely collapsed. This point is at a radial distance of 205 feet from the chamber, for the Rainier test, and at 820 and 870 feet, for the Logan and Blanca tests, respectively.

Portalward from the collapsed areas, the explosions formed new faults and joints, deformed the tunnels by movement of the tuffs along shear planes parallel to and dipping steeply away from the tunnel, and opened and extended pre-existing fractures.

The newly formed joints are most numerous in the competent tuff and are coincident with or parallel to preexplosion fractures. The most prominent new faults are bedding-plane thrust faults that dip 3° to 10° toward the chambers and have displaced the beds horizontally as much as 4 feet. Thrusting occurred most commonly where a layer of wet soft clay separates competent tuff beds.

The amount of radial displacement of the tuffs by the Rainier test increases abruptly within 400 feet of the chamber. The tuff beds 60 feet radially from the explosion were moved horizontally as much as 38 feet (fig. 191.5). Radial displacement of surveyed stations in the Rainier tunnel was 2.5 feet at 200 feet from the chamber, 1.0 foot at 400 feet, and less than 6 inches at 1,100 feet. In the Blanca test, the radial displacement of surveyed stations in the tunnel 1,100 feet from the chamber following was about ten times as great as in the Rainier test.

The tuff adjacent to the explosion chambers was brecciated and extensively fractured. The breccia zone around the Rainier chamber is, at the level of the explosion, roughly circular in plan and 190 feet in maximum diameter (fig. 191.5). In vertical sections through the chamber, the breccia zone is elliptical (figs. 191.6 and 191.7). This zone extends for about 80 feet below the chamber. According to Johnson and others (1959, p. 1465) it extends about 386 feet above the chamber. The estimated volume of the breccia zone is about 245,000 cubic yards. Where exposed in the Rainier tunnel, the breccia zone is separated by shear and fracture zones 2 to 6 feet wide from highly fractured tuff, which below the chamber extends as much as 70 feet outward from the breccia zone.

The breccia zone produced by the Logan explosion (fig. 191.8) is a nearly vertical prolate spheroid having an estimated volume of 190,000 cubic yards. The breccia zone produced by the Blanca explosion has not been so fully studied, but it appears to be similar in shape, size, and orientation to that produced by the Logan explosion.

The volume of a breccia zone produced by a nuclear explosion in tuff depends partly on the properties of

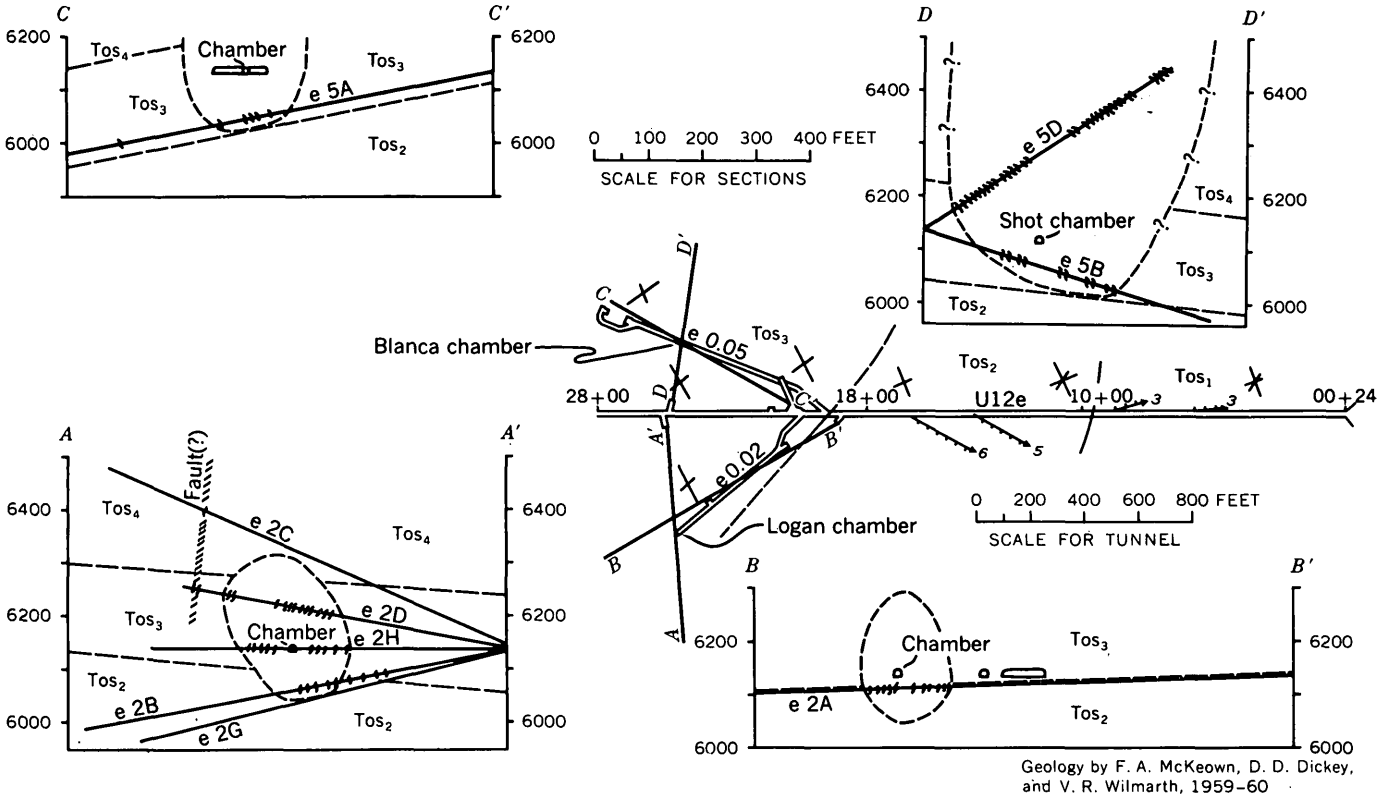

FIGURE 191.8.—Geologic map and sections of part of U12e tunnel complex, showing exploratory drill holes and some effects of the Logan and Blanca explosions.

the rock. The tuffs surrounding the Rainier explosion are friable, whereas those around the Logan are tough and compact, and as a result the volume of breccia formed per kiloton of yield is 3.4 times as large for the Rainier as for the Logan explosion.

REFERENCES

Glasstone, Samuel, ed., 1957, The effects of nuclear weapons: U.S. Atomic Energy Comm., Washington, U.S. Govt. Printing Office, 579 p.

Johnson, G. W., and others, 1959, Underground nuclear detonations: Jour. Geophys. Research, v. 64, no. 10, p. 1457–1470.

192. BRECCIATION AND MIXING OF ROCK BY STRONG SHOCK

By EUGENE M. SHOEMAKER, Menlo Park, Calif.

Work done in cooperation with the U.S. Atomic Energy Commission

Investigation of the fragmentation and displacement of earth materials engulfed by strong shock reveals that complex movement of these materials behind the shock front extends out to a fairly sharply defined limit. Within this limit is a domain in which fragments that were originally at widely different distances from the origin of the shock are mixed; beyond this limit the rocks are fractured, but the fragments, though dis-

placed outward, are not mixed. The mixed debris formed in small-scale explosions is commonly unconsolidated, and in some cases it is expelled from the region of strong shock. The mixed debris, where preserved, and its contact with unmixed material are most easily observed in craters.

NUCLEAR EXPLOSIONS IN ALLUVIUM

At the Nevada Test Site, two nuclear explosions (Jangle U and Teapot ESS experiments), of 1.2±0.5 kiloton (TNT equivalent) yield (Johnson, 1959, p. 10) have been detonated by the U.S. Atomic Energy Commission at shallow depth in alluvium. The particles of which the alluvium is composed are about 50 percent felsic tuff and about 50 percent quartzite. The floors and lower walls of the two craters formed by these explosions are underlain by a compact breccia consisting of slightly to strongly compressed and sheared blocks of alluvium, set in a matrix of smaller blocks and alluvial detritus. The original bedding of the alluvium is partially preserved in the breccia, but in some places individual blocks derived from one stratigraphic horizon have been introduced into parts of the breccia composed mainly of blocks from another horizon. Glass, formed by fusion of alluvium resulting from shock, is dispersed through the matrix of the breccia in the form of droplike, spindle-shaped, and irregular lapilli. Bedding in the breccia is overturned and is locally in fault contact with less disturbed beds along the walls. The base of the breccia in the Teapot ESS crater is 61 feet below the center of the detonated nuclear device, but its depth in the Jangle U crater is not known. A thin patchy layer of material formed by falling back of ejected debris overlies the breccia in both craters.

METEOR CRATER, ARIZONA

The structure of the Teapot ESS crater (Shoemaker, 1960) is closely similar to that of Meteor Crater, in Arizona. Rocks intersected by Meteor Crater include, in descending order, about 50 feet of sandstone and shale, 265 to 270 feet of sandy dolomite, and several hundred feet of quartzose sandstone. The lower walls and floor of the crater are underlain by a lens of breccia composed chiefly of shattered, twisted, and compressed blocks of sandstone. Glass, composed of sandstone and dolomite fused by shock, is dispersed in the breccia; the glass derived from dolomite contains minute particles of meteoritic nickel-iron. The base of the breccia lies at an average depth of about 1,100 feet from the original ground surface. The breccia is overlain by about 30 feet of debris formed by falling back of ejected fragments. The total energy released by meteorite impact, estimated by scaling of horizontal crater dimensions from the Teapot ESS crater, was about 1.4 to 1.7 megatons, and the center of gravity of the energy released is estimated to have been between 320 and 400 feet from the surface along the path of meteorite penetration (Shoemaker, 1960).

UNDERGROUND EXPLOSIONS IN BEDDED TUFF

The effects of three underground explosions in pumiceous bedded tuff at the Nevada Test Site have been described in detail by various workers, and I have studied them independently. These explosions were: (a) the Rainier experiment, in which a nuclear device of 1.7±0.5 kiloton yield was detonated (Johnson, 1959, p. 10); (b) explosion of 50 tons of dynamite (60 percent nitroglycerin gelatin); and (c) explosion of 10 tons of dynamite (60 percent nitroglycerin gelatin).

The Rainier experiment produced a breccia of mixed fragments containing dispersed glass in various forms, that closely resembles the mixed breccia in the Jangle U and Teapot ESS craters. Where the breccia was intersected in an exploratory drift, the distance from the nearest wall of the original explosion chamber to the limit of the domain of mixing ranges from 62 to 72 feet (measured from Diment and others, 1959, fig. 4.4).

In the 50-ton dynamite shot a mixed breccia was formed, whose edge is about 23 feet from the nearest wall of the explosion chamber where intersected by an exploratory drift (measured from map transmitted by J. M. Cattermole, 1958).

In the 10-ton dynamite shot, rock compressed and disaggregated by shock was expelled from the vicinity of the shot chamber by venting the explosion gases. Rocks in the walls of the cavity thus formed are not mixed. The fragments in the expelled debris are very similar in size, frequency distribution, and degree of shearing to those in the mixed breccia of the nuclear explosion craters. Except on the side of the original entryway, the horizontal distance from the walls of the original explosion chamber to the walls of the resultant cavity ranges from 10 to 15 feet and averages about 12 feet (measured from map transmitted by J. M. Cattermole, 1958).

EXPLOSIONS IN SANDSTONE

Vertical drill holes 1.8 inches in diameter in sandstone in Unaweep Canyon, Colorado, sprung with charges of dynamite, have been transformed into elongate cavities 8 to 9 inches in diameter surrounded by an aureole of fractured rock. The horizontal distance from the walls of the original drill holes to the walls of the cavities produced by the dynamite explosions ranges from about 0.2 to 0.3 feet. Most of the

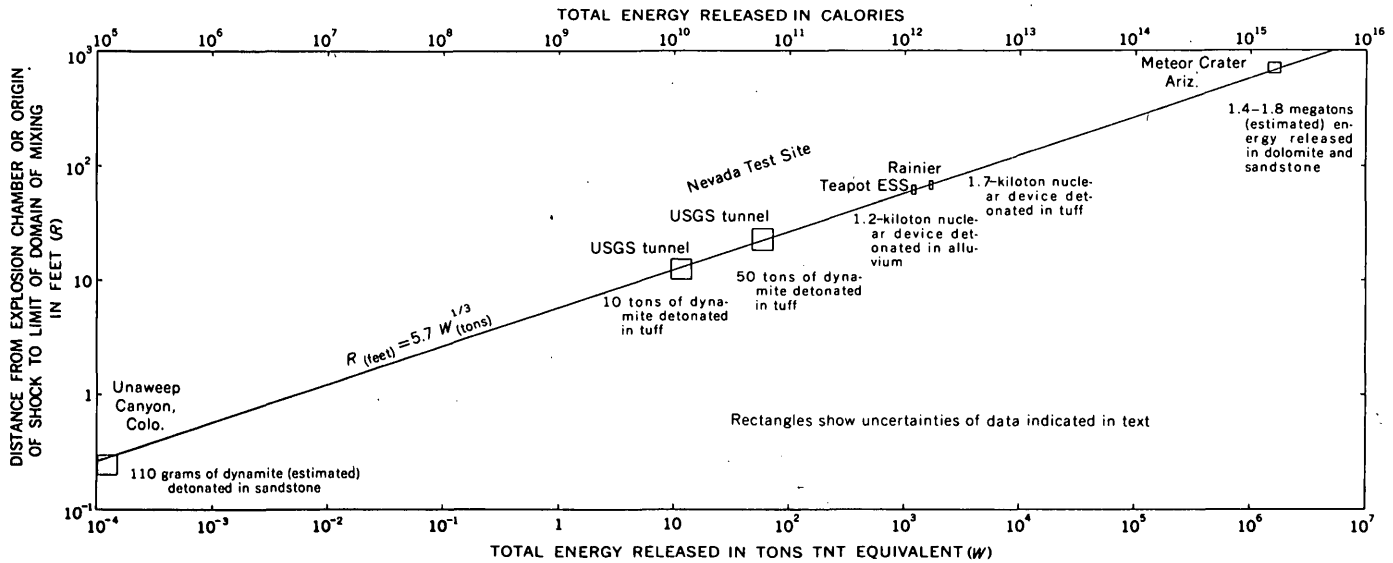

FIGURE 192.1.—Distance from origin of shock to limit of domain of mixing as a function of total energy released.

rock crushed and disaggregated by shock has been expelled from the holes. A right circular cylinder of dynamite having the diameter of the drill holes and a height equal to its diameter would weigh about 110 grams.

SCALING LAW FOR DOMAIN OF MIXING

The mixed breccia underlying the nuclear explosion craters and Meteor Crater, Arizona, is here interpreted as strictly homologous with the mixed breccia produced by the contained nuclear and dynamite explosions, with the debris expelled from the sprung drill holes and the cavity produced by the 10-ton dynamite shot. The mixing appears to have occurred in the shock wave (compare with Johnson and others, 1958, and Kennedy and Higgins, 1958). The limit of the domain of mixing initially extends in all directions to roughly equal distances from the origin of the shock or from the walls of the shot chamber. This distance obeys a simple scaling law with respect to the total energy released (fig. 192.1), which appears to be virtually independent of the character of the material affected and of the mechanism by which the shock is generated.

In the explosions that form craters, the mixed breccia is probably at first in the form of a roughly spherical shell, but the upper part of the shell is ejected and the lower part is sheared out laterally into the form of a deep concavo-convex lens. Only the vertical distance from the origin of the shock to the base of the lens, therefore, is directly comparable with the dimensions of shells formed in contained explosions. In figure 192.1 an uncertainty of 5 feet has been arbitrarily assigned to this distance for the Teapot ESS crater and to the lateral dimensions of the shell for the 50-ton dynamite shot. Twenty percent uncertainty has been arbitrarily assigned to the total energy released in the dynamite shots. For the sprung drill holes the effect on scaling of differences between conical and spherical divergence of the shock has been neglected.

The following equation gives the relation between the limit of the domain of mixing and the energy released:

$$\frac{R}{W^{1/3}} = K = 5.7 \frac{\text{feet}}{\text{tons}^{1/3}},$$

where R is the distance in feet from the explosion chamber or origin of shock to the limit of the domain of mixing, and W is the total energy released in tons TNT equivalent.

REFERENCES

Diment, W. H., and others, 1959, Effects of the Rainier underground explosion: U.S. Geol. Survey open-file report, TEI–355, 134 p., May 12, 1959.

Johnson, G. W., 1959, Mineral resource development by the use of nuclear explosives: California Univ., Lawrence Radiation Lab. Rept. UCRL–5458, 18 p.

Johnson, G. W., Pelsor, G. T., Preston, R. G., and Violet, C. E., 1958, The underground nuclear detonation of September 19, 1957, Rainier Operation Plumbbob: California Univ., Lawrence Radiation Lab. Rept. UCRL–5124, 27 p.

Kennedy, G. C., and Higgins, G. H., 1958, Temperatures and pressures associated with the cavity produced by the Rainier event: California Univ., Lawrence Radiation Lab. Rept. UCRL–5281, 9 p.

Shoemaker, E. M., 1960, Impact mechanics at Meteor Crater, Arizona, *in* Kuiper, G. P. (ed.), The solar system, v. 4, Planets and comets, part 2: Chicago, Illinois, Chicago Univ. Press (in press); also U.S. Geol. Survey open-file report, 55 p., Dec. 28, 1959.

557753 O—60——28

193. PALEOMAGNETISM, POLAR WANDERING, AND CONTINENTAL DRIFT

By RICHARD R. DOELL and ALLAN V. COX, Menlo Park, Calif.

Most recently workers in the field of paleomagnetism have concluded that paleomagnetic evidence indicates movements of the earth's axis of rotation as well as large-scale relative displacements of continents. India and Australia, for example, are thought to have been displaced 5,000 and 1,000 kilometers, respectively, with respect to Europe and North America since Eocene time.

In an attempt to evaluate these interpretations critically, the available paleomagnetic data have been reviewed with special attention to evidence for stability and paleomagnetic applicability of the observed remanent magnetizations; moreover, because of the importance of statistics in these interpretations, statistical analyses have been made of original data when these were available and when the original workers did not use the standard methods.

We have concluded, from the paleomagnetic data now available, that the earth's magnetic field had vastly different characteristics during the following periods: post-early Pleistocene, Oligocene to early Pleistocene, Mesozoic to early Tertiary, late Paleozoic, early Paleozoic, and Precambrian. If paleomagnetic results are to be used as evidence supporting or refuting continental drift, it is first essential to determine the configuration of the earth's magnetic field during the time when contemporaneous rocks from different continents were magnetized. For only a few of the above temporal subdivisions has the configuration of the geomagnetic field been established with sufficient certainty to justify application to the problem of continental drift.

Rocks of late Pleistocene to Recent age have yielded, in scores of studies, directions of magnetization consistent with positions of the geomagnetic pole that frequently differ significantly from that of the present geomagnetic pole, but rarely differ from that of the present geographic pole. These data offer strong evidence in favor of the dynamo theory which relates the earth's main magnetic field to the axis of rotation and they indicate that the present inclined dipole field must be regarded as only a transient feature. Moreover, the directions of magnetization in these rocks are all of the same polarity as the present field, indicating a total absence of processes causing self-reversal of the remanent magnetization.

Measurements on rocks of Oligocene to early Pleistocene age differ from those on late Pleistocene rocks in that about half of the measured directions are nearly 180 degrees from the present field directions. The earth's magnetic field may have undergone at least a dozen complete reversals during this interval, the last occurring in the early Pleistocene. The geomagnetic poles calculated from measurements on Oligocene to early Pleistocene rocks on all continents are grouped around the present geographic poles, with somewhat more scatter than those calculated for late Pleistocene rocks. On the basis of the dynamo theory, polar wandering since the beginning of the Oligocene greater than about 10 degrees (the average confidence interval of most of these measurements) is excluded. These results similarly exclude continental displacements greater than about 10 degrees since the beginning of the Oligocene.

Measurements made on rocks of Precambrian age are in striking contrast with those on rocks of Oligocene age and younger. Of the more than 40 studies reported, not one of the virtual geomagnetic poles (the pole for a dipole field that would give the measured directions of magnetization) lies near the present geographic pole, and an impressive grouping of poles lies near the equator and slightly east of the 180th meridian. Measurements from different continents do not appear to differ significantly, which limits the amount of continental drift since Precambrian time. The North American measurements, however, which far outnumber all the others, do include some widely scattered average pole positions.

Virtual geomagnetic poles calculated from measurements on rocks of early Paleozoic age are much more scattered than the Precambian poles, altogether the latter span a much greater time interval. Continental drift interpretations based on these early Paleozoic data are extremely hazardous.

Of the pre-Tertiary rocks, those of Permian and Carboniferous age yield the most interesting and consistent virtual geomagnetic poles. All but a few of the poles lie between 30 and 40 degrees of latitude; all of the more than 40 poles calculated from measurements made on North American and European rocks lie between 90 and 180 degrees east longitude, whereas the 4 from Australia lie just west of Greenwich. Most of the North American Permian poles are west of the European Permian poles; the Carboniferous poles, however, from both continents are grouped to-

gether. On the assumption that the earth's field was dipolar, these measurements on late Paleozoic rocks have been interpreted in terms of large drift of Australia relative to the northern hemisphere continents since the Paleozoic, and a smaller westward drift of North America relative to Europe. Although this latter interpretation is suggested by the Permian poles, a simple westward drift of North America does not explain both the Permian and Carboniferous data. An interpretation based on continental drift would require rather improbable relative movements between North America and Europe, and more data from Permian and Carboniferous rocks are highly desirable.

Another interesting feature of the Permian data is that, with one poorly documented exception, all of the virtual geomagnetic poles have the same polarity; reversals are entirely absent. Since reversals are abundant in rocks of younger and older ages, the Permian field appears to be unique in having had a constant polarity over millions of years. To explain this fact on the self-reversal hypothesis requires that the special mechanisms and compositions necessary for self-reversal were entirely absent from Permian rocks but abundant in rocks of all other ages, which is rather unlikely.

Although over 50 measurements on rocks of Mesozoic and early Tertiary age have now been reported, no magnetic field configuration has emerged that is comparable in consistency and simplicity with that found in the late Paleozoic and late Tertiary rocks. Some of the virtual geomagnetic poles calculated from these measurements lie near the present geographic poles, but a significantly large number lie in very low latitudes. Although these rather divergent poles have recently been cited in support of large relative displacements of most of the continents, the character of the earth's magnetic field during this time has not, in our opinion, been sufficiently well delineated to justify interpretation of the paleomagnetic data as evidence either for or against continental displacement during this time.

194. PREPARATION OF AN ACCURATE EQUAL-AREA PROJECTION

By Richard R. Doell and Robert E. Altenhofen, Topographic Division, Menlo Park, Calif.

Many of the problems that arise in measuring remanent magnetism and in interpreting paleomagnetic data are essentially problems in spherical trigonometry or three-dimensional geometry. Nor is paleomagnetism unique in posing such problems; others arise in structural geology (Phillips, 1954) and structural petrology (Fairbairn, 1949), and even in the prediction of satellite orbits (Wallace, 1959). When many such problems arise in a given study, especially if not great accuracy is required, it is desirable to replace the tedious analytical methods of solution by graphical aids. By far the most useful of these aids are those which, by one means or another, project an orderly array of points from a hemisphere to a plane. The most common are the *stereographic* projection (often called a "Wulff net") and the *Lambert equal-area* projection (also known as a "Schmidt net").

The principal advantage of the stereographic projection is that it is direction-true—circles on the sphere project as circles on the projection, and angles between lines on the sphere are preserved on the projection. Its main disadvantage is that it is not area-true. The equal-area projection distorts directions and shapes, but, as its name implies, it gives the same areal relations on the projection that were on the sphere. A further slight advantage of the equal-area projection is that the accuracy with which points may be plotted on it is nearly uniform over the entire projection, whereas on the stereographic projection the accuracy of plotting varies by a factor of two.

There is little choice between the two projections when used for solving problems in spherical trigonometry or three-dimensional geometry; any problem that can be solved on one projection can also be solved on the other by exactly the same procedures. Which one is the more desirable depends on the particular problem at hand and the type of presentation desired. Phillips (1954) and Fairbairn (1949, p. 275–296) describe various methods of employing these projections in structural geology and structural petrology and give other references on the use of these projections for general and specialized studies.

The equal-area projection is generally preferable in studies of remanent magnetism and in paleomagnetic

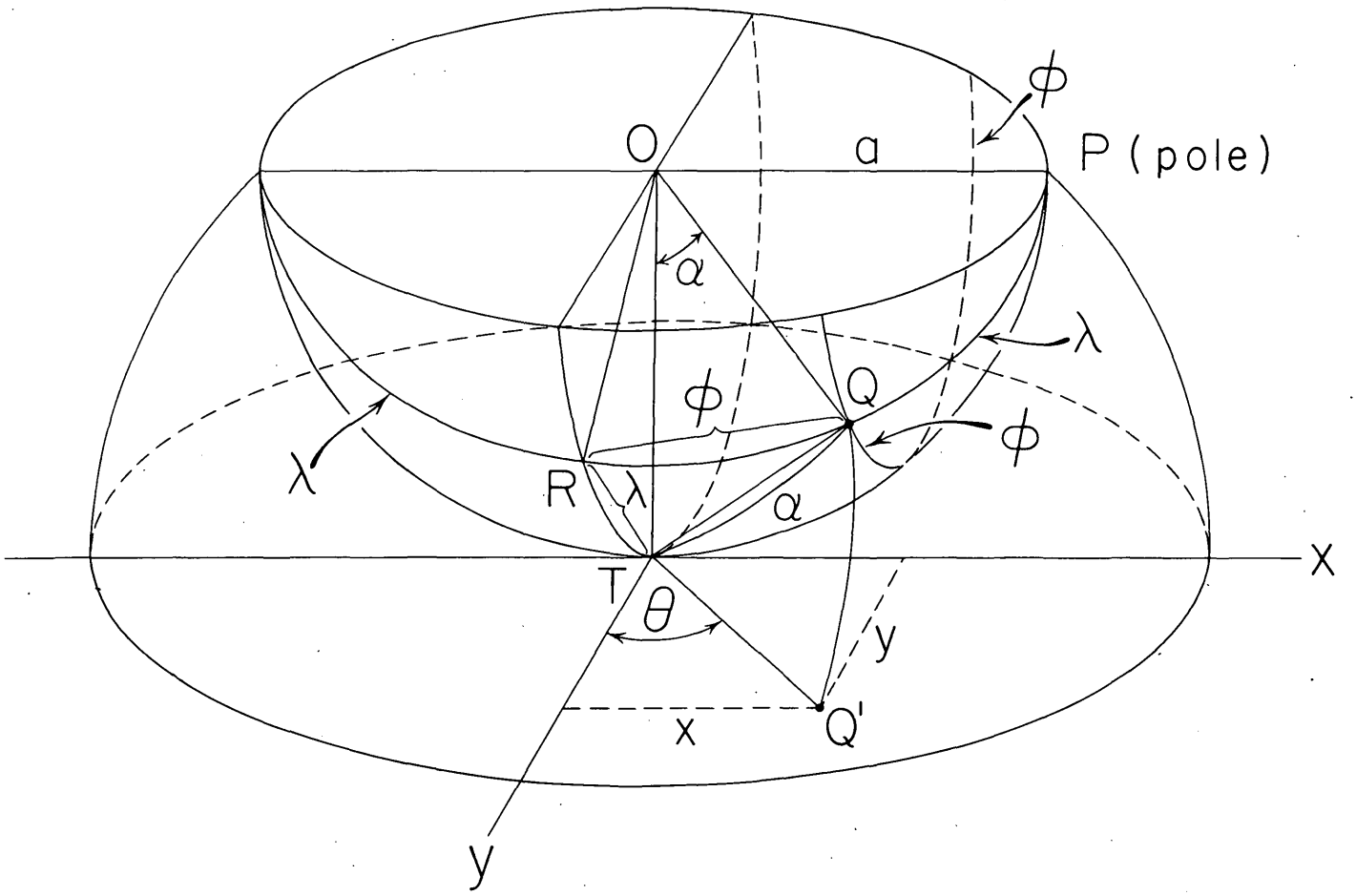

FIGURE 194.1.—Relations in the construction of a Lambert equal-area projection.

research, when it is usually necessary to present and compare groupings of directions. The significance of a separation between groups of directions is more easily determined on the equal-area projection than on the stereographic projection. Graphical methods of solving many of the problems that arise in research on remanent magnetism have been given by Graham (1949).

A Lambert equal-area projection may be constructed by rotating each point of intersection of the parallels and meridians on the hemisphere into a projection plane (a plane tangent to the hemisphere), about the point of tangency, in a plane normal to the projection plane. If the projection plane is tangent to the hemisphere at its pole, the projection is a polar equal-area projection, useful only for presentation of data and not for the solution of problems; and if the point of tangency lies on the equator the projection is called a meridional equal-area projection.

The construction of a meridional projection is depicted in figure 194.1, where xy is the projection plane, T the point of tangency, and Q the intersection of the parallel ϕ and the meridian λ. Q is to be rotated to Q' in the plane xy; $\overline{TQ}$ is used as a radius, and the rotation takes place in the plane TOQ. $\overline{TQ}$ is also the distance from the center of the projection (T) to the projected point Q', and we wish to find the coordinates x, y.

From the law of cosines of spherical trigonometry in ΔPTQ,

(1) $\cos \widehat{TQ} = \cos \widehat{PQ} \cos \widehat{PT} + \sin \widehat{PQ} \sin \widehat{PT} \cos \angle QPT$,

where $\frown$ is used to designate a side of the triangle and $\angle$ is used to designate an angle. Since $\widehat{PT} = \pi/2$, $\sin \widehat{PQ} = \cos \phi$, and $\angle QPT = \lambda$, equation (1) becomes

(2) $\cos \widehat{TQ} = \cos \phi \cos \lambda$.

Letting $\widehat{TQ} = \alpha$, we find the length of the line $\overline{TQ}$ to be

(3) $\overline{TQ} = 2a \sin \alpha/2$,

where a is the radius of the sphere. From the law of sines of spherical trigonometry in ΔTQR,

(4) $\sin \angle RTQ/\sin \phi = \sin \angle TRQ/\sin \alpha$.

Since $\angle RTQ = \theta$ and $\angle TRQ = \pi/2$, equation (4) becomes

(5) $\sin \theta = \sin \phi/\sin \alpha$.

We may then get the desired coordinates from

(6) $x = \overline{TQ} \sin \theta$

$y = \overline{TQ} \cos \theta$.

Since each quadrant of the projection is a mirror image of the adjacent quadrants, only the points in one quadrant of the hemisphere need be computed, but even so there are 8011 intersections of the integral-degree parallels and meridians in a single quadrant. For this reason the computations for the projection described here were made by Walter Anderson with the Geological Survey's Datatron, which computed the 8011 coordinate pairs in 3½ hours.

The points for one quadrant were then plotted on a stable transparent mylar sheet by a rectilinear coordinate plotter. Finally, four quadrants were fitted together by precise photographic methods to furnish a master negative for the entire projection. Positive copies on stable film may now be obtained by standard photographic means.

For ease of use, a short segment of the meridian is drawn through every other point on the 10° longitude lines, and every fifth longitude and latitude intersection (except those north and south of 75°) is marked by a small cross.

Near the center of the 15-inch standard-size projection the integral degree points are 0.093 inch apart, and near the edges, 0.068 inch—averaging about 0.08 inch. Because positions on the projection may be estimated to about one-tenth degree, or 0.008 inch on the average, the points were plotted to an accuracy of 0.001 inch. No distortions, misalignments, or composing errors greater than a few thousandths of an inch have been detected, so that calculations to an accuracy of one-tenth degree may be made with confidence.

REFERENCES

Fairbairn, H. W., 1949, Structural petrology of deformed rocks, 2nd ed.: Cambridge, Mass., Addison-Wesley Press, 344 p.

Graham, J. W., 1949, The stability and significance of magnetism in sedimentary rocks: Jour. Geophys. Research, v. 54, p. 126–136.

Phillips, F. C., 1954, The use of stereographic projection in structural geology: London (publishers, Edward Arnold), 86 p.

Wallace, R. E., 1959, Graphic solution of some earth satellite problems by use of the stereographic net: Jour. British Interplanetary Soc., v. 17, p. 120–123.

MINERALOGY, GEOCHEMISTRY, AND PETROLOGY

195. CRYSTAL HABIT OF FRONDELITE, SAPUCAIA PEGMATITE MINE, MINAS GERAIS, BRAZIL

By Marie Louise Lindberg, Washington, D.C.

Frondelite, $Mn''Fe_4'''(PO_4)_3(OH)_5$, was described some years ago as a new mineral from the Sapucaia pegmatite mine, Minas Gerais, Brazil (Lindberg, 1949). The specimens on which the description was based consisted of brown botryoidal masses with a radiating fibrous structure. Frondelite forms an isomorphous series with rockbridgeite, $Fe''Fe_4'''(PO_4)_3(OH)_5$. Botryoidal masses of minerals in this series are of widespread occurrence, but no single crystals of any of them have yet been described.

Minute, doubly terminated, stubby crystals of frondelite (fig. 195.1) with high luster have been found, together with crystals of avelinoite, (=cyrilovite) (Lindberg, 1957a), metastrengite, and leucophosphite (Lindberg, 1957b). These form loose aggregates of sugary grains in a vuggy zone in the larger botryoidal masses of frondelite. The crystals are up to 0.2 mm in length. The crystal forms include {100}, {010}, {110}, and {101} (table 195.1).

TABLE 195.1.—*Morphological data for frondelite*

Crystal class: 222 Space group $B22_12$

Calculated data

$a:b:c = 0.8166:1:0.3063$ $p_0:q_0:r_0 = 0.3751:0.3063:1$

$q_1:r_1:p_1 = 0.8166:2.666.1$ $r_2:p_2:q_2 = 3.265:1.225:1$

Forms	φ	ρ=C	φ1	ρ1=A	φ2	ρ2=B
010	0°00′	90°00′	90°00′	90°00′	--------	0°00′
100	90°00′	90°00′	--------	0°00′	0°00′	90°00′
110	50°46′	90°00′	90°00′	39°14′	0°00′	50°46′
101	90°00′	20°34′	0°00′	69°26′	69°26′	90°00′

Frondelite is orthorhombic; its space group is $B22_12$; $a=13.89$, $b=17.01$, $c=5.21$ A (Lindberg, 1949). Similarities in the powder pattern to that of manganoan lipscombite, $(Mn'',Fe'')Fe'''_2(PO_4)_2(OH)_2$, (Lind-

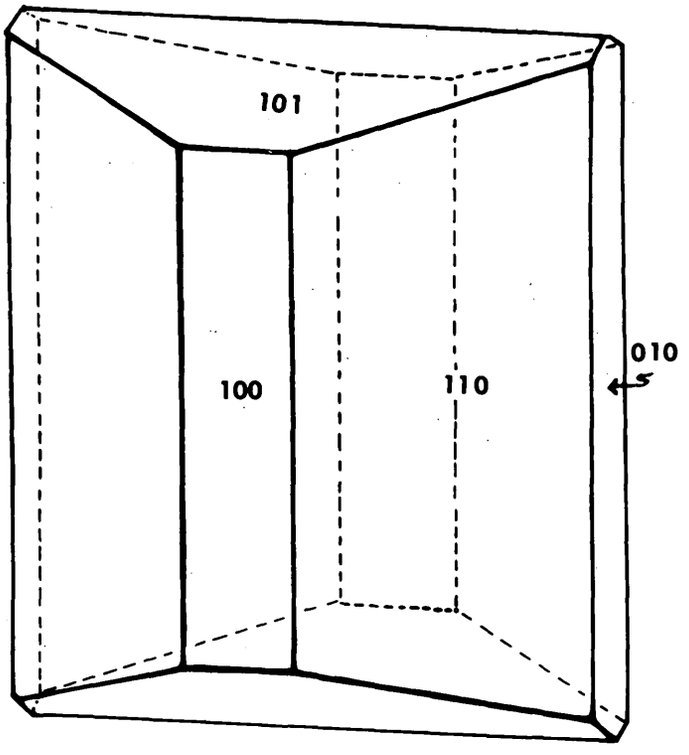

FIGURE 195.1.—Crystal habit of frondelite.

berg and Pecora, 1958) suggest that the crystal structure may be derived from that of lipscombite (Katz and Lipscomb, 1951) by systematic omission in the filling of octahedral and tetrahedral spaces, in a manner similar to that by which the crystal structure of the lazulite-scorzalite-barbosalite series can be derived from that of lipscombite (Lindberg and Christ, 1959). Intensity data for the determination of the crystal structure are being collected from the frondelite crystals.

REFERENCES

Katz, Lewis, and Lipscomb, W. N., 1951, Crystal structure of iron lazulite, a synthetic mineral related to lazulite: Acta Cryst., v. 4, p. 345–348.

Lindberg, M. L., 1949, Frondelite and the frondelite-rockbridgeite series: Am. Mineralogist, v. 34, p. 541–549.

——— 1957a, Relationship of the minerals avelinoite, cyrilovite, and wardite: Am. Mineralogist, v. 42, p. 204–213.

——— 1957b, Leucophosphite from the Sapucaia pegmatite mine, Minas Gerais, Brazil: Am. Mineralogist, v. 42, p. 214–221.

Lindberg, M. L., and Christ, C. L., 1959, Crystal structures of the isostructural minerals lazulite, scorzalite, and barbosalite: Acta Cryst., v. 12, p. 695–697.

Lindberg, M. L., and Pecora, W. T., 1958, Phosphate minerals from the Sapucaia pegmatite mine, Minas Gerais: Soc. Brasileira Geologia Bol., v. 7, no. 2, p. 5–14.

196. SOME CHARACTERISTICS OF GLAUCONITE FROM THE COASTAL PLAIN FORMATIONS OF NEW JERSEY

By JAMES P. OWENS and JAMES P. MINARD, Washington, D.C.

Glauconite concentrates were collected from most of the formations of the New Jersey coastal plain near Trenton, N.J. A sample was collected from each of 9 formations of Late Cretaceous to early Tertiary age, and 2 samples were taken from the Cape May formation of Quaternary age. The 11 samples were subjected to a variety of tests to determine whether chemical or physical properties provide criteria for distinguishing between primary and reworked glauconite. A method for differentiating the two types is proposed, based chiefly on grain morphology and chemical characteristics. In addition, it is proposed that the reworked glauconite can be further subdivided into two types: the marine detrital and the fluvial detrital.

All the samples were concentrated by magnetic separation, and final purification was made by a heavy liquid separation.

BINOCULAR EXAMINATION

The dominant grain morphology for each concentrate was determined microscopically. The major types were found to be (a) rounded or subrounded grains with smooth to grooved surfaces (botryoidal) and (b) elongate grains which appear to be stacks of green micaceous plates—"accordion" forms of Galliher (1935) or "tabular" forms of Light (1952).

All the concentrates consist chiefly of the rounded grains, but the presence of the accordion forms in quantity in some of the suites suggests that much of the glauconite is primary. High concentrations of accordion forms occur in the Merchantville and Marshalltown formations and in the Red Bank sand.

The rounded types are decidely larger than the other types, commonly occurring as coarse sands, whereas the accordion forms rarely exceed medium sand size.

CHEMICAL ANALYSES

The concentrates were chemically analyzed and the structural formulas computed for each (table 196.1). The samples containing abundant accordion forms show a significant deficiency in the total interlayer ions as compared with the reworked sands.

The glauconite samples from the reworked fluvial sands of Quaternary age also show a much higher ferric to ferrous ratio than the older primary and reworked sands of marine origin.

X-RAY STUDIES

X-ray diffractometer studies were undertaken to determine the homogeneity of the glauconite concentrates and the degree of ordering in the structure (following Burst's (1958) classification).

Contamination by other minerals such as clay and quartz was notably low. Small amounts of apatite were detected in some samples, however, particularly those from the Manasquan and Mount Laurel formations. Because of this, the P_2O_5 determined by chemical analysis in all the concentrates was combined with an equal amount of CaO before computing the formulas.

Four X-ray classes of glauconite were defined by Burst (1958), two of these, the "well-ordered" (1 M mica structure) and "disordered" (1 Md mica structure), reflected a high degree of homogeneity for this mineral. X-ray analyses of all the concentrates showed them to be either the "well-ordered" or "disordered" types.

No consistent relationship could be established by this method to differentiate between the primary and reworked types.

INFRARED ANALYSES

An attempt was made to characterize the glauconites by means of infrared analyses. The results obtained from all the specimens are fairly similar, as was true with the X-ray analyses. A typical pattern has well-developed troughs at the wave lengths 9.4 and 10.2 microns, and a weak reflection at 12.5 microns. Small differences in the magnitude of the troughs are espe-

TABLE 196.1.—*Structural formulas computed from chemical analyses of glauconite concentrates from formations of the coastal plain*

Pleistocene	Cape May formation:		
	$[K_{.667}Na_{.013}][Mg_{.333}Fe''_{.088}Fe'''_{1.327}Al_{.249}Ti_{.075}][Si_{3.507}Al_{.493}O_{10}](OH)_2$		
	$\Sigma=.680$	$\Sigma=2.07$	$\Sigma=4.00$
	Cape May formation:		
	$[K_{.70}Na_{.009}][Mg_{.38}Fe''_{.07}Fe'''_{1.22}Al_{.38}Ti][Si_{3.62}Al_{.38}O_{10}](OH)_2$		
	$\Sigma=.709$	$\Sigma=2.02$	$\Sigma=4.0$
Miocene	Kirkwood formation:		
	$[K_{.747}Na_{.008}][Mg_{.47}Fe''_{.536}Fe'''_{.90}Al_{.34}Ti][Si_{3.76}Al_{.24}O_{10}](OH)_2$		
	$\Sigma=.755$	$\Sigma=2.046$	$\Sigma=4.0$
Eocene	Manasquan formation:		
	$[K_{.722}Na_{.018}Ca_{.10}][Mg_{.46}Fe''_{.16}Fe'''_{.925}Al_{.42}Ti_{.003}][Si_{3.69}Al_{.31}O_{10}](OH)_2$		
	$\Sigma=.84$	$\Sigma=1.968$	$\Sigma=4.0$
Paleocene	Vincentown formation (basal member):		
	$[K_{.65}Na_{.01}Ca_{.08}][Mg_{.38}Fe''_{.23}Fe'''_{1.03}Al_{.31}Ti_{.05}][Si_{3.67}Al_{.33}O_{10}](OH)_2$		
	$\Sigma=.74$	$\Sigma=2.00$	$\Sigma=4.00$
	Hornerstown sand:		
	$[K_{.764}Na_{.009}Ca_{.007}][Mg_{.384}Fe''_{.204}Fe'''_{1.08}Al_{.36}Ti_{.003}][Si_{3.68}Al_{.32}O_{10}](OH)_2$		
	$\Sigma=.780$	$\Sigma=2.031$	$\Sigma=4.00$
Upper Cretaceous	Red Bank sand:		
	$[K_{.636}Na_{.009}Ca_{.01}][Mg_{.35}Fe''_{.18}Fe'''_{1.0}Al_{.48}Ti_{.004}][Si_{3.68}Al_{.32}O_{10}](OH)_2$		
	$\Sigma=.655$	$\Sigma=2.014$	$\Sigma=4.00$
	Navesink formation:		
	$[K_{.678}Na_{.009}Ca_{.05}][Mg_{.35}Fe''_{.25}Fe'''_{1.1}Al_{.34}Ti_{.003}][Si_{3.69}Al_{.31}O_{10}](OH)_2$		
	$\Sigma=.737$	$\Sigma=2.04$	$\Sigma=4.0$
	Mount Laurel sand:		
	$[K_{.727}Na_{.004}Ca_{.03}][Mg_{.31}Fe''_{.21}Fe'''_{1.14}Al_{.36}Ti_{.006}][Si_{3.59}Al_{.41}O_{10}](OH)_2$		
	$\Sigma=.761$	$\Sigma=2.026$	$\Sigma=4.0$
	Marshalltown formation:		
	$[K_{.634}Na_{.008}Ca_{.015}][Mg_{.33}Fe''_{.18}Fe'''_{.91}Al_{.58}Ti_{.004}][Si_{3.73}Al_{.27}O_{10}](OH)_2$		
	$\Sigma=.657$	$\Sigma=2.004$	$\Sigma=4.0$
	Merchantville formation:		
	$[K_{.621}Na_{.009}Ca_{.025}][Mg_{.293}Fe''_{.16}Fe'''_{.99}Al_{.58}Ti_{.005}][Si_{3.61}Al_{.39}O_{10}](OH)_2$		
	$\Sigma=.655$	$\Sigma=2.028$	$\Sigma=4.0$
	Idealized formula (Hendricks and Ross): $(K, Ca½, Na)_{.84}(Al_{1.47}Fe'''_{.97}Fe''_{.19}Mg_{.4})(Si_{3.65}Al_{.35}O_{10})(OH)_2$		
	$\Sigma=.84$	$\Sigma=2.03$	$\Sigma=4.00$

cially noted from the glauconite in the Kirkwood. The reason for this difference is still not known, but a possible explanation may be in the Fe''' to Fe'' ratio. Of all the samples, this ratio is lowest in the Kirkwood, about 3:1. The ratio in most specimens ranges from 6: or 8:1, but in the fluvially reworked glauconites it is as much as 20:1.

EXCHANGE CAPACITY STUDIES

The exchange capacity for glauconite from two of the Coastal Plain formations (table 196.2) shows the stability of the major interlayer ion, potassium, in the glauconite structure.

TABLE 196.2.—*Exchange capacity and exchangeable cations of glauconite concentrates from Sewell, N.J.*

[Analyst, Dorothy Carroll]

Formation	Sieve size	Meq per 100 g							Total K_2O in sample (percent)
		Na	K	Ca	Mg	Total (sum)	A	B	
Hornerstown	+35	0.06	0.03	15.4	9.8	25.3	21	22.3	7.4
Hornerstown	+60	.12	.02	15.4	7.0	22.4	22.0	24.0	
Navesink	+35	.05	.02	15.8	4.9	20.8	23.0	26.4	7.2
Navesink	+60	.03	.02	15.4	5.6	21.0		22.8	
Navesink	+120	.07	.02	18.5	7.7	26.3	25	26.4	

A = Determined after leaching with NH_4Cl.
B = Colorimetric manganese method.

These data suggest that if a primary grain (low but stable interlayer ion total) is reworked in an environment where the necessary interlayer ions are readily available, an increase in the interlayer summation should be expected. This is clearly shown in table 196.1.

SUMMARY

In summary, those glauconites with low interlayer ion summation, medium to fine grain size, and large concentrations of accordion forms are thought to represent primary types. The glauconites of the Merchantville, Marshalltown, and Red Bank are chiefly this type. Those glauconites with high interlayer ion summations, rounded shapes, and coarse grain sizes, are considered to be reworked marine types. The glauconites of the Mount Laurel, Navesink, Hornerstown, Vincentown, and Manasquan are mostly this type. Those glauconites with a high Fe''' to Fe'' ratio are considered to be subaerially altered and are of fluvial origin. The glauconite of the Cape May is this type.

REFERENCES

Burst, J. F., 1958, Mineral heterogeneity in glauconite pellets: Am. Mineralogist, v. 43, p. 481–497.

Galliher, E. W., 1935, Geology of glauconite: Am. Assoc. Petroleum Geologists Bull., v. 19, no. 11, p. 1569–1601.

Light, Mitchell, 1952, Evidence of authigenic and detrital glauconite: Science, v. 115, no. 2977, p. 73–75.

197. X-RAY DETERMINATIVE CURVE FOR NATURAL OLIVINE OF COMPOSITION Fo_{80-90}

By EVERETT D. JACKSON, Menlo Park, Calif.

X-ray diffraction determinative curves for the entire range of olivine composition between forsterite and fayalite have recently been published by Yoder and Sahama (1957, p. 475–491), Eliseev (1957, p. 657–670), and Heckroodt (1958, p. 377–386). Yoder and Sahama state that the error attached to an individual estimate of composition on their determinative curve is ±3 or 4 mol percent Fo. Although Eliseev and Heckroodt have not carried out statistical analysis of their data, the errors in their curves appear to be of the same order of magnitude. A more precise curve has been constructed to determine the Fo content of a large number of olivines from the Peridotite member of the Stillwater complex, where the entire range of olivine composition is only 10 mol percent.

Olivine concentrates from five specimens of olivine-bearing rocks of the Peridotite member were crushed to −325 mesh and cleaned by centrifuging in Clerici solution. Optical grain counts indicate that the samples thus obtained are more than 99 percent pure olivine. Two of the samples were split to make hidden duplicates, which were then treated as separate samples. All seven samples were analyzed by a spectrogravimetric method devised by Stevens and others (Art. 228), and the Fo content was calculated as the atomic ratio of Mg to total octahedral cations. Splits of each of the 7 samples were further divided into 3 subsamples for X-ray examination. These subsamples were assigned random numbers to determine run order, mixed with about 10 percent lithium fluoride (reagent), and

prepared as slurrys on cover glasses 7/8 inch in diameter. The cover glasses containing the slurrys were placed in a rotating sample holder, and sample heights were adjusted by placing prepared disks of the proper thickness under the sample. Each of the 21 subsamples was allowed to oscillate twice up and down between 62° and 67°2θ on a Norelco diffractometer using copper radiation and a nickel filter. One degree divergent and scatter slits were used; the receiving slit was 0.006 inch wide, the scan speed 1/4° per minute, and the chart speed 1 inch per degree 2θ. The distance between the olivine (062) peak and the lithium fluoride (220) peak was measured directly in degrees from the charts and compiled, and means and standard deviations of Δ 2θ were calculated from them. Fo content, calculated from the analyses, and X-ray data are summarized in table 197.1.

TABLE 197.1.—*X-ray measurements and Fo content of seven olivine samples from the Stillwater complex*

Field No.	Lab. No.	Fo [1]	Mean of 12 readings $\Delta 2\theta$ (062) olivine-(220) lithium fluoride (degrees) [2]	Standard deviation of 12 readings (degrees) [3]
55MV-49	9	89.7	2.857	0.0014
55MV-40	8	85.8	2.926	.0010
55BE-44 [4]	11	85.8	2.928	.0013
55MV-26	6	84.9	2.947	.0025
55BE-37 [5]	10	84.7	2.945	.0019
55MV-29	7	84.0	2.958	.0015
52MV-9	5	80.5	3.019	.0015

[1] Atomic ratio of Mg to total octahedral cations.
[2] For Cu radiation.
[3] There appear to be no significant run and smear differences.
[4] Hidden duplicate of 55MV-40.
[5] Hidden duplicate of 55MV-26.

The information in table 197.1 forms the basis for the determinative curve in figure 197.1. It was most convenient to plot X-ray measurements directly as $\Delta 2\theta$ (Cu) on the ordinate. A regression analysis of the data in table 197.1 was made, considering each of the seven measurement sets to be individual determinations and taking the chemically derived Fo value as the independent variable. The equation for the straight line curve is:

$$\Delta 2\theta \text{ (062) olivine—(220) lithium fluoride} = 4.4587 - 0.017855 \text{ Fo}$$

The 95 percent confidence intervals (based on assumed normal distribution) for the regression equation are $\pm 0.006°2\theta$ at 85 mol percent Fo and $\pm 0.0075°2\theta$ at 80 and 90 mol percent Fo. These limits correspond to an uncertainty of about ± 0.35 mol percent Fo at the center of the curve and ± 0.43 mol percent Fo at the limits of the curve.

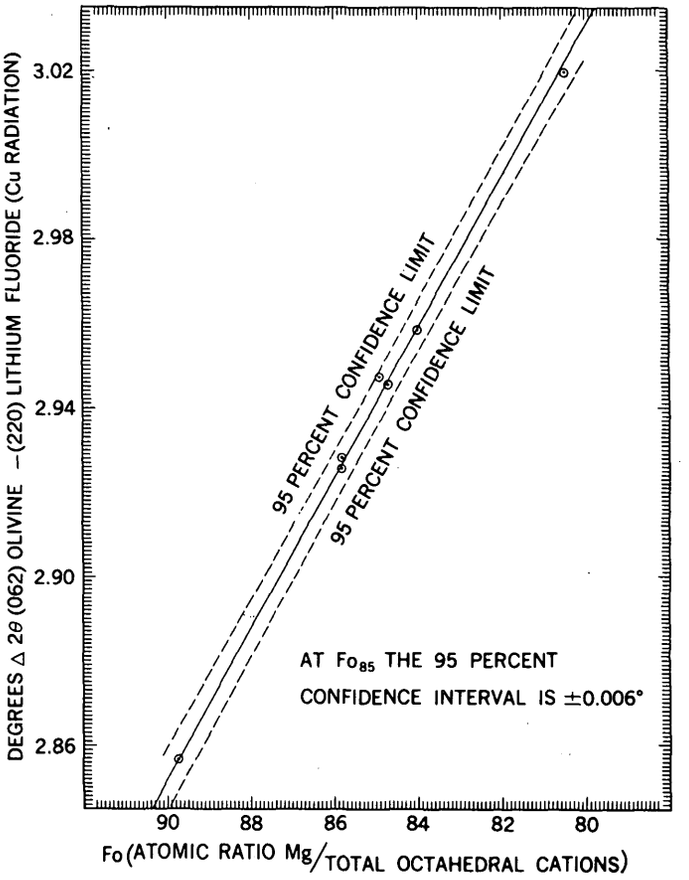

FIGURE 197.1.—X-ray determinative curve for natural olivine of composition Fo_{80-90}.

The absolute values of d_{130} were also determined by means of a silicon internal standard, after the method of Yoder and Sahama (1957, p. 475–491), but the standard deviations and the standard error obtained by this method were considerably greater. Measurements of the (062) peak are inherently more precise than measurements of (130), because (062) appears at a larger 2θ angle and because the (062) spacing changes more over the range forsterite-fayalite (Eliseev, 1957, p. 660–661). Disadvantages of (062) as compared with (130) are that it is less intense and more subject to interference from reflections of some commonly associated minerals.

The determinative curve shown in figure 197.1 is based on olivine from a single petrographic province. Yoder and Sahama (1957, p. 487) have shown that X-ray parameters of olivines are sensitive to variation in minor element content and possibly to temperature of formation. The curve therefore should be used with caution in estimating or comparing compositions of olivine from diverse environments.

REFERENCES

Eliseev, E. N., 1957, Rentgenometricheskoye izucheniye mineralov isomorfnogo ryada forsterit-fayalit [X-ray investigation of the minerals of the isomorphous series forsterite-fayalite]: Zapiski Vsesoyuznogo Mineralogicheskogo Obshchestva, v. 86, no. 6, p. 657–670.

Heckroodt, R. O., 1958, An X-ray method for the determination of olivine: Geol. Soc. South Africa Trans. and Proc., v. 61, p. 377–386.

Yoder, H. S., Jr., and Sahama, Th. G., 1957, Olivine X-ray determinative curve: Am. Mineralogist, v. 42, p. 475–491.

198. ACIDIC PROPERTIES OF FITHIAN "ILLITE"

By Dorothy Carroll and Alfred M. Pommer, Washington, D.C.

Work done partly in cooperation with the U.S. Atomic Energy Commission

If the pH values obtained by discontinuous potentiometric titration of the H-form of Fithian "illite" (A.P.I. reference clay mineral No. 35) are plotted against log NaOH concentration, curves are obtained that are unlike those found for H-montmorillonite (Pommer and Carroll, 1960). The principal differences are in slope and in the positions of equivalence points for the two clay acids which, theoretically, should be present. The pH values obtained change with time, apparently because the "illite" reacts slowly with the base. These differences are shown in figure 198.1.

Garrels and Christ (1956) showed that "illite" behaves as a mixture of two clay acids, and suggested that both interlayer and edge sites of the mineral may contribute to its acidity. Hendricks (1945) believes that cation exchange in micaceous minerals is due primarily to neutralization of charges at the surfaces and edges of mineral platelets, and secondarily to replacement of cations in between the sheets. These sheets are firmly held together by K^+ ions as in muscovite, but as the K^+ ions are leached out by weathering other cations enter to make up the total positive charge required to keep the mineral electrically neutral. The total exchange capacity of these micaceous minerals and the ease with which their exchangeable cations can be replaced is very much less than for montmorillonite.

The structural formula of the "illite" sample used for the titration was calculated from a chemical analysis by W. W. Brannock. The charge deficiency of the cations is almost equally divided between the octahedral and tetrahedral layers:

$$\overset{-.34}{(Al_{1.44}\overset{3+}{Fe}_{.32}\overset{2+}{Mg}_{.19})}\overset{-.33}{(Si_{3.67}Al_{.33})}O_{10}(OH)K_{2.46}(Ca,Na)_{.13}$$

The exchange capacity determined experimentally, 26 milliequivalents per 100 grams, agrees satisfactorily with the calculated figure of 20 milliequivalents per 100 grams.

In recording successive pH values for the 32 samples in the discontinuous titration (table 198.1) it became apparent that the values were steadily decreasing. Part of this decrease was undoubtedly due to reaction of atmospheric CO_2 with the NaOH, as explained elsewhere (see Art. 199). The pH figures for the "illite" sample suspended in distilled water decreased steadily from 5.0 to 2.90 over a period of 75 days, and this lowering of pH values cannot have resulted from CO_2 absorption by the water, because the pH values are much too low. Apparently the "illite" releases H ions very slowly.

The data plotted in figure 198.1, curve (*A*), obtained after 1 day, showed that the "illite" reacted to the NaOH as a monobasic acid. The pK value was calculated to be 6.9 and this value is not consistent with the low pH of the distilled water in contact with "illite". The material even initially appeared to have a higher acidity than an acid with a pK of 6.9. Curve (*B*) has no definite inflection point; in fact it is almost a straight line. The "illite" here reacts as a substrate with an infinite number of exchange sites, and the exchange can be considered a surface reaction. Curve (*C*), obtained as a result of 75 days reaction of the "illite" samples with NaOH solutions, shows three distinct breaks. This curve resembles somewhat vaguely that obtained for H-montmorillonite (Pommer and Carroll, 1960). Its principal intersection point is at pH 3.8; an inflection point appears at pH 5.6. The first part of each of the three titration curves is similar in slope, although at different pH values. The pH values suggest that some of the H^+ ions are very loosely

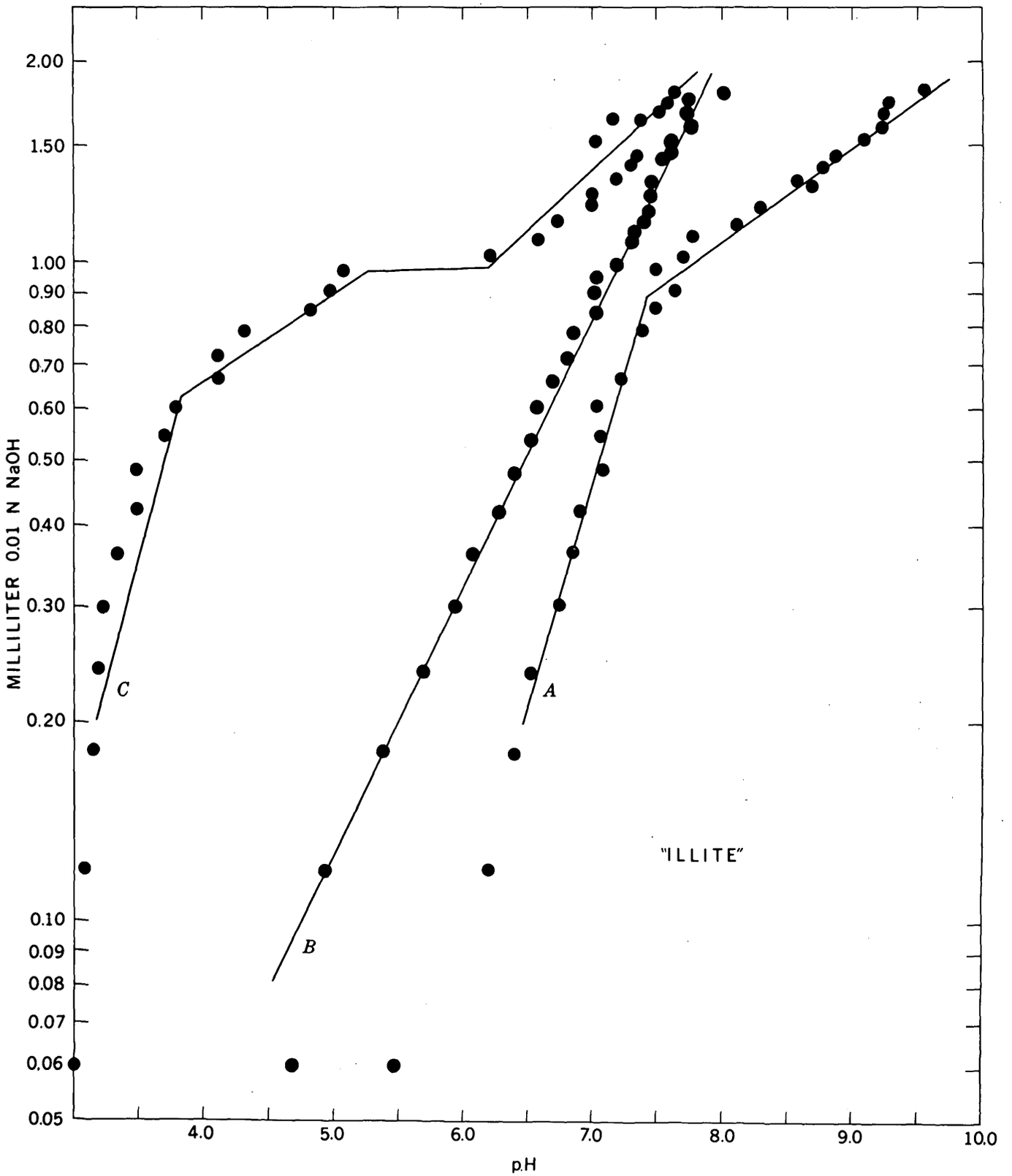

FIGURE 198.1.—Discontinuous potentiometric titration of 1-percent suspensions of H-"illite" with 0.01*N* NaOH (each sample has a volume of 6.8 ml). *A*, Curve obtained 1 day after NaOH increments were added; *B*, average curve for the succeeding 5 days; *C*, curve obtained after NaOH had been in contact with the "illite" samples for 75 days.

TABLE 198.1.—*pH values for the titration of 70 mg samples of H-"illite" with 0.01 N NaOH*

[Total volume per sample is 6.8 ml. n.d.=not determined.]

Sample	NaOH added (ml)	pH after number of days indicated							Na ppm per 100 ml [4]
		1 [1]	3	4	6	7	3–7 [2]	75 [3]	
1	nil	5.0	4.70	4.55	4.31	4.08	4.40	2.90	[5] 0.71
2	0.06	5.45	5.00	4.80	4.60	4.45	4.71	3.00	.68
3	.12	6.20	4.75	5.25	5.01	4.70	4.92	3.10	.81
4	.18	6.40	5.90	5.20	5.31	5.05	5.36	3.15	.86
5	.24	6.52	6.02	5.85	5.65	5.30	5.70	3.20	.67
6	.30	6.75	6.32	6.02	5.90	5.40	5.91	3.25	.77
7	.36	6.85	6.45	6.10	6.05	5.62	6.05	3.35	.25
8	.42	6.90	6.60	6.21	6.28	6.00	6.27	3.51	.77
9	.48	7.10	6.60	6.45	6.45	6.05	6.38	3.50	.84
10	.54	7.05	6.63	6.55	6.58	6.33	6.52	3.71	.91
11	.60	7.05	6.75	6.55	6.65	6.25	6.55	3.81	.94
12	.66	7.25	6.70	6.65	6.83	6.50	6.67	4.15	1.16
13	.72	7.30	6.95	6.69	6.90	6.60	6.78	4.13	1.20
14	.78	7.42	6.97	6.75	7.03	6.72	6.86	4.35	4.19
15	.84	7.51	7.10	6.98	7.12	6.83	7.01	4.85	4.27
16	.90	7.65	7.10	6.97	7.15	6.82	7.01	5.00	4.09
17	.96	7.50	7.20	6.95	7.23	6.88	7.06	5.10	4.13
18	1.02	7.70	7.25	7.05	7.37	7.05	7.18	6.20	4.13
19	1.08	7.80	7.31	7.25	7.45	7.10	7.27	6.60	n.d.
20	1.14	8.12	7.35	7.30	7.40	7.13	7.30	6.75	4.21
21	1.20	8.30	7.43	7.35	7.51	7.20	7.37	7.00	1.16
22	1.26	8.70	7.62	7.45	7.55	7.25	7.46	7.05	2.24
23	1.32	8.58	7.50	7.40	7.60	7.38	7.47	7.20	1.96
24	1.38	8.80	7.08	7.51	7.65	7.41	7.56	7.30	1.92
25	1.44	8.89	7.80	7.55	7.69	7.42	7.61	7.35	3.20
26	1.50	9.10	7.75	7.55	7.77	7.45	7.63	7.05	4.30
27	1.56	9.25	7.83	7.67	7.71	7.52	7.68	7.45	4.42
28	1.62	9.30	7.98	7.70	7.82	7.55	7.76	7.15	4.44
29	1.68	9.25	7.80	7.77	7.80	7.61	7.74	7.52	4.53
30	1.74	9.30	8.00	7.81	7.90	7.65	7.74	7.60	4.33
31	1.80	9.55	8.20	7.98	8.00	7.75	7.98	7.65	4.45
32 [6]	1.80	10.61	9.68	9.18	8.50	8.20	8.89	8.12	4.89

[1] Readings for curve *A*, figure 198.1.
[2] Average of 3–7 days. Readings for curve *B*, figure 198.1.
[3] Readings for curve *C*, figure 198.1.
[4] Determined in 100 ml filtrate removed from "illite" after 75 days.
[5] Sample 1, blank; contains 70 mg illite in water.
[6] Sample 32, blank; contains 1.8 mg. 0.01 *N* NaOH in water but no "illite."

held by the "illite". The lowering of the inflection point from curve (a) to curve (c) appears to show a decrease in the exchange capacity, perhaps caused by flocculation and consequent loss of exchange sites by the clays.

The solutions were removed from the "illite" samples and sodium was determined in the filtrates (table 198.1, column 7). The results indicate that during addition of the first 12 increments of sodium hydroxide the "illite" removed sodium from the solutions. The solutions from samples 14 to 31 contained considerably higher amounts of sodium than those from the other samples.

The results of the potentiometric titration emphasize the difficulty and slowness with which micaceous minerals react, probably because of the presence of K^+ ions that hold the octahedral sheets firmly together. Fithian "illite" is much more compact than montmorillonite and has a high inherent charge (Marshall, 1949, p. 22). Chemical analyses of micaceous minerals show that they form a series in which the exchange reaction will increase as K^+ ions are removed and are replaced by other cations such as Ca^{2+} and Mg^{2+}.

REFERENCES

Garrels, R. M., and Christ, C. L., 1956, Application of cation exchange reactions to the beidellite of the Putnam silt loam soil: Am. Jour. Sci., v. 254, p. 372–379.

Hendricks, S. B., 1945, Base exchange of crystalline silicates: Indus. and Eng. Chemistry, v. 37, p. 625–630.

Marshall, C. E., 1949, The colloid chemistry of the silicate minerals: New York, Academic Press, 195 p.

Pommer, A. M., and Carroll, Dorothy, 1960, Interpretation of potentiometric titration of H-montmorillonite: Nature, v. 185, p. 595–596.

199. CARBON DIOXIDE AND ALUMINA IN THE POTENTIOMETRIC TITRATION OF H-MONTMORILLONITE

By DOROTHY CARROLL, Washington, D.C.

Work done in cooperation with the U.S. Atomic Energy Commission

Interpretation of the results of potentiometric titrations of hydrogen-clays with a base may be somewhat uncertain for two reasons: (a) pH values are influenced by the chemical reaction of atmospheric CO_2 with the base; and (b) alumina in the exchange positions of the mineral may interfere with the replacement of H^+ ions by other cations in the neutralization of the clay acid.

Discontinuous potentiometric titrations of H-montmorillonite (Pommer and Carroll, 1960) with NaOH yield values in the range of pH 4 to 12. A number of blanks containing NaOH solutions without clay samples were inserted among the samples to show the effect of their reaction with CO_2. The samples were all in glass weighing bottles with tightly closed but not air-

tight covers. The bottles were opened to make pH reading. In accordance with the experimental design the pH was determined after the solutions had been mixed and allowed to stand for 1 day and for 12 days (table 199.1).

TABLE 199.1.—*pH values of solutions to which increments of 0.1N* NaOH *were added*

[Total volume of each is 6.2 ml]

Sample	NaOH added (ml)	NaOH, micromoles in solution	pH values after number of days indicated					Difference in pH in 11 days
			1	2	5	7	12	
1a	0.02	0.32	7.60	6.40	6.10	6.10	6.05	1.55
6a	.10	1.61	9.85	9.50	7.80	7.45	7.20	2.65
12a	.22	3.54	10.50	10.30	9.75	9.15	8.00	2.50
18a	.44	7.10	11.00	10.95	10.90	10.60	9.70	1.30
24a	.68	10.96	11.50	11.35	11.40	11.35	11.35	.15
30a	.92	14.83	11.75	11.58	11.52	11.65	11.65	.10
38	1.20	19.35	11.85	11.65	11.75	11.75	11.85	nil

A semilog plot of pH values against concentration of NaOH shows the effect of CO_2 in this particular titration by the divergence of the lines for the first and second series of pH readings (fig. 199.1).

A plot such as figure 199.1 can be used to estimate the maximum deviations due to CO_2 absorption. These values are helpful in deciding whether CO_2 absorption affects the results of such titration experiments to a significant degree.

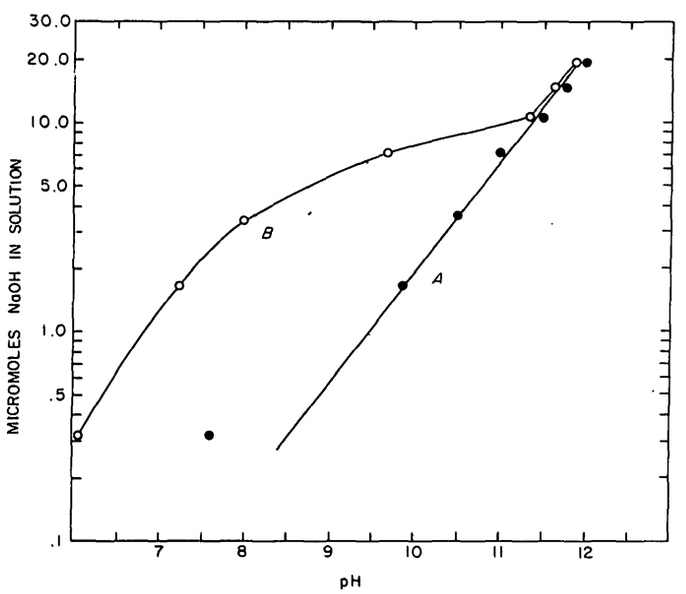

FIGURE 199.1.—Effect of reaction of CO_2 with very dilute NaOH solutions in closed glass containers. *A*, pH readings 1 day after mixing; *B*, pH readings 12 days after mixing. The lowest point on curve *A* indicates a lower pH than was theoretically expected, because reaction with CO_2 is more strongly shown in such dilute solutions than in more concentrated solutions.

The figures in table 199.1 show that under experimental conditions, even with carefully closed containers, there may be appreciable lowering of pH values in potentiometric titrations of H-clays. It has been found, however, that this does not necessarily interfere with the interpretation of curves for clay acids.

The second difficulty that may occur in titration of an H-clay with a base is caused by movement of alumina from the octahedral layer of the mineral to the exchange positions during the preparation of the H-clay. The clay has then become an H-Al-clay and behaves differently from an H-clay on titration with a base. Paver and Marshall (1934) first drew attention to the release of Al_2O_3 from clay minerals by electrodialysis. Subsequently various investigators (Low, 1955; McAuliffe and Coleman, 1955; Aldrich and Buchanan, 1958; Higdon and Marshall, 1958) have described the effect of titration of H-Al-clays with bases. Thompson and Culbertson (1959) have said that autodigestion takes place if H-montmorillonite is stored after preparation. No additional alumina is released, however, if all traces of HCl are removed by careful washing, and Taylor (1959) has shown that the decay of acid-washed clays from H- to Al-systems cannot be inhibited by washing out the excess acid with water. Higdon and Marshall (1958) conclude from a series of experiments that true H-clays can be prepared by treatment with H-exchange resins but not by electrodialysis.

Samples of H-montmorillonite from Chambers, Ariz., prepared by treatment with 1 *N* HCl at room temperature, were used for a discontinuous potentio-

TABLE 199.2.—Al_2O_3 *found in filtrates from the titration of H-montmorillonite with 0.1* N NaOH

[65 mg samples in a total volume of 6.2 ml]

Sample	NaOH added (ml)	Al_2O_3 (mg)	Sample	NaOH added (ml)	Al_2O_3 (mg)
1	nil	0.06	19	0.48	2.32
2	0.02	nil	20	.52	2.87
3	.04	.06	21	.56	3.53
4	.06	nil	22	.60	3.95
5	.08	nil	23	.64	3.11
6	.10	nil	24	.68	3.95
7	.12	.25	25	.72	3.95
8	.14	.37	26	.76	3.11
9	.16	.50	27	.82	2.99
10	.18	.82	28	.86	2.39
11	.20	.99	29	.90	4.31
12	.22	.99	30	.94	3.53
13	.24	1.75	31	.98	3.05
14	.28	2.75	32	1.06	4.19
15	.32	4.13	34	1.10	4.31
16	.36	3.92	35	1.14	5.38
17	.40	3.69	36	1.16	4.84
18	.44	.87	37	1.20	5.26

metric titration with 0.1 *N* NaOH (Pommer and Carroll, 1960). The filtrates of 36 samples from this titration were analyzed for Al_2O_3. If Al_2O_3 had been moved from the octahedral layers of the clay to the exchange positions during the preparation of the H-form, it should either prevent the replacement of H^+ ions during titration or be present in the solutions that had been in contact with the clay samples. The titration curve obtained indicates that the clay titrated was an H-clay and not an H-Al-clay. A negligible amount of Al_2O_3 was removed during the titration of the first clay acid, and amounts up to the second equivalence point remained small. The Al_2O_3 found in the filtrates towards the end of the titration is due to decomposition of the montmorillonite by NaOH. The amounts of Al_2O_3 found in the filtrates are given in table 199.2. It is concluded that this method of preparation with 1 *N* HCl formed H-montmorillonite and not H-Al-montmorillonite.

REFERENCES

Aldrich, D. G., and Buchanan, J. R., 1958, Anomalies in techniques for preparing H-bentonites: Soil Sci. Soc. America Proc., v. 22, p. 281–285.

Higdon, W. T., and Marshall, C. E., 1958, Electrochemical properties in relation to two methods of preparation of colloidal clays: Jour. Chem. Physics, v. 62, p. 1204–1209.

Low, P. F., 1955, The role of aluminum in the titration of bentonite: Soil Sci. Soc. America Proc., v. 19, p. 135–139.

McAuliffe, Clayton, and Coleman, N. T., 1955, H-ion catalysis by acid clays and exchange resins: Soil Sci. Soc. America Proc., v. 19, p. 156–160.

Paver, H., and Marshall, C. E., 1934, The role of aluminum in the reactions of the clays: Jour. Chem. Industry, v. 53, p. 750–760.

Pommer, A. M., and Carroll, Dorothy, 1960, Interpretation of potentiometric titration of H-montmorillonite: Nature, v. 185, p. 595–596.

Taylor, A. W., 1959, Concentrations of ions at the surfaces of clays: Am. Ceramic Soc. Jour., v. 42, p. 182–184.

Thompson, A. C., and Culbertson, J. L., 1959, Acidic properties of bentonite: Jour. Chem. Physics, v. 63, p. 1917–1920.

200. CHANGES IN THERMOGRAVIMETRIC CURVES OF CALCIUM SULFATE DIHYDRATE WITH VARIATIONS IN THE HEATING RATE

By Charles A. Kinser, Washington, D.C.

One of the most valuable functions of the recording thermogravimetric balance is the making of a permanent and continuous record of the rate at which a sample loses weight while its temperature is raised at a uniform rate. This technique has been especially valuable in the study of hydration states of various minerals and chemical compounds.

As a sample passes, during the heating process, from one stable hydration state to another, there is usually a change in the rate of water loss, and this is indicated on the thermogravimetric curve by a change in slope.

It was surprising, therefore, that the thermogravimetric curve (fig. 200.1, curve *A*) obtained for a 0.4-gram sample of synthetic gypsum gave no evidence of a transition at the point corresponding to hemihydrate (plaster of Paris) composition, after 1.5 moles of water had been evolved. This curve was recorded as the temperature was raised at the rate of 4° C per minute, which is a slower rate than that generally reported by other workers in this field. Duval (1953, p. 59) used a temperature rise of about 7° C per minute for most of his reported experiments.

When a second run was made with the rate of temperature rise reduced to 1° C per minute (fig. 200.1, curve *B*), a significant break appeared in the curve at the point corresponding to hemihydrate composition. When a third run was made, with a temperature rise of 0.5° C per minute, the transition occurred at the same point and was even more pronounced than before (fig. 200.1, curve *C*). The slopes of curves *B* and *C* thus indicate that the hemihydrate loses water at a slower rate than the dihydrate.

These findings indicate that in thermogravimetric study of hydration states it is very important to consider the speed at which dehydration proceeds. This has also been pointed out by Charlot and Bézier (1957, p. 180). Although experiments conducted by others have shown that satisfactory thermogravimetric curves can generally be obtained at rates of 7° to 12°C per minute, the present study indicates that some transitions are not revealed by the curves unless the temperature is raised at a much slower rate.

REFERENCES

Charlot, G., and Bézier, Denise, 1957, Quantitative inorganic analysis (translated by R. C. Murray): New York, John Wiley, 691 p.

Duval, Clement, 1953, Inorganic thermogravimetric analysis: New York, Elsevier, 531 p.

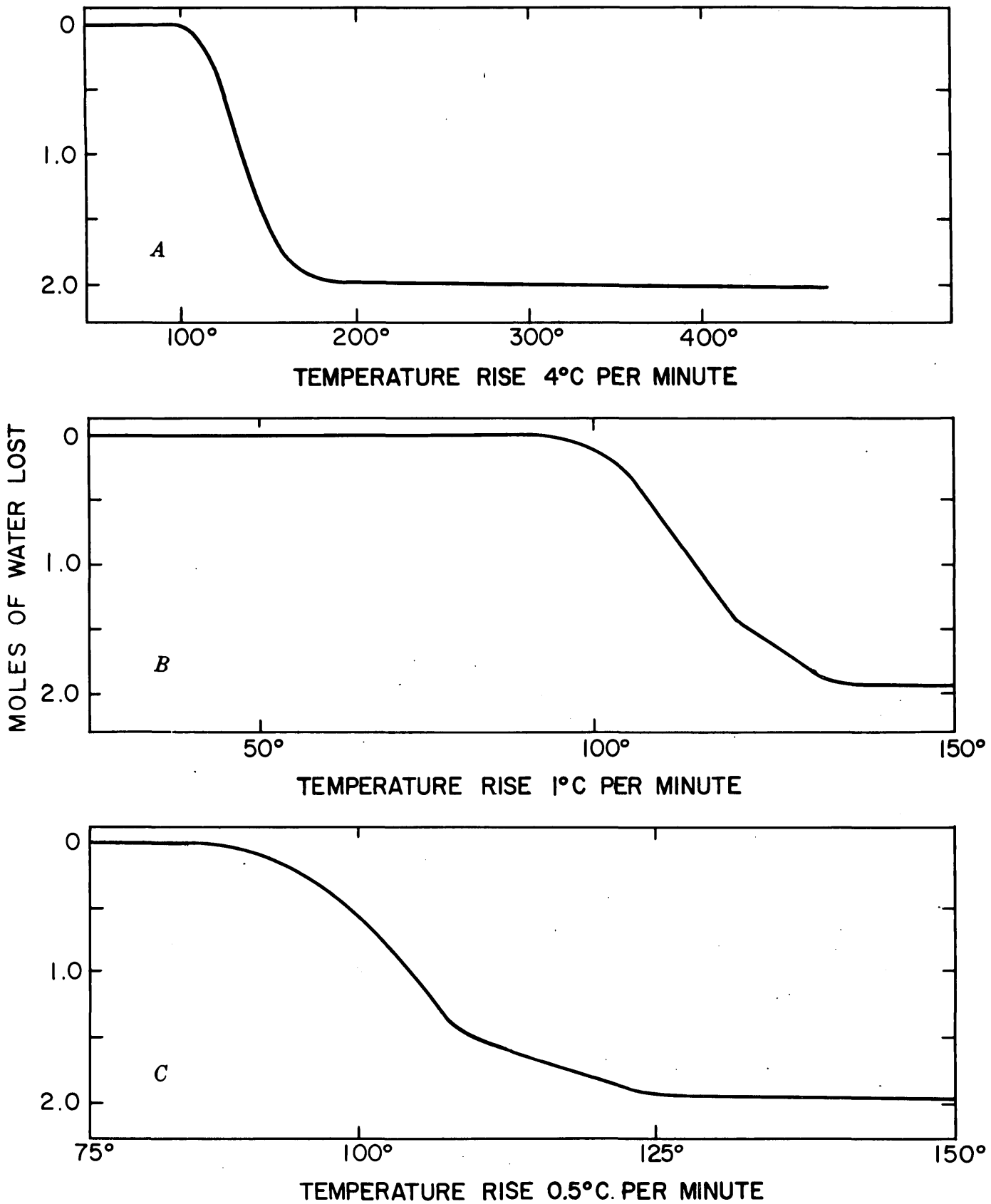

FIGURE 200.1.—Thermogravimetric curves for calcium sulfate dihydrate. *A*, Temperature rise 4° C per minute; *B*, temperature rise 1° C per minute; *C*, temperature 0.5° C per minute.

201. SYNTHETIC BAYLEYITE

By Robert Meyrowitz and Marie Louise Lindberg, Washington, D.C.

Bayleyite, $Mg_2UO_2(CO_3)_3 \cdot 18H_2O$, was first synthesized by Axelrod and others (1951). They prepared the synthetic compound by (a) allowing an aqueous solution containing stoichiometric amounts of $Mg(NO_3)_2$, $UO_2(NO_3)_2$, and K_2CO_3 (adjusted faintly alkaline to phenolphthalein) to evaporate at room temperature and (b) "by first preparing the insoluble silver uranyl carbonate, reacting an excess of the silver uranyl carbonate with magnesium chloride, filtering off the precipitate of AgCl and excess silver uranyl carbonate, and allowing the filtrate to crystallize" at room temperature. The crystals obtained by evaporation for a long time were very small and were identified as bayleyite by their X-ray diffraction powder patterns.

Bachelet, Cheylan, Davis, and Goulette (1952) prepared $Mg_2UO_2(CO_3)_3$ by bubbling CO_2 gas through an aqueous suspension of uranium oxide (Hemi-hydrate) and basic magnesium carbonate. After solution of the reactants, the magnesium uranylcarbonate was precipitated in three ways: (a) by evaporating the solution at room temperature, (b) by bubbling dry air through the solution, and (c) by adding acetone. The material obtained was further purified by recrystallization from water. The synthetic compound was identified by partial chemical analysis. No optical or X-ray diffraction data were given.

Crystals of solutes can be caused to form by cooling the solution until part of solvent has crystallized. Crystals of the solute then form slowly in the remaining super saturated solution. We have synthesized large amounts of bayleyite in a relatively short time by applying this method in the manner described below.

An aqueous solution (100 ml), approximately 0.1 M as $Mg_2UO_2(CO_3)_3$, containing Na_2CO_3, $UO_2(NO_3)_2$, and $Mg(NO_3)_2$ was adjusted with Na_2CO_3 to pH 8.0. The solution, contained in a plastic bottle, was for a few days alternately frozen solid and then slowly thawed in a refrigerator. The crystals formed were filtered from the cold solution and pressed dry. Because of the great solubility of bayleyite the crystals were not washed with water. These crystals were easily seen with a hand-lens, and were identified as bayleyite by their X-ray diffraction powder patterns. Experiments with 100 ml of 0.2 M and 0.3 M $Mg_2UO_2(CO_3)_3$ solutions were equally successful. Small crystals of bayleyite were also prepared by substituting K_2CO_3 for Na_2CO_3 in a solution of about 0.1 M $Mg_2UO_2(CO_3)_3$. When these crystals were dissolved in water and then recrystallized by evaporation large crystals with good terminal faces were produced. Some of these crystals were 1 by ⅛ inch and were identified as bayleyite by their X-ray diffraction powder patterns.

Bayleyite is monoclinic. The observed extinctions on single crystal X-ray patterns ($h0l$, $h=2n$; $0k0$, $k=2n$) suggest the space group $P2_1/a(C_{2h}^5)$, but neither a mirror plane of symmetry nor a two-fold axis of symmetry has been confirmed by crystallographic measurements. The unit cell measurements ($a=26.55$, $b=15.28$, $c=6.50$A, all ± 0.5 percent; $\beta=92°58' \pm 10'$) are smaller than those obtained by Axelrod and others (1951) ($a=26.65 \pm 0.05$ A, $b=15.31 \pm 0.05$A; $c=6.53 \pm 0.02$A; $\beta=93°04' \pm 20'$). The newly synthesized crystals deteri-

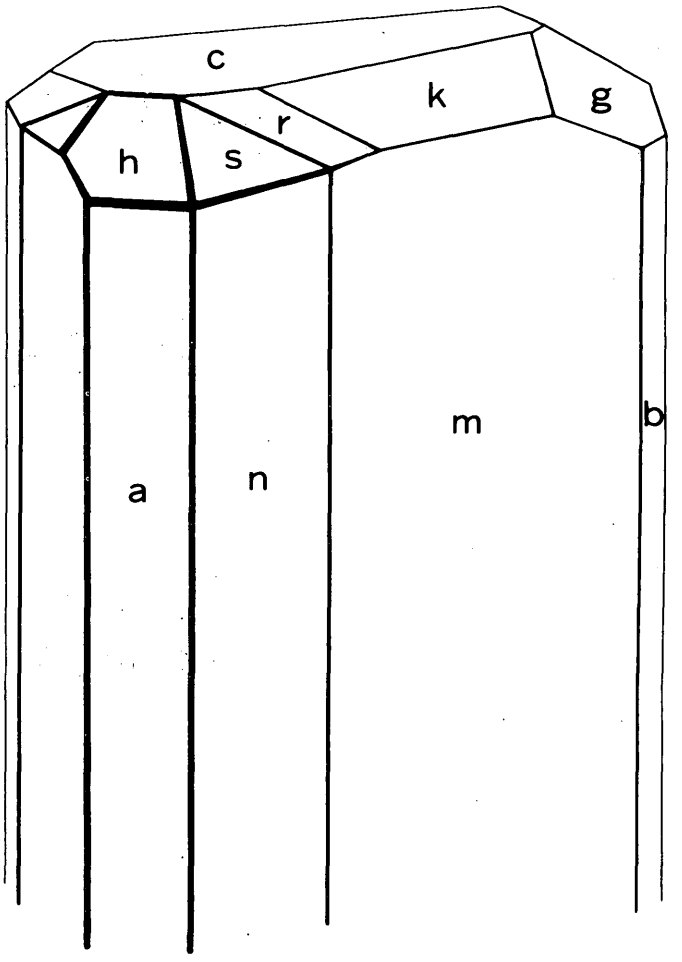

Figure 201.1.—Crystal habit of synthetic bayleyite.

TABLE 201.1.—*Crystallographic Elements and angle table (calculated from X-ray data) Monoclinic*

a : b : c=1.7376 : 1 : 0.4254 β=92°58′; p_o : q_o : r_o=0.2448 : 0.4248 : 1
r_3 : p_2 : q_2=2.3540 : 0.5763 : 1; μ=87°02′; p_o' 0.2451, q_o' 0.4254, x_o' 0.0518

Forms		ϕ	ρ	ϕ_2	ρ_2=B	C	A
c	001	90°00′	2°58′	87°02′	90°00′	----------	87°02′
b	010	0 00	90 00	----------	0 00	90°00′	90 00
a	100	90 00	90 00	0 00	90 00	87 02	----------
m	110	29 57	90 00	0 00	29 57	88 31	60 03
n	210	49 03	90 00	0 00	49 03	87 46	40 57
g	021	3 29	40 26	87 02	49 39	40 21	87 45
h	401	90 00	45 54	44 06	90 00	42 56	44 06
k	111	34 55	27 25	75 14	67 49	24 59	74 47
r	211	51 52	34 34	61 32	69 29	32 17	63 30
s	311	61 37	41 49	51 48	71 31	39 13	54 04
v	$\bar{2}11$	−45 52	31 25	113 40	68 43	33 36	111 58
e	$\bar{3}11$	−58 06	38 50	124 21	70 39	41 22	122 10

orated during the X-ray study, as shown by the broadening and weakening of reflections in successive patterns.

Bayleyite crystals grow in clusters of singly terminated radiating fibers. Individual fibers are asymmetrical in habit; they are tabular parallel to (110) and ($\bar{1}\bar{1}0$), and the faces (001) and (111), parallel to the same zone-axis, are well developed. Prism faces ($1\bar{1}0$) and ($\bar{1}10$), are narrow, and the pyramid face, ($1\bar{1}1$) has not been noted on any of the six crystals measured. Faces of the forms {210}, {021}, {211}, {311}, {211}, and {311}, are unequally developed (fig. 201.1). Table 201.1 lists the crystallographic elements and angle table for the observed forms, as calculated from the X-ray data.

REFERENCES

Axelrod, J. M., Grimaldi, F. S., Milton, Charles, and Murata, K. J., 1951, The uranium minerals from the Hillside Mine, Yavapai County, Arizona: Am. Mineralogist, v. 36, p. 1–22.

Bachelet, M., Cheylan, E., Davis, M., and Goulette, J. C., 1952, Préparation et propriétés des uranylcarbonates: Soc. Chim. France Bull., 1952, p. 565–569.

202. SYNTHETIC HYDROUS BORON MICAS

By HANS P. EUGSTER and THOMAS L. WRIGHT, Johns Hopkins University, Baltimore, Md.

Work done in cooperation with the National Science Foundation

It is well known that boron occurs in fourfold coordination in silicates, including danburite (Dunbar and Machatschki, 1930), reedmergnerite (Milton and others, 1960), and many others. Noda, Daimon, and Toyoda (1944) synthesized a boron-fluoro-phlogopite, $KMg_3BSi_3O_{10}F_2$. (See also Comeforo, Hatch, Humphrey, and Eitel, 1953, and Hatch, Humphrey, and Worden, 1956.) The role of boron in hydrous phyllosilicates is less clear. Harder (1959 a and b) found as much as 2,000 ppm boron in natural micas. J. R. Porter (written communication, 1959) has pointed out that montmorillonites from the Kramer boron deposit in southern California contain over 1,500 ppm boron.

To test the possible extent of replacement of tetrahedrally coordinated aluminum by boron in hydrous phyllosilicates, we have synthesized aluminum-free boron phlogopite and biotite, and probably boron-bearing muscovite.

Boron phlogopite, $KMg_3BSi_3O_{10}(OH)_2$, was grown from a mixture of $K_2O \cdot 6SiO_2 + MgO + H_3BO_3$ (K:Mg:B:Si=1:3:1:3) in sealed gold tubes at a water pressure of 2,000 bars and at temperatures between 250° and 800°C. The results of our experiments are given in table 202.1. Boron phlogopite grows readily and crystallizes well, though not nearly as well as boron-free phlogopite. Traces of forsterite are present in the products formed above 400°C because the vapor phase differs appreciably in composition from pure water. Table 202.2 gives powder X-ray data for a boron phlogopite grown at 600°C and 2,000 bars. Reflections are not sharp enough to warrant further refinement of the cell dimensions, which are listed in table 202.3. No single crystals were available on which we could study polymorphism. Calculations were based on a 1M modification (Yoder and Eugster, 1954). Boron phlogopite shows a distinctly smaller b spacing than boron-free phlogopite. The approximate indices of refraction were measured in white light, the material being too finely divided to permit an accurate determination of $n\alpha$ and $n\gamma$; the results are as follows: Minimum index, n_1,=1.546±0.002, maximum index, n_2,=1.568±0.002, and birefringence=0.022. Measure-

TABLE 202.1.—*Results of hydrothermal experiments, all performed at a water pressure of 2,000 bars*

[In all experiments the material was in an aqueous fluid.]

Starting material	Temperature (degrees C)	Time (hours)	Products
Boron muscovite mix (K_2O-$6SiO_2$+MgO+H_3BO_3)	800	139	Boron phlogopite+forsterite.
	750	144	Boron phlogopite+forsterite.
	710	305	Boron phlogopite+forsterite.
	700	622	Boron phlogopite+trace of forsterite.
	600	315	Boron phlogopite+trace of forsterite.
	400	648	Boron phlogopite.
	300	660	Boron phlogopite.
	250	1,152	Boron phlogopite.
Boron annite mix ($K_2O{\cdot}6SiO_2$ +$FeC_2O_4{\cdot}2H_2O$+H_3BO_3).	820	133	Magnetite+glass.
	700	622	Magnetite+trace of boron annite.
	550	300	Boron annite+magnetite.
Boron muscovite mix (K_2O-$6SiO_2$+Al_2O_3+H_3BO_3).	710	144	Sanidine+leucite+glass.
	400	648	Boron-bearing muscovite+sanidine.
	300	660	Boron-bearing muscovite+sanidine.

TABLE 202.2.—*X-ray powder measurements on synthetic boron phlogopite*

d in A	I	hkl	Q×10 5
10. 163	54	(001)	+5
5. 063	12	(002)	−4
4. 571	14	(020)	−24
3. 660	6	(11$\bar{2}$)	−60
3. 377	55	(002)	−3
3. 155	8	(112)	+4
2. 930	7	(11$\bar{3}$)	−30
2. 719	3	(023)	−1
2. 619	32	(200)	−2
2. 534	5	(004)	+16
2. 434	15	(201)	−6
2. 287	3	(040)	−72
2. 172	10	(13$\bar{3}$)	−56
2. 027	14	(005)	+14
1. 679	5	(13$\bar{5}$)	−61
1. 528	15	(060)	+28
1. 512	3	(061)	+92

ments were easiest on the forsterite-free phlogopite grown at 400°C, which has a distinctly smaller birefringence than the other synthetic phlogopites.

Boron annite, $KFe_3BSi_3O_{10}(OH)_2$, was also synthesized under similar conditions. It crystallizes somewhat more reluctantly than boron phlogopite, but its X-ray powder pattern shows strong basal mica peaks.

TABLE 202.3.—*Cell dimensions (in angstrom units) of synthetic phlogopites*

	1M phlogopite [1]	1M fluorphlogopite [1]	1M boron phlogopite
a	5. 314±0. 01	5. 310±0. 01	5. 32 ±0. 01
b	9. 204± . 02	9. 195± . 02	9. 165± . 02
c	10. 314± . 005	10. 136± . 005	10. 29 ± . 01
β	99°54′±5′	100°4′±3′	100°10′±10′

[1] Yoder and Eugster (1954).

We are not quite sure that we synthesized boron muscovite, $KAl_2BSi_3O_{10}(OH)_2$, for an appreciable amount of sanidine remains in the products of all our experiments. These products, however, have a smaller *b* spacing than boron-free muscovite, which indicates that some boron has entered the muscovite lattice. It would be difficult to prove the absence of Al in fourfold coordination, unless 100 percent yield could be achieved.

Boron micas are of great interest not only from a crystallographic, but also from a petrologic point of view. Although in natural minerals the replacement of tetrahedral aluminum by boron will rarely, if ever, go to completion, many micas from boron-rich environments can be expected to contain significant amounts of boron.

REFERENCES

Comeforo, J. E., Hatch, R. A., Humphrey, R. A., Eitel, W. 1953, Synthetic mica investigations: Am. Ceramic Soc. Jour., v. 36, p. 286–294.

Dunbar, C., and Machatschki, F., 1930, Structure of danburite, $CaB_2Si_2O_8$: Zeitschr. Kristallographie, v. 76, p. 133–146.

Harder, H., 1959a, Beitrag zür Geochemie des Bors. I.: Akad. Wiss. Göttingen Nachr., Math.-phys. Kl., no. 5, p. 67–122.

——— 1959b, Beitrag zür Geochemie des Bors. II.: Akad. Wiss. Göttingen Nachr., Math.-phys. Kl., no. 6, p. 123–183.

Hatch, R. A., Humphrey, R. A., and Worden, E. C., 1956, Synthetic mica investigations. VIII: U.S. Bur. Mines Rept. Inv. 5283, p. 1–48.

Milton, C., Chao, E.C.T., Axelrod, J. M., and Grimaldi, F. S., 1960, Reedmergnerite, $NaBSi_3O_8$, the boron analogue of albite, from the Green River formation, Utah: Am. Mineralogist. (in press)

Noda, Tokichi, Daimon, Nobutoshi, and Toyoda, Hitoshi, 1944, Synthesis of boron mica: Jour. Soc. Chem. Industry Japan, v. 47, p. 499–502. (From Chem. Abs., 1949, v. 43, 6544d.)

Yoder, H. S., and Eugster, H. P., 1954, Phlogopite synthesis and stability range: Geochim. et Cosmochim. Acta, v. 6, no. 4, p. 157–185.

203. RECENT DEVELOPMENTS IN THE CRYSTAL CHEMISTRY OF VANADIUM OXIDE MINERALS

By Howard T. Evans, Jr., Washington, D.C.

Work done in cooperation with the U.S. Atomic Energy Commission

It is now firmly established that most of the vanadium of the Colorado Plateau ores was first deposited as a constituent of montroseite, a hydrated vanadium oxide isostructural with goethite and diaspore (Evans and Block, 1953). This mineral was the source of all the other vanadium minerals in these ores except vanadium silicates. The first step in the weathering process was determined through study of crystal structure (Evans and Mrose, 1955) to be a solid-state transformation to paramontroseite, which is metastable and is readily decomposed by further weathering. The course of alteration to other secondary minerals has been traced with the help of thermodynamic studies by Evans and Garrels (1958). The weathering pattern is summarized by them in terms of oxidation potential and pH in a diagram a portion of which is reproduced in figure 203.1 in slightly modified form. The mineralogy of vanadium in the Colorado Plateau ores has been well summarized by Weeks, Coleman, and Thompson (1959), and an earlier survey of the crystal chemical background of vanadium mineralogy has been given by Evans (1959).

Numerous studies of crystal structure in this and other laboratories show that each of the valence states of vanadium has associated with it a characteristic

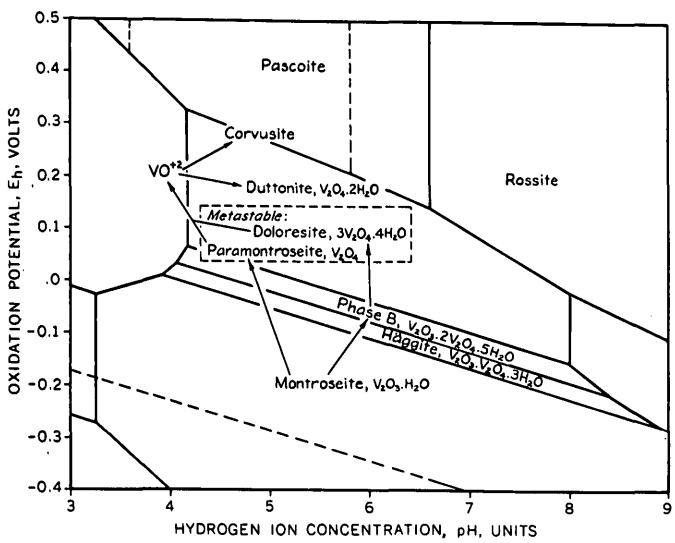

Figure 203.1.—Oxidation potential—pH equilibrium diagram for vanadium minerals modified from Evans and Garrels (1958), showing stability relationships among oxide minerals.

crystal chemistry, and on this basis the oxide minerals may be divided into three groups. In this paper recent work in the first two of these groups will be described, and some speculations based on this will be offered, which I hope will tend to clarify the confusing and complex chemistry of vanadium-oxide minerals in general.

THE MONTROSEITE-DOLORESITE GROUP

The chemical compositions of all the minerals listed in table 203.1 have been established by analysis of crystal structures. All these structures are based on a chain of octahedra joined by sharing edges along the fibre axis of the mineral crystal, which has therefore a characteristic fibre spacing of 3.0 A. Each represents a different arrangement of single and double chains, in which hydrogen bonding plays a major role (Evans, 1959). A recent extension of this work has greatly clarified the nature of the common mineral doloresite (Stern, Stieff, Evans, and Sherwood, 1957). All attempts to determine the structure of this mineral were thwarted for a time because its monoclinic symmetry was hidden by submicroscopic lamellar twinning; it was assumed to be orthorhombic. When untwinned material was discovered near Carlile, Wyoming, it was readily shown to be monoclinic (fig. 203.2) (Evans and Mrose, 1958). The relation of such material (termed "phase B," and always found intimately intergrown with häggite) to the common form of doloresite is still unclear, but the Wyoming mineral apparently contains trivalent vanadium, with two more hydrogen atoms per unit cell than doloresite. I now believe that phase B, which may tentatively be designated "protodoloresite," is thermodynamically stable, as shown in figure 203.1, while doloresite is metastable. Doloresite, therefore, is probably derived from protodoloresite by a solid-state transformation, just as paramontroseite is derived from montroseite (Evans and Mrose, 1955). Protodoloresite is derived from montroseite through a replacement process, in such a way that the structure of the former always has one of the two possible orientations with respect to the latter (fig. 203.3). This accounts for the lamellar twinning. A more detailed description of these investigations will be given elsewhere.

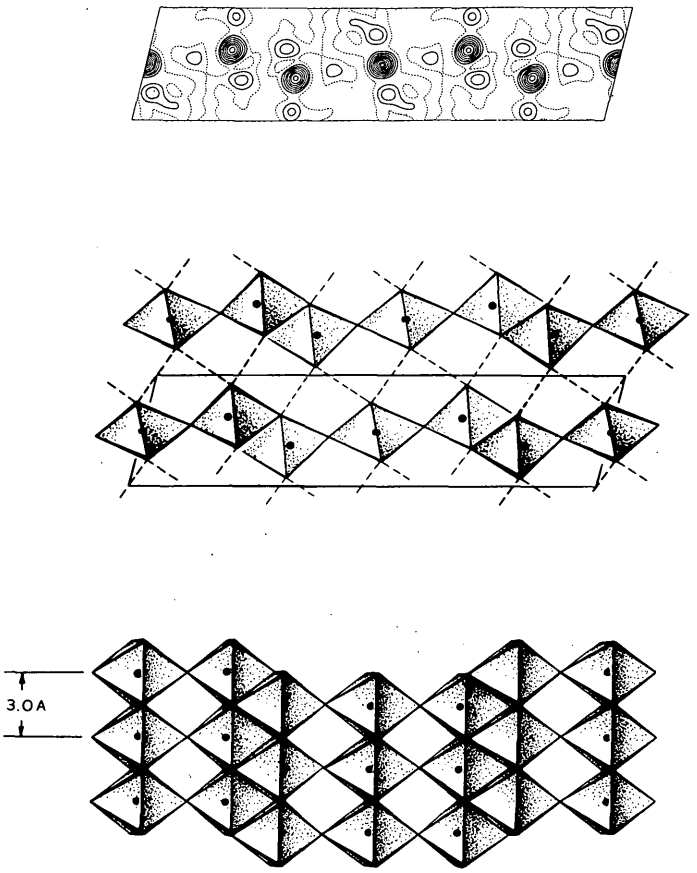

FIGURE 203.2.—Crystal structure of protodoloresite: Top, electron density projected along the fibre (b) axis; center, schematic view of the structure viewed along the b axis showing VO_6 groups as octahedra, hydrogen bonds as dashed lines; bottom, schematic view of one layer viewed normal to center view.

TABLE 203.1.—*Minerals of the montroseite and duttonite groups*

Mineral	Formula	Cell content	Reference
Montroseite	$V_2O_3 \cdot H_2O$	$H_4V_4O_8$	1, 2, 3
Häggite	$V_2O_3 \cdot V_2O_4 \cdot 3H_2O$	$H_6V_4O_{10}$	4
"Protodoloresite"	$V_2O_3 \cdot 2V_2O_4 \cdot 5H_2O$	$H_{10}V_6O_{16}$	4
Doloresite	$3V_2O_4 \cdot 4H_2O$	$H_8V_6O_{16}$	4, 5
Paramontroseite	V_2O_4	V_4O_8	3
Duttonite	$V_2O_4 \cdot 2H_2O$	$H_8V_4O_{12}$	4, 6
"Paraduttonite"	$V_2O_5 \cdot H_2O$	$H_4V_4O_{12}$	----------

1. Weeks, Cisney, and Sherwood (1953)
2. Evans and Block (1953)
3. Evans and Mrose (1955)
4. Evans and Mrose (1958)
5. Stern, Stieff, Evans, and Sherwood (1957)
6. Thompson, Roach, and Meyrowitz (1957)

THE DUTTONITE GROUP

Duttonite (Thompson, Roach, and Meyrowitz, 1957) is a quadrivalent hydrated oxide of vanadium, $V_2O_4 \cdot 2H_2O$ or $VO(OH)_2$, stable in absence of air. Its structure (Evans and Mrose, 1958) contains octahedral strings similar to those in the lower oxides, but the octahedra are strongly polarized (fig. 203.4). It may be regarded as consisting of rows of vanadyl ions (VO^{+2}) held together by zigzag hydrogen-bonded chains of hydroxyl ions. The occurrence of crystals of duttonite in vugs indicates that the mineral was precipitated from acid solutions of vanadyl ions through hydrolysis.

There are three known types of duttonite: (a) light-brown square crystal plates from the Peanut mine, Montrose County, Colo., which are monoclinic

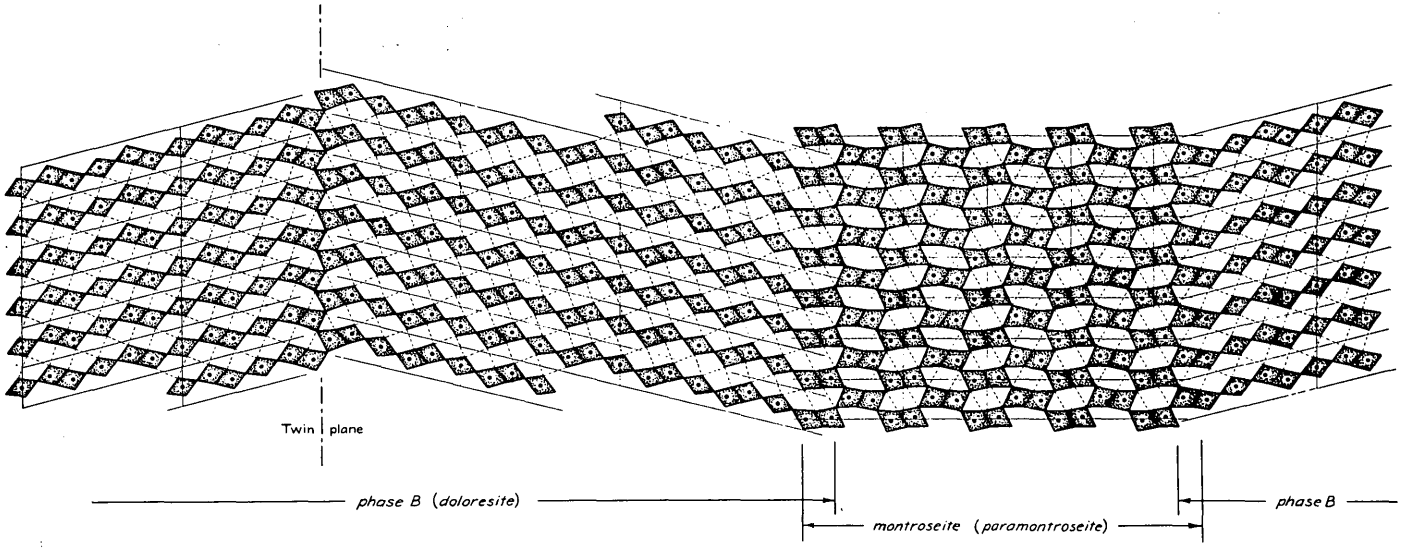

FIGURE 203.3.—Demonstration of the alteration mechanism of protodoloresite (phase B), showing the origin of two relative orientations and lamellar twinning.

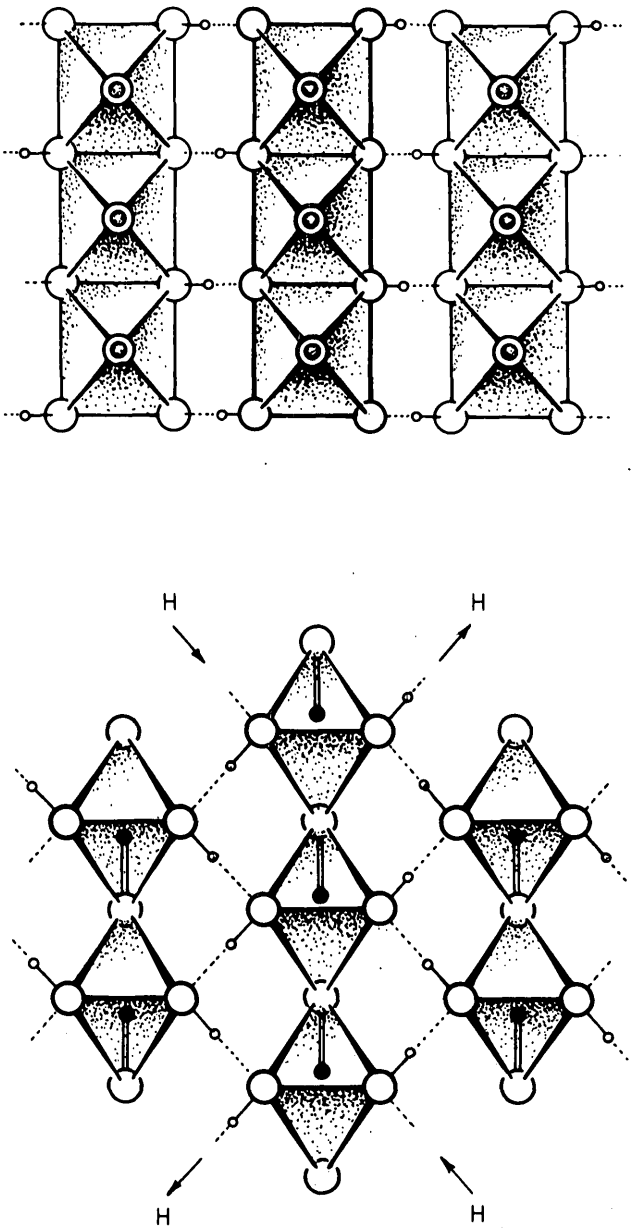

FIGURE 203.4.—Crystal structure of duttonite: Top, view along monoclinic (b) axis; bottom, view normal to top view, showing ordered polarization of zigzag hydroxyl chains (H–H). Vanadyl groups (VO^{+2}) are emphasized by double lines.

(β=90°40′); (b) synthetic vanadyl hydroxide (powder) which is orthorhombic (β=90°); and (c) black radiating prismatic crystals from the Monument No. 2 mine, in Monument Valley, Ariz., which are crystallographically identical with the Peanut mine crystals. These observations are explained by the critical role of hydrogen in the duttonite structure. The zigzag hydrogen bond chains referred to above must be polarized, and if the polarizations of the chains in the structure are ordered, the symmetry must be monoclinic. This presumably is true of the natural crystals from the Peanut mine. If the chains are disordered, then the average symmetry becomes orthorhombic, as we can reasonably expect it to be in the synthetic material. Further, we may imagine that some of the hydrogen atoms in the hydroxyl chains are absent. If the crystal structure is to be preserved, the loss of hydrogen must be accompanied by a concomitant oxidation of some of the vanadium atoms. If this process were carried to the limit, the reaction:

$$V_2O_4 \cdot 2H_2O \rightarrow V_2O_5 \cdot H_2O$$
duttonite "paraduttonite"

would result, following a solid-state transformation again reminiscent of the oxidation of montroseite to paramontroseite. When light-brown duttonite is heated, it first turns green, then dark green, and finally brownish black. At about 170°C the structure breaks down and duttonite is converted to V_2O_5. Up to this point there is no noticeable change in the X-ray powder diffraction pattern. Their change in optical properties is considerable, but it has not yet been followed quantitatively. Chemical analysis of duttonite synthesized in the presence of air always shows the presence of V_2O_5 in varying amounts. The black mineral found at Monument Valley is probably close to $V_2O_5 \cdot H_2O$, which I will tentatively designate "paraduttonite." The habit of the mineral suggests that it was deposited directly in this oxidized form, under conditions quite different from those prevailing at the Peanut mine.

REFERENCES

Evans, H. T., Jr., 1959, The crystal chemistry and mineralogy of vanadium: *in* Garrels, R. M., and Larson, E. S. 3d, Geochemistry and mineralogy of the Colorado Plateau uranium ores, U. S. Geol. Survey Prof. Paper 320, p. 91–102.

Evans, H. T., Jr., and Block, Stanley, 1953, The crystal structure of montroseite, a vanadium member of the diaspore group: Am. Mineralogist, v. 38, p. 1242–1250.

Evans, H. T., Jr., and Garrels, R. M., 1958, Thermodynamic equilibria in aqueous systems as applied to the interpretation of the Colorado Plateau ore deposits: Geochim. et Cosmochim. Acta, v. 15, p. 131–149.

Evans, H. T., Jr., and Mrose, M. E., 1955, A crystal chemical study of montroseite and paramontroseite: Am. Mineralogist, v. 40, p. 861–875.

——— 1958, The crystal structures of three new vanadium oxide minerals: Acta Cryst., v. 11, p. 56–57.

Stern, T. W., Stieff, L. R., Evans, H. T., Jr., and Sherwood, A. M., 1957, Doloresite, a new vanadium oxide mineral from the Colorado Plateau: Am. Mineralogist, v. 42, p. 587–593.

Thompson, M. E., Roach, C. H., and Meyrowitz, R., 1957, Duttonite, a new quadrivalent vanadium oxide from the Peanut mine, Montrose County, Colorado: Am. Mineralogist, v. 42, p. 455–460.

Weeks, A. D., Cisney, E., and Sherwood, A. M., 1953, Montroseite, a new vanadium oxide from the Colorado Plateaus: Am. Mineralogist, v. 38, p. 1235–1241.

Weeks, A. D., Coleman, R. G., and Thompson, M. E., 1959, Summary of the ore mineralogy [of the Colorado Plateau] *in* Garrels, R. M., and Larsen, E. S., 3d, Geochemistry and mineralogy of the Colorado Plateau uranium ores: U. S. Geol. Survey Prof. Paper 320, p. 65–79.

204. AUTHIGENIC RHODOCHROSITE SPHERULES FROM GARDNER CREEK, KENTUCKY

By E. C. T. Chao and William E. Davies, Washington, D.C.

Zen (1959) reported the occurrence of rhodochrosite in marine bottom sediments of the Peru-Chile Trench where many crystals appear to be skeletal and subhedral. To our knowledge, authigenic spherulitic rhodochrosite from sediments has never been reported in the literature.

Rhodochrosite spherules were found in sediments as an authigenic mineral in the channel of Gardner Creek, 3.5 miles west-southwest of Park City, Barren County, Ky. Gardner Creek flows in a karst valley on the Pennyroyal Plain that terminates in a large sink hole where the stream goes underground. The mineral occurs in an orange-yellow clayey quartz silt that contains about 0.5 percent of heavy minerals. About 20 percent of the heavy fraction is rhodochrosite; the remainder is goethite, chromite, leucoxene, and tourmaline.

The rhodochrosite occurs as spherical grains, usually in clusters of two or more as shown in figure 204.1. Most of the grains are about 0.1 mm in diameter and

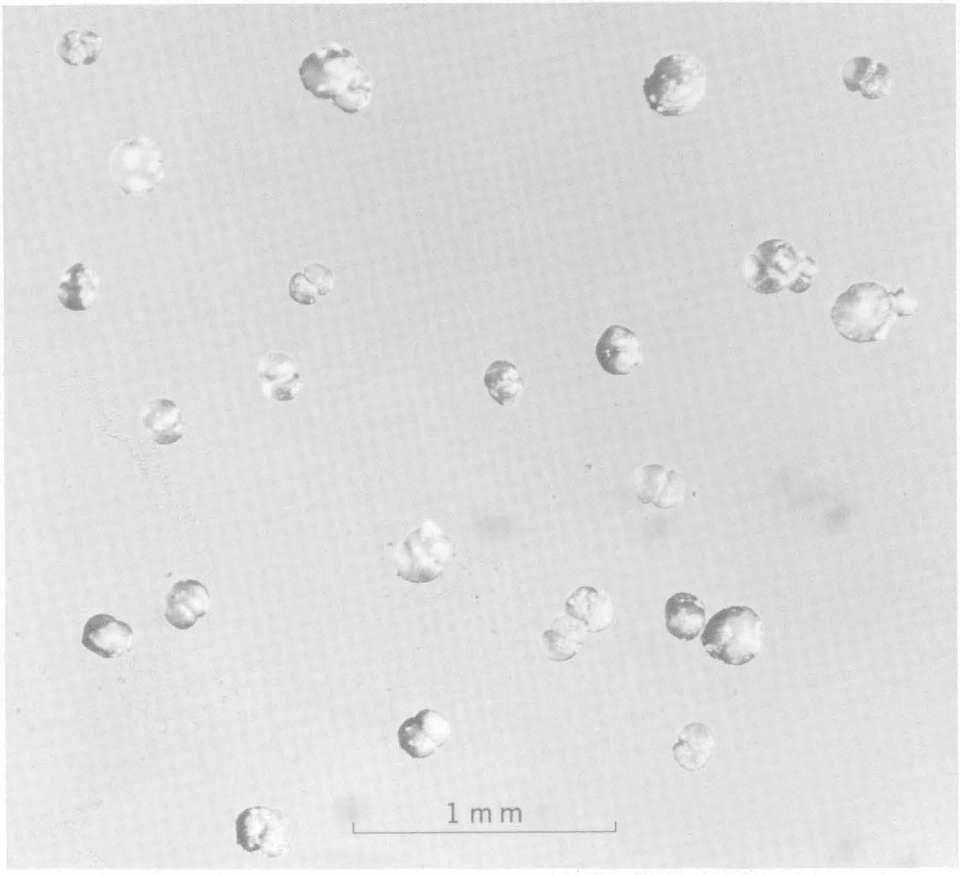

Figure 204.1.—Rhodochrosite spherules, Gardner Creek, Ky.

the clusters are about 0.2 mm across. It is pale yellowish to reddish brown in color. The indices of refraction are $\omega=1.815$ and $\epsilon=1.598$ (both $\pm$ .002) which indicate that the mineral is nearly a pure rhodochrosite (Wayland, 1942). This is also substantiated by a semiquantitative spectrographic analysis made by our colleague Janet D. Fletcher:

Element	*Percent*
Mn	XO.
Fe	X.
Al	0.X
Si	0.X
Ca	0.X
Mg	0.0X

The X-ray powder diffraction pattern gives a unit cell with a=4.78 and c=15.82 A. The *d*-spacing for the 10T4 reflection is 2.86 A which is within the range of cell size for nearly pure rhodochrosite reported by Ehrenburg (1957).

The typical spherulitic character is shown by the extinction relations when the spherules are viewed under the microscope with crossed nicols.

These rhodochrosite spherules are of sedimentary origin and are believed to be forming today. Unfortunately when this sample was collected, we were not aware of the presence of the rhodochrosite spherules so that no attempt was made to determine its chemical environment.

REFERENCES

Ehrenburg, B. G., 1956, Nekotoriye vozmojenosti premenenia rentgenovskgo analiza polikristallov pri geologicheskih issledovaniya: Akad. Nauk SSSR Izv., Ser. fiz., v. 20, no. 7, p. 764–769.

Wayland, R. G., 1942, Composition, specific gravity and refractive indices of rhodochrosite; rhodochrosite from Butte, Montana: Am. Mineralogist, v. 27, no. 9, p. 614–628.

Zen, E-An, 1959, Mineralogy and petrography of marine bottom sediment samples off the coast of Peru and Chile: Jour. Sed. Petrology, v. 29, no. 4, p. 513–539.

205. STRATIGRAPHIC VARIATIONS IN MINERALOGY AND CHEMICAL COMPOSITION OF THE PIERRE SHALE IN SOUTH DAKOTA AND ADJACENT PARTS OF NORTH DAKOTA, NEBRASKA, WYOMING, AND MONTANA

By Harry A. Tourtelot, Leonard G. Schultz, and James R. Gill, Denver, Colo.

Investigations of the Pierre shale are based on about 100 measured sections of parts of the Pierre shale along the Missouri River and around the Black Hills, 700 electric and gamma ray logs, X-ray mineralogical analyses of 500 samples, and chemical and spectrographic analyses of 69 samples. Stratigraphic studies have been made in an area of about 150,000 square miles and interpretations of mineralogical and chemical data apply to about 100,000 square miles.

STRATIGRAPHY

The Pierre shale is between 500 and 1,000 feet in thickness in central and southern South Dakota (fig. 205.1, sections *A–A′* and *B–B′*), about 2,200 feet in southeastern Montana, and about 3,900 feet in east-central Wyoming. Beds of marlstone that are distinctive units in central South Dakota disappear to the west. Silty and sandy beds, largely absent in central South Dakota, are locally prominent in the Black Hills area, and constitute well-defined stratigraphic units farther to the west.

Much of the westward and northward thickening of the lower part of the Pierre shale (fig. 205.1) takes place in the Gammon ferruginous member. The Gammon is a much thickened lateral equivalent of part of the Niobrara formation (fig. 205.1, section A–A′) and also includes rocks equivalent to the Eagle and Telegraph Creek formations of Montana. The Sharon Springs and Mitten black shale members of the Pierre, and the Claggett shale, are contemporaneous units of organic-rich black shale and beds of nonswelling bentonite that constitute a useful gamma-ray and electric log datum throughout the region. Silty and sandy beds overlying the Mitten member along the west side of the Black Hills are 400 to 600 feet thick, and are the eastward equivalents of the nonmarine Judith River and Mesaverde formations of Montana and Wyoming; these beds seem to be represented by less than 100 feet of shale of the Gregory member of the Pierre in central South Dakota. The top of the silty and sandy beds is a convenient horizon on which to divide the Pierre into upper and lower parts for examination of mineralogical data.

The upper part of the Pierre shale in the southern Black Hills area is about 1,400 feet thick and is the equivalent of the Bearpaw shale in central Montana and the DeGrey, Verendrye, Virgin Creek, and Mobridge members of the Pierre along the Missouri River in central South Dakota. The Elk Butte member of the Pierre lies on the Mobridge member, and grades vertically and laterally into the overlying Fox Hills sand-

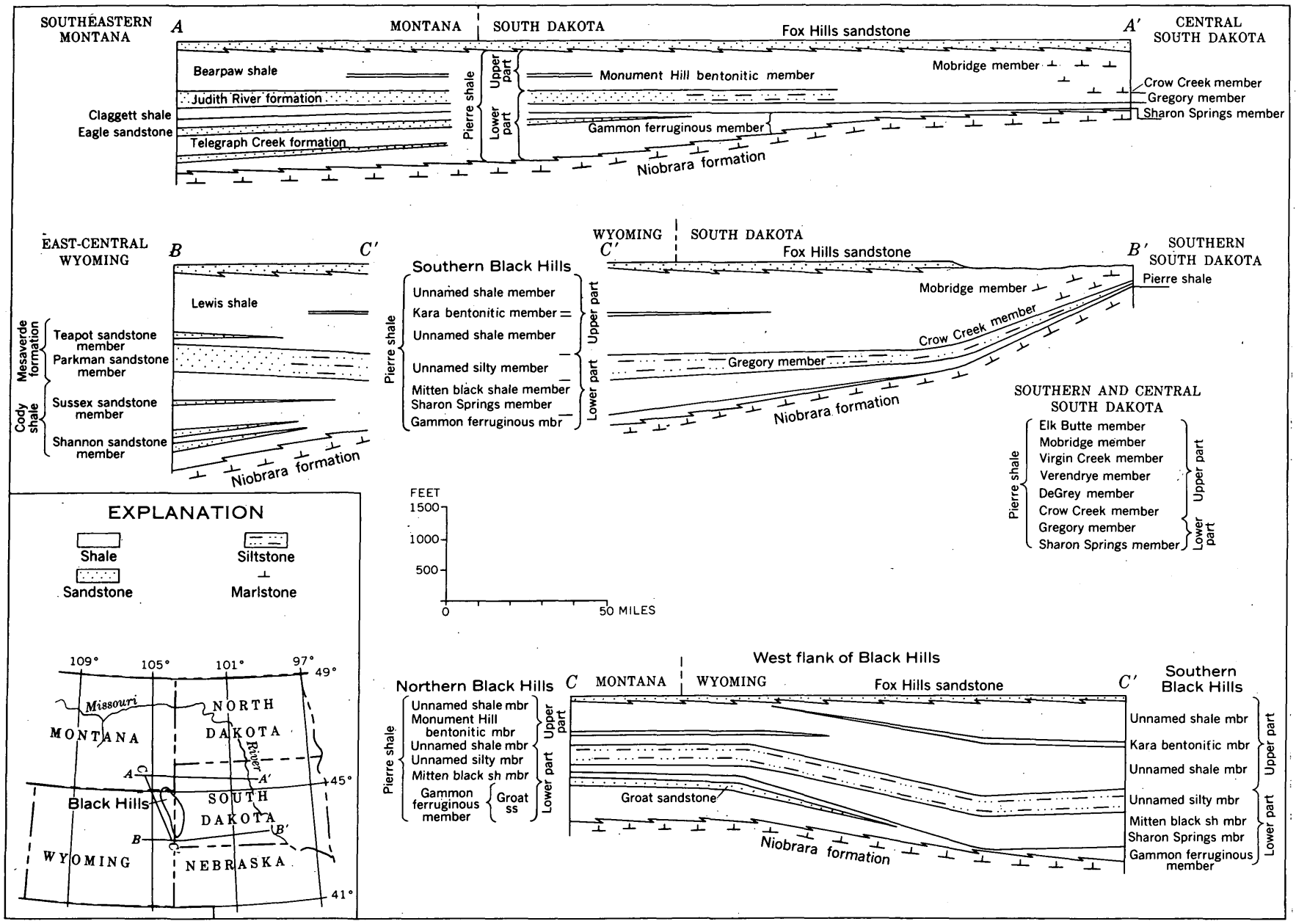

FIGURE 205.1.—Generalized sections showing relations of Pierre shale and equivalent rocks in South Dakota and adjacent parts of North Dakota, Nebraska, Wyoming, and Montana.

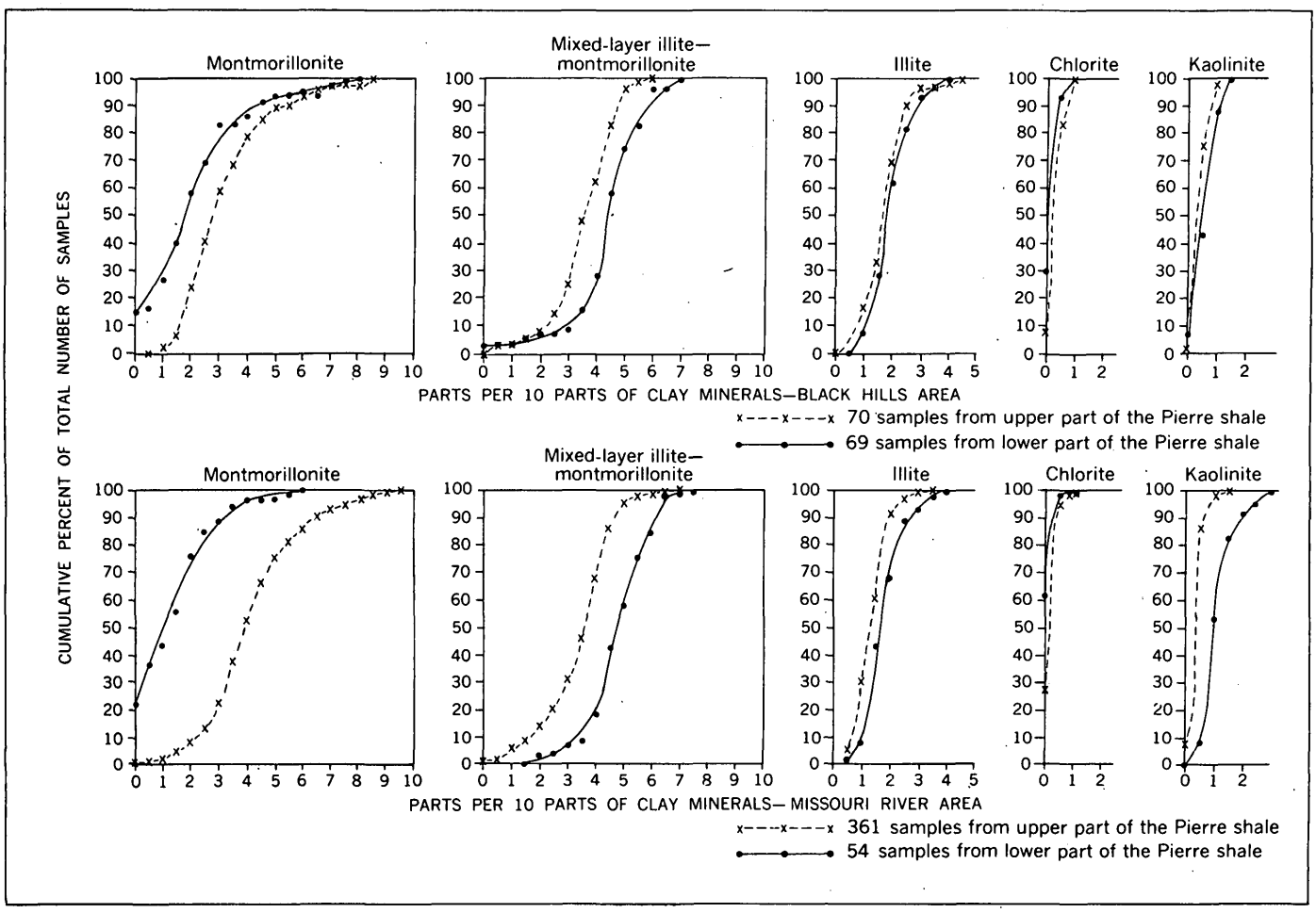

FIGURE 205.2.—Relative abundance of minerals in clay fraction of samples of the Pierre shale in South Dakota and adjacent parts of North Dakota, Nebraska, Wyoming, and Montana.

stone. The Elk Butte member is absent in the Black Hills region, where the Fox Hills sandstone lies conformably on rocks in the Pierre older than the Elk Butte.

MINERALOGY

Most samples of Pierre shale consist of 65 to 80 percent clay minerals, 15 to 25 percent quartz, a few percent feldspar, and commonly small amounts of calcite, dolomite, biotite, pyrite, gypsum, jarosite, clinoptilolite, and organic matter. However, carbonates may constitute as much as 75 percent of some marlstones, cristobalite as much as 40 percent of some siliceous shales, and organic matter as much as 15 percent of some organic-rich shales. The clay fraction of a typical shale consists of 25 to 45 percent montmorillonite, which is predominantly of the calcium-rich variety; 35 to 45 percent mixed-layer illite-montmorillonite; 15 to 25 percent illite; and about 5 percent each of kaolinite and chlorite (fig. 205.2). Principal variations from this typical composition are in frothy-weathering rocks containing abundant sodium montmorillonite, and in organic-rich shales in the Sharon Springs and Mitten members which contain relatively little montmorillonite and chlorite, but contain abnormally large amounts of kaolinite and mixed-layer clay.

Montmorillonite is more abundant in the clay fraction of samples from the upper part of the Pierre than in samples from the lower part. Mixed-layer illite-montmorillonite is more abundant in the lower part of the Pierre. In the upper part of the Pierre shale the amount of montmorillonite in the clay-mineral fraction generally is highest in the Missouri River area of central South Dakota where the Pierre is thin.

The beds of bentonite consist predominantly or entirely of montmorillonite; a few beds contain a little kaolinite. Many beds of bentonite also contain small amounts of feldspar and biotite. At several localities, beds of bentonite in the lower part of the Pierre shale contain large amounts of clinoptilolite, and at one locality phillipsite. Uncommonly low swelling properties

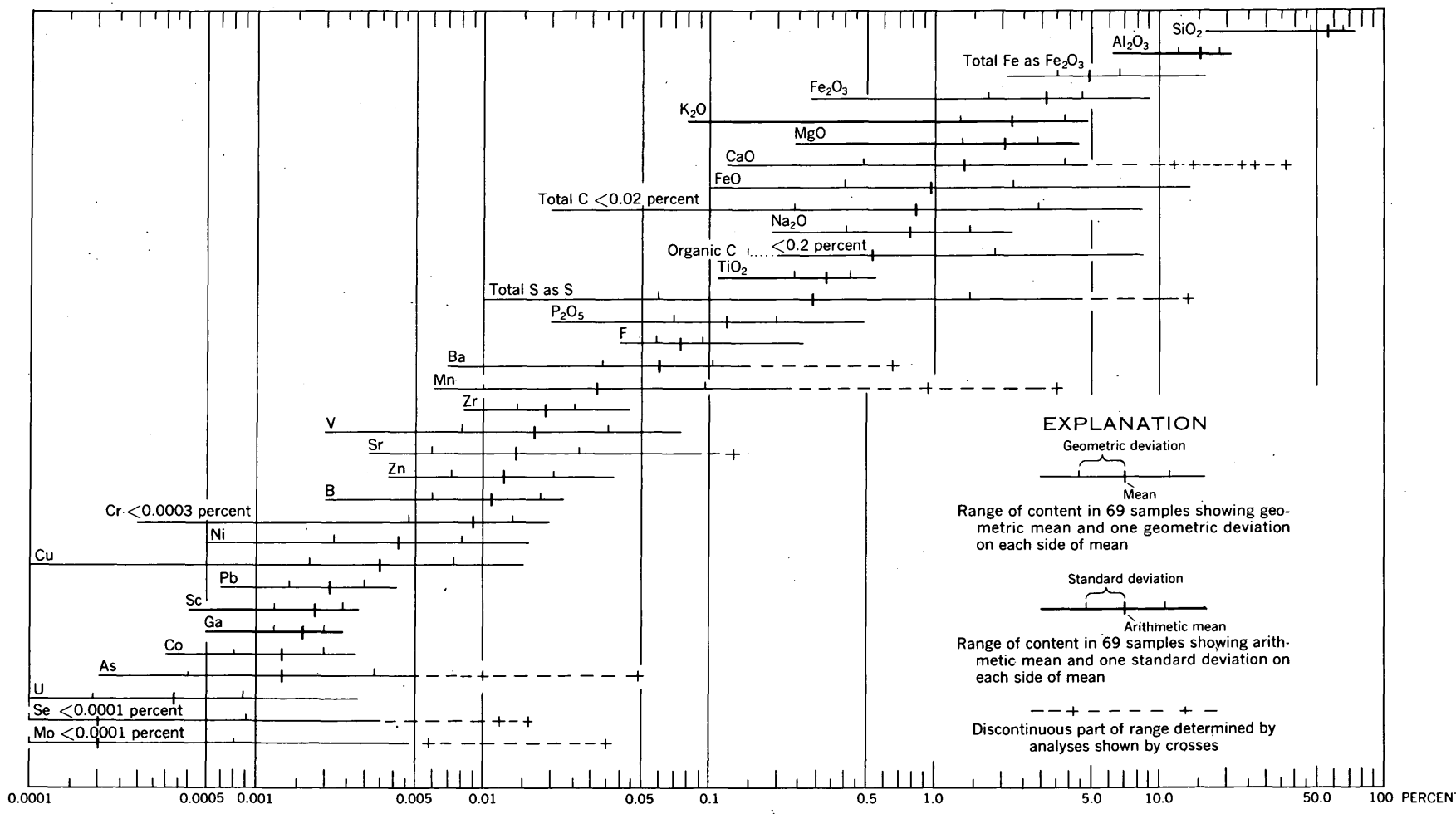

FIGURE 205.3.—Bulk chemical composition of 69 samples of bentonite, shale and claystone, and marlstone from the Pierre shale, South Dakota and adjacent parts of North Dakota, Nebraska, Wyoming, and Montana.

TABLE 205.1.—*Average contents of minor elements in bentonite, in shale and claystone, and in marlstone from the Pierre shale, South Dakota and adjacent parts of North Dakota, Nebraska, Wyoming, and Montana*

[Values are given in parts per million. $\bar{x}$=arithmetic mean; $\bar{s}$=standard deviation.]

Minor elements	Bentonite		Shale and claystone						Marlstone		Value of sample(s) excluded
			Organic carbon								
			<0.5 percent		0.5-1.0 percent		>1.0 percent				
	Content, in parts per million, in number of samples indicated										
	10		19		20		14		6		
	$\bar{x}$	$\bar{s}$	$\bar{x}$	$\bar{s}$	$\bar{x}$	$\bar{s}$	$\bar{x}$	$\bar{s}$	$\bar{x}$	$\bar{s}$	
B	90	67	125	32	130	30	145	34	70	30	
B	72	52									230
Sc	9	3	17	5	21	4	21	5	22	3	
Ti	2, 300	1, 000	3, 000	550	3, 500	560	3, 500	540	2, 600	690	
V	100	170	170	50	200	60	400	180	200	120	
V	50	20									580
Cr	4	3	94	23	100	18	125	27	90	18	
Mn	295	170	1, 000	2, 100	2, 000	7, 700	260	340	1, 400	1, 500	
Mn			315	190							1,200, 1,500, 2,300, and 9,400
Mn					290	145					34, 600
Mn							175	100			1, 400
Mn									860	640	4, 200
Co	10	6	14	3	16	4	14	7	16	5	
Ni	40	35	55	32	50	31	53	39	55	14	
Ni							45	24			160
Cu	15	11	34	10	40	14	80	33	45	28	
Zn	110	98	130	25	160	65	150	96	140	56	
Zn	62	26									230, 330
Ga	18	2	14	4	17	4	17	4	15	6	
As	10	10	11	6	13	8	69	120	20	13	
As							31	15			100, 490
Se	1	4					33	47	17	17	
Se							15	12			120, 160
Se									20	16	<1
Sr	210	140	160	57	140	31	115	54	620	410	
Zr	260	130	180	30	200	46	210	62	140	35	
Mo	3	3	2	2	1	1	43	90	4	5	
Mo							20	20			350
Ba	1, 200	1, 900	650	200	720	280	630	210	450	220	
Ba	500	390									6, 600
Pb	30	8	21	5	23	5	19	7	20	11	
U	6	3	3	1	4	2	12	8	5	3	

of some samples of bentonite seem to be due to magnesium as the chief exchangeable cation, or an aluminum hydroxide layer in the normal position of the exchangeable cations of the montmorillonite.

CHEMICAL COMPOSITION

The bulk chemical composition of 69 samples of bentonite, shale and claystone, and marlstone is shown in figure 205.3. Silica and alumina are the only constituents with a mean content of more than 10 percent. The constituents that have mean contents greater than 1 percent are total iron as ferric oxide, ferric oxide determined separately, and the oxides of potassium, magnesium, and calcium. Ferrous oxide, total carbon, sodium oxide, and organic carbon have mean contents greater than 0.5 percent.

The 69 samples have been divided into five groups according to rock type and the amount of organic carbon, and the arithmetic means and standard deviations for minor elements in each rock type are shown in table 205.1. Bentonite has the lowest mean contents of scandium, chromium, and copper; if isolated high values

are excluded from the mean, bentonite also has the lowest contents of vanadium, and zinc. Bentonite probably has the highest contents of zirconium and lead. The group of samples with more than 1.0 percent organic carbon has the highest mean contents of vanadium, copper, arsenic, selenium, molybdenum, and uranium, although there is some overlap of standard deviations with those of other groups. The group of organic-rich samples tends to have the highest contents of boron, chromium, and probably zinc. The marlstone group has the highest mean contents of strontium and manganese, although the values for manganese have a very wide range. Generally higher mean contents of scandium, cobalt, nickel, and gallium are present in the marlstone group if analyses of these samples are calculated to a carbonate-free basis. The remaining minor elements seem to show no significant differences from group to group.

206. SUMMARY OF CHEMICAL CHARACTERISTICS OF SOME WATERS OF DEEP ORIGIN

By Donald E. White, Menlo Park, Calif.

Probably all changes that occur in rocks from diagenetic, metamorphic, and magmatic processes are reflected in some way in the compositions of the waters associated with the rocks or magmas during the changes. Tentative characteristic concentrations and ratios of critical components are here proposed to assist in distinguishing some "deep" waters of different origin (table 206.1). These data are refinements of criteria previously proposed (White, 1957b, p. 1666), and are a product of a review by Donald E. White, John D. Hem, and G. A. Waring on chemical compositions of ground waters, prepared as a chapter for the revision of Data of Geochemistry (Clarke, 1924).

The elements of the alkali and halogen groups, as well as boron and chemically combined nitrogen, are of particular interest because in general they are highly

TABLE 206.1.—*Approximate median ratios and contents by weight of analyses of waters of different types*

	Number of analyses	Ca/Na	Mg/Ca	K/Na	Li/Na	HCO_3*/Cl	SO_4/Cl	F/Cl	Br/Cl	I/Cl	B/Cl	Total reported ppm	SiO_2 ppm	Total reported N as NH_4, in ppm	pH
Ocean	----------	0.038	3.2	0.036	0.00001	0.0074	0.14	0.00007	0.0034	0.000003	0.00024	34,500	7	0.05	8.0
Oil-field brines:															
NaCl type	11	.04	.4	.015	.0003	.02	.0005	.0002	.003	.002	.003	30,000	30	40	7.0
Na-Ca-Cl type	13	.3	.15	.02	.0002	.001	.0008	.00002	.005	.00008	.0002	120,000	10	200	6.7
Springs that may contain connate water:															
NaCl type	12	.05	.5	.03	.0003	.2	.002	.0003	.0015	.002	.015	20,000	30	40	7.8
Na-Ca-Cl type	15	.2	.1	.05	.0005	.03	.005	.00005	.002	.0001	.0005	20,000	25	7	7.1
Springs that may contain volcanic water:															
Geyser waters	14	.03	.06	.10	.01	.15	.1	.003	.002	.0000	.02	2,000	300	1±	8.4
Non-geyser NaCl type	8	.06	.1	.13	.002	.3	.06	.001	.003	.0006	.01	10,000	110	1±	7.2
Acid SO_4-Cl type	13	.8	.3	.2	.01	.00	.7	.01	.0006	.0000	.01	9,000	300	6	2.2
Acid SO_4 type	11	1.5	.4	.4	.00	.00	400	.03	.004	.000	.3	2,000	200	30	1.9
HCO_3-SO_4 type	5	1	.2	.4	.005	50	10	.0	----------	----------	.4	500	70	1±	7.0
Springs that may contain metamorphic water:															
$NaHCO_3$-boron type	10	.05	.6	.02	.002	5	.05	.001	.002	.002	.1	12,000	80	5	6.8
Miscellaneous waters:															
Springs associated with Hg deposits	6	.04	.5	.03	.001	2	.4	.006	.002	.003	.1	3,000	90	20	7.0
Springs associated with Mn and W deposits	6	.5	.3	.07	.001	.3	.5	.02	.001	.000	.002	2,000	60	1±	6.8
Springs depositing travertine	6	1	.3	.15	.002	.2	1.4	.01	----------	----------	.02	2,000	60	1	6.5
Heated meteoric waters	6	.2	.2	.1	---------	15	4	.06	----------	----------	.1	200	50	---------	9.2

*Includes CO_3 as equivalent HCO_3.

soluble. The quantities present in a water are therefore determined by the local supply of each element throughout the history of origin and migration of the water and not in general by low solubility. Absorption, ion exchange, and influence of organic activity are considered as special factors not included in the term "low solubility."

Because saline waters can be diluted, and dilute waters can be concentrated by evaporation, the absolute quantity of a minor element in solution is considered in general to be much less significant than the ratio of the minor element to its geochemically most closely related major element.

No claim is made for exact precision or for any high degree of reliability for any one component or ratio, but if the characteristics of an unknown water agree within an order of magnitude with those of one of the types of table 206.1, the probability for such an origin is considered to be very good.

CONNATE WATERS AND OIL-FIELD BRINES

The existence of connate or "fossil" water has been questioned, but most geologists assume that many saline brines in deep sedimentary basins contain some water that is not greatly different in age from the enclosing rocks and is connate (White, 1957b, p. 1661–1678). Most connate waters are with little doubt ocean water associated with marine sediments; a few nonmarine connate waters are known.

Many of the chemical changes that take place in ocean water after its incorporation in sediments and isolation from oceanic circulation have been considered by White (1957b, p. 1662–1674).

Most deep brines of Tertiary oil fields are high in Na and Cl. On the other hand, the deep brines of most oil fields of pre-Tertiary age throughout the world are of the Na-Ca-Cl type; the distinction between these two types is arbitrarily based on a Ca/Na ratio of 0.1 by weight.

Some oil field waters of types not summarized in table 206.1 are characteristically high in sulfate and (or) bicarbonate rather than chloride. Sulfate and bicarbonate waters, although studied only slightly, are believed by the present author to develop after the connate chloride waters were largely flushed out by circulating meteoric water.

VOLCANIC OR MAGMATIC WATERS

It is clear that deep magmatic waters cannot be sampled directly at their sources except perhaps from fluid inclusions in minerals in igneous rocks and veins, and that volcanic emanations can be sampled only at the surface where pressures are low and compositions are perhaps much different than at depth where pressures are high (White, 1957a). Waters of spring systems characterized by especially high temperatures and heat flow and located in areas of active or relatively recent volcanism are of great interest because they may contain at least some volcanic or magmatic steam condensed at depth, where hydrostatic pressure is sufficiently high for substances of low volatility to be transported in solution in a dense vapor phase. The possible origins of the greatly differing types of waters in volcanic hot spring areas have been reviewed by White (1957a); the principal chemical characteristics of these types are summarized in table 206.1. Geyser waters are considered separately from other chloride waters because the very high geothermal gradient characterizing geyser areas is believed to increase the probability that some magmatic water, rather than entirely nonmagmatic waters, is involved.

WATERS OF POSSIBLE METAMORPHIC ORIGIN

Some spring waters of high mineral content have chemical characteristics that are not clearly indicative of any of the groups previously considered. One type of particular interest is characterized by high concentrations of Na, HCO_3, and B, and by relatively low Cl. White (1957b, p. 1678–1679) has suggested that these waters may be driven from hydrous minerals of sedimentary rocks that are being reconstituted during progressive metamorphism, after interstitial connate water high in chloride has been largely driven off during compaction of the sediments. These spring waters high in HCO_3, B, and Na are generally low in temperature; they are also relatively high in ratios of I/Cl and are notably lower in ratios of Li/Na and K/Na than the volcanic chloride waters. These characteristics suggest a relationship at least as close to connate as to volcanic waters.

OTHER SPECIAL GROUPS

Thermal and mineral waters associated with quicksilver deposits are in general more nearly similar in chemical composition to connate waters of the NaCl type and to waters of possible metamorphic origin than to volcanic waters (table 206.1). Of analyzed thermal waters associated with quicksilver deposits in California, Nevada, and New Zealand, 3 have characteristics suggesting a relation to connate NaCl water, 6 suggest a metamorphic origin, 3 are dominantly rather dilute meteoric water without clearly diagnostic characteristics, and only 1 is a recognizable volcanic water of the NaCl type.

Spring waters depositing Mn and in general some W (table 206.1) are dominantly meteoric water with some of the diagnostic characteristics of volcanic waters and of metamorphic(?) waters.

Little attention has been given to the minor element composition of meteoric waters that are known to have been in contact with salt deposits. The few available analyses indicate that K/Na is generally less than 0.005, Br/Cl is generally less than 0.0003, and B/Cl is generally less than 0.0002.

REFERENCES

Clarke, F. W., 1924, The data of geochemistry: U.S. Geol. Survey Bull. 770, p. 1–841.

White, D. E., 1957a, Thermal waters of volcanic origin: Geol. Soc. America Bull., v. 68, p. 1637–1658.

——— 1957b, Magmatic, connate, and metamorphic waters: Geol. Soc. America Bull., v. 68, p. 1659–1682.

207. GEOCHEMICAL INVESTIGATION OF MOLYBDENUM AT NEVARES SPRING IN DEATH VALLEY, CALIF.

By F. N. Ward, H. M. Nakagawa, and Charles B. Hunt, Denver, Colo.

In the course of a general geologic and geochemical study, a part of Death Valley, Calif., was discovered to be characterized by salts, brines, and other less saline natural waters that contain more than average amounts of molybdenum. To account for these amounts, field determinations were made on the salts, brines, plants, and waters along a traverse between Nevares Spring and the edge of the salt pan. A geologic cross section along the traverse is shown in figure 207.1.

Nevares Spring is a major hot spring in the area of molybdenum enrichment. Its waters, flowing at about 50 gallons per minute, rise along faults that separate Tertiary shales from Paleozoic rocks on the east side of the valley. The barren slope below Nevares Spring is mostly mantled with Pleistocene gravel. On a small bench where the gravel thins and exposes the underlying Tertiary beds, a second spring zone has developed. The springs in this zone are cold and include Cow Springs and the spring above Shadeless Acres. Travertine mounds built by Nevares Spring and springs of the second zone support mixed stands of phreatophytes, plants that send their roots to a permanent water table.

The gravel fan extending panward from the second spring zone is of late Pleistocene and Recent age. Its highly permeable surface supports a stand of desert holly (*Antriplex hymenelytra*), a xerophyte that depends on vadose water.

At the edge of the salt pan, where the gravel grades into sand and silt, the ground water is dammed by the silt and rises to the surface to form a third spring zone. The water issuing from this zone is cold and is depositing sodium carbonate and sodium sulfate. As the water moves panward, the proportion of dissolved sodium chloride increases, and the phreatophytes are zoned according to their increasing salinity tolerances. Identical species of plants such as arrowweed, tamarix, and desert holly, collected at Nevares Spring, Shadeless Acres (second spring zone), and the mouth of Cow Creek (third spring zone), contain identical amounts of molybdenum, even though the water taken up by the plants differs greatly in molybdenum content from one locality to another. Moreover, arrowweed and tamarix collected on the west side of the Valley contain the same amount of molybdenum as the same species do at Nevares Spring. This suggests that these species are saturated with molybdenum and therefore do not reflect differences in the molybdenum content of the water.

Data on the molybdenum content of the water, the dissolved solids, and the amount of dissolved solids are given in table 207.1.

TABLE 207.1.—*Molybdenum in waters and dissolved solids*

Sample	Location	pH	Total dissolved solids (ppm)	Molybdenum	
				Relative content of dissolved solids (ppm)	Relative content of water (ppb)
DV-1	Nevares Spring	7.4	700	25	18
2	Cow Spring	8.2	1,100	31	34
4	Mouth Cow Creek	8.4	14,000	18	270
5	Cow Creek Marsh	9.0	48,000	7	340

These data are obtained by a technique in which molybdenum from a brine or other natural water sample collects on a chelating resin, known commercially as A–1, according to a technique recently described by Nakagawa and Ward (1960). This resin shows a marked affinity for heavy elements. Because the affinity is unaffected by salt concentration, the resin is remarkably applicable to brines. Dilute alkali removes the molybdenum from the resin and the quantity of molybdenum is determined by its reaction with thio-

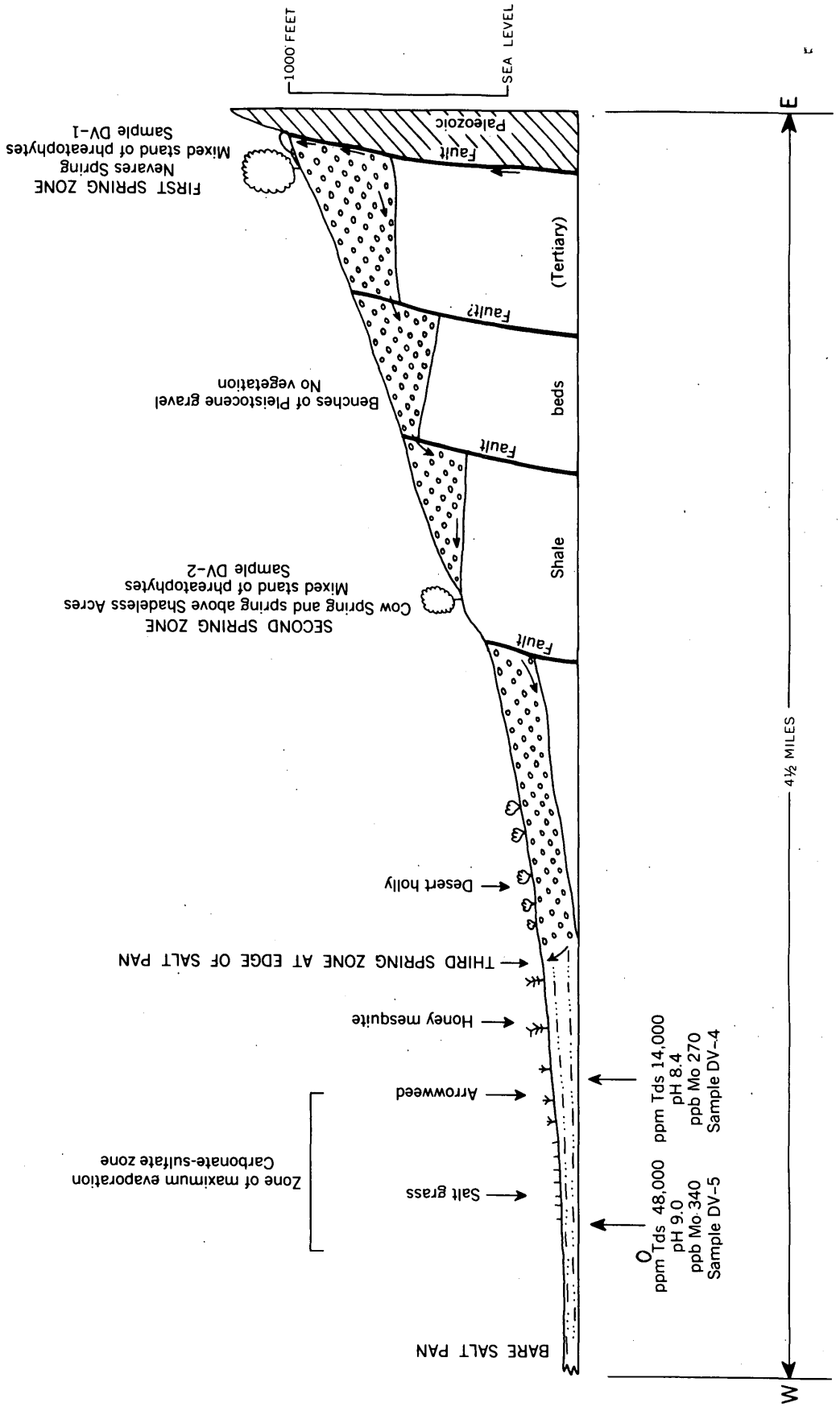

FIGURE 207.1.—Diagrammatic cross section from Nevares Spring to the Death Valley salt pan. Arrows show direction of movement of ground water.

cyanate to form a colored complex whose intensity is proportional to the concentration. The molybdenum content of salts and plants is measured similarly after special sample preparation. Salts are leached with hot water, and plants are ashed prior to leaching with dilute acid.

The molybdenum content increases from 18 ppb (parts per billion) in Nevares Spring water to more than 300 ppb at the mouth of Cow Creek, at the edge of the salt pan (sample DV–5). The increase parallels the increase in pH. Both the molybdenum and the pH reach a maximum in the carbonate-sulfate zone, where maximum evaporation occurs and the carbonate and sulfate precipitate (samples DV–4 and 5).

The increase in molybdenum content of the water might be attributed to the entry of molybdenum-rich waters from the faults in the Tertiary shale beds. The increase in total dissolved solids is greater than the increase in molybdenum, however, so the other dissolved solids would have to be introduced in larger amounts. The preferred hypothesis is that the increase in the concentration of solids is chiefly the result of evaporation. In Death Valley, the evaporation rate is about 150 inches per year (0.4 inches per day); the entire discharge from Nevares Spring could thus be balanced by evaporation over an area only 600 feet square, confirming as reasonable that part of the hypothesis. The 69-fold increase in the total solids and only 19-fold increase in the molybdenum between Nevares Spring and Cow Creek marsh is attributed to the concentration of molybdenum in the salts deposited during evaporation. The salt efflorescence at the mouth of Cow Creek and Cow Creek marsh (samples DV–4 and DV–5) contains 15 ppm of molybdenum (the sand immediately beneath it contains only 1 ppm molybdenum); in that sample, the salt contains appreciably more molybdenum than the water from which it formed, furnishing permissive evidence for the balance of the preferred hypothesis.

REFERENCE

Nakagawa, H. M., and Ward, F. N., 1960, Determination of molybdenum in water after collection on ion exchange resin: Abstracts of The Pittsburgh Conference on Analytical Chemistry and Applied Spectroscopy, p. 36.

208. THE DEATH VALLEY SALT PAN, A STUDY OF EVAPORITES

By Charles B. Hunt, Denver, Colo.

The Death Valley salt pan, California, one of the largest in the world, covers more than 200 square miles. All of it is below sea level. The salt crust on the pan ranges from a few inches to a few feet in thickness and lies on silt and clay. At the center, the salts in the crust and in the brines are mostly chlorides. These are surrounded by a narrow zone in which the salts are mostly sulfates, and these in turn by a zone containing carbonate salts. This zoning, which reflects the solubility of the salts, can be illustrated by evaporating a brine in a dish in a laboratory. When this is done (*A* in fig. 208.1), the first salts to precipitate are carbonates (*c*), which form at the edge of the dish and across the bottom. As the water level drops and the salinity of the brine increases, sulfates (*s*) are deposited. Finally, when maximum salinity is reached, chlorides, principally halite (*h*), are deposited.

The Death Valley salt pan consists of such concentric zones, but to continue the analogy on a laboratory scale, two complexities must be introduced. First, the floor of Death Valley has been tilted while the salts were being deposited, so the rings are crowded against the east side (*B* in fig. 208.1). Further, since the crust formed, fresh water entering the pan has reworked the salts (fig. 208.1*C*) by washing them from areas subject to frequent flooding (*f*) and concentrating them in irregular growths around those areas.

The salts are also layered in an orderly way where ground water is evaporating. At such places the most soluble salts, the chlorides, form a crust on the surface. Below this crust is a layer containing sulfate salts, and below this is a layer containing carbonate salts.

A different layering occurs in areas frequently flooded by surface water. In these areas a layer of mixed salts containing a high percentage of sulfates accumulates near the surface; the repeated floods wash the more soluble salts, including chlorides, from the layer.

The minerals are orderly too with respect to their degree of hydration. The less hydrated salts occur in two very different kinds of environments: they occur, as would be expected, on dry high surfaces subject to

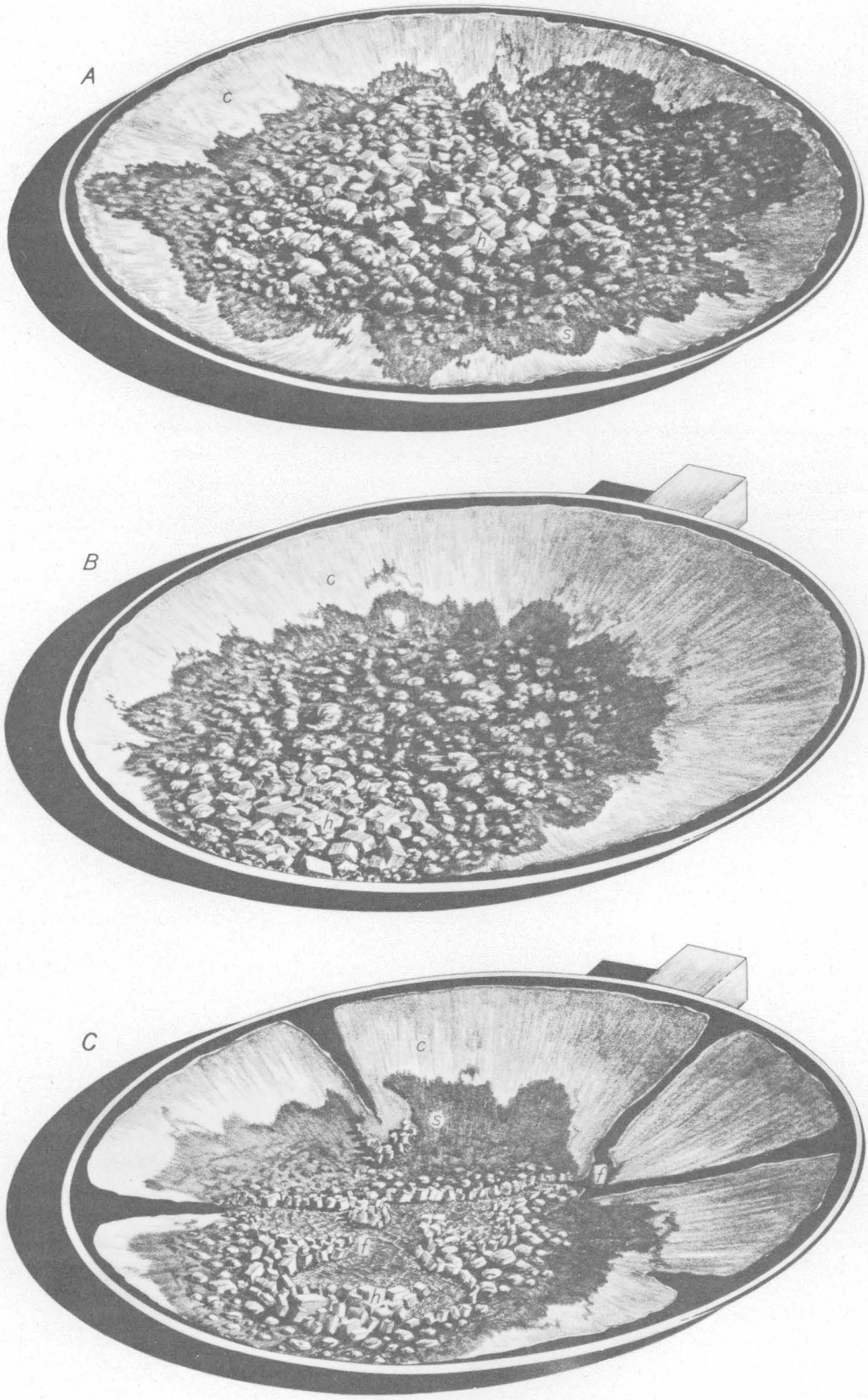

FIGURE 208.1.—Diagram illustrating chemistry and history of the salt pan in Death Valley.

557753 O—60——30

very high ground temperatures, but they also occur in wet environments that are highly saline.

The variations in composition of the salts are due to such factors as: differences in source of waters entering the salt pan, position in the pan, whether the water is ground water or surface water, whether it is standing or flowing, and seasonal and other long-range changes in temperature, precipitation, and evaporation. In wet periods, for example, when considerable water is entering the salt pan, the most soluble salts are washed to the middle. In dry periods, the brines become concentrated and deposit salts nearer the edge of the pan.

209. EARLY STAGES OF EVAPORITE DEPOSITION

By E-AN ZEN, Silver Spring, Md.

The minerals precipitated in the early stages of evaporation of sea water are the carbonates, halite, gypsum, and anhydrite. With the exception of the carbonates, these phases can all be referred to the ternary system $CaSO_4$–NaCl–H_2O. Figure 209.1, compiled from the literature, is an approximately correct polythermal liquidus diagram for this system at one atmosphere pressure, plotted for convenience on a semi-log scale. Within this system and at fixed pressure, there are seven invariant points, labeled a to g; these are shown in table 209.1. The temperature and composition of the binary eutectic ice-gypsum-solution is as yet unknown. Because of the low solubility of gypsum, however, its temperature is probably not much below 0°C, and its composition is probably not much different from what it is at 0°C. The univariant curves, *c-g* and *d-g*, are conjectural. A less probable alternative arrangement is shown in inset 2 of figure 209.1. These uncertainties, however, are not important to the main argument.

In figure 209.2*A* the system is portrayed in a conventional triangular diagram. For the sake of clarity, there is considerable scale distortion in this diagram, but the topological arrangement is unaltered. Three isothermal, isobaric sections are shown in figures 209.2*B*, 209.2*C*, and 209.2*D*.

To relate the phase diagrams to natural evaporite deposits, several features common to many of these deposits should be remembered.

First, the mineralogy of individual beds is simple. Unimineralic beds of anhydrite or gypsum, for example, are common; polymineralic beds are rarer.

Second, these unimineralic beds are commonly very thick; anhydrite beds up to several hundred feet in thickness are well known.

Third, distinct types of unimineralic beds may interlaminate and attain considerable cumulative thicknesses.

Unimineralic beds suggest deposition of evaporites in systems open to material exchange. For such thermodynamically open systems, and at arbitrary temperature and pressure, Gibbs' Phase Rule takes the form (Korzhinskii, 1950, p. 52)

$$\phi \text{max.} = c - c'$$

TABLE 209.1—*Data used for constructing the isobaric liquidus diagram (fig. 209.1)*

Point	Phases	Temperature (degrees C)	Soln comp., g/kg H_2O		References
			$CaSO_4$	NaCl	
a	Ice (I), gypsum (G), solution (L)	<0	≈ 1.75	0	Posnjak, 1938, p. 267.
b	Anhydrite (A), G, L	42	2.1	0	Idem, p. 268.
c	Sodium chloride dihydrate (H.2W), I, L	−21.1	0	303.9	Internat. Crit. Tables v. 4, p. 235, 1928.
d	Halite (H), H.2W, L	.15	0	356.5	Idem, p. 235.
e	H, A, G, L	14	≈ 4.4	359	Idem, p. 286 (extrapolated by present writer); MacDonald, 1953, p. 891.
f	G, H, H.2W, L	$t_f < -21.1$	----	----	
g	G, I, H.2W, L	$t_g < t_f$	----	----	
h	I, G, H, L	$t_h < t_j$	----	----	
j	I, H, H.2W, L	$t_j < -21.1$	----	----	

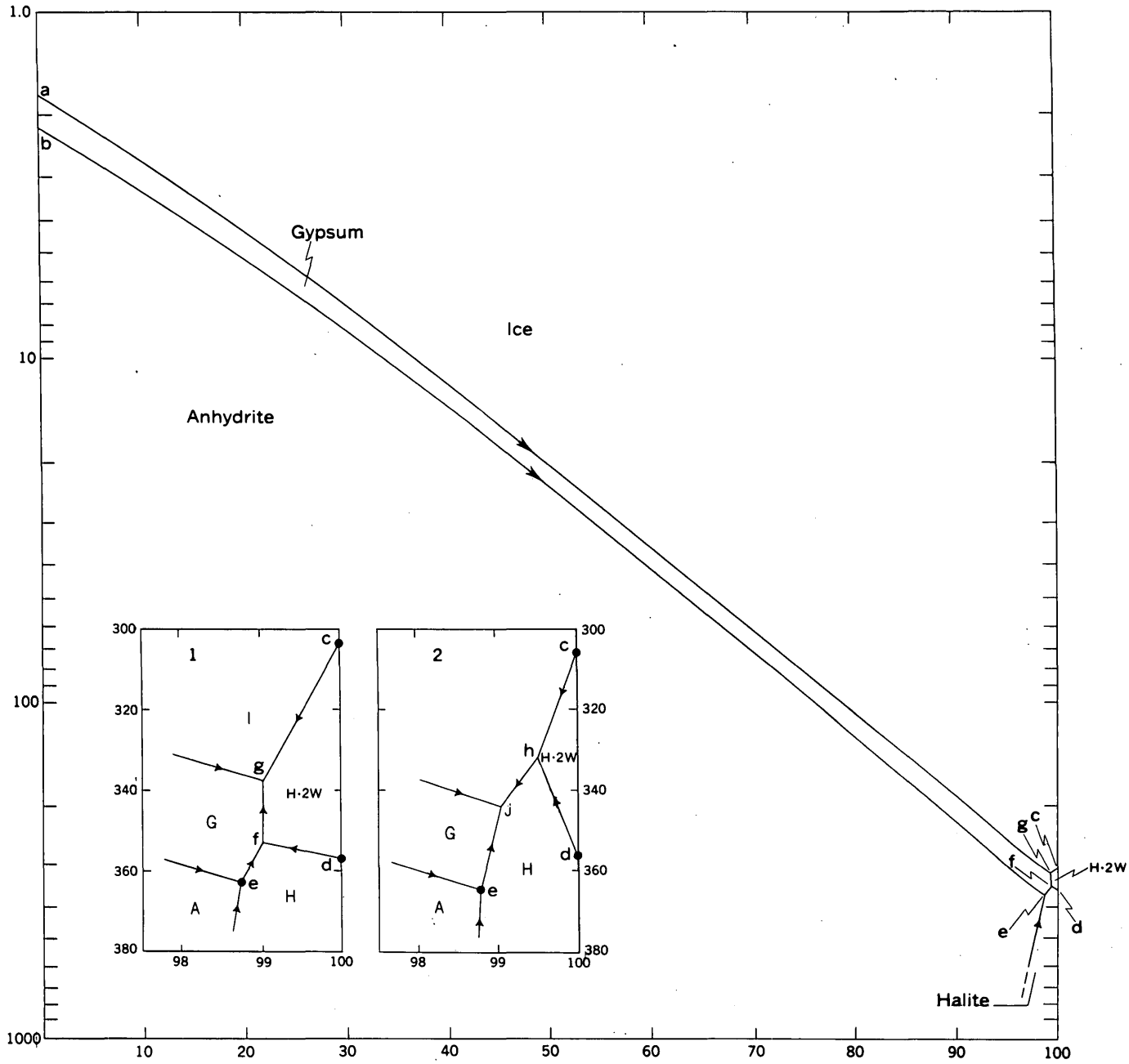

FIGURE 209.1.—Isobaric liquidus diagram for the system $CaSO_4$-NaCl-H_2O.

where ϕ is the number of phases in the system, c the number of distinct chemical components, and c' the number of components capable of exchange with their surroundings. The prevalence of unimineralic rocks thus indicates that there are only a few components that do not commonly undergo material exchange with their surroundings; it seems to rule out evaporation in a static basin with occasional replenishment of water, for such a setup is essentially a thermodynamically closed system.

The deposition of any unimineralic bed hundreds of feet thick requires that hydrologic, climatic, and bottom conditions remain more or less constant a long time; thick beds made up of interlamination of thin unimineralic layers show, however, that periodic fluctuations of environmental conditions can also occur.

A model of steady-state evaporation of sea water and precipitation of salts in a thermodynamically open system may help to explain these facts. Imagine that an ocean current of constant composition is generated from a fixed source, and concentrates as it flows and

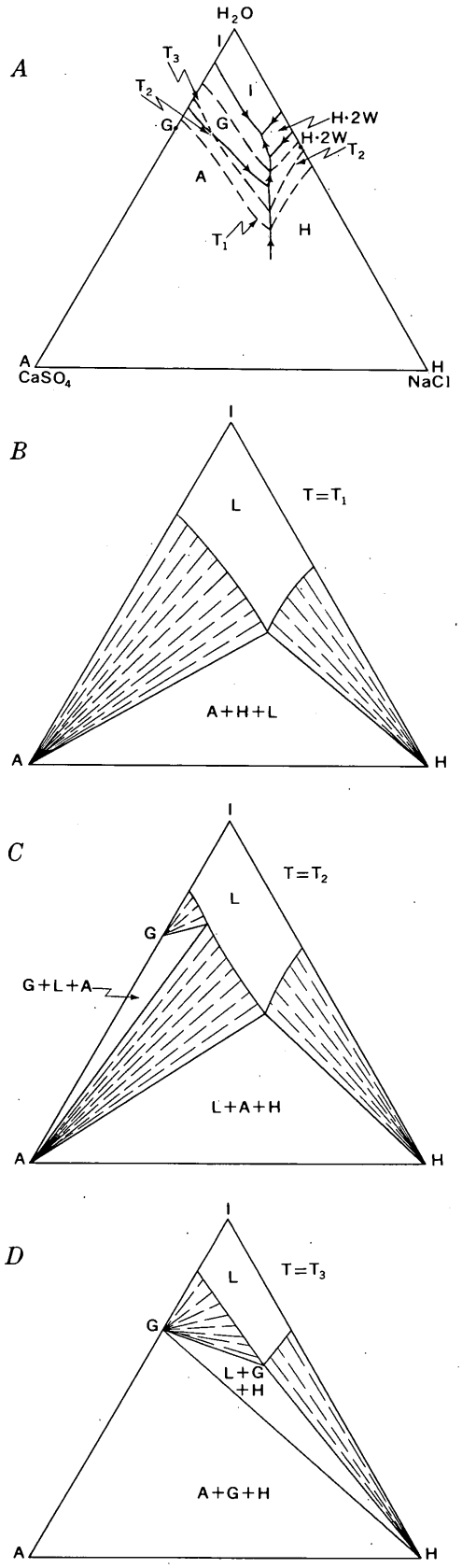

FIGURE 209.2.—Schematic liquidus diagram for the system $CaSO_4$–NaCl–H_2O with three isothermal sections.

evaporates. Suppose the chemical as well as physical conditions to be so balanced that the environment is constant at each point in space, although these conditions may change along the current. As a result, every mass of water arriving at a given spot will have exactly the same composition, temperature, and pressure as every other mass of water arriving at that spot, and will therefore precipitate the same salt. Each solid phase, however, can be precipitated from a range of water composition (fig. 209.2). Since the water composition must change gradually, a range of composition corresponds to an area in space; this is a way to get areally extensive beds of evaporite salts.

If, however, we follow a particuar mass of water along, the situation is more complex. If no mixing of waters of different origins occurs, the water will ordinarily first become saturated with one salt, then another is added, and so on, within one system, as isothermal evaporation proceeds; the solution will thus change in composition along a particular isotherm until a point like P in figure 209.2B is reached, and its composition will thereafter remain constant.

In our present model, however, precipitated salts settle to the bottom and become removed from the reacting system, which thus is thermodynamically open. In nature, moreover, physical conditions are expected to vary from one part of the current to another. Therefore, since the solution is not in contact with its precipitates, when changes in temperature or pressure occur, it cannot remain exactly saturated by reacting with these solids, as it could in a closed system. If the solution is initially in equilibrium with both halite and gypsum along the cotectic (such as at point P in figure 209.2B a change of temperature, let us say, will tend to cause it to become saturated with only one of these solids. Therefore, although multimineralic evaporite rocks can be derived by precipitation in a closed system through the mutual adjustment of solids and solution, in an open system such rocks can be derived only at specific temperatures and pressures, and are therefore of no importance geologically; the field geologist usually would see sharp contacts between unimineralic beds.

If the physical conditions fluctuate, the solution at a given point in space will alternately become saturated with one salt and then another; interlamination of unimineralic beds can therefore result, such as is found in the Castile formation (Permian) in Texas: in the lower part of this formation calcite and anhydrite laminae a few millimeters thick alternate for over 200 feet (Udden, 1924, p. 348–350; Adams, 1944, p. 1604). Moreover, if we trace these beds along a time plane, these salts should change laterally into one another, owing

to the combined effects of variations in T, P, and in water composition, resulting in onlap-offlap relations. Detailed mapping of the salts in a given deposit might produce a picture of the distribution of the physical variables during deposition, and of their changes with time.

REFERENCES

Adams, J. E., 1944, Upper Permian Ochoa series of Delaware Basin, West Texas and southeastern New Mexico: Am. Assoc. Petrol. Geologists Bull., v. 28, p. 1596–1625.

International Critical Tables, 1926–1933. New York, McGraw-Hill Book Co.

Korzhinskii, D. S., 1950, Phase rule and geochemical mobility of elements: Internat. Geol. Cong. 18th, London 1948, Proc., Sec. A. Problems of Geochemistry, p. 50–57.

MacDonald, G. J. F., 1953, Anhydrite-gypsum equilibrium relations: Am. Jour. Sci., v. 251, p. 884–898.

Posnjak, E., 1938, The System $CaSO_4$–H_2O: Am. Jour. Sci., 5th ser., v. 35A, p. 247–272.

Udden, J. A., 1924, Laminated anhydrite in Texas; Geol. Soc. America Bull., v. 35, p. 347–354.

210. SPATIAL RELATIONS OF FOSSILS AND BEDDED CHERTS IN THE REDWALL LIMESTONE, ARIZONA

By Edwin D. McKee, Denver, Colo.

The most distinctive lithologic unit in the Redwall limestone (Early Mississippian) of northern Arizona is the second member above the base, commonly referred to as the *B* member. This unit consists of thin beds of white chert and gray carbonate rock in an alternating sequence. Because of marked contrasts in color between the two types of rock this member is especially conspicuous in the walls of Grand Canyon where it forms a banded cliff with a height ranging from 70 feet in the east to 120 feet in the west. This member also is easy to recognize in well cuttings from the subsurface both east and north of Grand Canyon.

Alternating layers of chert and carbonate rock in the *B* member commonly give the impression, as seen from a distance, of even, flat bedding, but detailed examination proves that these layers have highly irregular top and bottom surfaces, and, in many places, they terminate laterally within short distances. Locally, the chert forms series of disconnected lenses or irregularly shaped masses. Beds of both rock types have a general horizontal attitude, however, and range in thickness from 2 to 8 inches. Fossils, common in the white porcelainlike chert, are preserved as external molds. The carbonate rock is pure limestone in the western part of the region, but uniformly fine grained dolomite in the eastern part.

A semiquantitative study has been made of the *B* member at selected localities to determine relations and distributional trends of rock types and of fossils throughout the Grand Canyon region. At each of 22 sites, considered representative of the member as a whole in this region, a 4- by 4-foot square was marked off on a vertical outcrop face for analysis. The pattern of chert distribution and the location and type of all recognizable fossils within the square, or sample plot, were then recorded on a chart (fig. 210.1).

Analysis of the sample plots indicates several significant features. First, fossils associated with the rock in eastern Grand Canyon, for example at Tanner Trail (fig. 210.1a), are dominantly bryozoans; those in central Grand Canyon, for example at Diamond Creek (fig. 210.1b), are largely crinoids; and those in western Grand Canyon, for example at Bridge Canyon and Whitmore Wash (figs. 210.1c, 210.1d), include both of these groups and many other types in addition. Furthermore, in western Grand Canyon the total number of all fossils is very much greater than farther east. Thus, differences in type and relative abundance of fossils, as determined from the sample plots, form a pattern representative of faunal facies on the shallow sea floor; this facies pattern is believed to have extended westward across a shelf toward the deeper waters of a geosyncline.

A second trend in the sample squares concerns fossil distribution in each of the two rock types. Fossils of all varieties are very much more numerous in the chert than in the associated carbonate rock. In eastern Grand Canyon this may be the result of fossil destruction during dolomitization, although this is not certain as moderately well preserved individuals are scattered through the dolomite. In western Grand Canyon, on the other hand, the carbonate rock as seen in thin section is fine to coarse grained limestone; therefore, the relative scarcity of fossils in carbonate rock seems to represent a feature of the original environment of deposition. Thus, the presence and distribution of beds

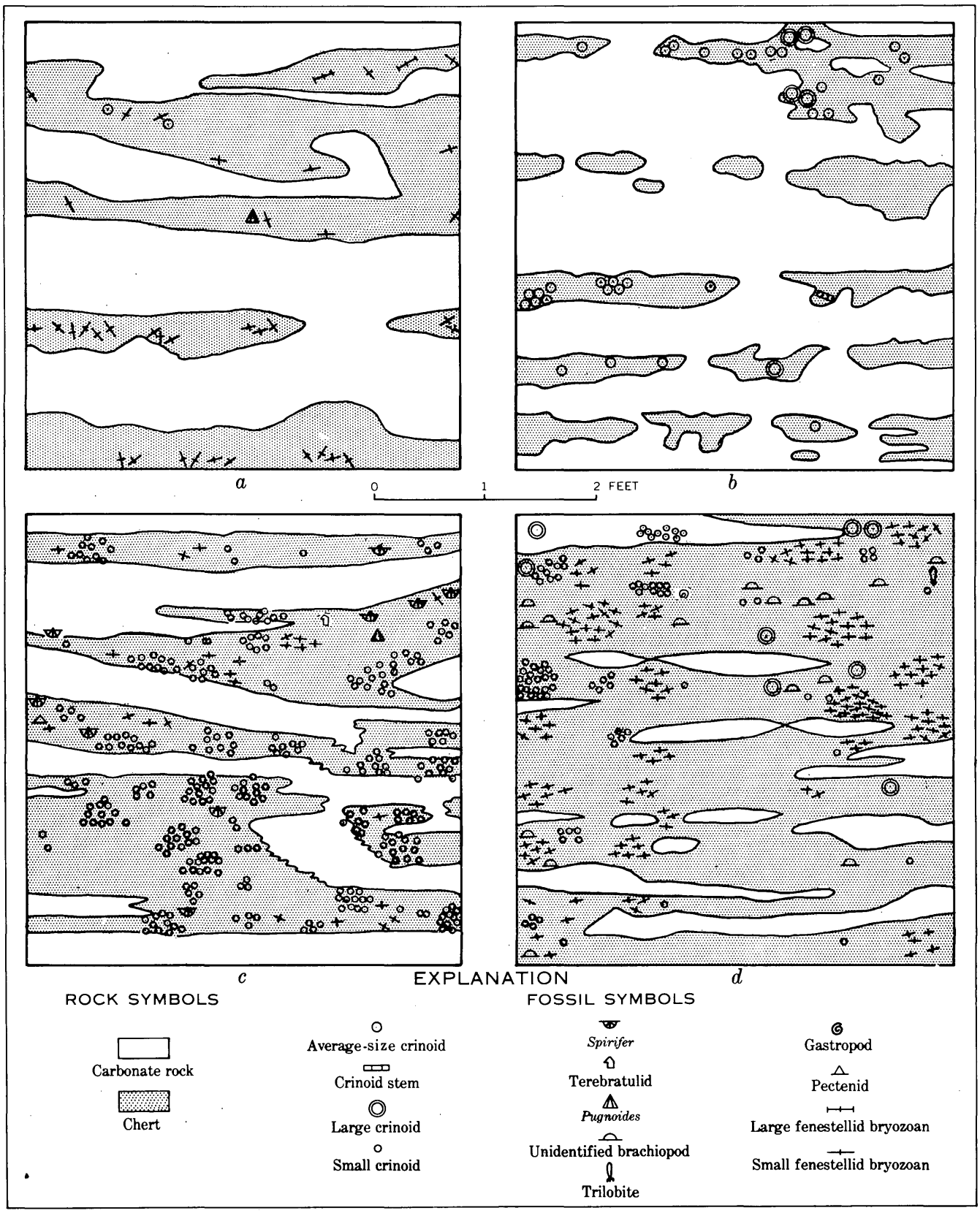

FIGURE 210.1.—Sample plots from four vertical outcrop faces of the *B* member of the Redwall limestone in Arizona, showing distribution of chert, carbonate rock, and associated fossils. *a*, Tanner trail, lower part of member; *b*, Diamond Creek, middle part of member; *c*, Bridge Canyon, upper part of member; *d*, Whitmore Wash, upper part of member.

and lenses of chert are related to distribution and abundance of fossils; locally abundant fossils may have formed zones of maximum permeability and therefore zones most favorable for silicification.

Because dolomite in the *B* member of the Redwall limestone is confined to the landward or easternmost sections of Grand Canyon, and for other reasons, such as the presence of protodolomite and the manner of fossil preservation, this rock is considered, in the classification of Dunbar and Rodgers (1957, p. 238), to be an S-dolostone rather than a T-dolostone, and is interpreted as having formed by replacement of calcium carbonate on or beneath the sea floor prior to lithification. The sample-plot study shows, however, that the chert was formed before the dolomite, for external molds in the chert show preservation of delicate details of shell structure, whereas molds in the dolomite are much less perfectly preserved. Because of this and supporting petrographic evidence, a very early stage of chertification is postulated for the bedded cherts of the Redwall limestone.

REFERENCE

Dunbar, C. O., and Rodgers, John, 1957, Principles of stratigraphy: New York, John Wiley and Sons, 356 p.

211. STRUCTURALLY LOCALIZED METAMORPHISM OF MANGANESE DEPOSITS, AROOSTOOK COUNTY, MAINE

By Louis Pavlides, Beltsville, Md.

GENERAL CHARACTER OF THE DEPOSITS

Layered manganese- and iron-bearing deposits in eastern Aroostook County, Maine, occur as sedimentary lenses, chiefly in folded rocks of Silurian age. They are grouped in three ill-defined areas that form a discontinuous belt about 65 miles long. In the central or Maple and Hovey Mountains area the lenses are in slate, which overlies a sequence of volcanic rocks and slate interlayered with graywacke. The rocks are in the greenschist facies of regional metamorphism.

The deposits in the Maple and Hovey Mountains area are of two primary lithologic types: (1) a hematitic type, which consists mostly of hematitic shale, slate, and banded hematite ironstone, and (2) a siliceous carbonate type. The deposits contain, on the average, about 7 percent manganese and 13 percent iron, but the lithologic units included in the deposits differ widely in grade, and so do the various kinds of rock within a given unit.

In deposits of the hematitic type, hematite is commonly the most abundant mineral, and braunite ($3Mn_2O_3 \cdot MnSiO_3$) and rhodochrositic carbonate the principal manganese minerals. Spessartite, bementite, cryptocrystalline apatite, quartz, muscovite, chlorite, and alkali feldspar are present in lesser amounts, along with local barite, phlogopite, chert, and hausmannite.

In the deposits of the siliceous carbonate type, the chief manganese minerals are rhodochrositic and sideritic carbonates. Chlorite is widespread and abundant. Pyrite is locally abundant, and some quartz, alkali feldspar, and cryptocrystalline apatite are present.

Magnetite of metamorphic origin is locally abundant in both primary facies, and it is possible to distinguish magnetite-bearing and magnetite-free varieties of both facies. The chief manganese mineral of the magnetite-bearing deposits is manganoan carbonate close to rhodochrosite in composition. Chlorite is abundant, and the accessory constituents include cryptocrystalline apatite, quartz, alkali feldspar, biotite, muscovite, stilpnomelane(?), and bementite(?). Deposits that originally consisted of siliceous carbonate also contain accessory pyrite and, in a few places, a very little pyrrhotite. Some unreplaced hematite remains in deposits that were originally of the hematitic type, but braunite is generally absent.

METAMORPHISM IN THE MAPLE-HOVEY DEPOSIT

The Maple-Hovey deposit, which is the largest in the area and the only one that will be discussed here, consists mainly of three superposed continuous units of manganese-bearing hematitic rock, but at its base in many places there is a thin and discontinuous layer of manganiferous siliceous carbonate. The total thickness of manganiferous rocks in the deposit averages about 150 feet. The deposit occurs in a doubly plunging syncline with numerous secondary folds.

Most of the magnetite occurs on or near the axes of secondary folds, both at the ends of the main syncline and along its flanks. Typically the magnetite occurs in

TABLE 211.1.—*Chemical analyses of manganese-bearing hematitic ironstones and manganiferous, magnetite-bearing ironstones from the Maple-Hovey deposit*

Laboratory No. / Field No.	51-1626CD [1] T-5-A	51-1627CD [1] T-12-A	51-1628CD [1] T-12-B	51-1629CD [1] T-42-A	51-1630CD [1] T-43-A	51-55SC [2] T-12+142E	Arithmetic average
A. Hematitic ironstones							
SiO_2	19. 19	19. 77	14. 64	13. 30	37. 14	21. 02	20. 84
Al_2O_3	3. 53	3. 31	2. 53	3. 20	9. 67	2. 53	4. 13
Fe_2O_3	38. 65	27. 10	55. 16	56. 67	5. 66	57. 10	40. 06
FeO	. 00	. 00	. 00	. 00	. 00	. 00	. 00
MgO	1. 49	1. 59	1. 08	1. 29	2. 36	1. 15	1. 49
CaO	5. 91	5. 04	5. 99	5. 31	2. 54	5. 02	4. 97
Na_2O	. 76	. 02	. 97	1. 32	1. 42	[4] . 18	. 78
K_2O	. 76	. 50	. 44	. 57	2. 74	[4] . 24	. 88
H_2O-	. 06	. 09	. 30	. 16	. 06	. 14	. 14
H_2O+	. 57	1. 05	. 94	. 71	. 70	1. 08	. 84
TiO_2	. 16	. 13	. 11	. 14	. 39	[4] . 16	. 18
CO_2	4. 78	4. 50	2. 96	4. 49	6. 85	1. 62	4. 20
P_2O_5	4. 02	3. 17	4. 15	3. 25	. 15	3. 70	3. 07
MnO	19. 87	33. 67	10. 37	9. 47	29. 93	6. 31	18. 27
S [3]	. 01	. 01	----	----	----	----	----
O	----	----	----	----	----	. 18	----
Total	99. 76	99. 95	99. 64	99. 88	99. 61	100. 43	99. 85

Laboratory No. / Field No.	51-1631CD [1] T-19-C	51-1632CD [1] T-23-B	51-1633CD [1] T-23-A	51-1634CD [1] T-23-C	51-1635CD [1] T-23-D	51-54SC [2] T11+270W	Arithmetic average
B. Magnetite-bearing ironstones							
SiO_2	8. 96	18. 62	19. 90	16. 63	13. 57	26. 41	17. 35
Al_2O_3	3. 59	3. 60	2. 25	3. 40	3. 73	4. 59	3. 53
Fe_2O_3	45. 52	40. 51	20. 09	42. 21	40. 21	39. 21	37. 96
FeO	17. 71	20. 86	3. 45	17. 24	1. 47	15. 53	12. 71
MgO	1. 35	2. 33	1. 54	1. 14	. 92	1. 78	1. 51
CaO	5. 98	4. 00	8. 09	4. 18	6. 56	4. 11	5. 49
Na_2O	. 03	. 04	. 02	. 03	. 10	[4] . 07	. 05
K_2O	. 26	. 23	. 63	1. 30	. 88	[4] . 45	. 63
H_2O-	. 08	. 58	. 57	. 57	1. 00	. 14	. 49
H_2O+	2. 07	2. 78	1. 88	1. 64	1. 95	2. 12	2. 07
TiO_2	. 14	. 14	. 10	. 09	. 03	[4] . 22	. 12
CO_2	2. 17	. 28	13. 26	3. 06	7. 22	. 00	4. 33
P_2O_5	4. 80	3. 13	5. 52	2. 94	4. 62	3. 16	4. 03
MnO	6. 98	2. 66	21. 99	5. 75	17. 27	1. 78	9. 41
S [3]	. 03	. 02	. 06	. 007	. 01	. 05	. 03
Total	99. 67	99. 78	99. 35	100. 187	99. 54	99. 63	99. 71

[1] Robert N. Echer, analyst, Denver, Colo.
[2] Charlotte M. Warshaw, analyst, Washington, D.C.
[3] Determined by M. K. Carron, Washington, D.C.
[4] Determined by S. M. Berthold, Washington, D.C.

layers that mark the original bedding, but none of the magnetite-bearing layers are stratigraphically continuous for more than a very short distance; most of them appear to cut across lithologic boundaries and to extend discontinuously along different stratigraphic levels. This distribution of the magnetite demonstrates that it is of metamorphic origin, and because the metamorphism which resulted in the formation of magnetite is closely associated with tight folds it is here called structurally localized metamorphism.

Where rocks of the hematitic type, such as the manganiferous banded hematite ironstones of the middle unit in the Maple-Hovey deposit, have undergone structurally localized metamorphism, they generally differ from their less metamorphosed equivalents in the following respects: (a) they contain virtually no braunite;

(b) they contain much magnetite but little or no hematite, indicating that the magnetite was derived from hematite; (c) they contain abundant chlorite, notably in certain layers and in the pressure shadows of magnetite; (d) they contain biotite; and (e) muscovite is coarser and more abundant in them than in the less metamorphosed rocks.

In siliceous carbonate rocks that have been affected by structurally localized metamorphism, the most conspicuous and apparently the most abundant metamorphic mineral is magnetite. The magnetite is mostly in the carbonate layers, and its iron apparently came from the iron-bearing carbonate. Pyrite grains are larger in the more highly metamorphised rocks than elsewhere.

CHEMICAL CHANGES

The chemical changes accompanying structurally localized metamorphism can be evaluated only for the originally hematitic rocks, because no comparable chemical analyses are available for the siliceous carbonate rocks. These chemical changes are indicated approximately by comparing the chemical analyses, given in table 211.1, of hematitic and of magnetite-bearing ironstones from the middle manganiferous unit of the Maple-Hovey deposit. They are believed to include: (a) formation of FeO (there is no FeO in the banded hematite ironstones), (b) increase in H_2O, and (c) decrease in Na_2O. These are the only chemical differences that persist in all the samples in table 211.1. Some of the apparent increases and decreases of other oxides may be significant, but none of them affect all the specimens listed in the table.

Other chemical data and field and petrographic relationships suggest that structurally localized metamorphism consisted essentially in a reorganization of the constituents within the deposits, without appreciable addition or subtraction of constituents except for the addition of H_2O.

The chief chemical changes in the hematitic-type deposits involved reduction of Fe^{3+} to Fe^{2+} to form magnetite from hematite, and simultaneous reduction of the higher valence manganese oxides to MnO, resulting in the destruction of braunite. Hydration, whose chief result was formation of chlorite, also occurred. In the siliceous carbonate rocks the reactions involved a partial oxidation of the Fe^{2+} radical of the carbonate Fe^{3+} to form magnetite.

Structurally localized metamorphism is believed to have occurred in tight folds because they facilitated the movement of regional fluids and acted as local thermal nodes. The conditions necessary to form magnetite were presumably achieved where the chemical potential of the oxygen in fluids permeating and moving through the deposits was such that magnetite was the stable mineral phase at a certain critical temperature. In order for the systems fluid-hematite and fluid-$FeCO_3$ to adjust towards equilibrium at the prevailing oxidation-reduction potential of the environment, hematite was reduced to magnetite and the iron in the carbonate was oxidized to magnetite.

212. MIGRATION OF ELEMENTS DURING METAMORPHISM IN THE NORTHWEST ADIRONDACK MOUNTAINS, NEW YORK

By A. E. J. Engel, and Celeste G. Engel, La Jolla, Calif.

Work done in cooperation with the California Institute of Technology, Pasadena, California, the University of California, La Jolla, California, and the National Science Foundation

The sialic segment of the Earth's crust and many associated hypogene mineral deposits are presumably extracts or differentiates from subjacent, more mafic rock. The extraction of felsic, volatile, and ore-forming substances from simatic subcrust or mantle clearly involves transfer by magma, migma, and metamorphic fluids—although the relative roles of igneous and metamorphic processes remain enigmatic. One way of better understanding the origin, growth, and regeneration of the sial and its mineral deposits is to examine the changes in common crustal rocks induced by progressive, regional metamorphism, and to study the changes in properties of these rocks as they seem to approach and cross threshold conditions for melting.

The present study, in the northwest Adirondack Mountains, is an attempt to evaluate the changes in

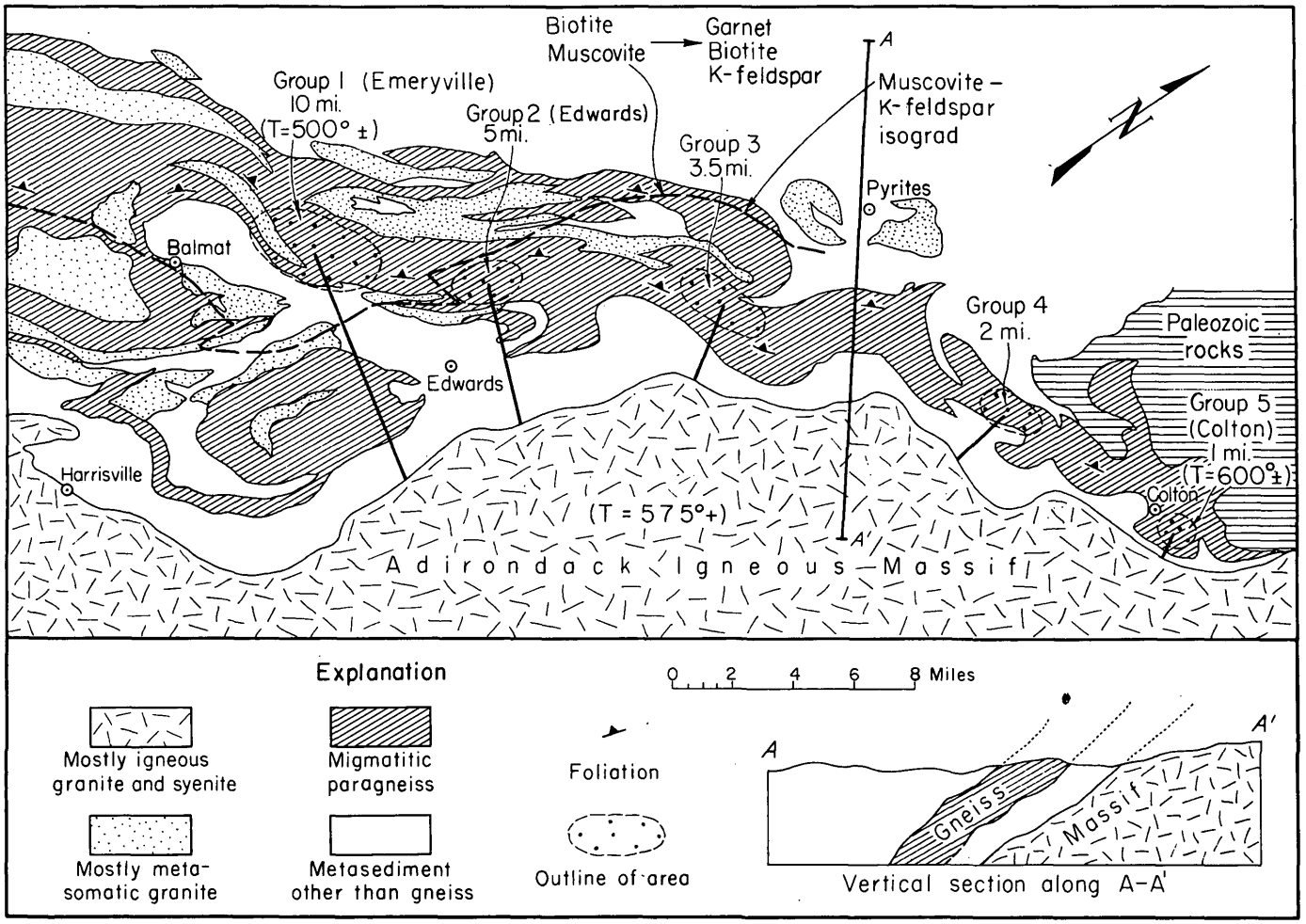

FIGURE 212.1.—Sketch map of the northwest Adirondack Mountains showing the relations of the paragneiss, marble, and associated granite to the Adirondack massif. The amphibolites described in the text occur within the gneiss complex. The lines drawn approximately normal to the perimeter of the massif indicate the relative distances of the several sample localities from the massif. Emeryville is in the area of group 1 and Colton in group 5.

composition and characteristics of three common rock types—basalt, graywacke, and siliceous magnesium limestone—as these are traced some 40 miles into the core of the Adirondack orogen (fig. 212.1).

The geological features of these three rock types and their stratigraphic and structural relations have been previously described (Engel and Engel, 1953; Brown and Engel, 1956; Engel and Engel, 1958, 1960). Geological thermometers indicate that temperatures of metamorphism were about 500° C at the southwest end of the belt, and at or slightly above 600° C near the perimeter of the massif (Engel and Engel, 1958) Depths of metamorphism are inferred to be from 5 to 10 miles.

The metamorphism of graywacke has been described in a series of publications (Engel and Engel, 1953, 1958, 1960). At the lower temperature end of the belt the graywacke is metamorphosed to a quartz-biotite-oligoclase-muscovite gneiss whose bulk composition seems to be that of the parent metasedimentary rock, fig. 212.2). With increasing temperature of metamorphism the mineral and chemical composition of the graywacke changes as shown graphically in figure 212.2. Muscovite disappears, garnet appears, plagioclase increases in abundance and in average An content, and quartz and biotite decrease (fig. 212.2). Complementary changes in chemical composition include a decrease in K, Si, Fe^{+++}, H_2O, and Ba. There is a well-defined complementary increase in Al, Fe^{++}, total Fe, Mg, Ca, Cr, Ga, Ni, and V. The ratio $Si+K+Na+H_2O/Ca+Mg+Fe$ changes from about 6.4 at Emeryville to about 4.5 at Colton. These changes amount to a degranitization or basification of the gneiss which appears to be anatectic in origin. The process of basification begins at about 550° C and is well-defined at 600° C. The mobilized Si, K, Ba, and H_2O appear to be partly liberated and partly trapped as veinitic migmatite. The basaltic rocks at the southwest end of

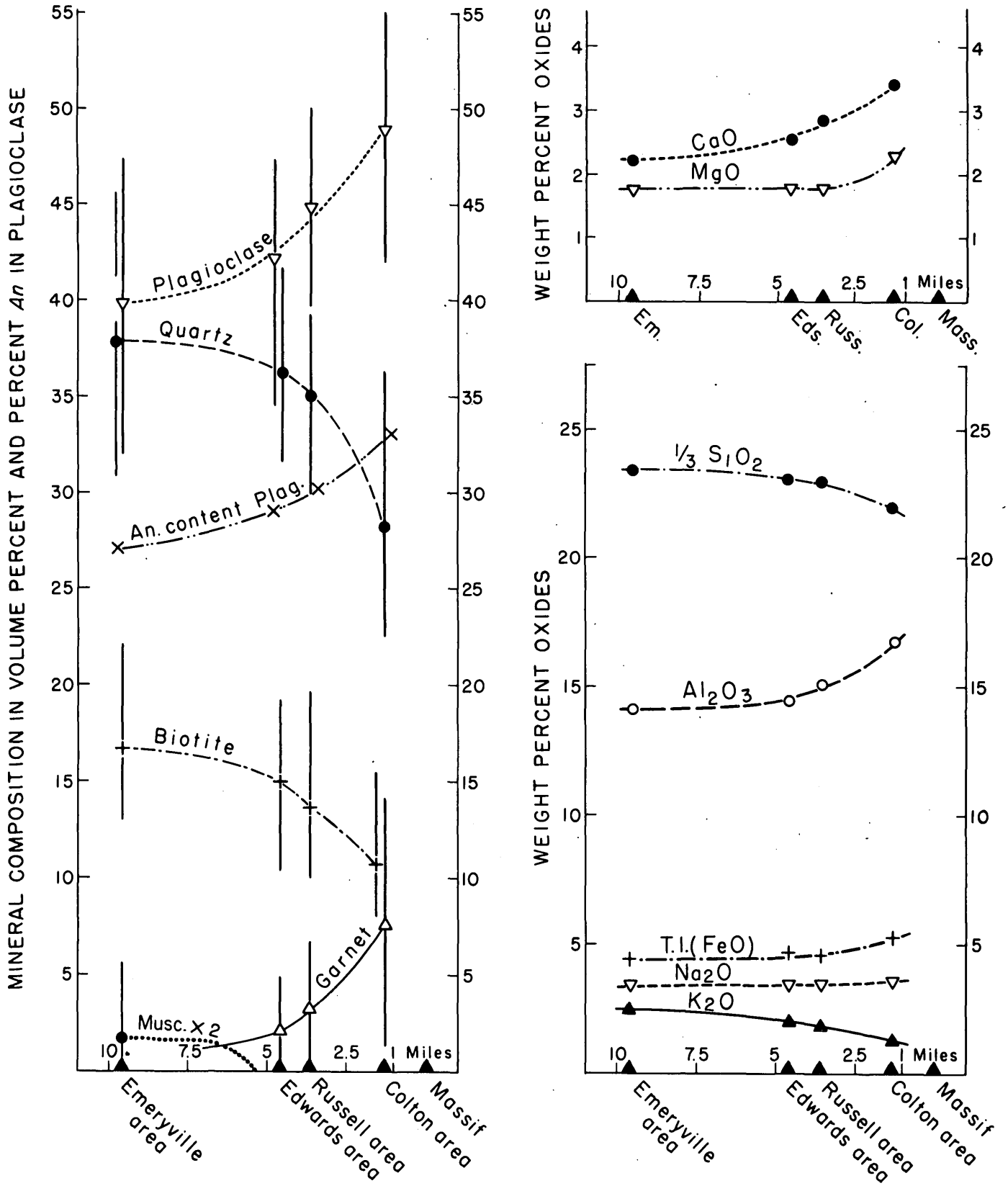

FIGURE 212.2.—Generalized curves indicating changes in mineral and major-element composition of 73 samples of paragneiss in the Emeryville-Colton region, New York. Points indicate the mean composition of the gneiss in each area. The vertical lines drawn through the points at Emeryville and Colton indicate the maximum range or dispersion of values from the mean. Distances between areas on the horizontal coordinate are measured along horizontal lines drawn normal to the trace of the perimeter of the massif to the center of each area or group (fig. 212.1).

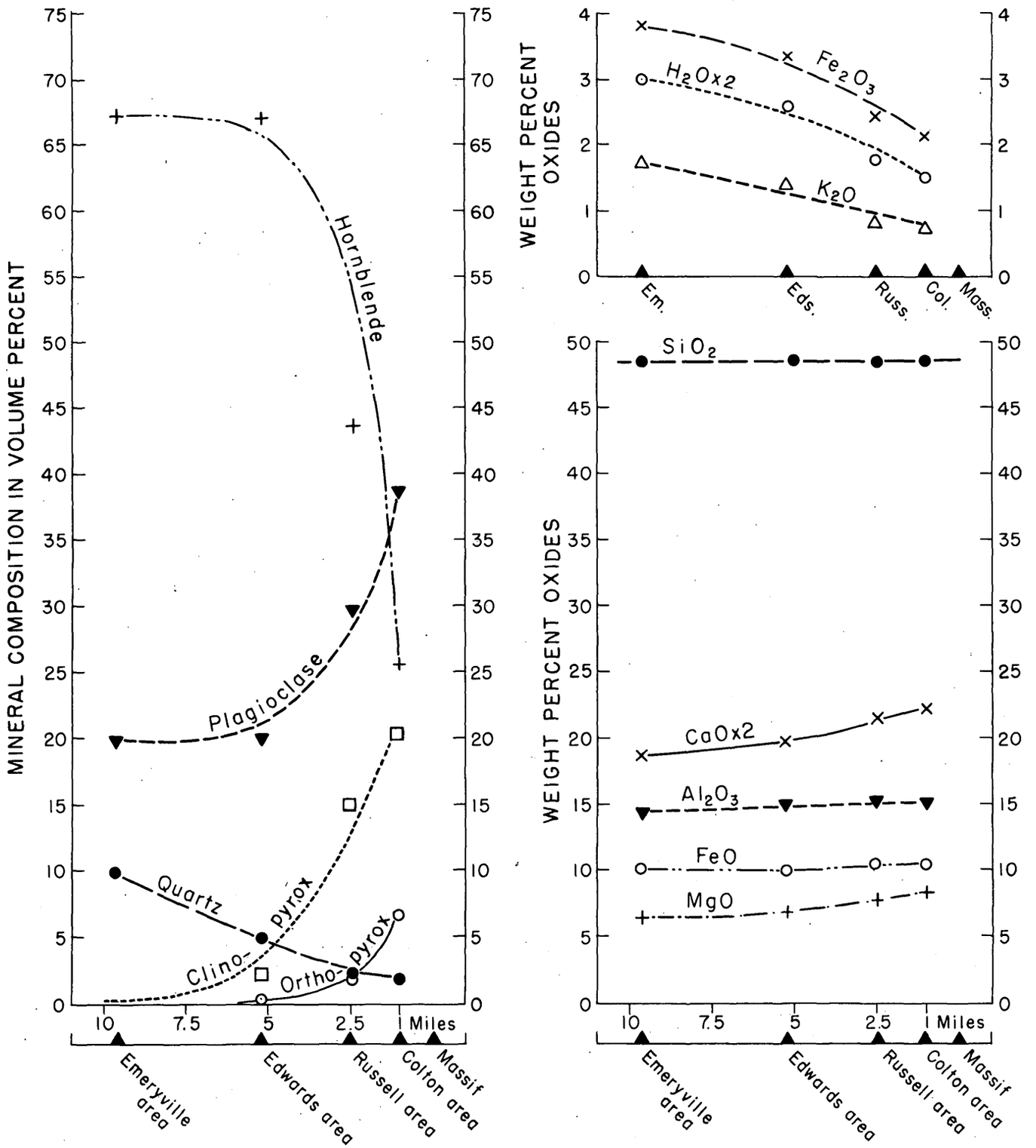

FIGURE 212.3.—Generalized curves indicating changes in mineral and major-element compositions of 76 samples of amphibolite in the Emeryville-Colton region, New York. The form of this graph is identical with that of figure 212.2, with which this should be compared.

the belt, where temperature and pressure were lowest, are metamorphosed to dark-green to black, coarse grained hornblende-andesine amphibolites with about 10 percent quartz, 2 percent ilmenite, and 0.4 percent sphene (fig. 212.3). The bulk chemical composition is that of a slightly oversaturated basalt. At Colton, New York, 30 miles to the northeast, where higher temperature and pressure prevailed, the amphibolites are greenish-black, coarse grained labradorite-two pyroxene-hornblende gneiss, with about 2 percent quartz and 2 percent ilmenite; here the chemical composition is that of an olivine basalt. With increasing grade of metamorphism, there is a decrease in K_2O, H_2O, and in the ratio Fe^{+++}/Fe^{++}. Amounts of Ca and Mg have increased and the ratio K/Ca decreases from 1.3 at Emeryville to 0.4 at Colton.

In the thick siliceous marbles associated with the rocks described above, diopside has formed as the highest rank mineral at both Emeryville and Colton. Commonly, the diopside occurs as reaction rims or coronas separating metasedimentary quartz and dolomite. These rims thicken as the marble is traced to the northeast. Consequently, there is good evidence that progressive metamorphism is accompanied by progressive decarbonation of the marble (fig. 212.4).

The systematic changes in composition of the three contrasting rock types—basalt, graywacke, and marble—with progressive metamorphism appear almost certainly to be metamorphic in origin, rather than fortuitous properties of the premetamorphic rock sequence. Although this conclusion is based primarily on the field relations and measured properties of the rocks, it also is consistent with predictions from laboratory and theoretical studies (Tuttle and Bowen, 1958, p. 117).

Assuming that this interpretation is correct, it is of interest to examine the amounts and relative proportions of the liberated substances and their capability to form significant rock and mineral deposits. Volume changes in the system during metamorphism may be inferred from detailed field studies. Theoretically all three units may be expected to decrease in volume with the decrease being greatest in marble, intermediate in gneiss, and least in amphibolite. Actually, field studies indicate that the marble and gneiss decrease in total thickness by about 30 and 15 percent respectively between Emeryville and Colton. There is no well-defined change in the volume of amphibolite.

Assuming that two-thirds of the volume changes in the gneiss and marble are due to loss of constituents during metamorphism, and that no decrease in the volume of amphibolites has occurred, a cubic kilometer of these rocks in their relative proportions, have released on the order of 53 million tons of SiO_2, 7.8 million tons of K_2O, 4.4 million tons of H_2O, and 160 million tons of CO_2.

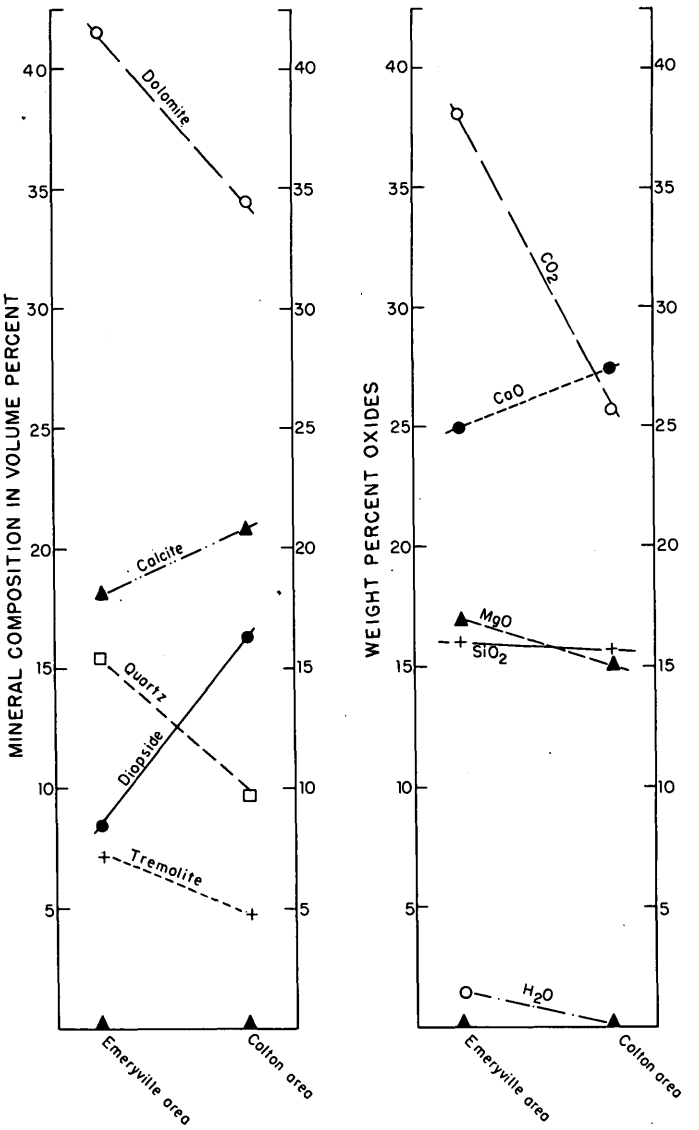

FIGURE 212.4.—Graph illustrating the approximate extent of decarbonation of marble, due to the growth of metamorphic silicates, especially diopside, in the Emeryville and Colton areas.

Some conception of the volume of mobilized material is indicated by the fact that at least 10,000 cubic kilometers of combined gneiss, marble, and amphibolite appear to have undergone this type of high grade metamorphism and partial melting in the exposed Adirondack orogen; and an equivalent or greater amount was even more completely fluxed and variously assimilated.

The amounts and kinds of trace elements that have accompanied these major elements are most difficult to assess in view of the errors inherent in our calculations.

TABLE 212.1.—*Estimated amounts of alkalis, silica, water, and carbon dioxide emitted from paragneiss, amphibolite, and marble during regional metamorphism in the Colton area, New York*

[Expressed in tons per cubic kilometer]

Oxide	Rock type [1]			
	Gneiss	Amphibolite	Marble	Total [2]
SiO_2	21×10^7	trace	----------	525×10^5
K_2O	26×10^6	13×10^6	----------	78×10^5
H_2O	10×10^6	19×10^6	----------	44×10^5
CO_2	----------	----------	25×10^7	163×10^6

[1] Includes 80 percent of the total Grenville-like metasedimentary rocks and associated volcanics in the northwest Adirondacks.

[2] A weighted average in which gneiss constitutes 25 percent, amphibolite 10 percent, and marble 65 percent.

There is no doubt, however, that large volumes of Ba, B, Pb, Zn, and Mn have been released during metamorphism. The amount released from the gneiss alone are on the order of 100 thousand tons of Ba per cubic kilometer, 25 thousand tons of Mn, and 10 thousand tons of Pb. Analyses of samples from other rock types are not completed.

The processes of mobilization of these elements, their mode of migration, sites of distribution and deposition, and related phenomena remain speculative. Probably the gneiss in the area between Russell and Colton was partly molten during the most intense phase of metamorphism, and at least incipient melting must have occurred at Emeryville. The experimental work of Tuttle and Bowen suggests that with 1 percent constituent H_2O, about 10 percent of the paragneiss could have been liquid at the temperatures and pressures pertaining at Colton.

Tuttle (in Tuttle and Bowen, 1958, p. 126) notes:

> As melting (of felsic rocks in the crust) may take place at temperatures as low as 600° C in the presence of water vapor, and at still lower temperatures when other volatiles are also present, it seems reasonable to consider partial melting as an important agent for promoting regional metamorphism.

The suggested fluxing and emission of volatiles and alkali silicates in the Adirondack rocks appears to be documented by the migmatite and granite intimately associated with the gneiss complex.

The ratio of K_2O/SiO_2 which seems to have been liberated from the gneiss is about 1:8, very close to that in associated congealed migma. The ratio of K_2O/SiO_2 emitted from the amphibolite seems very much larger—probably 2:1.

Whether or not the potassic minerals formed during retrograde metamorphism and whether the deposits of Pb, Zn, and Ba at Emeryville were also derived from the gneiss is uncertain. The amounts of Pb, Zn, and Ba emitted from the gneiss alone seem to be large enough—if concentrated—to form all the known deposits of these metals in the northwest Adirondacks; but studies of the migmatites suggest that a large fraction—one-half to three-fourths—of these elements have remained associated with the K-feldspar, muscovite, and related metamorphic silicates of the migmatites.

SUMMARY

In the metamorphic sequence of the Adirondack orogen, H_2O and CO_2 are the first common constituents expelled in large volume. Probably this is a generalization applicable to most terranes. And very little else may be expelled during any regional metamorphism that does not exceed intermediate grade. Certainly the accumulating evidence from diverse terranes is that the other common rock-forming elements do not migrate very far in the lower and middle grade of metamorphism (Shaw, 1956; Raychaudhuri [1]; Schwartz [2]). Data from the Emeryville-Colton region suggest that if other common rock-forming elements are considered, the alkalis, especially K, and its cogeners, appear to be mobilized first, followed by silica. Studies are to be continued with the aim of refining the data we have and amplifying them with information from other rock units in the Adirondack orogen, and elsewhere.

REFERENCES

Brown, J. S., and Engel, A. E. J., 1956, Revision of Grenville stratigraphy and structure in the Balmat-Edwards district, northwest Adirondacks, N.Y.: Geol. Soc. America Bull., v. 67, p. 1599–1622.

Engel, A. E. J., and Engel, C. G., 1953, Grenville series in the northwest Adirondack Mountains, N.Y.—Part II, Origin and metamorphism of the major paragneiss: Geol. Soc. America Bull., v. 64, p. 1049–1097.

——— 1958, Progressive metamorphism and granitization of the major paragneiss, northwest Adirondack Mountains, N.Y.—Part I, Total rock: Geol. Soc. America Bull., v. 69, p. 1369–1414.

——— 1960, Progressive metamorphism and granitization of the major paragneiss, northwest Adirondack Mountains, N.Y.—Part II, Mineralogoy: Geol. Soc. America Bull., v. 71, p. 1–58.

Shaw, D. M., 1956, Geochemistry of pelitic rocks—Part III, Major elements and general geochemistry: Geol. Soc. America Bull., v. 67, p. 919–934.

Tuttle, O. F., and Bowen, N. L., 1958, Origin of granite in the light of experimental studies in the system $NaAlSi_3O_8$–$KAlSi_3O_8$–SiO_2–H_2O: Geol. Soc. America Mem. 74, 152 p.

[1] Raychaudhuri, Bimalendu, 1960, Studies of amphibolites and constituent hornblendes from an area of progressive metamorphism near Lead, South Dakota: California Inst. Tech. Ph.D. thesis.

[2] Schwartz, H. P., 1960, Geochemical investigations of an arkosic quartzite in the Winchester-Hemet area, California: California Inst. Tech. Ph.D. thesis.

213. CHILLED CONTACTS AND VOLCANIC PHENOMENA ASSOCIATED WITH THE CLOUDY PASS BATHOLITH, WASHINGTON

By Fred W. Cater, Jr., Denver, Colo.

The Cloudy Pass batholith, a post-Eocene intrusive remarkable for a number of features not normally associated with batholiths, lies along the crest of the Northern Cascade Mountains in north-central Washington. The batholith is about 11 miles wide, has a known length of about 15 miles, and is exposed to a depth of about 4,000 feet below its roof; it intrudes pre-Tertiary crystalline rocks, mostly gneisses, although some satellitic dikes intrude Eocene rocks. Only the southeastern part of the batholith, in the Holden quadrangle, was studied in detail (see fig. 213.1). In this quadrangle the batholith is cut by intrusive breccias and is bordered in many places by porphyritic chilled rocks. Although such chilled borders have been reported on other batholiths, they are rare. The southeastern end of the batholith cuts off a large graben and plunges beneath pre-Tertiary gneisses that are pierced by a southeast-trending line of porphyry plugs, irregular breccia pipes, and a volcanic neck, all of which are believed to rise from an underlying part of the batholith. The volcanic neck is the only one known to me that can be tied with reasonable assurance to a visible batholith.

In addition to the fact that in places the border rocks grade into the main body of the batholith, several lines of evidence support the belief that border rocks, plugs, and the volcanic neck are consanguineous to the batholith: (a) The chemical compositions of the chilled and batholithic rocks are closely similar; (b) certain distinguishing mineralogic features are common to all, such as sodic labradorite crystals of identical habit that characteristically show marked oscillatory zoning, and grains of quartz that are either euhedral or rounded by resorbtion; (c) rocks of the chilled border, plugs, and volcanic neck are microscopically identical except for the closer packing of phenocrysts in some phases; (d) locally the interior rocks of some of the plugs are closely similar to the rocks of the main mass of the batholith; and (e) the spatial relation suggests that the plugs and the volcanic neck rise from the plunging end of the batholith. Some of this evidence is discussed at greater length below.

The main body of the batholith is a granogabbro, for the constituent minerals are sodic labradorite, quartz, orthoclase, hornblende, biotite, and minor augite. The labradorite characteristically shows marked oscillatory zoning; orthoclase replaces earlier formed minerals or is interstitial and normally occurs only in the main body of the batholith. The texture of the batholithic rocks is typically igneous. Leucocratic granodiorite, a late differentiate, occurs in dikes and also as the matrix of intrusive breccias, both of which cut the batholith. The contact of the interior part of the batholith with the marginal porphyritic border rocks is sharp and intrusive in most places but in a few it is gradational.

The border rocks are thickest along the steeply dipping eastern contact of the batholith. They consist in general of phenocrysts of sodic labradorite, rounded or euhedral quartz grains, hornblende, and augite in a groundmass of fine-grained andesine, quartz, and hornblende. Orthoclase is rare and occurs principally as fracture fillings. Locally the groundmass has a pilotaxitic texture.

Three layers of border rocks were mapped, each differing somewhat in megascopic appearance. The outer layer is most extensive and not only borders the northeast side of the batholith as far as it has been traced but, southeast of Hart Lake, diverges as a prong from the batholith. The rock in this layer is mesocratic and has a peculiar texture because of close packing of the phenocrysts from which most of the matrix appears to have been squeezed out while still liquid. The other two layers are aphanitic, almost black, and contain fewer phenocrysts; the central layer differs from the inner layer by possessing a fragmental texture like that of a volcanic flow breccia, although all the border rocks show a protoclastic texture. The contact of the outer layer with the gneissic host rocks is roughly conformable and sharp; gneiss adjacent to the contact is crumpled and brecciated. The contact between the central and outer layer is intrusive, the central layer intruding the outer, but as intrusion occurred before the outer layer had completely solidified, the contact is not everywhere sharp. The contact between the central and inner layers is gradational.

The outer layer of the border zone was evidently injected as a dike slightly ahead of the advancing batholith, as it diverges from the batholith south of Hart Lake, rises to levels higher than the batholithic roof at places, and unlike the other layers, nowhere laps over the top of the batholith. The central layer and especially the inner layer are conformable with the side and

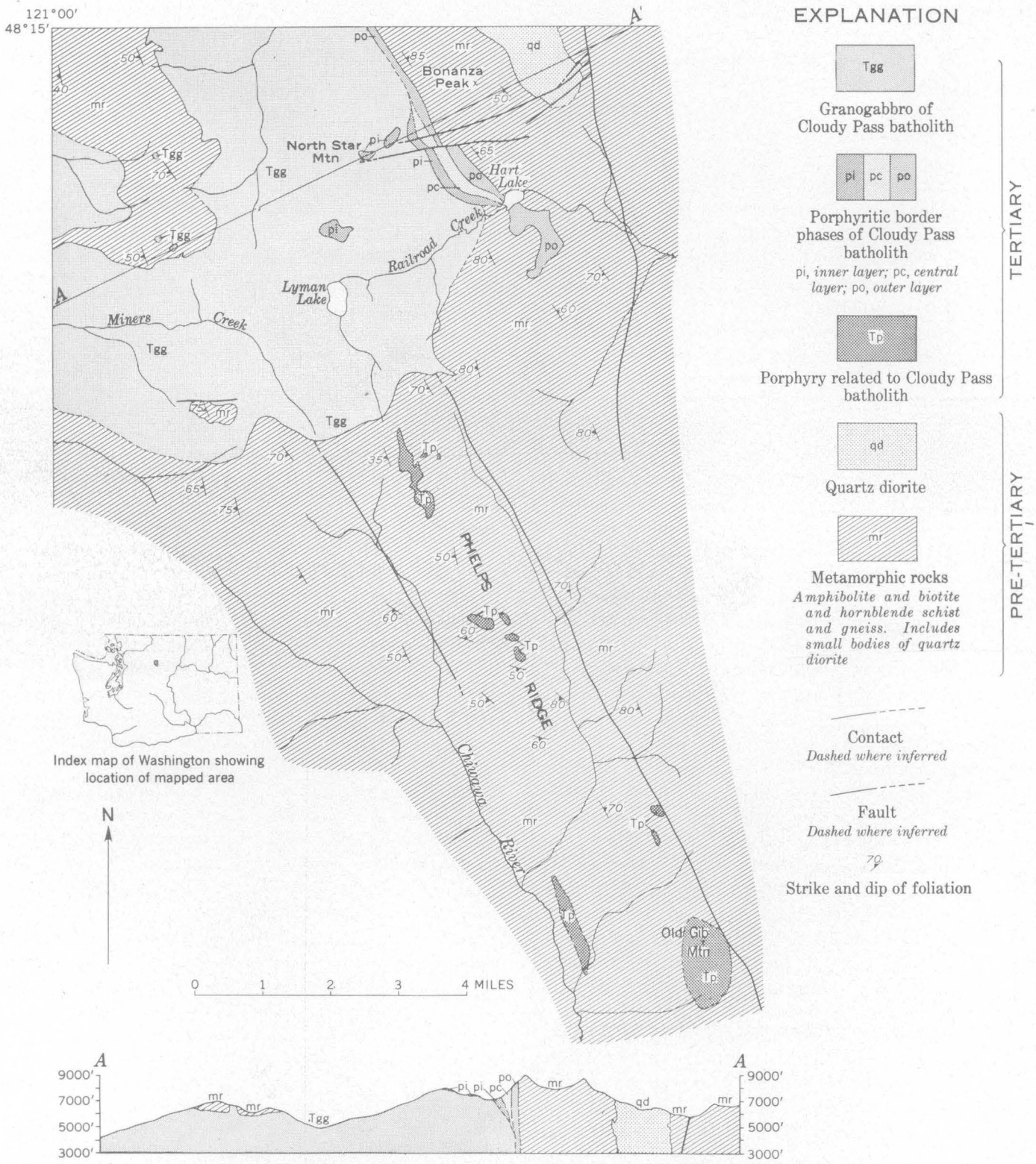

FIGURE 213.1.—Geologic map of part of the Cloudy Pass batholith and related rocks, Holden quadrangle, Washington.

roof of the batholith and evidently constitute a chilled border that formed during the last stages of advance of the batholith. The central layer appears to have formed as the chilled but only partly solidified margin of the batholith dragged against and mixed with the only partly solidified rocks of the outer layer.

Two types of intrusive breccias are related to the batholith. One consists of rounded fragments of the

batholithic rocks set in a matrix of leucocratic granodiorite and is restricted to the batholith. The other consists of fragments of both batholithic and gneissic wall rocks set in a matrix of mineral grains and finely comminuted material. This second type occurs along Phelps Ridge as extremely irregular masses and dikes in the gneiss and in the porphyry plugs. The intrusive breccias seem to have formed after the batholith had largely solidified. As the magma crystallized, vapor pressures increased to the point where "second boiling" occurred, thereby producing the breccias.

The volcanic neck on Old Gib mountain is several miles southeast of the plunging end of the batholith and adjacent to the fault bounding the northeast side of a graben. This graben predates the batholith, and the bounding fault may have been effective in localizing the volcanic neck. The volcanic neck consists of porphyritic chilled rocks microscopically identical to the two inner layers of batholithic border rocks but is gray rather than black. It contains the same conspicuously zoned sodic labradorite as the batholith, and large phenocrysts of quartz, many of them rounded by resorbtion. Within the volcanic neck is a Peléan spine about 800 feet long and 500 feet wide that has a vertically fluted slickensided contact with the surounding porphyry. Much of the rock in the spine is highly altered, some of it to large masses of clay.

The evidence indicates that the Cloudy Pass batholith reached a high level in the earth's crust, and, in so doing, solved its room problem—to the depths visible at least—by lifting the overlying rocks; the batholith abruptly cuts off rather than wedges apart the enclosing gneiss, and evidence for either stoping or large scale granitizing is utterly lacking. Because the batholith ascended to levels where volcanic processes became effective, it illustrates well the interrelations that can exist between batholiths and volcanic activity. Thanks to the fortunate exposure of its upper part, the batholith can be classed as unequivocally igneous; yet, if it were exposed only at deeper levels, who knows but what it might show evidence of other origin.

214. THE ROLE OF IMPERMEABLE ROCKS IN CONTROLLING ZEOLITIC ALTERATION OF TUFF

By A. B. Gibbons, E. N. Hinrichs, and Theodore Botinelly, Denver, Colo.

Work done in cooperation with the U.S. Atomic Energy Commission

In the Tippipah Spring NW quadrangle, northern Nevada Test Site, in Nye County, Nev., relatively impermeable rocks, namely quartzite, argillite, and dolomite of Paleozoic age and a small stock of quartz monzonite, unconformably underlie volcanic rocks of the Oak Spring formation of Tertiary age. The prevolcanic rocks were folded, faulted, and eroded to a surface of high relief before the volcanic rocks were deposited.

The Oak Spring formation (Johnson and Hibbard, 1957, p. 367) is in places as much as 2,200 feet thick. It consists chiefly of bedded and nonbedded silicic tuff, with some flows of impermeable rhyolite and basalt. Some of the nonbedded tuff is firmly welded and relatively impermeable. Although the welded tuff is almost all vitric, the nonwelded tuffs are of two contrasted types, one type being vitric—that is, unaltered—and the other zeolitized (table 214.1).

Vitric tuff constitutes most of the upper part of the Oak Spring formation, and zeolitic tuff most of the lower part, but the contacts between these kinds of tuff cross-bedding planes, and also cross contours ranging in altitude from 5,400 to 7,000 feet. Significantly, all the nonwelded tuff that directly overlies prevolcanic rocks is zeolitic, regardless of which unit of the Oak Spring formation it belongs to, and regardless of the altitude of the contact. At most localities, moreover, tuff that overlies a layer of welded tuff or rhyolite is zeolitic, whereas tuff that underlies such a layer is vitric (figs. 214.1 and 214.2).

This preferential zeolitization of tuffs that overlie prevolcanic rocks and dense volcanic rocks is presumably due to the contrast in permeability between the prevolcanic rocks and the dense volcanic rocks on the one hand and the poorly consolidated vitric tuff on the other.

The consistent association of the zeolitized tuff with relatively impermeable rocks indicates that the zeolitization was caused by solutions migrating along the contacts of the less permeable rocks. The great influ-

557753 O—60——31

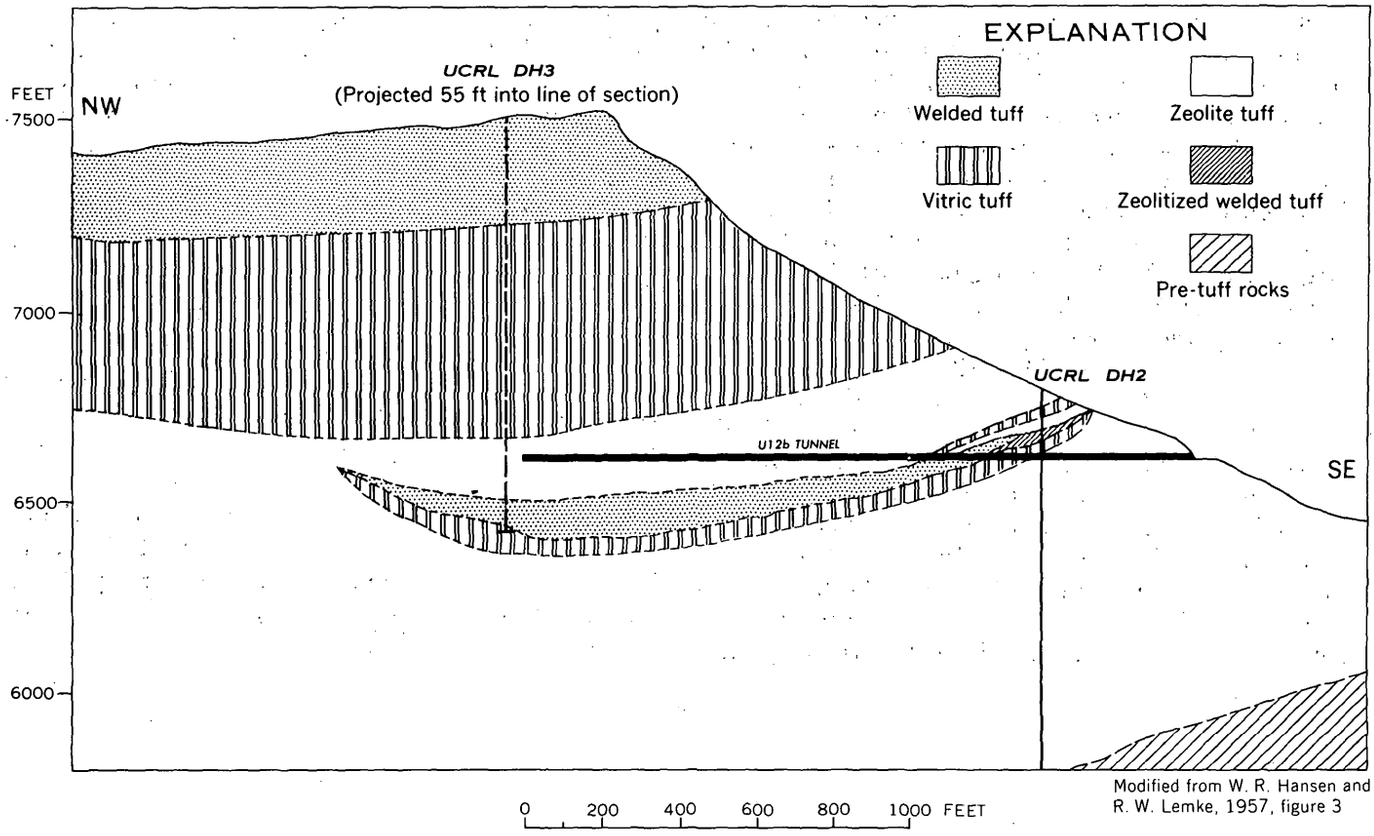

TABLE 214.1.—*Mineral composition, permeability, and cation-exchange capacity of three kinds of tuff, Tippipah Spring NW quadrangle, Nye County, Nev.*[1]

Property	Zeolitized tuff	Nonwelded vitric tuff	Uppermost welded tuff (figs. 214.1 and 214.2)
Mineral composition	Zeolite [2], cristobalite montmorillonite, phenocrysts of sanidine, quartz, plagioclase, mica, and iron oxides.	Glass (n=1.48 to 1.50), phenocrysts of sanidine plagioclase, quartz, mica, and iron oxides.	Glass, phenocrysts of potassian feldspar, quartz, plagioclase, mica, and iron oxides.
Permeability (millidarcies)	0.072 (0.00076–17) 28 [3]	82 (15–224) 7 [4]	0.33 (0.00092–58) 10.
Cation-exchange [5] capacity (milliequivalents/100 g).	90 (25–132) 5	17 (5–50) 11	(Not analyzed).

[1] Data from Diment and others (1958), except where noted.

[2] Determined by X-ray diffractometer analyses. Fine-grained zeolite with refractive indices 1.475 to 1.480 and an X-ray powder pattern very similar to that of heulandite, but stable to a higher temperature (about 700° C) than heulandite. This is probably clinoptilolite, as redefined by Mumpton (1960).

[3] First number is arithmetic mean; range is in brackets; last is number of samples.

[4] Water permeability determined by C. H. Roach (1960, written communication). Others are brine permeabilities.

[5] Analyses by H. C. Starkey. Ammonium chloride leach for 16 hours.

FIGURE 214.1.—Geologic section along U12b tunnel, showing relations of zeolitic tuff to welded tuff and prevolcanic rocks.

ence of permeability is shown by the notable rarity of alteration in firmly welded tuffs, which are nearly all fresh even where the surrounding nonwelded tuff is completely zeolitized. Yet the chemical characteristics of the glassy welded tuffs are such that they could be zeolitized in some places—for example in the part of the lower welded tuff penetrated by UCRL DH 2 (fig. 214.1). The alteration here may be the result of increased permeability due to incomplete welding toward the thinned edge of the tuff.

The zeolitizing solution was probably a circulating fluid rather than a large body of stagnant ground water, for the great irregularity of the top of the zeolitized tuff indicates that the alteration was not controlled by

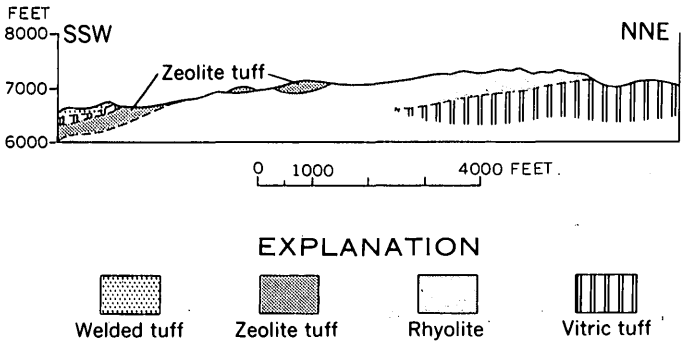

FIGURE 214.2.—Geologic section across the rhyolite area between Rainier and Pahute Mesas, showing the relations of rhyolite to zeolite and vitric tuff. The welded tuff is the same as the lower welded tuff of figure 214.1.

the nearly horizontal upper surface that a body of stagnant ground water would have. Masses of zeolite tuff overlying impermeable rocks, and masses of unaltered vitric tuff underlying welded tuff and rhyolite, suggest alteration by downward-moving water that was most active where its movement was impeded by impermeable rocks. As no evidence has been found of hydrothermal activity in the Oak Spring formation in this district, the altering agent was probably meteoric water moving in the zone of vadose circulation. Ground water evidently still flows along the prevolcanic erosion surface, for every one of the six known springs in the Tippipah Spring 15-minute quadrangle issues from the tuff within about 100 feet of that surface.

Ground water in the Oak Spring formation is low in dissolved solids, the principal ones being sodium and bicarbonate ions and silica (Clebsch, 1959, p. 70), and is generally mildly alkaline (pH 6.9 to 8.4) (Clebsch, 1959, p. 72, and written communication). We believe that the zeolitizing solutions were similar to recent ground water. This contrasts with the view of other investigators, who think that strongly alkaline water is necessary for the crystallization of zeolites (Stringham, 1952, p. 662). Deffeyes (1959, p. 607) suggests, however, that the hydrolysis of volcanic glass makes the water in contact with the glass sufficiently alkaline to cause precipitation of zeolites. His idea is extrapolated from experimental evidence obtained by Hovestadt (1902), but is supported by the discovery of authigenic zeolites in volcanic sediment from deep-sea cores (Arrhenius and Goldberg, 1955, p. 226); these zeolites have crystallized below room temperature in sea water which is only mildly alkaline (pH 7.5 to 8.4, Rankama and Sahama, 1950, p. 291).

In summary, we believe that the vitric tuff was probably zeolitized by percolating meteoric water of mild alkalinity at near-surface temperatures, and that the confining effect of impermeable layers of welded tuff and rhyolite and of the impermeable prevolcanic rocks helped to make the alteration especially intense in tuff overlying such rocks. Just when the alteration took place is uncertain, but it was after deposition of the tuff and before most of the normal faulting that affected the Oak Spring formation.

REFERENCES

Arrhenius, Gustav, and Goldberg, E. D., 1955, The distribution of radioactivity in pelagic clays: Tellus, v. 7, p. 226–231.

Clebsch, Alfred, Jr., 1959, Part V, Ground water, *in* Diment, W. H., and others, Geological Survey investigations in the U12b.03 and U12b.04 tunnels, Nevada Test Site: U.S. Geol. Survey TEM–996, open-file report.

Deffeyes, K. S., 1959, Zeolites in sedimentary rocks: Jour. Sed. Petrology, v. 29, no. 4, p. 602–609.

Diment, W. H., and others, 1958, Properties of Oak Spring formation in Area 12 at the Nevada Test Site: U.S. Geol. Survey TEI–672, open-file report.

Hansen, W. R., and Lemke, R. W., 1957, Geology of the USGS and Rainier tunnel areas, Nevada Test Site: U.S. Geol. Survey TEI–716, open-file report.

Hovestadt, H., 1902, Jena glass and its scientific and industrial applications [Translated by J. D. and H. Everett]: London, Macmillan and Company, 419 p.

Johnson, M. S., and Hibbard, D. E., 1957, Geology of the Atomic Energy Commission Nevada Proving Grounds area, Nevada: U.S. Geol. Survey Bull. 1021–K.

Mumpton, F. A., 1960, Clinoptilolite redefined: Am. Mineralogist, v. 45, p. 351–369.

Rankama, Kalervo, and Sahama, T. G., 1950, Geochemistry: Chicago, Ill., Univ. of Chicago Press, 912 p.

Stringham, Bronson, 1952, Fields of formation of some of the common hydrothermal alteration minerals: Econ Geology, v. 47, no. 6, p. 661–664.

ANALYTICAL AND PETROGRAPHIC METHODS

215. DETERMINATION OF TOTAL IRON IN CHROMITE AND CHROME ORE

By JOSEPH I. DINNIN, Washington, D.C.

The iron content of chromite and chrome ore is important to both the geologist and the industrial metallurgist. The variation of the Cr/Fe ratio in chromite from different localities can aid in the study of the geochemistry of chromite, and it can also provide a clue to the genesis of the deposit from which the sample came. The Cr/Fe ratio in an ore deposit has a dollar and cents meaning, for it helps to determine whether the ore will meet specifications for chemical, metallurgical, or refractory grades.

The common procedures for determining this ratio have been described by Hartford (1953). Chromite is almost invariably fused with sodium peroxide, leached with hot water, and boiled, and the ferric hydroxide is filtered out and washed with hot water. The iron is then dissolved with acid, reduced with stannous chloride, and titrated with a standard oxidizing agent. This separation of iron hydroxide is important, because a high concentration of the deep-green chromic ion would obscure the disappearance of the yellow ferric chloride color which occurs when stannous chloride is added.

Losses of iron may occur at several stages. The hot alkaline leaching solution and the hot wash water peptize a measurable amount of iron. Some ferric hydroxide adheres to the walls of the crucible and may not be completely removed by policing. Some iron alloys with the metal crucible, and no special provision is made to recover it.

The two most common methods of decomposing chromite are fusion with sodium peroxide and digestion with hot concentrated perchloric acid. Both methods oxidize chromium to the sexivalent state, and if the solutions are to be reduced with a silver reductor and no provision is made for prior reduction of chromium an inordinate amount of silver would be required. The silver reductor can be used directly, however, if a mixture of phosphoric and sulfuric acid is used as the dissolving agent. The amount of silver reduced varies only with the amount of iron in solution, and the chromium is not oxidized; it is therefore unnecessary to separate the chromium, and the major source of error in the usual procedure is thus avoided.

EQUIPMENT AND REAGENTS FOR SILVER REDUCTOR METHOD

Silver reductor: The construction and use of the reductor are described by Kolthoff and Belcher (1957, p. 12–16).

Acid mixture: Equal volumes of concentrated phosphoric and sulfuric acids.

Sodium chloride solution: 20 percent (w/v).

Hydrochloric acid wash solution: 1 *N*.

Sodium diphenylaminesulfonate indicator solution: 0.02 percent (w/v).

Standard potassium dichromate solution: 0.1000 *N*.

PROCEDURE

1. Transfer 0.5000 g chromite or chrome ore sample to a 125-ml Erlenmeyer flask.
2. Add 25 ml of the acid mixture and swirl until the sample is completely wetted.
3. Cover with a watch glass and heat the mixture on a hot plate or a flame (200° to 300° C) until the sample is completely dissolved.
4. Allow the solution to cool to about 50° C and dilute with approximately 75 ml water.
5. Add 5 ml sodium chloride solution.
6. Pass the cooled solution (20° to 50° C) through the reductor.
7. Rinse the flask with hydrochloric acid solution and wash the column by passing through it 5 increments containing 25 ml each of the HCl wash solution.
8. Add 2 ml indicator solution.
9. Titrate immediately with standard dichromate solution to the distinct purple-blue end point.
10. Calculation of percent Fe:

$$\text{Percent Fe} = \text{ml dichromate} \times \frac{0.005585 \times 100}{0.5000}$$

ACCURACY AND PRECISION

An estimate of the accuracy of the method was obtained by analyzing the metallurgical chrome ore standard (Hartford, 1953) and the National Bureau of Standards Standard Sample No. 103, chrome refractory. Determinations performed over a period of several months, using several reductor columns, were in excellent agreement with the certificate values.

A measure of the precision of the method was obtained by repeated analysis of a laboratory substandard. The iron content of the sample was determined 17 times during a period of three months, using several reductor columns. The average iron content was found to be

TABLE 215.1.—*Percentage of iron in 14 samples of chrome ore*

Sample	Conventional method $Fe(OH)_3$ separation (Dinnin, 1959)	Colorimetric (orthophenanthroline) (Dinnin, 1959)	Silver reductor
1	12. 43, 12. 99	13. 3	13. 34, 13. 24, 13. 20
2	10. 62, 10. 61	10. 9	10. 84, 10. 92, 10. 81
3	19. 26	19. 4	19. 39, 19. 38, 19. 43
4	12. 69, 12. 93	13. 1	12. 93, 12. 81, 12. 81
5	12. 46	12. 9	12. 64, 12. 59, 12. 66
6	19. 21, 19. 22	19. 3	19. 44, 19. 50
7	20. 09, 20. 33, 20. 15	20. 3	20. 50, 20. 46, 20. 50
8	15. 36	15. 4	15. 47, 15. 49
9	13. 38, 13. 52, 13. 48	13. 6	13. 65, 13. 66
10	19. 19	19. 3	19. 46, 19. 50
11	15. 31, 15. 41	15. 7	15. 59, 15. 65, 15. 60
12	20. 26, 20. 31	20. 4	20. 39, 20. 50, 20. 50
13	19. 30	19. 8	19. 67, 19. 67, 19. 75
14	15. 44, 15. 48	15. 6	15. 54, 15. 49, 15. 54

14.10 percent, the standard deviation 0.06, and the coefficient of variation 0.4 percent.

An idea of what can be done by routine use of this method may be obtained from table 215.1. This gives the iron percentage of 14 samples of chrome ore, (a) as determined by several commercial laboratories using conventional methods, (b) as previously determined colorimetrically in this laboratory, and (c) as determined by means of the silver reductor.

The results obtained by the proposed method, and also by the colorimetric method, are consistently a little higher than those obtained by the conventional method (table 215.1). This difference was to be expected because of the separation involved in the conventional method.

The precision offered by the silver reductor method and its relative ease of manipulation should make it attractive to those concerned with analysis of either minerals or ores containing chromium.

REFERENCES

Dinnin, J. I., 1959, Rapid analysis of chromite and chrome ore: U.S. Geol. Survey Bull. 1084–B, p. 31–68.

Hartford, W. H., 1953, Industrial chrome ore analysis—An industry standard sample of metallurgical chrome ore: Anal. Chemistry, v. 25, p. 290–295.

Kolthoff, I. M., and Belcher, R., 1957, Volumetric analysis, v. III, Titration methods: oxidation-reduction reactions: New York, Interscience Publishers, Inc., 714 p.

216. DETERMINATION OF ZINC IN BASALTS AND OTHER ROCKS

L. F. RADER, W. C. SWADLEY, H. H. LIPP, and CLAUDE HUFFMAN, JR., Denver, Colo., Washington, D.C., Denver, Colo., and Denver, Colo.

Zinc is one of the trace metals in silicate rocks for which only very limited data have been published. Particularly lacking are reliable determinations of zinc in rocks that have also been analyzed for major elements.

Sandell and Goldich (1943) have reported determinations of minor elements, including zinc determined by the dithizone method (Sandell, 1937), in 29 acidic and 25 basic rocks. Their results are almost the only chemical data for zinc reported in the literature for 30 years or more, and are widely quoted in reference texts (Goldschmidt, 1954, p. 261). Spectrographic data for zinc in silicate rocks are conspicuously lacking in the literature, owing in part at least to the volatility of zinc and its lack of spectographic sensitivity. The work of Lundegardh (1948) and Wedepohl (1953), both of whom used special techniques to enhance the sensitivity of their spectrographic methods for determination of zinc, are exceptions. Without special techniques the lower limit of detection for zinc by the spectrographic procedures now in general use is about 200 ppm (0.02 percent). Zinc has been determined chemically in the range below 200 ppm to a limited extent, as one of several trace metals looked for in the field by means of geochemical prospecting methods (Lakin and others, 1952). These methods, however, are only semiquantitative, and are intended primarily for rapidly scanning large numbers of samples while seeking anomalous areas.

A highly sensitive and precise chemical method for the determination of zinc combines selected features of several published procedures and has been thoroughly tested and adapted to the determination of trace amounts of zinc. This procedure is particularly designed to determine zinc even in rocks containing 10 to 20 percent of iron and containing many other ele-

TABLE 216.1.—*Precision of the zinc determination, showing freedom from interference by selected elements in different materials*

The standard deviations for the 3 sets of samples respectively are 0.0005, 0.0002, and 0.0003 percent zinc.

Zinc was determined by C. Huffman and H. Lipp; semiquantitative spectrographic analyses on Klondike Ridge samples by J. C. Hamilton; quantitative spectrographic analyses on G–1 and W–1 are averages from Ahrens and M. Fleischer (written communication); shale analyses are averages of chemical and quantitative spectographic analyses from Rader and F. S. Grimaldi (unpublished data).

Sample	Zinc, percent by method described			Other elements, percent				
	Run 1	Run 2	Run 3	Fe	Mn	Cu	Pb	Ti
Conglomerates, Klondike Ridge, San Miguel County, Colo.								
258712	0.0056	0.0056	0.0060	1.5	0.07	7.0	0.015	0.03
258724	.0068	.0058	----------	1.5	7.0	.07	.15	.007
258719	.0033	.0040	.0037	.7	.7	.3	.07	.07
258721	.0021	.0029	----------	.7	.15	7.0	.3	.15
258711	.015	.016	.015	.3	.15	1.5	.007	.03
258713	.016	.015	.015	.3	.007	1.5	.003	.07
258716	.018	.018	.019	.3	7.0	.3	.15	.007
258723	.010	.010	----------	.3	.07	3.0	.0015	.07
Granite G-1 and diabase W-1								
G–1	0.0041	0.0039	0.0042	1.4	0.021	0.0013	0.005	0.14
W–1	.0076	.0080	.0078	7.8	.13	.011	.0005	.74
Pierre shale								
259528	0.0059	0.0059	----------	1.5	0.43	0.0020	0.0016	0.15
259533	.018	.017	----------	2.9	3.5	.0033	.0015	.20
259537	.0026	.0031	----------	3.1	.020	.0005	.0030	.15
259539	.012	.014	----------	3.0	.029	.0027	.0027	.25
259546	.017	.018	----------	3.9	.039	.0038	.0027	.38
259548	.030	.029	----------	2.3	.025	.0040	.0031	.14
259549	.010	.0094	----------	11.1	.016	.0071	.0036	.27
259563	.0031	.0037	----------	1.9	.008	.0071	.0018	.44
259592	.016	.016	----------	4.5	.012	.0041	.0025	.41
259594	.012	.012	----------	2.9	.017	.0027	.0023	.42

ments in amounts that interfere with the determination of zinc by other methods.

The principles of the method are as follows: Zinc in a 1.2 M solution of hydrochloric acid, when passed through an ion-exchange column containing anion-exchange resin in the chloride form, is absorbed on the resin (Kraus and Moore, 1953). The only other metals absorbed under these conditions are lead, six-valent molybdenum, and varying but small portions of uranium, three-valent iron, and cadmium (Kraus and Nelson, 1955). All other metals in solution at this acidity pass through the column and are discarded if conditions are optimum. The zinc is removed from the resin by passing 45 ml of 0.01 M hydrochloric acid through the column. Cadmium, if present, is not removed under these conditions, but trace amounts of other metals may accompany the zinc. Zinc is precipitated with sodium diethyldithiocarbamate at a pH of 8.5, and the precipitate extracted into chloroform (Stewart and Bartlet, 1958). The zinc is then stripped from the chloroform with 0.16 M hydrochloric acid, and after adjusting the pH of the solution to 9.0 it is determined directly with zincon (2-carboxy-2-hydroxy-5-sulformazylbenzene) (Rush and Yoe, 1954). The absorbance of the color complex is determined spectrophotometrically at 620 mμ. A reagent blank correction, including all acids and solutions added to the samples, must be determined with each suite of samples.

Zinc recoveries and separations were checked during development of the method by radiometric tracer methods employing the radioactive isotopes Zn^{65} and Cd^{115}.

Zinc determinations were made on highly mineralized sedimentary sandstones and conglomerates from Klondike Ridge, near Gypsum Valley, Colorado, on the granite G–1 and the diabase W–1, and on Pierre shale

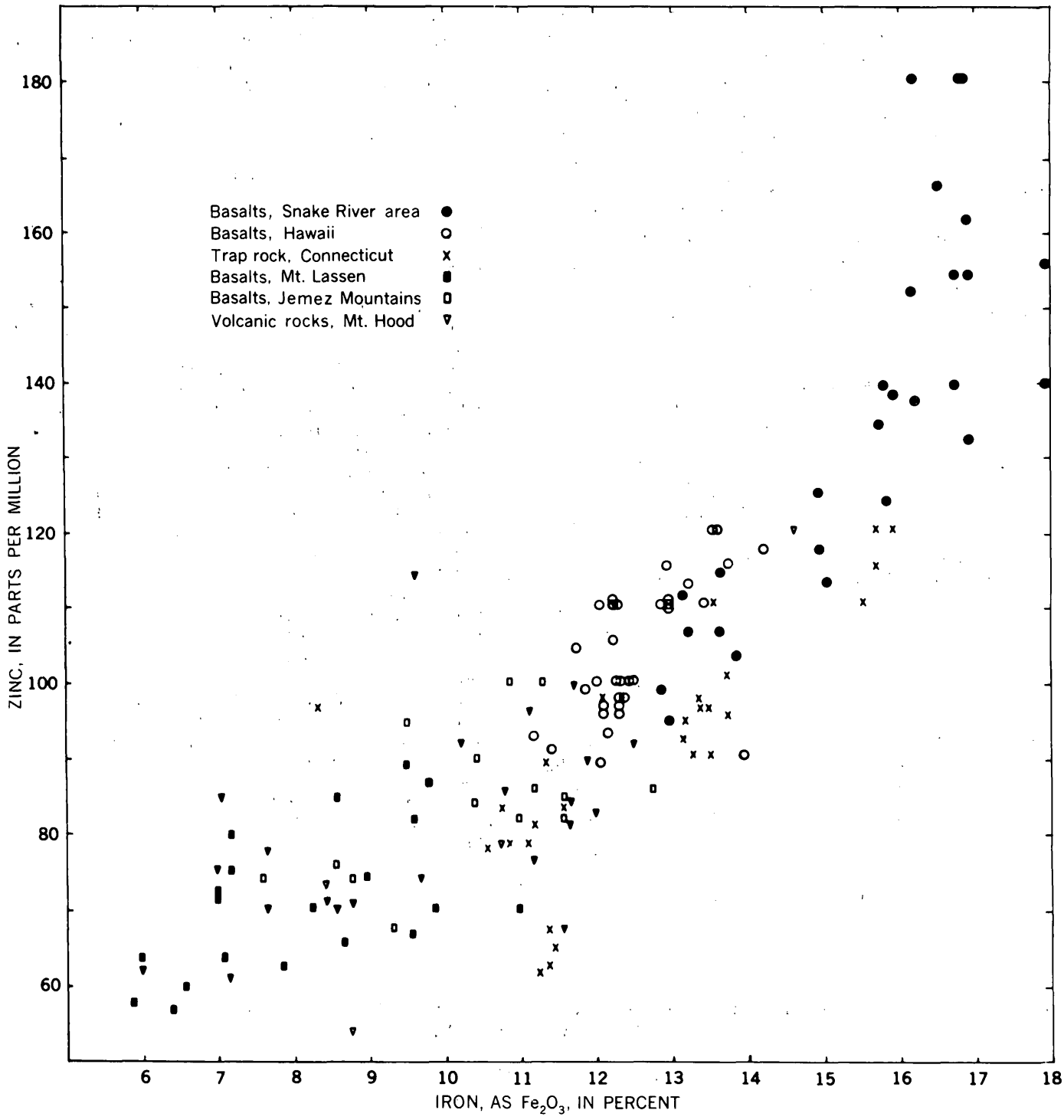

FIGURE 216.1.—Ratio of zinc to total iron, calculated as Fe_2O_3, in basalts from six different areas in the United States.

(table 216.1). Replicate determinations for zinc made at different times are shown in the table opposite results obtained by others for Fe, Mn, Cu, Pb, and Ti, in order to show the relative degree of mineralization that might influence the zinc determination. No interference with the zinc determination was found in these samples, which contain up to 11 percent Fe, 7 percent Mn, 7 percent Cu, 0.3 percent Pb, and 0.7 percent Ti. The standard deviations of the method for three different types of rock calculated from the data in table 216.1 (Dixon and Massey, 1951, p. 239) were found to be 0.005 percent zinc for the sandstones and conglomerates, 0.0002 percent zinc for the granite and diabase, and 0.0003 percent zinc for the shale.

Table 216.2 gives the average zinc content and range of zinc concentration in 25 basalts and 7 olivine basalts from the Snake River area in Idaho, in 16 basalts and 18 olivine basalts from the Island of Hawaii in the Hawaiian Islands, in 21 basalts and 10 diabases from central Connecticut, in 4 basalts and 10 olivine basalts from the Jemez Mountains area about 50 miles west of Santa Fe in north central New Mexico, in 6 basalts, 10 olivine basalts, 11 andesites, and 1 dacite from the Mount Hood area in Oregon, and in 20 basalts from the Mount Lassen area in California. The standard deviation for the zinc determinations on these rocks, based on 68 replicated determinations made at different times, was 0.0006 percent zinc.

TABLE 216.2.—*Range and average zinc content for 159 basalts and related rocks from six areas*

[The standard deviation of the analyses, based on 68 replicated determinations, is 0.00062 percent zinc]

	No. of samples	Zinc content, percent	
		Average	Range
Snake River area, Idaho	32	0.014	0.0093 to 0.018
Island of Hawaii, Hawaii	34	.010	.0089 to .012
Connecticut	31	.0090	.0064 to .012
Jemez Mountains area, New Mexico	14	.0084	.0068 to .010
Mt. Hood area, Oregon	28	.0080	.0048 to .012
Mt. Lassen area, California	20	.0072	.0057 to .0089
Total	159	0.0094	0.0048 to 0.018

Plots of zinc against the major oxides were used to determine general relationships between zinc and the major elements of the basalts. Only the plot of zinc against total iron (expressed as Fe_2O_3) showed a significant relationship that is of interest with regard to the geochemistry of zinc. This plot is shown as figure 216.1. It will be seen that 90 percent of the points plotted in figure 216.1 fall within a narrow band. This indicates that for a given value of total iron, the amount of zinc in the sample is given by the diagram to within ±15 ppm zinc.

REFERENCES

Dixon, W. J., and Massey, F. J., 1951, Introduction to statistical analysis: New York, McGraw-Hill Book Company, Inc.

Goldschmidt, V. M., 1954, Geochemistry: Oxford, Clarendon Press (edited by Alex Muir).

Kraus, K. A., and Moore, G. E., 1953, Anion exchange studies VI. The divalent transition elements manganese to zinc in hydrochloric acid: Am. Chem. Soc. Jour., v. 75, p. 1460–1462.

Kraus, K. A., and Nelson, F., 1955, Anion exchange studies of the fission products: International conference on the peaceful uses of atomic energy, A. Conf. 8/p/837, U.S.A., 23 June.

Lakin, H. W., Almond, Hy, and Ward, F. N., 1952, Compilation of field methods used in geochemical prospecting by the U.S. Geological Survey: U.S. Geol. Survey Circ. 161.

Lundegardh, Per H., 1948, Some aspects to the determination and distribution of zinc: The Annals of the Royal Agricultural College of Sweden (Lanlbrukshogskolans Annaler), v. 15, p. 1–36 (in English).

Rush, R. M., and Yoe, J. H., 1954, Colorimetric determination of zinc and copper with 2-carboxy-2′-hydroxy-5′-sulforneazylbenzene: Anal. Chemistry, v. 26, p. 1345–1347.

Sandell, E. B., 1937, Determination of copper, zinc, and lead in silicate rocks: Ind. Eng. Chemistry, Anal. Ed., v. 9, p. 464–469.

Sandell, E. B., and Goldich, S. S., 1943, The rarer metallic constituents of some American igneous rocks: I and II: Jour. Geology, v. 50, p. 99–115 and p. 167–189.

Stewart, J. A., and Bartlet, J. C., 1958, Determination of zinc and separation from ashed biological material: Analytical Chemistry, v. 30, p. 404–409.

Wedepohl, K. H., 1953, Untersuchungen zür Geochemie des Zinks: Geochim. et Cosmochim. Acta, v. 3, p. 93–142.

217. COMPARISON OF THREE METHODS FOR THE DETERMINATION OF TOTAL AND ORGANIC CARBON IN GEOCHEMICAL STUDIES

By I. C. FROST, Denver, Colo.

The determination of the organic matter in sedimentary rocks and any associated ores presents some challenging and difficult analytical problems. Not only is the organic matter itself chemically complex and intimately associated with inorganic minerals, but further difficulties arise from the presence of carbon, hydrogen, oxygen, nitrogen, and sulfur in both organic and inorganic compounds. For these reasons a satisfactory separation into organic and inorganic fractions is difficult or impossible. It is much easier to determine organic carbon rather than organic matter. Organic carbon, the most abundant element of organic matter, is determined directly on carbonate-free samples, and by the difference between total and mineral carbon on samples that contain carbonates. Three different analytical methods, adapted from published

procedures, are used routinely. Table 217.1 compares for these methods the time required for a determination, sample-size limitations, and the precision obtained with various proportions of organic carbon. Choice of method to be used is based on a visual examination of the sample. During the past five years these methods have been applied to several hundred rock samples in which organic carbon content ranged from nearly zero to nearly 100 percent.

TABLE 217.1.—*Comparison of relative time per analysis, sample size limitations, and precision for various proportions of organic carbon*

	Method		
	1	2	3
Relative time per determination	Slow	Rapid	Intermediate.
Analyses per day	2–3	10	5–6
Sample size, grams	0.0050–2.0	0.0050–0.40	2.0–10.0.
Precision (Range of percent C):			
30–100	±0.34	±0.74	
0.25–4.00	±0.018	±0.033	±0.034.
<0.6			±0.035.

METHOD 1

Tube-furnace combustion with gravimetric determination of evolved carbon dioxide has been described in detail by Pregl (1937). This method is best suited to organic substances, but it can be applied to rocks and soils. Samples containing carbonate minerals are generally analyzed with the addition of a flux, such as vanadium pentoxide or potassium dichromate, to insure complete removal of carbonate minerals and promote oxidation of the organic carbon. Carbon in minerals and total carbon must be determined separately; the difference between them is the organic carbon. Additional apparatus is required for determining mineral carbon. Samples containing metal sulfides require frequent changing of the reagents used for removing sulfur, but a preliminary acid treatment can be used for removing carbonate minerals as well as sulfides. Method 1 is recommended for control purposes.

METHOD 2

Gasometric method. Parr (1904) determined total carbon in coal and soil by a modification of a volumetric method commonly used to determine mineral carbon. He oxidized organic carbon to alkali carbonate by fusion with sodium peroxide in a closed bomb. In the Survey laboratory this method has been expanded and adapted to the determination of organic carbon in amounts of 0.2 percent or more in a wide variety of rocks. Samples containing more than 30 percent organic carbon are easily oxidized, but those containing less generally require addition of a combustion aid such as powdered aluminum or magnesium to provide the heat necessary for insuring complete oxidation of the carbon. Total or organic carbon can be determined about 5 times as rapidly by this method as by method 1. Carbon in carbonate minerals, when it is present in amounts greater than 0.01 percent is determined separately and the organic carbon calculated as the difference between it and total carbon. Mineral sulfides, if present, are oxidized to sulfates and cause no interference. The apparatus used is relatively inexpensive, and it may also be used for the measurement of carbon dioxide in carbonate minerals. As only a small sample (0.4 gram or less) can be oxidized in a micro-bomb, and as sodium peroxide tends to absorb carbon dioxide from the air with the resulting reagent blank correction, this method is suitable only for samples containing more than 0.2 percent organic carbon. The method has been used extensively since 1956 to determine organic carbon in samples collected for uranium investigations in the Ambrosia Lake area and for investigating the Pierre shale.

Table 217.2 gives analytical values determined by methods 1 and 2 for 10 samples of carbonaceous shale containing 28 to 80 percent total carbon. Standard deviation of replicate determinations for method 1 is ±0.34 percent carbon and for method 2 is 0.74 percent. The deviation between the mean values obtained by the two methods is 0.67 percent carbon. Standard de-

TABLE 217.2.—*Comparison of total carbon of carbonaceous shales determined by tube-furnace combustion and gasometric methods*

[Replicate determinations by each method]

Sample	Total carbon, percent			
	Method 1 (tube-furnace combustion)		Method 2 (gasometric)	
7	28. 68	28. 56	27. 7	28. 2
8	59. 87	60. 90	60. 6	58. 8
1	64. 32	64. 49	63. 4	64. 5
3	67. 74	67. 61	65. 9	65. 5
10	67. 83	68. 29	68. 0	66. 9
2	72. 04	72. 28	73. 1	73. 1
5	73. 46	73. 04	73. 5	73. 5
9	78. 97	78. 99	79. 4	81. 1
6	80. 71	79. 95	80. 7	82. 1
4	80. 40	80. 75	80. 5	80. 4
Standard deviation [1]				
	0. 34		0. 74	

[1] Standard deviation between mean values of Method 1 and Method 2 is 0.67.

viations were estimated by the scheme given by Youden (1951) for paired values.

METHOD 3

Modified combustion. Studies have recently been made of combustion techniques applied to large samples (5 grams or more), carbon dioxide being absorbed in a solution of barium hydroxide. The excess barium hydroxide is titrated with standard hydrochloric acid, using phenolphthalein as the indicator. The barium hydroxide concentration and the titration procedure are given by Lundell, Hoffman, and Bright (1931, p. 172–174). The simplicity of this titration and its good sensitivity lowers the minimum of determinable organic carbon from the 0.2 percent measurable by the gasometric method to 0.03 percent. Carbonate minerals, sulfides, and most of the silicate and clay minerals are removed by chemical treatment before combustion. Five-gram samples are digested overnight with hydrofluoric acid in a plastic centrifuge tube, and then for 6 hours with cold 15 percent nitric acid. After each digestion the sample is centrifuged and the clear solution removed by suction. Each digestion is made in two cycles. No significant loss of organic carbon is apparent from the data given in table 217.3. The values obtained by method 2 on untreated samples agree, within the limits of error of the methods, with those obtained by method 3 on acid-treated samples. The insoluble residue is washed free of acid, dried at a temperature of 65° C, and transferred to a combustion boat. The last traces of sample are scrubbed from the centrifuge tube into a Selas porcelain crucible having a ceramic disk bottom of fine porosity. After drying, the crucible is placed in the tube of the furnace with the combustion boat. Combustion for eight minutes, with an oxygen flow of approximately 1000 cubic centimeters per minute and a furnace temperature of 900°C, usually causes the sample to become completely oxidized.

The 42 samples selected for comparing method 2 with method 3 were collected for the Pierre shale investigations. Their organic carbon, as determined by method 2, ranged downward from 0.6 percent; for 15 of them it could only be reported as less than 0.2 percent (table 217.3). Replicate determinations by method 3 on 16 Pierre shale samples, with a mean value of 0.33 percent, gave a standard deviation of 0.034 percent carbon.

Five standard synthetic samples, containing 0.25, 0.50, 1.00, 2.00, and 4.00 percent organic carbon were also prepared by thoroughly mixing weighed amounts of sodium oxalate and reagent-grade silica flour. Total carbon determinations were made in duplicate by methods 1 and 2, and also by method 3 with the omission of the acid treatment, as the samples contained no carbonates or sulfides. The results are given in table 217.4. The standard deviations are 0.018 for method 1, 0.033 for method 2, and 0.035 for method 3. As with samples

TABLE 217.3.—*Comparison of organic carbon of Pierre shale determined by the gasometric and the modified combustion method*

[Sixteen replicate determinations by method 3 give a standard deviation of ±0.034 percent carbon]

Sample	Organic carbon, percent: Method 2 (gasometric)	Method 3 (modified) combustion	
528	0.2	0.11	0.16
529	.5	.46	
530	.4	.48	
531	.4	.39	
533	.6	.57	.62
534	.2	.23	
535	.4	.43	
536	.4	.23	.24
537	<.2	.07	.04
538	.3	.40	.42
539	<.2	.12	.22
540	.2	.28	
541	<.2	.05	.03
542	<.2	.16	
544	<.2	.08	
546	.4	.37	.45
548	<.2	.05	.04
550	<.2	.24	
551	.2	.30	
552	.5	.53	.51
554	<.2	.05	.02
557	<.2	.10	
559	.3	.21	
565	.2	.25	
566	.3	.36	
567	<.2	.03	
572	<.2	.04	
575	.6	.55	
576	.4	.54	
577	.5	.65	.67
580	.2	.32	
581	.4	.78	.71
583	.3	.18	
584	.4	.41	
586	.4	.36	
588	<.2	.05	
589	.5	.58	
593	<.2	.02	
597	.5	.60	.67
598	<.2	.23	.26
600	<.2	.27	
605	.4	.38	.36

TABLE 217.4.—*Comparison of total carbon determined by three methods in synthetic samples*

[Replicate determinations by each method]

Theoretical	Total carbon, percent					
	Method 1 (tube furnace combustion)		Method 2 (gasometric)		Method 3 (modified combustion)	
0.25	0.27	0.26	0.22	0.20	0.23	0.22
0.50	.53	.53	.44	.51	.50	.47
1.00	1.02	1.02	1.00	.96	.95	.98
2.00	2.07	2.03	1.97	2.02	2.05	1.96
4.00	3.97	4.01	4.02	3.98	4.00	4.05
Standard deviation						
Standard deviation	0.018		0.033		0.035	

of higher total carbon content, method 1 is most precise. Standard deviations were calculated according to the method for duplicate determinations given by Youden (1951, p. 17).

On a routine basis, samples submitted for the determination of organic carbon are first ranked visually; those estimated to contain more than 0.5 percent organic carbon are then analyzed by method 2 and those estimated to contain less than 0.5 percent by method 3. Visual estimation is not always reliable, however, because sulfides of iron, vanadium, and molybdenum, and possibly other minerals, may be mistaken for organic carbon.

REFERENCES

Lundell, G. E. F., Hoffman, J. I., and Bright, H. A., 1931, Chemical analysis of iron and steel: New York, John Wiley and Sons, 641 p.

Parr, S. W., 1904, Determinations of total carbon in coal and soil: Am. Chem. Soc. Jour., v. 26, p. 294–297.

Pregl, F., 1937, Quantitative organic microanalysis: Philadelphia, Pa., P. Blackston's Sons.

Youden, W. J., 1951, Statistical methods for chemists: New York, John Wiley and Sons, 126 p.

218. THE DETERMINATION OF LEAD IN IRON-BEARING MATERIALS

By JESSE J. WARR and FRANK CUTTITTA, Washington, D.C.

Work done in cooperation with the U.S. Atomic Energy Commission

Methods for the spectrophotometric determination of lead with dithizone as summarized by Sandell (1959) show that the dithizonate of lead is accompanied by dithizonates of thallium, stannous tin, and bismuth, and that the lead value obtained by these methods is in error to an extent equivalent to the amount of tin, bismuth, or thallium present. These errors would be reflected in calculations of geologic age.

This paper describes a method by which trace amounts of lead can be determined in iron-bearing materials. The procedure eliminates any increase of lead values due to thallium or tin, and most of that due to bismuth. It also provides a means for the total removal of large amounts of iron, which interfere in the extraction of lead with dithizone.

This work was undertaken to supplement or modify existing procedures for the separation and determination of lead with dithizone in iron-bearing materials such as limonite and steel (Sandell, 1959).

The method utilizes extraction of cupferrates (Furman and others, 1949) as a preliminary separation of interfering metallic ions. Ferric iron, copper, bismuth, thallium (III), and tin are removed from a 1:9 HCl solution by extraction with chloroform using excess cupferron. Lead is not precipitated as the cupferrate from acidities as low as 0.5*N* (Pinkus and Belche, 1927) and is insoluble in organic solvents (Baudisch and Furst, 1917). The excess of cupferron is largely removed from the aqueous layer by extraction with chloroform.

The acidity of the remaining aqueous phase is adjusted to 1.5*N* HCl and the lead separated from Tl(I) by extraction with a 1 percent solution of diethylammonium-diethyldithiocarbamate in chloroform (Maynes and McBryde, 1957). After evaporation of the lead-bearing extracts and subsequent destruction of organic matter by wet-ashing with HNO_3-$HClO_4$ mixture, the lead is further isolated with dithizone and then determined spectrophotometrically as the dithizonate as described by Sandell (1959). Standard calibration curves, used in the spectrophotometric determination of lead and prepared directly from pure

solutions, agree with those obtained when known quantities of lead are carried through the cupferron-carbamate steps.

In the course of obtaining these data, the following additional observations were made:

1. Multiple extractions with cupferron in chloroform are necessary in order to remove about 95 percent of the bismuth when small amounts (<500 micrograms) are present.
2. When deemed practicable, the lead-dithizone determination can be made directly on a solution that has undergone a cupferron separation, followed by a chloroform extraction of the excess cupferron.
3. Our data confirm the usefulness of methyl isobutyl ketone (hexone) as an extractant for Fe(III) from 6*N* HCl (Specker and Doll, 1958). Only one extraction can be made; any attempt to make a second produces an emulsion.
4. Our data also confirm the results of Maynes and McBryde (1957), who found that Fe(III), Cu, and Bi can be extracted and separated from Pb in 6*N* HCl with a chloroform solution of carbamate.

PROCEDURE

1. *Preparation of solutions and elimination of interferences.*—A sample containing approximately 15 micrograms of lead is weighed into a 150-ml Teflon beaker. (Platinum is not used because of the solvent action of ferric iron in strong HCl and of aqua regia.) Ten milliliters of aqua regia and 5 ml of HF are added. The beaker is covered with a Teflon cover and left for 1½ hours on the steam bath. The cover is removed and the solution is evaporated to dryness. The salts are converted to chlorides by evaporation to dryness several times with HCl. Twenty-five milliliters of 1*N* HCl are added and the covered solution is heated on the steam bath until all the chloride salts are dissolved. The beaker is placed in a refrigerator and chilled to 5°–10° C.

The chilled solution is transferred to a 125-ml separatory funnel. Two rinsings of the beaker are made, the first with approximately 0.5 gram of cupferron and 10 ml of chilled chloroform, and the second with 10 ml of chilled chloroform. Both rinses are added to the contents of the separatory funnel. The funnel is then shaken for 2 minutes and the layers allowed to separate. The lower layer is drained off and discarded. Small quantities (<5 ml) of chloroform are added to the aqueous layer. This is shaken, and drained off until the aqueous phase becomes colorless.

The acidity of the aqueous phase is then increased from 1*N* HCl to approximately 1.5*N* HCl by adding 3 ml of 6*N* HCl. Ten milliliters of 1 percent diethylammonium-diethyldithiocarbamate in $CHCl_3$ is added and the solution is shaken for 1 minute. The lower carbamate layer is then transferred to a 50-ml beaker. A second carbamate extract is made with a fresh 10-ml portion and this is combined with the first extract. The beaker is placed on a steam bath and the lead carbamate solution is evaporated nearly to dryness. The organic matter is destroyed by wet ashing with 3 ml concentrated HNO_3 and 0.5 ml $HClO_4$, the acids being added cautiously to prevent spattering. The solution is evaporated to dryness on a hot plate to remove oxides of nitrogen and excess perchlorates. One milliliter of (1+1) HNO_3 and 5 ml of water are added and brought to a boil to dissolve salts.

The solution is cooled and filtered into a separatory funnel through glass wool tightly packed in the stem of a small funnel. The beaker is rinsed several times with 1:99 HNO_3, and the rinse solutions are filtered into the separatory funnel. The resulting volume of the filtrate and rinsings is about 25 ml.

2. *Spectrophotometric determination.*—The lead is then determined by the dithizone procedure as described by Sandell (1959), using chloroform as the solvent. The samples, reagent blanks, and lead standards used in the preparation of the standard spectrophotometric curve are carried through the procedure simultaneously.

REFERENCES

Baudisch, O., and Furst, R., 1917, Über innere Metallkomplexsalzen. Über Nitroso-arylhydroxylamine: Deutsche Chem. Gesell. Ber., v. 50, p. 324–327.

Furman, N. H., Mason, W. B., and Pekola, J. S., 1949, Extraction of cupferrates: Anal. Chemistry, v. 21, p. 1325–1330.

Maynes, A. D., and McBryde, W. A. E., 1957, Determination of traces of lead in igneous minerals: Anal. Chemistry, v. 29, p. 1259–1263.

Pinkus, A., and Belche, E., 1927, Determination of aluminum by cupferron: Soc. chim. Belgique Bull., v. 36, p. 277.

Sandell, E. B., 1959, Colorimetric determination of traces of metals, 3d ed., p. 555–559, 563–571: New York, Interscience Publishers, Inc.

Specker, H., and Doll, W., 1958, Photometrische Eisenbestimmung im Reinmetallen: Zeitschr. Anal. Chemie, v. 152, p. 128.

219. DETERMINATION OF LEAD IN PYRITES

By Frank Cuttitta and Jesse J. Warr, Washington, D.C.

Work done in cooperation with the U.S. Atomic Energy Commission

METHOD

Some geochronological studies require the determination of traces of lead in pyrite. This paper describes a method for the separation and purification of pyritic lead for chemical or mass spectrometric analysis. The chemical determination is made by means of the lead-dithizone mixed-color system.

The dithizone data summarized by Sandell (1959) show that iron is a major interference, and that lead dithizonate is accompanied by dithizonates of Tl(I), Sn(II), and Bi(III), which cause the lead values found to be too high. The method was therefore modified to separate the lead from large quantities of iron by means of a sulfide precipitation, in which copper acts both as a carrier for the lead sulfide and as a catalyst for the reduction of iron with hydroxylamine at pH 0.4–0.5. Lead is separated from the copper carrier and any bismuth and tin present by simultaneously reprecipitating the sulfides of those three metals from 1.5*M* HCl, and is then extracted from the remaining 1.5*M* HCl solution with 1 percent diethylammonium diethyldithiocarbamate in chloroform. The organic content of the lead-bearing extracts is destroyed by wet-ashing with HNO_3–$HClO_4$. The lead is further isolated and then determined spectrophotometrically with dithizone as described by Sandell (1959).

Standard curves prepared directly from pure lead solutions were in excellent agreement with those prepared from known amounts of lead carried through the sulfide-carbamate separations. Results obtained for a few samples of pyrite agree with those obtained by other methods.

PROCEDURE

Preparation of sample solution and separation of lead.—Transfer a weighed amount of pyrite (60–80 mesh) containing from 5 to 15 micrograms of lead to a 150-ml Teflon beaker. Add 15 ml aqua regia and 5 ml HF, cover the beaker with a Teflon disc, and allow the mixture to digest at room temperature for half an hour. Transfer the beaker to a steam bath and heat gently until all apparent action has subsided. Replace the Teflon disc covering the beaker with a ribbed Teflon cover and evaporate the liquid to dryness. Convert the salts to chlorides by several times adding a small quantity of HCl and evaporating to dryness. Add 20 mg copper as the chloride in 75 ml 0.2*N* HCl. Reduce iron with hydroxylamine hydrochloride (catalyzed by copper at this acidity) and precipitate the sulfides with H_2S. Separate the lead from the copper carrier and any bismuth and tin present by simultaneously reprecipitating the sulfides of those three metals from 1.5 *M* HCl. Boil out the H_2S and completely remove the lead from the 1.5 *M* HCl solution by extracting two or three times with 10-ml portions of 1-percent diethylammonium diethyldithiocarbamate in $CHCl_3$. Thallium remains in the aqueous phase. Evaporate the combined carbamate extracts to incipient dryness on a steam bath, and destroy the organic matter by wet-ashing with 3 ml concentrated HNO_3 and 0.5 ml $HClO_4$. Remove oxides of nitrogen and excess perchlorates by fuming to near dryness on a hot plate. Dissolve the salts in 5 ml 1 : 9 HNO_3. Filter the cooled solution quantitatively directly into a separatory funnel through glass wool tightly packed in the stem of a small funnel. Use 1 : 99 HNO_3 as a wash. The total volume of filtrate and rinsings is about 25 ml. The lead is separated by extraction and determined spectrophotometrically with dithizone dissolved in chloroform as described by Sandell (1959).

Analytical control is obtained by means of sample solutions spiked with known amounts of lead. The samples (spiked and unspiked), the reagent blanks, and the lead standards used in the preparation of the calibrated spectrophotometric curve are subjected to the procedure simultaneously.

Preparation of lead iodide for mass spectrometry.—The amount of lead isolated, purified, and converted to lead iodide ranges from 25 to 200 micrograms. After the determination of the lead content of the pyrite, an amount of sample containing the desired quantity of lead is carried through the procedure described above to the point preceding the spectrophotometric determination. The lead is then extracted as the dithizonate into chloroform from an alkaline-cyanide medium. The lead is back-stripped into 5 ml 0.001*N* HCl, rejecting the organic dithizone phase. Any dithizone in the aqueous lead-bearing phase is removed by several ex-

tractions with 5-ml portions of $CHCl_3$. The acid solution of lead is evaporated to dryness, the residue is dissolved in 5 ml of 25-percent sodium acetate, and the lead is precipitated as the sulfide with H_2S. The lead sulfide is converted to the nitrate with concentrated HNO_3 in a 5-ml round bottom beaker supported by a borosilicate glass sleeve. Just before the isotopic composition is determined, freshly prepared alcoholic NH_4I is used to convert the trace quantity of lead nitrate to the iodide.

REFERENCE

Sandell, E. B., 1959, Colorimetric determination of traces of metals, 3d ed.: New York, Interscience Publishers, Inc., p. 555–571.

220. DETERMINATION OF LEAD IN ZIRCON WITH DITHIZONE

By Frank Cuttitta and Jesse J. Warr, Washington, D.C.

Work done in cooperation with the U.S. Atomic Energy Commission

The determination of lead in such minerals as zircon for geochronologic studies by classical methods is difficult, especially if the sample is small and its lead content very low. We believe the best chemical procedure with such samples to be separation and spectrophotometric determination of lead with dithizone. Experimental factors relating to application of this reagent to the determination of lead are summarized by Sandell (1959). Several samples of zircon were analyzed by this method to provide data for intralaboratory comparison of lead analyses made on zircons to be used in cross-checking analytical methods. The results are presented in table 220.1.

Studies were also made to determine the loss of lead by volatilization from zircon undergoing decomposition by fusion. No loss was detected when the zircon was fused with a carbonate-borate flux, or when it was decomposed by sintering with sodium peroxide in platinum for 30 minutes in an electric muffle maintained at 460°±15°C (Rafter, 1950).

Table 220.1.—*Intralaboratory comparison of average lead in zircon samples*

Zircon	Lead (percent)				
			Chemical		
	Spectrographic [1]	Isotope dilution [2]	Mean of n determinations	n	Standard deviation
NBS–197	0.0034		0.0034	51	
ZS–4	.0038		.0038	7	0.0003
9	.030	0.031	.028	16	.0028
10	.0049		.0047	6	.0002
12	.012		.011	6	.0008
2	.0034		.0035	5	

[1] Rose and Stern, 1960.
[2] Analysis by L. R. Stieff.

PROCEDURE

Grind the sample to an impalpable powder in a boron carbide mortar and mix thoroughly. Small particle size is necessary to insure complete fusion in a reasonable time. Weigh a 0.1000-gram sample (should contain 8 to 15 micrograms lead) into a 15-ml platinum crucible and add 1 gram of carbonate-borate flux, prepared by mixing equal portions by weight of anhydrous sodium carbonate and anhydrous sodium borate (Ampt, 1935). Mix thoroughly. Cover the crucible, place it in a furnace and heat to 150° or 200°C, to drive off any moisture. Gradually increase the temperature until the mass is a viscous liquid (approximately 925°C). Keep the crucible at this temperature for 20 to 30 minutes. Cool to room temperature and place the crucible and melt in a 100-ml beaker, add 20 ml water, cover, and digest on a steam bath until the melt has completely disintegrated to a fine silt. Then add 15 ml (3+7) HNO_3, cover, and digest on a steam bath until the silt just dissolves. Transfer the solution quantitatively to a 125-ml Teflon-stoppered separatory funnel, removing and washing the crucible. Adjust volume to 50 ml; the final HNO_3 concentration is 7 percent v/v. A reagent blank is processed along with the samples.

Sample solutions spiked with known amounts of lead are also used as a means of process control. The sample (spiked and unspiked), the reagent blanks, and the lead standards used in the preparation of the calibrated spectrophotometric curve are simultaneously subjected

to the same procedure. The lead is separated by extraction with chloroform, and determined spectrophotometrically with dithizone, in the manner described by Sandell (1959).

REFERENCES

Ampt, G. A. 1935, Determination of zirconium: Australian Chem. Inst. Jour. and Proc., v. 2, p. 321–334.

Rafter, T. A., 1950, Sodium peroxide decomposition of minerals in platinum vessels: Analyst, v. 75, p. 485–492.

Rose, H. J., Jr., and Stern, T. W., 1960, Spectrochemical determination of lead in zircon for lead-alpha age determination: Am. Mineralogist. (in press)

Sandell, E. B., 1959, Colorimetric determination of traces of metals, 3d ed.: New York, Interscience Publishers, Inc., p. 563–571.

221. PREPARATION OF LEAD IODIDE FOR MASS SPECTROMETRY

By Frank Cuttitta and Jesse J. Warr, Washington, D.C.

Work done in cooperation with the U.S. Atomic Energy Commission

The determination of geologic age by the lead-uranium or lead-lead methods is based on a knowledge of the Pb^{206}/U^{238}, Pb^{207}/U^{235}, and Pb^{207}/Pb^{206} ratios. The lead is isolated from samples and is converted to lead iodide, which is used to determine the isotopic composition with a mass spectrometer. In the case of pure galena, PbS, the lead iodide is prepared directly. Other materials of geologic interest for geochronological studies, such as allanite, asphaltite, autunite, brackebuschite, brannerite, cerussite, clausthalite, coffinite, coronadite, davidite, descloizite, feldspar, impure galena, limonite, microlite, parsonite, phosphorite, pitchblende, polycrase, psilomelane, pyrite, samarskite, thorianite, thorite, uraninite, yttrotantalite, and zircon require isolation and purification of lead content by conversion to one of three intermediate forms, PbS, $PbSO_4$, or $Pb(NO_3)_2$, prior to final conversion to PbI_2.

When the amount of lead is expected to be less than 1 mg, reagent blanks are carried along. The procedures described are adequate for most applications. However, they may be modified or simplified where experience indicates this to be necessary.

An intensely yellow precipitate of lead iodide, PbI_2, is formed when iodide ions are added to lead salt solutions. Recrystallization from hot water changes the lead iodide into beautiful, golden, sparkling leaflets. Although the compound is yellow, its aqueous solution is quite colorless. Some physical constants (Remy, 1956) are: Density=6.2, mp=412°C, bp=900°C, and solubility at 25°C (brucite-type PbI_2) =0.331 gram per liter or 1.6 millimoles per liter and at 100°C=1.865 grams per liter or 9 millimoles per liter. The iodide is insoluble in alcohol but moderately soluble in solutions of alkali iodides. It is decomposed by ether. Crystallization from solutions containing hydriodic acid produces the addition compound $HI \cdot PbI_2 \cdot 5H_2O$ which is orange yellow in color.

Lead iodide was prepared by the following procedures:

1. Directly from pure galena (PbS).—PbS is dissolved and transformed with excess hot concentrated hydriodic acid to iodoplumbous acid, $HPbI_3$, with the evolution of H_2S. The operation is carried out in a 15-ml centrifuge tube immersed in a water bath, heating until the sulfide dissolves and no further evolution of H_2S can be detected. A copious yellow precipitate will form on dilution of the clear amber-yellow solution (1 to 2 ml in volume) with 10 ml of ice-cold lead-free water. The iodide is centrifuged, and the centrifugate is discarded. The PbI_2 is dried in the centrifuge tube at 80°C. For small amounts of galena (<5 mg), the procedure is scaled down to a semimicrolevel using 2- to 3-ml centrifuge tubes and long stemmed capillary tube medicine droppers for delivering reagents.
2. From pure lead sulfate.—$PbSO_4$ dissolves and transforms in hot (Caley, 1933) or cold (Caley and Burford, 1936) concentrated HI to iodoplumbous acid, $HPbI_3$. The resulting solution has a faint yellow to dark-golden yellow color depending on the lead concentration. A copious precipitate of lead iodide is formed on dilution with ice-cold water. The lead sulfate used for the preparation is contained in a 5-ml porous porcelain filter crucible after having been prepared for the gravimetric determination of lead. The lead sulfate is dissolved either in hot or

cold concentrated HI, using a total of 2 ml in portions. It is filtered directly into a 15-ml centrifuge tube using suction. Ten to twelve milliliters of hot boiling water is used as a wash solution. Lead iodide precipitates on cooling to 5° to 10°C.

3. From impure lead sulfate.—In the course of preparing sample solutions in H_2SO_4 for the volumetric determination of uranium, insoluble sulfates form and these are reserved for the isolation of lead.

   Lead may be separated from silicon dioxide, calcium, strontium, barium, tin, and antimony by extraction of the precipitated sulfates and oxides with ammonium acetate (20 percent w/v solution containing 3 percent v/v acetic acid). $CaSO_4$ is extracted to a considerable extent and about 95 percent of the lead is separated from $BaSO_4$ even when the lead-barium ratio is 1:100 (Scott and Aldridge, 1931). The lead is precipitated as the sulfide from the acetate medium, centrifuged, washed free of salts, and then converted to the nitrate with nitric acid. The nitrate is converted to the iodide with a freshly prepared saturated alcoholic solution of ammonium iodide.
4. From uranium-bearing materials.—Samples are dissolved as described in the literature and converted to chloride in an HCl medium. The sample solutions are adjusted to pH 0.4 to 0.5. Iron and vanadium are reduced with hydroxylamine hydrochloride in the presence of 10 to 20 mg of copper which serves as a catalyst for the reduction of iron at this pH and as a carrier for lead when precipitated as the sulfide. After precipitation of the sulfide, the lead is then separated from the copper carrier and from any bismuth present by simultaneously reprecipitating the latter two as the sulfides from 2*M* HCl. The lead is then extracted from the 2*M* HCl solution (50 ml volume) with 2 to 3 10-ml portions of 1 percent w/v diethylammonium-diethyldithiocarbamate in chloroform. Thallium remains in the aqueous phase. After evaporation of the chloroform, the lead carbamate is wet-ashed, and the lead is cycled through another sulfide precipitation from a small volume in a sodium acetate medium. As little as 10μg of lead is precipitated in this manner. The lead sulfide is converted to the nitrate by treatment with concentrated HNO_3. After evaporation to dryness, the lead nitrate is transposed to the iodide with alcoholic NH_4I just before the mass spectrometric analysis.
5. From feldspars and zircons.—Feldspars are dissolved by an HF–HCl attack in Teflon; zircon or any insoluble residue remaining from the acid attack of feldspars is decomposed by a carbonate-borate fusion in platinum at 925°C for 20 to 30 minutes. Zircon samples are decomposed directly with carbonate-borate fusion. After the preparation of the sample solution in HCl medium, the procedure is similar to that used in the separation and purification of lead from uranium-bearing materials described in step 4 above. Blanks are run simultaneously with samples. Occasionally, circumstances may warrant the introduction of a dithizone extraction of the lead from an alkaline-cyanide medium just before the final sulfide step.

REFERENCES

Caley, E. R., 1933, Action of hydriodic acid on the difficultly soluble sulfates: Am. Chem. Soc. Jour., v. 55, p. 3947–3952.

Caley, E. R., and Burford, M. G., 1936, Detection and separation of difficultly soluble compounds by concentrated HI: Indus. and Eng. Chemistry, Anal. Ed., v. 8, p. 63–67.

Remy, H., 1956, Treatise on inorganic chemistry, v. 1, p. 550–551: New York, Elsevier Publishing Co.

Scott, W. W., and Aldridge, S. M., 1931, Investigation of ammonium acetate separation of sulfates of lead, barium, and calcium: Indus. and Eng. Chemistry, Anal. Ed., v. 3, p. 32.

222. DETERMINATION OF SMALL QUANTITIES OF OXYGEN ADSORBED ON ANATASE

By Frank Cuttitta, Washington, D.C.

Work done in cooperation with the U.S. Atomic Energy Commission

Measurements of the magnetic susceptibility of the anatase and rutile form of TiO_2 have recently been made by F. E. Senftle, T. Pankey, and F. Grant (written communication, 1960) on synthetic crystals. Their results show an increase in the magnetic susceptibility of from 0.04 to 0.25 x 10^{-6} emu per gram for anatase from room temperature to 77° K whereas the magnetic susceptibility of rutile was found to be

temperature independent. The anomalous change noted for anatase could be explained if about 0.35 percent oxygen was adsorbed onto the surface of the anatase powder from impurities in the tank gas used in making the magnetic measurements. In an attempt to test this possibility, the amount of oxygen adsorbed on portions of the same anatase sample used for the magnetic susceptibility determination was measured by two methods, and the purity of the tank gas used in the magnetic measurements was tested also.

One of the methods used to determine the oxygen content of powdered anatase consisted of desorbing the oxygen at 925° C and sweeping it out with oxygen-free nitrogen. The results of two experiments showed the adsorbed oxygen content to be 0.40 and 0.34 percent. It was noted that TiO_2 (white powdered synthetic anatase) turned yellow on heating and inverted to rutile at this temperature but the sample color was restored to white on cooling to room temperature. This is the normal color variation observed when converting anatase to rutile.

The second method, based on the work of Czanderna and Honig (1959) who reported that nitrogen is strongly adsorbed on anatase at room temperature, was to replace adsorbed oxygen by flowing a current of oxygen-free nitrogen at room temperature over the powdered anatase. Two measurements of the oxygen content of anatase determined by this means were 0.37 and 0.38 percent. These agree with the results of the first experiment and confirm the observations of Czanderna and Honig (1959).

The purity of tank gas of the type used in the magnetic measurements was tested by removing adsorbed oxygen in a dynamic high vacuum (using a Welch duo-seal pump) at room temperature. After maintaining a continuous dynamic vacuum for 15 minutes at room temperature, the oxygen was swept out and determined as described below. Results were comparable to measurements of blanks—no oxygen being detected by the method. It was also observed that during outgassing the sample turned gray. After the admission of nitrogen, the sample color was restored to white. The gray color was due to a loss of a small amount of oxygen from the TiO_2 lattice, that is, production of oxygen vacancy sites. If the tank nitrogen admitted had been pure, no change in color would have taken place, so the fact that the TiO_2 again regained its white color indicates that the tank nitrogen probably was contaminated with a small amount of oxygen. This was later confirmed by further magnetic measurements.

The above experiments showed that the amount of oxygen adsorbed to the anatase surface was about 0.35 to 0.40 percent—approximately the same amount as that theoretically calculated as being necessary to produce the anomalous magnetic susceptibility at 77°K. The experiment on outgassing pointed to the impurity in the tank gas as a likely source of the oxygen. This was subsequently eliminated and the anomaly disappeared.

557753 O—60——32

PROCEDURE FOR MEASURING THE OXYGEN CONTENT OF GAS

The oxygen content of the nitrogen gas was measured in all of these experiments by a procedure that utilizes the reaction of the oxygen with copper as described by MacHattie and Maconachie (1937) and Urig, Roberts, and Levin (1945). Oxygen can be determined in gases and liquids by copper moistened with ammonia-ammonium chloride salt solution:

$$2Cu + O_2 + 8NH_3 + 4H^+ \rightarrow 2Cu(NH_3)_4^{++} + 2H_2O$$

Colorimetric measurement of the intensity of the blue cupriammine complex permits determination of 0.1 to 2 ml of oxygen. The copper-oxygen conversion factor is defined as the milliliters of pure oxygen at 0°C and 760 mm of mercury pressure equivalent to 1 mg of copper and is theoretically equal to 0.088 ml (0.126 mg O_2) corresponding to the formation of cuprous oxide. However, data published by MacHattie and Maconachie (1937), Powell and Joy (1949), and Deinum and Dam (1949) indicate that apparently some cupric oxide is also formed. Powell and Joy and Deinum and Dam obtained an average factor of 0.099 ml (0.142 mg) by introducing known volumes of oxygen into their apparatus. Powell and Joy (1949) have also shown that the rate for the complete absorption of oxygen from a gas passed through the absorption tube should not exceed 350 ml of gas per minute and that under these conditions the method is probably accurate to within at least 2.5 percent of the true value.

The preparation of reagents and copper calibration curves are described by Powell and Joy (1949). Their apparatus for determining low concentrations of oxygen in gas has been modified to obtain data for the work listed above. The pertinent details of the apparatus are given in figure 222.1.

OPERATION OF APPARATUS

Assemble the apparatus as shown in figure 222.1 and purge it with oxygen-free nitrogen. Connect the delivery tube of the reagent bottle to the right arm of stopcocks *A*. Fill the absorption tube to the mark near stopcock *C*. Allow the solution to pass back through the left arm of stopcock *A* into a 200-ml volumetric flask using a positive nitrogen pressure through the left arm of stopcock *C*. Return the apparatus to its original position and repeat the washings until the solution, when taken from the apparatus, has only a

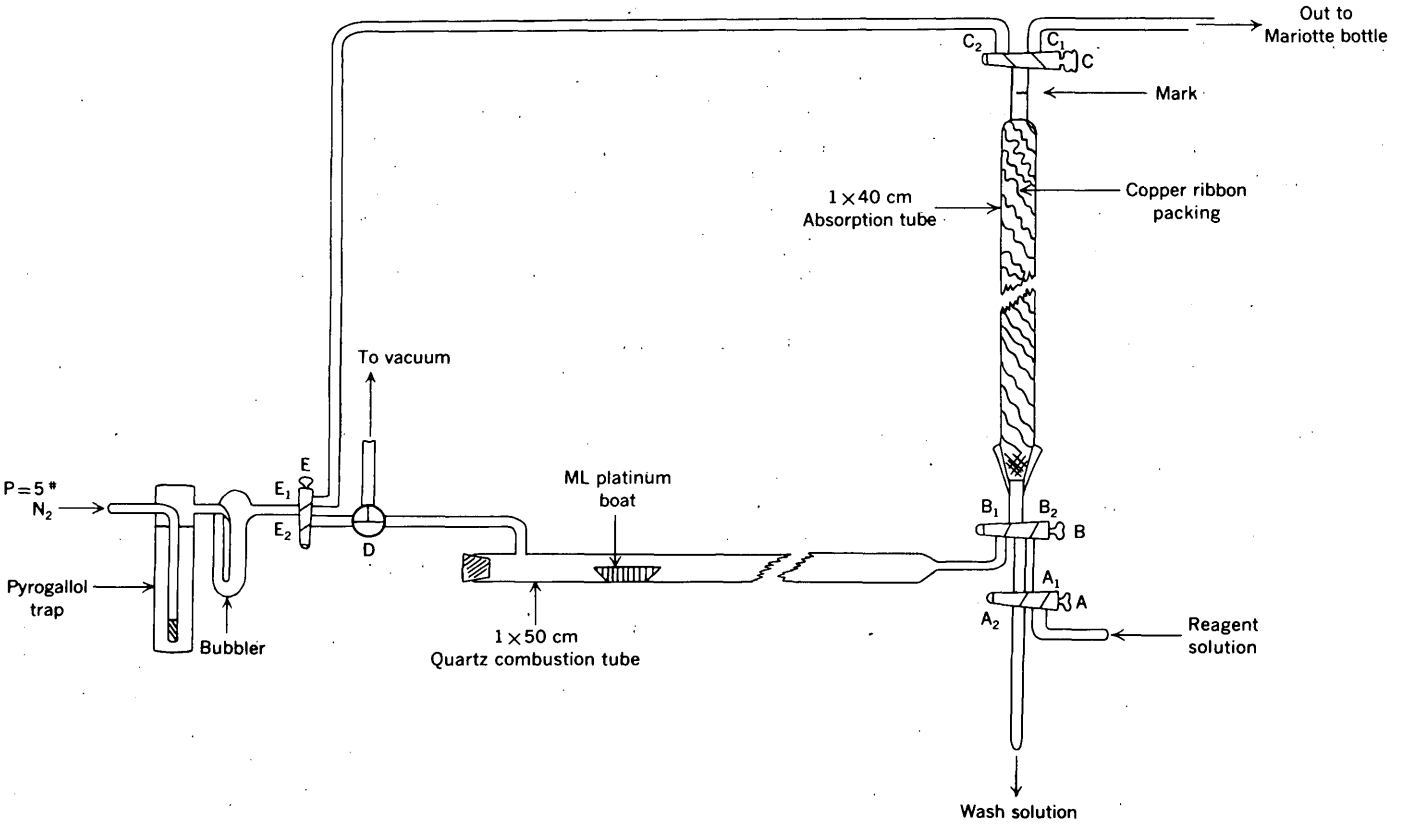

FIGURE 222.1.—Apparatus for determining low concentrations of oxygen adsorbed on anatase.

slight constant color due to the oxygen in the reagent. The apparatus is now ready for use.

Run reagent blanks and samples, using a nitrogen gas flow, through stopcocks E_2, B_2, C_1, and out to the Mariotte bottle. Exactly 450 ml of nitrogen is passed in a 20 minute period under a 5 pound positive pressure.

After the prescribed volume of gas has been passed through the apparatus, close E_2 and B_2 and open E_1, B_1, and A_1. Pass reagent solution into the absorption tube to the mark near stopcock *C*. Discharge the solution through the left arm of stopcock *A* (A_2) into a 200-ml volumetric flask. Repeat this operation four times more. The apparatus is now ready for re-use. Make up the combined washings to 200-ml with the ammonia reagent. Determine the absorbance of this solution at 640 mμ, setting the spectrophotometer to 100 percent transmission with the reagent solution. Our experiences show that reagent blanks are remarkably constant.

REFERENCES

Czanderna, A. W., and Honig, J. M., 1959, Interaction of oxygen with titanium dioxide: Jour. Phys. Chemistry, v. 63, p. 620–626.

Deinum, H. W., and Dam, J. W., 1949, Determination of small quantities of oxygen: Anal. Chimica Acta, v. 3, p. 353–359.

MacHattie, I. J. W., and Maconachie, J. E., 1937, Determination of small quantities of oxygen in gases and liquids: Indus. and Eng. Chemistry, Anal. Ed., v. 9, p. 364–366.

Powell. J. S., and Joy, P. C., 1949, Determination of small quantities of oxygen in hydrocarbon gases: Anal. Chemistry, v. 21, p. 296–297.

Urig, K., Roberts, F. M., and Levin, H., 1945, Determining oxygen in hydrocarbon gases: Indus. and Eng. Chemistry, Anal. Ed., v. 17, p. 31–34.

223. PRELIMINARY TESTS OF ISOTOPIC FRACTIONATION OF COPPER ADSORBED ON QUARTZ AND SPHALERITE

By Frank Cuttitta, Frank E. Senftle, and E. C. Walker, Washington, D.C.

Work done in cooperation with the U.S. Atomic Energy Commission

Isotopic fractionation may result from the adsorption of a gaseous or ionic species on a solid surface. Caldirola and Rossi (1957a, b) studied these effects for a gaseous mixture in the light of the Lennard-Jones theory on the interaction of atoms and molecules with solid surfaces. Their computations agree with the experimental results of Trawick and Berman (1956) who studied the fractionation of elemental gases by adsorption on silicon powder.

The conditions that are favorable for adsorption are also favorable for ion exchange. Fractionation of isotopes by exchange reactions is well known, as has been shown by Betts and others (1956), who separated Na^{22} and Na^{24} on Dowex resins.

The adsorption by mineral grains of ions contained in ground water is a common process associated with the migration of atoms in nature. For instance, ion exchange and adsorption most certainly take place at grain surfaces in a sandstone or other rock through which ground water percolates. And from results of the above-mentioned laboratory experiments, it is reasonable to speculate that isotopic fractionation does take place in nature under these conditions.

The following preliminary experiments were performed with copper as a tracer to determine the extent of isotopic fractionation on cellulose, quartz, and sphalerite. Richardson and Hawkes (1958) found that the total adsorption of copper on quartz amounted to about 3×10^{-12} moles of copper per square centimeter of quartz. Experiments by Gaudin and others (1951) indicate that a gram of sphalerite in the size range of 48 to 325 mesh will adsorb about 1.9×10^{-6} moles of copper. However, it is not clear from their data whether this was due to a true adsorption mechanism.

Results are generally quoted as the deviation, Δ, from the standard ratio (Cu^{63}/Cu^{65}=2.223) in parts per mil (o/oo), where

$$\Delta = 1000 \times \frac{(Cu^{63}/Cu^{65})\ \text{standard} - (Cu^{63}/^{65})\ \text{sample}}{(Cu^{63}/Cu^{65})\ \text{standard}}$$

An enrichment of the heavy isotope or the light isotope is indicated by a positive or a negative number, respectively.

EXPERIMENT 1

A chromatographic column (40 cm long by 2 cm diameter) was "packed" with an aqueous slurry of Whatman ashless chromatographic paper (batch 1274–78–83) to a height of 30 cm and allowed to drain by gravity. An aqueous solution of $CuSO_4$ (5 mg Cu/ml) was made from reagent grade, fine crystal $CuSO_4 \cdot 5H_2O$ (Baker and Adamson) and the isotopic abundance ratio, Cu^{63}/Cu^{65}, was determined to be 2.223 (Walker and others, 1958). Seventy-five milliliters of this solution was passed through the quasi-drained moist column at room temperature under gravity flow and various fractions of the effluent were collected as shown in the following tabulation. The final fraction was obtained by allowing the column to drain until no further collection could be made.

Aqueous fraction	Volume (ml)	Color
1	25	No color
2	20	No color
3	20	Very faint blue
4	3	Light blue
5	3	Blue
6	3	Slightly darker blue
7	3	Very blue
8	3	Dark blue

The first four fractions were then combined, the copper extracted and converted to Cu_2I_2 as discussed by Walker and others (1958), and a mass spectrographic analysis was made. An enrichment of a little better than 1 part per mil of the heavy isotope (Cu^{65}) over the normal isotopic abundance for reagent grade $CuSO_4$ was found for the combined fractions. This variation is about twice as large as the largest experimental error observed in previous measurements and justified further experimental work.

EXPERIMENT 2

A glass column (105 cm long by 1.5 cm in diameter) was "dry-packed" with 40 to 50 mesh sea sand to a volume of 185 ml. The sand was first washed with 1:1 HCl and then with distilled water until the effluent gave no test for chloride. The head solution (different from that used in experiment 1) contained 0.1 mg Cu

per ml at a pH of 4.9 and was prepared from $CuSO_4$ (Baker and Adamson, Lot 6071). The mean of two mass spectrographic analyses on this solution showed an enrichment of Cu^{65} of $+1.45 \pm 0.09$ parts per mil from our previous copper standard.

This solution (250 ml) was gravity fed through the column and various fractions of the effluent were collected as before. The copper in each fraction was isolated as Cu_2I_2 and analyzed with a mass spectrometer. The results indicate a definite fractionation and enrichment of Cu^{63} in the effluent and acid washings relative to the "head" liquor. The enrichment of the heavy isotope shown in the water washings is less than the actual enrichment on the surface of the adsorbent because of the dilution effect of the fluid remaining in column. The results of this experiment and the corresponding values for delta are tabulated below. If delta (Δ) is larger than 1.45 (value for the "head" liquor) there is an enrichment of Cu^{65}, if smaller a depletion of Cu^{65}.

Solution	Volume (ml)	Number of isotopic analyses	Δ
Head	------	------	$+1.45 \pm 0.09$
Effluent fraction 1	10	[1]	----------
2	30	2	$+.45 \pm .14$
3	40	1	$+.4 \pm .1$
4	80	1	$+.64 \pm .5$
5	[2]	1	$+.6 \pm .06$
Distilled water	[3] 500	1	$+1.54 \pm .33$
1*M* H_2SO_4 at 75° C	[3] 500	2	$+.17 \pm .25$

[1] Sample lost.
[2] Remainder.
[3] Five 100-ml washings.

EXPERIMENT 3

The procedure outlined in experiment 2 was repeated as closely as possible. The column was packed with sphalerite instead of quartz sea sand. A mesh size of 30 to 40 was used to facilitate the flow of the copper solution. The sphalerite (Joplin, Mo.) was picked to exclude any large pieces of other minerals and was estimated to be about 95 percent pure. Another 250 ml of the same head solution (enriched 1.45 ± 0.09 parts per mil relative to the standard) as used in the previous experiment was passed through the column. The following tabulation shows an enrichment of the effluent fractions in Cu^{63} similar to that found in experiment 2:

Solution	Volume (ml)	Remarks	Δ
Head	------	0.1 mg Cu per ml.	1.45 ± 0.09
Effluent fraction 1	40	No Cu detected	----------
Effluent fraction 2	60	----do--------	----------
Effluent fraction 3	80	Slight blue color	$.94 \pm .04$
Effluent fraction 4	[1]	Light blue	$.94 \pm .04$
Distilled water	[2] 500	Colorless	$2.2 \pm .9$
1*M* H_2SO_4 at 75° C	[2] 500	----do--------	----------

[1] Remainder.
[2] Five 100-ml washings.

DISCUSSION

Three exploratory experiments indicate that a solution of copper ion can be isotopically fractionated by passage through a suitable column. However, the data are limited and a number of questions are raised especially as to the mechanism.

In experiment 2, one would not expect any major exchange between the quartz and copper. This is born out by the experiments of Hensley and others (1949) and Long and Willard (1952) on the adsorption of sodium ions on fused silica and glass. One must, therefore, assume a physical adsorption mechanism, which leads to the heavy isotope being preferentially adsorbed and the effluent being enriched in the light mass Cu^{63}. The experiment tends to bear this out. Cu^{65} in a solution of moderate concentration of copper is adsorbed preferentially to Cu^{63}, but in solutions of low copper concentration, as in the water washings, it is apparently more easily stripped from the quartz than Cu^{63}. This would account for the lighter copper in the acid washings. However, only a very small amount of copper ($\approx$0.1 mg) was acid leached from the sand, and the mass spectrometric analysis was made with some difficulties. We therefore consider this to be of qualitative value only.

In experiment 3, the pattern of the results was the same as in experiment 2. However, in this case one would expect that there would be a significant exchange of zinc ions by copper ions as well as adsorption. Evidently this was the case as relatively large amounts of zinc were found in the effluent solutions. However, we believe that the adsorption process as reported by Halfawy and Senftle (1957) is the major enrichment mechanism for the following reasons:

1. If copper replaced zinc one would expect water insoluble copper sulfide to be formed and this would not be removed by the water washings.
2. Since adsorption does take place on sphalerite one would expect an enrichment of the heavy isotope as was found.

These experiments show that some fractionation does take place by adsorption on solid surfaces. Further work should be done to substantiate these data.

REFERENCES

Betts, R. H., Harris, W. E., and Stevenson, M. D., 1956, The partial separation of sodium-22 from sodium-24 by ion-exchange chromatography: Canadian Jour. Chemistry, v. 34, p. 65–74.

Caldirola, P., and Rossi, G., 1957a, Isotopic effects due to adsorption of a gas on a solid: Nuovo Cimento, v. 5, no. 5, p. 1316–1332.

Caldirola, P., and Rossi, G., 1957b, Influence of adsorption and surface migration on isotopic separation in the diffusion of a gas through a porous wall: Nuovo Cimento, v. 5, no. 5, p. 1374–1376.

Gaudin, A. M., Spedden, H. R., and Corriveau, M. P., 1951, Absorption of silver ion by sphalerite: Am. Inst. Mining Metall. Engineers Trans., Tech. Pub. No. 3142–B (*in* Mining Eng., v. 3, p. 780–784).

Halfawy, M., and Senftle, F. E., 1957, Adsorption of radionuclides on minerals for ore beneficiation purposes: Zeitschr. Phys. Chemie, Neue Folge, v. 12, p. 196–205.

Hensley, J. W., Long, A. O., and Willard, J. E., 1949, Reactions of ions in aqueous solution with glass and metal surfaces: Indus. and Eng. Chemistry, v. 41, p. 1415–1421.

Long, A. O., and Willard, J. E., 1952, Reactions of ions in aqueous solution with glass: Indus. and Eng. Chemistry, v. 44, p. 916–920.

Richardson, P. W., and Hawkes, H. E., 1958, Adsorption of copper on quartz: Geochim. et Cosmochim. Acta, v. 15, p. 6–9.

Trawick, W. G., and Berman, A. S., 1956, Separation of isotopes by flow through powder packs with high ratio of surface area to void volume: Oak Ridge Gaseous Diffusion Plant K–1236, 34 p.

Walker, E. C., Cuttitta, Frank, and Senftle, F. E., 1958, Some natural variations in the relative abundance of copper isotopes: Geochim. et Cosmochim. Acta, v. 15, p. 183–194.

224. WATER-SOLUBLE BORON IN SAMPLE CONTAINERS

By Claude Huffman, Jr., Denver, Colo.

Paper cartons of various sizes and qualities ranging from small 1-oz pillboxes to quart size waxed-paper ice cream cartons are used as sample containers in the Denver laboratory of the U.S. Geological Survey. These containers were selected because they are cheap, nonbreakable, easily stored, adapted to Denver's low humidity, and their cylindrical shape with no neck lends itself to the mechanical mixing of the sample.

A systematic study was made by P. R. Barnett (oral communication) of possible sources of boron contamination that might explain high and erratic spectrographic results obtained for boron in a study of the Pierre shale. The paper pillbox sample container was suspected as a possible source of contamination. A pillbox was leached with water and semiquantitative spectrographic analysis of the evaporated solution showed a significant boron content.

Quantitative data obtained by a chemical method were desirable to explore further the extent of the possible contamination of analytical splits by water-soluble boron from paper cartons. A series of leaching tests with water on various paper containers was made. Water-soluble boron was extracted from the cardboard by heating one-fourth-inch squares of cardboard in water on a steam bath for 3 hours. The volume was adjusted to 100 ml per 2 grams of cardboard treated. Boron was determined on the solutions spectrophotometrically using the carminic acid method of Hatcher and Wilcox (1950). All water leaching experiments were made in boron-free polyethylene plastic beakers to avoid any possible contamination from chemical glassware (Wichers, Finn, and Clabaugh, 1941).

Sample cartons analyzed for boron are described and the water-soluble boron content is given in table 224.1. The results show that water-soluble boron ranging from 90 to 550 ppm was leached from the containers. This amount, no doubt, could contaminate Pierre shale samples having a boron content of 20 to 320 ppm. The 4-oz drug-packer commonly used for storing sample pulps in the Denver laboratory contains about 550 ppm boron; the cap from this container contains about 200 ppm. The cardboard mixing baffle inserted inside the 4-oz drug-packer during the mechanical mixing of the sample pulp contains about 140 ppm water-soluble boron. The 1 oz drug-packer (round pillbox) used by the spectrographic laboratory as sample storage containers for both quantitative and semiquantitative analyses contains about 190 ppm boron. The ice cream carton showed no appreciable water-soluble boron, probably because of its water-proofing. Boron could possibly

Table 224.1.—*Water-soluble boron content in cardboard containers*

[Based on 2 grams of paper leached with 100 ml water]

Description of sample material tested	Water-soluble boron (parts per million)
Drug-packer, 4-oz, 3½ by inches	550
Drug-packer cap, from 4-oz packer above	200
Cardboard mixing-baffle inserted in 4-oz packer while mixing samples	140
Drug-packer, 1-oz round, flat pillbox 1½ by ½ inch (spectrographic sample storage container)	190
Colored code ribbon from outside 1-oz pillbox above	420
Drug-packer, 2-oz 2½ by 1½ inch	90
Drug-packer cap, from 2-oz packer above	125
Waxed paper, quart, ice cream carton, 7 by 3½ inches	<5

be picked up by the abrasive effect of rock powders on the cardboard containers. This would be particularly true where the container is used for mechanical mixing of the sample.

DISCUSSION

It seems reasonable to assume that soluble boron from sample containers is at least partly responsible for high and erratic spectrographic data for boron. Salts of boron or boric acid are probably added to prevent mold and bacterial decay of the adhesives used in manufacturing the cardboard. This study indicates that sufficient boron to contaminate samples containing small amounts of boron is present in most of the sample containers used in the Denver laboratory. Containers used for samples for low boron determination should be tested. Most glass containers contain some boron; the most suitable container is probably a cheap boron-free plastic.

REFERENCES

Hatcher, J. T., and Wilcox, L. V., 1950, Colorimetric determination of boron using carmine: Anal. Chemistry, v. 22, p. 567–569.

Wichers, E., Finn, A. N., and Clabaugh, W. S., 1941, Comparative tests of chemical glassware: Indus. and Eng. Chemistry, Anal. Ed., v. 13, p. 419–422.

225. DILUTION-ADDITION METHOD FOR FLAME SPECTROPHOTOMETRY

By F. S. Grimaldi, Washington, D.C.

A more or less serious weakness inherent in the flame photometric method is the "matrix" effect. By this is meant that the emission intensity from a given element may depend on the nature and concentration of the accompanying elements in the sample. The method described here, a synthesis of several desirable features of methods reviewed by Gilbert (1959) plus some added features, requires no prior knowledge of the chemical composition of the sample. In this method matrix effects are largely overcome by sufficient dilution of the sample, and residual matrix effects are corrected for by a "spiking" technique. The resulting plot of intensity vs. concentration defines the upper region of a working curve characteristic of the given sample matrix mixed with differing amounts of test element. The curve is usually linear but may show a slight but regular curvature where sufficient dilution of the sample cannot be made. The shape of the curve for lower concentrations of the element is deduced by extrapolation from the known portion to zero intensity, thus defining at the same time the point of zero concentration. This is the only assumption made.

The extrapolation to zero intensity is simplified by choosing a concentration for a standard such that, if the standard is set at 100, the unspiked sample reads in the range of 20 to 35 percent transmission. Before plotting, the intensities obtained are corrected for background by reading emissions to the left or to the right of the chosen line or both, the extent to the left or right depending on the concentration and nature of the element and the slit width used. Minimum slit widths should be used to obtain the best resolving power and thus decrease or eliminate line interference from other elements.

PROCEDURE

1. Prepare a 3-percent v/v $HClO_4$ solution of the sample. For silicate rocks a 0.5-gram sample can be decomposed directly with HF and $HClO_4$ and made to 100-ml volume in a volumetric flask.
2. Obtain approximate concentrations of all elements in question as follows: Set 100-ppm standards at 100 on the flame spectrophotometer and read each element at its most sensitive wavelength. The concentrations obtained are used as a guide for dilution, if needed, and proper increments of spike to be used.
3. Take four aliquots for each element to be determined, maintaining a 3-percent concentration of $HClO_4$ acid. Add to the second, third, and fourth aliquots such definite multiples of spike that the fourth sample will contain a total of about three times the concentration of the test element estimated to be present in the sample.
4. Adjust to a definite volume and record the transmission.
5. Record the background emission at the wavelengths indicated in table 225.1.
6. Plot the net intensity (total intensity minus background intensity minus the reading of the blank at the optimum wavelength (against concentration, setting the concentration of the unspiked sample at an arbitrary point. Draw a smooth curve

through the points and extrapolate the curve to zero intensity. This locates the point of zero concentration. The concentration for the sample can then be read off the curve.

Table 225.1 indicates the concentration useful for each of the alkali metals for the 100-percent setting on an instrument such as the Beckman DU flame spectrophotometer, and the various wavelengths at which readings are made. These figures are given on the assumption that no element is present which gives line or band interference.

TABLE 225.1.—*Concentration for 100-percent setting and selected wavelengths for emission and background readings*

Element	Concentration parts per million as oxide	Wavelength mμ	
		Emission	Background
Na	10	589. 5	575, 600
K	25	768	750, 780
Li	25	671	660, 680
Rb	50	780	750, 815
Cs	50	852	815, —

The data for a typical run, given in table 225.2, were obtained as follows: A 0.5-gram sample of silicate rock was dissolved and made to 100 ml. Five milliliter aliquots were taken, spikes were added, and the solutions were then diluted to 50 ml before aspiration. A 25 ppm K_2O standard was set at 100 at 768 mμ, a slit opening of 0.12 being used on the Beckman DU.

TABLE 225.2.—*Typical data for determination of K_2O, hydrogen flame*

Sample aspirated	Emissions, percent transmission at			Net emission, percent transmission
	768 mμ	750 mμ	780 mμ	
Alone	28. 3	0	0	26. 5
+5 ppm K_2O	48. 3	0	0	46. 5
+10 ppm K_2O	68. 2	0	0	66. 4
+15 ppm K_2O	88. 4	0	0	86. 6
Blank	1. 8	0	0	----------

In figure 225.1 the net emissions are plotted against concentration of K_2O, setting the concentration of the unspiked sample arbitrarily at 10 ppm. The extrapolated portion of the curve, shown dashed, intercepts the abscissa at 3.3 ppm of K_2O; the sample thus contains 6.7 ppm of K_2O. This corresponds to 1.34 percent K_2O in the original rock.

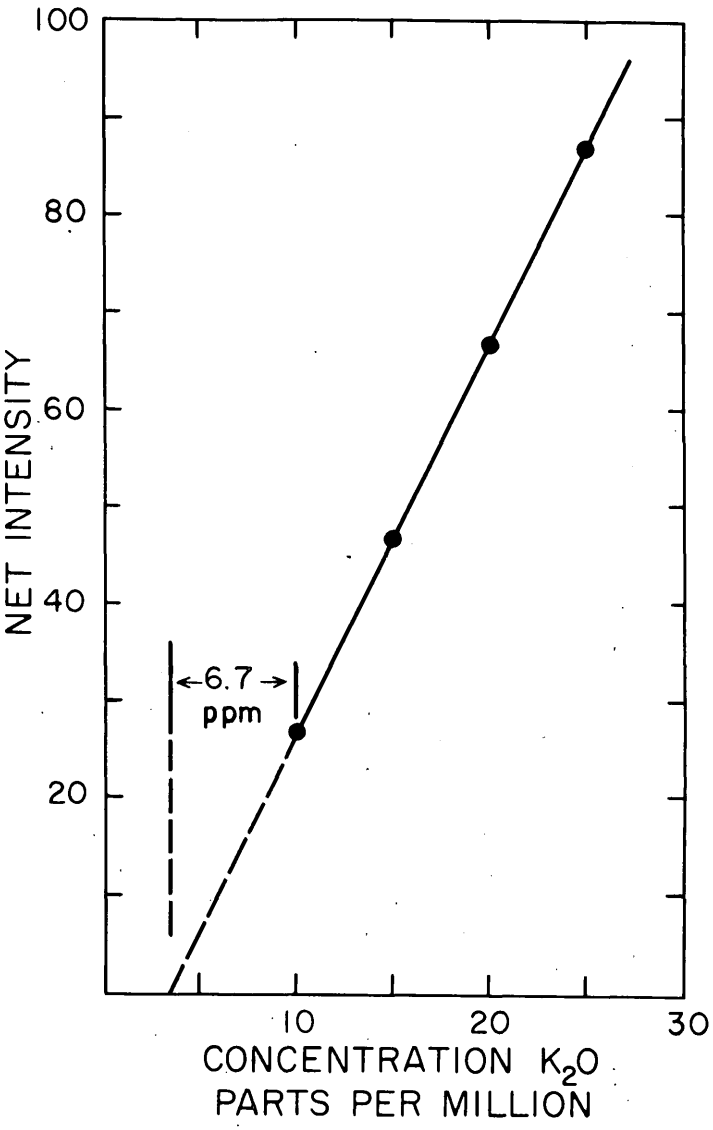

FIGURE 225.1—Determination of K_2O, typical data.

At present, only limited comparative data are available on samples, but these data show excellent agreement with results obtained by more conventional methods.

REFERENCE

Gilbert, P. T., 1959, Analytical flame photometry: New developments: Beckman Instruments, Inc., Paper 227, 77 p.

226. A SPECTROPHOTOMETRIC METHOD FOR THE DETERMINATION OF FeO IN ROCKS

By LEONARD SHAPIRO, Washington, D.C.

The most common procedure for determining ferrous iron in rocks consists of decomposing the rock with a boiling mixture of sulfuric and hydrofluoric acid and then titrating the solution with potassium dichromate or permanganate. Although this procedure has some disadvantages, arising from the fact that ferrous iron is easily oxidized by air and that ferric iron can easily be reduced by organic matter as it is brought into solution, it can give satisfactory results in much of the work for which it is used, provided it is carried out with great care and only a few samples are analyzed at a time.

In revising the methods of Shapiro and Brannock (1956), a method of determining FeO has been devised that is less subject to the difficulties encountered with the titration procedure, when applied to a large batch of samples, and easier to perform.

To avoid errors due to oxidation of the ferrous iron before titration, procedures have been proposed in which a measured excess of oxidant is added to the sample, so that the ferrous iron is immediately oxidized as it is dissolved, and the resulting Fe_2O_3, which may be more stable, is measured (Wilson, 1955). But this use of oxidants, though it gives very good results with some samples, is unreliable where other oxidizable materials such as organic matter or sulfides are present. In general, therefore, it is better to use a color-forming reagent rather than an oxidant.

In the method to be described, powdered orthophenanthroline is added to the weighed sample, and followed by H_2SO_4 and HF. The attack is carried out on a steam bath, the orthophenanthroline complexing the ferrous iron as it goes into solution. After the attack, buffer is added and absorbance of the resulting color is measured in a spectrophotometer.

REAGENTS AND EQUIPMENT

Orthophenanthroline: The pure powdered reagent. Crush to a powder if necessary.

Sulfuric acid: 50 ml of the concentrated acid to 450 ml of water.

Hydrofluoric acid: 48 percent.

Boric acid: 5 percent solution.

Sodium citrate: 10 percent solution.

A metal dipper: A scoop with a hole 3/16 inch in diameter, drilled deep enough so that when full it holds about 20 mg of the orthophenanthroline powder.

Plastic bottles, 1 oz: Two to three dozen polyethylene bottles ½ inch in outer diameter should be available to take full advantage of the procedure.

Steam-bath covers: Drill ½-inch holes into sheets of plastic or metal to fit on the top of a steam bath to support the plastic bottles.

A rock sample having a known FeO content between 5 and 10 percent, to be used as a standard.

PROCEDURE

1. For each sample, carefully weigh 10.0 mg. of rock powder (200 mesh) and transfer to a dry plastic bottle. Do the same to the rock standard.
2. Add 1 dipper of powdered orthophenanthroline to each of the bottles, and to another one to serve as a blank.
3. Add 3 ml of the H_2SO_4 solution.
4. Add ½ ml of the HF with a plastic safety pipet, swirling to ensure complete wetting of the sample.
5. Place on a steam bath in a fixed order, so that the first one on will be the first one off. Leave on steam for 30 minutes.
6. While the samples are on the steam bath, transfer 5 ml of the boric acid solution to a series of 100-ml volumetric flasks.
7. Following the same order as used previously, remove samples from the steam bath, and rapidly add 20 ml of sodium citrate to each. It is desirable to have the steaming time as nearly uniform as possible.
8. Transfer the contents of the bottles to the volumetric flasks, using water to rinse the bottles.
9. Make up to the mark and mix.
10. Determine the absorbances in a spectrophotometer at a wavelength of 555 mμ, using the blank as a reference. A cell path of 25 mm is suitable.
11. Read all the absorbances also at 640 mμ against the blank as reference. This serves as a measurement of the "cloud" of any undecomposed material or of any fine precipitate formed, especially with limestone samples. These corrections are generally quite small.
12. Calculate as follows: For each solution subtract the absorbance at 640 mμ from the absorbance at 555 mμ to obtain absorbance due to the color. Divide the known FeO value for the standard rock by the absorbance of its color to obtain a factor. Multiply the factor by the color absorbance for each sample to obtain percent FeO.

DISCUSSION AND RESULTS

Two factors were studied which seemed pertinent to the procedure. The small sample size made it seem likely that particle size might be a problem by giving nonuniformity of sampling. This was tested by using a sample containing approximately 10 percent FeO. Six weighings were made from an 80-mesh portion, and six weighings from a 200-mesh portion of the same sample. The 12 samples were then run for FeO at one time. Both sets gave precisely the same average value, but the results from the 80-mesh set showed a spread of 0.5 percent absolute, and those from 200-mesh

set a spread of only 0.1 percent absolute. In the procedure adopted, therefore, samples are ground to 200 mesh.

The second factor to be studied was the stability of the ferrous-orthophenanthroline color under the conditions of steaming used in the procedure. It was found that there was a progressive though fairly slow change with time of steaming, of the order of about one percent loss in color per three minutes of steaming. Too short a steaming period might fail to decompose all the silicates; too long a period of steaming would result in a greatly reduced sensitivity. A 30-minute steaming time was chosen as a satisfactory compromise. The effect of difference in steaming time was minimized by steaming all the samples and the standards for the same length of time.

An evaluation of the procedure was attempted by making spectrophotometric analyses of 25 rocks which had been analyzed by the titration procedure. The spectrophotometric procedure was used by three analysts at different times. The results obtained by the three analysts were generally in very good agreement; where they were not, two of the three agreed well and the other was sharply off. This might be explained by an occasional nonhomogeneous sample. Agreement with the titration procedure was good for most of the samples but not as good as the precision among the three analysts. As the true value of FeO is unknown, a measure of accuracy is not obtainable. Precision, except for an occasional large deviation, with within 2 percent of the amount present above 1 percent FeO and ±0.1 percent FeO (absolute) below 1 percent FeO of the average for the three analysts.

A collaborative study comparing the results of analyses of the same material from a large number of laboratories (Fairbairn and others, 1951) showed a wide spread of results in the reported value for FeO by the titration procedure, pointing up the difficulty of obtaining agreement. The procedure here presented may reduce this interlaboratory spread.

REFERENCES

Fairbairn, H. W., and others, 1951, A cooperative investigation of precision and accuracy in chemical, spectrochemical, and modal analysis of silicate rocks: U.S. Geol. Survey Bull. 980, p. 8–11.

Shapiro, Leonard, and Brannock, W. W., 1956, Rapid analysis of silicate rocks: U.S. Geol. Survey Bull. 1036–C, p. 19–56.

Wilson, A. D., 1955, A new method for the determination of ferrous iron in rocks and minerals: Great Britain Geol. Survey Bull. 9, p. 56–58.

227. SPECTROCHEMICAL ANALYSIS USING CONTROLLED ATMOSPHERES WITH A SIMPLE GAS JET

By C. S. Annell and A. W. Helz, Washington, D.C.

The normal spectrochemical procedure for analyzing rock and similar material involves the excitation in air of the sample mixed with graphite. Intense cyanogen band spectra are produced, which make useless for spectrochemical analysis much of the spectral region from 3500 to 4200 A. The interfering bands may be eliminated by excluding either carbon or nitrogen from the arc. However, it has been demonstrated many times that graphite or carbon is a very desirable admixture for rocklike samples, and therefore a more desirable solution is to exclude nitrogen from the arc in order to eliminate the cyanogen bands. Many methods for excluding nitrogen have been reported and in most methods the arc is placed in an enclosed chamber (Thiers, 1953). More recently, controlled atmospheres have been used with an air jet that had been designed primarily to improve stability of the direct-current arc (Shaw and others, 1958).

Two modifications of a simple gas jet have been studied extensively and will be described in detail in a later publication. This report is to show the effectiveness of one of these in reducing the cyanogen band intensity and to list observations of prominent lines of some elements found in the cyanogen band region.

The controlled atmosphere jet used is shown in figure 227.1. The normal type of ¼-inch sample-carrying electrode is clamped by rotating the lever shown at the base of the jet. Gas enters through the rubber and copper tubing illustrated, surrounds the base of the electrode, and rises through the annular space between the electrode and the ½-inch opening of the ceramic "welding" tip. This simple device is very effective, and easy to use and keep clean. The top of the sample electrode is shown projecting about 5 mm above the rim of the jet. The gas mixture selected after studying carbon dioxide and mixtures of helium or argon with

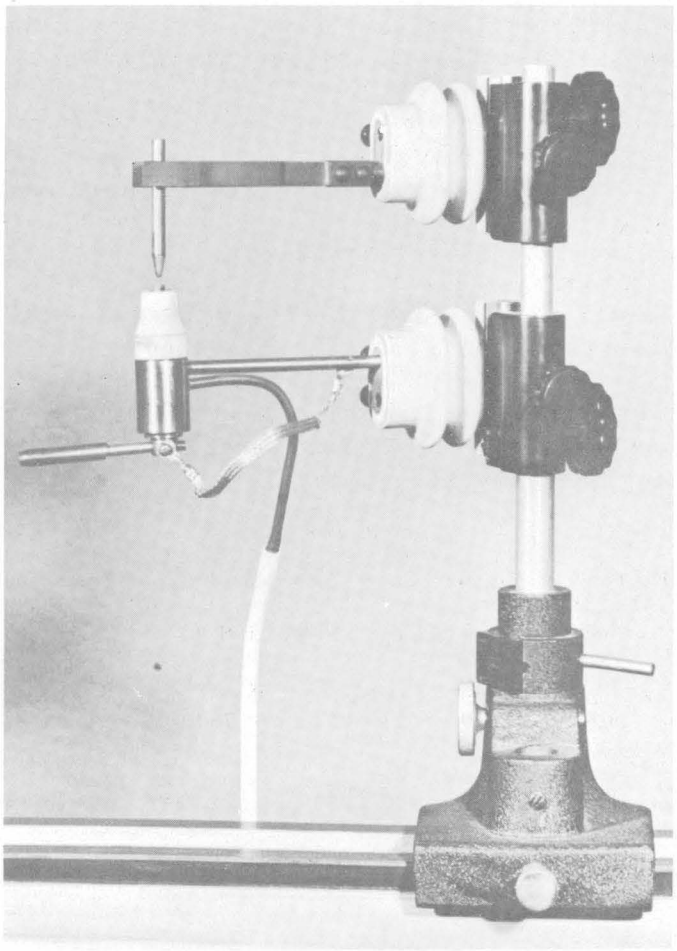

FIGURE 227.1.—Controlled-atmosphere jet for ¼-inch electrodes, shown in position on an arc stand.

oxygen, is four parts argon and one part oxygen flowing at a rate of 20 cubic feet per hour. Figure 227.2 illustrates how effective the above gas mixture, flow rate, and jet are for excluding nitrogen from the surrounding atmosphere of a 15 ampere direct-current arc.

Arc stability and rate of sample and electrode consumption are factors also considered in determining the gas mixture and flow rate. The use of greater proportions of argon or helium prolongs the arcing period. This versatility of controlled atmospheres can be advantageous, as when special problems associated with volatile elements are considered. The arc conditions used for the illustration show low-energy atom lines depressed and high-energy lines enhanced in the "Ar–O_2" spectra relative to the arcs in air. The excitation may be altered over a considerable range by changing the proportion and kind of gas mixture.

Several spectrograms have been prepared using standards for silicate rock analysis as the samples. These spectra are being studied to select lines in the cyanogen region that might be preferred over lines of the same elements in other regions of the spectrum for one or more of the following reasons: (a) lines may have a higher intensity than those normally used (Bastron and others, 1960) for determining a given element; (b) lines normally used for determinations of an element may have interferences requiring the use of other less sensitive lines; and (c) elements desired as internal standards for determining another element may not normally have lines suitable with respect to intensity, excitation energy, or spectral location.

A list of selected lines in the cyanogen region of several elements that have been studied is given below. Comparisons are also made with normally used lines in other spectral regions.

Ce II 4137.6 Ce II 4186.6	Both lines have similar intensities that are slightly greater than Ce II 4222.6, which has a detectability at 0.02 percent Ce.
La II 3949.1	Same order of intensity as La II 4333.7, which is detectable at about 0.001 percent La.
Sm II 3609.48	Has detectability at about 0.002 percent Sm.
Sm II 3885.3	Has detectability at about 0.01 percent Sm.
Pr II 4179.4	Has detectability at about 0.005 percent Pr, which is better than Pr II 3245.46 by a factor of 10.
Nd II 4156.1	Intensity similar to Nd II 4303.6, which is detectable at about 0.01 percent Nd.
Eu II 3819.66	Detectability below 0.001 percent Eu, ion line.
Eu I 3971.99	Detectability of about 0.001 percent Eu, atom line.
Tm 3700.26 Tm 3717.92 Tm 3795.77	All these lines have detectabilities at about 0.001 percent Tm.
Tl 3519.24 Tl 3775.72	Both lines are detectable at 0.002 percent Tl.
W 4008.75	This line has a detectability at about 0.003 percent W with possible interference from Ti I 4008.93.
W 4074.4	Slightly more intense than W 4294.61, which is detectable at 0.02 percent W.
Ru 3498.942 Ru 3661.35 Ru 3728.03	All three lines have detectable limits close to 0.002 percent Ru.
Ti I 3653.496 Ti I 3642.675 Ti I 3635.463	Three persistent atom lines with detectabilities at about 0.002 percent Ti.
Ti II 3759.295 Ti II 3761.323	These lines are slightly less intense than Ti II 3372.80, which has a detectability at about 0.0005 percent Ti.

Although the chief objective of the controlled atmosphere is to reduce the cyanogen band intensity, special applications to geological studies are suggested. The use of inert atmospheres of helium and argon have been shown to have a pronounced enhancing effect on

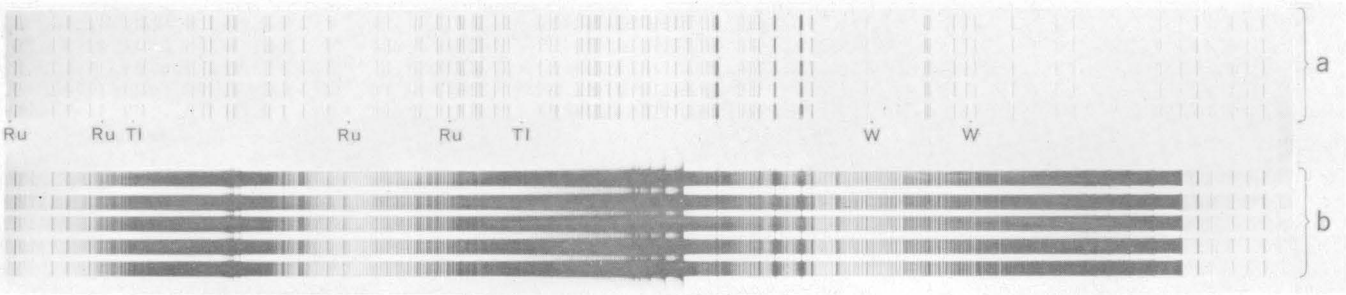

FIGURE 227.2.—Spectra, cyanogen region, of silicate rock standards containing tungsten, thallium, and ruthenium: *a*, in air, *b*, in controlled atmosphere of 4 parts of argon and 1 part of oxygen.

ion lines and high energy atom lines (Thiers and Vallee, 1957). This effect upon lines of the volatile Group V elements (P, As, Sb, and Bi), for example, may increase their detectability. Persistent ion lines of rare earth and other transition elements may be enhanced.

The suppression of excessive background caused by incandescent carbon and sample particles is usually sufficient to eliminate background corrections that are occasionally required when the sample electrode is arced in the air. This frequently enables the analyst to extend the working curves of affected spectral lines to a lower concentration range.

In conclusion, the effect of different controlled atmospheres upon the excitation and vaporization of sample constituents should lead to many useful applications to geochemical problems. The use of a simple gas jet demonstrates how readily a valuable portion of the spectrum can be utilized in spectrochemical analyses.

REFERENCES

Bastron, Harry, Barnett, P. R., and Murata, K. J., 1960, Method for the quantitative spectrochemical analysis of rocks, minerals, ores, and other materials by a powder d-c arc technique: U.S. Geol. Survey Bull. 1084–G.

Shaw, D. M., Wickremasinghe, O., and Yip, C., 1958, A simple device for the spectrochemical analysis of minerals in an inert atmosphere using the Stallwood jet: Spectrochimica Acta, v. 13, p. 197–201.

Thiers, R. E., 1953, The advantages of controlled atmospheres for arc spectroscopy: Applied Spectroscopy, v. 7, p. 157–163.

Thiers, R. E., and Vallee, B. L., 1957, The effect of noble gases on the characteristics of the d. c. arc: Coll. Spectroscopicum Internat. VI, Amsterdam, 1956, Proc., London, Pergamon Press, p. 179–185.

228. COMBINATION OF GRAVIMETRIC AND SPECTROGRAPHIC METHODS IN THE ANALYSIS OF SILICATES

By ROLLIN E. STEVENS, ARTHUR A. CHODOS, RAYMOND G. HAVENS, ELISABETH GODIJN, and SARAH T. NEIL, Menlo Park, Calif.; California Institute of Technology, Pasadena, Calif.; Denver, Colo.; California Institute of Technology, Pasadena, Calif.; and Menlo Park, Calif.

Results of analyses of the granite, G–1, and the diabase, W–1, submitted to laboratories throughout the world, seem to indicate that conventional methods of silicate analysis can give accurate values but in practice results vary widely because of personal and other errors (see Fairbairn and others, 1951, and Stevens and others, 1960). Many of the apparent errors in these analyses may have been caused by assuming that all of a given constituent was collected in a precipitate and that the precipitate was pure. Errors from these causes can be eliminated by analysis of the precipitates and the analysis of the material left after precipitation.

In the present study precipitates and other separates, obtained in a system of wet chemical separations, are analyzed spectrographically. Spectrographic analysis is well suited for the analysis of the separates, because of the large number of elements that can be determined in this way. The accuracy needed in the analysis of the separates varies directly with the percentage of contaminant found. When a contaminant is shown to be present in appreciable quantity in a separate, the contaminant can then be determined by wet chemical methods. This combination of wet chemical separations with spectrographic and chemical analysis of

separates will herein be called spectrogravimetric analysis.

The plan being developed for spectrogravimetric analysis is aimed at accomplishing the following: (a) measurement of all nonvolatile constituents; (b) correction of the weight of each precipitate or separate for material other than the constituent sought; (c) correction of each determination for the quantity of the constituent which failed to separate; and (d) correction of each determination for materials added as reagents, filter paper, and airborne dust, by a blank analysis made at the same time.

The wet separations are made in vessels of platinum, plastic, or fused quartz to prevent contamination from the material of the vessels, and the vessels are kept covered with plastic covers to reduce airborne contamination to a minimum. Only volatile reagents are used in the wet chemical separations for constituents other than SiO_2, in order to show more direct material balance of sample weight with the total weight of the separates.

An outline of the wet chemical separations for main constituents follows:

A. SAMPLE FOR SiO_2

A 1 g sample is heated to constant weight at 105°–110°C, fused with 5 g Na_2CO_3, leached with water, acidified with HCl, and evaporated to dryness. Soluble salts are dissolved in hot dilute HCl, and the silica is removed by filtering. The solution is again evaporated to dryness, baked at 105°–110°C, dissolved in hot dilute HCl, and filtered to remove residual silica.

Combined precipitates.—The precipitates are ignited to constant weight at 1100°C as impure SiO_2. The silica is volatilized with HF and the weight of SiO_2 calculated by difference.

Combined filtrates.—The filtrates are again evaporated to dryness, and Na_2CO_3 solution is added to make alkaline to render less hygroscopic; the solution is again evaporated to dryness and baked at 105°–110° C. The dry salts are submitted for spectrographic determination of the SiO_2 remaining.

B. SAMPLE FOR CONSTITUENTS OTHER THAN SiO_2

Solution of sample.—A 1 g sample is heated to constant weight at 105°–110°C, decomposed with HF+H_2SO_4, HF is removed by repeated evaporations with H_2SO_4 to dryness, and the residue is dissolved in dilute HCl. The constituents are separated from this solution by the following steps:

B1.—Ammonia precipitate—oxides of Al, Fe, Ti, V, Cr, etc.—plus impurities. These are collected by double precipitation with NH_4OH vapor in the cold. The precipitate is ignited to constant weight at 1100° C, and submitted for spectrographic analysis. Major constituents are determined chemically.

B2.—CaO plus impurities. Collected by double precipitation as oxalate in the combined filtrates from B1. The precipitate is ignited to constant weight as CaO, and converted to $CaSO_4$ or CaF_2 for spectrographic analysis.

B3.—MgO plus impurities. Collected by double precipitation and recovery precipitation of magnesium ammonium carbonate in the combined filtrate from B2, to which alcohol is added to repress the solubility. The precipitate is ignited to constant weight at 900° C, and converted to $MgSO_4$ or MgF_2 for spectrographic analysis.

B4.—Alkalies—$(Na,K)_2SO_4$ plus impurities. The combined filtrates from B3 are evaporated to dryness in a fused quartz beaker, and heated to remove the ammonium salts and the excess of sulfuric acid. The residue is dissolved in water, transferred to a platinum crucible, again evaporated to dryness, and heated to constant weight at 800° C. The salts are analyzed spectrographically, and Na, K, and other alkali elements determined with the flame photometer.

SPECTROGRAPHIC ANALYSIS OF SEPARATES

The spectrographic equipment is that described by Engel and Engle (1958) for separates A, B1, B4, and blanks, and essentially that described by Myers and Barnett (1953) for separates B2 and B3. An accuracy of ± 15 percent has been attempted in the spectrographic analyses. When a constituent of a separate is present in appreciable amount, it is determined by wet chemical methods. The spectrographic analyses of the separates are made as follows:

A. SiO_2 in salts from SiO_2 separations and blanks.—25 mg of a 1:4 mixture of sample and graphite is arced to completion in duplicate in a 19-ampere (short circuit) d-c arc. Standards are made by adding quartz to a NaCl base. Standards and samples are exposed on the same plate. Each plate is calibrated and a working curve is established by densitometry.

B1 and B4. The ammonia precipitates and the alkali sulfates and blanks.—Samples are diluted with graphite in the proportions 1:9, 1:99, and 1:999; 20 mg of the diluted samples and standards are arced to completion in duplicate in a 19-ampere (short circuit) d-c arc. Standards are made from mixtures of the oxides of the elements in a graphite base. Each plate is calibrated and working curves are established by densitometry.

B2 and B3. Ca *and* Mg *separates.*—Samples diluted with boron-graphite base in the proportions 1:9, 1:99, 1:299, and 1:999. 20 mg of the diluted samples and standards are arced to completion in duplicate in a 300-volt, 17 ampere d-c arc. Standards made from mixtures of the oxides of the elements in a boron-graphite base. Each plate is calibrated and working curves are established by densitometry.

CALCULATIONS

Calculations are illustrated by those for SiO_2 and for MgO in Olivine 55MV–40 for E. D. Jackson, and the summary of the analysis is given together with that of a hidden duplicate.

		Weight (grams)	
SiO_2	Wt sample at 105°–110° C	0.7440	
	Wt SiO_2 collected	.2982	
	Wt salts in filtrate 6.9 g		
	Percent SiO_2 in salts (spectrographic) <0.001		
	Correction for SiO_2 in salts	<+.0001	
	Correction for SiO_2 in blank	—.0008	
	Corrected wt SiO_2	.2975	
	Percent SiO_2		39.99

			Weight (grams)	
MgO	Wt sample at 105°–110° C			0.7503
	Wt MgO			.3468
	+MgO elsewhere (spectrographic):			
			Percent	
	In ammonia precipitate (wt 0.1114 g)		33	+.0003
	In $CaCO_3$ (wt 0.0003 g)		14	+.00004
	In $(Na, K)_2SO_4$+quartz (wt 0.0270 g)		8.3	+.0022
	Total MgO			.3493
	—impurities in MgF_2 (wt 0.4817 g) (spectrographic):			
			Percent	
	SiO_2		.02	
	Al_2O_3		.10	
	Fe_2O_3		.14	
	CaO		.04	
	MnO		.26	
	$BaSO_4$		.03	
	CoO		.01	
	NiO		.01	
	$SrSO_4$		.01	
			.62	—.0030
	—MgO in blank (spectographic)			—.0001
	Corrected wt MgO			.3462
	Percent MgO			46.14

Summary of analysis: Olivine from poikilitic harzburgite, Peridotite member, Mountain View area, Stillwater complex, Montana.

[Na_2O+K_2O not determined because determination of small quantities in separates not developed at time of analysis]

	55MV-40	55BE-44 (hidden duplicate)
SiO_2	39.99	40.01
Al_2O_3	.11	.14
Fe_2O_3	None	None
FeO	13.12	13.14
MgO	46.14	46.13
CaO	.04	.04
H_2O+	.12	.05
TiO_2	.007	.005
MnO	.17	.19
BaO	.03	.03
NiO	.19	.14
CoO	.03	.03
Cr_2O_3	.02	.02
CuO	.007	.002
Sc_2O_3	.01	.01
SrO	.002	.002
ZnO	.02	----------
ZrO_2	.001	.001
	100.01	99.95
H_2O−	.03	.02

CONCLUSIONS

The precision shown in the analysis of the olivine and its hidden duplicate may not be typical of spectrogravimetric analysis at present, but further development of the methods *may* yield such precision consistently. The results shown here also do not indicate the accuracy of the method, for they have not been compared with known or previously determined values. However, the system of analysis is of wet chemical separations, proven elsewhere, corrected by spectrographic and chemical determinations which are also well established. Nevertheless, the accuracy needs to be determined by results on materials of known composition.

Spectrogravimetric analysis seems to offer the following advantages over conventional procedures:

1. Essentially eliminates the possibility of gross error in the analysis for major constituents.
2. Improves the accuracy of the determinations of major constituents by determining the corrections needed to make them accurate.
3. Assures that nonvolatile constituents that can be determined chemically or spectrographically have not been overlooked.
4. Concentrates elements present in small quantity so that they can be measured.

Spectrogravimetric analysis, in its present state of development, is too costly to use for any but special samples although there are a number of geological problems requiring very precise data that may be approached in this way. The comparative cost of this type of analysis, however, is less than appears at first glance because analyses do not usually need to be checked by duplicate determinations.

REFERENCES

Engel, A. E. J., and Engel, C. G., 1958, Progressive metamorphism and granitization of the major paragneiss, Northwest Adirondack Mountains, New York: Geol. Soc. America Bull., v. 69, p. 1369–1414.

Fairbairn, H. W., Schlecht, W. G., Stevens, R. E., Dennen, W. H., Ahrens, L. H., and Chayes, F., 1951, A cooperative investigation of precision and accuracy in chemical spectrochemical, and modal analysis of silicate rocks: U.S. Geol. Survey Bull. 980, 71 p.

Myers, A. T., and Barnett, P. R., 1953, Contamination of rock samples during grinding as determined spectrographically: Am. Jour. Sci., v. 251, p. 814–830.

Stevens, R. E., and others, 1960, Second report on a cooperative investigation of the composition of two rocks: U.S. Geol. Survey Bull. 1113.

229. SODIUM-SENSITIVE GLASS ELECTRODES IN CLAY TITRATIONS

A. M. Pommer, Washington, D.C.

The study of the titration of clay acids, an important part of the investigation of the ion-exchange properties of clays (Marshall, 1949), is complicated. The reaction of the solid clays with the titrant is not instantaneous, because it takes place across a phase boundary. This raises a rate problem, but this can be minimized by resorting to discontinuous or "bottle" titrations. In this type of titration, individual reaction mixtures are kept in closed vessels (hence the name "bottle titration"); samples of identical weight are then placed in each vessel, but different amounts of titrant are added to these samples. Each of the reaction mixtures can then be analyzed at any time thereafter, and a titration curve plotted from which the end point is determined. If the method of analysis is nondestructive, as is the case in pH measurement, the determinations can be repeated as often as desired, and as a steady state is approached, the change between successive measurements becomes smaller and disappears. Other advantages of discontinuous titrations are these: It is possible to titrate at constant volume and constant ionic strength and thus eliminate dilution factors or changes in activity coefficients. If a single determination is ruined, it does not affect the value of the other determinations, which can still be plotted. The results of discontinuous pH titrations of clays has been reported (Pommer and Carroll, 1960).

In addition to the rate problem there is another complicating factor in the study of clay acids: it arises from the fact that these phases belong to multivariant systems, involving not only replacement of hydrogen by a cation such as sodium, but also release of exchangeable aluminum and the decomposition of the clays to soluble or insoluble aluminates and silicates (Marshall, 1949). For this reason a pH titration is best supplemented by further determinations, in which the sodium content of the reagent solutions in contact with the clay may supply important clues. Such determinations may be conveniently made in parallel with pH studies by means of a sodium-sensitive glass electrode. The same reference electrodes and measuring instruments (pH meters) are used in each case. It is not necessary to withdraw and consume solutions, and the clay-solution ratio is not significantly disturbed during consecutive determinations.

Glass electrodes sensitive to hydrogen ions have long been known. Their properties are reviewed by Dole (1941). Lengyel and Blum (1934) had noted that the potential of glass electrodes containing Al_2O_3 or B_2O_3 depends on the concentration of several cations in addition to H^+. Nikolskii (1953) extended the mathematical theory of glass electrodes, and Shults (1954) described a series of glasses of varying sensitivity to sodium which could be used in hydrochemical investigations (Kryukov and others, 1955; Goremykin and Kryukov, 1957). Eisenman and others (1957) developed a glass electrode suitable for measuring sodium ions, which was useful in biological problems (Friedman and others, 1959). An electrode of this type is now commercially available under the name "78137V Experimental cationic-sensitive glass electrode" (Beckman Instruments, 1959). Bower (1959) gives instructions for the use of this electrode; they require that the pH of the solution be adjusted to 7 before the sodium is measured.

Eisenman found that a sodium-sensitive glass electrode functions primarily as a hydrogen electrode if the pH drops below 4 and this finding was confirmed by Leonard (1959), who also stated that it was necessary to suppress the hydrogen activity to a value about four orders of magnitude below the expected sodium level. In discontinuous clay titrations, where the pH cannot be changed without spoiling the experiment, it is necessary to determine the sodium activities without an adjustment of pH.

It is possible, though tedious, to evade these difficulties by calibrating the sodium electrode in a series of solutions that differ in pH and sodium concentrations, but before this task was undertaken, an attempt was made to see whether the millivolt readings of a sodium-sensitive glass electrode, read against a standard calomel reference electrode, could be utilized in a study of clays. Figure 229.1 shows that this is so for a montmorillonite.

It has already been shown (Pommer and Carroll, 1960) that the titration of H-montmorillonite with NaOH can be plotted semilogarithmically (pH on the linear scale against volume of titrant on the logarithmic scale) to yield three apparoximately straight lines intersecting at the two points that represent the neutralization of two clay acids. It has been suggested that the first, or C^- acid, represents the neutralization of the interlayer positions, and the second, or E^- acid, represents the neutralization of the edge positions (Garrels and Christ, 1956). Figure 229.1 shows such

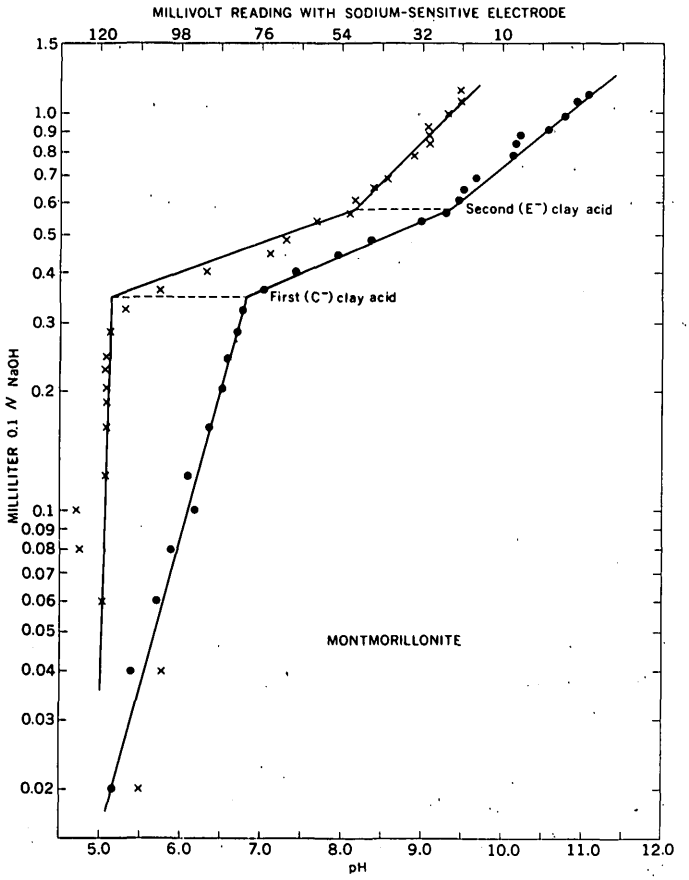

FIGURE 229.1.—Semilogarithmic plot of pH and potential difference readings between a sodium-sensitive glass electrode and a calomel electrode for the titration of a montmorillonite with sodium hydroxide. Dots represent pH; ×'s represent Na-millivolt readings.

a titration for a montmorillonite from Chambers, Arizona (A.P.I. Standard No. 23, Kerr and others, 1950). In addition to the pH values, millivolt readings from a Beckman 78137V Experimental Cationic-sensitive Glass Electrode/Calomel couple are also plotted on a semilogarithmic scale. It can be seen that again, except for abnormality at the low end of the curve, three approximately straight lines are formed which intersect at the two points representing the neutralization of the clay acids. The abnormality at the low end, where there is very little sodium in solution, may be due to the high sensitivity of the electrode to minute amounts of sodium in this region, or may be caused by pH effects. Table 229.1 relates millivolt readings to sodium content determined by flame photometry.

Though it is yet too early to draw firm conclusions, figure 229.1 indicates that as the first clay acid is neutralized virtually all the sodium added is taken up from the solution. This is shown by the marked steepness of the sodium curve in this region, which indicates

TABLE 229.1.—*Comparison of readings, in millivolts, with electrodes of calomel and sodium sensitive glass and with sodium values determined by flame photometry*

[Analyst, Dorothy Carroll]

pH	Na millimoles per liter	Na electrode millivolts	pH	Na millimoles per liter	Na electrode millivolts
4.80	0.53	89	8.50	3.5	53
5.30	.55	109	8.60	3.8	51
5.25	.60	104	8.60	4.2	45
5.80	.55	120	8.65	4.2	42
6.00	.55	120	8.75	4.8	38
6.10	.69	120	8.80	5.7	35
6.15	.70	122	8.90	6.4	31
6.00	.70	104	8.90	7.0	31
6.40	.76	118	8.75	7.0	31
6.55	.70	118	9.05	7.8	24
6.65	.90	118	9.05	7.2	25
6.70	.98	118	9.10	8.8	22
6.80	1.4	116	9.10	9.1	20
7.00	1.8	113	9.05	11	18
7.40	2.0	104	9.20	11	18
7.60	2.4	91	9.20	11	15
8.25	2.4	69	9.45	19	7
8.35	2.5	61			

a constant sodium concentration in the supernatant solution in equilibrium with the clay. As the second acid is neutralized this is no longer true, and the millivolt reading therefore changes more rapidly with addition of sodium hydroxide. Studies are now under way which, it is hoped, will elucidate this phenomenon.

REFERENCES

Beckman Instruments, Inc., 1959, 78137V Experimental cationic-sensitive glass electrode: Beckman Instruments, Inc., Bulletin 741–A, Fullerton, Calif.

Bower, C. A., 1959, Determination of sodium in saline solutions with a glass electrode: Soil Science Soc. America Proc., v. 23, p. 29–31.

Dole, Malcolm, 1941, The glass electrode. Methods, applications, and theory: New York, John Wiley and Sons, 332 p.

Eisenman, George, Rudin, D. O., and Casby, J. U., 1957, Glass electrode for measuring sodium ion: Science, v. 126, p. 831–834.

Friedman, S. M., Jamieson, J. D., Nakashima, Miyoshi, and Friedman, C. L., 1959, Sodium- and potassium-sensitive glass electrodes for biological use: Science, v. 130, p. 1252–1254.

Garrels, R. M., and Christ, C. L., 1956, Application of cation-exchange reactions to the beidellite of the Putnam silt loam soil: Am. Jour. Sci., v. 254, p. 372–379.

Goremykin, V. E., and Kryukov, P. A., 1957, Potentiometric method of determining sodium ions by means of a glass electrode with a sodium function: Akad. Nauk SSSR Izv. Otdel. Khim. Nauk, no. 11, p. 1387–1389.

Kerr, P. F., and others, 1950, Analytical data on reference clay minerals: Am. Petroleum Inst. Proj. 49, Prelim. Rept. 7, 160 p.

Kryukov, P. A., Shults, M. M., and Goremykin, V. E., 1955, Use of glass electrodes having a sodium function for water analysis: Gidrokhim. Materialy, v. 24, p. 23–27.

Lengyel, B., and Blum, E., 1934, The behavior of the glass electrode in connection with its chemical composition. Faraday Soc. Trans., v. 30, p. 461–471.

Leonard, J. E., 1959, Glass electrodes for the direct measurement of sodium ion activity, in aqueous solution; Instrumental Analysis Symposium, 5th, Houston, Texas, Instrument Soc. America: Beckman Instruments, Inc., preprint R–6148, 5 p.

Marshall, C. E., 1949, The colloid chemistry of the silicate minerals: New York, Academic Press, 195 p.

Nikolskii, B. P., 1953, Theory of the glass electrode V., Generalized theory of the glass electrode: Zhur. Fiz. Khimii, v. 27, p. 724–743.

Pommer, A. M., and Carroll, Dorothy, 1960, Interpretation of potentiometric titration of H-montmorillonite: Nature, v. 185, p. 595–596.

Shults, M. M., 1954, Investigation of the sodium function of the glass electrode: Leningrad Univ. Uchenye Zapiski no. 169, ser. Khim. Nauk no. 13, p. 80–156.

230. PRECIPITATION OF SALTS FROM SOLUTION BY ETHYL ALCOHOL AS AN AID TO THE STUDY OF EVAPORITES

By R. A. Gulbrandsen, Menlo Park, Calif.

If the origin of evaporites is to be well understood, accurate and extensive data must be obtained regarding the composition of sea water and other natural saline solutions and the salts precipitated from them at various stages of evaporation. One of the chief reasons why these data are not available arises from the mechanical difficulties encountered in performing carefully controlled and detailed evaporation experiments. Evaporation itself, apart from its exasperating slowness, creates a difficult problem by causing precipitation on the sides of the container, and the difficulty is increased by the strong tendency of highly saline solutions to creep up the walls. Such difficulties are avoided by a method in which ethyl alcohol "extracts" water from the solution. The process is analogous to evaporation, and causes precipitation of the salts.

The method is based on the well-known "salting-out" or "solubility-depressant" effect, which is due to the comparative insolubility of salts in one member of a pair of completely miscible liquids. In this case the two liquids are water and ethyl alcohol, and the inorganic salts soluble in water solutions are essentially insoluble in ethyl alcohol. The addition of ethyl alcohol to a saline solution, therefore, reduces the salts' solubility and causes precipitation.

Some of the principal salts are precipitated from sea water by this method in the same sequence as they would be by evaporation. Gypsum precipitates abundantly when the ethyl alcohol content of the solution is about 35 percent by volume, and halite begins to be precipitated when the content is about 65 percent. Although the method appears promising at this point, much testing remains to be done before its usefulness and applicability are established.

231. A GAMMA-RAY ABSORPTION METHOD FOR THE DETERMINATION OF URANIUM IN ORES

By Alfred F. Hoyte, Washington, D.C.

Work done in cooperation with the U.S. Atomic Energy Commission

The conventional method of determining the uranium content of rocks by radioactivity measurements yields a value for equivalent uranium—that is, the amount of uranium that would produce the observed radioactivity if perfect equilibrium existed. Many ores and minerals, however, are out of equilibrium, and where that is true this method fails to show the actual amount of uranium present. An attempt has therefore been made

to devise a new, nondestructive, radioactivity method of uranium analysis that would be virtually independent of the state of equilibrium of the sample.

Eichholz and others (1953) described a method which they claim is capable of making uranium analyses irrespective of the equilibrium condition of the uranium and its daughter products in the sample, and they have shown that this method works satisfactorily for most Canadian ores. It has recently been found, however, that this method gives erroneous results when applied to certain disequilibriated ores from other localities. This is so because the assumptions made regarding source of radiation and type of disequilibrium are not always valid.

In the hope of devising a method free from these objections, I have experimented with beta- and gamma-ray counting methods, both of which are easily applied, and found that the gamma-ray method was most successful.

U^{238} is an alpha emitter and cannot be conveniently measured directly. The method must therefore be capable of measuring a daughter product that is known to be in equilibrium with uranium. The first two daughters of U^{238} are Th^{234} ($T\frac{1}{2}=24.1$ d) and Pa^{234} ($T\frac{1}{2}=1.18$ m). Secular equilibrium is assured because both of these nuclides have very short half-lives. The third daughter product, U^{234}, has a half-life of $T\frac{1}{2}=25\times10^5$ y, which is too long to assure equilibrium. The 93 kev gamma-ray peak from Th^{234} was therefore used for the determination of uranium.

With the NaI(Tl) crystals currently available, it is difficult to resolve the 93 kev (Th^{234}) and the 68 kev (Th^{230}) peaks, and it is virtually impossible to resolve the Compton peak, a gamma ray of energy about 80 kev produced in the crystal by the radium–226 gamma ray of energy 188 kev.

The solution, then, would seem to lie in so setting the pulse-height selector as to detect only three peaks. Absorption of the gamma rays in various metals could then be used to formulate a method for determining the uranium content.

DESCRIPTION OF APPARATUS

The scintillation detector consists of a NaI(Tl) crystal optically coupled to an RCA 5819 photomultiplier tube operated at 1200 volts.

The negative pulses emitted by the photomultiplier (the amplitude of these pulses being proportional to the energy of the incident gamma-ray) are fed into a linear nonoverload amplifier, and these pulses are amplified so that they fall within the range of the pulse-height analyzer.

557753 O—60——33

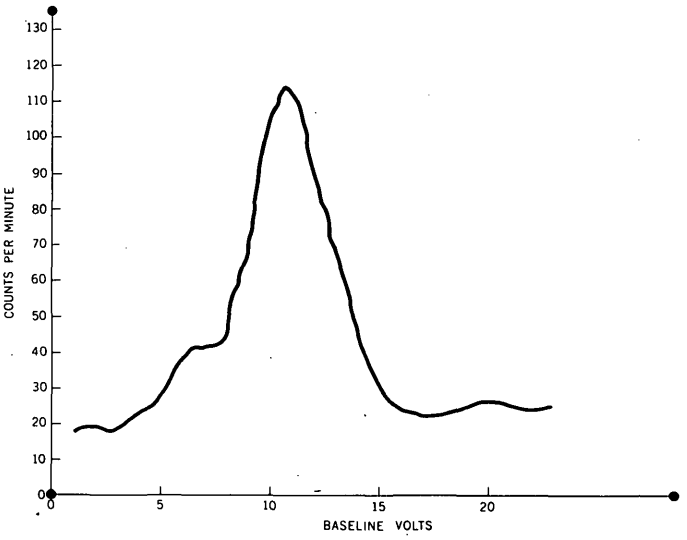

FIGURE 231.1.—The unresolved peak (68 kev, 80 kev, 93 kev).

The pulse-height analyzer is an instrument that measures the number of pulses per unit time of magnitude V volts as a function of V (Birks, 1953)—in other words it plots N(V) against V. Figure 231.1 is a plot of the unresolved peak made by means of this pulse-height analyzer, which was a single-channel one. To calibrate this instrument I used the 1.17 Mev and 1.33 Mev peaks from cobalt–60, the 0.67 Mev peak from cesium–137, and the 0.08 Mev peak from thorium–228. I checked the apparatus once a day for drift by plotting the distribution of some known peak.

The sample of ore to be assayed is crushed to powder, thoroughly mixed, then put into a cardboard pillbox two inches in diameter that has previously been weighed. The weight obtained for the sample is correct to 0.1 milligram.

THE METHOD

It is assumed that the counting rate (counts per minute per gram) of a sample at a given setting of the pulse-height analyzer is directly proportional to the percentages of (a) uranium, (b) equivalent thorium, and (c) equivalent radium in a sample of ore, where the equivalent of any daughter product is the amount of uranium that would be required in the sample to support it (Rosholt, 1957).

To check this assumption, a sample that is in radioactive equilibrium and two other samples that are out of equilibrium to a known extent were used to determine (a) the uranium counting rate, (b) the thorium counting rate, and (c) the radium counting rate in each of these samples. By using this information on these three standards a system of equations was developed, and the theoretical counting rates of several other sam-

ples were computed from the known radiochemical data. As shown in the following tabulation, the results are in good agreement with the measured counting rates:

Sample	Composition (percent)			Total number of counts per minute per gram	
	U	Th	Ra	Calculated	Experimental
229176	3. 02	15	14. 7	58. 9	59. 1
229184	. 75	8. 76	6. 07	26. 1	26. 8
253133	. 3	9. 12	6. 62	27. 6	27. 4
211894	. 01	5. 85	5. 17	19. 9	21. 4
234600	2. 01	2. 02	1. 99	11. 7	11. 5
234601	. 61	. 59	. 24	2. 3	2. 13
234052	. 13	. 091	1. 90	10. 61	10. 43
248147	17	13. 9	13. 2	87. 13	85. 92

ABSORPTION IN LEAD

As the counting rates for uranium, thorium, and radium have been computed and checked in a large number of samples, it is possible to get a relationship from them that enables one to determine quantitatively the absorption of each of the three radiations in lead.

A number of other absorbers have been tried, but lead was chosen as most desirable because of its k-absorption edge at 88 kev, which greatly attentuates the 93 kev peak of thorium–234.

For a given thickness of absorber, let the ratio between transmitted (I) and incident (I_o) radiation be as follows:

$$\text{for 93 kev } \frac{I}{I_o}=P, \text{ where}$$

$$P=\frac{\text{U counts per minute per gram with absorber}}{\text{U counts per minute per gram without absorber}}$$

Similarly for the 68 kev peak (thorium–230)

$$\text{put } \frac{I}{I_o}=q,$$

and for the 188 kev peak put

$$\frac{I}{I_o}=r.$$

Thus for the standard sample it may be shown that

$$pN_U+qN_{Th}=rN_{Ra}=N_D \quad (1)$$

where N_D is the number of counts per minute per gram with absorber.

Similarly for the first sample, which is out of equilibrium, the equation is

$$paN_U+qbN_{Th}+ncN_{Ra}=N_D \text{ (counts per minute per gram)} \quad (2)$$

and for the second

$$pxN_U+qyN_{Th}+rzN_{Ra}=N_D'' \quad (3)$$

from equations (1), (2), and (3) it is possible to determine the values of the coefficients p, q, and r.

From the nature of the equations it is obvious that p, q, and r are really the transmission coefficients for the radiations from the three nuclides—uranium, thorium, and radium respectively. These values can readily be checked by using the tables in the Handbook.

To derive three equations in three unknowns (uranium, thorium, and radium), one needs but to measure the transmission coefficients for two thicknesses of absorber. With some refinement, this method can be used to determine the amounts of U, Th, and Ra in the sample.

The system of equations thus obtained should be as follows (units are in counts/minute/gram):

$$N_U+N_{Th}+N_{Ra}=C'$$
$$\alpha N_U+\beta N_{Th}+\gamma N_{Ra}=C''$$
$$\zeta N_U+\eta N_{Th}+\lambda N_{Ra}=C'''$$

(α, β, γ, ζ, η, λ) are the measured transmission coefficients.

It is then possible to determine the number of counts per minute per gram due to each component of the radiation. A calculation of the ratios of the counts in the sample to those of the standard will give a determination of the percent uranium, percent equivalent thorium, and percent equivalent radium in the sample; the equations are as follows:

$$\text{Percent U sample}=\frac{\text{Uranium counts per minute per gram of sample}}{\text{Uranium counts per minute per gram of standard}}\times \text{percent U of standard}$$

CONCLUSION

The method gives good results with samples of uranium content of about 0.30 percent or more, as is shown in the following tabulation:

Sample	eTh^{230}	eRa	U (chemical) (percent)	U (this method) (percent)
F–30063	----------	----------	0. 280	0. 283
253133	9. 12	6. 62	. 300	. 296
F–18734	----------	----------	. 32	. 369
F–30016	----------	----------	. 55	. 590
F–20031	----------	----------	. 68	. 614
229184	8. 76	6. 07	. 75	. 713
229176	15. 0	14. 7	3. 02	2. 96
248147	13. 9	13. 2	17. 00	17. 40

The method is unreliable, however, for samples that contain less than 0.30 percent U. The reason for this, in our opinion, is the instability of the equipment. In trying to recheck some of the counts, the magnitude of the error in the total number of counts per minute per

gram was much greater than the number of counts that would be produced by the uranium in the sample, and it is therefore obvious that the uranium counts could easily be lost.

As there is a large error in the channel width of the pulse-height selector, the method should be improved by omitting this part of the equipment and using only a lower discriminator. A thin crystal should be used to eliminate the higher energy gamma rays.

REFERENCES

Birks, J. B., 1953, Scintillation counters: New York, McGraw-Hill Book Co., 148 p.

Eichholz, G. G., Hilborn, J. W., and McMahon, C., 1953, The determination of uranium and thorium in ores: Canadian Jour. Physics, v. 31, p. 613–628.

Rosholt, J. N., Jr., 1957, Patterns of disequilibrium in radioactive ores, *in* Dunning, J. R., and Prentice, B. R., eds., Advances in nuclear engineering, v. 2, pt. 2: New York Pergamon Press, p. 300–304.

232. METHOD OF GRINDING CESIUM IODIDE CRYSTALS

By Prudencio Martinez, Washington, D.C.

Work done in cooperation with the U.S. Atomic Energy Commission

For scintillation counting, it has been found that the resolution of cesium iodide for alpha particles is a function of the thickness of the scintillator. For this work, unmounted crystals ranging from 75 microns to 12 millimeters in thickness were required. As cesium iodide is very soft, it is difficult to grind and polish this material into very thin crystals by ordinary lapping methods. A brief description of the equipment and technique used to prepare thin unmounted crystals of cesium iodide and other soft crystalline material is given.

A minature lap shown in figure 232.1, was constructed for this work. During the grinding operation, the crystal blank is held in a jig as shown in figure 232.2. The crystal jig consists of a brass cylindrical housing into which the crystal blank is inserted, and a brass plunger that fits into the housing exerts a pressure against the crystal. It is necessary to provide a groove above the crystal end of the plunger to collect any excess grinding compound which may ooze past the edge of the crystal. Without the groove, the plunger tends to bind against the housing. When in operation the crystal jig rests on the lap and bears against two miniature ball bearings mounted on a perpendicular V-block. The bearings allow the jig to rotate uniformly during the grinding operation.

The crystal blanks were cut and faced on a lathe before lapping. In the lapping operation, a grinding paste made of ten- to fifteen-micron carborundum powder and light machine oil was used. Final polishing of the crystal after grinding was done with ethylene glycol. A glycol soaked wad of cotton is rubbed gently over the crystal which is then wiped dry with another piece of cotton. The crystal should not be rubbed with glycol any longer than 15 or 20 seconds. Polishing takes

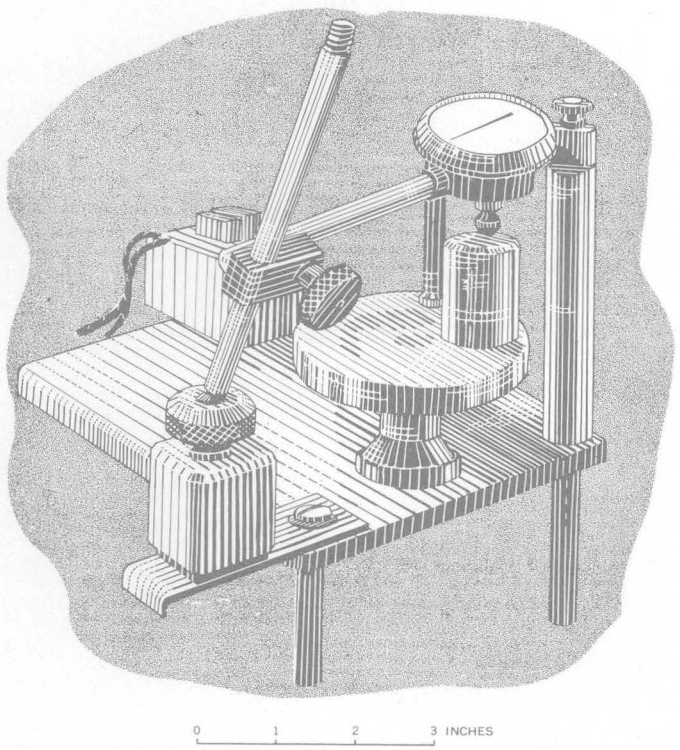

Figure 232.1—The minature lap showing jig in operating position.

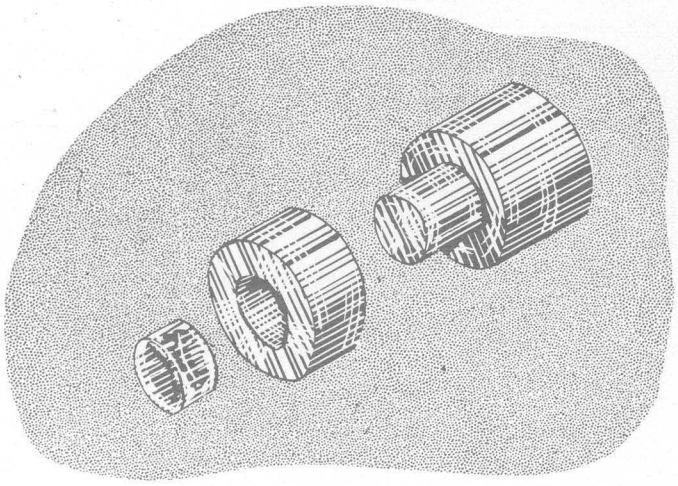

FIGURE 232.2.—Exploded view of crystal blank and jig.

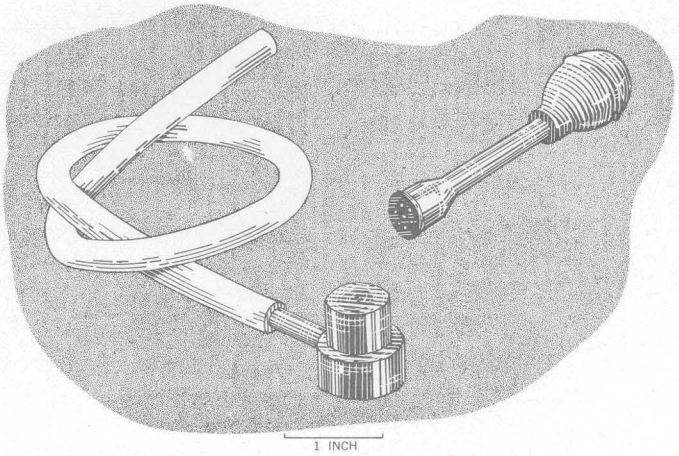

FIGURE 232.3.—The vacuum manipulator and pad.

place because of the partial solubility of CsI in glycol. Prolonged exposure to glycol will dissolve too much of the crystal, causing unevenness of the surface as well as feathering of the edges.

Owing to the softness and solubility of CsI, it is possible to handle the crystals manually only down to about 0.25 mm in thickness. Below this thickness, fracture of the crystal is probable, and a 75 micron thick crystal, for instance, will dissolve significantly if exposed to moist hands. To circumvent the problem of handling crystals thinner than 0.25 mm two vacuum handling devices as shown in figure 232.3 were made. The vacuum that can be produced by mouth is sufficient to operate them. If toxic hydrocarbons such as xylene, toluene, or benzene are to be used for washing the grinding compound from the crystal, these devices should be operated with a rubber bulb.

Crystals having thicknesses greater than 0.25 mm can be measured directly with a micrometer. For measuring crystals below 0.24 mm a dial gauge can be placed above the center of the plunger and the thicknesses of the crystal can be read directly as the grinding operation progresses. When the grinding is finished, the whole jig is slid off the lap and placed upside down on a table. The crystal is now supported by the plunger and protrudes from the housing. The vacuum holder is then used to transfer the crystal to a beaker containing the solvent. After the washing is completed, the crystal is deposited on a wad of cotton to dry. If polishing is required it can be done on the vacuum pad. For very thin crystals it is better to use cotton wrapped on a stick instead of a cotton wad as described earlier.

INDEX

[Numbers refer to articles]

U.S. GOVERNMENT PRINTING OFFICE: 1960 O—557753